

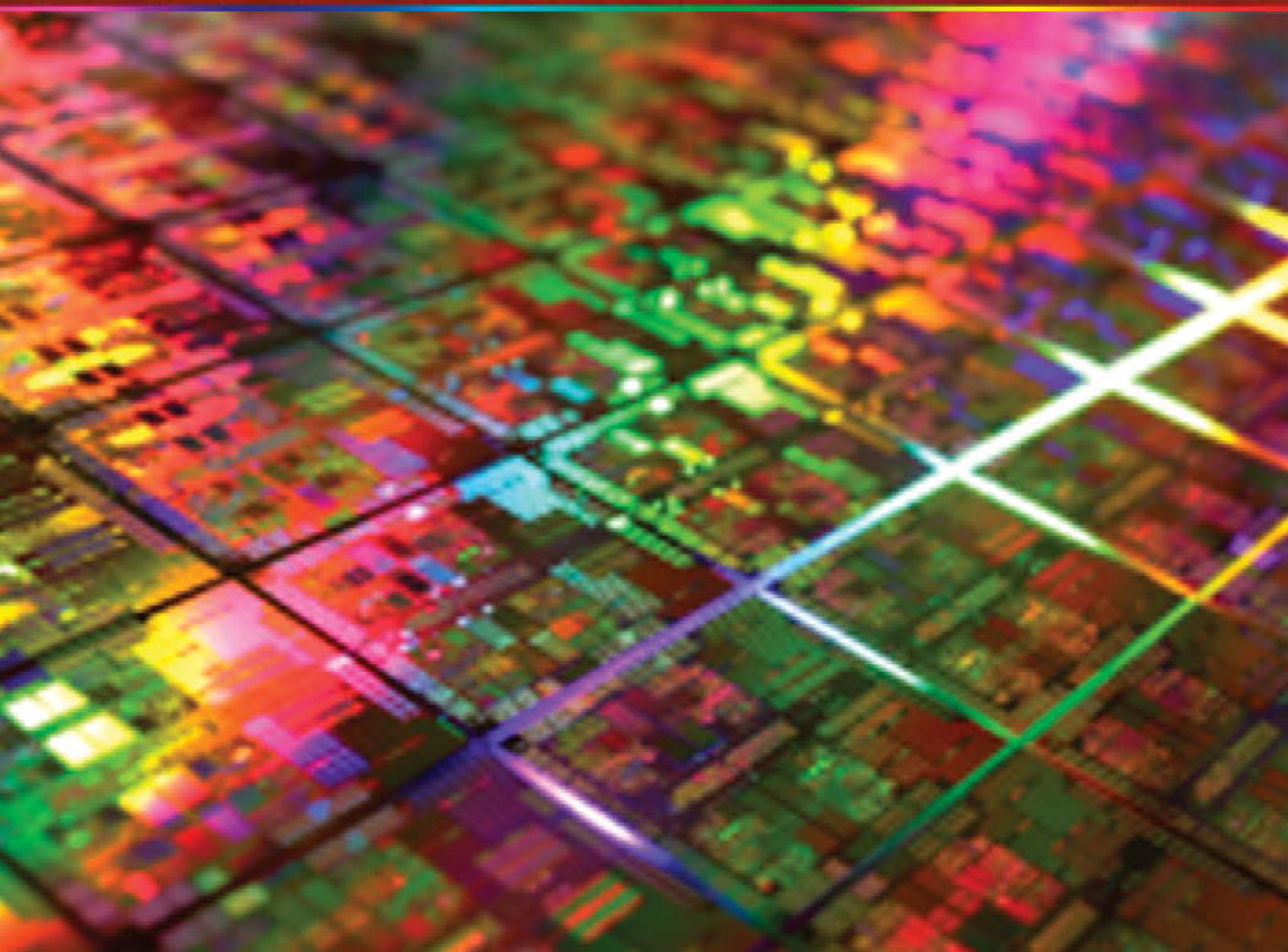
SPIE PRESS



SPIE

Chemistry and Lithography

Uzodinma Okoroanyanwu



Chemistry and Lithography

Chemistry and Lithography

Uzodinma Okoroanyanwu



WILEY

SPIE
PRESS

Bellingham, Washington USA

Library of Congress Cataloging-in-Publication Data

Okoroanyanwu, Uzodinma.

Chemistry and lithography / Uzodinma Okoroanyanwu.

p. cm. -- (Press monograph ; 192)

ISBN 978-0-8194-7562-6

1. Lithography. 2. Chemistry, Technical. I. Society of Photo-optical Instrumentation Engineers. II. Title.

NE2425.O38 2010

621.3815'31--dc22

2009036266

Published by

SPIE

P.O. Box 10

Bellingham, Washington 98227-0010 USA

Phone: +1 360.676.3290

Fax: +1 360.647.1445

Email: Books@spie.org

Web: <http://spie.org>

and

John Wiley & Sons, Inc.

111 River Street

Hoboken, New Jersey 07030

Phone: +1 201.748.6000

Fax: +1 201.748.6088

ISBN: 9781118030028

Copyright © 2010 Society of Photo-Optical Instrumentation Engineers

All rights reserved. No part of this publication may be reproduced or distributed in any form or by any means without written permission of the publisher.

The content of this book reflects the work and thought of the author(s). Every effort has been made to publish reliable and accurate information herein, but the publisher is not responsible for the validity of the information or for any outcomes resulting from reliance thereon.

Printed in the United States of America.



Dedicated to the memory of the late Professor William C. Gardiner, Jr.,
of The University of Texas at Austin, under whom I studied.

Contents

Preface	xxi
Acronyms and Abbreviations	xxv
Part I: Origins, Inventions, and the Evolution of Lithography	1
1 Introduction to Lithography	3
2 Invention of Lithography and Photolithography	9
2.1 Introduction	9
2.2 Invention of Lithography	11
2.3 Invention of Photolithography	17
2.4 Pioneers of Photography	18
2.4.1 Joseph Nicéphore Niépce—The inventor of photography and photolithography	19
2.4.2 Louis Jacques Mandé Daguerre	25
2.4.3 William Henry Fox Talbot	26
3 Optical and Chemical Origins of Lithography	29
3.1 Introduction	29
3.2 Key Developments that Enabled the Invention and Development of Lithography	33
3.2.1 Developments in optical physics	33
3.2.1.1 Tactile and emission theories of light	33
3.2.1.2 Early studies in optics and catoptrics	34
3.2.1.3 On the nature of light	38
3.2.1.4 Electromagnetic theory	50
3.2.1.5 Electromagnetic spectrum	55
3.2.1.6 Absorption of light	58
3.2.1.7 Chemical effects of light	58
3.2.1.8 The discovery of electrons	61
3.2.1.9 The discovery of x rays	62
3.2.1.10 Radioactivity	63

3.2.1.11	The beginnings of quantum theory	64
3.2.1.12	Molecular theory of matter	65
3.2.1.13	Blackbody radiation	66
3.2.1.14	Planck's quantum hypothesis for blackbody radiation	67
3.2.1.15	Einstein's quantum hypothesis for the photoelectric effect	69
3.2.1.16	Bright and dark line spectra	71
3.2.1.17	Nuclear model of the atom	74
3.2.1.18	Bohr's model of the hydrogen atom	75
3.2.1.19	Implications of Bohr's theory	78
3.2.1.20	Quantum theory of light	79
3.2.1.21	Einstein's theory of relativity	83
3.2.2	Developments in optical instruments and glassmaking technologies	85
3.2.3	Developments in chemistry	95
3.2.3.1	The four-element theory	95
3.2.3.2	Chemistry as a distinct discipline	97
3.2.3.3	Alchemy	98
3.2.3.4	Early theories of combustion and calcination	99
3.2.3.5	Phlogiston theory	100
3.2.3.6	Discovery of simple gases in common air	102
3.2.3.7	Foundation of modern chemistry	104
3.2.3.8	Post-Lavoisian evolution of chemistry	109
3.2.3.9	Development of various fields in chemistry	117
4	Evolution of Lithography	137
4.1	Introduction	137
4.2	Offset Lithography	141
4.3	The Printed Circuit Board and the Development of the Electronics Industry	142
4.4	The Transistor and Microelectronics Revolution	145
4.4.1	The invention of the transistor	145
4.4.2	Limits of discrete transistors	147
4.5	The Integrated Circuit	148
4.6	Other Notable Developments in Transistor Technology	148
4.7	Overall Device Technology Trends	152
4.8	Semiconductor Lithography	157
4.8.1	Optical lithography	160
4.8.2	Challenges of decreasing exposure wavelength in optical lithography	165
4.9	X-ray Lithography	165
4.10	Electron-Beam Lithography	167
4.11	Ion-Beam Lithography	169
4.12	Extreme Ultraviolet Lithography	170

4.13	Soft Lithography	170
4.13.1	Microcontact printing	171
4.13.2	Micromolding in capillaries	172
4.13.3	Nanoskiving	172
4.13.4	Step-and-flash imprint lithography	172
4.13.5	Nanoimprint lithography	172
4.14	Proximal Probe Lithography	173
4.15	Atom Lithography	175
4.16	Stereolithography	176
4.17	Molecular Self-Assembly Lithography	176
 Part II: Lithographic Chemicals		 179
5	Lithographic Chemicals	181
5.1	Introduction	181
5.2	Resists	181
5.2.1	Resist solvents	184
5.2.2	Manufacture of resists	184
5.3	Antireflection Coatings	186
5.4	Resist Developers and Rinses	187
5.5	Resist Strippers and Cleaners	189
5.6	Offset Lithographic Inks and Fountain Solutions	193
5.6.1	Offset lithographic inks	193
5.6.2	Fountain solutions	194
6	Negative Resists	195
6.1	Introduction	195
6.2	Resins	196
6.3	Types of Negative Resists	199
6.3.1	Non-radiation-based negative resists	199
6.3.1.1	Wax-lampblack-soap resists	199
6.3.2	Radiation-induced negative resists	200
6.3.2.1	Negative resists based on radiation-induced cross-linking reactions	200
6.3.3	Chemically amplified cross-linking negative resists	224
6.3.3.1	Chemically amplified negative phenolic resists based on acid-catalyzed condensation/intermolecular dehydration cross-linking reactions	224
6.3.3.2	Chemically amplified negative resists based on radiation-induced polarity changes	226
6.3.4	Non-chemically amplified negative resists based on radiation-induced polarity changes	227
6.3.4.1	Metal-chalcogenide resists	227

6.3.4.2	Ylide resists	232
6.3.4.3	Diazo resists	233
6.3.5	Chemically amplified negative resists based on radiation-induced polarity changes	234
6.3.5.1	Chemically amplified negative resists based on acid-catalyzed pinacol rearrangement	234
6.3.5.2	Chemically amplified negative resists based on acid-catalyzed intramolecular dehydration	236
6.3.5.3	Chemically amplified condensation/intermolecular dehydration negative resists based on acid-catalyzed cross-linking with acid-sensitive electrophile (cross-linking agent)	238
6.3.5.4	Chemically amplified methacrylate negative resists based on acid-catalyzed esterification	246
6.3.5.5	Chemically amplified methacrylate negative resists based on acid-catalyzed deprotection and development in supercritical CO ₂	247
6.4	General Considerations on the Chemistry of Cross-Linking	252
6.5	Negative Resists Arising from Polymerization of Monomers in the Presence of Polyfunctional Components	256
6.6	General Considerations on the Chemistry of Photoinitiated Radical Polymerization Employed in Negative Resist Systems	257
6.6.1	Photogeneration of radicals	258
6.6.1.1	Initiators based on photofragmentation	258
6.6.2	Radicals generated by hydrogen abstraction	262
6.6.2.1	Other practical initiator systems based on hydrogen abstraction	263
6.6.3	Dye-sensitized initiation	266
6.6.4	The initiation step	269
6.6.5	Propagation versus termination and the kinetic chain length	270
6.6.5.1	The steady state approximation	270
6.7	General Considerations on Photoinitiated Condensation Polymerization	272
6.7.1	The thiol-ene system	272
6.8	General Considerations on the Photoinitiated Cationic Polymerization Employed in Negative Resist Systems	273
6.8.1	Initiation by onium salts	273
6.8.1.1	Initiation	273
6.8.1.2	Propagation	274
6.9	Practical Negative Resist Compositions Arising from Photopolymerization of Monomers in the Presence of Polyfunctional Components	280
6.9.1	Negative resist composition	280
6.9.2	Binders	280

6.10	Lithographic Applications of Photopolymerization Negative Resists	280
6.10.1	Lithographic offset plates	281
6.10.2	Dry resists	281
6.10.3	Printed circuit boards	282
6.10.4	Solder mask	283
6.10.5	IC device fabrication	283
7	Positive Resists	285
7.1	Introduction	285
7.2	Types of Positive Resists	286
7.2.1	Non-chemically amplified positive resists	286
7.2.1.1	Non-chemically amplified positive resists based on functional group polarity switch	286
7.2.1.2	Non-chemically amplified positive resists based on main chain scission	323
7.2.2	Chemical amplification positive resists: the chemical amplification concept	335
7.2.2.1	Acid generators	336
7.2.2.2	Chemical amplification positive resists and their imaging mechanisms	343
7.2.2.3	Chemical amplification positive resists based on deprotection	343
7.2.2.4	Chemical amplification positive resists based on Claisen rearrangement	385
7.2.2.5	Chemical amplification positive resists based on depolymerization	387
7.3	Resist Materials for Multilayer Resist Systems	391
7.3.1	Hard mask resist materials	392
7.3.2	Top surface imaging resists	393
7.3.3	Bilayer resists	393
8	General Considerations on the Radiation and Photochemistry of Resists	395
8.1	Interaction of Radiation with Resists	395
8.2	Excited State Complexes	397
8.2.1	Excimers	397
8.2.2	Exciplexes	398
8.3	Energy Transfer	399
8.3.1	Dipole resonance transfer	400
8.3.2	Exchange transfer	401
8.3.3	The Perrin formula	402
8.4	Energy Migration in Resist Polymers	403
8.5	Spectral Sensitization	406
8.6	Sensitization by Energy Transfer	407

8.6.1	Triplet sensitization	407
8.6.2	Sensitization by electron transfer	408
8.7	Radiation Chemistry Versus Photochemistry of Resists	409
8.8	Radiation Chemical Yield and Dosimetry	411
8.9	Radiation Chemistry of Polymers	411
8.9.1	Backbone scission and cross-linking	411
8.9.2	Determination of the scission yield	412
8.9.3	Determination of the cross-linking yield G_x	413
8.10	Sensitivity and Exposure Radiation	414
8.11	Exposure Mechanisms of Resists and Exposure Radiation	415
9	Antireflection Coatings and Reflectivity Control	419
9.1	Introduction	419
9.2	Antireflection Coating Strategies	421
9.2.1	Top antireflection coatings	421
9.2.2	Theory of top antireflection coatings	424
9.2.3	Reflection and transmission amplitudes	424
9.3	Bottom Antireflection Coatings	428
9.3.1	Organic bottom antireflection coatings	428
9.3.1.1	Design approaches to organic bottom antireflection coatings	428
9.3.2	Inorganic bottom antireflection coatings	431
9.4	Applications of Bottom Antireflection Coatings	432
9.4.1	Suppression of standing waves and reflectivity effects	432
9.4.2	Feature CD trimming	435
9.4.3	Damascene applications involving silicon-containing resists and silicon-containing hard mask materials with antireflection properties	437
9.5	Organic versus Inorganic Bottom Antireflection Coating and Rework/Stripping Issues	438
9.6	Bottom Antireflection Coating–Resist Interactions	438
9.7	Theory of Bottom Antireflection Coatings	440
9.7.1	Reflectivity of absorbing layers	440
9.7.2	Electric field in photoresist films	441
9.7.3	Bulk standing wave intensity	444
9.7.4	Substrate reflectivity and photoresist absorbance	445
9.7.5	Relative swing amplitude	446
9.8	Bottom Antireflection Coatings for High-NA Imaging	448
	Part III: The Practice of Lithography	449
10	Stone, Plate, and Offset Lithography	451
10.1	Stone and Plate Lithography	451
10.2	Offset Lithography	455

10.3	The Offset Lithographic Press	456
10.4	Components of an Offset Lithographic Press	457
10.4.1	Paper-feeding system	457
10.4.2	Damping system	457
10.4.3	Inking system	457
10.5	Types of Offset Lithographic Inks	458
10.6	Fabrication of Lithographic Offset Plates	458
10.7	The Offset Lithographic Process	459
10.8	Waterless Offset Lithography	460
11	The Semiconductor Lithographic Process	463
11.1	Introduction	463
11.2	Adhesion Promotion	464
11.2.1	Priming of silicon dioxide surface with HMDS	466
11.3	Resist Coating	468
11.3.1	The resist spin-coating process	468
11.4	Characterizing Ultrathin Resist Processes	472
11.4.1	Instabilities in ultrathin resist films	473
11.4.2	Spin coating and instabilities in ultrathin resist films	473
11.4.3	Hydrodynamics of ultrathin resist films	474
11.4.4	Instabilities and thermophysical properties of ultrathin resist films	476
11.4.5	Ultrathin films and defectivity	482
11.5	Soft Bake/Prebake	485
11.6	Alignment	488
11.7	Exposure	489
11.8	Postexposure Bake	491
11.8.1	Deprotection kinetics of representative resist polymer systems	493
11.9	Monitoring Photoacid Generation in Thin Photoresist Films by Means of Fluorescence Spectroscopy	498
11.10	Postexposure Bake Sensitivity	501
11.11	Consequences of Acid Diffusion	502
11.12	Development	504
11.12.1	Resist development methods	505
11.12.2	Types of development processes	506
11.12.2.1	Chemical development	506
11.12.2.2	Physical development	507
11.12.3	Development rate characterization	507
11.12.3.1	Laser interferometry	507
11.12.3.2	Quartz crystal microbalance	509
11.13	Dissolution Mechanism of Resist Polymers	511
11.14	Dissolution Mechanism of Phenolic Resists	513
11.15	Comparison of Dissolution Characteristics of Novolac and Poly(hydroxystyrene)-based Resists	513

11.16	General Facts about the Dissolution Mechanism of DNQ/Novolac Resists	515
11.16.1	Mechanistic models for DNQ/novolac dissolution	517
11.16.1.1	The membrane model	518
11.16.1.2	The secondary structure model	519
11.16.1.3	The critical deprotonation model	522
11.16.1.4	The percolation model of resist dissolution	525
11.16.1.5	The critical ionization model	527
11.16.1.6	The stone wall model of novolac dissolution	527
11.16.1.7	Effects of resin and inhibitor structure on dissolution rate	527
11.17	Resist Development Issues	532
11.17.1	Pattern collapse	532
11.18	Postdevelopment Bake and Resist Stabilization Treatments	536
11.18.1	Postdevelopment bake	536
11.18.2	UV radiation curing	537
11.18.3	Electron-beam curing of resists	540
11.18.3.1	Radiation chemistry of electron-beam curing	542
11.18.3.2	Effects of electron-beam curing	542
11.19	Measurement and Inspection	543
11.20	Etching	544
11.20.1	Wet etching	544
11.20.2	Dry etching	545
11.20.2.1	Plasma etching	546
11.20.2.2	Reactive-ion etching	547
11.21	Rework/Stripping	548
12	Lithographic Modeling	551
12.1	Introduction	551
12.2	Historical Background	551
12.3	Structure of a Lithographic Model	554
12.3.1	Aerial image	556
12.3.2	Standing waves	556
12.3.3	Prebake	556
12.3.4	Exposure	556
12.3.5	Postexposure bake	556
12.3.6	Development	557
12.4	Basic Imaging Theory	557
12.5	Accounting for Aberrations	560
12.6	Aerial Image Formation Models	563
12.6.1	Scalar models for calculating aerial image intensity	563
12.6.1.1	Zero-order scalar model	564

12.6.1.2	First-order scalar model	564
12.6.1.3	High-NA scalar model	565
12.6.2	Full scalar and vector models	565
12.7	Standing Wave Models	566
12.8	Exposure Models	570
12.8.1	Adapting exposure kinetics of DNQ to the Dill equations	574
12.9	Postexposure Bake Models	579
12.9.1	Adapting exposure kinetics of chemical amplification resists to the Dill equations	582
12.10	Development Models	589
12.10.1	The kinetic development model or Mack model	590
12.10.2	The enhanced kinetic development model or enhanced Mack model	592
12.10.3	The lumped parameter model	593
12.10.4	Resist profile	598
12.11	Accuracy of Lithographic Models	599
12.12	Applications/Uses of Lithographic Modeling	600
12.12.1	Research applications	601
12.12.2	Process development applications	602
12.12.3	Manufacturing and instructional applications	603
13	Optical Lithography	605
13.1	Introduction	605
13.2	Elements of Optical Lithography	606
13.2.1	Radiation sources	608
13.2.1.1	High-pressure arc lamps	608
13.2.1.2	Excimer and excimer laser sources	609
13.2.2	Illumination system	616
13.2.3	Mask and reticles	618
13.2.3.1	Classification of masks	620
13.2.3.2	Mask types and mask materials	620
13.2.3.3	Fabrication of photomasks	623
13.2.3.4	Mask-making resists	626
13.2.3.5	Etching of mask-making resists	626
13.2.4	Pellicles	627
13.2.5	Exposure optics system	628
13.3	UV Photochemistry in the Exposure Chamber Environment of Optical Lithographic Tools	629
13.3.1	UV absorption properties of typical gases in lithographic exposure tools	630
13.3.2	Photodissociation of molecular oxygen	632
13.3.3	Photo-oxidative degradation of photoresist polymers	636
13.3.3.1	General mechanism of patterned resist polymer photo-oxidative degradation	637

13.3.4	Inorganic salt formation on DUV exposure tool lenses and reticles	641
13.3.4.1	Mechanism of ammonium sulfate crystal formation on DUV lithographic exposure lenses and reticles	642
13.3.5	Corrosion and oxidation of chrome structures in DUV lithographic masks	645
13.3.5.1	Mechanism of lithographic mask chrome structure oxidation	646
13.4	Optical Materials for UV and Visible Light Lithographies	648
13.4.1	Fused silica	651
13.4.1.1	Fused-silica degradation mechanisms	652
13.4.2	Calcium fluoride	655
13.4.3	Optical coatings	657
13.4.3.1	Aluminum mirrors	657
13.4.3.2	Dielectric optical coatings	658
13.4.4	Pellicle materials	658
13.5	Printing Modes	658
13.5.1	Contact and proximity printing	659
13.5.2	Projection printing	660
13.6	General Considerations on Optics Relevant to Lithography	665
13.6.1	Image formation	665
13.6.1.1	The role of the objective lens	668
13.6.1.2	Partial coherence theory of image formation	670
13.6.2	Image quality	673
13.6.2.1	Contrast	674
13.6.2.2	Modulation transfer function	674
13.6.2.3	Exposure latitude	675
13.6.2.4	Normalized image log-slope	676
13.6.2.5	Depth of focus	676
13.6.2.6	Exposure-defocus window	677
13.6.2.7	Critical dimension uniformity	677
13.7	Optical Lithographic Technologies and Their Performance	677
13.7.1	i-line (365-nm) lithography	677
13.7.2	KrF (248-nm) lithography	678
13.7.3	Dry ArF (193-nm) lithography	678
13.7.3.1	ArF resist material chemistry	681
13.7.3.2	ArF lithographic patterning issues	682
13.7.4	Water immersion ArF (193-nm) lithography	692
13.7.4.1	Resists and topcoats	694
13.7.4.2	Postexposure bake delay stability	696
13.7.4.3	Defectivity	696
13.7.5	F ₂ excimer laser (157-nm) lithography	700

14	X-Ray and Extreme Ultraviolet Lithographies	703
14.1	Introduction	703
14.2	Proximity X-Ray Lithography	704
14.2.1	Synchrotron sources	705
14.2.2	X-ray masks	706
14.3	Extreme Ultraviolet Lithography	707
14.3.1	EUV multilayer mirrors	710
14.3.2	Fabrication of Mo-Si multilayer mirrors	713
14.3.3	EUV masks	714
14.3.4	The EUV exposure system	715
14.3.5	Sources for EUV lithography	716
14.3.5.1	Laser-produced plasma sources	717
14.3.5.2	Discharge-produced plasma sources	718
14.4	Optics Lifetime	719
14.5	Contamination Processes	721
14.5.1	Carbon deposition	721
14.5.2	Oxidation	725
14.5.3	Impact of contamination	728
14.6	Contamination Mitigation Strategies	730
14.6.1	Exposure chamber environment control	731
14.6.2	Use of oxidation-resistant capping layers	731
14.6.3	Thermal processes used in EUV optics contamination mitigation	731
14.6.4	Nonthermal processes used in EUV optics contamination mitigation	733
14.6.5	Reactive-ion etching processes for cleaning contaminated optics	737
14.6.6	Debris-mitigation schemes	737
14.7	EUV Resists and Imaging Performance	737
15	Charged Particle Lithography	741
15.1	Introduction	741
15.2	Electron-Beam Lithography	741
15.2.1	Electron scattering	742
15.2.2	Electron-beam lithography systems	746
15.2.2.1	Electron sources	747
15.2.2.2	Electron optical components	748
15.2.2.3	Exposure stage	748
15.2.2.4	Computer	749
15.3	Types of Electron-Beam Lithographies	749
15.3.1	Electron-beam direct-write lithography	750
15.3.2	Scanning strategies	751
15.4	Electron Projection Lithography	751
15.4.1	Scattering with angular limitation projection electron-beam lithography (SCALPEL)	753
15.4.1.1	SCALPEL technology challenges	757

15.4.2	Projection reduction exposure with variable axis immersion lens (PREVAIL) lithography	759
15.5	Ion-Beam Lithography	759
15.5.1	Types of ion-beam lithographies	761
15.5.2	Ion projection lithography	763
15.5.3	Stochastic blur	766
16	Lithography in Integrated Circuit Device Fabrication	767
16.1	Introduction	767
16.2	Fabrication of a 90-nm CMOS Microprocessor	773
16.2.1	Twin-well process	773
16.2.1.1	n -well formation	773
16.2.1.2	p -well formation	775
16.2.2	Shallow trench isolation process	776
16.2.2.1	STI oxide fill	777
16.2.2.2	STI oxide polish and nitride strip	777
16.2.3	Polysilicon gate process	778
16.2.4	Lightly doped drain implant processes	778
16.2.4.1	n^- LDD implant	779
16.2.4.2	p^- LDD implant	779
16.2.5	Sidewall spacer formation	779
16.2.6	Source/drain implant process	780
16.2.6.1	n^+ S/D implant	780
16.2.6.2	p^+ S/D implant	781
16.2.7	Contact formation	782
16.2.8	Via-1 and tungsten plug formation	782
16.2.8.1	Via-1 formation	783
16.2.8.2	Tungsten plug formation	783
16.2.9	Copper interconnect wiring formation by means of the dual damascene technique	784
16.2.10	Bond pad metal formation and packaging	790
16.2.11	Wafer testing and sorting	790
17	Advanced Resist Processing and Resist Resolution	
	Limit Issues	791
17.1	Introduction	791
17.2	Resist Systems	792
17.2.1	Single-layer resist systems	792
17.2.2	Multilayer resist systems	792
17.2.2.1	Hard mask resist system	794
17.2.2.2	Top surface imaging resist system	794
17.2.2.3	Bilayer resist system	796
17.3	Advanced Resist Processing Techniques	797
17.3.1	Single-exposure techniques	797
17.3.1.1	Hyper-NA imaging resist processing techniques	798

17.3.1.2	EUV lithography resist processing technique	799
17.3.1.3	Postexposure-based CD shrink techniques	799
17.3.2	Reflow CD shrink techniques	800
17.3.2.1	Thermal reflow shrink technique	800
17.3.2.2	Electron-beam-induced CD shrink techniques	801
17.3.3	Chemically induced CD shrink techniques	803
17.3.3.1	Chemically induced CD shrink techniques based on sidewall formation	803
17.3.3.2	Chemically induced CD shrink techniques based on sidewall erosion	806
17.3.3.3	Plasma-assisted CD shrink technique	808
17.3.4	Double-exposure techniques	809
17.3.5	Double-patterning techniques	811
17.3.5.1	Lithography-etch-lithography-etch patterning scheme	813
17.3.5.2	Lithography-freeze-lithography-etch patterning scheme	813
17.3.5.3	Self-aligned double-patterning (SADP) scheme	815
17.4	Resolution Limit Issues of Resists	818
17.4.1	Resolution limits due to chemical amplification in resists	819
17.4.1.1	Elucidating how photoacid diffusion leads to resist contrast and resolution loss	823
17.4.2	Resolution limits due to line edge roughness	825
17.4.2.1	Base quenchers	826
17.4.2.2	Polymer size	827
17.4.2.3	Shot noise	828
17.4.3	Resolution limits due to confinement effects in resists	829
17.4.4	Resolution limits due to resist polymer molecular properties	830
17.4.5	Resolution–line edge roughness–sensitivity trade-off	831
17.5	Resist Materials Outlook for the 22-nm and Smaller Technology Nodes	833
17.6	Resist Processing Outlook for the 22-nm and Smaller Technology Nodes	834
	Afterword	835
	Index	837

Preface

It is my intention to provide in this book a concise treatment of chemical phenomena in lithography in a manner that is accessible to a wide readership. While the emphasis is placed on how lithography is mediated through chemical phenomena, topics in optical and charged particle physics as they are practiced in lithography are also presented, with a broader view to illustrate how the marriage between chemistry and optics has made possible the print and electronic revolutions on which our digital age depends.

The link between chemistry and lithography is essentially fourfold. First, several important chemical and physical principles were involved in the invention of lithography and photolithography. This theme is explored in Part I, covering Chapters 1–4. Chapter 1 introduces the role of lithography in print and electronic revolutions. Chapter 2 deals with the invention of lithography and photolithography. Chapter 3 provides the background surrounding the discovery of the chemical and optical principles that made possible the invention of lithography and photolithography. Chapter 4 traces the evolution of lithography from its invention to the various forms in which it is practiced today.

Second, the processes for the synthesis, manufacture, usage, and handling of lithographic chemicals and materials are all chemical transformations, involving distinct chemical reactions that follow well-established chemical principles. This theme is explored in Part II, covering Chapters 5–9. Chapter 5 deals with synthesis and formulation of the chemicals used in lithography such as inks, fountain solutions, resists, antireflection coatings, solvents, developers, resist strippers and removers, etc. Chapters 6 and 7 explore the chemistry of negative and positive resist materials, respectively, in terms of their synthesis, physical characterization, radiation chemistry, imaging mechanism, and lithographic applications. Chapter 8 explores in a general manner the radiation and photochemistry of resist materials. Chapter 9 deals with the theory and application of antireflection coatings in reflectivity control.

Third, several important chemical and physical principles are involved in the various modules that constitute lithography, covering preparation of the lithographic substrates (be they lithographic plates or silicon wafers), coating and deposition of resist solutions on appropriate substrates affording thin dry films, exposure of the dry films to actinic radiation, thermal processing of the exposed films, development of the exposed and baked films to afford the

lithographic relief images, and postdevelopment processes designed to stabilize the relief images against subsequent processes. These themes are explored in detail in Part III, dealing with the practice of lithography as exemplified in stone plate and offset lithography on one hand, and semiconductor lithography on the other. These topics are covered in Chapters 10–17.

Chapter 10 deals with stone and offset lithographic processing that is employed in the printing of fine art images, newspapers, textbooks, advertisements, etc. By far, the most advanced form of lithography practiced today is semiconductor lithography, used in the fabrication of logic and memory integrated circuit (IC) devices that power computers, cell phones, telecommunications systems, and a host array of other devices. For this reason, Chapter 11 is entirely dedicated to a discussion on the overview of the semiconductor lithographic process, covering all of the chemical and physical phenomena involved in all of the related unit operations. In particular, the physical characterization of these processes as well as the photochemistry and photophysics involved in the exposure processes are highlighted. Chapter 12 deals with lithographic modeling. Chapter 13 in turn deals with optical lithography, which by far is the most dominant of all of the semiconductor lithographic techniques. Covering g-line, i-line, KrF, ArF, and F₂ lithographies, the discussion here focuses on the physics and chemistry of the exposure sources, the construction of the exposure tool, mask making, and application of these lithographies in device manufacture. Chapter 14 deals with x-ray and EUV lithographies. Chapter 15 presents charged particle lithographies based on electron beams and ion beams.

Chapter 17 explores the chemistry underlying advanced resist processing techniques, including resist-based resolution enhancement techniques (such as double patterning, chemical amplification of resist line or the CARL process, hydrophilic overlayer or the HOL process, reflow techniques, etc.) and stabilization techniques (such as UV, e-beam curing, and ion implantation) used to improve the quality of semiconductor lithographic patterning. In such techniques, the chemistry is often quite different from that used in conventional resist processing. This is one of the most active areas of current research, and one in which it appears likely that employing postexposure resist chemical modifications might prove successful in overcoming resolution limits imposed by the constraints of the geometric optics of the exposure tool.

Chapter 17 also discusses the chemical and physical basis of emerging patterning challenges confronting lithography as the industry transitions to lithographic nodes where the physical properties of the resist become extremely sensitive to the substrate and interfacial and confinement effects. These effects begin to manifest as the thickness of the resist film approaches a few multiples of the radius of gyration of the polymers from which they are constituted. Such challenges include resolution loss due to uncontrolled diffusion, thin-film instabilities and confinement effects, line edge roughness, etc. Other equally important challenges, but not altogether related to resist film thickness, include the impact of oxygen on lithographic patterning, contamination (airborne, water, resist outgas, particle, inorganic salts, etc.), pattern collapse, line width slimming, etc. These are covered in Chapter 13.

The fourth link between chemistry and lithography concerns the principles governing the chemical transformations utilized in process-integration schemes that are part of the implementation of lithography in IC device fabrication. This theme, discussed in Chapter 16, explores how lithography is used to define and pattern the various front end of lithography (FEOL) and back end of lithography (BEOL) layers of a state-of-the-art Advanced Micro Devices (AMD) microprocessor based on a complementary metal-oxide semiconductor (CMOS) device.

An attempt has been made throughout the book to provide examples illustrating the diversity of chemical phenomena in lithography across the breadth of the scientific spectrum, from fundamental research to technological applications. The format of this book is not necessarily chronological, but is such that related aspects of lithography are thematically organized and presented with a view to conveying a unified view of the developments in the field over time, spanning many centuries, from the very first recorded reflections on the nature of matter to the latest developments at the frontiers of lithography science and technology. Nonetheless, the emphasis is predominantly placed on applications that have relevance in the semiconductor industry. The enormous wealth of materials from which these illustrations and examples have been drawn means that this author's choice is inherently peculiar, although each example is intended to provide deeper insight into the underlying principles involved.

A great many of the pioneers of chemistry and lithography are not represented herein at all. I can only record my immense debt to them and all who have contributed to the development of the two fields to the state in which I have reported it.

I am indebted to a number of people who in one way or another made this book possible. My academic mentor, the late Professor William C. Gardiner, Jr. of The University of Texas at Austin, distinguished teacher and physical chemist, himself the author of numerous books, introduced me to physical chemistry and guided my academic development in the field.

Professor C. Grant Willson of The University of Texas at Austin introduced me to lithography and supervised my doctoral thesis. I learned the intricacies of resist processing under the tutelage of the late Dr. Jeffrey Byers of SEMATECH.

A number of colleagues and associates proofread the entire manuscript or some chapters of the book, and provided valuable suggestions and corrections. These include Dr. Harry J. Levinson, my manager at AMD and also at GlobalFoundries, and Dr. Chris Mack, developer of PROLITH and founder of the FINLE Corporation, both of whom read the entire manuscript. Dr. Jim Thackeray of Rohm and Haas Electronic Materials read Chapters 5–8; these are the chapters dealing with lithographic chemicals. Dr. Witek Maszara of GlobalFoundries read Chapter 16, which deals with the application of lithography in IC device fabrication. These reviewers should not be blamed for any errors that may remain, which are strictly my responsibility.

In a less direct way, I have benefited throughout my professional career from scientific and technical discussions in the area of advanced lithography with colleagues at the strategic lithography technology departments of both AMD and GlobalFoundries, as well as at the lithography department of

IMEC (Inter-University Microelectronics Center). I have also benefited from scientific discussions in the area of polymers and photochemistry with Professor Katharina Al-Shamery of Univeristät Oldenburg in Germany, and in the area of physical methods of polymer characterization with Professors Jim Watkins and Todd Emrick of the University of Massachusetts at Amherst.

I also want to express my sincere thanks to the editorial staff of SPIE, and especially to Dara Burrows and Tim Lamkins, who have been most sympathetic and helpful at all times during the course of writing this book. They remained undismayed by the long delays as the length of the book expanded far beyond what we originally agreed to. The book is a much better book because of their editorial assistance.

Portions of this book were written in libraries and museums in a number of locations within the United States and Germany. I am particularly grateful to the staff of the archives of the Deutsches Museum in Munich, especially to Dr. Eva Mayring, Margrit Prussat, and Wolfgang Schinhan, for the assistance they rendered to me during my research at their facility in locating archival materials on and by some of the seminal individuals whose research in decades and centuries gone by greatly contributed to the invention and development of lithography.

The permission granted to me by AMD and extended by GlobalFoundries, the two companies for which I work, made it possible for me to write this book. I am indebted to Michela Jacob, the librarian in the AMD Fab30 facility and GlobalFoundries Fab1 in Dresden, Germany, for the numerous books and articles she was able to procure for me, sometimes from libraries far-flung from Dresden. I am also indebted to the individuals and publishers who granted me the permission to reproduce in this book some of their copyrighted figures and tables.

Finally, I must acknowledge the assistance I have received from my family members. Writing a book of this size takes undue toll on everyone directly or indirectly involved with it, particularly family members who have had to endure all kinds of inconveniences too numerous to mention. I wish therefore to acknowledge their helpful support. For these and other blessings, I am truly grateful.

*Uzodinma Okoroanyanwu
Florence Village, Northampton, Massachusetts
November 2010*

Acronyms and Abbreviations

AEE	aminoethoxy ethanol
AFM	atomic force microscope
AIBN	azobis(isobutyronitrile)
AMC	airborne molecular contaminant
APM	atomic processing microscope
AR	antireflection
ARC	antireflection coating
att-PSM	attenuated phase-shifting mask
BARC	bottom antireflection coating
BEOL	back end of line
BIM	binary intensity masks
BJT	bipolar junction transistor
BLR	bilayer resist
BOCST	butoxycarbonyloxystyrene
BOP	benzyloxy-protected poly(<i>p</i> -hydroxystyrene)
BPO	benzoyl peroxide
CaF ₂	calcium fluoride
CAD	computer-aided design
CAR	chemically amplified resist
CARL	chemical amplification of resist lines
CBN	carbo- <i>t</i> -butoxy norbornene
CD	critical dimension
CFC	chlorofluorocarbon
CH	cyclohexanone
CMN	carbomethoxy norbornene
CMOS	complimentary metal-oxide semiconductor
CMP	chemical mechanical polishing
CMTF	critical modulation transfer function
CO	cycloolefin
COG	chromium-on-glass
COMA	cycloolefin-maleic anhydride
COP	crystal-originated pit
CPU	central processing unit
CVD	chemical vapor deposition

DC	direct current
DEA	dissociative electron attachment
DEAP	diethoxyacetophenone
DMAc	dimethylacetamide
DMF	dimethylformamide
DMI	dimethyl-2-imidazolidinone
DMPA	dimethoxy phenylacetophenone
DMSDMA	dimethylsilyldimethylamine
DMSO	dimethylsulfoxide
DNQ	diazonaphthoquinone
DOF	depth of focus
DP	degree of polymerization
DPD	diazopyrazolidine dione
DPP	discharge-produced plasma
DPPH	diphenyl picrylhydrazyl
DRAM	dynamic random access memory
DRLS	development rate log slope
DRM	development rate monitor
DTBP	di- <i>tert</i> -butyl peroxide
DTBPIONf	di(<i>tert</i> -butylphenyl) iodonium perfluorobutanesulfonate (nonaflate)
DUV	deep ultraviolet
EBES	electron-beam exposure system
EBL	electron-beam lithography
ECR	electron cyclotron resonance
EFM	electric-field-induced migration
EL	ethyl lactate
EOC	etalon output coupler
EOL	end of line
EPR	electron projection lithography
ESCAP	environmentally stable chemically amplified photoresist
ESD	electrostatic discharge
EUV	extreme ultraviolet
FEOL	front end of line
FET	field-effect transistor
FIB	focused ion beam
FRP	free radical polymerization
FTIR	Fourier transform infrared
FWHM	full width half maximum
HDPCVD	high-density chemical vapor deposition
HEPA	high-efficiency particulate air
HF	hydrofluoric acid
HMDS	hexamethyldisilazane
HOL	hydrophilic overlayer
HSQ	hydrogen silesquioxanes

HVM	high-volume manufacturing
IC	integrated circuit
IGFET	insulated gate field-effect transistor
ILD	interlayer dielectric
IMS	ion microfabrication system
IPL	ion projection lithography
ITRS	International Roadmap for Semiconductors
JFET	junction field-effect transistor
KRS	ketal resist system
KTFR	Kodak Thin Film™ resist
LBNL	Lawrence Berkeley National Laboratories
LEE	low-energy electron
LEEPL	low-energy electron projection lithography
LELE	lithography-etch-lithography-etch
LER	line edge roughness
LFLE	lithography-freeze-lithography-etch
LLD	lightly doped drain
LPCVD	low-pressure chemical vapor deposition
LPP	laser-produced plasma
L/S	line/space
LWR	line width roughness
Mac	methylacetamide
MEA	monoethanolamine
MEBES	multiple electron-beam exposure system
MEEF	mask error enhancement factor
MEMS	microelectromechanical system
MET	microexposure tool
MIBK	methylisobutyl ketone
MIF	metal-ion-free
ML	multilayer
MMA	methyl methacrylate
MOCVD	metal-organic chemical vapor deposition
MOP	methoxypropyl-protected poly(<i>p</i> -hydroxystyrene)
MOS	metal-oxide semiconductor
MOSFET	metal-oxide semiconductor field-effect transistor
MTF	modulation transfer function
MW	molecular weight
NA	numerical aperture
NBHFA	norbornene hexafluoroisopropanol
NHA	numerical half-aperture
NH ₄ HF	ammonium fluoride
NILS	normalized image log-slope
nMOS	<i>n</i> -channel metal-oxide semiconductor
NMP	N-methylpyrrolidone
NVSM	nonvolatile semiconductor memory

OPC	optical proximity correction
OPD	optical path difference
OPE	optical proximity effect
PAC	photoactive compound
PAG	photoacid generator
PBOCST	poly(<i>tert</i> -butoxycarbonyl oxystyrene)
PBS	poly(butene sulfone)
PCB	printed circuit board
PCM	portable conformable mask
PDMS	polydimethylsiloxane
PE	photoelectron
PEB	postexposure bake
PECVD	plasma-enhanced chemical vapor deposition
PFOS	perfluorooctane sulfonic acid
PGMA	poly(glycidyl methacrylate)
PGME	propylene glycol monomethylether
PGMEA	propyleneglycol monomethyl ether acetate
PHOST	polyhydroxystyrene
PMIPK	poly(methyl isopropenyl ketone)
PMMA	poly(methyl methacrylate)
pMOS	<i>p</i> -channel metal-oxide semiconductor (field-effect transistor)
PMPS	poly(methylpentene sulfone)
ppb	parts per billion
PPDA	<i>p</i> -phenylenediacrylic acid
PREVAIL	projection reduction exposure with variable axis immersion lens
PROLITH	positive resist optical lithography
PSM	phase-shifting mask
PVD	physical vapor deposition
PVP	poly(vinyl pyridine)
PWB	printed wiring board
RB	rose bengal
RC	resistance capacitance
RELACS	resolution enhancement of lithography assisted by chemical shrink
RIE	reactive-ion etching
ROMP	ring-opening metathesis polymerization
SADP	self-aligned double patterning
SAM	self-assembled monolayer
SCALPEL	scattering with angular limitation projection electron-beam lithography
S/D	source/drain
SEMC	single-electron memory cell
SLM	spatial light modulator
SLR	single-layer resist
SNS	sulfone/novolak system

SPM	sulfuric acid and hydrogen peroxide mixture
STI	shallow trench isolation
STM	scanning tunneling microscope
TBEST	<i>tert</i> -butyl ester-protected 4-hydroxystyrene
TBMA	<i>tert</i> -butyl methacrylate
TBTFMA	<i>tert</i> -butyl-2-trifluoromethylacrylate
TCAD	technology computer-aided design
TE	transverse electric
TEM	transmission electron microscopy
TFE	tetrafluoroethylene
THF	tetrahydrofuran
THP	tetrapyranal
TM	transverse magnetic
TMAH	tetramethylammonium hydroxide
TMS	trimethylsilyl
TMSDEA	trimethylsilyldiethylamine
TMSDMA	trimethylsilyldimethylamine
TPSHFA	triphenylsulfonium hexafluoroantimonate
TSI	top surface imaging
ULPA	ultralow-penetration air
UTR	ultrathin resist
UV	ultraviolet
VAP	vinyl addition polymerization
VEMA	poly(vinyl ether- <i>alt</i> -maleic anhydride)
VUV	vacuum ultraviolet
WET	wafer electrical test
XRR	x-ray reflectivity

Chapter 1

Introduction to Lithography

I have imposed upon myself, as a law, never to advance but from what is known to what is unknown, never to form any conclusion which is not an immediate consequence necessarily flowing from observation and experiment; and always to arrange the facts, and the conclusions which are drawn from them, in such an order as to render it most easy for beginners in the study of chemistry thoroughly to understand them.

Antoine Lavoisier, *Traité Élémentaire de Chimie*

It is hard to think of an invention that has had a greater influence on the mass production of devices that have enabled humankind to communicate information with printed matter or with photons or with electrons or with ions or even with atoms than lithography. The information highways and pathways of our present age—the information age—are literally paved with chips of crystalline silicon made by lithography. Nearly every book, magazine, newspaper, brochure, flyer, catalog, and other print piece that has been produced during the last three hundred years has been printed with offset lithography. Nearly every integrated circuit (IC) in the chips that run the computers and telecommunication systems that power the information highway, as well as medical devices, electronics, home and industrial appliances, automobiles, and airplanes—to mention but a few—is made by semiconductor lithography. Without such integrated circuits, we would have no powerful computers, no large-scale automation, no communication satellites, or even space exploration. There would certainly be no electronic calculators or digital watches, no transistor radios, portable tape recorders, personal digital assistants, Internet, cell phones, etc. Many diagnostic procedures in medicine and dentistry rely on integrated circuits, as does the heart pacemaker and the modern hearing aid. The impact of all these things on our lives is tremendous. For instance, we can watch events on our television sets or mobile phones or on the Internet as they are happening thousands of miles away. We can withdraw our money from automatic teller machines almost everywhere in the world, without the aid of a bank clerk, whose function has been transformed from that of an accounts keeper to one of an intermediary between the customer and the computer.

Many products are now manufactured, assembled, and shipped today by automatic machines that rely on integrated circuits for their operations. Airplanes are guided by computer-controlled systems and even airline seats are reserved worldwide by an instantaneous computer booking system. The list is almost endless and is growing every day. A world without lithography would be unrecognizable to any one of us today, although we may not always be cognizant of its pervasiveness and reach in our daily lives.

How did we get to where we are today? It all started with the invention of lithography in 1798, of photolithography and photography simultaneously in 1826, and subsequent developments in lithography ever since, all of which were made possible by antecedent developments in chemistry and optical physics over a period spanning more than 30 centuries, since records began to be kept. Through this unique marriage of chemistry and optics, the science and technology of lithography have evolved and made possible the mass production of printed materials, starting from the late eighteenth century during the industrial revolution and culminating in the microelectronics revolution that ushered in the mass production of microelectronic equipment, starting from the middle of the twentieth century with the invention of the transistor in 1947 and the invention of the integrated circuit 12 years later. Innovations in lithography, new materials, and scaling to ever-smaller dimensions have led to many orders of magnitude of improvement in the capability of transistors to carry out computation, thus paving the way for the information age in which we currently live. All of these developments have radically influenced the course and trajectory of human civilization and development.

This book therefore deals with how chemistry mediates lithography, a topic that has not been previously discussed at length. In particular, it traces the arc of developments in lithography from a chemical perspective, starting from its invention and reaching back in an unmistakably continuous line to a period much earlier still. Like an arc, it has a beginning, a bow, and a tip. The beginning of this arc is the invention of lithography in 1798, the bow of the arc is the invention of photolithography in 1826, and the tip of the arc coincides with the development of semiconductor lithography in the 1950s and culminates in the state of the art in the field today.

The objective of this book is not to lay out 30 centuries of the history of science, particularly that of physics and chemistry, like a long piece of wallpaper, and divide it into so many superficial categories after the manner of the encyclopedist and the abridger. Instead, we will focus on the lines of strategic change and carefully examine those moments in the history of physics and chemistry that seem consequential and uncover the intellectual knots that had to be untied, which directly or indirectly aided the development of lithography. The treatment therefore needs not follow in chronological order and linear fashion, but rather must be organized around similar coherent themes.

It is very useful to learn from the mistakes of early scientists, to examine particular intellectual hurdles associated with given periods, as well as the course of scientific developments that ran into blind alleys, but that nonetheless affected the progress of science in general and lithography in particular.

Since its invention, lithography has witnessed tremendous evolution. Many of its variants are now practiced, ranging from stone plate lithography used in fine art printing, to offset lithography used in the printing of newspapers and the like, and to semiconductor lithography, which utilizes a variety of exposure radiations to print integrated circuits. While all of these variants of lithography are covered in this book, our emphasis will be on semiconductor lithography, since it is the most scientifically and technically advanced form of lithography. And within semiconductor lithography, optical lithography is the most dominant technique used in fabrication of integrated circuits. Most importantly, relative to other lithographic techniques, semiconductor lithography best exemplifies the marriage of chemistry and optics—a theme that we explore in depth in this book.

Lithography in its very essence is a series of chemical transformations—a fact recognized by its inventor who called it chemical printing. Like all chemical transformations, its currency of transaction is the electron—outer-shell electrons of the atoms, molecules, and compounds of the material (also called resist) on which the image of the mask or the object to be printed is recorded, to be precise. These electrons orchestrate distinct bond-breakage and bond-formation events in all of the process steps in lithography that ultimately lead to the contrast between the clear (exposed) area and the dark (unexposed) area of the image-recording medium. Preparation of the substrate, coating of the resist, the actual exposure, and subsequently the postexposure thermal and related processing are all characterized by distinct chemical processes that taken together are ultimately about chemical bond breakage and formation.

In the substrate preparation step involving priming, the surface chemistry of the substrate is modified to promote the adhesion between the substrate and the resist material during coating. In the exposure process proper, exquisite radiation chemistry takes place inside the radiation sources in order to generate the exposure radiation, but also because of the interaction of these radiations—be they photons, ions, electrons, x rays—with the outer-shell electrons of the radiation-sensitive compounds and molecules in the resist, leading to bond breakage and/or bond formation.

In the postexposure thermal processing steps, thermally driven diffusion and reaction of the active species that catalyze deprotection, bond scission, or cross-linking reactions in the resist are engendered. In the development step, appropriate areas of the resist film are dissolved away either through physical dissolution (involving no chemical reaction) or through acid-base neutralization reactions between the exposed areas of the resist and the developing solvent (depending on polarity). This is the basis of the contrast between the exposed and unexposed areas of the resist film.

The main attribute of optical lithography that made it the manufacturing technology of choice for ICs since the beginning of the IC era is the tremendous throughput advantages it offers through its ability to reproduce an entire IC layout from a master (or reticle) in a single exposure, in contrast to other technologies that address a field point by point. In addition to the compelling throughput advantages, there were resolution and cost advantages as well. The infrastructure for light sources, lenses, reticles, photosensitive polymers, and other optical materials developed for other optical and photographic applications were

appropriated and applied to IC lithography, allowing development resources to be shared.

In 1965, Gordon Moore¹ postulated that the exponential growth in the number of transistors in an IC led to certain technical and economic advantages. Smaller transistors switch faster, allowing more operations per second. And more transistors with more interconnections enable computations of much greater complexity to be achieved. This postulate has since been codified as Moore's law,² which states that the complexity of ICs as measured by the number of transistors approximately doubles every two years (see Fig. 1.1). This law has led to unprecedented growth in the computer industry. Technologies that were once available only in supercomputers are now commonly available in children's toys. Satellite communications networks that were once the domain of the military now help drivers find their way to their locations.

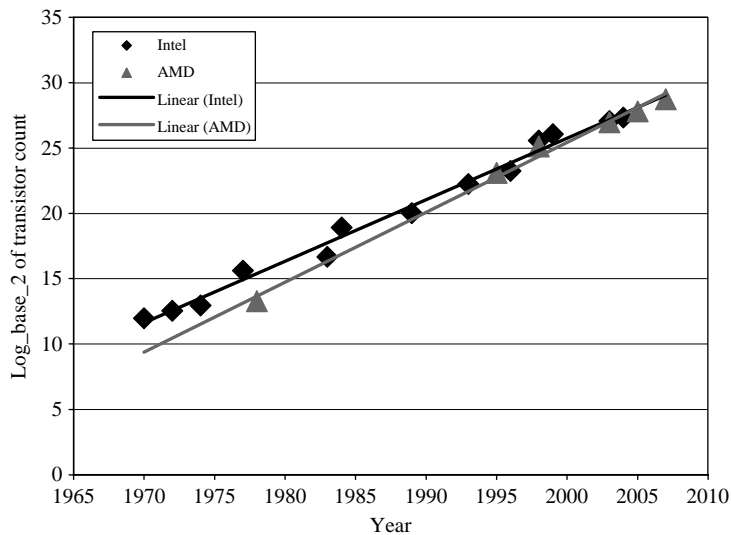


Figure 1.1 Plot of the number of transistors versus year for microprocessors manufactured by Advanced Micro Devices, Inc. and Intel Corporation microprocessors.³

A good metric for measuring progress in IC lithography is resolution, the ability to resolve and distinguish two neighboring features on the chip. Two main approaches for improving resolution include decreasing the wavelength of

¹G.E. Moore, "Cramming more components onto integrated circuits," *Electronics* **38**(8), 114–117 (1965).

²G.E. Moore, "Progress in digital electronics," IEEE Meeting 1975, *Tech. Digest* 11–13 (1975); G.E. Moore, "Lithography and the future of Moore's law," *Proc. SPIE* **2440**, 2–17 (1995).

³For information on transistor count number versus year of manufacture for AMD's microprocessors, please see <http://www.amd.com>; for Intel Corporation's microprocessors, please see <http://www.intel.com/museum/archives/history/docs/Moore.htm>/Intel Microprocessor Transistor Count Chart.

the optical source and increasing the numerical aperture of the optical system, as derived from Rayleigh's resolution criterion⁴ and shown in Eq. (1.1).

$$w = k_1 \frac{\lambda}{\text{NA}}, \quad (1.1)$$

where w is the half pitch of the feature being printed, k_1 is a process-dependent parameter, λ is the exposure wavelength, and NA is the numerical aperture of the optical system, which is defined in terms of the maximum cone angle of rays (θ_{max}) subtended by the maximum pupil diameter at the image plane as: $\text{NA} = n \sin \theta_{\text{max}}$ (where n is the refractive index in image space). Equation (1.1) unites chemistry with optics in lithography, for it is the interaction of the exposure photons, electrons, ions, or x rays transmitted through the numerical aperture of the optics, with the electrons of the high-contrast recording medium—photosensitive materials (resists)—that mediates chemical phenomena on which lithographic patterning is based. The exposed part of the resist is altered relative to the unexposed part, leading to contrast between the two regions during development.

The progress of optical lithography is partly, then, the result of decreasing the exposure wavelength. From the initial broadband sources, the IC industry made a migration first to the mercury g-line (436 nm), then to the i-line (365 nm), and then switched to exciplex⁵ laser sources—first KrF (248 nm) and now ArF (193 nm). A migration to an F₂ excimer laser source was contemplated by the IC industry, but did not materialize, even after significant investments, primarily because of issues associated with the availability of IC industry-grade calcium fluoride (CaF₂), used in the lens elements. The migration toward shorter wavelengths

⁴Lord Rayleigh, "Investigations in optics, with special reference to the spectroscope," *London, Edinburgh, Dublin Phil. Mag. J. Sci.*, Series 1 6, **18**(49), Pt. XXXI, 261–274, Pt. XLVI, 403, 411, and Pt. LVI, 477–486 (1879); Lord Rayleigh, "Investigations in optics, with special reference to the spectroscope," *London, Edinburgh, Dublin Phil. Mag. J. Sci.*, Series 7, **9**(53), Pt. V, 40–55 (1879); Lord Rayleigh, "On the theory of optical images, with special reference to the microscope," *London, Edinburgh, Dublin Phil. Mag. J. Sci.* **42**(255), Pt. XV, 167–195 (1896).

⁵The term "exciplex" refers to a combination AB* of two different atoms; it exists only in an electronically excited state and dissociates as soon as the excitation is lost. It differs from an "excimer," an excited state dimer of two similar atoms AA*. The exciplex lasers that have found widespread applications in lithography are based on KrF* and ArF* formed in electrical discharge in a mixture containing krypton and fluorine in KrF lasers and argon and fluorine in ArF lasers, respectively. The only true excimer laser that has found application in lithography is based on excited state F₂* dimers (lasing at 157 nm). The KrF* and ArF* exciplex and F₂ excimer survive for a few nanoseconds, long enough to participate in laser action. As soon as the excitation is gone, the atoms separate because the potential energy curve of their ground state is repulsive. Unfortunately, the widely used misnomer "excimer laser" appears in the literature to describe exciplex lasers XeCl* (lasing at 308 nm), KrF* (lasing at 248 nm), and ArF* (lasing at 193 nm) when "exciplex laser" is appropriate. In this book, we will use the appropriate terms. [For the photochemistry of excimers and exciplexes, please see, for example, P.W. Atkins, *Physical Chemistry*, 5th ed., p. 609, W.H. Freeman, New York (1994); P. Suppan, *Chemistry and Light*, pp. 104–110, Royal Society of Chemistry, Cambridge, England (1994)].

naturally limits the pool of available photosensitive materials that could be employed in resist formulations.

Because the NA of the optical system limits the spatial frequencies that can be transmitted to expose the resist, the NA of lens designs has migrated from 0.2 to 0.42 to 0.63 to 0.75 to 0.95. With a fundamental limit of NA = 1.0 for a conventional optical system, the introduction of immersion ArF lithography has enabled the migration to hyper-NA (>1.0) optical systems. It is noteworthy that the drive toward high NA is at a cost of decreased depth of focus and increased difficulty in fabricating a lens with adequate field size.⁶

Today, the leading-edge microelectronic devices are being made with photolithography at 193 nm, which is inevitably a continuation of the progression from longer-wavelength lithographies and is dictated by the requirements for higher resolution and the drive in the IC industry toward greater packing density and higher speeds, as noted earlier.

The resolution that will be necessary for the manufacture of future generations of ICs with feature sizes below 22 nm is beyond the limits of 365-, 248-, and 193-nm UV lithographies. According to the International Technology Roadmap for Semiconductors (ITRS),⁷ extreme ultraviolet (EUV) lithography at 13.5 nm is a promising candidate for achieving such high resolution. With EUV lithography, sub-22-nm devices can be fabricated with conventional masks using reflective optics of 0.25–0.45 NA.

As stated above, this book attempts to systematically reappraise the main developments in chemistry and optics that have ultimately led to lithography as practiced today, especially in semiconductor lithography—the most advanced form of lithography.⁸ The task is no doubt an onerous one, but one that must be done in order to unearth the hidden connections between the various streams of thoughts that materialized as lithography and subsequently as semiconductor lithography.

⁶M.J. Bowden, “The lithographic process: the physics,” Chapter 2 in *Introduction to Microlithography*, L.F. Thompson, C.G. Willson, and M.J. Bowden, Eds., pp. 19–138, American Chemical Society, Washington, DC (1994).

⁷<http://www.itrs.org>

⁸Although the emphasis of this book is on semiconductor lithography, attempts will be made where necessary to highlight relevant aspects of the low technology variants of lithography as practiced in offset lithography and fine art lithography.

Chapter 2

Invention of Lithography and Photolithography

God grant that it [lithography] may soon spread all over the world; that it may prove useful to mankind, and contribute to its improvement; and that it may never be abused to any dishonourable or wicked purpose; and I shall then never cease to bless the hour in which I invented it.

Alois Senefelder,¹ 1771 1834

2.1 Introduction

Before beginning this journey through how lithography and subsequently photolithography came into existence, and how the technology has evolved ever since, it is necessary to review the cultural, scientific, and technological framework out of which these planographic printing techniques emerged. A great deal has already been written about the artistic and sociological impacts of the fine art lithographers and photographers of the nineteenth and twentieth centuries, which will not be reviewed here. The introduction of lithography at the end of the eighteenth century and of the simultaneous introduction of photolithography and photography in the third decade of the nineteenth century greatly influenced every facet of human endeavor, particularly in scientific and technological pursuits.

With the rise during the seventeenth and eighteenth centuries of many scientific fields based on visual observations—systematics (or the taxonomy of biological organisms), topology, and geology—the ability to make illustrative drawings of scientific observations became an increasingly important skill. A very high premium was also placed on the ability to make realistic and accurate drawings of mechanical arts and engineering. Concomitant with these developments was the rapid industrialization brought about by the industrial revolution in Britain

¹A. Senefelder, *A Complete Course of Lithography*, p. 85, Da Capo Press, New York (1997). [This book is an unabridged republication of the first English edition published in London in 1819, which was originally published in German under the title, *Vollständiges Lehrbuch der Steindruckerey*.]

and its influence elsewhere during the late eighteenth century, which increased the need for draftsmen to produce drawings to aid in the production and use of the ever-expanding number of machines needed for the industries.²

These factors naturally increased the value of individuals who were able to record images directly as seen in nature without interpretation by an artist or a draftsman. Being able to draw provided one with upward social mobility in an era where class and social distinctions determined one's worth in a society. The origins of this exact form of drawing stem from art conventions of perspective drawings set forth in the early Renaissance, which were in turn derived from Euclid's geometry. The removal of artifice from art through the codification of a system of drawing that produced what was understood to be scientifically accurate reflections of the world was the main goal of the rules of perspective. And by the seventeenth century, these Renaissance rules were brought to their apex by the great Dutch artists. In addition to rules of perspectives, artists and draftsmen were aided by a variety of mechanical drawing devices or drawing machines like perspectograph, (invented in 1816 by Thomas Alason³), physiognotrace (invented in 1786 by Gilles Luis Chretien), and cameras, mostly camera obscura and camera lucida.⁴

The camera obscura was the most common camera in use then. Although it was referred to in writings dating from antiquity, the camera obscura was first described in detail by Johann Baptista Porta in 1533. Literally meaning "dark room," the camera obscura is basically a dark chamber or box, with an opening through which light passes. The light entering the camera opening falls onto the wall opposite the opening to form an image. A camera obscura with small opening requires no lens to be operational. However, larger openings outfitted with a lens produce very bright images.⁵

Another type of camera, the camera lucida, which means "light room" and may refer to the fact that the instrument did not require any enclosure, box, or lens as in the camera obscura, was first described in 1807 by William Hyde Wollaston, although the exact source of the name is unknown. There are basically two main types of *camerae lucidae*. The first one is a device with a reflective glass mounted on a stand, such that the glass is positioned at a 45-deg angle to the paper. This allows the artist or draftsman to see the reflection of the scene on the glass and also to look through the glass to the paper. The scene is thus perceived to be superimposed on the paper and can be easily copied. Images made with this type of camera lucida are laterally reversed. The other type of camera lucida uses a four-sided prism fastened to a small stand. The use of this type of instrument calls for the artist or draftsman to position the eye so that it sees both the image

²M.S. Barger and W.B. White, *The Daguerreotype: Nineteenth Century Technology and Modern Science*, pp. 4–10, Johns Hopkins University Press, Baltimore (1991).

³T. Alason, in *Trans. Soc. Arts*, pp. 145–147 (1816).

⁴M.S. Barger and W.B. White, *The Daguerreotype: Nineteenth Century Technology and Modern Science*, pp. 4–5, Johns Hopkins University Press, Baltimore (1991).

⁵*ibid.*, pp. 6–8.

of the scene reflected directly on the retina and the scene on which the paper is copied.⁶

Being more portable and convenient to use than the camera obscura because it was a very simple device with only a few parts and it did not require a darkened surrounding, and that once its operation had been learned it was easy to use, the camera lucida quickly found wide use among draftsmen, especially for tasks such as enlarging or reducing drawings and for copy work. Its portability made the camera lucida useful to both professional artists and amateurs making topological and architectural views. In particular, the camera lucida had special appeal to travelers because it could be used to make “correct representations”⁷ of the places visited even by those who could not draw as well as artists. The renowned traveler and British naval officer Col. Basil Hall wrote a laudatory book about the camera lucida, in which he claimed that once the operation of this camera was mastered, the user “could rove where he pleases, possessed of the magical secret of recording the features [scenes] and freed from the triple misery of Perspective, Proportion and Form, all responsibility respecting these taken off his hands.”⁸

Equally significant was the increased demand during this period not only for unique works of art such as portraits and drawing, but also for reproductions of works of art such as prints. Demand for printed books also witnessed a phenomenal rise during this period. By sheer necessity, new printing methods and new methods of making the paper needed for the mass production of inexpensive art works and books were developed during this time. Lithography, the only new printing method discovered since the invention of movable type some three hundred years earlier, was introduced during this period. It revolutionized printmaking in every facet because it was faster and cheaper than any of the previous printing processes.⁹

2.2 Invention of Lithography

The invention of lithography dates from 1798 when the playwright Alois Senefelder¹⁰ (see Fig. 2.1) writing with ink¹¹ prepared with wax, soap, and

⁶ibid., pp. 6–8.

⁷B. Hall, *Forty Etchings, from Sketches Made with the Camera Lucida in North America in 1827 and 1828*, Cadell & Co., Edinburgh (1829), memorandum.

⁸M.S. Barger and W.B. White, *The Daguerreotype: Nineteenth Century Technology and Modern Science*, pp. 6–8, Johns Hopkins University Press, Baltimore (1991).

⁹ibid., pp. 8–9.

¹⁰A. Senefelder, *Vollständiges Lehrbuch der Steindruckerey*, “Karls Thienemann and Gerold, Munich, Vienna,” (1818), a complete course in lithography (in German).

¹¹The lithographic ink is used for writing or drawing immediately on the stone, or for covering the surface of it, or for transferring drawings, executed on the paper, to the stone. The ink functions principally to fill the pores of the stone in those places to which it is applied with an oily greasy substance, and it also resists the action of *aqua fortis* and other acids. Inks are generally of two kinds: one of a thicker nature for drawing on the stone; and another of a more liquid nature for transferring drawings to the stone. Senefelder discloses the following eight recipes as making the best ink compositions: (1) white beeswax (8 parts by weight), soap (2 parts by weight), lampblack (1 part by weight);

lampblack on a tablet of polished Kellheim limestone,¹² the border of which he lined with wax,¹³ and on the entire surface of which he applied an acid solution¹⁴ for a short period of time, led him to the serendipitous discovery that the limestone was etched away in areas on which he had not written. The wax writing solution resisted¹⁵ the acid. On removing the acid, he observed that the written or image

(2) wax (12 parts by weight), common tallow (4 parts by weight), soap (4 parts by weight), lampblack (1 part by weight); (3) wax (12 parts by weight), shellac (4 parts by weight), soap (4 parts by weight), lampblack (1 part by weight); (4) tallow (8 parts by weight), shellac (8 parts by weight), soap (4 parts by weight), lampblack (1 part by weight); (5) wax (8 parts by weight), shellac (4 parts by weight), mastic (4 parts by weight), soap (4 parts by weight), lampblack (1 part by weight); (6) wax (8 parts by weight), tallow (4 parts by weight), shellac (4 parts by weight), soap (4 parts by weight), lampblack (1 part by weight); (7) wax and gum guaicum melted together in equal quantities (12 parts by weight), tallow (4 parts by weight), soap (4 parts by weight), lampblack (1 part by weight); (8) wax (6 parts by weight), shellac (4 parts by weight), tallow (2 parts by weight), mastic (3 parts by weight), Venetian turpentine (1 part by weight), soap (4 parts by weight), lampblack (1 part by weight). Preparation of the ink calls for mixing together all of the different ingredients (in the manner listed above for each composition) except the soap, in an iron saucepan, and exposing the mixture to a strong fire until the whole of the mass ignites. When the quantity of the mixture is reduced to one half, the saucepan is carefully covered, or poured into a container of water, to extinguish the flame and cool the substance. Colorants for the ink, besides lampblack, may include indigo, blue lake, vermilion, and red ochre, and various other colors, provided they do not alter the nature of the soap. Distilled water is recommended for dissolving the ink. [A. Senefelder, *A Complete Course of Lithography*, pp. 110–118, Da Capo Press, New York (1997).]

¹²The best Kellheim stones for making lithographic stone plates, Senefelder reported, came from Solenhofen, a village in Bavaria, Germany. Chemically, these stones consist of calcium carbonate. In nitric and other acids, they can be almost entirely dissolved, with the carbonic acid escaping in the form of gas. The demand for these stones at the time was very high, but their availability was restricted by political and economic events such as the continental blockade and the various military campaigns of the period. Thus, early on it became a matter of national priority to find either local sources of limestone or suitable substitutes for printing stones in order to free countries like England and France from their dependence on German limestone. [Cited in M.S. Barger and W.B. White, *The Daguerreotype: Nineteenth Century Technology and Modern Science*, p. 9, Johns Hopkins University Press, Baltimore (1991).]

¹³A substance that is sometimes used for covering the stones, which like the ink compositions, resists the action of *aqua fortis*, is known under the name of etching ground, as it differs very little from that which engravers use for their copper plates. Senefelder's recipe for this calls for: wax (12 parts by weight), mastic (6 parts by weight), asphaltum (4 parts by weight), colophony (2 parts by weight), tallow (1 part by weight). Preparation of the etching ground involves melting all of the above ingredients together on the fire in an iron saucepan, and exposing the latter to heat until the asphaltum is completely dissolved. Then, the mass is left burning until it is reduced to about two thirds; after which the fire is extinguished and the product cooled and formed into different shapes and preserved for use. Alternatively, a good etching ground can be prepared from plain wax, if it is left boiling and burning until nearly five parts of it are consumed. [A. Senefelder, *A Complete Course of Lithography*, pp. 122–123, Da Capo Press, New York (1997).]

¹⁴*Aqua fortis*, or nitric acid, muriatic acid, vinegar, tartaric acid, malic acid, and oxalic acid are typical acids used in stone plate lithography to etch away nonimage, nonwritten areas of the stone, i.e., areas that are not properly covered with grease.

¹⁵Because the wax resisted the etching action of the acid, materials behaving as such within the field of lithography have since then been called resists.



Figure 2.1 Portrait of Alois Senefelder, the inventor of lithography. (Published with permission from the Deutsches Museum, Munich.)

areas were raised by about 1/10 inch above the rest of the stone. By carefully rolling ink over the stone surface, he could deposit ink pigments only on the image areas of the stone, which he could easily transfer to a sheet of paper with little pressure (see Fig. 2.2 for the first lithographic press constructed by Senefelder and Fig. 2.3 for a portable hand press also constructed by Senefelder in 1818). Senefelder called his invention *steindruck*, which means “stone printing.”¹⁶

¹⁶According to Senefelder, the invention of lithography draws its direct origin under the most trifling of circumstances in a story he narrated thus: “I had just succeeded in my little laboratory in polishing a stone plate, which I intended to cover with etching ground, in order to continue my exercises in writing backwards, when my mother entered the room, and desired me to write her a bill for the washer woman, who was waiting for the linen; I happened not to have even the smallest slip of paper at hand, as my little stock of paper had been entirely exhausted by taking proof of impressions from the stones; nor was there even a drop of ink in the inkstand. As the matter would not admit of delay, and we had nobody in the house to send for a supply of the deficient materials, I resolved to write the list with my ink prepared with wax, soap, and lampblack, on the stone which I had just polished, and from which I could copy it at leisure.

Some time after this I was just going to wipe this writing from the stone, when the idea all at once struck me, to try what would be the effect of such a writing with my prepared ink, if I were to bite in the stone with *aqua fortis* [nitric acid]; and whether, perhaps, it might not be possible to apply printing ink to it, in the same way as to wood engravings, and so take impressions from it. I immediately hastened to put this idea in execution, surrounded the stone with a border of wax, and covered the surface of the stone, to the height of two inches, with a mixture of one part of *aqua fortis*, and ten parts of water, which I left standing 5 minutes on it; and on examining the effect of this experiment, I found the writing elevated about a 10th part of a line (or 1 120th part of an inch.) Some of the finer, and not sufficiently distinct, lines, had suffered in some measure, but the greater part of the letters had not been damaged at all in their breadth, considering their elevation; so that I confidently hoped to obtain very clear impressions, chiefly from printed characters, in which there are not many fine strokes.

I now proceeded to apply the printing ink to the stone, for which purpose I first used a common printer’s ball; but, after some unsuccessful trials, I found that thin piece of board, covered with fine cloth, answered the purpose perfectly, and communicated the ink a more equal manner, than any



Figure 2.2 Wooden lithographic press constructed by Alois Senefelder and used in his invention of lithography. (Published with permission from the Deutsches Museum, Munich.)



Figure 2.3 Lithographic stone and small hand press constructed by Alois Senefelder in 1818 and used for fast production of lithographic prints. Note the copy made from the handwritten note on the lithographic stone. (Published with permission from the Deutsches Museum, Munich.)

other material I had before used. My further trials of this method greatly encouraged my perseverance. The application of the printing ink was easier than in the other methods, and I could take impressions with a fourth part of the power that was requisite for an engraving, so that the stones were not at all liable to the danger of breaking; and, what was the greatest moment for me, this method of printing was an entirely new invention, which had occurred to nobody before me". [A. Senefelder, *A Complete Course of Lithography*, pp. 9–11, Da Capo Press, New York (1997) (originally published in 1819).]

Because Senefelder was printing in relief, this method is not the same as what we call lithography today. Nevertheless, Senefelder's invention was a significant advancement over the older copper plate engraving printing method, which was rather laborious, slow, and costly. But the basis of all modern lithography derives also from another observation of his,¹⁷ which was that when a greasy (oily) image is drawn on a slab of limestone surface of appropriate size ground flat to desired texture, perhaps with a pencil, following which a solution of gum arabic¹⁸ (preferably acidic in the pH range between 3.5 and 5) is applied, and when an ink roller is subsequently rolled over the entire stone surface, ink would deposit only on the image areas on the stone (i.e., areas on the stone drawn with the greasy pencil) and would be repelled in the nonimage areas (i.e., areas of the stone without the drawings from the greasy pencil). With a little pressure, he could easily transfer the image on the stone to a paper laid face down on the stone. This invention—based on the fact that oil and water repel each other—is the basis of all contemporary lithographic printing. He called this invention *chemische druckerey*, which means “chemical printing” because the process depends on the chemical interaction of grease, dilute acid, gum arabic, and water, rather than the stone from which the name lithography is derived.

¹⁷According to Senefelder, “My whole process was therefore, as follows: To wash the polished stone with soap water, to dry it well, to write or draw upon it with the composition of ink of soap and wax, then to etch it with *aqua fortis*; and lastly, to prepare it for printing with an infusion of gum water. I had hoped to have been able to dispense with the gum water, but was soon convinced that it really enters into chemical affinity with the stone, and stops its pores still more effectually against the fat, and opens them to the water. In less than three days after my first idea, I produced as perfect and clear impressions, as any that has since been obtained”. [A. Senefelder, *A Complete Course of Lithography*, pp. 31–32, Da Capo Press, New York (1997).]

¹⁸The lithographic stone, being made of limestone and therefore containing numerous pores, is equally capable of imbibing greasy as well as watery substances through these pores. These substances have the quality of adhering to the particles that make up the stone, but can be easily separated from them, so long as the nature of the stone is not altered. This alteration is effected by sulfuric, tartaric, and phosphoric acids. Water evaporates gradually from the pores when the stone dries; but gum arabic and other greasy substances do not. Printing ink cannot adhere to the stone, so long as it contains a sufficient quantity of water. In general, it adheres only faintly to the calcium carbonate surface, and does not get stronger affinity to it, until its pores are filled with the greasy hydrophobic etching ground (resist) to which the ink, also hydrophobic, can favorably unite. This affinity of adhesion of the printing ink with the resist on the stone takes place only when the two hydrophobic substances can directly contact each other. If this contact is interrupted (which may happen when the etching ground has penetrated too deep into the stone and has left the surface), the etching ground will not take the printing ink until direct contact has been reestablished between these two greasy substances. When applied to a well polished stone, the solution of gum arabic, being very hydrophilic, produces the effect that the wetted spot will not accept the hydrophobic ink as long as it remains wet. But as soon as the spot dries up, the ink adheres to it, but can be easily wiped off with a sponge and water. The gum arabic does impart to the stone the quality of rejecting the printing ink, a quality that is made all the more durable if the acid has been previously applied to this spot, before the application of the gum arabic. On this principle lies lithographic printing. [A. Senefelder, *A Complete Course of Lithography*, pp. 146–147, Da Capo Press, New York (1997).]

The process has been variously called *steindruckerey*, polyautography, engraving or printing from stone, and *imprimerie chimique*. The French were the first to call the process by its current name, *lithographie*,¹⁹ which means “writing with stone,” and derived from Greek words *lithos* meaning stone and *graph* meaning to write.

Not long after Senefelder’s original discovery, artists across Europe employed it to make reproductions of the works of old masters and, in time, recognized it as a valuable medium for their own original works. “Not only was it the first printing process to be introduced after the invention of the movable type three hundred years earlier,” Barger and White²⁰ assert, “it was also based on chemical, not mechanical, principles.” Descriptions of the process were widely disseminated in scientific and technical journals, as well as in the popular press. By 1815, Mulhouse, France, had developed into a major center for lithography in Europe, and many people came there from England and Germany to learn the process.²¹ By 1825, A. Hyatt Mayor asserts that “lithography matured its classic style when Goya, as an exile in Bordeaux, drew four big stones of bullfights. At 79, when most men are happy if they can refine what they invented years earlier, Goya created the first great works of art in the medium, the first that combine the freedom of a sketch with a black-and-white as rich and as satisfying as a painting. The road that he opened was soon followed by great artists like Delacroix, Daumier, Degas, Lautrec, Bonnard, Vuillard, Matisse, Picasso, and practically every prominent painter in France, and ultimately by those in other countries.”²²

From France, lithography spread westward to the United States and eastward to Persia. Remarkably, British engravers and aquatinters fought the adoption of lithography in England, fearing that it threatened their monopoly of reproducing paintings and drawings, and so they persuaded Parliament to exclude the excellent German limestones with a prohibitive import duty. On their part, American engravers were under the impression that lithography was just a shortcut to what engravers did, but since they were not part of an organized body that could lobby the U.S. Congress, Currier and Ives were left free to exploit the process for reproducing thousands of paintings and drawings.²³

The first steam lithographic press was invented in France in 1850 and introduced into the United States by R. Hoe around 1868.²⁴ Lithographic stones were used for the image and a blanket-covered cylinder received the image from the plate and transferred it to the substrate in the steam lithographic press. Direct rotary presses for lithography using zinc and aluminum metal plates were

¹⁹M.S. Barger and W.B. White, *The Daguerreotype: Nineteenth Century Technology and Modern Science*, pp. 8–10, Johns Hopkins University Press, Baltimore (1991).

²⁰*ibid.*, p. 9.

²¹*ibid.*, p. 9.

²²A.H. Mayor, in A. Senefelder, *A Complete Course of Lithography*, pp. V–VI, Da Capo Press, New York (1997) [Mayor provides an excellent introduction to the 1977 edition of Senefelder’s classic book].

²³*ibid.*

²⁴[http://4dps.dynodan.com/printing process explained/index.html](http://4dps.dynodan.com/printing%20process%20explained/index.html)

introduced in the 1890s.²⁵ The first offset press was independently invented in 1903 by Ira A. Rubel (a paper manufacturer) and A.F. Harris.²⁶

The offset process rose to become the most popular form of printing during the 1950s as quality of plates, inks, paper, etc. improved tremendously. Beginning from the late 1950s, it became the dominant printing technique because it produces sharper, cleaner image reproductions over letterpress, and it was also less expensive in comparison to gravure. Today, the majority of printing, including newspapers, is done by the offset process.

It must be emphasized that lithographic printing is a planographic printing technique in that the inked imaged areas are on the same level as the uninked, nonprinting areas. It differs from relief or raised-image processes (e.g., letterpress) and intaglio or incised-image processes.²⁷

As the popularity of lithography grew soon after it had been invented, some of the literature reports about the lithographic process suggested that it might be possible to transfer designs directly onto the stone if the design could be made translucent and if the lithographic stone could be varnished with a light-sensitive substance. Light passing through the design could then be transferred to the prepared stone below.²⁸ This idea came to fruition at the hands of Joseph Nicéphore Niépce around 1826, who succeeded in making the first permanent photograph of nature, using photolithographic techniques.

2.3 Invention of Photolithography

Photography and photolithography share a common history. They were both invented with the same technique by the same man—Joseph Nicéphore Niépce—who succeeded in taking the first permanent photograph from nature, using the action of light on a photosensitive substrate. Although the invention of photography has been variously ascribed to Thomas Wedgwood, who in the 1790s conceived the original idea of permanently fixing the images of the camera through the darkening action of silver salts in light, but was unsuccessful in practice, to Fox Talbot, who in 1835 introduced the negative/positive process, the principle still employed in photography today, to Daguerre, who in 1837 invented the first practical process of photography (daguerreotype process), the credit alone belongs to Joseph Nicéphore Niépce, who obtained the first permanent recorded image from nature in 1826.²⁹

²⁵ibid.

²⁶ibid.

²⁷L. Stroebel and R. Zakia, Eds., *Encyclopedia of Photography*, 3rd ed., p. 310, Focal Press, Boston (1993).

²⁸M.S. Barger and W.B. White, *The Daguerreotype: Nineteenth Century Technology and Modern Science*, p. 10, Johns Hopkins University Press, Baltimore (1991).

²⁹H. Gernsheim and A. Gernsheim, *The History of Photography: From the Camera Obscura to the Beginning of the Modern Era*, p. 1, Thames & Hudson, London (1969).

To understand the invention of photolithography, it is necessary to examine the work of those who had been conducting experiments that could lead to permanent photographic imaging with light. These men have been variously referred to as pioneers or fathers of photography and include Thomas Wedgwood (1771–1805), Joseph Nicéphore Niépce (1765–1833), Louis Jacques Mandé Daguerre (1789–1851), and William Henry Fox Talbot (1800–1877).

2.4 Pioneers of Photography

The first recorded attempts at imaging using light-sensitive materials were made by Johann Heinrich Schulze (1687–1744), who discovered the light sensitivity of silver nitrate in 1723.³⁰ Following Schulze's experiment, the knowledge of the chemical and optical principles of photography was fairly widespread and published in serious scientific treatises and even popular books of amusing parlor tricks. However, the circumstance that photography was not invented earlier remains the greatest mystery of its history.³¹ Influenced by Schulze's work, subsequent experimenters used light-sensitive materials as part of their light-sensitive inks. Imaging on a more sophisticated level was done sometime during the 1790s by Thomas Wedgwood,³² who in his first attempt sought to use the sun to produce images on light-sensitive paper and leather. Although he was successful in producing silhouettes, he did not have a way of stopping the action of light on his papers, resulting in his silhouettes gradually darkening and eventually fading away and disappearing. The primary light-sensitive material he reported using was silver nitrate,³³ as well as silver chloride, which he stated had no advantages over silver nitrate. He also noted that the images obtained in a camera obscura were too faint to be recorded with his sensitive paper.³⁴

Although Wedgwood was the first to unite the two main ingredients of photography—the darkening of silver salts in light and the image of the camera

³⁰M.S. Barger and W.B. White, *The Daguerreotype: Nineteenth Century Technology and Modern Science*, p. 16, Johns Hopkins University Press, Baltimore (1991).

³¹H. Gernsheim and A. Gernsheim, *The History of Photography: From the Camera Obscura to the Beginning of the Modern Era*, p. 1, Thames & Hudson London (1969).

³²According to Barger and White, there are conflicting reports as to when Wedgwood stopped his experimentation because of ill health [*The Daguerreotype: Nineteenth Century Technology and Modern Science*, p. 16, Johns Hopkins University Press, Baltimore (1991)]. They cite John Werge who noted that Wedgwood had given up his activities as early as 1792 [*Evolution of Photography with a Chronological Record of Discoveries, Inventions, Etc.*, p. 9, Piper and Carter, London (1890)]. They also cite Wedgwood's biographer, R.B. Litchfield, who places the date later, in 1799 [R.B. Litchfield, *Tom Wedgwood, the First Photographer*, Duckworth and Co., Convent Garden (1903)].

³³T. Wedgwood and H. Davy, "An account of a method of copying painting on glass and of making profiles by the agency of light on nitrate of silver, invented by T. Wedgwood, Esq., with observations by H. Davy," *J. R. Inst. (Lond.)* **1**, 170 (1802).

³⁴M.S. Barger and W.B. White, *The Daguerreotype: Nineteenth Century Technology and Modern Science*, p. 16, Johns Hopkins University Press, Baltimore (1991).

obscura—it was others such as Niépce, Daguerre, Talbot, and others who filled in the fine details in the ever-complex tapestry of ideas that eventually materialized as photography. Apparently, it never occurred to any of the great number of artists of the seventeenth and eighteenth centuries who were using the camera obscura to try to fix its image permanently. It was only when scientific men such as those mentioned above wanted to make pictures and turned to the camera obscura for assistance that the sciences of chemistry and optics were at last successfully married and united in photography.³⁵

Perhaps aware that the solution to producing a permanent photographic image lay in arresting the action of light on the photochemical reactions of the silver nitrate, the pioneers of photography sought for ways to accomplish just that. An account of their enormous contributions to the invention and development of photography, although a result of an evolution rather than any sudden discovery by any one of them, is presented below. For given knowledge of the same principles, it is only natural to expect that people working quite separately and without knowledge of each other should generate the same invention at about the same time, and this is in fact borne out by the numerous different processes for which claims of priority were made in various parts of Europe immediately after the announcement by François Dominique Arago of Daguerre's discovery on January 7, 1839.³⁶ An excellent account of the events surrounding the invention of photography has been provided elsewhere.³⁷ Here, we will summarize the main events that are pertinent to the invention of photolithography.

2.4.1 Joseph Nicéphore Niépce—The inventor of photography and photolithography

The singular honor for the invention of photography as well as photolithography goes to Joseph Nicéphore Niépce (1765–1833) (see Fig. 2.4), who was born in Chalon-sur-Saône, France, to a wealthy bourgeois family. Although trained for the priesthood, he, like many other members of religious orders, was forced to abandon his profession during the French Revolution. In 1792 he joined the army, but his career as a soldier was cut short because of a bout with yellow fever. He moved to Nice in 1794, where he married and became a petit bureaucrat. In 1801, he and his family returned to the family estate in Gras outside of Chalon-sur-Saône. His older brother, Claude, joined them a little later, where together they occupied themselves with inventions.³⁸

Their first major invention was the *pyréolophore*, a boat with an internal combustion engine that was patented in 1807. Their efforts to market and sell

³⁵H. Gernsheim and A. Gernsheim, *The History of Photography: From the Camera Obscura to the Beginning of the Modern Era*, pp. 1–2, Thames & Hudson, London (1969).

³⁶*ibid.*

³⁷M.S. Barger and W.B. White, *The Daguerreotype: Nineteenth Century Technology and Modern Science*, Chapter 3, Johns Hopkins University Press, Baltimore (1991).

³⁸*ibid.*, pp. 17–20.



Figure 2.4 Portrait of Joseph Nicéphore Niépce, the inventor of photolithography. (Published with permission from the Deutsches Museum, Munich.)

the *pyréolophore* lasted well over 20 years and took Claude to Paris in 1816 and then to England in 1817. They also discovered new methods for the cultivation and extraction of dye from the woad plant, for which they received recognition from the French government. During this time, indigo had become scarce and expensive as a result of the continental blockade, while the demand for blue dye for military uniforms did not diminish in equal measure. In 1817, Joseph Nicéphore Niépce also became an inventor of a machine that was the forerunner of the bicycle.³⁹

In 1813, the interest of the Niépce brothers shifted to lithography. The first patent for the lithographic process had been granted in France in 1802, and the process was then primarily used for printing music. Its spread was due to French contacts made in Germany during Napoleon's occupation of Bavaria. Due to the occupation, lithography aroused more interest in France than it did in England; however, its practice was hindered by the French political situation until after the restoration of Louis XVII to the throne in 1815. It was after that time that French lithography took off in popularity, so much so that by the end of 1817, the government, alarmed by the spread of the new technology and the relative ease of making broadsides with it, placed restrictive regulations on the process for reasons of state security. In spite of these restrictions, the French became the leading practitioners of the art by 1820.⁴⁰

Another factor that led to the popularization of lithography in France and that was also an incentive for the Niépce brothers was the institution of premiums by the *Société d'Encouragement des Arts et Métiers* for improvements to the lithographic process. Yearly premiums were consistently offered from the time of the introduction of lithography in France until well into the 1840s for devising better methods of transferring designs to lithographic stones, finding a suitable

³⁹ibid., p. 17.

⁴⁰ibid., p. 18.

substitute for the German limestone traditionally used as lithographic stones, and producing materials to ink lithographic stones. The prizes for the premiums ranged from 1,000 to 3,000 francs, depending on the year and the objective. The *English Society of Arts* also offered similar premiums throughout the 1820s and 1830s, with prizes ranging from 20 to 50 pounds.⁴¹

Motivated by the premiums from the *Société d'Encouragement*, during the early course of his research on lithography, Joseph Nicéphore Niépce wedded the two objectives of improving both lithography and methods of transferring designs to stone. For several years, he worked sporadically on various aspects of lithography, the first fruit of which was outlined in a letter he sent to the *Société d'Encouragement* with local stone samples suitable for lithography found in the region of Chalon-sur-Saône in September 1816. Much to his relief, these stones were judged by the *Société d'Encouragement* to be of sufficient quality to use for lithography.⁴²

Also around 1816, Joseph Nicéphore Niépce was successful in capturing images using a camera obscura and silver chloride papers. However, and like Thomas Wedgwood before him, he did not find a way to stop the action of the light, nor did he overcome a second serious problem—the images he produced were negative mirror images, reversed in both tone and geometry, of the scenes captured by his camera.⁴³

Discouraged with the results he obtained on paper, Joseph Nicéphore Niépce abandoned that avenue of investigation and turned to producing images on stone, metal plates, and glass. He experimented with various resin and varnish concoctions, such as gum guaiacum, which turned color and had altered solubility properties when exposed to sun, to produce these images. He also searched for materials that would bleach rather than darken in the sun, so that the image created by the camera could be viewed directly in positive tone. Furthermore, he reasoned that if a method that was more along the lines of printing could be devised, it would not matter that the images recorded by the camera were totally reversed because they would be reversed again in the printing process. And very significantly, with such a method, it would be possible to obtain multiple copies from an original.⁴⁴

At last, Joseph Nicéphore Niépce made the fundamental leap when he understood that these plates could be objects in and of themselves, not just intermediaries to something else. He successfully copied engravings onto light-sensitive plates. He oiled these engravings to make them transparent and then laid them on lithographic stones or glass plates coated with his various concoctions of light-sensitive varnishes. After sufficient exposure he treated the plates with various solvents that washed away the unexposed portions of the varnishes. Using acid, he was then able to etch away the clear areas of the plate that were

⁴¹ibid., p. 18.

⁴²ibid., p. 18.

⁴³ibid., p. 18.

⁴⁴ibid., pp. 18–19.

not protected by the light-sensitive varnish. Once etched and stripped of all the varnish, he could then use the plate for printing.

In an 1824 letter he sent to his brother Claude, Nicéphore wrote that he had succeeded in obtaining direct images on stone and glass that then could be etched and used for printing. It turned out that he had spoken too soon about direct images, but success in this area, nevertheless, did not elude him for long.⁴⁵

At about that same time, Nicéphore began to experiment with pewter plates. Possessing a lighter and more natural color than the copper and zinc plates he had been using, pewter allowed him to attain a greater range of tones. In 1826, using a polished pewter plate to which he added a thin film of light-sensitive substance called asphalt or bitumen of Judea that was exposed to an image of his courtyard and garden from his window with the aid of a simple camera obscura, he obtained the first successful direct camera image—an image of the courtyard of his country estate *Le Gras* in the village of St. Loup-de-Varennes, near Chalon-sur-Saône in France (Fig. 2.5). After dissolving the unexposed parts of the photograph in turpentine oil and rinsing the plate, he obtained, without the need for any other fixing, a permanent bitumen image of the light drawing, in which the shadows were indicated by the bare pewter plate. To prevent a lateral reversal of the image, Niépce had employed a prism in front of his achromatic lens, both of which he had obtained from the Parisian optician Charles Chevalier when he purchased his first professional camera in January of 1826. He named his invention *heliography* and the direct camera image *point de vue du Gras* (view from the window at Le Gras).⁴⁶ This invention is a major milestone that marks the beginning of photography and photolithography.

This first photograph was in effect a projection printed lithographic image,⁴⁷ taken no doubt on a fine day since the image shows both sides of the courtyard to be illuminated. This is because the exposure took 8–10 hours, during which time the sun moved.

Bitumen of Judea is a tarlike petroleum substance that has been recovered in chunks from the Dead Sea since Egyptian times and has been used for embalming mummies, as a building material, and as a black varnish material. It has the peculiar property of softening when heated but hardening when exposed to light—essential properties of a negative resist. Earlier, the Niépce brothers had discussed using this material as part of a possible fuel mixture for the *pyréolophore*.

⁴⁵ibid.

⁴⁶H. Gernsheim, “The 150th anniversary of photography,” in *History of Photography*, Vol. 1, p. 1 (1977); M.S. Barger and W.B. White, *The Daguerreotype: Nineteenth Century Technology and Modern Science*, p. 19, Johns Hopkins University Press, Baltimore (1991).

⁴⁷H. Gernsheim and A. Gernsheim, *The History of Photography: From the Camera Obscura to the Beginning of the Modern Era*, London: Thames & Hudson (1969); J.L. Mangnier, in *Asphalt as the World’s First Photopolymer Revisiting the Invention of Photography in Processes in Photopolymer*, V.V. Krongaus and A.D. Trifunac, Eds., Chapman and Hall, New York (1995) [cited in C.G. Willson, R.A. Dammel, and A. Reiser, “Photoresist materials: a historical perspective,” *Proc. SPIE* **3050**, 38–51 (1997)]; H. Gernsheim and A. Gernsheim, *Photographic J. A* **118** (1952) [cited in C.G. Willson, R.A. Dammel, and A. Reiser, “Photoresist materials: a historical perspective,” *Proc. SPIE* **3050**, 38–51 (1997)].



Figure 2.5 The first photograph from nature (*Point de vue du Gras* or View from the window at Le Gras), taken in 1826 by Joseph Nicéphore Niépce of the courtyard in his country estate *Le Gras* in the village of St. Loup-de-Varennes, near Chalon-sur-Saône in France. This image was recorded on a polished pewter plate using heliography. (Published with permission from the Harry Ransom Humanities Research Center, The University of Texas at Austin.)

Nicéphore had discovered that bitumen of Judea is soluble in lavender oil and that high-quality coatings could be made from the solution. He used the material to coat a variety of substrates, but his best work was done on polished pewter.⁴⁸

As mentioned above, Nicéphore developed his image with a mixture of lavender oil and kerosene. The bitumen of Judea is rendered less soluble in the mixture of lavender oil and kerosene (it hardens) on exposure, and so during development, the unexposed parts are washed away, revealing to a varying degree the surface of the pewter. The photolithographic processes involved in the imaging thus effectively created a relief structure in the remaining organic media.⁴⁹

Two seminal events occurred in 1825 immediately after Nicéphore had made his fundamental invention in photography and photolithography to alter the course of his work. First, he established a working relationship with the Parisian lithographer A.F. Lémaitre, to whom, for the next several years, he sent lithographic plates, which the former etched and printed. Second, that same year a relative of Nicéphore, while visiting the opticians Charles and Vincent Chevalier of Paris to purchase a good camera to take back to Gras, mentioned that Nicéphore had some success in producing permanent images using a camera and showed the Chevaliers examples of his work. Quite impressed with the work, they

⁴⁸M.S. Barger and W.B. White, *The Daguerreotype: Nineteenth Century Technology and Modern Science*, pp. 19–20, Johns Hopkins University Press, Baltimore (1991).

⁴⁹H. Gernsheim, “The 150th Anniversary of Photography,” in *History of Photography*, Vol. 1, p. 1 (1977); C.G. Willson, R.A. Dammel, and A. Reiser, “Photoresist materials: a historical perspective,” *Proc. SPIE*, **3050**, 38–51 (1997).

mentioned it to another customer, Louis Jacques Mandé Daguerre, who was also interested in recording images made using a camera. Almost as soon as Daguerre heard of Nicéphore's work, he resolved to make contact with him and sent a letter in January 1826 requesting information about it. After two more letters from Daguerre, Nicéphore relented and sent one of his heliographs on pewter and a print pulled from the plate to the former.⁵⁰ The two men were later to form a partnership to promote and develop Nicéphore Niépce's process, which eventually led to the invention of daguerreotype process, the forerunner of modern-day photography.⁵¹

September 1827 saw Nicéphore take a trip to England to see Claude, who was very ill and probably dying. The trip brought grave disappointments, not only because of Claude's ill health, but also because Claude had made no progress in promoting the *pyréolophore*. For more than 30 years, the brothers had devoted the family fortune to promoting this machine, and it was during this trip that it became clear to Nicéphore that there was to be no return on these investments—the family fortune was lost.⁵²

While in England, Nicéphore tried to promote his latest invention, *heliography*. He made the acquaintance of Francis Bauer, a prominent botanical illustrator at the Royal Botanical Gardens at Kew and a fellow of the Royal Society, to whom he showed some examples of his heliographs, including the view taken from the window at Gras. Bauer encouraged Nicéphore to prepare a memoir about heliography to be presented to the Royal Society, but Nicéphore was reluctant to do this because he did not want to divulge his process publicly without some financial arrangements. His descriptions of the process were intentionally vague in order to prevent others from stealing his ideas. This secretiveness, however, ran counter to the Royal Society's rules of scientific disclosure, and thus his memoir was not presented to this organization. He also tried to gain the royal patronage of George IV, but this plan failed as well. He finally approached the Society of Arts, hoping to find some interest in his process there, but was not successful with them, either. He was very disappointed with this lack of interest in his invention, even in England, because he thought that he had a better chance of exploiting his new process in England than in France. He returned home disappointed, leaving with Bauer his memoir along with some samples of heliographs, including the view of his courtyard and garden, the first successful photograph ever taken.⁵³

When he started working again, he began to use polished, silver-plated copper plates for two main reasons, namely, (i) silver, as a whiter metal than pewter, would

⁵⁰M.S. Barger and W.B. White, *The Daguerreotype: Nineteenth Century Technology and Modern Science*, p. 19, Johns Hopkins University Press, Baltimore (1991).

⁵¹*ibid.*

⁵²*ibid.*, Chapter 3.

⁵³These items were shown several times during the nineteenth century but were thought lost since 1898. In 1952, through the efforts of Helmut and Alison Gernsheim, who have done extensive work in chronicling of the history and development of photography, they were found in a trunk that had belonged to the Bauer family and had been in storage since 1917.

increase the number of tones in his heliographs and (ii) copper made a more suitable plate for printing. He quickly discovered that he could make another kind of image on silver plate by treating an image made in bitumen of Judea with iodine vapor; this led to blackening of the uncovered areas of the plate. After removing the bitumen, a positive silver iodide image was left on the plate.⁵⁴

2.4.2 Louis Jacques Mandé Daguerre

As mentioned earlier, Nicéphore Niépce and Louis Jacques Mandé Daguerre (see Fig. 2.6) formed a partnership to promote and develop Nicéphore Niépce's process in December 1829. Niépce subsequently presented a complete description of the process to Daguerre, who using it as a foundation, pushed forward and developed the daguerreotype process. He discovered that silver iodide, which can be made by fuming silver plates with iodine, just as Nicéphore Niépce had done, was sensitive to light and that it alone could be used to make images. He also made the discovery that if an exposed plate with no apparent image was exposed to mercury vapor, a latent image appeared. With this method, he discovered the latent image. Unfortunately, Nicéphore Niépce did not live to see any of Daguerre's results. He died in 1833, and Daguerre came upon these improvements in 1835. At this point, Daguerre still could not produce permanent images, but in 1837



Figure 2.6 Portrait of Louis Jacques Mandé Daguerre, the inventor of daguerreotype, the forerunner of modern photography. (Published with permission from the Deutsches Museum, Munich.)

⁵⁴M.S. Barger and W.B. White, *The Daguerreotype: Nineteenth Century Technology and Modern Science*, Chapter 3, Johns Hopkins University Press, Baltimore (1991).

he finally made the discovery that he could stop the action of light by putting his plates in hot, saturated salt water. Daguerre called his new process *daguerreotype*,⁵⁵ and it is this particular process that is the forerunner of modern-day photography.

When news of the processes of the two partners reached the physicist François Dominique Arago (1786–1853), then not only the director of l’Observatoire in Paris and the permanent secretary of the Académie des Sciences, but also a member of the Chamber of Deputies in the French Parliament, the fortunes of the two partners took a turn for the better. Being interested in light and its properties, Arago had an immediate personal interest in these processes. He particularly felt that daguerreotype could be used as a tool to unlock some of the mysteries of light and that it would also be useful as a recording medium not only for artists and architects, but also for scientists, archeologists, and travelers. In addition, he had the vision to see that this process would have an impact far beyond the mere fact of its being able to record images. He thus set about to see that Daguerre and Nicéphore Niépce were duly rewarded and that this discovery brought both honor and glory to France. To this end, a brief notice about the daguerreotype process was published in the *Comptes Rendus*, the journal of the *Académie des Sciences*. It merely stated that a process had been devised and that details would be forthcoming.⁵⁶

This notice generated a great deal of public interest throughout western Europe and brought about two particular responses. First, Francis Bauer sent a letter to the *Literary Gazette* describing Nicéphore Niépce’s work and offering to show the heliographs that he had given to him 11 years earlier. Bauer wanted to make sure that his friend Nicéphore Niépce was accorded the recognition due him for his invention. Second, about this time, William Henry Fox Talbot published an account of his process for making images with light in order to establish his priority as the first discoverer of such a process.⁵⁷

2.4.3 William Henry Fox Talbot

The scientist William Henry Fox Talbot (1800–1877) (see Fig. 2.7) made his first imaging experiments with papers prepared with silver nitrate, which he found were not very sensitive. He then turned to silver chloride paper, and soon discovered that he could stop the action of light on his sensitive papers by soaking them in a strong solution of salt water, just as Daguerre had done earlier. During the summer of 1835, he was successful in making images of his house using his sensitive paper and a camera obscura, although with extremely long exposure time (on the order of several hours). He also experimented with a solar microscope in conjunction with his sensitive paper, which resulted in the first photomicrographs

⁵⁵:ibid.

⁵⁶:ibid.

⁵⁷:ibid.



Figure 2.7 Portrait of William Henry Fox Talbot. (Published with permission from the Deutsches Museum, Munich.)

ever taken, sometime during this period. As the publicity surrounding Arago's announcement mounted even in England, Talbot had to concede that the discoveries of Niépce and Daguerre did indeed have priority over his own.⁵⁸

The publicity surrounding the discoveries of Niépce, Daguerre, and Talbot also propelled others who had been thinking along the same lines to publicize their own discoveries. In May 1839, Mungo Ponton (1802–1880), a member of the Edinburgh Society of Arts, published a process based on dichromate salts, which he believed was a variant of Talbot's.⁵⁹

Thus, the period between 1826 and 1839 saw the birth of a new era—the world witnessed the introduction of photography, which used several processes to capture permanent images using cameras. None of these discoveries was the result of a concerted scientific research program based on the systematic application of knowledge of light-sensitive materials to the problem of imaging. Rather, the discoveries were the result of three men who were interested in solving problems—one an inventor (Niépce) trying to improve lithography by competing for premiums offered by the *Société d'Encouragement des Arts*; one an artist and promoter (Daguerre) trying to fulfill the need of capturing the images in his camera; and one a gentleman scientist (Talbot) trying to make up for his inability to draw as well as an artist. These men all drew on knowledge that was widely available during their time. They applied that knowledge in new ways to devise solutions to obstacles that had earlier prevented others from solving the problem. All three were able to produce images that had relatively short exposure times (i.e., on the order of minutes) and were able to

⁵⁸ibid.

⁵⁹M. Ponton, "Notice of a cheap and simple method of preparing paper for photographic drawing, in which the use of any salt of silver is dispensed with," *Edinburgh New Phil. J.* **27**, 169–171 (1839).

make these images permanent by stopping the action of light with some subsequent treatment.⁶⁰ For these contributions, these three men are the founding pioneers and fathers of photography. While Daguerre's and Talbot's contributions to photography are significant, the priority for the invention of photography and photolithography belongs to Niépce. Everything we do today in offset lithography as well as in optical lithography, and for that matter in other fields of semiconductor lithography, derive from Niépce's invention.

⁶⁰M.S. Barger and W.B. White, *The Daguerreotype: Nineteenth Century Technology and Modern Science*, p. 27, Johns Hopkins University Press, Baltimore (1991).

Chapter 3

Optical and Chemical Origins of Lithography

To understand a science, it is necessary to know its history.

Auguste Comte

3.1 Introduction

As stated in Chapter 1, the so-called information superhighway is paved with chips of crystalline silicon made by lithography, for it is the key technology process step with which we are able to create fine patterned structures that ultimately form the devices and interconnects of complex functional integrated circuits used in microelectronics. As a matter of fact, both circuit speed and integration density depend on the lithographic minimum printable feature. Today, lithography represents over 35% of the chip manufacturing cost in the semiconductor industry. The increasing cost of lithographic exposure tools is recognized as one of the most critical factors for keeping up with Moore's law.¹

Although lithographic patterning is not the only critical step in integrated circuit device manufacture, its specifications are by far the most stringent and also the most consequential. This arises not only from the requirements on a given patterning step for tight dimensional control and absence of defects, but also from the sheer number of patterning steps that a modern device structure undergoes. It is not uncommon for many integrated circuit structures to pass through 30 or more patterning steps in the course of fabrication. Under such conditions, the need for precise, reliable, and reasonably low-cost lithographic solutions is imperative.

Equally imperative are ways of overcoming the challenges presented by ever more demanding applications of sophisticated chemistry in semiconductor lithography, in terms of materials, processes, and tools. A modern lithography module clean room for patterning silicon chips is a masterpiece of automated chemical engineering, operating at its highest efficiency and effectiveness when

¹G.E. Moore "Lithography and the future of Moore's law," *Proc. SPIE* **2440**, 2 17 (1995).

it is operated by the fewest possible number of operators in order to minimize contamination and to improve both control and uniformity of lithographic processes. Moreover, the fabrication of increasingly powerful and sophisticated computers depends on advances in the design of circuits that match advances in the sophistication of IC device fabrication technologies, especially lithography.

It is therefore only reasonable to construct the chemical history of the developments that led to the emergence of lithography as the preeminent critical step in the fabrication of integrated circuits and the mass production of printed matter such as newspapers. But in order to arrive at a fuller understanding of the evolution of lithography, it is necessary to examine the work of a large number of scientists whose contributions to chemistry and physics, particularly optical physics, span a period of over 3000 years, and who were instrumental in shaping the invention of lithography in 1798 by Senefelder² and its subsequent development and progress. This story is really not only a triumph of advances in the understanding of materials science, but is also a product of the knowledge gained in the convergence of major areas of chemistry and physics (particularly those related to optical physics, semiconductor physics, and atomic physics).

Like every other technological innovation, lithography is “like a river—its growth and development depending on tributaries and on conditions it encounters on its way. The tributaries to [such] an innovation are inventions, technologies and scientific discoveries; the conditions are the vagaries of the market place.”³

There are several special features to the innovation that we might call lithography. First of all, it is not really a single innovation at all, but consists of a long series of linked innovations. There is a continuous chain of lithographic patterning techniques based on the simple idea that oil and water repel each other, which stretches from Senefelder’s stone plate lithography of 1798 to Niepce’s visible-light lithography of 1826, to offset lithography, to the most advanced semiconductor lithography of today. The major techniques that have evolved are extensions of photolithography. However, the diffraction limitations imposed by the wavelength of visible light are overcome by shorter-wavelength photons or electrons. Just about every conceivable particle with wavelengths shorter than a micrometer has been investigated as a potential exposure radiation. To date, only five have proven successful enough to have been generally useful in advanced lithography, namely, near-ultraviolet photons, deep-ultraviolet photons, electrons, soft x rays, and ions. Although deep-UV lithography uses some new materials and techniques, it is more of an evolutionary development from visible-light lithography. Electron-beam lithography, x-ray lithography, and ion-beam lithography, on the other hand, employ physical concepts, techniques, and equipment that are comparatively new to microfabrication.⁴

²A Senefelder, *Vollständiges Lehrbuch der Steindruckerey (A Complete Course in Lithography)*, Thienemann and Gerold, Munich (1818).

³E. Braun and S. MacDonald, *Revolution in Miniature: The History and Impact of Semiconductor Electronics*, Chapter 1, Cambridge University Press, Cambridge (1978).

⁴N.D. Wittels, “Fundamentals of electron and x ray lithography,” in *Fine Line Lithography*, R. Newman, Ed., pp. 1–104, North Holland Publishing, Amsterdam (1980).

The totality of these lithographic innovations and the innovations in semiconductor electronics that they have engendered are so massive as to make most single technological innovations pale in comparison. Apart from the scale of the innovations and the scale of its impact, lithographic technology and its associated semiconductor technology are distinguished by their very great dependence on science. In more ways than one, lithography and modern electronics, which it enables, owe their very existence to science; they are both truly innovations based on science.

In the remainder of the present chapter, our object is to consider, from a historical perspective, how key theoretical and technological developments in optical physics and chemistry have influenced the development of lithography. A summary of these developments is given in thematic order, but not necessarily in chronological order, in Fig. 3.1.

Since lithography as practiced in its many varied incarnations today involves essentially a series of chemical transformational processes mediated at some stage by some type of radiation, usually light, a narrative that traces the development and evolution of thought and ideas on the nature of light and chemical phenomena that ultimately went into the invention of and subsequent development of lithography is judged a good device for presenting this fascinating story. Along this journey we will examine fundamental theories on the nature of light and matter, spanning the earliest known human reflections on these subjects to modern quantum theory, while exploring how the marriage between chemistry and optics

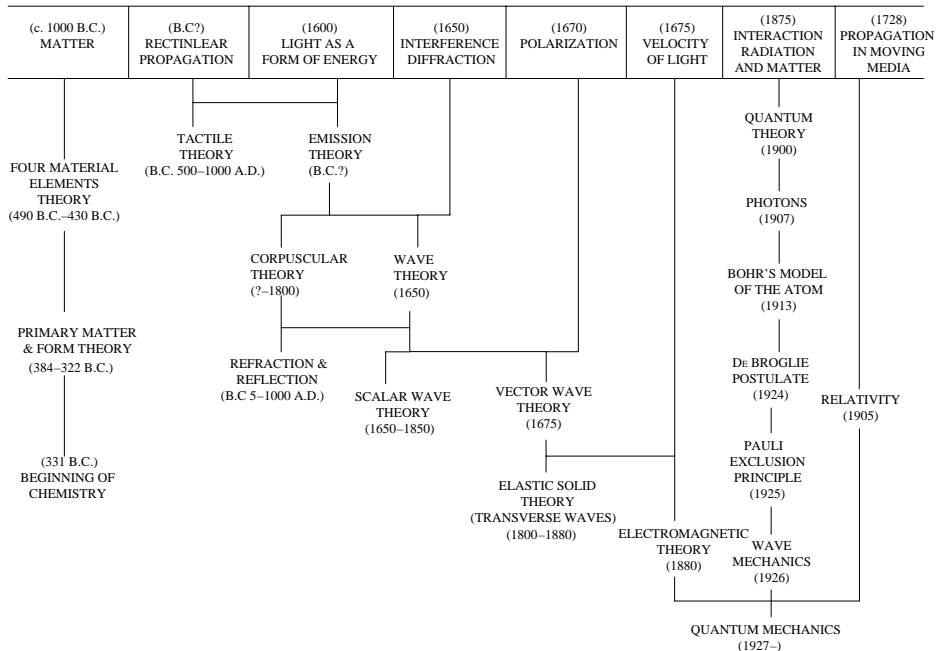


Figure 3.1 Key developments in optical physics and chemistry that led to the invention and development of lithography. (Figure continued on next page.)

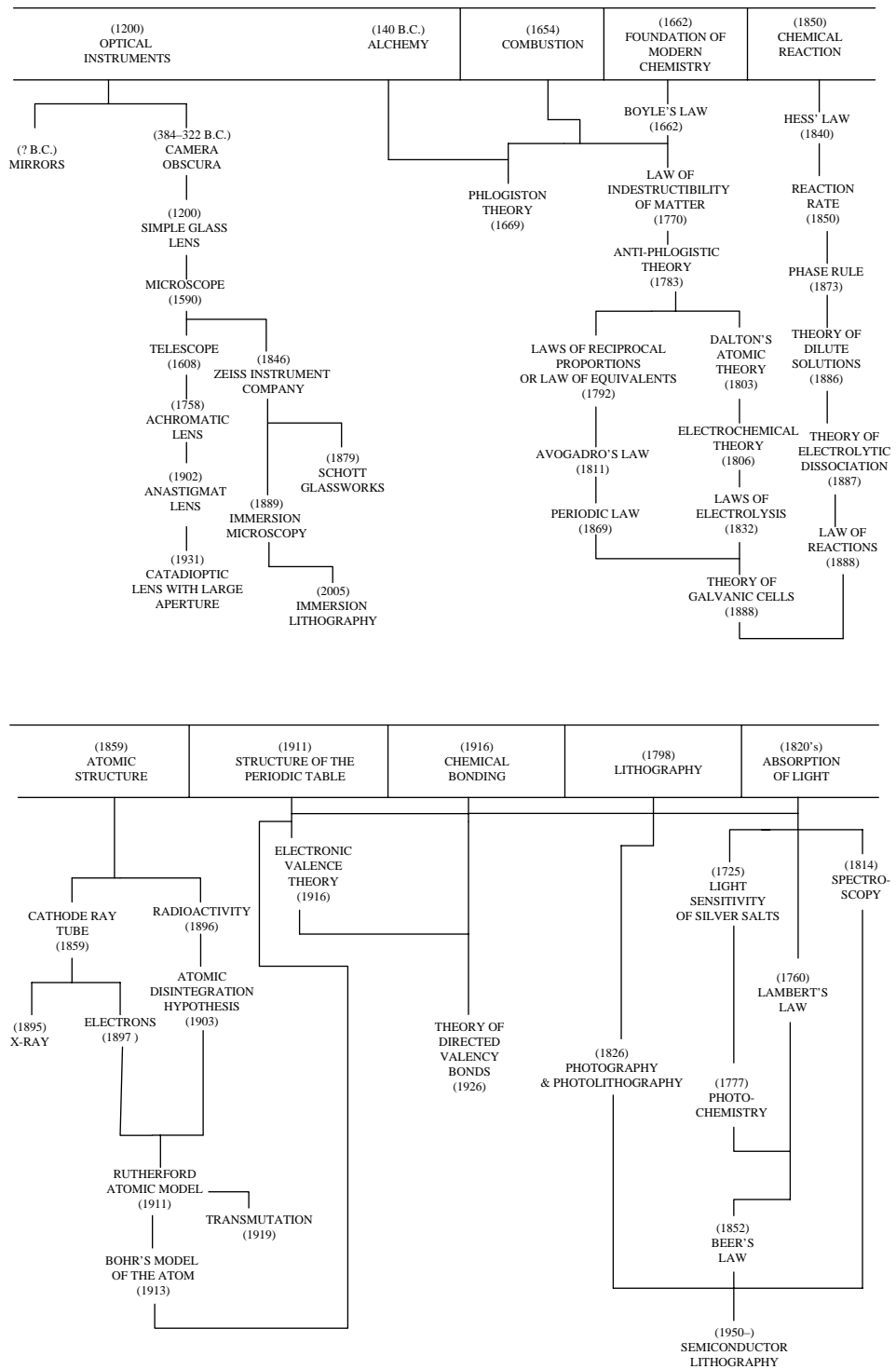


Figure 3.1 (Continued).

led to the invention and development of lithography. We will also examine how each key development on the chemical effects of light opened up many new fields. From photometry to photochemistry, a new world sprang to life after the invention of lithography, another after the invention of photography and photolithography. Furthermore, we will examine key developments in the optical instrument and glassmaking technologies—key critical technologies that enabled the development of instruments used in modern lithography. The whole story is one of fascinating science that has transformed human life.

3.2 Key Developments that Enabled the Invention and Development of Lithography

3.2.1 Developments in optical physics

A comprehensive treatment of the development of optical physics covering, among other topics, the theories of light has been given elsewhere.⁵ Here, only the key developments that directly or indirectly influenced the development of lithography as practiced today are covered. In such a treatment, it is convenient to disregard the chronological order in which the developments occurred, but rather to present the materials from the historical point of view and to show how each of the developments has been incorporated into the development and practice of lithography. A summary of these developments are given in Fig. 3.1.

3.2.1.1 Tactile and emission theories of light

Historically, it has been known since antiquity that the earliest speculations on the nature of light were theories of vision. One school held that the eye sends out invisible antennae or sensitive probes or visual rays and is thus able to feel objects that are too distant to be touched by hands or feet. This theory was called the “tactile” theory. An alternative hypothesis held that light consists of small particles that are emitted by bright objects and that, on entering the eye, are able to affect some sensitive part of the eye and so give rise to the sensation of sight. This theory was called the “emission” theory. Both of these theories were current among Greek thinkers about 500 BC.⁶

In its inherent simplicity, the tactile theory is able to describe the unknown in terms of the known. The mystery of vision is directly related to the simpler and more obvious sense of touch. The theory does, however, experience some

⁵R.W. Ditchburn, *Light*, Dover Publications, New York (1991); P. Mason, *The Light Fantastic*, Penguin Books, New York (1981); M.I. Sobel, *Light*, University of Chicago Press, Chicago (1987).

⁶Many variations and combinations of these theories were also suggested. We need not consider them since they are more complicated than the two theories we have described and have no important compensating advantages.

difficulty in explaining why things can be felt, but not seen, in the dark, and why bodies can be made visible in the dark by heating them. The fact that certain bright bodies are able to make neighboring bodies visible is also not explained by the tactile theory.⁷

Some of these difficulties of the tactile theory can be explained away by postulating that the visual probes are able to feel only certain kinds of surfaces and then making a series of assumptions that surfaces can be modified under various conditions. But this approach only ends up making the theory intolerably complicated, since the simple sense of relation to the sense of touch—the very important attribute of the theory—is lost. These conflicts can be resolved in a simple and satisfactory way by the emission theory if it is assumed that some bodies are able to emit a radiation to which the eyes are sensitive, and that others are able to reflect or scatter this radiation so that it enters the eye.⁸ For these and similar reasons, the tactile theory was gradually superseded by and eventually replaced with the emission theory. The process for this transformation was, however, very slow, and it was not until about 1000 AD that, under the influence of the Arabian astronomer Alhazen (discussed below), the tactile theory was finally abandoned.⁹

3.2.1.2 Early studies in optics and catoptrics

Another major notable development in the early studies of light phenomena is attributed to Euclid,¹⁰ the great Greek mathematician of the third century BC, who wrote two books on light, *Optics* and *Catoptrica* (meaning on reflection). Little is known of the latter book, but a review of it, written perhaps many centuries later—and possibly spurious—discusses the properties of mirrors and provides an accurate law of reflection (see Fig. 3.2), which states that a ray is reflected from a plane surface at the same angle with which it strikes the surface. Euclid was certainly aware that light travels in straight lines, a fact that he employed in his discussions on the laws of perspective.¹¹

⁷R.W. Ditchburn, *Light*, p. 4, Dover Publications, New York (1991).

⁸A modern interpretation of the emission theory will have light being defined as “visible radiation,” which takes part in the following general account of the visual process. Light being emitted, reflected, or scattered enters the eye and is focused by the lens of the eye on the retina, located at a surface situated at the back of the eye. The retina contains a large number of nerve endings, which on receiving light transforms the latter into electrical impulses through some chemical and physical action. A series of electrical impulses is thus sent from the retina along an appropriate nerve fiber to the brain.

⁹R.W. Ditchburn, *Light*, p. 4, Dover Publications, New York (1991).

¹⁰Greek science reached its highest peak in Euclid’s century. Archimedes of Syracuse was the greatest scientist of the era, and he made advances in mechanics, hydrostatics, and mathematics. [Cited in M.I. Sobel, *Light*, p. 2, University of Chicago Press, Chicago (1987)].

¹¹M.I. Sobel, *Light*, p. 2, University of Chicago Press, Chicago (1987).

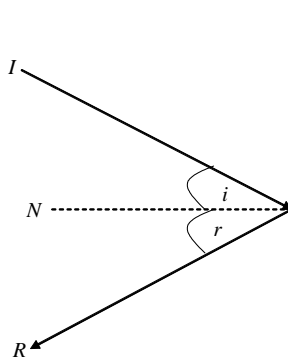


Figure 3.2 The law of reflection. An incident ray of light I upon hitting a mirror surface is reflected R such that the angle of incidence i equals the angle of reflection r . The dashed line, N , is the normal to the surface. The angle of incidence is the angle between the incoming ray and the normal; the angle of reflection is the angle between the reflected ray and the normal. I , N , and R are in the same plane.

3.2.1.2.1 Refraction

Another significant contribution to the early studies of light phenomena was due to Claudius Ptolemy, who made the first systematic study of refraction. In the second century AD in Greek Alexandria, he developed his cosmology in which the Earth is at the center of the universe with the Sun and the planets orbiting around it. This cosmology reigned undisputed for 13 centuries. Although the Ptolemaic system was actually a compilation of works of earlier Greek astronomers, notably Hipparchus, Ptolemy recognized that to correctly determine the location of a planet he must take into account the bending of light as it enters the Earth's atmosphere. He demonstrated that when light enters a dense medium from a less dense one, the ray is bent toward the normal and, conversely, it is bent away from the normal when entering a less dense medium.¹²

Ptolemy also studied air-water, air-glass, and water-glass interfaces, and made tables of the angle of incidence (the angle between the incoming light ray and the normal) and the corresponding angle of refraction (the angle between the refracted ray and the normal). He postulated, however incorrectly, that for a given interface the two angles were proportional. His *Optics*, only part of which has survived to the present day, is noteworthy, not so much for its data as for the very fact of its adherence to the experimental method.¹³

The next major figure in the story of light is found more than eight centuries later, during the height of Islamic civilization.¹⁴ Born in 965 AD,

¹²ibid., pp. 2–3.

¹³ibid.

¹⁴By the year AD 750, Islamic soldiers fanning out from Arabia had overrun many lands around their region and built an empire along the entire Mediterranean Sea and as far east as India. Among the great thinkers of this era were al Khwarizmi the mathematician, Avicenna the physician, Averroës

Alhazen¹⁵ experimented and wrote extensively on optics. In his writings on optics, he used highly developed algebra and geometry, as well as an experimental approach in a very modern sense, involving the use of sighting tubes, strings, and plane and curved glasses and mirrors to study the laws of reflection and refraction. He refuted Ptolemy's claim that the angle of incidence was proportional to the angle of refraction, although he himself did not obtain the correct mathematical relation. He showed that a convex lens (where each surface is a part of a sphere) can magnify an image. He carried out a rigorous mathematical treatment of reflection from spherical, cylindrical, and conical mirrors. He observed that if parallel rays of light strike a curved mirror that is a section of a sphere, the rays are not brought to a precise focus, a condition known as spherical aberration; but a mirror in the shape of a paraboloid (a solid figure produced by rotating a parabola about its axis) can produce a sharp focus.¹⁶ Furthermore, he deduced that twilight, the persistence of daylight after the Sun has set, to be due to the refraction of sunlight from the upper layers of the Earth's atmosphere. By assuming that twilight ends when the Sun's rays are refracted from the very top of the atmosphere, he deduced that the atmosphere was 20 to 30 miles high, a fairly good estimate by modern standards.¹⁷

Also in Alhazen's writings we find reports of very detailed early dissection of the human eye. We also find speculations on the method of propagation of light that anticipates the seventeenth-century theory of Huygens. And we find the hints or rather the suggestion, demonstrated only in the nineteenth century, that light travels less easily (i.e., at lower velocity) when it enters a dense medium, and that this causes the ray to be bent toward the normal.¹⁸

It should be pointed out that the research and scholarship of the Muslim scholars were important not only in themselves, but also on account of the fact that they transmitted, in Latin translation, the spirit of learning to medieval philosophers such as Roger Bacon and Albertus Magnus, whose work foreshadowed the age of science in the West. Bacon was certainly familiar with Alhazen's works in optics, understood how to trace rays of light through lenses and mirrors, and may very well have been the first to use a lens for spectacles. He also suggested combining two lenses to make a telescope, although it is not certain that he actually built one.¹⁹

3.2.1.2.2 The invention of the microscope and telescope

Next, our journey through the history of studies in light phenomena takes us to the age of Copernicus, specifically the invention of the microscope by Zacharias

the philosopher, and Alhazen the physicist [cited in M.I. Sobel, *Light*, p. 5, University of Chicago Press, Chicago (1987)].

¹⁵Alhazen is actually the Latinized version of the great Arabic scholar Abu Ali al Hasan ibn al Hasan al Haitham, born in 965 AD.

¹⁶M.I. Sobel, *Light*, pp. 4 5, University of Chicago Press, Chicago (1987).

¹⁷ibid.

¹⁸ibid.

¹⁹ibid.

Janssen about 1590, the invention of the telescope by Hans Lippershey in 1608, and its quick deployment by Galileo Galilei.²⁰ The modern-day optical and electron microscopes that are widely used in the inspection of lithographically patterned wafers all trace their origins to Janssen's invention.

3.2.1.2.3 Laws of refraction

Around 1621, the Dutch scientist Willibrod Snell discovered the correct law of refraction, which both Ptolemy and Alhazen were unable to deduce.²¹ By applying heuristic momentum conservation arguments in terms of sines, Rene Descartes independently derived the law in his 1637 philosophical and mathematical treatise, *Discourse on Method*. Descartes was able to solve several optical problems with the aid of this law.

Snell's law provides the relation between the angle of incidence and the angle of refraction (see Fig. 3.3) in terms of a quantity, called the index of refraction, which is characteristic of the medium into which light travels. Specifically, the ratio of the sine of the incident angle to the sine of the refracted angle is equal to the refractive index of the medium. According to modern wave theory, the refractive index is the ratio of the speed of light in vacuum to the speed of light in the medium.²² Expressed another way, Snell's law states that the ratio of the sines of the angles of incidence and refraction is equivalent to the ratio of velocities in the two media, or equivalent to the inverse ratio of the indices of refraction,

$$\frac{\sin i}{\sin t} = \frac{v_1}{v_2} = \frac{n_2}{n_1} \quad (3.1)$$

or

$$n_1 \sin i = n_2 \sin t, \quad (3.2)$$

where $\sin i$ is the sine of the angle of incidence, $\sin t$ is the sine of the angle of refraction, v_1 and v_2 are the velocities of the light ray in medium 1 and 2, respectively, and n_1 and n_2 are the refractive indices of the light ray in medium 1 and 2, respectively.

Not long after the formulation of Snell's law, the French mathematician Pierre de Fermat unified the laws of reflection and refraction by showing that both could be deduced from the hypotheses that light travels a path of least time. In other words, given two points A and B in a region with mirrors or with different media, the path of a ray of light from point A to point B will be that for which the time of travel is least. The implication of Fermat's principle is that light travels at a finite speed.²³

²⁰ibid., p. 5.

²¹ibid.

²²ibid.

²³ibid.

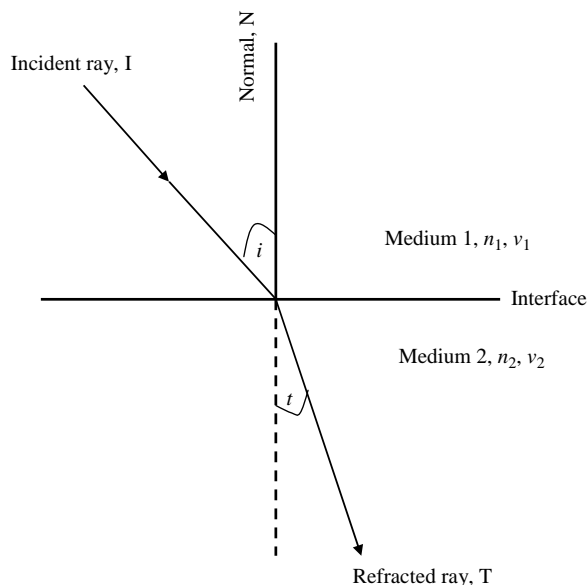


Figure 3.3 Refraction of light at the interface between two media of different refractive indices, with n_2 greater than n_1 . An incident light ray I travels from medium 1 into medium 2, making an incident angle i with the normal, N. It traverses the interface and travels into medium 2, as the refracted ray T, making a refracted angle t with the normal N in medium 2. Given that the velocity of light is lower in medium 2, the angle of refraction t is smaller than the angle of incidence i .

3.2.1.3 On the nature of light

From about the mid-seventeenth century, studies aimed at elucidating the nature of light consumed the attention of most scientists. Reasoning that light provides the primary information about the experience around them, these scientists thought that understanding what it is and how it works should provide the key to understanding the diversity of natural phenomena. Such studies (see below) were the purview of not only astronomers and physicists, but also of mathematicians, chemists, biologists, and even physicians. Other workers in related fields such as opticians, glass and lens makers, and instrument makers pursued theories of light derived from specific applications and improvements of their crafts.²⁴ This desire to understand what light is and how it works was the impetus behind the work that eventually resulted in the invention of photography and photolithography.

²⁴M.S. Barge and W.B. White, *The Daguerreotype: Nineteenth Century Technology and Modern Science*, p. 12, Johns Hopkins University Press, Baltimore (1991).

3.2.1.3.1 Light and color

In an attempt to elucidate why when sunlight is bent in a glass prism the colors of the rainbow are produced—a fact known since antiquity—Sir Isaac Newton (1641–1727) (see Fig. 3.4) in 1666 carried out a wide variety of experiments in which he allowed a narrow pencil of sunlight to pass through a small hole in a window shade of a darkened room, producing a small circle of light on the opposite wall. Next, he placed a prism in front of the hole and observed that the beams struck a different area of the wall. The displacement of the beams was not surprising because it resulted from the refraction of the entire beam by the prism. He observed that the spot of light was now elongated and was no longer a circle. He also observed that colors are spread out along its axis, red on one end, violet on the other. On measuring the angles subtended by the axes of the spot as seen from the hole, he found the long axis close to three degrees and the short axis about one-half a degree.²⁵

Next, he proceeded to analyze the beam by keeping the prism in place and introducing beyond it a barrier with a small hole. Through this hole he allowed only the red portion of the beam to pass; later the orange, the yellow, and so on. This allowed him to experiment separately with each color, which he did by placing a second prism beyond the barrier to refract light arriving through the small hole. He monitored the angle of refraction of red light alone, orange light alone, etc., and found that the angle is different for different colors; violet light is bent most, red least, the others falling in between, leading him to postulate two theorems: “Light which differ in color, differ also in their degrees of refrangibility [refraction],” and “The light of the sun consists of rays of differently refrangible.”²⁶

In another set of experiments, he took the beam emerging from a prism—separated into colors—and let it pass through a second prism, inverted with respect to the first. In this arrangement, the second prism performed the opposite function of the first. The result he obtained was a combination of the separated



Figure 3.4 Sir Isaac Newton (1641–1727), who among many things discovered the laws of universal gravitation and was a proponent of the particle theory of light. (Published with permission from the Deutsches Museum, Munich.)

²⁵M.I. Sobel, *Light*, pp. 6–8, University of Chicago Press, Chicago (1987).

²⁶Sir Isaac Newton, *Optics*, pp. 20, 26, Dover Publications, New York (1979).

colors, which produced a white spot on the wall. He was thus convinced that sunlight is a combination of colors of the rainbow.²⁷

In order to explain the basis of the colors of material objects, using a prism, he took light of a particular color (“uncompounded light,” as he called it) and let it shine on different objects. A red object in blue light, he observed, looks blue. In green light it looks green and in red it looks red, but in this case it appears brightest. This led him to conclude that a red object reflects all colors but reflects red more strongly, so that in the “compound” white light of the sun the object reflects red most strongly and appears red to the viewer.²⁸

3.2.1.3.2 Light as a wave or particle

Toward the end of the seventeenth century, two opposing theories of light were being investigated. These fall into two broad categories, namely, (i) particle (also called the corpuscular or emission) theory and (ii) wave (or undulatory) theory.²⁹ Knowing that light is a form of energy that can be transferred from one place to another, many scientists of the seventeenth and eighteenth centuries sought to describe it by analogy with other methods of energy transport. They distinguished between two methods of energy transport, that is, transport of matter or by wave. While energy transport by matter is associated with the movement of the material body or the medium in which the matter is contained, energy transport by waves is not accompanied by any bodily movement of the medium. When energy is transported, it is not easy to discern whether the mechanism of transport is matter or wave. But there is one fundamental difference—interference phenomenon—a difference that becomes the crucial factor in the history of the study of light phenomena.³⁰

Interference is the phenomenon that distinguishes waves from matter. While waves can interfere with one another in a constructive (when the superposition of the waves add up) or destructive (when the superposition of the waves cancel each other) manner, matter cannot. It was thus reasonable for many scientists of the seventeenth and eighteenth centuries to describe light either in terms of moving particles or of waves.³¹

3.2.1.3.3 Particle (or corpuscular) theory of light

The corpuscular theory of light, expounded by Sir Isaac Newton, states that light is made up of very small corpuscles or streams of particles that are emitted from

²⁷M.I. Sobel, *Light*, pp. 6–8, University of Chicago Press, Chicago (1987).

²⁸*ibid.*

²⁹*ibid.*; M.S. Barge and W.B. White, *The Daguerreotype: Nineteenth Century Technology and Modern Science*, pp. 12–13, Johns Hopkins University Press, Baltimore (1991); W. Ditchburn, *Light*, pp. 5–6, Dover Publications, New York (1991).

³⁰M.I. Sobel, *Light*, pp. 9–10, University of Chicago Press, Chicago (1987); R.W. Ditchburn, *Light*, pp. 6–7, Dover Publications, New York (1991).

³¹*ibid.*

one body and move at great speed through space and strike some receptive body. Founded on the premise that light travels in a straight line and therefore must cast complete shadows when it illuminates a barrier—in other words, light does not go around corners—he found it rather difficult to accept that light is a wave, even when his own experimental results should have led him to such a conclusion. For instance, his observation of the now famous Newton's rings, a concentric series of colored rings—alternately bright and dark—resulting from the reflected light from when a convex surface of a lens of large radius of curvature is placed in contact with a plane surface of glass (see Fig. 3.5), is a consequence of the wavelike character of light.³²

He did, however, recognize that these rings indicated the presence of some kind of periodicity and that this suggested a wave theory of light. He nevertheless believed that the rectilinear propagation of light was an insuperable objection to a simple wave theory. Instead, he suggested that light is made up of corpuscles that either possess an internal vibration of their own or are in some degree controlled by waves or vibrations of the medium through which they travel.³³ During most of the eighteenth century, the corpuscular theory was the dominant working theory for natural philosophers concerned with questions of light, largely because of Newton's influence.³⁴

It should be pointed out that the objection to a simple wave theory was removed when it was discovered that the propagation of light is not strictly linear. Light does indeed spread, though to a very small extent, from the edges of a beam defined by rays. As an example, the shadow of a straight edge formed by a small source is not perfectly sharp when viewed under high magnification. Some light does penetrate into the region that ought to be completely dark if light were propagated entirely in straight lines, and there exists a series of fine, light and dark bands at the edge of the region outside the shadow. The Jesuit Francesco Grimaldi who lived in Newton's lifetime made some observations of this kind, but it was not

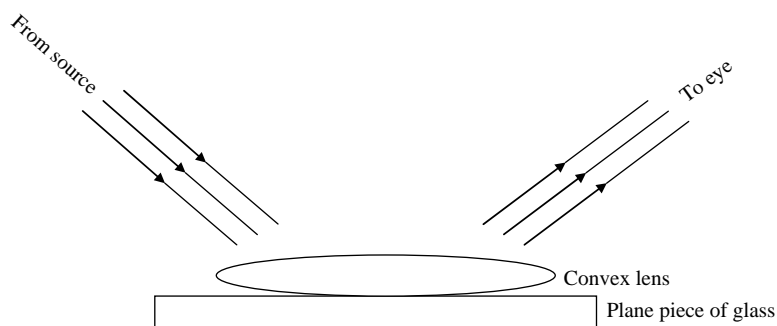


Figure 3.5 Apparatus for viewing Newton's rings.

³²M.I. Sobel, *Light*, p. 8, University of Chicago Press, Chicago (1987); R.W. Ditchburn, *Light*, pp. 7–8, Dover Publications, New York (1991).

³³R.W. Ditchburn, *Light*, Dover Publications, New York, pp. 7–8 (1991).

³⁴M.I. Sobel, *Light*, University of Chicago Press, Chicago, p. 8 (1987).

until 150 years later that the phenomenon (which is now called diffraction) was clearly elucidated. The discovery and elucidation of diffraction irrefutably showed that the propagation of light is not exactly rectilinear.³⁵

Today, leading-edge lithography is all about diffraction-limited printing. The design of lithographic exposure tools is such that they are designed to limit the effects of diffraction, either through materials selection or the way the materials are used.

3.2.1.3.4 Wave (or undulatory) theory of light

The earliest systematic wave theory was proposed by the Dutch astronomer Christian Huygens (1629–1695), a contemporary of Newton. Although Huygens did not fully develop his wave theory mathematically, he showed how a train of waves striking the edge of a barrier will be bent around the edge, thus making it possible for a wave of light to penetrate into regions behind a barrier. Huygens' theory was also able to explain Snell's law of refraction, if one assumes that waves travel more slowly in a dense medium than in air.³⁶

Although the bending of light around an edge, otherwise called diffraction, had been observed by Grimaldi and Newton, the amount of light bent into the shadow is so extremely small that Newton did not regard the effect as evidence for the existence of light waves, but rather some property of the edge.³⁷ By the time the optical researches of Newton (1672) and Huygens (1678) were published, it was already well established that sound was a pressure wave in air. It was not until the research of the English physician Thomas Young (1773–1829) (see Fig. 3.6)



Figure 3.6 Thomas Young (1773–1829), who laid the foundation of the wave theory of light and proposed the trichromatic theory of color vision. (Published with permission from the Deutsches Museum, Munich.)

³⁵R.W. Ditchburn, *Light*, pp. 7–8, Dover Publications, New York (1991).

³⁶M.I. Sobel, *Light*, p. 10, University of Chicago Press, Chicago (1987).

³⁷*ibid.*, p. 10.

in 1801 that the wave theory of light was revived and the similarities and differences between light and sound were explained.³⁸

The first scientist to suggest the trichromatic theory of color vision, Thomas Young, laid the foundation for the wave theory of light, stating that when a body becomes luminous it sends out waves of particular amplitude and wavelength. He noted that the length of these waves determines their color in much the same way that the wavelength of sound waves determines their pitch.³⁹ Furthermore, he felt that light waves were transported in a special medium, the luminiferous ether, which vibrates and transports the waves to some receptive body at a distance.⁴⁰

In his 1801 lecture on “The Theory of Light and Colors,” Young undertook to prove the wave theory of light by demonstrating interference effects; he also gave the first physical analysis of the nature of color. For instance, in explaining the basis of Newton’s rings, he postulated that there exists a thin layer of air between the convex lens and the flat surface beneath it. Light being reflected from any boundary between two media, and in this case from the upper and the lower boundaries of the air layer, results in two such beams on arriving at the eye, having traveled paths of different lengths to either destructively interfere in order to create the dark ring or constructively interfere in order to create the bright ring. He found that the difference between the bright and dark rays depends on the path difference of one-half the wavelength. Thus, by observing the separation between the light and dark rings, he was able to calculate the wavelength of light of different colors. He found a value of 0.00007 cm for red light, about 0.00004 cm for violet, and values between for the intermediate colors in the spectrum. With one stroke, he explained Newton’s rings and a number of similar effects associated with thin films, such as the colors seen in soap bubbles or in thin layers of oil floating on water.⁴¹

Furthermore, he performed the simplest interference experiment, allowing a light beam to fall on two parallel slits, and observed the pattern of light and dark stripes, often called fringes, on a screen placed a finite distance beyond the slits. His findings showed that each color in the prism’s spectrum corresponds to a light wave of a particular wavelength, with the longer wavelengths toward the red end of the spectrum and the shorter wavelengths toward the blue and violet.⁴²

When Young first presented his ideas, the main problem facing scientists was that the corpuscular and wave theories of light could not be resolved using available

³⁸M.I. Sobel, *Light*, p. 10, University of Chicago Press, Chicago (1987). Young had previously published work on sound and light during the 1790s, but his primary work on light and color was published in 1801 in a lecture he delivered to the Royal Society of London, entitled “The theory of light and colors.”

³⁹M.S. Barge and W.B. White, *The Daguerreotype: Nineteenth Century Technology and Modern Science*, p. 12, Johns Hopkins University Press, Baltimore (1991).

⁴⁰M.S. Barge and W.B. White, *The Daguerreotype: Nineteenth Century Technology and Modern Science*, p. 12, Johns Hopkins University Press, Baltimore (1991).

⁴¹M.I. Sobel, *Light*, pp. 10-12, University of Chicago Press, Chicago (1987); M.S. Barge and W.B. White, *The Daguerreotype: Nineteenth Century Technology and Modern Science*, pp. 12-13, Johns Hopkins University Press, Baltimore (1991).

⁴²M.I. Sobel, *Light*, p. 12, University of Chicago Press, Chicago (1987).

experimental knowledge—a fact made all the more difficult because the wavelength of light is so small, making its wave characteristics very difficult and hard to detect, unless the dimensions of the apparatus used are very small. For example, interference fringes can be seen only when the spacing between two reflection surfaces is very small. Diffraction can be easily seen only in the shadow of very small objects. That the path of a light beam deviates from a straight line by an extremely small angle makes it extremely difficult to detect diffracted light beams—those spreading around corners.⁴³

It was noted that while the wave theory cannot give a satisfactory account of exactly rectilinear propagation of light, it is well suited to describe approximately rectilinear propagation, provided that it is assumed that the wavelength of light is small in relation to the relevant dimensions of the apparatus.⁴⁴ Young's ideas did not win immediate acceptance; however, powerful mathematical derivations based on experimental work in France and England helped sway many scientists of this era to the wave theory. Most importantly, work in the areas of color, interference, polarization, refraction, diffraction, and absorption were often better described by those who espoused Young's wave theory of light than those who espoused Newton's corpuscular theory of light.⁴⁵

The period starting from about the late seventeenth century saw very important advances in the techniques of experimental physics, and the number and accuracy of experiments on light witnessed significant increase. The observations obtained were in agreement with the wave theory, which became more exactly defined in the nineteenth century.⁴⁶ We describe below three important observations.

3.2.1.3.5 The wavelength of light

Many detailed experiments on interference and diffraction were made, leading to a set of determinations of the wavelength of light. It was established that, in a spectrum, the wavelength is related to the color. The wavelength is about 6.5×10^{-5} cm for red, 5.6×10^{-5} cm for green, and 4.5×10^{-5} cm for blue light. When the wavelengths were measured with different methods, consistent results were obtained.⁴⁷

3.2.1.3.6 The velocity of light

In 1676, the Danish astronomer Olaus Roemer made the fundamental discovery that light is not propagated instantaneously, but that it travels with an enormously

⁴³ibid.

⁴⁴R.W. Ditchburn, *Light*, p. 8, Dover Publications, New York (1991).

⁴⁵M.S. Barge and W.B. White, *The Daguerreotype: Nineteenth Century Technology and Modern Science*, pp. 12–13, Johns Hopkins University Press, Baltimore (1991).

⁴⁶R.W. Ditchburn, *Light*, p. 8, Dover Publications, New York (1991).

⁴⁷ibid., pp. 8–9 (1991).

high, though finite speed. He had arrived at these conclusions from a long period of observing the rotation of the moons of Jupiter and timing their eclipses as they passed around that huge planet. He observed that the moons seemed to either slow down or speed up depending on whether Jupiter was moving away from the Earth or coming closer to it. This effect, he wrote,⁴⁸ was the result of the extra time that the light took to cover the distance between the planets when they were farther apart.⁴⁹

The French physicist Armand Hippolyte Louis Fizeau measured the speed of light in air to be 3×10^{10} cm/s from observing the length of time it takes light to traverse unobstructed through a pair of cogwheels set at the opposite ends of a long axis and made to spin at the rate of a few thousand revolutions per minute. By interposing three mirrors between the cogwheels, with one of the mirrors placed far away, he lengthened the light path, thereby making the effect observable.⁵⁰

Jean Foucault (Fizeau's friend and collaborator) succeeded in shortening the distance by substituting rotating mirrors instead of cogwheels, and was thus able to measure the velocity of light in many different media—air, water, or any transparent material. He observed that the velocity of light in material bodies is less than its velocity in vacuum, thus providing a belated support to Huygens' wave theory and against Newton's particle theory of light.⁵¹

Foucault's experiment was considered at the time to be very crucial, particularly in light of the fact that corpuscular theory held that light travels faster in a dense medium because the molecules of the medium attract the particles of light, speeding up their motion as they enter; and then when the light leaves the medium the same attractive force pulls the corpuscles back, retarding their motion as they enter the air. In contrast, the wave theory, according to arguments going back to Huygens, requires a slower speed in a dense medium than in air.⁵² As predicted by the wave theory, the velocity of light in water, glass, etc. turned out to be exactly its velocity in vacuum divided by the refractive index of the material in question.⁵³

⁴⁸In describing his experiments, Roemer states, "I have been observing the first satellite of Jupiter over eight years. The satellite is eclipsed during each orbit of the planet on entering its vast shadow. I have observed that the intervals between the eclipses vary. They are the shortest when the Earth moves towards Jupiter and longest when it moves away from it. This can only mean that light takes time for transmission through space. . .

The speed must be so great that the light coming to us from Jupiter takes 22 minutes longer to reach us at the farthest end of our orbit round the Sun, than at the other of the orbit when we are nearest Jupiter. That is to say, light takes about 10 minutes to travel from the sun to the Earth; it does not travel instantaneously as alleged by M. Descartes" [cited in P. Mason, *The Light Fantastic*, p. 83, Penguin Books, Middlesex (1981).

⁴⁹P. Mason, *The Light Fantastic*, p. 83, Penguin Books, Middlesex (1981).

⁵⁰G. Gamow, *The Great Physicists from Galileo to Einstein*, pp. 160–162, Dover Publications, New York (1961).

⁵¹G. Gamow, *The Great Physicists from Galileo to Einstein*, p. 161, Dover Publications, New York (1961).

⁵²M.I. Sobel, *Light*, p. 15, University of Chicago Press, Chicago (1987).

⁵³G. Gamow, *The Great Physicists from Galileo to Einstein*, p. 162, Dover Publications, New York (1961).

A very critical experiment, the full significance of which was, however, not realized until after the publication of Einstein's theory of relativity, was carried out in 1851 by Fizeau. Fizeau was interested in determining how the velocity of light is influenced by the motion of the medium through which it propagates. For these investigations, he derived the empirical formula for the velocity V of light in a fluid moving with velocity v ,

$$V = \frac{c}{n} \pm \left(1 - \frac{1}{n^2}\right)v, \quad (3.3)$$

where c is the speed of light in vacuum and n is the refractive index of the fluid in question. Neither Fizeau nor anyone else at that time understood the implications of this result, thus the case rested until one-half a century later when Einstein showed that the empirical formula is a direct result of the theory of relativity.⁵⁴

In 1887, the American physicist A.A. Michelson and his assistant E.W. Morley carried out another remarkable experiment, aimed at observing the effect of the Earth's motion through space on the velocity of light as measured on its surface; in other words to detect "the ether winds"—supposedly created from the motion of the Earth against the luminiferous ether. The apparatus consisted of a terrestrial light source in a device he had invented called an interferometer (see Fig. 3.7),⁵⁵ which measures interference—interference between two light beams that originate from the same light source (hence, are coherent). The initial beam was made to travel to a glass plate positioned at a 45-deg angle; part of the beam is reflected, part is transmitted. The two secondary beams travel at right angles and are eventually brought together by means of other mirrors and are then viewed through a telescope. Given that the two beams have traveled different paths—perhaps one traveled parallel to the Earth's motion and the other perpendicular to the earth's motion—the viewer sees an interference pattern, alternating fringes of light and dark, which itself is not surprising. However, in the final step of the experiment, the experimenters rotated the entire apparatus through 90 deg, effectively interchanging the paths of the two beams. They expected to see a shift in the fringes since the light paths through the ether have changed. Instead, the result they observed was negative, since no fringe shift was observed, implying that somehow the luminiferous ether remained stationary to the planet Earth in its annual circuit around the sun. In other words, no ether wind was created, suggesting perhaps that the luminiferous ether does not exist, and even more importantly, that the speed of light in space is constant.⁵⁶

How the speed of light is affected when the source of the light is moving became a question that attracted much theoretical speculation in the years after 1887. In 1905, Einstein found the solution lying at the heart of Maxwell's

⁵⁴ibid., pp. 162–164.

⁵⁵A.A. Michelson, *Studies in Optics*, pp. 20–32, Dover Publications, Mineola, New York (1995).

⁵⁶M.I. Sobel, *Light*, pp. 199–202, University of Chicago Press, Chicago (1987).

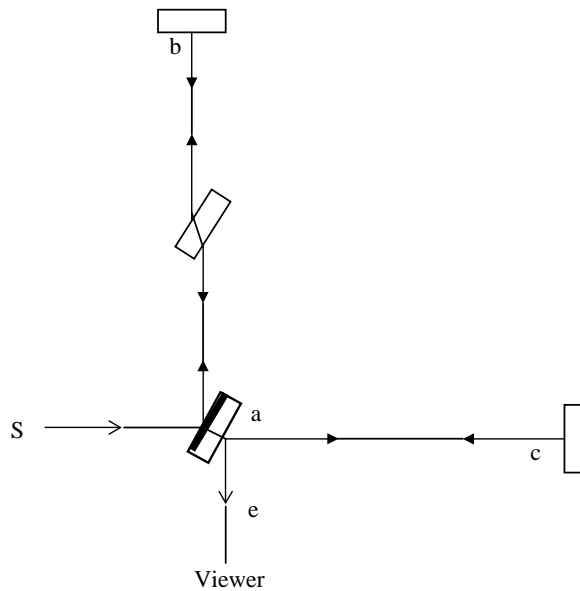


Figure 3.7 Michelson interferometer. Light from the source S is directed to the surface of a plane-parallel glass plate a, which separates it into two “coherent” pencil rays, one of which is transmitted through a glass plate en route to the surface b, from where it is reflected back to the separating surface a. The other pencil ray is reflected normally from the plane mirror c back to the separating surface a, and together with the reflected beam from b, return to the separating surface a, from where they both proceed in the direction ae where the resulting interference fringes may be projected on a screen or observed by the eye, with or without an observing telescope.

equations of electromagnetism⁵⁷ (see the sections on relativity and electromagnetic theories).

Today, interferometers are used widely in the alignment system of lithographic exposure tools for coordinating the movement of the exposure stage. In particular, they have found application in high-precision measurements of extremely small distances, between different objects in the exposure tool. Furthermore, interferometric lithography owes its very existence to the Michelson-Morley experiment.

3.2.1.3.7 The polarization of light

A rather curious observation was made in 1670 by Bartholinus, who discovered that when a beam of ordinary light passes through certain crystals, such as natural calcite or Icelandic spar, each ray splits into two. When he passed the two rays through a second crystal, he observed that the effect depends on the orientation

⁵⁷Einstein takes Maxwell’s electromagnetic theory as the starting point of his analysis. He does not make any reference to the Michelson Morley experiment.

of the crystal with respect to the beam. For certain orientations, the two rays each split into two. For others, the two rays pass through the crystal unchanged (see Fig. 3.8). This phenomenon is known as double refraction (or birefringence). It is an indication that a beam of light that has passed through a crystal is differentiated with respect to the planes, including the direction of propagation.⁵⁸

The simplest experiment on polarization was made much later (in 1808) by the French engineer Etienne Louis Malus, who was in Napoleon's army. He reflected a beam of light at the surfaces of two unsilvered pieces of glass (see Fig. 3.9) and observed that when the two reflections are in the same plane, a high proportion of the light incident on the second mirror (M_2) is reflected. If the mirror M_2 is turned so that the second reflection is directed out of the plane of the paper, the

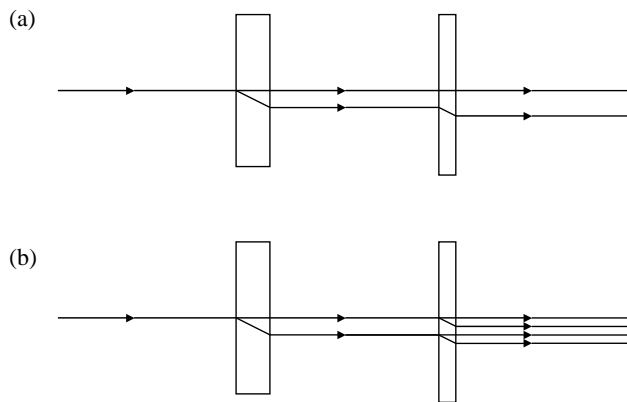


Figure 3.8 Double refraction: (a) two crystals with similar orientations; (b) two crystals with different orientations of crystal axes.

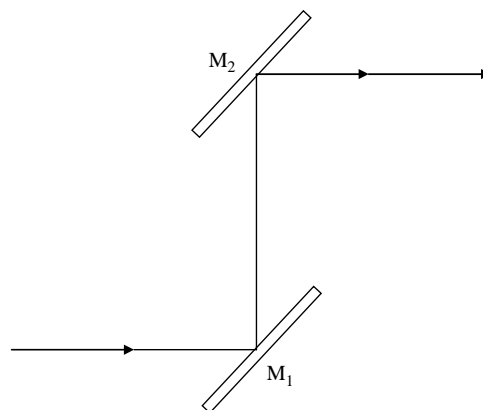


Figure 3.9 Malus's experiments. Note that M_1 and M_2 are unsilvered mirrors.

⁵⁸R.W. Ditchburn, *Light*, p. 9, Dover Publications, New York (1991).

reflected beam becomes weaker, approaching nearly zero brightness when the two reflections are in planes at right angles. This suggests that after the first reflection, the beam of light has a special property in relation to the plane of the paper, that is, it can be strongly reflected, at a glass surface, in this plane but not at right angles. A beam of light possessing this property is said to be plane polarized. Although this type of theory finds no place in a theory of longitudinal waves, it is, however, adequately represented in a theory of transverse waves.⁵⁹ Thus, although polarization is a subtle property of light, its elucidation was instrumental in establishing one of the basic characteristics of light waves, along with an important difference between light and sound—light is a transverse wave, the oscillations being perpendicular to the path of propagation. This was a fact realized by Huygens (1690), but it was not until the nineteenth century that it became possible to conduct experiments on the reflection and refraction of polarized light. Sound waves, on the other hand, were known in the nineteenth century to be longitudinal, consisting of oscillations of air in directions back and forth, along the direction of propagation. Being longitudinal, the motion of sound can be represented as the variation of a scalar quantity, while transverse wave motion must be represented by a vector whose direction is related to the plane of polarization.⁶⁰

The experimental and theoretical work of Thomas Young, and later, of Augustin Fresnel (1788–1827), on interference and polarized light during the first few years of the nineteenth century yielded new evidence that supported the wave theory of light. Both scientists observed that under certain conditions, light appeared to interfere with and be cancelled out by other light that arrived at an eye or a lens at the same time. Young called this phenomenon interference. Fresnel's mathematical treatment of the interference phenomenon was far more rigorous and complete than that of Young. He developed the mathematical wave theory of light so thoroughly that the particle theory was vanquished and literally not heard of again until the twentieth century.⁶¹

The mathematician Simeon Poisson predicted (and also experimentally verified) one of the consequences of Fresnel's theory, namely, that a circular disk placed in a parallel beam of light should not only throw a circular shadow with narrow diffraction fringes around it, but should also show a bright spot ring in the middle of the shadow.⁶² Fresnel also made extensive studies of diffraction, measuring fringes produced at the edges of shadows in various types of experiments, and he showed that his results could be fully explained by the wave theory, with his measured values for wavelengths of light in agreement with those calculated by Young.⁶³

⁵⁹R.W. Ditchburn, *Light*, pp. 9–10, Dover Publications, New York (1991).

⁶⁰*ibid.*, p. 10; M.I. Sobel, *Light*, pp. 15–16, University of Chicago Press, Chicago (1987).

⁶¹P. Mason, *The Light Fantastic*, pp. 43–45, Penguin Books, Middlesex (1981); M.S. Barge and W.B. White, *The Daguerreotype: Nineteenth Century Technology and Modern Science*, p. 13, Johns Hopkins University Press, Baltimore (1991).

⁶²P. Mason, *The Light Fantastic*, p. 44, Penguin Books, Middlesex (1981).

⁶³*ibid.*, pp. 43–45; M.S. Barge and W.B. White, *The Daguerreotype: Nineteenth Century Technology and Modern Science*, p. 13, Johns Hopkins University Press, Baltimore (1991).

The success of the wave theory⁶⁴ greatly influenced the progress of similar work in other areas of optics, which also proceeded at a rapid pace during this period. This very success stimulated the demand for new and improved lenses and optical instruments, which had the effect of feeding the increasing demand for instruments to aid in the accurate depiction and recording of nature. Although the physics of image formation in a lens was fairly well understood during this time, new mathematics derived from the study of other light phenomena led to improved lens design and likewise improved instruments such as telescopes, microscopes, and cameras. Three notable specific examples of instruments included the camera lucida, the “Wollaston doublet” lens for microscopes, and a singlet landscape lens corrected to produce a flat field of view, all of which were developed by William Hyde Wollaston (1766–1828).⁶⁵ New methods for manufacturing glasses were devised during this period as well, and a more empirical understanding of the relationship between glass composition and the quality of lenses was also established.⁶⁶

Today, in the regime of hyper-numerical-aperture imaging and immersion lithography, polarization effects have become very dominant. Understanding these effects and designing around them have relied enormously on the theories of Fresnel and Young.

3.2.1.4 Electromagnetic theory

The formulation of the wave theory of light predated the development of the fundamental laws of electromagnetism.⁶⁷ The notion of light waves traveling through vacuum was inconceivable to scientists of the nineteenth century, who were schooled on the properties of water waves and sound waves (which travel through air and through liquids and solids). They therefore felt it necessary to postulate the existence a medium that carried waves of light as transverse oscillations. This was the luminiferous ether, which pervaded all space, even out to the stars. The ether was imbued with properties that made it rarer than air, since starlight is refracted when entering the atmosphere. It was incompressible, or else it would dissipate a light ray in all directions. It was perfectly elastic, such that it would not retard the passage of matter (such as the planets in their orbits) and it possessed the same kind of rigidity as a solid because only a solid is able to propagate a transverse wave. Even Lord Kelvin likened it to a mold of transparent jelly.⁶⁸

⁶⁴The wave theory resulted from efforts on the two sides of the English Channel. The success of that theory was attested to by the election of Fresnel, in 1827, as a foreign member of the British Royal Society and the election of Young, in the same year, as a foreign member of the French Academy; see also M.I. Sobel, *Light*, University of Chicago Press, Chicago, p. 15 (1987).

⁶⁵M.S. Barge and W.B. White, *The Daguerreotype: Nineteenth Century Technology and Modern Science*, Johns Hopkins University Press, Baltimore, p. 13 (1991).

⁶⁶*ibid.*

⁶⁷R.W. Ditchburn, *Light*, p. 10, Dover Publications, New York (1991).

⁶⁸M.I. Sobel, p. 15–16, *Light*, University of Chicago Press, Chicago (1987).

It should be pointed out that natural philosophy in the nineteenth century was ripe for a bogus concept like the ether, because scientists had come to accept the existence of substances other than ordinary matter. Under the shadow of Newton, science in the previous century had been dominated by a mechanistic world view in which all phenomena were due to the interaction of matter. But research involving the properties of heat, light, electricity, and magnetism made it manifestly clear that although one might try to picture these as materials—fluids or corpuscles—they were nonetheless in some fundamental ways different from ordinary matter. Thus, these scientists thought that there were two types of matter, that is, normal or “ponderable” matter, and the “imponderables.” The ether was thus regarded as the most pervasive and subtle of the imponderables.⁶⁹

A theory of transverse waves in such a medium presented a rather qualitative description of the fundamental phenomena of interference—diffraction and polarization. In order to build the edifice of the wave theory, it was necessary to make special assumptions concerning the density and elasticity of this medium, and also concerning the conditions obtained at the surface separating two media such as glass and air. A close examination of these details revealed certain difficulties and appeared to indicate that there were some inconsistencies in the theory. All these difficulties were resolved by Maxwell’s electromagnetic theory of light—the great achievement of nineteenth century science—which unified the imponderables of electricity and magnetism.⁷⁰

Although this great theoretical synthesis was the work of James Clerk Maxwell (Fig. 3.10) in Scotland, it in fact grew out of the experimental researches of many scientists, including Hans Christian Oersted in Denmark, Charles Augustin de Coulomb, Jean-Baptiste Biot, and Andre-Marie Ampere in France, and Michael Faraday (Fig. 3.11) in England. Oersted was the first to show in 1820 that there was an intimate connection between electricity and magnetism when he observed



Figure 3.10 James Clerk Maxwell, who among many other things, consolidated and extended the equations of electromagnetism. (Published with permission from the Deutsches Museum, Munich.)

⁶⁹ibid.

⁷⁰R.W. Ditchburn, *Light*, pp. 10–11, Dover Publications, New York (1991).

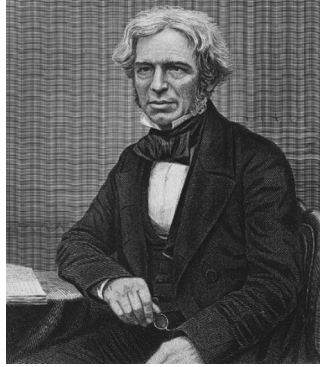


Figure 3.11 Michael Faraday, who among many things discovered electromagnetic induction in 1831 and established the connection between electricity, magnetism, and light; he also discovered electrolysis. (Published with permission from the Deutsches Museum, Munich.)

that a coil of wire carrying an electric current produces the same kind of magnetic field as a bar magnet. Faraday was the first to demonstrate the opposite phenomenon—electrical effects produced by magnets—when he observed that a magnet moved through a coil of wire induces a pulse of current in the wire (without the wire being attached to a battery or any source of electricity).⁷¹

Generalizing a set of empirical facts that include: (i) light is an electromagnetic wave with coupled electric and magnetic fields (\vec{E} and \vec{H}) traveling through space, (ii) these fields can interact with a material, resulting in four other quantities, that is, the electric displacement \vec{D} , the magnetic induction \vec{B} , the electric current density \vec{J} , and the electric charge density ρ , and (iii) a changing magnetic field creates in its vicinity a changing electric field, and a changing electric field similarly creates a changing magnetic field, he derived the famous equations [Eqs. (3.4)–(3.7)] that now bear his name, which connect the rate of change of the magnetic field with space distribution of the electric field and vice versa,⁷²

$$\vec{\nabla} \times \vec{H} = \frac{4\pi}{c} \vec{J} + \frac{1}{c} \frac{\partial \vec{D}}{\partial t}, \quad (3.4)$$

$$\vec{\nabla} \times \vec{E} = -\frac{1}{c} \frac{\partial \vec{B}}{\partial t}, \quad (3.5)$$

$$\vec{\nabla} \cdot \vec{D} = 4\pi\rho, \quad (3.6)$$

$$\vec{\nabla} \cdot \vec{B} = 0, \quad (3.7)$$

⁷¹M.I. Sobel, *Light*, p. 16, University of Chicago Press, Chicago (1987).

⁷²G. Gamow, *The Great Physicists from Galileo to Einstein*, p. 152, Dover Publications, New York (1961); P. Mason, *The Light Fantastic*, pp. 49–52, Penguin Books, Middlesex (1981); M.I. Sobel, *Light*, p. 16, University of Chicago Press, Chicago (1987); C.A. Mack, *Field Guide to Optical Lithography*, p. 11, SPIE Press, Bellingham, WA (2006); C.A. Mack, *Fundamental Principles of Optical Lithography: The Science of Microfabrication*, pp. 30–32, John Wiley & Sons, Hoboken, NJ (2007).

where c is the speed of light in vacuum. Equation (3.4) shows how a time-varying electric field (or displacement) causes a change in the magnetic field induction. In other words, a changing electric displacement produces a magnetic induction. Equation (3.5) shows how a time-varying magnetic induction causes a change in the electric field. In other words, a changing magnetic induction produces an electric field. Equation (3.6) shows how static charge affects the electric field, while Eq. (3.7) shows that there are no magnetic charges.⁷³

It is from the properties of the materials involved that relationships between current density and the electric field, the electric displacement and the electric field, and the magnetic induction and magnetic field are established. In the event that the material through which the electromagnetic radiation is propagating is isotropic, and is moving slowly relative to the speed of light, and the fields involved are time harmonic, then the three material equations become⁷⁴

$$\vec{J} = \sigma \vec{E}, \quad (3.8)$$

$$\vec{D} = \epsilon \vec{E}, \quad (3.9)$$

$$\vec{B} = \mu \vec{H}, \quad (3.10)$$

where σ , ϵ , and μ are the conductivity, dielectric constant, and magnetic permeability of the material, respectively. For transparent (or dielectric) materials, $\sigma = 0$. In general, materials used in lithography are nonmagnetic; thus $\mu = 1$.⁷⁵

One of the great insights that derive from Maxwell's equations is the realization that both electric and magnetic fields are manifestations of the same underlying phenomenon—electromagnetism. Maxwell also deduced that they can exhibit wavelike properties⁷⁶ (see Fig. 3.12). As an illustration, an oscillating electric charge will create around its vicinity a region of oscillating electric and magnetic fields, and these fields in turn create oscillating electric and magnetic fields around themselves in a process that gets repeated multiple times such that radiating spheres of electromagnetic fields proceed outward from the original charge. Given the periodic nature of the motion of the electric charge, the variation of the field out along a radius is also periodic, and the wave created in this way is a spherical wave.⁷⁷

⁷³ibid.

⁷⁴ibid.

⁷⁵C.A. Mack, *Field Guide to Optical Lithography*, p. 11, SPIE Press, Bellingham, WA (2006).

⁷⁶M.I. Sobel, *Light*, p. 17, University of Chicago Press, Chicago (1987).

⁷⁷G. Gamow, *The Great Physicists from Galileo to Einstein*, pp. 149–157, Dover Publications, New York (1961); M.I. Sobel, *Light*, pp. 15–21, University of Chicago Press, Chicago (1987); R.W. Ditchburn, *Light*, pp. 10–12, Dover Publications, New York (1991); E. Hecht, *Optics*, 4th ed., Pearson Education (2001); R.A. Serway and J.W. Jewett, *Physics for Scientists and Engineers*, 6th ed., Brooks/Cole (2004); P. Tipler, *Physics for Scientists and Engineers: Electricity, Magnetism, Light, and Elementary Modern Physics*, 5th ed., W.H. Freeman & Co., New York (2004); J. Reitz, F. Milford, and R. Christy, *Foundations of Electromagnetic Theory*, 4th ed., Addison Wesley, Menlo Park (1992); J.D. Jackson *Classical Electrodynamics*, 2nd ed., John Wiley & Sons, Hoboken, NJ (1975).

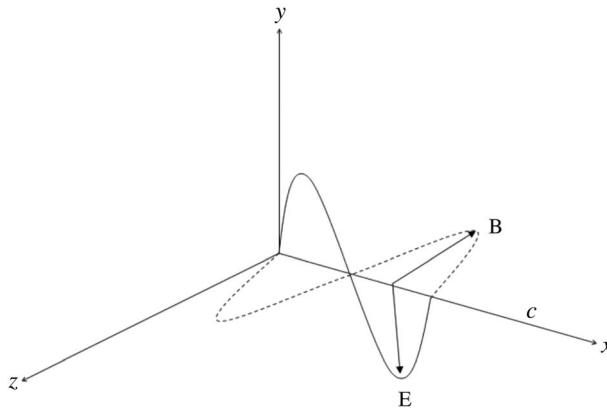


Figure 3.12 A schematic of a polarized electromagnetic wave at a fixed instant in time. The light wave travels along the x axis with velocity c .

In deriving his equations, Maxwell used electrostatic units for electric field, and electromagnetic units for magnetic field. The application of these equations for describing propagating waves led him to the conclusion that the propagation velocity is numerically equal to the ratio of the two units, i.e., 3×10^{10} cm/s,⁷⁸ which coincidentally is the velocity of light in vacuum measured by various methods long before Maxwell was born. Describing this numerical coincidence when he first published his theory of electromagnetism in the *Philosophical Magazine* in 1862, he stated, “This velocity is so nearly that of light, that it seems we have strong reason to believe that light itself (including radiant heat, and other radiations if any) is an electromagnetic disturbance in the form of waves propagated through the electromagnetic field according to electromagnetic laws.”⁷⁹ Coincidentally, in the same year as Maxwell’s publication, Jean-Bernard-Leon Foucault, using an improved method over the earlier work of Fizeau, determined a new, accurate value of the speed of light (differing by less than 1% from today’s best value).⁸⁰

In all, Maxwell formulated the equations of electromagnetism in a general form, and he showed that they are consistent with transverse electromagnetic wave propagation. He derived the velocity of propagation from constants measured in laboratory experiments on electricity and magnetism. He predicted that an oscillating electric charge will generate an electromagnetic wave and that the wave travels at the speed of light, given by $\sqrt{1/\mu_0\epsilon_0}$ (where ϵ_0 is electric permittivity of vacuum, μ_0 is the permeability of vacuum). The wavelength depends on how rapidly the charge oscillates. His theory included an account of the propagation of electromagnetic waves in media such as glass. He showed that his theory gave a general account of the phenomena of reflection and refraction, including

⁷⁸G. Gamow, *The Great Physicists from Galileo to Einstein*, p. 156, Dover Publications, New York (1961).

⁷⁹J.C. Maxwell, *A Dynamical Theory of the Electromagnetic Field; The Scientific Papers of James Clerk Maxwell*, pp. 1–535, New York: Dover Publications (1965).

⁸⁰M.I. Sobel, *Light*, p. 17, University of Chicago Press, Chicago (1987).

the formation of a spectrum by the dispersion of light. It is noteworthy to realize that he achieved all of this without introducing any arbitrary assumptions. The theory of light was transformed by him, into a part of the theory of electricity and magnetism.⁸¹

It cannot be overemphasized that because of Maxwell's electromagnetic theory, we now can understand the interaction of light and matter, including the phenomena of emission, propagation, and absorption of light, as resulting from forces acting between propagating short electromagnetic waves and electrons, busily buzzing around the positively charged atomic nuclei. And, with Maxwell's equations, it is possible to explain in the most minute detail all of the phenomena and laws of optics.⁸²

Today, the reach of Maxwell's electromagnetic theory extends all the way to lithography, where it guides the choice and usage of optical elements of lithographic exposure tools, as well as the interaction of these optical elements and radiation-sensitive resist materials with lithographic exposure radiations.

3.2.1.5 Electromagnetic spectrum

Even before the birth of Maxwell, the electromagnetic spectrum had been extended beyond the violet-to-red range revealed by the prism. As early as 1801, the astronomer William Herschel made the observation that as he moved a thermometer across the beam emerging from a prism, from yellow to orange to red, heating effects increased and that they increased still further when he moved to a region beyond the red. This observation established that there is radiation beyond the red, called infrared, which, following the work of Maxwell, we recognize as electromagnetic waves with wavelengths longer than 700 nm. Herschel also observed that infrared radiation obeys the same laws of reflection and refraction that light obeys. Later workers found infrared radiation to show polarization and interference phenomena as well.⁸³

At the opposite end of the spectrum, ultraviolet radiation (waves beyond the violet) was discovered on account of one of the chemical effects of light on certain salts. It had been known since early in the eighteenth century that light darkens silver nitrate and certain other salts. This phenomenon later became the basis of photography and was used in some of the early inorganic photoresists. Having learned of Herschel's infrared waves, the German physicist Johann Ritter in 1801 discovered the darkening of silver nitrate by waves in the region beyond the violet, with wavelengths shorter than those of visible light.⁸⁴

⁸¹M.I. Sobel, *Light*, pp. 15–21, University of Chicago Press, Chicago (1987); R.W. Ditchburn, *Light*, pp. 10–12, Dover Publications, New York (1991); P. Mason, *The Light Fantastic*, pp. 49–52, Penguin Books, Middlesex (1981).

⁸²G. Gamow, *The Great Physicists from Galileo to Einstein*, pp. 156–157, Dover Publications, New York (1961).

⁸³M.I. Sobel, *Light*, p. 19, University of Chicago Press, Chicago (1987).

⁸⁴*ibid.*

Maxwell's electromagnetic theory suggested the possibility of producing electromagnetic waves of other wavelengths beyond the visible. Although Herschel and Ritter demonstrated the effects of some of these waves, and by so doing, indirectly proved the existence of these waves, they were, however, not able to directly prove the existence of these waves since they did not produce them. It was not until 1887 that the required experimental evidence was provided by Heinrich Hertz (Fig. 3.13), who conclusively demonstrated the existence of electromagnetic waves. He showed how to produce such waves with wavelengths much greater than those of the visible spectrum, and thereby opened the door to the world of radio and television.⁸⁵

To generate electric sparks, Hertz used an induction coil with a vibrating spring as a contact breaker. The coil was connected to two brass balls that formed a spark gap. The balls were attached to long brass rods that acted as antennas. Because of the sudden and violent surge of electricity in a spark, the motion of charges corresponds to oscillations at very high frequency. The sparks generated in the gap induce an alternating current in the rod, and the rod now acts as a transmitting radio antenna.⁸⁶ To detect the electromagnetic waves emitted from the spark transmitter, Hertz used a secondary spark gap with its own antenna. In order to enhance the received signal, he made the secondary gap small and adjustable. The experiments were an immediate success, since he observed sparks in the secondary gap at distances of several meters from the transmitter. Using parabolic mirrors made from zinc sheet enabled him to detect the waves at a much greater distance. He found that the waves could be blocked by metal sheets or by human bodies, but not by insulating materials.⁸⁷



Figure 3.13 Heinrich Hertz, who demonstrated the existence of electromagnetic waves and thus confirmed Maxwell's electromagnetic theory. (Published with permission from the Deutsches Museum, Munich.)

⁸⁵P. Mason, *The Light Fantastic*, pp. 53–55, Penguin Books, Middlesex (1981).

⁸⁶M.I. Sobel, *Light*, p. 21, University of Chicago Press, Chicago (1987).

⁸⁷*ibid.*

Hertz was able to identify these electromagnetic rays as an invisible form of light by demonstrating that they displayed the wavelike phenomena of reflection, refraction, polarization, and interference. From interference measurements, he showed that the wavelength of the waves received by the detector was 66 cm, a million times longer than the wavelength of red light.⁸⁸ From both wavelength and frequency measurements of these electric waves, he was able to calculate the speed at which the waves travel, finding it to be precisely the speed of light.⁸⁹

A great deal of the progress of experimental physics since Hertz's great discovery has consisted of the discovery of methods of producing electromagnetic waves of different wavelengths, a good number of which are now employed in lithography: near-UV (365 nm), deep-UV (248 nm and 193 nm), vacuum UV (157 nm), extreme UV (13.4 nm), x ray (0.1–10 nm), etc. Some of the properties of these waves depend on their wavelength, but they all propagate with the same velocity (in vacuum) and they all obey Maxwell's equations. Modern technical advances have made it possible to produce or detect waves of nearly every wavelength from above 3000 m to well below 10^{-11} cm⁹⁰ (see Fig. 3.14).

In general terms, the electromagnetic spectrum is classified by wavelengths into electrical energy, radio, microwave, infrared, the visible region we perceive as light, ultraviolet, x rays, and gamma rays. The visible region occupies the band between approximately 400 nm and 700 nm, and is detected by the human eye and perceived as light. Radiation within the ultraviolet region are invisible, but affects the skin and causes sunburn. Infrared radiation is invisible but produces the sensation of heat.

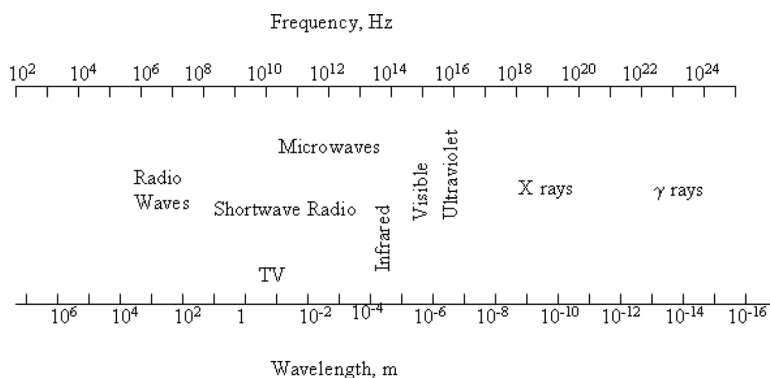


Figure 3.14 The electromagnetic spectrum, showing the frequency and wavelength of the radiations. Visible light encompasses the 400–700-nm band.

⁸⁸ibid.

⁸⁹M.I. Sobel, *Light*, p. 22, University of Chicago Press, Chicago (1987).

⁹⁰R.W. Ditchburn, *Light*, pp. 10–12, Dover Publications, New York (1991).

3.2.1.6 Absorption of light

The way in which light is absorbed was studied by Johann Heinrich Lambert (1728–1777), who first expressed it in the differential form,

$$\frac{dI}{dz} = -\alpha I, \quad (3.11)$$

where I is the intensity of light traveling in the z direction through a medium, and α is the absorption coefficient of the medium and has units of inverse length. In a homogenous medium (i.e., α is not a function of z), Eq. (3.11) may be integrated to yield

$$\frac{I(z)}{I_0} = e^{-\alpha z}, \quad (3.12)$$

which can be rearranged to yield

$$-\ln \frac{I(z)}{I_0} = \alpha z = A, \quad (3.13)$$

where z is the distance the light has traveled through the medium, I_0 is the intensity at $z = 0$, and A is the absorbance. The ratio of the transmitted light to the incident light [left-hand side of Eq. (3.12)] is the transmission of the light. In 1852, Augustus Beer (1825–1863) showed that for dilute solutions, the absorption coefficient is proportional to the concentration of the absorbing species in the solution as

$$\alpha_{\text{solution}} = ac, \quad (3.14)$$

where a is the molar absorption coefficient (sometimes called the molar extinction coefficient) of the absorbing species and c is the concentration.

Equations (3.12) and (3.13) are now referred to as Lambert's law, which in essence states that there is a logarithmic dependence between the transmission of light through a substance and the concentration of the substance, and also between the transmission and the length of the material that the light travels through. Today, Lambert's law serves as the starting point of all lithographic modeling, along with the radiation chemistry/photochemistry that go with it.

3.2.1.7 Chemical effects of light

To complement the research efforts targeted at elucidating and controlling the physical characteristics of light, active research was also conducted on the chemical effects of light, dating back to the early decades of the eighteenth century. In fact, the roots of the science of photochemistry date back to this era, when in 1727 Johann Heinrich Schulze (1687–1744) (Fig. 3.15) discovered that if a bottle of silver nitrate crystals was placed in the sun and part of the bottle



Figure 3.15 Johan Heinrich Schulz (1687–1744), who discovered the darkening of silver nitrate crystals under light irradiation. (Published with permission from the Deutsches Museum, Munich.)

covered with a stencil, the uncovered area would blacken. Inspired by Schulze's discovery, other experimenters discovered various metal compounds and other silver compounds, that, in time, were used in the production of silver nitrate ink and other inks, which were used to produce permanent designs on a variety of substrates including paper, textiles, bones, ivory, and leather. Silver nitrate was also used as a hair dye during this time.⁹¹

In 1777, Karl Wilhelm Scheele (1742–1786) (Fig. 3.16) published the first comprehensive book on the chemical effects of light. Considered the father of



Figure 3.16 Statue of Karl Wilhem Scheele (1742–1786), who is considered to be the founder of the science of photochemistry. (Published with permission from the Deutsches Museum, Munich.)

⁹¹M.S. Barge and W.B. White, *The Daguerreotype: Nineteenth Century Technology and Modern Science*, pp. 13–14, Johns Hopkins University Press, Baltimore (1991).

photochemistry, Scheele used his experiments to try to demonstrate that light was composed of or contained phlogiston,⁹² a fact he deduced rather erroneously when he observed that when silver oxide, gold oxide, or mercury oxide is placed at the focus of a burning glass (a parabolic mirror used to focus the rays of the Sun on an object to be burned), these salts are changed to metal.⁹³

Another major contributor to research in the chemical effects of light during this period was the Frenchman Antoine Lavoisier (1734–1794), who introduced accurate methods of weight measurements of materials undergoing chemical reactions into the field of chemistry. He believed that light was a true reagent, which when added to some compounds could alter their basic properties or cause a reaction. In time, testing for reactivity in light became part of the regular chemical routine of investigating new compounds and elements.⁹⁴

The science of photometry—the measurement of the effect of light intensity whether transmitted or absorbed on various materials—provided another impetus for research on chemical effects of light during this period. These studies⁹⁵ had broad focus, spanning research on astronomy and chemical effects of light. Very basic photometers were made with paper saturated with silver nitrate, silver chloride, or other light-sensitive solutions.⁹⁶

Another major development in the research on the chemical effects of light was spectral analysis, the forerunner of modern spectroscopy. This entails the study of the physical and chemical effects of light that has been dispersed into a spectrum by being passed first through a slit and then through a prism.⁹⁷ In 1752, the Scotsman Thomas Melvill, when studying the light of a flame passed through a prism, discovered that the spectrum was not continuous like that of the Sun; rather, parts of the spectrum were bright, and others were dark. He observed that the locations of the bright spots and their colors were different when different chemicals were placed in the flame.⁹⁸

⁹²Phlogiston was thought to be a substance that exists in all combustible materials, which on combustion is released. It was an important chemical concept introduced at the beginning of the eighteenth century and maintained until the death of Joseph Priestly in 1802. Although Priestly discovered oxygen in 1774, he, like many scientists of his era, did not recognize that it was the substance responsible for combustion. Consequently, the development of chemistry was stifled on account of this erroneous concept. Antoine Lavoisier made the connection that oxygen is responsible for combustion and in so doing sounded the death knell for phlogiston.

⁹³M.S. Barge and W.B. White, *The Daguerreotype: Nineteenth Century Technology and Modern Science*, p. 14, Johns Hopkins University Press, Baltimore (1991).

⁹⁴*ibid.*, p. 14.

⁹⁵Many illustrious scientists including Thomas Young, François Arago, John Herschel, and Simeon Poisson conducted such experiments in photometry [cited in François Arago, *Biographies of Distinguished Scientific Men*, translated by W.H. Smyth, B. Powell, and R. Grant, 2nd series, Tricknor & Fields, Boston (1859); M.S. Barge and W.B. White, *The Daguerreotype: Nineteenth Century Technology and Modern Science*, p. 14, Johns Hopkins University Press, Baltimore (1991)].

⁹⁶M.S. Barge and W.B. White, *The Daguerreotype: Nineteenth Century Technology and Modern Science*, p. 14, Johns Hopkins University Press, Baltimore (1991).

⁹⁷*ibid.*, p. 15.

⁹⁸M.I. Sobel, *Light*, p. 81, University of Chicago Press, Chicago (1987).

In addition, spectral light was used to study gases and flames colored by the addition of various metal salts and transparent liquids, as well as to monitor the effects of photochemical changes. Based on his work on spectral analysis, Scheele established that there is a difference between actions of light and heat. This line of research was subsequently to lead to the discovery of the infrared region of the spectrum in 1800 by Friedrich Wilhelm Herschel (discussed above), and the ultraviolet region in 1801 by J.W. Ritter (discussed above). It also led William Hyde Wollaston to discover the ultraviolet region of the spectrum in 1802; he referred to this discovery as chemical rays.⁹⁹

In the final analysis, a great deal of both theoretical and empirical activity concerning light and its effect on a wide variety of materials were already well established by the early part of the nineteenth century. In particular, many chemical discoveries that showed the range of both light-sensitive materials and their properties in a variety of conditions were made. These discoveries comprised light-sensitive materials such as silver nitrate, silver chloride, silver oxalate, mercury oxalate, chromate and citrate salts, iron salts, gold salts, and platinum salts; compounds that react with light-sensitive materials, such as sodium thiosulfate; and elements that react with other materials to form light-sensitive compounds, such as chlorine, iodine, and bromine.¹⁰⁰ During this period, the use of optical instruments was particularly widespread among artists, artisans, and scientists.¹⁰¹ It was in this milieu of abundant data on chemical effects of light on materials, along with the widespread availability of optical instruments in the early part of nineteenth century, that the invention of photolithography and its subsequent development were made possible.

3.2.1.8 The discovery of electrons

By the end of the nineteenth century, the properties of light waves were fairly well understood. Long-wavelength radiation such as infrared and radio waves were already discovered, along with short-wavelength ultraviolet radiation. Still, scientists sought to find out whether there were other shorter-wavelength radiations yet to be discovered; they also wondered about what properties these radiations might have, along with their possible applications.

It was in this climate that the cathode rays produced by electrical discharges in gases at low pressure were discovered by Plucker in 1859.¹⁰² Aided by improvements in vacuum pumps to provide a high degree of vacuum and the induction coil to provide high-voltage electricity, Sir William Crookes in 1876 built the first cathode ray tube, the forerunner of the television tube. With this equipment, he was

⁹⁹ibid., pp. 14 15, 81.

¹⁰⁰M.S. Barge and W.B. White, *The Daguerreotype: Nineteenth Century Technology and Modern Science*, pp. 15 16, Johns Hopkins University Press, Baltimore (1991).

¹⁰¹ibid., p. 16.

¹⁰²J.R. Partington, *A Short History of Chemistry*, 3rd ed., p. 357, Dover Publications, New York (1989).

able to investigate the peculiar bands of light that formed near the negative electrode (the cathode). He found that these bands could be moved about by moving a bar of magnet near the tube. He proposed that the movement of the bands showed that the cathode rays that formed the electrical discharge were actually streams of negatively charged particles.¹⁰³ In 1897, J.J. Thomson not only showed that the cathode rays consisted of negatively charged particles, but he even measured their mass, which he determined to be much smaller than that of the hydrogen atom (the currently accepted value is about 1/1850 that of the H atom), as well as the electric charge.¹⁰⁴ The name “electron” was coined for these particles by Johnston Stoney, who in 1874 calculated an approximate value for its charge.¹⁰⁵ The modern theory of atomic structure derives from the discovery of the electron and radioactivity.¹⁰⁶

The electronic revolution that has defined our modern world derives directly from the discovery of the electron. In particular, electron-beam lithography traces its very origin to this same discovery.

3.2.1.9 The discovery of x rays

While investigating the nature of cathode rays produced in a Crookes tube that he had covered with a shield of black cardboard, ostensibly to prevent the cathode rays from escaping, Roentgen (Fig. 3.17) observed in 1895 the luminescent effect on a



Figure 3.17 Wilhelm Conrad Roentgen, the discoverer of x rays and of radiography. (Published with permission from the Deutsches Museum, Munich.)

¹⁰³P. Mason, *The Light Fantastic*, p. 189, Penguin Books, Middlesex (1981).

¹⁰⁴J.R. Partington, *A Short History of Chemistry*, 3rd ed., p. 357, Dover Publications, New York (1989).

¹⁰⁵*ibid.*

¹⁰⁶*ibid.*; P. Mason, *The Light Fantastic*, pp. 189–190, Penguin Books, Middlesex (1981).

piece of barium platinocyanide paper lying a considerable distance away. Reasoning that this luminescent effect could only be produced by some invisible ray, different from the cathode rays, but yet emanating from the Crookes tube, while also penetrating the black cardboard shield, he gave them the “provisional” name of x rays.¹⁰⁷ That name is still in use everywhere in the world today, except in his native Germany, where they are called Roentgen rays. He determined many properties of the x rays and showed that they could pass through glass or wood; through aluminum, though not through lead; and even through human flesh. On emerging, the x rays would make a fluorescent screen glow or a photographic plate turn black.¹⁰⁸

It was George Stokes who proposed that x rays were electromagnetic radiation with even shorter wavelengths than the ultraviolet radiations. Roentgen himself erroneously thought that they were not transverse but longitudinal waves, like sound, while other scientists thought they were another kind of particle. A decade later, diffraction experiments carried out with crystals confirmed Stokes’ view of x rays as invisible form of radiation.¹⁰⁹ The roots of x-ray lithography stretch all the way back to Roentgen’s discovery.

3.2.1.10 Radioactivity

In 1896, Henri Becquerel (Fig. 3.18) made the serendipitous discovery of yet another unexpected phenomenon, revealing the existence of invisible radiations with wavelengths shorter than those of x rays. He had found that crystals of the

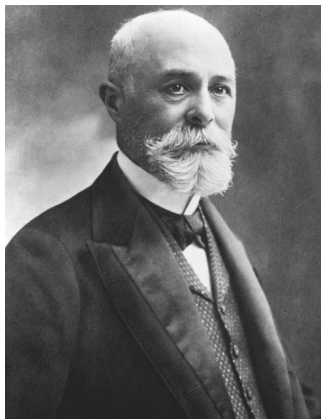


Figure 3.18 Antoine Henri Becquerel, who discovered natural radioactivity. (Published with permission from Deutsches Museum, Munich.)

¹⁰⁷ibid., pp. 190–191.

¹⁰⁸ibid.

¹⁰⁹ibid., p. 195.

salts of uranium could also blacken a photographic plate while it was still in its black paper wrapper.¹¹⁰ Subsequent work on this phenomenon of “radioactivity,” as Marie Curie called it, showed that certain elements, particularly radium (discovered by Pierre and Madam Curie in 1898), can spontaneously release energy. These elements constantly emit positively and negatively charged particles as well as electromagnetic waves of very short wavelength, the gamma rays.¹¹¹ In 1899, Madam Curie postulated that radioactive atoms are unstable and disintegrate with emission of energy, a hypothesis extended by Rutherford and Soddy in 1903 to explain radioactivity.¹¹² The identification of the α , β , and γ rays of radioactive substances were accomplished by Giesel, Becquerel, P. and Mme. Curie, and Rutherford between 1899 and 1903.¹¹³ Alpha rays were later proven by Regner and Rutherford to consist of positively charged helium atoms.¹¹⁴ The grandeur of the whole electromagnetic spectrum could finally be appreciated (see Fig. 3.14). From the short gamma rays of radioactivity to the long radio waves, the spectrum spanned more than 50 octaves.¹¹⁵

3.2.1.11 The beginnings of quantum theory

Although electromagnetic theory, the high point of nineteenth century physics, explains how light travels through space, it tells nothing about how light is created and destroyed—processes that take place only via light interaction with matter. As a result, the theory of light could not be complete without an understanding of the fundamental nature of matter.¹¹⁶

This understanding was finally achieved in the quantum theory of 1925, which provided for the first time an adequate explanation of how matter is constructed of atoms and molecules, how atoms are constructed of nuclei and electrons, and how atoms interact with light. Each of the major developments of nineteenth-century physical science played critical roles in leading up to quantum theory. These developments included electromagnetic theory, molecular theory of matter, and statistical thermodynamics.¹¹⁷

Influenced by the electromagnetic theoretical prediction that oscillating electric charges would emit radiation, which was demonstrated when Heinrich Hertz experimented with emitted long-wavelength radiation, prominent physicists of the late nineteenth and early twentieth centuries pursued the idea that the oscillation

¹¹⁰ibid.; J.R. Partington, *A Short History of Chemistry*, 3rd ed., p. 357, Dover Publications, New York (1989).

¹¹¹ibid.

¹¹²ibid.

¹¹³ibid.

¹¹⁴ibid.

¹¹⁵An octave is the span from any particular frequency to a frequency twice as great. For example, the frequency of violet light is only about 1.8 times that of the deepest red, so that the visible spectrum occupies less than a single octave out of the vast span of electromagnetic radiation.

¹¹⁶M.I. Sobel, *Light*, p. 73, University of Chicago Press, Chicago (1987).

¹¹⁷ibid., p. 73.

of individual molecules in a solid could be taken as the source of emitted light.¹¹⁸ The theoretical study of this problem marked one of the major turning points in the history of science, for it provided the final pieces of the puzzle in the construction of the modern theory of light, as well as the fundamental nature of matter, and for these reasons we will consider the historical developments surrounding it in detail.¹¹⁹ Along the way, quantum theory resolved important questions dealing with blackbody radiation, photoelectricity, etc. that could not be explained by classical physics.¹²⁰

3.2.1.12 Molecular theory of matter

In 1808, the English chemist John Dalton proposed the molecular theory of matter, which states that each element is made up of identical atoms, each compound of many identical molecules, and each molecule of a small number of atoms; and that a chemical reaction is the combination or recombination of several atoms to form molecules, the process multiplied many times to become observable in nature or in the laboratory.¹²¹ Applying the molecular theory to gases (with the assumption that a gas consists of widely separated molecules, interacting very little with each other and moving incessantly at high speeds in a random manner), James Joule, in 1848, explained the pressure of a gas on the walls of a container.¹²² Other theorists of the mid-nineteenth century were able to deduce properties of gases, including their expansion when heated and their diffusion through air from this kinetic molecular theory.¹²³

Between 1860 and 1870, the Austrian physicist Ludwig Boltzmann introduced the statistical theory of heat (statistical mechanics) into the molecular theory of matter. He postulated that although the molecules of a gas—or indeed any matter—are so numerous that one can never predict the exact path of each one, one can nevertheless predict the behavior of the gas as a whole by assigning a set of probabilities for each molecule being in a particular state. These laws of statistical thermodynamics provided a firm foundation for the kinetic theory of gases, and an explanation for the phenomena of temperature and heat. The laws defined temperature as a measure of the average speed of these random molecular motions, and heat as energy associated with the random speeds of molecular motion.¹²⁴ Today, the rational design of resist materials and optical elements used in lithography, as well as the interaction of radiation with these materials, are based on these same molecular theories of matter.

¹¹⁸ *ibid.*, p. 75.

¹¹⁹ *ibid.*, p. 76.

¹²⁰ *ibid.*, pp. 74–81.

¹²¹ *ibid.*, p. 73.

¹²² *ibid.*, p. 74.

¹²³ *ibid.*, p. 74.

¹²⁴ *ibid.*, p. 74.

3.2.1.13 Blackbody radiation

One of the difficulties encountered by physicists of the late nineteenth century, the resolution of which overturned the conceptual framework of physics, had to do with the radiation given off by material bodies when they are heated. It is well known that when a metal such as iron is heated in a fire to a very high temperature, say 3000°C, and then taken out of the flame, it first glows red hot—a self-luminous source. When it is heated even further, to say 6000°C, the radiation becomes white and even turns blue as the temperature is raised even higher. Thus, one sees that there is a continual shift of the color of a heated body from the red through the white and into the blue as it is heated to a higher and higher temperature.¹²⁵ On the basis of frequency, the emitted radiation ranges from a lower frequency to a higher frequency as the temperature increases. The exact frequency spectrum emitted by the body is dependent on the particular body itself. An ideal body, i.e., one that absorbs and emits all frequencies, is called a blackbody and serves as an idealization for any radiating material. The radiation emitted by a blackbody is referred to as blackbody radiation.¹²⁶

Detailed study of this radiation in the nineteenth century uncovered the following facts. (i) The spectrum is continuous like the Sun's and includes the infrared region and all colors of the visible and ultraviolet regions. (ii) A plot of intensity versus wavelength (see Fig. 3.19) shows maximum intensity at one wavelength and decreasing intensity at both higher and lower wavelengths. (iii) The hotter the object, the shorter is the wavelength of maximum intensity. (iv) The hotter the object, the greater is the total amount of radiation emitted from a given surface area. As an example, at 3000°C, maximum intensity occurs in the infrared, but the tail of the spectrum stretches into the red region of the visible region of the spectrum, hence we see the object as “red hot.” At a lower temperature, the maximum intensity falls within the far-infrared region, which we cannot see, but can feel as radiant heat. At 6000°C, the maximum wavelength falls within the blue, with substantial radiation stretching into the entire visible region. The distribution (variation of intensity with wavelength) looks very much like that of the Sun, and we see the object as “white hot.”¹²⁷

Many physicists of the late nineteenth century tried to derive expressions consistent with the experimental intensity-versus-frequency curves for several temperatures, as shown in Fig. 3.19, but without success. In fact, the Rayleigh-Jeans law gives the expression that is derived according to the laws of nineteenth century physics as¹²⁸

$$\rho(\nu, T)d\nu = \frac{8\pi kT}{c^3} \nu^2 d\nu, \quad (3.15)$$

¹²⁵D.A. McQuarrie, *Quantum Chemistry*, pp. 5–6, University Science Books, Mill Valley, CA (1983); M.I. Sobel, *Light*, pp. 74–75, University of Chicago Press, Chicago (1987).

¹²⁶D.A. McQuarrie, *Quantum Chemistry*, pp. 5–6, University Science Books, Mill Valley, CA (1983).

¹²⁷M.I. Sobel, *Light*, p. 75, University of Chicago Press, Chicago (1987).

¹²⁸D.A. McQuarrie, *Quantum Chemistry*, pp. 6–7, University Science Books, Mill Valley, CA (1983).

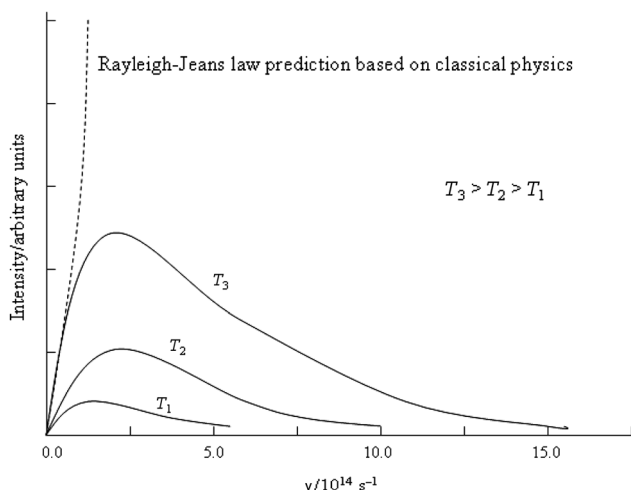


Figure 3.19 Spectral distribution of the intensity of blackbody radiation as a function of frequency for several temperatures. The dashed line is the prediction of classical physics. (Reprinted with permission from University Science Books.)¹³⁰

where $\rho(\nu, T)d\nu$ is the density of radiative energy between the frequency ν and $\nu + d\nu$, k is the Boltzmann constant, T is the absolute temperature, and c is the speed of light. The dashed line indicated in Fig. 3.19 is the prediction of the Rayleigh-Jeans law. (Fig. 3.20 shows a picture of Lord Rayleigh.)

It can be seen that the Rayleigh-Jeans law reproduces the experimental data at low frequencies fairly well. However, at high frequencies, the Rayleigh-Jeans law diverges as ν^2 . Since the frequency increases in the ultraviolet region of the spectrum, this divergence was called the “ultraviolet catastrophe,” a phenomenon that classical physics was unable to explain theoretically. This was the first such phenomenon to be observed in physics and did in fact mark a major milestone in the annals of physics.¹²⁹

3.2.1.14 Planck’s quantum hypothesis for blackbody radiation

In 1900, the German physicist Max Planck (Fig. 3.21) was the first person to offer a successful explanation of blackbody radiation. He, too, like Rayleigh and Jeans earlier, assumed that the radiation emitted by the body was due to the oscillations of the electrons in the constituent particles of the material body. He pictured these electrons to oscillate in an atom much like electrons oscillated in an antenna to give off radio waves, as Hertz had demonstrated. In the case of the atomic antennae, however, the oscillations occur at much higher frequency and hence are associated with frequencies in the visible, infrared, and ultraviolet regions rather than in the

¹²⁹ibid., p. 7.

¹³⁰D.A. McQuarrie, *Quantum Chemistry*, p. 6, University Science Books, Mill Valley, CA (1983).



Figure 3.20 Lord John William Strutt Rayleigh, a very influential physicist who made significant contributions in optical and radiation physics. The optical resolution criterion, so central in lithography for judging the capability of an exposure tool, is named after him. (Published with permission from Deutsches Museum, Munich.)

radio wave region of the spectrum. Implicit in the Rayleigh-Jeans' derivation is the assumption of the principle of continuity—a principle so obvious and axiomatic that it lies unspoken at the heart of classical physics—namely, that physically observable variables such as the energies of the electronic oscillators responsible for the emission of the radiation can take on a continuum of values. Planck's great insight was the realization that he had to move away from this mode of thinking in order to derive an expression that would fit the experimental data such as those shown in Fig. 3.19. He made the revolutionary assumption—one of the most daring and momentous departures in the history of physics—that the energies of the



Figure 3.21 Max Karl Ernst Ludwig Planck, who in 1900 proposed the quantum hypothesis that fully explains the physics of blackbody radiation. (Published with permission from the Deutsches Museum, Munich.)

oscillators had to be proportional to an integral multiple of the frequency or, in an equation, that

$$\varepsilon = nh\nu, \quad (3.16)$$

where n is an integer, h is a proportionality constant, now called Planck's constant, and ν is the frequency.¹³¹ Using statistical thermodynamic arguments, he was able to derive the expression

$$\rho(\nu, T)d\nu = \frac{8\pi h\nu^3}{c^3} \frac{d\nu}{e^{h\nu/kT} - 1}, \quad (3.17)$$

now called the Planck distribution law¹³² for blackbody radiation, where all of the symbols except h have the same meanings as in Eq. (3.16). The only adjustable constant is h . Planck showed that this equation gives excellent agreement with the experimental data for all frequencies and temperatures if h is assigned the value of $6.626 \times 10^{-34} \text{ J} \cdot \text{s}$.¹³³ Remarkably, he was initially reluctant to claim the physical reality of this quantization of energy.

3.2.1.15 Einstein's quantum hypothesis for the photoelectric effect

Heinrich Hertz first observed the photoelectric effect when he discovered that ultraviolet light causes electrons to be emitted from a metallic surface, while he was carrying out the experiments that confirmed Maxwell's theory of the electromagnetic nature of light in 1886 and 1887. The ejection of electrons from the surface of a metal by radiation is termed the photoelectric effect. Two experimental observations of the photoelectric effect cannot be adequately explained with the classical wave theory of light. First, the kinetic energy of the ejected electrons is independent of the intensity of the incident radiation, contrary to the prediction of classical physics. According to classical physics, electromagnetic radiation is an electric field oscillating perpendicular to its direction of propagation, whose radiation intensity is proportional to the square of the electric field. Therefore, as the intensity increases, so does the amplitude of the oscillating electric field. The surface electrons of the metal oscillate along with the field, so much so that as the intensity (amplitude) increases, the electrons oscillate more violently, eventually breaking away from the surface with a kinetic energy that depends on the amplitude (intensity) of the field. Second, there is a threshold frequency ν_0 , characteristic of the metallic surface, below which no electrons are ejected, and above which,

¹³¹D.A. McQuarrie, *Quantum Chemistry*, p. 7, University Science Books, Mill Valley, CA (1983); M.I. Sobel, *Light*, p. 77, University of Chicago Press, Chicago (1987).

¹³²D.A. McQuarrie, *Quantum Chemistry*, pp. 7–8, University Science Books, Mill Valley, CA (1983); M.I. Sobel, *Light*, p. 77, University of Chicago Press, Chicago (1987).

¹³³*ibid.*, pp. 7–12.

the kinetic energy of the ejected electrons is proportional to the frequency ν —a clear contradiction of classical physics, which predicts that the photoelectric effect should occur for any frequency of light as long as the intensity is sufficiently high.¹³⁴

In order to interpret these results, the German physicist Albert Einstein (about 1905) (see Fig. 3.22) applied Planck's hypothesis but extended it in an important way. In applying his energy quantization concept $\Delta\varepsilon = h\nu$ to the emission and absorption mechanism of the atomic electronic oscillators, Planck believed that once the light energy was emitted, it behaved like a classical wave. Einstein, on the other hand, suggested that the energy of a light beam is not evenly spread over the whole beam, but is concentrated in certain regions called photons.¹³⁵ In other words, the radiation itself existed as small packets of energy such that $\varepsilon = h\nu$.¹³⁶

The Einstein photons are light particles—they are localized concentrations of mass, momentum, and energy, and they are propagated like particles. There are usually a very large number of them in a light beam, the energy in any one photon being very small.¹³⁷



Figure 3.22 Albert Einstein, who among many things, explained the photoelectric effect and the Brownian motion, and proposed the special and general theories of relativity. (Published with permission from the Deutsches Museum, Munich.)

¹³⁴D.A. McQuarrie, *Quantum Chemistry*, p. 12, University Science Books, Mill Valley, CA (1983); R.W. Ditchburn, *Light*, pp. 13–14, 645–646, Dover Publications, New York (1991); M.I. Sobel, *Light*, pp. 78–81, University of Chicago Press, Chicago (1987).

¹³⁵Gilbert Luis coined the term *photon* in 1926.

¹³⁶D.A. McQuarrie, *Quantum Chemistry*, p. 12, University Science Books, Mill Valley, CA (1983); R.W. Ditchburn, *Light*, pp. 13–14, 645–646, Dover Publications, New York (1991); M.I. Sobel, *Light*, pp. 78–81, University of Chicago Press, Chicago (1987).

¹³⁷R.W. Ditchburn, *Light*, p. 13, Dover Publications, New York (1991).

Applying the conservation of energy argument, Einstein showed that the kinetic energy of the ejected electrons $[(1/2)mu^2]$, where m is mass and u is velocity] is equal to the energy of the incident radiation ($h\nu$) minus the minimum energy required to remove an electron from the surface of the particular metal (ϕ),

$$\frac{1}{2}mu^2 = h\nu - \phi, \quad (3.18)$$

where ϕ , called the work function of the metal, is similar to an ionization energy. The left-hand side of Eq. (3.18) cannot be negative, which implies that $h\nu \geq \phi$. The minimum frequency ν_0 that will eject an electron is just the frequency required to overcome the work function of the metal, and is given by¹³⁸

$$h\nu_0 = \phi. \quad (3.19)$$

The picture that emerges of the photoelectric effect is one in which after the collision of the photons with the electrons of the metal, the photon energies are absorbed by the electrons, resulting in the destruction of the photons and emission of the electrons from the metal. In escaping from the metal, the electron may lose some of that energy as it overcomes the forces that bind it to the metal. The electrons ejected in the photoelectric current are thus observed to have a range of energies—those least strongly bound originally in the metal (i.e., those that were closer to the surface) have the maximum energy. The maximum energy of these electrons depends only on the frequency of the light, which is consistent with the hypothesis that light deposits a fixed amount of energy on each liberated electron, the quantity of energy being proportional to the frequency of the light.¹³⁹

Further work on the photoelectric effect was done in 1916 by the American physicist Robert Mulliken, who succeeded in verifying Einstein's theory in detail. Specifically, he determined the value for Planck's constant h that was in agreement with the value obtained from blackbody radiation.¹⁴⁰ Resist imaging in EUV lithography is based on this photoelectric effect.

3.2.1.16 Bright and dark line spectra

The origin of spectroscopy lies in the spectral analytical work of Thomas Melville, already described above, and the development of the spectroscope by William Wollaston and Josef Fraunhofer (1787–1826) (see Fig. 3.23). Melville's observation in 1752 that the spectrum of light of a flame passed through a prism was not continuous like that of the Sun, but rather that parts of the spectrum were bright, while others were dark, with the locations of the bright spots and their

¹³⁸D.A. McQuarrie, *Quantum Chemistry*, p. 13, University Science Books, Mill Valley, CA (1983).

¹³⁹M.I. Sobel, *Light*, p. 80, University of Chicago Press, Chicago (1987).

¹⁴⁰*ibid.*, pp. 80–81.



Figure 3.23 Josef von Fraunhofer (1787–1826), the inventor of the diffraction grating and the spectroscope, and one of the founders of spectroscopy. (Published with permission from the Deutsches Museum, Munich.)

colors being different when different chemicals were placed in the flame, provided yet another clue to the nature of the atomic structure.¹⁴¹

The Fraunhofer's spectroscope was constructed to receive light that had been passed through a slit and a tube to create a narrow beam, resulting in a spectrum beyond the prism that was then viewed through a telescope. This instrument allowed Fraunhofer to construct for the first time a map of the dark line spectra from the Sun, the principal lines from which he named with the letters A through G—the now-familiar Fraunhofer lines. In 1814–1815, he published his Sun and stellar studies that gave spectral analysis a real boost.¹⁴²

The key to understanding the dark lines, also called absorption lines, came when it was discovered that the frequencies at which they occurred were the same as the frequencies in the bright line spectrum of glowing gases. Gustav Kirchhoff (1824–1887), in 1859, had shown that he could produce dark lines in the spectra of a blackbody by passing that light through a region of cool gas, which led him to deduce that such a process was responsible for the absorption spectrum of the Sun. Although the inner core of the Sun (photosphere) emits a continuous spectrum, by the time the radiation traverses the outermost layer of the Sun's body, known as the chromosphere, which contains rarefied hot gases, the elements contained in these hot gases absorb and scatter characteristic wavelengths corresponding to elements in them. This results in the dark line spectra of the Sun monitored on Earth. In other words, the spectrum of the transmitted light from the Sun contains dark lines at just those frequencies that are absorbed by hot gases surrounding the Sun.¹⁴³

¹⁴¹ibid., p. 81.

¹⁴²ibid., M.S. Barge and W.B. White, *The Daguerreotype: Nineteenth Century Technology and Modern Science*, p. 15, Johns Hopkins University Press, Baltimore (1991).

¹⁴³G. Gamow, *The Great Physicists from Galileo to Einstein*, p. 123, Dover Publications, New York (1961).

Kirchhoff also formulated the law that now bears his name—Kirchhoff’s law—which states that all substances absorb the same light frequencies that they can emit. This law has found widespread application in the study of composition of the Sun and other stars many light-years away,¹⁴⁴ as well as in the rational design of resist sensitizers and photoactive compounds used in lithography.

It has been determined that the Sun contains vapors of sodium, calcium, iron, and many other elements.¹⁴⁵ Working together in Heidelberg, Kirchhoff and Robert Wilhelm Bunsen (1811–1899) (see Fig. 3.24) established that each kind of atom has its own signature in a characteristic array of spectral lines.¹⁴⁶

Fraunhofer was also the inventor of diffraction grating, a series of parallel wires separated by variable distances as small as 0.005 cm, which acted like an enhanced version of Young’s two-slit experiment and could also be used as a replacement for the prism. Passing light through the spaces between the wires forms an interference pattern beyond the grating, and the direction of constructive interference is different for each wavelength.¹⁴⁷

In the 1820s, David Brewster (1781–1868), Sir John Herschel (1792–1871), and William Henry Fox Talbot performed similar types of experiments on the absorption of light to those by Fraunhofer. Independently, these researchers made the observation that flame spectra obtained by burning compounds of different compositions varied in systematic ways. These three researchers all produced line spectra, which they tried to relate to the dark lines observed by Fraunhofer



Figure 3.24 Gustav Robert Kirchhoff and Robert Wilhelm Bunsen, who working together made important contributions to spectroscopic analysis of substances. (Published with permission from the Deutsches Museum, Munich.)

¹⁴⁴ibid.

¹⁴⁵The power of this law is aptly illustrated in the discovery of the element helium, which was first discovered via a series of unexplained dark lines in the Sun’s spectrum, lines that were not related to emission lines then known on Earth. Later, helium gas was found on the Earth.

¹⁴⁶E. Hecht, *Optics*, 2nd ed., p. 10, Addison Wesley, Menlo Park (1990).

¹⁴⁷M.I. Sobel, *Light*, p. 81, University of Chicago Press, Chicago (1987).

from his solar spectrum. Although there was some agreement that the spectra contained chemical information characteristic of the flame analyzed, there was however no consensus on the role of light in the production of these spectra.¹⁴⁸ It was not until the early twentieth century that it was discovered that these line spectra are not the result of light interaction with specific compounds, but rather are related to their atomic structures, and therefore to chemistry.¹⁴⁹

As already stated, a common characteristic of all of the spectra of flames and electric discharges in gases analyzed in the spectroscopy in the nineteenth century was the presence of bright lines, located at positions characteristic of particular wavelengths. Each chemical element emits a unique set of wavelengths, which made it possible for the spectroscopy to become a device that could be used to identify the elements, just as fingerprints identify the individual.¹⁵⁰ The body of data on bright line spectra of gases obtained during this period presented a serious challenge to physicists and chemists as great as that of blackbody radiation—a challenge that in some ways was greater, since the continuous emission from hot solid objects was largely independent of the nature of the objects, whereas the line spectrum was different for each element.¹⁵¹

Being the simplest form of matter, since each atom or molecule is independent, and not affected by forces due to the other atoms, a gas therefore made an ideal candidate for studying line spectra. The hydrogen atom being the simplest atom—as revealed from the chemical experiments and observations of Dalton, Avogadro, Joseph-Louis Gay-Lussac, and others (described below)—was therefore chosen, and its line spectrum carefully studied. Between the years 1909 and 1912, the first successful theory of the hydrogen atom, and its line spectrum, was formulated, based on the experimental work of Ernest Rutherford and the theoretical insights of Niels Bohr.¹⁵²

3.2.1.17 Nuclear model of the atom

In 1911, Rutherford proposed the nuclear model of the atom, consisting of a very small positively charged nucleus surrounded by outer electrons at relatively large distances from the nucleus. He showed that this nuclear model can be used to explain the very large deflections sometimes suffered by α particles in passing through matter.¹⁵³ What holds the electrons in place is an attractive electrical

¹⁴⁸M.S. Barge and W.B. White, *The Daguerreotype: Nineteenth Century Technology and Modern Science*, p. 15, Johns Hopkins University Press, Baltimore (1991).

¹⁴⁹Line spectra do not give any information about the physics of light; rather, the lines are related to transitions between various energy levels in the atoms making up the compound analyzed. The elucidation of what gives rise to the lines in line spectra had to wait until after the introduction of quantum mechanics and the work of Niels Bohr in the early decades of the twentieth century.

¹⁵⁰M.I. Sobel, *Light*, p. 82, University of Chicago Press, Chicago (1987).

¹⁵¹*ibid.*, p. 83.

¹⁵²*ibid.*

¹⁵³J.R. Partington, *A Short History of Chemistry*, p. 360, 3rd ed., Dover Publications, New York (1989); M.I. Sobel, *Light*, pp. 82–85, University of Chicago Press, Chicago (1987).

force between each electron and the nucleus, and this force is what binds the atom together. This implies that the electrons cannot be stationary, for if they were, they would fall into the nucleus. Rather, just as the Earth orbits the Sun under the influence of the attractive gravitational forces, the electron orbits the nucleus. This is now referred to as Rutherford's planetary model of the atom.¹⁵⁴

In 1913, Moseley developed a method for determining the nuclear charge from the frequency of x rays emitted by an element on collision with high-velocity electrons.¹⁵⁵ Each element has its own characteristic x rays, which are almost like a fingerprint of the element.¹⁵⁶

The nuclei of atoms are now known to be made up of protons and neutrons, a neutron being a particle of approximately the same mass as the proton but without the charge. The mass of the atom has now been determined to be approximately equal to the sum of the masses of the protons and neutrons. The nuclear charge is equal to the atomic number, given by the position of an element in the periodic table. An element is now defined by this atomic number, and different isotopes of an element have the same atomic number.¹⁵⁷

3.2.1.18 Bohr's model of the hydrogen atom

Realizing that Rutherford's planetary model of the atom is incompatible with the classical Maxwell theory of radiation—which stipulates that a charged electron in circular motion will continually emit radiation and thereby lose energy, its orbit will shrink, and it will quickly spiral into the nucleus—Niels Bohr¹⁵⁸ in 1913 (see Fig. 3.25) asserted that an electron in an atomic orbit simply does not radiate; in other words Maxwell's theory does not apply at this level. Bohr's main contribution was to make two nonclassical assumptions.¹⁵⁹

First, he assumed the existence of stationary electron orbits, in defiance of classical physics. In other words, he postulated that, like the oscillators that produce blackbody radiation, the electron can exist in only certain quantized energy levels; and as long as it stays in a given level, it produces no light, and its energy does not change. He specified these orbits by invoking a quantization condition, where he assumed that the angular momentum l of the electron must be quantized according to the equation

$$l = mur = n \quad n = 1, 2, \dots \quad (3.20)$$

where m is the mass of the electron, u is the velocity of the electron, r is the radius of the electronic orbit, and \hbar is equal to $h/2\pi$. The force holding the electron in a

¹⁵⁴M.I. Sobel, *Light*, p. 85, University of Chicago Press, Chicago (1987).

¹⁵⁵H.G.J. Moseley, "The high frequency spectra of the elements," Part 1, *Phil. Mag.* **XXVI**, 102 (1913); Part 2, **XXVII**, 107 (1914); also cited in J.R. Partington, *A Short History of Chemistry*, 3rd ed., p. 360, Dover Publications, New York (1989).

¹⁵⁶ibid.

¹⁵⁷J.R. Partington, *A Short History of Chemistry*, 3rd ed., pp. 360–361, Dover Publications, New York (1989).

¹⁵⁸N. Bohr, "On the constitution of atoms and molecules," *Phil. Mag.* **XXVI**, 476, 857 (1913).

¹⁵⁹D.A. McQuarrie, *Quantum Chemistry*, p. 23, University Science Books, Mill Valley, CA (1983).

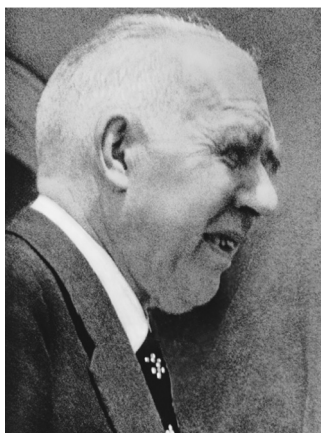


Figure 3.25 Neils Bohr, who in 1913 postulated the Bohr model of the hydrogen atom, from which derives the notion of electronic shells that initiated the modern atomic theory of chemical reactions, as well as the concept of energy levels that underlie the design of lasers. (Published with permission from the Deutsches Museum, Munich.)

circular orbit is the coulombic force ($e^2/4\pi\epsilon_0r^2$) of attraction between the proton and the electron, whereas the centripetal force (mu^2/r) keeps it moving in the circular orbit. An electron in a stationary circular orbit therefore experiences a coulombic force that is counterbalanced by the centripetal force due to its rotation around the nucleus. Equating these two forces, we obtain

$$\frac{e^2}{4\pi\epsilon_0r^2} = \frac{mu^2}{r}, \quad (3.21)$$

where e is the charge on the electron, and ϵ_0 is the permittivity of free space and is equal to $8.85419 \times 10^{-12} \text{ C}^2\text{N}^{-1} \cdot \text{m}^{-2}$. Solving Eq. (3.21) for u and substituting into Eq. (3.20), we obtain

$$r = \frac{4\pi\epsilon_0^2n^2}{me^2} \quad n = 1, 2, \dots, \quad (3.22)$$

which shows that the radii of the allowed orbits, now called Bohr orbits, are quantized. The value of the Bohr radius corresponding to $n = 1$ is the radius of the hydrogen atom in its ground state. Under the above-described scenario, the electron can move around the nucleus only in circular orbits with radii given by Eq. (3.22).

The total energy of the electron in the hydrogen atom, being the sum of the kinetic and potential energies, is therefore given by

$$E = \frac{1}{2}mu^2 - \frac{e^2}{4\pi\epsilon_0r}, \quad (3.23)$$

where the negative sign in front of the potential energy term indicates that the proton and electron attract each other, their energy being less than it is when

they are infinitely separated. Using Eq. (3.22) to eliminate the mu^2 in the kinetic energy term, Eq. (3.23) becomes

$$E = \frac{1}{2} \left(\frac{e^2}{4\pi\epsilon_0 r} \right) - \frac{e^2}{4\pi\epsilon_0 r} = -\frac{e^2}{8\pi\epsilon_0 r}. \quad (3.24)$$

Because the only allowed values of r are those given in Eq. (3.22), substituting Eq. (3.22) into Eq. (3.24), we obtain the expression for the only allowed energies as

$$E_n = -\frac{me^4}{8\epsilon_0^2 h^2 n^2} \quad n = 1, 2, \dots \quad (3.25)$$

It should be pointed out that the negative sign in this equation is an indication that the energy states are bound states; the energies given by Eq. (3.25) are less than when the proton and electron are infinitely separated. The state of the lowest energy for the hydrogen atom corresponds to $n = 1$, and is called the ground state. States with $n > 1$ have higher energies than the ground state and are called excited states. An electron, Bohr asserted, can spontaneously fall from a higher energy level to a lower one; and when it does, it releases an amount of energy that is the difference between the two energy levels. This energy is lost by the atom, and it goes to create a quantum of light. In this way, light is the child of the atom in the process of change and, in another way, is the mechanism of the atomic process; for if there were no light, the atom would not be able to go from one state to another.¹⁶⁰

Bohr also made the assumption that the observed spectrum of the hydrogen atom is due to transitions from one allowed energy state to another, with the energy difference between two levels given by

$$\Delta E = \frac{me^4}{8\epsilon_0^2 h^2} \left(\frac{1}{n_1^2} - \frac{1}{n_2^2} \right) = h\nu. \quad (3.26)$$

The equation $\Delta E = h\nu$ is called the Bohr frequency condition and is the basic assumption that as the electron falls from one level to another, the energy evolved is given off as a photon of energy $E = h\nu$. The energies and the energy differences are quantized, and so are the frequencies.¹⁶¹ The isolated atom emits light of only certain definite frequencies, as observed in the bright line spectrum.¹⁶²

The equations of Bohr's theory are in agreement with the observed frequencies in the hydrogen spectrum, as are the observed spectral series—Lyman series (when electrons excited to higher levels relax to the $n = 1$ state) and Balmer series (when electrons excited to higher levels relax to the $n = 2$ state, and so on). Working backward, the observations can also be used to determine the value of Planck's constant. The value obtained in this way was found to be in agreement with the result deduced from the blackbody radiation and photoelectric effect.¹⁶³

¹⁶⁰M.I. Sobel, *Light*, pp. 85–86, University of Chicago Press, Chicago (1987).

¹⁶¹D.A. McQuarrie, *Quantum Chemistry*, p. 25, University Science Books, Mill Valley, CA (1983).

¹⁶²M.I. Sobel, *Light*, pp. 86–87, University of Chicago Press, Chicago (1987).

¹⁶³*ibid.*, p. 87.

3.2.1.19 Implications of Bohr's Theory

Between 1912 and 1925, Bohr's theory of the atom gave rise to a conceptual framework for the study of matter on many fronts. Applying the theory to predict the energy levels and therefore the emission frequencies of atoms more complicated than hydrogen—say, helium with two electrons, lithium with three, and so on—led to the concept of electronic shells about the nucleus, the outer shell less tightly bound, and it is these outer-shell electrons that determine the element's spectrum.¹⁶⁴ It should be pointed out that the theory was not fully successful in predicting the spectral lines of the elements that are more complicated than hydrogen.

Furthermore, the concept of electronic shells initiated the modern atomic theory of chemical reactions. It is now well accepted that the electrons in the outer shells, transferring from one atom to another or being shared by two atoms, provide the machinery for chemical reactions and the binding of atoms to form molecules.¹⁶⁵

The concept of atomic energy levels also underlies the design of lasers, which depend on a way of exciting the electrons in atoms that could hardly have been discovered by chance.¹⁶⁶ Einstein predicted that light emission could be produced if the atoms were so highly energized that the majority of the electrons at a certain energy level were excited into a higher level. In this scenario, a photon emitted from an excited atom "collects" another photon from a neighboring excited atom and travels along with it, in phase and amplitude and in exactly the same direction. Next, these two photons in turn collect two more, and in this way a process that amplifies the number of photons is created that proceeds through the laser cavity, whether in the form of a solid crystal rod or a long tube of gas. By positioning a mirror at each end of the tube to reflect the light back and forth, an enormous intensity of these photons can be built up in a very short time. Making one of the mirrors partly reflecting allows a narrow, parallel, intense laser beam to emerge from it¹⁶⁷ as the new form of light that is now used in many fields—communications, surveying, range finding and welding, medical surgery, and even as light sources for lithography.

Despite its successes, Bohr's theory did not resolve the fundamental issues that lie at the heart of the quantum theory of Planck and Einstein: What is behind the quantization of oscillators and atoms? What happens when a system changes its state, resulting in the creation of a photon? How can the generated photon behave like a particle under certain conditions and like a wave under other conditions?

¹⁶⁴ibid., pp. 89–90.

¹⁶⁵ibid., p. 90.

¹⁶⁶Laser technology is one of those rare instances in scientific research, such as the development of nylon, atomic fission, or genetic engineering, where important technologies have sprung directly from scientific theory.

¹⁶⁷P. Mason, *Light Fantastic*, p. 232, Penguin Books, New York (1981).

3.2.1.20 Quantum theory of light

The answers to the above questions, not all of which need be presented here, were formulated between 1925 and 1926, in the revolution of modern quantum theory, which shook the foundations of physics and philosophy. Remarkably, the central theme of quantum theory was the nature of light, and what came to be called the wave-particle duality. But other broader implications of the new theory existed, and the first inkling of this was given in 1924 by Louis de Broglie (Fig. 3.26) in his doctoral dissertation. He postulated that particles may also possess wavelike properties¹⁶⁸ and that these wavelike properties would manifest themselves only in phenomena occurring on an atomic scale, as dictated by Planck's constant. He also postulated that the wavelength of these matter waves, for a given particle such as an electron or proton, would be inversely proportional to the particle's momentum p , which is a product of its mass m and speed v ,¹⁶⁹

$$\lambda = \frac{h}{mv} = \frac{h}{p}. \quad (3.27)$$



Figure 3.26 Louis Victor de Broglie, who in his 1924 doctoral thesis postulated that particles may also have wavelike properties. (Published with permission from the Deutsches Museum, Munich.)

¹⁶⁸De Broglie's hypothesis sounds rather strange at first sight, but it does suggest a beautiful symmetry in nature. Surely, if light can be particlelike at times, why should matter not be wavelike at times? Realizing that Einstein had shown from relativity theory that the momentum of a photon is given by $p = h/\lambda$, de Broglie argued that both light and matter obey the equation $\lambda = h/p$.

¹⁶⁹M.I. Sobel, *Light*, p. 92, University of Chicago Press, Chicago (1987); M.I. Sobel, *Light*, pp. 85, 86, 375–377, University of Chicago Press, Chicago (1987); D.A. McQuarrie, *Quantum Chemistry*, pp. 30–35, University Science Books, Mill Valley, CA (1983).

Experimental confirmation of de Broglie's hypothesis was soon obtained in 1927 by the observation that electron beams can be diffracted in much the same way as x rays.¹⁷⁰

It must be noted that today, de Broglie's hypothesis has practical applications not only in electron microscopy, but also in electron-beam lithography. The wavelength of the electrons are easily controlled with the aid of an applied voltage, and the small de Broglie wavelengths attainable offer a more precise probe (in microscopy applications) or higher resolution (in lithography applications) than systems using visible and UV photons. In addition, in contrast to electromagnetic radiation of similar wavelengths (x rays and UV), the electron beam can be easily focused by using electric and magnetic fields.¹⁷¹ Electron microscopes have found wide applications in chemistry and biology, where they are used to investigate atomic and molecular structures, as well as in the semiconductor industry to inspect and review integrated circuit features.

Building on de Broglie's hypothesis,¹⁷² theorists such as Erwin Schrödinger, Werner Heisenberg, Max Born, and others developed a new and fundamental theory.

In 1926, Erwin Schrödinger modified the classical wave equation describing a three-dimensional standing wave by imposing wavelength restrictions suggested by de Broglie's hypothesis. He obtained a second-order differential equation for a wave function ψ with second-order differential coefficients with respect to the coordinates x , y , and z for a particle of mass m moving in a potential field U . It is of the form¹⁷³

$$\frac{\partial^2 \psi}{\partial x^2} + \frac{\partial^2 \psi}{\partial y^2} + \frac{\partial^2 \psi}{\partial z^2} + \frac{8\pi m}{h^2}(E - U) = 0, \quad (3.28)$$

where h is Planck's constant and E represents the total energy of the particle.

¹⁷⁰M.I. Sobel, *Light*, p. 92, University of Chicago Press, Chicago (1987).

¹⁷¹D.A. McQuarrie, *Quantum Chemistry*, p. 34, University Science Books, Mill Valley, CA (1983).

¹⁷²De Broglie's hypothesis today not only has practical applications in electron microscopy and electron beam lithography, but was also a key step in our understanding of atomic structure. It can be seen as a simple, yet physical argument for the quantized Bohr orbit, if one assumes that as the electron revolves around the proton, it has a wavelength λ associated with it. For the orbit to be stable, the wave must be in phase as the electron makes one complete revolution. Otherwise, there will be cancellation of some amplitude on each revolution, leading to disappearance of the wave. For the stability condition of the wave pattern around an orbit requires that an integral number of complete wavelengths must fit around the circumference of the orbit. Because the circumference of a circle is $2\pi r$, we have the quantum condition, $2\pi r = n\lambda$ ($n = 1, 2, 3, \dots$). Substituting the de Broglie's relation into this equation leads to the Bohr quantization condition, $mvr = nh$ [see also, D.A. McQuarrie, *Quantum Chemistry*, p. 34, University Science Books, Mill Valley, CA (1983)].

¹⁷³K.W. Whitten and K.D. Gailey, *General Chemistry with Quantitative Analysis*, p. 87, Saunders College Publishing, Philadelphia (1981); J.R. Partington, *A Short History of Chemistry*, 3rd ed., p. 374, Dover Publications, New York (1989); D.A. McQuarrie, *Quantum Chemistry*, pp. 77-101, University Science Books, Mill Valley, CA (1983). This equation does not contain time and is therefore called the time independent Schrödinger equation, the solution of which yields stationary state wave functions. Although there is a more general Schrödinger equation that is time dependent, a great number of problems of chemical and lithographic interest can be described in terms of stationary state wave functions.

The equation also contains a term that in the ordinary equation for wave motion contains the wavelength λ . In this case, λ is taken as the wavelength defined by de Broglie's equation above, and is contained in the fourth term of the Schrödinger equation. The assumption is made that ψ is finite, continuous, and single valued in general for all values of the coordinates, and that the square of the wave function, ψ^2 , gives the density of charge at each point, the knowledge of which gives an indication of the directions in which bond formation may occur.¹⁷⁴

In pondering the implications of the wave-particle duality, Werner Heisenberg was led in the mid-1920s to consider a problem in the measurement of the position of an electron in the following way. If we wish to locate the electron within a distance Δx , then we must use light with a wavelength at least that small, since for the electron to be "seen," a photon must interact or collide in some way with it, otherwise the photon will just pass right by and the electron will appear transparent. The photon has a momentum $p = h/\lambda$, and during the collision some of this momentum will be transferred to the electron, which implies that the very act of locating the electron necessarily leads to a change in its momentum. Furthermore, if we wish to locate the electron more accurately, we must use light with a smaller wavelength, which implies that the photons in the light beam will have greater momentum because of the relation $p = h/\lambda$. Given that some of the photon's momentum must be transferred to the electron in the process of locating it, the momentum change of the electron therefore effectively becomes greater.¹⁷⁵

A careful analysis of this problem led Heisenberg to show that it is impossible to determine exactly how much momentum is transferred to the electron. This implies that if one wishes to locate an electron within a region Δx , then this causes an uncertainty in the momentum of the electron. He was able to show that if Δp is the uncertainty in the momentum of the electron, then

$$\Delta x \Delta p \approx h. \quad (3.29)$$

Equation (3.29) is called Heisenberg's uncertainty principle, a fundamental principle of nature, which states that if we wish to locate any particle to within a distance Δx , then we automatically introduce an uncertainty in the momentum of the particle that is given by Eq. (3.29).¹⁷⁶

It must be pointed out that this limitation on our knowledge of the physical world, embodied in the Heisenberg uncertainty principle, is not due to poor measurement or poor experimental technique, but is a fundamental property of the act of measurement itself; it is intimately associated with quantization.¹⁷⁷ For if light were not quantized, one could imagine making measurements with ever-smaller and smaller quantities of light and energy, until we would ultimately approach a measurement that would not disturb the system being measured; or at

¹⁷⁴J.R. Partington, *A Short History of Chemistry*, 3rd ed., p. 374, Dover Publications, New York (1989).

¹⁷⁵D.A. McQuarrie, *Quantum Chemistry*, pp. 36-37, University Science Books, Mill Valley, CA (1983).

¹⁷⁶*ibid.*, p. 37.

¹⁷⁷M.I. Sobel, *Light*, p. 92, University of Chicago Press, Chicago (1987).

least we could make the disturbance as small as we wished, so that the uncertainty principle could be reduced to negligible values. But nature imposes on us a physical limit h , Planck's constant, that determines the minimum energy content of a photon; this produces uncertainties that are not negligible and that are more significant on the atomic scale.¹⁷⁸

In the final analysis, quantum theory is a theory of measurements, for it tells us what we can measure within the limits of these uncertainties. If one is able to measure a quantity accurately, then he or she cannot be able to make a precise measurement of a second quantity. But the possible values of the second quantity are associated with probabilities, which he or she can calculate exactly from the equations of quantum theory. As an example, suppose that we know that the electron in the hydrogen atom is in its ground state, implying that we know its energy precisely. Then we cannot know precisely its other quantities such as the electron's position at a given time or its velocity. But we can calculate the probability of the electron being at any particular point in space with the equations of quantum theory. And thus emerges the concept of a wave—something that is distributed through space, in contrast to a particle, which is located at a point.¹⁷⁹

Today Bohr's concept of an electronic orbit is no longer tenable, but the modern quantum theory substitutes for the orbit a probability distribution, in which, in the case of the hydrogen atom, the probability is concentrated in the region where the Bohr orbit was. For a free electron (i.e., one not bound to the hydrogen nucleus), the probability distribution looks like that of a wave—a confined region of oscillations, called a wave packet. These wavelike properties are extremely difficult to observe under normal conditions because typical wavelengths of electrons are extremely short—around 10^{-9} or 10^{-10} m. Wavelike properties such as diffraction and interference are only observed when the typical dimensions of the measurement system are of a comparable dimension to the wavelength.¹⁸⁰

And so it was that in 1927 C.H. Davisson and L.H. Germer were able to demonstrate wave properties in a beam of electrons by using the latticework of atoms in a crystal as the equivalent of a diffraction grating (just as had been done 15 years earlier for x rays). On examining the electrons scattered by a nickel crystal, they observed a pattern of alternating minima and maxima, just like the pattern of constructive and destructive interference seen in light passed through a grating. And using the well-established equations of diffraction, these scientists calculated the wavelength of the electrons in the beam and found a value in agreement with the

¹⁷⁸ibid. An another way of looking at this problem, bearing in mind that h is fixed, is to imagine using photons of very low frequency; the photon's energy $h\nu$ becomes smaller, and its disturbance of the system being measured is thus minimized. But low frequency implies long wavelength, which for the optical instrument (e.g., a microscope) translates to poor resolving power. Effectively, we cannot obtain information about an object smaller than that wavelength; we cannot even locate the object, except with an uncertainty of the same dimension as the wavelength [also cited in M.I. Sobel, *Light*, p. 247, University of Chicago Press, Chicago (1987)].

¹⁷⁹M.I. Sobel, *Light*, pp. 92–93, University of Chicago Press, Chicago (1987).

¹⁸⁰ibid., p. 93.

theory of de Broglie. Soon, electron waves were confirmed by other researchers, including G.P. Thomson, the son of J.J. Thomson, who in 1897 had discovered the electron by observing its particlelike properties.¹⁸¹

Although the quantum theory of 1925 resolved the age-old dilemma of light by unifying the entities of light and matter and by asserting that wave-particle duality applies to both, it failed to address the issue of another fundamental distinction between the two: the photon is created out of nothing—in the flash of an atomic jump—while the electron is permanent.¹⁸²

All in all, the message of light since the quantum revolution of the twentieth century is the message of the atom, which has given us a new understanding of how humans interact with their surroundings. It is beyond the scope of this book to dwell on the philosophical implications of quantum theory, which extend even to epistemology and logic, or on its predictive success in fields as varied as astrophysics, chemistry, lithography, metallurgy, nuclear and elementary particle physics, materials science, as well as atomic physics and optics. It is enough, however, to say that it remains today the premier indispensable tool of the theorist in the realm of physical science.¹⁸³

3.2.1.21 Einstein's theory of relativity

With the Michelson–Morley experiment confirming that there is no ether filling the entire space of the universe and therefore no absolute motion since one cannot move in respect to nothing, Einstein in 1905 proposed the theory of relativity by denying any meaning of the concept of absolute rest, and then adding the postulate that light in empty space always travels with a definite speed that is quite independent of the movement of the source. He deduced that Lorentz space and time transformations for two coordinate systems (x, y) and (x', y') moving in respect to each other with a velocity v from an initial time t to a new time t' [Eqs. (3.21) and (3.22)] correspond to physical reality. This deduction formed the foundation of his theory of relativity.¹⁸⁴

$$x' = \frac{x + vt}{\sqrt{1 - (v/c)^2}}, \quad (3.30)$$

$$t' = \frac{t + (v/c^2)x}{\sqrt{1 - (v/c)^2}}. \quad (3.31)$$

Applying these relativistic formulas for adding velocities, he explained the experimental results obtained by Fizeau, described earlier in Eq. (3.3), which occurred half a century before. Substituting for v_1 the value of the velocity of

¹⁸¹ibid., pp. 93–94.

¹⁸²ibid., p. 95.

¹⁸³ibid.

¹⁸⁴G. Gamow, *The Great Physicists from Galileo to Einstein*, p. 180, Dover Publications, New York (1961).

light c/n in water, and replacing v_2 simply with v for the velocity of water in the pipe yields

$$V = \frac{c/n + v}{1 + cv/nc^2} = \frac{c/n + v}{1 + v/nc}. \quad (3.32)$$

By multiplying the numerator and denominator by $(1 - v/nc)$, we obtain

$$V = \frac{(c/n + v)(c/n - v)}{1 - v^2/n^2c^2} = \frac{c/n + v - v/n^2 + v^2/nc^2}{1 - v^2/n^2c^2}. \quad (3.33)$$

Given that v is much smaller than c , (v/c) is a very small number, and $(v/c)^2$ is even smaller. Neglecting the terms containing v^2/c^2 in the above formula, we obtain

$$V = \frac{c}{n} + v - \frac{v}{n^2} = \frac{c}{n} + v \left(1 - \frac{1}{n^2}\right), \quad (3.34)$$

which is exactly Fizeau's empirical formula [see Eq. (3.3)]. This result confirms that there is no "drag of the ether." It also shows that the resulting velocity is simply the relativistic sum of the velocity of light in the liquid and the velocity of the liquid's flow through the pipe.¹⁸⁵

Another important consequence of the new transformation principles of space and time engendered by relativistic mechanics is that the mass of a moving body does not remain constant as in the Newtonian system, but increases with increasing velocity, as given by¹⁸⁶

$$m = \frac{m_0}{\sqrt{1 - v^2/c^2}}, \quad (3.35)$$

where m_0 is the so-called "rest mass," i.e., the inertial resistance to the force that tends to move the particle initially at rest, and v is the velocity of the body. As the velocity of the material body increases, approaching the velocity of light, it becomes progressively more difficult to increase its velocity, and at $v \rightarrow c$, the resistance to further acceleration approaches infinity. In other words, given that mass is resistance to acceleration, as the body is pushed closer to the velocity of light, its resistance to that push becomes stiffer and stiffer. This gives rise to another aspect of the basic statement of relativity theory, to the effect that a material body must move at less than the velocity of light. Due to increased inertial resistance, the energy required to accelerate a material body and to make it to move with the velocity of light becomes infinite.¹⁸⁷

¹⁸⁵G. Gamow, *The Great Physicists from Galileo to Einstein*, pp. 9, 179–183, Dover Publications, New York (1961).

¹⁸⁶ibid., pp. 183–184.

¹⁸⁷ibid., pp. 183–184.

Einstein's relativity theory also predicts that mass and energy are interchangeable. His famous equation, $E = mc^2$, is a relation between E , the rest energy of a particle, and m , the mass of the particle when at rest (called the rest mass).¹⁸⁸ When the particle is in motion, both E and m increase, but they remain connected by this fundamental equation and the universal constant c^2 .¹⁸⁹

3.2.2 Developments in optical instruments and glassmaking technologies

The roots of optical technology date back to remote antiquity. The book of *Exodus*, written around 1200 BC, recounts how Bezalel, while preparing the ark and tabernacle, "made the laver [a ceremonial basin] and its base of bronze from the mirrors of ministering women who ministered at the door of the tent of the meeting."¹⁹⁰ In antiquity, mirrors were made of polished copper or bronze, and later on of speculum, a copper alloy rich in tin. The Greek dramatist Aristophanes alluded to the burning glass (a positive lens) in his comic play *The Clouds*, written in 424 BC. The Romans, as reported in the accounts of Pliny (23–79 AD), also made use of burning glasses. The Roman philosopher Seneca (3 BC–65 AD) wrote that a water-filled glass globe could be used for magnifying purposes.¹⁹¹

During the middle ages, the Franciscan Roger Bacon (1215–1294), considered to be the first scientist in the modern sense, was believed to have initiated the idea of using lenses for correcting vision and even hinted at the possibility of combining lenses to form a telescope. Medieval alchemists were believed to have produced an amalgam of tin and mercury that was rubbed onto the back of glass plates to make mirrors.¹⁹² Leonardo da Vinci (1452–1519) described the camera obscura, which was later popularized by the work of Giovanni Battista Della Porta (1535–1615), who in 1589 discussed multiple mirrors and combinations of positive and negative lenses in his *Magia naturalis*.¹⁹³

The pace of optical technology accelerated tremendously in the seventeenth century, aided by theoretical works on the nature of light (reported above). The

¹⁸⁸The Einstein mass energy equivalence law can be derived from considerations of light pressure, first experimentally verified by the Russian physicist P.N. Lebedev, and shown to be numerically equal to twice the amount of reflected energy E divided by the velocity of light c . Applying momentum arguments, one can show that a beam of light reflected from a mirror will experience a momentum equal to the product of the "mass of light" m falling on the mirror per unit time by its velocity, $P_{\text{light}} = 2mc$. Comparing this equation with Lebedev's empirical relation, $P_{\text{light}} = 2E/c$, we obtain $m = E/c^2$ or $E = mc^2$.

¹⁸⁹I. Sobel, *Light*, pp. 205–207, University of Chicago Press, Chicago (1987); G. Gamow, *The Great Physicists from Galileo to Einstein*, pp. 9, 184–188, Dover Publications, New York (1961); P. Mason, *The Light Fantastic*, p. 84, Penguin Books, Middlesex (1981).

¹⁹⁰*Holy Bible, The Book of Exodus*, Chapter 38, verse 8, p. 82, Rev. Standard Version, Catholic Ed., Camden, NJ (1966) [cited in E. Hecht, *Optics*, 2nd ed., p. 1, Addison Wesley, Menlo Park (1990)].

¹⁹¹E. Hecht, *Optics*, 2nd ed., p. 1, Addison Wesley, Menlo Park (1990).

¹⁹²*ibid.*, p. 2.

¹⁹³*ibid.*

refracting telescope, patented by Hans Lippershey (1586–1619), a Dutch spectacle maker, in 1608 was the first major optical instrument invented in this century. On hearing about this invention, Galileo Galilei (1564–1642), in Padua, built his own instrument within several months, grinding the lenses by hand. The compound microscope was invented at about the same time, possibly by the Dutchman Zacharias Janssen (1588–1632), and later improvements were made on this design by Francisco Fontana (1580–1656) of Naples, who replaced the concave eyepiece in Jansen’s microscope with a convex lens. A similar change was introduced in the telescope of Johannes Kepler (1571–1630). In 1668, Isaac Newton (1642–1727) invented the reflecting telescope as his solution to the problem of chromatic aberrations. John Dollond in 1758 combined two elements, one of crown glass and the other of flint glass, and succeeded in forming a single achromatic lens, used in correcting chromatic aberration.¹⁹⁴

By the nineteenth century, optical technology had progressed to such a level that it was recognized that further development depended on a perfect marriage between science and craftsmanship—an idea first proposed by Josef Fraunhofer and implemented by the trio of Carl Zeiss, Ernst Abbe, and Otto Schott, the triumvirate of the Carl Zeiss company, whose story has become synonymous with that of modern optical technology, which includes the principles used in the design and construction of lithographic exposure tools. This is an interesting story,¹⁹⁵ and aspects of it need to be retold here, if only for its didactic lessons.

The story begins on July 21, 1801, when a glazier’s workshop in a little village just outside of Munich suddenly collapsed, bringing down the whole building on top of it. The glazier’s assistant, Josef von Fraunhofer, had been buried under the great rubble of bricks, beams, and glass; but as if by a dint of miracle, the debris formed itself into an arch from which the lad had to be extricated, unhurt. Passing nearby in his carriage was none other than the Duke of Bavaria, who was attracted to the scene no doubt by the commotion. Sending for the lad, the Duke found him to be a bright, intelligent boy who, although not formally educated, had learned about glassmaking from his father. Greatly impressed by the young Fraunhofer, the Duke presented him with a bag of money, which he promptly used to buy himself a glassmaking machine, some books on optics, and a release from his apprenticeship. Throughout the remainder of his remarkably short life of 39 years, he made outstanding advances in glassmaking, in the construction of optical instruments, in the foundation of spectroscopy, and in the wave theory of light.¹⁹⁶

With a prism and a telescope that he manufactured by himself, he discovered numerous black lines in the spectrum of sunlight thrown by a prism. He made use of these lines as wavelength markers when he was developing his new lenses. Subsequently they would be recognized as “optical fingerprints” for identifying individual elements whose atoms absorbed only certain wavelengths from the sun. Soon after, he became one of the world’s premier scientific instrument makers.¹⁹⁷

¹⁹⁴ibid., pp. 2–5.

¹⁹⁵P. Mason, *The Light Fantastic*, pp. 151–166, Penguin Books, Middlesex (1981).

¹⁹⁶ibid., p. 151.

¹⁹⁷ibid.

With the goal of achieving a perfect marriage between science and craftsmanship in order to improve the quality of his instruments and to distinguish them from those of his competitors, he developed the following three basic principles that he assiduously followed: (i) the improvement of technical manufacturing methods for optical instruments and glasses, (ii) research and development of basic theories of optics, and (iii) the improvement of raw materials for making glass. Although each of these three principles was important in its own right, it was only by combining all three of them that he believed progress could be made beyond the old methods of trial and error used by his contemporaries. Unfortunately, when he died in 1826, the German scientific instrument industry went into decline, along with his approach.¹⁹⁸ The illustrious Fraunhofer's approach was lost and not resurrected until the optical team of Carl Zeiss (Fig. 3.27) and Ernest Abbe (Fig. 3.28) went into collaboration with Otto Schott (Fig. 3.29), the glassmaker, in 1882.¹⁹⁹

Carl Zeiss, after leaving high school in 1834 and spending an additional 12 years in apprenticeship, studying and working in various scientific workshops, set up his own instrument workshop in November of 1846 and immediately went into business as an instrument maker in the little university town of Jena. Jakob Schleiden, a founder of modern botany and professor at the University of Jena, offered him guidance in the manufacture of microscopes. Like many of his contemporaries in the same business, his method of manufacturing lenses relied on trial-and-error methods, which seemed rather wasteful and inefficient. Seeking to replace these old hit-or-miss methods with a true scientific understanding of the microscope, he enlisted the help of some of his friends at the University of Jena. First, he enlisted the help of the mathematician Barfus, who worked on it until



Figure 3.27 Carl Zeiss, founder of the Carl Zeiss optical company in Jena in 1846. (Published with permission from the Deutsches Museum, Munich.)

¹⁹⁸ibid., p. 152.

¹⁹⁹ibid., pp. 151–152 (1981).

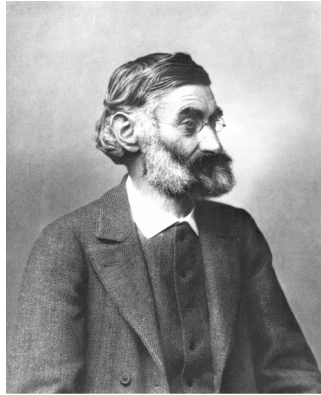


Figure 3.28 Ernst Abbe, who developed the Abbe sine condition—a design specification derived from wave theory for ensuring good image quality in microscopes. He also transformed the Zeiss optical company into the Carl Zeiss Foundation in 1889. The greatness of this company was not only in the quality of its optical products, but equally in the care it took of its workers at a time when exploitation and oppressive poverty were the rule. (Courtesy of the Carl Zeiss Archives.)

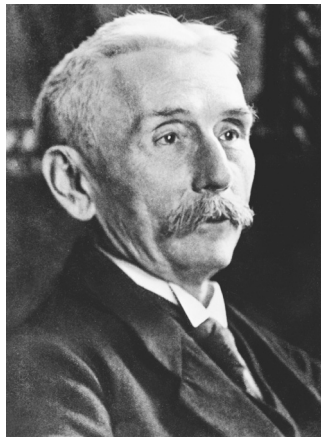


Figure 3.29 Otto Friedrich Schott, who along with Zeiss and Abbe established the Technical Glass Laboratory of Schott and Co. in Jena in 1884. He was also a partner in the Zeiss optical company. (Published with permission from the Deutsches Museum, Munich.)

his death, but without success. Finally, he enlisted the help of the young physics lecturer Ernst Abbe.²⁰⁰

In characteristic fashion, Abbe made a wide-ranging search of the available optical literature, but found nothing of help. After numerous visits to the Zeiss workshop, Abbe came to the conclusion that the main problem with existing

²⁰⁰ibid., p. 153.

microscopes of the day was that the rays of light passing through the outer parts of the lens came to a focus at a slightly different point from the rays passing through the middle, thereby degrading the sharpness of the image. He worked out theoretical ways of solving this problem and obtained an exact specification for the shapes, sizes, and positions of the lenses. He left absolutely nothing to the judgment of the instrument maker.²⁰¹

But when a dozen microscopes were built in 1868 in accordance with Abbe's specifications, it was determined that the performance of all of them was inferior to the standard trial-and-error instruments they had been producing. Undeterred, Zeiss encouraged Abbe to try again and stayed closely with him while he spent the next two years working in the shops, studying the techniques, and designing the measuring and testing equipment that would be needed if a satisfactory theory were to be found. At long last, he realized that the accurate theory for constructing microscope lenses was none other than the wave theory of light. He realized that the objects being examined under the microscope were so finely structured that the light from each tiny detail did not go simply in a straight line, but was diffracted into a pattern of light and dark bands, just as in Newton's interference experiments with pinholes or Young's experiments with slits. To obtain a true image of that detail, he determined that it was necessary to collect all of the light diffracted from it and to reassemble it with the system of lenses.²⁰²

Next, Abbe calculated the precise geometry of the lens system using the wave theory of light. The microscopes made to his new specification showed good improvement, but were still of poor quality. When he next recalculated the geometry of the lens system to ensure that points a little way off the direct axis were brought into the same sharp focus as points in the direct line of sight, he devised what is now referred to as the "Abbe sine condition"—a specification derived from the ray theory of light that is still a key feature in modern microscope design, which has greatly influenced the design of lithographic exposure tool lenses. When the Zeiss company built the "theoretical microscopes" according to the specification of the Abbe sine condition, while simultaneously meeting the specification that they collect enough diffracted rays from the object to resolve the finest possible detail, these microscopes were determined to be at least as good as the best microscopes of their day; and more importantly, each was made to a reproducible specification—a decided edge over competing microscopes from other companies, which were still made by repeated trial-and-error method. Needless to say, Abbe was greatly delighted, on examining a number of the best microscopes then available, to find that they all fulfilled the Abbe sine condition. Thus, in a way, the old craftsmen had successfully corrected their lens systems for off-axis imaging without even realizing it.²⁰³

With the lens design problem solved, Abbe turned his attention to the problem of how to get the right kind of glass. At that time, a lens designer had only two

²⁰¹ibid.

²⁰²ibid., p. 154.

²⁰³ibid.

distinct options when it came to the choice of glass, namely, crown glass, made of silica, soda, and potash, and flint glass, the same mixture made heavier by the addition of oxides of lead. Flint glass characteristically refracts light more strongly, while also showing a much greater difference between its refraction of the different colors than crown glass. It was customary during this period to combine a crown glass lens with a flint glass lens in a way that brought light of different colors to a focus at the same point in the “achromatic” microscope lenses being produced during this period. This helped to a certain extent in eliminating the confusing multicolored images that limited the performance of the earlier microscopes.²⁰⁴ It should be pointed out that Fraunhofer had earlier shown that a complete solution to the color problem was theoretically possible, and Abbe succeeded in finding this solution only to be hampered because of lack of glass with the required optical properties, as he wrote:²⁰⁵

“This discussion then leads to the conclusion that the deficiencies of present-day microscope objectives. . . are caused by the optical properties of the presently available raw materials. Therefore, perfection of the optical quality of the microscopes seems to depend primarily on the progress in the art of glassmaking.”

Quite auspiciously, in 1879, the solution to the high-quality glass availability problem materialized in a large parcel that Otto Schott sent to Abbe containing pieces of glass he had made by substituting lithium for the sodium or potassium in ordinary glass. Otto Schott, a young chemist whose father owned a plate glass works in Westphalia, had written his graduation thesis on the manufacture of window glass. He was more interested in using his basic chemical knowledge of minerals to discover entirely new kinds of glass than he was in making windows or in making money for that matter. So it was that he requested Abbe to measure the optical characteristics of the new glass materials he had sent him.²⁰⁶

When Abbe measured the optical characteristics of Schott’s new glass, he found them to differ from those of conventional glasses, though unfortunately not in the way required for Abbe’s achromatic lens design. Nevertheless, Abbe felt excited about the prospects he saw in the very existence of such an enterprising glassmaker, especially one who appreciated the importance of producing a number of small batches of glass with systematically varying composition. In no time, Schott joined the team of Zeiss and Abbe, and within three years he moved to Jena to operate a small glassmaking laboratory that the three set up jointly. In 1884, this laboratory was transformed into the Technical Glass Laboratory of Schott and Company. Two years later, it heralded a new era for optical instruments by issuing a catalog of 44 different types of glass, such as heat-resistant glasses, thermometer glass, borate, phosphate, and zinc glasses, as well as the special optical glasses that Abbe needed for his color-correction lenses.²⁰⁷

²⁰⁴ibid., pp. 154–155.

²⁰⁵E. Abbe, *Gesammelte Abhandlungen*, Vol. 1, p. 159, G. Fisher Verlag, Jena (1906).

²⁰⁶P. Mason, *The Light Fantastic*, pp. 155–156, Penguin Books, Middlesex (1981).

²⁰⁷ibid., p. 157.

The strong bond of friendship and trust between these three men stood up to some severe testing. Having established the glassmaking company largely with the help of a large government subsidy that was to be conditional on transfer of the works to Berlin, when faced with a decision to either abandon his colleagues and move the glassworks to Berlin to receive the full government subsidy or stay with his glassworks in Jena with his colleagues and lose the subsidy, Schott chose the latter. The government withdrew its condition.

Another severe test came when Herman von Helmholtz, the leading German biophysicist at the University of Berlin at the time, heard of Abbe's explanation of image formation in terms of the wave theory of light. Helmholtz had earlier worked on this problem, but without success, and so he set off eagerly for Jena to obtain a firsthand account from Abbe. Very much impressed with what he heard, he returned to Berlin and wrote to Abbe offering him a professorship at the university, but Abbe refused to accept the offer, just like Schott had done to the German government. Nothing—not even money or prestige—would deter the three partners from pursuing their work together in optical science.²⁰⁸

In 1889, shortly after the death of Carl Zeiss, Abbe developed his most advanced microscope—a microscope with a newly designed eyepiece and an oil-immersion objective, referred to as Abbe's "famous condenser," which directed the light onto the specimen. Together, these two components took the instrument to the ultimate limit of resolving power. Abbe's own theory had shown that no feature finer than about one-half a wavelength of the illuminating light could ever be resolved. Achieving the maximum resolving power in a microscope in 1889 was of the utmost importance for the study of microorganisms in the then rapidly growing field of bacteriology. Compared to the first observations of dental bacteria in 1683 by the Dutch pioneer Leeuwenhoek, who used a single-lens microscope to magnify the bacteria to perhaps 150 times, Abbe's new instrument could magnify up to 2000 times to resolve details in bacteria that are only a few wavelengths in size.²⁰⁹

It should be pointed out that the theoretical optical limits of resolution predicted by Abbe's theory probably saved many other microscope manufacturers from striving after the unattainable. This may also have unwittingly contributed to the belief that was common in Europe around 1890, that physical science was largely complete, and that all of the major discoveries had already been made; a belief no doubt shattered within a few years by a succession of unexpected discoveries of the greatest importance—discoveries such as radioactivity, the electron, x rays, etc.,²¹⁰ already discussed in the preceding sections of this book.

Roentgen's discovery of x rays opened the way to x-ray diffraction, a very effective tool for exploring the last elements of matter. It also opened the way to x-ray lithography. The discovery of the electron by J.J. Thompson opened the way to electron microscopy, influenced no doubt by one of the great surprises of twentieth-century physics—the discovery that matter, just like light, could

²⁰⁸ibid.

²⁰⁹ibid., pp. 157–158.

²¹⁰ibid., pp. 158–159.

behave as a particle or as a wave, depending on the circumstances (as discussed above). An electron can behave like a particle when accelerated from the filament in a television tube to produce a point of light on the screen; it can also behave like a wave. A beam of electrons can be focused, using electric or magnetic lenses, resulting in the image of a very small object being greatly magnified and projected as a picture on the screen.²¹¹ Similar principles are employed in exposure tools used in electron beam lithography.

In the 1890s, Abbe turned his attention to devising ways for ensuring the continued success of the Carl Zeiss enterprises, while ensuring the well-being of its workers. After having considered the limitations of the common forms of corporate structure, for example, the limited liability company or the cooperative, he found them to offer no guarantee that the social responsibility of the concern would not one day be submerged by selfish and profit-oriented motives. As a result, he created a new form of organization, the Carl Zeiss Foundation, drawing up the statutes of the Foundation himself. The guiding principle of the Foundation was that the material and scientific success of the Zeiss works did not stem from the activity of a few individuals, but rather from the participation of the entire body of personnel. Consequently, he stated that all of the employees should share in the benefits of the firm's operations and should be entitled to lifelong economic security. Noting that the Zeiss works could fulfill this objective only if its sound financial position was ensured, he included in the statutes precise regulations as to the way the income was to be distributed between maintenance, replacement, production, and scientific research.

Remarkably, the regulations that attracted the most controversy were those aimed at safeguarding the rights of the workers, namely, (i) an hourly wage or salary, once granted, cannot be reduced; (ii) all employees of more than five-years standing shall enjoy job protection; and (iii) hiring of employees must always be irrespective of race, political affiliation, or religious belief. He also introduced a nine-hour day, which was reduced in 1900 to eight hours, sickness pay, holiday pay, retirement benefits, health insurance, and a workers' council. He made all of the provisions in the statutes permanently binding on the employer, so that the personnel and economic status of the employees was not a matter of charity but an inalienable legal right.²¹²

In 1889, he established the Carl Zeiss Foundation, and two years later he transferred to the Foundation his ownership of the optical works and his half-share in the glassworks. By so doing, he gave up his position of owner to become one of the team of four managers who governed the company according to the statutes.²¹³

It is a lasting tribute to the inspiration of Abbe, as well as to the success of his plan, that 20 years later, at the end of World War I, Otto Schott followed in his footsteps when he presented his share of the glassworks to the Foundation, effectively exchanging his position of owner for that of a manager.²¹⁴

On March 19, 1945, during World War II, squadrons of British and American bombers bombed the town of Jena, destroying the Zeiss facilities. At the end of the

²¹¹ *ibid.*, pp. 158–160.

²¹² *ibid.*, pp. 160–162.

²¹³ *ibid.*, pp. 162–163.

²¹⁴ *ibid.*, p. 163.

war, 80 of the leading scientists and engineers of the Zeiss optical works and a similar group of 40 from the Schott glassworks were relocated to Oberkochen in the western part of Germany, in the Allied zone, where they began with whatever they managed to salvage from Jena to build up a new optical organization that they regarded not just as successor to the Carl Zeiss Foundation, but as the genuine article of the Foundation itself. Meanwhile in Jena, much of the damaged heavy equipment that the Russians had taken away under the reparations agreement were brought back when the factory was rebuilt; and soon after, the Carl Zeiss Company of Jena was back in business.²¹⁵

Following the collapse of the Berlin Wall in 1989, the two Carl Zeiss Foundations were reunited and are flourishing now as ever. Being at the forefront of modern technological developments, they are continually turning out new instruments for research and production, new microscopes, telescopes, spectrometers, lithographic exposure tool lenses, precision measuring instruments, etc.²¹⁶

Numerous other notable discoveries, inventions, and innovations in optical science and technology were made over the last 100 years by scientists and engineers who were not affiliated with the Zeiss Company. Some of these are outlined below.

The year 1930 witnessed the discovery of phase-contrast phenomena by Frits Zernike, the principle that underlies his invention of the phase-contrast microscope in 1938, and for which he won the Nobel Prize in physics in 1953. Phase-contrast microscopy made possible the production of high-contrast images of transparent specimens such as living cells, subcellular organelles, lithographic patterns, etc. Also, the same Frits Zernike introduced in 1934 the “Zernike polynomials,”²¹⁷ a set of orthogonal polynomials that arise in the expansion of a wavefront function for optical systems with circular pupils. Since 1960, these polynomials have found wide application in optical design, metrology, and image analysis.

Since World War II, developments in optical technology have spanned many fronts, ranging from optical element design to the incorporation of newfangled mathematics and approaches for analyzing image formation and quality, to new optical materials and processes for manufacturing them, to the use of computers in image processing and optical element design, to new optical devices and optical effects, etc. A few of the notable developments, starting from about the end of World War II, are outlined below.

From about the 1950s, several workers in different countries began to infuse optics with mathematical techniques and insights of communication theory. Bound together by Fourier’s mathematical analysis, the outgrowths of this approach (called Fourier optics) have been far-reaching, particularly in the areas of theory of image formation and evaluation, transfer functions, and spatial filtering. In particular, the use of techniques such as spatial frequency filters have offered a rich new way of appreciating a broad range of optical phenomena.²¹⁸

²¹⁵ibid., pp. 165–166.

²¹⁶ibid., p. 166.

²¹⁷F. Zernike, “Beugungstheorie des Schneidenverfahrens und seiner verbesserten Form, der Phasenkontrastmethode,” *Physica* **1**, 689 (1934).

²¹⁸E. Hecht, *Optics*, 2nd ed., p. 10, Addison Wesley, Menlo Park (1990).

In addition, the availability of high-speed digital computers has engendered a vast improvement in the design of complex optical systems. New practical uses were found for aspherical lens elements, and the diffraction-limited system with an appreciable field of view finally became a reality. The ion bombardment polishing technique, in which one atom is chipped away at a time, was introduced to meet the need for extreme precision in the manufacture of optical elements. Single and multilayer thin-film coatings (reflecting, antireflecting, etc.) became widely available. Fiber optics evolved into a practical tool, along with thin-film light waveguides. A great deal of attention was paid to the infrared region of the spectrum, with an eye to applications in surveillance systems, missile guidance, communications, etc., and these in turn have stimulated the development of infrared materials. Plastics began to be used in optics, particularly in lens elements, replica gratings, fibers, aspherics, etc. A new class of partially vitrified glass ceramics with exceedingly low thermal expansion coefficients was developed and is now widely in use.²¹⁹

The year 1960 saw the building of the first laser, and within a decade laser beams spanned the range from infrared to ultraviolet. The availability of high-power coherent sources led to the discovery of new optical effects such as harmonic generation, frequency mixing, etc., which in turn were incorporated into a slew of new devices. The technology required in the manufacture of practical optical communication systems also witnessed very fast evolution. The applications of crystals in devices such as second-harmonic generators, electro-optical and acousto-optic modulators, and the like have spurred a great deal of contemporary research in crystal optics. Holography, the wavefront reconstruction technique that produces three-dimensional images, was found to have numerous additional applications in nondestructive testing, data storage, etc.²²⁰

The 1980s and 1990s saw the development of lithographic exposure sources such as KrF and ArF exciplex lasers. Today, the majority of advanced IC circuits are fabricated with these laser-based exposure tools.

From about 1970 to the present, the applications of optics for military purposes has ranged across the spectrum from “smart bombs” and spy satellites to “death rays” and infrared gadgets that see in the dark. But profit motive, coupled with the need to improve the quality of life have also brought optical products into the consumer market place as never before. Today, lasers have found widespread applications in a variety of areas, including reading videodiscs in living rooms, cutting steel in factories, setting type in newspapers, scanning labels in supermarkets, performing surgery in hospitals, exposing resists used in patterning integrated circuits, etc.²²¹ The list of appliances that now rely on optics for their operations is truly staggeringly long.

²¹⁹ibid.

²²⁰ibid., p. 11.

²²¹ibid., p. 11.

3.2.3 Developments in chemistry

A comprehensive treatment of the history of chemistry has been given elsewhere.²²² In this section, we present only the key points, stretching from the very roots of the field, through the actual beginning of the field as a distinct discipline, and ultimately to the most advanced state of the field in the present era, which are directly related to the invention, development, and evolution of lithography.

The meaning and purpose of chemistry has undergone a lot of metamorphoses throughout recorded history. Muir writes that “the purpose of chemistry seems to have changed much from time to time. At one time chemistry might have been called a theory of life, and at another time a department of metallurgy; at one time as study of combustion, and at another time an aid to medicine; at one time an attempt to define a single word, the word element, and at another time, the quest for the unchanging basis of all phenomena. Chemistry has appeared to be sometimes a handicraft, sometimes a philosophy, sometimes a mystery, and sometimes a science.”²²³ Today, chemistry is viewed as the central, enabling science that enables other fields of science, including lithography.

3.2.3.1 The four-element theory

The beginning of the story of lithography can be traced all the way back to the roots of chemistry itself, in the first clear expressions of the idea of an element in the teachings of Greek philosophers, who sought to explain the material world around them. Foremost among these philosophers were Thales (640–546 BC), who proposed that all things were made of water; Anaximenes (560–500 BC) of air; and Herakleitos (536–470 BC) of fire. It was Empedocles (490–430 BC) who introduced the concepts of four “roots” of things, namely, fire, air, water, and earth, and two forces, attraction and repulsion, which joined and separated them.²²⁴

Plato (427–347 BC) was the first person to use the name “elements” (*stoicheia*); he assumed that things are produced from a formless primary matter, perhaps just space, taking on “forms.” The minute particle of each element, he believed, has a special shape—fire a tetrahedron, air an octahedron, water an icosahedron, and earth a cube—which are cut out of space by two kinds of right-angled triangles. To him, the elements change into one another in definite ratios, by resolution into triangles and reassociation of these. His dialogue *Timaeus*²²⁵ includes a discussion of the compositions of inorganic and organic bodies and can be regarded as an elementary treatise on chemistry.

²²²For a comprehensive treatment on the history of chemistry, see, for example, J.R. Partington, *A Short History of Chemistry*, 3rd ed., Dover Publications, New York (1989); M.M. Pattison Muir, *A History of Chemical Theories and Laws*, New York (1907).

²²³M.M. Pattison Muir, *A History of Chemical Theories and Laws*, p. vii, New York (1907).

²²⁴J.R. Partington, *A Short History of Chemistry*, 3rd ed., Chapter II, Dover Publications, New York (1989).

²²⁵Plato, “Timaeus,” in *The Dialogues of Plato, The Great Books of the Western World*, translated by B. Jowett and M.J. Adler, Ed., Encyclopedia Britannica, Inc., Chicago, pp. 442–477 (1993).

Summarizing the theories of earlier thinkers, Aristotle (384–322 BC) proposed that all substances consisted of primary matter called *hule*, from which different forms could be made, just like a sculptor can make different statues from one block of marble. He preferred to think of the form as evolving from within, as in organic growth. He called the form *eidos* and believed that these forms can be removed and replaced by new ones, thus giving rise to the ideas of the transmutation of the elements. He believed that the fundamental properties of matter were hotness, coldness, moistness, and dryness. By combining these in pairs, he obtained what are called the four elements, fire, air, earth, and water, which make up in varying proportions the vast multitude of different substances in nature.²²⁶ He also believed that a substance, for example, that burned more vigorously than another contained a higher proportion of the element fire, while one that has more fluid than another contained a higher proportion of the element water. To these four material elements, he later added a fifth, immaterial, one that appears in his latter writings as the *quintessence*, and which corresponds with the ether. The four material elements, he thought, were supposed to settle out naturally into earth (below), water (the oceans), air (the atmosphere), fire, and ether (the sky and heavenly bodies).²²⁷

He defined an element to mean “one of those of bodies into which other bodies can be decomposed and is itself is not capable of being divided into others.” He drew a distinction between mechanical mixture, solution, and chemical change with complete change of properties. He said that vapor from sea water evaporated in a vessel condenses as fresh water on the cool lid, and (wrongly) that wine would give water in a similar way, suggesting that he knew of a primitive method of distillation. He classified several chemical processes, thought that metals are mostly water (a clear influence of Plato), and listed the “homogenous” parts of animals and plants, thus constituting a primitive organic chemistry.²²⁸

The four-elements theory lasted well into the end of the eighteenth century, and the concept of the ether as a medium for the transmission of light lasted to the end of the nineteenth century.²²⁹ The remarkable longevity of the four-element theory for several millennia highlights the lack of a chemical proof that earth, water, air, and fire were elements, or that nature’s enormous variety of materials were made up of only four substances. To the ancient mind, the theory helped to explain many facts in ways that were easily understood.

Applying Aristotle’s theory to medicine, Galen of Pergamos (129–199 AD) proposed that in a healthy body, the four elements, which appear as four humors (blood, phlegm, bile, and black bile) are in equilibrium (an idea going back to Anaxogoras, 450 BC). Disease, he said, is caused by the predominance of an element and is cured by the opposite element.²³⁰

²²⁶J.R. Partington, *A Short History of Chemistry*, 3rd ed., pp. 13–14, Dover Publications, New York (1989).

²²⁷*ibid.*, p. 14.

²²⁸*ibid.*

²²⁹*ibid.*, pp. 14–15.

²³⁰*ibid.*

3.2.3.2 Chemistry as a distinct discipline

Chemistry as a distinct discipline had its origin around the beginning of the Christian era, in the city of Alexandria in Egypt, which was founded by Alexander the Great at the mouth of the Nile in 331 BC. In Alexandria, the ancient Egyptian industrial arts of metallurgy, dyeing, and glassmaking were fused with the philosophical speculations of ancient Greece, which at that time had undergone many changes, and had assimilated elements of Eastern mysticism. In particular, Plato's teachings were transformed into Neoplatonism. The Gnostic sects grew during the early centuries of the Christian era, also in Alexandria. Most importantly, the technical arts, i.e., the imitation and falsification of precious metals, gems, and dyes, gradually was transformed during this time (influenced by the theoretical views on the nature of matter) into the "divine" or "sacred" art of making gold or silver. It was precisely in this very development, which contained in its very essence the germ of chemistry, that a considerable body of positive, practical chemical knowledge came into existence.²³¹

It is noteworthy that before the commencement of the Christian era, we find no indication of the existence of chemistry in Europe or the Near East, although chemical operations were known to technologists of the time. The name "chemistry" first appears in an edict of the Emperor Diocletian in 296 AD, given by Suidas (tenth century) from an older source, in which the books of the Egyptians (in Alexandria) on *chemeia*, on making (i.e., imitating) gold and silver, are ordered to be burned. The word also appears in the writings of Greek authors such as Plutarch, who in his treatise *On Isis and Osiris*, written about 100 AD, called Egypt *chemeia* on account of the black color of its soil.²³² Partington writes that the word probably meant Egyptian art.²³³

It is also interesting that the art of chemistry was commonly ascribed to the mysterious Hermes Trismegistos, whose name is still preserved in the expression "hermetically sealed," and who was invoked by the Gnostics as the source of all wisdom.²³⁴

Quite a good number of Greek treatises on the divine were in existence as early as the first century AD. These chemical treatises written in Greek in Egypt, at Alexandria, are generally considered to be the earliest known books in chemistry. Zosimos (300 AD) was the most prolific of these authors. The books contained many examples of interesting practical chemical information, which appear for the first time, and also many diagrams of chemical apparatuses. They contained information on operations such as fusion, calcinations, solution, filtration, crystallization, sublimation, and especially distillation; and methods of heating include the open fire, lamps, and the sand and water baths.²³⁵

²³¹J.R. Partington, *A Short History of Chemistry*, 3rd ed., pp. 19–20, Dover Publications, New York (1989).

²³²*ibid.*, p. 20.

²³³*ibid.*, p. 20.

²³⁴*ibid.*

²³⁵*ibid.*, pp. 21–22.

3.2.3.3 Alchemy

It is generally accepted that alchemy began in China around 140 BC. In 1144, it appeared in Europe by way of translations made in Spain from Arabic works.²³⁶ Partington asserts that the Arabic name *alchemy* is merely the Alexandrian-Greek *chemeia* with the Arabic definite article *al* prefixed. Both Roger Bacon and Albert the Great (Albertus Magnus) wrote about it in 1250.²³⁷

Alchemy was based on the concept of transmutation of substances, an idea that was derived from the marked effects of arsenic, mercury, and sulfur in changing the color of metals. It was quite a rational idea at the time, for many alchemists believed that they could produce gold from the action of the above substances on baser metals such as lead or that they could produce silver from copper by turning the color of copper white with arsenic. The transmuting agent was called by the Arabs *aliksir* (elixir), perhaps from the Greek *xerion*, which meant a dusting powder or cosmetic; later, it was called the philosopher's stone, or tincture (i.e., an agent for changing the color of substances) by the European alchemists.²³⁸

Other notable developments in chemistry between the twelfth and nineteenth centuries are outlined below. In the thirteenth century, Bacon describes gunpowder, which became known in Europe (perhaps from China by way of the Arabs) as being composed of seven parts saltpeter, five parts wood charcoal, and five parts sulfur. Theophrastus Bombast von Hohenheim, commonly called Paracelsus (1493–1541), founded iatochemistry, or chemistry applied to the service of medicine. In 1556, Georg Agricola (1494–1555), a German physician, wrote *De Re Metallica* on mining and metallurgy. Johann Baptista van Helmont (1579–1644) clearly expressed for the first time the law of indestructibility of matter, and emphasized that metals when dissolved in acids are not destroyed but can be recovered again by suitable means. He invented the name gas and was the first person to describe carbon dioxide. He regarded air and water as the fundamental elements. In 1597, Andreas Libavius (1540–1616), a German schoolmaster, wrote *Alchemia*, the first textbook of chemistry. Between 1646 and 1649, Johann Rudolph Glauber (1604–1670) published the *New Philosophical Furnances*, in which he describes the preparation of salts and mineral acids. In 1675, Nicholas Lemery published a textbook *Cours de Chymie*, in which he classified substances into three “kingdoms of nature,” namely, mineral, vegetable, and animal. In 1666, Otto Tachenius published *Hippocrates Chemicus*, in which he gave a clear definition of a salt: “all salts are composed of two parts, of acid and alkali.” Johann Kunckel (1630–1703)

²³⁶In 640 AD, Egypt was conquered by the Arabs, who with the help of learned Greeks, Syrians, and Persians living under their rule made translations of Egyptian books on chemistry (which were written in Greek) into Arabic [cited in J.R. Partington, *A Short History of Chemistry*, 3rd ed., p. 27, Dover Publications, New York (1989)].

²³⁷*ibid.*

²³⁸J.R. Partington, *A Short History of Chemistry*, 3rd ed., pp. 34–40, Dover Publications, New York (1989).

described the preparation of gold ruby glass and in 1679 wrote a treatise on glass manufacture (*Ars Vitraryia*) based on an earlier work by an Italian, Neri.²³⁹

3.2.3.4 Early theories of combustion and calcination

The chemical and physical changes involved in combustion and calcination drew a great deal of interest for chemists of the sixteenth century, who observed that when metals are heated in open crucibles, they leave behind a *calx*, which when weighed was observed to be heavier than the metal. Partington reports that explanations typically given for this observation then were that some kind of “soul” escaped from the metal, or that the matter became denser, or that some kind of acid was absorbed from the fire, or that fire possessed weight and was absorbed by the metal during the formation of the calx.²⁴⁰ In the following, we sketch broad outlines of the most significant chemists of this era.

Robert Boyle (1627–1691) was one of the pioneering chemists of this era. A major problem that occupied his interest was elucidating what really constituted an element. He showed through experimentation that the four elements of Aristotle and the three principles of the alchemists (mercury, sulfur, and salt) did not deserve to be called elements or principles at all, since none of them could be extracted from bodies, e.g., metals. He defined an element as follows:

“I mean by Elements, as those Chymists that speak plainest to by their Principles, certain Primitive and Simple, or perfectly unmingled bodies; which not being made of any other bodies, or of one another, are the Ingredients of which all those call’d perfectly mixt Bodies are immediately compounded, and into which they are ultimately resolved.”²⁴¹

He believed in the atomic theory, which he used to explain chemical changes. In 1662, he discovered the law that bears his name, Boyle’s law (the volume of a gas is inversely proportional to the pressure).²⁴²

Robert Hooke (1635–1702)²⁴³ postulated a theory of combustion involving twelve propositions in which he stated, among other things:

“Air is the universal dissolvent of all sulfurous bodies; this action of dissolution produces a very great heat and that which we call fire; this dissolution is made by a substance inherent, and mixt with the air, that is like, if not the very same, with that which is fixt in saltpeter; in this dissolution of bodies by the air, a certain part

²³⁹ibid., p. 65, Chapter IV.

²⁴⁰Cf. J.C. Gregroy, *Combustion from Heraclitos to Lavoiser*, London (1934).

²⁴¹R. Boyle, *Sceptical Chymist: or Chymico Physical Doubts & Paradoxes, Touching the Spagyrist’s Principles commonly call’d Hypostatical as they are wont to be Propos’d and Defended by the Generality of Alchymists*, p. 350, London (1661).

²⁴²J.R. Partington, *A Short History of Chemistry*, 3rd ed., pp. 67–77, Dover Publications, New York (1989).

²⁴³Robert Hook claimed to have predicted the law of gravitation before Newton made his discovery of the law of gravitation, and is known for his discovery, in 1660, of Hooke’s law.

is united and mixt, or dissolved and turn'd into the air, and made to fly up and down with it.”²⁴⁴

John Mayow (1641–1679) recognized that combustion and respiration are analogous processes. He correctly stated that animal heat is developed in the muscles, and proved that arterial blood in a vacuum gives off a gas.²⁴⁵

3.2.3.5 Phlogiston theory

The phlogiston theory was first proposed in its rudimentary form by Johann Joachim Becher (1635–1682), who published in 1669 a book called *Physica subterranean*, in which he introduced the idea that the constituents of bodies are air, water, and three earths, one of which is inflammable (*terra pinguis*), the second mercurial, the third fusible or vitreous. These three earths correspond with the sulfur, mercury, and salt of the alchemists.²⁴⁶ He also introduced the idea of inflammable earth to explain combustibility (1669), which was extended into the *Theory of Phlogiston* (the name *phlogiston* given to Becher's *terra pinguis*) by Georg Stahl (1660–1734) (see Fig. 3.30). Stahl believed that all combustible and inflammable substances and metals contained a common principle of inflammability called phlogiston (ϕ), which was contained in all substances, and which escaped on



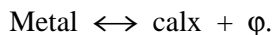
Figure 3.30 Georg Ernst Stahl (1660–1734), who formulated the phlogiston theory to explain combustion. He believed that all combustible substances and metals contained a common principle, phlogiston, which escaped on combustion or calcinations, but could be transferred from one substance to another, and restored to the metallic calx by heating with substances rich in phlogiston (such as charcoal, oil, etc.). (Published with permission from Deutsches Museum, Munich.)

²⁴⁴R. Hooke, *Micrographia: or some Physiological Descriptions of Minute Bodies made by Magnifying Glasses. With Observations and Inquiries thereupon*, London (1667).

²⁴⁵*ibid.*, p. 81.

²⁴⁶*ibid.*, p. 85.

combustion or calcinations in the forms of fire and flame; it could be transferred from one substance to another, and on heating with substances rich in phlogiston (such as charcoal, oil, etc.) can be restored to the metallic calx, reproducing the metal,²⁴⁷ illustrated by



A particular application of the “phlogiston” theory was eventually to lead chemists into much confusion and to help to finally bring about its downfall. This confusion arose in the following manner. When a metal such as copper or lead is heated, it turns into a powdery substance with no metallic properties. The same phenomenon takes place in the rusting of iron, but in the absence of heat. The chemists of the phlogistic era explained this glaring contradiction of the phlogiston theory by assuming that a metal was a kind of combustible material, which on heating loses its phlogiston, leaving the powdery residue, calx. They knew, however, that if this calx was reheated with charcoal it reconverted back into metal. Because charcoal would burn away almost entirely, they regarded it as being very rich in phlogiston. They explained that the heating of the calx with charcoal was responsible for restoring enough phlogiston to the calx to reconstitute the original metal. This led them to define a metal as a compound of calx and phlogiston, and calcination as the process of heating a metal to produce its calx, via decomposition, which they regarded as a kind of combustion in which phlogiston escaped from the metal.

It was well known, on the other hand, as early as the sixteenth century that metals increase in weight on calcinations. But how could the weight increase, since something material, namely, phlogiston, had been lost from the substance of the metal? This was a serious contradiction, and some of the chemists who supported phlogiston theory disregarded this fact, while others assumed that phlogiston had negative weight.²⁴⁸ Others concocted some rather inconsistent hypotheses to explain it. Lomonsov (1754) explained the increase in weight in terms of air being fixed by the metal.²⁴⁹ Laurent Bérault (1747)²⁵⁰ concluded that the increase in weight was due to the addition of certain foreign particles mixed with the air and separated by the action of heat.²⁵¹

Thus, the phlogiston theory went through a series of modifications throughout this period. In the old phlogiston theory, phlogiston was believed to be equivalent to *minus* oxygen; in the later theory, it was proposed to be hydrogen (Cavendish,

²⁴⁷ibid., p. 148.

²⁴⁸ibid.

²⁴⁹ibid., p. 149.

²⁵⁰L. Bérault, *Dissertation sur la Cause de l'Augmentation de Poids, que certaines Matières acquièrent dans leur Calcination*, Bordeaux (1747) [cited in J.R. Partington, *A Short History of Chemistry*, 3rd ed., p. 149, Dover Publications, New York (1989)].

²⁵¹J.R. Partington, *A Short History of Chemistry*, 3rd ed., Chapter V, Dover Publications, New York (1989).

1731–1810; Kirwan, 1735–1812; Priestly, 1733–1804), or the matter of light (Macquer, 1718–1784).²⁵²

It should be mentioned that even at its height of popularity, there were chemists who were skeptical of the phlogiston theory. Nicolas Lemery (1645–1715), for instance, did not adopt the theory of phlogiston.²⁵³

In spite of the fact that the phlogiston theory made it possible for a large number of facts to be coordinated into a system, it nevertheless retarded the progress of chemistry and prevented a number of the best chemists from seeing the correct explanation of the facts they uncovered.²⁵⁴ So until it, along with the four-element theory, were comprehensively rejected, modern chemistry remained unfounded; for earth, air, water, and fire are not the elements, and substances do not burn because of the presence in them of a common principle of inflammability.

3.2.3.6 Discovery of simple gases in common air

The history of the rejection of the phlogiston theories begins with the discovery of simple gases in common air, particularly the discovery of oxygen, which constitutes one-fifth of common air. The journey to these discoveries begins, oddly enough, in the phlogistic era, fueled by the works of a good number of exceptional chemists.

At first it was supposed that gases were different varieties of common air, with slightly different properties. In his *Vegetable Staticks* (1727), Stephen Hales (1677–1761) describes the production of “air” from a variety of substances, along with its collection and measurement, but he was not able to make any qualitative distinction between the different gases in air (such as oxygen, hydrogen, nitric oxide, carbon dioxide, coal gas, etc.) that he must have obtained.²⁵⁵ In 1754, Joseph Black (1728–1799) demonstrated the chemical differences between one kind of air from common air and gave it the name of “fixed air” (which is now known as carbon dioxide). He showed that it was produced in the combustion of charcoal, in respiration when air is exhaled from the lungs, and in fermentation.²⁵⁶ Carbon dioxide had been previously recognized and called *gas sylvestre* by van Helmont.²⁵⁷ Black’s other major contribution was the discovery of latent heat and specific heats.²⁵⁸

Another exceptional scientist during the phlogistic era was Henry Cavendish (1731–1810), who (i) recognized and named equivalents (1766–1788), (ii) investigated the properties of fixed air (CO₂) and inflammable air (H₂), which he erroneously identified with phlogiston, (iii) determined the (nearly constant)

²⁵²ibid., p. 149.

²⁵³ibid.

²⁵⁴ibid.

²⁵⁵J.R. Partington, *A Short History of Chemistry*, 3rd ed., pp. 90–93, Dover Publications, New York (1989).

²⁵⁶ibid.

²⁵⁷ibid., p. 48.

²⁵⁸ibid.

composition of the atmosphere (1781) and the volumetric composition of water (1748), and (iv) observed that nitric acid can be formed by sparking nitrogen (“phlogisticated air”) with an excess of oxygen (“dephlogisticated air”) over potash solution. A supporter of the phlogiston theory, he admitted that his results could be explained by Lavoisier’s oxygen theory²⁵⁹ (see Section 3.2.3.7).

Joseph Priestley (1733–1804) (see Fig. 3.31) was another exceptional chemist during the phlogistic era. He discovered oxygen in 1774, which he isolated from the decomposition of mercury oxide. He also discovered many other gases such as ammonia, hydrochloric acid gas, nitric oxide, nitrous oxide, nitrogen dioxide, nitrogen, carbon monoxide, and sulfur dioxide. He was among the first scientists to recognize that green plants make oxygen, which is responsible for restoring the goodness of air vitiated, by putrefaction or the burning of candles or the respiration of animals, through a process mediated by light. This process was elucidated in the twentieth century as photosynthesis. He also observed that inflammable air (H_2) is rapidly absorbed by heated metallic oxides (calces) in a process in which the latter are reduced, with water being formed if the gas is dry. He erroneously identified hydrogen with phlogiston. He also made the observation that water is formed in the explosion of inflammable air with common air or dephlogisticated air (known to us as oxygen).²⁶⁰

Carl Wilhelm Scheele (1742–1786) was another phenomenal chemist of the phlogistic era. He was actually the first discoverer of oxygen (1772–1774), on which he first published in 1777. He made other important discoveries including (i) chlorine and manganese, (ii) silicon fluoride and hydrofluoric acid from fluorspar, (iii) phosphorus from bone ash, phosphoric acid from the action of nitric acid on phosphorus, (iv) arsenic acid, molybdic acid, tungstic acid, arsenic

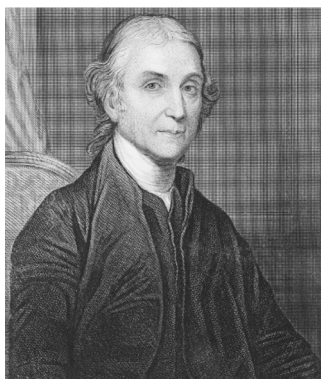


Figure 3.31 Joseph Priestley (1733–1804). (Published with permission from the Deutsches Museum, Munich.)

²⁵⁹ibid., pp. 150–152.

²⁶⁰J. Priestley, *Experiments and Observations on Different Kinds of Air*, (3 vols.) London (1774–1777); J. Priestley, *Experiments and Observations Relating to Various Branches of Natural Philosophy* (3 Vols., Vol. I London, Vols. II–III Birmingham) (1779–1786) [Also cited in J.R. Partington, *A Short History of Chemistry*, 3rd ed., pp. 110–121, Dover Publications, New York (1989)].

anhydride, copper arsenite (also called “Scheele’s green”), and the distinction between molybdenite (MoS_2) and graphite, (v) several organic compounds, including tartaric acid, mucic acid, lactic acid, uric acid, prussic acid, oxalic acid, citric acid, malic acid, gallic acid, and pyrogallic acid, (vi) glycerol and casein, (vii) hydrogen sulfide, (viii) the action of light on silver salts, (ix) the distinction between nitrous and nitric acid, nitric oxide, nitrous oxide, nitrogen dioxide, and nitric acid, and (x) the formation of cyanide by the action of ammonia on a mixture of charcoal or graphite and potassium carbonate. He proposed the peculiar theory that phlogiston + fire air (oxygen) $\xrightarrow{\text{heat}}$.²⁶¹

3.2.3.7 Foundation of modern chemistry

Antoine Laurent Lavoisier (1743–1794)²⁶² (see Fig. 3.32) is universally acknowledged as the founder of modern chemistry. Although he discovered no new substances, devised no really novel apparatuses, and worked out no improved



Figure 3.32 Antoine Laurent Lavoisier (1743–1794), the founder of modern chemistry. His method of rigid quantification, as well as his analytical definition of an element, along with his theory of combustion initiated the “chemical revolution.” Both chemistry and physiology owe their modern forms to him. (Published with permission from the Deutsches Museum, Munich.)

²⁶¹ibid., pp. 104–109.

²⁶²Recent biographies include A. Donovan, *Antoine Lavoisier: Science, Administration, and Revolution*, Blackwell, Oxford (1993); J. P. Poirier, *Lavoisier: Chemist, Biologist, Economist*, University of Pennsylvania Press, Philadelphia (1996) [originally published as *Antoine Laurent de Lavoisier, 1743–1794*, Editions Pygmalion/Gerard Watelet, Paris (1993)]. For an excellent review of these books, see E.M. Melhado, “Scientific biography and scientific revolution: Lavoisier and eighteenth century chemistry,” *Isis* **87**, 688–694 (1996). For a guide to earlier biographies, see Henry Guerlac, “Lavoisier and his biographers,” *Isis* **45**, 51–62 (1954). Other notable references include M. Beretta, Ed., *Lavoisier in Perspective*, Deutsches Museum, Munich (2005); E. Grimaux, *Lavoisier*, Paris (1888); D. Mckie, *Antoine Lavoisier* (1935, 1953); Notes and Records of the Royal Society, **VII**, 1 (1949); *Œuvres de Lavoisier*, 6 vols., Paris (1864–1893); Tilden, *Famous Chemists*, p. 63 (1921); J.A. Cochran, “Lavoisier (1931); Hartog, *Ann. Sci.* **V**, 1 (1941); Partington, *Nature* **clii**,

methods of preparation, modern chemistry and physiology could not exist in their present form without the contributions of Lavoisier. It has been said that “Lavoisier, though a great architect in the science, labored little in the quarry; his materials were chiefly shaped to his hand, and his skill was displayed in their arrangement and combination.”²⁶³ He brought the work of Black, Priestley, and Cavendish to their logical conclusions, and provided accurate interpretation of their experimental results.²⁶⁴

Although he did not discover oxygen, he was certainly the first person to recognize the consequences of its discovery, the first person to realize its true nature as an element, and by ingenious quantitative experiments, he was the first person to establish the true chemistry of combustion and calcinations of metals that had been foreshadowed by the works of Hooke and Mayow.²⁶⁵ The following is a brief account of how he made the above accomplishments.

History records that in October of 1774 Priestly visited Paris. There he met Lavoisier, to whom he described his latest discovery—the new “air” in which the flame of a candle burned much more brilliantly than in common air. He also told Lavoisier how he obtained it by heating the calx of mercury or the calx of lead.²⁶⁶

Lavoisier, it should be noted, had long been working on the related problems of combustion and calcination, and as early as 1772, he had reached the conclusion that air played an important part in combustion and that the two inflammable substances, phosphorus and sulfur, combined with air when they were burned and that their weight was increased by this combination of air. He showed that tin and lead increase in weight on calcinations and an equal weight of air is absorbed (1774).²⁶⁷ Earlier, he proved (1770) that water cannot be converted into earth,²⁶⁸ as van Helmont had previously thought.²⁶⁹

Through many months of the year 1773, he made further experiments; and in 1774–1775, after his meeting with Priestly, he concluded that the gain in weight of metals on calcination was as a result of their combination with air; but he still got no further than supposing that it was combination with common air in a pure state, without suspecting that only a part or constituent of the common air was involved.²⁷⁰

The year 1777 saw him in further experimentations, in which he reached the seminal conclusion that only a part of the air was involved in combustion,

207 (1943); Duveen and Klisckstein, *Bibliography of Lavoisier*, (1955), cited in J.R. Partington, *A Short History of Chemistry*, 3rd ed., p. 122, Dover Publications, New York (1989).

²⁶³Brande, *Manual of Chemistry*, 6th ed., pp. i xxxv (1848), cited in J.R. Partington, *A Short History of Chemistry*, 3rd ed., p. 122, Dover Publications, New York (1989).

²⁶⁴J.R. Partington, *A Short History of Chemistry*, 3rd ed., p. 123, Dover Publications, New York (1989).

²⁶⁵ibid., pp. 129–130.

²⁶⁶ibid., p. 126.

²⁶⁷ibid., pp. 125–126.

²⁶⁸ibid., p. 124.

²⁶⁹ibid., p. 41.

²⁷⁰ibid., p. 127.

respiration, and calcination—the heavier part of the air—and that air itself was not a simple substance but rather consisted of two “airs.” One of these was respirable, supported combustion, and combined with metals on calcination; this he called the “salubrious part” of the air. The other part, he concluded, was incapable of supporting combustion or respiration, it was inimical both to fire and to life, and it played no part in calcination.²⁷¹

On May 3, 1777, Lavoisier read to the Paris Academy of Sciences an account of one of the most significant experiments in the entire annals of science. On a charcoal furnace, he heated four ounces of mercury for 12 days in an apparatus consisting of a glass vessel, the neck of which is bent to connect with the air in a bell jar, inverted over a mercury trough. After 12 days, he observed that a red calx or oxide of mercury formed in the glass vessel and the level of water rose in the bell jar to a level corresponding to a decrease of about one-fifth of the total volume of air in the apparatus. The residual air extinguished lighted candles and asphyxiated animals. He called it “azote” (now called nitrogen).²⁷²

He then heated the red particles of mercuric oxide in a separate apparatus and collected the gas evolved from them. It amounted to about one-fifth of the original air and it supported combustion and respiration. He called it “oxygen.” On mixing the oxygen with the air from which it had been removed, he was able to reconstitute the common air once again. Thus, in this classic experiment, Lavoisier was able to show that common air consisted largely of nitrogen and oxygen, both of which have strikingly different, indeed opposite, properties; and he separated them one from the other.²⁷³

In 1780, he formally presented his theory of combustion, as follows:²⁷⁴

- (1) In every combustion there is disengagement of the matter of fire or of light.
- (2) A body can burn only in pure air (oxygen gas).
- (3) There is “destruction or decomposition of pure air,” and the increase in weight of the body burnt is exactly equal to the weight of the air “destroyed or decomposed.”
- (4) The body burnt changes into an acid by addition of the substance which increases its weight.
- (5) Pure air is a compound of the matter of fire or of light with a base. In combustion the burning body removes the base, which attracts more strongly than does the matter of heat, and sets free the combined matter of heat, which appears as flame, heat and light.

²⁷¹ibid., pp. 127–128.

²⁷²ibid., p. 128.

²⁷³ibid., pp. 128–129.

²⁷⁴A.L. Lavoisier, *On Combustion in General* (1780), cited in *Œuvres de Lavoisier*, II, p. 225, Impr. Impériale, Paris (1864–1893); also in J.R. Partington, *A Short History of Chemistry*, 3rd ed., p. 131, Dover Publications, New York (1989).

In experiments designed to elucidate the composition of water (1783–1784), he decomposed water into its constituent parts: oxygen and inflammable air, which he later renamed “hydrogen” (i.e., “water former”).²⁷⁵

Using an ice calorimeter, he and Laplace in 1783 measured the specific heats and the heat evolved in combustion and respiration, thus laying the foundations of thermochemistry, both on experimental and theoretical grounds, since the authors stated the principle that “as much heat is required to decompose a compound as is liberated on its formation from the elements.”²⁷⁶

He also showed that in chemical reactions, matter was neither created nor destroyed; the total weight of the products of a chemical reaction was equal to the total weight of the starting reactants. All of these are encapsulated in the law of indestructibility of matter, in which in 1789 he stated the following:

...“for nothing is created in the operations either of art or nature, and it can be taken as an axiom that in every operation an equal quantity of matter exists both before and after the operation; that the quality and quantity of the principles remain the same and that only changes and modifications occur. The whole art of making experiments in chemistry is founded on this principle: we must always suppose an exact equality or equation between the principles of the bodies examined and those of the products of the analysis.”²⁷⁷

Chemistry was thus effectively established on a quantitative basis, and the first chemical balance sheet was now drawn up.

A very significant immediate result of these great advances was the reform of the language of chemistry. The old names of substances had, of course, no relation to their chemical composition, since that was unknown at the time; and their chemical composition could not have been determined until it had been discovered of what elements they were composed.

Lavoisier defined an “element or principle” as the “last point which analysis is capable of reaching, since we have not hitherto discovered the means of separating them, they act with regard to us as simple substances, and we ought never to suppose them compounded until experiment and observation have proved them to be so,”²⁷⁸ which is essentially our modern definition of a chemical element. It must be pointed out that he adopted Robert Boyle’s 1661 definition that an element was a substance that could not be decomposed into anything simpler. He applied this idea in a very cautious way, not asserting that such substances, as they appeared to be incapable of further decomposition were, in fact, elements, but that they should be regarded as elements until evidence to the contrary was forthcoming. He generated the first table of chemical elements, which included

²⁷⁵J.R. Partington, *A Short History of Chemistry*, 3rd ed., pp. 142–147, Dover Publications, New York (1989).

²⁷⁶*Œuvres de Lavoisier*, II, p. 283, Impr. Impériale, Paris (1864–1893).

²⁷⁷A.L. Lavoisier, *Traité Élémentaire de Chimie*, p. 140, Chez Cuchet, Paris (1789).

²⁷⁸*ibid.*, p. 192 (1789).

oxygen, hydrogen, nitrogen, sulfur, phosphorus, and carbon, and a large number of metals.²⁷⁹

Having thus determined what substances were to be regarded as elements, Lavoisier and some of the French chemists who had adopted his view set on themselves the further task of devising a suitable system of chemical nomenclature that emphasized giving every known substance a name that corresponded to its chemical composition. The old names before Lavoisier's chemical nomenclature were often coined to indicate some physical property of a substance or its mode of preparation, or to perpetuate its discoverer's name or the place where it had been found as a mineral.

The language of science, Lavoisier, maintained in his *Méthode de Nomenclature Chimique*, was itself an analytical instrument. The system of chemical nomenclature that he devised gave us for every substance, in a word or two, a clean indication of its chemical nature and composition. That even after more than two centuries of further discovery since he devised this system, it has survived until today, with very little modification, is but a testament to his exceptional vision. Lavoisier's influence on the course of modern chemistry indeed cannot be overemphasized.

In all, Lavoisier's contributions span the entire field of modern chemistry—from the concept of chemical elements to the law of indestructibility of matter and conservation of mass in chemical transformations, from the theories of combustion to the foundation of thermochemistry, from chemical nomenclature to the mathematization and quantification of chemistry. Bertholet describes Lavoisier's influence on chemistry as "*La révolution chimique*." It has been noted that a book on chemistry written before his time would not be intelligible to a student unacquainted with the history of chemistry, while Lavoisier's *Traité élémentaire de Chimie* reads like a rather old edition of a modern textbook.²⁸⁰

The revolution in chemistry was complete; modern chemistry dates from the publication of Lavoisier's great classic, the *Traité élémentaire de Chimie*,²⁸¹ in Paris in 1789. From this work, which ranks with Newton's *Principia* as one of the greatest of all scientific books, we may quote one sentence that particularly reveals its author's method, and which embodies his fondness for mathematical precision, his determination to give priority to experimental evidence, and his mistrust of ideas: "I have imposed upon myself, as a law, never to advance but from what is known to what is unknown, never to form any conclusion which is not an immediate consequence necessarily flowing from observation and experiments; and always to arrange the facts and the conclusions which are drawn from them, in such an order as to render it most easy for beginners in the study of chemistry to thoroughly understand them."²⁸²

Equally impressive is Lavoisier's role in the discovery of the one element that is at the heart of the entire semiconductor industry and that through the agency of

²⁷⁹J.R. Partington, *A Short History of Chemistry*, 3rd ed., pp. 134–135, Dover Publications, New York (1989).

²⁸⁰*ibid.*, p. 130.

²⁸¹*ibid.*

²⁸²*ibid.*

lithography is fabricated into digital and analog devices—silicon. Having generated or reduced several oxides, he had suggested in 1789 that quartz, or silica (or silicon dioxide), was probably the result of the union of oxygen with an as yet unidentified element. Since his life was cut short,²⁸³ it was left to others to isolate and investigate the chemistry, as well as the technological applications of silicon.

3.2.3.8 Post-Lavoisian evolution of chemistry

Chemistry under the influence of Lavoisier became a distinct discipline—a discipline with its own instruments, techniques, and a specific technical language.²⁸⁴ Even if pre-Lavoisian chemistry could be regarded as a discipline, as a set of investigative and interpretive practices, as a livelihood, and as a tradition of texts, according to Donovan, it lacked the methodological rigor to become a science.²⁸⁵ In the post-Lavoisier era, chemistry developed into chemical principles such as stoichiometry, affinity, the law of reaction (such as definite proportions used in determining chemical compositions), and a variety of chemical equivalents, to mention but a few. It was the successive evolutions of these doctrines that led to the atomic theory, Dalton's grand idea that changed the face of the science for good.²⁸⁶

... this hypothesis of atoms forms at present the foundation of all our theories, the solid base of our system of chemical knowledge. It gives a striking simplicity to the laws relating to the composition of bodies; it enables us to look into their intimate structure; it intervenes in the interpretation of their properties, reactions, and transformation; and will doubtless at some future time furnish points of support for the science of molecular mechanics.²⁸⁷

Today, the most advanced chemical principles are based on quantum mechanics and have led to remarkable developments in spectroscopy, materials synthesis, etc. All of these developments have aided the discovery and isolation of new elements, compounds, and molecules. We briefly outline a few of these developments in the following sections.

The first marginally successful synthesis of elemental silicon was carried out in 1811 by Joseph Louis Gay-Lussac and Louis J. Thenard, who passed silicon fluoride over heated potassium. However, a much more successful method was used by Swedish chemist Jöns Jacob Berzelius in 1824, which involved the reduction of potassium fluorosilicate with metallic potassium. The element silicon was eventually recognized to be one of the most abundant in the lithosphere, that is, the crust of the Earth. Remarkably, even at that early stage, a debate developed as to whether silicon was a metal or an insulator, with Berzelius taking the view that

²⁸³Lavoisier was guillotined in 1794 during the reign of terror of the French Revolution.

²⁸⁴M. Crosland, "Research schools in chemistry from Lavoisier to Wurtz," *Br. J. History Sci.* **36**, 333–361 (2003).

²⁸⁵A. Donovan, "Lavoisier as chemistry and experimental physicist: a reply to Perrin," *Isis* **81**, 270–272 (1990).

²⁸⁶A. Wurtz, *A History of Chemical Theory*, Preface, Macmillan, London (1869).

²⁸⁷*ibid.*, p. 194.

it is a metal and Humphrey Davy that it is an insulator. This issue was not fully resolved until World War II, along with a deeper understanding of crystalline solids.²⁸⁸

The scientific study of silicon continued to advance during the nineteenth century. Notable contributions were made by Friedrich Wöhler (Fig. 3.33), who developed crystalline forms of silicon between 1856 and 1857. Although the chemistry of silicon compounds occupied a central position in the field of inorganic chemistry through much of the nineteenth century, precious little seems to have been reported in the literature about the elemental crystalline form until it became of interest to the metallurgists during the last quarter of the century.²⁸⁹

3.2.3.8.1 Laws of chemical reactions

After establishing chemistry on its modern course following the demise of the phlogistic theory of matter, chemists of the late eighteenth century and early nineteenth century turned their attention to formulating laws and theories governing chemical reactions. Some of these laws and theories are briefly outlined below.

- (1) The law of definite proportions—The first of these chemical reaction laws, the law of constant or definite proportions, was recognized by Joseph Louis Proust (1754–1826) in 1797, who stated it in 1799 as follows:

“We must recognize an invisible hand which holds the balance in the formation of compounds. A compound is a substance to which Nature assigns fixed ratios;



Figure 3.33 Friederich Wohler, the founder of modern organic chemistry when in 1828 he succeeded in producing urea (an organic substance) by evaporating a solution of isomeric ammonium cyanate (an inorganic substance). He also succeeded in producing crystalline silicon and boron between 1856 and 1857. (Published with permission from the Deutsches Museum.)

²⁸⁸F. Seitz and N.G. Einspruch, *Electronic Genie: The Tangled History of Silicon*, p. 3, University of Illinois Press, Urbana (1999).

²⁸⁹*ibid.*, p. 3; J.R. Partington, *A Short History of Chemistry*, 3rd ed., pp. 230–232, 238, Dover Publications, New York (1989).

it is, in short, a being which Nature never creates other than balance in hand, *pondere et mensura*.”²⁹⁰

Proust had been led to this law from his observation that several metals can form more than one oxide and sulfide, each of which has a definite composition.

- (2) The law of multiple proportions—First recognized by John Dalton in 1803 as a consequence of his atomic theory, this law states that when two elements combine to form more than one compound, the weights of one element that unite with identical weights of the other are in simple multiple proportions.²⁹¹
- (3) The law of reciprocal proportions or the law of equivalents—Cavendish established in 1766 that identical weights of a given acid require different weights of different bases for neutralization, and he called these weights of the bases equivalents.²⁹² It was Richter who in 1795 generalized these observations into the law of the reciprocal proportions thus:

“If P is the mass of a determining element, where the masses of its elements determined are a, b, c, d, e , etc., Q the mass of another determining element, where $\alpha, \beta, \gamma, \delta, \epsilon$, etc., are the masses of its element determined, so that a and α, b and β, c and γ, d and δ, e and ϵ shall represent the same elements; and further if the neutral masses $P + a$ and $Q + \beta, P + a$ and $Q + \gamma, P + c$ and $Q + \alpha, P + a$ and $Q + \gamma$, etc., are decomposed by double affinity, so that the resulting products are neutral, then the masses a, b, c, d, e , etc., have the same quantitative ratio among one another as the masses $\alpha, \beta, \gamma, \delta, \epsilon$, etc., or conversely.”²⁹³

3.2.3.8.2 Atomic theory

The origin of atomic theory dates back to the early Greek philosophers.²⁹⁴ Boyle in 1661 wrote of “those theories of former philosophers, which are now with great applause revived, as discovered by latter ones.”²⁹⁵

Anaxagoras of Klazomenai (near Smyrna) (498–428 BC) held that bodies are divisible without limit and retain their characteristics.²⁹⁶ Zeno of Elea (around 489 BC), who was part of the Eleatic school, believed that matter is continuous,

²⁹⁰J.R. Partington, *A Short History of Chemistry*, 3rd ed., pp. 153–154, Dover Publications, New York (1989).

²⁹¹*ibid.*, pp. 158–159.

²⁹²*ibid.*, pp. 159–160.

²⁹³J.B. Richter, *Über die neuern Gegenstände der Chymie* IV, 67 (1795); also quoted in J.R. Partington, *A Short History of Chemistry*, 3rd ed., pp. 162–163, Dover Publications, New York (1989).

²⁹⁴J. Burnet, *Early Greek Philosophy*, 3rd ed., (1920); I. Freund, *The Study of Chemical Composition*, Cambridge (1904); J.R. Partington, *Ann. Sci.* IV, 245 (1939); J.R. Partington, *A Short History of Chemistry*, 3rd ed., p. 164, Dover Publications, New York (1989).

²⁹⁵R. Boyle, *Sceptical Chymist*, p. 23 (1661).

²⁹⁶J.R. Partington, *A Short History of Chemistry*, 3rd ed., pp. 165–166, Dover Publications, New York (1989).

and since the universe is full of matter, there is no motion. He invented a number of ingenious paradoxes, such as that of “Achilles and the tortoise,” to prove that things do not really move; we only think they do. The Eleatics held that “without vacuum there is no motion; there is no vacuum, hence there is no motion.”²⁹⁷

Aristotle credits Leukippos (about 450 BC) with founding atomic theory. Aristotle wrote that starting from the same premise as the Eleatics, Leukippos arrives at an opposite conclusion from them, articulated as: “without vacuum there is no motion; there is motion, hence there is vacuum.”²⁹⁸

The greatest exponent of atomic theory in antiquity was Demokritos of Abdera (460–370 BC), who adopted and extended it. According to Aristotle, Demokritos believed that atoms are hard, and have form and size. Demokritos also believed that atoms are indivisible by reason of their very small size; that they have no color, taste, or smell, since these are merely secondary or subjective properties. To Demokritos, atoms move spontaneously and ceaselessly in the vacuum; they come together by necessity and form aggregates by a sort of hook and eye mechanism, not by attractive forces. The motion of atoms, according to Demokritos, is “like that of dust particles seen in a sunbeam in still air in a room.”²⁹⁹ This “necessity” of Demokritos is not unlike the statistical considerations of the kinetic theory of gases postulated by Boltzmann and Maxwell more than 2000 years later.

Epikouros (341–270 BC) adopted the atomic theory and attributed weights to the atoms. To him, the atoms fall perpendicularly through the vacuum, but at undetermined times and in undetermined places they “swerve” and so enter into collision. The concept of “swerve” has some resemblance to the modern theory of indeterminacy.³⁰⁰

Following the early Greek era, interest in atomic theory waned and was only revived by the writings of Gassendi (1592–1655). For instance, Boyle and Lemery made extensive use of it.³⁰¹ Boyle states, “It seems not absurd to conceive that at the first Production of mixt Bodies, the Universal matter whereof they among other Parts of the Universe consisted, was actually divided into little particles of several sizes and shapes variously mov’d.”³⁰²

Another ardent atomist was Newton. He assumed that “particles attract one another by some force, which in immediate contact is exceedingly strong, at small distances performs the chymical operations, and reaches not far from the particles with any sensible effect.”³⁰³ With the assumption that a gas is made of particles repelling one another with a force varying inversely as the distance, Newton deduced Boyle’s law.³⁰⁴ Furthermore, he rejected Descartes’ idea that by their

²⁹⁷ibid., p. 164.

²⁹⁸ibid.

²⁹⁹ibid., p. 165.

³⁰⁰ibid., 165.

³⁰¹J.C. Gregory, *A Short History of Atomism: from Democritus to Bohr*, Black Ltd., London (1931).

³⁰²R. Boyle, *Sceptical Chymist*, p. 37, J. Cadwell, London (1661).

³⁰³I. Newton, *Opticks*, Query 31, p. 364 (1730).

³⁰⁴I. Newton, *Principia*, Book 2, prop. 23, theorem 18, p. 301, London (1687).

endless encounters some of the particles might have suffered attrition, and become “old worn particles” different from the rest.³⁰⁵

The modern formulation of atomic theory is attributed to John Dalton (1766–1844), who stated it in this form.³⁰⁶

- (1) The chemical elements are made of very minute indivisible particles of matter, called atoms, which preserve their individuality in all chemical changes.
- (2) All the atoms of the same element are identical in every respect, particularly in weight. Different elements have atoms that differ in weight. Each element is characterized by the weight of its atom.
- (3) Chemical combination occurs by the union of the atoms of the elements in simple numerical ratios, e.g., 1 atom A + 1 atom B; 1 atom A + 2 atoms B; 2 atoms A + 1 atom B; 2 atoms A + 2 atoms B, etc.

The above assumptions of atomic theory explain very well the laws of constant, multiple, and equivalent proportions. However, the theory could not predict the relative weights of atoms from the combining proportions unless the number of atoms in the particle of the compound is known, and this for many years remained the main point of dispute³⁰⁷ in the theory.

3.2.3.8.3 Electrochemical or dualistic theory

Two main contributors to electrochemical theory were Sir Humphrey Davy (1778–1829) in 1806 and Jons Jakob Berzelius (1779–1848) (Fig. 3.34) starting in 1811. Dualism was the basis of electrochemical theory. Oxygen, according to Lavoisier, was the central element in the system, so much so that he defined an acid as a compound of a radical with oxygen. Davy extended this concept by showing that a base was a compound of a metal with oxygen, and Berzelius (1779–1848) completed the dualistic system by assuming that, in all cases, a salt was a compound of an acid

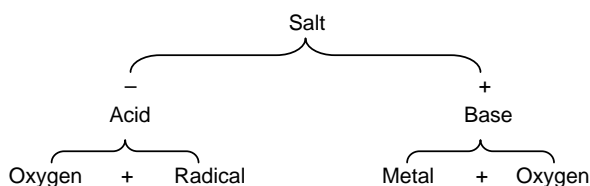
³⁰⁵I. Newton, *Opticks*, p. 376, William Innys, London (1730).

³⁰⁶J.R. Partington, *A Short History of Chemistry*, 3rd ed., p. 169, Dover Publications, New York (1989). In a lecture at the Royal Institution in 1810, Dalton attributed the origin of this atomic theory to attempts to explain his law of partial pressures (1801–1802), which states that the pressure exerted by a mixture of perfect gases is the sum of the pressures exerted by the individual gasses occupying the same volume. The partial pressure of a gas is the pressure a gas would exert if it occupied the container alone and if it behaved perfectly. Dalton's law of partial pressure is a more general form of Henry's law, which states that the amount of gas absorbed by a liquid is proportional to the pressure.

³⁰⁷Dalton attempted to resolve the discrepancy by making use of the general rules: (i) If only one compound of two elements is known, it is presumed to be binary (1 atom A + 1 atom B), unless some cause appears to the contrary. (ii) When two compounds exist, they are assumed to be binary (A + B) and ternary (A + 2B or 2A + B). When three compounds are observed, one is binary, two are ternary, and one quaternary (3A + B or A + 3B) [cited in J.R. Partington, *A Short History of Chemistry*, 3rd ed., pp. 169–170, Dover Publications, New York (1989)].



Figure 3.34 Jöns Jakob Berzelius (1779–1848), the great Swedish chemist and a major proponent of the electrochemical or dualistic theory. He produced elemental silicon in 1824. Silicon remained a chemical curiosity for about 60 years, until the metallurgical chemists took an interest in alloy steels. (Published with permission from the Deutsches Museum, Munich.)



Scheme 3.1 Illustration of the dualistic or electrochemical theory of the formation of chemical compounds as consisting of two distinct species that are of opposite polarities. An acid is a compound of oxygen and a radical. A base is a compound of oxygen and a metal. A salt is a compound of an acid and a base.

(actually an acid anhydride) with a base (actually a basic oxide), as illustrated in Scheme 3.1.³⁰⁸

Berzelius further noted that a similar dualism exists in electricity, influenced by his observation that salts in solution are decomposed by the electric current into bases, which travel to the negative pole and therefore seem to carry a positive charge, and acids, which travel to the positive pole and seem to carry a negative charge, and by so doing succeeded in linking the above conception with electrical polarity. Bases were thus seen as electropositive oxides, acids as electronegative oxides, or, as Berzelius expressed it, they are electropositive and electronegative substances, respectively.³⁰⁹

Davy postulated that chemical changes and electrical changes are distinct phenomena; both are produced by the same power acting in one case (electrical)

³⁰⁸J.R. Partington, *A Short History of Chemistry*, 3rd ed., p. 196, Dover Publications, New York (1989).

³⁰⁹*ibid.*, p. 197.

on masses, in the other case (chemical) on particles. The origin of electromotive force, he says, is contact, but when the metals are connected, the charges tend to become neutralized, and the chemical change restores the electromotive force. He observes that even apparently insoluble substances, such as glass, when moist, can be decomposed by the current, and acids may be transported through alkaline solutions provided they are not precipitated on the way.³¹⁰

Based on his studies of electrolysis, Berzelius in 1803 reported the following conclusions:³¹¹

- (1) Chemical compounds are decomposed by the electric current, and their components collect at the poles.
- (2) Combustible bodies (hydrogen), alkalis, and earths and metals travel to the negative pole; oxygen, acids and oxidized compounds travel to the positive pole.
- (3) The extent of decomposition is in compound proportion to the affinities and the surfaces of the poles. It is proportional to the quantity of electrical conductivity.
- (4) The chemical changes in decomposition depend firstly on the affinities of the components for the poles (metals), secondly on the affinities of the components for one another, and thirdly on the cohesion of the compounds formed.

According to Berzelius, elements may be divided into two groups on the basis of the charges they take up on contact. The arrangement of elements according to electron affinities is called the electrochemical series. He regarded oxygen as the most electronegative element, as evidenced by the fact that in an oxygen compound, oxygen was always negative. He arranged all of the elements in a series with oxygen at the top and potassium (the most electropositive element) at the bottom, and with hydrogen separating the two classes as follows. (The arrangement does not differ much from modern tables of electrode potentials.)³¹²

O, S, N, F, Cl, Br, I, Se, P, As, Cr, Mo, W, B, C, Sb, Te, Ta, Ti, Si, H;
 Au, Os, Ir, Pt, Rh, Pd, Hg, Ag, Cu, U, Bi, Sn, Pb, Cd, Co, Ni, Fe, Zn, Mn,
 Ce Th, Zr, Al, Y, Be, Mg, Ca, Sr, Ba, Li, Na, K

The order may vary with temperature. He believed that the strength of an acid or base is greater the more pronounced the electrochemical character of the radical. Berzelius also believed that a weak base may act as an acid toward a strong base (e.g., alumina and caustic soda), and a weak acid may act as base toward a strong acid (e.g., boric acid and sulfuric acid).³¹³

³¹⁰H. Davy, *Elements of Chemical Philosophy*, p. 160, Johnson and Co., London (1812).

³¹¹J.J. Berzelius and Hisinger, "Versuch, betreffend die Wirkung der elektrischen Säule auf Salze und auf einige von von ihren Basen," *N. Allgem. J. Chem.* **I**, 115 (1803) [cited by J.R. Partington, *A Short History of Chemistry*, 3rd ed., p. 192, Dover Publications, New York (1989)].

³¹²*ibid.*, p. 200.

³¹³*ibid.*

3.2.3.8.4 Laws of electrolysis

Michael Faraday³¹⁴ (1791–1867) postulated the laws of electrolysis as (i) the amount of decomposition in electrolysis is proportional to the current strength and the time, i.e., to the quantity of electricity passing (in 1832), and (ii) the weights of substances deposited by the same current are in the proportion of their chemical equivalent weights (in 1833).³¹⁵

William Whewell invented these names for Faraday, including electrolysis, electrolyte, anode, cathode, anion, and cation,³¹⁶ while von Grotthus proposed in 1805 a theory of the mechanism of current conduction in solutions.³¹⁷

3.2.3.8.5 Avogadro's hypothesis

Amedeo Avogadro (1776–1856) (Fig. 3.35) postulated (in 1811) that equal volumes of all gases, at the same temperature and pressure, contain identical numbers of particles (molecules). The molecules of elementary gases, e.g., oxygen, hydrogen, and chlorine, he says, consist of two (or perhaps a multiple of



Figure 3.35 Amedeo Avogadro (1776–1856), who postulated in 1811 that equal volumes of all gases, at the same temperature and pressure, contain the same number of molecules. (Published with permission from the Deutsches Museum.)

³¹⁴A chemist physicist, Michael Faraday made enormous contributions to physics and chemistry. His discoveries of electromagnetic induction and of specific inductive capacity, and in electrolysis are especially noteworthy. His papers on physics are collected in his *Experimental Researches in Electricity* (3 vols, 1839; 2nd ed., 1849); those on chemistry are collected in his “Researches in Chemistry and Physics” (1859), and include the discovery of carbon perchloride (C_2Cl_6) in 1821, of the liquefaction of gases (1823–1845), of benzene in 1825, of the isomeric sulphonic acids of naphthalene in 1826, and the preparation of colloidal gold (including the description of the so called Tyndall phenomenon in 1857 [cited in J.R. Partington, *A Short History of Chemistry*, 3rd ed., pp. 193–194, Dover Publications, New York (1989)].

³¹⁵*ibid.*, p. 194.

³¹⁶*ibid.*

³¹⁷*ibid.*; also cited in *Ann. Chimie* **LVIII**, 54 (1806); *Ostwald's Klassiker*, No. 152.

two) atoms, and not (as Dalton believed) of single atoms.³¹⁸ He showed that his hypothesis reconciles Dalton's atomic theory with Gay-Lussac's law of combining volumes, if one assumes that very simple relations also exist between volumes of gaseous substances and the numbers of simple or compound molecules that form them.³¹⁹

3.2.3.9 Development of various fields in chemistry

In this section we briefly review some of the important developments in the key fields of chemistry—organic, physical, and polymer chemistry—that enabled and continue to enable lithographic science and technology.

3.2.3.9.1 Development of organic chemistry

The foundation of organic chemistry as practiced today dates back to 1828 when Friedrich Wöhler (1800–1882) (see Fig. 3.33) showed that urea, a typical organic compound, could be produced by merely heating ammonium cyanate, an inorganic compound; both compounds are isomeric. The prevailing view at the time was that in the organic world, the existence of a mysterious “vital force” was responsible for the formation of compounds, and their preparation in the laboratory could hardly be expected.³²⁰ The impact of Wöhler's discovery resulted in a paradigmatic shift in the way organic chemistry and organic reactions have been practiced and analyzed, respectively, ever since. The majority of resists in use today in lithography are made of organic polymeric materials. The first steps on the path to these materials were no doubt laid by Wöhler.

Jean Baptiste Dumas (1800–1884) formulated the theory of substitution thus:³²¹

- (i) When a substance containing hydrogen is submitted to the dehydrogenating action of chlorine, of bromine, of iodine, of oxygen, etc., for each atom of hydrogen that it loses it gains an atom of chlorine, of bromine, or half an atom of oxygen.
- (ii) When the compound contains oxygen the same rule holds good without modification.
- (iii) When the hydrogenized body contains water, this loses its hydrogen without replacement, and then, if a further quantity of hydrogen is replaced, then substitution takes place, as in the former cases.

³¹⁸J.R. Partington, *A Short History of Chemistry*, 3rd ed., Dover Publications, New York, pp. 208–210 (1989).

³¹⁹*ibid.*, p. 209.

³²⁰*ibid.*, p. 220.

³²¹*ibid.*, p. 241.

Other notable discoveries in organic chemistry that directly influenced the development of lithography include Peter Greiss' discovery in 1860 of azo compounds, which are obtained by the action of nitrous acid in the cold on solution of salts of aromatic amines such as aniline. These azo compounds form the starting point in the preparation of numerous organic compounds, including azo dyes, the first member of which (aminoazo-benzene, "aniline yellow") was obtained by Mène in 1861, and even diazonaphthoquinone (DNQ) sensitizer used in resist applications for g-line lithography, h-line lithography, and i-line lithography and lithographic printing plates.

3.2.3.9.2 The formula of benzene

August Kekulé (1829–1896) postulated the hexagonal formula³²² for benzene in 1866 (see Fig. 3.36), in which the six atoms of carbon in the benzene ring were regarded as being joined alternatively by single and double linkages, so as to preserve the tetravalency of carbon.³²³ The importance of Kekulé's benzene formula in organic chemistry cannot be overemphasized. It explains isomerism in the derivatives of benzene and has proved sufficiently useful during years of intensive work since it was proposed. X-ray studies of the structure of aromatic compounds have also confirmed the existence of the flat hexagonal ring of carbon atoms.³²⁴ Today, benzene is a major feedstock used in the manufacture of a great majority of resists used in all lithographic technologies, except ArF lithography.

Optical activity involving the ability to rotate the plane of polarized light was first observed by Biot in 1815–1835 in a number of naturally occurring organic compounds, such as turpentine, camphor, sugars, and tartaric acid. Since optically active compounds exhibited this property both in their crystalline form as well as in solutions, it was reasoned that this property is inherent in the molecules. Mitscherlich in 1844 observed that although tartaric and racemic acids are isomeric, the former and its salt are optically active, while racemic acid is inactive.³²⁵

In an attempt to elucidate the observation of Mitscherlich, Pasteur in 1848 observed that the crystals of tartaric acid are characterized by small facets that

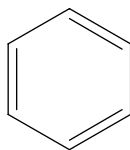


Figure 3.36 Structural formula of benzene proposed by Kekulé.

³²²Kekulé reports that the origin of the discovery of the structure of benzene appeared to him while he was asleep in his study in Ghent, whereby he saw the long chains of carbon atoms like snakes twisting and curling until one "gripped its own tail and the picture whirled scornfully before my eyes" [cited in Benzolfest: Rede, *Berichte XXIII*, 1302 (1890)].

³²³J.R. Partington, *A Short History of Chemistry*, 3rd ed., p. 290, Dover Publications, New York (1989).

³²⁴*ibid.*, p. 292.

³²⁵*ibid.*, p. 300.

had unaccountably been overlooked by Mitscherlich and were similar to the hemihedral facets observed by Haüy on optically active quartz. Quartz crystals are in two forms, i.e., right and left handed, depending on the position of the facets. The two forms are related to each other by the same relation that an object has with its own mirror image. Herschel pointed out in 1821 that this was probably related to Biot's observation that some quartz crystals rotated the plane of polarized light to the right and some to the left.³²⁶

Pasteur's other main important discovery, among many others in this field, was the resolution of sodium ammonium racemate, an optically inactive compound, by crystallization (1848–1850). In describing his discovery, he remarks:³²⁷

“I carefully separated the crystals which were hemihedral to the right from those which were hemihedral to the left, and examined their solutions separately in the polarizing apparatus. I then saw with no less surprise than pleasure that the crystals hemihedral to the right deviated the plane of polarization to the right, and that those hemihedral to the left deviated it to the left; and when I took an equal weight of each of the two kinds of crystals, the mixed solution was indifferent towards the light in consequence of the neutralization of the two equal and opposite individual deviations.”

The interpretation of Pasteur's results in terms of the relation of optical activity to the presence of an asymmetric carbon atom was given independently in 1874 by van't Hoff and LeBel, and in so doing, laid the foundation of stereochemistry. According to van't Hoff:³²⁸

“In the case where the four affinities of an atom of carbon are saturated by four different univalent groups, two and only two different tetrahedra can be obtained, of which one is the mirror image of the other. . . two structural formulae of isomers in space.”

Earlier in 1867 Kekulé had described the tetrahedral model of the carbon atom, with a central sphere as the atom and four wires pointing to the corners of the tetrahedron as the valencies. Van't Hoff also stated that “Every carbon compound which in solution impresses a deviation on the plane of polarization possesses an asymmetric carbon atom,” i.e., one in which the four groups attached to the carbon are all different.³²⁹

It has since been established that optical activity can exist in compounds with no asymmetric carbon atoms, as long as they can form two nonsuperimposable molecular configurations. For instance, optical activity has been established in the case of compounds of selenium, tin, sulfur, chromium, etc., some of the compounds being quite free of carbon.³³⁰ Optical activity in modern chemistry is believed to originate in the enantiomorphous molecular configurations of compounds that possess it.

³²⁶ibid., pp. 300–301.

³²⁷Alembic Club Reprint No. 14; *Delephine, Bull. Soc. Chim.* **XXXVII** (1925) [cited in: J.R. Partington, *A Short History of Chemistry*, 3rd ed., p. 302, Dover Publications, New York (1989)].

³²⁸J.R. Partington, *A Short History of Chemistry*, 3rd ed., p. 304, Dover Publications, New York (1989).

³²⁹ibid., p. 305.

³³⁰ibid., pp. 306–307.

3.2.3.9.3 Development of physical chemistry

Influenced by the revolution in chemistry engendered by Lavoisier in the late eighteenth century, prominent chemists and physicists who succeeded him sought to understand the physical basis of chemical phenomena, from which they formulated many significant theories that laid the foundation of the main branches of modern physical chemistry, and for that matter, the whole of chemistry. Some of these theories and related developments are reviewed below.

(1) *Law of mass action*—The law of mass action was first proposed³³¹ with full generality by Guldberg and Waage in 1864.³³² They postulated that the “force” responsible for the equilibrium reaction/transformation is proportional to the product of the masses involved in the equilibrium reaction,



which is given by kpq (for the forward reaction) and $k'p'q'$ for the reverse reaction, where k and k' are the activity coefficients for the forward and backward reaction, p and q are the active masses (defined as number of molecules per unit volume) for substances A and B , and p' and q' are active masses for substances A' and B' , respectively. The value of the active masses can be determined experimentally, from which the ratio k/k' can be easily determined for any original condition of the four substances.³³³

In 1877 van't Hoff replaced the indefinite “force” by the velocity of reaction. The velocity with which A and B react to form A' and B' he expressed as $v' = kpq$, and the velocity with which A' and B' react to form A and B he expressed as $v = k'p'q'$. The actual velocity of the complete reaction is therefore given by $V = v - v'$; $kpq - k'p'q'$. At equilibrium, $V = 0$ and $p'q'/pq = k/k'$.³³⁴

Kinetics, the branch of physical chemistry dealing with rates of chemical reactions, therefore had its origins in the above-mentioned works of Guldberg and Waage as well as van't Hoff. Today, the techniques developed by these scientists are used to study rates of various reactions involved in lithographic patterning. A few examples include deprotection kinetics of chemical amplification resists, development kinetics of resists, kinetics of photolysis of photoacid generators in

³³¹Earlier in 1850, Ludwig Wilhelmy was the first person to investigate the rate of progress of a chemical reaction, i.e., the inversion of cane sugar by water in the presence of an acid. This reaction is particularly suited to experimental investigation because its progress can be followed by the polarimeter, without disturbing the conditions of the reacting system. Wilhelmy found that in the presence of a large and practically constant mass of water, the amount of sugar changed in a small interval of time, dt , is proportional to the amount, M , actually present, $dM/dt = kM$, where k is a constant, and leading to the equation after integration, $\log M = kt + \text{const}$. Also in 1850, Williamson pointed out the dynamical character of a chemical equilibrium, namely, that it is the result of two opposite changes taking place at equal rates [cited in J.R. Partington, *A Short History of Chemistry*, 3rd ed., p. 324, Dover Publications, New York (1989)].

³³²J.R. Partington, *A Short History of Chemistry*, 3rd ed., pp. 325–327, Dover Publications, New York (1989).

³³³*ibid.*, pp. 326–327.

³³⁴*ibid.*, p. 327.

chemical amplification resists, and color center formation in quartz glass of lithographic exposure tools, to mention but a few.

(2) *Thermochemistry*—The foundations of the branch of physical chemistry dealing with thermochemistry was laid by Lavoisier and Laplace, who through their collaborative efforts showed that the heat evolved in a reaction is equal to the heat absorbed in the reverse reaction. They investigated the specific and latent heats of a number of substances, as well as the amount of heat generated in combustion. It was Hess who in 1840 enunciated the law that now bears his name—Hess's law³³⁵—that the evolution of heat in a reaction is the same whether the process is accomplished in one step or in a number of stages. As an illustration, the heat of formation of CO₂ is the sum of the heat of the formation of CO and the heat of oxidation of CO to CO₂.³³⁶

When the mechanical theory of heat was enunciated, Hess's law was soon realized to be a consequence of the law of conservation of energy, which states that energy cannot be created nor destroyed, but can be transformed from one form to the other. A consideration of the second law of thermodynamics, enunciated by Carnot in 1824, influenced Helmholtz in 1882 to estimate the work done by the chemical forces as not the heat evolved in the reaction, but the largest quantity of work that can be gained when the reaction is carried out in a reversible manner, e.g., electrical work in a reversible cell. This maximum work is regarded as the diminution of the free or available energy of the system, while the heat evolved is regarded as a measure of the diminution of the total energy of the system.³³⁷

The application of the second law of thermodynamics to chemistry, first occurring notably in the study of dissociation phenomena in solids, influenced Horstman in 1873 to point out that such changes are exactly similar to physical changes of state, and that the thermodynamic equation derived by Clapeyron and Clausius for changes of state are also applicable here, i.e., $dp/dT = Q/T(v' - v)$, where p is the dissociation pressure, Q is the heat of dissociation, T is the absolute temperature, and v' and v are the volumes of the system after and before dissociation. In the case in which a gas or vapor formed is supposed to behave as an ideal gas, and the volume of the solids is neglected in comparison with that of the gas, the equation becomes $d \log p/dT = Q/RT^2$, where R is the universal gas constant.³³⁸

Between 1884 and 1886, van't Hoff generalized this equation so as to make it applicable to all cases of chemical equilibrium between gases or substances in dilute solution. Here, he replaces p with the equilibrium constant K in the above equation.³³⁹ However, although the integration of this equation gives a means of

³³⁵G.H. Hess, "Thermochemische Untersuchungen," *Ann. Phys.* **1**, 385 (1840); *Ostwald's Klassiker* No. 9 [cited in J.R. Partington, *A Short History of Chemistry*, 3rd ed., pp. 327–328, Dover Publications, New York (1989)].

³³⁶J.R. Partington, *A Short History of Chemistry*, 3rd ed., p. 327, Dover Publications, New York (1989).

³³⁷*Ostwald's Klassiker* No. 124 [cited in J.R. Partington, *A Short History of Chemistry*, 3rd ed., p. 328, Dover Publications, New York (1989)].

³³⁸J.R. Partington, *A Short History of Chemistry*, 3rd ed., pp. 328–329, Dover Publications, New York (1989).

³³⁹*ibid.*, p. 329.

finding Q from measurements of the effect of temperature on K , it does not solve the problem of calculating K from the heat of reaction Q , since the equation contains an unknown constant of integration: $\log K = -Q/RT + \text{constant}$. It was in 1906 that Nernst showed that by making another assumption it was possible to calculate the value of this constant, and the problem of finding K and hence the affinity from the heat of reaction was solved.³⁴⁰

(3) *The phase rule*—The phase rule enunciated by Gibbs in 1876 is the most useful guide for predicting equilibrium in systems that are not homogenous. The rule deals with systems containing more than two different bodies, called phases, which are separated by boundaries, e.g., liquid and gas, or liquid and solid. Such a system can be built up from a certain minimum number of chemical substances called components. In order that a system shall be in equilibrium, Gibbs asserts, certain conditions of temperature, pressure, and the concentrations in the various phases must be satisfied. He called the number of these variables that must be fixed before there is equilibrium the number of degrees of freedom of the system. If P is the number of phases, C is the number of components, and F is the number of degrees of freedom, then Gibbs' phase rule states that $P + F = C + 2$.³⁴¹

(4) *Theory of solutions*—The modern theory of solutions is primarily based on the research works of Raoult and Pfeffer. Raoult had shown that the depression of the freezing point or of the vapor pressure of a solvent by the dissolved substance could be used to calculate the molecular weight of the latter in the following manner. If C represents the depression due to P grams in 100 grams of solvent, then $CM/P = K$, where M is the molecular weight and K is a constant representing the value of C when $P = M$, i.e., the molecular depression of the freezing point, which is the same for a given solvent for all dissolved substances.³⁴²

Pfeffer's research had been on osmotic pressure. It had been well established from early in the eighteenth century that when a solution is separated from pure water by a semipermeable membrane such as a bladder, the water permeates the membrane and dilutes the solution, setting up a pressure if the volume of the latter is prevented from increasing. This pressure was termed osmotic pressure. Pfeffer in 1877 was able, by depositing copper ferrocyanide on the walls of a porous pot, to prepare semipermeable membranes that were permeable to water, but were not permeable to dissolved sugar. Using these semipermeable membranes, he was able to measure the osmotic pressures of solutions.³⁴³

Interpreting Pfeffer's results, van't Hoff showed in 1886 that the osmotic pressure exerted by a dissolved substance is equal to the pressure that it would exert as a gas confined in a space equal to the volume of the solution. He remarks, "It gradually appeared that there is a fundamental analogy, nay almost an identity, with gases, more especially in their physical aspect, if only in solutions we consider

³⁴⁰ibid., p. 329.

³⁴¹ibid., pp. 330–331.

³⁴²ibid., pp. 331–332.

³⁴³ibid., p. 332.

the so-called osmotic pressure instead of the ordinary gaseous pressure . . . we are not here dealing with a fanciful analogy, but with one which is fundamental.”³⁴⁴

By applying the principles of thermodynamics, van't Hoff was able to deduce a quantitative connection between osmotic pressure and the depression of the freezing point or lowering of the vapor pressure.³⁴⁵ However, like Raoult before him, he was not able to explain why solutions of salts in water exhibit higher osmotic pressures than they would be expected to do on the basis of van't Hoff's theory. The full explanation of this phenomenon was offered in the theory of electrolytic dissociation³⁴⁶ of Arrhenius (Fig. 3.37), which was based on the fact that solutions that showed abnormally high osmotic pressures were conductors of electricity.³⁴⁷

(5) *Theory of electrolytic dissociation*—Between 1853 and 1859, Hittorf showed by numerous experiments, to which Arrhenius drew attention, that the current in electrolysis is carried unequally by the two ions, which move with different speeds; he called the fraction carried by the anion the transport number n . Extending Hittorf's findings, Friedrich W.G. Kohlrausch showed in 1874 that the equivalent conductivity, i.e., the specific conductivity κ divided by the concentration of the solution in equivalents per cubic centimeter, $\kappa/c = \Lambda$, of a very dilute solution of a salt is the sum of two terms, one depending only on the cation and the other only on the anion: $\Lambda = l_c + l_a$. He called l_c and l_a the mobilities of the ions. If n is Hittorf's transport number, then $l_a = n\Lambda$.³⁴⁸



Figure 3.37 Svante Arrhenius (1859–1927), who proposed the theory of electrolytic dissociations (1887), investigated the viscosity of solutions, the effect of temperature on reaction rates (1889), etc. (Published with permission from the Deutsches Museum, Munich.)

³⁴⁴ibid., p. 333.

³⁴⁵ibid.

³⁴⁶The full statement of the theory of electrolytic dissociation was first published in the *Zeits. Phys. Chem.* **1**, 631 (1887).

³⁴⁷ibid., pp. 332–333.

³⁴⁸ibid., p. 324.

When Raoult's results were examined in the light of Hittort's and Kohlrausch's results, it became apparent that in solutions, salt dissociated into its two ions in a process called ionization. The electric current serves to drive the positively and negatively charged ions toward the electrodes of opposite polarity. Given that the number of particles in a given salt solution is increased by ionization, the abnormally high osmotic pressures and the related abnormal depressions of the freezing point were thus explained.³⁴⁹

Arrhenius showed that the degree of ionization calculated from the electrical conductivity, Λ/Λ_{∞} , where Λ_{∞} is the equivalent conductivity at infinite dilution (when there is complete ionization), was approximately the same as that calculated from the deviations from Raoult's law in the case of the freezing point measurement. Obtaining nearly identical results with two independent methods substantiated Arrhenius' theory. Today, there is a slight modification to the original formulation of Arrhenius's theory in some respects, involving mostly strong acids, bases, and salts, which are now supposed to be practically completely ionized in fairly dilute solutions, the deviations from the results for complete ionization being ascribed to interaction between the ions of the opposite charge, which causes a reduction in the mobilities of the ions and hence a diminution of Λ (Debye and Huckel, 1923).³⁵⁰

Important extensions of Arrhenius' theory were made by Walther Nernst (1864–1941) (see Fig. 3.38), who put forward the theory of galvanic cells in 1889, which states that the production of electromotive force in galvanic cells could be explained in terms of a "solution pressure" of the metal electrodes, tending to throw off charged ions into the solution, this tendency being balanced by the osmotic pressure of the dissolved ions. He also introduced in 1889 the theory of solubility product, which explains precipitation reactions. In addition, he investigated diffusion in solutions, including liquid contact potentials (1888–1889), and he postulated the so-called heat theorem ("third law of thermodynamics") (1906), which states that the entropy change is zero at absolute zero.³⁵¹

Today, these theories of solutions and of electrolytic solutions are used in the analysis of the solvent development of exposed resists, lithographic mask degradation due to corrosion, electromigration of chromium ions, etc.

(6) *Law of reactions*—Henry Le Chatelier (1850–1936) put forward the law of reaction, which governs the effects of pressure, temperature, concentration, and catalyst on reaction equilibrium. It states that "if a change of conditions (stress) is applied to a system at equilibrium, the system will respond in the way that best reduces the stress in reaching a new state of equilibrium."³⁵²

(7) *Periodic law and the periodic table*—The periodic law, which first disclosed a chemical and material relationship among chemical elements, represents one of the highest achievements of the revolution in chemistry that Lavoisier started. Its roots stretch all the way back to Johann Wolfgang Döbereiner

³⁴⁹ibid., p. 335.

³⁵⁰ibid., pp. 335–336.

³⁵¹ibid., pp. 336–338.

³⁵²K.W. Whitten and K.D. Gailey, *General Chemistry with Qualitative Analysis*, p. 427, Saunders College Publishing, Philadelphia (1981).



Figure 3.38 Walther Hermann Nernst (1864–1941), showed in 1889 that the production of electromotive force in galvanic cells could be explained in terms of a “solution pressure” of the metal electrodes. He made substantial contributions to chemical thermodynamics. (Published with permission from the Deutsches Museum, Munich.)

(1780–1849), who in 1817 and 1829 reported that in certain groups of three elements, e.g., Ca, Sr, and Ba, the atomic weight of the middle element was approximately the mean of those of the first and the third. These were called Döbreiner’s triads.³⁵³

The periodic law was proposed almost simultaneously and quite independently by Dmitri Ivanovich Mendeleev³⁵⁴ (see Fig. 3.39) in Russia and Julius Lothar Meyer³⁵⁵ (see Fig. 3.40) in Germany. In 1869 Mendeleev published his periodic law, which states that “the properties of the elements are in periodic dependence upon their atomic weights.” Lothar Meyer had previously reported (also in 1869) that certain triads of elements such as lithium, sodium, and potassium, as well as magnesium, calcium, and strontium, exhibit similar chemical properties. He had published in 1870 his well-known atomic volume curve, in which the periodic dependence of a quantitative property was shown as a function of the atomic weight, revealing that, as the atomic weight steadily increases, the property alternately rises and falls over definite periods of the elements. Following leads of this type, Mendeleev gave each known element a position in a single grand ensemble

³⁵³For the Döbreiner triads, see “Auszug eines Briefes vom Hofrath Wurzer, Prof. der Chemie zu Marburg,” *Ann. Phys.*, **LVI**, 331 (1817) (Ca, Sr, Ba); “An attempt to group elementary substances according to their analogies,” *Ann. Phys.*, **XV**, 301 (1829) (other triads); *Ostwald Klassiker* No. 66; J.R. Partington, *A Short History of Chemistry*, 3rd ed., p. 343, Dover Publications, New York (1989).

³⁵⁴D.I. Mendeleev, “Essai d’une système des elements,” *J. Russ. Phys. Chem. Soc.* **I**, 60 (1869); see also J.R. Partington, *A Short History of Chemistry*, 3rd ed., p. 348, Dover Publications, New York (1989).

³⁵⁵J.R. Partington, *A Short History of Chemistry*, 3rd ed., pp. 348–349, Dover Publications, New York (1989).

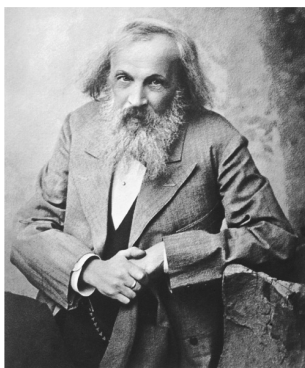


Figure 3.39 Dmitri Ivanovich Mendeleev (1834–1907), who independently formulated the periodic law of the elements and constructed the periodic table. (Published with permission from the Deutsches Museum, Munich.)

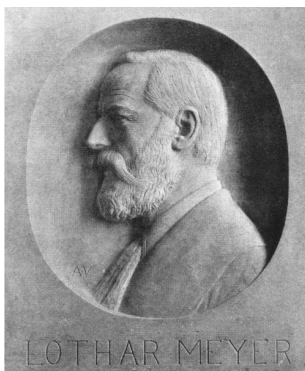


Figure 3.40 Julius Lothar Mayer (1830–1895), who pointed out that triads of elements, such as lithium, sodium, and potassium, and magnesium, calcium, and strontium, had similar chemical properties. He independently formulated the periodic law of the elements at about the same time as Mendeleev. (Published with permission from the Deutsches Museum, Munich.)

now called the periodic table, and identified gaps that he predicted would be filled by yet undiscovered elements. These then-undiscovered elements included gallium (discovered in 1875), scandium (discovered in 1879), and germanium.³⁵⁶

The modern periodic table, in which the elements are arranged according to the atomic numbers in columns (groups) and rows (periods) and presented so as to emphasize their periodic properties,³⁵⁷ from hydrogen 1 to lawrencium 103, is

³⁵⁶F. Seitz and N.G. Einspruch, *Electronic Genie: The Tangled History of Silicon*, p. 3, University of Illinois Press, Urbana (1999); J.R. Partington, *A Short History of Chemistry*, 3rd ed., pp. 346–349, Dover Publications, New York (1989).

³⁵⁷The periodic law unearthed a number of previously unsuspected analogies among the elements, and as a result, stimulated the study of inorganic chemistry, which had been rather neglected in the second half of the nineteenth century owing to the popularity of organic chemistry at that time.

shown in Table 3.1.³⁵⁸ While Dmitri Mendeleev is usually credited with the form of the modern periodic table, many other excellent chemists made profound contributions to its development, including Johann Döbereiner, John Newlands, Lothar Meyer, Sir William Ramsay, and others.³⁵⁹

The modern statement of the periodic law is that the chemical and physical properties of the elements vary in a periodic manner with their atomic numbers.³⁶⁰ The periodic table is now an indispensable reference tool for scientists because of its ability to predict the chemical behavior of elements. The high frequency of its use by scientists highlights the central role it plays in making sense out of what otherwise might be a chaotic jumble of facts about the elements and their molecular combinations,³⁶¹ bearing in mind the fact that even with the variety and complexity of our world, everything in it—air, water, rocks, living tissue, and the almost infinite number of other objects and materials around us—is actually made up of only a limited number of chemical elements. We know today that only 92 such elements exist naturally on the Earth, although several new artificial elements have been created under laboratory conditions.

What is then responsible for the periodic behavior of the elements? And why do elements within a particular group have similar chemical behavior? The explanation stems from the fact that atoms are attracted to each other by electric forces. The atomic number, i.e., the number of positively charged protons in the nucleus, determines how many negatively charged electrons are contained in the atoms of a particular element, and it is the outer-shell electrons, also called valence electrons, that determine the reactivity, or how strongly and in what way the atoms will bind with other atoms. The chemical behavior of an element is thus ultimately determined by the way in which the electrons orbiting its nucleus are structured.³⁶²

Elements in the same group of the periodic table possess the same number of electrons in their outer shells and are therefore said to have the same valence electronic configuration, and consequently similar chemical and physical properties. As electrons are filled into the inner shells of an atom, the outer shell takes on a specific valence configuration that is determined by the rules that govern how many electrons can occupy a particular shell, as described above in the section on quantum mechanics. It is this very regularity in the number of outer-shell electrons that explains the periodic behavior shown by the elements as the atomic number increases. Similarly, properties such as atomic size are determined by the number of shells an atom contains. For example, the radius of the atoms of the elements within a particular group in the periodic table increases from the top of the group to the bottom.³⁶³

³⁵⁸A. Stwertka, *A Guide to the Elements*, p. 6, Oxford University Press, Oxford (2002).

³⁵⁹J.R. Partington, *A Short History of Chemistry*, 3rd ed., pp. 342–349, Dover Publications, New York (1989).

³⁶⁰A. Stwertka, *A Guide to the Elements*, pp. 6–15, Oxford University Press, Oxford (2002).

³⁶¹*ibid.*, p. 15.

³⁶²*ibid.*, p. 13.

³⁶³*ibid.*, pp. 14–15.

Table 3.1 Modern Periodic Table.³⁶⁴

Group	1	2	3	4	5	6	7	8	9	10	11	12	13	14	15	16	17	18	
Period																			
1	^1H																		^2He
2	^3Li	^4Be											^5B	^6C	^7N	^8O	^9F		^{10}Ne
3	^{11}Na	^{12}Mg											^{13}Al	^{14}Si	^{15}P	^{16}S	^{17}Cl		^{18}Ar
4	^{19}K	^{20}Ca	^{21}Sc	^{22}Ti	^{23}V	^{24}Cr	^{25}Mn	^{26}Fe	^{27}Co	^{28}Ni	^{29}Cu	^{30}Zn	^{31}Ga	^{32}Ge	^{33}As	^{34}Se	^{35}Br		^{36}Kr
5	^{37}Rb	^{38}Sr	^{39}Y	^{41}Zr	^{41}Nb	^{42}Mo	^{43}Tc	^{44}Ru	^{45}Rh	^{46}Pd	^{47}Ag	^{48}Cd	^{49}In	^{50}Sn	^{51}Sb	^{52}Te	^{53}I		^{54}Xe
6	^{55}Cs	^{56}Ba	^{57}La	^{72}Hf	^{73}Ta	^{74}W	^{75}Re	^{76}Os	^{77}Ir	^{78}Pt	^{79}Hg	^{80}Hg	^{81}Tl	^{82}Pb	^{83}Bi	^{84}Po	^{85}At		^{86}Rn
7	^{87}Fr	^{88}Ra	$^{**89}\text{Ac}$	^{104}Rf	^{105}Db	^{106}Sg	^{107}Bh	^{108}Hs	^{109}Mt	^{110}Uun	^{111}Uun	^{112}Uub		^{114}Uuq					
* Lanthanides			^{58}Ce	^{59}Pr	^{60}Nd	^{61}Pm	^{62}Sm	^{63}Eu	^{64}Gd	^{65}Tb	^{66}Dy	^{67}Ho	^{68}Er	^{69}Tm	^{70}Tb	^{71}Lu			
* Actinides			^{90}Th	^{91}Pa	^{92}U	^{93}Np	^{94}Pu	^{95}Am	^{96}Cm	^{97}Bk	^{98}Cf	^{99}Es	^{100}Fm	^{101}Md	^{102}No	^{103}Lr			

Today, in lithography, knowledge of the periodic table is employed in the rational design of lithographic chemicals and materials. Specifically, H, Si, C, O, N, F, and S are the most commonly used elements in lithography. Si is primarily used in the fabrication of wafer substrates and organosilicon resists, as well as in the synthesis of optical glass/quartz elements of lithographic exposure tools. C, O, F, and S are widely used in the synthesis of resists and resist sensitizers.

(8) *Electronic theory of valency*—Influenced by Bohr’s model of the atom and developments in quantum physics, in 1916, G.N. Lewis proposed a simple model of the atom in which the outer layer of electrons is eight in the atoms of inert gases, and tends to become eight in other atoms either (i) by gain or loss of outer electrons, forming negative or positive ions, or (ii) by sharing electrons in pairs with other atoms, forming ordinary valency bonds.³⁶⁵ This theory was extended to heavier atoms by I. Langmuir in 1919.³⁶⁶

Two types of bonds,³⁶⁷ namely, ionic and nonionic (covalent) bonds, were recognized early on in the formulation of the electronic theory of valency. Lewis made clear distinctions between ionic and covalent bonds. The first are formed by transfer of electrons and production of separate charged ions (as explained by Kossel, 1916), the second, according to Lewis, by sharing of electrons in pairs, a single bond consisting of one shared pair, a double bond of two, and a triple bond of three.

A type of bond produced when both electrons of a pair come from the same atom was first described by Langmuir (1919).³⁶⁸ G.A. Perkins (1921)³⁶⁹ drew special attention to it, as did Lowry (1923),³⁷⁰ who called it a “mixed double bond” or “dative bond,” and Sidgwick (1923),³⁷¹ who called it a “coordinated link,” since such bonds are present in the so-called coordination compounds. In

³⁶⁴ibid., p. 6.

³⁶⁵G.N. Lewis, “The atom and the molecule,” *J. Amer. Chem. Soc.* **XXXVIII**, 762 (1916); W. Kossel, “Über Molekülbildung als Frage des Atombaus,” *Ann. Phys.* **XLIX**, 229 (1916).

³⁶⁶I. Langmuir, “The arrangement of electrons in atoms and molecules,” *J. Amer. Chem. Soc.* **XLI**, 868 (1919); **XLII**, 274 (1920); J.R. Partington, *A Short History of Chemistry*, 3rd ed., pp. 360–362, Dover Publications, New York (1989).

³⁶⁷J.R. Partington, *A Short History of Chemistry*, 3rd ed., Dover Publications, New York, pp. 361–362 (1989).

³⁶⁸I. Langmuir, “The arrangement of electrons in atoms and molecules,” *J. Amer. Chem. Soc.* **XLI**, 868 (1919); **XLII**, 274 (1920); J.R. Partington, *A Short History of Chemistry*, 3rd ed., Dover Publications, New York, pp. 360–362 (1989).

³⁶⁹G.A. Perkins, “The expression of the octet theory of valence in structural formulas,” *Philippine J. Sci.* **XIX**, 1 (1921); also cited in J.R. Partington, *A Short History of Chemistry*, 3rd ed., Dover Publications, New York, pp. 366–367 (1989).

³⁷⁰T.M. Lowry, “The electronic theory of valency. Part I. Intramolecular ionisation,” *Trans. Faraday Soc.* **XVIII**, p. 285 (1923); “Studies of Electrovalency, Part I. The polarity of double bonds,” *J. Chem. Soc.* **CXXIII**, 822 (1923); *J. Soc. Chem. Ind.* **XLII**, “Coordination and the election,” 1004R, “Coordination and acidity,” 1048R (1923); also cited in J.R. Partington, *A Short History of Chemistry*, 3rd ed., p. 368, Dover Publications, New York (1989).

³⁷¹N.V. Sidgwick, “Coordination compounds and Boron atom,” *J. Chem. Soc.* **CXIII**, 725 (1923); *The Electronic Theory of Valency*, Oxford (1927); W.G. Palmer, *Valency, Classical and Modern*, Cambridge (1944); also cited in J.R. Partington, *A Short History of Chemistry*, 3rd ed., Dover Publications, New York, p. 368 (1989).

1933, Pauling³⁷² proposed that different types of bonds in molecules can become equalized by rapid shifting of electrons, through a process called “resonance.” The resulting “resonance hybrid” contains contributions from the different possible electronic configurations.³⁷³

Coordination compounds, also called “molecular compounds,” formed by the addition of molecules in which the valencies of the atoms are apparently satisfied, were first investigated by Werner in 1893, who showed that the number of atoms or groups associated with a central atom is often four or six, the “coordination number” (other coordination numbers, up to a maximum of eight, occur, but less often).³⁷⁴ Various types of isomerism, including optical isomerism, are fairly well explained by Werner’s theory. Sidgwick showed in 1923 that groups that coordinate with metals do so by contributing electron pairs to the valency shell of the metal, hence the name “coordinate link” given to this type of bond.³⁷⁵

(9) *Theory of the periodic table*—The structure of the periodic table was explained by Bohr and others on the basis of four quantum numbers and Pauli’s exclusion principle, described below. These four quantum numbers represent the solution of the Schrödinger equation (described in the previous section) for hydrogen atoms, which describes the various states available to hydrogen’s single electron. The electrons are described as point charges revolving around the central positive nucleus of the atom in circular orbits, just like the planets revolve around the Sun. The energy state of the electron is described by a principal quantum number n , with each orbit having a particular value of n . It may take any integral value, i.e., $n = 1, 2, 3, 4, \dots$. By analogy with the planetary orbits (which obeys the inverse square law of attraction), the orbits would be expected to be ellipses, and for a given value of n , ellipses of varying eccentricity are therefore possible.³⁷⁶

³⁷²L. Pauling, “The nature of the chemical bond. Application of results obtained from the quantum mechanics and from a theory of paramagnetic susceptibility to the structure of molecules,” *J. Amer. Chem. Soc.* **LIII**, 1367, 3225 (1931); “The nature of the chemical bond. IV. The energy of single bonds and the relative electronegativity of atoms,” **LIV**, 988, 3570 (1932); *The Nature of the Chemical Bond*, New York (1939); also cited in J.R. Partington, *A Short History of Chemistry*, 3rd ed., pp. 368–369, Dover Publications, New York (1989). This phenomenon was recognized earlier in some theoretical discussions by other researchers, but its application in chemistry is largely due to Pauling.

³⁷³J.R. Partington, *A Short History of Chemistry*, 3rd ed., pp. 367–369, Dover Publications, New York (1989).

³⁷⁴A. Werner, “New ideas in inorganic chemistry,” *Z. Anorg. Chem.* **III**, 267 (1893); *Ber.* **XL**, 15 (1905); also cited in J.R. Partington, *A Short History of Chemistry*, 3rd ed., pp. 369–373, Dover Publications, New York (1989).

³⁷⁵N.V. Sidgwick, “Coordination compounds and the Bhor atom,” *J. Chem. Soc.* **CXIII**, 725 (1923); *The Electronic Theory of Valency*, Oxford (1927); W.G. Palmer, *Valency, Classical and Modern*, Cambridge (1944); also cited in J.R. Partington, *A Short History of Chemistry*, 3rd ed., p. 373, Dover Publications, New York (1989).

³⁷⁶J.R. Partington, *A Short History of Chemistry*, 3rd ed., pp. 362–365, Dover Publications, New York (1989); K.W. Whitten and K.D. Gailey, *General Chemistry with Qualitative Analysis*, pp. 69–101, Saunders College Publishing, Philadelphia (1981); P.W. Atkins, *Physical Chemistry*, 3rd ed., pp. 340–370, W.H. Freeman and Co., New York (1986).

Sommerfeld introduced the subsidiary (or azimuthal) quantum number l in 1925 to designate the geometric shape of the region in space that an electron occupies. Within each energy level (defined by the value of n), l may take integral values from 0 up to and including $(n - 1)$, i.e., $l = 0, 1, 2, \dots (n - 1)$. The maximum value of l is thus $(n - 1)$. The subsidiary quantum number designates a sublevel, or a specified kind of atomic orbital that an electron may occupy. For each value of l , a letter has become associated, each corresponding to a different kind of atomic orbital, i.e., $l = 0$ (s), 1 (p), 2 (d), 3 (f) $\dots (n - 1)$. The s , p , d , and f designations arise from the characteristics of spectral emission lines produced by electrons occupying the orbitals, i.e., s (sharp), p (principal), d (diffuse), and f (fine) structure.³⁷⁷

If the plane of the ellipse is defined by a weak magnetic field, it can assume a number of discrete positions that are defined by the magnetic quantum number m , which designates the spatial orientation of an atomic orbital. Within each sublevel, m takes all integral values from $-l$ through 0 up to and including $+l$, i.e., $m = (-l) \dots 0 \dots (+l)$. The maximum value of m depends on the value of l . For example, when $l = 1$, which designates the p sublevel, there are three permissible values of m , namely, $-1, 0$, and $+1$. There are thus three distinct regions of space, called atomic orbitals, associated with a p sublevel. Atomic orbitals are defined as regions of space where there is a high probability of finding electrons.³⁷⁸

A fourth quantum number, s , is used to define the spin of the electron about its own axis and the orientation of the magnetic field produced by the motion of an electron. It has two possible values, $\pm 1/2$, corresponding with two opposite directions of spin.³⁷⁹

The values of n, l, m , and s describe a particular atomic orbital, and each atomic orbital can accommodate no more than two electrons, one with $s = -1/2$ and a second with $s = +1/2$. The Pauli's exclusion principle (1925) states that no two electrons in an atom may have identical sets of four quantum numbers n, m, l , and s . No exceptions have been uncovered to date.³⁸⁰

By taking the values 1, 2, 3, and 4 for n and making use of the above relations, it can be shown that the maximum numbers of electrons with these values of n are 2, 8, 18, and 32, and these follow a general formula, $2n^2$. These correspond to the numbers in the periods of the periodic table (see Table 3.1) as follows:³⁸¹

- $n = 1$, hence $l = 0$ and $m = 0$; $s = \pm 1/2$, corresponding with two electrons.
- $n = 2$, hence l is 1 or 0. For $l = 0, m = 0$; for $l = 1, m$ is $-1, 0$, or 1 . There are four values of m and for each s is $\pm 1/2$, making a total of eight.
- $n = 3$, hence $l = 2, 1$, or 0 ; for these three cases, m is $(2, 1, 0, -1, -2), (1, 0, -1)$, and 0 ; there are nine cases, for each of which $s = \pm 1/2$, making 18 in all.
- $n = 4$, hence l is 3, 2, 1, or 0, giving 16 values of m , making 32 in all.

³⁷⁷ibid.

³⁷⁸ibid.

³⁷⁹ibid.

³⁸⁰ibid.

³⁸¹ibid.

The electronic structures of the atoms of all the elements have now been elucidated with a reasonable degree of certainty from spectroscopic data. Although Bohr's atomic model, with electrons revolving in orbits, is no longer accepted, the significance of the quantum numbers, with rather different interpretations, remains valid even today. Today, the electrons are believed to be distributed in "shells" corresponding with special values of n , the maximum numbers of electrons in these shells, starting with the one next to the nucleus, being 2, 8, 18, and 32. The end of a period is occupied by an inert gas, and the number of electrons in the outer shell of an inert gas is two for helium and eight for all the others.³⁸²

It is now well established that the atomic nucleus is made up of protons and neutrons, with the number of protons giving the positive charge of the nucleus or the atomic numbers. The electrons outside the nucleus, with an equal number of negative charges as there are positive charges in the protons of the nucleus, make the atom neutral. These electrons have principal quantum numbers n of 1, 2, 3, etc. There exists a well-defined scheme³⁸³ for building up the periodic table with elements, starting from the simplest element, hydrogen, to the heaviest elements.

(10) *Theory of directed valencies*—The theory of directed valencies derives from Schrödinger's equation, the solution of which represents mathematically the distribution of charge of an electron regarded as distributed through space with a certain density of charge at a particular point. The solution to this equation is the wavefunction ψ , which is assumed to be finite, continuous, and single valued in general for all values of the coordinates, and that the square of which, ψ^2 , gives the density of charge at each point. It thus follows that since the electron is in an atom, knowledge of the charge distribution gives an indication of the directions in which bond formation may occur.³⁸⁴

Thus, the Schrödinger wave equation led to the theory of directed valency, which states that the charge density of an electron in an atom may be either spherically symmetrical (as in the hydrogen atom), or more prominent in certain directions, in other words, have decided directions in space, corresponding with the directions of the valency bonds. The formation of a valency bond is thus interpreted as the pairing of an electron in one atom with another electron having an opposite spin in another atom. Chemists had earlier assumed, on the basis of the facts of stereochemistry, that valency bonds have definite directions in space, a fact now borne out also by Schrödinger's wave theory. This theory also correctly predicts the energy levels in the hydrogen atom.³⁸⁵

The application of the modern theory of valency in organic chemistry has led to new remarkable formulations of many compounds, such as ethylene and benzene, two main building blocks of materials used as resist resins in lithography. Today,

³⁸²ibid., p. 364.

³⁸³The scheme discussed here is excerpted from the descriptions rendered in J.R. Partington, *A Short History of Chemistry*, 3rd ed., pp. 364–365 Dover Publications, New York (1989).

³⁸⁴J.R. Partington, *A Short History of Chemistry*, 3rd ed., p. 374, Dover Publications, New York (1989).

³⁸⁵ibid.

valence bonds are regarded as examples of bonds produced by hybridization instead of the conventional double bonds.³⁸⁶

(11) *The transmutation of elements*—Transmutation of elements was first achieved by Rutherford (1919), who showed that when nitrogen atoms are bombarded with alpha particles, hydrogen nuclei or protons are emitted from them. In 1922, Blackett showed that the change occurs by an alpha particle penetrating the nucleus of the nitrogen atom, raising the nuclear charge from 7 to 9, and thereby forming an isotope of fluorine. The process emits a proton, leaving a nucleus of charge 8, an isotope of oxygen. Since then, many artificial elements have been formed by bombardment with various types of fast particles. In some cases, positive electrons (or positrons) are emitted in the processes. In this way, elements not known in nature have been discovered, filling previously vacant spaces in the periodic table, and elements heavier than uranium (the “transuranium elements”) have been made artificially from uranium.³⁸⁷

It should be mentioned that the uranium isotope 235, when bombarded with neutrons, undergoes fission, liberating more neutrons in what can become a self-supporting chain reaction with a very large liberation of energy. This is the principle of the atomic bomb and the production of nuclear energy. The fusion of protons and neutrons to form helium nuclei at the enormous temperature of an atomic bomb explosion is the basis of the principle of the hydrogen bomb.³⁸⁸

The dream of the alchemists of transmuting baser metals into gold was at last realized when, in 1941, Sherr, Bainbridge, and Anderson artificially produced gold from mercury.³⁸⁹

3.2.3.9.4 Development of polymer chemistry

From very early in their history to the present time, humans have used polymeric materials to satisfy many needs, i.e., wood; hide; natural resins and gums; and fibers such as cotton, wool, silk, resins used in lithography, and so forth. All forms of life, including ours, depend on polymer molecules, i.e., carbohydrates, proteins, nucleic acids, and so on. In spite of these critical roles polymers play in our lives and activities, precious little was known about them until very recently.

Early attempts, at least in the modern era, to characterize polymeric substances generally indicated that polymers possess high molecular weights, even if the results were not particularly accurate. These early investigators found it easier to interpret the results in terms of colligative properties than to simply accept the possibility that these substances were high-molecular-weight compounds, composed from smaller units that are held together by covalent bonds.

As early as 1826, Faraday had already arrived at C_5H_8 as the empirical formula of rubber, and by 1860, isoprene was identified as a product of the destructive

³⁸⁶ibid., p. 376.

³⁸⁷ibid., pp. 377–378.

³⁸⁸ibid., p. 379.

³⁸⁹ibid.

distillation of rubber. However, the idea that a natural polymer such as rubber somehow “contained” isoprene gradually emerged, but the nature of its involvement was more elusive and sometimes outright contentious.³⁹⁰

The late and slow development of polymer chemistry is generally agreed to be due mainly to lack of interest on the part of organic and physical chemists—the main two types of chemists whose research interests should naturally intersect with polymer chemistry. On the one hand, organic chemists were more interested in determining the structure of ordinary-sized organic molecules during the early years of the twentieth century, and this probably contributed to their reluctance to look beyond structures of convenient size. Physical chemists, on the other hand, were more interested in intermolecular forces at this period, and the idea that polymers were the result of some sort of association between low-molecular-weight constituent molecules prevailed for far much longer than it should have.³⁹¹

Hermann Staudinger (Fig. 3.41) is generally credited with being the father of modern polymer chemistry, although a foreshadowing of his ideas can be traced through older literature. In 1920, he proposed the chain formulas we use today, maintaining that structures are held together by covalent bonds that are equivalent in every way to those in low-molecular-weight compounds. These were rather controversial ideas at the time. Nevertheless, over time, these ideas were slowly accepted, culminating in his being awarded the Nobel Prize in 1953.

In addition to the intramolecular covalent bonds that keep the polymer molecules intact, we now know that intermolecular forces—hydrogen bonds,



Figure 3.41 Hermann Staudinger, the father of polymer chemistry. (Published with permission from Deutsches Museum, Munich.)

³⁹⁰For excellent books on polymer chemistry, see for example, P.C. Hiemenz, *Polymer Chemistry: The Basic Concepts*, p. 1, Merce! Dekker, New York (1984); H.R. Allcock and F.W. Lampe, *Contemporary Polymer Chemistry*, 2nd ed., Prentice Hall, Englewood Cliffs, NJ (1990); P.J. Flory *Principles of Polymer Chemistry*, Cornell University Press, Ithaca (1953).

³⁹¹ibid.

dipole-dipole interactions, and London forces—hold assemblies of these molecules together in the bulk state.

By the 1930s, Carothers started synthesizing polymers by applying well-established reactions of organic chemistry such as esterification and amidation. His products—polyesters and polyamides—contained many ester and amide linkages, in contrast to the single ester or amide linkages in products formed from simple organic molecules undergoing similar reactions. Physical chemists such as Flory, Kuhn, Guth and Mark, and a host of others eventually turned their attention to polymers, and soon they were applying thermodynamics, statistics, and crystallography to describe the multitude of forms that long-chain molecules could assume.³⁹²

Today, studies on and about polymers span the entire gamut of physical sciences and engineering: polymer chemistry, polymer physics, polymer engineering, and so on. Improvements in the manufacture and the processing of the resins used in all forms of lithography derive directly from advances in these fields of polymer science.

³⁹²ibid.

Chapter 4

Evolution of Lithography

The old order changeth, yielding place to new.

Alfred Tennyson, *The Idylls of the King*

4.1 Introduction

From the time of Senefelder to the present time, lithography has undergone major evolutions, but overall, its basic principle remains intact. It remains a planographic printing process in which the image and nonimage areas are on the same plane of the printing substrate.¹ Just as in Senefelder's time, today, the contrast between the image and nonimage areas depends on the interfacial tension of oily inks and water-retaining surfaces. This is in fact the very same principle that governs the immiscibility of oil and water—hydrophobic–hydrophilic interactions between the image and nonimage areas. The inks (or resist) are naturally hydrophobic and can be made resistant to the action of etchants when dry.

Lithography has evolved into a broad family of techniques that are distinctly different in many respects, yet share similar attributes as to their ultimate goal—a method to transfer information from one substrate to another with a high degree of fidelity and throughput relative to other comparable printing techniques. Senefelder's original direct stone plate lithography of the late eighteenth century evolved into offset lithography in the nineteenth century and is now what is primarily used in the printing industry. Offset lithography in turn evolved into semiconductor lithography in the twentieth century, where it is now used in the fabrication of integrated circuits.

Another notable evolution in lithography relates to the manner in which the image is created. While Senefelder drew his image by hand, using ink pencils, today, this mode of lithographic printing is practiced only by fine art lithographers. Most lithographic images today are done through radiation-induced chemical reactions on appropriate sensitive substrates, using photons, electrons, ions, and even atoms.

¹Lithography is one of the three basic printing methods, the other two being intaglio (gravure or engraving) and typography (relief printing).

Still another aspect of the evolution of lithography relates to the speed with which it is carried out. While Senefelder's stone plate lithography took hours, if not an entire day to complete just one print, today, an IC device layer on a silicon wafer substrate containing hundreds of devices, each of which may have nearly one billion transistors, can be patterned in just under one minute.

In spite of the tremendous evolutionary changes and developments that lithography has undergone, at its fundamental core, its printing and patterning action is ultimately about chemical transformations brought about by the interactions of electrons within the ink or resist material, or any lithographic patterning media, as the case may be. Such electronic interactions may be on the basis of affinity of oil for oil and the repulsion of oil and water as in stone lithography (solid plate printing); it could also be mediated by photons (as in photolithography), by electrons (as in electron-beam lithography), and by ions (as in ion-beam lithography). Where photoradiations (such as visible light photons, UV photons, x-ray photons, etc.), electrons, and ions are employed in the imaging process, they function primarily to excite the electrons of the sensitized lithographic substrates or radiation-sensitive materials in resists to appropriate energy levels, altering their physical properties such as solubility in an appropriate solvent, and thereby providing the basis of the contrast between the exposed and unexposed areas of the substrate or the resist. When such interactions are done properly, the result is a successful marriage between the exciting agent (electrons, photons, ions, etc.) and the electrons of the lithographic substrate, whose offspring is a well-resolved and well-patterned planographic feature. The tone of this feature could be either positive (when the exposed area is washed or dissolved away from the substrate) or negative (when the exposed area remains on the substrate).

Relative to other patterning techniques, how and why did lithography become the dominant printing method for the fabrication of integrated circuits? An adequate answer to this question must as a necessity trace the evolution of lithography from its invention through all of its myriad incarnations as have been practiced ever since its invention, through the invention of the transistor and the integrated circuit as well as the appropriation of its techniques in the large-scale fabrication of semiconductor devices. This journey must perforce highlight the unique properties of this patterning technique, with particular emphasis on semiconductor lithography, which has made it the dominant patterning technique used in the fabrication of integrated circuits.

Shown in Fig. 4.1 is a schematic of the major evolutionary trends and developments in lithography, starting from its very invention in 1798 and extending all the way to its role in the development of microelectronics—first the printed circuit board, next the transistor, and then the integration of the transistors into microprocessors, memory chips, and controllers—which have ushered in a cornucopia of machines that manipulate information by streaming electrons through silicon. Today, the entire microelectronics industry rests on lithographic techniques that routinely fabricate structures smaller than 45 nm across (that is, 45 billionths of a meter). This size is tiny by the standards of everyday experience—about

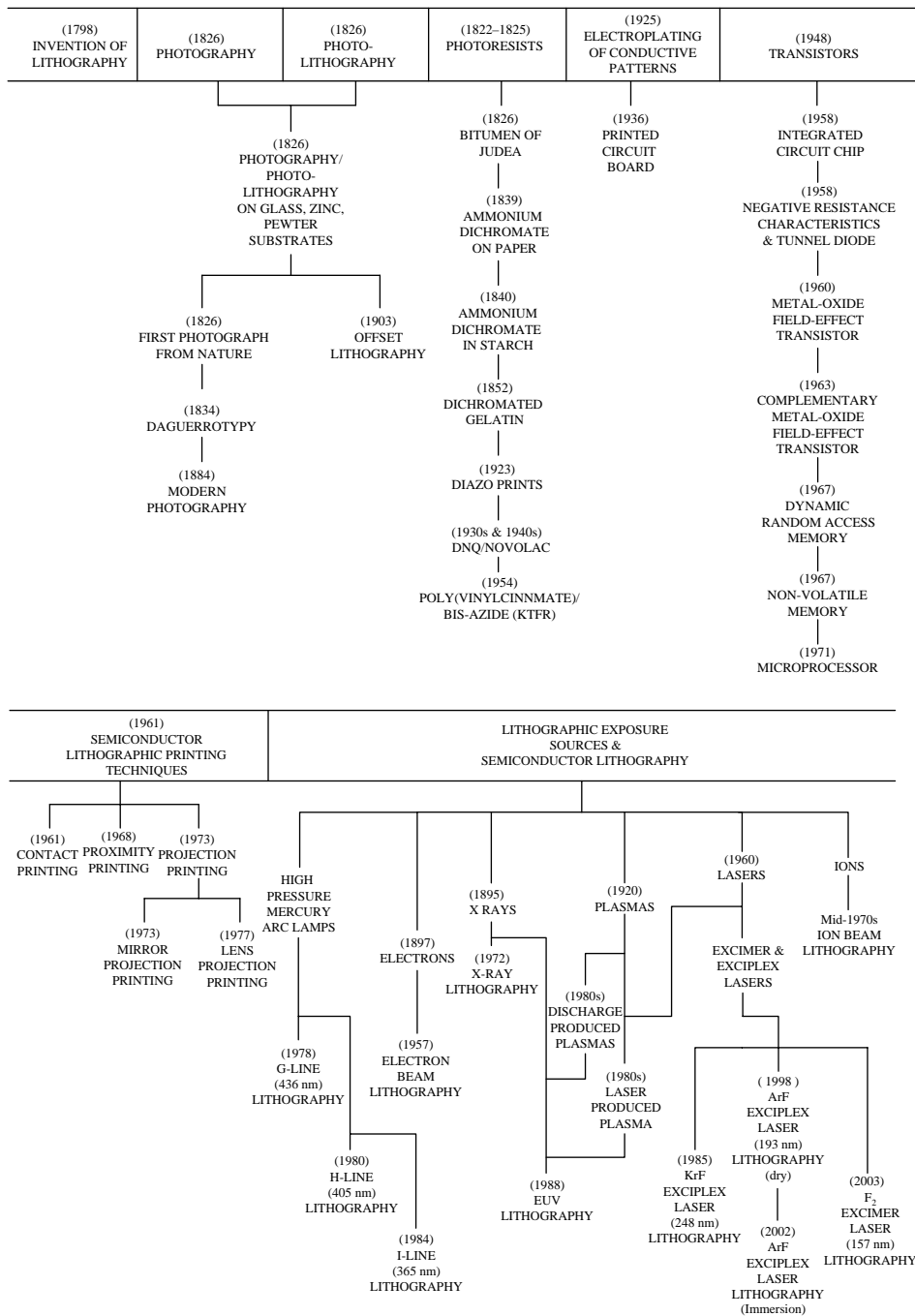


Figure 4.1 Evolution of lithography.

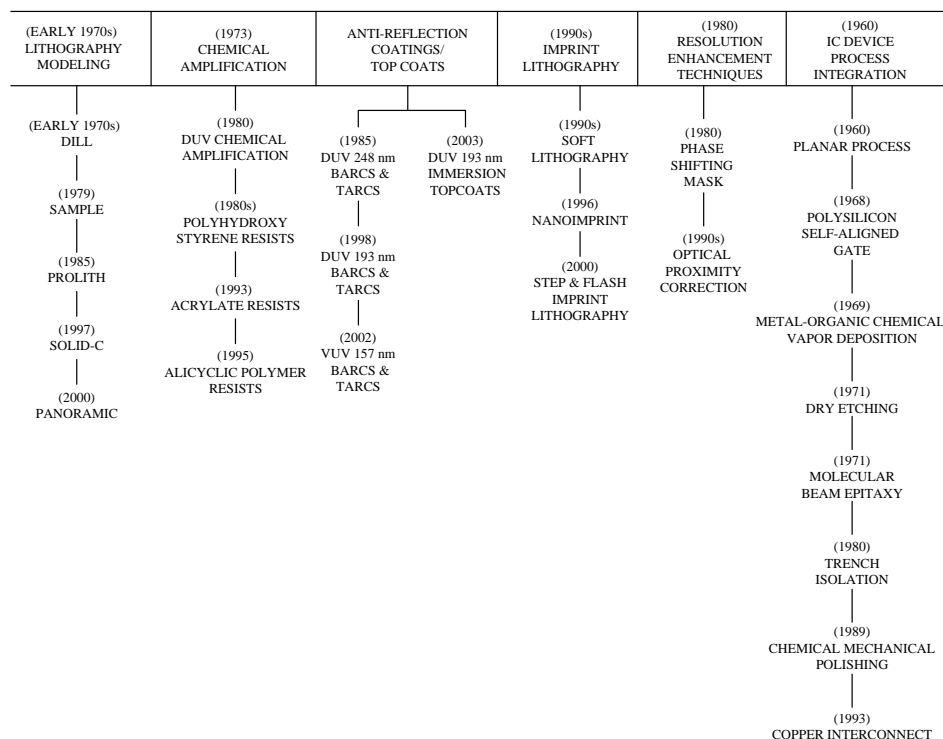


Figure 4.1 Continued.

one-thousandth the width of a human hair—but is comparatively large on the scale of atoms and molecules. A 45-nm-wide wire will span about 250 atoms of silicon.

The early history of the invention of lithography, photography, and photolithography has already been covered in Chapter 2 and will not be repeated here. Instead, our starting point shall be the developments that took place after the invention of photolithography in 1826 by Niépce. While the developments in fine art lithography² and offset lithography³ are interesting subjects in their own rights, our emphasis here will be on how developments in these lithographies were expropriated and employed in the development of printing plate technology, offset lithography, and subsequently semiconductor lithography, the most advanced form of lithography.

²The most notable exponent of fine art lithography was Toulouse Lautrec. For literature on key developments in fine art lithography, see J. Renard, *Histoire Naturelles (Natural History)*, English Transl. by R. Howard, Horizon Press, New York (1966); M. Joyant, *Henri de Toulouse Lautrec*, Arno Press, New York (1968).

³See, for example, H. Gernsheim and A. Gernsheim, *The History of Photography: From the Camera Obscura to the Beginning of the Modern Era*, Vol. 1, Thames & Hudson, London (1969).

4.2 Offset Lithography

We have come a long way from the stone plate lithography that Senefelder invented. As you can very well imagine, it would be quite difficult to mount a piece of stone on modern high-speed lithographic presses. While Senefelder's press was flat, which made the use of stone plates rather easy, modern lithographic printing presses, on the other hand, use curved cylinders to hold the offset plates—image carriers such as thin paper, plastic, or metal sheet—which, once exposed and processed, can be wrapped around a cylinder of a press for printing. Offset lithography therefore refers to a printing method in which the inked lithographic plate prints the image on a rubber blanket or roller (the offset), which in turn prints the image on the object (e.g., a newspaper or a circuit board).

The image areas of a modern offset plate accept ink and are hydrophobic, while the nonimage areas accept water and are hydrophilic. While this basic principle is common to all forms of offset lithography, there are many differences between offset plates and the method they use to separate the image from the non-image areas.⁴

Today, most lithographic plates are made of aluminum sheets of varying thickness with a granular finish. The grains serve to imbue the plate with water-carrying properties and anchorage to the image-forming material. The plates are typically presensitized, i.e., coated with light-sensitive diazo compounds and photopolymer resins that make them able to be responsive to light exposure.⁵ This photopolymer coating reacts with ultraviolet radiation, much like photographic film. On exposure to UV radiation through a film negative (see Fig. 10.3), the exposed part of the photopolymer on the plate (i.e., the part under the transparent section of the film negative) is cross-linked and “hardened,” while the unexposed part (i.e., the part under the dark areas of the film negative) remains unaffected by the UV radiation and thus can be easily removed in an appropriate solvent, resulting in a printing plate that can be used for offset lithography.

The major types of lithographic plates that are commonly used in the printing industry today include diazo plates, photopolymer plates, silver halide plates, electrophotographic plates, bimetallic plates, waterless plates, spark discharge plates, laser (digital waterless) plates, and plates made by the computer-to-plate (CTP) method in various materials. In addition to digital information from computers, film positives and negatives are used in making or exposing most types of offset plates today. While there are several types of offset plates, they are all generally classified as either positive or negative working plates, depending on the tone of their printing.⁶

The ink used in offset lithography has similar properties to those used in a letterpress in that both inks are very viscous. The water solution, called a “fountain solution,” is used to keep the ink from adhering to the nonimage areas of the

⁴http://4dps.dynodan.com/printing_process_explained/lithography_files/index.html

⁵ibid.

⁶ibid.

offset plate. The fountain solution is formulated from materials such as desensitizing gums, cleaners, buffering agents, etc.⁷ Offset lithographic printing is the dominant printing method used in the printing of newspapers, textbooks, and the like.

4.3 The Printed Circuit Board and the Development of the Electronics Industry

The printed circuit board (PCB)⁸ and modern resist technologies are both outgrowths of the printing industry, where resists have long been known, for more than a century before the invention of PCBs. In early PCB processes, etch resists were applied by offset lithographic printing, resulting inevitably in the transfer of printing technologies to the PCB industry.⁹ To better understand the role that lithography, specifically offset lithography, played in the development of PCBs, a brief discussion on the invention and development of PCBs is presented.

The roots of circuit boards stretch all the way back to 1925, when Ducas was granted a patent for a method of forming electroplated conductor patterns in copper, gold, or silver on a nonconductive base material. Although he formed the conductor patterns by stenciling rather than photoetching, these patterns are of interest because of their remarkable resemblance to modern-day circuit patterns. He stenciled a conductive paste on a plastic base and electroplated it with the aforementioned metals.¹⁰

Ducas designed these conductors to interconnect circuit elements in place of wires, while using the base as an insulator, in a method he described in one of the claims of the invention for “constructing electrical circuits arranged . . . upon the panel surfaces . . . for interconnecting terminals of electrical instruments secured to [the] surfaces.”¹¹ Remarkably, there exists no evidence that extensive commercial use was made of this invention, nor of any subsequent circuit board invention, until World War II.¹²

The year 1936 saw Eisler,¹³ in England, conceiving what are probably the earliest PCBs as we know them today. In 1948, he was granted a patent¹⁴ for a manufacturing process of a component of an electric circuit that involved printing the circuit pattern on a foil bonded to an impervious insulating backing

⁷ibid.

⁸The account rendered here is adapted from a similar one given in W.S. DeForest, *Photoresist: Materials and Processes*, Chapter 1, McGraw Hill, New York (1975).

⁹ibid., p. 6.

¹⁰C. Ducas, “Electrical Apparatus and Method of Manufacturing the Same,” U.S. Patent No. 1,563,731 (1925).

¹¹ibid.

¹²W.S. DeForest, *Photoresist: Materials and Processes*, pp. 6, 7, McGraw Hill, New York (1975).

¹³P. Eisler, *The Technology of Printed Circuits*, pp. 3–6, Heywood and Co., London (1959).

¹⁴P. Eisler, “Manufacture of electric components,” U.S. Patent No. 2,441,960 (1948).

using a medium (ink) that was adherent to the foil and capable of protecting the covered metal surfaces from chemical attack. He formed the pattern where the unprotected foil was etched away to the base. Today, this process is generally referred to as “print and etch.” He subsequently filed other patents dealing with circuit boards.¹⁵

Following the end of World War II, it was revealed in 1947 that large numbers of circuit boards had been manufactured for use in ordnance devices in the United States during the war, which spurred a lot of interest in PCBs, resulting in the development of numerous processes for making PCBs by the early 1950s. The most popular techniques for fabricating both PCB circuitry and interconnections during this early phase were mechanical fabrication techniques;¹⁶ these later gave way to plated-foil processes in the latter part of the decade.¹⁷ The use of eyelets for interconnection was the preferred method until electroless processes for metallizing through holes were introduced.¹⁸ Conductive ink patterns¹⁹ applied by stenciling or screening also found reasonable acceptance and were quite often used in both the plated and unplated conditions well into the late 1950s.

Plating as a means of forming a conductive path from one side of a board to the other of a circuit pattern evolved rather slowly during that decade in spite of the fact that methods for metallizing the through holes were available. As early as 1948, the two-step catalyzing process for electroless copper deposition for copper metallization of nonconductors was already in use.²⁰ Such a process involved first sensitizing glass or other nonconductive surfaces with a dilute stannous chloride solution that acted as a mordant, followed by a reduction of a precious metal such as gold from a subsequent acid-activating solution. These early

¹⁵P. Eisler, “Electric capacitor and method of making it,” U.S. Patent No. 2,607,825 (1952); P. Eisler, “Apparatus for regeneration of etching media,” U.S. Patent No. 2,748,071 (1956); P. Eisler, “Method of making printed circuits,” U.S. Patent No. 2,747,977 (1958).

¹⁶J.T. Beck, “Contacts for electrical circuits and methods for making same,” U.S. Patent No. 2,823,286 (1958); J.B. Little and B.E. Phelps, “Printed circuit connection and method of making same,” U.S. Patent No. 2,902,629 (1959); O.I. Steigerwalt and H.I. Ashry, “Method of making a printed circuit,” U.S. Patent No. 2,912,745 (1959); H.I. Ashry, O.I. Steigerwalt, and J.D. Heibel, “Method of making printed circuit panels,” U.S. Patent No. 2,912,746 (1959); H.I. Ashry, O.I. Steigerwalt, and J.D. Heibel, “Connecting means for etched circuitry,” U.S. Patent No. 2,912,747 (1959); W.D. Frazier, “Electrical mounting devices,” U.S. Patent No. 2,915,678 (1959); R.B. Gray, “Method of making printed circuit panels,” U.S. Patent No. 2,912,748 (1959); N.N. Berger, “Connecting means for etched circuitry,” U.S. Patent No. 2,889,393 (1959).

¹⁷H. Shapiro, *Plating*, pp. 607–611 (June 1957).

¹⁸J.T. Beck, “Contacts for electrical circuits and methods for making same,” U.S. Patent No. 2,823,286 (1958); W.D. Frazier, “Electrical mounting devices,” U.S. Patent No. 2,915,678 (1959); N.N. Berger, “Connecting means for etched circuitry,” U.S. Patent No. 2,889,393 (1959).

¹⁹D.K. Cardy, “Method of forming a printed circuit,” U.S. Patent No. 2,864,156 (1958); R.C. Sanders, “Electrical components,” U.S. Patent No. 2,876,392 (1959); M. Martin and C.S. Bojanowski, “Electrically conductive body and method of making same,” U.S. Patent No. 2,861,911 (1958); S.K. Tally and V.F. Dahlgren, “Printed circuit baseboard,” U.S. Patent No. 2,876,393 (1959); W.G. Lee, “Printed electric circuits,” U.S. Patent No. 2,940,018 (1960).

²⁰S. Wein, “Metal finishing,” p. 58 (Aug. 1948).

electroless copper deposition processes were plagued by instability, cost, and reliability problems that mitigated deploying them in high-volume production. A reliable activating and plating process was eventually developed by Atkinson²¹ in the mid-1950s, which was followed by a few others.²² The year 1960 saw the introduction of the colloidal catalyst²³ by the Shipley Company. This catalyst quickly became the standard sensitizing-activating process for the PCB industry, and it remains so today.²⁴

In the early and mid-1960s, multilayer boards arrived on the scene, particularly for military uses, where cost was not an issue; the premium was on compactness, weight, and reliability. These boards evolved with advances that occurred in metallizing and photoresist processes.²⁵ Standards and specifications were prepared for conventional boards²⁶ in the early 1960s, and in the latter part of that decade for multilayers.²⁷ Because of migration problems, silver was permanently eliminated as a competitor for copper in metallizing circuit board holes.²⁸

As already implied, the early selection of offset lithographic printing as a means of applying etching resists was quite natural, considering the nature of the inks that must be used for lithography and other available methods. The rubber image conforms more easily to uneven surfaces than the metal lithographic plate, and very little moisture is transferred with the ink compared to direct lithographic printing. Copper is receptive to most printing inks and is often used in lithographic plates. In spite of all the good attributes of offset lithographic printing, there exist some problems associated with this technique: (i) The process results in a thin coating, which usually necessitates two or more passes. (ii) Coatings are generally nonuniform, particularly when used for large areas. (iii) In some instances, misalignment and poor registration occur.²⁹

Another very important method for fabricating PCBs is screen printing. Perhaps more PCBs have been made using screen printing than any other method. Screen

²¹R.B. Atkinson, "Material and method for electroless deposition of metal," U.S. Patent No. 3,119,709 (1964).

²²M.C. Agens, "Process of stabilizing autocatalytic copper plating solutions," U.S. Patent No. 2,938,805 (1960); R.M. Lukes, "Copper plating process and solution," U.S. Patent No. 2,996,408 (1961).

²³"How to bond to copper while metallizing plastics," Shipley Co., Data Sheet DS 124 (Jan. 1960); C.R. Shipley, Jr., "Method of electroless deposition on a substrate and catalyst solution therefor," U.S. Patent No. 3,011,920 (1961).

²⁴W.S. DeForest, *Photoresist: Materials and Processes*, p. 9, McGraw Hill, New York (1975).

²⁵*ibid.*

²⁶"Military specifications for printed wiring boards," MIL P 55110A; "Printed wiring for electronic equipment," MIL STD 273A.

²⁷"Plated through hole multilayer circuit boards," MIL P 55640. Also see "Printed wiring for electronic equipment," MIL STD 1495.

²⁸D.E. Yost, in *Symposium on Printed Circuits*, University of Pennsylvania, Jan. 20, pp. 53–56 (1955); S.W. Chaikin, J. Janney, F.M. Church, and C.W. McClelland, *Ind. Eng. Chem.* **51**(3), 299–304 (March 1959).

²⁹W.S. DeForest, *Photoresist: Materials and Processes*, p. 12, McGraw Hill, New York (1975).

printing can be used to form thick, inexpensive, chemically resistant images with reasonable accuracy and at an exceptionally high production rate. Once a screen is prepared, it can be used to print many boards in rapid succession, with the aid of automatic equipment. Images are formed on tensioned screens with naturally occurring colloid resists such as gelatin and albumin, or with synthetic polymers such as polyvinyl alcohol, polyacrylics, etc., which are rendered photosensitive by dichromate or other means. Silk, stainless steel, nylon, and polyester screens are typically used. Processing following image formation can take the form of baking in order to harden the features before they are subjected to etching.³⁰

In screen printing, the image is formed when a supply of ink is moved across the screen surface by a squeegee and forced through the screen opening onto the board. The screen is depressed against the board at a point of contact by the squeegee, and as the squeegee passes a given point, the screen lifts, leaving behind ink forced through the openings. The squeegee blade forms a seal with the binder/resin and forces the ink ahead of it, while wiping clean the smooth surface. Screened resist images are compatible with most processes for either pattern plating or etching, and are applicable to most single- and double-sided board processes.³¹ As a general rule, screen printing of PCBs is done with negative resists.³²

Resists as different as naturally occurring colloids (such as gelatin, albumin, and shellac) or synthetic polymers (such as polyvinyl alcohol, polyacrylics, polyvinyl pyrrolidone, and polyvinyl butyral) rendered photosensitive by dichromate or other means, as well as synthetic photosensitive polymers such as polyvinyl cinnamates (Kodak positive resists), diazonaphthoquinone/novolac, and solid-film resists such as Riston® (introduced by Dupont in 1968) have all been used in PCB fabrication. Some of these resists are still being used today.

4.4 The Transistor and Microelectronics Revolution

4.4.1 The invention of the transistor

In 1947, John Bardeen and Walter Brattain,³³ both research scientists at Bell Telephone Laboratories, while trying to understand the nature of the electrons at the interface between a metal and a semiconductor, made a startling discovery. They found that by making two point contacts very close to one another, they could make a three-terminal device—the first “point contact” transistor³⁴ (see Fig. 4.2). They made the two point contacts at the bottom of a triangular quartz crystal from two strips of gold foil separated by about 50 μm , and pressed it

³⁰ibid., p. 12.

³¹ibid.

³²ibid., pp. 13, 14.

³³J. Bardeen and W.H. Brattain, “The transistor, a semiconductor triode,” *Phys. Rev.* **71**, 230 (1948).

³⁴The Nobel Foundation, http://nobelprize.org/educational_games/physics/transistor/history/index.html (2007).



Figure 4.2 The first point-contact transistor. It was invented at Bell Laboratories on December 23, 1947. (Reprinted with permission from Alcatel-Lucent.)

onto a semiconductor surface of germanium. With one gold contact biased forward (i.e., positive voltage with respect to the third terminal) and the other reverse biased, they observed transistor action. In other words, they observed the amplification of the input signal.³⁵

The researchers quickly made a few of these transistors and connected them with some other components to make an audio amplifier. Showing this audio amplifier to executives at Bell Telephone Company, who were very impressed that it didn't need time to "warm up" (like the heaters in vacuum tube circuits), they quickly realized the power of this new technology.³⁶ It should be mentioned that the original motivation for this invention was to find a way to amplify voices in telephones, a key product sold by the Bell Telephone Company—a goal that the inventors ably met.

This invention ignited a huge research effort in solid state electronics across the world. Bardeen and Brattain received the Nobel Prize in physics in 1956,³⁷ together with Shockley, "for their researches on semiconductors and their discovery of the transistor effect." Shockley had developed a so-called junction transistor in 1949,³⁸ which was built on thin slices of different types of semiconductor materials pressed together. The junction transistor was easier to understand theoretically, could be manufactured more reliably, and became the preferred semiconductor device, which ushered in the modern electronic era.³⁹

Transistors eventually made their way into portable radios and other electronic devices, and are most prominently used today as building blocks of integrated circuits. Remarkably, the invention of the point-contact and *p-n* junction transistors,

³⁵G.S. May and S.M. Sze, *Fundamentals of Semiconductor Fabrication*, Chapter 1, John Wiley & Sons, Hoboken, NJ (2004).

³⁶The Nobel Foundation, http://nobelprize.org/nobel_prizes/physics/laureates/1956/index.html (2007).

³⁷*ibid.*

³⁸The Nobel Foundation, http://nobelprize.org/educational_games/physics/transistor/history/index.html (2007).

³⁹*ibid.*

followed by Shockley's classic paper⁴⁰ on p - n junctions and bipolar transistors, also in 1949, spawned the microelectronics revolution that has had profound impact on our technological society over the latter half of the twentieth century and into the twenty-first century in such diverse fields as automobiles, computers and communications, medicine, energy, and home entertainment, to mention but a few.

What, then, really is a transistor? The transistor is a three-terminal, solid state electronic device. It consists of a three-layer structure that comprises an n -type semiconductor layer sandwiched between p -type layers (p - n - p configuration) or a p -type layer between n -type layers (n - p - n configuration) (see Chapter 16).

In such a three-terminal device, electric current or voltage between two of the terminals can be controlled by applying an electric current or voltage to the third terminal. In this way, a transistor regulates current and voltage flow and acts as a switch or gate for electronic signals. A small change in the current or voltage of the inner semiconductor layer (which acts as the control electrode) can produce a large, rapid change in the current passing through the entire component.⁴¹

The three-terminal character of the transistor makes it possible for one to use it as an amplifier for electrical signals, such as the one in a radio. With the three-terminal transistor, one can also make an electric switch that can be controlled by another electrical switch. By cascading these series of switches (i.e., switches that control switches, which in turn control other switches, etc.), one can build up very complicated logic circuits,⁴² resulting in switching times that are extremely short, on the order of nanoseconds, today. Such logic chips are at the heart of the personal computer and many other electronic gadgets in use today.⁴³

4.4.2 Limits of discrete transistors

Following the invention of the transistor, for many years, they were made as individual, discrete electronic components and were connected to other electronic components (resistors, capacitors, inductors, diodes, etc.) on printed circuit boards to make an electronic circuit. The transistor's small size and low power consumption made it an ideal candidate to replace the bulky vacuum tubes then used to amplify electrical signals and switch electrical currents. These beneficial attributes of transistors made it possible for them to be used in making ever more complex electronic circuits in place of vacuum tubes. However, it did not take long before the limits of this approach of building circuits were reached. Circuits

⁴⁰W. Shockley, "The theory of p n junction in semiconductors and p n junction transistors," *Bell Syst. Tech. J.* **28**, 435 (1949).

⁴¹Nobel Foundation, http://nobelprize.org/educational_games/physics/transistor/history/index.html (2007).

⁴²ibid.

⁴³ibid.

based on many individual, discrete transistors became too large, too cumbersome, and too difficult to assemble and produce for the simple reason that they contained too many electronic components. In addition, because the transistor circuits were faster than vacuum tube circuits, noticeable problems due to time delays for electric signals to propagate a long distance in these large circuits were observed. To make the circuits even faster, one needed to pack the transistors closer and closer together, a task that became all the more daunting, if not outright impossible, to accomplish.⁴⁴

4.5 The Integrated Circuit

In 1958, Jack Kilby⁴⁵ at Texas Instruments and, in 1959, Robert Noyce⁴⁶ at Fairchild Semiconductor independently invented the integrated circuit as a solution to the problem of building electronic circuits with large numbers of components. Instead of making transistors one by one, several transistors could be made with this technique at the same time, on the same piece of semiconductor. In addition to transistors, other electric components such as resistors, capacitors, and diodes could be made by the same process with the same set of materials.⁴⁷

The rudimentary IC that Kilby made contained one bipolar transistor, three resistors, and one capacitor, all made in germanium and connected by wire bonding. For his invention of the IC, Jack Kilby was awarded the Nobel Prize in physics in 2000.⁴⁸ The monolithic (monolith means “single stone”) IC that Noyce proposed in 1959 was a flip-flop circuit containing six devices, in which the aluminum interconnection lines were obtained by etching an evaporated aluminum layer over the entire oxide surface using a lithographic technique.⁴⁹

Since the invention of the IC, the pace of innovation has been scorching. The IC is now the foundation of microprocessors, memory chips, and myriad other kinds of semiconductor devices.

4.6 Other Notable Developments in Transistor Technology

Since the invention of the point-contact transistor in 1947, the number and variety of semiconductor devices have witnessed a tremendous increase as advanced

⁴⁴The Nobel Foundation, http://nobelprize.org/educational_games/physics/transistor/history/index.html (2007).

⁴⁵J.S. Kilby, “Invention of the integrated circuit,” *IEEE Trans. Electron Dev.* **ED-23**, 648 (1976); U.S. Patent No. 3,138,743 (1964).

⁴⁶R.N. Noyce, “Semiconductor device and lead structure,” U.S. Patent No. 2,981,877 (1961).

⁴⁷The Nobel Foundation, http://nobelprize.org/educational_games/physics/transistor/history/index.html (2007).

⁴⁸*ibid.*

⁴⁹R.N. Noyce, “Semiconductor device and lead structure,” U.S. Patent No. 2,981,877 (1961).

technology, new materials, and broadened comprehension have been applied to the creation of new devices. Without exception, all of these new devices⁵⁰ operate on the same basic principles of transistor action discovered in 1947. Some of the most notable ones are outlined below.

The year 1952 saw Ebers⁵¹ develop the basic model for the thyristor, an extremely versatile switching device. Chapin and co-workers⁵² developed the solar cell in 1954, using a silicon p - n junction. The solar cell is a device for harnessing energy from the Sun that can convert sunlight directly into electricity in a very environmentally benign manner. Kroemer,⁵³ in 1957, proposed the heterojunction bipolar transistor (potentially one of the fastest semiconductor devices) to improve transistor performance. Esaki,⁵⁴ in 1958, observed negative resistance characteristics in a heavily doped p - n junction, which ultimately led to the discovery of the tunnel diode, which is important for ohmic contacts and carrier transport through thin layers.

The year 1960 saw the invention of the planar process by Hoerni.⁵⁵ This process involves the formation of an oxide layer over a semiconductor surface. And with the aid of lithography, windows are defined on the oxide surface, from which portions of the oxide layer is subsequently removed. Impurity atoms are diffused only through the exposed semiconductor surface, and p - n junctions are formed in the oxide window areas.

The MOSFET (metal-oxide semiconductor field-effect transistor), first reported by Kahng and Atalla⁵⁶ in 1960, is the most important device for advanced ICs.⁵⁷ With the increase in the complexity of ICs, device fabrication technology transitioned from nMOS (n -channel MOSFET) to CMOS (complimentary metal-oxide semiconductor), which employs two complementary transistors per gate—nMOS and pMOS (p -channel MOSFET)—to form logic elements. The CMOS device was invented by Wanlass and Sah⁵⁸ in 1963. The CMOS technology offers the advantage that its logic elements draw significant current only during the transition from one state to another (e.g., from 0 to 1) and draw very little current

⁵⁰A short review on the invention of these devices is provided in G.S. May and S.M. Sze, *Fundamentals of Semiconductor Fabrication*, Chapter 1, John Wiley & Sons, Hoboken, NJ (2004). A good number of the classic papers on devices are collected in S.M. Sze, Ed., *Semiconductor Devices: Pioneering Papers*, World Scientific, Singapore (1991).

⁵¹J. Ebers, "Four terminal $p n p n$ transistors," in *Proc. IRE*, **40**, p. 1361 (1952).

⁵²M.D. Chapin, C.S. Fuller, and G.L. Pearson, "A new silicon $p n$ junction photocell for converting solar radiation into electrical power," *J. Appl. Phys.* **25**, 676 (1954).

⁵³H. Kroemer, "Theory of a wide gap emitter for transistors," in *Proc. IRE*, **45**, p. 1535 (1957).

⁵⁴L. Esaki, "New phenomenon in narrow germanium $p n$ junctions," *Phys. Rev.* **109**, 603 (1958).

⁵⁵J.A. Hoerni, "Planar silicon transistors and diodes," presented at IRF Int. Electron Devices Meeting, Washington, DC (1960).

⁵⁶D. Kahng and M.M. Atalla, "Silicon silicon dioxide surface device," presented at IRE Device Res. Conf., Pittsburgh (1960).

⁵⁷G.S. May and S.M. Sze, *Fundamentals of Semiconductor Fabrication*, p. 4, John Wiley & Sons, Hoboken, NJ (2004).

⁵⁸F.M. Wanlass and C.T. Sah, "Nanowatt logics using field effect metal oxide semiconductor triodes," in *Tech. Dig. IEEE Int. Solid State Circuit Conf.*, p. 32 (1963).

between transitions, thus making it possible for power consumption to be minimized. CMOS technology is the dominant technology for advanced ICs in the world today.⁵⁹

An extremely small MOSFET with a channel length of 15 nm was demonstrated by Yu and co-workers⁶⁰ at Advanced Micro Devices, Inc. (AMD) in 2001. This device may serve as the basis for the most advanced IC chips containing well over one trillion devices.⁶¹

The dynamic random access memory (DRAM) device, a two-element circuit, was invented by Dennard⁶² in 1967. The DRAM cell contains one MOSFET and one charge-storage capacitor. The MOSFET functions as a switch to charge or discharge the capacitor. Although a DRAM is volatile and consumes relatively high power, it is expected that DRAMs will continue to be the semiconductor memory of choice for nonportable electronic systems in the foreseeable future.⁶³

The nonvolatile semiconductor memory (NVSM) device was invented by Kahng and Sze⁶⁴ in 1967. The NVSM can retain its stored information when the power supply is switched off. Although very similar to the conventional MOSFET, it differs from the latter by the use of a “floating gate,” which makes possible semipermanent charge storage. Attributes such as nonvolatility, high device density, low power consumption, and electrical rewritability (i.e., the stored charge can be removed by applying voltage to the control gate) have made the NVSM the dominant memory for portable electronic systems such as cellular phones, notebook computers, digital cameras, and smart cards.⁶⁵

The ultimate floating-gate nonvolatile memory is the single-electron memory cell (SEMC), which requires only one electron for information storage. SEMCs can be fabricated by reducing the length of the floating gate to ultrasmall dimensions on the order of 10 nm. At this dimension, when an electron enters into the floating gate, the potential of the gate is altered such that it prevents the entry of another electron. Yano et al.,⁶⁶ in 1994, were the first to demonstrate the operation of an SEMC at room temperatures. The operation of a SEMC may one day serve as the basis for the most advanced semiconductor memories, which may contain well over one trillion bits.⁶⁷

⁵⁹G.S. May and S.M. Sze, *Fundamentals of Semiconductor Fabrication*, p. 8, John Wiley & Sons, Hoboken, NJ (2004).

⁶⁰B. Yu, et al., “15 nm gate length planar CMOS transistor,” *IEEE IEDM Tech. Dig.* p. 937 (2001).

⁶¹G.S. May and S.M. Sze, *Fundamentals of Semiconductor Fabrication*, Chapter 1, John Wiley & Sons, Hoboken, NJ (2004).

⁶²R.M. Dennard, “Field effect transistor memory,” U.S. Patent No. 3,387,286 (1968).

⁶³G.S. May and S.M. Sze, *Fundamentals of Semiconductor Fabrication*, p. 8, John Wiley & Sons, Hoboken, NJ (2004).

⁶⁴D. Kahng and S.M. Sze, “A floating gate and its application to memory devices,” *Bell Syst. Tech. J.* **46**, 1283 (1967).

⁶⁵G.S. May and S.M. Sze, *Fundamentals of Semiconductor Fabrication*, p. 5, John Wiley & Sons, Hoboken, NJ (2004).

⁶⁶K. Yano et al., “Room temperature single electron memory,” *IEEE Trans. Electron. Dev.* **41**, 1628 (1994).

⁶⁷G.S. May and S.M. Sze, *Fundamentals of Semiconductor Fabrication*, p. 5, John Wiley & Sons, Hoboken, NJ (2004).

With a view to improving device performance, Kirwan and co-workers⁶⁸ proposed the polysilicon self-aligned gate process in 1969. This process not only improved device reliability, it also reduced parasitic capacitances. Furthermore, in 1969, the metal-organic chemical vapor deposition (MOCVD) process was developed by Manasevit and Simpson,⁶⁹ which found widespread adoption in the fabrication of compound semiconductors such as GaAs.

In order to support the ever-shrinking device dimensions, a dry etching technique was developed to replace wet chemical etching for high-fidelity pattern transfer by Irving and co-workers⁷⁰ in 1971 in a process that involved the use of a CF_4/O_2 gas mixture to etch silicon wafers. Molecular beam epitaxy, developed also in 1971 by Cho,⁷¹ offers the advantage of near-perfect vertical control of composition and doping down to atomic dimensions, and is now applied extensively in the fabrication of photonic devices and quantum effect devices.⁷²

The year 1971 saw the invention of the microprocessor by Hoff et al.,⁷³ who put the entire central processing unit (CPU) of a simple computer on one chip. A four-bit microprocessor (Intel 4004) with a chip size of $3 \text{ mm} \times 4 \text{ mm}$ containing 2300 MOSFETs, it was fabricated with a *p*-channel polysilicon gate process using an $8\text{-}\mu\text{m}$ design rule. Remarkably, this microprocessor performed as well as their much larger counterparts, the IBM mainframe computers of the early 1960s, each of which needed a CPU the size of a large desk. The invention of the microprocessor was a major breakthrough for the semiconductor industry. Currently, microprocessors constitute the most advanced segment of the IC industry.⁷⁴ The Intel Corporation and Advanced Micro Devices, Inc. are the two companies that make more than 95% of all the microprocessors in the world.

Since the early 1980s, many new technologies have been developed to support the requirements of ever-shrinking minimum feature lengths. The three most significant technologies that were developed during this period include trench isolation, chemical mechanical polishing (CMP), and copper interconnect. Trench isolation was developed by Rung and co-workers⁷⁵ in 1982 to isolate

⁶⁸R.E. Kerwin, D.L. Klein, and J.C. Sarace, "Method for making MIS structure," U.S. Patent No. 3,475,234 (1969).

⁶⁹H.M. Manasevit and W.I. Simpson, "The use of metal organic in the preparation of semiconductor materials. I. Epitaxial gallium V compounds," *J. Electrochem. Soc.* **116**, 1725 (1969).

⁷⁰S.M. Irving, K.E. Lemons, and G.E. Bobos, "Gas plasma vapor etching process," U.S. Patent No. 3,615,956 (1971).

⁷¹A.Y. Cho, "Film deposition by molecular beam technique," *J. Vac. Sci. Technol.* **8**, S31(1971).

⁷²G.S. May and S.M. Sze, *Fundamentals of Semiconductor Fabrication*, Chapter 1, John Wiley & Sons, Hoboken, NJ (2004).

⁷³The inventors of the microprocessor include M.E. Hoff, F. Fagin, S. Mazor, and M. Shima. For a profile of M.E. Hoff, see R. Slater, *Portraits in Silicon*, p. 175, MIT Press, Cambridge (1987).

⁷⁴G.S. May and S.M. Sze, *Fundamentals of Semiconductor Fabrication*, p. 8, John Wiley & Sons, Hoboken, NJ (2004).

⁷⁵R. Rung, H. Momose, and Y. Nagakubo, "Deep trench isolated CMOS devices," *Tech. Dig. IEEE Int. Electron Dev. Meet.*, p. 237 (1982).

CMOS devices. This technique eventually replaced all other prior isolation methods for fine-featured ICs. In 1989, Davari and co-workers⁷⁶ developed the CMP technique for global planarization of interlayer dielectrics, a key enabling process technique for multilevel metallization. Electromigration, the transport of metal ions through a conductor due to passage of an electrical current, is a widely known device failure mechanism, particularly at submicron dimensions. Although aluminum has been in use since the early 1960s as an interconnect material, it suffers from electromigration at high electrical current; it is also too resistive. Paraszczak and co-workers⁷⁷ introduced copper interconnect in 1993 to replace aluminum for minimum feature lengths approaching 100 nm and smaller.⁷⁸

4.7 Overall Device Technology Trends

Device technology trends over the last 50-odd years are illustrated in Fig. 4.3, which shows the growth curves for different technology drivers. The bipolar transistor drove the IC device technology at the beginning of the modern electronic era (1950–1970). Between 1970 and 1990, the DRAM and the microprocessor based on MOS devices were the technology drivers, due largely to the rapid growth of personal computers and advanced electronic circuits. The nonvolatile semiconductor memory has been the technology driver since 2000, due mainly to the rapid growth of portable electronic systems.⁷⁹

The fact that demand for memory has continued to be an important driving force within the IC industry over the last 40 years and is expected to remain so for the foreseeable future is a testament to the heightened sensitivity of these devices to yield factors. Yield depends significantly on the surface area of the device and is often negatively impacted by contaminants—either from particulates outside the process equipment or generated by the process equipment, or re-deposits of process materials during processing. For this reason, yield is heavily affected by packing density, which in turn is a most apparent restriction in memory devices, making memory devices the technology drivers in the IC industry.⁸⁰ Memories lead the industry in both device density and line width.⁸¹ Packing density is determined by line width, and increases in memory size therefore require smaller line widths or larger die size or both.⁸² These call for lithographic exposure tools such as high-NA

⁷⁶B. Davari et al., “A new planarization technique, using a combination of RIE and chemical mechanical polish (CMP),” *Tech. Dig. IEEE Int. Electron Devices Meet.*, p. 61 (1989).

⁷⁷J. Paraszczak et al., “High performance dielectrics and processes for ULSI interconnection technologies,” *Tech Dig. IEEE Int. Electron Devices Meet.*, p. 261 (1993).

⁷⁸G.S. May and S.M. Sze, *Fundamentals of Semiconductor Fabrication*, p. 8, John Wiley & Sons, Hoboken, NJ (2004).

⁷⁹ibid.

⁸⁰VLSI Research Inc., “Wafer fabrication equipment,” Report No. 2233 11P (1989).

⁸¹ibid.

⁸²ibid.

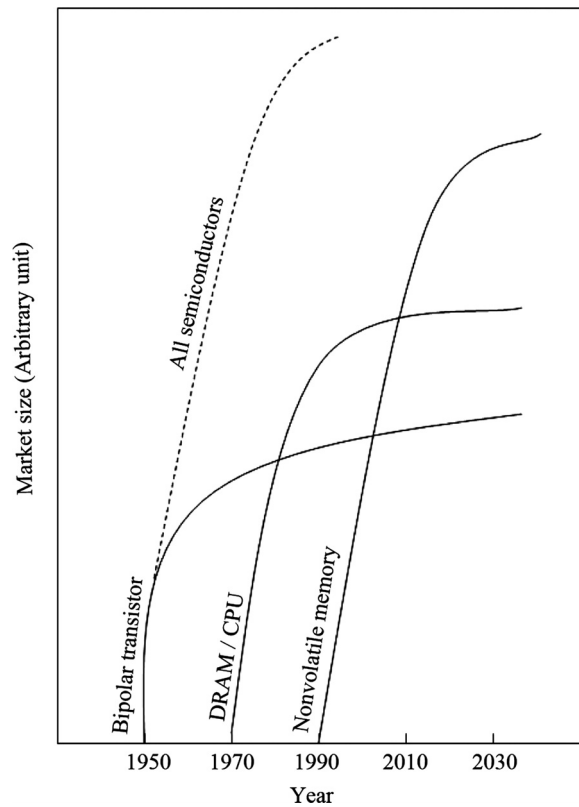


Figure 4.3 Growth curves for different technology drivers. (Reprinted with permission from Electron Devices and Materials Association.)⁸⁴

scanners and steppers that can reliably expose larger die sizes with a high degree of fidelity and without significant yield losses.⁸³

Since the beginning of the microelectronics era, the smallest line width (or minimum feature length) of an IC has shrunk at a rate of about 13% per year, motivated no doubt by the inherent advantages of device miniaturization. Device miniaturization leads to increased reduced unit cost per circuit function. For example, the cost per bit of memory chips has decreased by half every two years for successive generations of DRAM circuits. Also, as device dimensions shrink, the intrinsic switching time also decreases. Device speed has in fact improved by four orders of magnitude since 1959. Higher speeds lead to increased performance. Furthermore, as devices become smaller, they consume less power. The energy dissipated per logic gate has decreased by a factor of over one million since 1959.⁸⁵

⁸³ibid.

⁸⁴F. Masuoka, "Flash memory technology," in *Proc. Int. Electron Devices Mater. Symp.*, 83, Hsinchu, Taiwan (1996).

⁸⁵G.S. May and S.M. Sze, *Fundamentals of Semiconductor Fabrication*, Chapter 1, John Wiley & Sons, Hoboken, NJ (2004).

In the 39 years since the microprocessor was invented, microprocessor computational power has increased by a factor of two every 18 months since 1970,⁸⁶ so much so that computer clock speeds have increased by a factor of a thousand (from a few megahertz to a few gigahertz) and memory capacity has grown even more (from kilobytes to gigabytes). These facts are illustrated in Fig. 1.1 for microprocessors made by Intel Corporation and Advanced Micro Devices, Inc. Even in the face of this relentless drive toward miniaturization of computer chips over the last four decades, one aspect of computer hardware has remained largely unchanged. Until recently, most general-purpose computers were equipped with only one CPU, where programs are executed and calculations are performed. Now a major shift is underway. Many of the latest general-purpose computers from AMD and Intel are equipped with multiple processor chips that are fabricated onto a single slab of silicon. These multiple processors are meant to share the work of computation and multiply the machine's power.⁸⁷ Examples of such processor systems include the AMD Quad-Core Opteron™ processor (see Fig. 4.4).

A natural question to ask is this: Why build chips with multiple processors? Why not just keep increasing the speed of the single CPU? If the latter option were feasible, the chipmakers would have adopted it. Instead, they are turning to multicore systems only because the path to higher clock speeds seems to be very difficult, at least for now.⁸⁸

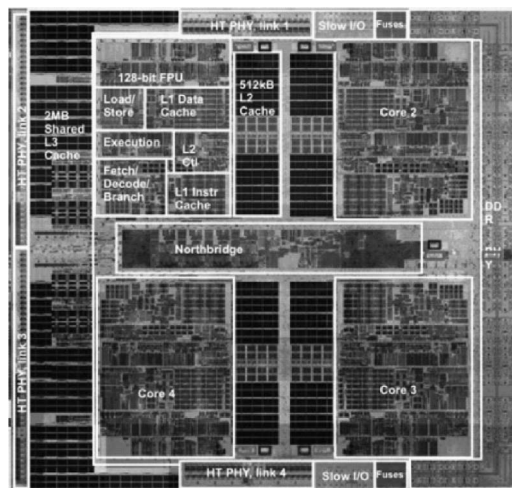


Figure 4.4 The AMD Quad-Core Opteron™ microprocessor chip has four separate processors that act in parallel. The cores are the four large areas of irregular geometry, while the cache memory is shown in the gridlike regions and holds cache memory. The total silicon area of 285 mm² holds 463 million transistors. The critical dimension is 65 nm. (Courtesy of AMD.)

⁸⁶See Fig. 1.1.

⁸⁷B. Hayes, "Computing in a parallel universe," *Am. Scientist*, pp. 476–480 (Nov.–Dec. 2007).

⁸⁸*ibid.*

The causes of this impasse derive from the peculiar physical and economic laws that govern the design of ICs.⁸⁹ The most celebrated of these laws stipulates that as transistors or other components are made smaller and are packed more densely on the surface of a silicon chip, the cost of producing the chip remains nearly constant, so much so that the number of transistors on a state-of-the-art chip doubles every year or two, as already alluded to. In effect, the cost per transistor steadily declines over time. This extraordinary fact is the basis of Moore's law,⁹⁰ formulated in 1965 by Gordon E. Moore, one of the founders of the Intel Corporation. The law reflects the fantastic progression of circuit fabrication that has unleashed previously unimagined computational power.⁹¹

Less famous than Moore's law but equally influential are several "scaling laws" first formulated in 1974 by Robert H. Dennard and co-workers⁹² at IBM, who asked the following questions: When the size of a transistor is reduced, how should the other factors such as voltages and currents that control its operation be adjusted? And what effect will the changes have on performance? Dennard and co-workers found that voltage and current should be proportional to the linear dimensions of the device, implying that power consumption (the product of voltage and current) will be proportional to the area of the transistor. This was a very significant discovery, which meant that even as the number of devices on a chip increased, the total power density would remain constant.⁹³

The conclusion drawn by Dennard and co-workers about performance was even more startling, but in a good way. Their scaling laws show that switching delay—the time it takes a transistor to go from the conducting to the nonconducting state, or vice versa, is proportional to size. This implies that as circuits shrink they can be operated at higher speed. The switching delay is a crucial measure of transistor performance.⁹⁴

Taken together, these observations suggest that the laws of nature seem to work in our favor in microelectronics. Moore's law and Dennard's scaling rules promise circuits that gain in both speed and capability, while cost and power consumption remain constant. From this favorable circumstance arises the whole bonanza of modern microelectronics.⁹⁵ But as with every bonanza, there are limits and trade-offs.

Over the last decade, chip designers have struggled with such limits and trade-offs, best exemplified by the twin problems of memory bottleneck and power management. Although CPUs are a thousand times faster today than they were

⁸⁹ibid.

⁹⁰See for example, D.C. Brock, ed., *Understanding Moore's Law: Four Decades of Innovation*, Chemical Heritage Press, Philadelphia (2006).

⁹¹See Fig. 1.1.

⁹²R. Dennard, F. Gaensslen, H. N. Yu, V.L. Rideout, E. Bassous, and M. LeBlanc, "Design of ion implanted MOSFETs with very small physical dimensions," *IEEE J. Solid State Circuits* **SC-9**(5), 256–268 (1974).

⁹³B. Hayes, "Computing in a parallel universe," *Am. Scientist*, pp. 476–480 (Nov.–Dec. 2007).

⁹⁴ibid.

⁹⁵ibid.

39 years ago, memory speed has increased only by a factor of one or so within the same period. As far back as the 1980s, reading a bit from main memory took a few hundred nanoseconds, which also corresponded to the time needed to execute a single instruction in a CPU. Then the memory and the processor cycles were well matched. Currently, a processor can execute a hundred instructions in the time required to obtain data from memory.⁹⁶

A strategy employed by chip designers for tackling the memory bottleneck is to transfer data in large blocks rather than single bits or bytes. This strategy improves throughput (bits per second), but not latency (the delay before the first bit arrives). To tackle the latency problem, computers are now equipped with an elaborate hierarchy of cache memories, which surround the processor core. Data instructions that will be executed immediately are held in the innermost, first-level cache, which has only a small capacity but is built for very high speed. For slightly less urgent information, there is a second-level cache, which is larger but a little slower than the first-level cache. Some processor systems even have a third-level cache.⁹⁷

Overreliance on cache memory presents some difficulties in predicting which data instructions a program will call for next, a wrong prediction being rather catastrophic. Devoting a large fraction of the silicon of processor chips to caches and logic circuits that control them means that fewer processors will be made from a given silicon wafer on a unit basis. In addition, the lithographic patterning of such processors is fraught with many difficult challenges in terms of defectivity, overlay control, and critical dimension control. As the disparity between memory and CPU speed widens even farther, at some point, all the benefits of any further increase in processor speed will be used up by the demand for more cache.⁹⁸

The second problem that now plagues chip designers is a power crisis. The scaling laws of Dennard and co-workers predict that power density should remain constant even as the number of transistors and their switching speed increase. However, for that prediction to hold, voltages have to be reduced in proportion to the linear dimensions of the transistor. In reality, chip manufacturers have not been able to lower operating voltages that steeply.⁹⁹

Historically, for each successive generation of processor chips, the linear dimensions (such as gate width of a transistor) has been scaled by a factor of 0.7, which yields an area reduction of one-half. In other words, chip density has doubled for every successive generation. Moreover, switching delay (the reciprocal of processing speed) is proportional to the linear size. If the operating voltage could also be lowered by a factor of 0.7, a transistor's power consumption should be proportional to this surface area, and the power density of the entire chip should therefore remain constant. However, in reality, the scaling factor for voltages has been 0.85 rather than 0.7, with the result that power density has been rising steadily with each new generation of chips, so that power and heat

⁹⁶ibid.

⁹⁷ibid.

⁹⁸ibid.

⁹⁹ibid.

have now become limiting factors, so much so that computers are now equipped with fans to cool them.¹⁰⁰

Going forward, even the 0.85 voltage reduction strategy is problematic because as voltage is lowered, transistors become leaky, like valves that cannot completely shut off. Presently, the leakage current now accounts for roughly a third of total power consumption; with further reductions in voltage, leakage could become even more unmanageable. On the other hand, without reducing the voltage, the clock rate cannot be increased.¹⁰¹

Some have taken to viewing these problems with memory latency and power density as signaling the end of Moore's law, which might not be entirely accurate. After all, chip manufacturers can still pack more transistors onto a chip and manufacture it for a roughly constant cost. In fact, the semiconductor industry "road map"¹⁰² calls for increasing the number of transistors on a microprocessor from a few hundred million today to more than 12 billion by 2020. What happens to be ending, or at least slowing down dramatically, is the scaling law that allows processor speed to keep climbing. The chip industry can still make smaller circuits, thanks to lithography, but not faster ones. And therein lies the reason behind the strategy of multicore chips, in which lots of little processors work in parallel to perform ever more complex computational tasks.¹⁰³

An illustration of this new strategy of having multiple processors on the same slab of silicon working in parallel is provided by the AMD Quad-Core Opteron™ microprocessor, the first native quad-core microprocessor (see Fig. 4.4). Released in 2007, this quad-core processor has nearly half a billion transistors, each one of which has three electrical contacts, totaling a total of 1.5 billion contacts per chip. In AMD's fabrication facilities, these electrical contact holes are made at the rate of roughly 35 billion per second with the aid of lithography. Imagine drilling a hole every three seconds, perhaps with the aid of an electrical drill. It would take one over 3000 years to drill 35 billion electrical contact holes, and at the end of which one would have produced the contacts for just one chip.¹⁰⁴ Again, this illustrates the speed and efficiency of semiconductor lithography. But how did the ancient art of lithography make the transition from the printing industry, where it was used for reproducing artistic impressions, blueprints, newspapers, and the like, into a technique for patterning of integrated circuits?

4.8 Semiconductor Lithography

The beginning of semiconductor lithography dates to 1957, when Andruss, using etch-resistant photoresist, successfully transferred patterns of a device into a

¹⁰⁰ibid.

¹⁰¹ibid.

¹⁰²International Technology Roadmap for Semiconductors, <http://www.itrs.net/Links/2005ITRS/Home2005.htm> (2005).

¹⁰³B. Hayes, "Computing in a parallel universe," *Am. Scientist*, pp. 476–480 (Nov.–Dec. 2007).

¹⁰⁴H.J. Levinson, Private Communication (2007).

semiconducting substrate.¹⁰⁵ Since then, lithography has evolved to become a key technology in the semiconductor industry. The phenomenal growth of the semiconductor industry derives, to a significant extent, from improvements in lithographic technology. Lithography also constitutes a significant economic factor, currently representing well over 35% of IC manufacturing costs.¹⁰⁶

Borrowed from the printing industry, semiconductor lithography is ideally suited for the fabrication of ICs, which requires the patterning of many layers of thin-film materials used in building up the device on a semiconductor substrate. Looked at another way, semiconductor lithography is basically an extension of photography. In semiconductor lithography, one first fabricates the equivalent of a photographic negative/positive containing the pattern required for some part of the microchip's circuitry. This negative/positive, called the mask, is then used to copy the pattern onto the semiconductor substrate of an IC. The process comprises two parts, namely, the preparation of the mask (a one-time event that can be slow and expensive) and the transfer of the mask pattern to the semiconductor substrate. In effect, the semiconductor lithographic process involves transferring a circuit pattern—as might, for example, be contained in a mask—into a radiation-sensitive film (resist) and subsequently replicating that pattern in an underlying thin conductor or dielectric film of the semiconductor substrate.¹⁰⁷

To make a mask for a part of an IC, a manufacturer first designs the pattern of the circuitry on a conveniently large-scale format and converts it into a pattern of opaque metallic film (usually chromium) on a transparent plate (usually glass or quartz). Semiconductor lithography is then used to reduce the size of the pattern and to transfer it onto a semiconductor substrate such as silicon wafer in a process that resembles that used in photography. This process is shown schematically in Fig. 4.5 and comprises a number of steps. First, an ultrahigh-purity wafer substrate, usually silicon wafer (“the stone”) is coated with radiation-sensitive resist (typically made of organic polymer or inorganic compounds), baked to evaporate the casting solvent, and exposed to radiation through a mask. The exposure process involves directing a beam of radiation (typically ultraviolet light from a mercury arc lamp or deep-ultraviolet light from excimer and excimer lasers or electrons, or even ions) to a mask, creating a transmitted or reflected image that then is made to pass through a set of lenses or mirrors, as the case may be, which in turn focuses the image onto the resist on the surface of a semiconductor substrate such as a silicon wafer.¹⁰⁸

Following exposure, the exposed resist film may be baked again, causing the catalytic photoacid¹⁰⁹ generated from the photoactive compound contained in

¹⁰⁵J. Andrus, “Fabrication of semiconductor devices,” U.S. Patent No. 3,122,817 (1964).

¹⁰⁶G.S. May and S.M. Sze, *Fundamentals of Semiconductor Fabrication*, Chapter 1, John Wiley & Sons, Hoboken, NJ (2004).

¹⁰⁷G.M. Whitesides and J.C. Love, “The art of building small,” *Sci. Am. Reports* **17**(3), 13–21 (2007); W.M. Moreau, *Semiconductor Lithography: Principles, Practices, and Materials*, Plenum, New York (1988); L.F. Thompson, C.G. Willson, and M.J. Bowden, *Introduction to Microlithography*, 2nd ed., American Chemical Society, Washington, DC (1993).

¹⁰⁸ibid.

¹⁰⁹Applicable only to chemically amplified resists.

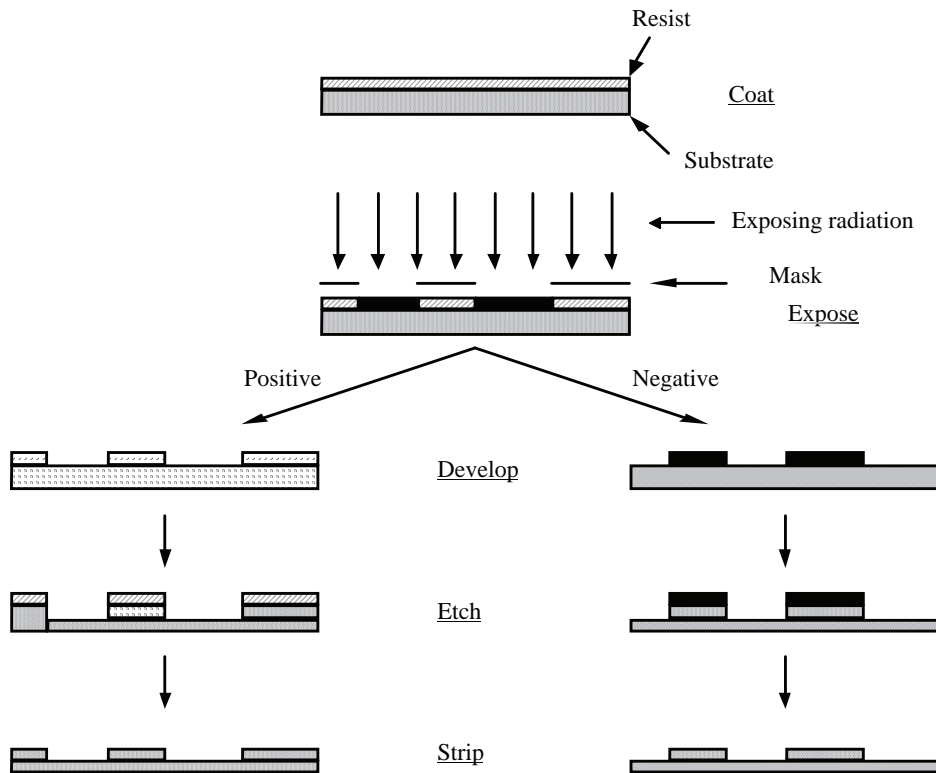


Figure 4.5 Schematic representation of the photolithographic process sequence.

the photoresist to act on the polymers. Next, the exposed resist film is developed in a solvent to produce a three-dimensional relief replica of the mask pattern. Finally, the image in the resist is etched into the underlying substrate by liquid-based substrate etching systems or a variety of plasma (dry) etch processes.¹¹⁰ And at the end of the process, the remaining resist is stripped off, leaving the patterned features on the semiconductor substrate, which then undergoes subsequent processing to transform it into an actual IC device.

Resists function by radiation-induced alteration of the solubility of the materials. There are two basic classes of resist materials, namely, negative and positive resists (see Fig. 4.5). Negative resists become less soluble on exposure to radiation; i.e., the unexposed areas can be selectively removed by treatment with an appropriate developer solvent. Positive resists selectively undergo an increase in solubility on exposure, enabling the exposed regions to be selectively removed in the developer. Both types of resists are formulated from polymers designed to have physical and chemical properties consistent with semiconductor

¹¹⁰G.M. Whitesides and J.C. Love, "The art of building small," *Sci. Am. Reports* **17**(3), 13–21 (2007); W.M. Moreau, *Semiconductor Lithography: Principles, Practices, and Materials*, Plenum, New York (1988); L.F. Thompson, C.G. Willson, and M.J. Bowden, *Introduction to Microlithography*, 2nd ed., American Chemical Society, Washington, DC (1993).

processing. Negative resists that undergo radiation-induced cross-linking often suffer from solvent-induced swelling, which imposes a limit on their resolution. Positive resists do not usually suffer from swelling problems and have thus dominated the fabrication of leading-edge devices. Details of these processes are described by Moreau¹¹¹ and Thompson et al.,¹¹² In the following section, we briefly review the various semiconductor lithographic techniques that are either currently being used to manufacture IC devices or are under development for potential future lithographic applications.

4.8.1 Optical lithography

Optical lithography (also called photolithography), which uses visible and ultraviolet radiation (436–157 nm) to transfer the pattern from the mask to a photosensitive resist, is the dominant technology today for the fabrication of ICs. The technology was adopted during the early days of planar transistor development and is still the dominant technology of choice.¹¹³ Since its introduction, photolithography has undergone many innovations and evolutions, as shown in Table 4.1 and Fig. 4.6.

The oldest photolithographic technique is contact printing,¹¹⁴ whereby the mask is placed close to the wafer surface and visually aligned to the previous pattern on the wafer, in a process called registration and alignment. The mask is then pressed into hard contact with the resist-coated wafer, following which the resist is flood exposed through the mask with ultraviolet light.¹¹⁵ The theoretical resolution of contact printing is given by¹¹⁶

$$\text{CD} = \frac{3}{2} \sqrt{\frac{\lambda z}{2}}, \quad (4.1)$$

where CD is the critical dimension (provided the feature is a grating with a period of twice the CD), λ is the exposure wavelength, and z is the thickness of the photoresist.

¹¹¹W.M. Moreau, *Semiconductor Lithography: Principles, Practices, and Materials*, Plenum, New York (1988).

¹¹²L.F. Thompson, C.G. Willson, and M.J. Bowden, *Introduction to Microlithography*, 2nd ed., American Chemical Society, Washington, DC (1993).

¹¹³W.S. DeForest, *Photoresist Materials and Processes*, McGraw Hill, New York (1975).

¹¹⁴W.M. Moreau, *Semiconductor Lithography: Principles, Practices, and Materials*, Plenum, New York (1988); W.S. DeForest, *Photoresist Materials and Processes*, McGraw Hill, New York (1975).

¹¹⁵L.F. Thompson, C.G. Willson, and M.J. Bowden, *Introduction to Microlithography*, 2nd ed., p. 9, American Chemical Society, Washington (1993).

¹¹⁶M.J. Bowden, "The lithographic process: the physics," in *Introduction to Microlithography*, L.F. Thompson, C.G. Willson, and M.J. Bowden, Eds., Section 2.1.1, pp. 22, 23, American Chemical Society, Washington, DC (1994).

Table 4.1 Evolution of lithography from 1967 to 2007.

Year of introduction	Lithography	Resist	Device	Minimum feature (μm)
1967	Contact printing	Cyclized rubber	256 bit DRAM	15 20
1971	Near contact printing	Cyclized rubber	1 Kbit DRAM	8 12
1971	Near contact printing	DNQ/Novolac	1 Kbit DRAM	8 12
1974	Near contact printing	DNQ/Novolac	4 Kbit DRAM	6
1977	436 360 nm, 1:1 projection printing	DNQ/Novolac	16 Kbit DRAM	4
1980	436 360 nm, 5 10 \times S&R	DNQ/Novolac	64 Kbit DRAM	2
1982	436 nm (g line), 5 \times S&R	DNQ/Novolac	256 Kbit DRAM	1.4
1985	g line, 5 \times S&R	DNQ/Novolac	1 Mbit DRAM	1
1988	365 nm (i line), 5 \times S&R	DNQ/Novolac	4 Mbit DRAM	0.7
1992	365 nm (i line), 5 \times S&R	DNQ/Novolac	16 Mbit DRAM	0.5
1995	365 nm (i line), 5 \times S&R	DNQ/Novolac	64 Mbit DRAM	0.35
1998	DUV (248 nm, KrF laser), 4 \times (i line), 5 \times S&R	PBOCST	256 Mbit DRAM	0.25
2001	DUV (248 nm/KrF laser), 4 \times S&R	PBOCST	1 Gbit DRAM	0.18
2005	DUV (193 nm/ArF laser)	Acrylate and alicyclics	4 Gbit DRAM	0.13
2007	DUV (193 nm/ArF laser), 4 \times S&R	Acrylate and alicyclics	16 Gbit DRAM	0.1

S&R: Step and repeat.
 DNQ: diazonaphthoquinone.
 PBOCST: poly(butoxycarbonate styrene).

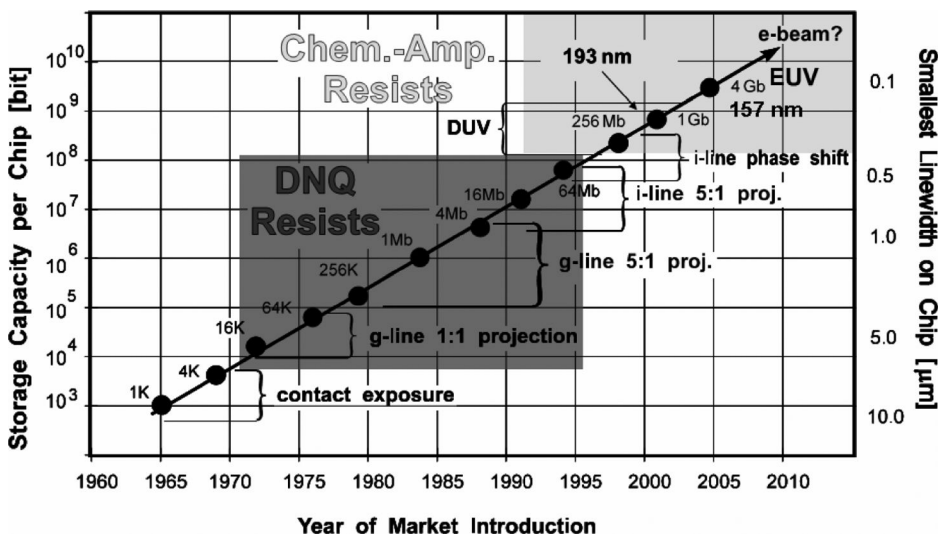


Figure 4.6 Evolution of semiconductor lithography. (Courtesy of R. Dammel.)

Unfortunately, contact printing was plagued by a number of practical and technical difficulties. Bringing the mask and the wafer into direct contact causes damage to the mask and creates defects, which are reproduced in subsequent exposures. In addition, nonflatness of the wafer and mask results in alignment error, which further limits the resolution capability of the technique.¹¹⁷

Practical and technical difficulties associated with contact printing led to a modification of the latter technique, such that the mask and the wafer were separated by a small, accurately controlled gap of 10–25 μm during exposure. Introduced in the early 1970s, this technique, known as proximity printing,¹¹⁸ minimizes mask and wafer damage caused by contact, but at the expense of resolution. This gap, however, limited resolution because of diffraction. The theoretical resolution of proximity printing is given by¹¹⁹

$$\text{CD} = \frac{3}{2} \sqrt{\lambda \left(g + \frac{z}{2} \right)}, \quad (4.2)$$

where g is the separation distance between the mask and the resist surface.

Around 1973, a technique known as projection printing, in which the mask image was projected onto the wafer by means of a 1:1 reflective or refractive optical system, was developed.¹²⁰ Given that the mask was no longer in direct contact with the wafer, the technique offered greatly increased mask lifetimes and marked reductions in defect density. The early projection systems were designed to image the full-wafer exposure without demagnification. Being $1\times$ projection systems, they were amenable to simple optical designs that permitted the use of a relatively broad light spectrum. With increasing wafer size, projection printing was incapable of imaging all features onto a wafer simultaneously. The image field therefore had to be partitioned.¹²¹

One of the first partitioning approaches was based on scanning projection printing,¹²² in which the reticle was projected onto the wafer by scanning a ring-shaped image field, consisting of two concentric spheres with a radii ratio such that the image field was well corrected for aberrations.¹²³ The exclusive use of

¹¹⁷A.K. K. Wong, *Resolution Enhancement Techniques in Optical Lithography*, p. 14, SPIE Press, Bellingham, WA (2001).

¹¹⁸D.O. Massetti, M.A. Hockey, and D.L. McFarland, "Evaluation of deep UV proximity mode printing," *Proc. SPIE* **211**, 32 (1980).

¹¹⁹M.J. Bowden, "The lithographic process: the physics," in L.F. Thompson, C.G. Willson, and M.J. Bowden, Eds., *Introduction to Microlithography*, Chapter 2, American Chemical Society, p. 24 (1994).

¹²⁰D.A. Markle, "The future and potential of optical scanning system," *Solid State Technol.* **27**(9), 159–166 (1984); M.C. King, *IEEE Trans. Electron Devices*, **ED-26**, 711 (1979).

¹²¹A.K. K. Wong, *Resolution Enhancement Techniques in Optical Lithography*, p. 14, SPIE Press, Bellingham, WA (2001); M.J. Bowden, "An introduction to microlithography," in *Introduction to Microlithography*, L.F. Thompson, C.G. Willson, and M.J. Bowden, Eds., pp. 9, 10, American Chemical Society, Washington, DC (1994).

¹²²R.M. Scott, "Annular field optical imaging system," U.S. Patent No. 3821763 (1974); A. Offner and C.T. Darien, "Unit power imaging catoptric anastigmat," U.S. Patent No. 3748015 (1973).

¹²³D.A. Markle, "The future and potential of optical scanning system," *Solid State Technol.* **27**(9), 159–166 (1984); M.C. King, *IEEE Trans. Electron Dev.* **ED-26**, 711 (1979).

mirrors during this time permitted the use of relatively broadband illumination, since chromatic aberration was not a concern. This technique was introduced in the 1970s.

Due to the continuous increase in wafer size and reduction of feature dimensions, full-wafer printing without demagnification became increasingly difficult to implement because of mask dimension control and pattern placement difficulties. These led to the introduction of reduction projection printing toward the end of the 1970s in order to alleviate these problems.¹²⁴ Known as step-and-repeat photolithography, this reduction projection printing technique involved exposing a smaller area (on the order of 1–2 cm²) and stepping this pattern over a large-diameter wafer. It improves resolution and alignment accuracy compared to full-wafer printing.¹²⁵ These step-and-repeat exposure systems, or steppers, were designed with either 1:1 or reduction optics (10×, 5×, and 4×).¹²⁶

In spite of the strategy of image field reduction, design of reduction projection optics still presented difficult technical challenges, exacerbated by the drive toward higher-numerical-aperture (NA) lenses for improved resolution and the need for aberration correction over the (still) substantial field area. For exposure wavelengths below 300 nm, fused silica and calcium fluoride were and still remain the only practical lens-making material, making chromatic aberration correction impossible in refractive exposure systems. Although reflective or catadioptric¹²⁷ systems could be used, the required surface finish of the aspheric mirrors in such systems is extremely difficult to achieve, but easily achieved in lenses used in immersion ArF (193 nm) lithography.¹²⁸

Line narrowing of the incident radiation was also adopted by the semiconductor industry as a solution for the design problems associated with reduction projection printing. The reasoning here involves the fact that narrowing the spectral width of the illumination light effectively minimizes chromatic aberration to the point that color correction is not needed in refractive systems. The degree-of-spectral-purity requirement increases with increasing NA, so much so that 248-nm exposure systems with a 0.7 NA have a spectral bandwidth on the order of a picometer. Such a narrow spectrum requires high spectral power, which can be obtained with high-repetition-rate laser sources.¹²⁹

¹²⁴V. Pol, "High resolution optical lithography: a deep ultraviolet laser based wafer stepper," *Solid State Technol.* **30**(1), 71–76 (1987).

¹²⁵L.F. Thompson, C.G. Willson, and M.J. Bowden, *Introduction to Microlithography*, 2nd ed., p. 10, American Chemical Society, Washington, DC (1993).

¹²⁶*ibid.*; A.K. K. Wong, *Resolution Enhancement Techniques in Optical Lithography*, p. 15, SPIE Press, Bellingham, WA (2001); M.J. Bowden, "An introduction to microlithography," in *Introduction to Microlithography*, L.F. Thompson, C.G. Willson, and M.J. Bowden, Eds., pp. 9, 10, American Chemical Society, Washington, DC (1994).

¹²⁷Using both reflective and refractive elements.

¹²⁸A.K. K. Wong, *Resolution Enhancement Techniques in Optical Lithography*, p. 15, SPIE Press, Bellingham, WA (2001).

¹²⁹A.I. Ershov, T. Hoffmann, W.N. Partlo, I.V. Formenkov, G. Everage, P.R. Das, and D. Myers, "Feasibility studies of operating KrF lasers at ultra narrow spectral bandwidths for 0.18 μm line widths," *Proc. SPIE* **3334**, 1021–1030 (1998); U. Stamm, R. Pätzelt, K. Kleinschmidt, K. Vogler,

Furthermore, the trend toward increase in chip size and the ever more stringent critical dimensional control requirements presented additional technical challenges that had to be overcome, even as stepper technology was being stretched to its limits. The imaging issues associated with this trend were again mitigated by reducing the exposure area with step-and-scan exposure systems,¹³⁰ which are essentially a hybrid of the early full-wafer scanning systems and step-and-repeat systems. In the step-and-scan exposure systems, the reticle is scanned rather than exposed all at once. Through repeated stepping and scanning, an entire wafer can be exposed.¹³¹

The size of the feature that can be printed with optical lithography is ultimately limited by the wavelength of the exposing radiation, hence the continuous shift to shorter wavelengths that the semiconductor industry has witnessed over the last 40 years, and illustrated in Fig. 4.6 and Table 4.1. During this period, exposure tools that operate in the near-UV (405–360 nm), deep-UV (250–190 nm) and vacuum-UV (157 nm) regions of the spectrum were commercialized. Because the materials used in conventional refractive optical systems are too opaque at these wavelengths, quartz and CaF₂ reduction lenses were introduced for the deep-UV (DUV) and vacuum-UV (VUV) exposure tools, respectively. The near-UV systems use filtered Hg arc lamps at 405 nm and 365 nm as the light source, while the DUV systems use line-narrowed KrF and ArF excimer lasers at 248 nm and 193 nm, respectively, as light sources. The VUV systems use the line-narrowed F₂ excimer laser at 157 nm as a light source.

Currently, DUV 193-nm (ArF) lithography dominates the lithographic technology in terms of market share, closely followed by DUV 248-nm (KrF) lithography. Dry ArF lithography is being used to fabricate the critical dimensions of 90-nm and 65-nm device technology nodes. Water-immersion ArF lithography is currently being used to fabricate devices at the 45-nm technology nodes and is planned to be extended to both the 32-nm and possibly 22-nm technology nodes. Immersion ArF lithography is expected to be the dominant technology for the rest of the 2010s and beyond, possibly pushing out the insertion of extreme ultraviolet (EUV) lithography to the 16-nm node sometime in 2016.¹³²

W. Zschocke, I. Bragin, and D. Basting, "ArF excimer laser for 193 nm lithography," *Proc. SPIE* **3334**, 1010–1013 (1998).

¹³⁰S. Hirukawa, K. Matsumoto, and K. Takemasa, "New projection optical system for beyond 150 nm patterning with KrF and ArF sources," *Proc. SPIE* **3334**, 414–422 (1998); D. Cote, K. Andersen, D. Cronin, H. Harrold, M. Himmel, J. Kane, J. Lyons, L. Markoya, C. Mason, D. McCafferty, M. McCarthy, G. O'Connor, H. Sewell, and D. Williamson, "Microscan III performance of a third generation, catadioptric step and scan lithographic tool," *Proc. SPIE* **3051**, 806–816 (1997); J. van Schoot, F. Bornebroek, M. Suddendorf, M. Mulder, J. Van der Spek, J. Stoeten, and A. Hunter, "0.7 NA step and scan system for 150 nm imaging with improved overlay," *Proc. SPIE* **3679**, 448–463 (1999); N. Deguchi and S. Uzawa, "150 nm generation lithography equipment," *Proc. SPIE* **3679**, 464–472 (1999).

¹³¹A.K. K. Wong, *Resolution Enhancement Techniques in Optical Lithography*, pp. 15, 16, SPIE Press, Bellingham, WA (2001).

¹³²International Roadmap for Semiconductors, <http://www.itrs.org> (2005).

4.8.2 Challenges of decreasing exposure wavelength in optical lithography

The strategy of shifting to ever-shorter wavelengths as a means of improving resolution in photolithography cannot continue indefinitely because of a number of factors. The first concerns the lack of exposure radiation sources with adequate output in the VUV and EUV regions of the spectrum. The second factor limiting resolution particularly as feature sizes get considerably smaller than the exposure wavelength is diffraction, which causes blurring of printed features. Various resolution enhancement techniques such as off-axis illumination, phase-shifting masks, and the use of immersion optics that have enabled hyper-NA imaging have made it possible to push the limits of photolithography to the realm of 45-nm and 32-nm technology nodes. But these technical improvements may not be sufficient to push the limits of photolithography to the sub-22-nm technology nodes.

The third limitation factor is cost and follows from the second in that because it is technically difficult to pattern features using short-wavelength photons, it is also very expensive to do so. True, the use of phase-shifting masks (alternating, attenuated, chromeless, etc.), optical proximity correction (OPC) schemes, and off-axis illumination schemes have enabled the extension of the useful life span of photolithography; however, the complexity of mask production and mask inspection presents difficult challenges whose solutions have not been found. In addition, mask cost is extremely high. The photolithographic tools that will be used to make chips well below the 22-nm technology node will invariably be extremely expensive, which may preclude some device manufacturers from buying them.

These inherent limitations of photolithography have thus necessitated the search for alternative semiconductor lithographic technologies. Electron beams, x rays, and ion beams have been employed in conventional semiconductor lithography, leading to the development of electron-beam, x-ray, and ion-beam lithographies. By subjecting soft rubbery materials such as polydimethylsiloxane to mechanical processes of printing such as stamping, molding, embossing, and cutting, a new form of semiconductor lithography called soft lithography has been developed within the last 15 years. And finally, semiconductor lithography has been further extended into the realm of proximal probe techniques based on atomic force microscopy and scanning tunneling microscopy, collectively called scanning probe lithography. In the remaining section, we briefly review each of these new extensions of semiconductor lithography.

4.9 X-ray Lithography

Lithography using x rays with wavelengths between 0.1 nm and 10 nm was first described by Spears and Smith¹³³ in 1972, and since then, significant research

¹³³E. Spears and H.I. Smith, "High resolution pattern replication using soft X rays," *Electron Lett.* **8**, 102 (1972); E. Spears and H.I. Smith, "X ray lithography: A new high resolution replication process," *Solid State Technol.* **15**(7), 21 (1972).

efforts have been devoted to it in many research institutes and IC companies across the globe, with the motivation of using it as a possible replacement for optical lithography. There are quite a few reasons why x-ray lithography is theoretically more attractive than optical lithography. Because x rays have much shorter wavelengths than the ultraviolet radiation currently used in optical lithography, they reduce wavelength-related diffraction problems, which limit resolution in optical lithography. Also, because resist films are transparent to x rays, high-aspect-ratio patterns can be fabricated with x-ray lithography. Furthermore, there is practically no field size limitation associated with x-ray lithography. And because the index of refraction is practically the same for all materials (close to unity) in the x-ray spectral region, standing wave effects and other reflection-related problems that plague optical lithography are eliminated in x-ray lithography.

Early x-ray systems employed conventional impact sources, which were relatively low-brightness sources. These systems were designed to expose an entire wafer in a single exposure, but the low brightness of the source necessitated the use of very sensitive resists. High-brightness sources such as synchrotron storage rings or pulsed laser-induced plasmas¹³⁴ became available over the last two decades, and several companies even attempted to incorporate these sources into step-and-repeat systems, which improved registration and relaxed the resist sensitivity requirements. Many problems still exist, however, including the fabrication of stable x-ray masks, alignment, and the commercial availability of suitable resist systems.¹³⁵

In spite of all the efforts that have been expended in the development of x-ray lithography, it has not yet been employed in any meaningful manner in IC device production. The difficulty of fabricating defect-free and stable x-ray masks presented nearly insurmountable challenges. The extension of optical lithography (photolithography) to technology nodes that were once deemed beyond its resolution limits, barely two decades ago, have also helped to consign x-ray lithography to the sidelines of IC device manufacture. In addition, conventional lenses are not capable of focusing x rays. Furthermore, many of the materials used in the fabrication of masks and lenses are rapidly degraded by the highly energetic x-ray radiation. Consequently, there are no current efforts to develop a production-worthy x-ray lithography capability within the semiconductor industry.

¹³⁴D.W. Peters, J.P. Drumheller, R.D. Frankel, A.S. Kaplan, S.M. Preston, and D.N. Tomes, "Application and analysis of production suitability of a laser based plasma x ray stepper," *Proc. SPIE* **923**, 28 (1988); D.W. Peters and R.D. Frankel, "X ray lithography: The promise of the past and reality of the present," *Solid State Technol.* **32**(3), 77 (1989); A. Heuberger, "X ray lithography," *J. Vac. Sci. Technol.* **B6**, 107 (1988); R. Hollman, "X ray lithography using broadband sources," *J. Vac. Sci. Technol.* **B6**, 186 (1988).

¹³⁵M.J. Bowden, "An introduction to microlithography," in *Introduction to Microlithography*, L.F. Thompson, C.G. Willson, and M.J. Bowden, Eds., pp. 11, 12, American Chemical Society, Washington, DC (1994).

4.10 Electron-Beam Lithography

Lithography using beams of electrons to expose resist is today a mature technology, having evolved from the scanning electron microscope developed in the mid-1950s.¹³⁶ In fact, it was one of the earliest processes used for fabricating ICs, dating back to 1957.¹³⁷ Almost from its very beginning, sub-100-nm resolution was reported with the technique. Broers reported 50-nm lines ion milled into metal films using a contamination resist patterned with a 10-nm-wide e-beam as early as 1964.¹³⁸ The year 1976 saw the fabrication of 8-nm lines on Au-Pd with a 0.5-nm probe and a 10-nm-thick carbon membrane substrate with e-beam.¹³⁹ In 1985, Murray et al., reported 1–2-nm features patterned on metal halide resists with e-beam.¹⁴⁰ Except for more recent reports on atomic scale resolution with proximal probe techniques, the resolution of e-beam lithography has been unsurpassed by any other lithographic technique.¹⁴¹

Although today all of the high-volume production of ICs is done with optical lithography, electron-beam lithography nevertheless continues to dominate two small but vital segments of the overall semiconductor lithography field. First, it is used to generate the masks that are used in optical lithography. Second, it is used in low-volume manufacture of specialty, high-resolution devices, custom

¹³⁶K.C.A. Smith and C.W. Oatley, Jr., “The scanning electron microscope and its fields of application,” *Br. J. Apply Phys.* **6**, 391 (1955); T.E. Everhart, “Persistence pays off: Sir Charles Oatley and the scanning electron microscope,” presented at the 40th Int. Conf. on Electron, Ion, and Photon Beam Technology and NanoFabrication, Atlanta, May 28–31 (1996); A.N. Broers, in *Proc. Symp. Electron Ion Beam Sci. Technol.*, pp. 3–25 (1972); A.N. Broers, “A new high resolution electron probe,” *J. Vac. Sci. Technol.* **10**, 979 (1973); D.S. Alles, F.R. Ashley, A.M. Johnson, and R.O. Townsend, “Control system design and alignment methods for electron lithography,” *J. Vac. Sci., Technol.* **12**, 1252 (1975); D.R. Herriot, R.J. Collier, D.S. Alles, and J.W. Stafford, “EBES: A practical electron lithographic system,” *IEEE Trans. Electron Dev.* **ED-22**, 385 (1975); H.C. Pfeiffer, T.R. Groves, and T.H. Newmann, “High throughput, high resolution electron beam lithography,” *IBM J. Res. Dev.* **32**(4), 494 (1988); J.T. Clemens, “Electron beam lithography: A gating item,” *Solid State Technol.* **32**(3), 69 (1989); A.N. Broers, “Resolution limits for electron beam lithography,” *IBM J. Res. Dev.* **32**(4), 502 (1988); H.C. Pfeiffer, “Variable spot shaping for electron beam lithography,” *J. Vac. Sci. Technol.* **15**, 887 (1978); D.R. Herriot and G.R. Brewer, “Electron beam lithography machines,” in *Electron Beam Technology in Microelectronic Circuit Fabrication*, pp. 141–216, Academic Press, Orlando (1981).

¹³⁷D.A. Buck, K. Shoulders, “An approach to microminiature printed systems,” *Proc. of Eastern Joint Computer Conf.*, p. 55, ATEE, New York (1957).

¹³⁸A.N. Broers, “Micromachining by sputtering through a mask of contamination laid down by an electron beam,” *Proc. of the First Int. Conf. on Electron and Ion Beam Technology*, R. Bakish, Ed., p. 181, John Wiley & Sons, Hoboken, NJ (1964).

¹³⁹A.N. Broers, W.W. Molzen, J.J. Cuomo, and N.D. Wittels, “Electron beam fabrication of 80 Å metal structures,” *Appl. Phys. Lett.* **29**, 596 (1976).

¹⁴⁰A. Murray, M. Scheinfein, M. Isaacson, and I. Adesida, “Radiolysis and resolution limits of inorganic halide resists,” *J. Vac. Sci. Technol. B* **3**, 367 (1985).

¹⁴¹E.A. Dobisz, F.K. Perkins, and M.C. Peckerar, “E beam and proximal probe processes for nanolithography,” in *Microlithography: Science and Technology*, J.R. Sheats and B.W. Smith, Eds., pp. 715–775, Marcel Dekker, New York (1998).

circuits, and prototype devices. These two vital functions performed by electron-beam lithography will in all probability not diminish in importance in the foreseeable future.¹⁴²

The main drawbacks of electron-beam lithography are its low throughput and high cost. The major advantages of electron-beam lithography include its ability to register accurately over small areas of a wafer, low defect densities, direct generation of patterns from circuit design data, and lack of diffraction issues of the type that limit resolution in optical lithography because electrons do not diffract at atomic scales.¹⁴³

The two principal modes of operation of electron-beam exposure systems include the maskless direct-write electron-beam machines and the mask-based electron-beam machines. Direct-write electron-beam machines operate directly from design data and are capable of extremely high resolution.¹⁴⁴ Mask-based electron-beam systems utilize masks in their imaging process. The implementation of electron-beam lithography in mix-and-match mode with optical lithography in a manufacturing environment has been demonstrated.¹⁴⁵

Several innovations in electron-beam reduction projection systems aimed at improving the low throughput of electron-beam writing machines have been reported.¹⁴⁶ For instance, workers at Hitachi developed the cell-projection electron-beam system, which projects entire transistor “cells” in a single exposure, which are then sequentially stepped over the entire device area.¹⁴⁷ This technique appears to be best suited for devices that are composed primarily of identical transistor elements, as found in DRAMs. In addition, workers at AT&T developed a reduction projection method known as SCALPEL (scattering with angular limitation projection electron-beam lithography) that uses a mask that scatters high-energy (70–200 KV) electrons through a thin patterned mask. The SCALPEL mask is made of a thin and low-atomic-number membrane and a high-atomic-number metal scattering element that is patterned. The scattered electrons are removed from the imaging systems through a back focal plane aperture.¹⁴⁸ The

¹⁴²M.J. Bowden, “An introduction to microlithography,” in *Introduction to Microlithography*, L.F. Thompson, C.G. Willson, and M.J. Bowden, Eds., p. 11, American Chemical Society (1994).

¹⁴³ibid.

¹⁴⁴ibid.

¹⁴⁵W.W. Flack, D.H. Cameron, V.J. Alameda, and G.C. Malek, “Mix and match lithography in a manufacturing environment,” *Proc. SPIE* **1671**, 126 (1992).

¹⁴⁶Y. Sohda, Y. Makayama, N. Saitou, H. Itoh, and H. Todokoro, “Electron optics for high throughput electron beam lithography system,” *J. Vac. Sci. Technol.* **B9**(6), 2940 (1991); H.W.P. Koops, *Micro circuit Eng.* **88**, 217, North Holland, New York (1989); S.D. Berger and J.M. Gibson, “New approach to projection electron lithography with demonstrated 0.1 μm linewidth,” *Appl. Phys. Lett.* **57**, 153 (1990); S.D. Berger, J.M. Gibson, R.M. Camarada, R.C. Farrow, H.R. Huggins, J.S. Kraus, and J.A. Liddle, “Projection electron beam lithography: A new approach,” *J. Vac. Sci. Technol.* **B5**, 2996 (1991).

¹⁴⁷H. Itoh, H. Tadokoro, Y. Sohda, Y. Nakayama, and N. Saitou, “Cell projection column for high speed electron beam lithography system,” *J. Vac. Sci. Technol.* **B10**, 2799 (1992).

¹⁴⁸S.D. Berger and J.M. Gibson, “New approach to projection electron lithography with demonstrated 0.1 μm linewidth,” *Appl. Phys. Lett.* **57**, 153 (1990); S.D. Berger, J.M. Gibson,

SCALPEL technology suffers from space-charge effects, which make it nearly impossible to achieve both high resolution and high throughput simultaneously with the system. As a result, the SCALPEL technology is no longer being pursued by the semiconductor industry. It should be pointed out, however, that when compared with conventional serial scanning systems, both the Hitachi and AT&T innovations provide for the simultaneous printing of a much larger number of pixels.¹⁴⁹

4.11 Ion-Beam Lithography

Lithography using beams of ions has been investigated by several researchers,¹⁵⁰ motivated by the fact that ion-beam lithography can achieve higher resolution than electron-beam lithographic techniques because ions have a higher mass and therefore scatter less than electrons. The technique also allows the use of resists with lower sensitivities than the other lithographic approaches. One major drawback of ion-beam lithography is that it may suffer from random (or stochastic) space-charge effects, causing broadening of the ion beam. The most important application of ion-beam lithography to date is the repair of optical lithographic masks.¹⁵¹

There are two types of ion-beam lithography systems, namely, a scanning focused-beam system and a large-area projection system. The former is similar to the electron-beam machine, in which the ion source can be Ga^+ or H^+ , the major differences being in the source and deflection lenses.¹⁵² The latter system is similar to an optical $5\times$ reduction projection step-and-repeat system, which projects 100-KeV light ions such as H_2^+ through a stencil mask.¹⁵³ It must, however, be stated that before these ion-beam lithographic techniques can become competitive with electron-beam lithography, there must be significant

R.M. Camarada, R.C. Farrow, H. R. Huggins, J.S. Kraus, and J.A. Liddle, "Projection electron beam lithography: A new approach," *J. Vac. Sci. Technol. B* **5**, 2996 (1991).

¹⁴⁹M.J. Bowden, "An introduction to microlithography," in *Introduction to Microlithography*, L.F. Thompson, C.G. Willson, and M.J. Bowden, Eds., pp. 11, 12, American Chemical Society, Washington, DC (1994).

¹⁵⁰T.M. Hall, A. Wagner, and L.F. Thompson, "Ion beam exposure characteristics of resists," *J. Vac. Sci. Technol.* **16**, 1889 (1979); T. Kaneko, T. Umegaki, and Y. Kawakomi, Microelectronics Seminar, in *Proc. Kodak Interface 80*, p. 25 (1980).

¹⁵¹G.S. May and S.M. Sze, *Fundamentals of Semiconductor Fabrication*, pp. 79, 80, John Wiley & Sons, Hoboken, NJ (2004).

¹⁵²J. Melngailis, "Focused ion beam technology and applications," *J. Vac. Sci. Technol. B* **5**, 469 (1987); K. Hosond, H. Morimoto, Y. Watanabe, and T. Kato, *Proc. SPIE* **923**, 84 (1988).

¹⁵³G. Stengl, W. Loschner, and P. Wolf, "Ion projection lithography machine IPLM 01: A new tool for sub 0.5 micron modification of materials," *J. Vac. Sci. Technol. B* **6**, 194 (1986); G. Stengl, G. Bosch, A. Chalupka, J. Fegerl, R. Fischer, G. Lammer, H. Loschner, L. Malek, R. Nowak, C. Traher, P. Wolfe, P. Mauger, A. Shimkunas, S. Sen, and H.C. Wolfe, "Ion projector wafer exposure results at 5X ion optical reduction obtained with nickel and silicon stencil masks," *J. Vac. Sci. Technol. B* **10**(6), 2824 (1992).

advances in high-brightness sources, high-speed deflection systems for the scanning system, and stable masks and large lenses for the projection tools.¹⁵⁴

4.12 Extreme Ultraviolet Lithography

Extreme ultraviolet lithography (EUV) is a promising next-generation lithographic technique for replacing optical lithography, perhaps at the sub-22-nm technology nodes. Invented independently in the mid-1980s by researchers at NTT and AT&T Bell Laboratories,¹⁵⁵ who were inspired by the availability of mirrors of reasonable efficiency at soft x-ray wavelengths ($\lambda \approx 10\text{--}15\text{ nm}$), it offers distinct advantages of wide process margins and extendibility to multiple lithographic nodes. Its main drawback is the enormous cost of bringing up its infrastructure.

The soft x rays with wavelengths of 10–14 nm used in EUV lithography are produced from a laser-produced plasma or synchrotron radiation. A mask that is produced by patterning an absorber material deposited on multilayer-coated flat silicon is used to reflect the EUV radiation from the nonabsorbing regions of the mask through a 4 \times reduction camera and imaged onto a thin layer of resist on the wafer. Due to the strong absorptivity of all materials at EUV wavelengths, the lithography process is performed in vacuum. In particular, the mirrors are coated with multiple layers that produce distributed quarter-wave Bragg reflectors. The mask blank is also multilayer coated to maximize its reflectivity at wavelengths of 10–14 nm.¹⁵⁶

The major problems of EUV lithography include low source power and mask defects, exacerbated by the difficulty of producing defect-free mask blanks and protecting the fabricated masks from contaminants and defects, given the lack of pellicles to protect the masks. Also, mask defect inspection and repair are extremely difficult. Furthermore, producing resists that simultaneously meet the resolution, line edge roughness, and sensitivity requirements for sub-22-nm half-pitch patterning is proving to be extremely difficult.

4.13 Soft Lithography

Soft lithography, developed in the 1990s in George Whitesides' Laboratories at Harvard University, involves printing, molding, and other mechanical processes

¹⁵⁴M.J. Bowden, "An introduction to microlithography," in *Introduction to Microlithography*, L.F. Thompson, C.G. Willson, and M.J. Bowden, Eds., pp. 11, 12, American Chemical Society (1994).

¹⁵⁵D.M. Tennant, J.E. Bjorkholm, R.M D'Souza, L. Eichner, R.R. Freeman, J.Z. Pastalan, L.H. Szeto, O.R. Wood, T.E. Jewell, W.M. Mansfield, W.K. Waskiewicz, D.L. White, D.L. Windt, and A.A. MacDowell, "Reflective mask technologies and imaging results in soft x ray projection lithography," *J. Vac. Sci. Technol. B* **9**(6), 3176 (1991).

¹⁵⁶G.S. May and S.M. Sze, *Fundamentals of Semiconductor Fabrication*, pp. 79, John Wiley & Sons, Hoboken, NJ, 80 (2004).

carried out using an elastic stamp to fabricate patterns with very fine resolutions. Photolithography or electron-beam lithography is used to fabricate the stamp in a resist layer on the surface of a silicon wafer; this results in a bas-relief master in which islands of resist stand out from the silicon. Patterning of features with this stamp is accomplished by pouring dimethylsiloxane—a free-flowing liquid—over the bas-relief master and curing it into the rubbery solid polymer called polydimethylsiloxane (PDMS). With this stamp, several techniques including microcontact printing, micromolding in capillaries, and nanoskiving can be used to fabricate nanostructures. Related techniques, based on step-and-flash imprint lithography and nanoimprint lithography that use hard masters instead of elastic PDMS have also been developed and have shown excellent resolution.¹⁵⁷

Soft lithography, it must be pointed out, is not well suited for fabricating structures with multiple layers that stack precisely on top of one another, as is the case in conventional ICs. Deformations and distortions of the soft PDMS stamp can result in errors in the replicated pattern and a misalignment of the pattern with any underlying pattern previously fabricated. The use of rigid stamps in imprint lithography has proved reasonably successful in correcting this shortcoming. However, it remains extremely difficult to produce rigid masters without defects, which, given that this is a $1\times$ printing technique, are reproduced on the wafer with a high degree of fidelity.¹⁵⁸

One significant advantage of imprint lithography over standard photolithography is the ability to pattern three-dimensional topographies in a single step, thus reducing the cost of fabricating such a device. Such topography is critical for connecting different layers on an IC.¹⁵⁹

4.13.1 Microcontact printing

In this technique, the PDMS stamp is inked with a reagent solution consisting of organic molecules called thiols. Next, the stamp is brought into contact with a thin film of gold on a glass, silicon, or polymer plate, resulting in a reaction between the thiols and the gold surface that forms a highly ordered film [a self-assembled monolayer (SAM)] that replicates the stamp's pattern. Given that the thiol ink spreads somewhat beyond the pattern area after it contacts the surface, the resolution of the monolayer cannot be quite as high as that of the PDMS stamp. But when performed correctly, microcontact printing can produce patterns with features as small as 50 nm.¹⁶⁰

¹⁵⁷G.M. Whitesides and J.C. Love, "The art of building small," *Sci. Am. Reports* **17**(3), 13–21 (2007); B.D. Gates, Q.B. Xu, M. Stewart, D. Ryan, C.G. Willson, and G.M. Whitesides, "New approaches to nanofabrication: molding, printing, and other techniques," *Chem. Rev.* **105**(4), 1171–1196 (2005).

¹⁵⁸*ibid.*

¹⁵⁹*ibid.*

¹⁶⁰G.M. Whitesides and J.C. Love, "The art of building small," *Sci. Am. Reports* **17**(3), 13–21 (2007).

4.13.2 Micromolding in capillaries

The PDMS stamp in this technique is placed on a hard surface containing liquid polymer, such that through capillary action the liquid polymer flows into the recesses between the surface and the stamp. On solidification, the polymer takes the form of the desired pattern. Patterning is completed when the stamp is released from the solidified polymer. This technique can replicate features smaller than 10 nm.¹⁶¹

4.13.3 Nanoskiving

In this technique, a PDMS stamp is first used to mold a hard plastic such as epoxy—with cylindrical posts, for example. Coating the molded epoxy with a thin (~ 50 nm) film of metal, followed by the coating of more epoxy, and cutting parallel to the plane of the sandwich structure, creates a thin sheet of plastic containing nanostructures shaped like the cross section of the original molded structures—for cylindrical posts, the resulting shapes are rings. The thickness of the slice determines their height and the deposited film their thickness. These techniques are well suited for fabricating subwavelength optical devices, waveguides, and optical polarizers on the one hand, and on the other hand, biochips based on nanofluidics and microfluidics, which are used in biochemical research.¹⁶²

4.13.4 Step-and-flash imprint lithography

The step-and-flash imprint lithography technique developed by C. Grant Willson of the University of Texas at Austin around 2000 differs from the soft lithographic techniques developed by George Whitesides in that in step-and-flash imprint lithography, lithography is used to pattern a quartz plate, yielding a rigid bas-relief master, which is directly pressed against a thin film of liquid polymer (thus eliminating the step of making the elastic PDMS stamp from the master as in Whitesides' approach), which fills the master's recesses. Then, the master is exposed to ultraviolet radiation, which cures and solidifies the polymer to create the desired replica. Releasing the quartz plate from the hardened polymer provides the patterned structures with resolution down to 20 nm.¹⁶³

4.13.5 Nanoimprint lithography

Developed by Stephen Chou of Princeton University in the 1990s, this technique uses a rigid, hard master that is placed on a film of polymer that has been heated

¹⁶¹ibid.

¹⁶²ibid.

¹⁶³B.D. Gates, Q.B. Xu, M. Stewart, D. Ryan, C.G. Willson, and G.M. Whitesides, "New approaches to nanofabrication: molding, printing, and other techniques," *Chem. Rev.* **105**(4), 1171–1196 (2005).

to a temperature near its melting point to facilitate the embossing process. This technique has shown resolution down to 20 nm with good fidelity.¹⁶⁴

4.14 Proximal Probe Lithography

One of the newest additions to lithographic patterning techniques is proximal probe lithography.¹⁶⁵ Not long after the very invention of the scanning tunneling microscope (STM) by Heinrich Rohrer and Gerd K. Binnig of the IBM Zurich Research Laboratories in 1981,¹⁶⁶ researchers began to investigate the application of proximal probes to lithography.¹⁶⁷ Proximal probes are attractive from a number of standpoints because they offer the potential for atomic-scale resolution. They have been used to define lithographic patterns in commercial resists, surface oxide, surface modification, electrochemical etching, and chemical vapor deposition. Furthermore, simple electronic structures have been made with proximal probe lithography and their transport properties measured.¹⁶⁸

Proximal probes are defined as tools in which a tip is held close to or in intimate contact with a surface so that there is an interaction between the atoms on the tip and the substrate.¹⁶⁹ The most widely used proximal probes include the STM, in

¹⁶⁴G.M. Whitesides and J.C. Love, "The art of building small," *Sci. Am. Reports* **17**(3), 13–21 (2007).

¹⁶⁵C.R.K. Marrian, Ed., *Technology of Proximal Probe Lithography*, SPIE Optical Engineering Press, Bellingham, WA (1993).

¹⁶⁶G. Binnig and H. Rohrer, "Scanning tunneling microscopy," *Helv. Phys. Acta* **55**, 726 (1982); G. Binnig, H. Rohrer, C.H. Gerber, and W. Weibel, "Tunneling through a controllable vacuum gap," *Appl. Phys. Lett.* **40**, 178 (1982); G. Binnig, H. Rohrer, C.H. Gerber, and E. Weibel, "Surface studies by scanning tunneling microscopy," *Phys. Rev. Lett.* **49**, 178 (1982).

¹⁶⁷M.A. McCord and R.F.W. Pease, "High resolution, low voltage probes from a field emission source close to the target plane," *J. Vac. Sci. Technol. B* **3**, 198 (1985).

¹⁶⁸E.E. Ehrichs, W.F. Smith, and A.L. de Lozanne, "Four probe resistance measurements of nickel wires written with a scanning tunneling microscope/scanning electron microscope system," *J. Ultra microsc.* **42–44**, 1438 (1992); L. Stockman, I. Heyvaert, C. van Haesendonck, and Y. Bruynseraede, "Submicrometer lithographic patterning of thin gold films with a scanning tunneling microscope," *Appl. Phys. Lett.* **62**, 2935 (1993); K. Matsumoto, M. Ishii, K. Segawa, Y. Oka, B.J. Vartanian, and J.S. Harris, "Room temperature operation of a single electron transistor made by the scanning tunneling microscope nanooxidation process for the TiO_x/Ti system," *Appl. Phys. Lett.* **68**, 34 (1996); T. Fayfield and T.K. Higman, "Fabrication and transport measurements of atomic force microscope modified silicon metal oxide semiconductor field effect transistors," *J. Vac. Sci. Technol. B* **13**, 1285 (1995); P.M. Campbell, E.S. Snow, and P.J. McMarr, "Fabrication of nanometer scale side gated silicon field effect transistors with an atomic force microscope," *Appl. Phys. Lett.* **66**, 1388 (1995); S.C. Minne, H.T. Soh, P.H. Flueckiger, and C.F. Quate, "Atomic force microscope lithography for fabricating a 0.1 μm metal oxide field effect transistor," *Appl. Phys. Lett.* **66**, 703 (1995); K. Matsumoto, S. Takahashi, M. Ishii, M. Hoshi, A. Kurokawa, S. Ichimura, and A. Ando, "Application of STM nanometer size oxidation process to planar type Mim Diode," *Jpn. J. Appl. Phys.* **34**, 1387 (1996).

¹⁶⁹C.J. Chen, *Introduction to Scanning Tunneling Microscopy*, Oxford University Press, New York (1993).

which current is induced to flow across a potential difference between a sharp tip and the substrate, and the atomic force microscope (AFM), in which an electric field potential is established between the tip and substrate, resulting in overlapping repulsive atomic potentials. In both STM and AFM, a conducting tip is held in close proximity to a substrate and potential is applied between the tip and the sample.¹⁷⁰

In STM lithography, the tip-to-sample separation is adjusted to maintain a constant current of approximately 0.003–3 nA between the tip and the sample. The tip-to-sample current is fed into the circuitry that drives the piezoelectric transducer, which in turn controls the tip height. Lateral piezoelectric transducers scan the tip across the surface.¹⁷¹

In AFM lithography, the tip rests on the end of a cantilever, with the force (1–100 nN) between the tip and sample being determined by measurement of the deflection of the cantilever. This measurement can be optical, capacitive, or piezoresistive. Here, the tip-to-sample separation is adjusted to maintain constant force between the tip and the sample.¹⁷²

Several physical approaches to writing patterns by STM and AFM have been reported. For AFM, these include moving nanoparticles around and arranging them in patterns by AFM tips, scratching a surface (or, more commonly, in monolayer films of atoms or molecules that coat the surface). For STM, by increasing the currents flowing from the tip of the STM, the microscope becomes a very small source for an electron beam, which can be used to write nanometer-scale patterns by probe-induced chemical vapor deposition,¹⁷³ lithography in resists,¹⁷⁴ and surface modification.¹⁷⁵ The STM tip can also push individual atoms around on a surface to build patterns.¹⁷⁶

There are several challenges that must be addressed before proximal probe lithography can make the transition into mainstream lithographies. The most

¹⁷⁰E.A. Dobisz, F.K. Perkins, and M.C. Peckerar, “E beam and proximal probe processes for nano lithography,” in *Microlithography: Science and Technology*, J.R. Sheats and B.W. Smith, Eds., p. 737, Marcel Dekker, New York (1998).

¹⁷¹*ibid.*, pp. 737, 738.

¹⁷²*ibid.*, p. 738.

¹⁷³F.K. Perkins, M. Onellion, S. Lee, and P.A. Dowben, “Demonstrating the utility of boron based precursor molecules for selective area deposition in a scanning tunneling microscope,” *Mater. Res. Soc. Proc.* **236**, 153 (1992); D.S. Scully, A. Ermakov, E.L. Garfunkel, and P.A. Dowben, “Electron beam induced patterned deposition of allylcyclopentadienyl palladium using scanning tunneling microscopy,” *J. Appl. Phys.* **76**, 7639 (1994).

¹⁷⁴E.A. Dobisz, F.K. Perkins, and M.C. Peckerar, “E beam and proximal probe processes for nano lithography,” in *Microlithography: Science and Technology*, J.R. Sheats and B.W. Smith, Eds., pp. 715–775, Marcel Dekker, New York (1998).

¹⁷⁵G.M. Shedd and P. Russel, “The scanning tunneling microscope as a tool for nanofabrication,” *Nanotechnology* **1**, 67 (1990).

¹⁷⁶J.A. Stroscio and D.M. Eigler, “Atomic and molecular manipulation with the scanning tunneling microscope,” *Science* **254**, 1319–1326 (1991). For pictures of atom manipulation, please see <http://www.almaden.ibm.com:80/vis/stm/gallery.html>.

important issues deal with the availability of good-quality resists or imaging layers, control and maintenance of the integrity of the tip, and throughput.¹⁷⁷

A new scanning probe method, called dip-pen lithography, was developed by Chad A. Manning of Northwestern University over the last decade. In this technique, the tip of an AFM is coated with a thin film of thiol molecules that are insoluble in water but react with a gold surface. When the device is placed in an atmosphere containing an appreciable concentration of water vapor, a minute drop of water condenses between the gold surface and the microscope's tip. Surface tension pulls the tip to a fixed distance from the gold, and this distance remains fairly fixed as the tip moves across the surface. The drop of water effectively acts as a bridge over which the thiol molecules migrate from the tip to the gold surface, where they form a self-assembled monolayer. Lines that are few nanometers across have been successfully written with this procedure.¹⁷⁸

Although dip-pen lithography is a relatively slow technique, it has great versatility with respect to the many varieties of molecules it can use as "inks," which makes it an attractive candidate for introducing chemical flexibility to nanometer-scale writing. Parallel arrays of independent scanning probes have improved the throughput of dip-pen lithography significantly in recent times.¹⁷⁹

4.15 Atom Lithography

A variety of direct atom manipulations have been demonstrated with proximal probes.¹⁸⁰ The electric field strength in the vicinity of a probe tip is very strong and inhomogenous, so much so that it can be used to manipulate atoms, including sliding atoms over surfaces and transferring atoms by pick (erase) and place (write). These atomic manipulation processes can be classified as parallel processes and perpendicular processes. In parallel processes, an adsorbed atom or molecule is induced to move along the surface (sliding). In perpendicular processes, the atom or molecule is transferred from the surface to the tip of a proximal probe or vice versa. While the theoretical resolution of this technique is a single atom, its major drawback is the extremely long time it takes to generate even the simplest of features.¹⁸¹ The use of the atomic processing microscope (APM) by Kamerski et al.,¹⁸² in 1993 has opened up new methods for shortening the time considerably.

¹⁷⁷E.A. Dobisz, F.K. Perkins, and M.C. Peckerar, "E beam and proximal probe processes for nano lithography," in *Microlithography: Science and Technology*, J.R. Sheats and B.W. Smith, Eds., p. 739, Marcel Dekker, New York (1998).

¹⁷⁸G.M. Whitesides and J.C. Love, "The art of building small," *Sci. Am. Reports* **17**(3), 13–21 (2007).
¹⁷⁹*ibid.*

¹⁸⁰J.A. Stroscio and D.M. Eigler, "Atomic and molecular manipulation with the scanning tunneling microscope," *Science* **254**, 1319–1326 (1991).

¹⁸¹M.J. Madou, *Fundamentals of Microfabrication: The Science of Miniaturization*, 2nd ed., p. 61, CRC Press, New York (2002).

¹⁸²Editorial, "Ingenious STM puts atoms right where you want them," *Res. Dev.*, p. 71, (April, 1993).

They succeeded in imaging selected atoms on a surface, stripping them off, and replacing them with other atoms, all in a matter of minutes. The APM relies on some important technical innovations such as photon biasing, whereby a precise voltage and photon pulse is “tuned” to a specific atom to strip it from the surface. Optical biasing (called “optical tweezers”) has been used to manipulate a variety of individual particles on a variety of surfaces.¹⁸³

4.16 Stereolithography

Stereolithography, a technique in which light exposure is used to solidify a special liquid resin into a desired three-dimensional shape, has been developed in recent years.¹⁸⁴ This is accomplished by polymerizing monomers (such as acrylates) contained in a mold of the desired pattern in stepwise fashion with UV radiations or e-beam radiations until the desired pattern is realized. Following polymerization and solidification, the formed pattern is released from the mold. Complex objects with a resolution better than 5 μm in the x , y , and z directions have been fabricated in this manner.¹⁸⁵ The key to this three-dimensional imaging is the use of photon resists that are capable of undergoing two-photon photochemistry. Such resists can respond to the square of the radiation intensity. This necessitates the use of extremely high-power radiation. Remarkably, this approach enables lithographic patterning on nonplanar substrates.

4.17 Molecular Self-Assembly Lithography

Molecular self-assembly, a chemical process in which molecules spontaneously organize to form larger-ordered structures, represents one of the newest emerging lithographic techniques. In one form of this technique, self-assembling precursor molecules from solutions or vapor phases react at interfaces to produce layers of monomolecular thickness that are chemically bonded to solid surfaces through thermodynamically favorable bond formation involving chemisorption. Such layers belong to a class of SAMs and make good ultrathin film resist candidates. These SAM films can be molecularly engineered to be patterned by various types of energetic radiation including DUV, soft x rays, ion beams, and low-energy electrons.¹⁸⁶ Scratching and microcontact printing (see Section 4.13.1) have been

¹⁸³M.J. Madou, *Fundamentals of Microfabrication: The Science of Miniaturization*, 2nd ed., p. 61, CRC Press, New York (2002).

¹⁸⁴K. Ikuta and K. Hirowatari, “Real three dimensional micro fabrication using stereolithography,” in *Proc. IEEE Micro Electro Mechanical Systems (MEMS '93)*, Ft. Lauderdale, pp. 42–47 (1993); K. Ikuta, K. Hirowatari, and T. Ogata, “Three dimensional integrated fluid systems (MIFS) fabricated by stereo lithography,” in *IEEE Int. Workshop on Micro Electro Mechanical Systems (MEMS '94)*, Oiso, Japan, pp. 1–6 (1994).

¹⁸⁵M.J. Madou, *Fundamentals of Microfabrication: The Science of Miniaturization*, 2nd ed., pp. 66, 67, CRC Press, New York (2002).

¹⁸⁶C.R.K. Marrian and E.S. Snow, “Proximal probe lithography and surface modification,” *Microelectron. Eng.* **32**, 173–189 (1996).

used to pattern SAMs. Device features smaller than 20 nm have been successfully patterned on SAMs with STMs and conventional electron-beam lithography systems.¹⁸⁷

Resists based on SAMs have also been successfully deposited on metals such as gold, aluminum, titanium, zirconium, silver, copper, and platinum as well as SiO₂, GaAs, and other surfaces,¹⁸⁸ inspired no doubt by the first demonstration of the formation of long-chain ω -substituted dialkyldisulfides on gold in 1983.¹⁸⁹ Alkane thiols and dialkyldisulfides, which are lipidlike organic molecules having the general formula HS-(CH₂)_n-X and X-(CH₂)_m-SS-(CH₂)_m-Y, respectively, where *n* and *m* indicate alkyl chain length and X, Y indicate the end groups [-CH₃, -azobenzene, -OH, etc.],¹⁹⁰ are well-known precursor materials for SAMs on gold, the most extensively studied substrate. Organosilanes are often used to form SAMs on Si surfaces through Si-O-substrate siloxane bond; the alkyl group R is responsible for the ordered nature of the film.¹⁹¹

A new variant of this technique, called directed self-assembly lithography, pioneered within the last five years in Tom Russel's group at the University of Massachusetts at Amherst and Paul Nealy's group at the University of Wisconsin, Madison, involves the use of external fields (such as interfacial interactions, electric fields, thermal fields, capillary force, solvent evaporation, and flow fields), internal fields, gradient fields, and coupled fields to direct the self-assembly of appropriate precursors, typically block copolymers, on surfaces into desired patterns that can be imaged with various types of energetic radiation including DUV, soft x rays, and electron beams, and be transferred into underlying substrates.

¹⁸⁷H.U. Muller, C. David, B. Volkel, and M. Gunze, "Nanostructuring of alkanethiols with ultrasharp field emitters," *J. Vac. Sci. Technol.* **B13**, 2846–2849 (1995).

¹⁸⁸H.A. Biebuyck, N.B. Larsen, E. Delamarche, and B. Michel, "Lithography beyond light: micro contact printing with monolayer resists," *IBM J. Res. Dev.* **41** (1997).

¹⁸⁹R.G. Nuzzo and D.L. Allara, "Adsorption of bifunctional organic disulfides on gold surfaces," *J. Am. Chem. Soc.* **105**, 4481 (1983).

¹⁹⁰E. Delamarche, B. Michel, H.A. Biebuyck, and C. Gerber, "Golden interfaces: the surface self assembled monolayers," *Adv. Mater.* **8**, 719–729 (1996).

¹⁹¹M.J. Madou, *Fundamentals of Microfabrication: The Science of Miniaturization*, 2nd ed., pp. 62, 63, CRC Press, New York (2002).

Chapter 5

Lithographic Chemicals

Why is the grass so cool, fresh and green?
The sky so deep, and blue?
Get to your Chemistry,
You dullard, you!

Walter de la Mare, *The Dunce*

5.1 Introduction

Present-day lithographic chemicals, including inks, resists, antireflection coatings, casting solvents, developers, strippers, etc., evolved largely from technologies developed in the printing industry. Integrated circuits and circuit boards were unheard of in 1798 when Senefelder invented lithography and in 1826 when Niepce invented photolithography. Since those early days, lithographic chemicals have evolved from being extracted from natural sources to being derived almost exclusively from synthetic sources today. They have also grown in importance along with the electronics industry, since even the simplest electronic systems today are patterned with resists, using ever more sophisticated arrays of lithographic chemicals. In this chapter, we present an overview of lithographic chemicals used in patterning integrated circuit devices and printing newspapers, textbooks, posters, and the like, while making historical references to similar materials used in lithography in earlier times.

5.2 Resists

Resist formulations may generally contain these components: (i) film-forming resin, (ii) solvent, (iii) sensitizer or photoinitiator or photoacid generator, and (iv) additives. The dried film coated from a solution containing the above ingredients undergoes changes when exposed to radiation of a certain wavelength or electrons or even ions; this exposure alters the solubility in the developer of the exposed areas relative to the unexposed areas. If the resist prints in a negative tone, the exposed areas are hardened, whereas positive-tone resists are made more soluble in the developer solvent by the exposure. The changes in the exposed areas

are due to some chemical reactions brought about by the absorbed radiation.¹ Historically, it is possible that the resin itself is intrinsically photosensitive (e.g., bitumen of Judea or Syrian asphalt), in which case it would be classified as a one-component resist; but much more commonly some substance or substances that are capable of absorbing radiation energy and bringing about an insolubilizing reaction (e.g., ammonium dichromate, DNQ) have been added to the formulation, in which case the resist would be classified as a multicomponent resist (see Fig. 5.1). These substances are referred to as “sensitizers” or “photoinitiators” and are invariably present in modern-day resist formulations. A related group of compounds used in chemically amplified resists, but that all the same function in an analogous fashion to sensitizers, are called photoacid generators (e.g., onium salts). Additives are substances that enhance or improve the performance of the resist. Examples include leveling agents, surfactants, antioxidants, stabilizers, and related chemicals.² A typical advanced resist today may comprise 50%–90% by weight of solvent, 10%–40% by weight of resins, 1%–8% by weight of sensitizers or photoacid generators, and less than 1% by weight of surfactants, antioxidants, leveling agents, and other additives.

It should be emphasized that one-component resists consisting of pure radiation-sensitive materials, which in modern times are comprised primarily of polymers that combine all of the necessary attributes of a resist, have now fallen out of favor. In contrast, modern advanced lithography relies almost exclusively on the multicomponent design concept in which resist functions are provided by separate components, comprising the resin/binder on the one hand, and the photoactive compounds on the other. In these multicomponent systems, the resins/binders are polymers and are typically inert to radiation, but can undergo radiation-induced reactions initiated by the photoactive components of the resists.³

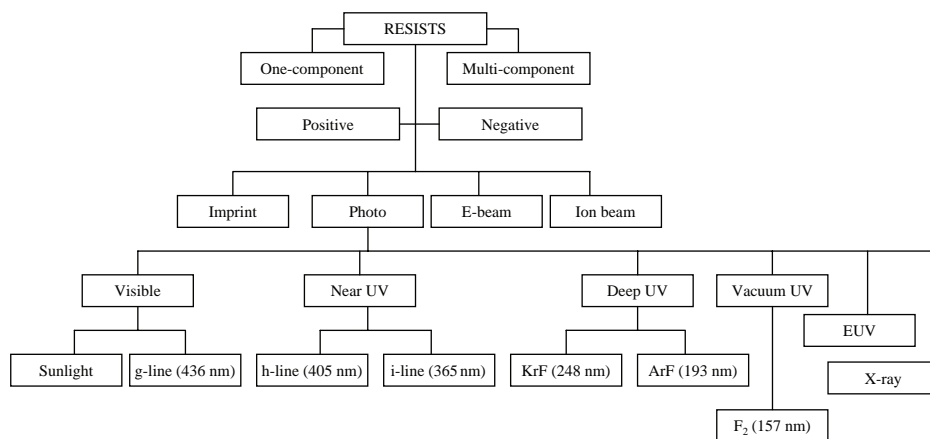


Figure 5.1 Resist classifications.

¹W.S. DeForest, *Photoresist: Materials and Processes*, p. 20, McGraw Hill, New York (1975).

²*ibid.*

³H. Ito, “Chemical amplification resists for microlithography,” *Adv. Polym. Sci.* **172**, 45, (2005).

In addition to classifying resists based on their imaging tone or on the basis of the number of components they contain, resists can also be classified on the basis of the radiation types used to expose them (see Fig. 5.1). Here we have UV resists (generally called photoresists), extreme-UV resists, x-ray resists, electron-beam (e-beam) resists, ion-beam resists, etc. Photoresists can be further divided into near-UV (350–450 nm) resists, mid-UV (300–350 nm) resists, deep-UV (250–190 nm) resists, and vacuum-UV (157 nm) resists, depending on exposure wavelength. Because EUV resists are actually exposed by secondary electrons generated by the soft x-ray photons used in EUV lithography at 13.5 nm, they are technically not called photoresists, and EUV lithography is also not technically considered to be an extension of photolithography.⁴

The aforementioned classification scheme reflects the semiconductor industry's quest for fine resolution. The development of modern resists has followed in lockstep the migration of semiconductor lithography from the visible light region of the electromagnetic spectrum at 436 nm of the mercury discharge lamp g-line to the near-UV region at 365 nm of the mercury discharge lamp i-line, to DUV at 248 nm and to 193 nm, using KrF and ArF exciplex lasers, respectively. As shown in Fig. 4.6, cyclized rubber resists dominated the industry between 1960 and 1970, during the era of contact printing based on i- and h-line lithography. Diazoanthraquinone (DNQ)/novolac resists dominated the industry between 1970 and 1996, spanning the g-, h-, and i-line lithographies. By 1997, resolution requirements for advanced ICs at the 250-nm technology node were beyond the capabilities of i-line lithography, paving the way for the introduction of polyhydroxystyrene (PHOST) resists based on chemical amplification and exposed with DUV 248-nm KrF exciplex lasers into high-volume production. Beyond i-line, resist chemistry for optical lithographies is dominated by the demands of the base polymer absorption; novolac is too opaque to be used as a 248-nm resist. PHOST-based resists, being reasonably transparent at 248 nm, became the new standard resin.

The switch to PHOST-based resists required the invention of a new imaging scheme, namely, chemical amplification with high sensitivity, in order to accommodate the low output power of early KrF lasers, as well as the fact that unlike DNQ/novolac, PHOST-based resists do not exhibit dissolution inhibition behavior. By the time 193-nm ArF, exciplex-laser lithography was implemented in high-volume production at the 90-nm technology node in 2003, and PHOST resist resins were replaced with aliphatic and alicyclic polymers, which are reasonably transparent at this wavelength, unlike PHOST. Again, the imaging mechanism was based on chemical amplification. Because aliphatic polymers based on acrylates etch somewhat too fast, copolymerizing them with the more etch-resistant alicyclic norbornene-derived monomers improved the overall etch stability of these polymers. Resist formulations based entirely on alicyclic polymers have also been developed and deployed in the high-volume manufacturing environment. The technology nodes covering 90 nm and 65 nm with dry ArF lithography, as well as 45 nm with immersion ArF lithography, are all based on these groups of polymers.

⁴ibid.

With F₂ excimer laser lithography at 157 nm, even polymers based on acrylates and norbornenes are too opaque to be of any useful value in resist applications. Therefore, fluorocarbons and silanol polymers are the two main classes of polymers that have reasonable transparency at this wavelength. Again, like their 193-nm and 248-nm counterparts, the 157-nm resists employ chemical amplification in their imaging mechanism, for quite similar reasons.

Because the absorption phenomenon at EUV is atomic, almost every element is opaque at EUV, except thin films of polymers with high carbon content (as in aromatic PHOST-based polymers, as well as in acrylate and alicyclic polymers) and silicon. Polymers containing high amounts of oxygen and fluorine have very high absorptivity at EUV.⁵

Although photoresists remain the dominant resists used in the fabrication of all kinds of IC devices, electron-beam resists are widely used in the fabrication of photomasks and x-ray masks, as well as in niche applications in the fabrication of exploratory research devices.

Among the many parameters (resolution, contrast, sensitivity, etch resistance, storage stability, thermal stability, radiation absorption, adhesion to appropriate substrates, solubility in appropriate solvents, etc.) that are used to describe resists, contrast and sensitivity are the two that are most used to describe resist performance. In the next two chapters, the four constituents of resists are discussed in detail for each resist platform.

5.2.1 Resist solvents

Resist solvents are chosen based on their ability to dissolve the resist resins, compounds, sensitizers, and additives, as well as cast good dry films of the resist from solution. They have evolved over the years from being sourced exclusively from naturally occurring compounds such as linseed oil and turpentine as used in the bitumen of Judea resists of the early days of photolithography in the early part of nineteenth century, to water used in the dichromate resists in the mid-nineteenth to early twentieth centuries, to synthetic organic solvents now used in resists in the semiconductor industry. Today, resist solvents fall into a narrow range of boiling points and evaporation rates. Table 5.1 contains some of the most popular resist solvents currently in use in semiconductor lithography. There is only a limited selection of suitable organic solvents available for use as casting solvents. In fact, some organic solvents with otherwise good properties such as xylene, cyclohexanone, chlorobenzene, etc. that were used in earlier times are no longer being used today due to toxicological concerns.

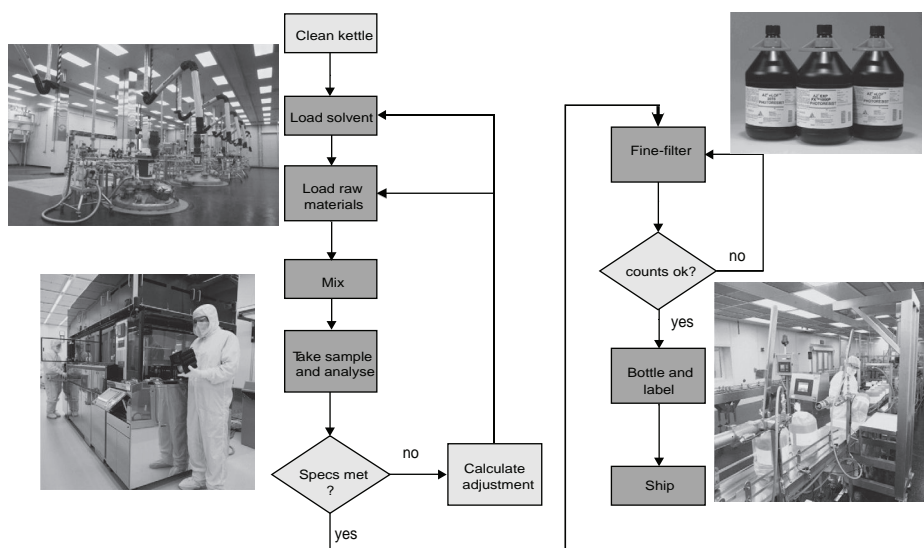
5.2.2 Manufacture of resists

The process flow for the large-scale manufacturing of advanced commercial resists is shown in Fig. 5.2. The process begins with cleaning the reaction vessel or kettle,

⁵The absorption properties of EUV resists are covered in Chapter 14.

Table 5.1 Commonly used resist solvents.

Chemical and common names and formula	Boiling point (°C)	Viscosity (cP)	Comments
2 Ethoxymethyl acetate (Ethyl cellulosolve acetate) $C_2H_5O(CH_2)_2 OCOCH_3$	156	1.2	Widely used in the past, but now considered unsafe
2 Methoxyethylether (Diglyme) $CH_3OCH_2CH_2OCH_2CH_2OCH_3$	162		Widely used in the past, but now considered unsafe
Ethyl lactate $CH_3CH(OH)COOC_2H_5$	154	2.4	Currently commercially available and considered safe
Propyleneglycol monoethylether acetate (PGMEA) $CH_3O(CH_2)_2CH_2OCOCH_3$	146	1.2	Currently commercially available and considered safe
Methylmethoxy propionate $CH_3O(CH_2)_2COOCH_3$	145		Currently commercially available and considered safe
Ethyl pyruvate $CH_3COCOOC_2H_5$	155		Currently commercially available and considered safe
2 Heptanone $CH_3(CH_2)_4COCH_3$	121		Currently commercially available and considered safe
2 Ethylethoxy propionate $CH_3CH_2O(CH_2)_2COOC_2H_5$	170	1.1	Used often as cosolvent in currently commercially available solvents.
Diacetone alcohol (4 Hydroxy 4 methyl 2 pentanone) $CH_3COCH_2C(OH)(CH_3)_2$	168	2.9	Safe solvent, but not currently in use for positive resists
Cyclohexanone $(CH_2)_5O$	157	2.0	Safe solvent, but not currently in use for positive resists
Amyl acetate $CH_3COO(CH_2)_4CH_3$	142	0.8	Used only as cosolvent. Although considered safe, it is not currently in use for positive resists

**Figure 5.2** Typical process flow for the large-scale manufacturing of advanced commercial resists. (Courtesy of R. Dammel.)

into which the appropriate resist solvent is subsequently loaded, followed by the resins, sensitizers, and additives. After properly mixing and dissolving of the solid contents of the resist into the solvent, aliquots of resist solution are withdrawn and analyzed to make sure that the components meet the vendor's specification. Solutions that meet these specifications are then filtered, bottled, and labeled, before being shipped to their prospective customer. Solutions that do not meet the manufacturer's material specification are reformulated and the components adjusted appropriately to meet the specification. This iteration loop is executed as many times as necessary until the manufacturer's specification is met.

5.3 Antireflection Coatings

As patterning resolution entered submicron regimes, it quickly became obvious that substrate reflectivity posed significant problems that degraded critical dimension (CD) control and process latitude. Materials that suppressed reflectivity from the substrate were developed to mitigate this problem. They are called antireflection coatings, of which there are two types: organic and inorganic antireflection coatings.

Most antireflection coatings are organic polymers that are highly absorbing or contain highly absorbing dyes. They can be applied at the resist-substrate interface, in which case they are called bottom antireflection coatings, or they can be applied at the surface of the resist, in which case they are called top antireflection coatings.

Top antireflection coatings are made of polyfluoroalkylethers⁶ and Teflon-based materials,⁷ and are used to reduce swing curve effects. Additionally, they have been reported to improve the signal-to-noise ratio and shape of some stepper alignment signals.⁸ Earlier generations of top antireflection coatings were designed to be coated from organic solvents that do not attack the resist layer and must be removed before development since they are not aqueous-base soluble. In principle, chlorofluorocarbons (CFCs) may be used for both purposes, since they do not attack the resist.⁹

Inorganic antireflection coatings are typically deposited by sputtering, and as opposed to organic antireflection coatings, may in some cases be left in the finished device. Typical inorganic antireflection coatings include silicon oxynitride, amorphous silicon, tantalum silicide, titanium nitride, etc.

⁶T. Tanaka, N. Hasegawa, H. Shiraishi, and S. Okazaki, "A new photolithography technique with antireflective coating on resist ARCOR" in *Proc. SPE Reg. Tech. Conf. Photopolym.*, Ellenville, pp. 195–203 (1991).

⁷T.A. Brunner, "Optimization of optical properties of resist processes," *Proc. SPIE* **1466**, 297–308 (1991).

⁸T. Tanaka, N. Hasegawa, H. Shiraishi, and S. Okazaki, "A new photolithography technique with antireflective coating on resist ARCOR," in *Proc. SPE. Reg. Tech. Conf. Photopolym.*, Ellenville, pp. 195–203 (1991).

⁹In spite of this quality, CFCs cannot be used as solvents for top antireflection coatings because they are now banned for their role in the depletion of the ozone layer.

5.4 Resist Developers and Rinses

Resist developers fall into two main categories, depending on whether they are used for developing negative or positive resists. Negative resist developers are typically organic solvents in which the resist resins are soluble. Because the exposed area of the negative resist film is cross-linked and remains on the substrate, the unexposed part, still retaining the solubility characteristics of the parent resist resin, is dissolved away with the developing solvent. The actual negative-resist-developing operation involves the selective dissolution of the unexposed areas. Chemically, the cross-linking caused by the exposure process does not significantly alter the resist polymer enough to prevent a strong interaction with solvents capable of dissolving the unexposed and uncross-linked polymer. Consequently, swelling of the exposed areas will occur and can affect resist adhesion¹⁰ if it is severe enough; it will continue until equilibrium is reached.¹¹ Ways of minimizing the swelling problem of negative resists include applying adequate exposure to afford sufficient cross-linking, which in turn acts to limit the swelling, as well as using developing solvents that are not too active. It is known that the weaker the developing solvent, the lower the swelling, but the greater the probability of scum formation from inadequate development. Examples of negative resist developers include xylene, cyclohexanone, cellosolve acetate, heptanone, etc.¹²

Following the developing process of negative resists, a rinse is used to remove the excess developing solvents and the undissolved resist film from the patterned features. After developing, the negative-acting resist image is swollen, as already stated above, with absorbed solvents and is very susceptible to damage or lifting around the edge during rinsing. Most rinse solvents are nonaqueous, partly because water has a very strong polar attraction for the silica on the wafer surface and may tend to undermine the swollen image and cause adhesion loss. In earlier times, normal butyl acetate was commonly used as a rinse solvent for negative resists immediately after development.¹³ Mixtures of the lower aliphatic alcohols and developers were also sometimes used in earlier times as rinse solvents for both the negative ester- and hydrocarbon-resist resins after development.¹⁴

It has also been reported that water in the developing solvents may cause scumming with negative resists, particularly on silica surfaces. It tends to concentrate at the silica surface of wafers during the develop process. This is a location with high local resin concentration in the developing solvent, and, as a nonsolvent, it can cause precipitation in the form of a thin resin scum under some conditions.¹⁵

Positive resist developers, comprised entirely of solutions of alkaline metal or amine salts and bases, dissolve away the exposed areas of the resist, leaving

¹⁰E.B. Davidson, *Tech. Papers, Reg. Tech. Conf. Soc. Plast. Eng.*, Mid Hudson Sec., p. 141 (Oct. 1970).

¹¹W.S. DeForest, *Photoresist: Materials and Processes*, p. 242, McGraw Hill, New York (1975).

¹²*ibid.*, pp. 242–243.

¹³*ibid.*, p. 243.

¹⁴*ibid.*

¹⁵*ibid.*

largely untouched the unexposed areas, unlike their negative resist counterparts. The unique changes occurring in positive resists, described earlier, result in the formation of carboxylic acid groups in the sensitizer molecules or base polymer resins, which form alkaline-metal or amine salts in the developer solvent and are thereby dissolved away. There is little or no affinity between the unexposed areas and the developer solvent, which is in stark contrast to the negative resists, where both the exposed and unexposed areas tend to attract and retain the solvents. Solvent retention, which tends to cause swelling and pattern distortion in negative resist images, does not occur to any significant extent in positive resists. However, side reactions may occur in the exposed areas of positive resists, particularly in resists based on novolac resins (which contain phenolic groups) and DNQ sensitizers, where the likelihood of coupling reactions exists.¹⁶

During the developing process, coupling reaction, which has long been known in the formation of azo dyes, occurs at a very rapid rate at the proper pH with the formation of azo linkage between the sensitizer and phenol resin of novolac resists. Quinone diazides are quite stable and are resistant to coupling at neutral or acidic pH. Excessive alkalinity may impede coupling through the formation of other compounds. However, at the proper pH range, coupling could function to reduce the loss of the phenol resin from the surface.¹⁷

Positive resist developer solutions include, at least, a source of alkalinity in an aqueous medium and may or may not include a surfactant. Additionally, buffering agents, such as glycol ethers,¹⁸ and a coupling agent may also be present. During the developing process, the carboxylic acid groups formed by the exposed sensitizer or from the deprotection of the resist polymer resin is neutralized by the alkali substance present in older developers of bygone eras or a tetramethylammonium hydroxide (TMAH) base in modern developers, forming salts.¹⁹

Salts thus formed are dissolved in the developing solution, resulting in the decrease of the pH of the solution as the developing process proceeds. The absorption of carbon dioxide from the ambient air by the developer also consumes the free alkalinity in the developer, an occurrence that is not generally problematic in strongly buffered developers, but does affect dilute nonbuffered developer solutions appreciably.²⁰

Another factor that affects the positive resist developing process is temperature. Generally, temperatures in the low or mid-teens or above 26°C may tend to cause changes in the required developing time for a given resist. Developer temperatures much higher than 26°C may cause pattern resist feature damage, whereas incomplete developing or scumming may occur at low developer temperatures.²¹

¹⁶ibid., p. 157.

¹⁷ibid.

¹⁸F. Endermann and W. Neugebauer, "Light sensitive omicron quinone diazides and the photomechanical preparation of printing plates therewith," U.S. Patent No. 3,148,983 (1964).

¹⁹W.S. DeForest, *Photoresist: Materials and Processes*, p. 157, McGraw Hill, New York (1975).

²⁰ibid.

²¹ibid.

Rinsing of positive resists after developing is done with deionized water. The primary purpose of rinsing positive resists following development in basic solutions such as an aqueous base is to remove water-soluble substances from the exposed parts. In contrast to negative resists that require a forceful rinse to remove the insoluble solvent-logged portions of the image, the reaction products of the exposed areas of positive resists are water-soluble acidic salts. Water purity does not appear to have a significant effect on the quality of the rinsing operation of positive resists, although the possibility of calcium in the rinse water forming acidic salts of low solubility, which might manifest as scumming, poses a potential problem.²² Hence, only deionized water is used for rinsing developed positive resists in modern semiconductor lithographic practices.

Another classification scheme of resist developers is based on whether they are made of inorganic or organic compounds (see Fig. 5.3). While inorganic developers such as potassium hydroxide were popular during the early days of semiconductor lithography, in modern semiconductor lithography, organic developers are the preferred option because unlike their inorganic counterparts, they do not contain metallic ions, which can cause electrical failures in devices fabricated with them. Both developer types can be buffered or nonbuffered; both may contain surfactants or not.

5.5 Resist Strippers and Cleaners

At the end of the lithographic and etch patterning processes, as well as implant processes for the front end of lithography (FEOL) layers and back end of lithography (BEOL) layers, the remaining resists will have to be stripped and cleaned off

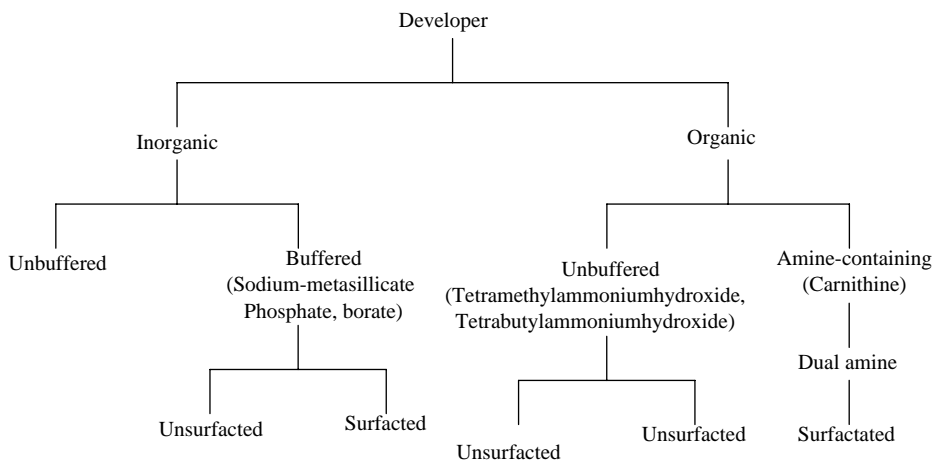


Figure 5.3 Resist developers.

²²ibid.

from the wafer before the wafer is subjected to further processing in the BEOL layers. The FEOL layers comprise those device layers in which lithographic and etch patterning processes, as well as implant and diffusion processes, are used in the definition of critical components such as the active, gate, source, and drain regions of the transistor, along with their associated implant regions. The BEOL layers comprise those layers in which lithographic and etch patterning processes are used to define the via openings for the interconnection between device layers or local interconnection within a given layer for the metallization and wiring of the active devices so as to form integrated circuits, or the contact openings used to electrically connect the active devices to the outside world.

Two broad categories of resist strippers and cleaners are employed. These are solvent-based (wet) and plasma-based (dry) strippers. Depending on whether the wet stripping is to be done for the FEOL processes or BEOL processes, different types and combinations of resist strippers may be used in order not to damage the devices.

A number of resist stripping solutions have been developed over the years. Early broad-spectrum (i.e., effective for both negative and positive resists) resist strippers used in semiconductor lithography contained one or more components such as halogenated hydrocarbons (methylene chloride, trichloroethylene, tetrachloroethylene, chloroform), phenols and phenolic compounds, glycol ethers, ketones (acetone, methylethyl ketone), dioxane, nitromethane, formamides, sulfonic acids,²³ hot concentrated solutions of sulfuric acid saturated with chromic acid, and the like. The common resist strippers for positive resists then included equal volumes of sulfuric acid and hydrogen peroxide (30%), acetone, hot dimethyl formamide, methyl ethyl ketone, methyl isobutyl ketone, dioxane, hot butyl cellosolve, butyl carbitol, and aqueous caustic application following UV light exposure.

Some of these strippers suffered from one or more drawbacks such as potential toxicity to workers exposed to them, environmental and pollution problems in disposal after use, volatility, corrosion of equipment, and the safety hazard of operating at temperatures above the flash point of the stripper. They were also plagued by difficulties and the high cost associated with disposing of them in an environmentally acceptable manner after use. The semiconductor industry has to a large extent migrated away from them for the aforementioned reasons, and some of the chlorinated resist strippers such as chloroform are now banned from the semiconductor industry.

In modern times, resist stripping for FEOL layers is typically accomplished with first the application of sulfuric acid and hydrogen peroxide mixture (SPM) solution, followed by the application of ammonium hydroxide and hydrogen peroxide mixture (APM) solution. This combination of solutions is able to strip off almost every kind of resist, except those that have been used in implant processes or have been hard baked or modified by plasma gases during dry etching

²³J.E. Vander Mey, "Phenol free and chlorinated hydrocarbon free photoresist stripper comprising surfactant and hydrotropic aromatic sulfonic acids," U.S. Patent No. 4,165,294.

or O₂-ashing processes. For BEOL layers, resist stripping is accomplished with dilute hydrofluoric acid (HF) solutions. At times, organic acids such as oxalic and citric acids are mixed into the dilute HF solutions. The choice of these solutions for BEOL layers is mandated by the need to prevent corrosion of the copper wirings.

The latest evolution of resist strippers is based on compositions comprising organic amine compounds and organic solvents as diluents. Typical organic amines in such formulations comprise monoethanolamine (MEA), 2-(2-aminoethoxy) ethanol (AEE), monopropylamine, methylamylethanol, ethylenediamine, piperidine, benzyl amine, etc. Choline is sometimes added to enhance the activity of MEA. Typical polar organic solvents that are used in combination with the aforementioned amine compounds include N-methylacetamide (Mac), N,N-dimethylacetamide (DMAc), N,N-dimethylformamide (DMF), N-methylpyrrolidone (NMP), dimethylsulfoxide (DMSO), carbitol acetate, methoxyacetoxyp propane, N,N-dimethylformamide (DMF), N,N-dimethylpropionamide, N,N-diethylbutylamide, N-methyl-N-ethylpropionamide, diethylene glycol monoethyl ether, diethylene glycol dialkyl ether, γ -butyrolactone and 1,3-dimethyl-2-imidazolinone, etc. Even nonprotonic polar solvents such as 1,3-dimethyl-2-imidazolidinone (DMI), 1,3-dimethyl-tetrahydropyrimidinone, etc. are also used in combination with the organic amine compounds, as well as sulfone compounds such as sulforane, and glycol monoalkyl ethers such as diethylene glycol monoethyl ether, diethylene glycolmonobutyl ether, etc. The proportions of the above constituents in a typical modern resist stripper are dependent on the application to which they are targeted.²⁴

A particular resist stripping challenge is the removal of hard-baked positive resists and sidewall resist polymers that have been exposed to and modified by plasma gases during dry etching or an ashing process. Conventional strippers based on the compositions described above are not very effective in removing these types of modified resists. Broad-spectrum resist stripper compositions containing as their principal active components a mixture of (i) morpholine or certain derivatives thereof such as N-methylmorpholine, N-ethylmorpholine N-(2-hydroxyethyl)morpholine, and the like and (ii) pyrrolidone or certain of its derivatives such as N-methylpyrrolidone,²⁵ N-ethylpyrrolidone, N-(2-hydroxyethyl) pyrrolidone, and the like possess markedly improved properties in terms of their ability to strip a wide variety of resists including resists that have been exposed to processing temperatures on the order of 180°C or higher, or have even been subjected to plasma ashing. These stripper compositions or variations thereof can be employed effectively at temperatures approximating room temperature in most cases and at temperatures that are safely below the flash point of the composition. In addition to the above principal components in the compositions of this class of resist strippers, there may also be present one or more diluents, provided that such diluents are free from corrosive properties, do not attack the

²⁴I.E. Ward, "Stripping compositions containing an alkylamide and an alkanolamine and use thereof," U.S. Patent No. 4,770,713 (1988).

²⁵N methylpyrrolidone causes poisoning of chemically amplified resists and is today not used within the lithography bay of modern clean rooms. However, it is still used in some resist stripping applications, often in bays that are not connected to the lithography bay.

substrate, and do not present any significant toxicity or environmental hazards or interfere in any way with the efficacy of the compositions of the active ingredients in the resist strippers. Such diluents comprise polar organic solvents such as glycols, of which ethylene glycol, propylene glycol, dipropylene glycol, tripropylene glycol, tetrapropylene glycol, and the like are typical examples. Other typical examples include glycol mono-alkyl ethers such as the monomethyl, monoethyl, monopropyl, and monohexyl ethers of diethylene glycol and dipropylene glycol, glycol esters such as ethyleneglycol monoacetate, ethyleneglycol diacetate, and the like, and glycol ether esters such as 2-ethoxyethyl acetate (cellosolve acetate), 2-butoxyethyl acetate (butylcellosolve acetate), and the like. These diluents are incorporated into the stripper alone or in mixtures of two or more, provided that their total amount does not limit the effectiveness of the active ingredients in the strippers.²⁶

The broad-spectrum modern-day resist stripper compositions are employed to strip any of a wide variety of resists, including both positive and negative resists, from a substrate after the resist has performed its protective function with respect to the substrate. They are capable of stripping a wide variety of resists from metallic and other substrates without attacking the substrate or any circuitry. They are effective in stripping resists that have been subjected to a postbake treatment at temperatures greater than 200°C or other thermal hardening techniques known, before being subjected to further processing such as etching, ion implantation doping, metal deposition, and the like.

For the most efficient resist strippers, stripping can be accomplished in many cases at temperatures approximating ambient temperature (~20–25°C) in a relatively short time, on the order of a few minutes. However, where the resist has been subjected to relatively high temperatures, up to about 180°C or higher, in hard-bake processes, or have been implanted or used in O₂ plasma etching, stripper compositions are typically employed at elevated temperatures up to about 250°C in order to ensure a fast completion of the stripping process. The exact temperature and time to employ the stripper composition in any given instance is principally a function of the temperature to which the resist has been exposed during postbake and/or other resist hardening techniques. The temperature of stripping is designed to be less than the flash point of the stripper composition.²⁷ It should be mentioned that resists used in implant lithography tend to be carbonized, especially at the interface between the resist layer and the substrate and at wafer bevels, which makes it extremely difficult to strip off such carbonized residues with SPM/APM solutions. For this reason, implanted resists are removed with hot SPM at 250°C, followed by cold APM solution. The cold APM solution is effective in preventing pitting of the substrate that can result from hot APM application.

The mode of contacting the stripper composition with the resist to be stripped can be by spraying the stripper on or immersing the resist and substrate in a bath

²⁶E.J. Turner, "Photoresist stripper composition and process of use," World Int. Property Organization, Patent Application, WO/1987/005314 (1987).

²⁷ibid.

of the stripper, which is maintained at the appropriate temperature. Completion of stripping is typically determined by visual inspection of the substrate, and if necessary with the aid of a microscope or like means. Following the completion of the stripping operation, the wafer substrate is washed with deionized water or a dilute aqueous solution of surfactant in order to remove any residual stripper solution, the latter being soluble in, or miscible with, water.

These modern resist strippers pose no significant toxicity hazard to qualified personnel handling them. The compositions are miscible with water and are therefore readily washed from the substrate after the stripping operation has been completed. The stripping bath is stable and can be reused many times over a prolonged period without losing its efficacy. Furthermore, the principal components of these strippers are readily recoverable by distillation and thus can be recycled.

Resist coatings are also removed with oxygen plasmas that oxidize the resist to volatile compounds such as water and carbon dioxides. Oxygen-containing gases at low pressures are passed through an RF field to produce atomic oxygen, electrons, and various other excited-state molecules and atoms. These reactive species produced in the plasma convert the resist film into the above-mentioned volatiles, which are easily pumped away from the chamber.²⁸

On volatilization of the organics, inorganic impurities are left on the surface of the substrate, which are easily removed with the use of dilute HF solutions or by other means. One advantage of dry stripping of resists is the lack of dependence on the resist type or prior processing. Even the toughest, most thoroughly cured and cross-linked resist films are easily removed with plasma stripping. Temperatures of the components usually are kept below 150°C, and most metals, with the exception of copper and nichrome, are not significantly affected by the plasma bombardment. The resistance values of the latter metal are often affected, probably through the conversion of the resistor metal to oxides; copper oxidizes readily in such an environment.²⁹

5.6 Offset Lithographic Inks and Fountain Solutions

5.6.1 Offset lithographic inks

Inks used in offset lithographic printing vary widely in their composition due mainly to the intended purpose of the finished product. An ink used to print on cartons differs significantly from that used for printing on metal for beverage cans, and even from that used for printing textbooks and newspapers. The inks can be either petroleum based or vegetable oil based. These inks are generally composed of resins, pigments, drying and nondrying oils, waxes, catalysts, etc. Common resins include synthetics such as phenolics, urethanes, maleics, and

²⁸W.S. DeForest, *Photoresist: Materials and Processes*, p. 246, McGraw Hill, New York (1975).

²⁹*ibid.*

epoxides. Nondrying ink oils serve to control the ink rheology and the rate of ink film setting. Catalysts are used to initiate the polymerization of the resins.

Petroleum-based ink oils are mainly normal paraffins and naphthenic fractions of petroleum distillate. They possess a very low vapor pressure. Vegetable-based ink oils are mainly soy oil, although tung, linseed, corn, safflower, canola, castor, coconut, cottonseed, and sunflower oils are also sometimes used. These vegetable oils do not have a measurable vapor pressure at room temperature, and their boiling points are also not measurable at atmospheric pressure. The vegetable oils do typically undergo decomposition, discoloration, charring, and ultimately evolution of smoke before reaching their boiling points.

5.6.2 Fountain solutions

The role of fountain solutions in offset lithography presses is to keep the ink from adhering to the nonimage areas of the offset plate. Their composition may vary from press to press, but as a general rule, they contain some type of desensitizer, either synthetic or Sudanese gum arabic, acids or bases, buffering agents, corrosion inhibitors, fungicides, antifoaming agents, drying stimulators, and wetting agents. The wetting agents serve to reduce the surface tension and increase the viscosity of the fountain solution. Common wetting agents used in fountain solution include isopropyl alcohol or alcohol substitutes such as glycol ethers and ethylene glycol.

Chapter 6

Negative Resists

“... How charming it would be if it were possible to cause these natural images to imprint themselves durably, and remain fixed upon the paper! And why should it not be possible? I asked myself.”

William Henry Fox Talbot, *The Pencil of Nature*

6.1 Introduction

As the enabling factor/component for each lithographic printing technique, resists have oftentimes determined the successful implementation of each lithography. At times, new resists and related processes developed in anticipation of yet to be developed lithographic tools and methods. Other times, the invention of new lithographic tools and methods have preceded the invention of the corresponding resists. In Chapters 6 and 7, we trace the evolution of resist materials and processes throughout the entire history of lithography. In Chapter 8, we discuss general aspects of radiation chemistry of resist polymers. We pay particular attention to the factors that necessitated the changes and sometimes transitions in the evolution of lithographic resist materials and processes. The treatment on each representative class of resists is rendered here in a manner that employs a brief narrative of the historical background covering the invention of the resist to contextualize its usage, while also presenting detailed chemistry of the resist materials covering their synthesis, formulation, radiation chemistry, and image formation mechanisms, as well as the processing and applications of such materials in printing and fabrication. Because the resins of modern resists are almost exclusively composed of polymers, a generalized treatment of the fundamentals of radiation chemistry of resist polymers is provided in Chapter 8 as a way of highlighting the unique properties of these materials that make them ideal candidates for resist applications in semiconductor fabrication and general printing.

The evolution of resist materials and resist processes over time has closely paralleled the evolution of lithography. Generally, the evolution of resists can be divided into two main eras, namely, the dichromate era and the modern era (see Fig. 6.1). There have been many important discoveries in resist materials and processes, some of the most significant of which are covered in this chapter and the next.

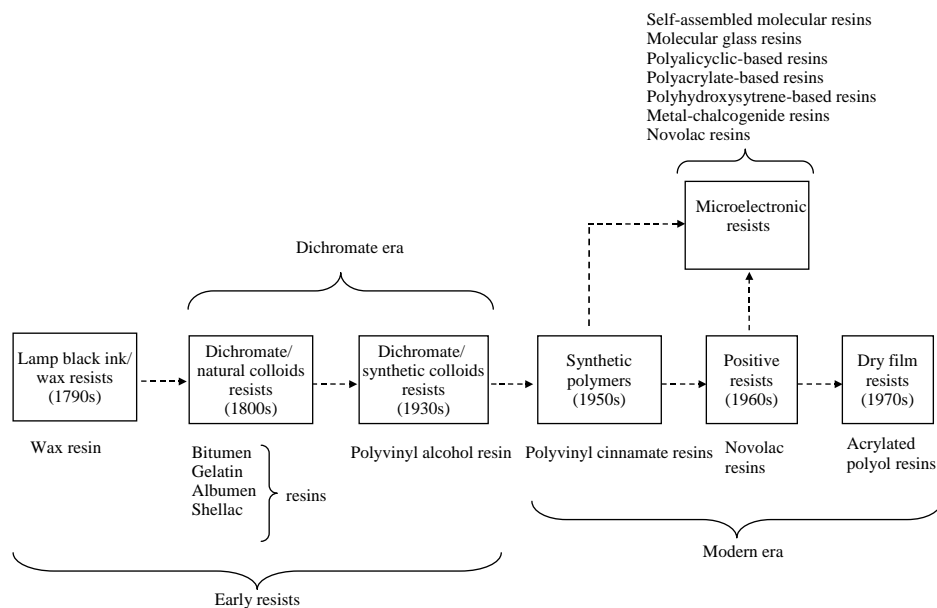


Figure 6.1 Historical evolution of resists.

The early resist materials, such as bitumen of Judea, dichromated gelatin, and other dichromated colloids, were all negative resists. The mechanism by which they functioned was not well understood at the time of their discovery. It was only in the 1920s that it was recognized that gelatin and other natural colloids were macromolecules¹ and that rubber vulcanization is a cross-linking process. Only then did the idea begin to take hold that the hardening and the insolubilization that occur on exposure of dichromated gelatin are brought about by radiation-induced cross-linking.²

Characteristically, negative resists of the modern era (since 1950) have high chemical resistance and good image reproduction qualities. They were widely used in the manufacture of circuit boards and microelectronic devices for these reasons before the advent of positive resists. Because of their high chemical resistance, negative resists are generally more difficult to strip and clean than other resists, although there are some satisfactory resist strippers as described in Chapter 5. In the following sections, components of negative resists are considered individually.

6.2 Resins

Negative resist resins, as a rule, do not have to be sensitive to actinic radiation (although some are), but they do have to be capable of insolubilization through a

¹H. Morawetz, "Difficulties in the emergence of the polymer concept – an essay," *Angew. Chem. Int. Ed. Engl.* **26**, 93 (1987).

²A. Reiser, *Photoactive Polymers: The Science and Technology of Resists*, p. 22, John Wiley & Sons, Hoboken, NJ (1989).

reaction with the sensitizer molecule that has been activated by absorbed radiation energy.³ Other additional properties of negative resist resins include solubility in a solvent system before exposure, capability of wetting and adhering to a variety of substrate surfaces, ability to form a uniform coherent film without losing its solubility in the solvent on evaporation of the latter, and ability of the processed resin image to be resistant to aqueous solutions.⁴

Of particular interest is the process by which the resist is rendered insoluble to the developing solution on exposure. The process can be non-radiation based (as in hydrophilic-hydrophobic interactions in wax-lampblack-soap resists) or it can originate from the interaction of radiation with the resin (as in optical and charged particle resists). With the exception of the dichromated resists, one characteristic that modern-day resists possess is that their resins are organic polymers, typically with unsaturated double bonds between two carbon atoms, in which two pairs of electrons are shared between two carbon atoms in the same molecule. On activation, perhaps through interaction with actinic radiation or heat, the one electron pair can be shared by carbon atoms of adjacent polymer molecules that are similarly unsaturated, leading to the cross-linking of the two polymers, and ultimately transforming the physical properties of the polymers in which it occurs. Cross-linking increases the hardness, chemical resistance, and adhesion to the substrate of the polymers in which it occurs.⁵

Since polymers constitute the majority of modern resist resins, we provide here a brief general description of their physical and chemical properties, which make them ideal candidates for resist applications. Furthermore, we review how these properties are used in resists.

As their name implies, polymers are large molecules with repetitive sequences of monomers—groups of atoms—connected in a linear or branched fashion, as illustrated in Fig. 6.2. The linear polymers contain a basic backbone structure, which may have various functional groups attached to them. In coated resist films, these linear polymers are attached only loosely to each other by secondary forces that are significantly weaker than electronic bonds. When sufficiently heated, these polymers absorb thermal energy, which breaks the secondary forces between individual polymer chains, resulting in enhanced mobility of these chains over and around each other, eventually resulting in the melting of the polymer into a liquid state. Polymers that melt in this manner are called “thermoplastics.” Branched polymers behave generally in a manner similar to the linear polymers. If, however, the functional groups on the backbone of the polymer contain unsaturated groups, heat or thermal polymerization may take place before melting occurs. This results in a polymer that is a highly cross-linked network similar to Fig. 6.2(c). This cross-linked or network polymer is quite different from the linear polymers from which it is synthesized; it is generally stronger and more brittle, it possesses greater thermal and chemical resistance, and does not

³W.S. DeForest, *Photoresist: Materials and Processes*, pp. 20, 21, McGraw Hill, New York (1975).

⁴*ibid.*, p. 21.

⁵*ibid.*, p. 21.

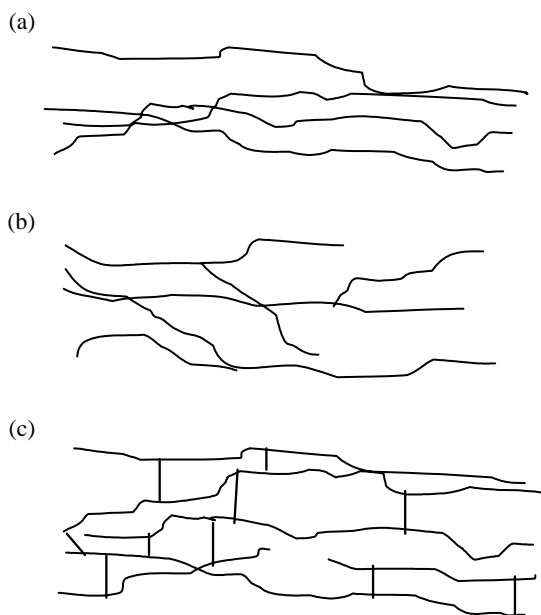


Figure 6.2 Forms of polymers: (a) Linear polymers; (b) Branched polymers; (c) Cross-linked or network polymers.

soften on heating. The interconnected structure of the cross-linked or network polymer prevents the individual molecules from moving around relative to each other when thermal energy is absorbed, as in the case of the linear polymer. As a result, instead of melting, the cross-linked polymer remains a solid until enough energy is absorbed to cause its chemical bonds to rupture and form different lower-molecular weight compounds. With prolonged heating of the cross-linked polymer at high temperature, charring and total decomposition will occur. Polymers of this type are referred to as “thermosets.” After exposure to actinic radiation, negative resist coatings act in a similar manner to a thermoset resin. Instead of heat, radiation-chemical energy is responsible for the cross-linking reactions in negative resist systems. Postexposure baking of the image may result in additional polymerization.⁶

As stated earlier, when the exposed part of the negative resist film is developed in an appropriate solvent, areas that have not been exposed retain their original linear (or branched) solvency and are removed by the developer solution. Exposed areas, on the other hand, having been cross-linked, are able to resist the developer action, and are therefore not removed. In this way, a negative image is formed by the selective solvency of the exposed and unexposed areas in the developer.⁷

⁶W.S. DeForest, *Photoresist: Materials and Processes*, pp. 22–23, McGraw Hill, New York (1975).

⁷*ibid.*, pp. 22–25.

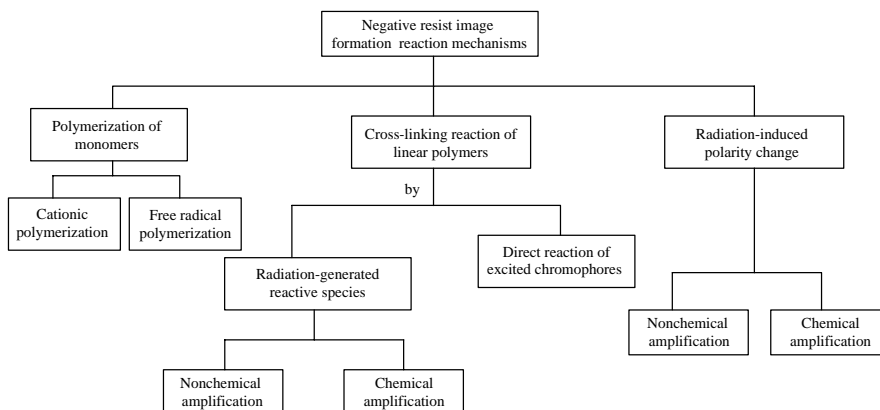


Figure 6.3 Reactions used to generate negative resist images.

In addition to having the ability to be cross-linked and resisting the action of the developer in the exposed areas, negative resist resins must be adherent to wafer substrate surfaces and capable of wetting them thoroughly. Wetting occurs when the polymer molecules have a stronger attraction for the substrate surface than they have between themselves. Poor wetting occurs when the polymer molecules have stronger attractive forces between themselves than the substrate surface, which reduces their attraction for the latter. Adhesion is therefore the result of an attraction between sites on the substrate surface and the polymer molecule.⁸

Figure 6.3 shows the three main classes of reactions used to generate images in negative-working resist systems. Because the dissolution rate of a polymer decreases as the molecular weight increases, common approaches used in the design of negative resists include cross-linking of high-molecular-weight linear polymers, radiation-induced polarity changes in the functional groups of linear polymers, and polymerization of multifunctional monomers. These techniques have been fairly well reviewed.⁹

6.3 Types of Negative Resists

6.3.1 Non-radiation-based negative resists

6.3.1.1 Wax-lampblack-soap resists

An oily, greasy solution of wax, soap, and lampblack, which Senefelder used in making a drawing on a polished limestone slab surface, with which he invented

⁸ibid., p. 23.

⁹J.L.R. Williams, *Fortschritte der chemischen Forschung*, Springer Verlag, Berlin, Bd 13(2), pp. 227–250 (1969); G.A. Delzenne, "Synthesis and photocrosslinking of light sensitive polymers," *Eur. Polym. J., Suppl.*, pp. 55–91 (1969); G.A. Delzenne, "Photocrosslinkable polymeric systems and their technical applications," *Makromol. Chem., Suppl.* 2, 169–188 (1979).

lithography in 1798, must as a necessity be classified as the first resist used in lithography. After drawing on the polished slab, he applied an acidified gum arabic solution (preferably acidic in the pH range between 3.5 and 5) to the slab, and then rolled an ink roller soaked in ink over the entire stone surface, whereupon he discovered that the ink deposited only on the image areas on the stone (i.e., areas on the stone drawn with the greasy pencil) and was repelled in the nonimage areas (i.e., areas of the stone without the drawings from the greasy pencil). With a little pressure, he could easily transfer the image on the stone to a paper laid face down on the stone. This oily, greasy material of wax solution of soap and lampblack was the first resist (specifically, the first negative resist) because it was the first material ever used in human history to protect the printed image on the lithographic stone from the action of the etching solution (in this case, the gum arabic solution), which washed away the unprotected or undrawn areas of the stone, resulting in a clear planographic negative-tone image fixed on the stone after the process was completed. The wax writing solution resisted¹⁰ the acid!

6.3.2 Radiation-induced negative resists

6.3.2.1 Negative resists based on radiation-induced cross-linking reactions

Generally, the reactions that generate cross-links in polymeric systems are classified into two types, namely, those where cross-links are formed by the direct reaction of an excited molecule or group, and those where cross-links are formed through the action of a radiation-generated reactive species in the ground state.¹¹ The following describes both types.

6.3.2.1.1 Negative resists based on cross-link formation by direct reactions of excited chromophores

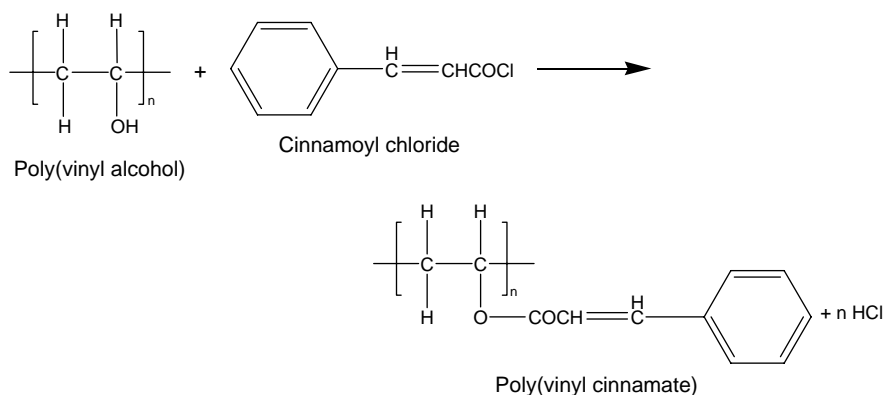
Realizing that it might be possible to print and transfer designs onto a lithographic stone with light, if the design could be made translucent and if the lithographic stone could be varnished with a light-sensitive substance, early lithographers sought to find photosensitive materials that could be employed in such a manner, thus freeing one from the drudgery of drawing the images by hand. Light passing through the design could then be transferred to the prepared stone below. This idea came to fruition at the hands of Nicéphore Niépce around

¹⁰Because the wax resisted the etching action of the acid, materials behaving as such within the field of lithography have since then been called resists.

¹¹A. Reiser, *Photoactive Polymers: The Science and Technology of Resists*, p. 24, John Wiley & Sons, Hoboken, NJ (1989).

1824, who succeeded in making the first permanent photograph of nature¹² using photolithographic techniques. The resist he used, bitumen of Judea,¹³ is now universally accepted as the first photoresist that was successfully used in photolithography as well as in photography. It is a tarlike petroleum substance that has been recovered in chunks from the Dead Sea since ancient Egyptian times and has been used for embalming mummies, as a building material, and as a black varnish material. It has the peculiar property of softening when heated but hardening when exposed to light—essential properties of a negative resist. It is soluble in lavender oil, and high-quality films of it on a variety of substrates such as polished pewter and glass can be coated from lavender solution, as Joseph Nicéphore Niépce discovered.¹⁴ He coated it on a polished pewter plate and projected onto it an image of his courtyard in Chalon-sur-Saône on a bright sunny day, with the aid of a camera obscura. Next, he developed the image by immersing the exposed bitumin-of-Judea-coated pewter plate in lavender oil, which washed away the unexposed part of the bitumen film, revealing to varying degrees the surface of the pewter, while leaving intact the hardened (cross-linked) exposed parts of the bitumen of Judea resist. In this way, Niépce was able to capture and record the image of his courtyard. Effectively, light cross-linked the unsaturated bitumen coating, making it insoluble in the mineral spirits. Thus photolithographic processes involved in the imaging effectively created a relief structure in the remaining organic media.¹⁵

The poly(vinyl cinnamate) (**I**) (see Scheme 6.1) resist represents the simplest example of cross-linking in a negative resist system by an excited chromophore.



Scheme 6.1 Synthesis of poly(vinyl cinnamate) (**I**).

¹²See Figs. 2.4 and 2.5.

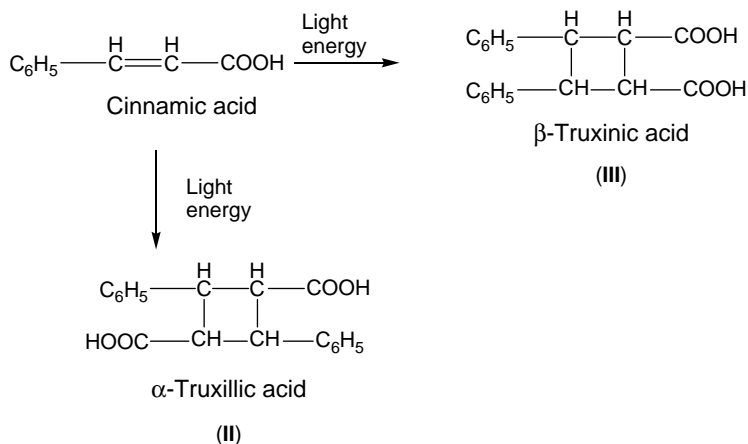
¹³The role of bitumen of Judea in the invention of photolithography and photography is described in Chapter 2, for it was the resist that was used to capture the first permanent image from nature.

¹⁴M.S. Barger and W.B. White, *The Daguerreotype: Nineteenth Century Technology and Modern Science*, pp. 19–20, Johns Hopkins University Press, Baltimore (1991).

¹⁵C.G. Willson, R.A. Dammel, and A. Reiser, "Photoresist materials: a historical perspective," *Proc. SPIE* **3050**, 38–51 (1997).

The poly(vinyl cinnamate) resin is made by the esterification of poly(vinyl alcohol) with cinnamoyl chloride. The reaction takes place in pyridine, a solvent that has an affinity for hydrogen chloride, the by-product of the reaction, and in so doing prevents it from reacting with the starting materials. At the end of the reaction, the solution is diluted with acetone to dissolve the poly(vinyl cinnamate). After washing, the resin is dried and dissolved in ethylene glycol monoethyl ether acetate (also called cellusolve acetate). The polymer synthesized by this method is intrinsically photosensitive and solvent soluble. By dissolving it in cellusolve acetate to form a dilute (2.5–3.5 wt%) solution and adding a sensitizer, a suitable coating solution for lithographic plates could be obtained. When coated on such lithographic plates and exposed, the image can be developed by swabbing with cellusolve acetate or by using trichloroethylene vapor. Resist images thus formed are reportedly ink receptive, accurate, tough, and adherent.¹⁶

The photosensitivity of poly(vinyl cinnamate) derives from the reactivity of the cinnamoyl group. Cinnamic acid is a naturally occurring compound (found in oil of cinnamon, from which it derives its name) and is readily synthesized. Its photosensitivity has long been known, though little use was made of this property until Mink and co-workers, while reviewing the literature in search of a potential cross-linking reaction, found it to be the only solid state photodimerization that was known at the time.¹⁷ On irradiation, the cinnamate groups can dimerize to yield a truxillate (II) or truxinate (III) (Scheme 6.2). If cinnamates from two chains are involved, the cyclic product represents a cross-link.



Scheme 6.2 Photodimerization of cinnamic acid to produce α -truxillic acid (II) and β -truxinic acid (III).

¹⁶W.S. DeForest, *Photoresist: Materials and Processes*, pp. 24–26, McGraw Hill, New York (1975).

¹⁷H. Stobbe and A. Lehfeldt, "Polymerisationen und depolymerisationen durch licht verschiedener Wellenlänge II. a und b trans Zimtsäure, allo Zimtsäure und ihre dimere," *Chem. Ber.* **58**, 2415 (1925).

The photodimerization reaction concept was thus adapted by Mink and co-workers in the design of a poly(vinyl cinnamate) resist system. Cross-links are formed by photoaddition between an excited (*) cinnamoyl group of one chain with a ground state cinnamoyl group belonging to another chain (Scheme 6.3).¹⁸

It is noteworthy that the [2 + 2] cycloaddition in the ground state of two C=C double bonds is forbidden by orbital symmetry (Woodward-Hoffmann), but it is a symmetry allowed as long as one of the reactants is in the excited state. The cross-linking of poly(vinyl cinnamate) by the photodimerization reaction of α -truxillic acid is therefore suitable as a photo-cross-linking mechanism. It is very effective in the cinnamoyl group and its analogs, where the carbonyl provides the desirable polarization of the reactive double bond; the phenyl group increases the polarizability and enhances the light-absorbing power of the chromophore.¹⁹

It must be mentioned that the poly(vinyl cinnamate) resist system makes excellent film and, unlike the dichromated gelatin resists, which they replaced, do not suffer from dark reaction, and thus can be stored indefinitely in the absence of light.

When the poly(vinyl cinnamate) resist system was introduced into the marketplace, it enjoyed immediate success. Sharp images with clean edges were easily generated, and the images withstood the etching action of strong etchants such as hydrofluoric acid. Encouraged by these positive attributes of the poly(vinyl cinnamate) resist system, researchers at Bell Laboratories used it in a small pilot production of semiconductor devices, but quickly were hit by a severe yield loss caused by the inadequate adhesion of the resist to the glassy surface of the oxidized wafers. In the words of Willson et al, "Eastman Kodak had their first [resist] customer complaint."²⁰

The imaging performance of poly(vinyl cinnamate) when exposed by a medium-pressure mercury arc lamp is poor. This is due to the mismatch between the absorption spectrum of the cinnamoyl group (with absorbance maximum at 280 nm) and the spectral emission of the mercury arc. The absorption spectrum of poly(vinyl cinnamate) does not overlap with most of the strong emission lines of a mercury arc lamp. This problem can be overcome by spectral sensitization, for example, with the addition of 5% of Michler's ketone,²¹ or by the replacement of the cinnamoyl group with a chromophore such as in poly(vinyl cinnamylidene acetate) (**IV**) that absorbs at longer wavelengths.²²

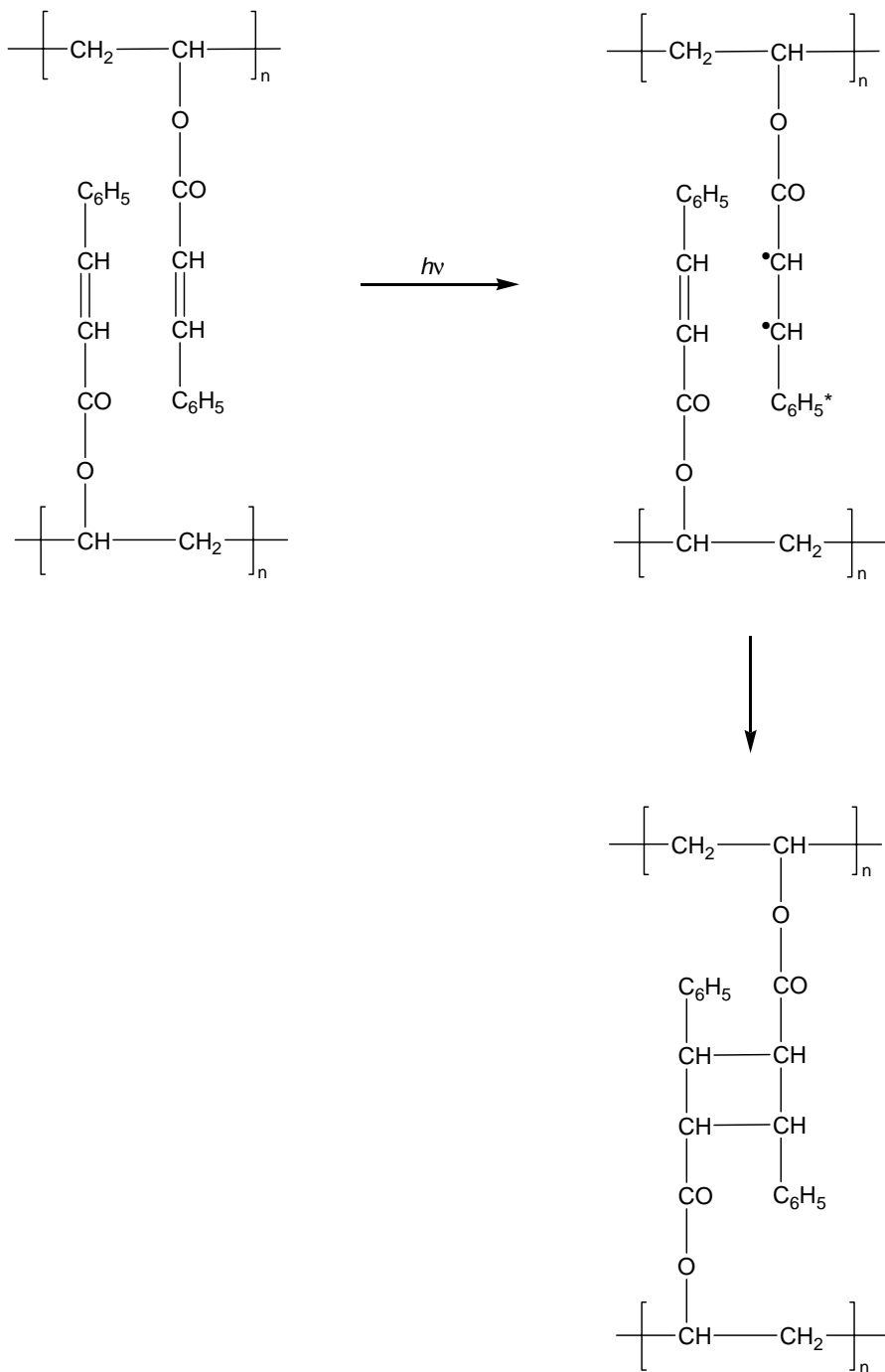
¹⁸A. Reiser, *Photoactive Polymers: The Science and Technology of Resists*, p. 25, John Wiley & Sons, Hoboken, NJ (1989).

¹⁹ibid., p. 26.

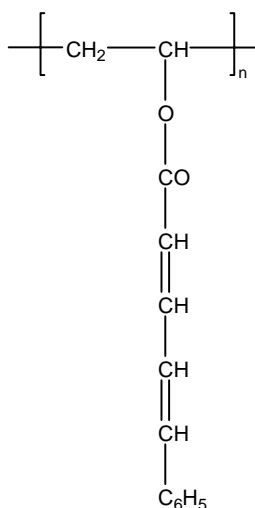
²⁰C.G. Willson, R.A. Dammel, and A. Reiser, "Photoresist materials: a historical perspective," *Proc. SPIE* **3050**, 38–51 (1997).

²¹E.M. Robertson, W.P. van Deusen, and L.M. Minsk, "Photosensitive polymers. II. Sensitization of poly(vinyl cinnamate)," *J. Appl. Polym. Sci.* **2**, 308 (1959).

²²A. Reiser, *Photoactive Polymers: The Science and Technology of Resists*, p. 26, John Wiley & Sons, Hoboken, NJ (1989).



Scheme 6.3 Photoinduced cross-linking reactions of poly(vinyl cinnamate) by α -truxillic dimerization.



Poly(vinyl cinnamylidene acetate) (IV).

Poly(vinyl cinnamylidene acetate) resin, introduced by Leubner and Unruh²³ in 1966, absorbs at 360 nm and has a higher sensitivity than unsensitized poly(vinyl cinnamate). Remarkably, only the double bond adjacent to the carbonyl group is reactive.²⁴ Furthermore, the cycloaddition reaction in this material is reversible; the cyclobutanes formed on irradiation at 365 nm can be cleaved by irradiation with the 254-nm mercury line.²⁵

Other photoreactive chromophores that have been investigated as replacements for cinnamoyl groups in resist resins include the chalcones with the general structure (V)²⁶ and polyesters such as phenylene diacrylates (VI). These can be used either as pendant groups, for example, attached to an ester linkage to poly(vinyl alcohol),²⁷ or in the backbone of a polyester resin.²⁸ Of particular importance is a polyester of *p*-phenylenediacrylic acid (PPDA) (VII),²⁹ which has been used extensively as the photosensitive material of precoated lithographic printing plates from

²³C.W. Leubner and C.C. Unruh, "Light sensitive polymers," U.S. Patent No. 3,257,664 (1966).

²⁴H. Tanaka, M. Tsuda, and H. Nakanishi, "Photochemistry of poly(vinyl cinnamylideneacetate) and related compounds," *J. Polym. Sci., Part A 1* **10**, 1729 (1972).

²⁵H. Tanaka and K. Honda, "Photoreversible reactions of polymers containing cinnamylideneacetate derivatives and the model compounds," *J. Polym. Sci., Polym. Chem. Ed.* **15**, 2685 (1977).

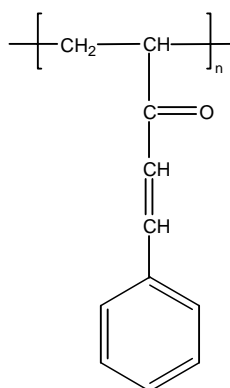
²⁶C.C. Unruh and A.C. Smith, "Condensation of poly(4 vinylacetophenone) with various aralde hydes," *J. Appl. Polym. Sci.* **3**, 310 (1960).

²⁷J.L.R. Williams, S.Y. Farid, J.C. Doty, R.C. Daly, D.P. Specht, R. Searle, D.G. Borden, J.J. Chang, and P.A. Martic, "The design of photoreactive polymer systems for imaging processes," *Pure Appl. Chem.* **49**, 523 (1977).

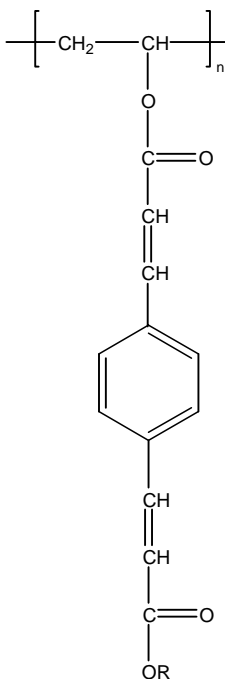
²⁸P.L. Egerton, J. Trigg, E.M. Hyde, and A. Reiser, "Photocycloaddition at excimer sites in a solid polyester of *p* phenylenediacrylic acid," *Macromol.* **14**, 100 (1981).

²⁹ibid.

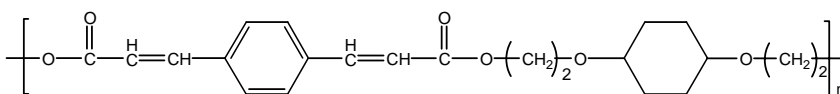
Eastman Kodak. Its bifunctional chromophore absorbs strongly at 365 nm. Its cross-linking reaction has a quantum yield of 0.1.³⁰



Chalcone (V)



Phenylene diacrylate (VI)



Para-phenylenediacyrylic acid (PPDA) (VII)

High-temperature resists have been formulated from a group of polyesters based on styrylpyridine,³¹ which are thermally stable up to 450°C. Such resists have found applications as fine-line solder masks or when the polymer is intended as a permanent component of the final device, be it as insulator, interlayer dielectric, or α -particle barrier.³²

Resist materials based on photoimageable polyimides have also been reported³³ containing polyamic acids to which photopolymerizable units have

³⁰A. Reiser, *Photoactive Polymers: The Science and Technology of Resists*, p. 28, John Wiley & Sons, Hoboken, NJ (1989).

³¹K. Ichimura, "Photosensitive poly(methacrylates) having styrylpyridinium and styrylquinolinium groups," *J. Polym. Sci., Polym. Chem. Ed.* **25**, 3063 (1987).

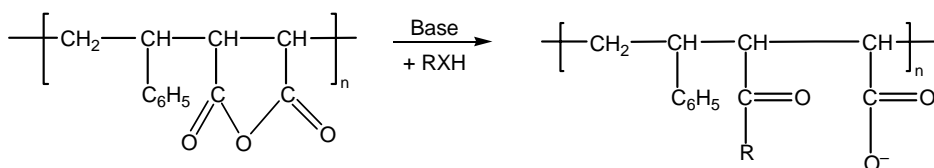
³²A. Reiser, *Photoactive Polymers: The Science and Technology of Resists*, p. 29, John Wiley & Sons, Hoboken, NJ (1989).

³³*ibid.*

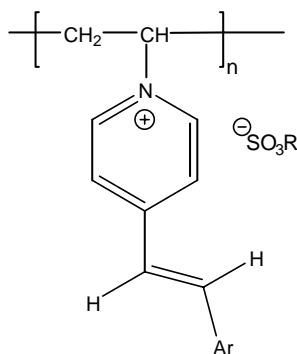
been added. Under UV irradiation through a lithographic mask, the exposed part of the film of the photoimageable polyimides is polymerized and cross-linked through the photopolymerizable units of their respective polymers, while the unexposed part of the film is not polymerized and is thus removed during solvent development. Such photoimageable polyimides are used in the encapsulation of IC devices to protect them against particulate and environmental contamination. They have also found applications as interlayer dielectric materials in IC devices.

Water-processable negative-acting resists with directly excitable chromophores have also been reported.³⁴ These resists are prepared by incorporating ionic or ionizable groups (acids or bases) in the polymer structure. Examples are shown in the following reaction (Scheme 6.4), where a copolymer of styrene and maleic anhydride is hydrolyzed in the presence of a photosensitive graft unit.³⁵ The hydrolysis of the anhydride group results in the generation of the aqueous soluble carboxylic acid and carboxylate ion moieties in the copolymer, both of which aid in the solubility of the anhydride copolymer in water.

Another approach that has been reported for making water-processable resists is via polymeric quaternary pyridinium salts (**VIII**), which are made light sensitive by reaction with an aldehyde.³⁶



Scheme 6.4 Base-catalyzed hydrolysis reactions of an anhydride group in a copolymer of styrene and maleic anhydride, which renders the latter soluble in water.



Polymeric quaternary pyridinium salts (**VIII**)

³⁴ibid.

³⁵J.L.R. Williams, "Photoreactive Polymers," in *Polyelectrolytes*, E. Selegny, Ed., Reidel, Dordrecht (1974).

³⁶G. Leubner, J.L.R. Williams, and C.C. Unruh, "Light sensitive polymeric stilbazoles and quaternary salts thereof," U.S. Patent No. 2,811,510 (1957).

Photoreactive chromophores based on pyridinium and other heteroaromatic bases have been incorporated into negative resist polymers as side chains.³⁷ Styrylpyridinium and styrylquinolinium are examples of such heteroatomic bases with photoreactive side chains.

6.3.2.1.2 Negative resists based on cross-link formation by radiation-generated reactive species

In a number of negative resist systems, cross-links are formed by the reaction of radiation-generated reactive species. When these reactive species mediate one cross-linking event per each unit of radiation received, the reaction is termed a non-chemical amplification reaction, and the resists thus formed are called nonchemically amplified cross-linking resists. Examples include (i) dichromate resists in which cross-links of the resin are formed by the coordinative bonding of Cr^{3+} ions generated from the dichromate photoactive compound with the amide groups of the protein resin; (ii) azide resists in which cross-links are formed from thermal reactions of photogenerated nitrenes (electron-deficient species) with the poly(*cis*-isoprene) rubber resin, or with polyimide resin; (iii) acylsilane resists in which siloxycarbenes mediate the grafting of acylsilyl groups onto suitable polymers such as poly(vinyl alcohol) and poly(vinyl pyridine), causing the cross-linking of these polymers; (iv) functionalized polystyrene-based resists where radicals are coupled to form cross-links.

However, when the reactive species mediate multiple cross-linking events per unit of radiation, the reaction is termed chemically amplified, and the resists thus formed are termed chemically amplified cross-linking resists. Examples of such chemical amplification reactions employed in negative resist design include pinacol rearrangement, intramolecular dehydration, condensation/intermolecular dehydration, esterification, and cationic polymerization of polymers with polymerizable pendant groups or cross-linking agents added as additives to the resist resin.

Briefly described below are some resists based on the above classes of reactions used in the design of negative resists, that is, nonchemically amplified cross-linking negative resists.

- (i) Dichromate resists based on cross-linking by chromium (III) ions—
Although bitumen of Judea resist material was favored by the inventor of

³⁷J.L.R. Williams and D.G. Borden, "The preparation and properties of photoreactive polymers I. 2 (arylviny) N vinylpyridinium arylsulfonate polymers," *Makromol. Chem.* **73**, 203 (1964); D.G. Borden and J.L.R. Williams, "Photopolymer design: Photocrosslinkable styrylpyridinium substituted vinyl polymers with absorption maxima from 270 nm to 540 nm," *Makromol. Chem.* **178**, 3035 (1977); K. Ichimura and N. Oohara, *J. Polym. Sci., Polym. Chem. Ed.* **25**, 3063 (1987); K. Ichimura and S. Watanabe, "Immobilization of enzymes with use of photosensitive polymers having the stilbazolium group," *J. Polym. Sci. Polym. Chem., Ed.* **18**, 891 (1980); K. Ichimura, "Preparation of water soluble photoresist derived from poly(vinyl alcohol)," *J. Polym. Sci. Polym. Chem., Ed.* **20**, 1411 (1982); "Preparation and characteristics of photocross linkable poly(vinyl alcohol)," **20**, 1419 (1982).

photolithography, it soon gave way to more light-sensitive formulations, the most important of which was dichromated gelatin,³⁸ whose introduction and usage in photolithography is a rather complicated affair. It appears that the Scotsman Mungo Ponton was the first to recognize the potential application of dichromate chemistry in photolithography when in 1839 he demonstrated the photosensitivity of a system that consisted of paper soaked in ammonium dichromate solution.³⁹ He was not, however, successful in generating any relief image on the paper soaked in ammonium dichromate solution. That honor goes to Henry Becquerel, who in 1840 succeeded in generating relief images based on a formulation of ammonium dichromate and starch.⁴⁰ He is credited with coining the term “resist,” which he used in describing his formulation, since it resisted the action of etching solvents on the relief images.⁴¹

It was William Henry Fox Talbot who first formulated a resist based on a solution of ammonium dichromate and gelatin. The solution of gelatin and ammonium dichromate resist is quite sensitive to light, casts fine films from water, and after exposure can be developed with water. In lithographic applications, the exposed area of the film remains on the stone, while the unexposed area is washed off with warm water. After drying, the gelatin image becomes hydrophobic and can accept printing ink. This was the first real practical resist system,⁴² which made possible the photomechanical preparation of lithographic plates. Talbot showed that high-quality images could be generated in dichromated gelatin resist materials that he successfully transferred to polished stone surfaces. Recognizing the importance of his discovery, he applied for and was granted an early British patent (Number 565) in 1852. His work on dichromated gelatin resists spawned the photolithography industry, so much so that starting in the mid-1800s, dichromated gelatin was the medium of choice for recording and transferring images onto printing plates made of metal and stone for over 100 years.⁴³

Remarkably, gelatin was not the only substrate explored for use with dichromates; egg albumen, agar, casein, fish glue, shellac, and starch have all been tried and used. In modern times, synthetic polymers such as poly(vinyl alcohol), poly(vinyl pyrrolidone), and poly(vinyl butyral) have, to a significant extent, displaced the above natural materials for use with dichromates; only gelatin and albumen have remained in use until quite recently. A typical modern recipe for dichromated albumen is given in Table 6.1.

³⁸Gelatin is a colloidal protein obtained by the thermal denaturation of collagen, which is isolated from animal skins and bones with very dilute acid. It can also be extracted from fish skin.

³⁹A. Becquerel, “Expériences sur la chaleur rayonnante,” *Compte Rend.* **10**, 469 (1840).

⁴⁰*ibid.*

⁴¹E. Courmont, *La Photogravure: Histoire et Technologies*, Gauthier Villars, Paris (1974).

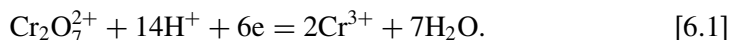
⁴²C.G. Willson, R.A. Dammel, and A. Reiser, “Photoresist materials: a historical perspective,” *Proc. SPIE* **3050**, 38–51 (1997).

⁴³J.G. Jorgensen and M.H. Bruno, *The Sensitivity of Bichromated Coatings*, Lithographic Technical Foundation, New York (1954).

Table 6.1 Dichromated albumen coating.⁴⁴ (Data used with permission from John Wiley & Sons.⁶⁶)

A. Dichromate Solution	
(NH ₄) ₂ Cr ₂ O ₇	758 g
Make up with water to	3758 g
B. Colloid Solution	
Egg Albumen	454 g
Ammonia (20% in water)	60 mL
Make up with water to	2360 mL
C. Coating Solution	
A	946 mL
B	192 mL
Water	237 mL

The mechanism that underlies the cross-linking of dichromated coatings remained a mystery for a very long time until Biltz and Eggert⁴⁵ established that the process involves the photoreduction of Cr(VI) to Cr(III):



Datta and Sollern⁴⁶ established that the detailed fate of the Cr(VI) depends somewhat on the colloidal medium, but that the final stage of the photoprocess always yields Cr³⁺ ions. Given that trivalent chromium is a well-known powerful coordination center, it was thought that cross-links may be formed by the coordinative bonding of Cr³⁺ with the amide groups of the protein. This view is, incidentally, supported by the fact that all polymers that have been used as gelatin substitutes, such as other proteins, starch, poly(vinyl alcohol), poly(vinyl pyrrolidone), and poly(vinyl butyral), carry ligands capable of forming complexes with Cr(III). In fact, Duncalf and Dunn's studies on coordinative bonding of gelatin to Cr(III) revealed that cross-linking occurs only in dry coatings of dichromated gelatin, but not in concentrated aqueous solutions where Cr³⁺ preferentially coordinates water to form CrCl₃ · 6H₂O and does not interact with the protein.⁴⁷

It must be mentioned that the exposure requirements of dichromated gelatin are orders of magnitude less than those of bitumen of Judea resist material. In 1855, A.L. Poitevin demonstrated photolithography on stone sensitized with dichromated gelatin, glue, albumen, and gum.⁴⁸

⁴⁴ibid. [cited in A. Reiser, *Photoactive Polymers: The Science and Technology of Resists*, p. 5, John Wiley & Sons, Hoboken, NJ (1989)].

⁴⁵M. Biltz and J. Eggert, "The spectral sensitivity of photographic layers," *Trans. Faraday Society*, **34**, 892–901; 908–912 (1928) [cited in A. Reiser, *Photoactive Polymers: The Science and Technology of Resists*, p. 24, John Wiley & Sons, Hoboken, NJ (1989)].

⁴⁶P. Datta, B.R. Soller, "Study of photo chemical reactions in a dichromated photoresist," *18th SPSE Fall Symp.*, Nov. 1978 [cited in A. Reiser, *Photoactive Polymers: The Science and Technology of Resists*, p. 23, John Wiley & Sons, Hoboken, NJ (1989)].

⁴⁷Cited in A. Reiser, *Photoactive Polymers: The Science and Technology of Resists*, pp. 22–24, John Wiley & Sons, Hoboken, NJ (1989)].

⁴⁸L. Stroebel and R. Zakia, Eds., *Encyclopedia of Photography*, 3rd ed., p. 7, Focal Press, Boston (1993).

Although dichromated gelatin resist material was a tremendously successful material, it had some peculiar shortcomings, chief among which include the fact that it suffers from a “dark reaction.” When ammonium dichromate and gelatin are mixed, the mixture undergoes a slow cross-linking reaction even in the dark. This peculiar characteristic of this resist limits its useful life to only a few hours after formulation, thus preventing it from being used in presensitized lithographic plate applications. In addition, being a protein, gelatin suffers from the problem that it does not have good etch resistance to strong acids and bases. However, it can be stabilized by “burning in” the images after development, which involves heating the developed images to 300°F, which causes them to char and effectively degrades the image quality.⁴⁹

Resist folklore has it that dichromated gelatin was the first resist the inventors of the transistor tried to use when they sought to fabricate many transistors on the same substrate.⁵⁰ To their surprise, they found that the resist had the necessary resolution, but was not very effective in resisting the hydrofluoric acid etching of silicon dioxide (their semiconducting substrate on which the resist was coated), a key process step in the fabrication of their device. Seeking help to the solution of this problem, the Bell Laboratories Team contacted Dr. Kenneth Mees, then the director of the Eastman Kodak Research Laboratory in Rochester, New York, who in turn turned to Dr. Louis Minsk and his research group. Minsk knew that gelatin was a polymeric material and had surmised that the hardening (tanning) of the dichromated gelatin was caused by light-induced cross-linking between adjacent chains of the protein molecules in gelatin.⁵¹

Numerous attempts were made to improve the adhesion of poly(vinyl cinnamate) resist on the semiconducting substrates, but it soon became apparent that a new-materials approach was needed in order to satisfactorily resolve this problem.⁵²

(ii) Negative azide resists based on cross-linking of isoprenoids by nitrenes—In a bid to solve the adhesion problem of poly(vinyl cinnamate), Mees requested the help of Martin Hepher, the head of the graphic arts department of Kodak Ltd. in Harrow, England. An experienced printing plate maker, Hepher quickly diagnosed the reason for the adhesion failure and promised to find a way of making a light-sensitive rubber adhesive. Hepher discussed this problem with Hans Wagner, an organic chemist, also at Kodak Ltd., who a few weeks earlier had read some papers by Professor Horner from Mainz University that described the photochemistry of azido compounds. Horner had discovered that azides undergo photolysis to generate very reactive intermediates that easily graft onto substrates.⁵³

Wagner’s main contribution in this story was the idea to synthesize a few bis-azides and mix them with a low-molecular-weight rubber of the sort used in the

⁴⁹C.G. Willson and R.A. Dammel, A. Reiser, “Photoresist materials: a historical perspective,” *Proc. SPIE* **3050**, 38–51 (1997).

⁵⁰*ibid.*

⁵¹*ibid.*

⁵²*ibid.*

⁵³*ibid.*

familiar rubber cements that are still sold today. He synthesized these bis-azides, formulated them with rubber, and found that they produced excellent images that had perfect adhesion to glass and other surfaces, including even oxidized silicon wafers. Thus was the adhesion problem solved at Eastman Kodak Company.⁵⁴

This resist system is based on the photodecomposition of organic azides into reactive species called nitrenes (electron-deficient nitrogen species analogous to carbenes), which under application of heat mediate the cross-link formation between chains of cyclized poly(isoprene) rubber.⁵⁵ The mechanism of this reaction was not well understood at the time of the invention of the cyclized poly(*cis*-isoprene)-bisazide negative resists. It was only in 1964 that the real existence of nitrenes and their role as reaction intermediates in this particular cross-linking reaction was established by Wasserman et al. and by Reiser and Frazer in 1965.⁵⁶ But before we dive into the details of this mechanism, we provide here a brief history surrounding the invention of this resist system.

With time, the rubber in the formulation was replaced with a well-defined and cyclized poly(*cis*-isoprene) of molecular weight of about 150,000 Daltons. The cyclization process is carried out by treating the synthetic rubber with a Lewis acid. The cyclization process imparts many positive attributes to the rubber.⁵⁷

(i) It reduces the degree of unsaturation in the rubber and stabilizes it against oxygen-mediated cross-linking, thereby improving the shelf life of the resist. (ii) It causes some chain scission in the rubber, thereby lowering its intrinsic viscosity and allowing the formulation of coatings with higher solid content. (iii) It also functions to raise the softening point of the polymer from about 30°C to nearly 60°C.⁵⁸

As it turned out, many bis-azides were evaluated for this resist application, but as is so often the case, the first one that Wagner ever made, 2,6-bis(4-azidobenzal)-4-methylcyclohexanone (**IX**) (see Scheme 6.5) turned out to be the best one. The resist formulation based on this very material was sold by Kodak as “Kodak Thin Film resist” (KTFR)⁵⁹ and became the workhorse of the semiconductor industry from 1957 until about 1972, when the critical dimensions of the IC devices reached about 2 μm, the resolution limit of KTFR.⁶⁰

The mechanism of the cross-linking reaction of cyclized rubber by photo-generated nitrenes, in other words, the photoprocess and the subsequent thermal reactions of azide photolysis in a polymeric substrate, are described by the following reactions (Scheme 6.6).⁶¹

⁵⁴ibid.

⁵⁵M. Hepher and H.M. Wagner, British Patent No. 762,985 (1954); A. Reiser and H.M. Wagner, “Photochemistry of the azido group,” *The Chemistry of the Azido Group*, S. Patai, Ed., Interscience, New York (1971).

⁵⁶A. Reiser, *Photoactive Polymers: The Science and Technology of Resists*, p. 33, John Wiley & Sons, Hoboken, NJ (1989).

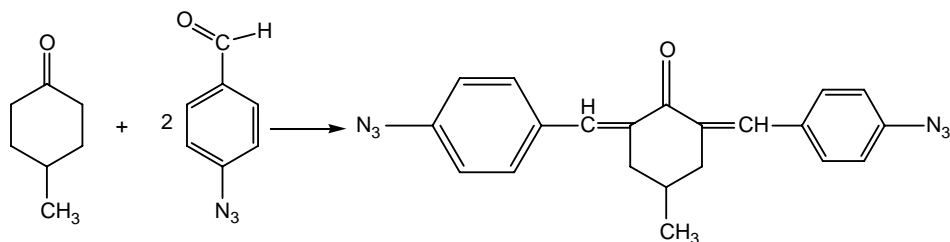
⁵⁷ibid.

⁵⁸ibid.

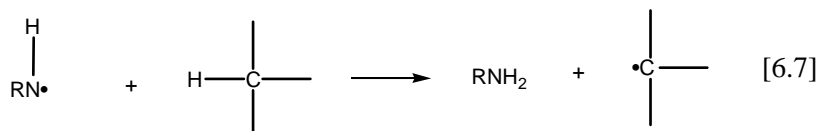
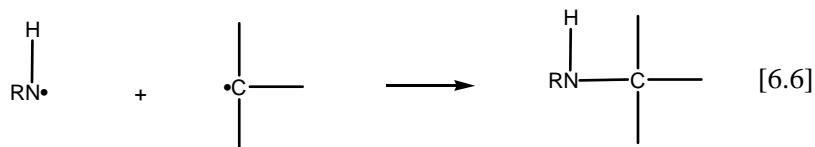
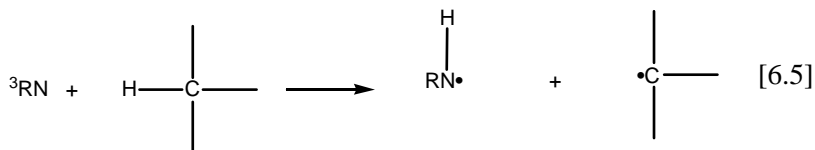
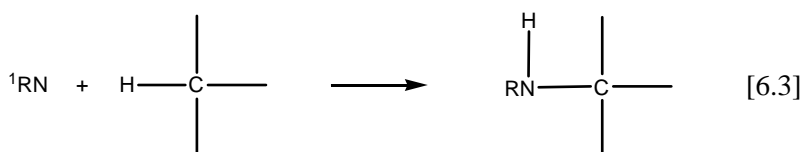
⁵⁹M. Hepher and H.M. Wagner, British Patent No. 762,985 (1954).

⁶⁰R.K. Agnihotri, D.L. Falcon, F.P. Hood, L.G. Lesoine, C.D. Needham, and J.A. Offenbach, “Structure and behavior of cyclized rubber photoresist,” *Photogr. Sci. Eng.* **16**, 443 (1972).

⁶¹A. Reiser, *Photoactive Polymers: The Science and Technology of Resists*, p. 33, John Wiley & Sons, Hoboken, NJ (1989).

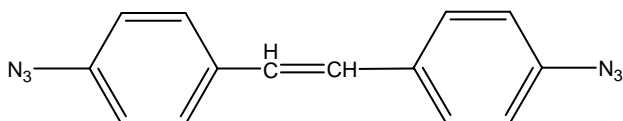
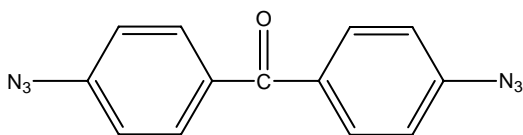
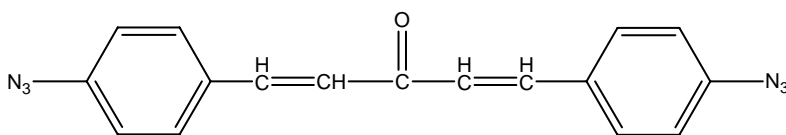


Scheme 6.5 Synthetic scheme of 2,6-bis(4-azidobenzal)-4methylcyclohexanone (**IX**)(Hans Wagner's bis-aryl azide that was the basis of Kodak's KTR resist system).



Scheme 6.6 Reaction mechanism of the cross-linking reaction of cyclized rubber by photogenerated nitrenes.

synthesis,⁶⁶ some other bis-azides have also found meaningful applications in commercial resists, and these include 4,4'-diazidostilbene (**X**), 4,4'-diazidobenzophenone (**XI**), and 4,4'-diazidobenzalacetone (**XII**). These resists are chosen for their compatibility with common resist resins such as poly(*cis*-isoprene), as well as for their spectral absorption.⁶⁷

4,4'-Diazidostilbene (**X**)4,4'-Diazidobenzophenone (**XI**)4,4'-Diazidobenzalacetone (**XII**)

The most commonly used resin in bis-azide resists is poly(*cis*-isoprene), which is cyclized by treatment with a mineral acid (Scheme 6.7). The cyclization reaction is quite similar to cationic polymerization. In the first reaction step, the acid cation adds to a double bond, producing a carbocation. The reaction of a nearby double bond with this ion leads to cyclization.⁶⁸

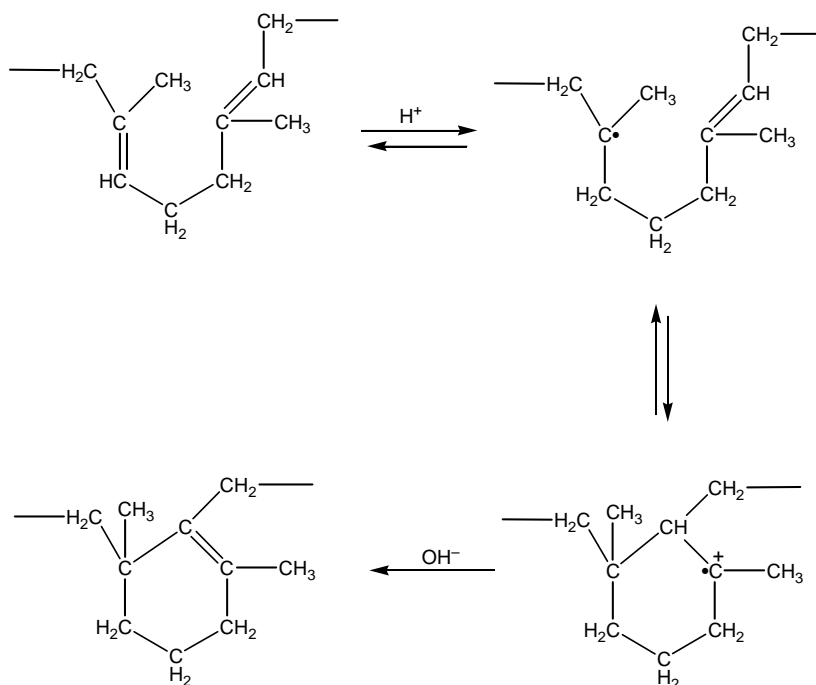
It should be mentioned that cyclization reduces the degree of unsaturation of the polymer, alleviating in the process the problem of spontaneous thermal cross-linking, as it introduces alicyclic units, which make the polymer less flexible and increase its softening temperature. The acid treatment also breaks some of the C—C bonds of the chain and lowers the molecular weight and with it the intrinsic viscosity, thus making possible the coating of solutions with a higher solids content.⁶⁹

⁶⁶ibid., p. 36.

⁶⁷ibid.; W.S. DeForest, *Photoresists: Materials and Processes*, McGraw Hill, New York (1975).

⁶⁸ibid.

⁶⁹A. Reiser, *Photoactive Polymers: The Science and Technology of Resists*, p. 37, John Wiley & Sons, Hoboken, NJ (1989).



Scheme 6.7 Cyclization of poly(*cis*-isoprene).

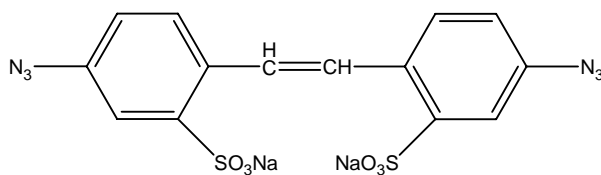
Furthermore, being a delicate process, the outcome of which determines the properties of resists formulated with rubbers made with it, cyclization procedures tend to be proprietary to the various manufacturers, who take great care to characterize it. The principal criteria they use include the degree of unsaturation and cyclicity (whether the structure has monocyclic, bicyclic, or tricyclic motifs in the polymer). The double bonds can be located inside (endo) or outside (exo) of the rings. The ratio of endocyclic to exocyclic double bonds has some effect on the physical properties of the resin.⁷⁰

Although the original KTRF resist based on 2,6-bis(4-azidobenzal)-4-methylcyclohexanone in poly(*cis*-isoprene) rubber resin that dominated the IC industry between 1957 and 1972 was organic solvent developed, in the 1980s, water-processable azide resists were described by Nonogaki and co-workers.⁷¹ These

⁷⁰ibid., p. 38.

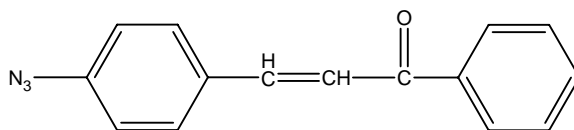
⁷¹M. Agaki, S. Nonogaki, T. Kohashi, Y. Oba, M. Oikawa, and Y. Tomita, "A water soluble, reciprocity law failing photoresist," *Polym. Sci. Eng.* **17**, 353 (1977); T. Kohashi, M. Agaki, S. Nonogaki, N. Hayashi, and Y. Tomita, "Water soluble, reciprocity law failing photoresist composed of poly(acrylamide co diacetone acrylamide) and water soluble bisazide," *Photogr. Sci. Eng.* **23**, 168 (1979); T. Iwayanagi, M. Hashimoto, S. Nonogaki, S. Koibuchi, and D. Makino, "Azide phenolic resin UV resist (MRL) for microlithography," *Polym. Eng. Sci.* **23**, 935 (1983); S. Nonogaki, M. Hashimoto, T. Iwayanagi, and H. Shiraishi, "Azide phenolic resin resists sensitive to visible light," *Proc. SPIE* **539**, 189 (1985); M. Hashimoto, T. Iwayanagi, H. Shiraishi, and S. Nonogaki, "Photochemistry of azide phenolic resin photoresists," presented at *Tech. Pap., Photo polym. Conf. SPE*, Ellenville, NY, Oct. 1985.

water-processable azide resists were based on poly(acrylamide) or poly(vinyl pyrrolidone) resins together with water-soluble bis-azides such as (XIII).

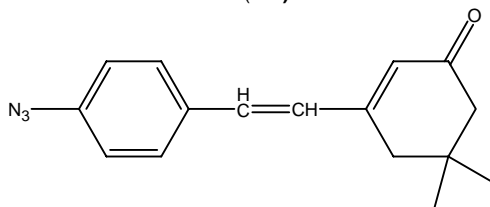


(XIII)

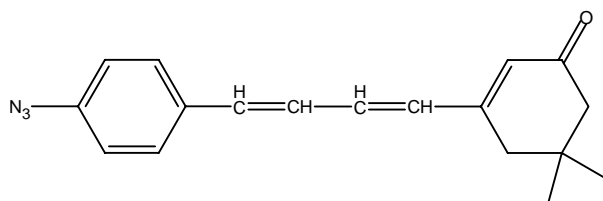
Several negative resists based on polymeric resin binders and azides as the photoactive compound have also been reported. These include resists based on poly(vinyl phenol) as the polymeric resin and various mono-azides as the photosensitive component such as 4-azidochalcone and its homologs (XIV, XV, XVI).⁷²



(XIV)



(XV)



(XVI)

Even resists based on poly(4-hydroxyl styrene) have been shown to be cross-linked in the DUV using 3,3'-diazodiphenylsulfone⁷³ and other bisazides⁷⁴ as the

⁷²A. Reiser, *Photoactive Polymers: The Science and Technology of Resists*, pp. 38–39, John Wiley & Sons, Hoboken, NJ (1989); N.J. Turro, *Modern Molecular Photochemistry*, Benjamin Cummings, Menlo Park, CA (1978); S. Nonogaki, M. Hashimoto, T. Iwayanagi, and H. Shiraishi, "Azide phenolic resin resists sensitive to visible light," *Proc. SPIE* **539**, 189 (1985); M. Hashimoto, T. Iwayanagi, H. Shiraishi, and S. Nonogaki, "Photochemistry of azide phenolic resin photoresists," presented at *Tech. Pap., Photopolym. Conf. SPE*, Ellenville, NY, Oct. 1985.

⁷³H. Tomioka, "Submicron optical lithography utilizing a negative deep UV resist MRS," *Proc. SPIE* **539**, 151 (1985).

⁷⁴T. Iwayangi, T. Kohashi, S. Nogaki, T. Matsusawa, K. Douta, and H. Yonazawa, "Azide phenolic resin photoresists for deep UV lithography," *IEEE Trans. Electrochem. Dev.* **28**, 1306 (1981).

photoactive compounds. Resins such as novolac and acrylic acid copolymers designed for DUV exposure are all cross-linkable with bisazides. These azido compounds are typically added to the resin in large quantities (20% by weight). On irradiation, the photogenerated nitrenes abstract hydrogen from the polymer backbone, producing carbon radicals, which on recombination provide the cross-linking mechanism. Remarkably, these cross-linked resins do not swell in the aqueous developer, unlike earlier negative tone resists. Submicron resolution has been reported with them.⁷⁵

It should be mentioned that the reaction of nitrenes with oxygen is a very important reaction that competes with cross-link formation in azide resists.⁷⁶



It is in fact possible to apply this reaction with oxygen to achieve complete image reversal in azide resists through the following procedure. First, the resist film is exposed in an oxygen atmosphere to a positive original, during which all of the azido groups in the irradiated areas are destroyed without producing cross-links. Next, by irradiating the film under vacuum, those parts that had been shielded during the first image exposure and therefore still contain azido groups will now be cross-linked. A positive image of the original is formed after development.⁷⁷

- (iii) Negative acylsilane resists based on cross-linking by carbenes—Cross-linking reactions of suitable polymeric resins by siloxycarbenes generated from the photoisomerization of acylsilanes can be the basis of negative resist imaging. When irradiated, acylsilanes exist in photostationary equilibrium with siloxycarbenes.⁷⁸ These siloxycarbenes in turn can insert into OH bonds or add to the pyridine nitrogen (Scheme 6.8), and so on.⁷⁹

“R” may represent any monomer or polymer [such as poly(vinyl alcohol)] with OH groups. The reaction can be used to good advantage to either graft acylsilyl groups or bifunctional acylsilanes onto suitable polymers such as poly(vinyl alcohol), poly(vinyl pyridine), etc. This results in cross-linking. Both methods have been reported to lead to efficient resists with good sensitivity.⁸⁰

⁷⁵A. Reiser, *Photoactive Polymers: The Science and Technology of Resists*, p. 39, John Wiley & Sons, Hoboken, NJ (1989).

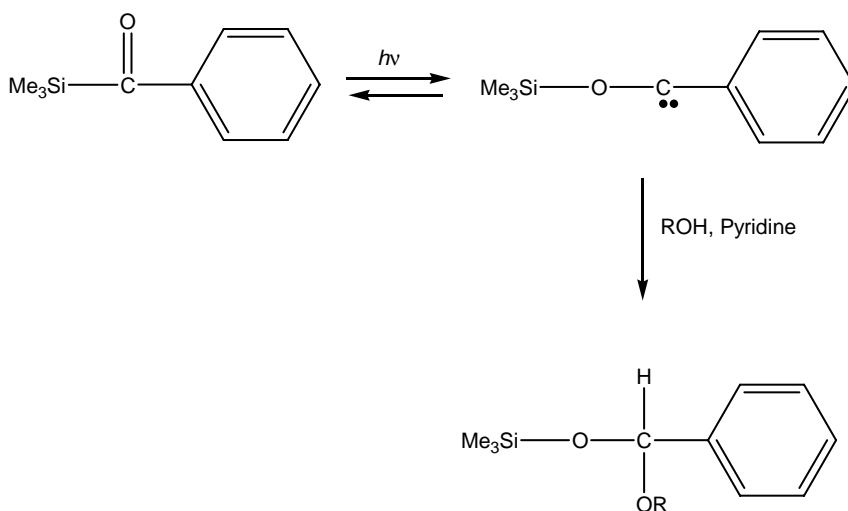
⁷⁶A. Reiser, G.C. Terry, and F.W. Willets, “Observation of the nitrene in the flash photolysis of 1 azidoanthracene,” *Nature* **211**, 410 (1966).

⁷⁷A. Reiser, *Photoactive Polymers: The Science and Technology of Resists*, p. 39, John Wiley & Sons, Hoboken, NJ (1989).

⁷⁸J.M. Duff and A.G. Brook, “Photoisomerization of acylsilanes to siloxycarbenes, and their reactions with polar reagents,” *Can. J. Chem.* **51**, 2869 (1973).

⁷⁹A. Reiser, *Photoactive Polymers: The Science and Technology of Resists*, p. 40, John Wiley & Sons, Hoboken, NJ (1989).

⁸⁰*ibid.*, p. 41.



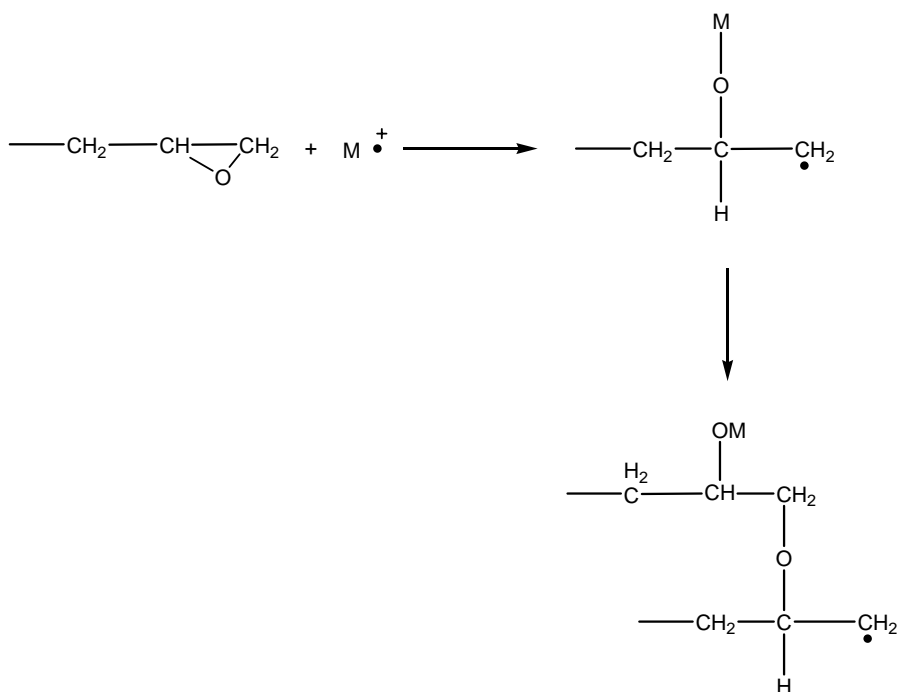
Scheme 6.8 Cross-linking reactions mediated by siloxycarbenes.

- (iv) Negative resists based on cross-linking by radicals—A substantial proportion of negative resists are based on radiation-induced cross-link formation initiated by radicals. Polymers such as polyethylene, various rubbers, polystyrene, and poly(vinyl chloride) are known to cross-link on irradiation; but from a lithographic standpoint, their radiation sensitivity is too low. The cross-linking efficiency of these materials can be significantly enhanced by introducing specific radiation-sensitive (labile) groups (for example, epoxy groups) or bonds.⁸¹ In this section, we briefly discuss a few important examples of negative resists whose imaging action is due to radical-initiated cross-linking of polymeric resins.
- (a) Acrylated polyol-based negative resists based on free radical-initiated cross-link formation—The free-radical-initiated cross-linking of acrylated polyols has been exploited as the basis of the mechanism responsible for negative tone imaging in dry film resists such as Riston,⁸² used widely in printed circuit board and printed wiring board manufacture.
- (b) Epoxy-based negative resists based on cross-link formation by radicals—Epoxy groups in polymers can undergo radical-mediated cross-link formation under exposure with an electron beam (Scheme 6.9)—but, remarkably, not with light. The radiation chemical yield⁸³ of such systems tends to be high

⁸¹M.P.C. Watts, "Electron beam resist systems A critical review of recent development," *Solid State Technol.* **27**(2), 111 (1984).

⁸²Riston[®] was introduced by Dupont in 1970. [See, for example, A. Reiser, *Photoactive Polymers: The Science and Technology of Resists*, p. 163, John Wiley & Sons, Hoboken, NJ (1989)].

⁸³The radiation chemical yield is defined in terms of *G* value, which is defined as the number of moles of product resulting from 100 eV of energy deposited into the system.



Scheme 6.9 Radical-mediated cross-linking of epoxy resin.

due to a chain mechanism in the cross-linking process, initiated by ions or radical ions, $\text{M} \cdot^+$, which are the primary products of irradiation.⁸⁴

That polymerization is observed in this system even after irradiation has ceased is evidence of the occurrence of a chain reaction mechanism. This postirradiative polymerization leads to the gradual enlargement of features in the imaged resist, which degrades the resolution.⁸⁵ The use of radical scavengers such as 1,1-diphenyl-2-picrylhydrazyl (DPPH) has been demonstrated as an effective way of inhibiting this reaction.⁸⁶

A good number of very successful epoxy resists have been developed from polymers carrying glycidyl groups and have found widespread application in electron-beam lithography.⁸⁷ Common resist resins based on this approach include poly(glycidyl methacrylate) (PGMA), a copolymer of glycidyl methacrylate with

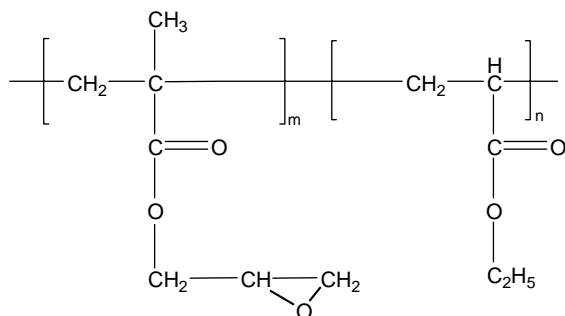
⁸⁴A. Reiser, *Photoactive Polymers: The Science and Technology of Resists*, p. 311, John Wiley & Sons, Hoboken, NJ (1989).

⁸⁵*ibid.*, p. 331.

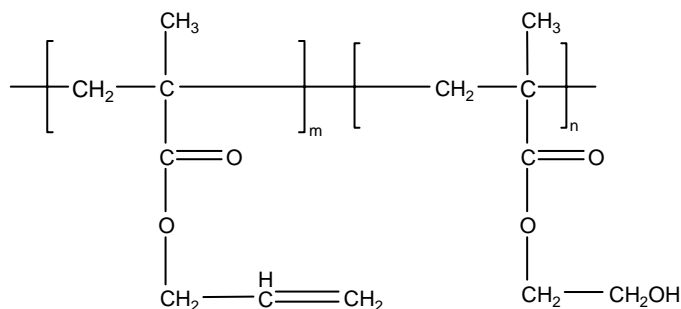
⁸⁶Y. Ohnishi, M. Itoh, K. Mizuno, H. Gokan, and S. Fujiwara, "Postirradiation polymerization of e beam negative resists: Theoretical analysis and method of inhibition," *J. Vac. Sci. Technol.* **19**, 1141 (1981).

⁸⁷Y. Taniguchi, Y. Hatano, S. Shiraishi, S. Horigone, S. Nonogaki, and K. Naraoka, "PGMA as a high resolution, high sensitivity negative electron beam resist," *Jpn. J. Appl. Phys.* **18**, 1143 (1979).

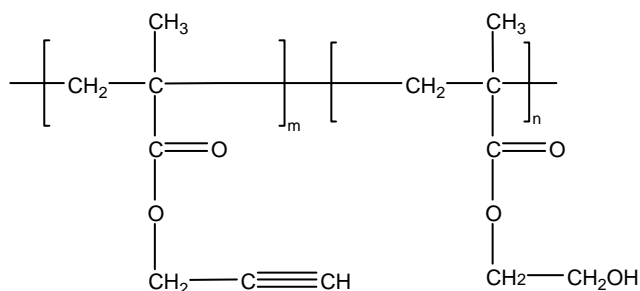
ethylacrylate (**XVII**) (marketed under the trade name of “COP”),⁸⁸ and copolymers of allyl methacrylate (**XVIII**) and propargyl methacrylate (**XIX**) with hydroxyethyl methacrylate.⁸⁹



Poly(glycidyl methacrylate-co-ethylacrylate) (**XVII**) “COP™”



Poly(allyl methacrylate-co-hydroxyethyl methacrylate) (**XVIII**)



Poly(propargyl methacrylate-co-hydroxyethyl methacrylate) (**XIX**)

⁸⁸L.F. Thompson, J.P. Balantyne, and E.D. Feit, “Molecular parameters and lithographic performance of poly(glycidyl methacrylate co ethyl acrylate): A negative electron resist,” *J. Vac. Sci. Technol.* **12**, 1280 (1975).

⁸⁹Z.C.H. Tan, R.C. Daly, and S.S. Georgia, “Novel, negative working electron beam resist,” *Proc. SPIE* **469**, 135 (1984); R.C. Daly, M. Hanrahan, and R.W. Blevins, “Negative working e beam copolymers,” *Proc. SPIE* **539**, 138 (1985).

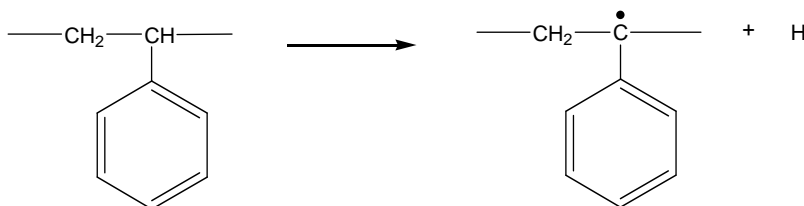
It should be pointed out that although PGMA and its derivatives are highly sensitive and have excellent resolution, they suffer from poor plasma etch stability. This led to the investigation of the plasma-resistant polystyrene and some of its derivatives as electron-beam resists.⁹⁰

- (c) Polystyrene-based negative resists derived from cross-link formation by radicals—It is well known that polystyrene cross-links slowly under irradiation (G-value for cross-linking, $G_x = 0.04$) and its cross-linking mechanism is centered around the tertiary C atom of the backbone (Scheme 6.10).⁹¹

When some or all of the phenyl rings are substituted with halogen (Scheme 6.11), the radiation sensitivity and the cross-linking efficiency of polystyrene can be enhanced significantly. Negative electron-beam resist formulated from iodinated⁹² and chlorinated⁹³ polystyrene and based on this approach have been reported. Sensitivity of about $2 \mu\text{C}/\text{cm}^2$ and resolution of about $1\text{-}\mu\text{m}$ features have been demonstrated with these materials.⁹⁴

The most important step in the mechanism is the opening of the weaker C—I bond, which produces a phenyl radical that abstracts a hydrogen atom from the tertiary carbon of the backbone, forming a cross-link by radical coupling.⁹⁵

The highest sensitivity ($0.5 \mu\text{C}/\text{cm}^2$) demonstrated with this class of materials was achieved with poly(chloromethylstyrene) (XX).⁹⁶ Other notable



Scheme 6.10 Cross-linking of polystyrene.

⁹⁰S. Imamura, T. Tomamura, K. Sugekawa, O. Kogure, and S. Sugarawa, "Crosslinking reactions in negative electron resists composed of halogenated aromatic polymers," *J. Electrochem. Soc.* **131**, 1122 (1984).

⁹¹P. Alexander, R.M. Black, and A. Charlesby, "Radiation induced changes in the structure of poly isobutylene," *Proc. R. Soc. London, Ser. A* **232**, 31 (1955).

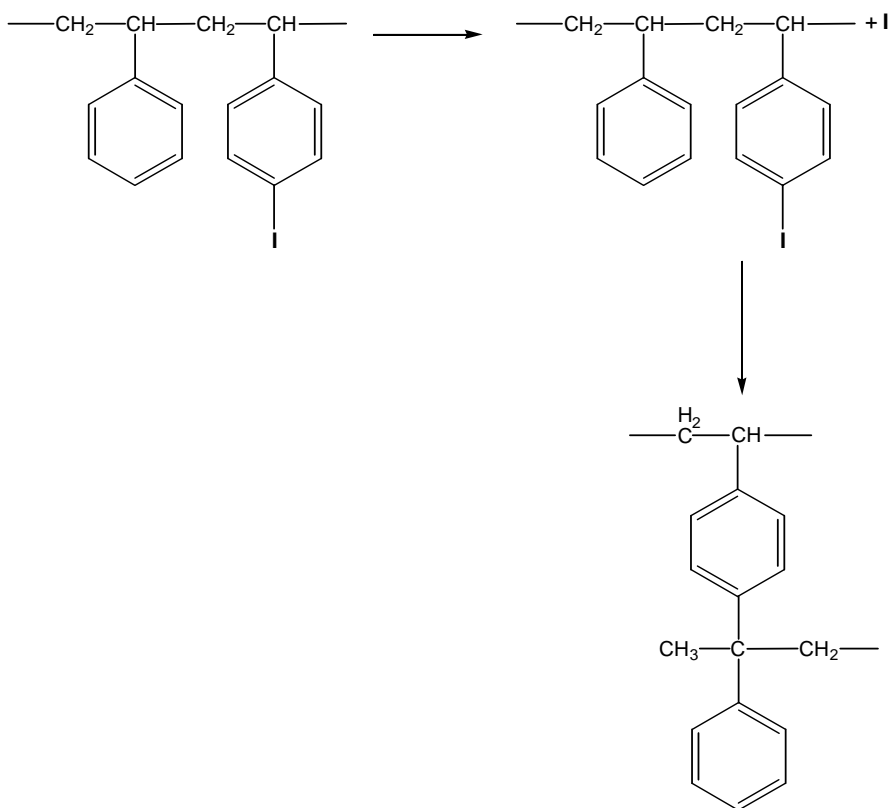
⁹²H. Shirashi, Y. Taniguchi, S. Horigome, and S. Nonogaki, "Iodinated polystyrene: An ion millable negative resist," *Polym. Eng. Sci.* **20**, 1054 (1980).

⁹³T. Ueno, H. Shirashi, and S. Nonogaki, "Insolubilization mechanism and lithographic characteristics of a negative electron beam resist iodinated polystyrene," *J. Appl. Polym. Sci.* **29**, 223 (1984).

⁹⁴*ibid.*

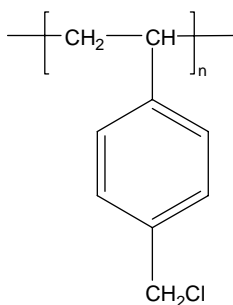
⁹⁵*ibid.*

⁹⁶E. Feit and L. Stillwagon, "Electron beam lithography of chlorinated polystyrenes with narrow molecular weight distributions," *Polym. Eng. Sci.* **20**, 1058 (1980); H.S. Choong and F.J. Kahn, "Molecular parameters and lithographic performance of poly(chloromethylstyrene) a high performance negative electron resist," *J. Vac. Sci. Technol.* **19**, 1121(1981).



Scheme 6.11 Mechanism of radiation-induced cross-linking of halogenated polystyrene derivative.

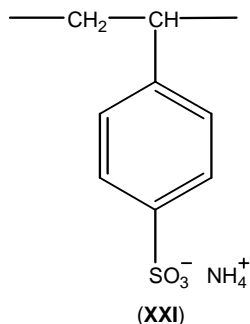
electron-beam resists based on aromatic polymers have been described, including poly(vinyl naphthalene) and poly(chloromethyl styrene-*co*-2-vinyl naphthalene). These resists have demonstrated high dry etch resistance.⁹⁷



Poly(chloromethylstyrene) (XX)

⁹⁷Y. Ohnishi, "Poly(vinylnaphthalene) and its derivatives as e beam negative resist," *J. Vac. Sci. Technol.* **19**, 1136 (1981).

Also worthy of mention is the introduction of conductive electron-beam resists that eliminate the charging effect that is so troublesome in electron-beam lithography. Todokaro et al.⁹⁸ accomplished this by using a partially chloromethylated poly(diphenylsiloxane) as the top imaging resist in a bilayer system, and using the ionically conductive ammonium salt of poly(*p*-styrene sulfonate) (XXI) as the bottom layer.



Lee and Jopson,⁹⁹ on the other hand, used a different approach involving poly(vinylpyridine) (PVP), which is fairly insensitive to electrons, but whose sensitivity could be improved by quaternizing it with methyl iodide. On irradiation of PVP with electrons, cross-links are generated in two steps. First, the methyl iodide splits off and is cleaved into radicals by a second electron. The methyl radicals so created produce backbone radicals that ultimately lead to cross-linking as shown in Scheme 6.12.¹⁰⁰

6.3.3 Chemically amplified cross-linking negative resists

6.3.3.1 Chemically amplified negative phenolic resists based on acid-catalyzed condensation/intermolecular dehydration cross-linking reactions

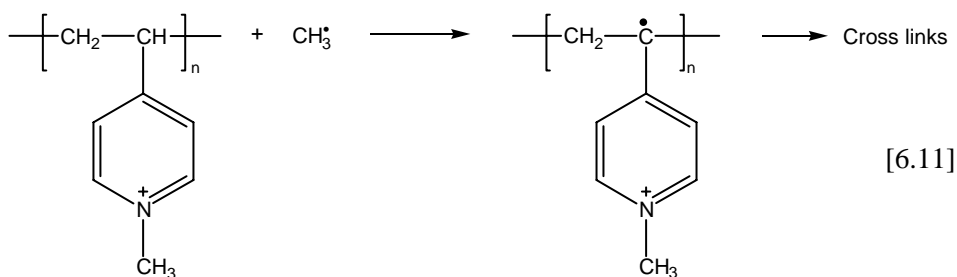
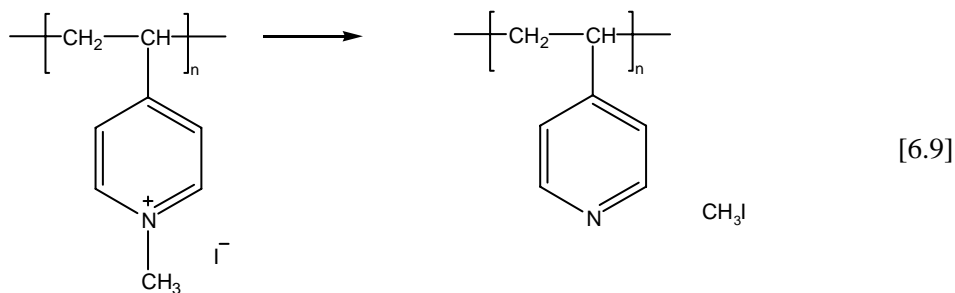
Negative tone resists based on acid-catalyzed cross-linking reactions in a chemical amplification fashion have been known for some time. These resists do not suffer from swelling since they are formulated from phenolic resins and developed with an aqueous base. One example of such a system comprises a phenolic resin (such as novolac), an acid generator (such as diazoquinone), and an alkoxyethylmelamine derivative (such as hydroxymethylmelamine) cross-linker. Irradiation with DUV photons, x rays, and electron beam generates acid from the acid generator, leading to the cross-link formation between the cross-linker and the phenolic resin.¹⁰¹

⁹⁸Y. Todokaro, A. Kajiyama, and H. Watanabe, "Conductive two layer resist system for electron beam lithography," *J. Vac. Sci. Technol. B* **6**, 357 (1988).

⁹⁹K.I. Lee and H. Jopson, "Electron beam chemistry of poly(4 vinyl pyridine) and its quaternized salts," *Polym. Bull.* **10**, 39 (1983).

¹⁰⁰A. Reiser, *Photoactive Polymers: The Science and Technology of Resists*, p. 315, John Wiley & Sons, Hoboken, NJ (1989).

¹⁰¹J. Lignau, R. Dammel, and J. Theis, "High resolution x ray and electron beam resists using chemical amplification," *Solid State Technol.* **10**, 9 (1989); "Recent trends in x ray resist: part II," **10**, 107 (1989).

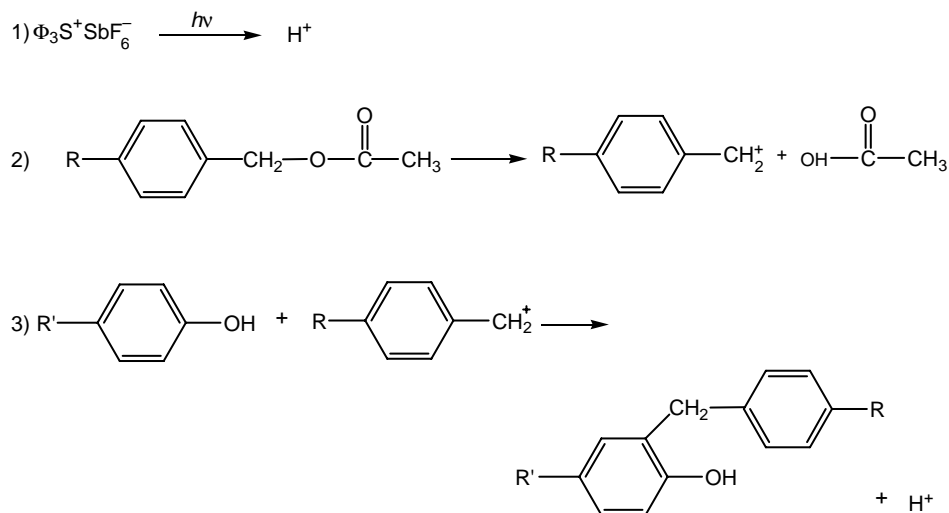


Scheme 6.12 Cross-linking mechanism of poly(vinyl pyridine).

Another interesting chemically amplified negative resist that functions on the basis of acid-catalyzed cross-linking comprises a photoacid generator and polymers bearing substituted phenol and benzyl acetate functionalities.¹⁰² On exposure, a latent image of acid is generated, and during postexposure bake, the acid catalyzes the thermolysis of the benzyl acetate to produce a benzyl carbocation. This reactive species adds to the electron-rich aromatic rings in its environment via electrophilic aromatic substitution to form a new carbon-carbon bond, while at the same time regenerating the acid. The regenerated acid continues the catalytic cycle as shown in Scheme 6.13.¹⁰³

¹⁰²J.M.J. Frechet, S. Matsuzczak, B. Reck, H.D. Stoever, and C.G. Willson, "Chemically amplified imaging materials based on electrophilic aromatic substitution: poly[4 (acetoxymethyl)styrene co 4 hydroxystyrene," *Macromolecules* **24**(8), 1746 (1991); H.D.H. Stoever, S. Matsuzczak, C.G. Willson, and J.M.J. Frechet, "Design of polymeric imaging materials based on electrophilic aromatic substitution: model studies," *Macromolecules* **24**(8), 1741-1745 (1991); R. Beck, R. Allen, R. Twieg, C.G. Willson, S. Matsuzczak, H.D.H. Stoever, N. Li, and J.M.J. Frechet, "Novel photo resist design based on electrophilic aromatic substitution," *J. Polym. Eng. Sci.* **14**, 960 (1989).

¹⁰³C.G. Willson, "Organic resist materials," in *Introduction to Microlithography* 2nd ed., L.F. Thompson, C.G. Willson, and M.J. Bowden, Eds., pp. 228-230, American Chemical Society, Washington, DC (1994).



Scheme 6.13 Chemical amplification mechanism involving acid-catalyzed cross-linking of a benzyl carbocation (from benzyl acetate) and a substituted phenol. Note that in step 1, photolysis of the acid generator produces a latent image of acid, while in step 2, acid-catalyzed thermolysis of the acetate produces a carbocation ion. Step 3 shows the carbocation reacting with an appropriately substituted aromatic compound in an electrophilic substitution reaction that produces a covalent linkage and regenerates the acid. There is no net consumption of acid.

6.3.3.2 Chemically amplified negative resists based on radiation-induced polarity changes

Radiation-induced changes in the polarity of inorganic compounds or molecules or polymer-bound functional groups can significantly alter the dissolution properties of the polymer.¹⁰⁴ This idea has been used widely in the design of a very important class of negative resists, spanning both photolithography and charged particle lithographies. The most prominent examples of non-chemically amplified resists and chemically amplified resists are illustrated below. We follow the approaches reported by D.A. Doane and A. Heller¹⁰⁵ for the non-chemically amplified resists, and the approaches reported by both Reiser¹⁰⁶ and Ito¹⁰⁷ for the chemically amplified resists.

¹⁰⁴The classical example of radiation induced polarity change is the photodecomposition of diazoquinone into an ionizable compound, the indene carboxylic acid. This reaction is the basis of one of the important positive photoresists discussed in Chapter 7. Attaching diazoquinone units to a polymer backbone, for example, via acrylic side groups, makes the unexposed polymer soluble in organic solvents and the exposed polymer soluble in dilute aqueous basic solutions.

¹⁰⁵D.A. Doane and A. Heller, eds., in *Proc. Symp. on Inorganic Resist Systems*, Vol. 82 9, The Electrochemical Society, Pennington, NJ (1982).

¹⁰⁶A. Reiser, *Photoactive Polymers: The Science and Technology of Resists*, pp. 44–46, John Wiley & Sons, Hoboken, NJ (1989).

¹⁰⁷H. Ito, "Chemical amplification resists for microlithography," *Adv. Polym. Sci.* **172**, 149–174, (2005).

6.3.4 Non-chemically amplified negative resists based on radiation-induced polarity changes

6.3.4.1 Metal-chalcogenide resists

Metal-chalcogenide inorganic resists are based on a photodoping phenomenon occurring in chalcogenide glass films, a phenomenon first reported in 1966 by M.T. Kostyshin and co-workers,¹⁰⁸ who showed that chalcogenide films deposited on metal substrates produce visible images on UV irradiation. It was Shimizu et al.¹⁰⁹ who were the first group to extensively study various metal-chalcogenide systems as imaging materials; they introduced the term “photodoping” in 1971 to refer to the migration of a metal into the chalcogenide, or other photosensitive material on exposure to radiation compatible with its bandgap energy.¹¹⁰

The idea of using Ge-Se, chalcogenide glass, as a resist for microelectronics fabrication was first reported in 1976 by A. Yoshihawa and co-workers.¹¹¹ They produced the first relief images (positive and negative images) from this system by photodoping the chalcogenide films with silver metal, with image formation resulting from a differential etching rate between the photodoped glasses and the undoped film in alkaline solutions. And in a subsequent article,¹¹² they demonstrated that these resists have both high contrast and high resolution. Furthermore, they showed that these resists do not swell during solvent development, are opaque to actinic light, and are resistant to the various acids commonly used in microelectronics fabrication processes.

¹⁰⁸The original papers by Kostyshin and co workers can be found under M.T. Kostyshin, E.V. Mikhailovskaya, and P.F. Romanenko, “Photographic sensitivity effect in thin semiconducting films on metal substrates,” *Soviet Phys. Solid State* **8**, 451 (1966). [See, for example, D.A. Doane, A. Heller, “An introductory perspective on inorganic resist systems,” in *Proc. Symp. on Inorganic Resist Systems*, Vol. 82 9, D.A. Doane and A. Heller, Eds., The Electrochemical Society, Pennington, NJ (1982)].

¹⁰⁹I. Shimizu, H. Sakuma, H. Kokado, and E. Inoue, “The photo doping of metals into solids for new type imaging systems,” *Bull. Chem. Soc. Jpn.* **44**, 1173 (1971); H. Kokado, I. Shimizu, and E. Inoue, “Discussion on the mechanism of photodoping,” *J. Non Cryst. Sol.* **20**, 131 (1976); I. Shimizu, H. Sakuma, H. Kokado, and E. Inoue, “Metal chalcogenides systems as imaging materials,” *Photogr. Sci. Eng.* **16**, 291 (1972); “The optical and electrical properties of metal photo doped chalcogenide glasses,” *Bull. Chem. Soc. Jpn.* **46**, 1291 (1973); T. Shirakawa, I. Shimizu, H. Kokado, and E. Inoue, “Relief image in Ag chalcogenide glass sensors,” *Photogr. Sci. Eng.* **19**, 139 (1975).

¹¹⁰D. A. Doane, A. Heller, eds., *Proc. Symposium on Inorganic Resist Systems*, vol. 82 9, p. 3, The Electrochemical Society, Pennington, NJ (1982).

¹¹¹A. Yoshikawa, O. Ochi, H. Nagai, and Y. Mizushima, “A novel inorganic photoresist utilizing Ag photodoping in Se Ge glass films,” *Appl. Phys. Lett.* **29**, 677 (1976).

¹¹²A. Yoshikawa, O. Ochi, H. Nagai, and Y. Mizushima, “A new inorganic electron resist of high contrast,” *Appl. Phys. Lett.* **31**, 161 (1977).

Numerous compositions of metal-chalcogenide resists have been reported.¹¹³ Generally, these resist systems contain a source of silver on the surface of a chalcogenide glass, e.g., As_2S_3 ¹¹⁴ or $\text{Ge}_x\text{Se}_{1-x}$ ¹¹⁵ (see Fig. 6.4). The thin Ag source may be

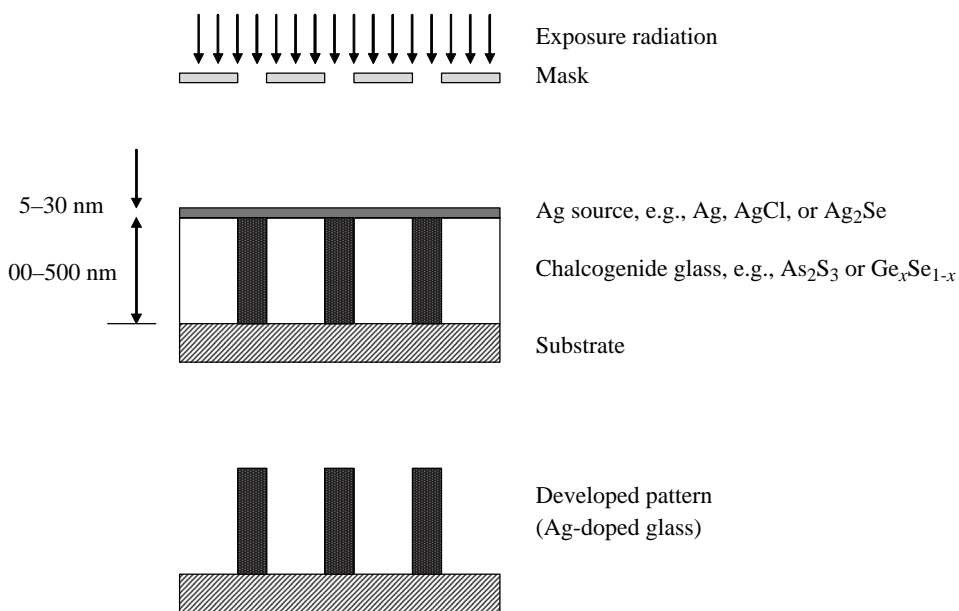


Figure 6.4 Generalized schematic of silver source/inorganic resist systems.

¹¹³An excellent review is provided by R.G. Vadimsky, K.L. Tai, and E. Ong, "Ag₂Se/Ge Se resist systems," in *Proc. Symp. on Inorganic Resist Systems*, Vol. 82 9, D.A. Doane and A. Heller, Eds., pp. 37–47, The Electrochemical Society, Pennington, NJ (1982).

¹¹⁴I. Shimizu, H. Sakuma, H. Kokado, and E. Inoue, "The photo doping of metals into solids for new type imaging systems," *Bull. Chem. Soc. Jpn.* **44**, 1173 (1971); *Photogr. Sci. Eng.* **16**, 291 (1972); T. Shirakawa, I. Shimizu, H. Kokado, and E. Inoue, *Photogr. Sci. Eng.* **19**, 139 (1975); M. Kasai and Y. Hajimoto, "The photodoping sensitivity in As S and Ge S films," *J. Appl. Phys.* **47**(8), 3594 (1976); M.S. Chang and J.T. Chen, "A dry etched inorganic resist," *Appl. Phys. Lett.* **33**(10), 892 (1978); M.S. Chang, T.W. Hou, J.T. Chen, K.D. Kolwicz, and J.N. Zemel, "Inorganic resist for dry processing and dopant applications," *J. Vac. Sci. Technol.* **16**(6), 1973 (1979); K.D. Kolwicz and M.S. Chang, "Silver halide chalcogenide glass inorganic resists for x ray lithography," *J. Electrochem. Soc.* **127**(1), 135 (1980).

¹¹⁵A. Yoshikawa, O. Ochi, H. Nagai, and Y. Mizushima, "A novel inorganic photoresist utilizing Ag photodoping in Se Ge glass films," *Appl. Phys. Lett.* **29**(10), 677 (1976); "A new inorganic electron resist of high contrast," **31**(3), 161 (1977); A. Yoshikawa, S. Hirota, O. Ochi, A. Takada, and Y. Mizushima, "Angstroms resolution in Se Ge inorganic photoresists," *Jpn. J. Appl. Phys.* **20**(2), L81 (1981); A. Yoshikawa, O. Ochi, and Y. Mizushima, "Dry development of Se Ge inorganic photoresist," *Appl. Phys. Lett.* **36**(1), 107 (1980); K. Balasubramanyam and A.L. Rouff, "Oblique deposition enhanced sensitivity in electron beam exposed $\text{Ge}_x\text{Se}_{1-x}$ inorganic resist," *J. Vac. Sci. Technol.* **19**(4), 1374 (1981); N. Funakoshi, S. Zembutsu, and T. Kasai, "Anomalous Ag surface diffusion in amorphous Se Ge/Ag inorganic resist," *Jpn. J. Appl. Phys.* **20**(9), L649 (1981); S. Zembutsu, "X ray photoelectron spectroscopy studies of Ag photodoping in Se Ge amorphous films," *Appl. Phys. Lett.* **39**(12), 969 (1981).

either pure, evaporated Ag,¹¹⁶ or a Ag compound such as AgCl¹¹⁷ or Ag₂Se.¹¹⁸ The compounds may be applied either by evaporation¹¹⁹ or by chemical reaction in solution.¹²⁰ During irradiation with UV,¹²¹ e-beam,¹²² or x-ray radiation,¹²³ Ag diffuses into the underlying chalcogenide glass, forming Ag-doped regions that exhibit enhanced etching resistance. A two-stage development process is used to define the pattern. First, Ag is removed from unexposed areas by immersion in either an acid¹²⁴ or in a fixer solution,¹²⁵ generating a negative-tone image. Next, the pattern is transferred into the glass by immersion in an alkaline solution, e.g., (CH₃)NH,¹²⁶

¹¹⁶I. Shimizu, H. Sakuma, H. Kokado, and E. Inoue, "The photo doping of metals into solids for new type imaging systems," *Bull. Chem. Soc. Jpn.* **44**, 1173 (1971); T. Shirakawa, I. Shimizu, H. Kokado, and E. Inoue, *Photogr. Sci. Eng.* **19**, 139 (1975); M. Kasai and Y. Hajimoto, "The photodoping sensitivity in As S and Ge S films," *J. Appl. Phys.* **47**(8), 3595 (1976); M.S. Chang and J.T. Chen, "A dry etched inorganic resist," *Appl. Phys. Lett.* **33**(10), 892 (1978).

¹¹⁷M.S. Chang, T.W. Hou, J.T. Chen, K.D. Kolwicz, and J.N. Zemel, "Inorganic resist for dry processing and dopant applications," *J. Vac. Sci. Technol.* **16**(6), 1973 (1979); K.D. Kolwicz and M.S. Chang, "Silver halide chalcogenide glass inorganic resists for x ray lithography," *J. Electrochem. Soc.* **127**(1), 135 (1980).

¹¹⁸K. Balasubramanyam and A.L. Rouff, "Oblique deposition enhanced sensitivity in electron beam exposed g Ge_xSe_{1-x} inorganic resist," *J. Vac. Sci. Technol.*, **19**(4), 1374 (1981).

¹¹⁹M.S. Chang, T.W. Hou, J.T. Chen, K.D. Kolwicz, and J.N. Zemel, "Inorganic resist for dry processing and dopant applications," *J. Vac. Sci. Technol.* **16**(6), 1973 (1979); K.D. Kolwicz and M.S. Chang, "Silver halide chalcogenide glass inorganic resists for x ray lithography," *J. Electrochem. Soc.* **127**(1), 135 (1980).

¹²⁰A. Yoshikawa, O. Ochi, H. Nagai, and Y. Mizushima, "A novel inorganic photoresist utilizing Ag photodoping in Se Ge glass films," *Appl. Phys. Lett.* **29**(10), 677 (1976); "A new inorganic electron resist of high contrast," **31**(3), 161 (1977).

¹²¹I. Shimizu, H. Sakuma, H. Kokado, and E. Inoue, "The photo doping of metals into solids for new type imaging systems," *Bull. Chem. Soc. Jpn.* **44**, 1173 (1971); I. Shimizu, H. Sakuma, H. Kokado, E. Inoue, *Photogr. Sci. Eng.* **16**, 291 (1972); T. Shirakawa, I. Shimizu, H. Kokado, and E. Inoue, *Photogr. Sci. Eng.* **19**, 139 (1975); M. Kasai and Y. Hajimoto, *J. Appl. Phys.* **47**(8), 3595 (1976); M.S. Chang and J.T. Chen, "A dry etched inorganic resist," *Appl. Phys. Lett.* **33**(10), 892 (1978).

¹²²K. Balasubramanyam and A.L. Rouff, "Oblique deposition enhanced sensitivity in electron beam exposed g Ge_xSe_{1-x} inorganic resist," *J. Vac. Sci. Technol.*, **19**(4), 1374 (1981).

¹²³K.D. Kolwicz and M.S. Chang, "Silver halide chalcogenide glass inorganic resists for x ray lithography," *J. Electrochem. Soc.* **127**(1), 135 (1980).

¹²⁴T. Shirakawa, I. Shimizu, H. Kokado, and E. Inoue, *Photogr. Sci. Eng.* **19**, 139 (1975); M.S. Chang and J.T. Chen, "A dry etched inorganic resist," *Appl. Phys. Lett.* **33**(10), 892 (1978).

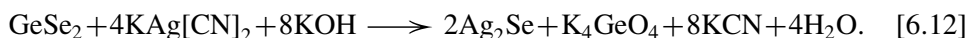
¹²⁵M.S. Chang, T.W. Hou, J.T. Chen, K.D. Kolwicz, and J.N. Zemel, "Inorganic resist for dry processing and dopant applications," *J. Vac. Sci. Technol.* **16**(6), 1973 (1979); K.D. Kolwicz and M.S. Chang, "Silver halide chalcogenide glass inorganic resists for x ray lithography," *J. Electrochem. Soc.* **127**(1), 135 (1980).

¹²⁶A. Yoshikawa, O. Ochi, H. Nagai, and Y. Mizushima, "A novel inorganic photoresist utilizing Ag photodoping in Se Ge glass films," *Appl. Phys. Lett.*, **29**(10), 677 (1976); **31**(3), 161 (1977); K. Balasubramanyam and A.L. Rouff, "Oblique deposition enhanced sensitivity in electron beam exposed g Ge_xSe_{1-x} inorganic resist," *J. Vac. Sci. Technol.* **19**(4), 1374 (1981); N. Funakoshi, S. Zembutsu, and T. Kasai, "Anomalous Ag surface diffusion in amorphous Se Ge/Ag inorganic resist," *Jpn. J. Appl. Phys.* **20**(9), L649 (1981); S. Zembutsu, "X ray photoelectron spectroscopy studies of Ag photodoping in Se Ge amorphous films," *Appl. Phys. Lett.* **39**(12), 969 (1981).

NaOH,¹²⁷ or KOH.¹²⁸ Dry development of the patterned feature in a CF₄ plasma is also possible.¹²⁹

In the following section, we delve into the imaging mechanisms of metal-chalcogenide resist systems, using Ag₂Se/Ge-Se as the illustrative case. Although there may be slight compositional variations in the makeup of the silver source or the chalcogenide in a plurality of metal-chalcogenide resist systems, in the main, the underlying reactions responsible for the imaging action of these resists remain essentially the same. Therefore, the imaging mechanism of Ag₂Se/Ge-Se resist exemplifies this class of resist systems rather well.

The source of the silver in this system is the Ag₂Se, formed as a thin layer on the surface of the Ge_xSe_{1-x} (i.e., GeSe₂·Se_y) chalcogenide glass by a chemical reaction in a bath containing Ag(CN)²⁻ anions¹³⁰ according to



The characteristics of the sensitized resist, Ag₂Se/Ge_xSe_{1-x}, include a broadband spectral sensitivity to all regions of UV light, opacity to light of all wavelengths up to 450 nm, and transparency to visible light.¹³¹ The broad spectral sensitivity of the resist makes it useful in a variety of multilevel configurations, its opacity eliminates problems associated with the reflection of light from reflective substrates, and its transparency to visible light makes possible precise alignment to previously defined patterns. Exposure of the resist causes photodoping of Ag in the Ge-Se, leading to the depletion of Ag in the exposed areas of the Ag₂Se layer. The effect is the reduction in the absorption of these areas (also called photobleaching), effectively increasing image contrast.¹³² It must be noted that the depletion of Ag in the exposed areas also results in Ag diffusing laterally from adjacent unexposed areas into exposed areas, photodoping these areas. This nonlinear resist response at image edges (also referred to as edge sharpening) compensates for light

¹²⁷T. Shirakawa, I. Shimizu, H. Kokado, and E. Inoue, *Photogr. Sci. Eng.* **19**, 139 (1975); M.S. Chang, T.W. Hou, J.T. Chen, K.D. Kolwicz, and J.N. Zemel, "Inorganic resist for dry processing and dopant applications," *J. Vac. Sci. Technol.* **16**(6), 1973 (1979); K.D. Kolwicz and M.S. Chang, *J. Electrochem. Soc.* **127**(1), 135 (1980).

¹²⁸K. Balasubramanyam and A.L. Rouff, "Oblique deposition enhanced sensitivity in electron beam exposed g Ge_xSe_{1-x} inorganic resist," *J. Vac. Sci. Technol.* **19**(4), 1374 (1981).

¹²⁹M.S. Chang and J.T. Chen, "A dry etched inorganic resist," *Appl. Phys. Lett.* **33**(10), 892 (1978); A. Yoshikawa, O. Ochi, and Y. Mizushima, "Dry development of Se-Ge inorganic photoresist," *Appl. Phys. Lett.* **36**(1), 107 (1980).

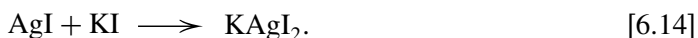
¹³⁰R.G. Vadimsky and K.L. Tai, "Wet chemical processing of the inorganic resist Ge_xSe_{1-x}," "Silver halide chalcogenide glass inorganic resists for x ray lithography," *ECS Ext. Abstr.* **80-2**, 824 (1980); R.G. Vadimsky, K.L. Tai, and E. Ong, "Ag₂Se/Ge-Se resist systems," in *Proc. Symp. on Inorganic Resist Systems*, Vol. 82-9, D. A. Doane and A. Heller, Eds., pp. 37-48, The Electrochemical Society, Pennington, NJ (1982).

¹³¹K.L. Tai, L.F. Johnson, D.W. Murphy, and M.S.C. Chung, "Sub 1000 Å linear lithographic patterns using Ag₂Se-GeSe₂ films," *J. Electrochem. Soc.* **126**(3), C118 (1979).

¹³²K.L. Tai, E. Ong, and R.G. Vadimsky "Inorganic resist systems for VLSI microlithography," in *Proc. Symp. on Inorganic Resist Systems*, Vol. 82-9, D. A. Doane and A. Heller, Eds., pp. 9-35, The Electrochemical Society, Pennington, NJ (1982).

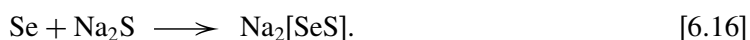
diffraction limitations and is a major factor in producing exceptional lithographic results.¹³³

The development of the latent image occurs in a two-stage process. First, the Ag₂Se is removed from the unexposed areas by immersion of the wafer in the KI/KI₃ solution,¹³⁴ leading to the conversion of the Ag₂Se to the soluble complex, KAgI₂, according to



This silver-specific stripping solution does not affect the integrity of the defined pattern, i.e., the photodoped regions, where Ag is bound to the Ge-Se matrix. Even when the optimal stripping time is substantially exceeded, these regions exhibit no sign of attack, which is indicative of extremely high selectivity, important for process control.

Complete delineation of the pattern in the Ge-Se glass is effected by dissolution of nonphotodoped areas in a two-component developer,¹³⁵ a strongly alkaline solution containing NaOH and a small amount of S²⁻ anions (required for glasses containing more than the stoichiometric amount of Se). The general development reactions may be written as¹³⁶



The effectiveness of the wet development stage depends highly on the structure of the glass. It has been shown that some Ge-Se layers possess an interlocked, phase-separated columnar structure that results in anisotropic, wet chemical etching.¹³⁷ This unique property, coupled with the thin imaging layer and the unique edge-sharpening property, is the reason behind the compelling lithographic performance of this inorganic resist.¹³⁸

¹³³K.L. Tai, W.R. Sinclair, R.G. Vadimsky, J.M. Moran, and M.J. Rand, "Bilevel high resolution photolithographic technique for use with wafers with stepped and/or reflecting surfaces," *J. Vac. Sci. Technol.* **16**(6), 1977 (1979).

¹³⁴R.G. Vadimsky and K.L. Tai, "Wet chemical processing of the inorganic resist Ge₂Se₃," *ECS Ext. Abstr.* **80-2**, 824 (1980); R.G. Vadimsky, K.L. Tai, and E. Ong, "Ag₂Se/Ge Se resist systems," in *Proc. Symp. on Inorganic Resist Systems*, Vol. 82 9, D.A. Doane and A. Heller, Eds., pp. 37-48, The Electrochemical Society, Pennington, NJ (1982).

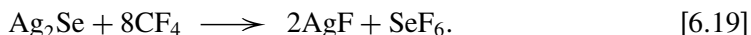
¹³⁵ibid.

¹³⁶ibid.

¹³⁷K.L. Tai, E. Ong, R.G. Vadimsky, C.T. Kemmerer, and P.M. Bridenbaugh, "Application of GeSe as a deep UV resist for submicron lithography," in *Proc. of Symp. on Inorganic Resist Systems*, Vol. 82 9, D.A. Doane and A. Heller, Eds., pp. 71-90, The Electrochemical Society, Pennington, NJ (1982); R.G. Vadimsky, K.L. Tai, and E. Ong, "Ag₂Se/Ge Se resist systems," in *Proc. of Symp. on Inorganic Resist Systems*, vol. 82 9, D.A. Doane and A. Heller, Eds., pp. 37-48, The Electrochemical Society, Pennington, NJ (1982).

¹³⁸R.G. Vadimsky and K.L. Tai, E. Ong, "Ag₂Se/Ge Se resist systems," in *Proc. of Symp. on Inorganic Resist Systems*, Vol. 82 9, D. A. Doane and A. Heller, Eds., pp. 37-48, The Electrochemical Society, Pennington, NJ (1982).

It is possible to dry develop Ag₂Se/GeSe, according to



AgF is not volatile and therefore protects and passivates the photodoped regions from attack.

The completely delineated Ag-doped Ge-Se pattern exhibits exceptional resistance to O₂ plasma,¹³⁹ thus allowing the use of reactive-ion etching (RIE) for the faithful transfer of the pattern to any underlying planarizing polymer layer. Combining the general attributes of metal-chalcogenide resist systems such as Ag₂Se/GeSe [namely, (i) diffraction compensation by edge sharpening, (ii) image contrast enhancement by photobleaching, (iii) substrate reflectivity elimination due to high absorbance of the Ge-Se, (iv) anisotropic wet chemical etching, and (5) accurate pattern transfer with dry etching due to O₂ resistance] with those of multilevel resist schemes has obvious advantages over organic multilevel schemes, primarily due to the opacity of the Ge-Se film to actinic light. This property allows the choice of conventional UV and DUV companion resists in a variety of configurations that are not applicable to organic polymer-based resist systems.¹⁴⁰

A major drawback of these chalcogenide resist systems is the contamination risk that their metallic ions and atoms pose to devices fabricated with them, should such contaminants not be properly cleaned off from such devices. Some of these chalcogenide resists are also very poisonous.

6.3.4.2 Ylide resists

Another important example of a resist based on radiation-induced polarity change employs the photochemical transformation of N-iminopyridinium ylides (**XXII**) to 1,2-diazepines (**XXIII**) as the basis of a negative non-chemically amplified resist (Scheme 6.14).¹⁴¹

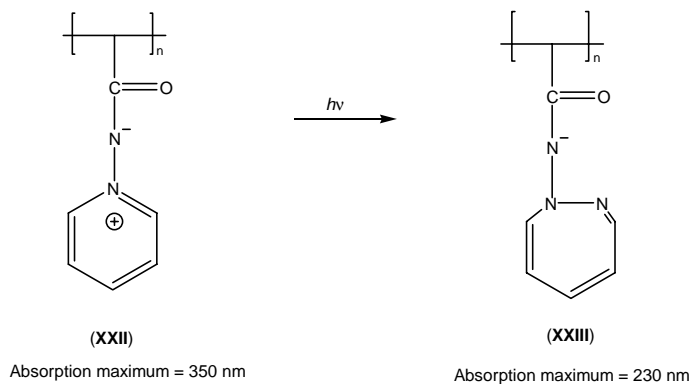
The polymer-bound ylides are water soluble while the diazepines are not, which makes it possible to develop this class of resists in aqueous developers. However, when the exposed resist is developed with organic solvents to produce a positive-tone image, the result is not satisfactory because of some adventitious cross-linking.¹⁴²

¹³⁹K.L. Tai, E. Ong, R.G. Vadimsky, J.M. Moran, and M.J. Rand, "Bilevel high resolution photolithographic technique for use with wafers with stepped and/or reflecting surfaces," *J. Vac. Sci. Technol.* **16**(6), 1977 (1979).

¹⁴⁰R.G. Vadimsky, K.L. Tai, and E. Ong, "Ag₂Se/Ge Se resist systems," in *Proc. of Symp. on Inorganic Resist Systems*, Vol. 82 9, D.A. Doane and A. Heller, Eds., pp. 37–48, The Electrochemical Society, Pennington, NJ (1982).

¹⁴¹R. Schwalm, A. Böttcher, and H. Koch, "Mid UV resist materials containing pyridinium ylides," *Proc. SPIE* **920**, 21–28 (1988).

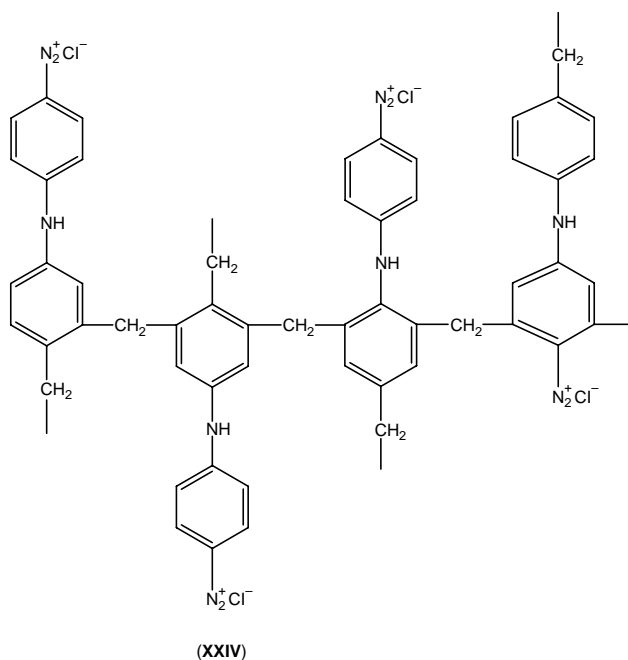
¹⁴²ibid.



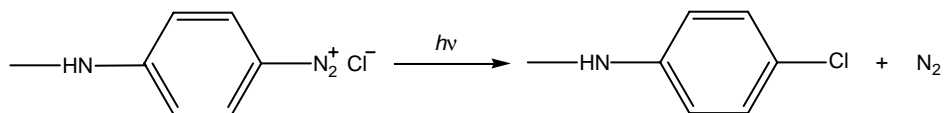
Scheme 6.14 Photochemical transformation of N-iminopyridinium ylides.

6.3.4.3 Diazo resists

Diazo resists based on diazoquinone photochemistry represent a very important group of non-chemically amplified negative resists based on radiation-induced polarity change. It should be pointed out that the driving force of the diazoquinone photochemistry is the great stability of N_2 , which makes the N_2 substituent a very effective leaving group. A very good example of a negative resist based on this very principle is the diazoresin produced by the diazotization of an aniline-formaldehyde resin with the indicated structure (XXIV).¹⁴³



¹⁴³A. Reiser, *Photoactive Polymers: The Science and Technology of Resists*, p. 45, John Wiley & Sons, Hoboken, NJ (1989).



Scheme 6.15 Photoinduced elimination of nitrogen in a diazoresin.

When this resin is irradiated, the diazonium ion eliminates nitrogen, leaving behind a carbocation that then reacts by substitution with the chloride ion (Scheme 6.15).

The chlorinated resin is not water soluble and reacts as a negative resist with an aqueous developer. This resist is widely used in the printing of lithographic plates and for the preparation of silverless negatives.¹⁴⁴

In addition to this radiation-induced polarity switch in the diazoresin, cross-links are also formed on exposure, which helps to make the image mechanically and thermally resistant. This cross-linking occurs at sites where a diazonium ion is located near a secondary amine and where the substitution reaction may produce a quaternary ammonium ion and lead to a cross-link (**XXIV**).¹⁴⁵

Another interesting variation on negative diazo resists involves compositions of aqueous acetic acid solution of 4-dimethylaminophenyldiazonium chloride and zinc chloride in a poly(N-vinyl pyrrolidone) binder; this is coated over cresol novolac film on a silicon wafer substrate.¹⁴⁶ The diazonium compound diffuses into the phenolic layer and is eventually partitioned in a uniform layer between the top layer and the phenolic resin. On exposure, the diazonium compound in the top layer bleaches and acts as a contrast-enhancement dye, while in the bottom it decomposes to the nonpolar 4-dimethylaminochlorobenzene, which acts as a dissolution inhibitor of the phenolic resin during development in aqueous-base solution. Line and space feature resolution of 0.5 μm has been reported for this material.¹⁴⁷

6.3.5 Chemically amplified negative resists based on radiation-induced polarity changes

6.3.5.1 Chemically amplified negative resists based on acid-catalyzed pinacol rearrangement

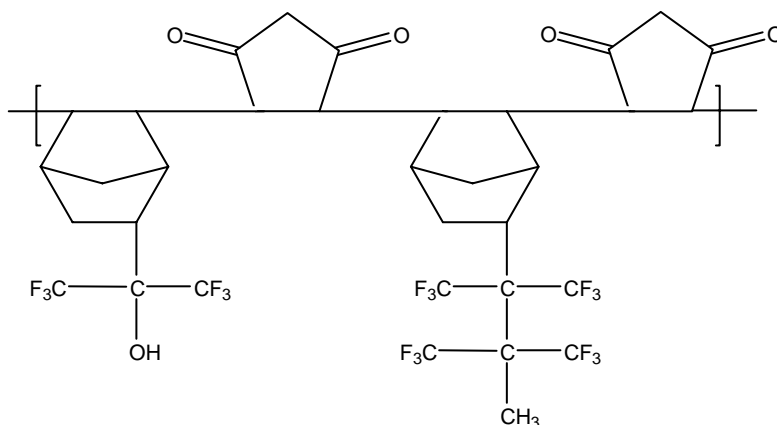
A pinacol-pinacolone rearrangement reaction involving polarity switch of a polar to a nonpolar functional group in a resist polymer has been exploited in

¹⁴⁴ibid.

¹⁴⁵ibid.

¹⁴⁶S. Uchino, T. Iwayanagi, and M. Hashimoto, "Photobleachable diazonium salt/phenolic resin two layer resist systems," *Proc. SPIE* **920**, 100 (1988).

¹⁴⁷A. Reiser, *Photoactive Polymers: The Science and Technology of Resists*, p. 46, John Wiley & Sons, Hoboken, NJ (1989).



Scheme 6.17 Pinnacol rearrangement polymer used in negative tone in 193-nm lithography.

pinacol rearrangement principle has also been extended to aqueous-base-developable negative tone resists designed for 193-nm lithography. The system comprises a copolymer of 5-(2-trifluoromethyl-1,1,1-trifluoro-2-hydroxypropyl)-2-norbornene (NBHFA) and norbornene bearing a pendant *vic*-diol (Scheme 6.17).¹⁵² Exposing a resist film comprising this resin and photoacid generator (PAG) to 193-nm photons results in the generation of photoacid, which in turn can convert the diol groups in the exposed part of the film to ketones, forming hydrogen bonding with the surrounding NBHFA hydroxyl groups, thus inhibiting the dissolution of the copolymer in an aqueous base, and resulting in negative tone images.¹⁵³

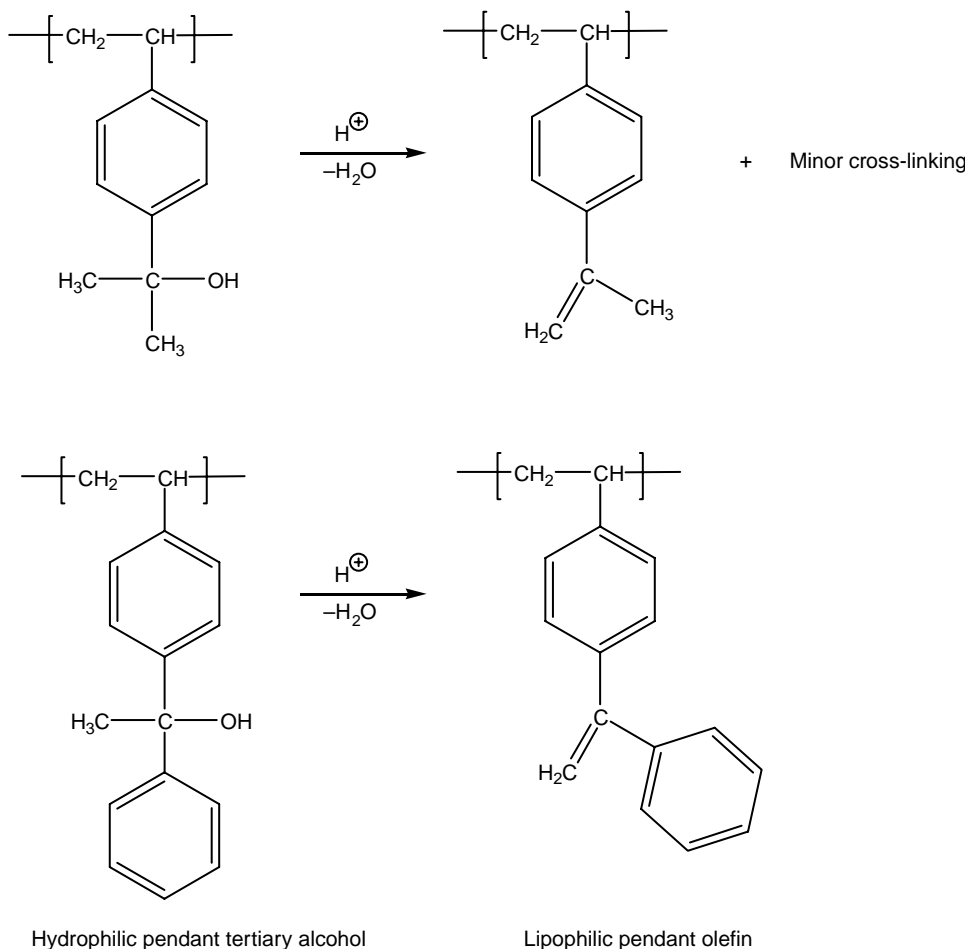
6.3.5.2 Chemically amplified negative resists based on acid-catalyzed intramolecular dehydration

The fact that tertiary alcohols can dehydrate intramolecularly with an acid as a catalyst to form olefins has been employed in the design of negative resists based on polarity switch. A good example is poly[4-(2-hydroxy-2-propyl)styrene], which undergoes acid-catalyzed dehydration to yield a stable tertiary benzylic carbocation, which subsequently eliminates a β -proton to form a pendant olefinic structure (Scheme 6.18).¹⁵⁴ This intramolecular dehydration reaction converts the

¹⁵²S. Cho, A.V. Heyden, J. Byers, C.G. Willson, "Negative tone 193 nm resists," *Proc. SPIE* **3999**, 62 (2000).

¹⁵³H. Ito, "Chemical amplification resists for microlithography," *Adv. Polym. Sci.*, **172**, 149 (2005).

¹⁵⁴H. Ito, Y. Maekawa, R. Sooriyakumaran, and E.A. Mash, "Acid catalyzed dehydration: A new mechanism for chemically amplified lithographic imaging," *Polymers for Microelectronics*, ACS Symp. Series 537, L.F. Thompson, C.G. Willson, and S. Tagawa, Eds., p. 64, American Chemical Society, Washington, DC. (1994).



Scheme 6.18 Intramolecular dehydration resulting in polarity change.

hydrophilic alcohol to a highly lipophilic olefin, which readily dissolves in a polar alcohol developer, resulting in negative tone image. It must be emphasized that the α -methylstyrene structure produced by the dehydration can undergo acid-catalyzed linear and cyclic dimerization, resulting in cross-linking.¹⁵⁵ However, the dimerization pathway is easily eliminated by replacing one of the methyl groups with a phenyl ring to generate a 1,1-diphenylethylene structure. A resist system based on this structure can be developed in a positive mode with the use of a nonpolar solvent such as xylene and in a negative mode with a polar alcohol.¹⁵⁶

¹⁵⁵ibid.

¹⁵⁶H. Ito, "Chemical amplification resists for microlithography," *Adv. Polym. Sci.* **172**, 152–153 (2005).

6.3.5.3 Chemically amplified condensation/intermolecular dehydration negative resists based on acid-catalyzed cross-linking with acid-sensitive electrophile (cross-linking agent)

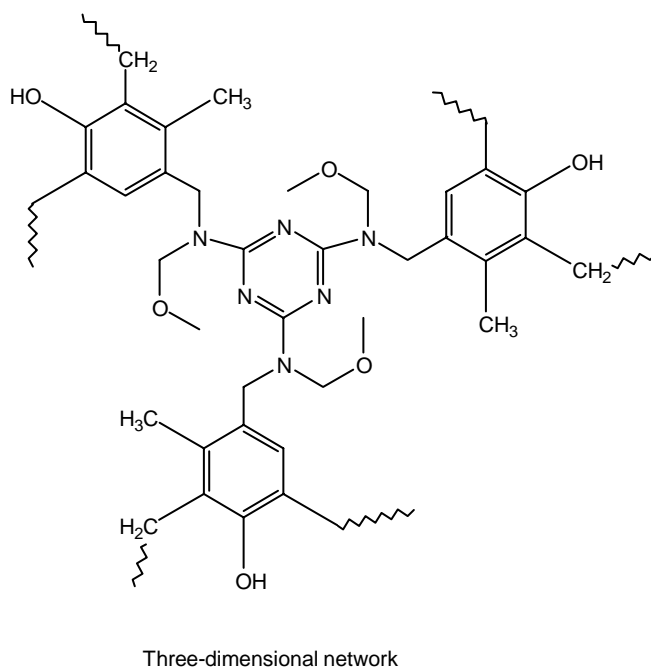
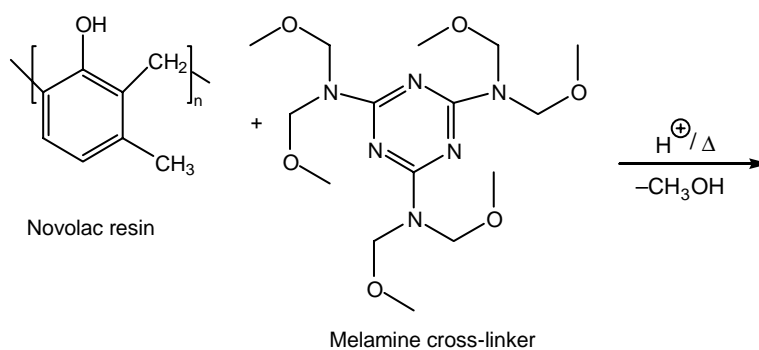
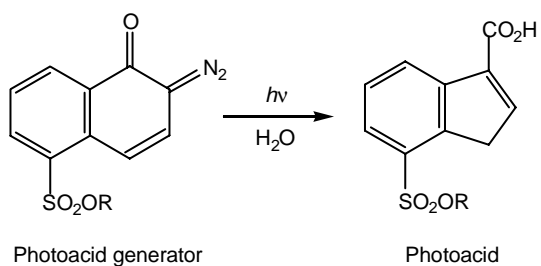
Acid-catalyzed condensation reaction mechanisms have been exploited in the design of aqueous-base-developable negative resist systems.¹⁵⁷ The condensation resists typically are composed of three components including a base soluble binder resin bearing reaction sites for cross-linking (typically phenolic resins), a radiation-sensitive acid generator, and an acid-sensitive latent electrophile that serves as the cross-linking agent.¹⁵⁸ The very first acid-catalyzed condensation resist system comprised a novolac/DNQ photoresist and an N-methoxymethylated melamine cross-linker. When exposed to near-UV photons, DNQ photolyzes to produce indene carboxylic acid, which reacts with the melamine cross-linker to generate an N-carbonium ion, along with methanol. The N-carbonium ion undergoes electrophilic substitution onto the electron-rich benzene ring of the novolac resin, regenerating a proton (Scheme 6.19). Cross-linking results because the melamine compound is multifunctional and can link up three different novolac polymer chains at each melamine molecule. Postexposure baking of the cross-linked resin followed by aqueous base development ensures that the exposed areas of the film remain insoluble, while the unexposed areas are dissolved away, generating a negative-tone relief image.¹⁵⁹ It should be pointed out that this resist can be developed in a positive-tone manner in the absence of a postexposure bake before the development step.¹⁶⁰

¹⁵⁷W.E. Feeley, J.C. Imhof, C.M. Stein, T.A. Fisher, and M.W. Legensa, "The role of the latent image in a new dual image, aqueous developable, thermally stable photoresist," *Polym. Eng. Sci.* **26**, 1101 (1986); H. Y. Liu, M.P. de Grandpre, and W.E. Feeley, "Characterization of a high resolution novolac based negative electron beam resist with 4 $\mu\text{C}/\text{cm}^2$ sensitivity," *J. Vac. Sci. Technol.* **B6**, 379 (1988); J.W. Thackeray, G.W. Orsula, J.F. Bohland, and A.W. McCullough, "Approaches to deep ultraviolet photolithography utilizing acid hardened resin photoresist systems," *J. Vac. Sci. Technol.* **B7**, 1620 (1989); A.K. Berry, K.A. Graziano, L.E. Bogan, Jr., and J.W. Thackeray, Chapter 6 in *Polymers in Microlithography*, ACS Symposium Series 412, E. Reichmanis, S.A. MacDonald, and T. Iwayanagi, Eds., p. 87, American Chemical Society, Washington, DC (1989); J. Lingnau, R. Dammel, and J. Theis, "Recent trends in x ray resist: part I," *Solid State Technol.* **32**(9), 105 (1989); "Recent trends in x ray resist: part II," **32**(10), 107 (1989); J.F. Bohland, G.S. Calabrese, M.F. Cronin, D. Canistro, T.H. Fedynshyn, J. Ferrari, A.A. Lamola, G.W. Orsula, E.K. Pavelcheck, R. Sinta, J.W. Thackeray, A.K. Berry, L.E. Boga, Jr., M.P. de Grandpre, K.A. Gran ziano, R. Olsen, S. Thompson, and M.R. Winke, *J. Photopolym. Sci. Technol.* **3**, 355 (1990); J.W. Thackeray, G.W. Orsula, M.M. Rajaratnam, R. Sinta, D. Herr, and E. Pavelcheck, "Dissolution inhibition mechanism of ANR photoresists: crosslinking vs. OH site consumption," *Proc. SPIE* **1466**, 39 (1991); M.T. Allen, G.S. Calabrese, A.A. Lamola, G.W. Orsula, M.M. Rajaratnam, R. Sinta, and J.W. Thackeray, "Further advances in chemistry and technology of acid hardened resists," *Photopolym. Sci. Technol.* **4**, 379 (1991).

¹⁵⁸H. Ito, "Chemical amplification resists for microlithography," *Adv. Polym. Sci.* **172**, 152 (2005).

¹⁵⁹*ibid.*, p. 153.

¹⁶⁰W.E. Feeley, J.C. Imhof, C.M. Stein, T.A. Fisher, and M.W. Legensa, "The role of the latent image in a new dual image, aqueous developable, thermally stable photoresist," *Polym. Eng. Sci.* **26**, 1101 (1986).



Scheme 6.19 Acid-catalyzed condensation reaction of novolac resins by melamine cross-linker.

The design principle of condensation resists has been extended to new platforms¹⁶¹ that include polyhydroxystyrene as the resin, chloromethyltriazine as HCl acid generator, and various other cross-linkers (XXV).¹⁶² Of particular importance are cross-linkers based on benzyl acetate derivatives, benzyl alcohol derivatives,¹⁶³ and vinyl cyclic acetals.¹⁶⁴ On acid treatment, these cross-linkers yield stable benzylic carbocation, which undergoes electrophilic substitution reactions onto the electron-rich benzene ring and cross-links the phenolic resin when the latent electrophile is multifunctional.¹⁶⁵

The cross-linker may be an additive (Scheme 6.20) or incorporated into a phenolic resin through copolymerization (Scheme 6.21). In the former case (known as a three-component system), the cross-linker, e.g., 1,4-di(acetoxymethyl) benzene, is added to the resist solution, along with the resin (e.g., PHOST, novolac) and PAG. In the latter case (known as a two-component system), the cross-linker (e.g., 4-vinylbenzyl acetate) is copolymerized with the resist's polymeric resin [e.g., butoxycarbonyloxystyrene (BOCST)], followed by selective removal of the *t*-BOC group in refluxing glacial acetic acid, to afford a copolymer bearing both the latent electrophile and the cross-linking site on the same polymer chain.¹⁶⁶ The formation of carbocation from the protonated ether moiety is the rate-determining step for cross-linking in these resists. Both the *C*-alkylation and *O*-alkylation are responsible for cross-linking and also result in the destruction of the base-solubilizing phenolic OH groups in the exposed areas of the film, and hence, the negative-tone imaging. These condensation negative resists have found widespread application in DUV 248-nm, electron-beam, and x-ray lithographies, where they

¹⁶¹J.W. Thackeray, G.W. Orsula, J.F. Bohland, and A.W. McCullough, "Approaches to deep ultra violet photolithography utilizing acid hardened resin photoresist systems," *J. Vac. Sci. Technol.* **B6**, 1620 (1989); A.K. Berry, K.A. Graziano, L.E. Bogan, Jr., and J.W. Thackeray, Chapter 6 in *Polymers in Microlithography*, ACS Symp. Series 412, E. Reichmanis, S.A. MacDonald, T. Iwayanagi, Eds., p. 87, American Chemical Society, Washington, DC (1989); J.W. Thackeray, G.W. Orsula, M.M. Rajaratnam, R. Sinta, D. Herr, and E. Pavelcheck, "Dissolution inhibition mechanism of ANR photoresists: crosslinking vs. OH site consumption," *Proc. SPIE* **1466**, 39 (1991).

¹⁶²B. Reck, R.D. Allen, R.J. Twieg, C.G. Willson, S. Matuszczyk, H.D.H. Stover, N.H. Li, and J.M.J. Frechet, "Novel photoresist design based on electrophilic aromatic substitution," *Polym. Eng. Sci.* **29**, 960 (1989); J.M.J. Frechet, S. Matuszczyk, H.D.H. Stover, C.G. Willson, and B. Reck, "Chemically amplified imaging materials based on electrophilic aromatic substitution: poly[4 (acetoxymethyl) styrene co 4 hydroxystyrene]," in *Polymers in Microlithography*, E. Reichmanis, S.A. MacDonald, T. Iwayanagi, Eds., ACS Symp. Series 412, p. 74, American Chemical Society, Washington, DC (1989); J.M.J. Frechet, B. Kryczka, S. Matuszczyk, B. Reck, M. Stanculescu, and C.G. Willson, "Chemically amplified imaging materials based on acid catalyzed reactions of polyesters or electrophilic crosslinking processes," *J. Photopolym. Sci. Technol.* **3**, 235 (1990).

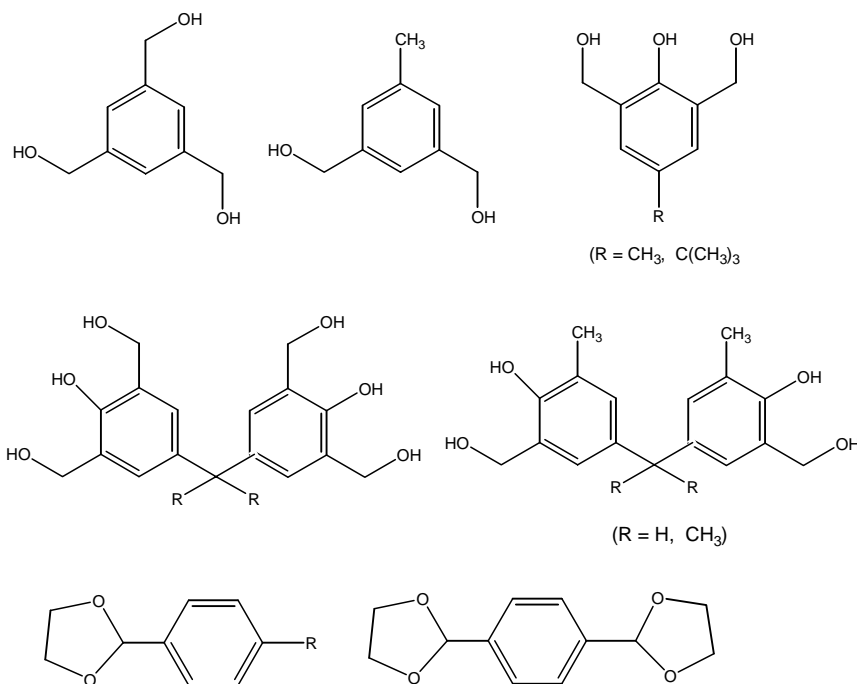
¹⁶³J.M.J. Frechet and S.M. Lee, "New three component aqueous base developable negative resist systems incorporating chemical amplification and tunable sensitivities," *Proc. SPIE* **1925**, 102 (1993).

¹⁶⁴U. Schedli, N. Muenzel, and H. Holzarth, "1,3 dioxolyl acetals as powerful crosslinkers of phenolic resin," *Proc. SPIE* **1925**, 109 (1993); W. S. Huang, K.Y. Lee, R.K. J. Chen, and D. Schepsis, "Negative tone resist system using vinyl cyclic acetal crosslinker," *Proc. SPIE* **2724**, 315 (1996).

¹⁶⁵H. Ito, "Chemical amplification resists for microlithography," *Adv. Polym. Sci.* **172**, 155 (2005).

¹⁶⁶*ibid.*, p. 156.

have provided excellent lithographic performance.¹⁶⁷ Calixerenes and dendrimers have also been used as matrix resins for negative-tone imaging through condensation.¹⁶⁸



(XXV) Examples of latent electrophiles (cross-linkers)

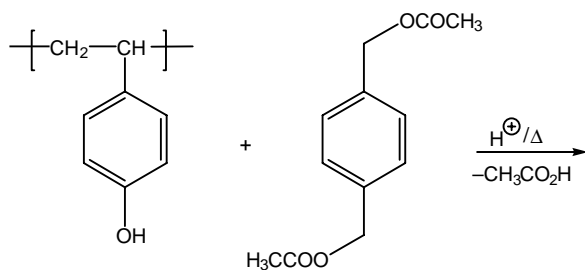
Variations on the condensation reaction concept that do not involve cross-linking have also been employed in the design of negative resists. The first set of these variations on the condensation reaction concept include the attachment of a bulky substituent to the phenolic group through *C*- or *O*-alkylation, which significantly decreases the dissolution rate of the phenolic resin in aqueous base (Scheme 6.22). Specific examples include *N*-hydroxy- and acetoxymethylimides, which although are monofunctional latent electrophiles, do undergo acid-catalyzed condensation reaction with phenolic resins, reducing their dissolution rate in the exposed areas and providing negative imaging on aqueous base development.¹⁶⁹

The second set of variations on the condensation reaction concept involves the acid-catalyzed methylation of phenols by aldehydes, with the aldehyde functioning as a latent electrophile (Scheme 6.23). Because the methylolated phenolic resin

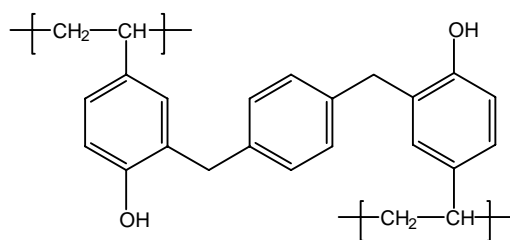
¹⁶⁷ibid., pp. 152–156.

¹⁶⁸ibid., p. 156.

¹⁶⁹H. Ito, K. Schildknegt, and E.A. Mash, "Negative chemical amplification resist systems based on polyhydroxystyrenes and *N* substituted imides or aldehydes," *Proc. SPIE* **1466**, 408 (1991); H. Ito, "Chemical amplification resists for microlithography," *Adv. Polym. Sci.* **172**, 156 (2005).

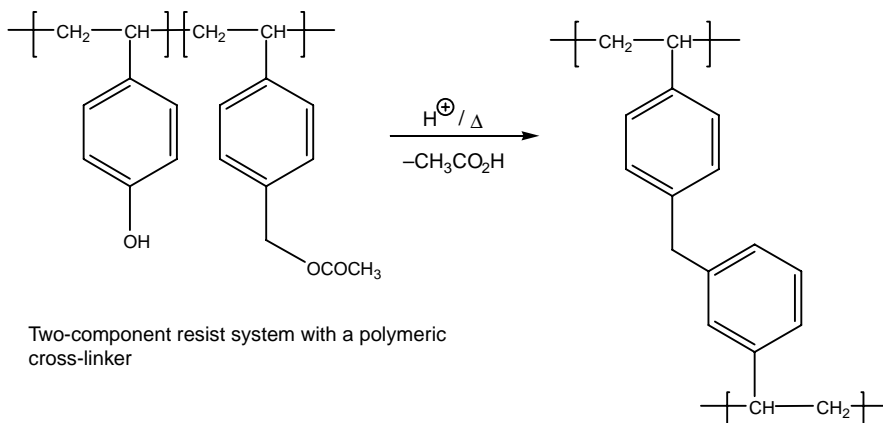


Three-component resist with a cross-linker



Cross-linked three-dimensional network

Scheme 6.20 Acid-catalyzed condensation cross-linking reaction of polystyrene by an added cross-linker.



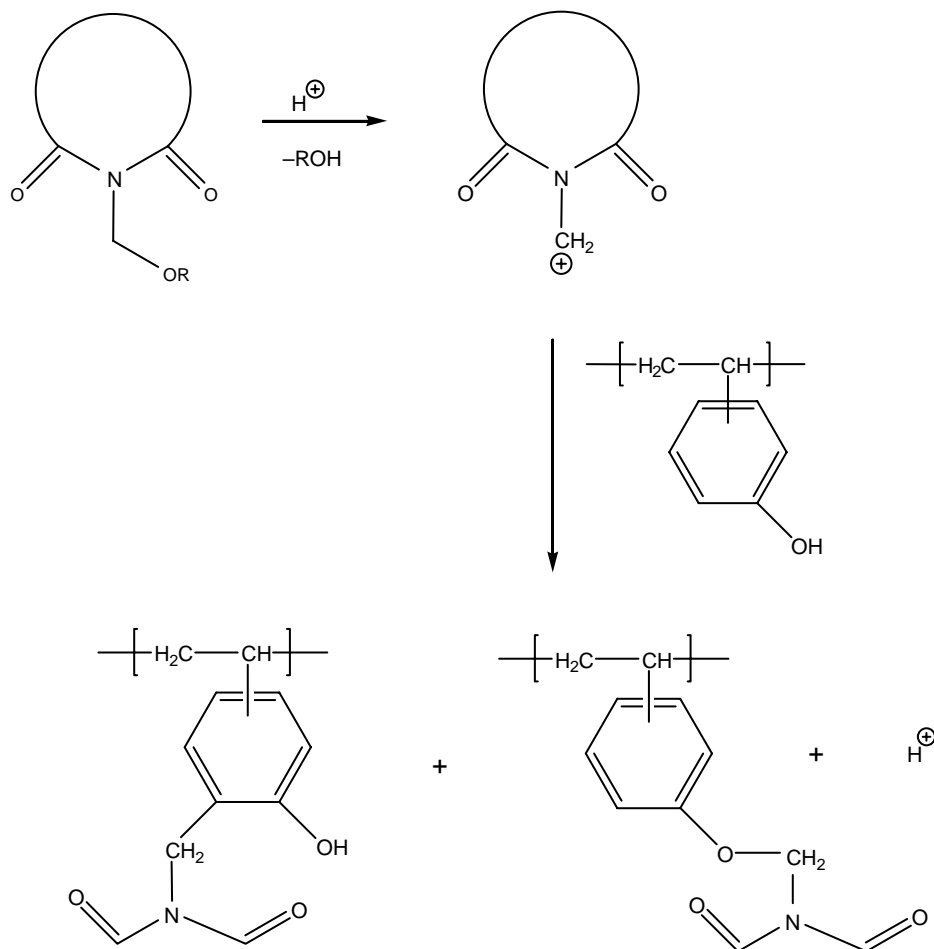
Two-component resist system with a polymeric cross-linker

Scheme 6.21 Acid-catalyzed condensation cross-linking reaction of polystyrene by a polymer-bound cross-linker.

dissolves much more slowly in aqueous base than its precursor resin, this concept is utilized in negative-tone imaging.¹⁷⁰ In addition, the methylolated phenol can undergo further cross-linking, which lowers the dissolution rate still further.¹⁷¹

¹⁷⁰H. Ito, "Chemical amplification resists for microlithography," *Adv. Polym. Sci.* **172**, 152–156 (2005).

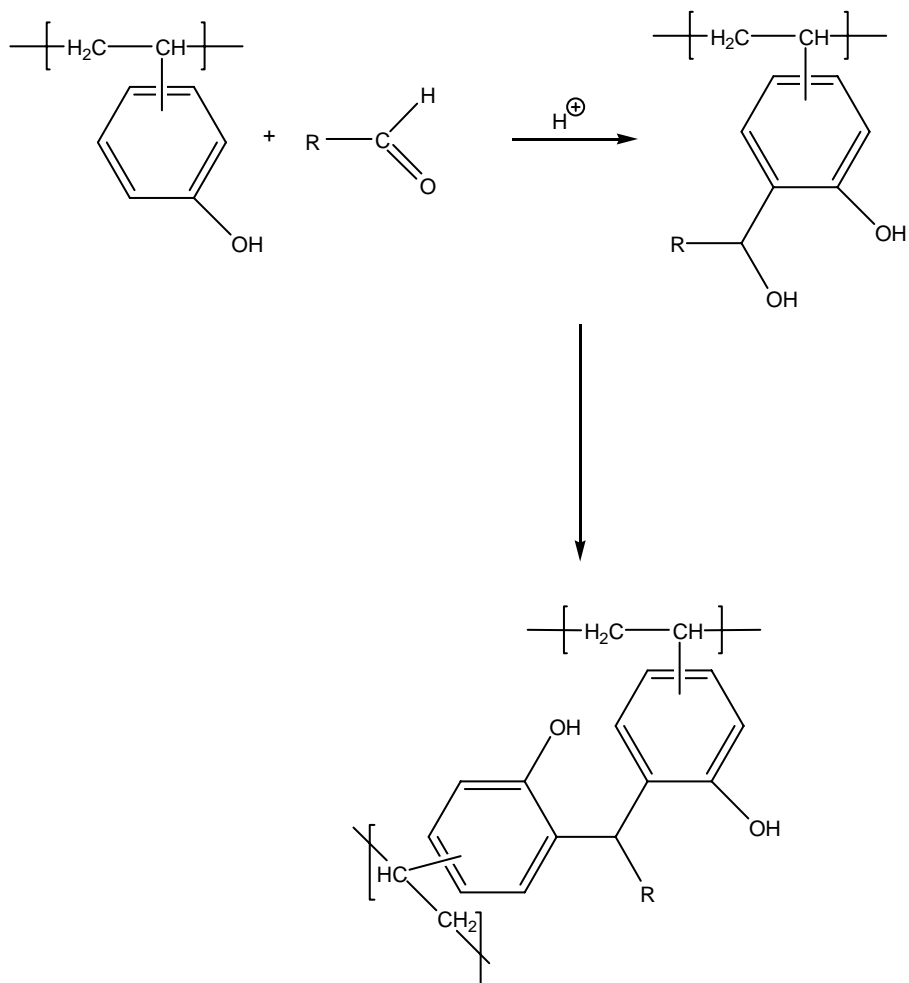
¹⁷¹ibid.



Scheme 6.22 C- and O-alkylation of phenol with monofunctional electrophile.

The third set of variations on the aqueous-base-developable condensation resist design concept involves self-condensation systems, typified by polymeric furan derivatives. A typical example is based on the copolymer poly[4-hydroxystyrene-*co*-4-(3-furyl-3-hydroxypropyl)styrene] (Scheme 6.24), which is prepared by radical copolymerization of the acetyl-protected furan monomer with BOCST, followed by base hydrolysis. In the presence of a photogenerated acid, the furan methanol residue, which is highly reactive toward electrophiles, attacks the ring carbons, a step that is facilitated by a mesomeric electron release from oxygen, resulting in a stable carbocation, which undergoes electrophilic substitution reactions onto the furfuryl ring, effectively cross-linking the chains and reducing the solubility of the exposed areas of the resin in aqueous base developer relative to the precursor (unexposed) resin, and resulting in a negative-tone image. In this way, the pendant furfuryl groups serve as both the latent electrophile and the nucleophile.¹⁷²

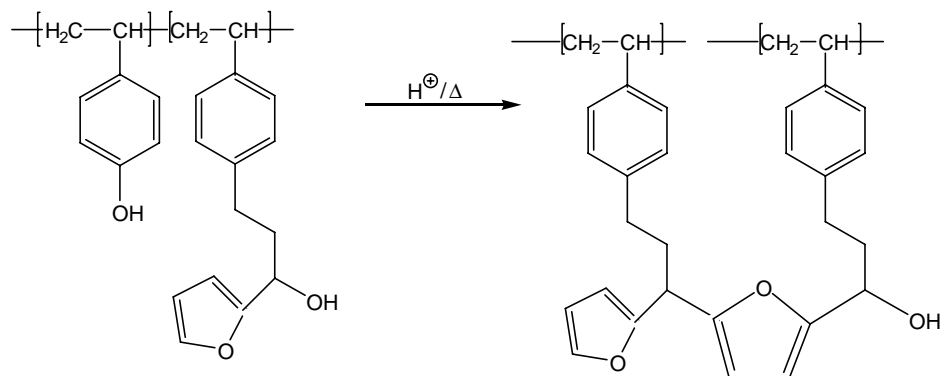
¹⁷²H. Ito, "Chemical amplification resists for microlithography," *Adv. Polym. Sci.* **172**, 157 (2005).



Scheme 6.23 Condensation of phenol with aldehyde.

Another example of a self-condensation negative resist system comprises poly[4-(1-hydroxyethyl)styrene] with a secondary alcohol pendant group, which cross-links through acid-catalyzed interchain dehydration, forming ether linkages. Development with alcohol produces negative-tone images. The aqueous-base-developable version of this resist is produced by copolymerizing styrenic secondary alcohol monomer with 4-acetoxystyrene, followed by base hydrolysis (Scheme 6.25).¹⁷³ On exposure, the photogenerated acid catalyzes intermolecular

¹⁷³H. Ito and Y. Maekawa, "Dual tone and aqueous base developable negative resists based on acid catalyzed dehydration," in *Polymeric Materials for Microelectronic Applications*, ACS Symp. Series 579, H. Ito, S. Tagawa, K. Horie, Eds., p. 70, American Chemical Society, Washington, DC (1994).



Scheme 6.24 Acid-catalyzed self-condensation of polymeric furan methanol.

dehydration of the resin, resulting in self-condensation to di(α -methylbenzene)ether, *O*-alkylation to α -methylbenzyl phenyl ether, and *C*-alkylation to *o*-(α -methylbenzyl)phenol. All of these condensation reactions are contributory to cross-linking and therefore to negative aqueous base development.¹⁷⁴

Self-condensation of silanol compounds in phenolic matrix resins has also been adapted for use in water-developable negative-tone resist applications (Scheme 6.26).¹⁷⁵ These resists function on the basis of polarity change instead of cross-linking. When formulated with phenolic resins, base-soluble silanol compounds such as phenylsilanediol function as dissolution promoters of the former, but on exposure and postexposure bake, these silanol compounds are converted to polysiloxanes through acid-catalyzed condensation, which, during aqueous base development, form a hydrophobic barrier surrounding the phenolic OH groups, leading to negative-tone imaging of the phenolic resins.¹⁷⁶ Silesquioxanes have also been employed in a similar manner in negative resist applications.¹⁷⁷

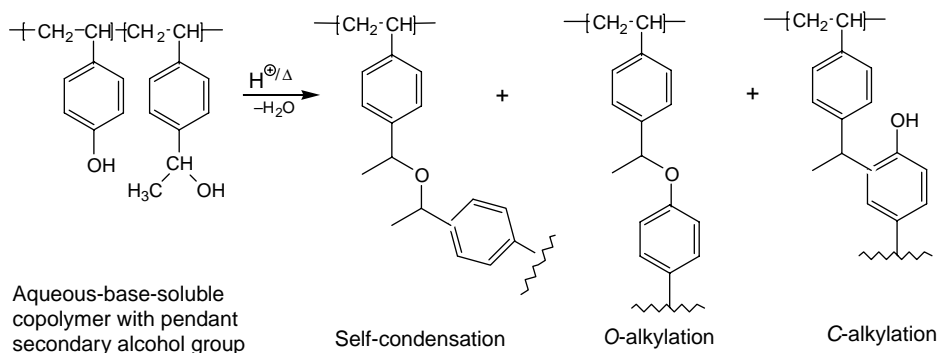
It is equally worthy to note that a resist based on hydrogen silesquioxanes (HSQs) and formulated in methylisobutyl ketone (MIBK) carrier solvent has recently been reported to have demonstrated pitch resolution down to 20 nm in a 30-nm-thick HSQ film with electron-beam direct-write lithography (exposure

¹⁷⁴H. Ito, "Chemical amplification resists for microlithography," *Adv. Polym. Sci.* **172**, 158 (2005).

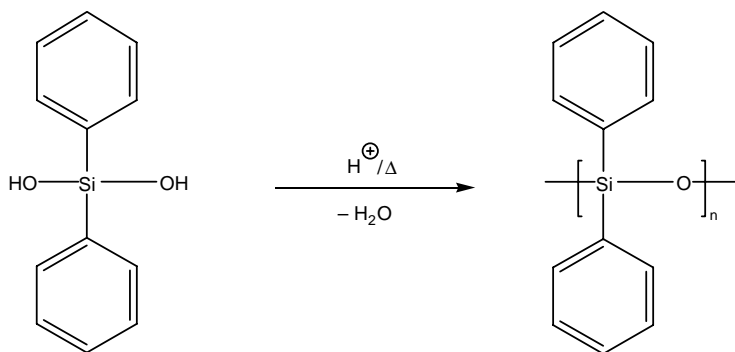
¹⁷⁵T. Ueno, H. Shiraishi, N. Hayashi, K. Tadano, E. Fukuma, and T. Iwayanagi, "Chemical amplification negative resist systems composed of novolac, silanols, and acid generators," *Proc. SPIE* **1262**, 26 (1990); H. Shiraishi, E. Fukuma, E. Hayashi, T. Ueno, K. Tadano, and T. Iwayanagi, "Acid catalyzed silanol condensation reaction mechanism in a chemical amplification negative resist system," *J. Photopolym. Sci. Technol.* **3**, 385 (1990); H. Shiraishi, E. Fukuma, N. Hayashi, K. Tadano, and T. Ueno, "Insolubilization mechanism of a chemical amplification negative resist system utilizing an acid catalyzed silanol condensation reaction," *Chem. Mater.* **3**, 621 (1991).

¹⁷⁶H. Ito, "Chemical amplification resists for microlithography," *Adv. Polym. Sci.*, **172**, 549 (2005).

¹⁷⁷D.R. McKean, N.J. Clecak, and L.A. Pedersen, "Highly etch resistant, negative resist for deep UV and electron beam lithography," *Proc. SPIE* **1262**, 110 (1990).



Scheme 6.25 Acid-catalyzed dehydration for negative tone aqueous base development.



Scheme 6.26 Silanol condensation for negative aqueous base development.

conditions: at 100 KV with $5000 \mu\text{C}/\text{cm}^2$).¹⁷⁸ A 350°C postexposure bake of this negative resist in N_2 was reported to enhance the contrast properties of the film, which can be developed in a normal aqueous developer (0.26 N tetramethylammonium hydroxide).

6.3.5.4 Chemically amplified methacrylate negative resists based on acid-catalyzed esterification

The esterification reaction of carboxylic acids and anhydrides has been exploited in the design of aqueous-base-developable negative resists because such a reaction changes the polarity of the resins from soluble to insoluble. A good number of negative resists designed for ArF lithography are based on this principle. Examples of such resists are based on the intramolecular esterification of resins bearing

¹⁷⁸D. Vogler, "Dow Corning targets maskless lithography with latest e beam photoresist," *Solid State Technol.* **51**(6), June 24, 2008: [http://www.electroiq.com/index/display/semiconductors/article/display/332554/articles/solid state technology/lithography/2008/06/dow corning targets maskless lithography with latest e beam photoresists.html](http://www.electroiq.com/index/display/semiconductors/article/display/332554/articles/solid%20state%20technology/lithography/2008/06/dow%20corning%20targets%20maskless%20lithography%20with%20latest%20e%20beam%20photoresists.html); Dow Corning XR 1541 E Beam Resist Product Information Sheet (2008): [http://www.dowcorning.com/content/publishedlit/XR 1541 E Beam resist.pdf](http://www.dowcorning.com/content/publishedlit/XR%201541%20E%20Beam%20resist.pdf).

γ -hydroxy acid moieties and prepared from the cyclopolymerization of dienes of norbornene and maleic anhydride in a reaction in which the anhydride is converted to γ -hydroxy acid using NaBH_4 , with a simultaneous formation of γ -lactone [Scheme 6.27(a)].¹⁷⁹ The γ -hydroxy acid moiety [in Schemes 6.27(a) and (b)] undergoes acid-catalyzed intramolecular esterification (known as ring closure) to form γ -lactone, effectively a polarity switch for negative-tone imaging with aqueous base developer. It should be pointed out that the presence of unreacted carboxylic acid units in the exposed regions of the film causes the penetration of water into the film, causing swelling-induced distortion.¹⁸⁰

The application of intramolecular esterification of resins bearing δ -hydroxy acid moieties¹⁸¹ has been demonstrated as a viable negative-imaging resist system for ArF lithography. Such resins are readily obtained from the free radical copolymerization of acrylates bearing pendant androsterone with δ -hydroxy acid and 3- β -acryloyloxyandrosterone, followed by oxidation with $\text{CH}_3\text{CO}_2/\text{H}_2\text{O}_2$ to form δ -lactone, and followed by hydrolysis in tetrahydrofuran with 0.2N aqueous NaOH (Scheme 6.28).¹⁸² This resin is able to overcome the above-mentioned problems associated with the γ -hydroxy acid system.¹⁸³

Furthermore, transesterification of hydroxyethyl ester moieties in methacrylate resists based on methacrylic acid and hydroxyethyl methacrylate resins has been demonstrated as a basis for negative-tone imaging in ArF lithography (Scheme 6.29).¹⁸⁴

6.3.5.5 Chemically amplified methacrylate negative resists based on acid-catalyzed deprotection and development in supercritical CO_2

A strategy based on the fact that polar polymers are not soluble in supercritical (SC) CO_2 has been exploited in the design of negative-tone resists. The strategy involves using fluorine-protected nonpolar polymers that are converted to polar polymers by acid-catalyzed deprotection, producing negative-tone images

¹⁷⁹T. Hattori, Y. Tsuchiya, Y. Yokoyama, and H. Shiraishi, "Design, synthesis, and evaluation of a novel amphiphilic alicyclic polymer having γ hydroxy acid structure," *Chem. Mater.* **10**, 1789 (1998); T. Hattori, Y. Tsuchiya, Y. Yokoyama, H. Oizumi, T. Morisawa, A. Yamaguchi, and H. Shiraishi, "Microswelling free negative resists for ArF excimer laser lithography utilizing acid catalyzed intramolecular esterification," *Proc. SPIE* **3678**, 411 (1999); T. Hattori, Y. Tsuchiya, Y. Yokoyama, H. Oizumi, T. Morisawa, A. Yamaguchi, and H. Shiraishi, "Micro swelling free negative resists for ArF phase shifting lithography utilizing acid catalyzed intramolecular esterification," *J. Photopolym. Sci. Technol.* **12**, 537 (1999).

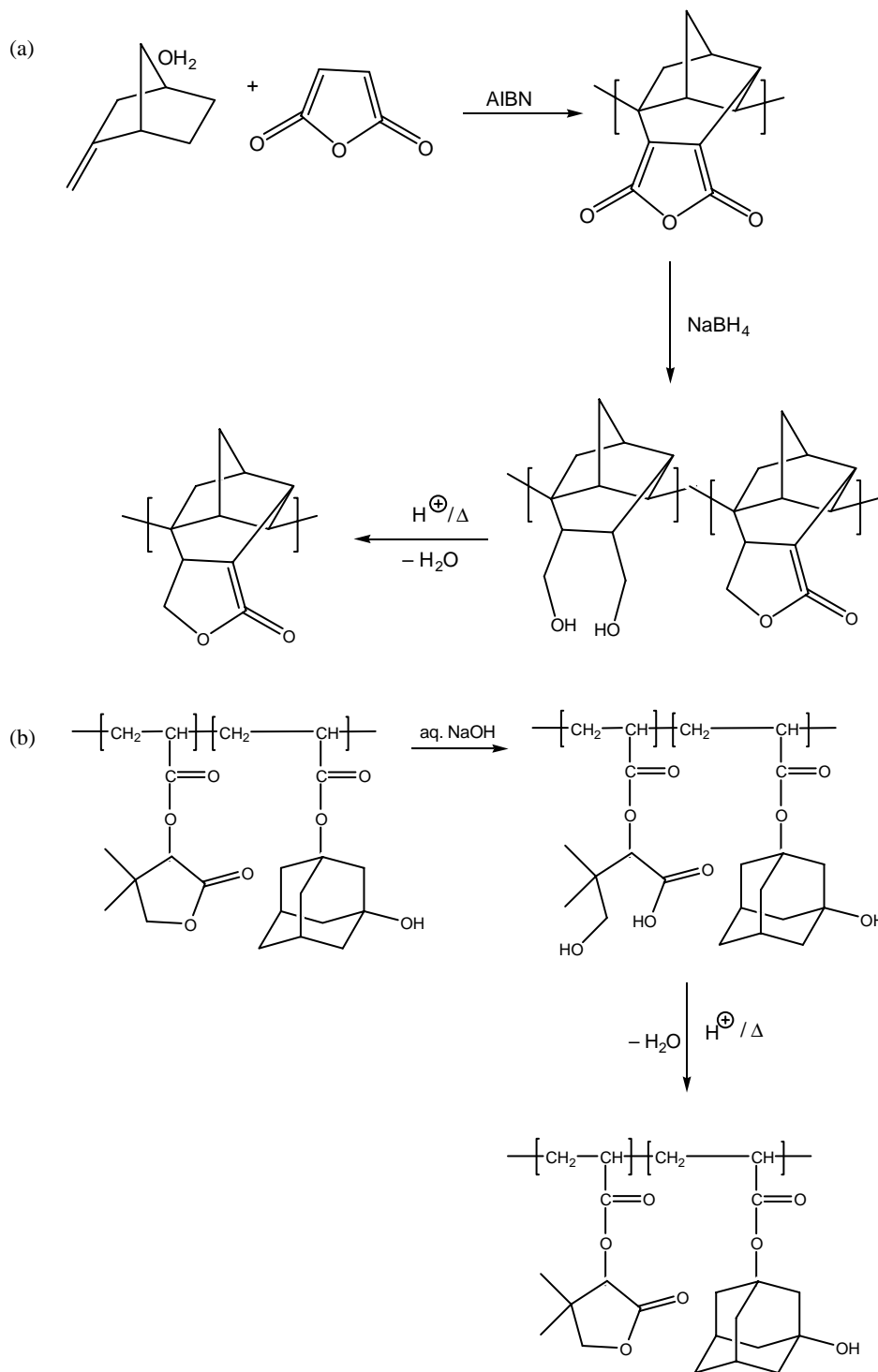
¹⁸⁰ibid.

¹⁸¹Y. Yokoyama, T. Hattori, K. Kimura, T. Tanaka, and H. Shiraishi, "Effect of comonomer structure on dissolution characteristics," *J. Photopolym. Sci. Technol.* **13**, 579 (2000); **14**, 393 (2001).

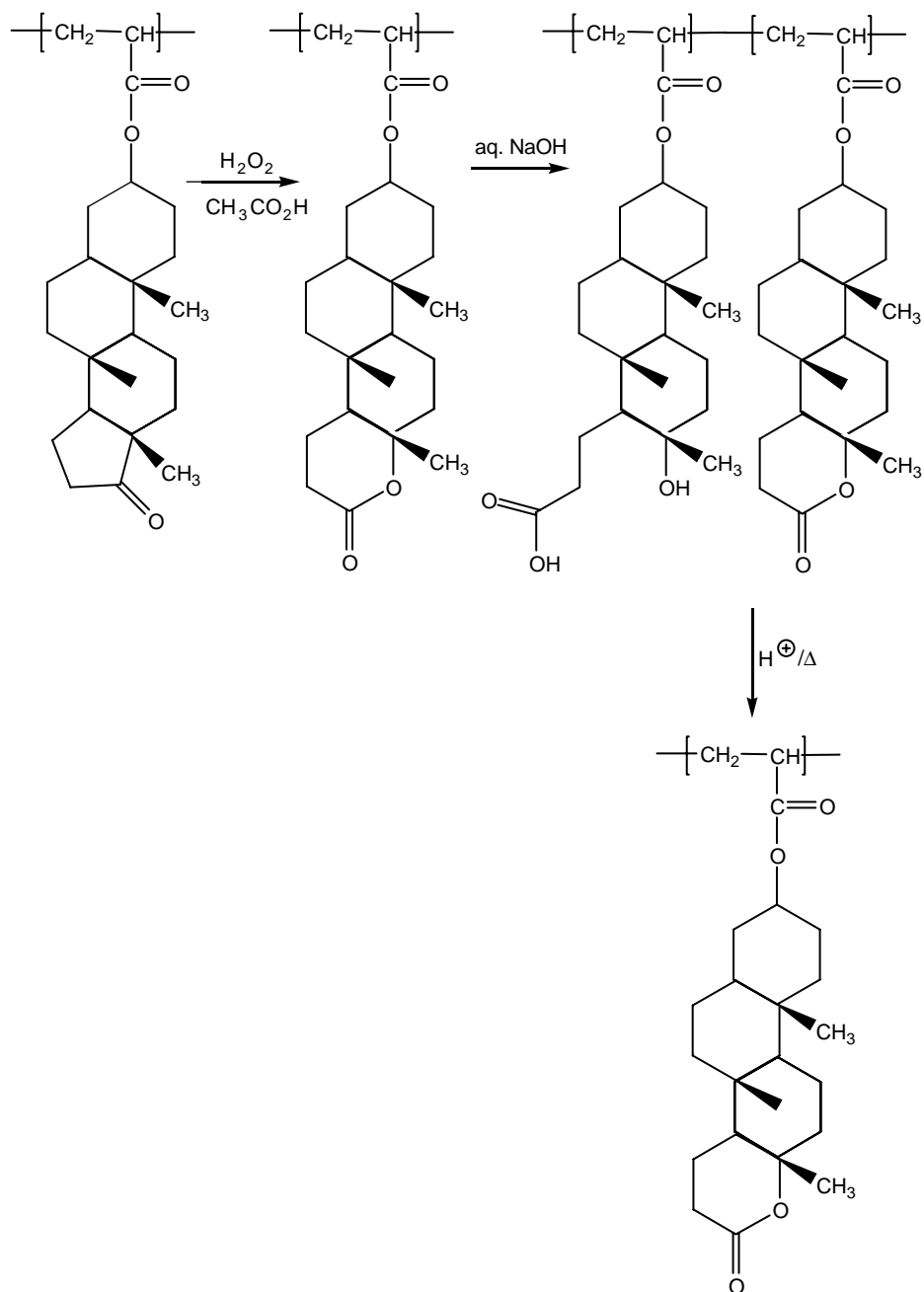
¹⁸²ibid.

¹⁸³H. Ito, "Chemical amplification resists for microlithography," *Adv. Polym. Sci.* **172**, 161–163 (2005).

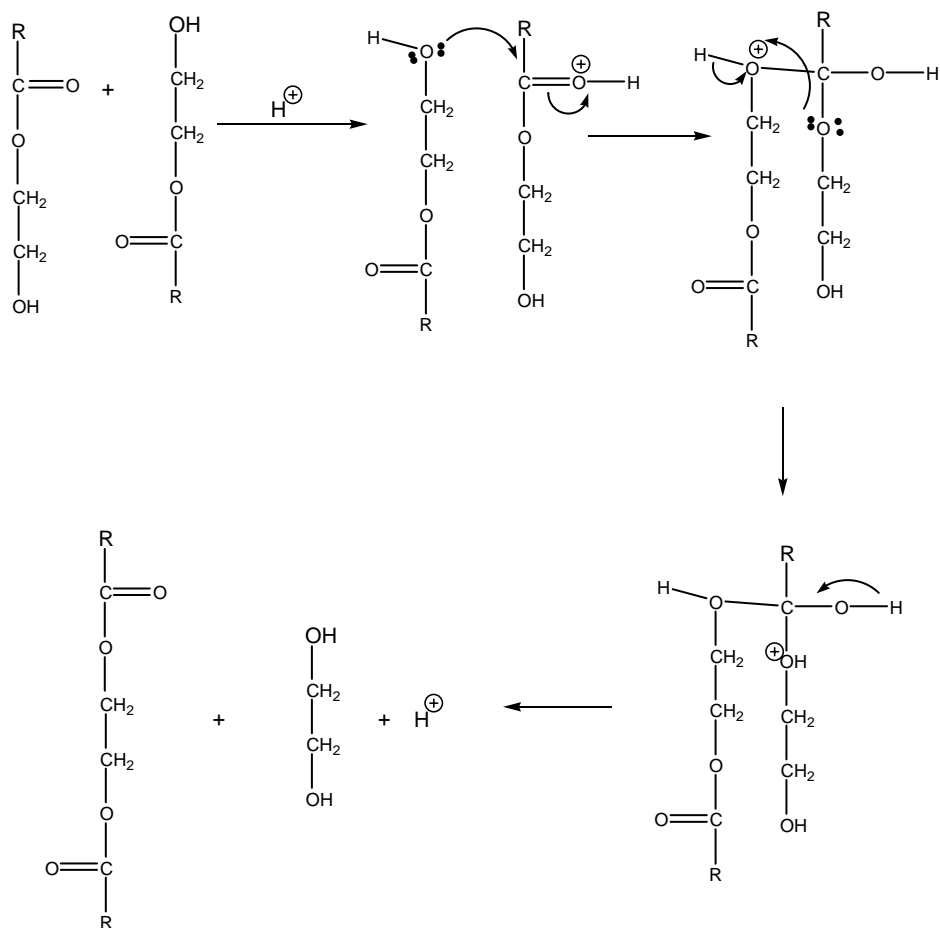
¹⁸⁴T. Aoai, J. S. Lee, H. Watanabe, S. Kondo, N. Miyagawa, S. Takahara, and T. Yamaoka, "Mechanism of acid catalyzed crosslinking reaction with hydroxyethyl group and application to microlithography," *J. Photopolym. Sci. Technol.* **12**, 303 (1999); S. Lee, A. Toshiaki, S. Kondo, N. Miyagawa, S. Takahara, and T. Yamaoka, "Negative working photoresist of methacrylate polymers based on the transesterification of the 2 hydroxyethyl group in the presence of an acid," *J. Polym. Sci. Part A* **40**, 1858 (2002).



Scheme 6.27 Examples of polarity changes (from polar to nonpolar state) resulting from intramolecular esterification of γ -hydroxy acid.



Scheme 6.28 Example of intramolecular esterification of δ -hydroxy acid.



Scheme 6.29 Polarity change from polar to nonpolar state resulting from transesterification reaction of hydroxyethyl ester moieties in methacrylate resists based on methacrylic acid and hydroethyl methacrylate polymers.

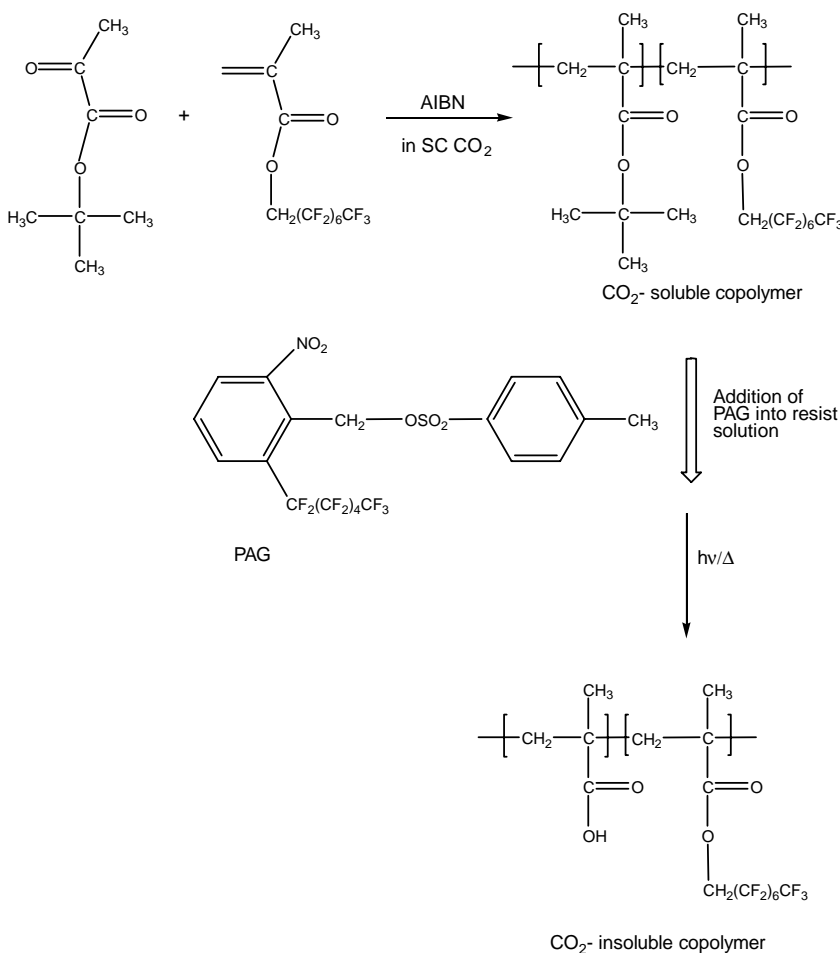
on development in SC CO₂. Examples of resist compositions utilizing this principle include polymethacrylates containing acid-labile groups and fluorine or siloxane esters,¹⁸⁵ block copolymers of tetrahydropyranal methacrylate and 1H,1H-perfluorobutyl or 1H,1H-perfluorooctyl methacrylate,¹⁸⁶ and copolymers of *t*-butyl methacrylate and 1H,1H-perfluorooctyl methacrylate.¹⁸⁷

¹⁸⁵R.D. Allen and G.M. Wallraff, "Herpes simplex virus type 2 glycoprotein G proteins and polypeptides," U.S. Patent No. 5,665,537 (1997).

¹⁸⁶N. Sundarajan, S. Yang, K. Ogino, S. Valiyaveetil, J. Wang, X. Zhou, C.K. Ober, S.K. Obendorf, and R.D. Allen, "Supercritical CO₂ processing for submicron imaging of fluoropolymers," *Chem. Mater.* **12**, 41 (2000).

¹⁸⁷J.M. Havard, N. Vladimirov, J.M.J. Frechet, S. Yamada, G. Willson, and J.D. Byers, "Photoresists with reduced environmental impact: Water soluble resists based on photo cross linking of a sugar containing polymethacrylate," *Macromolecules* **32**, 86 (1999).

While the above-named resist compositions are spin-coated from an organic solvent and developed in SC CO₂, a new resist composition whose resins are synthesized in SC CO₂ (Scheme 6.30) are able to be both spin-coated and developed in SC CO₂ has recently been reported.¹⁸⁸ The copolymer resins are made by radical polymerization of TBMA and 1H,1H-perfluorooctyl methacrylate



Scheme 6.30 All-supercritical-CO₂-processable (polymerization, casting, and development) negative-tone resist.

¹⁸⁸J.M. DeSimone, Z. Guan, and C.S. Elsbernd, "Synthesis of fluoropolymers in supercritical carbon dioxide," *Science* **257**, 945 (1992); C.L. McAdams, D. Flowers, E.N. Hoggan, R.G. Carbonell, and J.M. DeSimone, "All CO₂ processed 157 nm fluoropolymer containing photoresist systems," *Proc. SPIE* **4345**, 327 (2001).

with AIBN initiator in SC CO₂. Dissolving the resins with SC CO₂-soluble PAG and casting a film from the resulting solution (also from SC CO₂), exposing the film to 193 nm radiation, and developing in SC CO₂ affords negative tone images.¹⁸⁹

It must be mentioned that SC CO₂ has been touted as the solvent of choice for potentially replacing a few, if not all, wet processes in the semiconductor lithography clean room of the future because of a number of inherent advantageous attributes. It is nonhazardous and inexpensive. It has high diffusivity (very comparable to that of a gas), which may aid in rapid effective dissolution. It has no surface tension since its liquid and vapor state are not simultaneously present, which may thus aid in mitigating pattern collapse issues of high aspect ratio features. Its solution properties can be tuned with minor adjustments of temperature and pressure.¹⁹⁰

6.4 General Considerations on the Chemistry of Cross-Linking

It is well known that when a polymer resist undergoes radiation cross-linking, the weight-average molecular weight and the intrinsic viscosity initially increase proportionately with radiation dose, until they increase toward infinitely large values. If radiation dose increases further, a fraction that is insoluble in any solvent grows by the interconnection of the different polymer chains in the exposed area, resulting in network formation. This polymer network is called the gel, and this phenomenon is called gelation; the instant when an incipient gel is created is called the gel point. In the preceding sections, we have presented the chemical mechanisms by which this takes place; here, we concentrate on the physical consequences of the chemical process, following the approach of Reiser.¹⁹¹

A number of theories that attempt to explain the experimental behavior of cross-linked polymers have been proposed, and some of these are briefly reviewed here. A statistical theory of cross-linking was first proposed by Flory in 1941 and expounded on in 1942;¹⁹² in it, he showed that polymers of uniform molecules change the shape of molecular size distribution due to the formation of cross-links, creating an insoluble fraction after a certain number of cross-links has been formed. Stockmayer¹⁹³ proposed a theory dealing with the change in

¹⁸⁹H. Ito, "Chemical amplification resists for microlithography," *Adv. Polym. Sci.* **172**, 173 (2005).
¹⁹⁰ibid.

¹⁹¹A. Reiser, *Photoactive Polymers: The Science and Technology of Resists*, pp. 46–51, John Wiley & Sons, Hoboken, NJ (1989).

¹⁹²P.J. Flory, *J. Am. Chem. Soc.* **63**, "Molecular size distribution in three dimensional polymers. I. Gelation," 3083, "Molecular size distribution in three dimensional polymers. II. Trifunctional branch ing units," 3091, "Molecular size distribution in three dimensional polymers. III. Tetrafunctional branching units," 3096 (1941); *J. Phys. Chem.* **46**, 132 (1942).

¹⁹³W.H. Stockmayer, "Theory of molecular size distribution and gel formation in branched chain polymers," *J. Chem. Phys.* **11**, 45 (1943); "Theory of molecular size distribution and gel formation in branched polymers II. General cross linking," **12**, 125 (1944).

molecular size distribution due to cross-linking of polymers that have an initial arbitrary distribution of molecular sizes. Charlesby¹⁹⁴ proposed a solution, based on probability theory, to the problem of cross-linked polymers that have an initial arbitrary molecular size distribution. Although Charlesby's theory is preferable to those of Flory and Stockmayer in the ease of calculation, it is not successful in solving the problem of cross-linking as a whole. Saito¹⁹⁵ proposed a basic equation that governs the change in molecular size distribution of polymers due to cross-linking and from which many properties of cross-linked polymers are derived. Today, based on the research of the investigators mentioned above, along with many others, there is a universal agreement that the fundamental effect of cross-links on polymers is to change the molecular size distribution.¹⁹⁶

So how does cross-linking occur? According to Reiser,¹⁹⁷ cross-links are formed at the sites of individual chromophores. During the early stages of the process, their main effect is only to increase the average molecular weight of the polymer, resulting in a dramatic effect on the molecular weight distribution in the system. Given that all chromophores (polymer repeat units) have a priori the same probability of excitation, in a polydisperse system, large molecules are more likely to react than smaller ones. As a result, the largest molecule in the ensemble rapidly cross-links with other nearby molecules, forming a many-branched supermolecule that permeates the entire irradiated area. This produces a continuous three-dimensional network that the solvent may penetrate, but that it can no longer dissolve. This insoluble residue or gel in a solid matrix constitutes the image in negative-tone resist imaging. Image formation in cross-linking resists is thus identified as a process of photoinduced gelation.¹⁹⁸

It is important to note that at the gel point only an infinitesimally small fraction of the material is part of the network. As cross-linking continues, more and more of the original polymer chain molecules become linked to the network, and the weight

¹⁹⁴A. Charlesby, "Solubility and molecular size distribution of crosslinked polystyrene," *J. Polym. Sci.* **11**, 513 (1953); "The cross linking and degradation of paraffin chains by high energy radiation," *Proc. R. Soc.* **A222**, 60, "Gel formation and molecular weight distribution in long chain polymers," *Proc. R. Soc.* **A222**, 542; "Molecular weight changes in the degradation of long chain polymers," **A224**, 120 (1954).

¹⁹⁵O. Saito, *J. Phys. Soc. Jpn.* **13**, "On the effect of high energy radiation to polymers I. Cross linking and degradation," 198, "Effects of high energy radiation on polymers II. End linking and gel fraction," 1451, "Effects of high energy radiation on polymers III. Viscosity," 1465 (1958).

¹⁹⁶Many excellent reviews on cross linking in polymers have been written. See, for example, *The Radiation Chemistry of Macromolecules*, Vols. I and II, M. Dole, Ed., Academic Press, New York (1972); A. Reiser, *Photoactive Polymers: The Science and Technology of Resists*, pp. 46–51, John Wiley & Sons, Hoboken, NJ (1989).

¹⁹⁷A. Reiser, *Photoactive Polymers: The Science and Technology of Resists*, pp. 46–51, John Wiley & Sons, Hoboken, NJ (1989).

¹⁹⁸*ibid.*, p. 47.

fraction of the gel gradually increases.¹⁹⁹ Plotting the gel fraction against the exposure (radiation dose) that caused it generates the gel curve of the photopolymers (see Fig. 6.5).²⁰⁰

The progress of the cross-linking process is expressed by the weight fraction of the gel (see Fig. 6.5). The gel point marks the minimum exposure dose required for incipient image formation.²⁰¹

A relation between gel point exposure E_G and the molecular properties of the photopolymer can be derived from gelation theory²⁰² (see Fig. 6.6) using the following arguments. For a unit area of a resist film of thickness r , specific gravity d , and molecular weight of the monomer unit M_0 , the number of moles of photoreactive groups in unit area of the film is given by rd/M_0 . If in the irradiation process a fraction ρ of the available groups becomes cross-linked, the

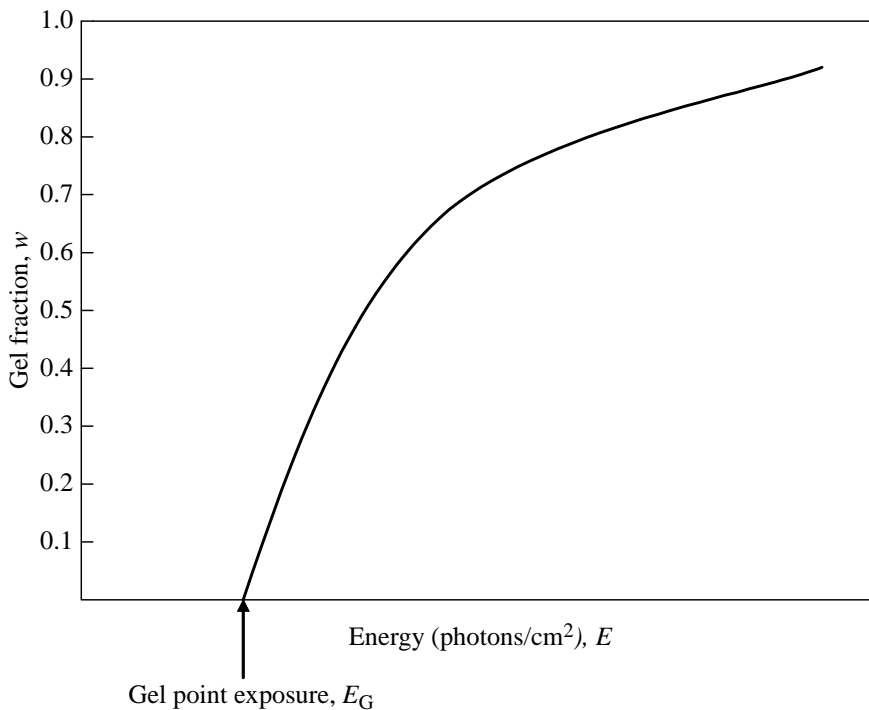


Figure 6.5 Generic resist gel curve, showing the gel point exposure, E_G .

¹⁹⁹ibid.

²⁰⁰ibid.

²⁰¹A. Reiser, "The physical chemistry of crosslinking photopolymers," *J. Chimie Physique Physico Chimie Biologique*, **77**(6), 469 (1980).

²⁰²A. Reiser and E. Pitts, "Characteristic curve of crosslinking photoresists," *Photogr. Sci. Eng.* **20**, 225 (1976); J. Finter, Z. Haniotis, K. Meier, and H. Zweifel, "A numerical method for calculation of gel point exposure energies from experimental gel curves: Photo cross linking of unsensitized poly[vinyl 3 (3,4 dihydro 1,2 naphthalene dicarboxylic acid imidyl) proprionate]," *J. Imaging Sci.* **30**, 259 (1986).

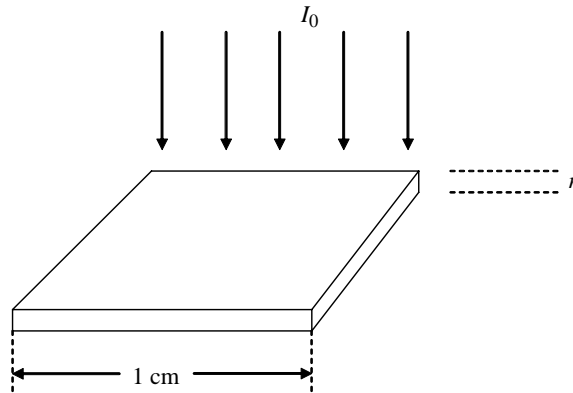


Figure 6.6 Unit area of a resist film of thickness r exposed to a photon flux I_0 .

number of cross-linked groups in a unit area is therefore given by $rd\rho/M_0$. Furthermore, if during irradiation a fraction A of the incident photons is absorbed, the photochemical balance equation can be expressed as

$$EA = \frac{rd\rho}{M_0\Phi}, \quad (6.1)$$

where E is the incident radiation dose in einsteins per square centimeter, A is the fraction of the incident energy that is absorbed, and Φ is the quantum yield of cross-link formation (defined as the number of groups or chromophores taking part in the intermolecular cross-links for each photon absorbed in the film²⁰³).

Equation (6.1) relates the cross-link density ρ to the exposure energy at any point in the cross-linking process. At the gel point, the cross-link density is such that on the average every macromolecule carries one cross-link, as expressed by Stockmayer's rule

$$\rho = \frac{M_0}{M_w}, \quad (6.2)$$

where M_w is the weight-average molecular weight of the polymer.

For the case where the incident radiation dose is very small, $D \ll 1$, the absorbed fraction of the radiation A can be approximated as

$$A = 1 - 10^{-D} \approx 2.303D = 2.303\epsilon mr. \quad (6.3)$$

The minimum exposure dose that takes the photopolymer to the gel point is obtained by combining Eqs. (6.1) and (6.2) and substituting the expression for A from Eq. (6.3) as

$$E_G = \frac{rd}{AM_w\Phi} \cong \frac{d}{2.303\epsilon m M_w \Phi}, \quad (6.4)$$

²⁰³The only cross links that contribute to network formation and thus to the polymer gel are intermolecular ones. Intramolecular links between two groups on the same chain do not contribute to network formation.

where ϵ is the molar extinction coefficient of the chromophore, m is the molarity of the chromophore in the solid film, and M_w is the weight-average molecular weight.

Equation (6.4) is the fundamental equation of cross-linking resists, for it relates the imaging characteristic, namely, the gel dose E_G , to molecular properties of the polymer. It expresses the fact that the resist sensitivity is proportional to the quantum yield of the cross-linking reaction, to the weight-average molecular weight M_w of the polymer, and to the radiation-gathering power ϵm of the chromophore.²⁰⁴

6.5 Negative Resists Arising from Polymerization of Monomers in the Presence of Polyfunctional Components

As described above, in cross-linking resists, radiation-induced changes in solubility are brought about by the formation of a three-dimensional network from an ensemble of linear polymeric chains. A similar result can be achieved by radiation-induced polymerization of monomers in the presence of polyfunctional components. Such results have found application in the field of lithographic imaging, especially with the aid of image amplification based on cross-linking, which results from the immobilization of large molecules by a small number of cross-links. In radiation-induced polymerization processes, the source of amplification is the chain reaction of the polymerization process. Although charged-particle-radiation-induced polymerization has been demonstrated mostly for curing applications, the applications of polymerization-mediated cross-linking in lithographic imaging have been weighted primarily in the direction of photoradiations. For this reason, the discussion in this section is devoted entirely to photoinduced polymerization cross-linking processes used in lithographic imaging applications. Reiser has provided an excellent overview of the photochemistry of these processes;²⁰⁵ here, we present only the salient facts that pertain to lithographic applications.

The earliest reports on the use of photoinitiated polymerization for the purpose of imaging were by Eggert et al.²⁰⁶ in 1938, Morton²⁰⁷ in 1949, and Oster²⁰⁸ in 1957. Plambeck²⁰⁹ invented the photopolymer printing plate probably sometime

²⁰⁴A. Reiser, *Photoactive Polymers: The Science and Technology of Resists*, pp. 49–50, John Wiley & Sons, Hoboken, NJ (1989).

²⁰⁵A. Reiser, *Photoactive Polymers: The Science and Technology of Resists*, Chapter 4, John Wiley & Sons, Hoboken, NJ (1989).

²⁰⁶J. Eggert et al., "Engraving roller for the manufacture of lenticular film," U.S. Patent No. 2,115,198 (1938).

²⁰⁷T.H. Morton, "The practical assessment of the light fastness of dyeings," *J. Soc. Dyers Colour* **65**, 597 (1949).

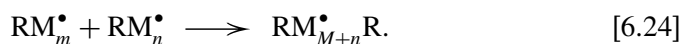
²⁰⁸G.K. Oster, G. Oster, and G. Prati, "Dye sensitized photopolymerization of acrylamide," *J. Am. Chem. Soc.* **79**, 595 (1957).

²⁰⁹L. Plambeck, Jr., "Photographic preparation of relief images," U.S. Patent No. 2,760,863 (1956).

in the early 1950s, but was granted the patent in 1956; this was followed in rapid succession by the patents of Leekely and Sorenson²¹⁰ in 1956 and by Hoerner and Olsen²¹¹ in 1958. All of the early work and almost all systems currently in use are based on free radical polymerization. Recently, cationic ring-opening polymerization has been developed to the point where it offers some distinct advantages.²¹²

6.6 General Considerations on the Chemistry of Photoinitiated Radical Polymerization Employed in Negative Resist Systems

Following the approach of Reiser, we present an overview of the photochemistry of photopolymerization.²¹³ In general, photoinitiated radical polymerization can be described by the following reaction sequence, where I stands for the initiator, and M for the monomer:²¹⁴



The first step in the sequence is the photogeneration of free radicals R_1^\bullet and R_2^\bullet (Reaction [6.20]). This is then followed by the interaction of the radicals with the monomer and the starting of the chain reaction, Reaction [6.21]. Reactions [6.20] and [6.21] together constitute the initiation process, while Reactions [6.22] and [6.23] represent the propagation of the radical function in the monomer, in other words, the growth of the polymer chain. Reaction [6.24] represents the many

²¹⁰R.M. Leekley, R.L. Sorensoen, "Verfahren zur herstellung lichtempfindlicher platten und aus ihnen druckplatten," German Patent No. 954,127 (1956).

²¹¹H. Hoerner and B. Olsen, "Plaques homogenes et polyamides en procede pour leur fabrication," Belgian Patent No. 575,159 (1958).

²¹²A. Reiser, *Photoactive Polymers: The Science and Technology of Resists*, p. 102, John Wiley & Sons, Hoboken, NJ (1989).

²¹³ibid., Chapter 4.

²¹⁴ibid., p. 46.

possible termination steps that end the reaction and set a limit to chain growth. We will now examine each of these steps.

6.6.1 Photogeneration of radicals

Photoinitiation is the first step in the formation of free radicals from photoinitiators (molecules capable of forming radicals on irradiation). Most photoinitiators in use today are based on one of two mechanisms, namely, photofragmentation and photoinduced hydrogen abstraction.²¹⁵

In photofragmentation, radicals are formed by the breaking of a covalent bond in the initiator I as



In photoinduced hydrogen abstraction, the excited initiator I^* reacts with a hydrogen donor (co-initiator) to produce free radicals as



6.6.1.1 Initiators based on photofragmentation

The main classes of initiators based on photofragmentation (scission of covalent bonds) are limited to UV applications, and they include peroxides, azo compounds, benzoin derivatives, acetophenone derivatives, ketoxime esters of benzoin, triazines, etc. On photolysis, these classes of initiators, depending on their wavelength of sensitivity, are able to initiate the polymerization of monomers such as methyl methacrylate in negative-tone lithographic imaging.

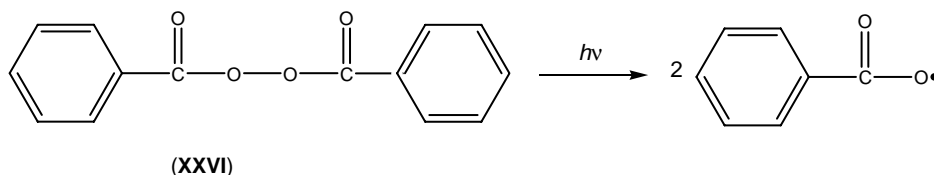
6.6.1.1.1 Peroxides

A good example of peroxides is benzoyl peroxide (BPO) (**XXVI**), which on excitation fragments into two benzoyl radicals (Scheme 6.31).²¹⁶ The excitation energy of this radical is roughly 100 kcal/mole, much higher than the energy of the —O—O— bond (30 kcal/mole). The radical has poor thermal stability, does not absorb well below 300 nm, and it is also not very reactive²¹⁷ and therefore not very effective in initiating polymerizations of interest in lithography.

²¹⁵ibid.

²¹⁶P.K. Sengupta and J.C. Bevington, "Photo dissociation of benzoyl peroxide," *Polymer* **14**, 527 (1973).

²¹⁷A. Reiser, *Photoactive Polymers: The Science and Technology of Resists*, p. 107, John Wiley & Sons, Hoboken, NJ (1989).



Scheme 6.31 Photodecomposition of benzoyl peroxide.

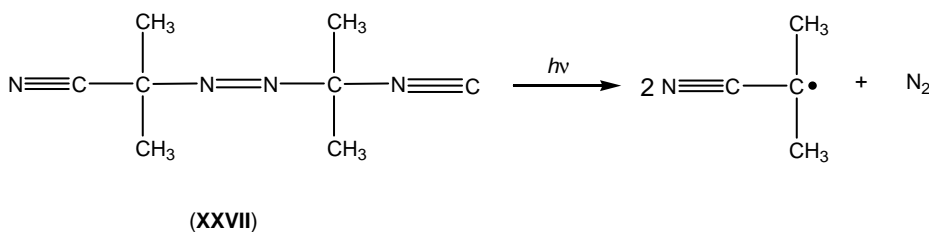
6.6.1.1.2 Azo compounds

The compound 2,2'-azobis(isobutyronitrile) (AIBN) (XXVII) is a good example of an azo compound that on absorption of light can fragment to yield a 2-cyanoisopropyl radical (Scheme 6.32). This is a much more reactive radical than the benzoyl radical and therefore is more effective in initiating polymerization than the latter. In addition, the fragmentation yield of AIBN is high because a molecule of nitrogen is eliminated in the photolytic process, and the two active radicals are formed at a distance of 3Å from each other, which increases their chances of escape from the primary cage.²¹⁸ This radical is not thermally stable, hence its popularity as a thermal initiator. Its main disadvantages include the fact that it absorbs only below 300 nm, which limits its wavelength range to imaging applications below 300 nm.²¹⁹

6.6.1.1.2.1 BENZOIN DERIVATIVES

Benzoin and its alkyl ether derivatives are known to undergo photoinitiated cleavage of the C—C bond adjacent to the carbonyl group, leading to the simultaneous formation of benzoyl radical and alkoxybenzyl radical (Scheme 6.33).

Photoscission is particularly efficient in the alkyl ethers of benzoin, and these are among the most widely used photoinitiators in the UV curing industry. The benzoyl alkyl ethers absorb between 330 and 350 nm.²²⁰ Both the benzoyl

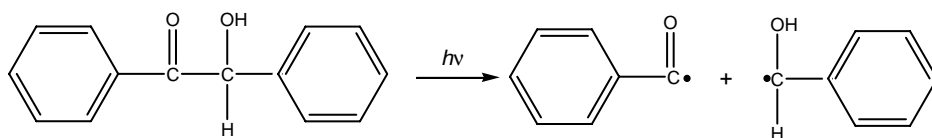


Scheme 6.32 Photodecomposition of AIBN.

²¹⁸ibid., p. 108.

²¹⁹ibid., pp. 107–108.

²²⁰ibid., p. 108.



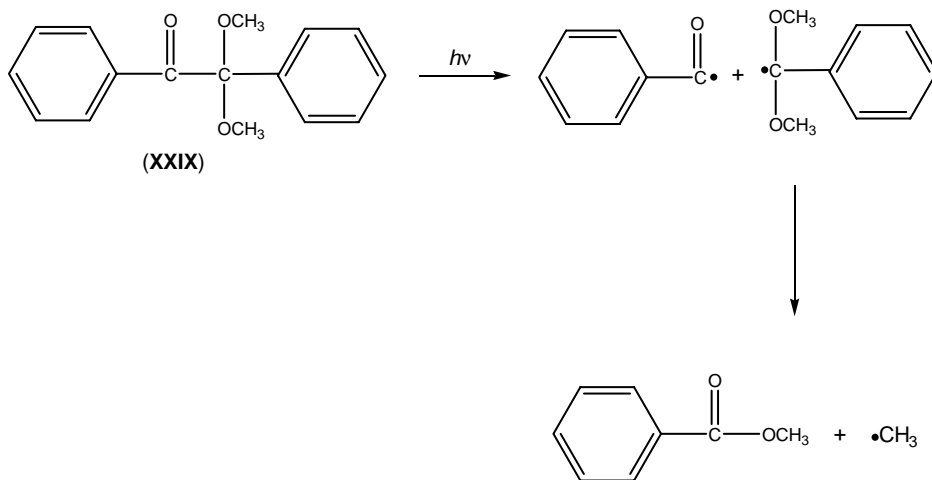
(XXVIII)

Scheme 6.33 Photodecomposition of benzoin.

radical and the alkoxybenzyl radicals take part in the initiation process.²²¹ It should be mentioned that generic benzoin ethers suffer from poor shelf life, which is linked to the presence of a labile hydrogen on the ether carbon.²²² The substitution of this labile hydrogen with benzyl ketals, such as 2,2'-dimethoxy-2-phenylacetophenone (DMPA) (XXIX) eliminates this problem (Scheme 6.34).²²³

6.6.1.1.2.2 ACETOPHENONE DERIVATIVES

The search for molecules that can absorb at 365 nm (the principal emission of the Hg arc in the UV) and that dissociate on excitation started with acetophenone.

**Scheme 6.34** Photodecomposition of DMPA.

²²¹S. Pappas and R.A. Asmus, "Photoinitiated polymerization of methyl methacrylate with benzoin methyl ether. III. Independent photogeneration of the ether radical," *J. Polym. Sci., Polym. Chem. Ed.* **20**, 2643 (1982).

²²²A. Reiser, *Photoactive Polymers: The Science and Technology of Resists*, p. 108, John Wiley & Sons, Hoboken, NJ (1989).

²²³ibid.

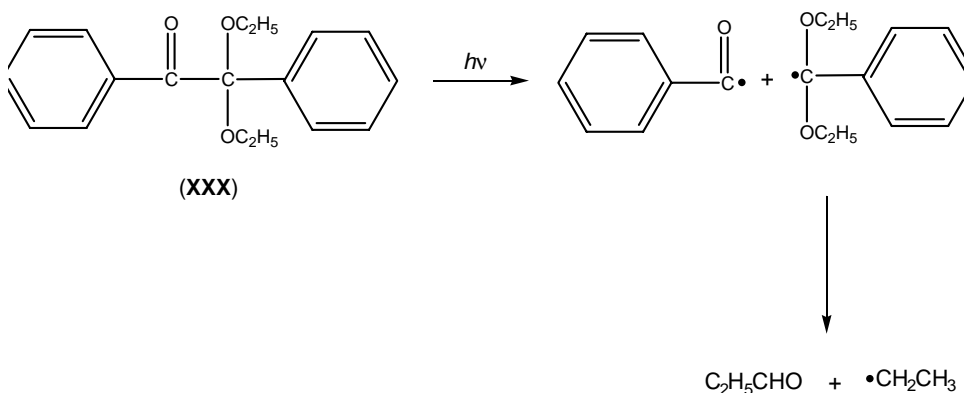
Many acetophenone derivatives have since been proposed, such as 2,2-diethoxyacetophenone (DEAP) (**XXX**), which fragments as in Scheme 6.35.²²⁴

Other acetophenone derivatives that have been proposed include 1-benzocyclohexanol, 4-methylmercapto- α,α -dimethyl-morpholino-acetophenone, which has a much stronger absorption at 365 nm than other benzoin ethers ($\epsilon \sim 10^4$ L/mole \cdot cm) and is therefore suitable as a photoinitiator for highly pigmented coatings.²²⁵

Ketoxime esters of benzoin, exemplified by 1-phenyl-1,2-propanedione-2-*O*-benzoyloxime (PPO) (**XXXI**), on photolysis eliminate two volatile fragments after the primary scission of the N—O bond (Scheme 6.36). The radical yield of PPO decomposition is very high ($\varphi = 0.9$). The phenyl radical, the final product of fragmentation, is an aggressive polymerization initiating species.²²⁶

6.6.1.1.2.3 TRIAZINES

Triazines (**XXXII**) are a class of symmetrical initiators where multiple fragmentations are brought about by a scission, which on excitation dissociate into three substituted nitriles (**XXXIII**) (Scheme 6.37).²²⁷ Specifically, the primary photoproducts are not radicals, but they dissociate into radicals in a secondary thermal step (Scheme 6.38).²²⁸



Scheme 6.35 Photodecomposition of DEAP.

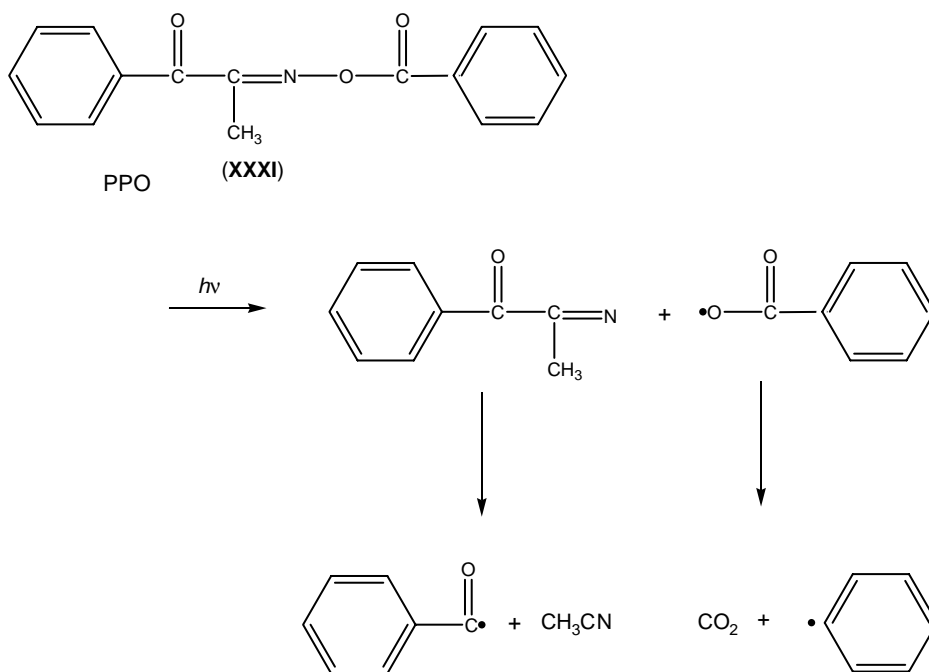
²²⁴C.L. Osborn, "Photoinitiation systems and their role in UV curable coatings and inks," *J. Radiat. Curing*, **3**(3), 2 (1976); M.R. Sander and C.L. Osborn, "Photochemistry of 2,2 dimethoxy 2 phenyla acetophenone triplet detection via 'spin memory,'" *Tetrahedron Lett.* 415 (1974).

²²⁵ibid.

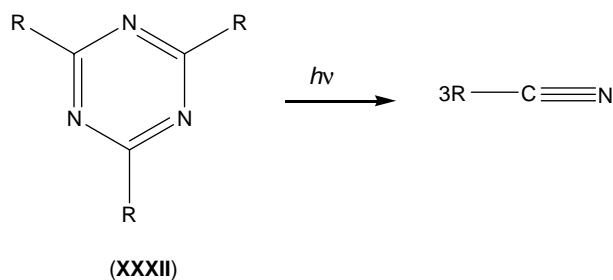
²²⁶A. Reiser, *Photoactive Polymers: The Science and Technology of Resists*, p. 112, John Wiley & Sons, Hoboken, NJ (1989).

²²⁷H. Sakuraji, M. Yoshida, H. Kinoshita, K. Utena, K. Tokumaru, and M. Yoshiro, "Structure reactivity relationships in triplet sensitized photolysis of aromatic ketone O acyloximes," *Tetrahedron Lett.* **20**, 1529 (1978).

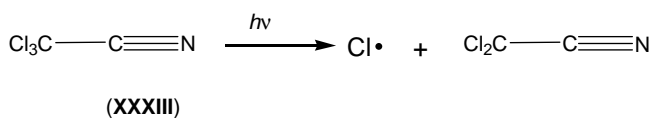
²²⁸A. Reiser, *Photoactive Polymers: The Science and Technology of Resists*, p. 113, John Wiley & Sons, Hoboken, NJ (1989).



Scheme 6.36 Photodecomposition of PPO.



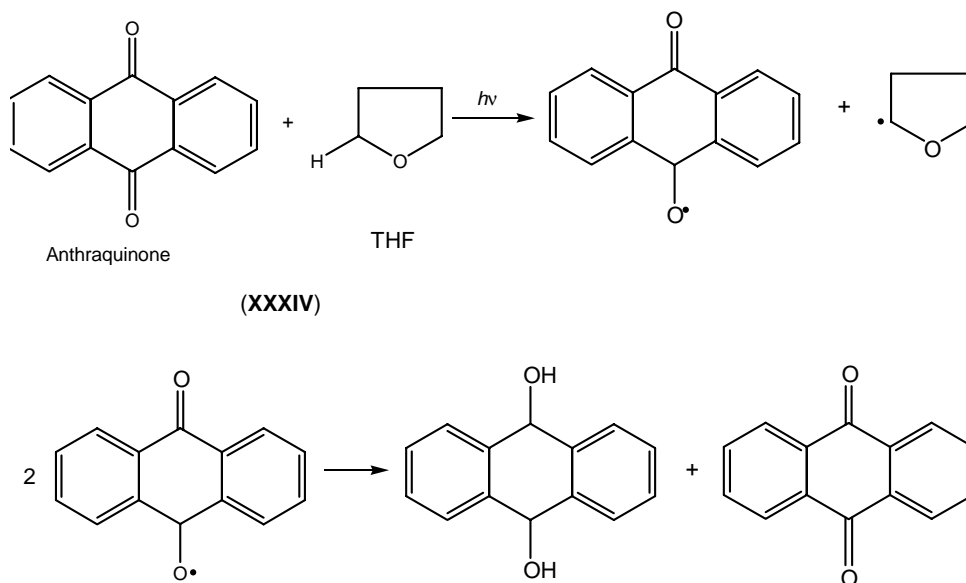
Scheme 6.37 Photodecomposition of triazine.



Scheme 6.38 Photodecomposition of nitriles.

6.6.2 Radicals generated by hydrogen abstraction

Abstraction of hydrogen by the excited state molecules makes possible the generation of radicals from molecules with low excitation energies, which effectively extends photoionization that can initiate photopolymerization of reactive monomers into the visible part of the spectrum. Examples of H-abstraction reactions



Scheme 6.39 Photoinduced abstraction of hydrogen from THF by anthraquinone.

include those by the excited triplet states of ketones such as anthraquinone (XXXIV). Photoirradiation of anthraquinone, for instance, in the hydrogen donor solvent tetrahydrofuran leads to the following processes (Scheme 6.39).²²⁹

In the presence of a reactive monomer, the radicals formed by hydrogen abstraction initiate chain polymerization. However, in the absence of any other reactive species, the radicals can combine to form dimers. The species that absorbs the radiation (anthraquinone) and gets promoted to an excited state is termed the initiator, while the hydrogen donor (THF) is termed the co-initiator. The tetrahydrofuryl radical is the principal initiating species.²³⁰

6.6.2.1 Other practical initiator systems based on hydrogen abstraction

6.6.2.1.1 Benzophenone and tertiary amines

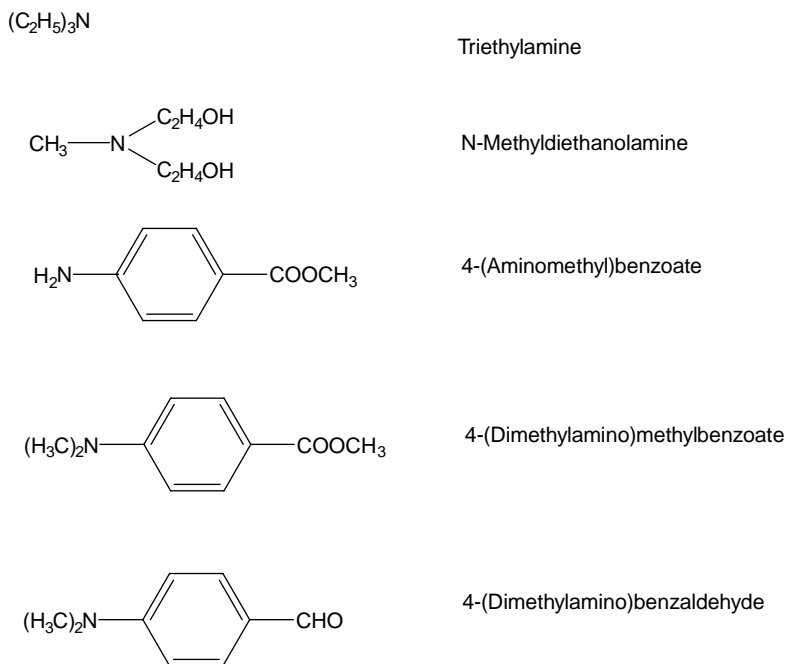
Addition of small amounts of tertiary amines to benzophenone-type initiators was reported by Sander et al.²³¹ to produce dramatic enhancement of initiating efficiency. This effect was determined to be caused not only by the good hydrogen bonding properties of the alkyl groups in the alpha position to nitrogen, but also by

²²⁹ibid., p. 113–114.

²³⁰A. Ledwith, G. Ndaalio, and A.R. Taylor, "Polymerization of methyl methacrylate photoinitiated by anthraquinone and 2-tert-butylanthraquinone," *Macromolecules* **8**, 1 (1975).

²³¹M.R. Sander, C.L. Osborne, and D.J. Trecker, "Benzophenone/triethylamine photoinitiated polymerization of methyl acrylate," *J. Polym. Sci., Part A* **10**, 3173 (1972).

the ability of the amines to act as electron donors to form exciplexes with the triplet excited state of benzophenone and other aromatic ketones.²³² The following amines are now frequently used as co-initiators (XXXV):



Amines used as coinitiators (XXXV)

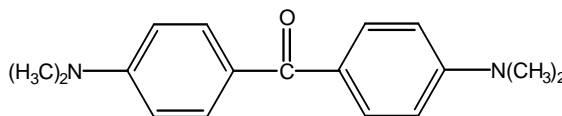
6.6.2.1.2 Michler's ketone

Michler's ketone, also called 4,4'-bis(dimethylamino)benzophenone (XXXVI), is an aromatic ketone as well as a tertiary amine, and is by itself a complete initiating system. It undergoes H abstraction on irradiation and is a useful photoinitiator.²³³ Its absorption at 365 nm is stronger than that of benzophenone. It is often

²³²A. Ledwith, in *The Exciplex*, M. Gordon and W.R. Ware, Eds., p. 209, Academic Press, New York (1975); A. Ledwith, "Photoinitiation of polymerisation," *Pure Appl. Chem.* **49**, 431 (1977); A. Ledwith, J.A. Bosley, and M.D. Purbrick, "Exciplex interactions in photoinitiation of polymerization by fluorenone amine systems," *J. Oil Colour Chem. Assoc.* **61**, 95 (1978).

²³³T.H. Koch and A.H. Jones, "A photochemical exchange reaction of Michler's ketone," *J. Am. Chem. Soc.* **92**, 7503 (1970); D.I. Schuster and M.D. Goldstein, "Photochemistry of ketones in solution. XXXVII. Flash photolysis of Michler's ketone in solution. Rate constants for decay and triplet excimer formation," *J. Am. Chem. Soc.* **95**, 986 (1973); V.D. McGinnis and D.M. Dusek, "Photopolymerization of methyl methacrylate with the use of 4,4' BIS (diethylamion) benzophenone as the photoinitiator," *ACS Polym. Prepr.* **15**(1), 480 (1974).

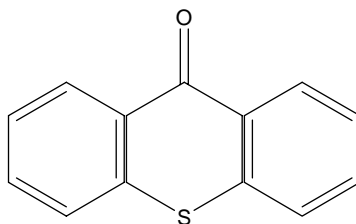
used as a co-initiator together with benzophenone, under which condition it acts as the hydrogen donor.²³⁴



Michler's ketone (XXXVI)

6.6.2.1.3 Thioxanthenes

Thioxanthenes (XXXVII) behave like aromatic ketones,²³⁵ and their lifetimes are relatively long, which makes their H-abstraction process efficient. Popular derivatives of this system include 2-chlorothioxanthone and 2-isopropylthioxanthone. They are typically used in conjunction with various tertiary amines.²³⁶



Thioxanthone (XXXVII)

6.6.2.1.4 3-Ketocoumarins

Originally developed as triplet sensitizers,²³⁷ ketocoumarins (XXXVIII) are equally useful as initiators and function here by abstracting hydrogen from suitable donors. Fine-tuning the absorption spectrum (and the triplet level) of this initiator is accomplished through varying the substituents R_1 , R_2 , and R_3 .²³⁸

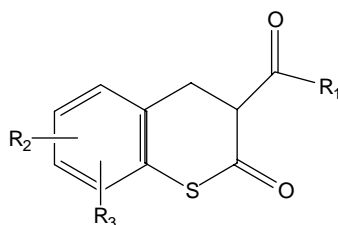
²³⁴A. Reiser, *Photoactive Polymers: The Science and Technology of Resists*, p. 117, John Wiley & Sons, Hoboken, NJ (1989).

²³⁵M.J. Davis, J. Doherty, A.A. Godfrey, P.N. Green, J.R.A. Yung, and M.A. Parrish, "The UV curing behavior of some photoinitiators and photoactivators," *J. Oil Colour Chem. Assoc.* **11**, 256 (1978).

²³⁶A. Reiser, *Photoactive Polymers: The Science and Technology of Resists*, p. 117, John Wiley & Sons, Hoboken, NJ (1989).

²³⁷D.P. Specht, C.G. Houle, and S.Y. Farid, "Photopolymerizable compositions featuring novel co initiators," U.S. Patent No. 4,289,844 (1981).

²³⁸A. Reiser, *Photoactive Polymers: The Science and Technology of Resists*, p. 118, John Wiley & Sons, Hoboken, NJ (1989).

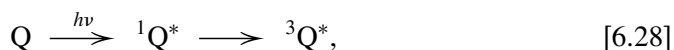


(XXXVIII)

6.6.3 Dye-sensitized initiation

The use of dye-sensitized initiation in polymerization dates to 1949 when Bamford and Dewar²³⁹ observed that some vat dyes could sensitize the photopolymerization of styrene. This was quickly followed up by Gerald Oster's discovery²⁴⁰ in 1954 that the polymerization of acrylonitrile and of acrylamide could be photoinitiated by fluorescein, rose bengal, and similar dyes, in the presence of reducing agents (such as phenylhydrazine, ascorbic acid) and oxygen. Remarkably, the amount of dye required for the photoinitiation event was extremely small ($\sim 0.1\%$ of the weight of monomer), and the quantum yield of monomer consumption was in excess of 4000 monomer units per photon.²⁴¹

Illustrated in the following reaction sequence is a description of the mechanism of dye-sensitized photoinitiation. Here, Q stands for the dye (a quinonoid structure) and HD represents the hydrogen or electron donor:



The donor radical D^\bullet represents the initiating species. Although the semiquinone radical HD^\bullet is usually not reactive enough to act as initiator, it may however disproportionate to generate Q and form the fully reduced hydroquinone H_2Q ,



The quinone can also be regenerated by the reaction of the semiquinone or the hydroquinone with atmospheric oxygen²⁴² as



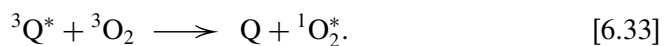
²³⁹C.H. Bamford and M.J.S. Dewar, "Photosensitization by vat dyes," *Nature* **163**, 214 (1949).

²⁴⁰G. Oster, "Dye sensitized photopolymerization," *Nature* **173**, 300 (1954).

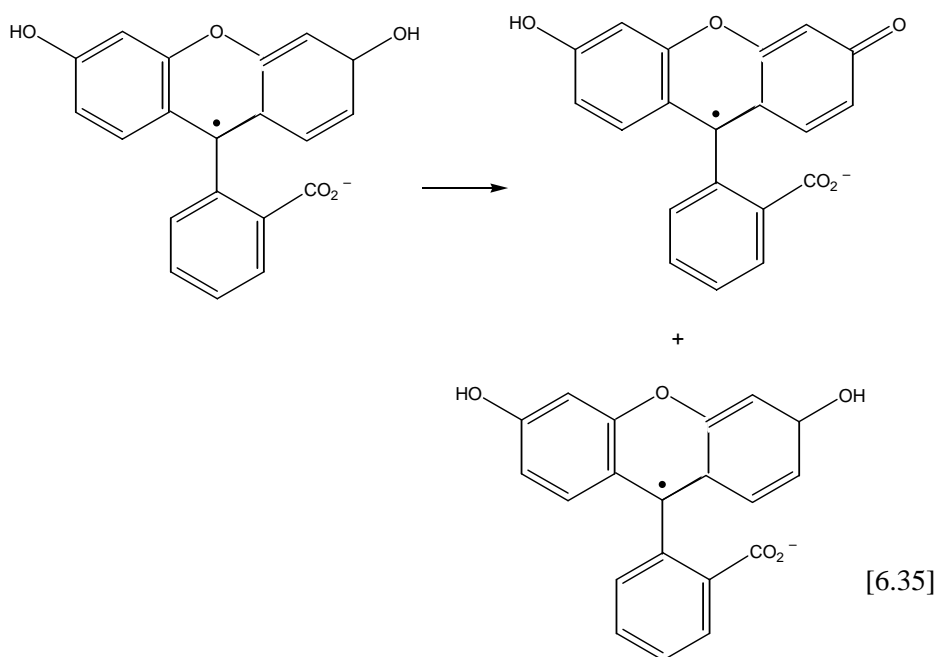
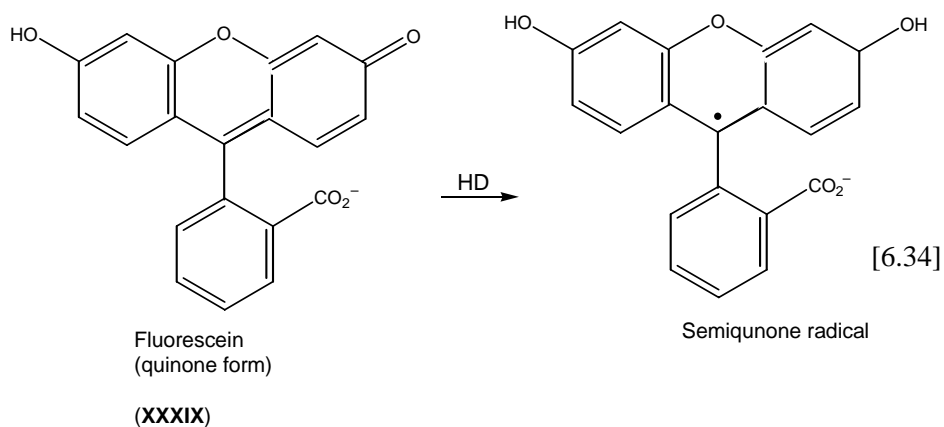
²⁴¹A. Reiser, *Photoactive Polymers: The Science and Technology of Resists*, p. 118, John Wiley & Sons, Hoboken, NJ (1989).

²⁴²R.S. Davidon and K.R. Tretheway, "The mechanism of the dye sensitised photo oxygenation of amines," *J. Chem. Soc., Commun.*, p. 674 (1975).

And finally, oxygen may react with the triplet state of the dye to produce singlet oxygen in a parallel process as



For fluorescein (**XXXIX**), in a medium pH ≈ 7 , Reactions [6.29] and [6.30] take the form shown in Reactions [6.34] and [6.35]:²⁴³



²⁴³ibid., p. 120.

Quite a number of the classes of photoreducible dyes have been identified.²⁴⁴ These include the xanthenes (fluorescein, rose bengal), the thiazines (methylene blue, thionine), the acridinium dyes (acriflavin), and some natural products, such as riboflavin.²⁴⁵

In addition, a wide range of electron and hydrogen donors have been discovered to work in these systems.²⁴⁶ A comprehensive list of these compounds has been compiled.²⁴⁷ In particular, tertiary amines are the most important of these donors²⁴⁸ since they transfer an electron from the lone pair of nitrogen to the acceptor, in a step that is followed immediately by the dissociation of a proton from the acidic α C—H bond to yield a resonance-stabilized radical.²⁴⁹

Other types of donors include arylsulfonates (such as ArSO_2NA),²⁵⁰ ethers such as isobenzofurane, and even suitably substituted aromatic hydrocarbons,²⁵¹ enolates of diketones such as dimedone,²⁵² carboxylates (ascorbic acid),²⁵³ and finally organometallics such as benzyltrimethylstannane, $\text{PhCH}_2\text{Sn}(\text{CH}_3)_3$.²⁵⁴

Typical lithographic applications of dye-sensitized photopolymerization today include direct laser imaging of printed wiring boards, based on a visible laser-sensitive resist (Riston LV[®]) developed by Dupont.²⁵⁵

²⁴⁴D.F. Eaton, "Dye sensitized Photopolymerization," in *Adv. Photochem.* **13**, 427 (1986); D.F. Eaton, "Electron transfer induced photofragmentation as a route to free radicals," *Pure Appl. Chem.* **56**, 1191 (1984).

²⁴⁵A. Reiser, *Photoactive Polymers: The Science and Technology of Resists*, p. 120, John Wiley & Sons, Hoboken, NJ (1989).

²⁴⁶G.A. Delzenne, H.K. Peeters, and U.L. Laridon, in *Non Silver Photographic Process*, R.J. Cox, Ed., p. 23, Academic Press, New York (1975); W.J. Tomlinson and E.A. Chandross, *Adv. Photochem.* **12**, 201 (1980).

²⁴⁷ibid.

²⁴⁸R.H. Kayser and R.H. Young, "The photoreduction of methylene blue by amines II. An investigation of the decay of semireduced methylene blue," *Photochem. Photobiol.* **24**, 39, 403 (1976).

²⁴⁹A. Reiser, *Photoactive Polymers: The Science and Technology of Resists*, p. 121, John Wiley & Sons, Hoboken, NJ (1989).

²⁵⁰U.L. Laridon, G.A. Delzenne, and H.K. Peeters, "Photopolymerisation of ethylenically unsaturated organic compounds," U.S. Patent No. 3,847,610 (1974).

²⁵¹U. Steiner, G. Winter, and H.E.A. Kramer, "Investigation of physical triplet quenching by electron donors," *J. Phys. Chem.* **81**, 1104 (1977).

²⁵²R.J. Allen and S. Chaberek, "Stirrer," U.S. Patent No. 3,488,769 (1970).

²⁵³G. Delzenne, S. Toppet, and G. Smets, "Photopolymerization of acrylamide. I. Formation of the initiating redox system," *J. Polym. Sci.* **48**, 347 (1960).

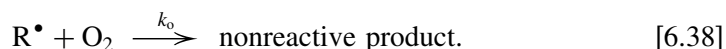
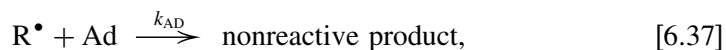
²⁵⁴D.F. Eaton, "Dye sensitized photopolymerization: Activation by trialkylbenzylstannanes," *Photogr. Sci. Eng.* **23**, 150 (1979).

²⁵⁵A. Reiser, *Photoactive Polymers: The Science and Technology of Resists*, p. 123, John Wiley & Sons, Hoboken (1989).

6.6.4 The initiation step

Once the radicals have been generated, the next step is for them to initiate polymerization. Some of them will be successful in this regard, while others will not. If the fraction of radicals that succeed in initiating polymerization is given by f_i , the quantum yield for each initiation reaction ϕ_i quantum yield of the chain initiation is given by $\phi_j = \phi_i f_i$.

The initiation step competes with the quenching (scavenging) of primary radicals by various additives (Ad) (such as stabilizers and antioxidants) and by oxygen, as



Thus, f_i can be expressed in the general form

$$f_i = \frac{k_r[\text{M}]}{k_r[\text{M}] + k_{\text{Ad}}[\text{Ad}] + k_o[\text{O}_2]}. \quad (6.5)$$

The reaction involving oxygen is the most important one, and in the presence of oxygen, the $k_o[\text{O}_2]$ term in the denominator of Eq. (6.5) is by far the largest term, suggesting that under these circumstances f_i tends to zero, resulting in the initiation process being completely inhibited. This, in fact, is the origin of the induction period that is often observed in polymerization processes.²⁵⁶

Oxygen readily reacts with most initiating radicals by forming peroxy radicals that do not effectively initiate polymerization, so much so that in the early stages of irradiation this reaction channel removes the photogenerated primary radicals:



It is only when most of the oxygen has been consumed that the primary radicals become available for initiation.²⁵⁷

Given that the rate of generation of primary radicals, at a given light flux, is a function of the concentration of photoinitiator, the induction period depends also on initiator concentration.²⁵⁸ In order to eliminate this induction period of polymerization in industrial scale applications, many photocuring processes are carried

²⁵⁶ibid., p. 127.

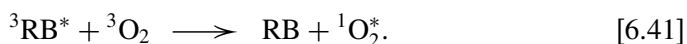
²⁵⁷ibid.

²⁵⁸R.D. Small, J.A. Ors, and B.S.H. Royce, "Photopolymer dielectrics: The characterization of curing behavior for modified acrylate systems," *ACS Symp. Ser.* **242**, 325 (1984).

out under a nitrogen or carbon dioxide atmosphere, or in films that are either protected from oxygen by an impermeable coversheet, or are exposed in a vacuum frame.²⁵⁹

Other approaches that are employed for removing oxygen from the system include chemical means, the most popular being the reaction with (tertiary) amines, which are often used as hydrogen donors in initiation and do form radicals that react with oxygen, and are thereby transformed into peroxy radicals.²⁶⁰

Another interesting way of removing oxygen was described by Decker²⁶¹ and involves the use of sensitizing dyes, such as rose bengal (RB), which transforms oxygen into singlet oxygen that can then be scavenged, for example, by diphenylbenzofuran,



6.6.5 Propagation versus termination and the kinetic chain length

6.6.5.1 The steady state approximation

As Reiser²⁶² describes it, once a radical chain is initiated, it propagates spontaneously until it is terminated by an encounter with another radical, by disproportionation, or in some other way. The average chain length, which ultimately determines the photosensitivity of the system, according to Reiser, is linked to the kinetic rate constants of the individual processes. Furthermore, the rate of initiation (i), propagation (p), and termination (t) can be fairly well described by the following equations:²⁶³

$$R_i = 2f_i\phi_i I_a = 2\phi_j I_a, \quad (6.6)$$

$$R_p = k_p[M][M^*], \quad (6.7)$$

$$R_t = 2k_t[M^*]^2, \quad (6.8)$$

²⁵⁹A. Reiser, *Photoactive Polymers: The Science and Technology of Resists*, p. 128, John Wiley & Sons, Hoboken, NJ (1989).

²⁶⁰ibid.

²⁶¹C. Decker, "A novel method for consuming oxygen instantaneously in photopolymerizable films," *Makromol. Chem.*, **180**, 2027 (1979).

²⁶²A. Reiser, *Photoactive Polymers: The Science and Technology of Resists*, p. 130, John Wiley & Sons, Hoboken, NJ (1989).

²⁶³M.J. Bowden, "Formation of macromolecules," in *Macromolecules*, F.A. Bovey and F.H. Winslow, Eds., Chapter 2, Academic Press, New York (1979).

where I_a represents the radiation flux absorbed by the initiator, ϕ_j represents the overall initiation efficiency, and k_p and k_t are the rate constants of propagation and termination, respectively. In order to express the rate of propagation and the average chain length in terms of measurable quantities, the radical concentration must be eliminated from Eqs. (6.7) and (6.8). This is readily done for a steady state regime such as the case in the photostationary state, where the rates of initiation and termination are equal. For these conditions, the steady state concentration of M^\bullet can be expressed as

$$[M^\bullet] = \left(\frac{\phi_j I_a}{k_t} \right)^{1/2}. \quad (6.9)$$

The rate of propagation can therefore be expressed in the form

$$R_p = k_p \left(\frac{\phi_j I_a}{k_t} \right)^{1/2} [M], \quad (6.10)$$

and the kinetic chain length, which is determined by the competition between propagation and termination, is expressed as

$$\nu = \frac{R_p}{R_t} = \frac{R_p}{R_i} = \frac{k_p}{2\sqrt{k_t}} (\phi_j I_a)^{1/2} [M]. \quad (6.11)$$

The ratio $k_p/\sqrt{k_t}$, Reiser asserts, defines the characteristic ratio of the monomer system.²⁶⁴ It is not dependent on the model of initiation, and it measures the ability of the monomer to support a radical chain reaction.

It should be mentioned that the above simple analysis does not take into consideration the attenuation of light intensity in the system, the depletion of the initiator, etc. Rather, it assumes that termination occurs only by bimolecular encounters between macroradicals, leading either to recombination or disproportionation. It does also imply that k_p and k_t indeed have constant values. This is particularly true in dilute solutions where the physical properties of the medium do not change appreciably during the reaction. However, in the transition from liquid monomer to highly viscous solution during polymerization, the physical properties of the cured polymer change gradually without any discontinuity. This is different from what happens when an amorphous system goes from its rubbery state to its glassy state. At the glass transition, almost all of the physical properties of the system change abruptly, as do its polymerization kinetics.²⁶⁵

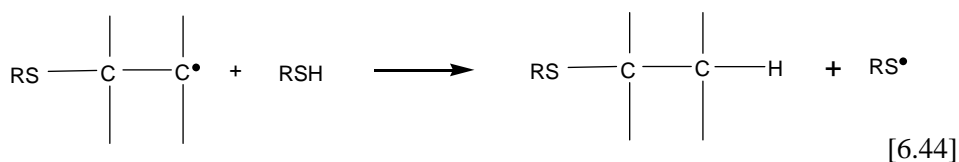
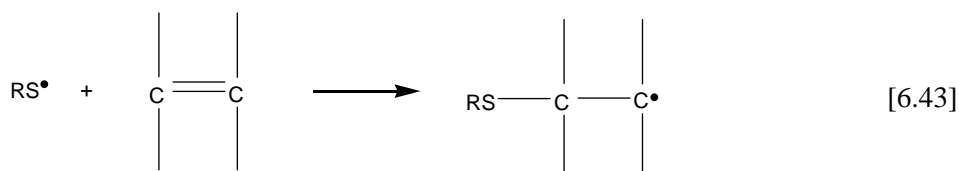
²⁶⁴A. Reiser, *Photoactive Polymers: The Science and Technology of Resists*, p. 130, John Wiley & Sons, Hoboken, NJ (1989).

²⁶⁵*ibid.*, pp. 131, 137–138.

6.7 General Considerations on Photoinitiated Condensation Polymerization

6.7.1 The thiol-ene system

As reported by Reiser,²⁶⁶ a unique system of photoinitiated polymerization is based on thiols (mercaptans) with olefinic double bonds according to the following scheme:



As shown above, this reaction system is a self-propagating chain reaction that can produce linear polymers if carried out with dithiols and with bifunctional olefins. The investigations of Marvel and Nowlin²⁶⁷ have demonstrated that the kinetics of this system follow those of condensation polymerization. Their report suggests that the average degree of polymerization (DP) for this system is not identical to the kinetic chain length of the radical reaction on which it is based, but is governed rather by Carruthers' equation,

$$DP = \frac{2}{2 - xf}, \quad (6.12)$$

where x is the degree of conversion, and f is the average functionality of thiols and olefins in the system. For dithiols and dienes, $f = 2$, which implies that for a conversion of 0.95, for example, the degree of polymerization is 20.²⁶⁸

It has been reported that if the average functionality is > 2 , cross-linking occurs in the system, and the reaction produces insoluble networks at comparatively low

²⁶⁶ibid., pp. 144–149.

²⁶⁷C.S. Marvel and G. Nowlin, "Polyalkylene sulfides. IV. The effect of pH on polymer size," *J. Am. Chem. Soc.* **72**, 5026 (1950).

²⁶⁸A. Reiser, *Photoactive Polymers: The Science and Technology of Resists*, p. 145, John Wiley & Sons, Hoboken, NJ (1989).

conversions.²⁶⁹ Although the linear polymers that can be formed from dithiols and dienes have not found any particular application, the polythiols and polyenes make highly photoreactive compositions, which have found useful applications in UV curing and in the manufacture of polymeric printing plates.²⁷⁰

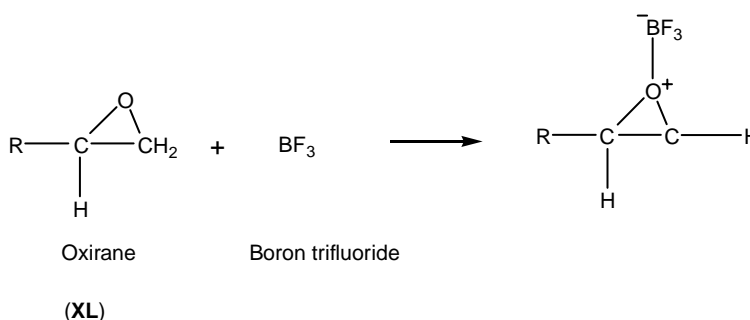
6.8 General Considerations on the Photoinitiated Cationic Polymerization Employed in Negative Resist Systems

Over the years, a number of compounds have been identified to photoinitiate cationic polymerization of monomers designed for radiation curing applications generally, and negative-resist applications specifically. The most prominent of these initiators are onium salts.

6.8.1 Initiation by onium salts

Epoxide monomers readily undergo cationic polymerization²⁷¹ whereby chain propagation is based on the attack of a carbocation on the negatively polarized oxygen of the oxirane (**XL**).²⁷² Chain initiation is either by another cation or by a strong electrophile, such as a Lewis acid (BF_3) or a protonic Brønsted acid. The process is illustrated in the reaction mechanism (Scheme 6.40).²⁷³

6.8.1.1 Initiation



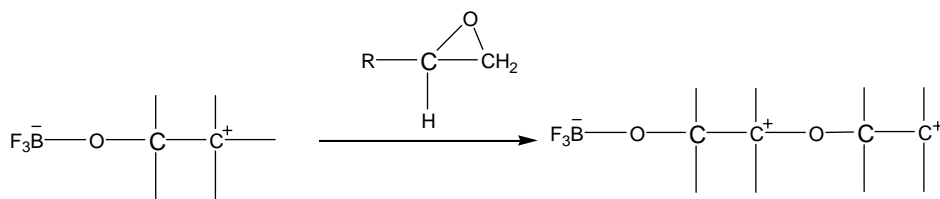
²⁶⁹C.B. Morgan, F. Magnotto, and A.D. Ketley, "Thiol/ene photocurable polymers," *J. Polym. Sci., Polym. Chem. Ed.* **15**, 627 (1977).

²⁷⁰A. Reiser, *Photoactive Polymers: The Science and Technology of Resists*, p. 148, John Wiley & Sons, Hoboken, NJ (1989).

²⁷¹J.V. Crivello, in *UV Curing: Science and Technology*, S.P. Pappas, Ed., pp. 24–75, Technology Marketing Corp., Norwalk, CT (1980).

²⁷²R.W. Lenz, *Organic Chemistry of Synthetic High Polymers*, p. 247, Interscience, New York (1967).

²⁷³A. Reiser, *Photoactive Polymers: The Science and Technology of Resists*, p. 147, John Wiley & Sons, Hoboken, NJ (1989).



Scheme 6.40 Mechanism of cationic polymerization of oxiranes.

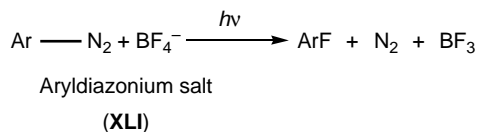
6.8.1.2 Propagation

The propagation step is fast, aided by the coulombic interaction between the carbocation and the negatively polarized ether oxygen, and the strain in the three-membered ring. Termination may occur by the reaction of the carbocation with an adventitious nucleophile (a base, for example) or, very occasionally, with the anion of the initiator.²⁷⁴

Reiser reports²⁷⁵ that in order not to terminate the reaction and hence inhibit propagation, the counter anion must have very low nucleophilicity, since strong nucleophiles or bases will terminate the reaction immediately. Nevertheless, the polymerization can tolerate a small amount of water (1–2%), which is important for the practical usefulness of the system. Oxygen, which acts as a biradical, shows no effect on cationic polymerization—quite an important practical advantage. Characteristically, the epoxy polymers that are the result of the curing process tend to have excellent mechanical properties, including thermal and dimensional stability, nontoxicity, and chemical inertness.

Furthermore, the propagating carbocations do not recombine, thus making possible the synthesis of high-molecular-weight polymers made by ionic polymerization. In purified and dry systems, termination can be eliminated altogether, and living polymers can be obtained.²⁷⁶

For imaging applications, a photochemical means of producing the Lewis or Brønsted acid photoinitiator is required. Aryldiazonium salts (**XLI**) were found to produce Lewis acids on photolysis:



[6.45]

²⁷⁴ibid., p. 148.

²⁷⁵ibid.

²⁷⁶ibid.

The fact that boron trifluoride (BF_3) is a Lewis acid capable of initiating cationic polymerization was not lost on Licari and Crepan,²⁷⁷ who were the first to realize the potential of the classical Schiemann reaction (Scheme 6.40 shown above) in the manufacture of printed circuit boards. It was Fischer²⁷⁸ who introduced aryldiazonium salts into UV curing of epoxy resins.

Almost all of the early initiators absorbed well below 200 nm. It was Schlessinger²⁷⁹ who prepared diazonium salts with an extended spectral range, and with them, was able to polymerize various mono- and bifunctional epoxy monomers, furans, dioxycyclopentadiene, and oxycyclohexene, as well as oligomers and epoxidized novolacs. Dose sensitivities on the order of 15–30 mJ/cm^2 have been demonstrated for some of these systems.²⁸⁰

The practical utility of these diazonium salts is limited by their short pot life; coatings have to be made from freshly mixed solutions. This has led to a search for alternative initiators. Today, diazonium salts have been displaced by iodonium and sulfonium salts, which are crystalline, stable, and colorless compounds that are soluble in common solvents as well as in many cationically polymerizable monomers. Crivello and Lam have prepared quite a large number of onium salts of which the following are but a tiny a selection (see Table 6.2).²⁸¹

Table 6.2 Examples of onium salts used in initiating cationic polymerization of resist resins. (Reprinted with permission from Wiley Inter-Science.²⁸¹)

Cations	Anions
	BF_4^-
	PF_6^-
	AsF_6^-
	SbF_6^-
	SnClF_5^+

R = H, CH_3 , CH_3O , isopropyl, *tert* butyl, Cl, Br

²⁷⁷J.J. Licari and P.C. Crepan, "Electromagnetic radiation polymerization," U.S. Patent No. 3,205,157 (1965).

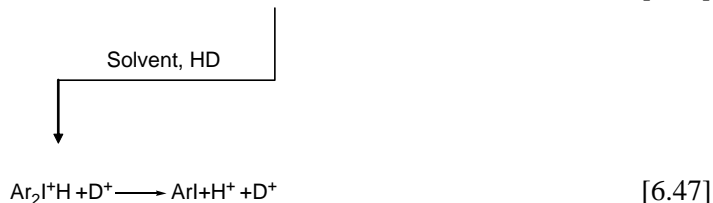
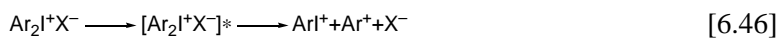
²⁷⁸E. Fischer, "Polymerization of cyclic ethers by diazonium salts of perchloric or perfluorocarboxylic acids," U.S. Patent No. 3,236,784 (1966).

²⁷⁹S.I. Schlessinger, "Photopolymerization of epoxides," *Photogr. Sci. Eng.* **18**, 387 (1974).

²⁸⁰A. Reiser, *Photoactive Polymers: The Science and Technology of Resists*, p. 149, John Wiley & Sons, Hoboken, NJ (1989).

²⁸¹J.V. Crivello and J.H.W. Lam, "New photoinitiators for cationic polymerization," *J. Polym. Sci., Polym. Symp.* **56**, 383 (1976); J.V. Crivello and J.H.W. Lam, "Photoinitiated cationic polymerization by dialkyl phenyl sulfonium salts," *J. Polym. Sci., Polym. Chem. Ed.* **17**, 977 (1979).

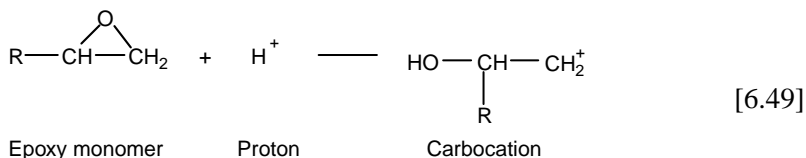
It should be pointed out that the photolysis of the diaryliodonium and triarylsulfonium salts proceeds differently from the photolysis of the diazonium systems. The reaction mechanism of the photolysis of iodonium salts is described by Reactions [6.46] and [6.47].



Triarylsulfonium salts behave in a similar manner as their iodonium salt counterparts (see Reaction [6.48]), as shown by the following facts:



The components do not get incorporated into the polymer during polymerization, and if fluorinated anions are used, no fluorinated aromatics are among the photoproducts, suggesting that the complex anions survive photolysis intact and that no strong Lewis acids are produced.²⁸² Rather, the corresponding Brønsted acids, for example, H^+BF_4^- , H^+PF_6^- , and so on, are generated, and these are the species that initiate cationic polymerization by the action of the proton on the epoxy monomer (Reaction [6.49]).²⁸³



It should also be mentioned that the absorption maxima of the diaryliodonium and the triarylsulfonium salts lie around 250 nm. These salts have no appreciable absorption above 300 nm. Dyes such as acridine yellow (λ_{max} 411 nm), benzoflavin (λ_{max} 460 nm), acridine orange (λ_{max} 539 nm), etc., can be used to spectrally sensitize iodonium salts.²⁸⁴ In contrast, triarylsulfonium salts are not sensitized by acridine derivatives or other common dyes; they can be sensitized by perylene and other polynuclear aromatic hydrocarbons.²⁸⁵

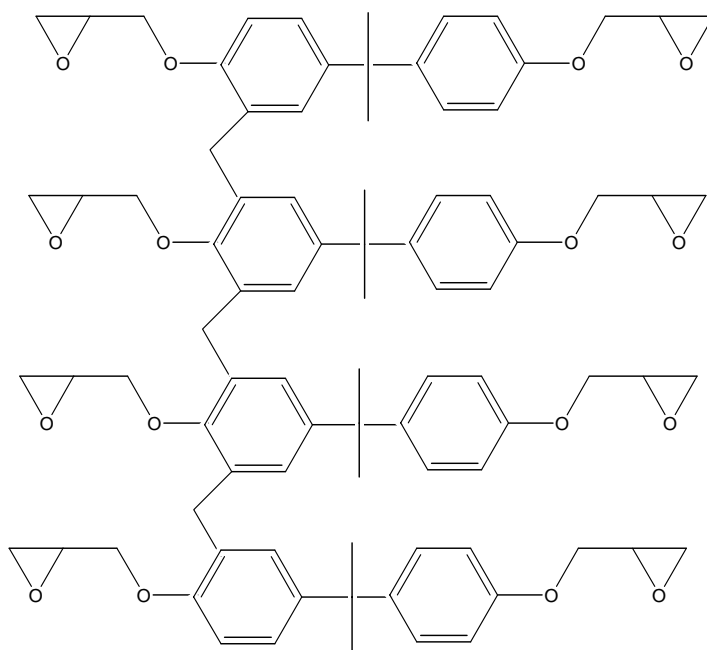
²⁸²A. Reiser, *Photoactive Polymers: The Science and Technology of Resists*, p. 150, John Wiley & Sons, Hoboken, NJ (1989).

²⁸³ibid.

²⁸⁴ibid.

²⁸⁵ibid.

A very important chemical amplification resist that has broad sensitivities to UV, e-beam, and x-ray radiations, marketed under the trade name of SU-8TM (**XLI**), is based on cross-linking of epoxy resins via cationic ring-opening polymerization of pendant epoxide groups.²⁸⁶ This resist currently remains the material of choice in thick resist imaging applications (50–100 μm)²⁸⁷ in microelectromechanical systems (MEMS). Resists based on styrene and allyl glycidyl ether copolymers have been demonstrated to be viable candidates for DUV applications.²⁸⁸ Pendant episulfides have also been shown to be cationically polymerizable for cross-linking in negative resist formulations (**XLII**).²⁸⁹



Epi-Res SU-8 (**XLI**)

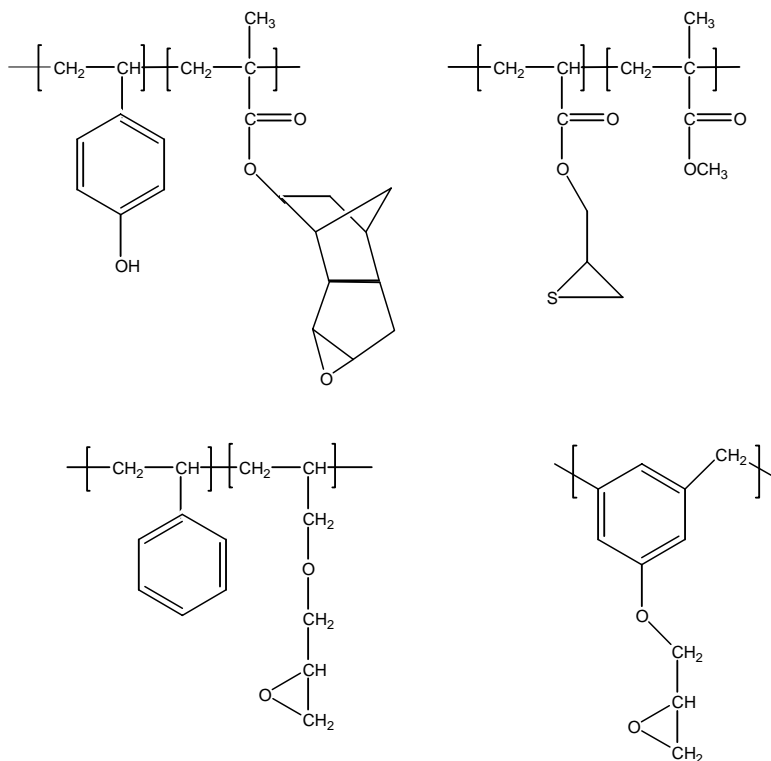
²⁸⁶H. Ito and C.G. Willson, in *Polymers in Electronics*, T. Davidson, Ed., p. 11, ACS Symp. Series 242, American Chemical Society, Washington, DC (1984).

²⁸⁷N.C. LaBianca and J.D. Gelorme, "Epoxy: Lithographic resists for thick film applications," *Proc. 10th Int. Conf. Photopolym.*, p. 239 (1994).

²⁸⁸K.J. Stewart, M. Hatzakis, J.M. Shaw, D.E. Seeger, and E. Neumann, "Simple negative resist for deep ultraviolet, electron beam, and x ray lithography," *J. Vac. Sci. Technol.* **B7**, 1734 (1989); K.J. Stewart, M. Hatzakis, and J.M. Shaw, "Epoxy resins for deep UV lithography," *Polym. Eng. Sci.* **29**, 907 (1989);

²⁸⁹J.C. Dubois, A. Eranian, and E. Datmanti, "New photoresists containing thiirane groups," *J. Electrochem. Soc.* **125**(3), C154 (1978); J.V. Crivello, "Applications of photoinitiated cationic polymerization to the development of new photoresists," in *Polymers in Electronics*, T. Davidson, Ed., p. 3, ACS Symp. Series 242, American Chemical Society, Washington, DC (1984).

A major limitation of polymerization-induced cross-linking in negative resists is swelling during organic solvent development, leading to feature distortions such as bridging, snaking, etc. Resist formulations comprising blends of PHOST with an epoxy-novolac resin (15 wt%) and triphenyl sulfonium hexafluoroantimonate (10 wt%) have been shown to be aqueous-base developable and are therefore fairly resistant to swelling.²⁹⁰



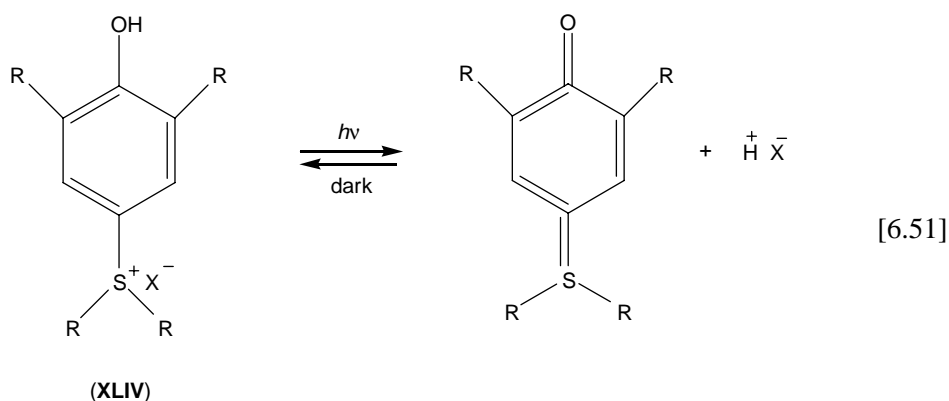
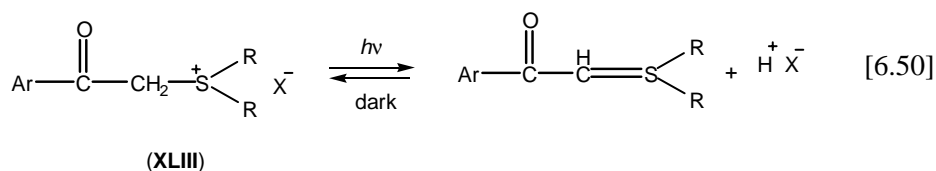
Examples of epoxy rings that are cross-linkable by cationic ring-opening polymerization (XLII)

Another remarkable fact about ionic polymerization in general, in contrast to other polymerization techniques, is that in the absence of adventitious terminators, ionic polymerization will go on after irradiation has ceased, and will often continue until most of the monomer has been exhausted. Although such post-irradiative polymerization may be an advantage in UV curing, it is undesirable in imaging applications where it limits resolution and degrades feature sharpness.²⁹¹

²⁹⁰W.E. Conley, W. Moreau, S. Perreault, G. Spinillo, and R. Wood, "Negative tone aqueous developable resist for photon, electron, and x ray lithography," *Proc. SPIE* **1262**, 49 (1990).

²⁹¹A. Reiser, *Photoactive Polymers: The Science and Technology of Resists*, p. 157, John Wiley & Sons, Hoboken, NJ (1989).

Crivello and Lam²⁹² have found a way to solve this problem with a new class of cationic initiators, the dialkylphenacylsulfonium salts (**XLIII**) (Reaction [6.50]), and the dialkyl-4-hydroxyphenyl sulfonium salts (**XLIV**) (Reaction [6.51]).



Unlike the photolysis of the triarylsulfonium ions that decompose irreversibly on irradiation, the photolysis of these new initiators is reversible. When irradiated, a photostationary state is established in these initiators, as indicated in Reactions (6.50) and (6.51). When the irradiation is stopped, the ilyd and the Brønsted acid revert to the original sulfonium salt. The acidity of the polymerization medium has to be maintained for the propagation of the ionic chain. When the acid is exhausted, the growth of the polymer chain is inhibited and polymerization stops.²⁹³

²⁹²J.V. Crivello and J.H.W. Lam, "Photoinitiated cationic polymerization with triarylsulfonium salts," *J. Polym. Sci., Polym. Chem. Ed.* **17**, 977 (1979); "Photoinitiated cationic polymerization by dialkylphenacylsulfonium salts," *J. Polym. Sci., Polym. Chem. Ed.* **17**, 2877 (1979); **18**, 1021 (1980); J.V. Crivello and J.L. Lee, "Photosensitized cationic polymerizations using dialkylphenacyl sulfonium and dialkyl(4 hydroxyphenyl)sulfonium salt photoinitiators," *Macromolecules*, **14**, 1141 (1981).

²⁹³A. Reiser, *Photoactive Polymers: The Science and Technology of Resists*, p. 152, John Wiley & Sons, Hoboken, NJ (1989).

6.9 Practical Negative Resist Compositions Arising from Photopolymerization of Monomers in the Presence of Polyfunctional Components

6.9.1 Negative resist composition

Given that the initiator and monomer are the only indispensable components of negative resists based on photopolymerization, practical systems are a good deal more complex. Such practical photopolymerization resists contain polyfunctional monomers (so-called cross-linkers) and polymeric or oligomeric binders, as well as various additives and modifiers such as antioxidants to stabilize the systems, radical scavengers to prevent thermal polymerization before exposure, amines to remove oxygen during irradiation, wetting agents, leveling agents, adhesion promoters, coating aids, and dyes.²⁹⁴

6.9.2 Binders

Binders are typically chemically inert or reactive polymers of moderate molecular weight. They are at least partially soluble in the monomer and in polymers of the monomer. They serve to increase the viscosity of the coating mixture and to allow the preparation of thick and thin layers with high solid content.²⁹⁵

Because the binder constitutes a large portion of the resist, it has a significant influence on the properties of the coating and on those of the cured film. For instance, if the binder is alkali soluble, the nonimage (i.e., nonexposed) areas of the exposed resist layer can be dissolved away with an aqueous developer. Also, some of the additives may be directly incorporated into the binder to improve specific physical properties, as in the incorporation of a small amount of free acrylic acid in a polymethacrylate binder to serve as an adhesion promoter for the binder. Most importantly, the binder contributes to lithographic imaging speed since the large macromolecule, caught in the network of the polymerizing monomer, enhances the mass-to-photon ratio of the system.²⁹⁶

Reactive binders are also sometimes used in practical negative resist systems. They are typically macromolecules of modest size that carry some unsaturation.

6.10 Lithographic Applications of Photopolymerization Negative Resists

Photoinitiated polymerization in negative resists used in lithography has found its main applications in lithographic offset plates in dry resists used in the printing of

²⁹⁴A. Reiser, *Photoactive Polymers: The Science and Technology of Resists*, p. 154, John Wiley & Sons, Hoboken, NJ (1989).

²⁹⁵ibid.

²⁹⁶ibid., pp. 155–156.

wire boards, printed circuit boards, solder masks, etc. Other emerging applications of this class of resists are in thick-film imaging for MEMS applications.

The process, as earlier described, is such that the polymerizable composition is in a liquid or in a semisolid, highly viscous state. The primary physical change associated with the early stages of polymerization is an increase in density, which manifests itself as an increase in the index of refraction. As polymerization progresses, the glass transition temperature of the system increases as well, and the coating changes from a rubbery (and possibly tacky) state to a glass. At this juncture, the coating is still relatively permeable to solvent; but gradually, as the cross-link density increases markedly, the material becomes solvent resistant, does not swell significantly, and remains mechanically strong even in the presence of the solvent.²⁹⁷

All lithographic imaging using photopolymerization negative resists relies on the difference between the solubility of the starting resin compositions and the cross-linked form. Following the methods of Delzenne and co-workers²⁹⁸ and Reiser,²⁹⁹ we will present the lithographic uses of photopolymerization in lithography.

6.10.1 Lithographic offset plates

Lithographic offset plates (see Chapter 10) are formulated from polymerizable components such as those described in earlier sections. They are typically coated to a film thickness of a few microns on substrates such as grained or anodized aluminum. Because the film is thin, inhibition of the photochemistry by oxygen presents a major problem. Therefore, exposure is usually done in a vacuum frame. In addition, tertiary amines are added to the composition in order to chemically scavenge oxygen during exposure. Resolution in lithographic plates is fairly good, better than 6 μm in the best plates.³⁰⁰ Lithographic plates are now the leading print medium for textbooks, catalogs, periodicals, and even newspapers.³⁰¹

6.10.2 Dry resists

Dry resist films are formulated from components described in earlier sections and are typically sandwiched between a polyester base sheet and a polyethylene protective cover foil. At the point of use, the resist film is separated from its base

²⁹⁷A. Reiser, *Photoactive Polymers: The Science and Technology of Resists*, pp. 158–159, John Wiley & Sons, Hoboken, NJ (1989).

²⁹⁸E. Brinkman, G. Delzenne, A. Poot, and J. Williams, *Unconventional Imaging Processes*, p. 32, Focal, London (1978).

²⁹⁹A. Reiser, *Photoactive Polymers: The Science and Technology of Resists*, pp. 162–167, John Wiley & Sons, Hoboken, NJ (1989).

³⁰⁰*ibid.*, p. 162.

³⁰¹*ibid.*

sheet and laminated onto the work piece, usually a copper-clad insulating support. The resist is exposed through the polyethylene film to a negative of the desired circuit pattern, after which the cover foil is removed, and the latent image formed on exposure is developed and dried. The metal support may then be etched through the resist mask, or the pattern can be plated with an etch-resistant material, following which the resist is stripped, before the copper is finally etched away.³⁰²

6.10.3 Printed circuit boards

The first major dry film resist was introduced in 1970 by the Dupont Corporation and was marketed under the trade name Riston. It has undergone many updates since then and remains fairly competitive to this day. Other dry film resists have been developed since the invention of Riston, and have found applications in printed circuit board (PCB) and printed wiring board (PWB) manufacturing.³⁰³

However, with the unrelenting introduction of ever-denser and more complex PCBs, the circuit pattern is now commonly generated by a computer. Here, the information is stored on disc and converted into raster scan image data, which are transferred by a laser scanner onto a dry resist film recording medium. Furthermore, laser scanning technology has also shown remarkable improvement, even to the point where laser direct imaging onto a laser-sensitive photoresist laminated onto the PCB has become economical. For this application, no intermediate photographic negatives are required, making the system extremely flexible and suitable for customization. The number of operations is effectively reduced, which improves the accuracy of the operation and reduces the number of defects.³⁰⁴

Two dry film resists designed to address the needs of the laser direct-write applications for PCBs and PWBs are Riston LUV[®] and Riston LV[®], developed by Dupont, and are reported to be sensitive to the UV and visible emission of argon lasers. In particular, Riston LV is based on the principles of dye-sensitized polymerization³⁰⁵ (presented earlier).

It should be noted that the increase in the operational speed of electronic devices has had a profound impact on wire board design. It has made possible the use of signal frequencies that are now in the microwave domain, ensuring that signals have to be routed essentially by microwave transmission lines rather than simply by electron conductors. Consequently, dimensional tolerances have

³⁰²ibid., pp. 162 163.

³⁰³ibid., pp. 163 165.

³⁰⁴ibid.

³⁰⁵ibid.

shrunk well below one mil, and the patterning technology used in printed circuit boards continues to follow in the footsteps of IC microlithography.³⁰⁶

6.10.4 Solder mask

Dry film resists have also found important applications in the fabrication of solder masks³⁰⁷ of IC devices, specifically, in the last phases of the manufacturing processes of IC devices such as calculators, processors, memories, etc., when all of the components of the circuit are in their proper place on the circuit board and they need to be interconnected by soldering. At that stage, a resist is applied to the back and/or to the front of the board where it covers everything, including the circuits as well as the contact pads. The resist may be applied as a liquid, or with more manufacturing convenience, as a dry resist film. Subsequently, the contact pads are uncovered by photoimaging. Next, a wave of liquid solder is sent across the board, which wets the contact pads and completes the interconnections in a single passage. The resist material must, as a necessity, be sufficiently heat resistant and mechanically stable. In some instances, the solder mask film is left in place after the operation, where it serves as a permanent protective encapsulant for the circuitry.³⁰⁸

6.10.5 IC device fabrication

Negative resists based on cross-linking of epoxy resins such as SU-8TM (see above) are used in thick resist (up to 2-mm thick) imaging applications in MEMS, microfluidics, and large-geometry IC devices, with aspect ratios as high as 10 or even greater. These resists are highly transparent to near ultraviolet radiations, which makes it possible to use them to fabricate relatively thick structures with nearly vertical sidewalls and high aspect ratios, using i-line lithography. When fully exposed and cross-linked, SU-8TM resists have extremely low resist outgassing in vacuum, are highly resistant to solvents, acids, and bases, and have excellent thermal properties, which make them well suited for permanent-use applications.

³⁰⁶W.S. Fujitsubo, "Lithography impact on printed wiring boards," *Solid State Technol.* **29**(6), 161 (1986); A. Reiser, *Photoactive Polymers: The Science and Technology of Resists*, p. 165, John Wiley & Sons, Hoboken, NJ (1989).

³⁰⁷F. Axon et al., "Achieving optimum performance with UV curable solder masks," *Circuit World*, **4**, 24 (1978).

³⁰⁸N.S. Fox, "UV solder masks as insulators for printed circuit boards," *ACS Symp. Ser.* **242**, 367 (1984); A. Reiser, *Photoactive Polymers: The Science and Technology of Resists*, p. 167, John Wiley & Sons, Hoboken, NJ (1989).

Chapter 7

Positive Resists

May not bodies receive much of their activity from the particles of light which enter into their composition.

Isaac Newton, *Opticks*

7.1 Introduction

Positive resists differ from their negative counterparts principally in their response to actinic radiation, despite the fact that the essential composition of the two resist types are similar in many ways: each contains sensitizers or appropriate radiation-sensitive compounds, resins, solvents, and additives. Unlike some negative resists, positive resists do not swell in developer. Moreover, the use of aqueous stripping and developing solutions greatly simplifies the equipment selection for positive resists in process equipment tooling by allowing low-cost readily available plastics to be used as containers. Problems from the use of flammable solvents are minimized with positive resists.¹

Although the early resists used in lithography were all negative resists, positive resist images have been produced on paper since the 1920s, starting with the ozalid process.² Resist coatings for positive and negative lithographic plates have been available for many years. It was not, however, until the early 1960s that positive photoresists made the transition from the lithographic plate industry to the semiconductor industry, occasioned by a licensing agreement that Shipley Company made with Azoplate Corporation. For many years the Shipley AZ resist series was the only available positive resist on the market. Several significant improvements were made by the Shipley Company with the cooperation of Azoplate Corporation during this period. In the later part of the 1960s, positive resist products were introduced into the market by Eastman Kodak, GAF, P.A. Hunt, and Dynachem Corporation. There is no gainsaying the fact that the introduction of positive resists was a significant contribution to the semiconductor industry and a major milestone in the evolution of photoresists.³

¹W.S. Deforest, *Photoresist Materials and Processes*, p. 47, McGraw Hill, New York (1975).

²G. Kögel and H. Neuenhaus, "Manufacture of light copy paper," U.S. Patent No. 1,444,469 (1923).

³W.S. Deforest, *Photoresist Materials and Processes*, p. 48, McGraw Hill, New York (1975).

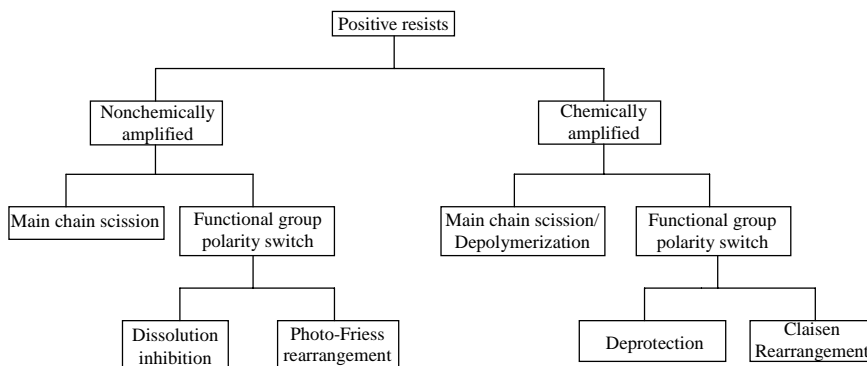


Figure 7.1 Classes of reactions used to generate positive resist imaging action.

Figure 7.1 shows the main classes of reactions used to generate images in positive working resist systems. Because the basis of the imaging action in positive resists lies in the enhanced solubility of the exposed part relative to the unexposed part, common approaches for designing positive resists rely on radiation-induced and photoinduced reduction of the molecular weight of the resin through main chain scission (for both non-chemically amplified and chemically amplified resists) or functional group polarity switch, including dissolution inhibition transformation of resist sensitizers and photo-Friess rearrangement (for non-chemically amplified positive resists); depolymerization, deprotection and Claisen rearrangement (for chemically amplified positive resists). These techniques have been fairly well reviewed.⁴ In the following sections, different classes of positive resist platforms and their components and chemical properties, as well as lithographic regimes of their applications, are considered individually.

7.2 Types of Positive Resists

7.2.1 Non-chemically amplified positive resists

7.2.1.1 Non-chemically amplified positive resists based on functional group polarity switch

7.2.1.1.1 Dissolution inhibition resists

7.2.1.1.1.1 DNQ-NOVOLAC RESISTS

The roots of DNQ-novolac resists stretches all the way back to the ozalid process,⁵ mentioned above, which dates to the invention around 1917 of the process for making architectural blueprint papers by Gustav Kögel (1882–1945) and

⁴A. Reiser, *Photoreactive Polymers: The Science and Technology of Resists*, John Wiley & Sons, Hoboken, NJ (1989); H. Ito, "Chemical amplification resists for microlithography," *Adv. Polym. Sci.* **172**, 37–245 (2005); L.F. Thompson, C.G. Willson, and M.J. Bowden, Eds., *Introduction to Microlithography*, American Chemical Society, Washington, DC (1994); T. Ueno, "Chemistry of

H. Neuenhaus.⁶ Kögel was a German monk who had been assigned the task of establishing the authenticity of several medieval vellum documents from the library of the monastery of Beuron. In this assignment, he often had to painstakingly copy medieval manuscripts letter by letter, a rather laborious process that made him wish for a better and more efficient one. After much experimentation, he found that using paper coated with certain diazo compounds such as diazoquinones, which were synthesized industrially at the Kalle AG Company of Wiesbaden, Germany, he could copy the visible illustrations with sunlight. Working with chemists from Kalle Company to exploit this diazo chemistry, he invented the process for making blueprints, which involves imbibing a paper with diazoquinone and a phenolic coupler such as naphthol and exposing it through a positive line drawing.⁷ On exposure, the diazoquinone is destroyed in the exposed area, and subsequent treatment of the paper with ammonia leads to the reaction of the unreacted diazoquinone with the phenolic coupler to produce the blue azo only in the unexposed parts, yielding a positive-tone image (Scheme 7.1). These were the first products based on light-sensitive organic compounds.⁸ At the time, the main compelling advantageous feature of the diazoquinones was their thermal stability, which gave the ozalid papers a reasonable shelf life. However, the coupling reaction was rather slow, and the diazoquinones were soon superseded by the more reactive diazonium salts, which are still in use today.⁹

Until the 1950s, all photomechanical reproductions were based on the negative-working dichromated colloid resists (described in Chapter 6). For a rather long time, the printing industry had been trying to develop a direct positive printing plate that would eliminate the need for the costly intermediate step. During World War II, researchers at the Kalle Laboratories in Wiesbaden, Germany, found that mixtures of phenolic resins with various diazoquinones produced useful positive-working reprographic plates, which were developable in aqueous alkali. Patents granted by the German authorities on these systems started to appear in 1949,¹⁰ while the corresponding American patents were later assigned to Azoplate Corporation in 1956 and 1962.¹¹

photoresist materials,” in *Microlithography: Science and Technology*, J.R. Sheats and B.W. Smith, Eds., pp. 429–514, Marcel Dekker, New York (1998).

⁵The history of this invention has been presented elsewhere; see for example, R. Dammel, *Diazo naphthoquinone based Resists*, Chapters 1–3, SPIE Press, Bellingham, WA, (1993); C.G. Willson, R.A. Dammel, and A. Reiser, “Photoresist materials: a historical perspective,” *Proc. SPIE* **3050**, 38–51 (1997). The account rendered here is adapted from these same sources.

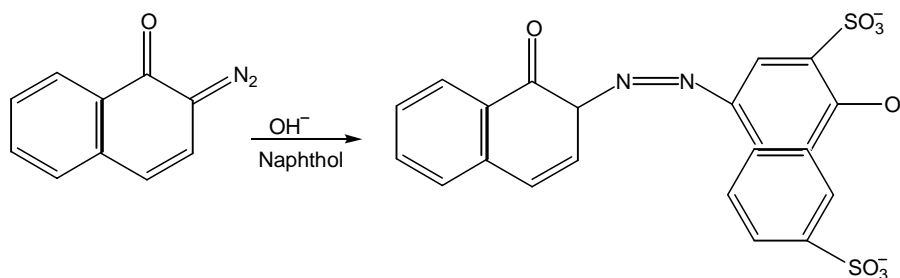
⁶G. Kögel and H. Neuenhaus, “Verfahren zur Herstellung von positiven lichtpausen,” German Patent No. 376,385 (1917); *Z. Wiss. Photogr.* **24**, 171 (1926).

⁷C.G. Willson, R.A. Dammel, and A. Reiser, “Photoresist materials: a historical perspective,” *Proc. SPIE* **3050**, 38–51 (1997).

⁸*ibid.*

⁹H. Zollinger, *Diazo and Azo Compounds*, Interscience, New York (1961); J. Kosar, *Light Sensitive Systems*, John Wiley & Sons, Hoboken, NJ (1965).

¹⁰Kalle AG, “Verfahren zur herstellung von kopien, besonders druckformen, mit hilfe von dizaoverbindungen und dafür verwendbares licht empfindliches material,” German Patent No. 879,205 (1949); M.P. Schmidt, “Verfahren zur herstellung von kopien, besonders druckformen, mit hilfe von dizaoverbindungen,” German Patent No. 865,109 (1956); O. Suss, M.P. Schmidt, “Verfahren



Scheme 7.1 The chemistry of the process for making blueprints.¹²

The diazoquinone-novolac positive plates were only a moderate commercial success, but interest in the diazoquinone-novolac systems was revived in the 1970s when the resolution requirements of the semiconductor industry outpaced the capabilities of the negative bis-azide resists then in use. It was during this time that the diazoquinone resists established themselves as nonswelling, high-resolution imaging materials in the semiconductor industry.

Sometime between 1930 and 1940, Oskar Süß of the Kalle Company invented the DNQ/novolac resist system, spurred on perhaps by the motivation of combining the two functional groups involved in the azocoupling reaction of their blueprint chemistry into one molecule.¹³

In formulating resists with the photosensitive DNQ materials, Oskar Süß and his colleagues at the Kalle Company used novolac¹⁴ obtained from the Albert Company, also in Wiesbaden, as a binder. Novolacs are condensates of phenol or cresols and formaldehyde, which had been independently discovered by Leo Baekeland, a Dutch chemist, and the German inventor C.H. Meyer. Both inventions led to two separate lines of products. Baekeland discovered that cross-linking the novolac with hardening agents yielded a thermoset, which he called Baekelite. C.H. Meyer, in turn, found that the initial exothermic reaction of formaldehyde with phenol could be moderated by adding collophonium to the

zur herstellung von kopien, besonders druckformen, mit hilfe von dizaoverbindungen und dafür verwendbares material," German Patent No. 894,959 (1951).

¹¹Azoplate Corp., "Light sensitive material for the photomechanical reproduction and process for the production of images," U.S. Patent No. 2,766,118 (1956) "Process of making printing plates and light sensitive material suitable for use therein," U.S. Patent No. 3,046,122 (1962).

¹²ibid.; C.G. Willson, R.A. Dammel, and A. Reiser, "Photoresist materials: a historical perspective," *Proc. SPIE* **3050**, 38 51 (1997).

¹³C.G. Willson, R.A. Dammel, and A. Reiser, "Photoresist materials: a historical perspective," *Proc. SPIE* **3050**, 38 51 (1997).

¹⁴The term "novolac" is believed to originate from shellac, a natural thermoplastic extracted from the sticky, resinous secretion of the tiny lac insect *Lucifer lacca*. Lac or Lak means lacquer or resin in a number of European languages, namely Dutch, German, or Swedish, and when prefixed by the Latin or Italian "novo," it denotes "new lacquer."

reagents.¹⁵ In addition, he found that the novolac resin could be mixed with linseed oil, which made it possible to use it as a base for lacquers and paints.¹⁶

The Albert Company commercialized the novolac resin under the brand name Albertol at about the same time the Baekelite Company in the United States and Baekelite GmbH in Germany started production in 1910. Albertol was intended to be used as a substitute for kopals,¹⁷ then used in the manufacture of oil paints. The Albertol novolacs performed very well as oil paint resins in terms of film hardness and gloss, but suffered from the unfortunate problem of smelling rather strongly even when dry, due mostly to residual and unreacted phenols. This is because in order to avoid gel formation during the polycondensation reactions involved in novolac synthesis,¹⁸ phenol must be used in excess (relative to the amount of formaldehyde in the starting reagents), as the solvent. In addition, the color of the film was not stable, turning initially from a clear coat, through various yellow intermediate stages, to a dark brown under the influence of light. The novolac resins were thus not commercially successful until World War I when Germany was cut off from its source of natural kopal resins. Occasioned by the exigencies of the war, novolac production at the Albert Company in Germany, the only factory in Germany that could provide raw materials needed for the paint industry at the time, witnessed a phenomenal increase. The odor problem was finally solved by another Albert Company chemist, Ludwig Berend, who invented a nonsmelling, solid phenol known today as bisphenol A, and in the process pioneered its use in specialized applications for novolacs.¹⁹

The search for an appropriate resin to impart film-forming properties and improved development properties to the DNQ lithographic materials invented by Oskar Süss and his colleagues at the Kalle Company, as stated earlier, led them to the novolac resins from the Albert Company. However, the mixture of novolacs with the new DNQ compounds gave only reddish-brown, dull tones in

¹⁵Following his invention of novolac, C.H. Meyer went to work for the Albert Company of Wiesbaden.

¹⁶C.G. Willson, R.A. Dammel, and A. Reiser, "Photoresist materials: a historical perspective," *Proc. SPIE* **3050**, 38–51 (1997).

¹⁷Kopals are semi fossilized natural resins, which were secreted by *Caesalpinaceae*, a treelike papilionaceous plant, thousands of years ago. Found as lumps embedded in sandy soil and collected manually in Tanzania, Congo, and the Philippines, the resin was used in the past in manufacturing oil paints [cited in C.G. Willson, R.A. Dammel, and A. Reiser, "Photoresist materials: a historical perspective," *Proc. SPIE* **3050**, 38–51 (1997)].

¹⁸Novolac manufacture during the first 60 years after its invention was a rather crude enterprise by today's standards. The reaction was carried out with excess phenol as solvent, which was removed at the end of the reaction by heating the resin to over 200°C. On cooling, the molten or semisolid resin was dropped onto the factory floor, where workers broke it up by hand with pick axes and sled gehammers. Lithographic resins based on novolacs were manufactured under essentially these same conditions at least until the late 1970s. For details on the modern methods of novolac manufacture, see, for example, R. Dammel, *Diazonaphthoquinone based Resists*, pp. 29–30, SPIE Press, Bellingham, WA (1993).

¹⁹C.G. Willson, R.A. Dammel, and A. Reiser, "Photoresist materials: a historical perspective," *Proc. SPIE* **3050**, 38–51 (1997).

the azocoupling reaction, not the brilliant blue desired for blueprint papers. By sheer serendipity, it was observed one day at the Kalle Company, some say when glassware were being cleaned, that a mixture of the DNQ-5-sulfonates with a novolac binder was much less soluble in aqueous bases when unexposed than in the exposed state. Oskar Süß correctly deduced that the intact DNQ-5-sulfonate was a dissolution inhibitor for novolac, while its photoproducts enhanced the dissolution rate of novolac.²⁰

The development contrast in aqueous base between the exposed parts of novolac films afforded by the photochemistry of the exposed DNQ in these parts relative to the unexposed DNQ in the unexposed part of the novolac film was quickly exploited by the Kalle company in the fabrication of positive lithographic printing plates based on the DNQ/novolac resist system. There had been a longstanding interest in positive-tone printing plates, since they made possible the immediate reproduction of an original without having to create an intermediate photographic negative. The first Kalle positive lithographic plate consisted of a DNQ/novolac resist system on an anodized aluminum sheet.²¹ It was introduced around 1950 under the Ozatec tradename, and met with immediate market success.²² Its main advantages included high contrast and resolution, while its main drawbacks were its fragility and a poor resistance to wear, compared to the negative-tone systems.²³

In the old days when wafers were handled with tweezers, before the advent of the automated wafer-handling systems of today, novolac resists were notorious for their particle generation problem, which eventually led to the introduction of automated wafer handling systems.²⁴

In their search for higher-resolution resists and potential replacements for KTRF, lithographers tested many photosensitive coatings, one of which was the positive-tone printing plate material from the Kalle Company of Wiesbaden, invented by Oskar Süß, and based on the DNQ-novolac resist system described above. This material turned out to be the first DNQ-novolac resist used in semiconductor lithography.

The story²⁵ surrounding how DNQ-novolac made the transition from the printing industry to the semiconductor industry is a fascinating one and needs to be retold here, if only to show how seemingly simple unconnected things can have very profound effects, when their potential is channeled and harnessed appropriately. Oddly enough, the nexus of the story runs through family ties, and begins in the early 1950s, in Murray Hill, New Jersey, in the offices of the Azoplate Company, the American outlet for Kale printing plates, which incidentally

²⁰ibid.

²¹ibid.

²²In the United States, these lithographic printing plates were sold by Azoplate, an affiliate of Hoechst AG (by then, Kalle had become a Hoechst AG subsidiary as well).

²³C.G. Willson, R.A. Dammel, and A. Reiser, "Photoresist materials: a historical perspective," *Proc. SPIE* **3050**, 38–51 (1997).

²⁴H.J. Levinson, AMD, Private Communication (2008).

²⁵The version of this story as narrated here is adapted from an account rendered in the report by C.G. Willson, R.A. Dammel, and A. Reiser, "Photoresist materials: a historical perspective," *Proc. SPIE* **3050**, 38–51 (1997).

was located right across the street from Bell Laboratories. The father of a technician at Azoplate was working at the time at Bell Laboratories, when apparently he (the father) had complained one day about the poor resolution of the solvent-developed KTFR resist systems then in use at Bell Laboratories. To this complaint, the son responded by touting the properties of the Azoplate DNQ/novolac coating, which he recommended to his father as a superior alternative to the KTFR resist that he was complaining about. Impressed by what he heard, the father one day took a bottle of the coating solution of the DNQ/novolac resist with him to Bell Laboratories and used it to pattern some devices. Thus began the age of DNQ/novolac resist systems in the semiconductor industry.

Azoplate marketed their DNQ/novolac resist materials designed for semiconductor lithographic application under the tradename AZ Photoresist.²⁶ The adoption of the DNQ/novolac resist systems in the semiconductor industry showed remarkable growth after the introduction of projection lithography in the early 1970s, so much so that by 1972 it began to supplant the cyclized rubber/bis-azide negative-tone resist, the old workhorse of the semiconductor industry (see Fig. 4.12 and Table 4.3). The changeover was rather dramatic and was driven by the inherent advantages of the new DNQ/novolac resist system relative to the old workhorse. These advantages include higher resist contrast and absence of swelling during development.²⁷

Other characteristics of DNQ/novolac resists that have contributed to their lasting success in the semiconductor industry include their high etch resistance and the fact that they can be developed in environmentally benign aqueous base developers. In addition, the cyclized rubber/bis-azide negative tone resists did not image well at the Hg g-line, the exposure wavelength of the earliest commercially available wafer steppers, the introduction of which effectively brought about the complete and wholesale conversion of the IC industry to novolac resists from the cyclized rubber/bis-azide.²⁸

For over a quarter of a century, starting in 1972, and spanning many technology nodes from 5 μm to 0.25 μm , DNQ/novolac resist systems have been employed in both wafer and mask fabrication. Although used predominantly in device fabrication, they have also been employed in mask-making applications, where sensitivity of $\sim 20 \mu\text{C}/\text{cm}^2$ at 10 KV has been reported.²⁹ They dominated the semiconductor lithographic resist market (see Fig. 4.3) during this period. The gradual and

²⁶Azoplate Corp., "Light sensitive material for the photomechanical reproduction and process for the production of images," U.S. Patent No. 2,766,118 (1956).

²⁷DNQ/novolac resist systems do not suffer from swelling during development because being positive acting resists, the exposed areas of the film are dissolved and washed away during development, leaving behind a positive image of the mask. In contrast, the cyclized rubber/bis azide resist is a negative resist, which means that the exposed areas of the film are cross linked, and during solvent development, do absorb solvent and swell as a result. This swelling action limits the resolution of such negative tone resists.

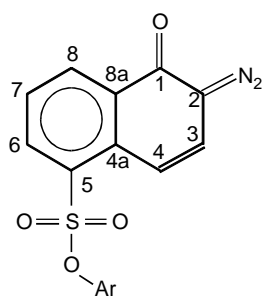
²⁸H.J. Levinson, AMD, Private Communication (2008).

²⁹D.R. Medeiros, A. Aviram, C.R. Guamieri, W. S. Huang, R. Kwong, C.K. Magg, A.P. Mahorowala, W.M. Moroeau, K.E. Petrillo, and M. Angelopoulos, "Recent progress in electro beam resists for advanced mask making," *IBM J. Res. Dev.* **45**(5), 639-650 (2001).

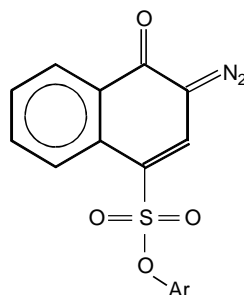
methodical incremental performance improvements in this resist system over the indicated period, coupled with advancements in resolution enhancement techniques, have been instrumental in prolonging the life of near-UV lithography by more than a decade beyond what “experts” had predicted as the end of its useful life.³⁰ Today, more than 35 years after their introduction into semiconductor industry, DNQ/novolac resists are employed in the less critical device layers, mostly in the back end because of their superior etch stability; they are also used for patterning ion implant areas of devices where features are often still large.

(i) The chemistry of DNQs

The most commonly used form of the photoactive component in DNQ resists are DNQs substituted in the 5-position (**I**) or in the 4-position (**II**) with sulfonic acid derivatives.



Diazonaphthoquinone-5-sulfonate ester (**I**)



Diazonaphthoquinone-4-sulfonate ester (**II**)

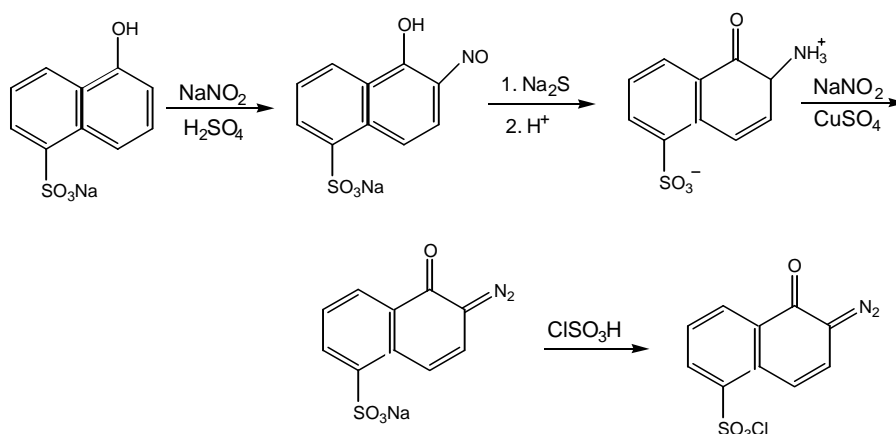
(ii) Synthesis

A review of synthetic methods for the most popular photoactive compounds used in diazoquinone resists—DNQ-5-sulfonate and DNQ-4-sulfonate—has been provided by Ershov et al.³¹ The synthesis typically begins with naphthalene derivatives, and proceeds via introduction of a sulfonic acid group, followed by diazotization and reaction with thionyl chloride to yield the sulfonic acid chloride (Scheme 7.2). In the next step, the chloride is reacted in a base-catalyzed esterification with a suitable ballast group or backbone, which usually is a multifunctional phenol, less frequently a monofunctional phenol or an aliphatic alcohol.³²

³⁰The story is a fascinating one that is explored in depth in Chapter 3.

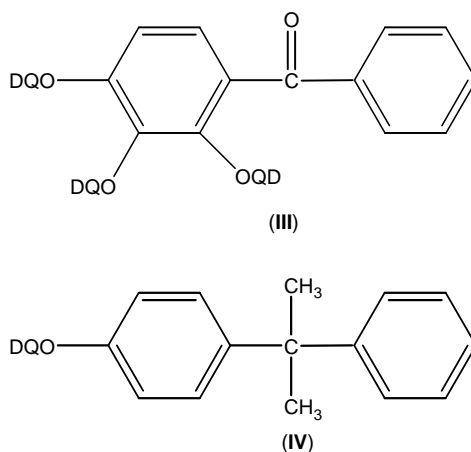
³¹V. V. Ershov, G. A. Nikiforov, and C. R. H. I. de Jonge, *Quinone Diazides*, Elsevier, Amsterdam (1981).

³²A. Reiser, *Photoreactive Polymers: The Science and Technology of Resists*, p. 187, John Wiley & Sons, Hoboken, NJ (1989); R. Dammel, *Diazonaphthoquinone based Resists*, pp. 13–15, SPIE Press, Bellingham, WA (1993).



Scheme 7.2 Synthesis of DNQ-5-sulfonates.³³

For resists designed for applications in the near-UV region, good absorption at 365 nm (i-line) and at 405 nm and 436 nm (g-line) is required, and aromatic substituents present the best option. The most commonly used ballast compound is polyhydroxybenzophenone, where one to three (or even four) hydroxyl groups can be esterified with diazoquinone sulfonyl-chloride, as discussed above. A popularly used dissolution inhibitor is a substituted 2,3,4-trihydroxy benzophenone of structure (III),³⁴ where DQ stands here for diazonaphthoquinone.³⁵ One other popular diazoquinone derivative found in commercial resists is the sulfonyl ester of cumylphenol. Similar materials such as shown in structure (IV) have also been employed in resist applications.³⁶



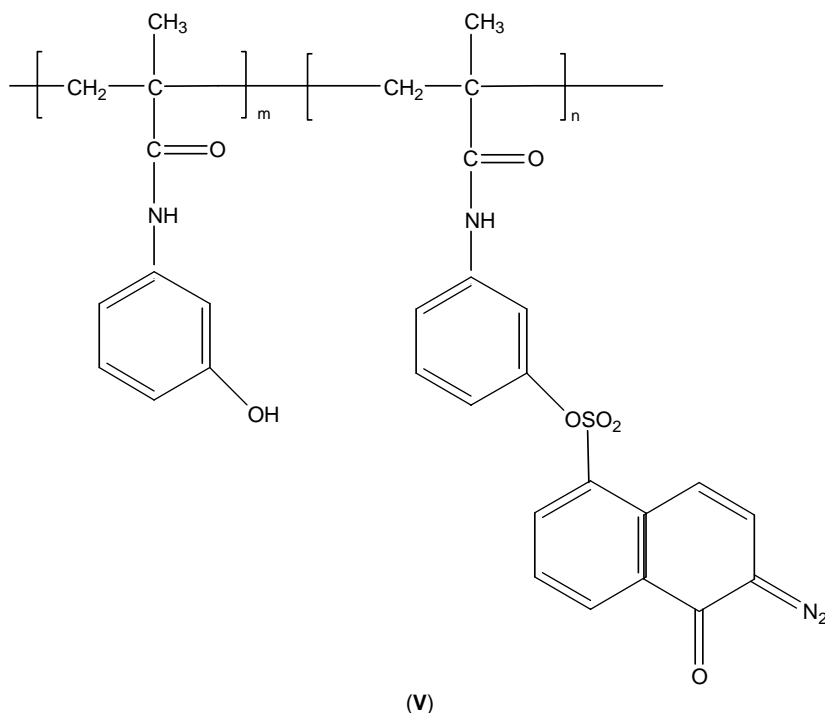
³³R. Dammel, *Diazonaphthoquinone based Resists*, p. 14, SPIE Press, Bellingham, WA (1993).

³⁴A. Reiser, *Photoreactive Polymers: The Science and Technology of Resists*, p. 187, John Wiley & Sons, Hoboken, NJ (1989).

³⁵ibid.

³⁶D.W. Johnson, "Thermolysis of positive photoresists," *Proc. SPIE* **469**, 72 (1984); A. Reiser, *Photoreactive Polymers: The Science and Technology of Resists*, p. 187, John Wiley & Sons, Hoboken, NJ (1989).

Reiser³⁷ asserts that in some resist formulations, the DNQ is directly attached to the phenolic resin, as is the case in the methacrylamide derivative shown in structure (V). This resist has found application in multilayer systems where the diffusion of the inhibitor into adjacent resist layers cannot be tolerated. However, this resist has poor thermal stability.



In recent times, higher esters of tetra- to hexahydroxy benzophenone derivatives have been reported to make good DNQ ballast compounds.³⁸

(iii) Physical properties of DNQs

DNQs have some physical attributes that make them ideal candidates as photoactive components for near-UV lithography. These attributes, according to Reiser,³⁹ include:

- (1) Their absorption spectra have good overlap with the emission spectrum of the irradiation source (usually a Hg arc).

³⁷A. Reiser, *Photoreactive Polymers: The Science and Technology of Resists*, p. 187, John Wiley & Sons, Hoboken, NJ (1989).

³⁸R. Dammel, *Diazonaphthoquinone based Resists*, p. 15, SPIE Press, Bellingham, WA (1993).

³⁹A. Reiser, *Photoreactive Polymers: The Science and Technology of Resists*, p. 188, John Wiley & Sons, Hoboken, NJ (1989).

- (2) They bleach, that is, they become more transparent during the course of the exposure, which makes it possible for the exposing radiation and hence the photoreaction to eventually penetrate to the bottom of the resist layer and reach the resist-substrate interface.
- (3) They are compatible with the novloac base resin, which enables them to affect the dissolution rate of the resist, since they form a single phase with the resin.
- (4) With a decomposition temperature at around 120°C and 130°C, they have a reasonable thermal stability over typical pre- and postbake processing temperature regimes.

(iv) Photochemistry of DNQs: absorption characteristics

Figure 7.2 shows the absorption spectra of 2,1,5-DNQ sulfonate and 2,1,4-DNQ sulfonate, covering the near-UV spectral region, and also shows the principal emission bands of a medium-pressure Hg arc lamp. Each figure shows the unexposed and exposed (bleached) spectra of these two isomers. The first two UV absorption bands of the DNQ moiety are assigned to the $n-\pi^*$ (S_0-S_1) and $\pi-\pi^*$ (S_1-S_2) transitions.⁴⁰ The fact that π states are involved is indicative of the dependence of the absorption maxima on the polarity of the environment. Given that only singlet states are involved, heavy atom effects are precluded, suggesting that the photochemistry of DNQs takes place on a singlet hypersurface.⁴¹

The absorption characteristics of DNQs depend strongly on the nature and location of substituents on the benzene ring. For instance, the typical absorption bands of DNQ-5-sulfonate lie at 350 and 400 nm, while those of its isomer, the DNQ-4-sulfonate, are blue-shifted to 310 and 390 nm. From the lithographic point of view, the position of these principal absorption peaks indicates that the DNQ-5-sulfonate is better suited for exposure with Hg g-line radiation, while DNQ-4-sulfonate, with a higher UV absorption yield, and thus more efficient coupling of energy into the resist, is better suited for Hg i-line radiation.⁴²

As seen in Fig. 7.2, the principal DNQ absorption peaks decrease dramatically on exposure because the main photolysis product of DNQ, indene carboxylic acid, is less absorbing at the irradiation wavelength than DNQ. This phenomenon is called bleaching.⁴³

⁴⁰H. Meier and K. Zeller, "The Wolff rearrangement of diazo carbonyl compounds," *Angew. Chem. Int. Ed. (English)* **14**, 32 (1975); M. Kaplan, D. Meyerhofer, "Response of diazoquinone resists to optical and electron beam exposure," *RCA Rev.* **40**, 169 (1979); "Sensitivity of diazoquinone resists to optical and electron beam exposure," *Polym. Eng. Sci.* **20**, 1073 (1980), D. Ilten, R. Sutton, "Spectrophotometric determination of photoresist photosensitivity," *J. Electrochem. Soc.* **119**, 539 (1972); B. Broyde, "Exposure of photoresists," *J. Electrochem. Soc.* **117**, 1555 (1970).

⁴¹R. Dammel, *Diazonaphthoquinone based Resists*, p. 15, SPIE Press, Bellingham, WA (1993).

⁴²ibid., p. 17.

⁴³ibid.

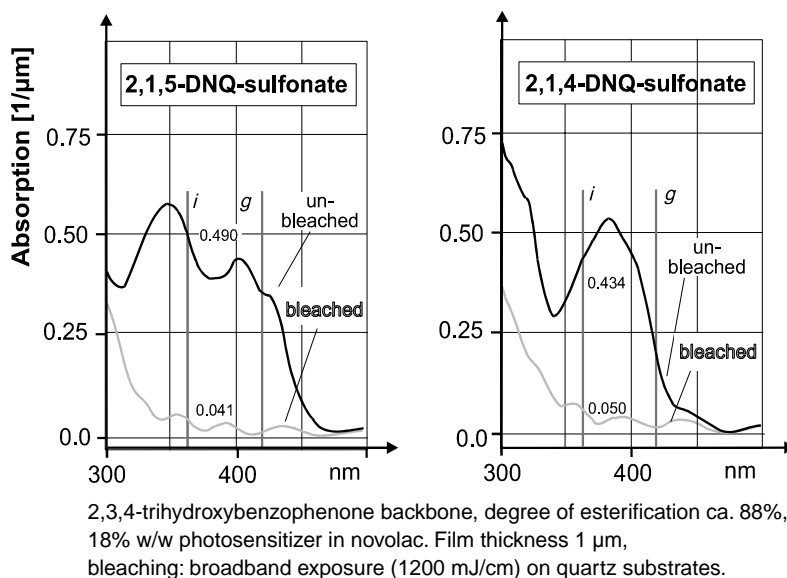


Figure 7.2 Absorption spectra of exposed (bleached) and unexposed films of 2,1,5-DNQ-sulfonate and 2,1,4-DNQ-sulfonate sensitizers attached to 2,3,4-trihydroxybenzophenone backbone in a novolac, around the near-UV spectral region. The spectra are shown together with the emission lines of the medium-pressure Hg arc. (Courtesy of R. Dammel.)

(v) Reactions of DNQs

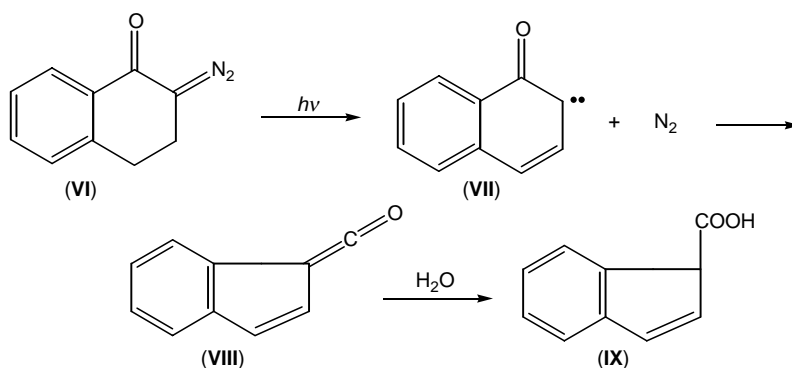
Süss,⁴⁴ in 1944, was the first person to systematically investigate the photoreactions of DNQs. He proposed the mechanism for the photolysis of DNQs indicated in Scheme 7.3.

The first step in the reaction scheme involves the elimination of nitrogen from the diazoquinone (**VI**), forming a carbene (**VII**). The carbene undergoes a Wolf rearrangement,⁴⁵ involving ring contraction, and leading to the formation of ketene (**VIII**). In the presence of small amounts of water in the novolac binder,⁴⁶ hydration of the ketene leads to the formation of indene carboxylic acid (**IX**). The main feature of the process is the transformation of a fairly hydrophobic

⁴⁴O. Süss, "Über die Natur der Belichtungsprodukte von Diazoverbindungen. Übergänge von aromatischen 6 Ringen in 5 Ringe," *Ann. Chem.* **556**, 65 (1944); "Über die Natur der Lichtzersetzungsprodukte von Diazoaminoverbindungen und Diazophenoläthern (III)," *Annalen Chem.* **557**, 237 (1947).

⁴⁵L. Wolff, "Ueber Diazoanhydride," *Ann. Chem.* **325**, 129 (1902); "Über Diazoanhydride (1,2,3 Oxydiazole oder Diazoxyde) und Diazoketone," **394**, 23 (1912); G. Schroeter. "Über die Hofmann Curtiusche, die Beckmannsche und die Benzilsäure Umlagerung," *Ber. Deutsch. Chem. Ges.* **42**, 2336 (1909); "Über die Beziehungen zwischen den polymeren Ketenen und dem Cyclobutan 1.3 dion und seinen Derivaten," **49**, 2697 (1916).

⁴⁶Under normal ambient working conditions, enough water is present in the novolac binder to ensure the formation of the carboxylic acid.



Scheme 7.3 Photolysis of DNQ.

and nonionizable compound (diazoquinone) to an ionizable hydrophilic species (indene carboxylic acid).⁴⁷

Scheme 7.3 describes a somewhat idealized picture of the chemistry underlying diazoquinone photolysis. Detailed investigations of this mechanism by a few researchers after Süss, notably Pacansky et al.⁴⁸ and Erlikh et al.,⁴⁹ have essentially confirmed the basic accuracy of the mechanism proposed by Süss, but with a few minor modifications. They identified side reactions that are associated with the process, a summary of which has been provided by Reiser (see Scheme 7.4).⁵⁰ Also, contrary to Süss' assumptions, these investigators established that it is not indene-1-carboxylic acid that is formed predominantly, but indene-3-carboxylic acid.⁵¹

These side reactions ultimately lead to cross-linking. In the first instance, in the presence of insufficient water content in the resist, the ketene (VIII) may react directly with the resin, producing cross-links that are highly undesirable in a positive resist. Suppression of this type of cross-linking is accomplished by the incorporation of ketene scavengers (amines) into the resist. These scavengers react with the ketene, thus preventing them from participating in cross-linking reactions. However, the scavengers may decarboxylate the acid on subsequent hydrolysis.⁵²

⁴⁷O. Süss, "Über die Natur der Belichtungsprodukte von Diazoverbindungen. Übergänge von aromatischen 6 Ringen in 5 Ringe," *Ann. Chem.* **556**, 65 (1944); A. Reiser, *Photoreactive Polymers: The Science and Technology of Resists*, p. 182, John Wiley & Sons, Hoboken, NJ (1989).

⁴⁸J. Pacansky and D. Johnson, "Photochemical studies on a substituted naphthalene 2,1,diazooxide," *J. Electrochem. Soc.* **124**, 862 (1977); J. Pacansky and J.R. Lyerla, "Photochemical decomposition mechanisms for AZ type photoresists," *IBM J. Res. Dev.* **23**, 42 (1979).

⁴⁹A.D. Erlikh, N.P. Protsenko, L.N. Kurovkaja, and G.N. Rodionova, *Zh. Vses. Khim. Obua.*, "Photolysis of onaphthoquinonediazides: Structure of substituted indenecarboxylic acids," **20**, 593 (1975) [cited in A. Reiser, *Photoreactive Polymers: The Science and Technology of Resists*, p. 187, John Wiley & Sons, Hoboken, NJ (1989); R. Dammel, *Diazonaphthoquinone based Resists*, pp. 13–15, SPIE Press, Bellingham, WA (1993)].

⁵⁰A. Reiser, *Photoreactive Polymers: The Science and Technology of Resists*, pp. 182–183, John Wiley & Sons, Hoboken, NJ (1989).

⁵¹R. Dammel, *Diazonaphthoquinone based Resists*, p. 23, SPIE Press, Bellingham, WA (1993).

⁵²A. Reiser, *Photoreactive Polymers: The Science and Technology of Resists*, p. 182, John Wiley & Sons, Hoboken, NJ (1989).

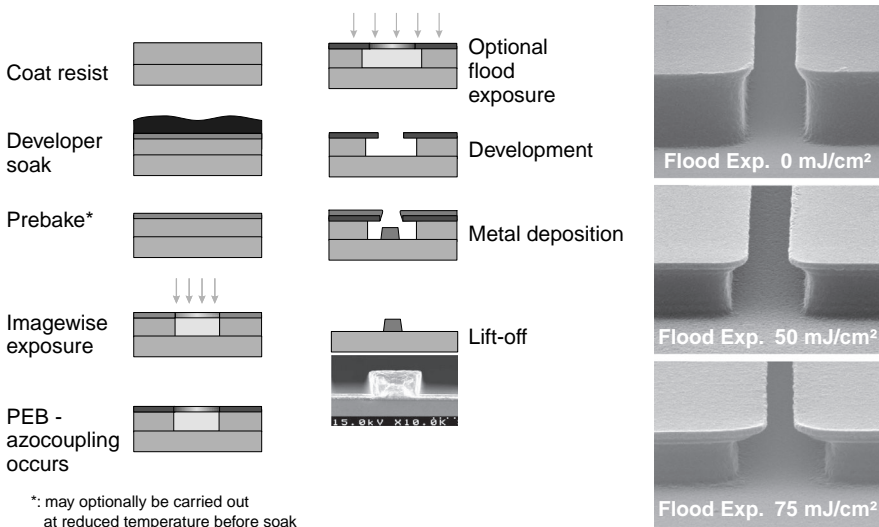
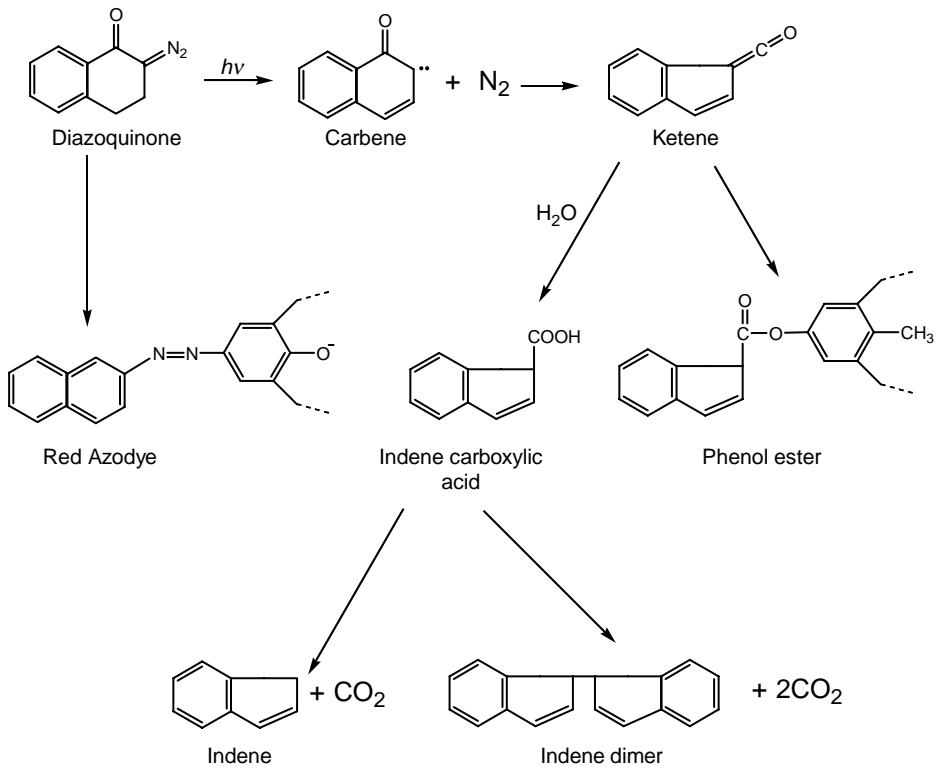
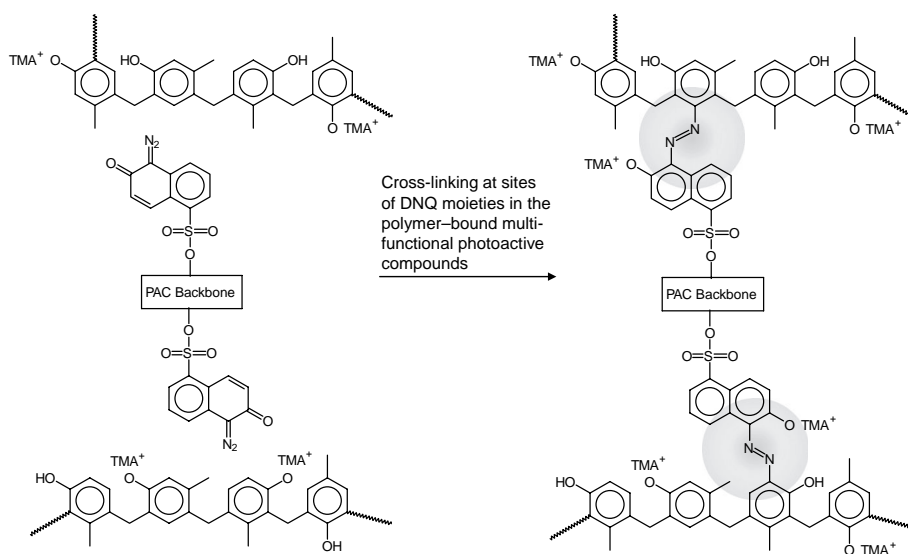


Figure 7.3 Use of azocoupling reaction in the lift-off process. (After R. Dammel.⁵³)

⁵³R. Dammel, "Diazonaphthoquinone based resists," SPIE Short Course No. SC104 (2003).

In point of fact, the reaction of ketene with the anhydrous base resin has been exploited to produce negative resist images with strongly undercut profiles, which have found applications in lift-off processes (Figure 7.3).⁵⁴ Furthermore, Itoh et al.⁵⁵ have reported that exposure of a novolac-DNQ positive resist to DUV (250 nm) radiation, to which it is very absorptive, leads to the creation of a cross-linked crust on the top of the resist.⁵⁶

A second side reaction involves the formation of red azo dye due to a slow coupling process between multifunctional DNQ and the phenolate ions of the novolac resin that are formed in the developer; this can create cross-links, thus reducing solubility. This may also occur during development in the unirradiated areas, during which stage cross-linking is no longer objectionable (see Scheme 7.5).⁵⁷



Scheme 7.5 Azocoupling reaction of unphotolyzed DNQ during development.⁵⁸

A third side reaction is the decarboxylation of indene carboxylic acid during postbake, leading to formation of indene and indene dimer.⁵⁹ This reaction

⁵⁴:ibid.

⁵⁵T. Itoh, Y. Yamashita, R. Kawazu, K. Kawamura, S. Ohno, T. Asano, K. Kobayshi, and G. Nagamatsu, "A negative resist, LMR (low molecular weight resist), for deep UV lithography," *Polym. Eng. Sci.* **26**, 1105 (1986).

⁵⁶A. Reiser, *Photoreactive Polymers: The Science and Technology of Resists*, p. 182, John Wiley & Sons, Hoboken, NJ (1989).

⁵⁷:ibid.; R. Dammel, *Diazonaphthoquinone based Resists*, p. 82, SPIE Press, Bellingham, WA (1993); M. Hanabata, Y. Uetani, and A. Furuta, "Novolac design for high resolution positive photoresists. II. Stone wall model for positive photoresist development," *Proc. SPIE* **920**, 349 (1988).

⁵⁸R. Dammel, "Diazonaphthoquinone based resists," SPIE Short Course No. SC104 (2003).

⁵⁹J. Pacansky and J.R. Lyster, "Photochemical decomposition mechanisms for Az type photoresists," *IBM J. Res. Dev.* **23**, 42 (1979).

is interesting on a number of grounds because it can be used in the design of a well-controlled image reversal process, where a negative image is produced with a conventional positive resist.⁶⁰ The decarboxylation process is base catalyzed and can be initiated at relatively low temperatures by the addition of a strong base (imidazole, monazoline, triethanolamine, and ammonia vapor)⁶¹ to the coating solution.⁶² In areas where the carboxylic acid has been removed, the original low dissolution rate of the inhibited novolac can be restored. By flood-exposing the film, carboxylic acid (which increases the dissolution rate) can be produced in the previously unexposed areas. Subsequent development in alkali leads to a negative-tone image of the original mask. This procedure has found application in lift-off processes where a negative and undercut resist image is required.⁶³ A schematic of the image reversal process that is acid catalyzed is shown in Fig. 7.4.⁶⁴ In this

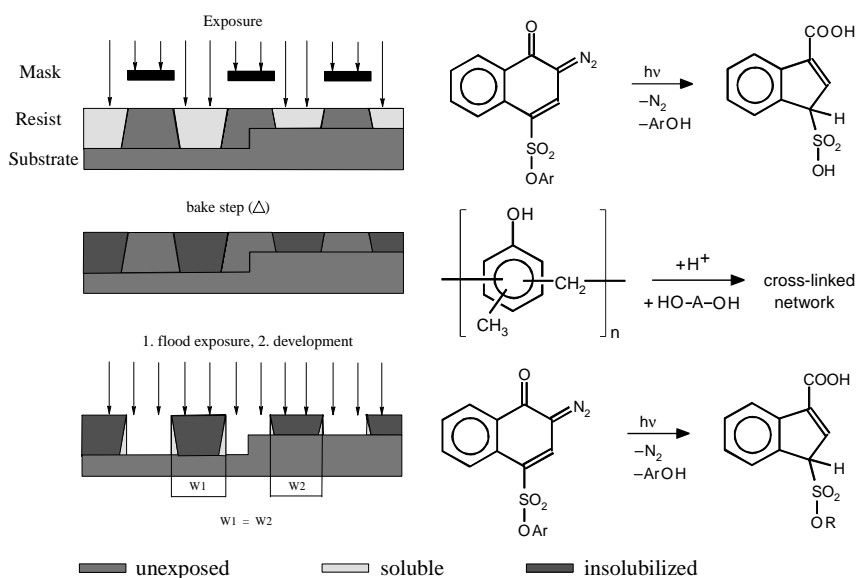


Figure 7.4 Process scheme for acid-catalyzed image reversal. (After R. Dammel.⁶⁵)

⁶⁰S.A. MacDonald, R.D. Miller, C.G. Willson, G.M. Feinberg, R.T. Gleason, R.M. Halverson, M.W. McIntire, and M.T. Motsiff, presented at Kodak Microelectron. Semin. Interface 1982, San Diego (1982).

⁶¹M.L. Long, "Image reversal techniques with standard positive photoresist," *Proc. SPIE* **469**, 189 (1984).

⁶²H. Moritz and G. Paal, "Method of making a negative photoresist image," U.S. Patent No. 4,104,070 (1978); C.G. Willson, in *Introduction to Microlithography*, L.F. Thompson, C.G. Willson, and M.J. Bowden, Eds., ACS Symp. Ser. 219, p. 117, American Chemical Society, Washington, DC (1984).

⁶³A. Reiser, *Photoreactive Polymers: The Science and Technology of Resists*, pp. 182-183, John Wiley & Sons, Hoboken, NJ (1989).

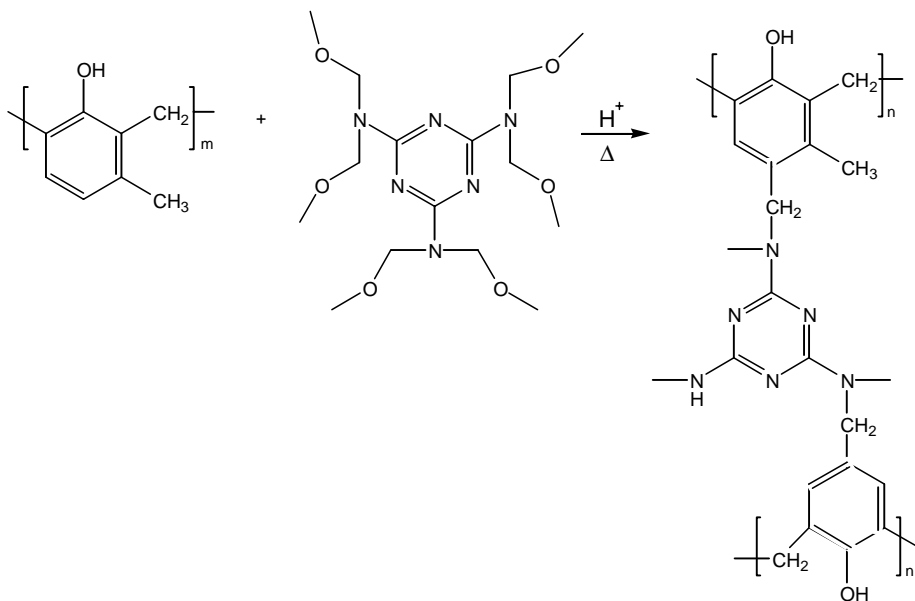
⁶⁴R. Dammel, *Diazonaphthoquinone based Resists*, pp. 140-141, SPIE Press, Bellingham, WA (1993); R.M.R. Gijzen, H.J.J. Kroon, F.A. Vollenbroek, and R. Vervoordeldonk, "A quantitative assessment of image reversal, a candidate for a submicron process with improved line width," *Proc. SPIE* **631**, 108 (1986).

⁶⁵R. Dammel, "Diazonaphthoquinone based resists," SPIE Short Course No. SC104 (2003).

process, DNQ-4-sulfonate/novolac resist containing an acid-activated cross-linking component leads to formation of indene sulfonic acid in the exposed areas, leaving the unexposed areas unaffected. Postexposure bake causes cross-linking of the novolac resin in the exposed areas, catalyzed by the strong sulfonic acid generated in the exposure step. In a subsequent flood exposure, the DNQ in the areas that had not been previously exposed is photolyzed to yield indene carboxylic acid, which enhances the dissolution of the novolac resin during development, while the cross-linked novolac in the areas that were exposed during the first exposure are not dissolved during development. The net result is a negative-tone image of the original mask.

The versatility of the diazoquinone photochemistry has been exploited in yet another interesting way by Feely et al.,⁶⁶ who have used the indene carboxylic acid generated in the photolysis of diazoquinone in hardening novolac resins to which melamine derivatives have been added as cross-linkers. Acid-hardening resins are usually cross-linked by strong protonic or Lewis acids. At high temperature, the indene carboxylic acid becomes effective in catalyzing the cross-linking reaction of the novolac resin with the melamine cross-linker (Scheme 7.6).⁶⁷

The comparative inactivity of indene carboxylic acid (as other carboxylic acids) in catalyzing this reaction at room temperature makes it possible to use



Scheme 7.6 Cross-linking reaction between novolac and melamine cross-linker.

⁶⁶W.E. Feely, J.C. Imhof, and C.M. Stein, "The role of the latent image in a new dual image, aqueous developable, thermally stable photoresist," *Polym. Eng. Sci.* **26**, 1101 (1986); W.E. Feely, "Micro plastic structures," *Proc. SPIE* **631**, 48 (1986).

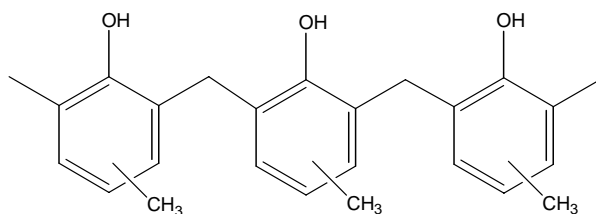
⁶⁷A. Reiser, *Photoreactive Polymers: The Science and Technology of Resists*, p. 184, John Wiley & Sons, Hoboken, NJ (1989).

the system in two different ways that can afford either positive-tone or negative-tone images. The indene carboxylic acid catalyst produced during exposure can be removed by a basic developer, and the system can be used as a normal positive resist. Alternatively, the irradiated areas can be cross-linked before development by heating them to between 80 and 100°C and subsequently flood exposing the whole wafer, followed by development in alkali to remove the unexposed area to yield a negative image of the original.⁶⁸

(vi) Resins for DNQ resists

The binder resin performs a very crucial function in the performance of the DNQ resist system. It must possess a lot of useful attributes, some of which include the following. It must be soluble in the proper casting solvents. The spin-coated films must adhere well to the underlying substrates and must have physical integrity to form continuous, pinhole-free coatings. For the DNQ-sulfonate photoactive compounds (PACs) to produce the discrimination necessary for high-resolution images, they must mix very well with the binder, and the exposed areas of the solid film of the binder polymer/PAC solution must be soluble in aqueous base developer. In this way, the exposed part of the film is washed away during development, affording a high-contrast resist. After the image has been formed, the polymer must provide the physical protection and “resist” damage associated with subsequent image transfer processes. Finally, the binder resin must be stripable when the image and image transfer steps are completed.

The resin most often used with DNQ resists is the reddish-colored novolac (cresol-formaldehyde condensation polymers).⁶⁹ The resins adhere well to most metal surfaces and form good films. Additionally, they are soluble in alkaline solutions and many common solvents, and they are capable of coupling with the DNQ sensitizer. The structure of novolac (**X**) is shown below.⁷⁰

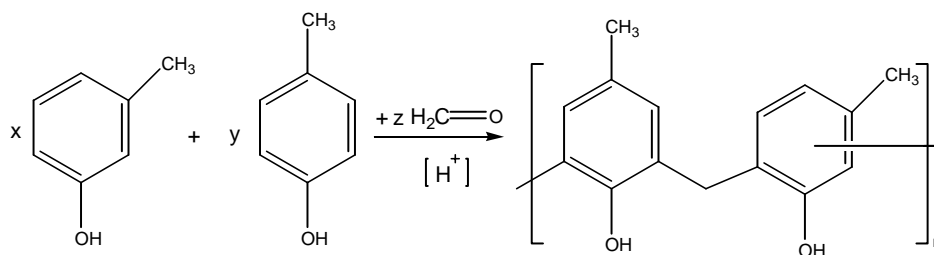


Novolac (**X**)

⁶⁸ibid., p. 185.

⁶⁹T.R. Pampalone, “Novolac resins used in positive resist systems,” *Solid State Technol.*, **27**(6) 115 (June 1984); Kalle Corp., “Verfahren zur herstellung von kopien, besonders druckformen, mit hilfe von diazo verbindungen und dafür verwendbares licht empfindliches material,” German Patent No. 879205 (1949).

⁷⁰The methylene links are not always *ortho* to the OH of the phenols; only in *m* cresol based novolacs is this the case.



Scheme 7.7 Synthesis of novolac.

Novolacs are linear polymers. Metacresol, a very reactive derivative of phenol, is typically used to prepare novolac resins. The presence of a methyl group at the *meta* (3 or 5) position of the benzene ring of phenol enhances the reactivity of the compound toward polymerization with formaldehyde. Novolac resins made with metacresol are also more moisture resistant than those with phenol. After preparation, novolac's ability to resist further polymerization is attributed to the fact that the chains terminate with phenol groupings, having been prepared with an excess of phenol.⁷¹

Novolac resins are produced commercially from cresol mixtures that contain amounts of *m*-cresol and *p*-cresol isomers in varying proportions, depending on the specific application. The reaction proceeds with both metal cation and acid catalysis (Scheme 7.7).⁷² Because of strict guidelines for metallic contaminants in semiconductor grade process materials and chemicals, acid catalysis is employed in the synthesis of novolacs used in photoresist applications. In a typical commercial production process, a mixture of *m*- and *p*-cresol isomers, formaldehyde (most often in the form of formalin, a 35–40% aqueous solution of formaldehyde) and an oxalic acid catalyst are reacted, following the description of Pampalone:⁷³

“The cresols are charged into the kettle and heated to 95°C, the catalyst is added and dissolved, and the formaldehyde is added over several hours to complete the exothermic reaction. The kettle is then heated to above 160°C and vacuum is drawn. Water and unreacted *p*-cresol are stripped off, residual oxalic acid decomposes to carbon dioxide, and only molten novolac resin remains in the kettle. The product is poured onto a cooling belt, and crushed.”

The condensation polymerization of the cresol with formaldehyde, it should be pointed out, is difficult to control and results in a relatively low-molecular-weight polymer. In general, these polymers are soluble in most spin-coating solvents, provide excellent adhesion to most substrates, and exhibit good film-forming and coating properties.

These novolac resins have exhibited enough balance in the needed binder properties mentioned above that they are now exclusively used in all commercial

⁷¹W.S. Deforest, *Photoresist Materials and Processes*, pp. 55–56, McGraw Hill, New York (1975).

⁷²R. Dammel, *Diazonaphthoquinone based Resists*, pp. 29–30, SPIE Press, Bellingham, WA (1993).

⁷³*ibid.*, p. 29; T.R. Pamplone, “Novolac resins used in positive resist systems,” *Solid State Technol.* **27**(6), 115 (1984).

DNQ-sulfonate positive-resist formulations. However, as the demands on these formulations increased over time due to the ever-continuous march to ever-smaller geometries, requiring new image transfer steps such as ion implantation and plasma etching, new improved binder resins were developed.

Novolacs as a general rule have two main shortcomings. First, their synthesis is often plagued with lot-to-lot variation, so much so that a specific chemical composition and molecular size is difficult to reproduce. This is because of inconsistent composition of the cresol starting material and also because the condensation polymerization is difficult to control. These variations can lead to irreproducible lithographic performance of the resists. Second, the low glass transition temperatures of the novolac polymers often lead to unacceptable image distortions during the plasma etching or ion implantation steps.

Attempts have been made over time to improve the physical properties of novolacs. The use of phenol formaldehyde resins prepared in alkaline medium in photoresist compositions is mentioned in a Kalle Co. AG patent.⁷⁴ The use of polyvinyl ethers in combination with novolacs to impart stickiness and plasticization action to the latter was patented by Christensen.⁷⁵ Steinhoff, Isaacson, and Roelants of the Shipley Company mention the use of vinyl ethers in a patent on roller coating.⁷⁶ Lower alkyl polyvinyl ethers, such as methyl, ethyl, butyl, and isobutyl, are added to novolac resins to improve coating flexibility and adhesion to metal surfaces as well as to improve resistance to mildly alkaline solutions. The use of styrene, methyl styrene, and styrene-maleic anhydride copolymers in combination with novolac was mentioned in several patents⁷⁷ of both Shipley and Kalle Co. AG. When novolac is copolymerized with maleic anhydride, a resin that is readily soluble in alkaline solutions is obtained.⁷⁸

Reiser⁷⁹ identifies the following four material factors that appear to influence the performance of novolac resist resins:

1. molecular weight,
2. the dispersity of the molecular weight distribution,
3. the isomeric composition of the cresoles, and
4. the relative position of the methylene linkages.

The molecular weight of novolac resins used in resist applications is typically in the range M_n 1000–3000, corresponding to 8 to 25 repeat units in the chain.

⁷⁴Kalle Co. AG, British Patent No. 7111,626 (1954).

⁷⁵C.W. Christensen, French Patent No. 1,542,334 (1968).

⁷⁶T.L. Steinhoff, C. Isaacson, and G.J. Roelants, "Method of coating printed board having through holes," U.S. Patent No. 3,535,157 (1970).

⁷⁷T.L. Steinhoff, C.R. Shipley, and J.A. MacDonald, "Light sensitive material and process for the development thereof," Canadian Patent No. 774,047 (1967); G. Friz, O. Suss, F. Uhlig, W. Neugebauer, and M.K. Reichel, "Toroidal transmission mechanism with torque loading cam means," U.S. Patent No. 3,184,983 (1964).

⁷⁸W.S. Deforest, *Photoresist Materials and Processes*, p. 57, McGraw Hill, New York (1975).

⁷⁹A. Reiser, *Photoreactive Polymers: The Science and Technology of Resists*, pp. 192–196, John Wiley & Sons, Hoboken, NJ (1989).

The polydispersity of the resin is fairly high, although it has been shown that a narrow molecular weight distribution improves lithographic performance.⁸⁰

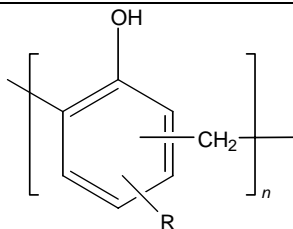
Hanabata et al.⁸¹ have also shown that a narrow molecular weight distribution, particularly in the absence of low-molecular-weight fragments, is beneficial for good image resolution in DNQ/novolac resists. In addition, they proposed the so-called “stone wall” model of resist dissolution, where low-molecular-weight fragments (the small stones in the wall) can be dissolved out from the bulk of the matrix and make the rest of the structure crumble over a wide range of development times and developer concentrations.⁸²

One of the main advantages of DNQ/novolac resists over the bis-azide/rubber resist system that was responsible for the former superseding the latter is the fact that novolac does not swell during development and is therefore suitable for the printing of high-resolution patterns. Additionally, novolac resin is reasonably resistant to plasma, a very important property in semiconductor device fabrication. However, the thermal and mechanical properties of novolac are not outstanding; its plastic flow temperature is around 120°C. Even here, the effects of isomer composition and of molecular weight play a role as can be seen from the data in Table 7.1.⁸³

A number of radiative treatment techniques have been identified to be successful in improving the image stability of diazoquinone resists. These radiative treatments introduce cross-links and increase the glass transition temperature (T_g), while also improving the mechanical strength of the polymer image. These

Table 7.1 Effect of novolac structure and degree of polymerization on flow temperature. (Reprinted with permission from Ref. 84. © 1989 John Wiley & Sons.)

R	n	T_{flow} (°C)
<i>o</i> Me	8	85
<i>p</i> Me	6	119
<i>o n</i> Pr	8	73
<i>o sec</i> Bu	9	69
<i>o tert</i> Bu	> 13	> 133
<i>o</i> Me (70%)	5	85
<i>p</i> Me (70%)	10	128



⁸⁰ibid., pp. 192–193.

⁸¹M. Hanabata, Y. Uetani, and A. Furuta, “Novolac design for high resolution positive photoresists. II. Stone wall model for positive photoresist development,” *Proc. SPIE* **920**, 43 (1988).

⁸²A. Reiser, *Photoreactive Polymers: The Science and Technology of Resists*, p. 193, John Wiley & Sons, Hoboken, NJ (1989).

⁸³ibid., pp. 195–197.

⁸⁴ibid., p. 195.

techniques, including DUV⁸⁵ and pulsed photomagnetic curing (flash exposure to a high-intensity UV arc in the presence of magnetic field)⁸⁶ have been used to prepare positive novolac resists for high-current ion implantation.

(vii) Solvents for DNQ/novolac resists

The most popular solvents used in the formulation of DNQ/novolac resists are propylene glycol monomethylether acetate, ethylene glycol monomethyl or monoethyl ether (cellosolve or methyl cellosolve), and ethyl lactate. For more hydrophobic resins, cellosolve acetate (ethylene glycol monoethyl ether acetate) is employed. Ester solvents, particularly acetates such as butyl acetate, are used as diluents, as are aromatic hydrocarbons, such as xylenes.⁸⁷

(viii) Additives

A main problem of DNQ/novolac resist solutions is their instability, and several stabilizing additives for diazo compounds are therefore added to the formulation to prevent this problem. Some of these additives include dyes and resin stabilizers.

In general, stabilizers are usually reducing agents or antioxidants such as thiourea,⁸⁸ sugars, and related compounds, organic acids,⁸⁹ etc. Oil-soluble dyes along with their stabilizing oils such as methyl violet BB in castor oil and roseaniline hydrochloride in sesame oil have also been mentioned as possible additives.⁹⁰

Because dyes tend to alter the exposure characteristics, they are used sparingly. Resin plasticizers such as phthalate esters have been employed as novolac resin plasticizers.⁹¹ Other additives include coating and leveling agents, designed to produce striation-free films. Such agents include perfluorooctyl sulfonates.

(ix) Dissolution behavior of DNQ/novolac resists

As stated earlier, photolysis of the DNQ-sulfonate ester PAC in novolac resins increases the solubility and the rate of development of the exposed areas of the latter in the aqueous base solution used for development relative to the unexposed areas (see Figs. 7.5 and 7.6). The difference between the dissolution rate of the unexposed area and the exposed area increases with DNQ loading. Good developer discrimination between the exposed and unexposed areas in this resist system produces high-contrast, high-resolution images (see Section 7.2.1.6).

⁸⁵W.H.L. Ma, "Plasma resist image stabilization technique (PRIST) update," *Proc. SPIE* **333**, 19 (1982).

⁸⁶P.A. Ruggiero, "Positive photoresist polymerization through pulsed photomagnetic curing," *Solid State Technol.* **27**(3), 165 (1894).

⁸⁷W.S. Deforest, *Photoresist Materials and Processes*, p. 59, McGraw Hill, New York (1975).

⁸⁸M.P. Schmidt, "Process of making printing plates and light sensitive material suitable for use therein," U.S. Patent No. 3,046,118 (1962).

⁸⁹Kalle Co. AG, British Patent No. 7111,626 (1954); M.P. Schmidt, "Process of making printing plates and light sensitive material suitable for use therein," U.S. Patent No. 3,046,118 (1962).

⁹⁰T.L. Steinhoff, C. Isaacson, and G.J. Roelants, "Method of coating printed board having through holes," U.S. Patent No. 3,535,157 (1970); F. Endermann, W. Neugebauer, and M.K. Reichel, "Light sensitive omicron quinone diazides and the photomechanical preparation of printing plates therewith," U.S. Patent No. 3,148,983 (1964).

⁹¹T.L. Steinhoff, C. Isaacson, and G.J. Roelants, "Method of coating printed board having through holes," U.S. Patent No. 3,535,157 (1970).

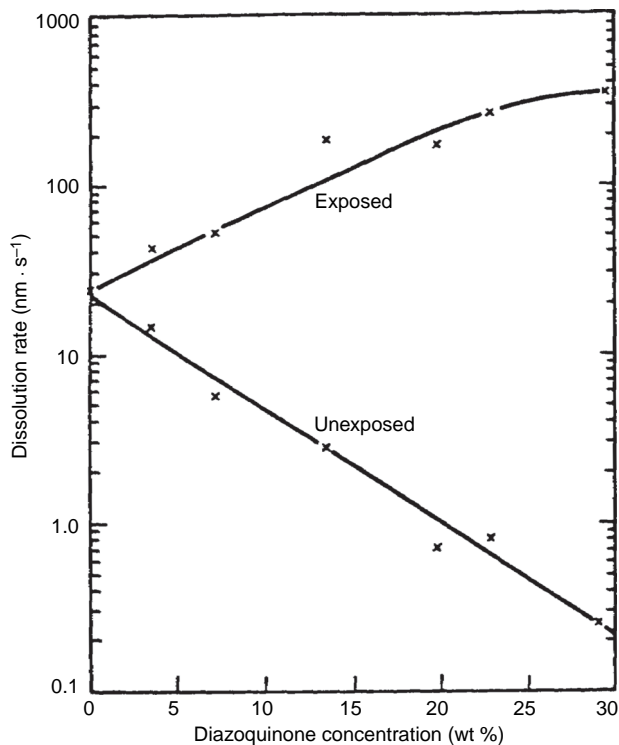


Figure 7.5 Dissolution rates of unexposed and fully exposed mixtures of DNQ and novolac as a function of DNQ loading. (Reprinted with permission from Ref. 92. © 1980 IEEE.)

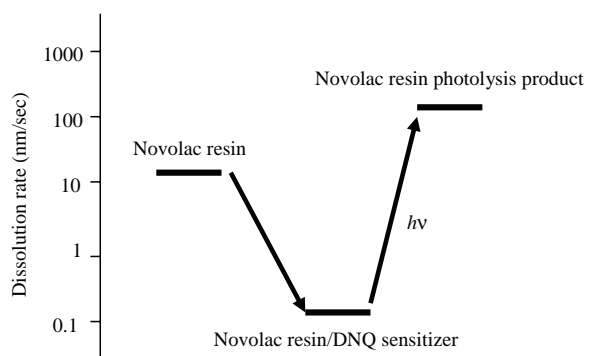


Figure 7.6 Three-level dissolution rate scheme for a commercial DNQ/novolac resist. (Reprinted with permission from Ref. 93. © 1982 Wiley-VCH Verlag GmbH & Co. KGaA.)

⁹²D. Meyerhofer, "Photosolubility of diazoquinone resists," *IEEE Trans. Electron. Dev.* **ED-27**, 921 (1980).

⁹³H. Steppan, G. Burr, and H.W. Vollman, "Resisttechnik ein Beitrag der Chemie zur Elektronik," *Angew. Chem.* **94**, 471 (1982); "The resist technique A chemical contribution to electronics," *Angew. Chem. Int. Ed. (English)* **21**, 455 (1982).

The detailed understanding of the chemical mechanism of image formation in DNQ/novolac resists continues to be an area of active research. The chemical basis of the image formation in this resist system is now generally agreed to result from large differences in the dissolution rate between the exposed and unexposed areas of the resist film. The use of the laser interferometry⁹⁴ and quartz crystal microbalance techniques⁹⁵ has established that DNQ-sulfonate is a dissolution inhibitor for novolac binder, presumably due to its hydrophobic nature. An earlier hypothesis stating that the unexposed DNQ-sulfonate in the masked areas of the resist readily couples with the novolac resin in the presence of the aqueous base to form azo dyes and that these actually inhibit the dissolution of the resin has been proven to be incorrect.⁹⁶ It is now established that the indene carboxylic acid formed from the photolysis of the DNQ-sulfonate PAC is the dissolution accelerator for the novolac binder. Therefore, this hydrophobic-to-hydrophilic switch in the resist is now the established mechanism that enables the high discrimination and high contrast obtainable in this resist system.

Experimental evidence obtained by Hinsberg and co-workers⁹⁷ suggests that the above simplistic picture may not account for all of the factors that lead to image discrimination in this resist system. In their experiment, they separately formulated the monofunctional PAC (**XIa**) and its indene carboxylic acid photoproduct, (**XIIb**), into a polymeric binder as a model resist system (Scheme 7.8). They then monitored with quartz crystal microbalance the dissolution rates of a film of the original novolac binder, the resist film before and after exposure, and the novolac film with the added acid. Table 7.2 shows the obtained results. A comparison of the dissolution rate of the unexposed resist film with the novolac film reveals the substantial inhibition effect of the dispersed DNQ-sulfonate in the film. Remarkably, the novolac film containing the externally synthesized indene carboxylic did not show a dissolution increase over the pure novolac resin itself. In contrast, the exposed resist showed an approximately 30% increase in dissolution rate over the pure novolac film that had the added externally synthesized indene carboxylic acid. The enhancement in dissolution rate was attributed to the gaseous nitrogen that is formed during the DNQ-sulfonate photolysis. The evolution of the nitrogen, the postulate goes, creates microvoids and stresses in the novolac film, which enhance the diffusion of the developer into the polymer film and lead to an increase in the dissolution rate. It should be mentioned that such a mechanism had been previously proposed for the development characteristics of poly(methyl methacrylate).⁹⁸

The role of the evolved nitrogen gas and the precise mechanism stir up heated debates and remain a subject of conjecture among researchers. The experiments by

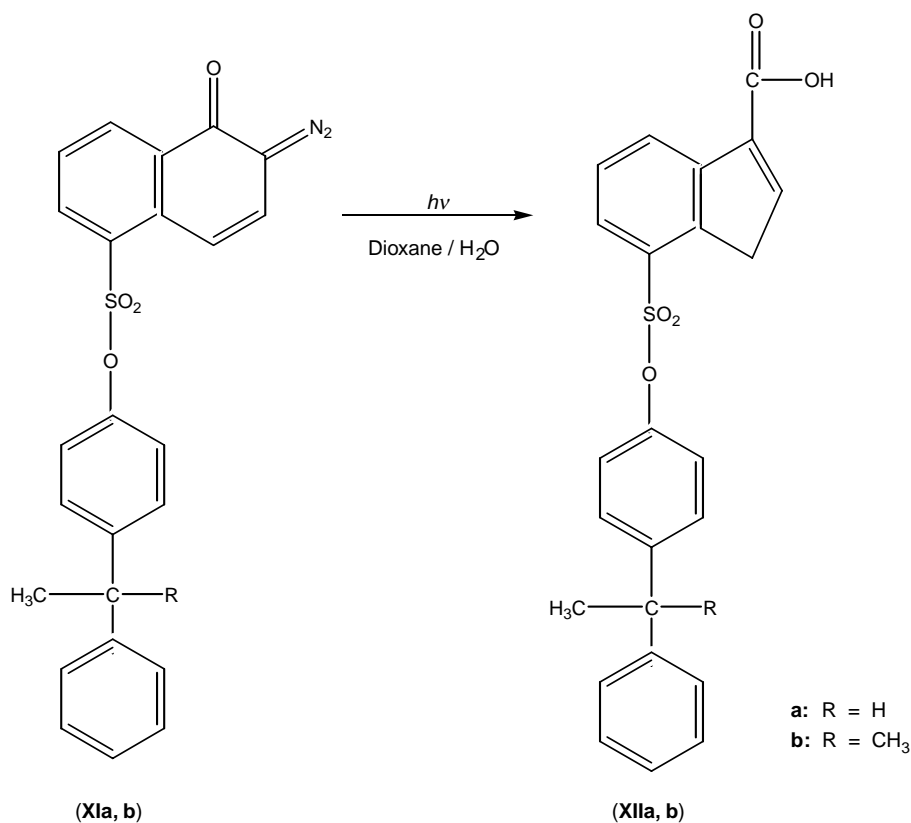
⁹⁴C.G. Willson, in *Introduction to Microlithography*, L.F. Thompson, C.G. Willson, and M.J. Bowden, Eds., pp. 152–157, American Chemical Society, Washington, DC (1994).

⁹⁵W.D. Hinsberg, C.G. Willson, and K.K. Kanazawa, "Measurement of thin film dissolution kinetics using a quartz crystal microbalance," *J. Electrochem. Soc.* **133**, 1448 (1986).

⁹⁶W.S. DeForest, *Photoresist Materials and Processes*, McGraw Hill, New York (1975).

⁹⁷W.D. Hinsberg, C.G. Willson, and K.K. Kanazawa, "Use of a quartz crystal microbalance rate monitor to examine photo product effects on resist dissolution," *Proc. SPIE* **539**, 6 (1985).

⁹⁸A.C. Ouano, in *Polymers in Electronics*, ACS Symposium Series No. 242, T. Davidson, Ed., Chapter 7, American Chemical Society, Washington, DC (1984).



Scheme 7.8 Radiation-induced generation of indene carboxylic photoproduct (**XII a,b**) from monofunctional photoactive compound (**XI a,b**).

Table 7.2 Dissolution rates of model photoresist coatings.⁹⁹

Coating	Dissolution rate ($\text{\AA}/\text{s}$) ¹⁰⁰
Novolac resin	1100
Novolac resin + XI (unexposed)	130
Novolac resin + XI (exposed)	1370
Novolac resin + XII	1000

Blum and co-workers,¹⁰¹ also involving doping novolac films with presynthesized indene carboxylic acid, confirm that the formation of the indene carboxylic acid is the important step leading to the dissolution rate enhancement in the exposed resist. In Blum's experiment, the novolac resin dissolved about five times more slowly

⁹⁹W.D. Hinsberg, C.G. Willson, and K.K. Kanazawa, "Use of a quartz crystal microbalance rate monitor to examine photo product effects on resist dissolution," *Proc. SPIE* **539**, 6 (1985).

¹⁰⁰These values were obtained by quartz crystal microbalance technique.

¹⁰¹L. Blum, M.E. Perkins, and A.W. McCullough, "Dissolution kinetics of a photoresist using organic acids to simulate exposed photoactive compounds," *Proc. SPIE* **771**, 148 (1987).

(as determined by laser interferometry) than that used in the previous Hinsberg's experiment (see Table 7.3). The dissolution rate of the unexposed resist with the DNQ-sulfonate PAC was determined to be 11 Å/s, whereas that of the fully exposed resist was 640 Å/s, corresponding to a nearly 60-fold increase between the exposed and unexposed film, and which is in agreement with other published results.¹⁰² Remarkably and in contrast to the results of Hinsberg et al.,¹⁰³ doping the novoac resin with the presynthesized indene carboxylic acid (**XIb**) produced a dissolution rate of 2650 Å/s, leading the authors to draw the following two conclusions. First, they believe that the evolution of nitrogen plays an insignificant role in the DNQ-sulfonate/novolac resist dissolution mechanism. Second, they believe that only about half of the PAC is photolyzed to carboxylic acid in the fully exposed resist, given that the dissolution rate is about four times slower than that of the novolac doped with presynthesized acid concentration (which is equivalent to 100% conversion of the DNQ-sulfonate PAC to acid). They proposed that the other half of the PAC couples with the polymeric phenol through the ketene to form an ester pendant to the novolac.

Table 7.3 Dissolution rates of model photoresist coatings.¹⁰⁴

Coating	Dissolution rate (Å/s) ¹⁰⁵
Novolac resin	185
Novolac resin + XI (unexposed)	11
Novolac resin + XI (exposed)	640
Novolac resin + XII	2650

The proposal of Blum et al.¹⁰⁶ appears to contradict the results of yet another group of researchers, namely, Daly and co-workers,¹⁰⁷ who used Fourier transform infrared (FTIR) spectroscopy to directly follow the formation of the ketene from the DNQ-sulfonate PAC photolysis in the novolac matrix. Under ambient conditions, they found that the ketene appeared to react quickly with water in the film to form indene carboxylic acid. Under dry conditions, with water excluded, however, the ketene appeared to be quite remarkably stable. Although the above experiments were qualitative in approach, they do indicate that the ketene reaction

¹⁰²R.C. Daly, T. DoMihn, R.A. Arcus, and M.J. Hanrahan, in *Polymers for High Technology*, ACS Symposium Series No. 346, M.J. Bowden and S.R. Turner, Eds., p. 237, American Chemical Society, Washington, DC (1987).

¹⁰³W.D. Hinsberg, C.G. Willson, and K.K. Kanazawa, "Use of a quartz crystal microbalance rate monitor to examine photo product effects on resist dissolution," *Proc. SPIE* **539**, 6 (1985).

¹⁰⁴L. Blum, M.E. Perkins, and A.W. McCullough, "Dissolution kinetics of a photoresist using organic acids to simulate exposed photoactive compounds," *Proc. SPIE* **771**, 148 (1987).

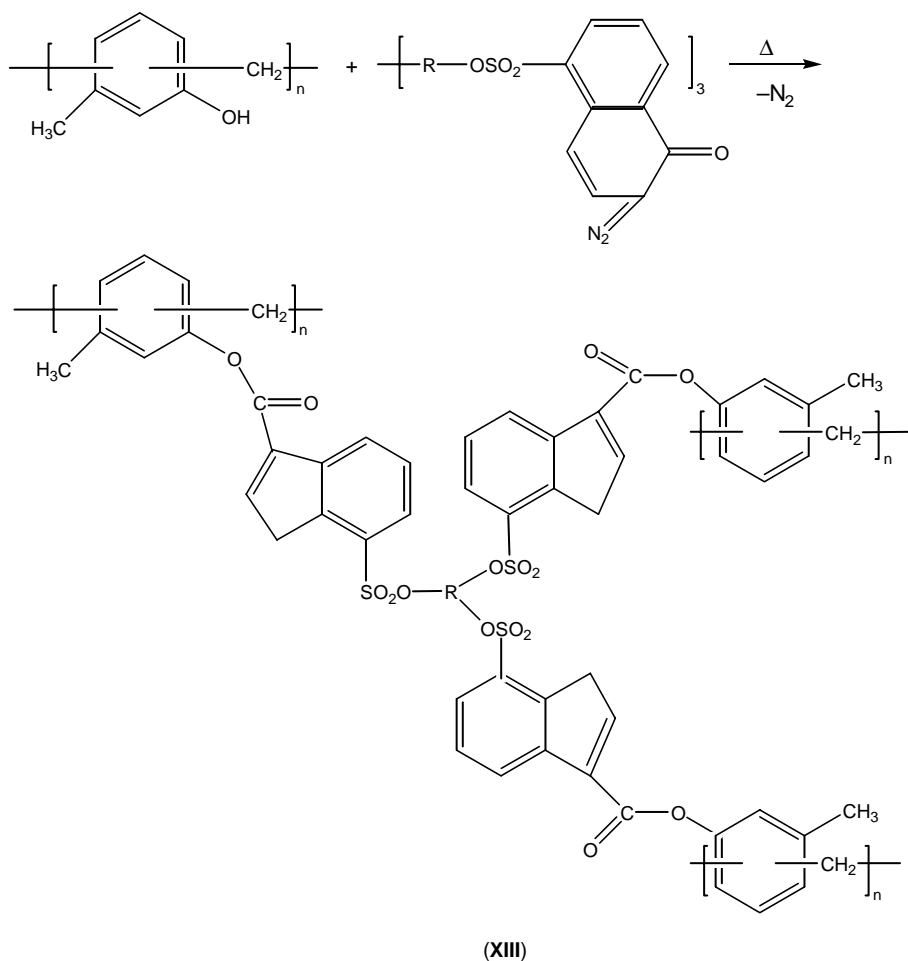
¹⁰⁵These values were obtained by laser interferometry technique.

¹⁰⁶L. Blum, M.E. Perkins, and A.W. McCullough, "Dissolution kinetics of a photoresist using organic acids to simulate exposed photoactive compounds," *Proc. SPIE* **771**, 148 (1987).

¹⁰⁷R.C. Daly, T. DoMihn, R.A. Arcus, and M.J. Hanrahan, in *Polymers for High Technology*, ACS Symposium Series No. 346, M.J. Bowden and S.R. Turner, Eds., p. 237 American Chemical Society, Washington, DC (1987).

with the polymeric phenol group is quite slow in comparison to the reaction with water. It must be emphasized that the conflicting picture painted by the above results indicates that the exact details of the image discrimination are not yet fully and satisfactorily resolved, despite the intense research interest in this technologically important group of resists.

One other important role the DNQ-sulfonate PAC plays, besides its primary role in image formation and development, relates to its contribution to enhanced image stability during the image transfer step in the microlithographic process. In normal processing, after the development step, the resist is hard baked at around 130°C for about 30 minutes to “harden” the novolac image. At this high temperature, the DNQ-sulfonate PAC is decomposed to ketene, with a large portion of it reacting with the phenolic groups in the novolac resin to form ester linkages (see Scheme 7.9). For multifunctional DNQ-sulfonate PACs, this esterification reaction leads to a cross-linked network (**XIII**) in the image area, which



Scheme 7.9 Cross-linking reaction scheme of novolac.

enhances the thermal flow stability of the resist film. This enhanced thermal stability in turn improves the performance of these hardened features in subsequent image transfer steps such as ion implantation and plasma etching by keeping the image from flowing or distorting at elevated temperatures.

(x) Resolution capability of DNQ/novolac resists

Figures 7.7 and 7.8 show the high-contrast and high-resolution capability, as well as the linearity plot, respectively, of a DNQ/novolac resist system.

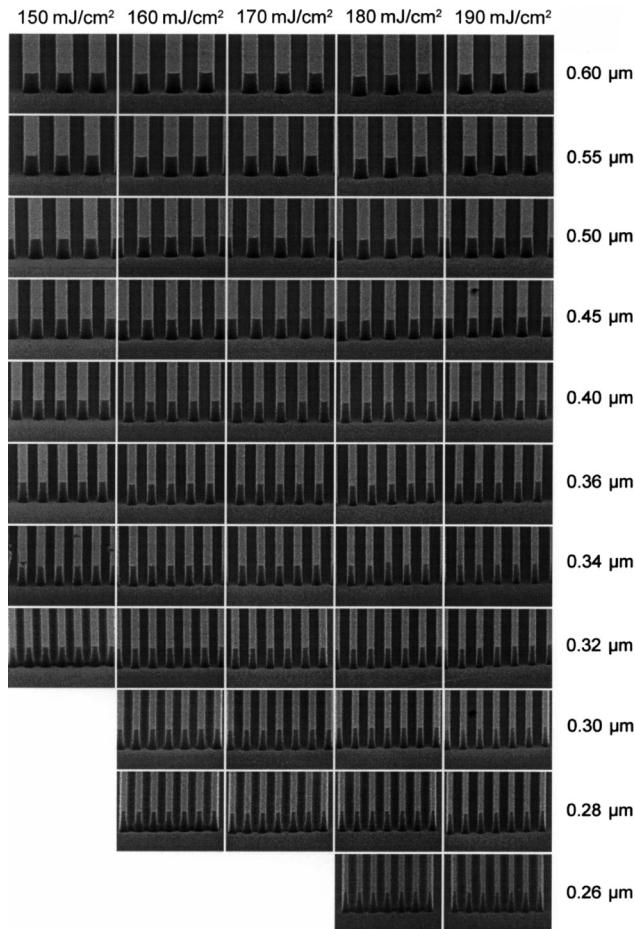


Figure 7.7 SEM of high-resolution images printed in AZ 7900 (DNQ-sulfonate/novolac positive i-line resist). Processing conditions: resist thickness 0.748 μm , BARC (BARLi) thickness 1920 \AA , soft bake at 90°C for 90 s, exposure tool Canon 3000i4, NA 0.63, sigma 0.65, PEB 110°C for 60-s, 64 s single puddle NMD-W developer at 20.5°C. (Courtesy of R. Dammel.¹⁰⁸)

¹⁰⁸R. Dammel, "Diazonaphthoquinone based resists," SPIE Short Course No. SC104 (2003).

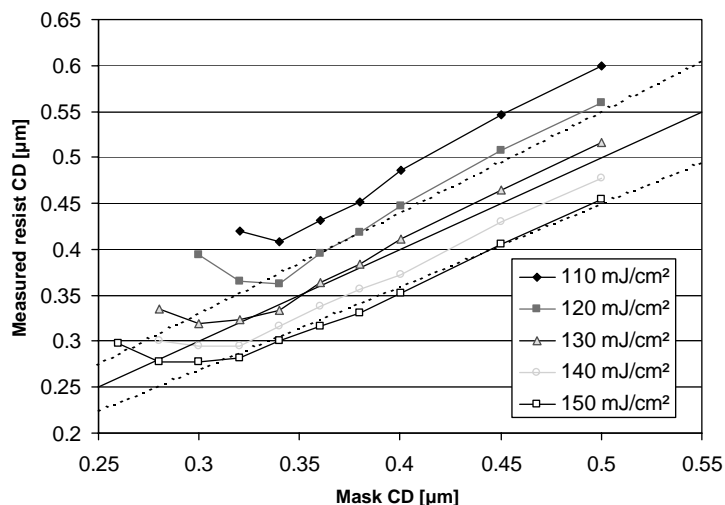


Figure 7.8 Linearity plot of features printed on AZ 7900 (DNQ-sulfonate/novolac positive i-line resist). (After R. Dammel.¹⁰⁹)

(xi) Post-DNQ/novolac resists

(a) DUV 248-nm resists

By the early 1990s, resolution requirements for printing device critical dimensions $\leq 0.25 \mu\text{m}$ mandated the switch to different classes of resist materials from the DNQ/novolac systems, with sensitivities to the DUV region of the spectrum. Research interest on DUV resists¹¹⁰ was inspired by a much earlier report¹¹¹ that showed that it is possible to print images in poly(methyl methacrylate) at 254 nm. Influenced by this report, a number of attempts were made by different groups to develop materials based on acrylates and vinyl ketones. Tokyo Ohka Kogyo (TOK) was the first resist supplier to market a commercial DUV resist, which was based on poly(methylisopropenyl ketone). They sold it under the

¹⁰⁹ibid.

¹¹⁰For excellent reviews on the history of DUV resists, see, for example, *Introduction to Microlithography* L.F. Thompson, C.G. Willson, and M.J. Bowden, Eds., American Chemical Society, Washington, D.C. (1994); *Radiation Curing in Polymer Science and Technology*, J. Fouassier and J. Rabe, Eds., Elsevier, London (1993); T. Iwayanagi, T. Ueno, S. Nonogaki, H. Ito, and C.G. Willson, in *Electronic and Photonic Applications of Polymers*, J.J. Bowden and S.A.R. Turner, Eds., ACS Advances in Chemistry Series 218, American Chemical Society, Washington, DC (1988); S.A. MacDonald, C.G. Willson, and J.M.J. Fréchet, "Chemical amplification in high resolution imaging systems," *Acc. Chem. Res.* **27**, 151 (1994); E. Reichmanis and L.F. Thompson, "Polymer materials for microlithography," *Chem. Rev.* **89**, 1273 (1989).

¹¹¹W.M. Moreau and R.R. Schmidt, "Photoresist for high resolution proximity printing," Extended Abstract 187, presented at 138th Electrochemical Society Meeting, Electrochemical Society, Pennington, NY (1970).

brand name of ODUR 10XX. Other remarkable approaches to the design of DUV resists were based on 1,3-diacyl-2-diazocompounds¹¹² and ortho nitrobenzylesters of carboxylic acids.¹¹³

It must be mentioned that these early DUV resists were not sensitive enough to be successfully imaged with the Perkin Elmer 500 Micrascan exposure tools, the first production-worthy exposure tools capable of DUV projection printing. These Perkin Elmer 500 exposure tools, equipped with high-pressure Hg lamps in their illuminators, generated less than 10% as much power in the DUV (240–260-nm or UV-2 mode) as they do in the near-UV (350–450-nm or UV-4 mode). This meant that DUV resists designed to be used in this tool must have an order-of-magnitude-higher sensitivity than the DNQ/novolac resists to ensure an acceptable level of productivity. This situation was the impetus that led to the design and development of “chemically amplified” resists¹¹⁴ for DUV 248-nm (KrF laser) lithography (see below).

As different resist platforms were investigated and evaluated for use in KrF lithography, the poly(hydroxy styrene) resist platform emerged as the most dominant because of some inherent advantages in terms of transparency (see Fig. 7.9), sensitivity, etch resistance, etc. It was in fact the resist platform used to pattern critical layers in the device technology nodes of 250 nm, 180 nm, and 130 nm. Unfortunately, the resolution requirements of device technology nodes ≤ 90 nm mandated the shift to the next lithographic wavelength at 193 nm, based on ArF lithography.

(b) Deep-UV 193-nm resists

The road to finding materials that could be used for imaging applications at 193 nm was fraught with difficult challenges. First, the pool of available materials is very limited, given that the aromatic polymers that have worked so well as resist resins in the 365-nm and 248-nm lithographic regimes are opaque at 193 nm—a consequence of the strong π - π^* electronic transition¹¹⁵ in that spectral region (see Fig. 7.9). Furthermore, the etch rate scales linearly with the carbon/hydrogen ratio,¹¹⁶ which favors the use of aromatics as well. Thus, for a while, it appeared that nature had conspired against the development of single-layer resist materials for ArF lithography.

¹¹²B.D. Grant, N.J. Clecak, R.J. Tweig, and C.G. Willson, “Deep UV photoresists I. Meldrum’s diazo sensitizer,” *IEEE Trans. Electron Devices* **ED-28**(11), 1300 (1981).

¹¹³E. Reichmanis, C.W. Wilkins, Jr., and E.A. Chandross, “A novel approach to o nitrobenzyl photo chemistry for resists,” *J. Vac. Sci. Technol.* **19**(4), 1338 (1981).

¹¹⁴H. Ito, C.G. Willson, and J.M.J. Fréchet, “New UV resists with negative or positive tone,” *Digest of Technical Papers, 1982 SPE Symp. on VLSI Technology*, p. 6 (1982); C.G. Willson, H. Ito, J.M.J. Fréchet, T.G. Tessier, and F.M. Houlihan, “Approaches toward the design of radiation sensitive polymeric imaging systems with improved sensitivity and resolution,” *J. Electrochem. Soc.* **133**, 181 (1986).

¹¹⁵R.M. Silverstein, G.C. Bassler, and T.C. Morrill, *Spectrometric Identification of Organic Compounds*, 4th ed., pp. 311–315, John Wiley & Sons, Hoboken, NJ (1981).

¹¹⁶H. Gokan, S. Esho, and Y. Ohnishi, “Dry etch resistance of organic materials,” *J. Electrochem. Soc.: Sol. State Sci. Technol.* **130**, 143 (1983).

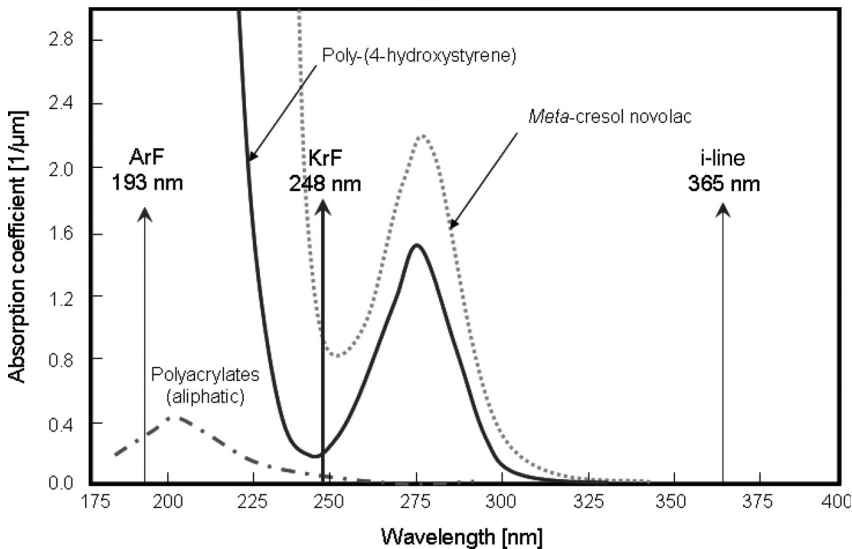


Figure 7.9 Absorption spectrum of different polymers used in ArF, KrF, and i-line lithographies. (After R. Dammal.¹¹⁷)

In addition to possessing high transparency at 193 nm and having high dry etch resistance (at least comparable to novolac-based resist systems), such resists must possess high sensitivity, fast photospeed, long process time delay latitude, good adhesion to silicon wafer substrates, and compatibility with the industry standard 2.38 wt% tetramethylammonium hydroxide developer solution. The very stringent nature of these requirements is connected with a significant number of process-related issues, particularly for the bulk-imaged (single-layer) 193-nm resist systems. A highly sensitive resist ($<10 \text{ mJ/cm}^2$) is required in order to protect the lens of the stepper from radiation damage from the strong 193-nm radiation. A resist with long process time delay latitude will have low sensitivity to environmental base contamination. Such a resist will therefore not be prone to T-topping and the consequent pattern deterioration problem. A resist with good adhesion to silicon wafer substrates is needed to prevent features from being blown away or collapsing during processing. This is a problem that becomes particularly acute as pattern sizes become smaller and the contact area of patterns to the substrate decreases, thereby increasing the capillary forces between the lines, and leading ultimately to pattern collapse. Thus, issues of sustainable aspect ratio and transparency place limitations on the imageable thickness for bulk-imaged ArF resist systems, so much so that the resist thickness approaches the total focal plane depth of the exposure optics, thereby reducing the process depth of focus to values that are impracticably small in a manufacturing environment.

Remarkably, regardless of the resist technology approach used, it should be mentioned that the imaging mechanisms of resists for ArF lithography use

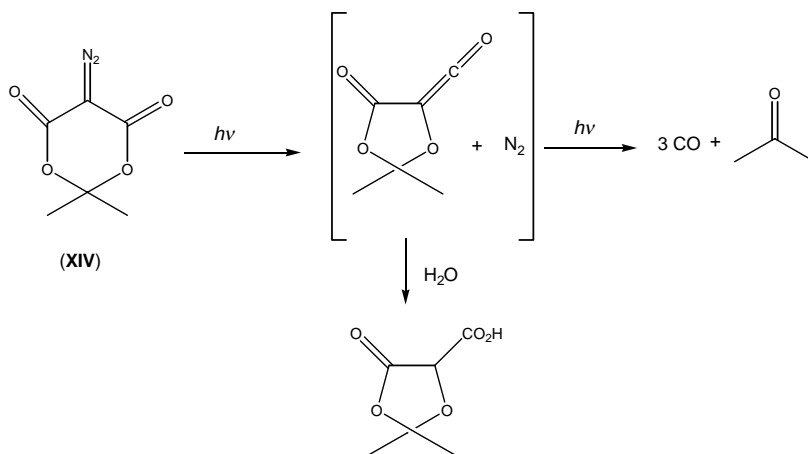
¹¹⁷R. Dammal, "Diazonaphthoquinone based resists," SPIE Short Course No. SC104 (2003).

chemically amplified deprotection chemistry.¹¹⁸ This suggests that the vast knowledge base generated with resists for KrF lithography was directly applied to the design and optimization of resist materials for ArF lithography, although some parameters such as balance of lipophilicity and hydrophobicity were more difficult to control in some of the 193-nm resist platforms relative to those of 248-nm resists.

In the following section, we consider in depth the chemistry governing the main platforms of single-layer resists designed for DUV 248-nm and DUV 193-nm, VUV (157-nm), and EUV (13.5-nm) lithographies, and as well as those for x-ray and charged particle (electron-beam and ion-beam) lithographies. Because some of these resist platforms have sensitivities to a broad spectrum of lithographic exposure radiations, the treatment here is organized around specific chemical functionalities and properties that are common to each resist platform and that determine its imaging mechanism and thus its lithographic usage. So, contrary to the standard method of organizing resists on the basis of their exposure sources such as “248-nm resists” or “x-ray resists,” we will here, where necessary, discuss the lithographic application of each resist type in the overall treatment of the chemistry of the main resist platforms.

7.2.1.1.1.2 DIAZO-MELDRUM'S ACID-BASED RESISTS

Resists with diazo-Meldrum's acid, like their DNQ counterparts, are based on the principle of transformation (or removal) of a dissolution inhibitor by a photoreaction. The photolabile inhibitor itself, diazo-Meldrum's acid, behaves like diazoquinone in that when formulated with novolac, it can inhibit the base solubility of the latter. On irradiation, it decomposes according to Scheme 7.10,¹¹⁹ forming an acid, which accelerates the dissolution of novolac in aqueous base.



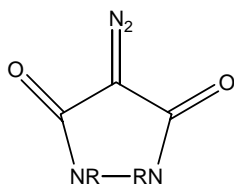
Scheme 7.10 Photodecomposition of diazo-Meldrum's acid.

¹¹⁸H. Ito and C.G. Willson, “Chemical amplification in the design of dry developing resist materials,” *Technical Papers of SPE Regional Technical Conference on Photopolymers*, p. 331, Society of Plastics Engineers, Brookfield, CT (1982).

¹¹⁹A. Reiser, *Photoreactive Polymers: The Science and Technology of Resists*, p. 262, John Wiley & Sons, Hoboken, NJ (1989).

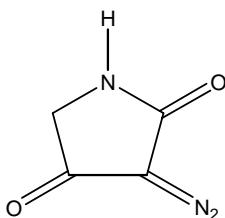
With an absorption peak almost exactly at 250 nm, and an ability to be bleached on irradiation, this sensitizer when formulated with suitable novolac resin makes an optically ideal resist for DUV exposure. Its reported sensitivity ($\sim 50 \text{ mJ/cm}^2$) compares favorably with the sensitivity of conventional DNQ/novolac resists ($\sim 100 \text{ mJ/cm}^2$).¹²⁰

Diazo-Meldrum's acid does have one serious drawback: it sublimates out of the coating during the prebake step. Enormous efforts were made with a view to finding related chromophores that do not sublime. Successful candidates include diazopyrazolidine dione (DPD) (XIV), diazotetramic acid (XV), and diazopiperidine dione (XVI).¹²¹



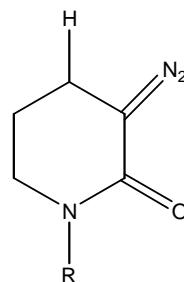
Diazopyrazolidine dione

(XIV)



Diazotetramic acid

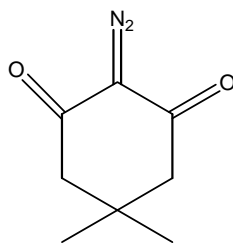
(XV)



Diazopiperidine dione

(XVI)

It has also been reported that the replacement of the lactone link (in diazo-Meldrum's acid) by a lactam improves hydrogen bonding in the acidic resin and lowers its vapor pressure.¹²² Furthermore, Schwarzkopf¹²³ has reported the synthetic route to 2-diazodimedones (XVII), which are highly photoreactive and which do not sublime at bake temperatures below 95°C .¹²⁴



2-Diazodimedones (XVII)

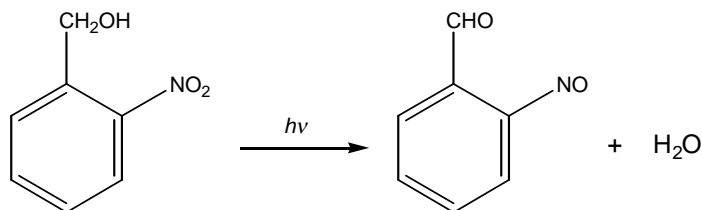
¹²⁰ibid.¹²¹ibid.¹²²For other thermally stable dissolution inhibitors based on diazo Meldrum's acid, see, for example, S.R. Turner, K.D. McKean, and L.A. Pedersen, "Thermally stable, deep UV resist materials," ACS Symposium Series 346, p. 200, American Chemical Society, Washington, DC (1987).¹²³G. Schwarzkopf, "New 2 diazocyclohexane 1,3 dione photoactive compounds for deep UV lithography," *Proc. SPIE* **920**, 7 (1988).¹²⁴A. Reiser, *Photoreactive Polymers: The Science and Technology of Resists*, p. 264, John Wiley & Sons, Hoboken, NJ (1989).

7.2.1.1.1.3 RESISTS BASED ON ORTHO-NITROBENZYL CHEMISTRY

Ortho-Nitrobenzyl photochemistry is the basis for another inhibition approach to designing and making several interesting DUV resists.¹²⁵ It derives from the intermolecular photo-oxidation by an *ortho*-nitro group in *o*-nitrotoluene and its derivatives, which was first reported by Ciamician and Silber in 1901¹²⁶ and rediscovered by Patchornik in 1973.¹²⁷ This reaction can lead to large changes in solubility between the exposed and unexposed parts of the resist film (Scheme 7.11).¹²⁸

Barzynski and Saenger¹²⁹ utilized this reaction to photochemically change the polarity of a compound by deprotecting a protective side group and exposing a free carboxylic acid, as illustrated in Scheme 7.12. While the unexposed polymer is soluble in common organic solvents, but not soluble in water, the exposed resist dissolves in dilute alkali due to the free carboxyl groups. In this system, it should be mentioned that image discrimination is not based on kinetics, but on a thermodynamic difference that involves the change from a truly insoluble substance to one that is soluble.¹³⁰

Another interesting variation on the application of *o*-nitrobenzyl chemistry in imaging application was reported by Reichmanis et al.¹³¹ The idea behind their approach is based on the fact that resist contrast (the change in film thickness corresponding to a small change in radiation dose) is dependent on the molar volume of the inhibitor that can be made hydrophilic by a single photon. So, by designing a dissolution inhibitor with a very large protecting group such as substituted cholic



Scheme 7.11 Photoinduced solubility change of *o*-nitrobenzyl ester.

¹²⁵E. Reichmanis, C.W. Wilkens, Jr., and E.A. Chandross, "A novel approach to *o* nitrobenzyl photo chemistry for resists," *J. Vac. Sci. Technol.* **19**, 1338 (1981); E. Reichmanis, R. Gooden, C.W. Wilkens, Jr., and H. Schonhorn, "A study of the photochemical response of *o* nitrobenzyl cholate derivatives in P(MMA MAA) matrices," *Polym. Sci. Poly. Chem. Ed.* **21**, 1075 (1983).

¹²⁶G. Ciamician and P. Silber, "Ciamician photodisproportionation," *Ber.* **34**, 2040 (1901).

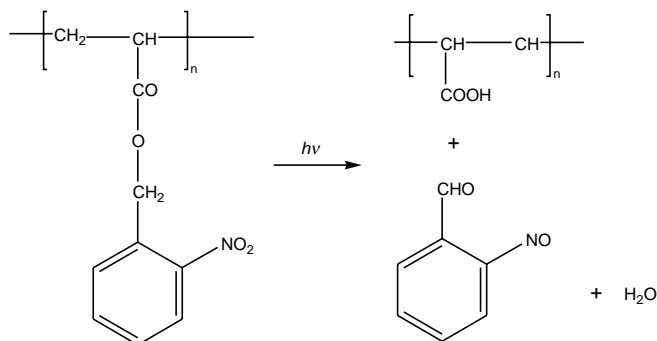
¹²⁷B. Amit and A. Patchornik, *Tetrahedron Lett.*, "The photorearrangement of *N* substituted *ortho* nitro anilides and nitroveratramides. A potential photosensitive protecting group," p. 2205 (1973); A. Amit, U. Zehavi, and A. Patchornik, "Photosensitive protecting groups a review," *Isr. J. Chem.* **12**, 103 (1974).

¹²⁸A. Reiser, *Photoreactive Polymers: The Science and Technology of Resists*, p. 264, John Wiley & Sons, Hoboken, NJ (1989).

¹²⁹H. Barzynski and D. Saenger, "Zur Photolyse von makromolekularen *o* Nitrobenzylderivaten," *Angew. Makromol. Chem.* **93**, 131 (1981).

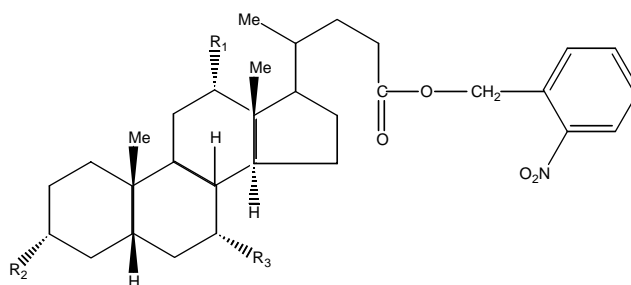
¹³⁰A. Reiser, *Photoreactive Polymers: The Science and Technology of Resists*, pp. 264-265, John Wiley & Sons, Hoboken, NJ (1989).

¹³¹E. Reichmanis, C.W. Wilkens, Jr., and E.A. Chandross, "A novel approach to *o* nitrobenzyl photo chemistry for resists," *J. Vac. Sci. Technol.* **19**, 1338 (1981).



Scheme 7.12 Photo-induced deprotection that leads to polarity change of a nitrobenzyl ester-functionalized acrylate polymer.

acids (XVIII) that could be deprotected via photoinduced *o*-nitrobenzyl reaction, they were able to realize lithographic imaging in these inhibitors in matrices of novolac resins (constituting 20 wt% of inhibitor) or with copolymers of methyl methacrylate and methacrylic acid (7:1). In these resists, the polymer binders are base soluble, and the dissolution inhibitor is the *o*-nitrobenzyl ester of substituted cholic acids. On exposure, the ester cleaves to produce products, which accelerates the resin's dissolution. These resists have demonstrated good absorption in the vicinity of 250 nm (DUV) and sensitivity comparable to that of diazoquinone resists ($\sim 100 \text{ mJ/cm}^2$).¹³²



1. (a) $R_1, R_2, R_3 = \text{OH}$

(b) $R_1, R_2 = \text{OH}, R_3 = \text{H}$

(c) $R_1, R_3 = \text{H}, R_2 = \text{OH}$

(d) $R_1, R_2, R_3 = \text{H}$

2. (a) $R_1, R_2, R_3 = \text{OSi}(\text{CH}_3)_3$

(b) $R_1, R_2, R_3 = \text{O}=\text{C}-\text{CF}_3$

(c) $R_1, R_2, R_3 = \text{O}=\text{C}-\text{C}(\text{CH}_3)_3$

(b) $R_1, R_2, R_3 = \text{O}=\text{C}-\text{CH}_3$

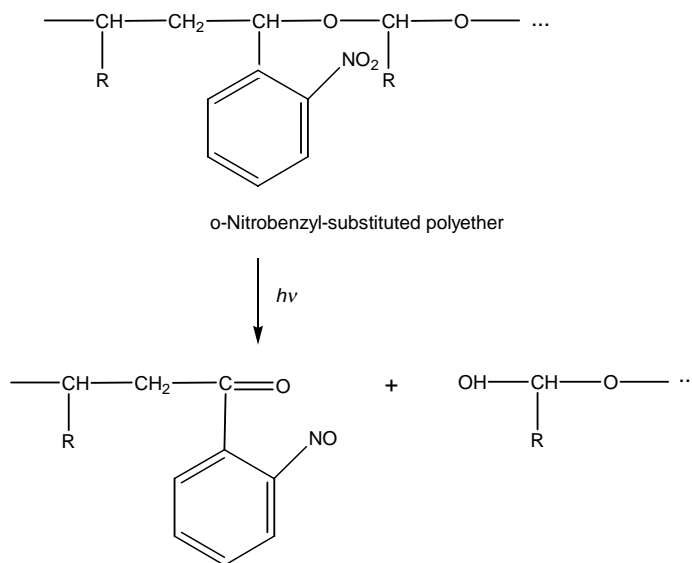
(XVIII)

¹³²A. Reiser, *Photoreactive Polymers: The Science and Technology of Resists*, p. 265, John Wiley & Sons, Hoboken, NJ (1989).

One other interesting variation on the use of *o*-nitrobenzyl chemistry in lithographic imaging applications involves the DUV photoinduced backbone fragmentation of *o*-nitrobenzyl-substituted polyether; this leads to the lowering of the molecular weight of the polymer sufficiently to enhance the solubility of the exposed part of the resist (Scheme 7.13).¹³³

Similar results involving backbone scission have also been obtained when the *o*-nitrobenzyl reaction is applied to a group of poly(N-alkyl-*o*-nitroamides), such as the *m*-poly(nitroanilide) (see Scheme 7.14).¹³⁴ In this system, the solubility switch is caused by two effects involving the lowering of the molecular weight due to backbone scission and by the generation of a free acid group on half of the fragments. This allows development of the resist in dilute alkali. Resist sensitivity in this system comparable to that of conventional diazoquinone resists ($\sim 100 \text{ mJ/cm}^2$) has been demonstrated.¹³⁵

And finally, *o*-nitrobenzyl chemistry has been demonstrated by Houlihan et al.¹³⁶ to be effective in uncoupling *p*-toluenesulfonic acid from its *ortho* nitrobenzyl ester (see scheme 7.15), which in turn is used to catalyze the



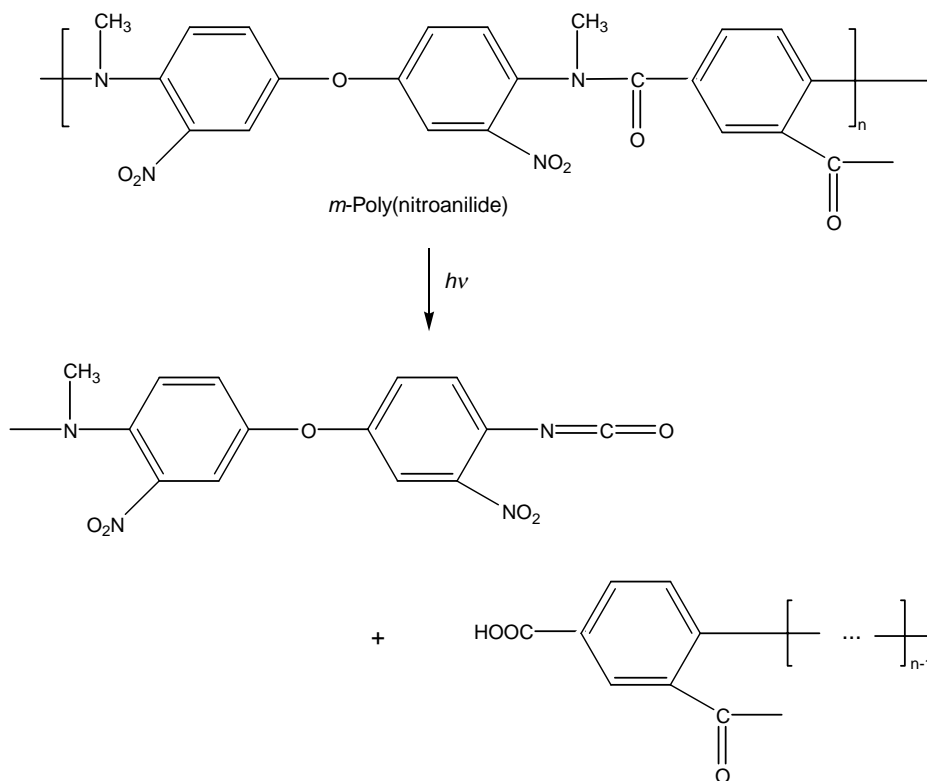
Scheme 7.13 Photo-induced backbone fragmentation of *o*-nitrobenzyl-substituted polyether.

¹³³C.C. Petropoulos, "Synthesis of novel photodegradable poly(*o* nitrobenzaldehyde acetal) polymers," *J. Polym. Sci., Polym. Chem. Ed.* **15**, 1637 (1977).

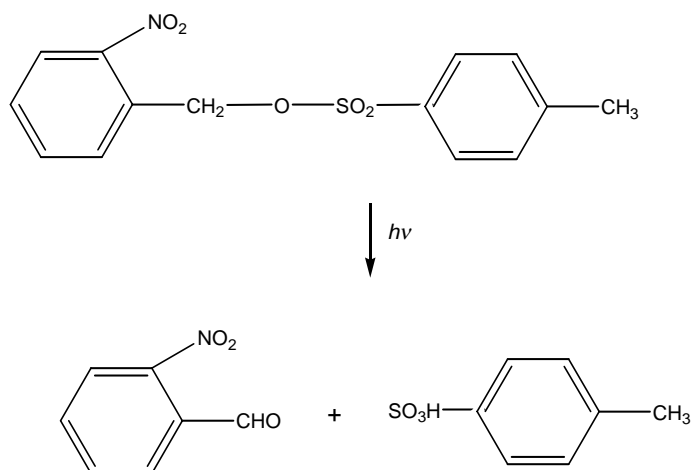
¹³⁴S.A. Macdonald and C.G. Willson, "Poly(N alkyl *o* nitroamides): A new class of thermally stable photosensitive polymers," in *Polymer Materials for Electronic Applications, ACS Symposium Series 184*, E.D. Feit and C. Wilkins, Jr., Eds., American Chemical Society, Washington, D.C., pp. 73–82 (1982).

¹³⁵A. Reiser, *Photoreactive Polymers: The Science and Technology of Resists*, p. 267, John Wiley & Sons, Hoboken, NJ (1989).

¹³⁶F.M. Houlihan, A. Shugard, R. Gooden, and E. Reichmanis, "An evaluation of nitrobenzyl ester chemistry for chemical amplification resists," *Proc. SPIE* **920**, 9 (1988).



Scheme 7.14 Photo-induced backbone scission of *m*-poly(nitroanilide).



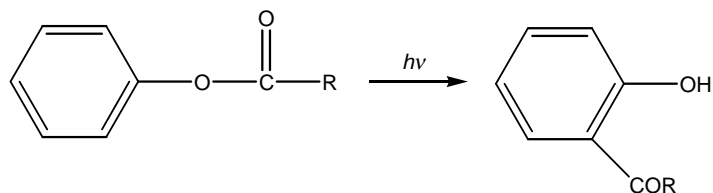
Scheme 7.15 Photo-induced uncoupling of *p*-toluenesulfonic acid from *ortho*-nitrobenzyl ester.

deprotection of poly(*tert*-butoxycarbonyloxystyrene) (PBOCST) resin, in yet another example of image discrimination based on polarity switch.

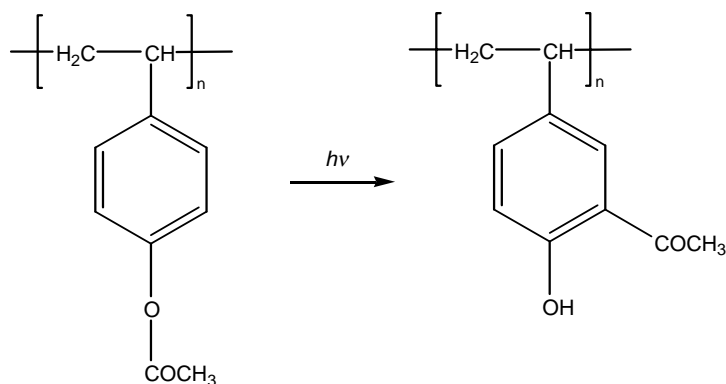
7.2.1.1.1.4 RESISTS BASED ON PHOTO-FRIESS REARRANGEMENT

Photo-Friess rearrangement is another mechanism that can be used to produce polarity changes in resist polymers. It is a photoreaction whereby the acid component of a phenolic ester or amide migrates to a position vicinal (or *ortho*) to the hydroxyl group (Scheme 7.16).¹³⁷

Tessier and co-workers have employed this reaction on derivatives of *p*-hydroxystyrene, such as poly(*p*-acetoxystyrene) and others. As shown in Scheme 7.17, the reaction uncovers the hydroxyl groups of the poly(vinyl phenol), thus making the exposed polymer soluble in alkali, or insoluble in common organic solvents, and can be used as a positive or a negative resist, depending on the developers. It should be pointed out that although poly(*p*-acetoxystyrene) is fairly insensitive, its homolog, poly(*p*-formylstyrene), has demonstrated reasonable speed (70 mJ/cm²) and good contrast.¹³⁸



Scheme 7.16 Photo-Friess rearrangement involving the photo-induced migration of the acid component of a phenolic ester to a position vicinal to the hydroxyl group.



Scheme 7.17 Photo-Friess rearrangement reaction of poly(*p*-acetoxystyrene) resulting in the formation of functionalized poly(vinyl phenol).

¹³⁷A. Reiser, *Photoreactive Polymers: The Science and Technology of Resists*, p. 268, John Wiley & Sons, Hoboken, NJ (1989).

¹³⁸*ibid.*

7.2.1.2 Non-chemically amplified positive resists based on main chain scission

Short-wavelength radiation emanating from the DUV region (<250 nm) to the x-ray region (0.1–10 nm) of the electromagnetic spectrum, as well as charged particles such as electron and ion beams, possess energy in excess of the binding energy of common C—C bonds¹³⁹ in resists (3.6 eV). Consequently, the interaction of these short-wavelength radiations and charged particles can lead directly to the scission of C—C bonds and to the formation of carbon-centered radicals, which is a characteristic of radiation chemistry (see Chapter 8). In particular, lithographic exposures utilizing DUV radiations (248 nm and 193 nm), VUV radiation (157 nm), EUV radiation (13.4 nm), x rays, electron beams, and ion beams can lead to the degradation of the resist polymer backbone and bring about a change in solubility by lowering the molecular weight. In this section, we review resists based on main chain scission events.

7.2.1.2.1 Resists based on poly(methyl methacrylate) and its derivatives

Poly(methyl methacrylate) (PMMA) is the most commonly used, studied, and best understood resist for exposures with ionizing radiations (x rays, electron beams, and ion beams), as well as DUV photons. It has many excellent lithographic properties, including the fact that it forms clear, pinhole-free thick films of moderate thickness that adhere well to many substrates, it has been shown to provide excellent resolution that is among the highest of any resist for any lithographic application, and it is easily and cleanly processed.¹⁴⁰ In particular, it has been the starting point in the development of electron-beam and DUV resists designed for mask-making and device fabrication since its initial use in the late 1960s.¹⁴¹ The resist is typically formulated in ketonic solvents or in cellosolve acetate, and after exposure, it is developed in 2-ethoxyethanol or in a mixture of 2-ethoxyethanol and ethanol.¹⁴²

It undergoes backbone scission as a secondary process following the cleavage of a C—C bond adjacent to carbonyl, in a Norrish-type I process as shown in Scheme 7.18.¹⁴³

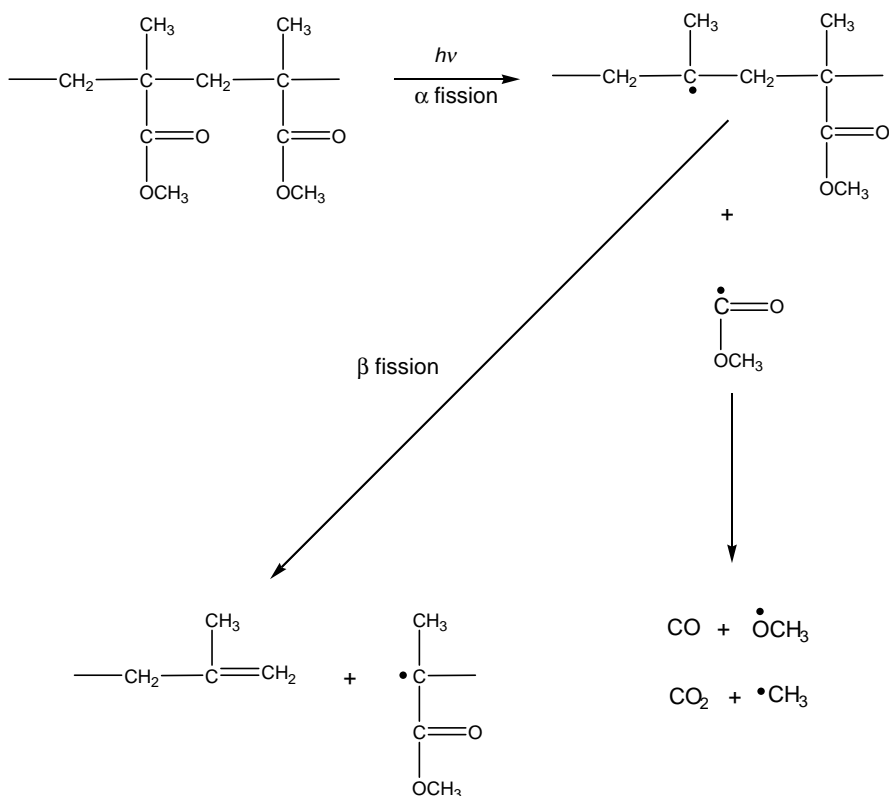
¹³⁹D.P. Shoemaker, C.W. Garland, and J.W. Nibler, *Experiments in Physical Chemistry*, p. 161, 6th ed., McGraw Hill, New York (1996).

¹⁴⁰I. Haller, M. Hatzakis, and R. Srinivasan, "High resolution positive resist for electron beam exposure," *IBM. J. Res. Dev.* **12**, 251 (1968); M. Hatzakis, "Electron resists for microcircuit and mask production," *J. Electrochem. Soc.* **116**, 1033 (1969).

¹⁴¹I. Haller, M. Hatzakis, and R. Srinivasan, *IBM. J. Res. Dev.* **12**, 251 (1968); K. Harada, T. Tamamura, and O. Kogure, "Detailed contrast (γ value) measurements of positive electron resists," *J. Electrochem. Soc.* **129**, 2576 (1982); M. Kakuchi, V.S. Sugawara, K. Murase, and K. Matsuyama, "Poly (fluoro methacrylate) as highly sensitive, high contrast positive resist," *J. Electrochem. Soc.* **128**, 1759 (1977).

¹⁴²K. Mochiji et al. "Negative patterning of AZ1350J by electron beam desensitization of photo sensitive compound," *Jpn. J. Appl. Phys.* **20**(Suppl. 20 1), 63 (1981); T.D. Berker, "The use of photo resists as negative electron resists," *Proc. SPIE* **469**, 151 (1984).

¹⁴³A. Reiser, *Photoreactive Polymers: The Science and Technology of Resists*, p. 319, John Wiley & Sons, Hoboken, NJ (1989).



Scheme 7.18 Radiation-induced main chain scission of PMMA.

The gaseous components formed in the process are believed to leave behind free volumes as they escape from the exposed areas of the film. In this way, they selectively speed up dissolution and enhance image discrimination.¹⁴⁴

It should be pointed out that Norrish-type I degradation is not efficient in PMMA, hence its rather low sensitivity to ionizing radiation, DUV radiation, and electron-beam radiation. For instance, it requires a dose of 3400 mJ/cm² at 240 nm to get it fully exposed and developable.¹⁴⁵ Experiments by Guillet and co-workers¹⁴⁶ have revealed that the cause of the inefficiency is the α -fission step in the chain scission mechanism.

PMMA has two main drawbacks, namely, it is rather insensitive (its scission yield $G_s = 1.3$) and it has poor plasma etch stability. Because of its outstanding physical properties and excellent resolution capability, attempts have been made

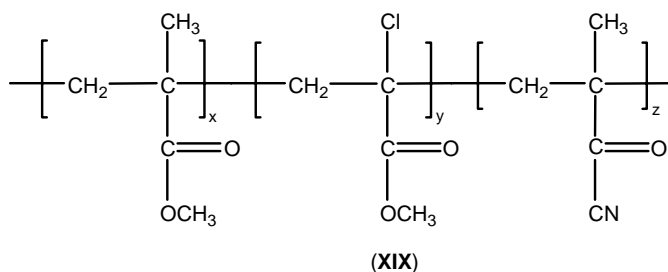
¹⁴⁴A.C. Ouano, "A study of the dissolution rate of irradiated poly (methyl methacrylate)," *Polym. Eng. Sci.* **18**, 306 (1978); L.E. Stillwagon, "Radiation degradation and film solubility rates of poly(butene 1 sulfone)," *Org. Coat. Plast. Chem.* **43**, 236 (1980).

¹⁴⁵A. Reiser, *Photoreactive Polymers: The Science and Technology of Resists*, p. 270, John Wiley & Sons, Hoboken, NJ (1989).

¹⁴⁶Y. Amerik and J.E. Guillet, "The Photochemistry of ketone polymers. IV. Photolysis of methyl vinyl ketone copolymers," *Macromolecules* **4**, 375 (1971); E. Dan and J.E. Guillet, "Photochemistry of ketone polymers. X. Chain scission reaction in the solid state," *Macromolecules* **6**, 230 (1973).

to find its derivatives or copolymers that retain its good qualities and yet have higher sensitivity to radiation.¹⁴⁷ The plasma etch resistance of PMMA cannot be significantly increased, but efforts to increase its sensitivity have been largely reported to be successful. These efforts are based on the idea of promoting the primary reaction step of the side chain scission either by introducing electron-withdrawing substituents (such as halogens) at the α position of the acrylate moiety to assist in the stabilization of a free radical, the first intermediate in the chain scission mechanism;¹⁴⁸ by substitution of the ester moiety; or by copolymerization with radiatively more labile components.¹⁴⁹

Examples of these general ideas include copolymers of methyl methacrylate with α chloroacrylate¹⁵⁰ and with acrylonitrile (XIX).¹⁵¹



The role of the electron-withdrawing substituent in the α position of the backbone is to stabilize the primary radical, as well as the radical that results from the Norrish rearrangements; this stabilization promotes decomposition.¹⁵² In the 1970s, such structural modifications led to PMMA derivatives that afforded resist formulations with sensitivities as low as $1 \mu\text{C}/\text{cm}^2$ at 10 kV.¹⁵³

Other examples include poly(fluorobutyl methacrylate) (XX) with reported sensitivity of $480 \text{ mJ}/\text{cm}^2$ at 240 nm¹⁵⁴ and copolymers of glycidyl methacrylate

¹⁴⁷For a comprehensive review of electron beam resists, see W.M. Moreau, *Semiconductor Lithography: Principles, Practices, and Materials*, Plenum Press, New York (1988), and references therein; A. Reiser, *Photoreactive Polymers: The Science and Technology of Resists*, pp. 269-270, John Wiley & Sons, Hoboken, NJ (1989).

¹⁴⁸C. Pittman, M. Ueda, C. Chen, C. Cook, J. Helbert, and J. Kwiatkowski, "Synthesis, radiation degradation, and electron beam resist behavior of fluorine containing vinyl polymers," *J. Electrochem. Soc.* **128**, 1759 (1981); M. Kakuchi, S. Sugawara, K. Murase, and K. Matsuyama, "Polymeric resist mask composition," U.S. Patent No. 4,125,672 (1978).

¹⁴⁹A. Reiser, *Photoreactive Polymers: The Science and Technology of Resists*, p. 320, John Wiley & Sons, Hoboken, NJ (1989).

¹⁵⁰J.N. Helbert, P.J. Kaplan, and F.H. Poindexter, "Radiation degradation of α substituted acrylate polymers and copolymers," *J. Appl. Polym. Sci.* **21**, 797 (1977); A.C. Ouano, "A study of the dissolution rate of irradiated poly (methyl methacrylate)," *Polym. Eng. Sci.* **18**, 306 (1978).

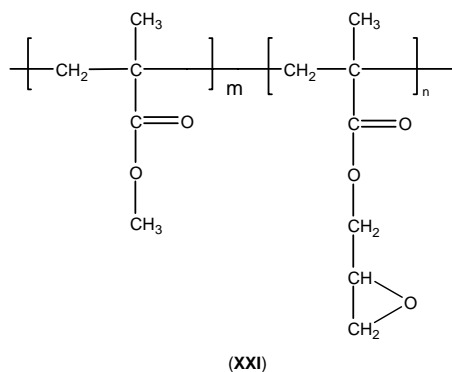
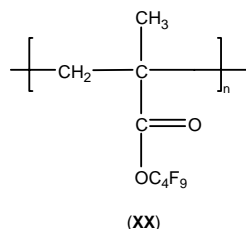
¹⁵¹A. Reiser, *Photoreactive Polymers: The Science and Technology of Resists*, p. 320, John Wiley & Sons, Hoboken, NJ (1989).

¹⁵²ibid.

¹⁵³S. Matsuda, et al., "Thermally reacted poly(methacrylamide) as a positive electron beam resist," *Polym. Eng. Sci.* **17**, 410 (1977).

¹⁵⁴Y. Mimura, T. Okhubo, T. Takeuchi, and K. Sekihawa, "Deep UV photolithography," *Jpn. J. Appl. Phys.* **17**, 541 (1978).

with methyl methacrylate (**XXI**), with reported sensitivity of 250 mJ/cm² at 250 nm (from a deuterium lamp).¹⁵⁵ It should be pointed out that poly(glycidyl methacrylate) undergoes main chain scission under DUV radiation, making it a positive resist; however, under electron-beam or x-ray exposure, it acts as a negative resist because of the ring opening and cross-linking at the epoxy moiety of the base resin.¹⁵⁶



One of the identified causes of the low sensitivity of PMMA to DUV radiation is the low absorption coefficient of the material in this region of the spectrum and the poor match of its absorption spectrum with the emission of the Xe-Hg lamp.¹⁵⁷ Incorporating acyloximino groups into the base polymer has been reported to overcome this deficiency and significantly enhance the photospeed of the resist (Scheme 7.19).¹⁵⁸ The α -keto-oxime chromophore, first introduced by Delzenne et al.,¹⁵⁹ has a strong broad absorption band in the DUV, centered around 225 nm; it is photolabile and is relatively thermally stable.¹⁶⁰ The incorporation

¹⁵⁵E.A. Chandross, E. Reichmanis, C.W. Wilkins, Jr., and R.L. Hartless, "Photoresists for deep UV lithography," *Solid State Technol.* **24**(9), 81 (1981).

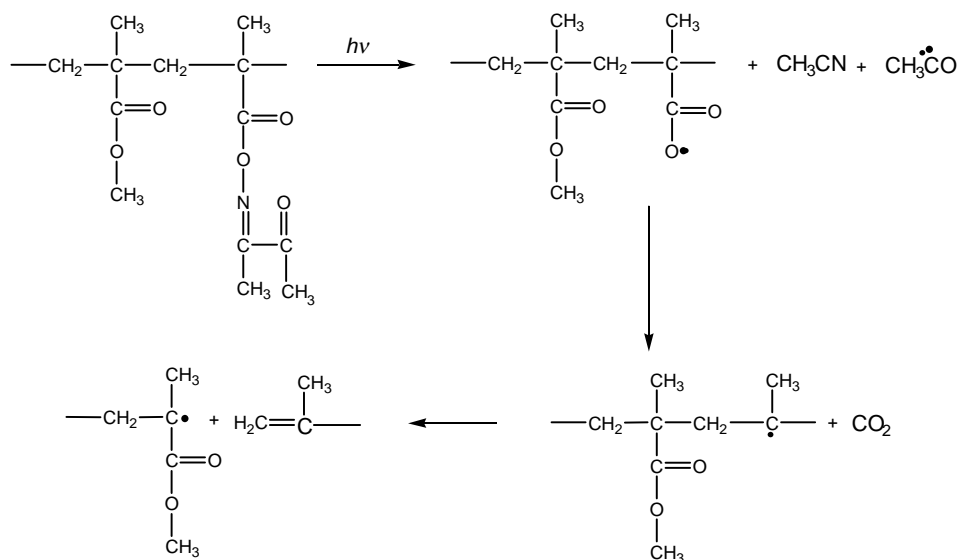
¹⁵⁶Y. Nakane, T. Tsumori, and T. Mifumi, in *Proc. Interface '78, Microelectronics Seminar*, Eastman Kodak, Rochester (1978).

¹⁵⁷A. Reiser, *Photoreactive Polymers: The Science and Technology of Resists*, p. 270, John Wiley & Sons, Hoboken, NJ (1989).

¹⁵⁸ibid.

¹⁵⁹G.A. Delzenne, U. Laridon, and H. Peeters, "Photopolymerization initiated by *O* acyloximes," *Eur. Polym. J.* **6**, 933 (1970).

¹⁶⁰C.W. Wilkins, Jr., E. Reichmanis, and E.A. Chandross, "The effect of sensitizers on the photo degradation of poly(methyl methacrylate co 3 oximino 2 butanone methacrylate)," *J. Electrochem. Soc.* **127**, 2514 (1980).



Scheme 7.19 Incorporating acyloximino groups into PMMA polymeric resins enhances the photospeed to UV radiation of resists formulated with them.

of 37% of the oximino monomer has been reported to produce a 50-fold increase in photospeed over PMMA at the same exposure condition.¹⁶¹

Another method that has been employed with a view to improving the DUV sensitivity in PMMA resists involves the copolymerization of methyl methacrylate with indenone.¹⁶² With a strong absorption in the 230–300-nm region of the spectrum, on irradiation of the resulting copolymer, the latter undergoes multiple chain scission events (see Scheme 7.20) that effectively enhance the sensitivity of the resist. Exposure sensitivity of 20 mJ/cm² at 240 nm has been demonstrated with this resist. The reason for the high radiation sensitivity of the system is believed to be due in part to the fact that the comparatively stable (highly conjugated) radical is formed in the primary step,¹⁶³ as well as to the release of the steric strain in the five-membered ketone ring.¹⁶⁴

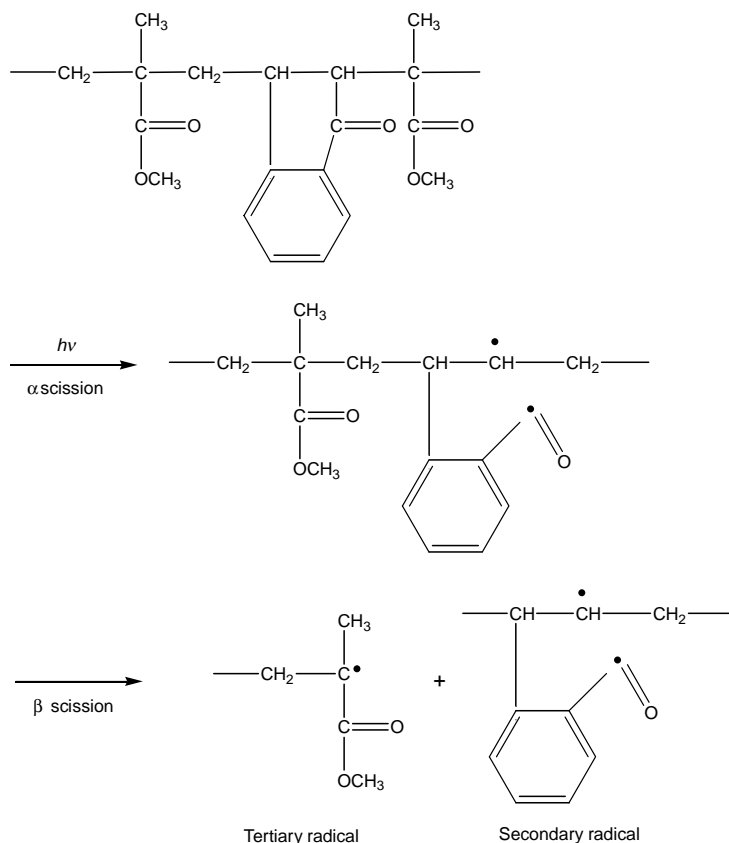
As indicated above, the introduction of electron-withdrawing groups is one of the strategies for improving the sensitivity of PMMA-type resists. This is best exemplified by fluorination in the ester moiety of PMMA, which has produced many useful electron-beam resists, such as poly(perfluorobutyl methacrylate) (XXII),

¹⁶¹E.A. Chandross, E. Reichmanis, C.W. Wilkins, Jr., and R.L. Hartless, "Photoresists for deep UV lithography," *Solid. State Technol.* **81** (Aug. 1981).

¹⁶²J.N. Helbert, P.J. Kaplan, and F.H. Poindexter, "Radiation degradation of α substituted acrylate polymers and copolymers," *J. Appl. Polym. Sci.* **21**, p. 797 (1977); A.C. Ouano, "A study of the dis solution rate of irradiated poly (methyl methacrylate)," *Polym. Eng. Sci.* **18**, 306 (1978).

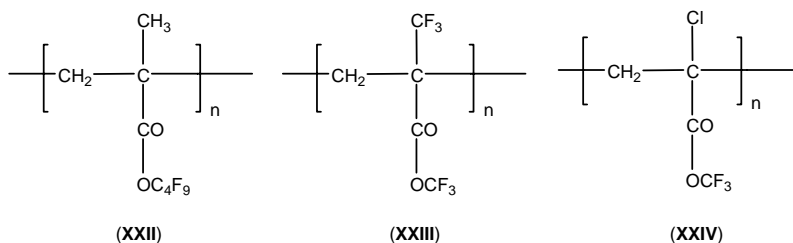
¹⁶³A. Reiser, *Photoreactive Polymers: The Science and Technology of Resists*, p. 272, John Wiley & Sons, Hoboken, NJ (1989).

¹⁶⁴R.L. Hartless and E.A. Chandross, "Deep UV photoresists: Poly(methyl methacrylate co indenone)," *J. Vac. Sci. Technol.* **19**, 1333 (1981).



Scheme 7.20 A copolymer of methyl methacrylate and indenone undergoing multiple radiation-induced chain scission events, resulting in the enhancement of the sensitivity of the resist relative to PMMA.

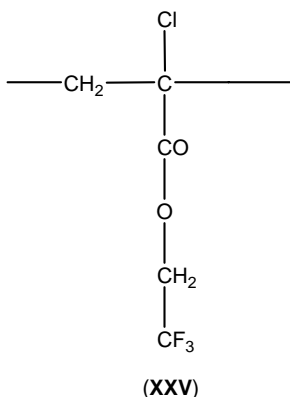
poly(hexafluoro methacrylate) (**XXIII**), poly(trifluoromethyl-*o*-chloroacrylate) (**XXIV**),¹⁶⁵ and in particular poly(2,2,2-trifluoroethyl- α -chloroacrylate) (**XXV**).¹⁶⁶ This resist has excellent electron-beam sensitivity ($0.8 \mu\text{C}/\text{cm}^2$ for 20 kV electrons)



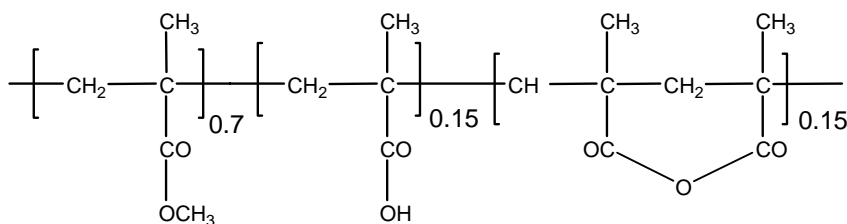
¹⁶⁵M. Kakuchi, S. Sugawara, K. Murase, and K. Matsuyama, "Poly (fluoro methacrylate) as highly sensitive, high contrast positive resist," *J. Electrochem. Soc.* **124**, 1648 (1977).

¹⁶⁶T. Tada, "Crosslinked poly(2,2,2 trichloroethyl methacrylate) as a highly sensitive positive electron resist," *J. Electrochem. Soc.* **126**, 1829 (1979).

and larger processing latitude than, for example, the electron-beam resist poly butene sulfone (PBS), discussed below, which has a comparable sensitivity.¹⁶⁷



Other strategies that have been reported for improving the sensitivity of PMMA resists include the introduction of substituents in the ester part of the PMMA and copolymerization with methacrylic acid,¹⁶⁸ with acrylonitrile, and with methacrylic anhydride. In particular, Moreau et al.¹⁶⁹ have described a resist based on the terpolymer of methacrylic acid, methacrylic anhydride, and methylmethacrylate (XXVI) that has demonstrated significantly faster speed than other resists based on PMMA, while maintaining desirable properties.



IBM's "Terpolymer" resist (XXVI)

Table 7.4 provides an overview of the radiation sensitivity of PMMA and its derivatives as DUV, as electron-beam, and as x-ray resists. Despite their excellent resolution and much improved sensitivity, PMMA-type resists suffer from poor etch resistance, necessitating the search for alternative resist materials for lithographic imaging applications.

¹⁶⁷A. Reiser, *Photoreactive Polymers: The Science and Technology of Resists*, p. 321, John Wiley & Sons, Hoboken, NJ (1989).

¹⁶⁸I. Haller, R. Feder, M. Hatzakis, and E. Spiller, "Copolymers of methyl methacrylate and methacrylic acid and their metal salts as radiation sensitive resists," *J. Electrochem. Soc.*, **126**, 154 (1979); M. Hatzakis, "PMMA copolymers as high sensitivity electron resists," *J. Vac. Sci. Technol.* **16**, 1984 (1979).

¹⁶⁹W. Moreau, D. Merrit, W. Mayer, M. Hatzakis, D. Johnson, and L. Pederson, "Speed enhancement of PMMA resist," *J. Vac. Sci. Technol.* **16**, 1989 (1979).

Table 7.4 Lithographic sensitivity of PMMA and derivatives. (Adapted with permission from Ref. 170. © 1989 John Wiley & Sons.)

	Sensitivity			
	G_s	E Beam ($\mu\text{C}/\text{cm}^2$)	DUV (mJ/cm^2)	X Ray (mJ/cm^2)
Poly(methyl methacrylate) ¹⁷¹	1.3	50	3400	4000
Poly(fluorobutyl <i>co</i> maleic anhydride) ¹⁷²	3	17	480	400
Poly(methyl methacrylate <i>co</i> methyl α chlorometh acrylate (38%)) ¹⁷³	3.5	6		
Poly(methyl methacrylate <i>co</i> acrylonitrile (11%)) ¹⁷⁴		4		
Poly(methyl methacrylate <i>co</i> indenone (50%)) ¹⁷⁵			40	
Poly(methyl methacrylate <i>co</i> oximino 2 butanone <i>co</i> methacrylonitrile (15%)) ¹⁷⁶			40	
Poly(methyl methacrylate <i>co</i> methacrylic acid (25%)) ¹⁷⁷	2	35		
Poly(methyl methacrylate <i>co</i> methacrylic acid <i>co</i> methacrylic anhydride) "IBM Terpolymer" ¹⁷⁸		4.5	8	
Poly(methyl methacrylate <i>co</i> Isobutylene (25%)) ¹⁷⁹			5	

¹⁷⁰This table is adapted from a similar one in A. Reiser, *Photoreactive Polymers: The Science and Technology of Resists*, p. 321, John Wiley & Sons, Hoboken, NJ (1989).

¹⁷¹M. Hatzakis, "Electron resists for microcircuit and mask production," *J. Electrochem. Soc.* **116**, 1033 (1969).

¹⁷²M. Kakuchi, S. Sugawara, K. Murase, and K. Matsugama, "Poly (fluoro methacrylate) as highly sensitive, high contrast positive resist," *J. Electrochem. Soc.* **124**, 1648 (1977).

¹⁷³T. Tada, "Crosslinked poly(2,2,2 trichloroethyl methacrylate) as a highly sensitive positive electron resist," *J. Electrochem. Soc.* **126**, 1635 (1979); J.N. Helbert, P.J. Caplan, and E.H. Poindexter, "Radiation degradation of α substituted acrylate polymers and copolymers," *J. Appl. Polym. Sci.* **21**, 797 (1977).

¹⁷⁴Y. Hatano, H. Morishita, and S. Nonogaki, *Org. Coat. Plast. Chem.* **35**, 258 (1975).

¹⁷⁵E. Reichmanis, C.W. Wilkins, Jr., and E.A. Chandross, "Preliminary evaluation of copolymers of methyl methacrylate and acyloximino methacrylate as deep UV resists," *J. Electrochem. Soc.* **127**, 2510 (1980).

¹⁷⁶R.L. Hartless and E.A. Chandross, "Deep UV photoresists: Poly(methyl methacrylate *co* indene none)," *J. Vac. Sci. Technol.* **19**, 1333 (1981).

¹⁷⁷M. Hatzakis, "PMMA copolymers as high sensitivity electron resists," *J. Vac. Sci. Technol.* **16**, 1984 (1979).

¹⁷⁸W. Moreau, D. Merrit, W. Moyer, M. Hatzakis, D. Johnson, and L. Pederson, "Speed enhancement of PMMA resist," *J. Vac. Sci. Technol.* **16**, 1989 (1979).

¹⁷⁹E. Gipstein, W. Moreau, and O. Need, "Poly(methyl methacrylate isobutylene) copolymers as highly sensitive electron beam resists," *J. Electrochem. Soc.* **123**, 1105 (1976).

7.2.1.2.1.1 POLY(METHYL ISOPROPENYL KETONE) RESISTS

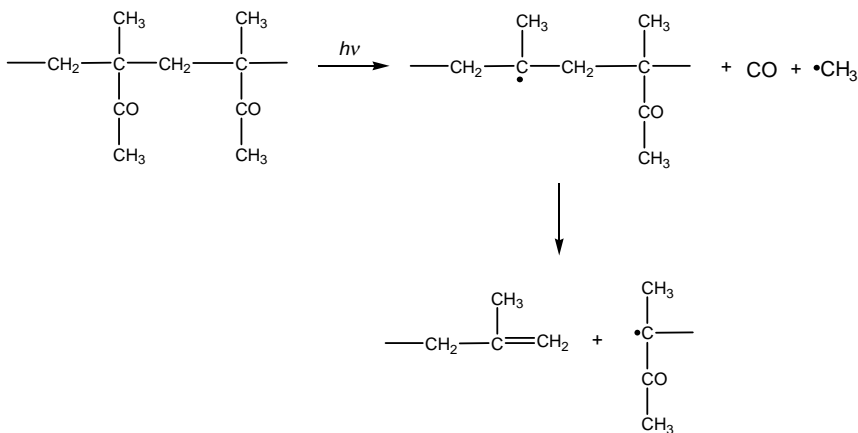
Another group of positive UV resists operating on the principle of radiation-induced main chain scission utilizes the efficient photochemistry of polymeric ketones, exemplified by poly(methyl isopropenyl ketone) PMIPK, to effect image discrimination. Scheme 7.21 shows the photolysis of this resist.¹⁸⁰

PMIPK is reported to be five times more sensitive than PMMA under the same exposure conditions. In addition, it has been reported that PMIPK can be chemically sensitized with substituted benzoic acids to yield exposure speeds that are 25 times faster than PMMA, depending on the exposure wavelength.¹⁸¹ The enhanced sensitivity of PMIPK resists has been attributed to be the consequence of a Norrish-type II process, where internal hydrogen abstraction is the primary reaction step (see Scheme 7.22).¹⁸²

A major drawback of the PMIPK resist system is its relatively low plasma resistance, even lower than that of PMMA. An approach that has been employed to improve its etch resistance is to blend it with more resistant aromatic polymers, but this is at the expense of decreased sensitivity.¹⁸³

7.2.1.2.1.2 POLY(OLEFIN SULFONE) RESISTS

One of the ways of promoting radiation-induced polymer main chain scission is to introduce a weak bond into the backbone, an idea behind resist systems based on



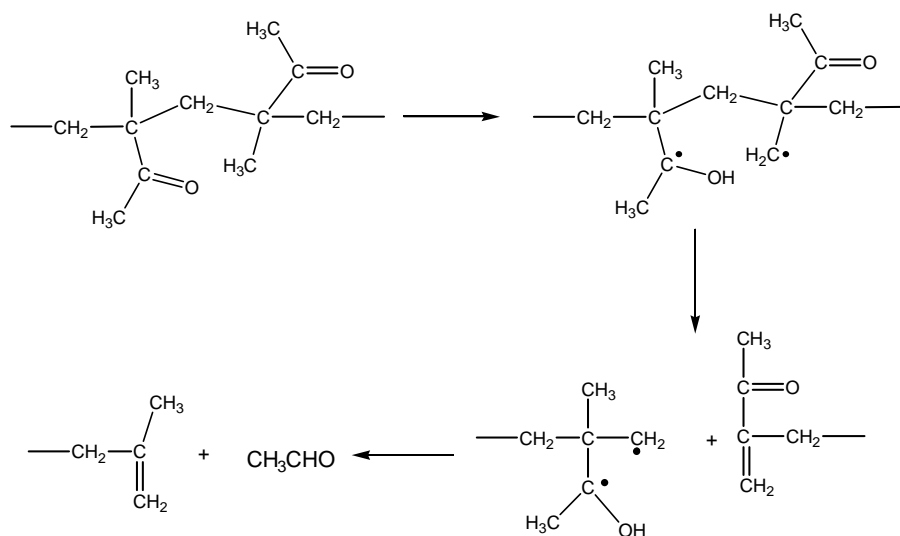
Scheme 7.21 Radiation-induced main chain scission of PMIPK.

¹⁸⁰A. Reiser, *Photoreactive Polymers: The Science and Technology of Resists*, p. 274, John Wiley & Sons, Hoboken, NJ (1989).

¹⁸¹Y. Mimura, T. Okhubo, T. Takeuchi, and K. Sekikawa, "Deep UV photolithography," *Jpn. J. Appl. Phys.* **17**, 541 (1978).

¹⁸²M. Tsuda, et al., "Spectrally sensitized decomposition of poly(methyl isopropenyl ketone): Novel deep UV resists," *Photogr. Sci. Eng.* **23**, 290 (1979).

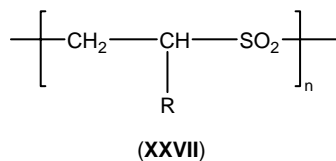
¹⁸³P. van Pelt, "Processing of deep ultraviolet (UV) resists," *Proc. SPIE* **275**, 150 (1981).



Scheme 7.22 Norrish-type II process in main chain scission of PMIPK.

poly(olefin sulfones) (**XXVII**). Remarkably, the unique property of poly(olefin sulfones) that make them suitable for this type of application, their weak C—S bond, was recognized in the 1930s by Marvel and co-workers.¹⁸⁴ The C—S bond has an energy of 2.7 eV compared with 3.6 eV of the average C—C bond.

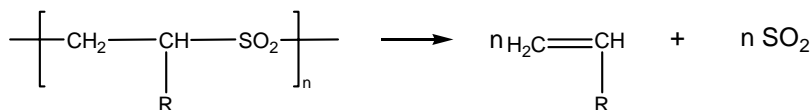
The use of poly(olefin sulfones) in resist applications was first demonstrated by Bowden and Thompson at Bell laboratories.¹⁸⁵ They prepared them by radical copolymerization of (liquid) SO₂ with a whole range of olefins,¹⁸⁶ at reaction temperatures deliberately kept low because of the low ceiling temperatures of poly(alkene sulfones). For poly(butene sulfone), T_c ~ 64°C. The resulting copolymers possess a regular 1:1 alternating composition.



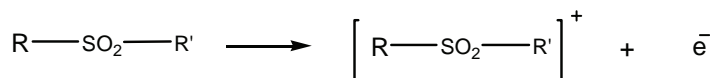
¹⁸⁴D.S. Frederick, H.D. Cogan, and C.S. Marvel, "The reaction between sulfur dioxide and olefins. Cyclohexene," *J. Am. Chem. Soc.* **56**, 1815 (1934).

¹⁸⁵M.J. Bowden and L.F. Thompson, "A new family of positive electron beam resists poly(olefin sulfones)," *J. Electrochem. Soc.* **120**, 1722 (1973); "Poly(styrene sulfone) A sensitive ion millable positive electron beam resist," *J. Electrochem. Soc.* **121** 1620 (1974).

¹⁸⁶M.J. Bowden and E.A. Chandross, "Process for fabricating a color cathode ray tube screen structure having superimposed optical filter means therein," U.S. Patent No. 3,884,695 (1975); C.G. Willson, J.M.J. Fréchet, and M.J. Farrel, IBM. Res. Report No. RJ 3259 (1981).



Scheme 7.23 Depolymerization of poly(butene sulfones).



Scheme 7.24 Generalized mechanism of acid generation in onium salts.

The exposure mechanism of this class of resists involves scission of the C—S bond, followed by the spontaneous depolymerization of the alternating polymer (Scheme 7.23).¹⁸⁷

The first step in the exposure mechanism is the loss of an electron from the molecule (Scheme 7.24),¹⁸⁸ probably from one of the $2p_i$ orbitals of sulfur; this results in a vacancy that is quickly filled from a higher orbital. The lost electron appears eventually in a σ (S—C) bonding orbital, effectively transforming the C—S into a weak one-electron bond that can be broken by thermal energy or by excess kinetic energy released in the ionization event.¹⁸⁹ Consequently, the scission yield of poly(alkene sulfones) is very high, which makes these resists very sensitive, both for electron-beam (less than $1 \mu\text{C}/\text{cm}^2$ at 10 kV) and for DUV (sensitivity of $5 \text{ mJ}/\text{cm}^2$ at 185 nm) lithographic exposures.¹⁹⁰

Following exposure, poly(olefin sulfones) can be developed by two main methods: by solvent development¹⁹¹ or by thermal development. The exposed areas of the resist simply evaporate on heating, or in some cases during exposure,¹⁹² in a phenomenon termed “self-development,” which negatively impacts the vacuum of the exposure tool’s electron column. The liquid development method is not without its drawbacks, as it requires a careful choice of solvent, since the development contrast depends only on molecular weight.¹⁹³

¹⁸⁷J.R. Brown and J.H. O’Donnell, “ γ radiolysis of poly(butene 1 sulfone) and poly(hexane 1 sulfone),” *Macromolecules* **5**, 109 (1972).

¹⁸⁸T.N. Bowner and J.H. O’Donnell, “Radiation degradation of poly(olefin sulfone)s—A volatile product study,” *Radiat. Phys. Chem.* **17**, 177 (1981).

¹⁸⁹A. Reiser, *Photoreactive Polymers: The Science and Technology of Resists*, p. 324, John Wiley & Sons, Hoboken, NJ (1989).

¹⁹⁰Y. Ohnishi, M. Itoh, K. Mizuno, H. Gokan, and S. Fujiwara, “Postirradiation polymerization of e beam negative resists: Theoretical analysis and method of inhibition,” *J. Vac. Sci. Technol.* **19**, 1141 (1981).

¹⁹¹M.J. Bowden and L.F. Thompson, “Electron irradiation of poly(olefin sulfones): Application to electron beam resists,” *J. Appl. Polym. Sci.* **17**, 3211 (1973).

¹⁹²M.J. Bowden and L.F. Thompson, “Effect of olefin structure on the vapor development of poly(olefin sulfones) under electron irradiation,” *Polym. Eng. Sci.* **17**, 269 (1977).

¹⁹³A. Reiser, *Photoreactive Polymers: The Science and Technology of Resists*, p. 324, John Wiley & Sons, Hoboken, NJ (1989).

Poly(1-butene sulfone) resist has been widely used in photomask manufacture since the 1970s and 1980s because it affords resolution down to about 500 nm (on the mask). It is marketed under the commercial name PBS and was extremely successful during this time.¹⁹⁴ However, the performance of the resist in terms of etch resistance, resolution, and critical dimension linearity and uniformity was found to be inadequate as the industry migrated to much smaller critical dimensions that required dry etch processing of the photomask Cr.¹⁹⁵

One reported approach to improving the etch resistance of PBS resists was the incorporation of novolac resins into the formulation, as in the poly(methylpentene sulfone) (PMPS) resist developed at Bell Laboratories and the sulfone/novolac system (SNS) resists developed at IBM in the 1980s.¹⁹⁶ Incorporation of novolac resins into this resist system imparted etch stability and aqueous base solubility to these resists. The olefin sulfone acted as a dissolution inhibitor in the unexposed regions, while the scissioned polymer in the exposed regions enhanced the solubility of the phenolic matrix in the base. Unfortunately, the SNS materials were less sensitive than PBS resists because the novolac matrix absorbed a substantial portion of the incident exposing electrons, making them unavailable for chain scission reactions by the olefin sulfones.¹⁹⁷

7.2.1.2.1.3 POLY(CHLOROACRYLATE-CO- α -METHYLSTYRENE) RESISTS

Because of the above limitations of PBS and SNS resist systems, poly(chloroacrylate-co- α -methylstyrene) (XXVIII) resist was developed at Nippon Zeon in the 1990s.¹⁹⁸ Based on chain scission events, the resist has found wide acceptance in mask-making applications, particularly for device design rule ≤ 180 nm at doses of $\sim 8 \mu\text{C}/\text{cm}^2$ on 10 kV electron-beam exposure tools.¹⁹⁹ It is marketed under the brand name ZEP. In spite of the widespread acceptance

¹⁹⁴ibid.

¹⁹⁵D.R. Medeiros, A. Aviram, C.R. Garnieri, W. S. Huang, R. Kwong, C.K. Magg, A.P. Mahorowala, W.M. Moreau, K.E. Petrillo, and M. Angelopoulos, "Recent progress in electron beam resists for advanced mask making," *IBM. J. Res. Dev.* **45**(5), 639 (2001).

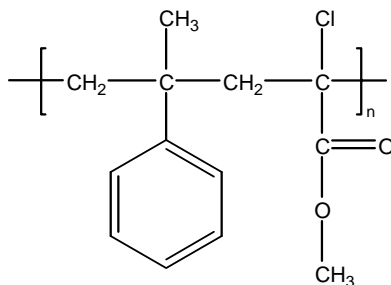
¹⁹⁶M.J. Bowden, L.F. Thompson, S. Fahrenholtz, and F. Doerries, "A sensitive novolac based positive electron resist," *J. Electrochem. Soc.* **128**, 1304 (1981); M.J. Bowden, "Contrast enhancement in multicomponent polymer systems," *J. Appl. Polym. Sci.* **126**, 1424 (1981); Y.Y. Cheng and B.D. Grant, "Terpolymer resist compositions," U.S. Patent No. 4,398,001 (1983).

¹⁹⁷E. Reichmanis, C.W. Wilkins, Jr., and E.A. Chandross, "Preliminary evaluation of copolymers of methyl methacrylate and acyloximino methacrylate as deep UV resists," *J. Electrochem. Soc.* **127**, 2510 (1980).

¹⁹⁸M. Lu, T. Coleman, and C. Sauer, "180 nm mask fabrication process using ZEP 7000, multipass gray, GHOST, and dry etch for MEBES 5000," *Proc. SPIE* **3546**, 98 (1998); K. Kwon, S. Kang, S. Park, H. Sung, D. Kim, J. Moon, "Additive oxygen effects in chrome films" *J. Mater. Sci. Lett.* **18**, 1197 (1999).

¹⁹⁹T. Inoue, Y. Matsuda, and Y. Tanaka, "Application of dry etching to 1 Gb DRAM mask fabrication," *Proc. SPIE* **3412**, 138 (1996); K. Harada, T. Tamamura, and O. Kogure, "Detailed contrast (γ value) measurements of positive electron resists," *J. Electrochem. Soc.* **129**, 2576 (1982).

and use of ZEP, it does not meet all of the industry's current and future mask-making requirements, particularly as the industry migrates to higher-voltage exposure systems: contrast >2 ,²⁰⁰ enhanced RIE resistance ($>2:1$ resist/Cr etch ratio), and improved sensitivity ($<8 \mu\text{C}/\text{cm}^2$ at 10 kV or $<25 \mu\text{C}/\text{cm}^2$ at 50 kV).²⁰¹



Poly(methyl- α -chloroacrylate-co- α -methylstyrene) (XXVIII), the polymer used in formulating ZEP electron-beam resist.

7.2.2 Chemical amplification positive resists: the chemical amplification concept

Resist sensitivity is a key parameter that determines the wafer throughput and ultimately the manufacturing cost of a device. Resists based on the classic DNQ/novolac system do not have the requisite sensitivity in the DUV, VUV, EUV, and x-ray regions of the spectrum, nor to electron and ion beams, to justify their use in these lithographic technologies. With a quantum yield between 0.2 and 0.3, the DNQ/novolac resists are not sensitive enough to be useful in the domain of low radiation intensity at the wafer planes of KrF and ArF DUV exposure tools, as well as exposure tools for the next-generation lithographic technologies such as EUV, e-beam, ion beam, and x ray. A resist sensitivity orders of magnitude higher than that provided by the DNQ/novolac resist system is required to make DUV, VUV, EUV, e-beam, ion-beam and x-ray lithography economically viable in terms of throughput. This sort of sensitivity improvement can only be achieved by a system with a gain mechanism or chemical amplification.²⁰²

²⁰⁰M. Kakuchi, V.S. Sagawara, K. Murase, and K. Matsuyama, "Poly (fluoro methacrylate) as highly sensitive, high contrast positive resist," *J. Electrochem. Soc.* **124**, 1648 (1977).

²⁰¹E. Reichmanis, C.W. Wilkins, Jr., and E.A. Chandross, "Preliminary evaluation of copolymers of methyl methacrylate and acyloximino methacrylate as deep UV resists," *J. Electrochem. Soc.* **127**, 2510 (1980).

²⁰²T. Iwayanagi, T. Ueno, S. Nonogaki, H. Ito, and C.G. Willson, in *Electronic and Photonic Applications of Polymers*, M.J. Bowden and R.S. Turner, Eds., Advances in Chemistry Series 218, pp. 109-224, American Chemical Society, Washington, DC (1988); G.A. Delzenne, "Organic photochemical imaging systems," *Adv. Photochem.* **11**, 1 (1979).

By definition, chemically amplified resists are those in which the initial photochemical or radiochemical exposure produces a catalyst, which acts on the surrounding matrix to mediate a cascade of reactions or initiate a chain reaction that modifies the properties of the matrix in a way that can be exploited in the generation of a relief image. The quantum efficiency for the formation of species responsible for the differential dissolution rate for such resists is the product of the quantum efficiency for the generation of the catalyst and the number of reactions that can be mediated by the catalyst before it is lost or inactivated.²⁰³ Because the catalytic chain length can be hundreds, if not thousands of turnovers,²⁰⁴ Willson²⁰⁵ asserts that the sensitivity of resists based on chemical amplification can be as high as two orders of magnitude greater than those of resists that consume at least one photon for every functional conversion, as is the case for DNQ/novolac resist systems.

In general, the chemical transformations associated with the chemical amplification mechanism in resists is effected through heating the exposed resist film, in a process called postexposure bake (PEB). Although, in principle, the active catalytic species (ions or radicals) could be generated from either photochemical (or radiochemical) acid or base generators, the acid generators are now used almost exclusively in advanced resist systems.²⁰⁶

7.2.2.1 Acid generators

A number of PAGs have been synthesized for use in chemically amplified resist systems. The choice of PAG to use for each specific application is dependent on a number of factors, including the nature of the radiation, quantum efficiency of acid generation, solubility, miscibility with resin, thermal and hydrolytic stability, plasticization effect, toxicity, strength and size of generated acid, impact on dissolution rates, cost, etc.²⁰⁷ Figure 7.10 shows classes, while Table 7.5 is a list of typical photochemical acid generators currently in use in chemical amplification resists.

²⁰³C.G. Willson, R.A. Dammel, and A. Reiser, "Photoresist materials: a historical perspective," *Proc. SPIE* **3050**, 38–51 (1997).

²⁰⁴M.J. Bowden and L.F. Thompson, "Electron irradiation of poly(olefin sulfones): Application to electron beam resists," *J. Electrochem. Soc.* **120**, 1722 (1973); "Poly(Styrene sulfone): A sensitive ion millable positive electron beam resist," *J. Electrochem. Soc.* **121**, 1620 (1974); D.R. McKean, U.P. Schaedeli, and S.A. MacDonald, "Acid photogeneration from sulfonium salts in solid polymer matrices," *J. Polym. Sci. Polym. Chem. Ed.* **27**, 3927 (1989); D.R. McKean, U.P. Schaedeli, P.H. Kasai, and S.A. MacDonald, "The effect of polymer structure on the efficiency of acid generation from triarylsulfonium salts," *J. Polym. Sci. Polym. Chem. Ed.* **29**, 309 (1991).

²⁰⁵C.G. Willson, "Organic resist materials," in *Introduction to Microlithography*, L.F. Thompson, C.G. Willson, and M.J. Bowden, Eds., p. 214, American Chemical Society, Washington, DC (1994).

²⁰⁶H. Ito, "Chemical amplification resists for microlithography," *Adv. Polym. Sci.* **173**, 48 (2005); C.G. Willson, "Organic resist materials," in *Introduction to Microlithography*, L.F. Thompson, C.G. Willson, and M.J. Bowden, Eds., p. 215, American Chemical Society, Washington, DC (1994).

²⁰⁷H. Ito, "Chemical amplification resists for microlithography," *Adv. Polym. Sci.* **173**, 48 (2005).

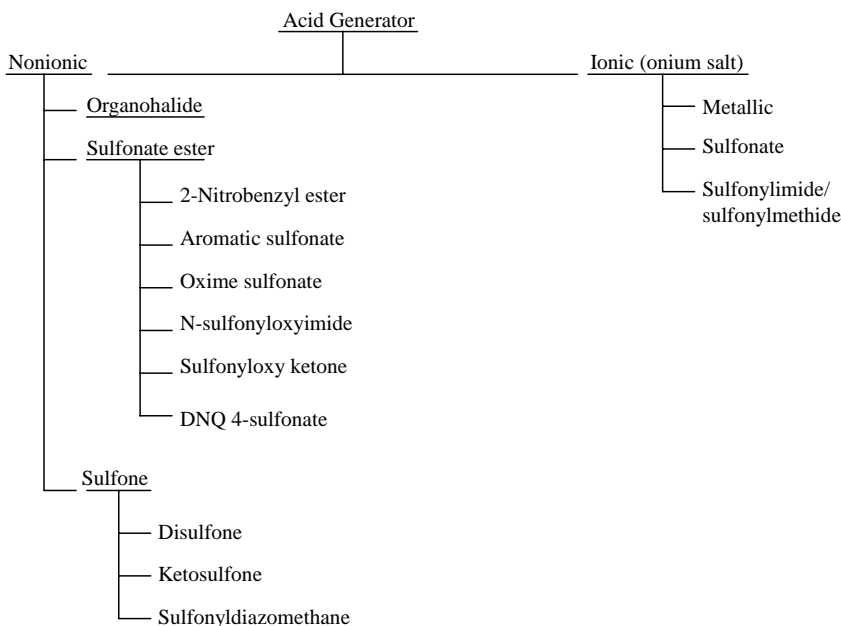


Figure 7.10 Classification of photochemical acid generators.

Rarely does an acid generator possess all of these attributes in the required measure. For instance, the diazonium salts produce Lewis acids (e.g., BF_3) and are not thermally stable; however, on the other hand, the sulfonium and iodonium salts are very thermally stable, but because they are ionic, can be particularly difficult to incorporate into resist formulations. The triazines and bromobisphenol-A produce halogen acids that are volatile, while the nitrobenzyl esters tend to undergo unwanted facile hydrolysis.²⁰⁸

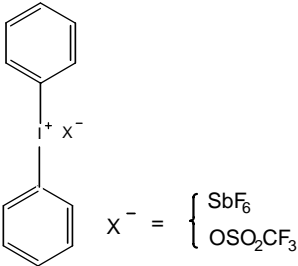
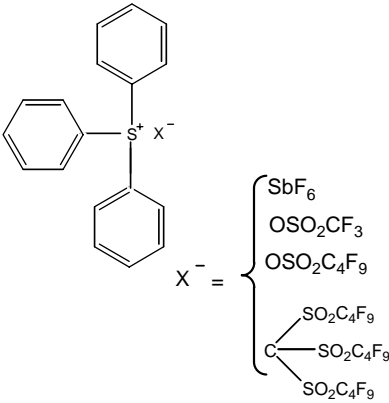
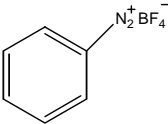
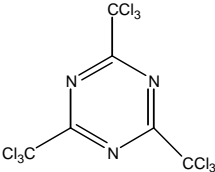
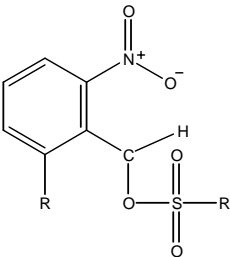
Photoacid generators fall into two main categories: ionic and nonionic PAGs. Ionic PAGs such as onium salts have broad sensitivity to DUV, e-beam, and x-ray radiation and can be red-shifted for near-UV applications by incorporating appropriate chromophores²⁰⁹ or through the use of sensitizers.²¹⁰ Although triphenylsulfonium hexafluoroantimonate was employed in the early chemical amplification

²⁰⁸H. Ito, "Chemical amplification resists for microlithography," *Adv. Polym. Sci.* **173**, 215 (2005).

²⁰⁹H. Ito and E. Flores, "Evaluation of onium salt cationic photoinitiators as novel dissolution inhibitor for novolac resin," *J. Electrochem. Soc.* **135**, 2322 (1988).

²¹⁰S.P. Pappas, "Photogeneration of acid: Part 6 A review of basic principles for resist imaging applications," *J. Imaging Technol.* **11**, 146 (1985); J.L. Dektar, N.P. Hacker, "Triphenylsulfonium salt photochemistry. New evidence for triplet excited state reactions," *J. Org. Chem.* **53**, 1833 (1988); S.P. Pappas, L.R. Gatechair, and J.H. Jilek, "Photoinitiation of cationic polymerization. III. Photosensitization of diphenyliodonium and triphenylsulfonium salts," *J. Polym. Sci. Polym. Chem. Ed.* **22**, 77 (1984); J.L. Dektar and N.P. Hacker, "Novel photoinduced electron transfer reactions between naphthalene and triphenylsulphonium salts," *J. Photochem & Photobiol.* **A 46**, 233 (1989); J.V. Crivello, "Cationic polymerization: Iodonium and sulfonium salt photoinitiators," *Adv. Polym. Sci.* **62**, 1 (1984).

Table 7.5 Compounds that generate acid on radiolysis.

Name	Representative Structure	Acid Generated
Diphenyliodonium salts	 $X^- = \begin{cases} \text{SbF}_6^- \\ \text{OSO}_2\text{CF}_3^- \end{cases}$	HSbF_6 HOSO_2CF_3
Triphenylsulfonium salts	 $X^- = \begin{cases} \text{SbF}_6^- \\ \text{OSO}_2\text{CF}_3^- \\ \text{OSO}_2\text{C}_4\text{F}_9^- \\ \text{C}(\text{SO}_2\text{C}_4\text{F}_9)_3^- \end{cases}$	HSbF_6 HOSO_2CF_3 $\text{HOSO}_2\text{C}_4\text{F}_9$
Diazonium salts		BF_3
Trichloromethyl triazine		HCl
o Nitrobenzyl esters		RSO_2OH

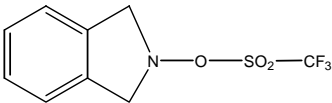
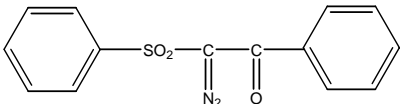
(Continued)

Table 7.5 Continued.

Name	Representative Structure	Acid Generated
α Hydroxymethylbenzoin sulfonic acid ester		RSO ₂ OH
Diazonaphthoquinone 4 sulfonate		
α Sulfonyloxy ketones		HOTos (<i>p</i> -toluene sulfonic acid)
Iminosulfonates		
N hydroxyimide sulfonates		TsOH
Disulfones		
Bromobisphenol A		HBr

(Continued)

Table 7.5 Continued.

Name	Representative Structure	Acid Generated
Hydroxyamic acid esters		CF ₃ SO ₂ OH
Diazosulfonates		RSO ₂ OH

resists,²¹¹ its use in device manufacture, along with those of other metallic acid generators, have been discontinued, largely because of contamination issues. Triphenylsulfonium trifluoromethanesulfonate (triflate), which generates the strongest organic acid, and triarylsulfonium salts, which are the most thermally stable salts with the onset of decomposition at $\sim 350^\circ\text{C}$, have since proved to be acceptable alternatives to the metallic salts. In particular, diaryliodonium sulfonates such as di(*tert*-butylphenyl) iodonium perfluorobutanesulfonate (nonaflate) (DTBPIONf) and perfluorooctanesulfonate are widely used in resist formulations for advanced lithography.²¹²

A new type of ionic PAGs based on imides and methides²¹³ has recently been proposed by 3M. The notable characteristic of these PAGs is that they do not contain perfluorooctyl sulfonates and related derivatives, which have recently been identified by the U.S. Environmental Protection Agency and environmental regulatory agencies in other countries to pose health hazards, as they are biopersistent and toxic, and bioaccumulate in mammalian tissues.²¹⁴

²¹¹J.G. Maltabes, S.J. Holmes, J. Morrow, R.L. Barr, M. Hakey, G. Reynolds, W.R. Brunsvold, C.G. Willson, N.J. Clecak, S.A. MacDonald, and H. Ito, "1X deep UV lithography with chemical amplification for 1 micron DRAM production," *Proc. SPIE* **1262**, 2 (1990).

²¹²T. Iwayanagi, T. Ueno, S. Nonogaki, H. Ito, and C.G. Willson, in *Electronic and Photonic Applications of Polymers*, M.J. Bowden and R.S. Turner, Eds., Advances in Chemistry Series 218, p. 51, American Chemical Society, Washington, DC (1988).

²¹³W.L. Lamanna, C.R. Kessel, P.M. Savu, Y. Cheburkov, S. Brinduse, T.A. Kestner, G.J. Lillquist, M.J. Paren, K.S. Moorhouse, Y. Zhang, G. Birznieks, T. Kruger, and M.C. Pallazzotto, "New ionic photo acid generators (PAGs) incorporating novel perfluorinated anions," *Proc. SPIE* **4690**, 817 (2002).

²¹⁴See, for example, *Hazard Assessment of Perfluorooctane Sulfonate (PFOS) and Its Salts*, Organization for Economic Co operation and Development (2002); S. Taniyasi, K. Kannan, Y. Horii, and N. Yamahita, "The environmental survey of perfluorooctane sulfonate (PFOS) and related compounds in Japan," presented at *Dioxin 2002*, Barcelona, Spain, August 11-16, 2002; S. Taniyasi et al., "A survey of perfluorooctane sulfonate and related perfluorinated organic compounds in water, fish, birds, and humans from Japan," *Env. Sci. Technol.* **37**(12), 2634-2639 (2003); R. Bossi et al., "Preliminary screening of perfluorooctane sulfonate (PFOS) and other fluorochemicals in fish, birds, and marine mammals from Greenland and The Faroe Islands," *Env. Pollution*, **136**(2), 323-329 (2005); G. Olsen et al., "Perfluorooctane sulfonate and other fluorochemicals in the serum of american red cross adult blood donors," *Env. Health Perspect.* **111**(16) (2003).

Nonionic PAGs in use in chemical amplification resists comprise organohalides such as tetrabromobisphenol A and 4,6-bis(trichloromethyl)-1,3,5-triazine. They generate hydrogen halide on irradiation (see Table 7.4) and were in fact employed in early negative-tone chemical amplification resists.²¹⁵ However, their volatility and limited acidolysis limited their widespread adoption. Organic nonionic PAGs based on sulfonate esters and sulfonyl compounds (see Table 7.4), which produce sulfonic acids or sulfinic acids,²¹⁶ have now been widely adopted in the industry. Even polymerizable and polymeric PAGs have been reported.²¹⁷

Some PAGs play quite diverse roles in addition to their primary function of generating photoacids. Some PAGs have been reported to act as dissolution inhibitors of phenolic and other acidic resins in aqueous developers.²¹⁸ Furthermore, the use of alkylsulfonium iodides in combination with PAGs has been reported to improve resist contrast and acid diffusion in electron-beam systems.²¹⁹

²¹⁵G. Buhr, R. Dammel, and C.R. Lindley, "Nonionic photoacid generating compounds," Abstracts of Papers of the American Chemical Society, *Poly. Mater. Sci. Eng.* **198**, 60 (1989).

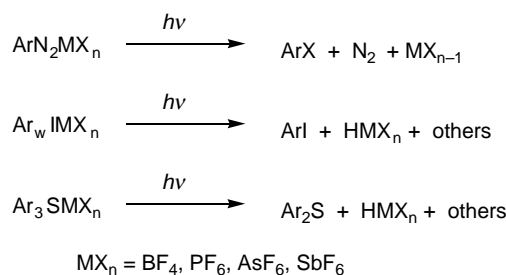
²¹⁶T. Aoi, Y. Aotani, A. Umehara, and T. Kokubo, "Application of silylether and silylester polymer for chemical amplification system," *J. Photopolym. Sci. Technol.* **3**, 389 (1990); M. Tsunooka, H. Yanai, M. Kitayama, and M. Shiraj, "Photo initiated acid formation and its applications the acid formation mechanism in photolysis of β ketosulfones in polymer matrices," *J. Photopolym. Sci. Technol.* **4**, 239 (1991).

²¹⁷R.D. Miller, A.F. Renaldo, and H. Ito, "Deoxygenation of sulfoxides promoted by electrophilic silicon reagents: preparation of aryl substituted sulfonium salts," *J. Org. Chem.* **53**, 5571 (1988); K. D. Ahn, C. M. Chung, and D. I. Koo, "Novel functional polymers from n (tosyloxy)maleimide. Photochemical acid generation in solid state and application as resist materials," *Chem. Mater.* **6**, 1452 (1994); C. M. Chung, D. I. Koo, and K. D. Ahn, "Terpolymers of tosyloxymaleimide for application as a polymeric photoacid generator single component resists," *J. Photopolym. Sci. Technol.* **7**, 473 (1994); K. D. Ahn, J. S. Koo, and C. M. Chung, "Photoacid generating polymers based on sulfonyloxymaleimides and application as single component resists," *J. Polym. Sci. Polym. Chem. Ed.* **34**, 183 (1996); S. T. Kim, J. B. Kim, C. M. Chung, and K. A. Ahn, "High resolution single component resists based on terpolymers having photoacid generating camphorsulfonyloxymaleimide units," *J. Photopolym. Sci. Technol.* **10**, 489 (1997); C. W. Lee, J. H. Shin, J. M. Kim, D. K. Han, K. D. Ahn, "New single component resists based on functional polynorborneneimides by chemical amplification for deep UV lithography," *J. Photopolym. Sci. Technol.* **11**, 405 (1998); J.E. Hanson, E. Reichmanis, F.M. Houlihan, and T.X. Neenan, "The synthesis and evaluation of copolymers of t butoxycarbonyloxystyrene and 2 nitrobenzylstyrene sulfonates: Single component chemically amplified deep UV imaging materials," *Chem. Mater.* **4**, 837 (1992); M. Shirai, M. Hayashi, and M. Tsunooka, "Photoinduced acid catalyzed silicon dioxide formation at the polymer surface by chemical vapor deposition," *Macromolecules* **25**, 195 (1992); M. Shirai, T. Sumino, and M. Tsunooka, "Surface imaging using photoinduced acid catalyzed formation of polysiloxanes at air polymer interface," in *Polymeric Materials for Microelectronic Applications*, H. Ito, S. Tagawa, and K. Horie, Eds., ACS Symposium Series 579, p. 183, American Chemical Society, Washington, DC (1994); K.E. Gonsalves, Y. Hu, H. Wu, R. Panepucci, and L. Merhari, in *Forefront of Lithographic Materials Research*, H. Ito, M.M. Khojasteh, and W. Li, Eds., p. 51, Society of Plastics Engineers, Mid Hudson Section, Hopewell Junction, NY (2001).

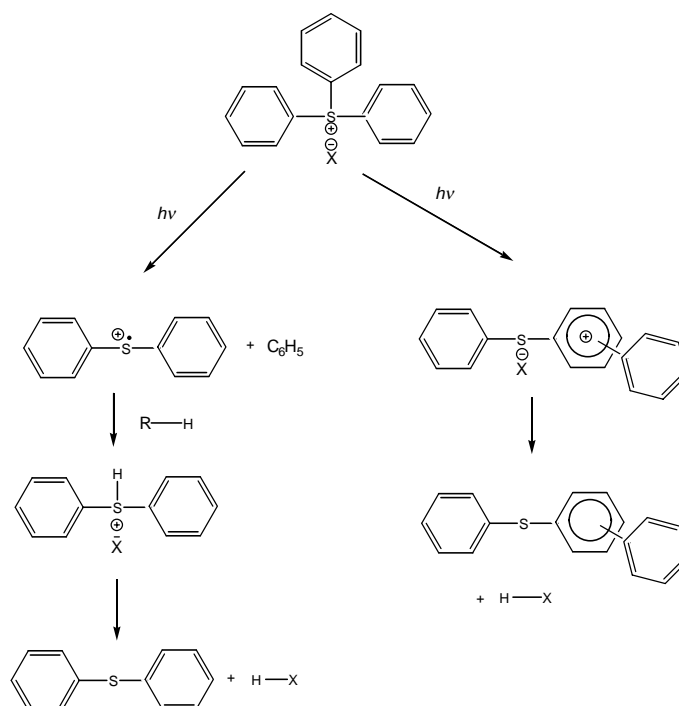
²¹⁸H. Ito and E. Flores, "Evaluation of onium salt cationic photoinitiators as novel dissolution inhibitor for novolac resin," *J. Electrochem. Soc.* **135**, 2322 (1988); H. Ito, "Aqueous base developable deep UV resist systems based on novel monomeric and polymeric dissolution inhibitors," *Proc. SPIE* **920**, 33 (1988).

²¹⁹T. Arai, T. Sakamizu, K. Katoh, M. Hashimoto, and H. Shiraishi, "A sensitive positive resist for 0.1 μm electron beam direct writing lithography," *J. Photopolym. Sci. Technol.* **10**, 625 (1997).

The mechanism of acid generation in some PAGs, particularly onium salts, has been studied extensively.²²⁰ Generally, Scheme 7.25 describes the photolytic



Scheme 7.25 Generalized mechanism of acid generation in onium salts.



Scheme 7.26 Photolysis mechanism of triphenylsulfonium salts.

²²⁰J.V. Crivello and J.H.W. Lam, *J. Polym. Sci. Polym. Lett. Ed.* **17**, 759 (1979); J.V. Crivello and J.L. Lee, "Photosensitized cationic polymerizations using dialkylphenacylsulfonium and dialkyl(4 hydroxyphenyl)sulfonium salt photoinitiators," *Macromolecules*, **14**, 1141 (1981); S.P. Pappas, "Photo generation of acid: Part 6 A review of basic principles for resist imaging applications," *J. Imaging Technol.* **11**, 146 (1985); J.L. Dektar and N.P. Hacker, "Triphenylsulfonium salt photochemistry. New evidence for triplet excited state reactions," *J. Org. Chem.*, **53**, (1988); J.L. Dektar and N.P. Hacker, "Photochemistry of triarylsulfonium salts," *J. Am. Chem. Soc.* **112**, 6004 (1990); G. Pohlers, J.C. Sciano, R.F. Sinta, R. Brainard, and D. Pai, "Mechanistic studies of photoacid generation from substituted 4,6 bis(trichloromethyl) 1,3,5 triazines," *Chem. Mater.* **9**, 1353 (1997).

reactions of diazonium, iodonium, and sulfonium salts—typical salts used as photoacid generators in chemical amplification resist systems.²²¹

For illustrative purposes, the photolysis of triphenyl sulfonium salts, one of the most popular acid generators, is presented in Scheme 7.26. In a viscous medium, a cage effect dominates the distribution of the photolysis products.²²²

7.2.2.2 Chemical amplification positive resists and their imaging mechanisms

As shown in Fig. 7.1, there are two broad categories of chemical amplification resists based on their imaging mechanisms, namely, (i) those based on acid-catalyzed main chain scission and (ii) those based on functional group polarity switch brought about by acid-catalyzed deprotection of lipophilic pendant groups, depolymerization, and Claisen rearrangement.

In this section, we consider in detail the chemistry that underlies the main classes of resists in each category. Where necessary, we will provide historical background relating to each resist type with a view to contextualizing the technological application of the given resist in device manufacture. The two main functional group polarity switching reactions utilized in chemical amplification resists include deprotection and Claisen rearrangement.

7.2.2.3 Chemical amplification positive resists based on deprotection

Chemical amplification resists based on deprotection rely on acid-catalyzed deprotection of pendant protecting groups of the resist matrix resin to generate aqueous base-soluble acidic functionalities such as those of phenols and carboxylic acids. The main structural requirements that enable this mechanism include a bond within the protecting group that forms a stable carbonium ion on heterolysis and an elimination mechanism for the formed carbonium ion to regenerate acid to continue the catalytic chain.²²³ Examples of systems that fulfill these requirements include carbonates, esters, and ethers.²²⁴ These systems have provided the basis for designing aqueous-base-developable positive resists that have now replaced diazoquinone/novolac resists in short-wavelength lithographic technologies. The most advanced positive resists in use today are built exclusively on this imaging mechanism. Examples of resists employing this imaging scheme are presented in subsequent sections under distinct categories of the main protecting group in each resist system.

The main resist polymer platforms used in this form of chemical amplification comprise poly(hydroxy styrene), acrylate, alicyclic, and hybrid acrylate-alicyclic systems. Because of the great versatility of polyhydroxystyrene (PHOST) in

²²¹A. Reiser, *Photoreactive Polymers: The Science and Technology of Resists*, p. 278, John Wiley & Sons, Hoboken, NJ (1989).

²²²J.L. Dektar and N.P. Hacker, "Photochemistry of triarylsulfonium salts," *J. Am. Chem. Soc.* **112**, 6004 (1990).

²²³C.G. Willson, "Organic Resist Materials," in *Introduction to Microlithography*, L.F. Thompson, C.G. Willson, and M.J. Bowden, Eds., p. 219, American Chemical Society, Washington, DC (1994).

²²⁴*ibid.*, pp. 219–220.

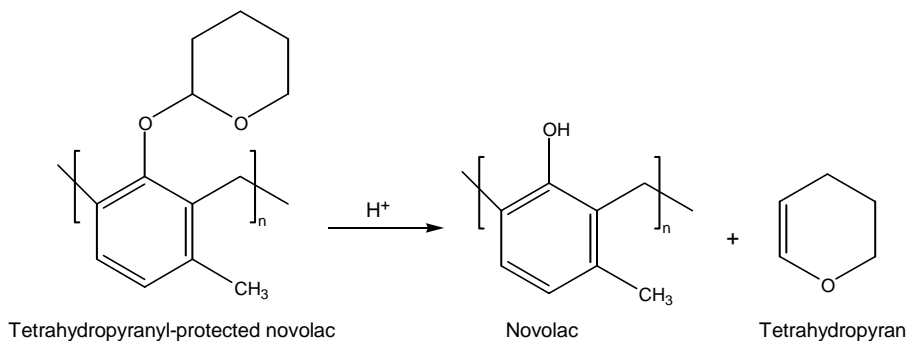
-serving as the platform for numerous variations on this theme of chemical amplification, we review here its general synthesis and attributes.

7.2.2.3.1 Ether-protected chemical amplification resists

7.2.2.3.1.1 POLY(TETRAHYDROFURAN-CO-NOVOLAC) RESISTS

The first chemically amplified resist was designed by G.H. Smith and J.A. Bonham of the 3M Company for which they were granted a U.S. patent in 1973.²²⁵ It was used in the acid-catalyzed deprotection of tetrahydropyranal ether from a polymer of tetrahydropyranal ether of novolac to generate a base-soluble phenol (novolac), as shown in Scheme 7.27. Incidentally, this work was never published in the open literature and was never exploited by 3M, and remained lost in the patent literature for a considerable length of time.

Other reported chemical amplification resist polymers based on the acid-catalyzed deprotection of ether-protected groups include the hydrolysis of trimethylsilyl (TMS) ether polymer²²⁶ and the alcoholysis of tetrahydropyranal (THP)²²⁷-protected group polymer; all of these lead to conversion to PHOST (see Scheme 7.28).²²⁸



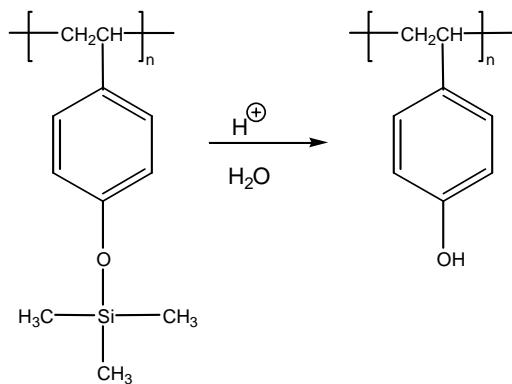
Scheme 7.27 The chemically amplified resist system invented by G.H. Smith and J.A. Bonham of 3M. The photogenerated acid cleaves the lipophilic tetrahydropyranal ether to generate the base soluble phenol.

²²⁵G.H. Smith and J.A. Bonham, "Photosolubilizable compositions and elements," U.S. Patent No. 3,779,778 (1973).

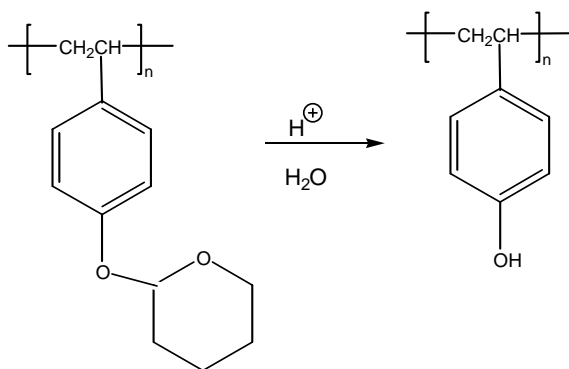
²²⁶T. Yamaoka, N. Nishiki, K. Koseki, and M. Koshiba, "A novel positive resist for deep UV lithography," *Polym. Eng. Sci.* **29**, 856 (1989); M. Murata, T. Takahashi, M. Koshiba, S. Kawamura, and T. Yamaoka, "Aqueous base developable novel deep UV resist for KrF excimer laser lithography," *Proc. SPIE* **1262**, 8 (1990).

²²⁷S.A.M. Hesp, N. Hayashi, and T. Ueno, "Tetrahydropyranal and furanyl protected polyhydroxystyrene in chemical amplification systems," *J. Appl. Polym. Sci.* **42**, 877 (1991); N. Hayashi, L. Schlegel, T. Ueno, H. Shiraishi, and T. Iwayanagi, "Polyvinylphenols protected with tetrahydropyranal group in chemical amplification positive deep UV resist systems," *Proc. SPIE* **1466**, 377 (1991).

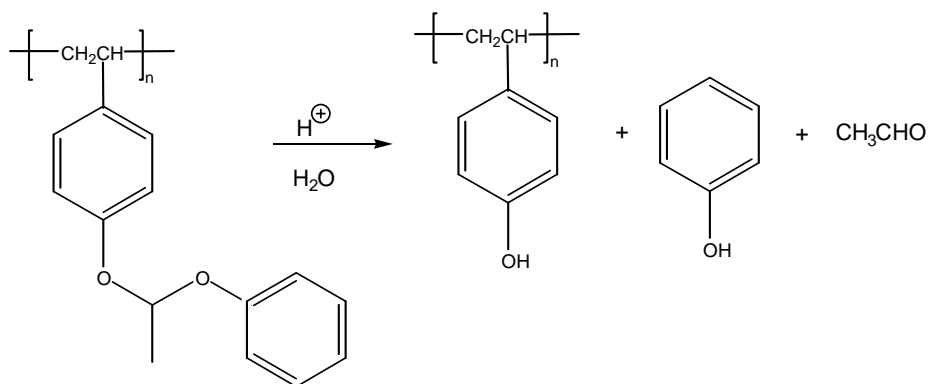
²²⁸H. Ito, "Chemical amplification resists for microlithography," *Adv. Polym. Sci.* **173**, 65 (2005).



Trimethylsilyl ether-protected PHOST



Tetrahydropyranyl ether-protected PHOST

Poly[4-(1-phenoxyethoxy) styrene]
(acetal-protected PHOST)**Scheme 7.28** Hydrolysis of TMS ether-, THP ether-, and acetal-protected PHOST.

7.2.2.3.2 Carbonate-protected chemical amplification resists

7.2.2.3.2.1 POLY(HYDROXYSTYRENE) RESIST PLATFORM

(i) Carbonate-protected poly(hydroxystyrene)-based resists

Faced with the shortcomings of the polyphthaldehyde resist (presented below in chemical amplification resists based on depolymerization),²²⁹ the search for chemically amplified DUV resists resulted in a quick switch to more stable materials based on poly(*p*-hydroxystyrene), a phenolic polymer that Willson et al. were studying as a potential replacement for novolac.²³⁰ They observed that poly(*p*-*tert*-butoxycarbonyloxystyrene) (PBOCST), which is poly(vinyl phenol) protected with *tert*-butoxycarbonyl groups (*t*-BOC),²³¹ is far more stable than the unprotected *p*-hydroxystyrene and could be purified and polymerized under controlled conditions. The resulting protected polymer could be easily deprotected thermally by heating it to 200°C²³² or to a much lower temperature (100°C) by treatment with acid generated from the exposure of onium salts, just as in the poly(phthaldehyde) systems.²³³

Deprotection of this polymer leads to a loss of about 45% of the original weight, corresponding to the disappearance of the volatile components formed in the reaction, namely, CO₂ and isobutylene (see Scheme 7.29).²³⁴

It has been reported that the deprotection event may follow two distinct pathways. The scission of the CO—O bond produces a *tert*-butoxy intermediate that generates acetone, *tert*-butyl alcohol, and methyl isopropenyl ether, while scission of the O—C bond leads to the formation of *tert*-butyl intermediates, which go on to generate isobutene as a gaseous product.²³⁵

²²⁹Although this resist system was invented almost a decade after the invention of the first chemical amplification resist, it was the first chemical amplification resist that was versatile and robust enough to support integrated circuit device manufacture.

²³⁰J.M.J. Fréchet, E. Eichler, H. Ito, and C.G. Willson, "Poly(*p*-*tert*-butoxycarbonyl styrene): a convenient precursor to *p*-hydroxystyrene resins," *Polymer* **24**, 995 (1983); C.G. Willson, H. Ito, J.M.J. Fréchet, T.G. Tessier, and F.M. Houlihan, "Chemical amplification in the design of polymers for resist applications," in *Proc. of IUPAC Macro '82, Int. Union of Pure and Applied Chemistry*, Oxford, England, p. 448 (1982); C.G. Willson, H. Ito, J.M.J. Fréchet, T.G. Tessier, and F.M. Houlihan, "Approaches to the design of radiation sensitive polymeric imaging systems with improved sensitivity and resolution," *J. Electrochem. Soc.* **133**, 181 (1986).

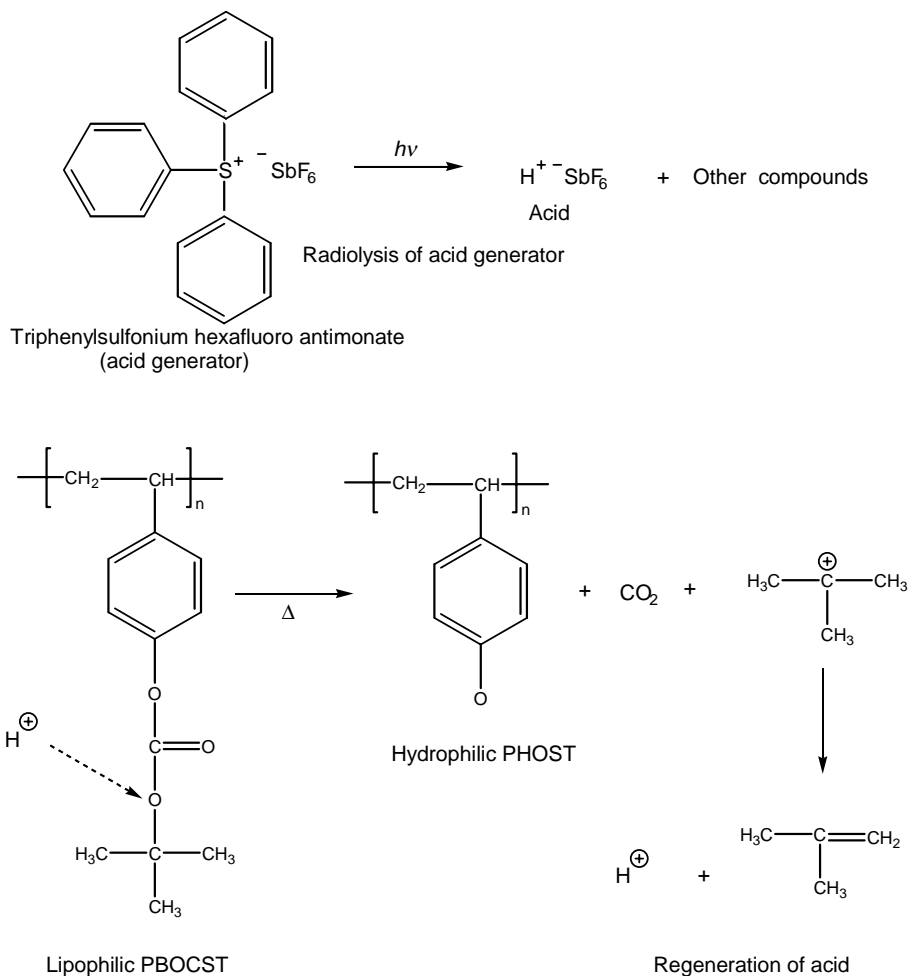
²³¹This protecting group is a very versatile one that is used extensively in peptide chemistry.

²³²A. Reiser, *Photoreactive Polymers: The Science and Technology of Resists*: p. 279, John Wiley & Sons, Hoboken, NJ (1989).

²³³C.G. Willson, R.A. Dammel, and A. Reiser, "Photoresist materials: a historical perspective," *Proc. SPIE* **3050**, 38–51 (1997).

²³⁴C.G. Willson, "Organic resist materials," in *Introduction to Microlithography*, L.F. Thompson, C.G. Willson, and M.J. Bowden, Eds., p. 218, American Chemical Society, Washington, DC (1994).

²³⁵F. Houle, G.M. Poliskie, W.D. Hinsberg, D. Pearson, M.I. Sanchez, H. Ito, and J. Hoffnagle, "Real time analysis of volatiles formed during processing of a chemically amplified resist," *Proc. SPIE* **3999**, 181 (2000); W.D. Hinsberg, F. Houle, M. Poliskie, D. Pearson, M. Sanchez, H. Ito, J. Hoffnagle, and M. Morrison, in *Forefront of Lithographic Materials Research*, H. Ito, M.K.



Scheme 7.29 Chemical amplification mechanism of acid-catalyzed deprotection of PBOCST.

The poly(*t*-butoxycarbonyl oxystyrene) or PBOCST formulated with triphenylsulfonium hexafluoroantimonate (as the photoacid generator) was an immediate success. It could be imaged in either positive or negative mode, depending on the developer used, with aqueous-based developers yielding positive images, while organic nonpolar solvent developers (which dissolve PBOCST but not the phenolic resin) yielded negative images. In combination with onium salt acid generators,

PBOCST is a very sensitive DUV resist. It can be sensitized to near-UV (365 nm) and also responds to electron exposure and EUV exposure. It also has very high dry etch resistance, as well as very high photosensitivity.²³⁶

The initial formulations of the resist gave better negative-tone images than positive ones, since the positive-tone images tended to have a T-topping profile caused by the neutralization of the photoacids in the top parts of the feature by airborne molecular bases. The first commercial application of the resist was in negative tone, and its first full-scale commercial application in DUV lithography was in the printing of the recessed oxide isolation level of IBM's 1-Mb DRAM with a critical dimension of 0.9 μm .²³⁷

(ii) Poly(hydroxystyrene)

PHOST is the main resist polymer platform for DUV 248-nm (KrF laser) lithography in the sense that acid-labile groups such as carbonates, esters, tetrahydropyran, acetals, and ketals are used to partially protect the hydroxyl group of some of its monomeric constituents in order to impart a lipophilic-to-hydrophilic polarity switch on radiation-induced deprotection/deblocking of these protecting groups, and subsequent development in an aqueous-base developer. The properties that make it such a very versatile resist platform for DUV 248-nm applications include its aqueous base developability, high DUV transparency, and high dry etch resistance.²³⁸ Given its very important and unique role in chemical amplification resists, we discuss here specific aspects of its synthesis and attributes.

Scheme 7.30 shows the synthetic pathways to PHOST, including radical, cationic, and anionic polymerization techniques.²³⁹ The polymerization behavior of the hydroxystyrene monomer (also called vinyl phenol) has been extensively investigated by Sovish,²⁴⁰ Overberger,²⁴¹ and Kato.²⁴² PHOST can be synthesized via direct radical polymerization of 4-hydroxystyrene, which in turn is obtained from catalytic dehydrogenation of 4-ethylphenol. This was the method used in the preparation of the first commercially available PHOST, which was sold by

²³⁶C.G. Willson, "Organic resist materials," in *Introduction to Microlithography*, L.F. Thompson, C.G. Willson, and M.J. Bowden, Eds., p. 218, American Chemical Society, Washington, DC (1994); C.G. Willson, R.A. Dammel, and A. Reiser, "Photoresist materials: a historical perspective," *Proc. SPIE* **3050**, 38–51 (1997).

²³⁷J. Maltabes, S.J. Holmes, J.R. Morrow, R.L. Barr, M. Hakey, G. Reynolds, W.R. Brunsvold, C.G. Willson, N.J. Clecak, S.A. MacDonald, and H. Ito, "1X deep UV lithography with chemical amplification for 1 micron DRAM production," *Proc. SPIE* **1262**, 2 (1990).

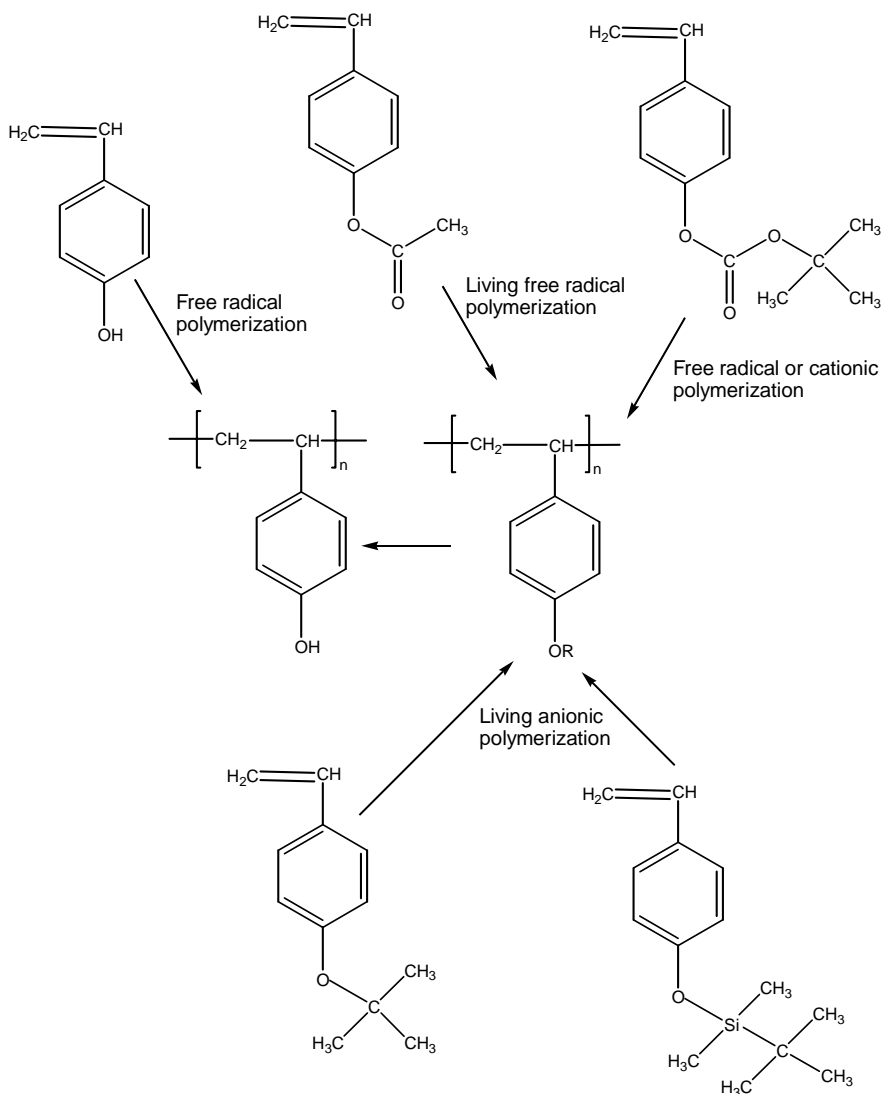
²³⁸H. Ito, "Chemical amplification resists for microlithography," *Adv. Polym. Sci.* **173**, 65 (2005).

²³⁹*ibid.*, p. 66.

²⁴⁰R.C. Sovish, "Notes: Preparation and polymerization of p vinylphenol," *J. Org. Chem.* **24**, 1345 (1959).

²⁴¹C.G. Overberger, J.S. Salamone, and S. Yaroslavsky, "Cooperative effects in the esterolytic action of synthetic macromolecules containing imidazole and hydroxyl functions," *J. Am. Chem. Soc.* **89**, 6231 (1967).

²⁴²M. Kato, "Radical polymerization behavior of hydroxystyrenes," *J. Polym. Sci. Part A* **7**, 2175 (1969).



Scheme 7.30 Synthetic routes to PHOST.

Maruzen Petrochemical of Japan in the early 1980s. Because the phenolic OH group is a radical scavenger, this synthetic approach yields rather low-molecular-weight polymers of Mw of a few thousand; the color of the polymer is dark red. The presence of aromatic rings on the repeating units of the polymer causes the polymer to significantly absorb in the DUV region. Catalytic hydrogenation of the polymer is effective in improving the transparency of the polymer in the DUV region.²⁴³

²⁴³H. Ito, "Chemical amplification resists for microlithography," *Adv. Polym. Sci.* **173**, 65–66 (2005).

The 4-hydroxystyrene monomer has poor storage stability since it undergoes rapid thermal oligomerization.²⁴⁴ Cationic polymerization of PHOST has also been reported by Kato.²⁴⁵

The very first reported PHOST that is transparent in the DUV was prepared by thermolysis or acidolysis of PBOCST, which is in turn prepared via radical polymerization of the BOCST monomer by 2,2-azobis(butyronitrile) (AIBN), benzoyl peroxide (BPO), or other radical initiators. The BOCST monomer can be prepared by the Wittig reaction on a protected 4-hydroxybenzaldehyde with a rather high yield due to the good stability of the *t*-BOC group toward a base catalyst.²⁴⁶ The PBOCST polymer thus obtained is readily converted to PHOST by heating the polymer to $\sim 200^\circ\text{C}$ or by treating the polymer with an acid such as acetic acid or HCl in solution. And PBOCST can be synthesized via cationic polymerization in liquid sulfur dioxide.²⁴⁷

Another route to PHOST synthesis, pioneered at Hoechst-Celanese, is the radical polymerization of 4-acetoxystyrene, followed by base hydrolysis in ammonium hydroxide. The 4-acetoxystyrene is readily prepared via Fries rearrangement of phenyl acetate to form 4-hydroxyacetophenone, followed by protection of the OH group with the acetyl group, and followed by reduction to carbinol, and finally, dehydration to yield the monomer.²⁴⁸

It has been reported that living radical polymerization of 4-acetoxystyrene with a TEMPO (2,2,6,6-tetramethylpiperidine-1-oxyl) adduct as the initiator, followed by base hydrolysis produces PHOSTs with narrow polydispersity, ~ 1.1 – 1.4 , which tend to have a 10 – 20°C higher T_g than their conventional PHOST counterparts (with polydispersity of 2.0 – 2.4), whose T_g ranges from 140 to 180°C .²⁴⁹

Hirao et al.²⁵⁰ have demonstrated the synthetic route to monodisperse PHOST, involving the living anionic polymerization of 4-*tert*-butyl(dimethyl)siloxystyrene

²⁴⁴R.C. Sovish, "Notes: Preparation and polymerization of p vinylphenol," *J. Org. Chem.* **24**, 1345 (1959); C.G. Overberger, J.S. Salamone, and S. Yaroslavsky, "Cooperative effects in the esterolytic action of synthetic macromolecules containing imidazole and hydroxyl functions," *J. Am. Chem. Soc.* **89**, 6231 (1967).

²⁴⁵M. Kato, "Radical polymerization behavior of hydroxystyrenes," *J. Polym. Sci. Part A 1* **7**, 2405 (1969).

²⁴⁶J.M.J. Fréchet, E. Eichler, H. Ito, and C.G. Willson, "H. poly(*p t* butoxycarbonyl styrene): a convenient precursor to *p* hydroxystyrene resins," *Polymer*. **24**, 995 (1983).

²⁴⁷ibid; H. Ito, "Chemical amplification resists for microlithography," *Adv. Polym. Sci.* **173**, 66 (2005).

²⁴⁸H. Ito, "Chemical amplification resists for microlithography," *Adv. Polym. Sci.* **173**, 67 (2005).

²⁴⁹G.G. Barclay, C.J. Hawker, H. Ito, and A. Orellana, P.R.L. Malenfant, R. Sinta, "Narrow polydispersity polymers for microlithography: synthesis and properties," *Proc. SPIE* **2724**, 249 (1996); G.G. Barclay, C.J. Hawker, H. Ito, and A. Orellana, P.R.L. Malenfant, R. Sinta, "The "living" free radical synthesis of poly(4 hydroxystyrene): physical properties and dissolution behavior," *Macromolecules* **31**, 1024 (1998).

²⁵⁰A. Hirao, K. Yamaguchi, K. Takenaka, K. Suzuki, S. Nakahama, and N. Yamazaki, "Polymerization of monomers containing functional groups protected by trialkylsilyl groups. 1. Synthesis of poly(4 vinylphenol) by means of anionic living polymerization," *Makromol. Chem. Rapid Commun.* **3**, 941 (1982); A. Hirao, K. Takenaka, S. Packirisamy, K. Yamaguchi, and S. Nakahama, "Polymerization of monomers containing functional groups protected by trialkylsilyl

in tetrahydrofuran (THF) under cryogenic temperature and high vacuum, and using butyllithium as the initiator. Desilylation of the resulting polymer with HCl yields the monodisperse PHOST. Replacing the THF solvent with cyclohexanone allows the anionic polymerization to be carried out at room temperature.²⁵¹

Commercial approaches to monodisperse PHOST that have been reported include the living anionic polymerization of 4-*tert*-butoxystyrene, which in turn may be synthesized via the reaction of styrenic Grignard reagent with *di-tert*-butyl peroxide,²⁵² followed by deprotection with a strong acid such as BBr.²⁵³

With respect to dissolution properties, PHOST dissolves much more rapidly than novolac resins in aqueous base developers; it is thus more difficult to inhibit its dissolution through the addition of a dissolution inhibitor such as DNQ. The dissolution rate of PHOST can, however, be modulated via partial protection of the OH group with acid-inert groups such as methyl or isopropyl carbonate, as well as with acid-labile groups such as carbonates, esters, acetals, and ketals. It can also be modulated through the choice of the appropriate isomers; *para*-PHOST isomers have higher aqueous base solubility than *meta*-PHOST isomers. The *ortho*-PHOST isomer is almost insoluble in an aqueous base.²⁵⁴ Substitution of the 3-position of 4-hydroxystyrene with a methyl group has also been shown to significantly reduce the dissolution rate of PHOST resins.²⁵⁵

groups, 4. Studies on anionic living polymerization of 4 (*tert* butyldimethylsilyloxy)styrene," *Makromol. Chem.* **186**, 1157 (1985).

²⁵¹H. Ito, A. Knebelkamp, S.B. Lundmark, C.V. Nguyen, and W.D. Hinsberg, "Silyl protected hydroxystyrenes: Living anionic polymerization at room temperature and selective desilylation," *J. Polym. Sci. Part A* **38**, 2415 (2000).

²⁵²D.A. Conlon, J.V. Crivello, J.L. Lee, and M.J. O'Brien, "The synthesis, characterization, and deblocking of poly(4 *tert* butoxystyrene) and poly(4 *tert* butoxy .alpha. methylstyrene)," *Macromolecules* **22**, 509 (1989).

²⁵³T. Iwayanagi, T. Ueno, S. Nonogaki, H. Ito, and C.G. Willson, in *Electronic and Photonic Applications of Polymers*, M.J. Bowden and R.S. Turner, Eds., Advances in Chemistry Series 218, p. 68, American Chemical Society, Washington, DC (1988).

²⁵⁴H. Ito, "Chemical amplification resists for microlithography," *Adv. Polym. Sci.* **173**, 69 (2005).

²⁵⁵K. Przybilla, H. Röschert, W. Spiess, C. Eckes, S. Chatterjee, D. Khanna, G. Pawlowski, and R. Dammel, "Progress in DUV resins," *Proc. SPIE* **1466**, 174 (1991); G. Pawloski, T. Sauer, R. Dammel, D. Gordon, W. Hinsberg, D. McKean, C.R. Lindley, H. J. Merrem, R. Vicari, and C.G. Willson, "Modified polyhydroxystyrenes as matrix resins for dissolution inhibition type photo resists," *Proc. SPIE* **1262**, 391 (1990); D.R. McKean, T.P. Sauer, W.D. Hinsberg, C.G. Willson, R. Vicari, and D. Gordon, "Synthesis, characterization, and lithographic behavior of methylated poly(4 hydroxystyrene)," *Polym. Preprints* **31**(2), 599 (1990); D.R. McKean, W.D. Hinsberg, T.P. Sauer, C.G. Willson, R. Vicari, and D.J. Gordon, "Methylated poly(4 hydroxystyrene): A new resin for deep ultraviolet resist application," *J. Vac. Sci. Technol.* **B8**, 1466 (1990); C.G. Willson, S.A. MacDonald, H. Ito, and J.M.J. Fréchet, "Recent progress in organic resist materials," in *Polymers for Microelectronics*, Y. Tabata, I. Mita, S. Nonogaki, K. Horie, and S. Tagawa, Eds., p. 3, Kodansha, Tokyo, Japan (1990); H. Ito, "Chemical amplification resists for microlithography," *Adv. Polym. Sci.* **173**, 69 (2005).

(iii) Synthesis of PBOCST

PBOCST is readily synthesized from the polymerization of *t*-butoxycarbonyl oxystyrene via radical or cationic polymerization in liquid sulfur dioxide²⁵⁶ or alternatively by reacting poly(hydroxystyrene) with *di-tert*-butyl dicarbonate in the presence of a base.²⁵⁷ PBOCST polymers with narrow dispersity have been prepared by living anionic polymerization of 5-*tert*-butyl(dimethyl)silyloxystyrene, followed by desilylation with HCl to form PHOST and protection with *di-tert*-butyl carbonate.²⁵⁸ PBOCST is very transparent around the 250-nm region of the spectrum (absorbance < 0.1/μm),²⁵⁹ thus making it an ideal candidate for DUV 248-nm lithography.

(iv) Other *t*-BOC-protected poly(hydroxy styrene)-based resists

The *t*-BOC protection group chemistry has been extended to other aqueous-base soluble polymers such as poly[styrene-*co*-N-(4-hydroxyphenyl)maleimide],²⁶⁰ poly(styrene-*co*-maleimide),²⁶¹ poly(4-hydroxystyrene sulfone),²⁶² and poly(4-hydroxy- α -methylstyrene)²⁶³ used in lithographic applications. Even novolac resins have been successfully protected with the *t*-BOC group,²⁶⁴ which has resulted in significant reduction of the DUV absorption of these resins.²⁶⁵

²⁵⁶J.M.J. Fréchet, E. Eichler, H. Ito, and C.G. Willson, "Poly(p *t* butoxycarbonyl styrene): a convenient precursor to p hydroxystyrene resins," *Polymer*, **24**, 995 (1983).

²⁵⁷F. Houlihan, F. Bouchard, J.M.J. Fréchet, and C.G. Willson, "Phase transfer catalysis in the *t* butyloxycarbonylation of alcohols, phenols, enols and thiols with di *t* butyl dicarbon" *Can. J. Chem.* **63**, 153 (1985).

²⁵⁸H. Ito, A. Knebelkamp, S.B. Lundmark, C.V. Nguyen, and W.D. Hinsberg, "Silyl protected hydroxystyrenes: Living anionic polymerization at room temperature and selective desilylation," *J. Polym. Sci. Part A: Polm. Chem.* **38**, 2415 (2000).

²⁵⁹H. Ito, "Chemical amplification resists for microlithography," *Adv. Polym. Sci.* **173**, 59 (2005).

²⁶⁰S.R. Turner, R.A. Arcus, C.G. Houle, and W.R. Schleigh, "High Tg base soluble copolymers as novolac replacements for photoresists," *Polym. Eng. Sci.* **26**, 1096 (1986); S.R. Turner, K.D. Ahn, and C.G. Willson, in *Polymers for High Technology*, M.J. Bowden and S.R. Turner, Eds., ACS Symposium Series 346, p. 200, American Chemical Society, Washington, DC (1987).

²⁶¹C.E. Osuch, K. Brahim, F.R. Hopf, A. McFarland, C.J. Mooring, and C.J. Wu, "A new class of resins for deep ultraviolet photoresists," *Proc. SPIE* **631**, 68 (1986); K. D. Ahn, D. I. Koo, S. J. Kim, "t boc maleimide copolymers for thermally stable deep UV resists by chemical amplification," *J. Photopolym. Sci. Technol.* **4**, 433 (1991).

²⁶²R.G. Tarascon, E. Reichmanis, F.M. Houlihan, A. Shugard, and L.F. Thompson, "Poly (t BOC styrene sulfone) based chemically amplified resists for deep UV lithography," *Polym. Eng. Sci.* **29**, 850 (1989).

²⁶³H. Ito, C.G. Willson, J.M.J. Fréchet, M.J. Farral, and E. Eichler, "Synthesis of poly(p hydroxy α methylstyrene) by cationic polymerization and chemical modification," *Macromolecules* **16**, 510 (1983); F.M. Houlihan, A. Shugard, R. Gooden, and E. Reichmanis, "An evaluation of nitrobenzyl ester chemistry for chemical amplification resists," *Proc. SPIE* **920**, 67 (1988).

²⁶⁴W. Brunsvold, W. Conley, W. Montgomery, and W. Moreau, in *Polymers for Microelectronics*, L.F. Thompson, C.G. Willson, and S. Tagawa, Eds., ACS Symposium Series 537, p. 333, American Chemical Society, Washington, DC (1994).

²⁶⁵A.S. Gozdz, J.A. Shelburne, and P.S.D. Lin, "Structure property relationships in *tert* butoxycarbonyl (t BOC) protected novolaks for resist applications," *Proc. ACS Div. Polym. Sci. Eng.* **66**, 192 (1992).

It should be noted that in addition to acid-catalyzed deprotection of some of the protected forms of the above-mentioned resins, namely, poly(4-*tert*-butoxy- α -methylstyrene)²⁶⁶ and poly(4-*tert*-butoxycarbonyloxystyrene sulfone),²⁶⁷ these resins are believed to undergo main chain scission under DUV irradiation. The poly(4-*tert*-butoxycarbonyloxystyrene sulfone) is believed to produce sulfinic or sulfonic acid through scission of the backbone C—S bond on x-ray irradiation, although it has a somewhat poor sensitivity to DUV.²⁶⁸ Because the resist polymer itself generates an acid that deprotects the *t*-BOC group, this system constitutes a rare example of a one-component chemical amplification resist (see Scheme 7.31).²⁶⁹

A major shortcoming of the series is their excessive shrinkage on exposure due to the loss of carbon dioxide and isobutene, which induces stress in the resist film and unacceptably high thickness loss during reactive-ion etching. A latter version of this resist comprising a terpolymer of poly(*t*-BOC-styrene-*co*-4-acetoxystyrene-*co*-styrene sulfone) has proven successful in mitigating this excessive shrinkage problem of the copolymer analog.²⁷⁰ Reportedly, the acetate group undergoes hydrolysis during aqueous-base development only in the presence of a phenolic functionality (i.e., only in the exposed regions) and the sulfone structure, while remaining inert to acidolysis (Scheme 7.32).²⁷¹

Polymers based on poly(hydroxyphenyl methacrylate), poly(*N*-hydroxyphenyl-methacrylate), and related copolymers have also been reported to be successfully protected with the *t*-BOC protecting group.²⁷² Other carbonates that have higher thermal stability than *t*-BOC-protected carbonates have also been reported,

²⁶⁶H. Ito, C.G. Willson, J.M.J. Fréchet, M.J. Farral, and E. Eichler, "Synthesis of poly(p hydroxy α methylstyrene) by cationic polymerization and chemical modification," *Macromolecules* **16**, 510 (1983).

²⁶⁷R.G. Tarascon, E. Reichmanis, F.M. Houlihan, A. Shugard, and L.F. Thompson, "Poly (*t* BOC styrene sulfone) based chemically amplified resists for deep UV lithography," *Polym. Eng. Sci.* **29**, 850 (1989).

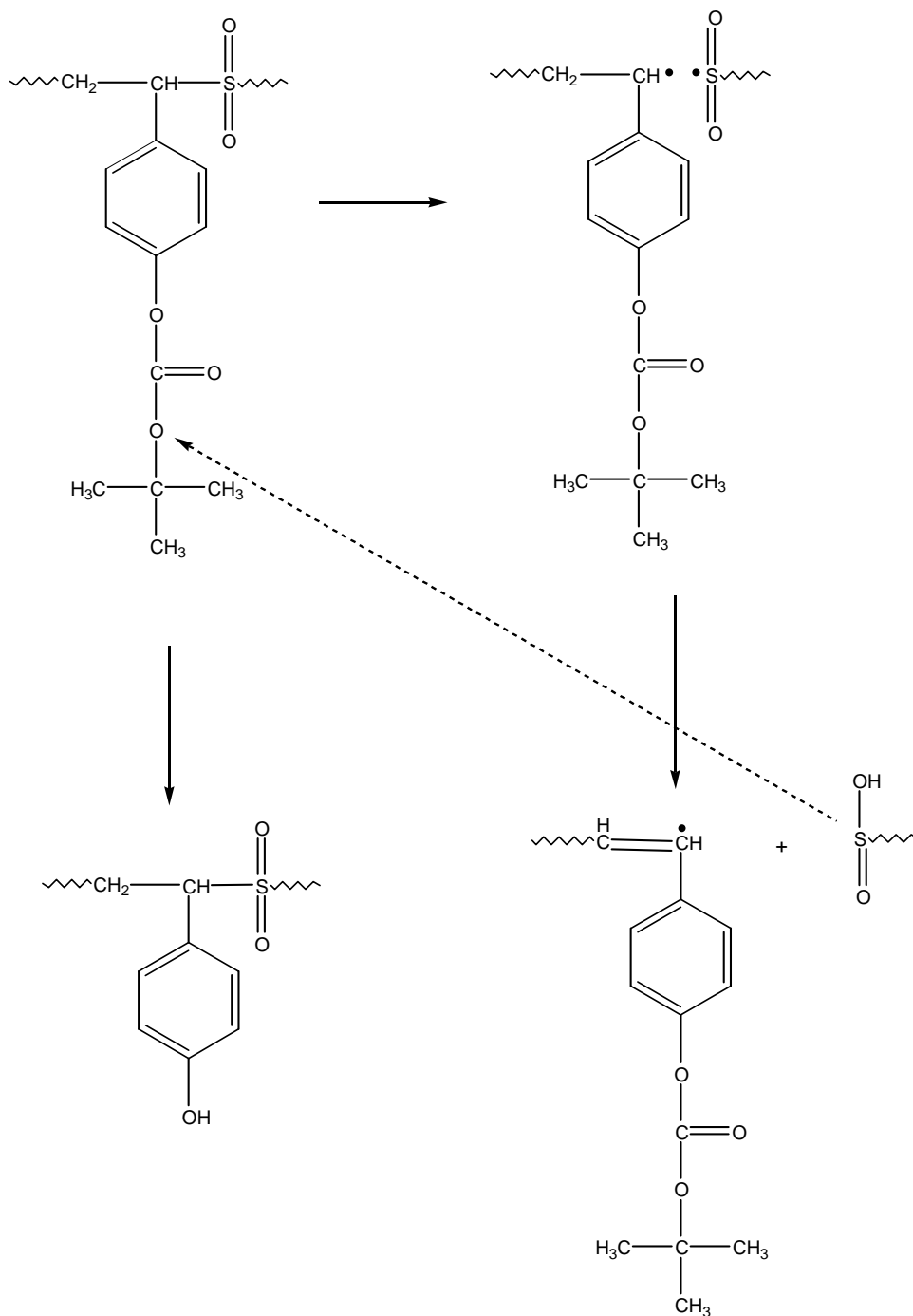
²⁶⁸A.E. Novembre, W.W. Tai, J.M. Kometani, J.E. Hanson, O. Nalamasu, G.N. Taylor, E. Reichmanis, and L.F. Thompson, "Preliminary lithographic characteristics of an all organic chemically amplified resist formulation for single layer deep UV lithography," *Proc. SPIE* **1466**, 89 (1991).

²⁶⁹T. Iwayanagi, T. Ueno, S. Nonogaki, H. Ito, and C.G. Willson, "A novel approach to inducing aqueous base solubility in substituted styrene sulfone polymers," in *Electronic and Photonic Applications of Polymers*, M.J. Bowden and R.S. Turner, Eds., Advances in Chemistry Series 218, p. 160, American Chemical Society, Washington, DC (1988).

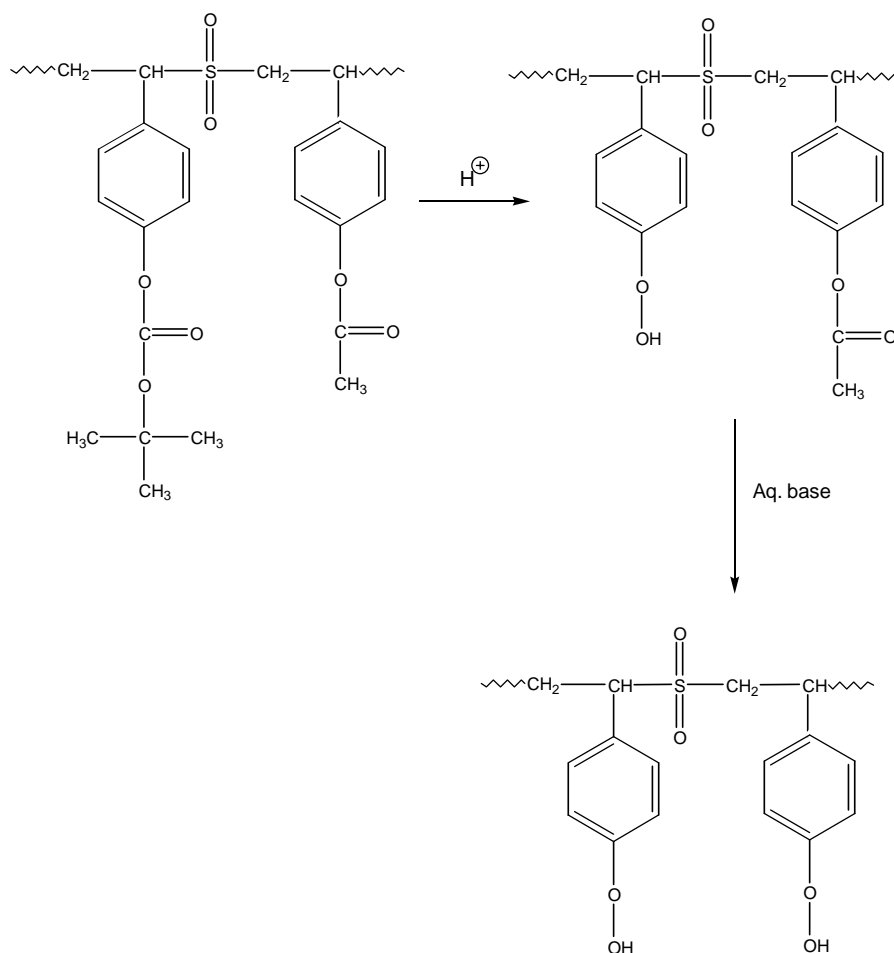
²⁷⁰J.M. Kometani, M.F. Galvin, S.A. Heffner, F.A. Houlihan, O. Nalamasu, E. Chin, and E. Reichmanis, "A novel approach to inducing aqueous base solubility in substituted styrene sulfone polymers," *Macromolecules* **26**, 2165 (1993).

²⁷¹T. Iwayanagi, T. Ueno, S. Nonogaki, H. Ito, and C.G. Willson, in *Electronic and Photonic Applications of Polymers*, M.J. Bowden and R.S. Turner, Eds., Advances in Chemistry Series 218, p. 160, American Chemical Society, Washington, DC (1988).

²⁷²K. Przybilla, R. Dammel, H. Röschert, W. Spiess, and G. Pawlowski, "New *t* boc blocked polymers for advanced lithographic applications," *J. Photopolym. Sci. Technol.* **4**, 421 (1991); K. Przybilla, H. Röschert, W. Spiess, C. Eckes, S. Chatterjee, D. Khanna, G. Pawlowski, and R. Dammel, "Progress in DUV resins," *Proc. SPIE* **1466**, 174 (1991).



Scheme 7.31 One-component x-ray positive resist based on t-BOC deprotection.



Scheme 7.32 Photoinduced acid-catalyzed deprotection, followed by base-catalyzed deacetylation during development.

including those with isopropyl, substituted α -methylbenzyl, and 1-(2-tetrahydrofurfuryl) ethyl groups.²⁷³

(v) Airborne poisoning of *t*-BOC-protected poly(hydroxy styrene)-based resists

A major drawback of *t*-BOC-protected PHOST-based resists, discovered somewhat late when the PBOCST was used for the first time in full-scale manufacturing

²⁷³W. Brunsvold, W. Conley, D. Crockatt, and N. Iwamoto, "Polyhydroxystyrene carbonate esters for high sensitivity photoresists having autodecomposition temperatures $> 160^\circ\text{C}$," *Proc. SPIE* **1086**, 357 (1989).

at IBM, was its propensity to postexposure delay (i.e., the time delay between exposure and postexposure bake) poisoning from airborne molecular bases. The problem manifested itself in the form of wild fluctuations in resist sensitivity. Experiments by S. MacDonald et al. elucidated the mechanism of this effect and determined its cause to be due to the gettering of airborne molecular bases by the resist film and subsequent neutralization of the photogenerated acids in the film, which prevents them from deprotecting the resist polymers.²⁷⁴ The researchers assembled a system that allowed wafers to be exposed to a controlled amount of the airborne molecular base with the highest concentration (several parts per billion) in the production facility, which was N-methylpyrrolidone (NMP). The experimental setup was such that a set of resist polymers were exposed to airstream samples containing radio-labeled NMP for a fixed length of time, following which the polymers were analyzed with scintillation counting techniques to ascertain how much of the NMP they had absorbed. Of all of the resist polymers tested, PBOCST was determined to be the fastest NMP getterer.²⁷⁵

The results also showed that the amount of absorbed NMP, or for that matter any airborne molecular base, depends on the solubility parameter of the polymer, on the nature of the contaminant, and on the T_g of the polymer.²⁷⁶ This was a remarkable result because it suggested that the environmental sensitivity of a resist polymer could be controlled by merely changing the T_g or the solubility parameter of the resist polymer. A verification of this result was obtained when the environmental stability of two polymers synthesized from two different isomers of BOCST monomers—the 3-BOCST and the 5-BOCST isomers—were found to have their environmental stability very well correlated with their T_g . The polymer with the significantly lower T_g —the 3-BOCST isomer—showed the least sensitivity to exposure to low levels of NMP.²⁷⁷

The implementation of the above-mentioned findings in the IBM production line as a way of combating the poisoning issue of chemically amplified resists came in the form of air filtration (for molecular bases) and the installation of controlled-environment storage spaces within the lithography clean room and within lithographic processing and exposure tools. Immediately following resist coating and baking in the track, wafers were transferred into these controlled-environment storage spaces, before they entered the exposure tool, which was also equipped with filtered-air enclosures to protect the wafers in the input cassettes on the exposure tool. Robotic transfer of the wafers from the output of the exposure tool to the postexposure bake plates of the track was also implemented, and was the

²⁷⁴S.A. MacDonald, W.D. Hinsberg, H.R. Wendt, N.J. Clecak, C.G. Willson, and C.D. Snyder, "Airborne contamination of a chemically amplified resist. I. Identification of problem," *Chem. Mater.* **5**, 348 (1993).

²⁷⁵C.G. Willson, R.A. Dammel, and A. Reiser, "Photoresist materials: a historical perspective," *Proc. SPIE* **3050**, 38–51 (1997).

²⁷⁶W.D. Hinsberg, S.A. MacDonald, N.J. Clecak, C.D. Snyder, and H. Ito, "Influence of polymer properties on airborne chemical contamination of chemically amplified resists," *Proc. SPIE* **1925**, 43 (1993).

²⁷⁷ibid.

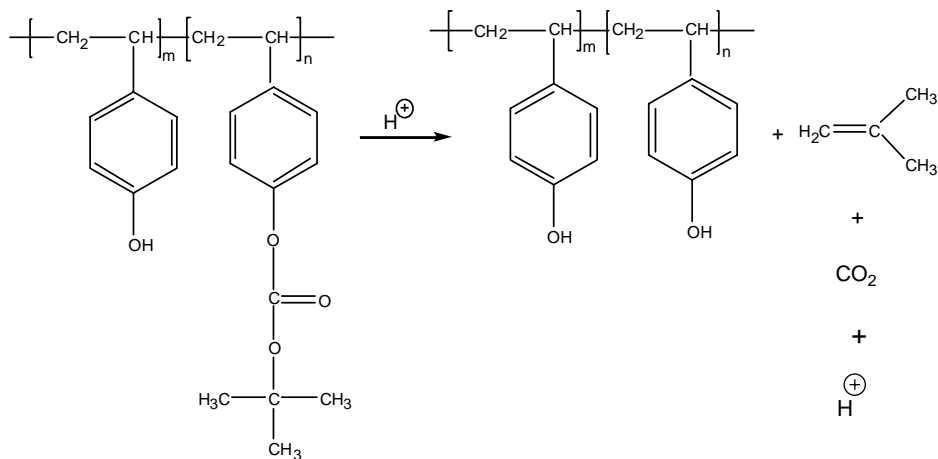
precursor of the cluster tool arrangements that are common in DUV exposure lines throughout the semiconductor industry today.²⁷⁸

7.2.2.3.3 Ester-protected chemical amplification resists

7.2.2.3.3.1 ESTER-PROTECTED POLY(HYDROXY STYRENE)-BASED RESISTS

Ester-protected carboxylic acid functional groups in resist resins can undergo photoinduced acid-catalyzed thermolysis in a chemical amplification scheme, just like carbonates, to form aqueous-base-soluble resins, and resulting in a change from a nonpolar to a polar state. The ester groups in these polymers are selected to generate on heterolysis of the C—O bond stable carbocations, which undergo spontaneous β -elimination to form olefins. The thermal and acidolytic stability can be tuned by changing the structure of the ester group.²⁷⁹

A very prominent example of this type of resist is a copolymer of 4-hydroxystyrene with *tert*-butyl ester-protected 4-hydroxystyrene (TBEST) (XXIX) (see scheme 7.33), developed at IBM and sold under the brand name of APEX-E by the Shipley Company. The synthetic route to copolymer (XXIX) can be through direct copolymerization of 4-hydroxystyrene with TBEST or via polymerization of TBEST, followed by partial deprotection to afford a copolymer with repeating units having about 20–30% protecting groups. Partial protection of copolymer



Scheme 7.33 Acid-catalyzed deprotection of poly(4-hydroxystyrene-co-4-polyhydroxystyrene-*tert*-butyl ester).

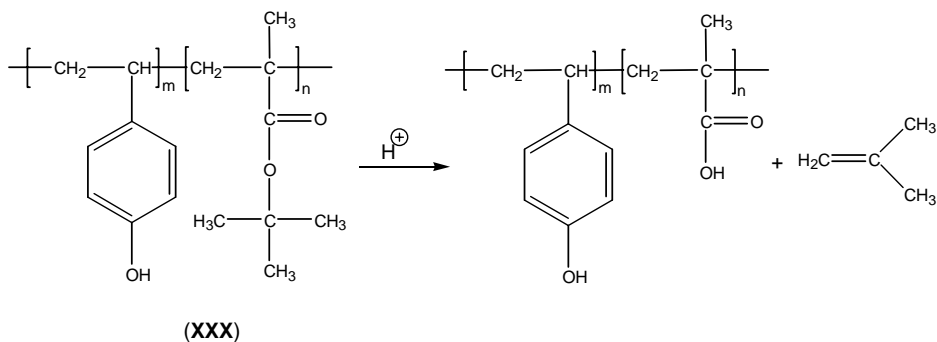
²⁷⁸C.G. Willson, R.A. Dammel, and A. Reiser, "Photoresist materials: a historical perspective," *Proc. SPIE* **3050**, 38–51 (1997).

²⁷⁹H. Ito, "Chemical amplification resists for microlithography," *Adv. Polym. Sci.* **173**, 62 (2005).

(XXIX) may also be accomplished by starting with the poly(hydroxystyrene) homopolymer and selectively protecting a fraction of the phenolic OH group.

Other ester-protected PHOST copolymers that have been employed in DUV resist applications include those protected with *tert*-butoxycarbonylmethyl²⁸⁰ and *tert*-butyl²⁸¹ groups. Poly(4-vinyl benzoate)²⁸² and poly(methyl methacrylate)²⁸³ are converted to poly(4-vinylbenzoic acid) and poly(methacrylic acid), respectively, by reactions with a photochemically generated acid.

One of the most important ester-protected polyhydroxystyrene-based resist copolymers, ESCAP (environmentally stable chemically amplified photoresist), developed at IBM, is based on the random copolymerization of 4-hydroxystyrene with *tert*-butyl acrylate (XXX).²⁸⁴ On exposure, this resist copolymer is converted to a copolymer of 4-hydroxystyrene with acrylic acid through photoinduced acid-catalyzed deprotection of the *tert*-butyl group (see Scheme 7.34). Because this resist system can be annealed at temperatures near its T_g in a process that fills up the free volumes (voids in the resist matrix), thus preventing the out-diffusion of photoacids from the matrix and in-diffusion of airborne bases into the resist, neutralization reactions between the photoacids and bases in the resist matrix (otherwise known as poisoning) are reduced, thus allowing



Scheme 7.34 Deprotection reaction of ESCAP resist polymer.

²⁸⁰Y. Ohnishi, H. Niki, Y. Kobayahi, R.H. Hayase, N. Oyasato, and O. Sasaki, "Postirradiation polymerization of e beam negative resists: Theoretical analysis and method of inhibition," *J. Photopolym. Sci. Technol.* **4**, 337 (1991).

²⁸¹D.A. Conlon, J.V. Crivello, J.L. Lee, and M.J. O'Brien, "The synthesis, characterization, and deblocking of poly(4 *tert* butoxystyrene) and poly(4 *tert* butoxy .alpha. methylstyrene)," *Macromolecules* **22**, 509 (1989).

²⁸²H. Ito, C.G. Willson, and J.M.J. Fréchet, "Positive/negative mid UV resists with high thermal stability," *Proc. SPIE* **771**, 24 (1987); H. Ito, M. L.A. Pederson, K.N. Chiong, S. Sonchik, and C. Tsai, "Sensitive electron beam resist systems based on acid catalyzed deprotection," *Proc. SPIE* **1086**, 11 (1989).

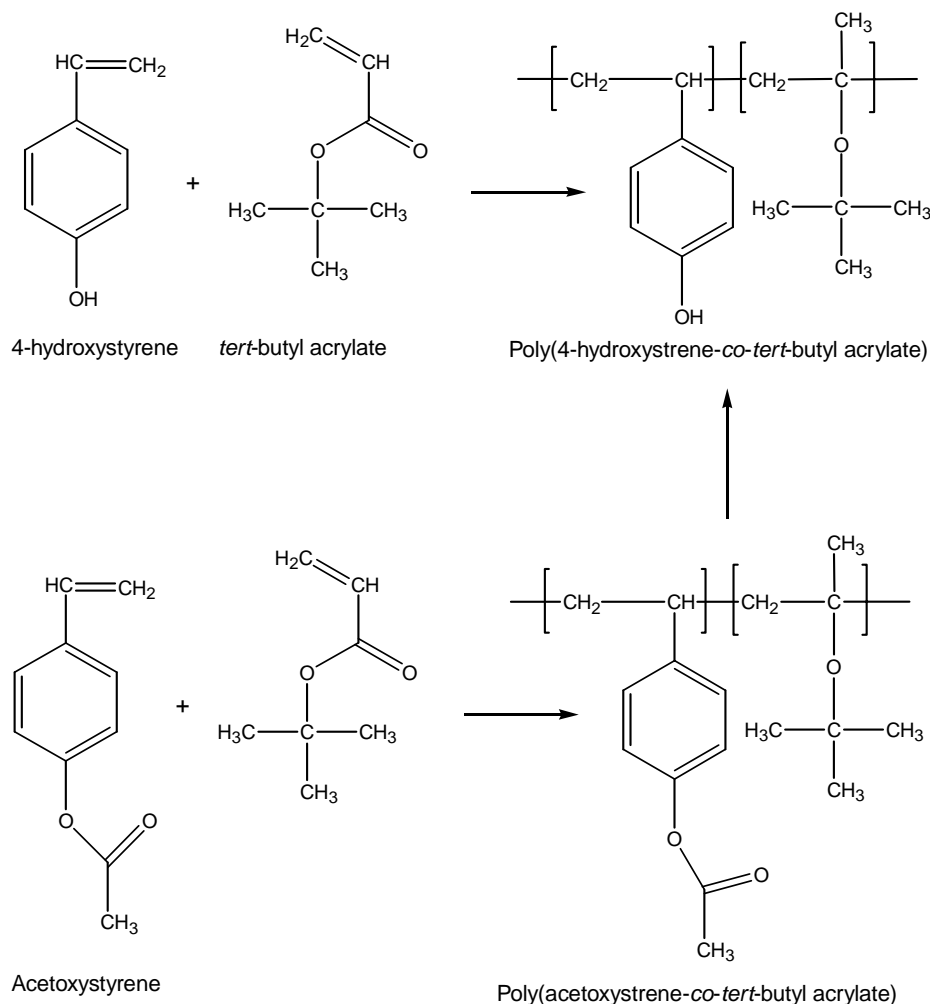
²⁸³H. Ito and M. Ueda, "Thermolysis and photochemical acidolysis of selected polymethacrylates," *Macromolecules* **21**, 1475 (1988).

²⁸⁴H. Ito, G. Breyta, D. Hofer, R. Sooriyakumaran, K. Petrillo, and D. Seeger, "Environmentally stable chemical amplification positive resist; Principle, chemistry, contamination resistance, and lithographic feasibility," *J. Photopolym. Sci. Technol.* **7**, 433 (1994).

the photoacids to participate in deprotection reactions that define the imaging mechanism of the system. The result is that this resist is extremely resistant to airborne contamination, in contrast to the early chemical amplification resists.

The poly(hydroxystyrene-*co-tert*-butyl acrylate) copolymer can be readily prepared by direct radical copolymerization of 4-hydroxystyrene with *tert*-butyl acrylate or alternatively via radical copolymerization of 4-acetoxystyrene with the *t*-butyl acrylate, followed by selective hydrolysis of the acetate group with ammonium hydroxide (see Scheme 7.35).²⁸⁵

In contrast to the partially protected PHOST copolymer, the ESCAP copolymers do not undergo thermal deprotection up to 180°C. Furthermore, the



Scheme 7.35 Synthetic routes to ESCAP resist polymer poly(4-hydroxystyrene-*co-tert*-butyl acrylate).

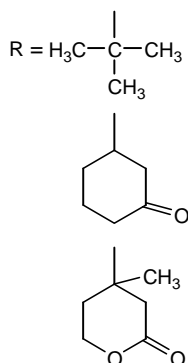
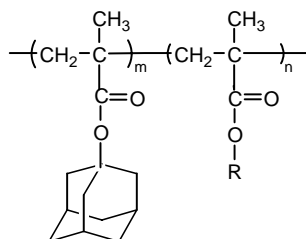
²⁸⁵H. Ito, "Chemical amplification resists for microlithography," *Adv. Polym. Sci.* **173**, 77 (2005).

photoacid-catalyzed conversion of the *tert*-butyl ester to carboxylic acid accelerates the dissolution rate in the exposed area relative to the unexposed area, effectively increasing the developer selectivity. ESCAP-type resists are by far the most widely used resists for DUV 248-nm lithography; some have found applications in EUV lithography as well.²⁸⁶

7.2.2.3.3.2 ESTER-PROTECTED POLY(METHACRYLATE)-BASED RESIST PLATFORM

Poly(methyl methacrylate)-based resists comprise a significant fraction of positive resists used in 193-nm and 157-nm lithographies. These resists are largely based on the acid-catalyzed deprotection of tertiary ester groups.

As already stated above, a major problem in the development of 193-nm single-layer resist (SLR) materials is the inherent trade-off between transparency and etch resistance. SLR resists for ArF lithography cannot contain aromatic groups (which characteristically have good etch resistance) if they are to meet transparency requirements. A breakthrough was made in 1992 when researchers at Fujitsu reported that acrylate polymers with pendant bi- and tricyclic units had comparable etch resistance to aromatic polymers²⁸⁷ (XXXI).



Acrylate polymers with pendant groups (XXXI) developed by researchers at Fujitsu over the period of 1992 to 1997.

Figures 7.11 and 7.12 show SEM images of line/space (L/S) and contact hole features printed in an early commercial version of this resist platform, based on

²⁸⁶ibid., pp. 77–78.

²⁸⁷Y. Kaimoto, K. Nozaki, S. Takechi, and N. Abe, "Alicyclic polymer for ArF and KrF excimer resist based on chemical amplification," *Proc. SPIE* **1672**, 66 (1992).

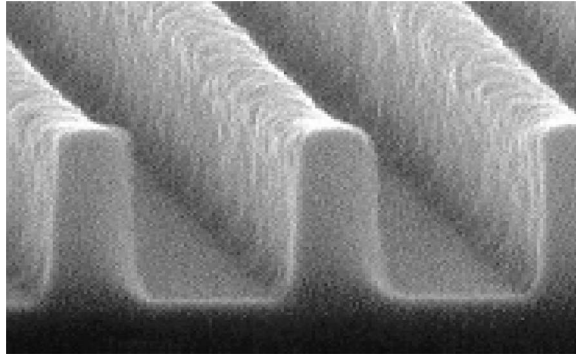


Figure 7.11 SEM images of 150-nm L/S features printed in Sumitomo's AX-210 resist, using ArF lithography.

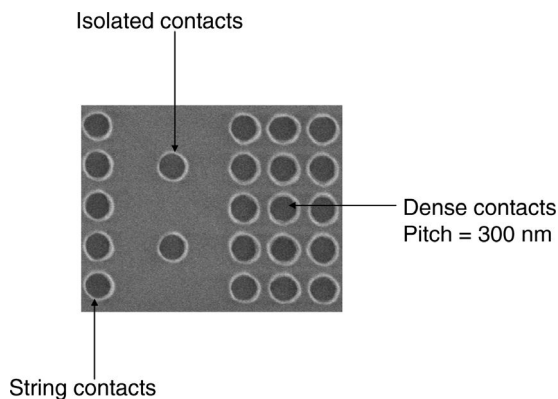


Figure 7.12 SEM images of 160-nm contact holes printed in Sumitomo's AX-655 resist, using ArF lithography.

poly(2-methyladamantyl methacrylate-*co*-gamma butyrolactone), and marketed under the trade names of AX-210 and AX-655, respectively, by Sumitomo Chemical. Figure 7.13 shows PEB delay stability of the very first commercial version of this resist platform, marketed under the brand name of PAR101 by Sumitomo. Notice the T-top profile in the images with 30- and 60-min delays before PEB, indicating the poisoning of the resist features that resulted from the neutralization of the photogenerated acid with ammonia and NMP, both of which were measured to be 0.64 ppb and 0.08 ppb, respectively, in the exposure tool at the time of the experiment.

In 1993, researchers at MIT Lincoln Labs and IBM reported that polymethacrylates were highly transparent to 193-nm radiation, and they were able to obtain excellent imaging performance at that wavelength.²⁸⁸ Their resist²⁸⁹ was

²⁸⁸R. R. Kunz, R.D. Allen, W.D. Hinsberg, and G.M. Wallraff, "Acid catalyzed single layer resists for ArF lithography," *Proc. SPIE* **1925**, 167 (1993).

²⁸⁹This resist was used for early ArF lithographic exposure tool testing purposes.

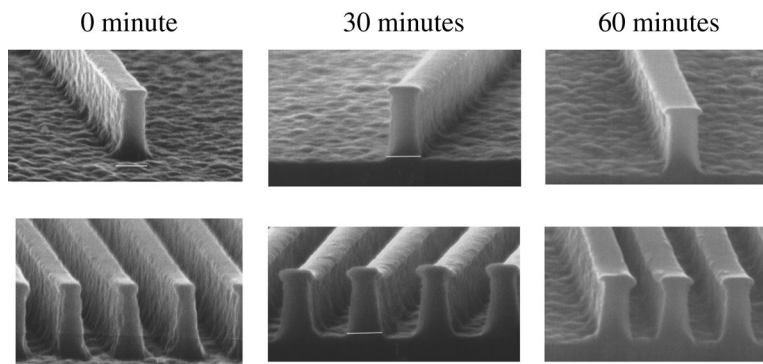
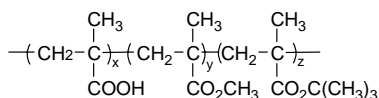


Figure 7.13 PEB delay stability of 160-nm lines printed on Sumitomo's PAR101 resist that is based on poly(2-methyladamantyl methacrylate-co-gamma butyrol lactone). Airborne molecular base concentration: NH_3 0.64 ppb; NMP 0.08 ppb. Processing conditions: PAB PEB $130^\circ\text{C}/60$ s. Resist thickness 4384 Å. Developer CD26 (2.38% TMAH). Dose $15 \text{ mJ}/\text{cm}^2$. NA 0.6, partial coherence 0.7.

a terpolymer of *tert*-butyl methacrylate (TBMA), methyl methacrylate (MMA), and methacrylic acid (MA) (**XXXII**) that was originally developed as a chemically amplified thick laser resist for laser direct writing of printed circuit board fabrication.²⁹⁰ The photogenerated acid induces acid-catalyzed deprotection of the *t*-butyl group to yield polymethacrylic acid, which is soluble in an aqueous base, resulting in a positive image. Unfortunately, this resist suffers from poor dry etch resistance and could only be developed with an extremely dilute developer.

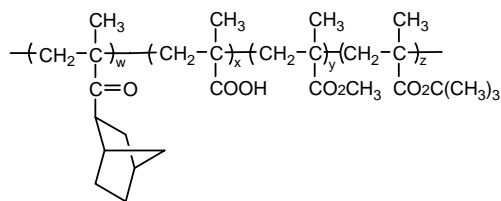
These findings prompted many research groups to incorporate alicyclic units and acid-labile ester functionality into polymethacrylates as pendant groups (see **XXXIII** and **XXXIV**).²⁹¹ These polymers were generally made by free radical



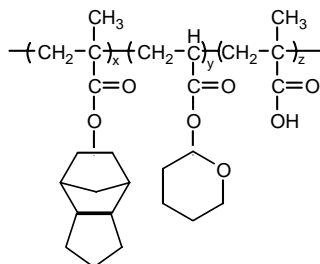
Acrylic terpolymer of methyl methacrylate, *t*-butyl methacrylate, and methacrylic acid (**XXXII**) developed by the IBM team and used for early ArF exposure tool testing purposes.

²⁹⁰R.D. Allen, G.M. Wallraff, W.D. Hinsberg, and L.L. Simpson, "High performance acrylic polymers for chemically amplified photoresist applications," *J. Vac. Sci. Technol. B* **9**, 3357 (1991).

²⁹¹K. Maeda, K. Nakano, T. Ohfuji, and E. Hasegawa, "Novel alkaline soluble alicyclic polymer poly (TCDMACOOH) for ArF chemically amplified positive resists," *Proc. SPIE* **2724**, 377 (1994); R.D. Allen, G.M. Wallraff, R.A. DiPietro, D.C. Hofer, and R.R. Kunz, "Single layer resists with enhanced etch resistance for 193nm lithography," *J. Photopolym. Sci. Technol.* **7**, 507 (1994); R.D. Allen, G.M. Wallraff, R.A. DiPietro, and D.C. Hofer, "193 nm single layer positive resists: building etch resist ance into a high resolution imaging system," *Proc. SPIE* **2438**, 474 (1995); M. Takahashi, S. Takechi, Y. Kaimoto, I. Hanyu, and N. Abe, "Evaluation of chemically amplified resist based on adamantyl methacrylate for 193 nm lithography," *Proc. SPIE* **2438**, 422 (1995); K. Nakano, K. Maeda, S. Iwasa, T. Ohfuji, and E. Hasegawa, "Positive chemically amplified resist for ArF excimer laser lithography composed of a novel transparent photoacid generator and an alicyclic terpolymer," *Proc. SPIE* **2438**,



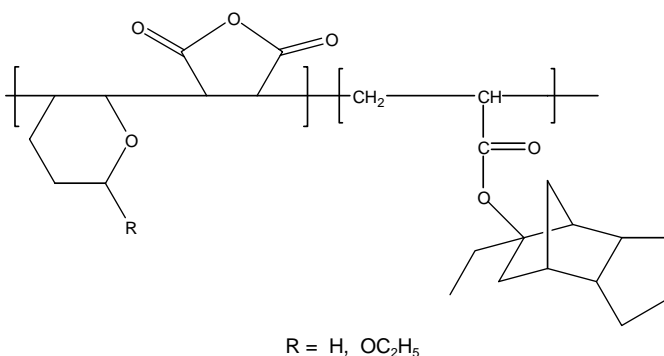
Acrylic tetrapolymer of isobornyl methacrylate, methyl methacrylate, *t*-butyl methacrylate, and methacrylic acid (**XXXIII**) developed by the IBM team in 1995.



Methacrylate terpolymer based on poly(ticyclodecanyl methacrylate-co-tetrahydropyranyl methacrylate-co-methacrylic acid) (**XXXIV**) developed at NEC in 1995.

polymerization. Because these resists have pendant alicyclic units on an acrylate backbone, we classify them as belonging to the acrylate platform.

A recently developed version of the methacrylate resist polymer platform is based on the radical copolymerization of vinyl ether, maleic anhydride, and acrylate monomers bearing appropriate functional groups.²⁹² Linear or cyclic alkyl vinyl ethers have been copolymerized with methacrylates bearing deprotectable ester groups (**XXXV**).



Acrylate terpolymer comprising vinyl ether, maleic anhydride, and alicyclic monomers (**XXXV**), developed at Samsung/Rohm Haas ca. 2001.

433 (1995); S. Takeshi, A. Kotachi, M. Takahashi, and I. Hanyu, "Approach to high aspect ratio patterning using cleavable adamantyl resist," *Proc. SPIE*, **3049**, 519 (1997).

²⁹²S. J. Choi, H. W. Kim, S. G. Woo, and J. T. Moon, "Design and synthesis of new photoresist materials for ArF lithography," *Proc. SPIE* **3999**, 54 (2000); H. W. Kim, S. J. Choi, D. W. Jung, S. Lee, S. H. Lee, Y. Kang, S. G. Woo, J. T. Moon, R. Kavanagh, G. Barclay, G. Orsula, J. Mattia, S. Caporale, T. Adams, T. Tanaka, and D. Kang, "A novel platform for production worthy ArF resist," *J. Photopolym. Sci. Technol.* **14**, 363 (2001).

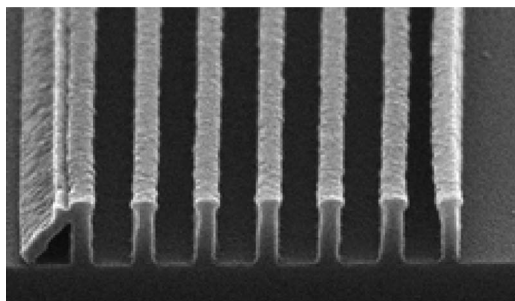


Figure 7.14 SEM images of 140-nm line and space features printed on Shipley's VEMA resist.

Figure 7.14 shows SEM images of 140-nm lines and space features printed in a first-generation resist based on poly(vinyl ether-*alt*-maleic anhydride) (VEMA) resins from the Shipley Corporation (now Rohm and Haas Corporation) around 2001.

7.2.2.3.3 ESTER-PROTECTED ALICYCLIC POLYMER RESIST PLATFORM

The second platform of ester-protected positive resists designed for ArF lithography is the alicyclic polymer platform,²⁹³ which was first developed at the University of Texas at Austin,²⁹⁴ and involves resists in which the alicyclic units with pendant ester-protecting groups, acidic groups, and adhesion-promoting groups constitute the backbone of the polymer. Resist polymers of this platform

²⁹³U. Okoroanyanwu, T. Shimokawa, J.D. Byers, and C.G. Willson, "Alicyclic polymers for 193 nm resist applications: synthesis and characterization," *Chem. Mater.* **10**(11), 3319 3327 (1998); U. Okoroanyanwu, J.D. Byers, T. Shimokawa, and C.G. Willson, "Alicyclic polymers for 193 nm resist applications: lithographic evaluation," *Chem. Mater.* **10**(11), 3328 3333 (1998); U. Okoroanyanwu, T. Shimokawa, J.D. Byers, and C.G. Willson, "Pd(II) catalyzed addition and ring opening metathesis polymerization of alicyclic monomers: routes to new matrix resins for 193 nm photolithography," *J. Mol. Catalysis A* **133**(1 2), 93 114 (1998); U. Okoroanyanwu, J.D. Byers, T. Shimokawa, K. Patterson, and C.G. Willson, "Alicyclic polymers for 193 nm lithography," in *Proc. of 11th Int. Conf. on Photopolymers*, 1, SPE, Mid Hudson Section of SPE, McAfee, NJ (1977); U. Okoroanyanwu, T. Shimokawa, D. Medeiros, C.G. Willson, J.M.J. Fréchet, Q.J. Niu, J.D. Byers, and R.D. Allen, "New single layer photoresists for 193 nm photolithography," *Proc. SPIE* **3049**, 92 (1997); Q.J. Niu, J.M.J. Fréchet, U. Okoroanyanwu, J.D. Byers, and C.G. Willson, "Novel functional polymers and copolymers for 193 nm and 248 nm chemically amplified resists," *Proc. SPIE* **3049**, 113 (1997); U. Okoroanyanwu, T. Shimokawa, S. Cho, P. Tsiartas, D. Medeiros, C.G. Willson, J.D. Byers, and R.D. Allen, "New single layer positive resists for 193 nm photolithography," in *Proc. of TECHCON '96*, Semiconductor Research Corp., p. 100 (1996); C.G. Willson, U. Okoroanyanwu, and D. Medeiros, "Photoresist compositions comprising norbornene derivative polymers with acid labile groups," U.S. Patent No. 6,103,445 (2000).

²⁹⁴For complete detail, please see, U. Okoroanyanwu, "Alicyclic polymers: chemistry and argon fluoride exciplex laser lithography," Ph.D. Thesis, The University of Texas at Austin (1997).

generally have higher plasma etch stability than their acrylate counterparts. The polymerization routes to the polymers of this platform include ring-opening metathesis polymerization [utilizing Ir(IV)-based catalysts], coordination cationic polymerization (or vinyl addition) [utilizing Pd(II)-based catalysts],²⁹⁵ and free radical polymerization [utilizing azobisisobutyronitrile (AIBN) and *di-tert*-butyl peroxide initiators]. Scheme 7.36 shows the synthetic pathways to these polymers.

The incorporation of cyclic olefins into the photoresist polymer backbone, it must be noted, represents a radical departure from the conventional 193-nm photoresist design concept, as typified by acrylate polymers²⁹⁶ or acrylate polymers with pendant cyclic olefins,²⁹⁷ or cyclic olefin/acrylate hybrid polymers.²⁹⁸ It is the unique architectures of the polymer backbones of these resist materials that impart properties (such as high etch resistance, low UV absorption at 193 nm, etc.)²⁹⁹ that make them very good candidates for 193-nm resist applications.

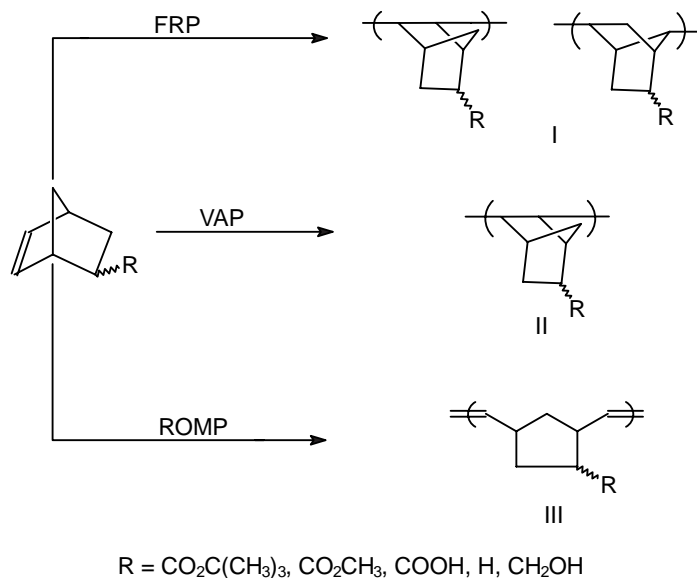
²⁹⁵The pioneering work on the synthesis of the coordination cationic ArF lithography resist polymers with catalysts based on Pd(II) and Ni(II) organometallic complexes was done by this author under the auspices of a joint collaborative project between The University of Texas at Austin and B.F. Goodrich Company of Brecksville, Ohio, in the summer of 1995, when the author was a visiting research scientist at the facilities of the latter, during his doctoral studies at UT Austin. By developing the synthetic pathways to these cationic coordination polymers and by demonstrating their exposure capabilities at 193 nm wavelength, the author paved the way for the subsequent exploitation of this class of resists in ArF lithography by IBM Corporation and JSR Corporation, who, working together with B.F. Goodrich, were able to make commercial resist products based on them; these resist products are now sold under the brand name of "COBRA." It should be mentioned that the Pd catalysts show a high tolerance toward polymerization of a wide variety of norbornene derivative monomers with functional groups, such as carboxylic acids and esters.

²⁹⁶K. Przybilla, R. Dammel, H. Röschert, W. Spiess, and G. Pawlowski, "New t-boc blocked polymers for advanced lithographic applications," *J. Photopolym. Sci. Technol.* **4**, 421 (1991); K. Przybilla, H. Röschert, W. Spiess, C. Eckes, S. Chatterjee, D. Khanna, G. Pawlowski, and R. Dammel, "Progress in DUV resins," *Proc. SPIE* **1466**, 174 (1991); R.D. Allen, G.M. Wallraff, W.D. Hinsberg, W.E. Conley, and R.R. Kunz, "Designing high performance KrF and ArF single layer resists with methacrylate polymers," *J. Photopolym. Sci. Technol.* **6**(4), 575 (1993); R.R. Kunz, S.C. Palmateer, A.R. Forte, R.D. Allen, G.M. Wallraff, R.A. DiPietro, and D.C. Hoffer, "Limits to etch resistance for 193 nm single layer resists" *Proc. SPIE* **2724**, 365 (1996).

²⁹⁷R.D. Allen, R. Sooriyakumaran, J. Opits, G. Wallraff, R. DiPietro, G. Breyta, D. Hofer, R. Kunz, S. Jayaraman, R. Schick, B. Goodall, U. Okoroanyanwu, and C.G. Willson, "Protecting groups for 193 nm photoresists," *Proc. SPIE* **2724**, 334 (1996); R.D. Allen, R. Sooriyakumaran, J. Opits, G. Wallraff, G. Breyta, R. DiPietro, D. Hofer, R. Kunz, U. Okoroanyanwu, and C.G. Willson, "Progress in 193 nm positive resists," *J. Photopolym. Sci. Technol.* **9**(3), 465 (1996).

²⁹⁸T.I. Wallow, F.M. Houlihan, O. Nalamasu, E. Chandross, T.X. Neenan, and E. Reichmanis, "Evaluation of cycloolefin maleic anhydride alternating copolymers as single layer photoresists for 193 nm photolithography," *Proc. SPIE* **2724**, 355 (1996).

²⁹⁹U. Okoroanyanwu, T. Shimokawa, J.D. Byers, and C.G. Willson, "Alicyclic polymers for 193 nm resist applications: synthesis and characterization," *Chem. Mater.* **10**(11), 3319-3327 (1998); U. Okoroanyanwu, J.D. Byers, T. Shimokawa, and C.G. Willson, "Alicyclic polymers for 193 nm resist applications: lithographic evaluation," *Chem. Mater.* **10**(11), 3328-3333 (1998); U. Okoroanyanwu, T. Shimokawa, J.D. Byers, and C.G. Willson, "Pd(II) catalyzed addition and ring opening metathesis polymerization of alicyclic monomers: routes to new matrix resins for 193 nm photolithography," *J. Mol. Catalysis A* **133**(1-2), 93-114 (1998); U. Okoroanyanwu, J.D.



Scheme 7.36 Synthetic scheme for the polymerization of norbornene and its derivatives via free radical polymerization (FRP), ring-opening metathesis polymerization (ROMP), and vinyl addition polymerization (VAP) techniques. Polymers I, II, and III are isomers that differ in their enchainment and physical properties. Co- and terpolymerization of norbornene and derivatives of norbornene with other alicyclic monomers such as maleic anhydride, methyltetracyclododecene carboxylic acid, etc. are also successfully synthesized with this scheme. (Note that 2, 3- and 2,7-enchainments of repeating units are reported in type I polymers.³⁰⁰)

The cycloaliphatic backbone of these polymers contributes to dry etch resistance and thermal stability and serves to tether the pendant functionalities required for imaging. The materials incorporate a pendant acid-cleavable group such as a *tert*-butyl ester that undergoes acid-catalyzed thermolysis accompanied by a

Byers, T. Shimokawa, K. Patterson, and C.G. Willson, "Alicyclic polymers for 193 nm lithography," in *Proc. of 11th Int. Conf. on Photopolymers*, 1, SPE, Mid Hudson Section of SPE, McAfee, NJ (1977); U. Okoroanyanwu, T. Shimokawa, D. Medeiros, C.G. Willson, and J.M.J. Fréchet, Q.J. Niu, J.D. Byers, and R.D. Allen, "New single layer photoresists for 193 nm photolithography," *Proc. SPIE* **3049**, 92 (1997); Q.J. Niu, J.M.J. Fréchet, U. Okoroanyanwu, J.D. Byers, and C.G. Willson, "Novel functional polymers and copolymers for 193 nm and 248 nm chemically amplified resists," *Proc. SPIE* **3049**, 113 (1997); U. Okoroanyanwu, T. Shimokawa, S. Cho, P. Tsiartas, D. Medeiros, C.G. Willson, J.D. Byers, and R.D. Allen, "New single layer positive resists for 193 nm photolithography," in *Proc. of TECHCON '96*, p. 100, Semiconductor Research Corp. (1996); C.G. Willson, U. Okoroanyanwu, and D. Medeiros, "Photoresist compositions comprising norbornene derivative polymers with acid labile groups," U.S. Patent No. 6,103,445 (2000).

³⁰⁰N.G. Gaylord, B.M. Mandal, and M.J. Martan, "Peroxide induced polymerization of norbornene," *Polym. Sci. Polym. Lett. Ed.* **14**, 555 (1976); N.G. Gaylord, A.B. Desphande, B.M. Mandal, and M.J. Martan, "Poly 2,3 and 2,7 bicyclo[2.2.1]hept 2 enes: Preparation and structures of polynorbornenes," *Macromol. Sci., Chem.* **A11**, 1053 (1977).

large change in polarity. They also incorporate a carboxylic acid group or maleic anhydride unit, which enhances the adhesion, wettability, and solubility of the material in an aqueous base developing solvent.

(i) Synthesis of alicyclic monomers

Carbo-*t*-butoxy norbornene (CBN) (*endo/exo* ratio 70/30) is readily synthesized by the Diels-Alder reaction between cyclopentadiene and *tert*-butyl acrylate.³⁰¹ Carbomethoxy norbornene (CMN) is also synthesized in similar manner.

(ii) Synthesis of alicyclic polymers

It has been known for some time that norbornene undergoes ring-opening metathesis polymerization in the presence of Ziegler-Natta catalysts,³⁰² reduced oxides of Cr, Mo, and W,³⁰³ and hydrated halides of Ru, Os, and Ir,³⁰⁴ resulting in an unsaturated polymer, poly(1,3-cyclopentylenevinylene). Norbornene also undergoes cationic polymerization in the presence of C₂H₅AlCl₂³⁰⁵, and FRP in the presence

³⁰¹U. Okoroanyanwu, T. Shimokawa, J.D. Byers, and C.G. Willson, "Alicyclic polymers for 193 nm resist applications: synthesis and characterization," *Chem. Mater.* **10**(11), 3319-3327 (1998); U. Okoroanyanwu, J.D. Byers, T. Shimokawa, and C.G. Willson, "Alicyclic polymers for 193 nm resist applications: lithographic evaluation," *Chem. Mater.* **10**(11), 3328-3333 (1998); U. Okoroanyanwu, T. Shimokawa, J.D. Byers, and C.G. Willson, "Pd(II) catalyzed addition and ring opening metathesis polymerization of alicyclic monomers: routes to new matrix resins for 193 nm photolithography," *J. Mol. Catal. A* **133**(1-2), 93-114 (1998); U. Okoroanyanwu, J.D. Byers, T. Shimokawa, K. Patterson, and C.G. Willson, "Alicyclic polymers for 193 nm lithography," *Proc. of 11th Int. Conf. on Photopolymers*, 1, SPE, Mid Hudson Section of SPE, McAfee, NJ (1977); U. Okoroanyanwu, T. Shimokawa, D. Medeiros, C.G. Willson, J.M.J. Fréchet, Q.J. Niu, J.D. Byers, and R.D. Allen, "New single layer photoresists for 193 nm photolithography," *Proc. SPIE* **3049**, 92 (1997); Q.J. Niu, J.M.J. Fréchet, U. Okoroanyanwu, J.D. Byers, and C.G. Willson, "Novel functional polymers and copolymers for 193 nm and 248 nm chemically amplified resists," *Proc. SPIE* **3049**, 113 (1997); U. Okoroanyanwu, T. Shimokawa, S. Cho, P. Tsiartas, D. Medeiros, C.G. Willson, J.D. Byers, and R.D. Allen, "New single layer positive resists for 193 nm photolithography," in *Proc. of TECHCON '96*, Semiconductor Research Corp., p. 100 (1996); C.G. Willson, U. Okoroanyanwu, and D. Medeiros, "Photoresist compositions comprising norbornene derivative polymers with acid labile groups," U.S. Patent No. 6,103,445 (2000).

³⁰²A.W. Anderson, N.G. Merckling, "Polymeric bicyclo (2, 2, 1) 2 heptene," U.S. Patent No. 2721,189 (1955); W.L. Truett, D.R. Johnson, I.M. Robinson, and B.A. Montague, "Polynorbornene by coordination polymerization," *J. Am. Chem. Soc.* **82**, 2337 (1960); T. Sujino, T. Saegusa, and J. Furukawa, "Polymerization of norbornene by modified Ziegler catalysts," *Makromol. Chem.* **85**, 71 (1965).

³⁰³H.S. Eleuterio, "Verfahren zur polymerisation cyclischer, insbesondere, mono-, di-, oder tricyclischer olefine," German Patent No. 1072811 (1960).

³⁰⁴F.W. Michelotti and W.P. Keaveney, "Coordinated polymerization of the bicyclo [2.2.1] heptene 2 ring system (norbornene) in polar media," *J. Polym. Sci. A* **3**, 895 (1965); R.E. Reinhart and H.P. Smith, *J. Polym. Sci. B*, **3**, 1049 (1965).

³⁰⁵J.P. Kennedy and H.S. Makowski, "Carbonium ion polymerization of norbornene and its derivatives," *Macromol. Sci. Chem.* **A-1**, 345 (1967).

of di-*tert*-butyl peroxide³⁰⁶ to reportedly yield poly(2,7-bicyclo[2.2.1]hept-2-ene), a saturated polymer, in both cases. Gaylord et al.³⁰⁷ attributed the unusual 2,7-enchainment of the polymer derived from free radical initiation to skeletal structural rearrangements of the bicyclic monomeric units that take place during the propagation reaction. Norbornene also undergoes vinyl addition polymerization in the presence of compounds of Pd(II)³⁰⁸ and Ti(IV),³⁰⁹ resulting in poly(2,3-bicyclo[2.2.1]hept-2-ene, a saturated polymer with 2,3-enchainment. Risse and co-workers³¹⁰ have reported on Pd(II)-catalyzed vinyl addition polymerization of norbornene derivatives bearing a variety of functional groups including esters.

Adapting the above-mentioned precedents in norbornene polymerization chemistry, the University of Texas research team was able to synthesize cycloaliphatic polymers with pendant-free carboxylic acid groups and carboxylic acids protected with acid-cleaveable groups, such as *tert*-butyl esters tailored for 193-nm resist use.³¹¹ They polymerized norbornyl derivatives such as CBN and

³⁰⁶H. Ito, "Chemical amplification resists for microlithography," *Adv. Polym. Sci.* **173**, 37 (2005).

³⁰⁷*ibid.*

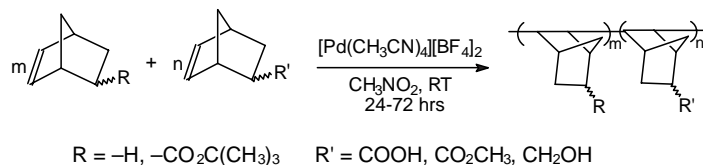
³⁰⁸W. Risse and S. Breunig, "Transition metal catalyzed vinyl addition polymerizations of norbornene derivatives with ester groups," *Makromol. Chem.* **193**, 2915 (1992); C. Mehler and M. Risse, "Addition polymerization of norbornene catalyzed by palladium(2+) compounds. A polymerization reaction with rare chain transfer and chain termination," *Macromol.* **25**, 4226 4228 (1992); R.G. Schulz, *Polym. Lett.* **4**, 541 (1966). C. Tanielian, A. Kiennemann, and T. Ospanpucu, "Influence de différents catalyseurs à base d'éléments de transition du groupe VIII sur la polymérisation du norbornène," *Can. J. Chem.* **57**, 2022 (1979); A. Sen and T. W. Lai, "Catalytic polymerization of acetylenes and olefins by tetrakis(acetonitrile)palladium(II) ditetrafluoroborate," *Organometallics* **1**, 415 (1982); C. Mehler and W. Risse, "Pd(II) catalyzed polymerization of norbornene derivatives," *Makromol. Chem. Rapid Commun.* **12**, 255 (1991).

³⁰⁹R.E. Rhinehart and H.P. Smith, *J. Polym. Sci. B*, **3**, 1049 (1965).

³¹⁰J.P. Mathew, A. Reinmuth, J. Melia, N. Swords, and W. Risse, "(η^3 Allyl)palladium(II) and palladium(II) nitrile catalysts for the addition polymerization of norbornene derivatives with functional groups," *Macromol.* **29**, 2755 (1996); W. Risse and S. Breunig, "Transition metal catalyzed vinyl addition polymerizations of norbornene derivatives with ester groups," *Makromol. Chem.* **193**, 2915 (1992).

³¹¹U. Okoroanyanwu, T. Shimokawa, J.D. Byers, and C.G. Willson, "Alicyclic polymers for 193 nm resist applications: synthesis and characterization," *Chem. Mater.* **10**(11), 3319 3327 (1998); U. Okoroanyanwu, J.D. Byers, T. Shimokawa, and C.G. Willson, "Alicyclic polymers for 193 nm resist applications: lithographic evaluation," *Chem. Mater.* **10**(11), 3328 3333 (1998); U. Okoroanyanwu, T. Shimokawa, J.D. Byers, and C.G. Willson, "Pd(II) catalyzed addition and ring opening metathesis polymerization of alicyclic monomers: routes to new matrix resins for 193 nm photolithography," *J. Mol. Catal. A* **133**(1 2), 93 114 (1998); U. Okoroanyanwu, J.D. Byers, T. Shimokawa, K. Patterson, and C.G. Willson, "Alicyclic polymers for 193 nm lithography," in *Proc. of 11th Int. Conf. on Photopolymers*, SPE, Mid Hudson Section of SPE, McAfee, NJ, p. 1 (1977); U. Okoroanyanwu, T. Shimokawa, D. Medeiros, C.G. Willson, J.M.J. Fréchet, Q.J. Niu, J.D. Byers, and R.D. Allen, "New single layer photoresists for 193 nm photolithography," *Proc. SPIE* **3049**, 92 (1997); Q.J. Niu, J.M.J. Fréchet, U. Okoroanyanwu, J.D. Byers, and C.G. Willson, "Novel functional polymers and copolymers for 193 nm and 248 nm chemically amplified resists," *Proc. SPIE* **3049**, 113 (1997); U. Okoroanyanwu, T. Shimokawa, S. Cho, P. Tsiartas, D. Medeiros, C.G. Willson, J.D. Byers, and R.D. Allen, "New single layer positive resists for 193 nm photolithography," in *Proc. of TECHCON '96*, Semiconductor Research Corporation, p. 100

its analogs via (i) vinyl addition polymerization (VAP) with bis-tetrafluoroborate-tetrakis (cyanomethane) palladium ($[\text{Pd}(\text{CH}_3\text{CN})_4][\text{BF}_4]_2$), in nitromethane at room temperature (see Scheme 7.37),³¹² (ii) FRP with di-*tert*-butyl peroxide at 118–130°C and AIBN at 65°C in THF (see Scheme 7.38),³¹³ and (iii) ROMP with dipotassium hexachloroiridate (K_2IrCl_6) in a mixture of water, acetic acid, and zinc at 50°C (see Scheme 7.39).³¹⁴ They hydrogenated the ROMP polymers using diimide, produced in situ from hydrazine (see Scheme 7.39).³¹⁵



Scheme 7.37 Vinyl addition copolymerization of various norbornene derivatives using $[\text{Pd}(\text{CH}_3\text{CN})_4](\text{BF}_4)_2$ in nitromethane at room temperature, using a procedure adapted from Risse and co-workers.³¹⁶

(iii) Thermal analysis

A thermogravimetric analysis (TGA) profile of a typical alicyclic copolymer resist resin, poly(CBN-co-NBCA), is shown in Fig. 7.15. All of the alicyclic resist co- and terpolymers show similar TGA profiles. The deprotection temperature and decomposition temperature for the polymers are roughly 250°C and 400°C, respectively. At the deprotection temperature, roughly 25% weight loss associated with the deprotection event and corresponding to the loss of isobutylene and carbon

(1996); C.G. Willson, U. Okoroanyanwu, and D. Medeiros, "Photoresist compositions comprising norbornene derivative polymers with acid labile groups," U.S. Patent No. 6,103,445 (2000).

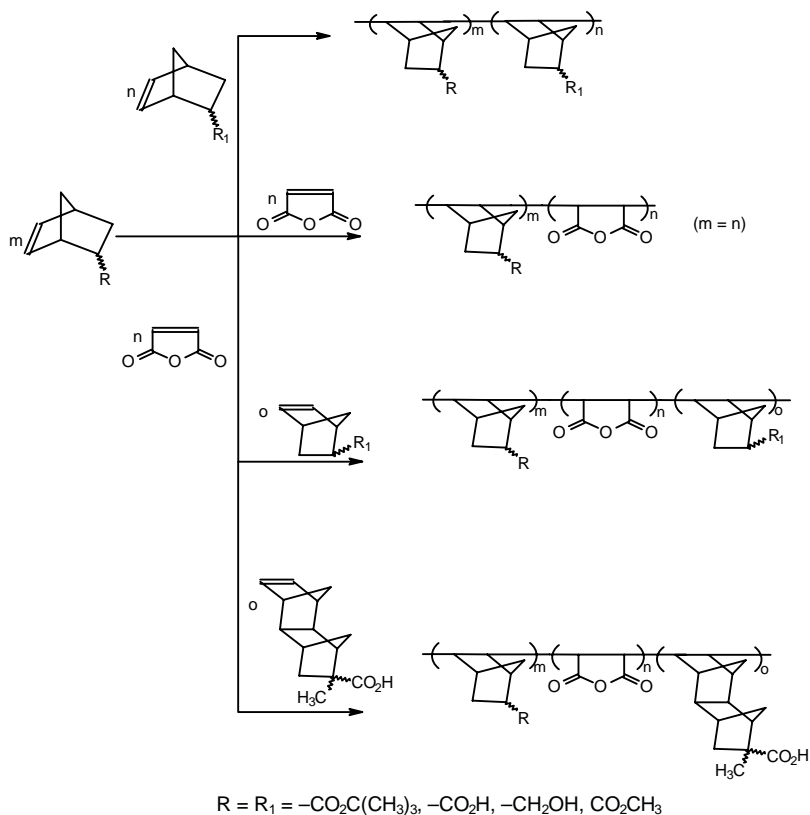
³¹²ibid.

³¹³ibid.

³¹⁴ibid.

³¹⁵ibid.

³¹⁶W. Risse and S. Breunig, S. "Transition metal catalyzed vinyl addition polymerizations of norbornene derivatives with ester groups," *Makromol. Chem.* 193, 2915 (1992); C. Mehler and M. Risse, "Addition polymerization of norbornene catalyzed by palladium(2+) compounds. A polymerization reaction with rare chain transfer and chain termination," *Macromol.* 25, 4226-4228 (1992); R.G. Schulz, "The chemistry of palladium complexes, III. The polymerization of norbornene systems catalyzed by palladium chloride (1)," *Polym. Lett.* 4, 541 (1966); C. Tanielian, A. Kiennemann, and T. Osparpucu, "Influence de différents catalyseurs à base d'éléments de transition du groupe VIII sur la polymérisation du norbornène," *Can. J. Chem.* 57, 2022 (1979); A. Sen and T. W. Lai, "Catalytic polymerization of acetylenes and olefins by tetrakis(acetonitrile)palladium(II) ditetrafluoroborate," *Organometallics* 1, 415 (1982); C. Mehler and W. Risse, "Pd(II) catalyzed polymerization of norbornene derivatives," *Makromol. Chem. Rapid Commun.* 12, 255 (1991).

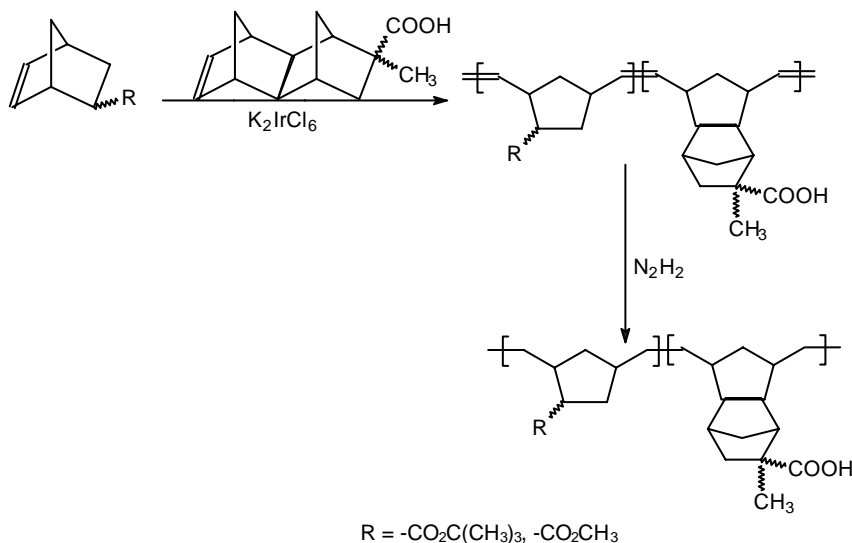


Scheme 7.38 Free radical copolymerization of various alicyclic monomers initiated by (1) azoisobutyronitrile (AIBN) in THF, and (2) di-*tert*-butyl peroxide (DTBP) in propylene glycol monomethylether acetate, and used in the synthesis of the alicyclic polymer resist materials for ArF lithography, pioneered at the University of Texas at Austin in 1995. Note that although only 2,3-enchainment of the cyclic olefins is shown above the scheme, 2,7-enchainment is also possible, as reported by Gaylord and co-workers.³¹⁷

dioxide from the starting copolymer is observed. The T_g of the ROMP-derived poly(CBN) is 90°C; the vinyl addition and free radical derived poly(CBN) show no thermal transition below the decomposition temperature at 250°C.³¹⁸

³¹⁷N.G. Gaylord, B.M. Mandal, and M.J. Martan, "Peroxide induced polymerization of norbornene," *Polym. Sci. Polym. Lett. Ed.* **14**, 555 (1976); N.G. Gaylord, A.B. Desphande, B.M. Mandal, and M.J. Martan, "Poly 2,3 and 2,7 bicyclo[2.2.1]hept 2 enes: Preparation and structures of polynorbornenes," *Macromol. Sci., Chem.* **A11**, 1053 (1977).

³¹⁸U. Okoroanyanwu, T. Shimokawa, J.D. Byers, and C.G. Willson, "Alicyclic polymers for 193 nm resist applications: synthesis and characterization," *Chem. Mater.* **10**(11), 3319 3327 (1998); U. Okoroanyanwu, J.D. Byers, T. Shimokawa, and C.G. Willson, "Alicyclic polymers for 193 nm resist applications: lithographic evaluation," *Chem. Mater.* **10**(11), 3328 3333 (1998); U. Okoroanyanwu, T. Shimokawa, J.D. Byers, and C.G. Willson, "Pd(II) catalyzed addition and ring opening metathesis polymerization of alicyclic monomers: routes to new matrix resins for



Scheme 7.39 Ring-opening metathesis polymerization of various alicyclic monomers using K_2IrCl_6 . Following polymerization, the polymer was hydrogenated with diimide produced in situ.

The other resist polymers, poly(CBN-alt-MAH), poly(CBN-co-MTDCA), and poly(CBN-alt-MAH-alt-NBE) show similar TGA profiles. Their decomposition temperatures are all in excess of 240°C.

A number of alicyclic polymers designed for resist applications and following the University of Texas at Austin approach have been reported. The most prominent among them include these listed below and marketed under the brand name

193 nm photolithography," *J. Mol. Catal. A* **133**(1-2), 93-114 (1998); U. Okoroanyanwu, J.D. Byers, T. Shimokawa, K. Patterson, and C.G. Willson, "Alicyclic polymers for 193 nm lithography," *Proc. 11th International Conference on Photopolymers*, SPE, Mid Hudson Section of SPE, McAfee, NJ, p. 1 (1977); U. Okoroanyanwu, T. Shimokawa, D. Medeiros, C.G. Willson, J.M.J. Fréchet, Q.J. Niu, J.D. Byers, and R.D. Allen, "New single layer photoresists for 193 nm photolithography," *Proc. SPIE* **3049**, 92 (1997); Q.J. Niu, J.M.J. Fréchet, U. Okoroanyanwu, J.D. Byers, and C.G. Willson, "Novel functional polymers and copolymers for 193 nm and 248 nm chemically amplified resists," *Proc. SPIE* **3049**, 113 (1997); U. Okoroanyanwu, T. Shimokawa, S. Cho, P. Tsiartas, D. Medeiros, C.G. Willson, J.D. Byers, and R.D. Allen, "New single layer positive resists for 193 nm photolithography," in *Proc. of TECHCON '96*, Semiconductor Research Corp., 100 (1996); C.G. Willson, U. Okoroanyanwu, and D. Medeiros, "Photoresist compositions comprising norbornene derivative polymers with acid labile groups," U.S. Patent No. 6,103,445 (2000).

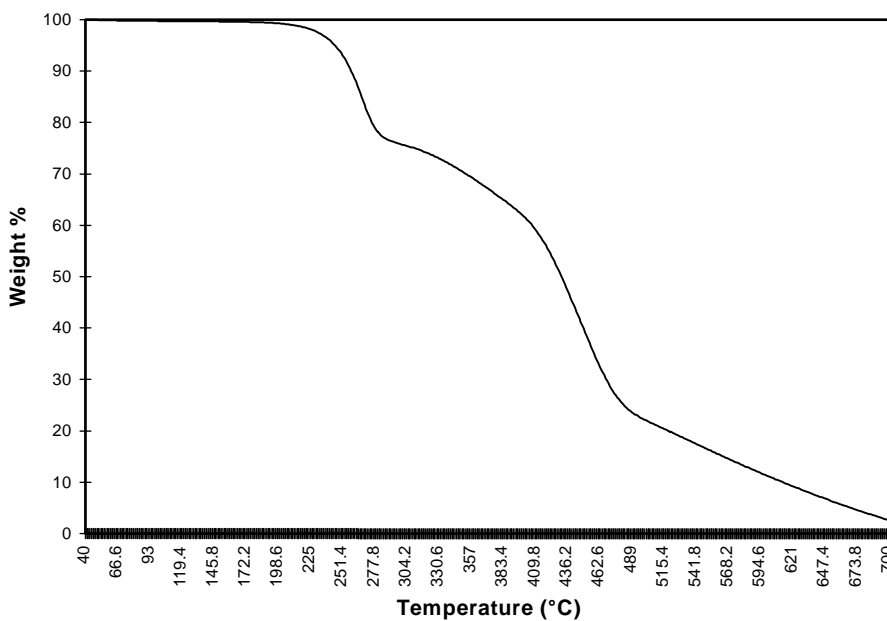
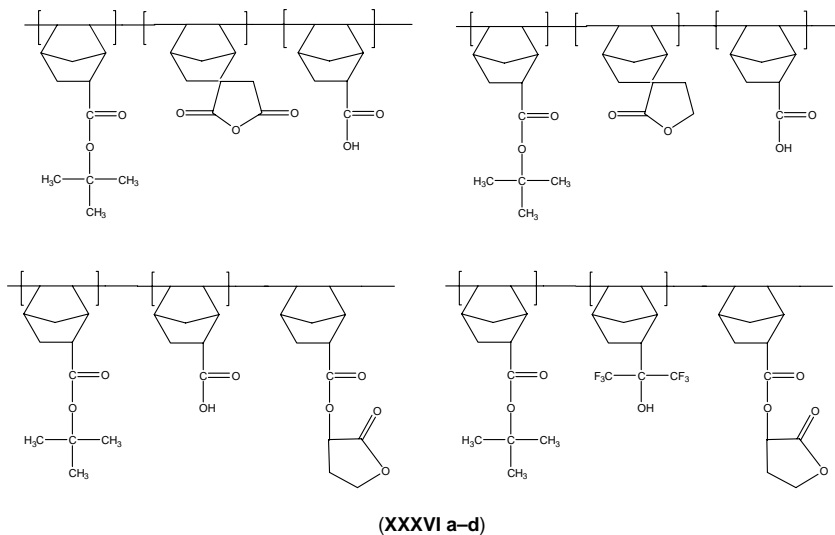


Figure 7.15 TGA curve of a typical resist copolymer poly(CBN-co-NBCA).

of COBRA (**XXXVI a–d**) by the JSR Corporation. The synthesis of these polymers are also catalyzed by Pd(II) catalysts.³¹⁹



³¹⁹H. Ito, "Chemical amplification resists for microlithography," *Adv. Polym. Sci.* **173**, 112–113 (2005); K. Hatada, T. Kitayama, S. Danjo, Y. Tsubokura, H. Yuki, K. Morikawa, H. Aritome, and S. Namba, "Polymers of alpha substituted benzyl methacrylates as a new type of electron beam resist," *Polym. Bull.* **10**, 45 (1983).

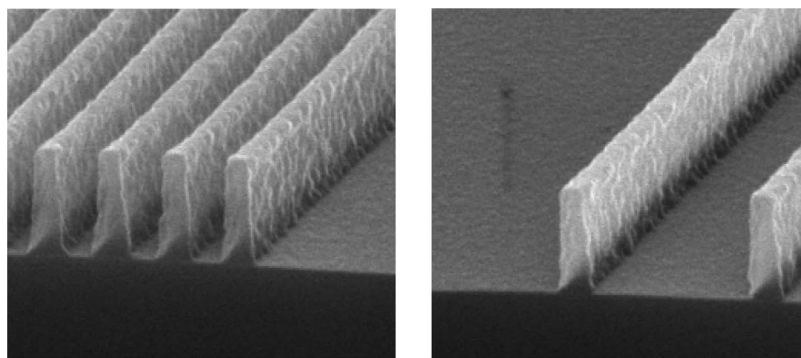


Figure 7.16 SEM images of 150-nm line features printed in the first commercial version of the alicyclic polymer resist platform, based on poly(dinorbornene-*alt*-maleic anhydride), and marketed under the brand name of AT01 by the JSR Corporation. Exposure wavelength was 193 nm.

Figure 7.16 shows SEM images of one of the first commercial versions of the alicyclic polymer resist platform, based on poly(dinorbornene-*alt*-maleic anhydride), and marketed under the brand name of AT01 by the JSR Corporation in 1998. Figures 7.17–7.19 show SEM images of other alicyclic platform resists, DHA-1001 and DHK-1000 series, exposed on ArF laser (193-nm) and electron-beam tools, respectively. These resists were produced by Dongjin Semichemical Co. Ltd.

A terpolymer of norbornene hexafluoroisopropanol, sulfur dioxide, and CBN (see Scheme 7.40) has been reported to be highly transparent at 193 nm (optical density $\sim 0.25/\mu\text{m}$) and successfully used in 193-nm resist application.³²⁰

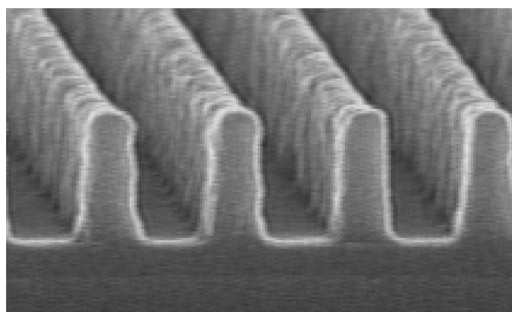


Figure 7.17 SEM images of 130-nm line and space features printed in a 350-nm thick Dongjin Semichem Co. Ltd. DHA-1001 resist with ArF lithography.

³²⁰H. Ito, N. Seehof, and R. Sato, "Synthesis and preliminary evaluation of substituted poly(norbornene sulfones) for 193 nm lithography," in *Proc. of ACS Div. Polym. Mater. Sci. Eng.*, Vol. 77, 449 (1977); H. Ito, R. Sato, T. Nakayama, and M. Ueda, in *Micro and Nanopatterning Polymers*, H. Ito, E. Reichmanis, O. Nalamasu, and T. Ueno, Eds., ACS Symposium Series 706, p. 208, American Chemical Society, Washington, DC (1998).

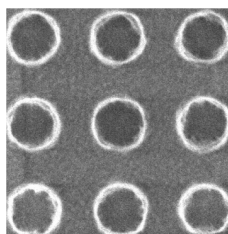


Figure 7.18 SEM image of 160-nm contact hole features printed in a 350-nm thick Dongjin Semichem Co. Ltd. DHA-1001 resist with ArF lithography with 28 mJ/cm².

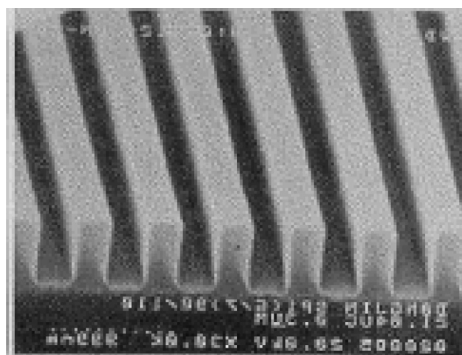
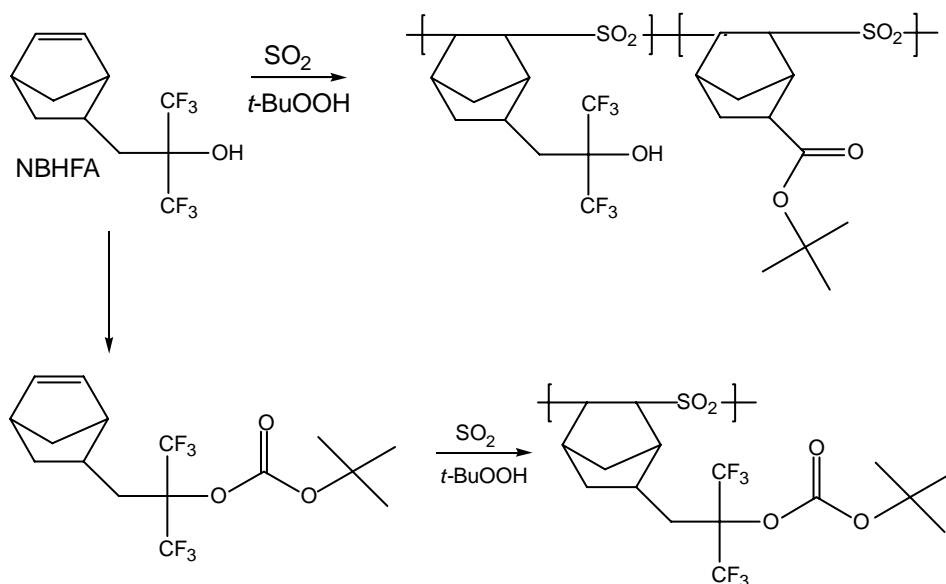


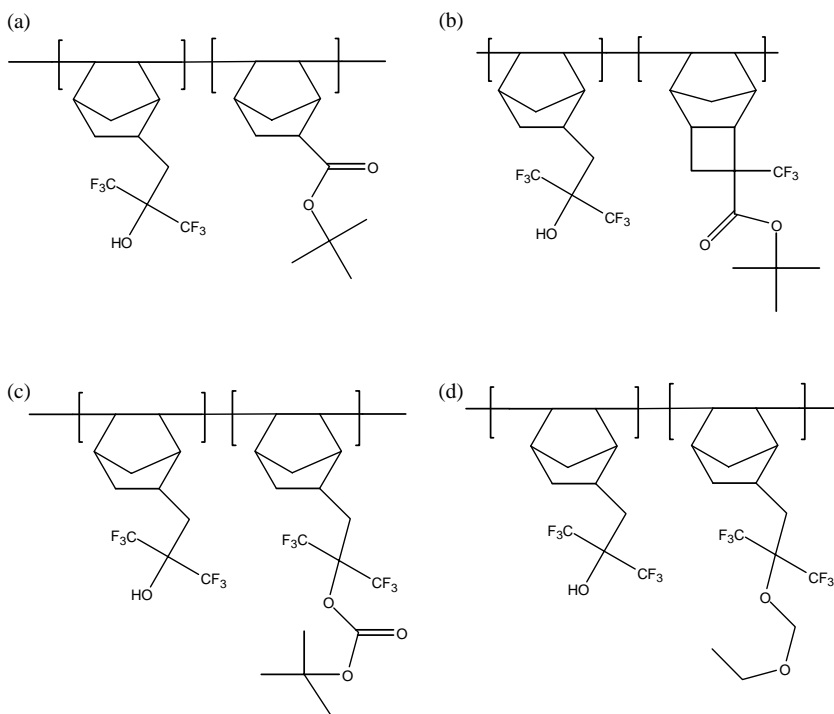
Figure 7.19 SEM image of 130-nm line and space features printed in a 350-nm thick Dongjin Semichem Co. Ltd. DHK-1000 resist with electron-beam lithography with 21 $\mu\text{C}/\text{cm}^2$.



Scheme 7.40 Synthetic routes to poly(NBHFA-co-SO₂).

A major drawback of this sulfone terpolymer resist is its poor plasma etch resistance.

Because fluoropolymers and polysilsesquioxanes are the only set of polymers with reasonable transparency at 157 nm, significant efforts were invested in finding lithographically useful fluorinated analogs of existing norbornene and metacrylate 193-nm resist platforms.³²¹ Fluorinated norbornenes with ester-protected groups comprising (i) polymers containing F in the backbone (typically prepared by copolymerization involving tetrafluoroethylene, TFE) and (ii) polymers containing F in the side chain as in NBHFA have been successfully synthesized and used in 157-nm lithography. In particular, NBHFA has been reportedly copolymerized with CBN and other norbornene monomers via VAP using Pd or Ni catalysts (XXXVIIa–d).³²²



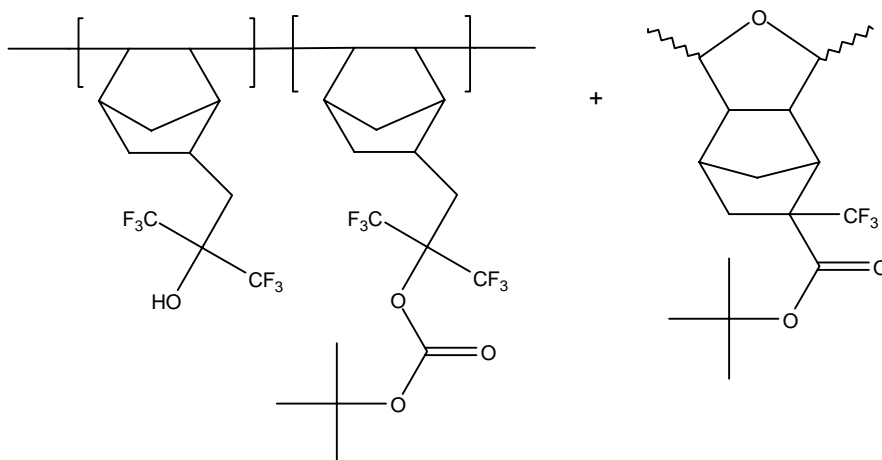
Representative copolymers of NBHFA copolymers synthesized by VAP
(XXXVII a-d). (Adapted with permission from Springer. 323)

³²¹An excellent review of these 157 nm resists has been written. See for example, H. Ito, "Chemical amplification resists for microlithography," *Adv. Polym. Sci.* **172**, 121–137 (2005).

³²²H. Ito, G.M. Wallraff, P. Brock, N. Fender, H. Truong, G. Breyta, D.C. Miller, M.H. Sherwood, and R.D. Allen, "Polymer design for 157 nm chemically amplified resists," *Proc. SPIE* **4345**, 273 (2001); H. Ito, G.M. Wallraff, P. Brock, N. Fender, C.E. Larson, H.D. Truong, G. Breyta, D.C. Miller, M.H.

This polymer generates hexafluoroalcohol on acid-catalyzed thermolysis and tends to have low contrast. Addition of *tert*-butyl ester oligomer into the formulation as a dissolution inhibitor helps to improve the development contrast of the resist; this particular version, marketed by Clariant Corporation, was the first commercially available resist designed for 157-nm lithography (XXXVIII).³²⁴

The other approach for making fluoropolymer norbornene resist was pioneered at Dupont and adopted by Daikin Kogyo of Japan. It involves either copolymerization of tetrafluoroethylene with NBHFA protected with an acid labile group or the



The first commercial 157-nm resist, sold by Clariant Corporation (XXXVIII)

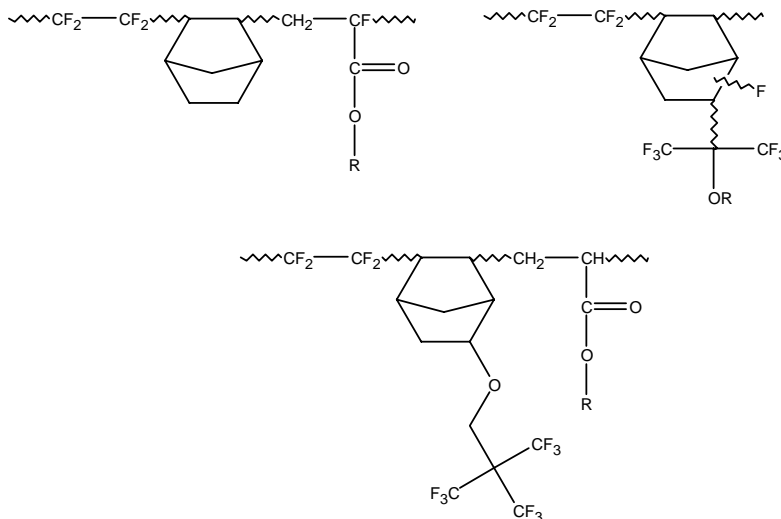
Sherwood, and R.D. Allen, "Novel fluoropolymers for use in 157 nm lithography," *J. Photopolym. Sci. Technol.* **14**, 583 (2001); H. Ito, G.M. Wallraff, N. Fender, P.J. Brock, W.D. Hinsberg, A. Mahorowala, C.E. Larsen, H.D. Truong, B. Breyta, and R.D. Allen, "Development of 157 nm positive resists," *J. Vac. Sci. Technol.* **B19**(6), 2678 (2001); K. Patterson, M. Yamachika, R. Hung, C. Bronsky, S. Yamada, M. Sommerville, B. Osborn, D. Hall, G. Dukovic, J. Byers, W. Conley, and C.G. Willson, "Polymers for 157 nm photoresist applications: a progress report," *Proc. SPIE* **3999**, 365 (2000); T. Chiba, R.J. Hung, S. Yamada, B. Trinique, M. Yamachika, C. Bronsky, K. Patterson, A.V. Heyden, A. Jamison, S. H. Lin, M. Sommerville, J. Byers, W. Conley, and C.G. Willson, "157 nm resist materials: A progress report," *J. Photopolym. Sci. Technol.* **13**, 657 (2000); R.J. Hung, H.V. Tran, B.C. Trinique, T. Chiba, S. Yamada, D.P. Sanders, E.F. Connor, R.H. Grubbs, J. Klopp, J.M.J. Fréchet, B.H. Thomas, G.J. Shafer, D.D. DesMarteau, W. Conley, and C.G. Willson, "Resist materials for 157 nm microlithography: an update," *Proc. SPIE* **4345**, 385 (2001); H.V. Tran, R.J. Hung, T. Chiba, S. Yamada, T. Mrozek, Y. T Hsieh, C.R. Chambers, B.P. Osborn, B.C. Trinique, M.J. Pinnow, D.P. Sanders, E.C. Connor, R.H. Grubbs, W. Conley, S.A. MacDonald, and C.G. Willson, "Fluoropolymer resist materials for 157 nm microlithography," *J. Photopolym. Sci. Technol.* **14**, 669 (2001).

³²³H. Ito, "Chemical amplification resists for microlithography," *Adv. Polym. Sci.* **173**, 123 (2005).

³²⁴ibid.

terpolymerization of TFE with NBHFA and acrylate-bearing acid-labile ester (XXXIX).³²⁵

Tert-butyl-2-trifluoromethylacrylate (TBTFMA) has been reportedly copolymerized with NBHFA (XL)³²⁶ or 5-trifluoromethyl-5-hydroxy-2-norbornene (XLI)³²⁷ to prepare 157-nm resist polymers with optical density $\sim 2.6/\mu\text{m}$. The



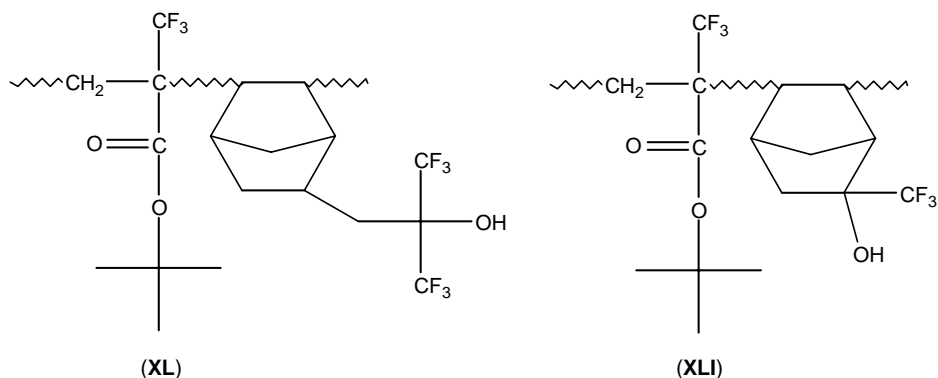
TFE-based 157-nm resist polymers used in 157-nm lithography (XXXIX).

³²⁵M.K. Crawford, A.E. Feiring, J. Feldman, R.H. French, M. Periyasamy, F.L. Schadt III, R.J. Smalley, F.C. Zumsteg, R.R. Kunz, V. Rao, L. Liao, and S.M. Holl, "157 nm imaging using thick single layer resists," *Proc. SPIE* **4345**, 428 (2001); M.K. Crawford, W.B. Farnham, A.E. Feiring, J. Feldman, R.H. French, K.W. Leffew, V.A. Petrov, F.L. Schadt III, and F.C. Zumsteg, "Fluoropolymers for 157 nm lithography: Performance of single layer resists," *J. Photopolym. Sci. Technol.* **15**, 677 (2002); T. Itani, M. Toriumi, T. Naito, S. Ishikawa, S. Miyoshi, T. Yamazaki, and M. Watanabe, "Characterization of fluoropolymers for 157 nm chemically amplified resist," *J. Vac. Sci. Technol.* **B19**(6), 2705 (2001); M. Toriumi, N. Shida, H. Watanabe, T. Yamazaki, S. Ishikawa, and T. Itani, "Fluoropolymer resists for 157 nm lithography," *Proc. SPIE* **4690**, 191 (2002); M. Toriumi, T. Yamazaki, T. Furukawa, S. Ire, S. Ishikawa, and T. Itani, "Fluoropolymer based resists for a single resist process of 157 nm lithography," *J. Vac. Sci. Technol.* **B20**, 2909 (2002).

³²⁶H. Ito, G.M. Wallraff, P. Brock, N. Fender, H. Truong, G. Breyta, D.C. Miller, M.H. Sherwood, and R.D. Allen, "Polymer design for 157 nm chemically amplified resists," *Proc. SPIE* **4345**, 273 (2001); H. Ito, G.M. Wallraff, P. Brock, N. Fender, C.E. Larson, H.D. Truong, G. Breyta, D.C. Miller, M.H. Sherwood, and R.D. Allen, "Novel fluoropolymers for use in 157 nm lithography," *J. Photopolym. Sci. Technol.* **14**, 583 (2001); H. Ito, G.M. Wallraff, N. Fender, P.J. Brock, W.D. Hinsberg, A. Mahorowala, C.E. Larsen, H.D. Truong, B. Breyta, and R.D. Allen, "Development of 157 nm positive resists," *J. Vac. Sci. Technol.* **B19**(6), 2678 (2001).

³²⁷B. Trinique, B.P. Osborn, C.R. Chambers, Y. T. Hsieh, S. Corry, T. Chiba, R.J. Huang, H.V. Tran, P. Zimmerman, D. Miller, W. Conley, and C.G. Willson, "Advances in resists for 157 nm micro lithography," *Proc. SPIE* **4690**, 58 (2002); C.G. Willson, B.C. Trinique, B.P. Osborn, C.R. Chambers, Y. T. Hsieh, T. Chiba, P. Zimmerman, D. Miller, and W. Conley, "The design of resist materials for 157 nm lithography," *J. Photopolym. Sci. Technol.* **15**, 583 (2002).

copolymer is extremely lipophilic and insoluble in an aqueous base. However, blending it with polyNBHFA increases its hydrophilicity and reduces the optical density to $\sim 2.0/\mu\text{m}$.³²⁸



It should be noted that the morphology of fluoropolymers tends to be different from those of hydrocarbon polymers of the kind we use in 193-nm and 248-nm lithography. Fluoropolymers tend to have much larger free volume than their hydrocarbon counterparts, largely on account of their relatively large fluorine atoms compared to hydrogen atoms in hydrocarbons. Therefore, diffusion and transport of species (photoacids, radicals, volatile photoproducts, etc.) through fluoropolymers appear to be somewhat more enhanced relative to their hydrocarbon counterparts. While transport of radical species occurs primarily by hopping transport in hydrocarbons, in fluoropolymers, the story appears to be quite different. It appears that cage effects play a far more significant role in 157-nm resists than in 193-nm resists. The above effects may be related to the enhanced environmental sensitivity, the higher propensity for outgassing, and even poor etch stability of 157-nm resists relative to their 193-nm and 248-nm counterparts.

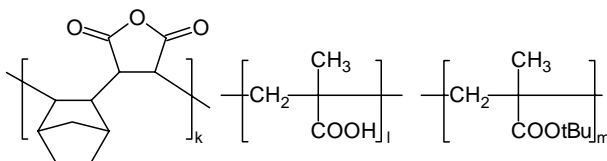
7.2.2.3.4 Ester-protected acrylic acid-alicyclic polymer hybrid resist platform

The third platform of resists for ArF lithography is the ester-protected acrylate/alicyclic polymer hybrid platform (XLII), which was pioneered at Bell labs.³²⁹ The polymerization route to polymers of this platform is free radical copolymerization of norbornene, maleic anhydride, and acrylic acid³³⁰ or norbornene, maleic

³²⁸H. Ito, "Chemical amplification resists for microlithography," *Adv. Polym. Sci.* **173**, 129 (2005).

³²⁹T.I. Wallow, F.M. Houlihan, O. Nalamasu, E.A. Chandross, T.X. Neenan, and E. Reichmanis, "Evaluation of cycloolefin maleic anhydride alternating copolymers as single layer photoresists for 193 photolithography," *Proc. SPIE* **2724**, 355 (1996).

³³⁰ibid.



The acrylate/alcyclic polymer hybrid polymer platform (XLII) pioneered at Bell Labs in 1996.

anhydride, and *t*-butyl acrylate.³³¹ Bile acids and steroids (XLIII) were added into the resist as dissolution inhibitors.³³²

Norbornenes-bearing pendant steroid³³³ and piperidyl³³⁴ groups have been successfully copolymerized with maleic anhydride and used in 193-nm resist formulations. Attaching the piperidyl base to the resist polymer improves the post-exposure delay stability of the resist, effectively helping to control acid diffusion. The most popular photoacid generators that have been employed in ArF resists have been mostly ionic and nonionic organic complexes of sulfonium and iodonium sulfonates, nonaflates, and triflates. A new acid generator based on bis(4-*tert*-butylphenyl)iodonium cyclamate, called “sweet PAG” (see Scheme 7.41) has been developed for use with a tetrapolymer of norbornene, maleic anhydride, acrylic acid, and *t*-butyl acrylate.³³⁵ This PAG generates a

³³¹T.I. Wallow, F.M. Houlihan, O. Nalamasu, E.A. Chandross, T.X. Neenan, and E. Reichmanis, “Evaluation of cycloolefin maleic anhydride alternating copolymers as single layer photoresists for 193 nm photolithography,” *Proc. SPIE* **2724**, 355 (1996); F.M. Houlihan, T.I. Wallow, A. Timko, E. Neria, B. Hutton, R. Cirelli, O. Nalamasu, and E. Reichmanis, “Recent advances in 193 nm single layer photoresists based on alternating copolymers of cycloolefins,” *Proc. SPIE* **3049**, 84 (1997); J. H. Park, S. J. Kim, S. Y. Park, and H. Lee, “ArF photoresist system using alicyclic polymer,” *Proc. SPIE* **3049**, 485 (1997).

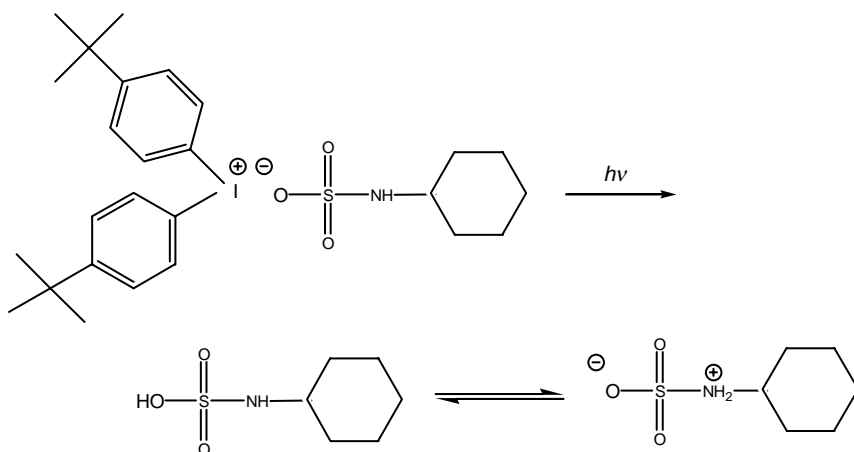
³³²F.M. Houlihan, T. Wallow, A. Timko, E. Neria, R. Hutton, R. Cirelli, J.M. Kometani, O. Nalamasu, and E. Reichmanis, “A commercially viable 193 nm single layer resist platform,” *J. Photopolym. Sci. Technol.* **10**, 511 (1997); G. Dabbagh, F.M. Houlihan, I. Rushkin, R.S. Hutton, O. Nalamasu, E. Reichmanis, A.H. Gabor, and A.N. Medina, “Model study by FT IR of the interaction of select cholate dissolution inhibitors with poly(norbornene *alt* maleic anhydride) and its derivatives,” *Proc. SPIE* **3678**, 86 (1999).

³³³J. B. Kim, B. W. Lee, J. S. Kang, J. H. Park, D. C. Seo, K. H. Baik, J. C. Jung, and C. H. Roh, “Chemically amplified resists based on the norbornene copolymers with steroid derivatives,” *Proc. SPIE* **3678**, 36 (1999); J. B. Kim, B. W. Lee, J. S. Kang, D. C. Seo, and C. H. Roh, “Poly(*t* butyl 3 α (5 norbornene 2 carbonyloxy) 7 α ,12 α dihydroxy 5 β cholan 24 oate co maleic anhydride) for a 193 nm photoresist,” *Polymer* **40**(26), 7423 (1999); J. B. Kim, B. W. Lee, H. J. Yun, and M. H. Y.G. Kwon, “193 nm photoresists based on norbornene copolymers with derivatives of bile acid,” *Chem. Lett.* **4**, 414 (2000).

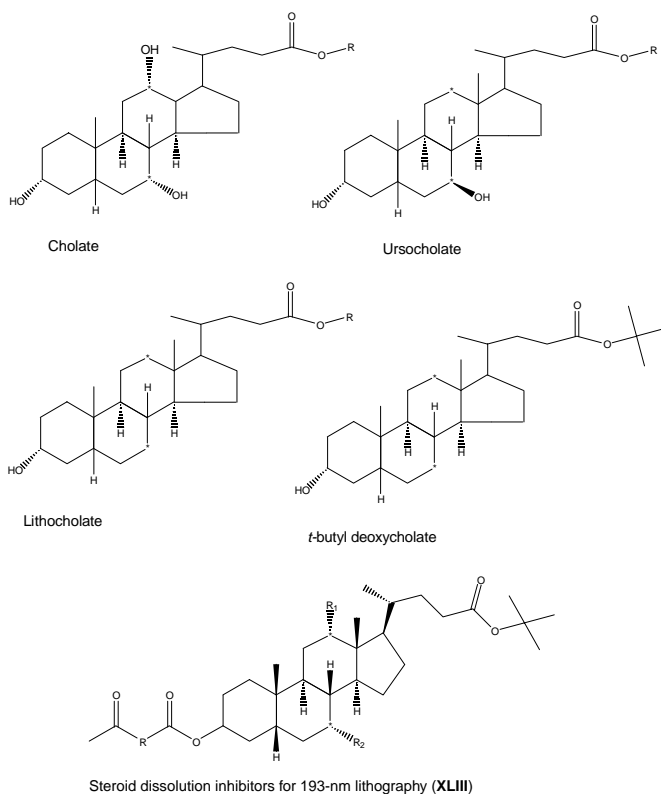
³³⁴J. B. Kim, M. H. Kwon, H. J. Yun, and M. H. Jung, “Postexposure delay effect in chemically amplified resists,” *J. Photopolym. Sci. Technol.* **14**, 401 (2001).

³³⁵F.M. Houlihan, J.M. Kometani, A.G. Timko, R.S. Hutton, R.A. Cirelli, E. Reichmanis, O. Nalamasu, A.H. Gabor, A. Medina, J. Biafore, and S. Slater, “193 nm single layer photoresists based on alternating copolymers of cycloolefins: The use of photogenerators of sulfamic acids,” *Proc. SPIE* **3333**, 73 (1998).

zwitterionic sulfamic acid on exposure to 248-nm and 193-nm radiations, while also acting as a photodecomposable base.³³⁶



Scheme 7.41 Photolysis of “sweet PAG” developed at Bell Labs.



³³⁶H. Ito, “Chemical amplification resists for microlithography,” *Adv. Polym. Sci.* **173**, 106 (2005).

7.2.2.3.5 Acetal- and ketal-protected chemical amplification resists

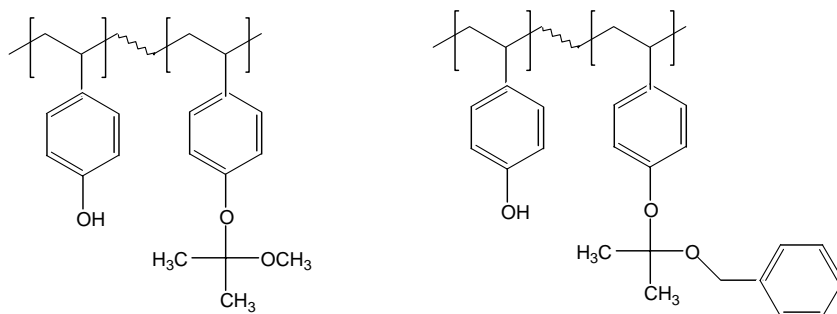
7.2.2.3.5.1 ACETAL AND KETAL-PROTECTED POLY(HYDROXY STYRENE)-BASED RESISTS

A number of acetal- and ketal-protected poly(hydroxy styrene) resists designed for 248-nm and 193-nm imaging have been demonstrated. Characteristically, these resists deprotect at much lower temperature than their high-temperature *t*-BOC-protected and *tert*-butyl ester-protected analogs. While the majority of chemical amplification resists require postexposure bake to accelerate the acid-catalyzed reactions, deprotection of acetal- and ketal-protected resist polymers proceeds at room temperature as soon as acid is generated during irradiation. At such a low temperature, the diffusion of the radiation-induced acid is limited to a rather short diffusion length, much shorter in fact than that of the high-activation energy *t*-BOC and *tert*-butyl ester-protected resist polymers. Acid diffusion in the resist matrix is, after all, a thermally driven process, implying that little, if any, generated acid will be available at the resist film surface to be neutralized by airborne bases, as occurs in T-topping (or environmental poisoning). As a result, the acetal- and ketal-protected polymers have greater PEB delay stability or environmental stability (less susceptibility to airborne base contamination) than their high-activation energy counterparts. The acetal- and ketal-protected resist polymers, however, tend to have poor hydrolytic and storage stability. They also tend to outgas more than their high-deprotection temperature counterparts. In addition, they tend to suffer from an excessive standing wave problem given their rather low deprotection temperature, and thus little or no thermally driven diffusion of the photoacids occurs to smooth out the standing waves. Consequently, this resist system must be paired up with extremely good bottom antireflection coatings to minimize the effect of standing waves, in order to harness their favorable properties.

An example of a ketal-protected resist polymer is the ketal resist system (KRS) from IBM, comprising two main resists: (i) formulated with a partially 2-methoxypropyl-protected poly(*p*-hydroxystyrene) (MOP) (XLIV) and (ii) formulated with a partially 2-benzyloxy-protected poly(*p*-hydroxystyrene) (BOP) (XLV). These resists have been largely used in electron-beam lithographic applications. Ketal resists based on structure (XLIV) have been reported to have excellent resolution (<100 nm), high sensitivity ($\sim 12 \mu\text{C}/\text{cm}^2$ at 50 kV), and high contrast (>10) without the need of PEB.³³⁷ However, this resist was found to have low thermal stability, excessive outgassing during exposure, and insufficient dissolution inhibition during development in the standard aqueous base developer, 0.26N

³³⁷U. Kumar, A. Pandya, R. Sinta, W. S. Huang, R. Bantu, and A. Katnani, "Probing the environmental stability and bake latitudes of acetal vs. ketal protected polyvinylphenol DUV resist systems," *Proc. SPIE* **3049**, 135 (1997); K.Y. Lee, and W. S. Huang, "Evaluation and application of a very high performance chemically amplified resist for electron beam lithography," *J. Vac. Sci. Technol.* **B**(11), 2808 (1993); W. S. Huang, R. Kwong, A. Katnani, M. Khojasteh, and K.Y. Lee, *Proc. of Tenth Conference on Photopolymers*, Ellenville, NY, p. 96 (1994); W. S. Huang, R.W. Kwong, W.M. Moreau, M. Chace, K.Y. Lee, C.K. Hu, D. Medeiros, and M. Angelopoulos, "Benzyloxypropene protected PHS resist system for e beam applications," *Proc. SPIE* **3678**, 1052 (1999).

tetramethylammonium hydroxide (TMAH).³³⁸ The ketal resist based on structure **XLV** was designed to address the above shortcomings of the resist based on **XLIV**, and met with somewhat reasonable success.³³⁹



Poly (4-hydroxystyrene-*co*-2-methoxypropoxystyrene) Poly (4-hydroxy-*co*-2-benzyloxypropyl styrene)
(**XLIV**) (**XLV**)

Early version of the ketal resist system (KRS) from IBM: partially 2-methoxypropyl (ketal)-protected PHOST, partially 2-benzyloxypropyl (ketal)-protected PHOST.

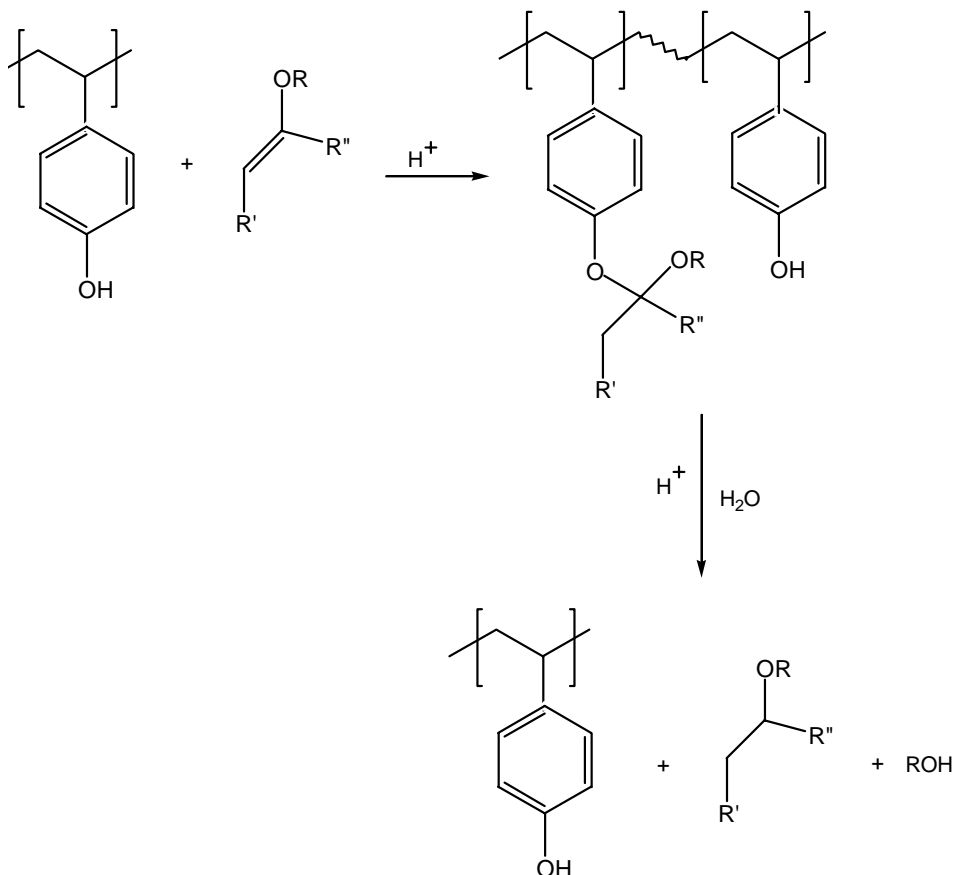
The latest evolution of the KRS resist, called KRS-XE, also from IBM, incorporates a novel ketal-protecting group that undergoes significantly less outgassing than MOP (Scheme 7.42).³⁴⁰ The ketal-protecting group is derived from enol ether to which the phenolic hydroxyl is added under acidic conditions. This resist system has exhibited excellent resolution (<60 nm) (see Fig. 7.20), is environmentally stable, exhibits large PAB (see Fig. 7.21) and PEB latitude (Fig. 7.22), and is compatible with the 0.26 N TMAH aqueous developer. In addition, the resist has demonstrated dry etch resistance comparable to that of the best DUV resists.³⁴¹

³³⁸U. Kumar, A. Pandya, R. Sinta, W. S. Huang, R. Bantu, and A. Katnani, "Probing the environmental stability and bake latitudes of acetal vs. ketal protected polyvinylphenol DUV resist systems," *Proc. SPIE* **3049**, 135 (1997); K.Y. Lee and W. S. Huang, "Evaluation and application of a very high performance chemically amplified resist for electron beam lithography," *J. Vac. Sci. Technol. B* **11**, 2807 (1993); W. S. Huang, R. Kwong, W.M. Moreau, M. Chace, K.Y. Lee, C.K. Hu, D. Medeiros, and M. Angelopoulos, "Benzyloxypropene protected PHS resist system for e beam applications," *Proc. SPIE* **3678**, 1052 (1999); R. Kwong, W. S. Huang, W. Moreau, R. Lang, C. Robinson, D.R. Medeiros, A. Aviram, R.C. Guarnieri, and M. Angelopoulos, "Materials issues and modeling for device nanofabrication," *Mater. Res. Soc. Symp. Proc.* **584**, 147 (2000).

³³⁹W. S. Huang, R. Kwong, W.M. Moreau, M. Chace, K.Y. Lee, C.K. Hu, D. Medeiros, and M. Angelopoulos, "Benzyloxypropene protected PHS resist system for e beam applications," *Proc. SPIE* **3678**, 1052 (1999).

³⁴⁰D.R. Medeiros, A. Aviram, C. Guarnieri, W. S. Huang, R. Kwong, C.K. Magg, A.P. Mahorowala, W.M. Moreau, K. E. Petrillo, and M. Angelopoulos, "Recent progress in electron beam resists for advanced mask making," *IBM J. Res. Dev.* **45**(5), 639 (2001).

³⁴¹ibid.



Scheme 7.42 Schematic of IBM's KRS-XE resist polymer synthesis and acid-catalyzed deprotection.

7.2.2.3.6 Evolution of poly(hydroxy styrene)-based resists

Not too long after its invention, the chemically amplified poly(*t*-BOC styrene) resist platform was widely adopted across the entire semiconductor industry, and many variations of it were developed by different resist companies for specific applications comprising line and space printing, isolated line printing, and contact hole printing. The three main platforms that animate the resist industry today are shown in Fig. 7.23, and are based on *t*-BOC chemistry (developed by IBM and Shipley, 1988), ESCAP chemistry (developed by IBM and Shipley, 1995), and acetal chemistry (developed by Wako and Shinetsu, 1995). All these resists have shown great environmental stability and excellent imaging and etch performance, and have been employed in patterning critical layers in the 250-nm and 130-nm device technology nodes, using KrF laser lithographic exposure tools, between 1997 and 2002 (see Table 4.1). Their usage has now been extended to EUV lithography.

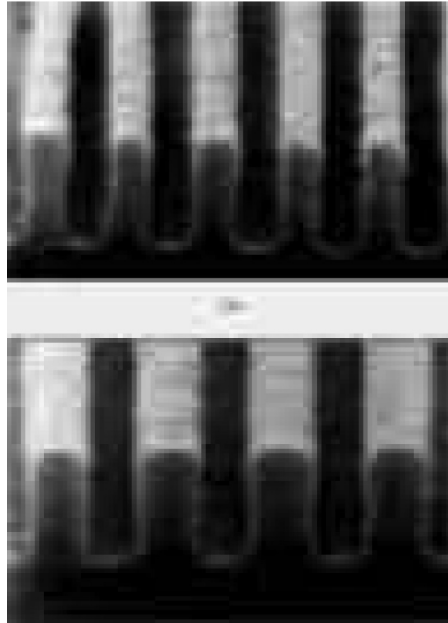


Figure 7.20 SEM images of a KRS-XE resist exposed on 75-kV EL4+ electron-beam exposure tool with (top) 55-nm equal lines and spaces, (bottom) 100-nm lines and 50-nm spaces. (Reproduced with permission from IBM Corp.³⁴²)

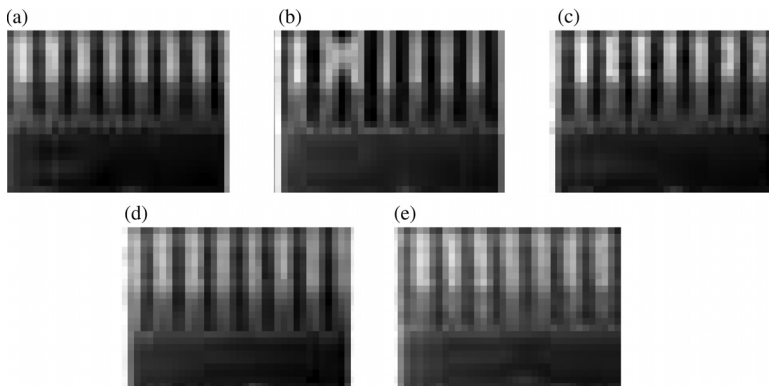


Figure 7.21 SEM images of 100-nm equal lines and spaces printed in a KRS-XE resist, showing the insensitivity of the resist image quality to variation in PAB temperatures: (a) 90°C, (b) 95°C, (c) 100°C, (d) 105°C, and (e) 110°C. (Reproduced with permission from IBM Corp.³⁴³)

³⁴²ibid.

³⁴³ibid.



Figure 7.22 SEM images of 100-nm lines and spaces printed in a KRS-XE resist: (a) no PEB, (b) 80°C PEB, (c) 110°C PEB. (Reproduced with permission from IBM Corp.³⁴⁴)

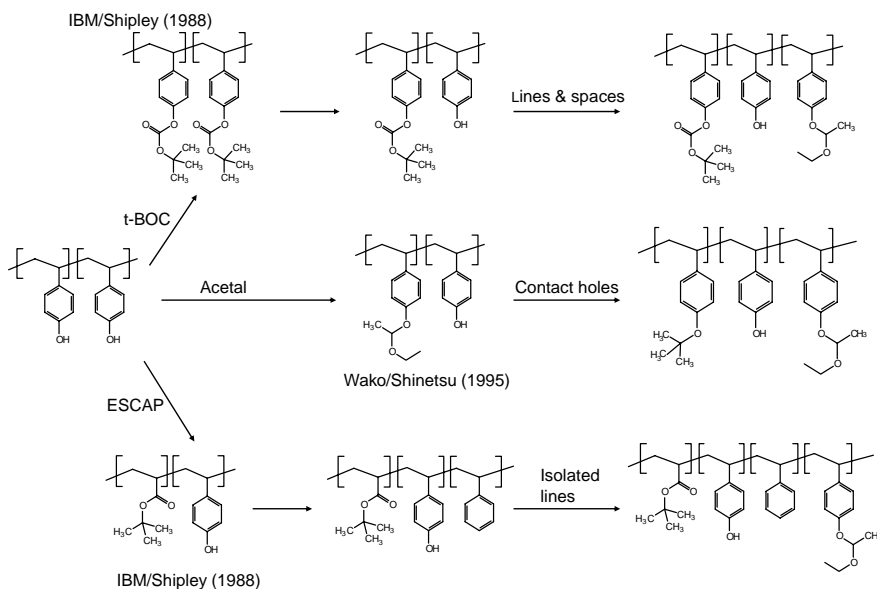


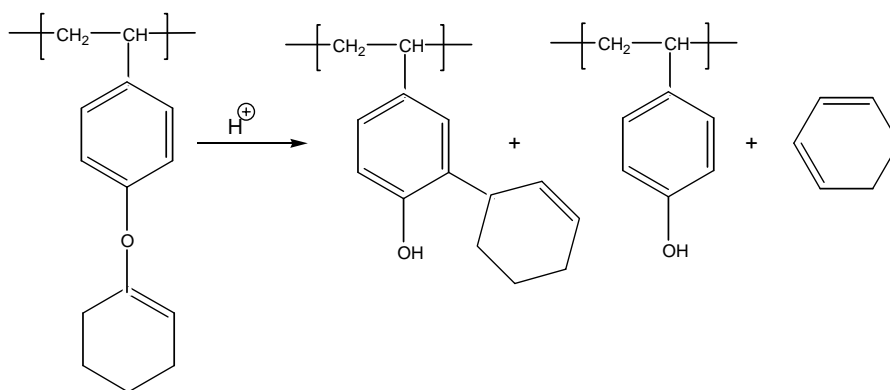
Figure 7.23 Common chemically amplified resist platforms based on poly(*p*-hydroxystyrene) and used in DUV lithographic applications. (Courtesy of R. Dammel.)

7.2.2.4 Chemical amplification positive resists based on Claisen rearrangement

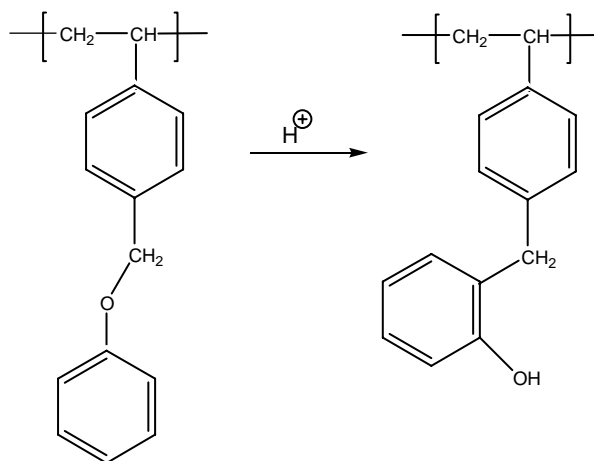
Acid-catalyzed rearrangements involving the deprotection of lipophilic protecting groups creating hydrophilic moieties, followed by the subsequent rearrangement of these lipophilic groups at distinct positions on the repeating unit of the polymer, have been employed in positive chemical amplification resists. A good example is the classic Claisen rearrangement, illustrated here for the specific case involving the photoinduced acid-catalyzed deprotection of cyclohexenyl-protected poly(*p*-hydroxystyrene), leading to a partial rearrangement of the cyclohexenyl-protecting group from the *para* to the *ortho* position in one of the

³⁴⁴ibid.

products; the other products being PHOST and hexadiene (Scheme 7.43).³⁴⁵ In this transformation, the resist polymer changes from the nonpolar to the polar state. Poly(4-phenoxyethyl styrene) is isomerized in a similar manner with an acid as a catalyst to a C-alkylated phenolic structure (Scheme 7.44).³⁴⁶



Scheme 7.43 Acid-catalyzed Claisen rearrangement of poly(4-cyclohexenyloxy styrene).



Scheme 7.44 Acid-catalyzed Claisen rearrangement of poly(4-phenoxyethyl styrene).

³⁴⁵H. Stover, S. Matuszczak, R. Chin, K. Shimizu, C.G. Willson, and J.M.J. Fréchet, "New design for self developing imaging systems based on thermally labile polyformals," in *Proc. of ACS Div. Polym. Mater. Sci. Eng.*, Vol. 61, p. 412 (1989).

³⁴⁶H. Ito, "Chemical amplification resists for microlithography," *Adv. Polym. Sci.* **173**, 148 (2005).

7.2.2.5 Chemical amplification positive resists based on depolymerization

7.2.2.5.1 Poly(phthaldehyde) resists

Unaware of the first patent on chemically amplified resist (granted to 3M Corporation), C.G. Willson et al. set out in the late 1970s to develop chemically amplified DUV resists. Their first attempt,³⁴⁷ which is the second chemically amplified resist invented for use in lithographic resist applications, involved the use of poly(phthaldehyde), which undergoes an equilibrium cyclopolymerization and has a ceiling temperature of about -40°C . Their idea was to prepare the polymer below its ceiling temperature, then cap it and isolate the intrinsically unstable product. Reasoning that any photochemical event that can generate the anionic chain end above the ceiling temperature should cause spontaneous depolymerization to the monomer, they prepared the polymer by anionic copolymerization of phthaldehyde and *o*-nitrobenzaldehyde monomers, and capped it with acylating agents. They incorporated *o*-nitrobenzaldehyde as a monomer into the polymer to render it photosensitive. Exposing the films of the capped copolymer to DUV radiation resulted in spontaneous relief image formation, but the resulting images could not be developed cleanly to the substrate. As expected, they observed that the polymer chain had undergone scission and had unzipped, but only in one direction because the photochemistry generates an *o*-nitrosoester capping unit as one chain end.³⁴⁸

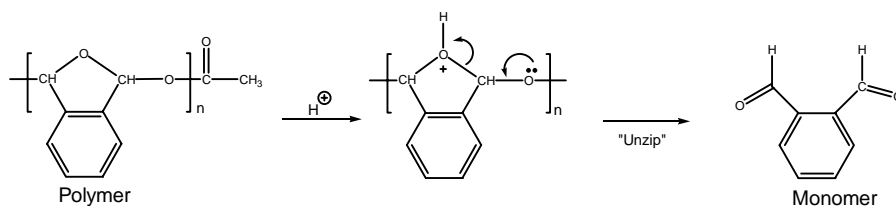
The solution to this problem was found when they used an anionic mechanism to prepare the poly(phthaldehyde) and a cationic mechanism involving the photo-generation of acid from a neutral species such as onium salts of the kind publicized by Crivello³⁴⁹ of General Electric, to unzip it (Scheme 7.45).³⁵⁰ Their first formulation of poly(phthaldehyde) with diphenyl hexafluoroarsenate provided a positive-tone resist with extremely high sensitivity. Exposure of this resist film to DUV radiation generated spontaneous relief image formation with doses as low as $2\text{ mJ}/\text{cm}^2$. The depolymerization reaction is reported to be exothermic and sufficiently energetic to cause the phthaldehyde monomer to vaporize. Self-developed

³⁴⁷This is the second chemical amplification resist invented for use in semiconductor lithography. Invented by Willson, Fréchet, and Ito, the resist on exposure spontaneously and uncontrollably depolymerizes in an exothermic reaction that is sufficiently energetic to evaporate the monomer. These inventors were unaware of a 3M Corporation patent on a similar concept, G.H. Smith and J.A. Bonham, "Photosolubilizable compositions and elements," U.S. Patent No. 3779,778 (1973).

³⁴⁸C.G. Willson and R.A. Dammel, A. Reiser, "Photoresist Materials: A Historical Perspective," *Proc. SPIE* **3050**, pp. 38–51 (1997).

³⁴⁹J.V. Crivello and J.H. Lam, "Photo initiated cationic polymerization with triarylsulfonium salts," *J. Polym. Sci.: Polym. Chem. Ed.* **17**, 977 (1979).

³⁵⁰H. Ito, C.G. Willson, and J.M.J. Fréchet, "New UV resists with negative or positive tone," *Digest of Technical Papers, 1982 SPE Symp. on VLSI Technol.*, p. 6 (1982); C.G. Willson, H. Ito, J.M.J. Fréchet, T.G. Tessier, F.M. Houlihan, "Approaches toward the design of radiation sensitive polymeric imaging systems with improved sensitivity and resolution," *J. Electrochem. Soc.* **133**, p. 181 (1986).

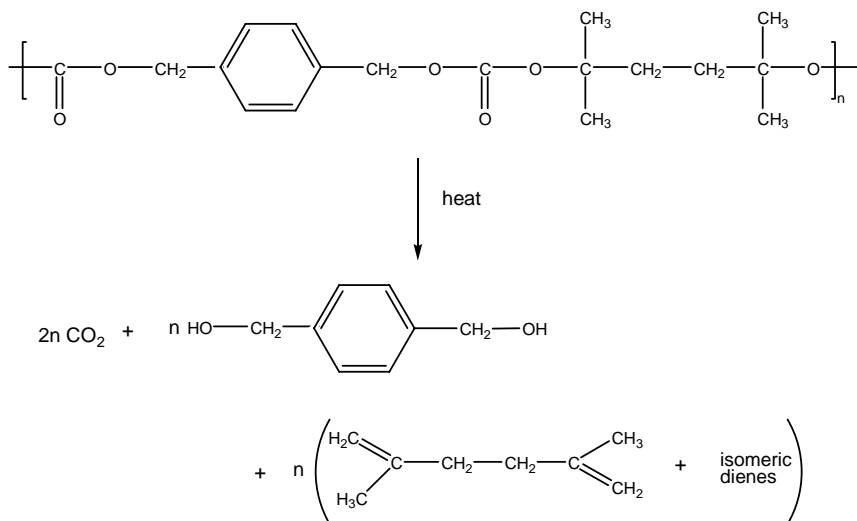


Scheme 7.45 Acid-catalyzed scission and unzipping of poly(phthalaldehyde).

images were also reported to have been generated at doses two orders of magnitude lower than those required to image typical DNQ/novolac resists.³⁵¹

Although this first formulation had very high photosensitivity, it had very little practical utility, since it was not able to function as a resist in the true sense of the word. Practically, very little film was left after spontaneous development of the exposed film.³⁵²

The hydrolysis of esters or carbonates of tertiary alcohols have also been employed to degrade resist polymer backbone, with a view to making them soluble in the developer. In particular, Fréchet et al.³⁵³ prepared resists based on thermally depolymerizable polycarbonates, such as the structure shown in Scheme 7.46, which exhibit great thermal lability and undergo multiple

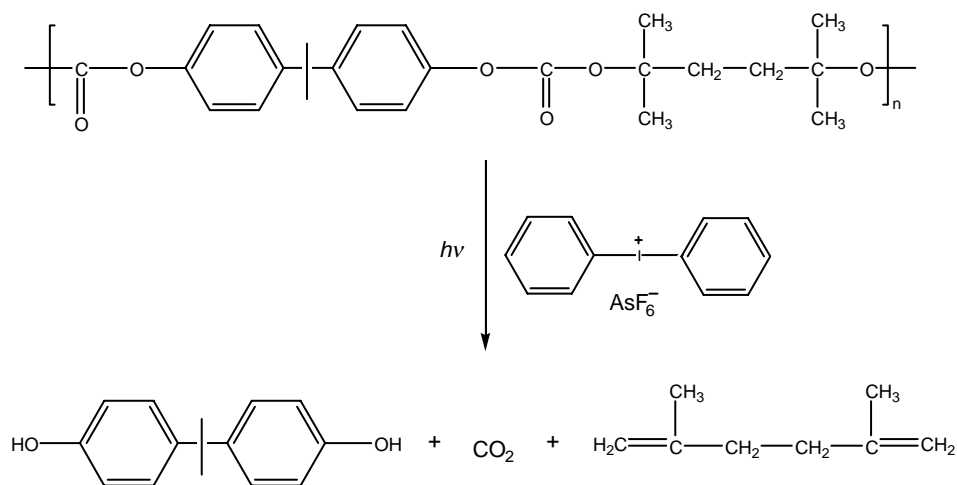


Scheme 7.46 Thermal depolymerization of polycarbonates.

³⁵¹C.G. Willson, R.A. Dammel, and A. Reiser, "Photoresist materials: a historical perspective," *Proc. SPIE* **3050**, 38 and 51 (1997).

³⁵²*ibid.*, pp. 38–51.

³⁵³J.M.J. Fréchet, F.M. Houlihan, F. Bouchard, B. Kryczka, and C.G. Willson, "Design, synthesis and study of novel thermally depolymerizable polycarbonates," *J. Chem. Soc. Commun.*, p. 1514 (1985); F.M. Houlihan, F. Bouchard, J.M.J. Fréchet, and C.G. Willson, "Thermally depolymer polycarbonates. II. Synthesis of novel linear tertiary copolycarbonates by phase transfer catalysis," *Macromolecules*, **19**, 13 (1986).



Scheme 7.47 Photoinduced depolymerization of polycarbonates.

backbone scissions when heated to a critical temperature $\sim 210\text{--}250^\circ\text{C}$. At these temperatures, the polymers decompose suddenly and cleanly into volatile products, with no solid residue left behind.³⁵⁴

It is worthwhile to note that the above reaction can take place at a much lower decomposition temperature in the presence of a catalytic amount of acid.³⁵⁵ Along the same lines, Narang and Attarwala³⁵⁶ have described a positive resist based on the previous polycarbonate (Scheme 7.47).

On irradiating this resin in the presence of diphenyliodonium hexafluoroarsenate, the resin decomposes at a bake temperature of 120°C , lasting only 60 s. Under these conditions, one of the products, bisphenol A, does not evaporate, but development in n-butanol produces positive-tone images of good quality.³⁵⁷

7.2.2.5.2 General considerations on the thermodynamics of radiation-induced depolymerization

Consider the formation of a polymer from its monomer as a reversible process indicated by³⁵⁸



The direction of this reaction is determined by its free energy change, ΔG , which can be expressed as the sum of the free energies of the activation of the

³⁵⁴A. Reiser, *Photoreactive Polymers: The Science and Technology of Resists*, p. 282, John Wiley & Sons, Hoboken, NJ (1989).

³⁵⁵J.M.J. Fréchet, F. Bouchard, F.M. Houlihan, E. Eichler, B. Kryczka, and C.G. Willson, "Design and synthesis of novel allylic and benzylic polycarbonates susceptible to acidolytic thermolytic depolymerization," *Makromol. Chem. Rapid Commun.* **7**, 121 (1986).

³⁵⁶S. Narang and S.T. Attarwala, "Chemical amplification in t diol poly carbonate resists," *ACS Polym. Prepr.* **26**(2), 323 (1985).

³⁵⁷A. Reiser, *Photoreactive Polymers: The Science and Technology of Resists*, p. 282, John Wiley & Sons, Hoboken, NJ (1989).

forward and the backward reaction. For a reaction to be feasible, its free energy change must be negative:

$$\Delta G = (\Delta G_p^\ddagger - \Delta G_{dp}^\ddagger). \quad (7.2)$$

However, ΔG is also given by

$$\Delta G = \Delta H - T\Delta S, \quad (7.3)$$

where ΔH is the change in enthalpy, T is temperature, and ΔS is the change in entropy.

Therefore,

$$\Delta G = (\Delta H_p^\ddagger - \Delta H_{dp}^\ddagger) + T(\Delta S_{dp}^\ddagger - \Delta S_p^\ddagger). \quad (7.4)$$

In the enthalpic terms of Eq. (7.4), ΔH_p is more negative than ΔH_{dp} , given that it is associated with the formation of a single bond from a double bond. Furthermore, the entropic change on depolymerization is much more positive than the entropic change of polymerization since the former is more disordered than the latter:

$$\Delta S_{dp}^\ddagger \gg \Delta S_p^\ddagger. \quad (7.5)$$

At low temperatures, the negative enthalpic term in Eq. (7.4) is dominant over the entropic term, but as the temperature increases, a point is reached where the two terms become equal and above which the positive entropy term will become dominant. The temperature,

$$T(\Delta S_{dp}^\ddagger - \Delta S_p^\ddagger) \geq (\Delta H_p^\ddagger - \Delta H_{dp}^\ddagger), \quad (7.6)$$

at which this occurs is referred to as the ceiling temperature T_c . Above T_c , the rates of the forward and the backward reactions are balanced, and the net rate of polymerization is effectively zero.³⁵⁹

It is impossible to synthesize a polymer from its monomers above T_c . If the polymer is synthesized below its ceiling temperature and then brought to a temperature above its T_c in the presence of traces of the polymerization catalyst, for instance, a free radical,³⁶⁰ it will spontaneously depolymerize.³⁶¹ It is this

³⁵⁸For a more detailed view of this analysis, please see, for example, A. Reiser, *Photoreactive Polymers: The Science and Technology of Resists*, pp. 285–286, John Wiley & Sons, Hoboken, NJ (1989).
³⁵⁹ibid.

³⁶⁰The requirement of the presence of the polymerization catalyst in the depolymerization process stems from the principle of microscopic reversibility. If, for example, all free radicals are removed from the system by simply endcapping the polymer, the thermodynamic equilibrium dictates that depolymerization state cannot be reached and the system will be stable. This was the approach employed by Ito and Willson in stabilizing polyphthaldehyde resists. [See for example, C.G. Willson, H. Ito, J.M.J. Fréchet, T.G. Tessier, F.M. Houlihan, "Approaches toward the design of radiation sensitive polymeric imaging systems with improved sensitivity and resolution," *J. Electrochem. Soc.* **133**, 181 (1986)].

³⁶¹A. Reiser, *Photoreactive Polymers: The Science and Technology of Resists*, p. 285, John Wiley & Sons, Hoboken, NJ (1989).

phenomenon of depolymerization that underlies the chemical amplification imaging action of polyphthaldehyde-based resists (described above).

It should be pointed out that T_c of practical resist polymers is well above room temperature, and their rate of depolymerization in normal circumstances is negligible. However, resist polymers such as polyphthaldehydes and some polysulfones, for example, have a low T_c and must therefore be prepared under cryogenic conditions. Endcapping these materials with alkyl or acyl groups, for example, while they are still at low temperatures, makes them stable at room temperature and higher. The T_c of poly(phthaldehyde) is -40°C , but if it is endcapped in these conditions, it is stable up to $\sim 180^\circ\text{C}$ and can be spin-coated and otherwise handled in the usual way.³⁶² Willson et al.³⁶³ have successfully prepared numerous samples of polyphthaldehyde ranging in molecular weights between 100,000 and 500,000 daltons by anionic polymerization in dry ice conditions (-78°C), using *n*-butyl lithium and similar reagents as catalysts; acetyl groups were used to endcap the polymer (see Scheme 7.48), which is remarkably stable up to 198°C .³⁶⁴

When resist films coated with formulations comprising this endcapped polymer with 10% by weight of various onium salts are exposed to DUV photons or an electron beam, acids are generated from the onium salts that go on to catalyze the hydrolytic scission process of the endcap moieties, as shown in Scheme 7.45, with the net result being the evaporation of the irradiated areas, with rather catastrophic implications for the contamination of the optical elements of exposure tools. In this mechanism, the acid attacks the lone electron pair on oxygen and brings about the depolymerization of the entire polymer. This, in essence, was the first resist system that self-developed reliably at room temperature without any further processing or special conditions.³⁶⁵

7.3 Resist Materials for Multilayer Resist Systems

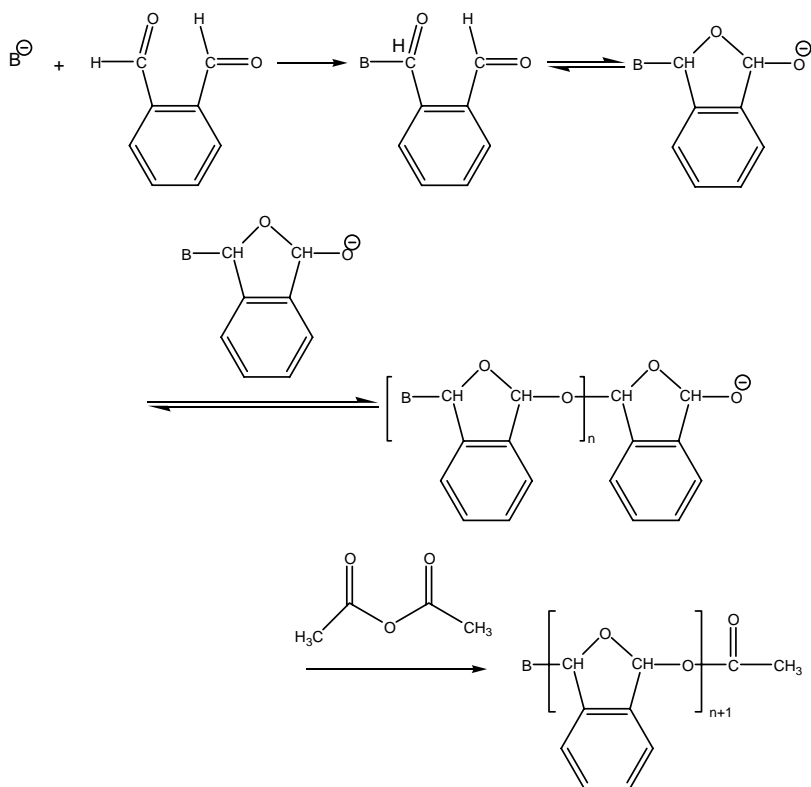
The three main approaches to multilayer resist imaging systems (see Chapter 16 for details) include: (i) hard mask (HM) processes, (ii) top surface imaging (TSI) processes requiring latent image formation only near the surface of the resist, thus circumventing any transparency requirements, and (iii) bilayer resist (BLR)

³⁶²ibid., p. 286.

³⁶³C.G. Willson, H. Ito, J.M.J. Fréchet, T.G. Tessier, and F.M. Houlihan, "Approaches toward the design of radiation sensitive polymeric imaging systems with improved sensitivity and resolution," *J. Electrochem. Soc.* **133**, 181 (1986).

³⁶⁴A. Reiser, *Photoreactive Polymers: The Science and Technology of Resists*, p. 296, John Wiley & Sons, Hoboken, NJ (1989).

³⁶⁵C.G. Willson, H. Ito, J.M.J. Fréchet, T.G. Tessier, and F.M. Houlihan, "Approaches toward the design of radiation sensitive polymeric imaging systems with improved sensitivity and resolution," *J. Electrochem. Soc.* **133**, 181 (1986).



Scheme 7.48 Endcapping of polyphthaldehyde resist polymers in order to prevent unwanted depolymerization.

processes that use thin imaging layers to accommodate strong absorption at the lithographic wavelength of interest. The materials used in multilayer resist systems are briefly discussed below.

7.3.1 Hard mask resist materials

The hard mask approach³⁶⁶ employs ultrathin resist films, typically ≤ 100 nm, as the imaging layer, which are coated over inorganic hard mask substrates such as silicon oxynitride, silicon nitride, amorphous carbon, etc.

³⁶⁶K.B. Nguyen, C. Lyons, J. Schefske, S. Bell, H.J. Levinson, and U. Okoroanyanwu, "Characterization of the manufacturability of ultra thin resist," *J. Vac. Sci. Technol. B* **17**(6), 3039 (1999); C. Pike, K.B. Nguyen, M.V. Plat, C.F. Lyons, P. King, K.A. Phan, U. Okoroanyanwu, H.J. Levinson, "Manufacturability of the ultrathin resist process," *J. Vac. Sci. Technol. B* **18**(6), 3381-3387(2000).

7.3.2 Top surface imaging resists

Typical vapor phase silylating agents used in top surface imaging systems include dimethylsilyldimethylamine (DMSDMA),³⁶⁷ trimethylsilyldimethylamine (TMSDMA),³⁶⁸ and trimethylsilyldiethylamine (TMSDEA).³⁶⁹ Typical liquid phase silylating agents used in top surface imaging systems include 1,1,3,3,5,5-hexamethylcyclotrisilazane³⁷⁰ and bis(dimethylamino)dimethylsilane with N-methyl-2-pyrrolidone (NMP) as a diffusion promoter.³⁷¹ Typical polymer resins include polyvinyl phenol and novolac/diazoquinone polymer resins.

7.3.3 Bilayer resists

Bilayer resists are formulated mostly from organosilicon polymers as the imaging layer and novolacs polymers as the underlayer. Many organosilicon resists for bilayer resist systems have been reported for use in near-UV, DUV, mid-UV, electron-beam, and x-ray applications, a good review of which has been provided by Ohnishi et al.³⁷² In recent times, negative-tone resist systems and processes based on silicon backbone polymers such as polysilanes,³⁷³ polysilynes,³⁷⁴ and plasma-deposited polymers³⁷⁵ have been developed for 193-nm lithography.

³⁶⁷S.C. Palmateer, R.R. Kunz, M.W. Horn, A.R. Forte, and M. Rothschild, "Optimization of a 193 nm silylation process for sub 0.25 μm lithography," *Proc. SPIE* **2438**, 455 (1995).

³⁶⁸M.A. Hartney, D.W. Johnson, and A.C. Spencer, "Evaluation of phenolic resists for 193 nm surface imaging," *Proc. SPIE* **1466**, 238 (1991); T.T. Dao, C.A. Spencer, D.W. Hess, "Study of silylation mechanisms and kinetics through variations in silylating agent and resin," *Proc. SPIE* **1466**, 257 (1991); D.W. Johnson, R.R. Kunz, and M.W. Horn, "Further developments in surface imaging resists," *J. Photopolym. Sci. Technol.* **6**, 593 (1993); D.W. Johnson, and M.A. Hartney, "Surface imaging resists for 193 nm lithography" *Jpn. J. Appl. Phys.* **31**, 4321 (1992).

³⁶⁹M.A. Hartney, D.W. Johnson, and A.C. Spencer, "Evaluation of phenolic resists for 193 nm surface imaging," *Proc. SPIE* **1466**, 238 (1991); T.T. Dao, C.A. Spencer, and D.W. Hess, "Study of silylation mechanisms and kinetics through variations in silylating agent and resin," *Proc. SPIE* **1466**, 257 (1991).

³⁷⁰M.A. Hartney, R.R. Kunz, L.M. Eriksen, and D.C. LaTulipe, "Comparison of liquid and vapor phase silylation processes for 193 nm positive tone lithography," *Proc. SPIE* **1925**, 270 (1993).

³⁷¹K. H. Baik, L. Van den Hove, and B. Roland, "Comparative study between gas and liquid phase silylation for the diffusion enhanced silylated resist process," *J. Vac. Sci. Technol. B* **9**, 3399 (1991); K. H. Baik, K. Ronse, L. Van den Hove, and B. Roland, "Liquid phase silylation for the DESIRE process," *Proc. SPIE* **1672**, 362 (1992).

³⁷²Y. Ohnishi, M. Suzuki, K. Saigo, Y. Saotome, and H. Gokan, "Silicon containing resists for bilayer resist systems," *Proc. SPIE*, **539**, 62 (1985).

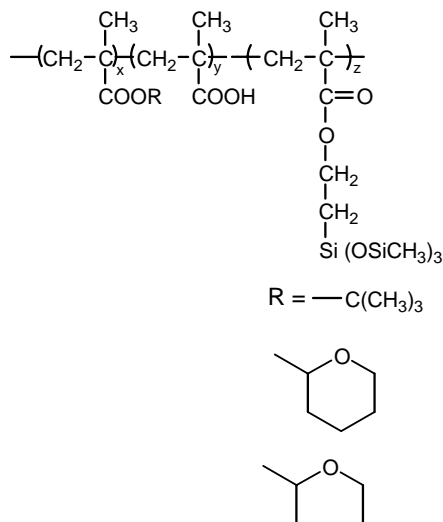
³⁷³R.R. Kunz, M.W. Horn, R.B. Goodman, P.A. Bianconi, D.A. Smith, J.R. Eshelman, G.M. Wallraff, R.D. Miller, and E.J. Ginsberg, "Surface imaged silicon polymers for 193 nm excimer laser lithography," *Proc. SPIE* **1672**, 385 (1992).

³⁷⁴R.R. Kunz, M.W. Horn, R.B. Goodman, P.A. Bianconi, D.A. Smith, and J.R. Eshelman, "Wet developed bilayer resists for 193 nm excimer laser lithography," *J. Vac. Sci. Technol. B* **10**, 2554 (1992).

³⁷⁵M.W. Horn, S.W. Pang, and M. Rothschild, "Plasma deposited organosilicon thin films as dry resists for deep ultraviolet lithography," *J. Vac. Sci. Technol. B* **8**, 1493 (1990).

It should be mentioned that these silicon backbone polymers are highly absorptive, and must therefore be used in very thin films (~ 30 nm), which can be prone to defects. Also, the principal electronic transition in these polysilanes (with two-dimensional silicon backbone) and polysilynes (three-dimensional silicon backbone) polymers when irradiated at 193 nm is most likely a $\sigma\text{-}\sigma^*$ transition involving the all-silicon backbone.³⁷⁶ Due to this excitation, reaction pathways leading to scission of the Si–Si bonds lead to photodegradation of the polymer. In the presence of oxygen, this photodegradation results in siloxane (Si–O–Si) formation within the polymer, and in the case of the three-dimensional network polymers, an increase in molecular weight is the result. This combination of both molecular weight and structural changes on irradiation allows for either solvent- or plasma-based development. Both approaches lead to negative-tone imaging.³⁷⁷

Promising positive-tone bilayer resists based on silicon-containing methacrylate polymers bearing acid labile side groups (Scheme 7.49), and designed for ArF lithography, were reported in 1996 by researchers at Olin Ceiba-Geigy Corporation.³⁷⁸



Scheme 7.49 Bilayer resist platform developed at Olin Ceiba Geigy/Olin Microelectronics Materials Company between 1996 and 1997.

³⁷⁶R.D. Miller and J. Michl, "Polysilane high polymers," *Chem. Rev.* **89**, 1359 (1989).

³⁷⁷R.R. Kunz, M.A. Hartney, M.W. Horn, C.L. Keast, M. Rothschild, and D.C. Shaver, "Resist processes for ArF excimer laser lithography," *J. Photopolym. Sci. Technol.* **6**, 473 (1993).

³⁷⁸U. Schaedeli, E. Tinguely, A.J. Blakeney, P. Falcigno, and R.R. Kunz, "Bilayer resist approach for 193 nm lithography," *Proc. SPIE* **2724**, 344 (1996).

Chapter 8

General Considerations on the Radiation and Photochemistry of Resists

Here the boundaries meet and all contradictions exist side by side.

Fyodor Dostoevsky, *The Brothers Karamazov*

8.1 Interaction of Radiation with Resists

The interaction of exposure radiation with amorphous solid films of resists and their constituents leads to distinct photophysical and photochemical processes that in turn underlie the basis of the contrast between the exposed and the unexposed sections of the resist film. A short section of this chapter is therefore devoted to the rudiments of photochemistry and photophysics of amorphous solid resist films. We can only provide here the most basic information required for understanding the subject.¹

It is necessary to introduce some terminology here. When the radiation-sensitive components of resists—the resins and components—are irradiated, they can absorb the energy and in turn get excited. It is the excited-state form of the radiation-sensitive components of the resist that plays the central role in these processes. These excited states of the molecules are identified by their multiplicity (the overall spin of the electrons in that state), by their molecular orbital character (indicating the involvement of π , n , σ , or other orbitals in the excitation process), and by their energy in relation to the energy of the ground state. The relevant excited states of a molecule include the singlet S_1 and triplet T_1 , and are typically

¹For a comprehensive treatment of the subject, the reader is referred to these excellent books: A. Reiser, *Photoreactive Polymers: The Science and Technology of Resists*, Chapter 3, John Wiley & Sons, Hoboken, NJ (1989); N.J. Turro, *Modern Molecular Photochemistry*, Benjamin Cummings, Menlo Park, CA (1978); J.A. Barltrop and J.D. Coyle, *Elements of Organic Photochemistry*, John Wiley & Sons, Hoboken, NJ (1975).

represented in a state diagram that shows their energy levels relative to the ground state singlet S_0 .²

A good way to picture the singlet and triplet states is to consider the configuration of a pair of $1s$ orbital electrons in the ground state, represented as $1s^2$. When excited, one of these electrons may be promoted into a $2s$ orbital, giving the configuration $1s^1 2s^1$. The two electrons need not be paired since they occupy different orbitals. According to Hund's rule of maximum multiplicity,³ the state of the atom or molecule in which the spins are parallel ($\uparrow\uparrow$) lies lower in energy than the state in which they are antiparallel or paired ($\uparrow\downarrow$). Both states are permissible, and can contribute to the photochemistry and photophysics of the atom or molecule.⁴

Electrons with parallel and antiparallel spins differ in their overall spin angular momentum. In the paired case, the two spin momenta cancel each other, resulting in zero net spin. The paired-spin arrangement is called a singlet. The triplet state is one in which the angular momenta of two parallel spins add together to give a nonzero total spin. In general, for states arising from the same configuration, the triplet state lies lower in energy than the singlet state. The origin of the energy difference between the singlet and triplet states arises from the effect of spin correlation⁵ on the coulombic interactions between electrons.⁶

The generation of an excited singlet state S_1 of a molecule in a resist is either by direct absorption of a photon or by energy transfer from another excited molecule. Once excited, the fate of the excitation energy acquired by the molecule can follow quite a number of pathways. The excited singlet state S_1 may either emit fluorescence or it may be deactivated by a nonradiative transition to the ground state. When nonradiative transitions occur between states of the same multiplicity (i.e., singlet to singlet or triplet to triplet), they are called internal conversions. When the transitions occur between states of different multiplicity, they are termed intersystem crossings. Intersystem crossings are spin-forbidden transitions that are due to the intervention (in aromatic systems) of out-of-plane vibrations or by the state-mixing effects of heavy atoms. The fraction of S_1 that emits fluorescence is a function of the competition between the radiative fluorescence transition, the internal conversion to ground state S_0 , and the intersystem crossing to T_1 . Furthermore, the excited triplet state may be deactivated by a radiative process (phosphorescence) and by nonradiative intersystem crossing to the ground state.⁷

²A. Reiser, *Photoreactive Polymers: The Science and Technology of Resists*, p. 65, John Wiley & Sons, Hoboken, NJ (1989).

³An atom in its ground state adopts a configuration with the greatest number of unpaired electrons.

⁴P.W. Atkins, *Physical Chemistry*, 5th ed., pp. 447–448, W.H. Freeman and Co., New York (1994).

⁵Spin correlation refers to the phenomenon in which electrons with parallel spins behave as if they have a tendency to stay well apart and hence repel each other less.

⁶P.W. Atkins, *Physical Chemistry*, 5th ed., pp. 447–448, W.H. Freeman and Co., New York (1994).

⁷A. Reiser, *Photoreactive Polymers: The Science and Technology of Resists*, pp. 65–66, John Wiley & Sons, Hoboken, NJ (1989).

8.2 Excited State Complexes

In lithographic exposure sources and resist photopolymer systems, an important type of excited state is the excited state complex, which consists of excimers and exciplexes.

8.2.1 Excimers

Excimers⁸ (excited dimers) are formed by pairs of molecules or atoms that do not significantly interact in the ground state, but are weakly bonded in the excited state. The bonding in the excimer takes place between an excited molecule and a ground state molecule of the same species. Its origin is in the change of orbital symmetry that accompanies excitation and leads to cooperative (positive) orbital overlap and hence to bonding between the two systems.⁹ Examples in resist systems can be found in aromatic and heteroaromatic molecules used in photoactive compounds. Excimers were first observed by Forster and Kasper in 1954 when they observed two kinds of fluorescence in fairly concentrated solutions (10^{-3} M) of pyrene.¹⁰

Figure 8.1 shows a schematic of the potential energy diagram of an excimer-forming pair of molecules. Worthy of note is the red shift and the loss of vibrational structure in this figure, which can be understood from the shape of the potential energy surfaces of the two molecules as they approach each other. In the ground state, as the two molecules come within the distance of their van der Waals radii, they repel each other, indicated in the graph by the rise in the potential energy; however, in the excited state, the attractive force of positive orbital overlap creates a potential energy well that defines the excimer. The depth of this well is the excimer-binding energy B , which equals the amount of energy by which the excimer is stabilized relative to the energy of the excited state of an isolated (monomeric) molecule. Through fluorescence emission, the paired molecule is returned to the shoulder of the repulsive branch of the potential energy curve. The change in energy corresponding to the fluorescence transition from the excimer (excitation energy of the excimer), ΔE_{FD} , is smaller than the change in energy in the fluorescence of the monomer (excitation energy of the monomer), ΔE_{FM} , hence the red shift in the emission. Furthermore, this energy change covers a continuous range of values and does not contain any vibrational fine structure of the molecular skeleton.¹¹

⁸A good example of the application of excimers is in lithographic exposure sources such as F_2 excimer lasers.

⁹A. Reiser, *Photoreactive Polymers: The Science and Technology of Resists*, pp. 67–68, John Wiley & Sons, Hoboken, NJ (1989).

¹⁰T. Forster and K. Kasper, "Ein Konzentrationsumschlag der fluoreszenz des pyrens," *Z. Phys. Chem. (N.F.)* **1**, 274 (1954).

¹¹A. Reiser, *Photoreactive Polymers: The Science and Technology of Resists*, p. 68, John Wiley & Sons, Hoboken, NJ (1989).

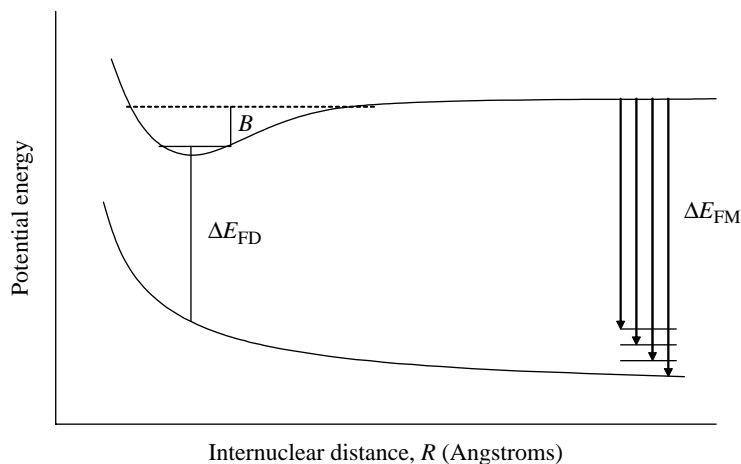


Figure 8.1 Schematic potential energy diagram of an excimer-forming pair of molecules. The lower curve shows both molecules in the ground state. The upper curve shows the excimer formation on the approach between an excited molecule and a molecule in the ground state. ΔE_{FM} is the excitation energy of the monomer, ΔE_{FD} is the excitation energy of the excimer, and B is the excimer-binding energy.

8.2.2 Exciplexes

The interaction on excitation of two similar molecules that do not have identical structures, for example, resist sensitizers such as anthracene and tetracene, can lead to the formation of heteroexcimers. If the two molecules differ significantly in their electron affinities such that one is an electron donor and the other an electron acceptor, the bonding process may be accompanied by a partial transfer of charge. Under this scenario, the interaction between the two molecules is stronger than in conventional excimers and the transient excited species formed as a result is termed an exciplex¹² (excited complex). Characteristically, exciplexes emit a structureless, red-shifted fluorescence, or phosphorescence, similar to that of an excimer.¹³

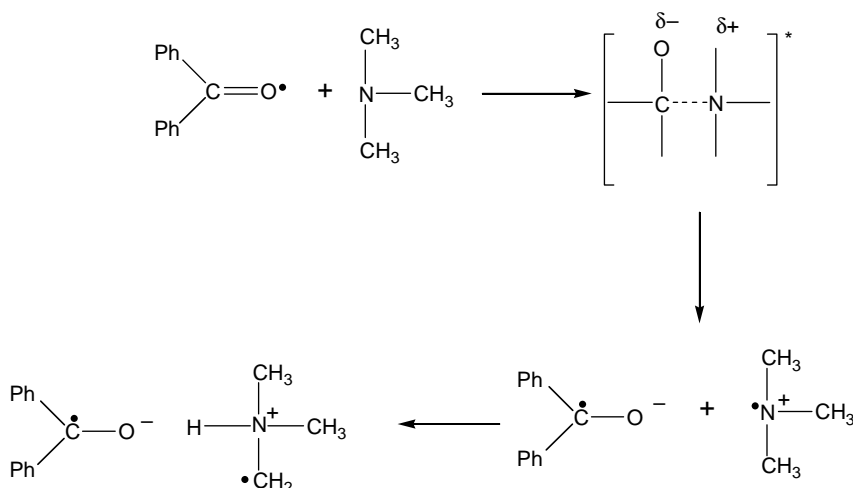
It should be pointed out that exciplexes are often stages in the complete transfer of an electron from one molecule to another, leading to the formation of radical ion pairs and finally of separated radical ions.¹⁴ An illustrative example is the photoreaction of benzophenone (a common resist sensitizer) with tertiary amine (a common resist quencher), as illustrated in Scheme 8.1.¹⁵

¹²Examples of the application of exciplexes in lithography include KrF and ArF exciplex laser light sources for 248 nm and 193 nm lithographies, respectively.

¹³A. Reiser, *Photoreactive Polymers: The Science and Technology of Resists*, p. 70, John Wiley & Sons, Hoboken, NJ (1989).

¹⁴*ibid.*, p. 70.

¹⁵R.F. Bartholomew, R.S. Davidson, P.F. Lambeth, J.F. McKellar, and P.H. Turner, "The photo reaction of aromatic carbonyl compounds with amines: evidence for electron transfer from tertiary aromatic amines to triplet benzophenone," *J. Chem. Soc. Perkin 2*, 577 (1972).



Scheme 8.1 Photoreaction of benzophenone and tertiary amine, illustrating electron transfer that leads to spatial transfer of charge typical of exciplexes.

8.3 Energy Transfer

Exposure-induced energy transfer in a resist matrix occurs not only between different states of a given radiation-sensitive resist molecule or component, but can also occur between such molecules or components when they are in close proximity to each other. It is customary to designate the molecule that carries the excitation energy as the donor (D) and the molecule that accepts the energy as the acceptor (A). The governing reaction is represented by Reaction [8.1]:



By nature, the energy transfer between molecules in resists is an electronic process, which is essentially adiabatic. Such a transfer will occur with reasonable probability only if the excitation energy of D^* is equal to or greater than that of A^* :¹⁶

$$E_{D^*} \geq E_{A^*} \quad (8.1)$$

At the point of transfer, donor and acceptor molecules are coupled and form a single quantum mechanical entity. The two distinct coupling mechanisms that have been recognized to mediate the transfer process¹⁷ include coulombic or

¹⁶Exceptions to this rule occur in reversible processes; see, for example, K. Sandros and H.L.J. Bäckstrom, "Transfer of triplet state energy in fluid solutions. II. Further studies of the quenching of biacetyl phosphorescence in solution," *Acta. Chem. Scand.* **16**, 958 (1962); "Transfer of triplet state energy in fluid solutions. III. Reversible energy transfer," *Acta. Chem. Scand.* **18**, 2355 (1964).

¹⁷For details on the experimental proof for various types of energy transfer, that is, between singlet states, between triplet states, and between singlet and triplet states, please see the following papers of Bennet, Kellog, and co workers at Dupont: R.G. Bennet, "Radiationless intermolecular

dipolar interaction (proposed by Förster¹⁸) and electron exchange or orbital interaction (proposed by Dexter¹⁹).

8.3.1 Dipole resonance transfer

Energy transfer by coulombic interactions is a dipole resonance effect, which according to Förster²⁰ may occur under favorable circumstances where the electronic transitions of two molecules may couple in a way similar to the coupling of two oscillating dipoles, with energy being transmitted from one to the other. For molecules in a resist, the rate of energy transfer for this kind of coupling is given by the expression

$$k_{\text{ET}}(\text{coulombic}) = \frac{\mu_{\text{D}}^2 \mu_{\text{A}}^2}{R_{\text{DA}}^6}, \quad (8.2)$$

where k_{ET} is a rate constant ($\text{M}^{-1} \text{s}^{-1}$), μ_{D} and μ_{A} are transition dipole moments of the fluorescence transition ($\text{D}^* - \text{D}$) and the absorption transition ($\text{A} - \text{A}^*$), respectively, and R_{DA} is the separation between the two molecular centers at the moment of transition.

Expressing the transition moments in terms of measurable quantities allows the Förster transfer rate to be written in the form²¹

$$k_{\text{ET}} = 8.8 \times 10^{-25} \frac{\kappa^2 \phi_{\text{F}}(\text{D})}{n^4 R^6 \tau_{\text{D}}^0} \int f_{\text{D}}(\nu) \epsilon_{\text{A}}(\nu) \frac{d\nu}{\nu^4}, \quad (8.3)$$

where n is the index of refraction of the medium, $\phi_{\text{F}}(\text{D})$ is the quantum yield of fluorescence of the donor, τ_{D}^0 is the fluorescence lifetime of the donor in the absence of the acceptor, and κ^2 is a geometric factor, which in a solid resist film medium has a value of approximately 0.457.²² The factor $f_{\text{D}}(\nu)$ is the fluorescence spectrum of the donor normalized to unity, while $\epsilon_{\text{A}}(\nu)$ is the absorption spectrum

energy transfer. I. Singlet \rightarrow singlet transfer," *J. Chem. Phys.* **41**, 3037 (1964); R.G. Bennet, R.P. Schwenker, and R.E. Kellog, "Radiationless intermolecular energy transfer. II. Triplet \rightarrow singlet transfer," *J. Chem. Phys.* **41**, 3040 (1964); R.E. Kellog and R.G. Bennet, "Radiationless intermolecular energy transfer. III. Determination of phosphorescence efficiencies," *J. Chem. Phys.* **41**, 3042 (1964); R.E. Kellog, "Radiationless intermolecular energy transfer. IV. Triplet \rightarrow triplet annihilation," *J. Chem. Phys.* **41**, 3046 (1964); "Radiationless intermolecular energy transfer. V. Singlet \rightarrow triplet transfer," **41**, 3048 (1964).

¹⁸T. Förster, "Zwischenmolekulare Energiewanderung und Fluoreszenz," *Ann. Phys.* **2**, 55 (1948); "I. Electron optical studies of imperfect crystals and their surfaces," *Discuss. Faraday Soc.* **27**, 7 (1959); T. Förster, *Die Fluoreszenz Organischer Verbindungen*, Vanderhoeck & Ruprecht, Göttingen (1951).

¹⁹D.L. Dexter, "A theory of sensitized luminescence in solids," *J. Chem. Phys.* **21**, p. 836 (1953).

²⁰T. Förster, "Zwischenmolekulare Energiewanderung und Fluoreszenz," *Ann. Phys.* **2**, 55 (1948); "I. Electron optical studies of imperfect crystals and their surfaces," *Discuss. Faraday Soc.* **27**, 7 (1959); T. Förster, *Die Fluoreszenz Organischer Verbindungen*, Vanderhoeck & Ruprecht, Göttingen (1951).

²¹M.Z. Maksimov and I.B. Rotman, "On energy transfer in solid solutions," *Opt. Spectrosc.* **12**, 337 (1962).

²²ibid.

of the acceptor (not normalized), ν are wave numbers, and R is the separation distance between the two molecular centers at the moment of transition.

From the above equations, it can be seen that in dipole resonance transfer, the rate of transfer is dependent on the fluorescence intensity and on the fluorescence lifetime of the donor, as well as on the spectral overlap between the fluorescence of the donor and the absorbance of the acceptor. Two very important features of this transfer mechanism are the sixth-power dependence on the separation of the two molecules as well as the fact that it is possible to transmit energy by resonance transfer over distances of up to 50 Å, a distance corresponding to several molecular diameters.²³

The tendency for energy transfer between a pair of molecules in resists is characterized by a critical distance R_0 at which the rate of energy transfer and the rate k_d of spontaneous deactivation of the donor are equal.²⁴ This leads to a condition that corresponds to an acceptor concentration, $[A]_{1/2}$, at which the fluorescence of the donor is reduced to half its original value (that is, the value it had in the absence of acceptor). The value of $[A]_{1/2}$ therefore can be derived from the equalities

$$k_{\text{ET}}[D^*][A]_{1/2} = k_d[D^*] \quad (8.4)$$

and

$$[A]_{1/2} = \frac{k_d}{k_{\text{ET}}}, \quad (8.5)$$

and the critical distance R_0 is linked to $[A]_{1/2}$ by the relation

$$R_0(\text{Å}) = \frac{7.35}{\sqrt[3]{[A]_{1/2}}}. \quad (8.6)$$

The transfer rate for a given molecular separation R in a resist matrix can be written in the following form:

$$k_{\text{ET}}(R) = \frac{1}{\tau_D} \left(\frac{R_0}{R} \right)^6. \quad (8.7)$$

8.3.2 Exchange transfer

This transfer mechanism is based on electron exchange between two molecules as indicated in the Hückel diagram of Fig. 8.2. According to Dexter,²⁵ the distance

²³A. Reiser, *Photoreactive Polymers: The Science and Technology of Resists*, p. 72, John Wiley & Sons, Hoboken, NJ (1989).

²⁴A. Lamola, "Electronic energy transfer in solution: Theory and applications," in *Energy Transfer and Organic Photochemistry*, A.A. Lamola and N.J. Turro, Eds. pp. 17-132, Interscience, New York (1969); A. Reiser, *Photoreactive Polymers: The Science and Technology of Resists*, p. 72, John Wiley & Sons, Hoboken, NJ (1989).

²⁵D.L. Dexter, "A theory of sensitized luminescence in solids," *J. Chem. Phys.* **21**, 836 (1953).

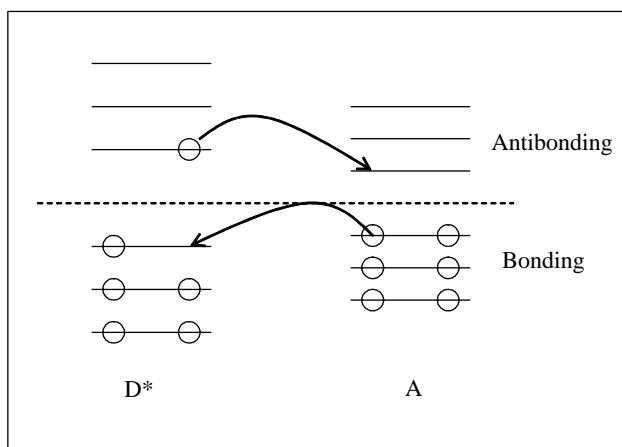


Figure 8.2 Energy transfer by electron exchange as represented in a Hückel orbital diagram.

dependence for this process is given by

$$K_{\text{ET}}(\text{exchange}) = KJ \exp\left(-\frac{2R_{\text{DA}}}{L}\right), \quad (8.8)$$

where K is a constant for a given donor-acceptor pair, J is a fully normalized spectral overlap integral, and L is the sum of the van der Waals radii of donor and acceptor. Reiser observes that the rate of exchange transfer falls off even more rapidly with increasing molecular separation than the rate of dipole resonance transfer.²⁶

By necessity, the exchange mechanism requires orbital overlap between donor and acceptor molecules, which means that it operates only over “collisional” distances, on the order of 10 Å. While the exchange transfer mechanism also depends on spectral overlap, it does not depend on the intensities of the radiative transitions and is therefore a more general energy transfer mechanism. Also, this type of energy transfer is rather nonspecific and occurs on almost every encounter, provided the process is exothermic [i.e., $(E_{\text{D}^*} - E_{\text{A}^*}) < 0$].²⁷

Furthermore, exchange transfer is also less sensitive to changes in spin multiplicity than resonance transfer. Therefore, it is the mechanism responsible for the triplet-to-singlet energy transfer in the spectral sensitization processes of organic photochemistry,²⁸ as seen in organic resist materials.

8.3.3 The Perrin formula

A simple formula for energy transfer based on the idea that energy transfer occurs between two molecules only if they find themselves together within a sphere of

²⁶A. Reiser, *Photoreactive Polymers: The Science and Technology of Resists*, p. 74, John Wiley & Sons, Hoboken, NJ (1989).

²⁷ibid.

²⁸P.J. Wagner, “Chemistry of excited triplet organic carbonyl compounds,” in *Creation and Detection of the Excited State*, A.A. Lamolda, Ed., Vol. 1A, p. 173, New York, Marcel Dekker (1971).

influence or “quenching sphere” was proposed early on by Perrin, who developed the formula²⁹

$$\frac{\phi_F}{\phi_F^0} = \exp(VN[A]), \quad (8.9)$$

where ϕ_F is the fluorescence quantum yield in the presence of the quencher concentration $[A]$, ϕ_F^0 is the fluorescence quantum yield in the absence of quencher, V is the volume of the quenching sphere, and N is Avogadro’s number. This model does not incorporate any coupling mechanism and was later extended by Terenin and co-workers,³⁰ who described energy transfer (quenching) in solid systems.

8.4 Energy Migration in Resist Polymers

Energy migration in resist polymer matrices plays a very important role by channeling energy to reactive sites, be they scissioning or cross-linking points on the polymer backbone or deprotection sites on the pendant groups of the polymer. The fundamental principles governing energy migration in polymers were originally formulated by Frenkel in 1931,³¹ long before they could be experimentally verified.³² It was Frenkel who introduced the term “exciton” for the energy quantum mobile in an ensemble of identical molecules. In 1935, Davydov described the spectral characteristics of such systems in more detail, illuminating in the attempt a number of unexplained phenomena in solid state physics.³³ Both Frenkel and Davydov predicted the possibility of energy migration not only in crystals, but also in partially ordered arrays and even in amorphous systems, of which resist polymers are a part. A few years later, Kallman and co-workers³⁴ reported observing long-range energy transfer in polystyrene (a common resist polymer platform in DUV lithography) and in some other polymers.

The thought then was that in these systems the exciton traveled along the phenyl groups in the side chains of the polymer in a process termed “down-chain migration.” This view was later confirmed by Fox et al.³⁵ and David et al.,³⁶

²⁹A. Reiser, *Photoreactive Polymers: The Science and Technology of Resists*, p. 75, John Wiley & Sons, Hoboken, NJ (1989).

³⁰E. Terenin and V. Ermolaev, “Sensitized phosphorescence in organic solutions at low temperature. Energy transfer between triplet states,” *Trans. Faraday Soc.* **52**, 1042 (1956); V.L. Ermolaev, “Energy transfer in organic systems involving the triplet state III. Rigid solutions and crystals,” *Sov. Phys. Usp.* (Engl. Transl.) **80**, 333 (1963).

³¹J.I. Frenkel, “On the transformation of light into heat in solids. II,” *Phys. Rev.* **37**, 1276 (1931).

³²The treatment here follows after the treatment in the excellent book, A. Reiser, *Photoreactive Polymers: The Science and Technology of Resists*, pp. 75–82, John Wiley & Sons, Hoboken, NJ (1989).

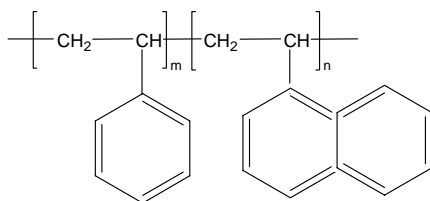
³³A.S. Davydov, *Theory of Molecular Excitons*, McGraw Hill, New York (1962).

³⁴F.H. Brown, M. Furst, and H. Kallmann, “Light and high energy induced energy transfer in liquid and rigid organic scintillators,” *Discuss. Faraday Soc.* **27**, 43 (1959).

³⁵R.B. Fox, T.R. Price, R.F. Cozzens, and J.R. McDonald, “Photophysical processes in polymers. IV. Excimer formation in vinylaromatic polymers and copolymers,” *J. Chem. Phys.* **57**, 534 (1972).

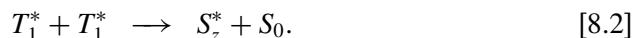
³⁶C. David, W. Demarteau, and G. Geuskens, “Energy transfer in polymers II Solid polyvinyl naphthalene benzophenone system and copolymers vinyl naphthalene vinylbenzophenone,” *Eur. Polym. J.* **6**, 1397 (1970).

who studied the fluorescence behavior of copolymers and of polymer blends, and also by Cozzens and Fox,³⁷ who observed that in copolymers of styrene and 1-vinylnaphthalene (**I**) containing only 1% of naphthalene and 99% of benzene units, naphthalene phosphorescence was observed almost exclusively.³⁸



Poly(styrene-*co*-1-vinylnaphthalene) (**I**)

In contrast, when 1% poly(1-vinylnaphthalene) is blended with 99% polystyrene, the result is mainly polystyrene phosphorescence. These results lend themselves to the conclusion that energy migration must occur intramolecularly via the manifold of phenyl groups attached to the polyvinyl backbone.³⁹ The same conclusion was also reached from the observation of delayed fluorescence in highly dilute solid solutions of poly(1-vinylnaphthalene) in organic glasses at 77 K. The delayed fluorescence in this system is attributed to the encounter of two triplet excited states, which in turn provides evidence for triplet migration along the chain. On encounter, the two triplet states are believed to disproportionate to form an excited state (which emits fluorescence) and a singlet ground state, as shown in Reaction [8.2]:⁴⁰



Furthermore, interrupting the sequence of naphthalene units, for example, by copolymerization with methyl methacrylate, results in diminution of the delayed fluorescence, which is observed only as long as significant blocks of naphthyl groups still remain.⁴¹ It is for similar reasons that delayed fluorescence, for example, in poly(2-vinylnaphthalene), is dependent on molecular weight, that is, on chain length.⁴²

Down-chain energy migration has since been widely investigated experimentally and confirmed, and is now known to be a common phenomenon that plays a significant role in the degradation and stabilization of polymers, including those

³⁷R.F. Cozzens and R.B. Fox, "Intramolecular triplet energy transfer in poly(1 vinylnaphthalene)," *J. Chem. Phys.* **50**, 1532 (1969).

³⁸A. Reiser, *Photoreactive Polymers: The Science and Technology of Resists*, p. 78, John Wiley & Sons, Hoboken, NJ (1989).

³⁹*ibid.*

⁴⁰*ibid.*

⁴¹*ibid.*, pp. 78–79.

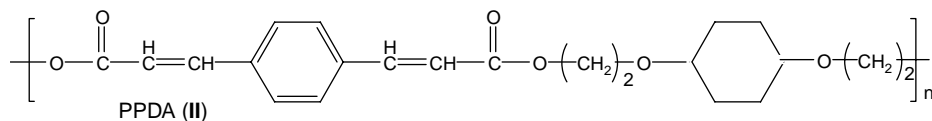
⁴²N. Kim and S.E. Webber, "Effect of molecular weight on triplet exciton processes. 4. Delayed emission of solid poly(2 vinylnaphthalene)," *Macromolecules* **13**, 1233 (1980).

used in resist applications. The polymer chain in these systems acts as an “antenna” that conducts energy either to a reactive site or away from the point of incidence to a quencher, where it can be harmlessly dissipated. The range of energy migration in some of these materials has been reported to be considerable.⁴³

It should be mentioned that side chain interaction in polystyrene and in similar polymers not only promotes energy migration, but also promotes the formation of excimers that occurs in solution mainly as a result of conformational transitions, which bring neighboring fluorophores into juxtaposition. In bulk polymers, excimer emission is much more pronounced, given that energy migration also occurs between chains. Reiser asserts that excimer emission occurs in bulk polymers from monomer pairs that have the required conformation already in the ground state.⁴⁴

Another characteristic of excimers in polymers is that they have a lower excitation energy than the isolated monomer, which implies that excimer sites in a polymer matrix can act as exciton traps. This is the reason polystyrene films, for example, exclusively emit excimer fluorescence although the concentration of the excimer sites is low, on the order of 1 mol%.⁴⁵ In these systems, the excimer sites are supplied with excitation energy by exciton migration. Of particular interest is the fact that the concentration of excimer sites tends to limit the exciton migration range in these systems.⁴⁶

A major distinction between the migration of energy in dilute solid solutions of polymers and solid films is that in the former the excitons are restricted to an intramolecular path along the polymer backbone, while in solid films of the neat material, they can migrate intermolecularly from one chain to another. An example of a material that illustrates this distinction rather well is the resist polymer PPDA (II),⁴⁷ which is based on the *p*-phenylene diacrylate chromophore that is described in Chapter 6.



In PPDA, the chromophores are part of the polymer backbone, and since they are not adjacent to each other, down-chain energy migration is not possible. Interestingly, when a dilute solution of this polymer is irradiated, a certain amount of excimer fluorescence is observed along with the predominant

⁴³A. Reiser, *Photoreactive Polymers: The Science and Technology of Resists*, p. 79, John Wiley & Sons, Hoboken, NJ (1989).

⁴⁴*ibid.*

⁴⁵W. Frank and L.A. Harrah, “Excimer formation in vinyl polymers. II. Rigid solutions of poly(2-vinylnaphthalene) and polystyrene,” *J. Chem. Phys.* **61**, 1526 (1974).

⁴⁶A. Reiser, *Photoreactive Polymers: The Science and Technology of Resists*, p. 79, John Wiley & Sons, Hoboken, NJ (1989).

⁴⁷*ibid.*, p. 80.

monomer fluorescence, which is indicative of the fact that the polymer chain folds on itself and that a few chromophores are able to assume a contact configuration that produces excimer emission.⁴⁸ However, when solid films of the same polymer are irradiated, no monomer fluorescence is seen, and only excimer fluorescence is observed.⁴⁹ This result suggests that excitation produced at the monomer sites must be freely mobile in the solid matrix to reach an excimer site within its lifetime.⁵⁰

8.5 Spectral Sensitization

The idea behind spectral sensitization of a resist system is to provide a means of utilizing radiative energy that is not directly absorbed by the reactants. Given that the most common lithographic exposure sources emit within rather narrow wavebands, resists, and in particular, photoresists, which do not absorb in one of these emission regions, will not respond to the radiation, resulting in the wastage of the radiative energy falling on them. A very good example of a resist system whose absorption spectrum is mismatched with the emission spectra of the exposure source is poly(vinyl cinnamate) under UV exposure from a medium-pressure Hg arc lamp. The strongest absorption peak of the poly(vinyl cinnamate) spectrum occurs in the DUV region (around 250 nm), missing most of the strong emission lines of the Hg arc lamp, which occur around 360 nm. It is this spectral mismatch between the emission lines of the Hg arc lamp and the poly(vinyl cinnamate) absorption that is the principal cause of the low sensitivity of the unsensitized poly(vinyl cinnamate) resist.⁵¹

It is possible to improve the light-collecting ability of the system through energy transfer by incorporating into the system (such as a resist) a component that absorbs the available energy efficiently and transmits it to the reactants. This process, which extends the action spectrum of the system, is referred to as “spectral sensitization” or “photosensitization.” The effect of sensitizers on the performance of a system can be quite dramatic. As a practical matter, spectral sensitization always extends the absorption range of the system to longer wavelengths, corresponding to lower excitation energies.⁵²

To achieve spectral sensitization by singlet energy transfer with a sensitizer that absorbs at a longer wavelength than the reactant would require endothermic energy transfer, which under normal circumstances is not a practical solution. However, it is possible to accomplish this with a sensitizer whose singlet excited state lies below that of the reactant, but whose triplet level lies above the triplet

⁴⁸M. Graley, A. Reiser, A.J. Roberts, and D. Phillips, “Excimer fluorescence as a probe into the solution behavior of a polyester of p phenylenediacrylic acid,” *Macromolecules* **14**, 1752 (1981).

⁴⁹P.L. Egerton, J. Trigg, E.M. Hyde, and A. Reiser, “Photocycloaddition at excimer sites in a solid polyester of p phenylenediacrylic acid,” *Macromolecules* **14**, 100 (1981).

⁵⁰A. Reiser, *Photoreactive Polymers: The Science and Technology of Resists*, p. 80, John Wiley & Sons, Hoboken, NJ (1989).

⁵¹*ibid.*, p. 83.

⁵²*ibid.*, p. 84.

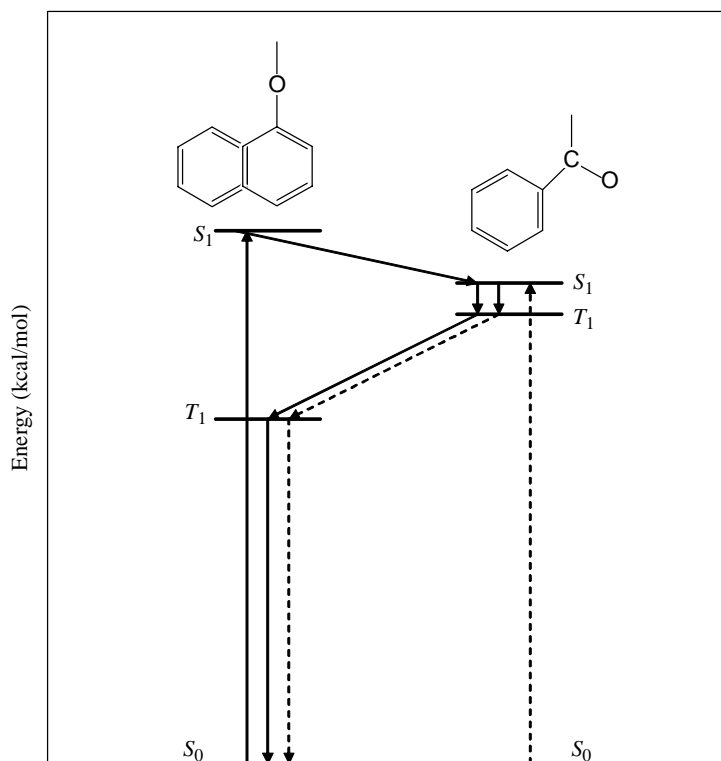


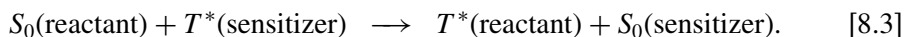
Figure 8.3 Schematic of an energy-level diagram for triplet sensitization for polymer-bound naphthyl groups and acetophenone. (Reprinted with permission from American Chemical Society.⁵³)

level of the reactant,⁵⁴ as schematically illustrated in Fig. 8.3 for the naphthalene (reactant)-acetophenone (sensitizer) pair.⁵⁵

8.6 Sensitization by Energy Transfer

8.6.1 Triplet sensitization

Triplet sensitization is associated with exothermic energy transfer from the triplet excited state of the sensitizer to the ground state of the reactant. The majority of sensitization processes in organic resist systems is based on the reaction



⁵³ibid.

⁵⁴A. Reiser, *Photoreactive Polymers: The Science and Technology of Resists*, p. 84, John Wiley & Sons, Hoboken, NJ (1989).

⁵⁵L. Merle Aubry, D.A. Holden, and J.E. Guillet, "Photophysics and photochemistry of naphthyl ester polymers in solution," *Macromolecules* **13**, 1138 (1980).

Given that the overall spin of the system is conserved, the transfer process is spin-allowed and occurs efficiently, provided only that transfer is exothermic, that is, $E_T(\text{sensitizer}) > E_T(\text{reactant})$. It must be mentioned that in triplet sensitization, only the triplet state of the reactants is populated. Consequently, the photoreaction occurs exclusively from the triplet state and may proceed by a different route from the singlet state reaction.⁵⁶

Reiser⁵⁷ has identified a number of attributes that candidates for triplet sensitizers must possess, as follows:

- (1) A high rate of intersystem crossing from S_1 to T_1 and consequently a high quantum yield ϕ_T of triplet formation.
- (2) An energy difference between the singlet excited state S_1 and the triplet excited state T_1 (referred to as singlet-triplet splitting) that is small.
- (3) Long triplet lifetime to increase the probability of energy transfer between sensitizer and reactant.
- (4) Ability to strongly absorb the available radiation in a spectral region where the reactant does not absorb.
- (5) Solubility in the reaction medium (solvent or polymer matrix).

As a general rule, these conditions are satisfied in the aromatic ketones where the $n\pi^*$ character of the excited states (triplets and singlet) favors intersystem crossing and high values of ϕ_T , as well as a small singlet-triplet splitting. This explains why the majority of common sensitizers are either ketones or contain the carbonyl group somewhere in their structure.⁵⁸

8.6.2 Sensitization by electron transfer

Sensitization by electron transfer can occur in resist systems. A good example is the sensitization of azide photolysis by aromatic hydrocarbons,⁵⁹ which proceeds by the coupled reactions,⁶⁰



and



⁵⁶A. Reiser, *Photoreactive Polymers: The Science and Technology of Resists*, p. 86, John Wiley & Sons, Hoboken, NJ (1989).

⁵⁷*ibid.*, pp. 86–88.

⁵⁸*ibid.*, p. 88.

⁵⁹L.J. Leyshon and A. Reiser, "Sensitized photodecomposition of phenyl azide and naphthyl azide," *Trans. Faraday Soc.* **68**, 1918 (1972).

⁶⁰A. Reiser, *Photoreactive Polymers: The Science and Technology of Resists*, p. 88, John Wiley & Sons, Hoboken, NJ (1989).

In this system, the hydrocarbon sensitizer is the electron acceptor, and the azide functions as the electron donor. The change in the free energy on charge transfer between two molecular species is given by an expression derived by Rehm and Weller:⁶¹

$$\Delta G_{CT} = E(D/D^+) - E(A^-/A) - \Delta E_{00}^* - e^2/\kappa a, \quad (8.10)$$

where $E(D/D^+)$ is the oxidation potential of the donor, $E(A^-/A)$ is the reduction potential of the acceptor (sensitizer), ΔE_{00}^* is the excitation energy of the sensitizer, e is the electronic charge, κ is the dielectric constant of the medium, and a is the distance between the molecular centers at the moment of transfer.

8.7 Radiation Chemistry Versus Photochemistry of Resists

Generally speaking, conventional photochemistry deals with valence or outer-shell electronic excitation associated with radiation lying in the approximate wavelength range 200–700 nm. Below 200 nm, higher-energy processes become progressively more dominant; photoionization, for instance, becomes predominant at 150 nm and below. In essence, photochemistry deals with the chemistry of electronically excited molecules, and ceases at around 90–100 nm; the region below this belongs to the province of radiation chemistry, i.e., the chemistry induced by the absorption of α , β , γ , or x rays.⁶²

In lithographic technologies utilizing charged particles such as electrons, ion beams, and high-energy ionizing radiations such as x rays, including EUV photons (otherwise called soft x rays), resist imaging exploits the chemical effects of these charged particles and radiations. A major characteristic of these charged particles and ionizing radiations is that the energy of the individual quanta is much higher than the energy of the chemical bonds in the resist material and larger than the ionization potentials of their constituent atoms. As a result, the primary result of the interaction between the high-energy radiations and charged particles with the material is ionization. A whole sequence of steps typically follows, ultimately leading to a variety of products. The description of these events falls within the subject of radiation chemistry.⁶³

Although radiation chemistry and photochemistry are clearly distinct, the boundary between them can be rather confusing at times. In resist photochemistry, radiation quanta applied to the resist as part of the exposure process are absorbed by specific chromophores in the resist molecules and compounds, which as a result

⁶¹D. Rehm and A. Weller, "Kinetik und Mechanismus der Elektronenübertragung bei der Fluoreszenzloschung in Acetonitril," *Ber. Bunsenges. Phys. Chem.* **73**, 834 (1969); A. Weller, "Photoinduced electron transfer in solution: Exciplex and radical ion pair formation free enthalpies and their solvent dependence," *Z. Phys. Chem. (N.F.)* **133**, 93 (1982).

⁶²J. Guillet, *Polymer Photophysics and Photochemistry: An Introduction to the Study of Photo processes in Macromolecules*, p. 347, Cambridge University Press, Cambridge, (1985); P. Suppan, *Chemistry and Light*, p. 8, The Royal Society of Chemistry, Cambridge (1994).

⁶³A.S. Davydov, *Theory of Molecular Excitations*, McGraw Hill, New York (1962).

get promoted into well-defined excited states. Because the energy of the delivered quanta exceeds some of the bond energies in the resist molecules and compounds, as in DUV and VUV lithographies, photochemistry leads to fragmentation and occasionally to ionization. The main characteristic feature of radiation chemistry of resists is that energy absorption is not associated with a particular chromophore, but occurs at random in the resist material. In concrete terms, radiation chemistry may be defined as being concerned with quantal energies far in excess of the ionization energy of common atoms and molecules—greater than 30 eV (700 kcal/mol)⁶⁴—corresponding to a wavelength of roughly 41 nm.

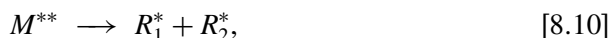
The typical course of radiation-induced chemical processes occurring during a resist exposure process may be described as follows. On exposure of resists by high-energy particles and radiations such as electrons, x rays, ions, etc., a number of cascading processes take place in the vicinity of the exposure point, and various product species are formed along its trajectory or in the spurs and side branches of it. The primary step is ionization, which is associated with the production of a large amount of kinetic energy that on encounter with neighboring atoms (Reaction [8.6]) leads to further ionization:



This process may be repeated over and over again with some of the secondary electrons recombining with their original partners (germinate recombination) and producing molecules in higher excited states:



These high-excited-state molecules can follow a number of paths. They can emit radiation, fragment into ions or radicals, decay to lower excited states by internal conversion, or finally return to the ground state (Reactions [8.8]–[8.11]):⁶⁵



Most often, this sequence leads to final products similar to those that occur under photochemistry. As the secondary electrons lose energy, they become thermalized and may have themselves attached either to specific molecules (thus forming molecular ions) or to the residual solvents in the resist film in the form of solvated electrons.⁶⁶

⁶⁴A. Reiser, *Photoreactive Polymers: The Science and Technology of Resists*, pp. 302–303, John Wiley & Sons, Hoboken, NJ (1989).

⁶⁵ibid., p. 303.

⁶⁶ibid.

8.8 Radiation Chemical Yield and Dosimetry

Because the energy of ionizing particles or radiations is not absorbed at a specific site or within a particular molecule, the quantum yield of a reaction involving one such particle or unit of radiation can be fairly well defined. The inherent efficiency of a radiation chemical process during resist exposure is measured in terms of a radiation chemical yield or G -value. For a process leading to a certain number of reaction products, the G -value of each is defined as the number of moles of that product resulting from 100 eV of energy deposited into the system. In a system of unit volume (1 L) the molarity of the product $[P]$ produced by a dose D is expressed as

$$[P] = G(P) \times \frac{D}{100} \text{ eV.} \quad (8.11)$$

In practice, the determination of the G -value requires the measurement of a product quantity and dose or dose rate.⁶⁷

8.9 Radiation Chemistry of Polymers

8.9.1 Backbone scission and cross-linking

The radiation chemistry of resist polymers is governed by two main processes, namely, backbone scission and cross-linking. Whether the polymer will act as a positive or negative resist resin under lithographic imaging depends on whether backbone scissioning or the cross-linking process is dominant.⁶⁸

Backbone scission leads to polymer degradation and to a decrease of the molecular weight of the polymer. It is associated with polymers containing weak bonds in their backbone (as exists in polyalkane sulfone) and/or in vinyl polymers containing tetra-substituted carbon, that is, carbon atoms that do not carry any hydrogen [as obtained in polymethylmethacrylate and poly(tetrafluoroethylene)]; all of these polymers degrade rapidly on irradiation. In contrast, vinyl polymer, rubber, and polyethylene, where each carbon of the main chain is bonded to at least one hydrogen atom, tend to cross-link when irradiated in the solid state.⁶⁹ The radiation yields of scission G_s and cross-linking G_x are polymer material properties used to characterize backbone chain scission and cross-linking phenomena in polymers.⁷⁰

⁶⁷ibid., p. 304.

⁶⁸M. Dole, *The Radiation Chemistry of Polymers*, Academic, New York (1972).

⁶⁹A. Reiser, *Photoreactive Polymers: The Science and Technology of Resists*, p. 307, John Wiley & Sons, Hoboken, NJ (1989).

⁷⁰ibid.

8.9.2 Determination of the scission yield

Under the condition of negligible or no cross-linking in a polymer during exposure, the backbone scission yield⁷¹ may be determined from the change in the molecular weight that occurs on irradiation. The pre-irradiation number of molecules of polymer in the sample can be expressed as

$$N^0 = N_A \frac{w}{M_n}, \quad (8.12)$$

where w is the weight of the sample (in grams), M_n is the number average molecular weight before irradiation, and N_A is Avogadro's number. After exposure to a given dose D , expressed in electron volts per gram, the number of scissions (N_{SC}), by definition of the scission yield G_s , is expressed as

$$N_{SC} = \frac{G_s}{100} Dw. \quad (8.13)$$

Each scission event increases N by one molecular unit so that the molecular weight M_n after exposure to a dose D can be expressed from Eqs. (8.12) and (8.13) by an equation of the form

$$\frac{1}{M_n} = \frac{1}{M_n^0} + \frac{G_s}{100N_A} D. \quad (8.14)$$

Table 8.1 contains values of G_s obtained in this way for a number of common resist polymers.

Experimentally, scission yield is often determined by exposing the material to γ radiation from a ^{60}Co source, and monitoring the molecular weight of the polymer in intervals during the process. These data are of great importance to

Table 8.1 Radiation yields of scission for a group of common polymers. (Data used with permission from Elsevier.⁷²)

Polymer	G_s
Poly(α methylstyrene)	0.3
Poly(isobutene)	4
PMMA	2
Cellulose	11
Poly(α methylcellulose)	16
Poly(tetrafluoroethylene)	Very high

⁷¹The method presented here is adapted from the treatment given in A. Reiser, *Photoreactive Polymers: The Science and Technology of Resists*, pp. 307–308, John Wiley & Sons, Hoboken, NJ (1989).

⁷²J.H. O'Donnell and D.F. Sangster, *Principles of Radiation Chemistry*, p. 121, Elsevier, New York (1970).

the lithographer because the radiation chemical procedure is simpler than a full lithographic evaluation, and correlates with G_s and lithographic sensitivity.⁷³

8.9.3 Determination of the cross-linking yield G_x

In the absence of scissioning, the radiation chemical yield of cross-linking⁷⁴ is readily determined by monitoring the insolubilization of the polymer. Charlesby and Pinner⁷⁵ showed that the soluble fraction s as a function of the irradiation dose received by the polymer can be described by an equation of the form

$$s + s^{1/2} = \frac{G_s}{2G_x} + \frac{9.65 \times 10^5}{M_n^0 G_x} \frac{1}{D}. \quad (8.15)$$

In the procedure, the polymer sample is irradiated and then extracted with a suitable solvent in which the soluble fraction, that is, the fraction of the material that is not cross-linked, can be determined. A plot of $(s + s^{1/2})$ against $1/D$ yields a straight line from which the value of G_x can be determined from either the intercept or the slope.

In a polymer in which both cross-linking and backbone scission are occurring to a significant degree, the G -values of both processes can be derived simultaneously by measuring the number-average and weight-average molecular weights, M_n and M_w , respectively, of the sample under irradiation. The M_n and M_w values can be expressed by the following two equations of similar form:

$$\frac{1}{M_n} = \frac{1}{M_n^0} + [G_s - G_x] \frac{D}{100N_A} \quad (8.16)$$

and

$$\frac{1}{M_w} = \frac{1}{M_w^0} + [G_s - 4G_x] \frac{D}{100N_A}. \quad (8.17)$$

A plot of the reciprocal molecular weight of the sample as a function of radiation dose yields straight lines, from which slope the values of $(G_s - G_x)$ and $(G_s - 4G_x)$ can be obtained, yielding the G -values.

⁷³A. Reiser, *Photoactive Polymers: The Science and Technology of Resists*, pp. 307–308, John Wiley & Sons, Hoboken, NJ (1989).

⁷⁴The method presented here is adapted from the treatment of the subject given in A. Reiser, *Photo reactive Polymers: The Science and Technology of Resists*, pp. 309–311, John Wiley & Sons, Hoboken, NJ (1989).

⁷⁵A. Charlesby and S.H. Pinner, "Analysis of the solubility behaviour of irradiated polyethylene and other polymers," *Proc. R. Soc. London, Ser. A* **249**, 367 (1959); P. Alexander, R.M. Black, and A. Charlesby, "Radiation induced changes in the structure of polyisobutylene," *Proc. R. Soc. London, Ser. A* **232**, 31 (1955).

8.10 Sensitivity and Exposure Radiation

Since the chemical effects of different ionizing radiations are essentially similar, it is expected that a resist that is sensitive to one ionizing radiation will also be sensitive to the other types of ionizing radiations. That is in fact the case—there is good correlation between electron sensitivities and x-ray sensitivities of most practical resists designed for these lithographies,⁷⁶ between electron and ion sensitivities,⁷⁷ and between electron-beam and EUV photon sensitivities. In other words, resists that are sensitive to electron-beam radiation are also sensitive to x-ray radiation, ion-beam radiation, and EUV photons. For instance, glycidyl ether bisphenol-A novolac is an epoxy-based negative-tone chemically amplified resist with sensitivity to x ray, electron-beam, DUV 248-nm, and i-line 365-nm radiations. Originally formulated by the IBM Corporation, this resist is now sold commercially under the brand name of SU-8 by the MicroChem Corporation for use in x-ray, electron-beam, DUV and i-line lithographies.

There is a physical basis for why resists show correlations and similarities in their exposure characteristics with their sensitivities to EUV, electron-beam, x-ray, and ion-beam radiations. Simply put, the resist sensitivity correlation between the different types of charged particle beams, x rays, and EUV photons suggests that the chemical reactions responsible for the generation of differential solubility in these systems do not stem directly from interaction of the resists with the primary beam. In all of the above-mentioned lithographic technologies, the energy of the primary beam greatly exceeds the bond strength and ionization potential of the components of the resist materials. That is, the energies of the primary beams are so high that, in principle, they can break any chemical bond in a resist, even accounting for the numerous energy relaxation modes in the resist polymer. If the primary beams were responsible for the chemical changes during exposure, no functional group selectivity would be expected.⁷⁸ Luckily, these high-energy primary beams do not directly couple with the bonds in the resist polymer and resist additives. So, here is one of the few instances in all of lithography where nature's interest and ours are aligned.

It is well established that the primary high-energy beam interacts with the resist material in a manner that is dependent only on the capture cross section of the atoms in the resist, and not on its molecular structure, to produce a cascade of

⁷⁶A. Terenin and V. Ermolaev, *Trans. Faraday Soc.* **52**, 1042 (1956); C.G. Willson, in *Introduction to Microlithography*, L.F. Thompson, C.G. Willson, and M.J. Bowden, Eds., pp. 212–213, American Chemical Society, Washington, DC (1994); J. Lignau, R. Dammel, and J. Theis, "High resolution x ray and electron beam resists using chemical amplification," *Solid State Technol.* **10**, 9 (1989); "Recent trends in x ray resist: part II," *Solid State Technol.* **10**, 107 (1989).

⁷⁷T.M. Hall, A. Wagner, and L.F. Thompson, "Ion beam exposure characteristics of resists," *J. Vac. Sci. Technol.* **16**, 1889 (1979); R.C. Brault, L.J. Miller, "Sensitivity and contrast of some proton beam resists," *Polym. Eng. Sci.*, **20**, 1064 (1980); Y. Wada, K. Mochiji, and H. Obayashi, "Reactive ion etching resistant negative resists for ion beam lithography," *J. Electrochem. Soc.* **130**, 187 (1983); J.E. Jensen, "Ion beam resists," *Solid State Technol.* **27**(6), 145 (1984).

⁷⁸C.G. Willson, in *Introduction to Microlithography*, L.F. Thompson, C.G. Willson, and M.J. Bowden, Eds., pp. 212–213, American Chemical Society, Washington, DC (1994).

lower-energy secondary and Auger electrons with short-range travel in the resist, inducing molecular structure-dependent reactions. Because the chemistry results from interaction of the secondary, low-energy electrons, the resist responds similarly to the source of these low-energy electrons, irrespective of the nature of the high-energy primary beam that engendered them. In other words, the secondary electrons produced by x ray, e-beam, ion beam, or EUV photons are all alike, physically and chemically, and all look alike to the resist molecules. Thus, the chemical response to high-energy radiation is essentially the same regardless of the nature of the primary beam, and the extent of response and sensitivity depends only on the efficiency with which the primary beam interacts with the resist film to produce the secondary electrons. This efficiency in turn depends only on the capture cross section, which is related to the beam energy and the atomic composition of the resist.⁷⁹

In specific terms, for lithographies based on these high-energy charged particles or EUV photons, the primary charged particles or photons do not expose resists. Instead, they generate secondary electrons on account of their interaction with resist polymers and PAGS, and which in turn expose the resists. For the specific case of EUV, the primary photons generate photoelectrons, which in turn generate secondary electrons. Absent these secondary electrons, we would not have EUV lithography, x-ray lithography, electron and ion-beam lithographies, etc.

8.11 Exposure Mechanisms of Resists and Exposure Radiation

The exposure mechanism of resists is determined by the nature of the interaction between the exposure radiation with the atoms and molecules of the resist matrix. For lithographic technologies using charged particles such as electrons, ion beams, and high-energy ionizing radiations such as x rays, including EUV photons, the exposure mechanism is driven by the ionization of the resist material, leading to either scissioning or cross-linking events in the exposed part of the resist. Whereas in lithographic technologies using low-energy photons as in UV, DUV, and VUV lithographies, the exposure mechanism is driven by photon absorption by specific chromophores in the resist, which in turn are promoted into well-defined excited states as a result, leading to the formation of photoproducts that are manifestly different from the components in the unexposed part of the resist.

Thus, broadly speaking, there are distinct differences in the exposure mechanism of resists used in the various lithographic technologies. Specifically, the exposure mechanism of aromatic-polymer-based chemically amplified resists designed for DUV 248-nm lithography proceeds via two pathways: (i) light is directly absorbed by the photoacid generator, followed by carbon-heteroatom bond cleavage and radical processes to generate photoacid,⁸⁰ or (ii) light can be absorbed by the aromatic polymer, which in turn sensitizes the photacid generator

⁷⁹ibid.

⁸⁰S.P. Pappas, B.C. Pappas, L.R. Gatechair, and W. Schnabel, "Photoinitiation of cationic polymerization, II. laser flash photolysis of diphenyliodonium salts," *J. Polym. Sci. Polym. Chem. Ed.* **22**(1), 69–76 (1984); J.L. Dektar and N.P. Hacker, "Photochemistry of triarylsulfonium salts," *J. Am. Chem.*

to decomposition. The exposure mechanism for chemically amplified resists designed for DUV 193-nm lithography and VUV 157-nm lithography is very similar to the 248-nm mechanism, except that the polymer does not participate in the sensitization of the PAG.⁸¹

A similar distinction exists between the exposure mechanism of aromatic-polymer-based chemically amplified resists and their non-chemically amplified counterparts that are based on dichromated gelatin, bis-azide/cis isoprene (both designed for visible-light lithography) and DNQ/novolac (designed for near-UV lithography). While direct sensitization of the photoactive compounds by the exposure photons is possible in these non-chemically amplified resists, indirect sensitization of the photoactive compounds by the resist resin is extremely rare. Chain scission resists such as those based on polymethyl methacrylate and its derivatives do not have sensitizers, and thus do not participate in sensitization processes. Instead, they undergo direct chain scissioning reactions initiated by the exposing radiations such as electron beams, x rays, etc.

In contrast, the exposure mechanism of chemically amplified resists designed for EUV 13.5-nm exposure occurs by an entirely different mechanism from the mechanisms described above for DUV 248-nm and 193-nm resists.⁸² For one thing, the energy of EUV photons (92.4 eV) is 18 and 14 times higher than 248-nm and 193-nm photons, respectively.

Although the complete picture of the mechanism of the EUV exposure mechanism is currently an active area of research, a consensus is quickly emerging as to how the process plays out. It is believed⁸³ that when an EUV photon interacts with a resist polymer or components in the resist, the dominant interaction is the photoelectric effect. Assuming an average ionization potential of ~ 10 eV for H, C, F... orbitals associated with resist atoms, this implies that on average, most initial excitations lead to the production of ~ 80 -eV primary electrons (photoelectrons) inside the resist film.⁸⁴ The photoelectrons rapidly move away from the excitation site and lose energy through a series of inelastic scattering events involving resist components, leading to the creation of a cascade of secondary electrons. In essence, the process of energy deposition in EUV lithography is based on the excitation of molecular transitions by the passing electrons.⁸⁵

Soc. **112**(6), 6004–6015 (1990); J.L. Dektar and N.P. Hacker, "Photochemistry of diarylsulfonium salts," *J. Org. Chem.* **55**(2), 639–647 (1990).

⁸¹J.F. Cameron, N. Chan, K. Moore, and G. Pohlert, "Comparison of acid generating efficiencies in 248 nm and 193 nm photoresists," *Proc. SPIE* **4345**, 106–118 (2001).

⁸²R.L. Brainard, G.G. Barclay, E.H. Anderson, and L.E. Ocola, "Resists for next generation lithography," *Microelectron. Eng.* **61–62**, 707–715 (2002).

⁸³This account is given by the late Prof. T. Madey of Rutgers, The State University of New Jersey, Private Communication (2007), before his untimely death in 2008.

⁸⁴T. Madey, Rutgers University, Private Communication (2007).

⁸⁵L.E. Ocola, "Electron matter interactions in x ray and electron lithography," Ph.D. Thesis, University of Wisconsin Madison (1996); G. Han, M. Khan, Y. Fang, and F. Cerrina, "Comprehensive model of electron energy deposition," *J. Vac. Sci. Technol. B* **20**(6), 2666–2671 (2002); G. Han, M. Khan, Y. Fang, and F. Cerrina, "Stochastic modeling of high energy lithographies," *J. Vac. Sci. Technol. B* **21**(6), 3166–3171 (2003).

As these photoelectrons move away from the site where they were created, along their tracks they can create excited atoms and molecules, radicals, ions, and secondary electrons. Since at ~ 80 eV energy losses by these photoelectrons are due mainly to ionization, secondary electrons are created in large quantities and carry most of the energy of the former. Regardless of the primary photon energy, secondary electrons in many materials have a low energy distribution with a most probable energy below ~ 10 eV,⁸⁶ as shown in Fig. 8.4.⁸⁷ At these energies, thermalization distances of electrons is on the order of 1–10 nm,⁸⁸ which defines the volumes of subsequent reactions (and effectively the resolution of the resist). In addition, more energetic secondary electrons can continue to ionize the medium, leading to a large total population of low-energy electrons (LEEs). These LEEs can produce a further generation of excited atomic, molecular, and

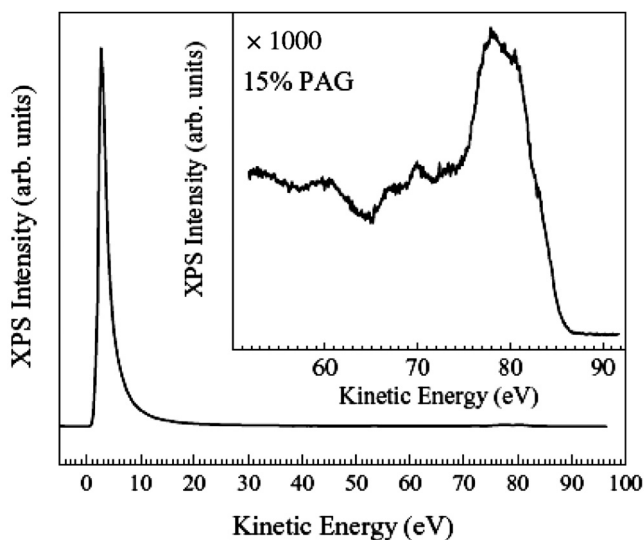


Figure 8.4 Photoinduced electron energy distribution curve for an EUV resist with 15% photoacid generator concentration, showing both the low-energy region and an inset of the blowup of the valence band region for a photon energy of 92 eV. (Courtesy of T. Madey.)

⁸⁶International Commission on Radiation Units and Measurements, ICRU Report No. 31, Washington, DC (1979); S.M. Pimblott and J.A. La Verne, "Production of low energy electrons by ionizing radiation," *Rad. Phys. Chem.* **76**, 1244 (2007).

⁸⁷The majority of the electrons emitted under EUV irradiation have low energies, < 10 eV. The inset in this figure shows a peak at ~ 80 eV in electron emission, which is probably due to photoelectrons emitted directly from the discrete absorption of EUV photons. The large peak in the secondary electron spectrum is due to the low energy secondary electrons, which are created by the photoelectrons that did not escape the surface immediately, in a process as described above.

⁸⁸V. Cobut, Y. Frongillo, J.P. Pataut, T. Goulet, M.J. Fraser, and J.P. Jay Gerin, "Monte Carlo simulation of fast electron and proton tracks in liquid water: I. physical and physicochemical aspects," *Radiat. Phys. Chem.* **51**, 229 (1998).

radical species and ions, which can induce nonthermal reactions within the femto-second time frame. In other words, the majority of reactive species that initiate chemical reaction are created by low-energy secondary electrons.⁸⁹

It has also been established that low-energy secondary electrons, i.e., electrons with kinetic energies in the range 0–15 eV, can effectively induce dissociation of organic molecules due to the high-dissociation cross sections.⁹⁰ The main process at play here is called dissociative electron attachment (DEA), and is especially effective for molecules containing fluorine atoms, such as photoacid generators, a major constituent of chemically amplified resists.⁹¹ Thus, in the final analysis, it is these low-energy secondary electrons that largely mediate the exposure of EUV resists, since they are directly involved either in the polarity-switching reactions (such as deprotection, rearrangement, depolymerization, etc.) or cross-linking reactions on which EUV positive-tone and negative-tone imaging, respectively, are based.

Experimental verification of the mechanism for EUV resist exposure has been largely provided by Madey and co-workers⁹² and Tagawa and co-workers.⁹³ Although described here for EUV exposures, the same processes are also at play in lithographies utilizing high-energy radiation and particles such as x rays on the one hand, and electron beams and ion beams on the other hand.

⁸⁹T. Madey, Rutgers University, Private Communication (2007).

⁹⁰M.N. Hedhili, P. Cloutier, A.D. Bass, T.E. Made, and L. Sanche, "Electron stimulated desorption of anionic fragments from films of pure and electron irradiated thiophene," *J. Chem. Phys.* **125**, 95704 (2006).

⁹¹T. Madey, Rutgers University, Private Communication (2007).

⁹²B.V. Yakshinskiy, R. Wasielewski, E. Loginova, and T.E. Madey, "Carbon accumulation and mitigation processes, and secondary electron yields of ruthenium surfaces," *Proc. SPIE* **6517**, 65172Z (2007); B.V. Yakshinskiy, R. Wasielewski, E. Loginova, M.N. Hedhili, and T.E. Madey, "DIET processes on ruthenium surfaces related to extreme ultraviolet lithography," *Surf. Sci.* **602**(20), 3220 (2008).

⁹³T. Kozawa and S. Tagawa, "Basic aspects of acid generation processes in chemically amplified resists for electron beam lithography," *Proc. SPIE* **5753**, 361–367 (2005); T. Kozawa and S. Tagawa, "Basic aspects of acid generation processes in chemically amplified resists for electron beam lithography," *J. Vac. Sci. Technol.* **18**(4), 471–474 (2005); S. Tagawa, S. Nagahara, T. Iwamoto, M. Akita, T. Kozawa, Y. Yamamoto, D. Werst, D.A. Trifunac, and D. Alexander, "Radiation and photochemistry of onium salts acid generators in chemically amplified resists," *Proc. SPIE* **3999**, 204–213 (2000); A. Nakano, K. Okamoto, Y. Yamamoto, T. Kozawa, S. Tagawa, T. Kai, H. Nemoto, and T. Shimokawa, "Deprotonation mechanism of poly(4 hydroxystyrene) and its derivatives," *Proc. SPIE* **5753**, 1034–1039 (2005); T. Kozawa, A. Saeki, and S. Tagawa, "Modeling and simulation of chemically amplified electron beam, x ray, and EUV resist processes," *J. Vac. Sci. Technol. B* **22**(6), 3522–3524 (2004); T. Kozawa, A. Saeki, A. Nakano, Y. Yoshida, and S. Tagawa, "Relation between spatial resolution and reaction mechanism of chemically amplified resists for electron beam lithography," *J. Vac. Sci. Technol. B* **21**(6), 3149–3152 (2003).

Chapter 9

Antireflection Coatings and Reflectivity Control

Between the idea
And the reality
Between the motion
And the act
Falls the shadow

T.S. Elliot, *The Hollow Men*

9.1 Introduction

As the exposure radiation propagates from the mask to the resist in the form of the aerial image, it encounters interfaces between the exposure medium (vacuum, air, or liquid in the case of immersion lithography) and the top resist surface, as well as between the bottom surface of the resist and the substrate. At each of the resist interfaces, transmission and reflection of the exposure radiation take place to varying degrees, depending largely on the absorbance of the resist. A major aspect of the image in the resist derives from the reflections off the substrate (or films coated on the substrate). The total energy in the resist is the sum of the downward-propagating image and the upward-propagating reflected image. The interference of these two images is dependent on the thickness of the resist, as well as that of other films above or below it. Two consequences of interference include standing waves (a sinusoidal variation of dose through the thickness of the resist) and swing curves (a sinusoidal dependence of the energy coupled into the resist as a function of the resist thickness).¹

¹Many excellent textbooks covering this subject have been written; see for example, C.A. Mack, *Fundamental Principles of Optical Lithography: The Science of Microfabrication*, John Wiley & Sons, Hoboken, NJ (2007); H.J. Levinson, *Principles of Lithography*, 2nd ed., pp. 117–123, SPIE Press, Bellingham, WA (2005); B.W. Smith and M. Hanratty, “Resist processing,” in *Microlithography: Science and Technology*, J.R. Sheats and B.W. Smith, Eds., pp. 575–590, Marcel Dekker, New York (1998); R. Dammel, *Diazonaphthoquinone based Resists*, pp. 126–133, SPIE Press, Bellingham, WA (1993).

Both standing waves and swing curve effects pose significant problems that negatively impact critical dimension control and significantly degrade depth of focus and exposure latitude. These problems are particularly acute in lithographic regimes where the resolution targets are significantly smaller than the wavelength of the exposure radiation, requiring tight critical dimension control. They are also acute for high-contrast resists.

Materials that suppress reflectivity from the substrate—otherwise called anti-reflection coatings²—were developed to mitigate these problems, in particular, swing curve effects (see the section on antireflection coatings below). In addition, these materials can help to reduce the effects of topographical variations; they also help to improve postexposure delay stability, and can help to mitigate missing contact problems, as well as scumming.

Furthermore, the adoption of optical proximity correction (OPC) across several layers, starting in the 180-nm technology node, greatly accelerated the adoption of antireflection coatings because OPC programs do not account for substrate reflectivity; it is implicitly assumed in these programs that substrate reflectivity is non-existent. Still further, pattern collapse due to capillary forces during solvent development becomes acute in the regime of subwavelength resolution lithography. Often resulting from the loss of adhesion at the base of the feature on account of the high aspect ratio associated with features in these subwavelength lithographic regimes, these features literally tumble over. To mitigate this problem, antireflection coatings are therefore designed to have good adhesion to the resist; such antireflection coatings are interposed between the resist layer and the substrate.

Antireflection coatings can be applied at the resist-substrate interface, in which case they are called bottom antireflection coatings (BARCs), or they can be applied at the surface of the resist, in which case they are called top antireflection coatings. The effect of top antireflection coatings on the swing amplitude S of resist materials is fairly well described by Brunner's formula:³

$$S = \sqrt[4]{R_b R_t} e^{-\alpha d}, \quad (9.1)$$

where R_b is the reflectivity at the resist-substrate interface (often reduced by BARCs), R_t is the reflectivity at the resist-air interface (often reduced by top antireflection coatings), α is the absorbance of the resist, and d is the resist thickness.

Bottom antireflection coatings, particularly organic ones, are used in many different applications, including reflectivity control (at both the first and second reflectivity minima, i.e., the first two lowest locations on the swing curve where reflectivity is insensitive to BARCs' thickness, in other words, the two lowest locations where the rate of change of BARCs' reflectivity with thickness is essentially zero) on highly reflective substrates such as silicon and aluminum; they also reduce swing curve and reflective notching, and standing waves. They

²Antireflection coatings were first invented for lenses in 1935 by Alexander Smakula (1900–1983) at Carl Zeiss Optics Company. They were a German military secret during the early stages of World War II.

³T.A. Brunner, "Optimization of optical properties of resist processes," *Proc. SPIE* **1466**, 297–308 (1991).

are also used as a conformal and planarizing layer, and in via-filling applications. Their surfaces can be adjusted to be compatible with a wide range of materials.

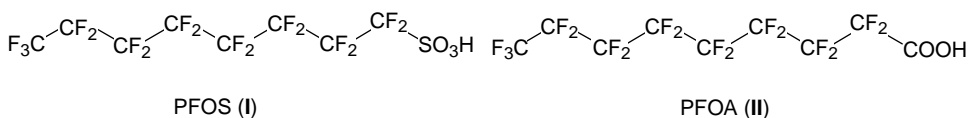
The performance metrics used to judge the quality of a given antireflection coating include optical parameters (n and k), plasma etch rate, coating properties (whether highly planarizing or somewhat conformal), reflectivity, thickness, and compatibility with the given resist to which it is paired.

Most antireflection coatings are organic polymers that are highly absorbing or contain highly absorbing dyes. They may be either wet developed or developer insoluble. In the first case, intermixing and undercut of resist lines (if the coating is more soluble than the resist) are typical problems observed. In the second case, the antireflection coating, often hard-baked, dye-loaded novolac, may not be removed in the developer, but instead be removed in the descum step or during dry etching. This technique, although quite effective, may result in loss of line width and resist thickness unless the etch rate of the antireflection coating is substantially higher than that of the novolac resist.⁴

9.2 Antireflection Coating Strategies

9.2.1 Top antireflection coatings

Top antireflection coatings were first proposed by Tanaka and co-workers at Hitachi in 1990.⁵ Top antireflection coatings are typically made of perfluorinated compounds such as perfluoroalkanoic acids or PFAA, in particular, perfluorooctanoic acid or PFOA (**II**), and perfluoroalkanesulfonic acids or PFAS, in particular, perfluorooctane sulfonic acid or PFOS⁶ (**I**).



⁴R. Dammel, *Diazonaphthoquinone based Resists*, pp. 127–130, SPIE Press, Bellingham, WA (1993).

⁵T. Tanaka, N. Hasegawa, and S. Okazaki, "A new photolithography technique with antireflective coating on resist: ARCOR," *J. Electrochem. Soc.* **137**, 3900 (1990).

⁶PFOS has been determined by the U.S. Environmental Protection Agency and other environmental regulatory agencies in many other countries and non governmental organizations to be biopersistent, bioaccumulating, and toxic to animals. [See, for example, "Hazard assessment of perfluorooctane sulfonate (PFOS) and its salts," Organization for Economic Co operation and Development (2002); S. Taniyasi, K. Kannan, Y. Horii, and N. Yamahita, "The environmental survey of perfluorooctane sulfonate (PFOS) and related compounds in Japan," presented at Dioxin 2002, Barcelona, Spain, Aug. 11–16, 2002; S. Taniyis et al., "A survey of perfluorooctane sulfonate and related perfluorinated organic compounds in water, fish, birds, and humans from Japan," *Environ. Sci. Technol.* **37**(12), 2634–2639 (2003); R. Bossi et al., "Preliminary screening of perfluorooctane sulfonate (PFOS) and other fluorochemicals in fish, birds, and marine mammals from Greenland and the Faroe Islands," *Environ. Pollut.* **136**(2), 323–329 (2005); G. Olsen et al., "Perfluorooctane sulfonate and other fluorochemicals in the serum of American Red Cross adult blood donors," *Environ. Health Perspect.* **111**(16) (2003).] It is therefore currently being regulated by the EPA with a significant new

Some are made of polyfluoroalkylethers⁷ and Teflon-based materials.⁸ They are used to reduce swing curve effects and have been reported to improve the signal-to-noise ratio and shape of some stepper alignment signals.⁹ The earlier generation of top antireflection coatings were designed to be coated from organic solvents that do not attack the resist layer and must be removed before development since they are not aqueous-base soluble. Thus, this additional process step necessary to remove them represents one of the drawbacks of using organic solvent-based top antireflection coatings. In principle, chlorofluorocarbons (CFCs) may be used for both purposes, since they do not attack the resist.¹⁰

The first-generation 248-nm and 193-nm lithographic top antireflection coatings used perfluorooctyl sulfonate (PFOS) compounds, which have been determined to be toxic and persistent in the environment. Recently introduced top antireflection coatings are PFOS-free and are environmentally friendly.

Top antireflection coatings serve multiple functions: reflectivity control (Fig. 9.1), defectivity control (although they can also be a source of defects), across-wafer line width variation control, improvement of process latitude (Fig. 9.2),¹¹ and postexposure delay stability (Fig. 9.3).

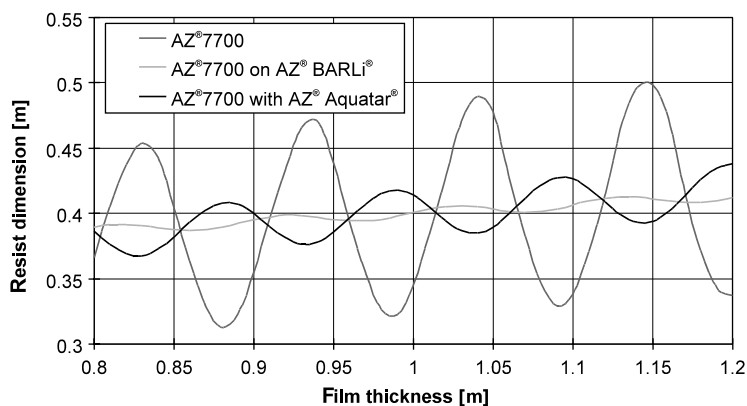


Figure 9.1 PROLITH/2 simulations showing the effects of top antireflection coating (AZ® Aquatar®) and BARC (AZ® BARLi®) on the swing curve of AZ®7700 resist on silicon wafer. (Courtesy of R. Dammel.)

use rule (SNUR). Lower molecular weight homologs of PFAS do not pose any environmental hazard and therefore are not being regulated.

⁷T. Tanaka, N. Hasegawa, H. Shiraishi, and S. Okazaki, in *Proc. SPIE. Reg. Tech. Conf. Photopolym.*, Ellenville, NY, pp. 195–203 (1991).

⁸T.A. Brunner, “Optimization of optical properties of resist processes,” *Proc. SPIE* **1466**, 297–308 (1991).

⁹T. Tanaka, N. Hasegawa, H. Shiraishi, and S. Okazaki, in *Proc. SPIE. Reg. Tech. Conf. Photopolym.*, Ellenville, NY, pp. 195–203 (1991).

¹⁰In spite of this quality, CFCs cannot be used as solvents for antireflection coatings because they are now banned due to their role in the depletion of the ozone layer.

¹¹M. Gehm, P. Jaenen, V. van Driessche, A.M. Goethals, N. Samarakone, L. Van den Hove, and B. Denturck, “Evaluation of methods to reduce linewidth variation due to topography for i line and deep UV lithography,” *Proc. SPIE* **1674**, 681 (1992).

The 1990s saw the introduction of commercial water-based top antireflection coating materials that do not require a solvent treatment but are removed during normal resist development in 0.26 N aqueous tetramethyl ammonium hydroxide developer solution¹² or simply dissolved with a water rinse. Specifically, they were introduced at 248-nm wavelength (KrF) lithography, with the first chemically

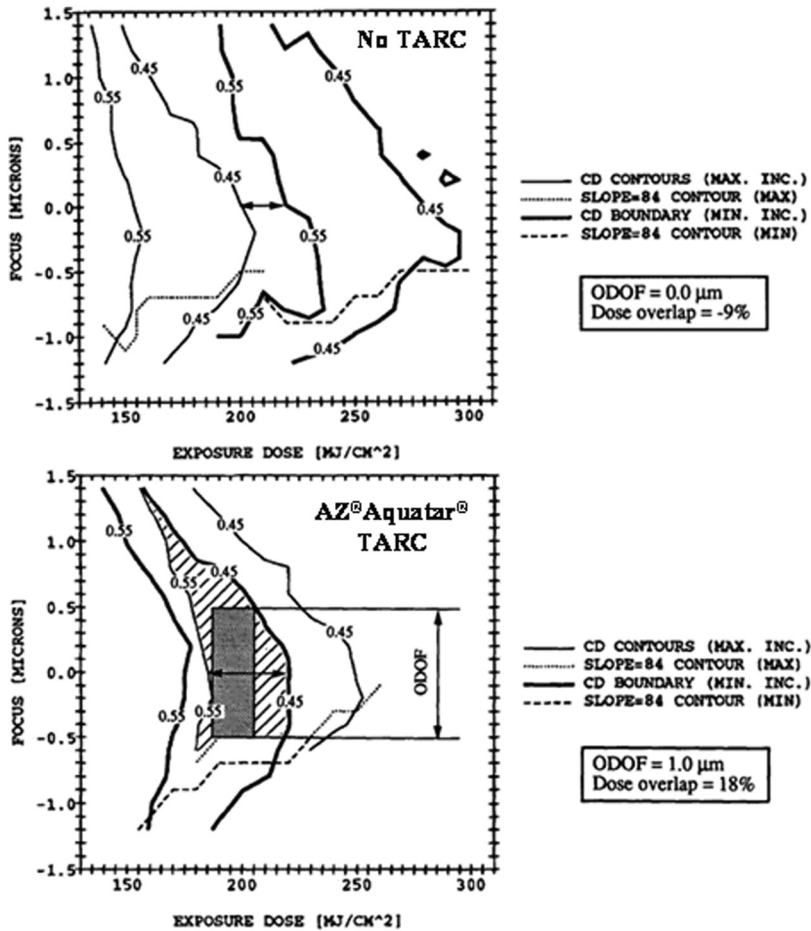


Figure 9.2 Process latitude (in terms of overlap depth of focus for 0.5- μm lines patterned with i-line lithography) of UCB-JSR 1 \times 500 resist with and without AZ[®] Aquatar[®] top antireflection coatings. Shown are the contour plots for the 0.5- μm line as a function of focus and exposure dose.¹³

¹²C.F. Lyons, R.K. Leidy, and G.B. Smith, "Practicing the top antireflector process," *Proc. SPIE* **1674**, 523 (1992); M. Gehm, P. Jaenen, V. van Driessche, A.M. Goethals, N. Samarakone, L. Van den Hove, and B. Denturck, "Evaluation of methods to reduce linewidth variation due to topography for i line and deep UV lithography," *Proc. SPIE* **1674**, 681 (1992).

¹³M. Gehm, P. Jaenen, V. van Driessche, A.M. Goethals, N. Samarakone, L. Van den Hove, and B. Denturck, "Evaluation of methods to reduce linewidth variation due to topography for i line and deep UV lithography," *Proc. SPIE* **1674**, 681 (1992).

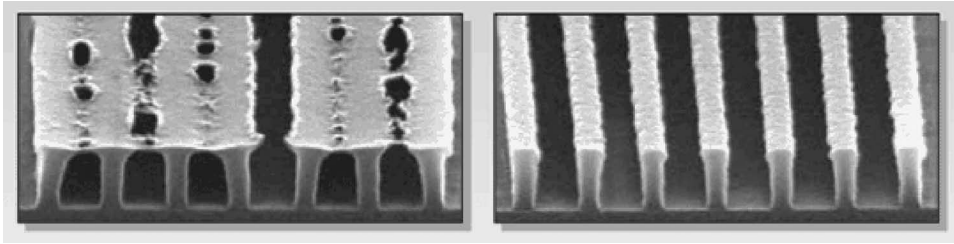


Figure 9.3 Top AR coatings improve postexposure delay stability (shown) and CD control. (Courtesy of M. Slezak.)

amplified resists. Delay time between the photoresist coating step and the exposure step is critical to CD control, and any airborne molecular base (ammonia, N-methyl pyrrolidone, etc.) within the exposure environment poses a contamination risk. Being on the surface of the resist, top antireflection coatings form a protective barrier to the transport of airborne molecular bases into the resist, where they may neutralize photoacids in the underlying chemical amplification resist (see Fig. 9.3).

9.2.2 Theory of top antireflection coatings

Absorptivity and reflectivity¹⁴ in materials can be fairly well characterized by the complex refractive index of the material in question, which is defined as

$$\tilde{n} = n - ik, \quad (9.2)$$

where the real part of the refractive index n is given by

$$n = \text{Re}(\tilde{n}), \quad (9.3)$$

and the imaginary part of the refractive index k is related to the absorbance of the material and it is given by

$$k = -\text{Im}(\tilde{n}) = \frac{\alpha\lambda}{4\pi}. \quad (9.4)$$

9.2.3 Reflection and transmission amplitudes

Consider a ray of light incident on a thin film of top antireflection coatings sandwiched between two semi-infinite media: air (or water) and the photoresist (Fig. 9.4). Assuming normal incidence, at the boundary between two media, say, medium 1 (air or water) and medium 2 (top antireflection coatings), the

¹⁴Excellent treatment of this subject can be found in, for example, M. Born and E. Wolf, *Principles of Optics*, 7th ed., pp. 43–70, Cambridge University Press, Cambridge (1999); E. Hecht, *Optics*, 2nd ed., pp. 94–104, Addison Wesley, Reading, MA (1990).

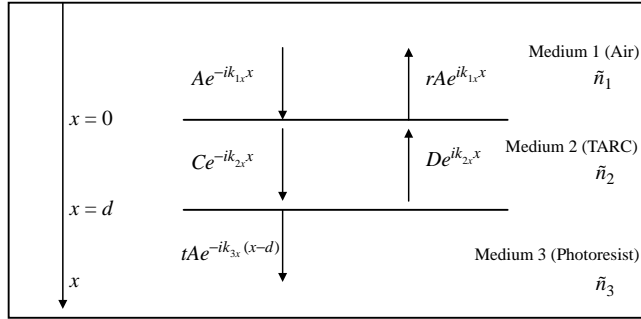


Figure 9.4 Schematic showing the transmission and reflectivity of light incident on a film stack of top antireflection coating (medium 2) coated on top of a photoresist film (medium 3) at normal incidence. The medium above the top antireflection coating is air (medium 1).

reflection (r_{12}) and transmission (t_{12}) coefficients are given by the Fresnel equations:

$$r_{12} = \frac{\tilde{n}_1 - \tilde{n}_2}{\tilde{n}_1 + \tilde{n}_2} = \frac{n_1 - n_2 - i(k_1 - k_2)}{n_1 + n_2 - i(k_1 + k_2)}, \quad (9.5)$$

$$t_{12} = \frac{2\tilde{n}_2}{\tilde{n}_1 + \tilde{n}_2} = \frac{2(n_2 - ik_2)}{n_1 + n_2 - i(k_1 + k_2)}. \quad (9.6)$$

Reflectivity R is given by

$$\begin{aligned} R &= rr^* = r_{12}r_{12}^* \\ &= \frac{n_1 - n_2 + i(k_1 - k_2)}{n_1 + n_2 + i(k_1 + k_2)} \cdot \frac{n_1 - n_2 - i(k_1 - k_2)}{n_1 + n_2 - i(k_1 + k_2)} = \frac{(n_1 - n_2)^2 + (k_1 - k_2)^2}{(n_1 + n_2)^2 + (k_1 + k_2)^2}. \end{aligned} \quad (9.7)$$

The reflection and transmission amplitudes A , C , and D can be derived from the condition that the electric field vector be continuous at the boundaries of the three media. It then follows that

$$C = t_{12}A + r_{21}D, \quad (9.8)$$

$$r_A = r_{12}A + t_{12}D, \quad (9.9)$$

$$t_A = t_{23}C \exp\left(-2\pi \frac{\tilde{n}_2 d}{\lambda}\right), \quad (9.10)$$

$$D \exp\left(2\pi \frac{\tilde{n}_2 d}{\lambda}\right) = r_{23}C \exp\left(-2\pi \frac{\tilde{n}_2 d}{\lambda}\right). \quad (9.11)$$

Eliminating the constants A , C , and D yields the Airy formulae for the reflectance and transmission amplitudes:¹⁵

$$r = r_{12} + \frac{t_{12}t_{21}r_{23}\tau_D^2}{1 + r_{12}r_{23}\tau_D^2} = \frac{r_{12} + r_{23}\tau_D^2}{1 + r_{12}r_{23}\tau_D^2}, \quad (9.12)$$

$$t = \frac{t_{12}t_{23}\tau_D}{1 + r_{12}r_{23}\tau_D^2}, \quad (9.13)$$

where

$$\tau_D = \exp(-i\phi) = \exp\left(-i\frac{2\pi\tilde{n}_2}{\lambda}d\right). \quad (9.14)$$

For the limiting case in which all the layers are transparent and nonabsorbing ($k = 0$), all refractive indices are real numbers, such that reflectivity is given by

$$R = r^2 = \frac{R_{12} + R_{23} + 2r_{12}r_{23} \cos(2\phi)}{1 + R_{12} + R_{23} + 2r_{12}r_{23} \cos(2\phi)}, \quad (9.15)$$

where

$$R_{ij} = r_{ij}^2. \quad (9.16)$$

To determine the conditions in which the reflectivity at the resist-air interface is zero, we must determine the extremal locations on the reflectivity curve, using the methods of differential calculus. R is an extremum if

$$\frac{dR}{d\phi} = \frac{2r_{12}r_{23}(R_{12} - 1)(R_{23} - 1) \sin(2\phi)}{[1 + R_{12}R_{23} + r_{12}r_{23} \cos(2\phi)]^2} = 0 \quad (\text{if } \sin(2\phi) = 0). \quad (9.17)$$

R is an extremum if $2\phi = m\pi$, which occurs when

$$d = \frac{m\lambda}{4n_2}. \quad (9.18)$$

Equation (9.18) is the phase match condition for zero reflectivity at the resist-air interface, and its significance lies in the fact that it encapsulates within it the optimal thickness of the top antireflection coating that is associated with the least reflectivity at the resist-air interface.

¹⁵G.B. Airy, "Remarks on Mr. Potter's experiment on interference," *Phil. Mag.* **2**, 20 (1833).

To determine whether the extremum is a minimum or a maximum, we take the second derivative of R with respect to ϕ :

$$\frac{d^2 R}{d\phi^2} \left(d = \frac{m\lambda}{4n_2} \right) = - \frac{4(-1)^m (r_{12}r_{23})(R_{12} - 1)(R_{23} - 1)}{[1 + (R_{12}R_{23})(-1)^m r_{12}r_{23}]^2} \quad (9.19)$$

$$= \frac{(-1)^{m+1} (n_1 - n_2)(n_2 - n_3) 64n_1(n_1 + n_2)(n_2 + n_3)}{\{(n_1 - n_2)(n_2 - n_3)(n_1 + n_2)(n_2 + n_3) + 2[4n_1n_2^2n_3 + (n_1^2 + n_2^2)(n_2^2 + n_3^2)]\}^2}. \quad (9.20)$$

R is a maximum if $(-1)^m (n_1 - n_2)(n_2 - n_3) > 0$ and a minimum if $(-1)^m (n_1 - n_2)(n_2 - n_3) < 0$. If m is odd, implying that $\tau_D^2 = \cos(2\phi) = -1$, then for normal incidence illumination, we obtain

$$R = \left(\frac{r_{12} - r_{23}}{1 - r_{12}r_{23}} \right)^2 = \left(\frac{n_1n_3 - n_2^2}{n_1n_3 + n_2^2} \right)^2. \quad (9.21)$$

The condition in which $R = 0$ occurs when the refractive index of the middle medium (top antireflection coating) is a geometric mean of the two outside media, provided $n_1 < n_2 < n_3$. In other words,

$$n_2 = \sqrt{n_1n_3} = \sqrt{n_3} \quad (n_1 = 1 \text{ for air}). \quad (9.22)$$

Equation (9.22) is the intensity match condition for the reflectance at the resist-air interface to be zero, and its significance lies in the fact that it encapsulates within it the optimal refractive index of the top antireflection coating that is associated with the least reflectivity at the resist-air interface.

Top antireflection coatings are typically coated very thin, in the range of a few tens of nanometers, over the resist. The optimum refractive index for top antireflection coating depends on the refractive index of the resist in the following manner:¹⁶

$$opt\ n_{\text{TARC}} = \sqrt{n_{\text{resist}}n_{\text{air}}} = \sqrt{n_{\text{resist}}} \quad (\text{for lithography in air}), \quad (9.22a)$$

$$opt\ n_{\text{TARC}} = \sqrt{n_{\text{resist}}n_{\text{water}}} = \sqrt{n_{\text{resist}}} \quad (\text{for lithography in water}). \quad (9.22b)$$

If m is even, implying that $\cos(2\phi) = 1$, then for normal incidence illumination,

$$R = \left(\frac{r_{12} + r_{23}}{1 + r_{12}r_{23}} \right)^2 = \left(\frac{n_1 - n_3}{n_1 + n_3} \right)^2. \quad (9.23)$$

R is at a maximum and is independent of the refractive index of the middle medium (top antireflection coating) (n_2), for the case where $n_1 < n_2 < n_3$.

In summary, for the reflectivity to be zero, both the phase match and the intensity match conditions must be satisfied.

¹⁶R. Dammel, *Diazonaphthoquinone based Resists*, p. 132, SPIE Press, Bellingham, WA (1993).

9.3 Bottom Antireflection Coatings

There are two main types of BARCs: organic and inorganic BARCs.

9.3.1 Organic bottom antireflection coatings

9.3.1.1 Design approaches to organic bottom antireflection coatings

Two primary design approaches for organic BARCs comprise binding the chromophore to the backbone of the polymer or simply mixing monomeric dyes with the BARC polymeric resins (see Fig. 9.5). Because the BARC is thermally cross-linked when applied to the substrate, in its design, efforts are made to balance the density of cross-linkable sites with film dissolution and strippability after baking. Also, highly etchable comonomers are copolymerized with the BARC resin polymer to improve overall etch rate of 248-nm and 193-nm lithographic BARCs (Fig. 9.5). A common problem associated with dyes is sublimation during the bake step. This has prompted efforts to bind the dyes to the polymer backbone or the use of large monomeric dyes, all in order to prevent them from sublimating.

Aromatics make excellent BARC chromophores at 193-nm wavelength because of their significant extinction coefficient at 193 nm due to the π - π^* transition. So, designing BARCs that work at both the first and second minima on silicon substrates does not present a great challenge. In contrast, aromatics do not have a very strong absorption at 248-nm wavelength, which makes it difficult to design a 248-nm wavelength aromatic BARC that is able to work at the first minimum. At 365-nm wavelength, aromatics are even less absorptive than at 248 nm; this makes it nearly impossible to design a 365-nm aromatic BARC that can work at the first reflective minimum on a silicon substrate.

The aromatics used in organic BARCs designed for 193-nm and 248-nm lithographies contain dyes that are typically multibenzoid aromatics based on anthracene (**III**) and monobenzoid aromatics based on benzene (**IV**). Structures (**V**) and (**VI**), respectively, show the 248-nm and 193-nm polymeric BARC design antireflection coating architectures. Typical examples of monomeric dyes are shown in (**VII**), along with their maximum absorption wavelength. The structures shown in

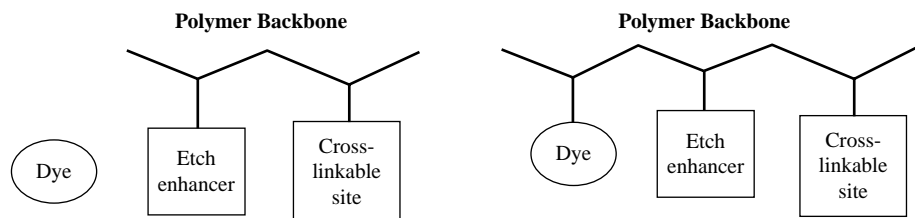
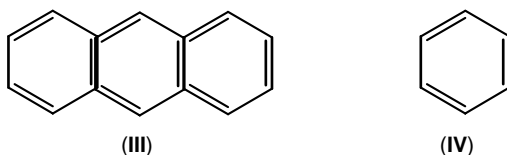
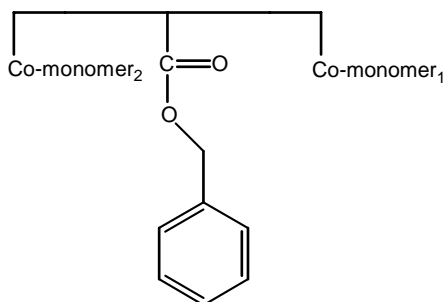


Figure 9.5 Two primary design approaches for organic BARCs.

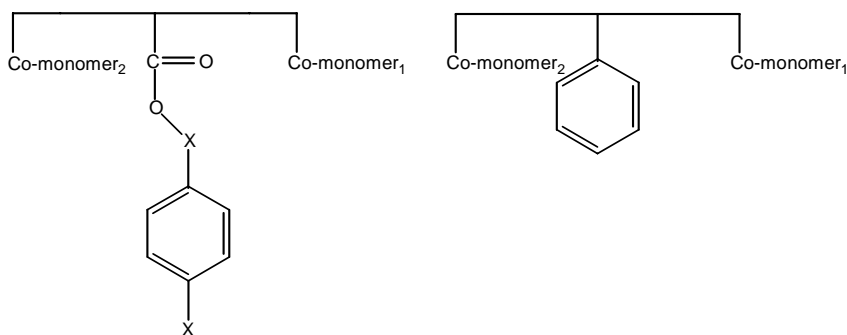
(VIII) are typical BARCs with polymer-bound dyes that are polymeric at spin-on, while Scheme 9.1 shows typical BARCs with polymer-bound dyes that are polymerized on the wafer. Dyed organosilicon glasses containing monobenzoid aromatics are also at times used as BARCs. They are highly planarizing with a slightly acidic surface, and are used mainly for dual damascene processes, specifically in “via-first” approaches, which benefit from the planarizing properties of this BARC.



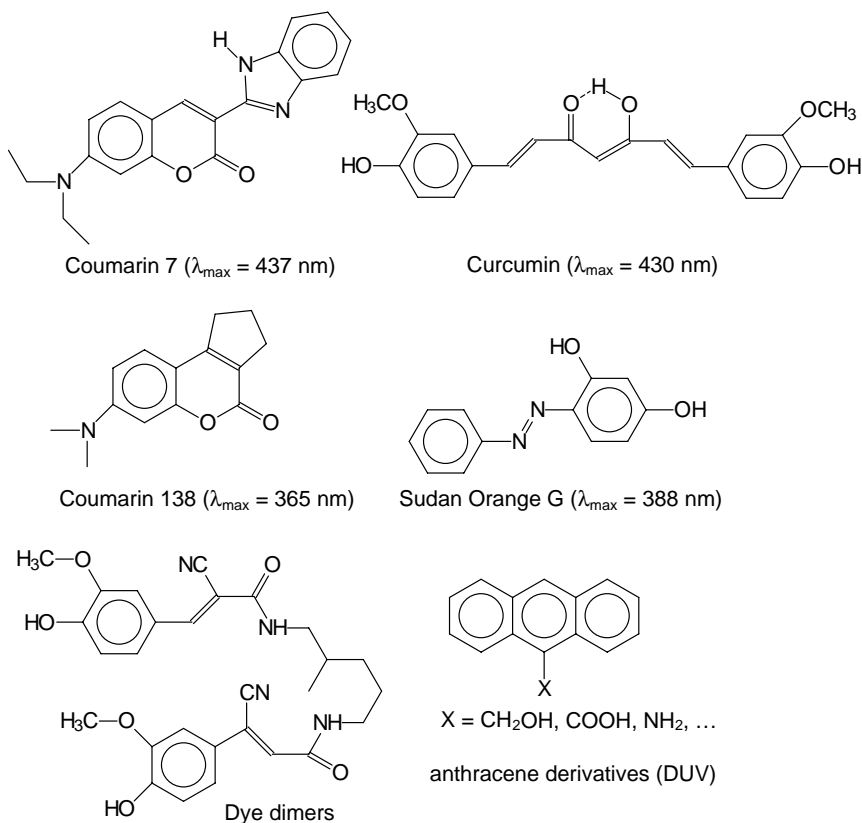
Chromophores for 248-nm (III) and 193-nm (IV) BARCs.



248-nm polymeric BARC
design antireflection coating architecture (V)



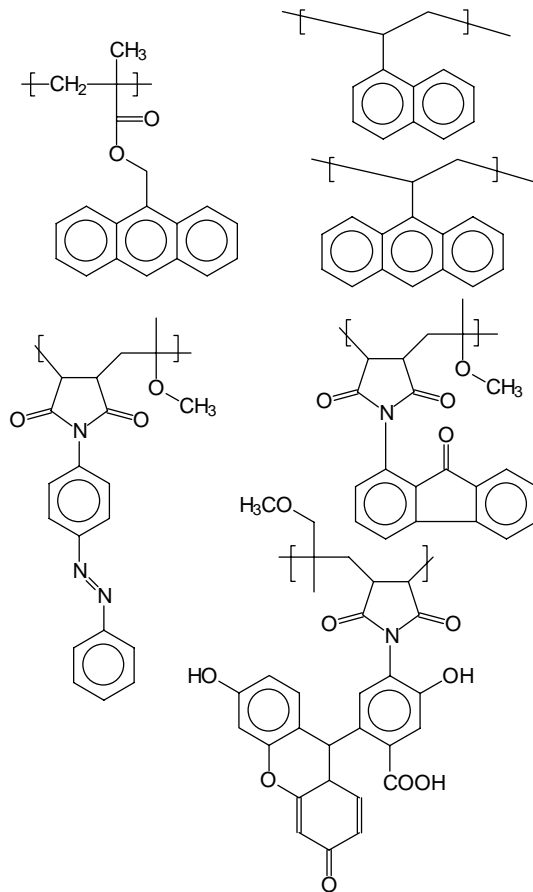
193-nm polymeric BARC
design antireflection coating architecture (VI)



Typical monomeric dyes (VII). (After R. Dammel.¹⁷)

Another approach in BARC design that is gaining in currency, particularly in recent times (although one of the earliest organic BARCs from Brewer Science was based on this principle as well), is to make the BARC developer soluble so that it can be removed during the development stage of the resist processing. These developer-soluble BARCs are used mainly at implant layers, where reactive-ion etching frequently cannot be used because of the possibility of device damage, and also because of cost considerations. The wet development, however, must be stopped at exactly the right moment to avoid footing or undercutting. This is typically accomplished by the use of a photosensitive BARC that is highly soluble in the exposed area, but insoluble in the unexposed area, resulting in a match between the resist and developer-soluble BARC, and producing a straight BARC wall.

¹⁷R. Dammel, "Anti reflection coatings: theory and practice," SPIE Short Course No. SC118 (2005).

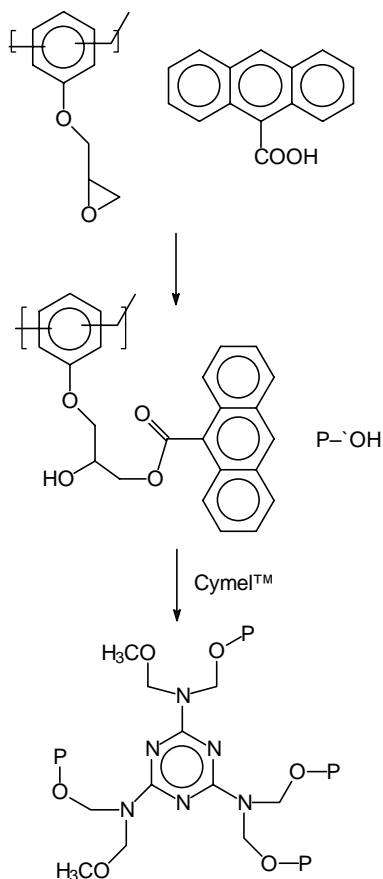


Bottom antireflection coatings with polymer-bound dyes that are polymeric at spin-on (VIII). (After R. Dammel.¹⁸)

9.3.2 Inorganic bottom antireflection coatings

Inorganic BARCs are thin inorganic sputtered layers, which, as opposed to their organic counterparts, may in some cases be left in the finished device or be removed during etch steps. Typical inorganic BARCs include silicon oxynitride, amorphous carbon, tantalum silicide, titanium nitride, etc. The type of inorganic BARC used depends on the nature of the reflecting substrate. The inorganic antireflection coatings such as SiON are intrinsically absorbing, with n and k values in the range of $n \approx 2.0$, $k \approx 0.5\text{--}2.0$ at 248-nm and 193-nm wavelengths. Only the first reflectivity minimum is possible with these antireflection coatings. They are highly conformal and can be prone to poisoning, necessitating the use of ashing or plasma treatment to cap the surface of the silicon wafer substrate.

¹⁸ibid.



Scheme 9.1 Polymerization of BARCs with polymer-bound dyes on the wafer. (After R. Dammel.¹⁹)

Inorganic BARCs are typically deposited by chemical vapor deposition (CVD) techniques, which affords the possibility of tuning the refractive index n and the extinction coefficient k by adjustments of the film composition and thickness.

9.4 Applications of Bottom Antireflection Coatings

9.4.1 Suppression of standing waves and reflectivity effects

Almost every single-layer resist system designed for DUV 248-nm (KrF) and DUV 193-nm (ArF lithography)²⁰ needs some kind of antireflection coating to mitigate

¹⁹ibid.

²⁰U. Okoroanyanwu, H.J. Levinson, A.M. Goethals, and F. Van Roey, "Progress in 193 nm photo resists and related process technologies," in *OMM Interface'98 Proc.*, 1 (1998).

substrate reflectivity problems. Absent a good antireflection coating, interference of the reflected and the incident 193-nm radiation results in standing wave effects (see Figs. 9.6 and 9.7), distorting the uniformity of the radiation flux reaching different points in the photoresist layer. The resulting swing curve is thus a periodic of a lithographic parameter with resist thickness, with the period given by $\lambda/2n$ (λ is the exposure wavelength and n is the refractive index of the resist). Problems arising from this include CD swing and the thickness dependence of profile and resolution.²¹ The swing effect is dominated by the optical constants of the photoresist materials and substrate. Different points in the photoresist layer undergo different levels of photochemical transformation, which ultimately is manifested as line width fluctuation.

The swing contrast of the thin-film interference effects in photoresists at 193 nm is almost the same as that at 248 nm,²² which suggests that the influence of thin-film interference effects in photoresists on line width control in both lithographic regimes are similar. Two promising inorganic antireflection coatings that have been reported in the literature are based on SiO_xN_y and $\text{SiO}_x\text{N}_y\text{:H}$.²³

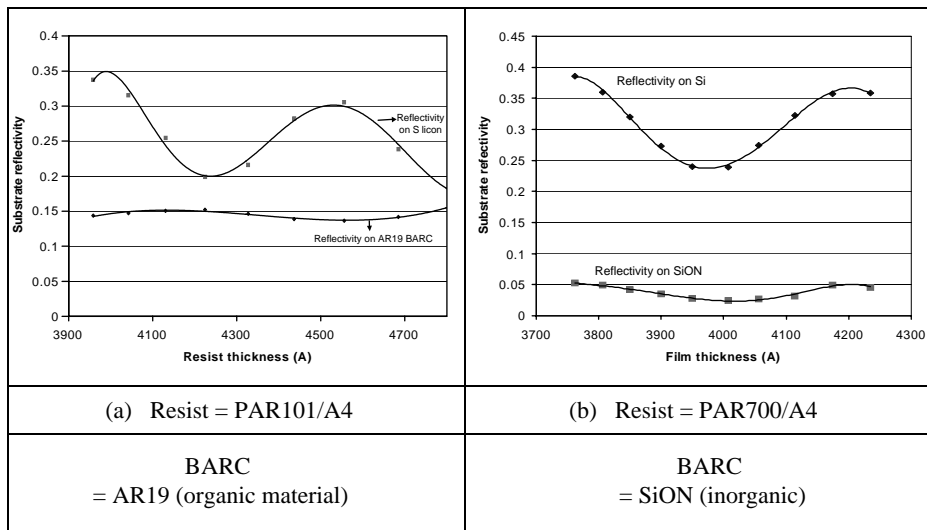


Figure 9.6 Substrate reflectivity as a function of thickness of (a) PAR101/A4 resist coated on AR19 BARC and (b) PAR700/A4 resist coated on silicon substrates. The dots represent the experimental points, and the solid lines represent polynomial fits.

²¹S. Hansen, R. Hurditch, and D. Brzowy, "Photoresist surface induction and its effect on swing behavior," *Proc. SPIE* **1925**, 626 (1985).

²²T. Ogawa, A. Sekiguchi, and N. Yoshizawa, "Advantages of a $\text{SiO}_x\text{N}_y\text{:H}$ anti reflective layer for ArF excimer laser lithography," *Jpn. J. Appl. Phys.* **35**, 6360 (1996); S. Kishimura, M. Takahashi, K. Nakazawa, T. Ohfuji, and M. Sasago, "ArF excimer laser lithography with bottom antireflective coating," *Proc. SPIE* **3334**, 310 (1998).

²³T. Ogawa, A. Sekiguchi, and N. Yoshizawa, "Advantages of a $\text{SiO}_x\text{N}_y\text{:H}$ anti reflective layer for ArF excimer laser lithography," *Jpn. J. Appl. Phys.* **35** 6360 (1996).

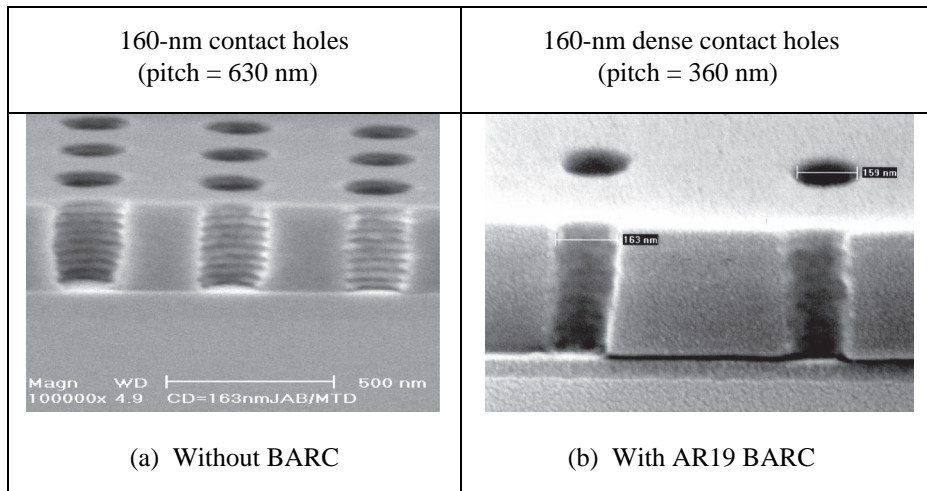


Figure 9.7 160-nm contact holes printed on 5000 Å of AX-655 resist with att-PSM. Pitch 630 nm. Dose 22 mJ/cm². Note the standing waves in (a) (without BARC) and no standing waves in (b) (with BARC).

Figure 9.6(a) shows the reflectivity swing oscillations with the thickness of a first-generation commercial 193-nm resist from Sumitomo Chemical, PAR101/A4 resist, coated on bare silicon and on an organic BARC from Shipley (AR19). Figure 9.6(b) shows the reflectivity swing oscillations with the thickness of PAR700/A4 resist (another early commercial 193-nm resist from Sumitomo Chemicals) on SiON-coated substrate. The significant swing amplitude in both figures constitutes a significant portion of the exposure latitude, particularly on highly reflective substrates such as Si. The AR19 antireflection coatings in Fig. 9.6(a) and the SiON antireflection coating in Fig. 9.6(b) both strongly suppress the thin-film interference relative to the silicon substrate.

Without BARCs, strong standing waves were obtained on the patterned resist sidewall [see Fig. 9.7(a)]. Applying AR19 BARC between the resist and the SiO₂ layer suppressed the standing waves [see Fig. 9.7(b)], resulting in a much smoother vertical sidewall of the contact holes.²⁴

Another application of BARCs, particularly for immersion and hyper-NA (NA > 1.0) lithography is the use of multiple layers in either a bilayer or trilayer configuration, with the top layer BARC having different optical properties from the bottom layer BARC, and so on and so forth. The configuration of the layers can be CVD hard mask (inorganic) BARC over an organic BARC or organic BARC over an organic BARC, etc. Figure 9.8 is a PROLITH (positive resist optical lithography) simulation showing the reflection contours for a dual-layer BARC at a scanner NA 1.35. This figure shows the capabilities of this BARC configuration in achieving a reflectivity of ~0.2%, which is a requirement for 45-nm node lithography.

²⁴U. Okoroanyanwu, H.J. Levinson, C. Y. Yang, S.K. Pangrle, J. Schefske, and E. Kent, "Integration considerations for 130 nm device patterning using ArF lithography," *Proc. SPIE* **4000**, 423 (2000).

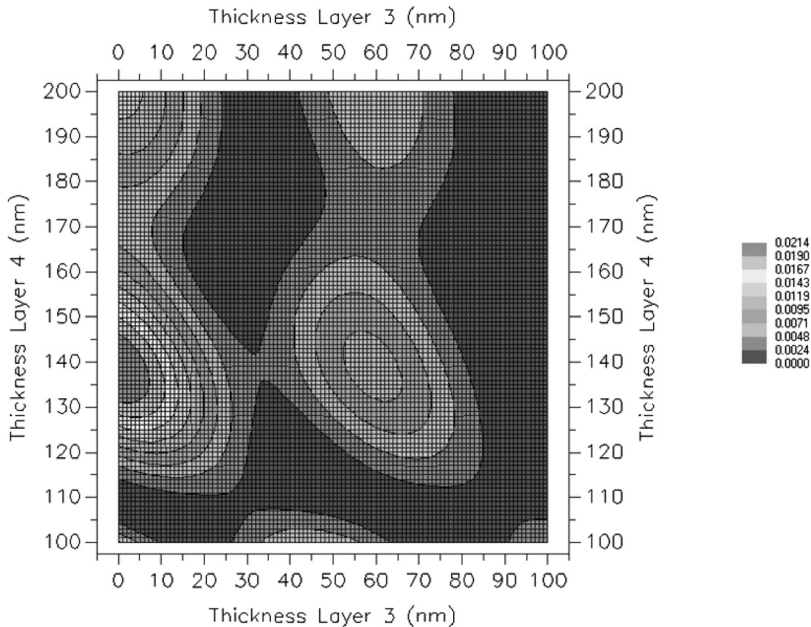


Figure 9.8 PROLITH simulation of reflectivity obtained on dual-layer BARC, comprising a top layer (layer 3) made of silicon-containing material and a bottom layer (layer 4) called ODL, all from Shinetsu Corporation. Exposure wavelength 193 nm, NA 1.35. (Courtesy of Ryoung-han Kim.)

One of the key challenges of hyper-NA imaging, it must be pointed out, concerns the very large range of angles of incidence from near vertical for a very large feature to 45 deg for an NA of 1.35 for a small feature. This is a scenario that makes it nearly impossible to sufficiently control reflectivity with a single-layer BARC for all of these different angles (see Fig. 9.9). One other approach for controlling reflectivity in hyper-NA systems is the use of a graded-index anti-reflection coating.

9.4.2 Feature CD trimming

Inorganic BARCs based on CVD hard masks can be used to trim the gate critical dimension and shrink the size of features such as contact holes after lithographic processing. Typically, in gate trimming, polysilicon is sometimes used as a hard mask, but then when the etch is completed, a hot phosphoric acid dip is used to strip the hard mask, which can attack the feature, causing CD erosion and loss of CD control. By replacing the poly hard mask with an amorphous carbon hard mask, all of the above problems are avoided, which allows one to trim the photoresist, and thus the final pattern, with larger process latitude than otherwise.²⁵

²⁵L. Peters, "How AR coatings stack up," *Semiconductor Int.* (2005).

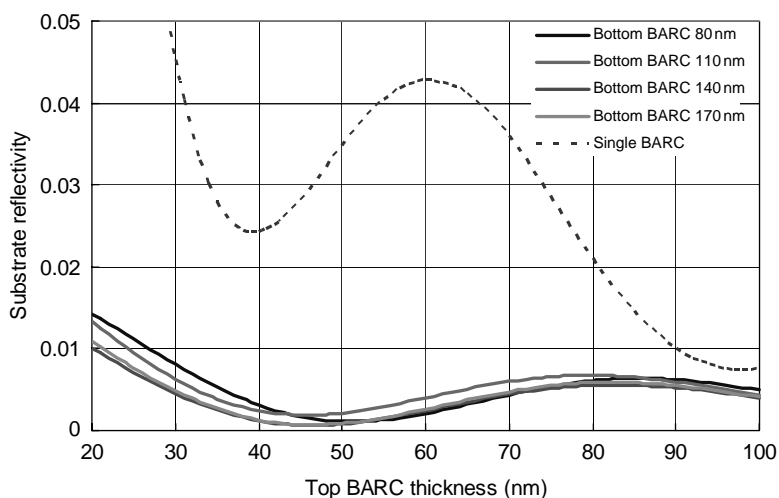


Figure 9.9 PROLITH simulation of reflectivity of single-layer BARC (ARC 29A from Brewer Science) and dual-layer BARC, comprising a top layer (SHB) with n 1.63, k 0.13 and a bottom layer (ODL) with n 1.5, k 0.3, both from Shinetsu. Exposure wavelength 193 nm. Target feature 50-nm lines per space at 100 nm pitch. Numerical aperture of exposure tool 1.35. (Courtesy of Ryoung-han Kim.)

The contact shrinking approach, pioneered at Applied Materials, Inc., involves a tapered hard mask scheme, in which the resist is first patterned over a hard mask, followed by a tapered hard mask etch rather than the conventional vertical etch. Depositing a dielectric CVD film at this stage over the tapered openings of the hard mask and subsequently doing an etch pattern transfer to the underlying amorphous carbon film affords a vertical etch pattern transfer with considerably smaller CD than the starting feature CD. This amorphous carbon CVD film has a similar composition to photoresist, but is able to withstand developer action during the development stage. Its greatest advantage lies in the fact that it can be readily removed after patterning, unlike SiON or SiOC masks, which must either stay in the device or be removed by hot phosphoric acid or other stripping methods.²⁶

There exist applications where the traditional hard mask can be left in place without any adverse effect on the performance of the device. For instance, in DRAM devices, SiON can be left on the gate layer, where it can serve as part of the self-aligning sequence of the storage cell and bit line contacts. It must be added, however, that amorphous carbon films do not require as much tuning as SiON films do.²⁷

²⁶ibid.

²⁷ibid.

The main drawback with CVD approaches has always been the need to move the wafers from the track to the CVD tool and back, with the attendant impact on throughput relative to all-track processing. But these drawbacks are offset by the inherent advantages of these films. Such advantages include the ease with which they can be reworked, as well as their good planarizing and conformal properties.²⁸

9.4.3 Damascene applications involving silicon-containing resists and silicon-containing hard mask materials with antireflection properties

The use of spin-on silicon-containing resists as well as silicon-containing hard mask materials is a new emerging reflectivity control strategy in the IC industry. These materials are designed to incorporate antireflection properties, effectively eliminating the need of an underlying antireflection coating, in a scheme that combines the traditional functions of hard mask and antireflection coating films into only one film. With these spin-on hard masks, the silicon content provides etch resistance, while distinct functional groups on the backbone of the polymer or pendant to the backbone provide antireflection properties.²⁹

The use of BARCs in dual damascene applications presents great challenges because of the high topography and transparent dielectrics used. Typically, during trench patterning in a via-first integration scheme, the via must be filled with a highly planarizing material. Low isolated/dense feature bias is very important, as is fast, efficient etching of this via fill material in order to reduce crowning or veiling defects. Two critical etch requirements for trench processing in this scheme include the ability to tune the dry etch rate of the material to that of the delicate dielectric, while protecting the via bottom, and while also ensuring that after etching, the material can be removed from the via without damaging the delicate dielectrics or leaving residues behind. Matching the etch rates of the Si-containing materials to that of the low-*k* dielectric is critical to yield because it eliminates problems such as shell defects and residue issues during etch, and pattern damage during cleaning of the vias; all of these problems can plague conventional materials.³⁰

The advantageous properties of these spin-on silicon-containing resists and hard mask materials with antireflection properties make these materials ideal candidates for dual damascene applications (see Fig. 9.10). They offer advantages over the conventional materials because they have better etch selectivity to the resists; they also tend not to suffer from the residue issues during etch and removal associated with conventional approaches. They now dominate in these applications, although spin-on carbon hard masks are emerging as worthwhile alternatives.³¹

²⁸ibid.

²⁹ibid.

³⁰ibid.

³¹ibid.

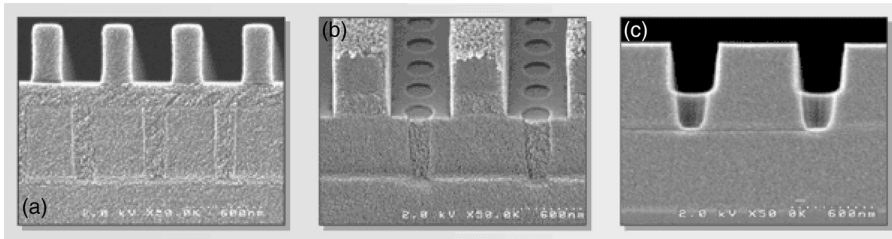


Figure 9.10 Via-first, trench-last patterning through a SiOCH low- k film using DUO248 AR coating, which is removed in one step using a commercially available wet chemistry. Shown is (a) pre-etch, (b) post-DUO248 open, and (c) post-resist and DUO coating strip. (Source: Honeywell Electronic Materials.)

One of the drawbacks of Si-containing resist and Si-containing hard mask materials is their propensity to outgas during exposure, which might lead to SiO₂ contamination of optical elements in the exposure tools. Silesquioxane-based materials appear not to suffer from this problem.

9.5 Organic versus Inorganic Bottom Antireflection Coating and Rework/Stripping Issues

One of the virtues of using organic BARCs is the ease with which they are coated and stripped after etch, in contrast to inorganic BARCs. A major shortcoming of the organic BARCs, however, is their considerable postetch CD bias in contrast to the inorganic ones. This poses a significant challenge in the optimization of BARC etch recipes and the eventual integration of organic BARCs in the manufacture of devices with extremely tight CD control requirements.

9.6 Bottom Antireflection Coating–Resist Interactions

Figure 9.11 shows the various BARC-resist interactions for specific BARC (BARC in the figure) types. Footing and notching are the two main interactions. While footing has both chemical and optical origins, notching is essentially optical in origin. Footing can result from the neutralization of photoacid by the nitrogen-containing bases in the BARC materials such as TiN and Si_xO_yN_z. Once neutralized, these photoacids are no longer available to participate in the imaging reactions of the resist, resulting in untransformed mass at the interface of the BARC and the resist feature.

When the footing has an optical origin, it is related to a phase jump of the reflected light at the interface between the BARC and the resist. The magnitude of the phase angle change depends on the film's optical constants and its thickness. The phase jump can result in a standing wave at the resist-BARC interface. A resist

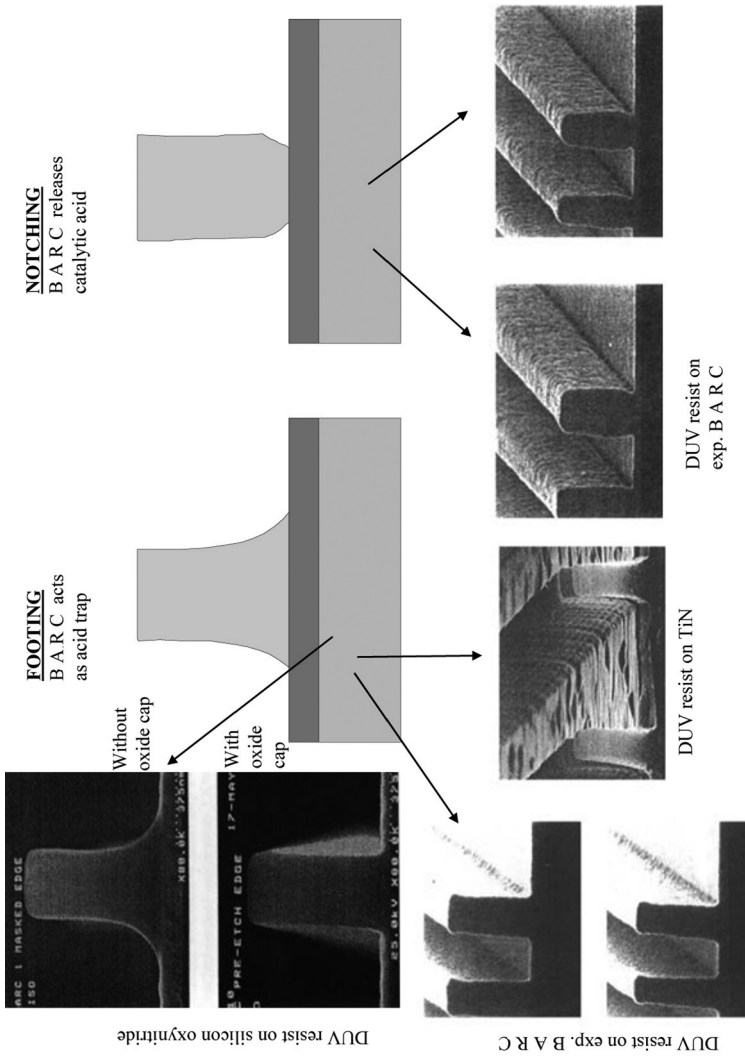


Figure 9.11 Bottom antireflection coating-resist interactions on different substrates: BARC, $\text{Si}_x\text{O}_y\text{N}_z$, TIN. (After R. Dammel.³²)

³²R. Dammel, "Anti-reflection coatings: theory and practice," SPIE Short Course No. SC118 (2005).

foot tends to form just before the reflectance minima. An undercut tends to form between the minima. Both the footing and notching effects tend to decrease with increasing BARC thickness.

9.7 Theory of Bottom Antireflection Coatings

9.7.1 Reflectivity of absorbing layers

Consider a ray of light incident on a thin absorbing film of BARC sandwiched between two semi-infinite media, namely, photoresist and the silicon wafer substrate (Fig. 9.12).

Using a similar approach as in the case of the top antireflection coating above, and assuming normal incidence at the boundary between two media, for instance medium 1 (photoresist) and medium 2 (BARC), the reflection (r_{12}) and transmission (t_{12}) coefficients are given by the Fresnel equations above [Eqs. (9.5) and (9.6)]. Multiplication of the reflection amplitude with its complex conjugate yields

$$R = r r^* = \frac{R_{12} + R_{23} e^{-2i(\phi - \phi^*)} + r_{12} r_{23}^* e^{2i\phi^*} + r_{12}^* r_{23} e^{-2i\phi}}{1 + R_{12} R_{23} e^{-2i(\phi - \phi^*)} + r_{12} r_{23}^* e^{2i\phi^*} + r_{12}^* r_{23} e^{-2i\phi}}$$

$$= \frac{R_{12} + R_{23} e^{-8\pi k_2 d / \lambda} + e^{-4\pi k_2 d / \lambda} [(r_{12} r_{23}^* + r_{12}^* r_{23}) \cos(4\pi n_2 d / \lambda) + i(r_{12} r_{23}^* - r_{12}^* r_{23}) \sin(4\pi n_2 d / \lambda)]}{1 + R_{12} R_{23} e^{-8\pi k_2 d / \lambda} + e^{-4\pi k_2 d / \lambda} [(r_{12} r_{23} + r_{12}^* r_{23}^*) \cos(4\pi n_2 d / \lambda) + i(r_{12} r_{23}^* - r_{12}^* r_{23}) \sin(4\pi n_2 d / \lambda)]} \quad (9.24)$$

Equation (9.24) can be simplified by the use of the following expressions for some of the terms:

$$C = r_{12} r_{23}^* + r_{12}^* r_{23}, \quad (9.25)$$

$$D = i(r_{12} r_{23}^* - r_{12}^* r_{23}), \quad (9.26)$$

$$G = r_{12} r_{23} + r_{12}^* r_{23}^*, \quad (9.27)$$

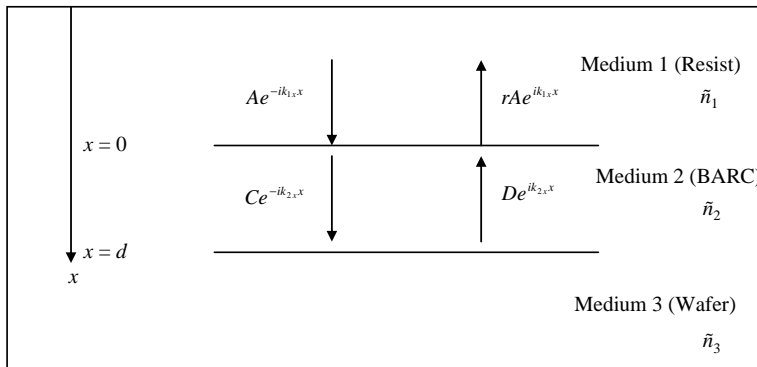


Figure 9.12 Schematic showing the transmission and reflectivity of light incident normally on a film stack of resist (medium 1) coated on top of a BARC film (medium 2), which in turn is coated on top of a silicon wafer substrate (medium 3).

$$H = i(r_{12}^* r_{23}^* - r_{12} r_{23}), \quad (9.28)$$

$$\alpha = \frac{4\pi k_2}{\lambda}, \quad (9.29)$$

$$\beta = \frac{4\pi n_2}{\lambda}. \quad (9.30)$$

Therefore, the reflectivity from the BARC layer is then conveniently expressed as

$$R = \frac{R_{12} + R_{23} e^{2\alpha d} + e^{\alpha d} (C \cos \beta d + D \sin \beta d)}{1 + R_{12} R_{23} e^{2\alpha d} + e^{\alpha d} (G \cos \beta d + H \sin \beta d)}. \quad (9.31)$$

For the limiting case of the infinitely thick layer 2 (photoresist),

$$\lim_{d \rightarrow \infty} R = R_{12}. \quad (9.32)$$

For the limiting case of the infinitely thin layer 2,

$$R(d \rightarrow 0) = \frac{R_{12} + R_{23} + C}{1 + R_{12} R_{23} + G} = \frac{(n_1 - n_3)^2 + (k_1 - k_3)^2}{(n_1 + n_3)^2 + (k_1 + k_3)^2} = R_{13}. \quad (9.33)$$

For the case in which all of the layers are nonabsorbing, $k_1 = k_2 = k_3 = 0$,

$$C_{\text{dielectric}} = G_{\text{dielectric}} = 2 \frac{n_1 - n_2}{n_1 + n_2} \cdot \frac{n_2 - n_3}{n_1 + n_3} = 2r_{12}r_{23}, \quad (9.34)$$

$$D_{\text{dielectric}} = H_{\text{dielectric}} = 0, \quad (9.35)$$

$$R \rightarrow \frac{R_{12} + R_{23}}{1 + R_{12} R_{23}}. \quad (9.36)$$

9.7.2 Electric field in photoresist films

The interference of the infinite series of reflections of an incoming ray in a thin film leads to the formation of standing waves. The electric field vector is then given by the sum of the rays as

$$\begin{aligned} E_s &= t_{12} E_0 e^{i(2\pi n_2 z/\lambda)} + t_{12} E_0 r_{23} \tau_D^2 e^{i(2\pi n_2 z/\lambda)} + t_{12} E_0 r_{23} r_{21} \tau_D^4 e^{i(2\pi n_2 z/\lambda)} \\ &\quad + t_{12} E_0 r_{23}^2 r_{21} \tau_D^6 e^{i(2\pi n_2 z/\lambda)} + t_{12} E_0 r_{23}^2 \tau_D^8 e^{i(2\pi n_2 z/\lambda)} + \dots \\ &= t_{12} E_0 [e^{i(2\pi n_2 z/\lambda)} + r_{23} \tau_D^2 e^{i(2\pi n_2 z/\lambda)}] \cdot (1 + r_{23} r_{12} \tau_D^2 (1 + r_{23} r_{21} \tau_D^2 (1 + r_{23} r_{21} \tau_D^2 \dots, \\ &= \frac{t_{12} E_0 [e^{i(2\pi n_2 z/\lambda)} + r_{23} \tau_D^2 e^{i(2\pi n_2 z/\lambda)}]}{1 - r_{23} r_{21} \tau_D^2} \\ &= \frac{t_{12} E_0 [e^{i(2\pi n_2 z/\lambda)} + r_{23} \tau_D^2 e^{i(2\pi n_2 z/\lambda)}]}{1 + r_{23} r_{12} \tau_D^2}, \end{aligned} \quad (9.37)$$

Table 9.1 Values of coefficients in the reflectivity equation for typical resist-BARC-silicon wafer substrate stack used at different lithographic wavelengths, where n_1 and k_1 are the optical constants for the resists; n_2 and k_2 are the optical constants for the coatings; and n_3 and k_3 are the optical constants for the silicon wafer substrate. (Source: R. Dammel.³³)

Wavelength	Opt. constants													
	n_1	k_1	n_2	k_2	n_3	k_3	R_{12}	R_{23}	α	β	C	D	G	H
435	1.690	0.025	1.833	0.150	4.850	0.192	0.002899	0.203309	4.3332	52.9520	0.036953	0.031501	0.039193	-0.028666
365	1.700	0.020	1.650	0.300	6.522	2.705	0.007144	0.389392	10.3285	56.8069	0.002605	0.105450	-0.019678	-0.103631
	1.700	0.020	1.650	0.600	6.522	2.705	0.029198	0.362493	20.6571	56.8069	0.024739	0.020427	0.015108	-0.205203
248	1.650	0.030	1.680	0.330	1.575	3.598	0.008103	0.410804	16.7214	85.1270	0.092598	0.068848	-0.057007	-0.100323
	1.650	0.030	1.680	0.600	1.575	3.598	0.028366	0.318908	30.4025	85.1270	0.152951	0.113092	-0.083593	-0.170869
193	1.710	0.023	1.600	0.300	1.010	2.909	0.008031	0.418181	19.5332	104.1770	0.067761	0.094030	-0.107428	-0.043512
	1.710	0.023	1.600	0.600	1.010	2.909	0.021339	0.333709	32.5554	104.1770	0.123819	0.114686	-0.138599	-0.096303
157	1.550	0.060	1.600	0.316	0.622	1.975	0.006704	0.364141	25.2928	128.0650	0.099137	-0.004335	-0.083021	-0.054355

³³R. Dammel, "Anti-reflection coatings: theory and practice," SPIE Short Course No. SC118 (2005).

where

$$\tau_D = \exp(-i\phi) = \exp\left(-i\frac{2\pi\tilde{n}_2}{\lambda}d\right), \quad (9.38)$$

$$\alpha = \frac{4\pi k_2}{\lambda}, \quad (9.39)$$

$$\beta = \frac{4\pi n_2}{\lambda}, \quad (9.40)$$

$$R_{23} = r_{23}r_{23}^*. \quad (9.41)$$

The standing wave intensity in the photoresist film is given by

$$I_s = E_s \cdot E_s^* \frac{t_{12}E_0[e^{-i(2\pi\tilde{n}_2z/\lambda)} + r_{23}\tau_D^2 e^{i(2\pi\tilde{n}_2z/\lambda)}]}{1 + r_{23}r_{12}\tau_D^2} \cdot \frac{t_{12}^*E_0[e^{-i(2\pi\tilde{n}_2z/\lambda)} + r_{23}^*\tau_D^{*2} e^{-i(2\pi\tilde{n}_2z/\lambda)}]}{1 + r_{23}^*r_{12}^*\tau_D^{*2}} \quad (9.42)$$

$$E_0^2 T_{12} e^{-\alpha z} \frac{e^{2\alpha d} + e^{2\alpha z} R_{23} + e^{-\alpha(d+z)} D \cos \beta(d-z) + e^{\alpha(d+z)} E \sin \beta(d-z)}{e^{2\alpha d} + R_{12}R_{23} + 2e^{\alpha d}(F \cos \beta d + 2G \sin \beta d)},$$

where

$$D = 2 \frac{k_2^2 - k_3^2 + n_2^2 - n_3^2}{(n_2 + n_3)^2 + (k_2 + k_3)^2}, \quad (9.43)$$

$$E = 4 \frac{n_3 k_3 - n_3 k_2}{(n_2 + n_3)^2 + (k_2 + k_3)^2}, \quad (9.44)$$

$$F = \frac{2}{[(n_1 + n_2)^2 + (k_1 + k_2)^2][(n_2 + n_3)^2 + (k_2 + k_3)^2]} [-k_2^4 - 4n_1 n_2 k_2 k_3 + 4k_1 n_2 (k_3 n_2 - k_2 n_3) + k_1^2 (k_2^2 - k_3^2 + n_2^2 - n_3^2) - (n_1 - n_2)(n_1 + n_2)(k_3^2 - n_2^2 + n_3^2) + k_2^2 (k_3^2 + n_1^2 - 2n_2^2 + 4n_1 n_3 + n_3^2)], \quad (9.45)$$

$$G = \frac{4}{[(n_1 + n_2)^2 + (k_1 + k_2)^2][(n_2 + n_3)^2 + (k_2 + k_3)^2]} \cdot \{-n_2 k_2^2 (k_1 + k_3) + k_2^3 (n_1 + n_2) - k_2 [k_3^2 n_1 + k_1^2 n_3 + (n_1 + n_3)(-n_2^3 + n_1 n_3)] + n_2 [k_1^2 k_3 + k_3 (n_1 - n_2)(n_1 + n_2)] + k_1 (k_3^2 - n_2^2 + n_3^2)\}. \quad (9.46)$$

In order to simplify the equation and to make it independent of the incident dose, it is customary to normalize it to the intensity at the top of the resist film (i.e., at $z = 0$):

$$I_s(z=0) = E_0^2 T_{12} \frac{e^{2\alpha d} + R_{23} + e^{-\alpha d} D \cos \beta(d) + e^{\alpha d} E \sin \beta(d)}{e^{2\alpha d} + R_{12}R_{23} + 2e^{\alpha d}(F \cos \beta d + 2G \sin \beta d)}. \quad (9.47)$$

The normalized intensity in the resist film (I_s^n) is given by

$$I_s^n = \frac{I_s}{I_s(z=0)} = e^{-\alpha z} \frac{e^{2\alpha d} + e^{2\alpha z} R_{23} + e^{-\alpha(d+z)} D \cos \beta(d-z) + e^{\alpha(d+z)} E \sin \beta(d-z)}{e^{2\alpha d} + R_{23} + e^{\alpha d} D \cos \beta d + e^{\alpha d} E \sin \beta d}. \quad (9.48)$$

As seen from the above equation, the normalized standing wave intensity is not dependent on n_1 and k_1 . This suggests that the change in the reflectivity at the top of the resist caused by a top antireflection coating can only lead to exposure dose changes (due to different amounts of light being reflected from the surface).

9.7.3 Bulk standing wave intensity

The equation for the standing wave intensity inside the resist has both a periodic and a nonperiodic component. For a resist film that is much thicker than the period $\lambda/4n_2$ of the standing wave, it is customary to think of the nonperiodic component of the standing wave as a “bulk” intensity, which is averaged over a period of the standing wave (see Fig. 9.13). The bulk intensity is given by

$$I_{\text{bulk}}(z) = e^{-\alpha z} \frac{e^{2\alpha d} + e^{2\alpha z} R_{23}}{e^{2\alpha d} + R_{23} + e^{-\alpha d} D \cos \beta d + e^{\alpha d} E \sin \beta d}. \quad (9.49)$$

The bulk intensity at the top of the resist film ($z = 0$) is given by

$$I_{\text{bulk}}(z = 0) = e^{-\alpha z} \frac{e^{2\alpha d} + R_{23}}{e^{2\alpha d} + R_{23} + e^{-\alpha d} D \cos \beta d + e^{\alpha d} E \sin \beta d}. \quad (9.50)$$

Normalizing the bulk intensity distribution to the value at $z = 0$, we obtain

$$I_{\text{bulk}}^n = \frac{I_{\text{bulk}}(z)}{I_{\text{bulk}}(z=0)} = e^{-\alpha z} \frac{e^{2\alpha d} + e^{2\alpha z} R_{23}}{e^{2\alpha d} + R_{23}} = e^{-\alpha z} \frac{1 + R_{23} e^{2\alpha(z-d)}}{1 + R_{23} e^{-2\alpha d}} = \frac{e^{-\alpha z} + R_{23} e^{-\alpha(2d-z)}}{1 + R_{23} e^{-2\alpha d}}. \quad (9.51)$$

Equation (9.51) is exactly the same as the case for when a single reflection from the resist-substrate interface is added incoherently to the incoming wave. Expanding the normalized bulk intensity in a McLaurin series in z , and truncating

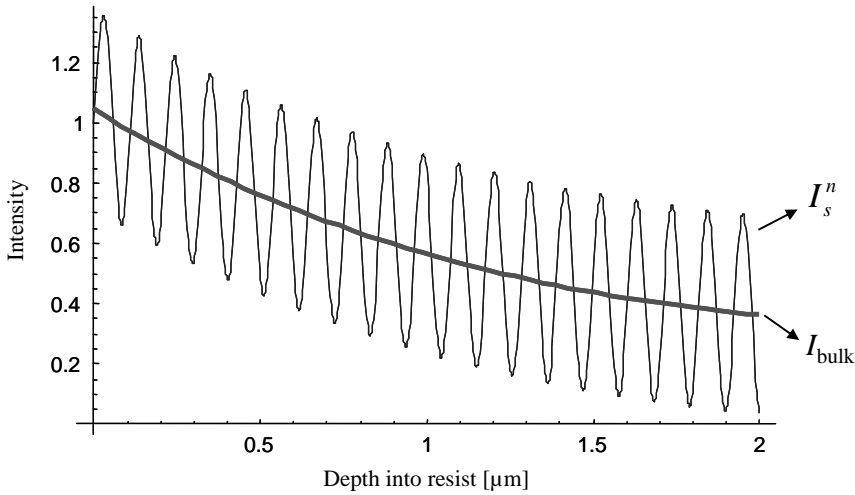


Figure 9.13 Computed normalized intensity and bulk intensity of standing waves in a resist film. Simulation parameters: λ 365 nm, \tilde{n}_2 1.71 0.02i, \tilde{n}_3 6.522 2.905i, D 1.2692, E +0.2535, R_{23} 0.41244, α 0.68857, β 58.8726. (After R. Dammel.³⁴)

the series after the linear term gives an approximation for an exponential function of the form

$$\begin{aligned}
 I_{\text{bulk}}^n &= \frac{e^{2\alpha d} - R_{23}}{e^{2\alpha d} + R_{23}} \alpha z + \frac{\alpha^2}{2!} z^2 - \frac{e^{2\alpha d} - R_{23}}{e^{2\alpha d} + R_{23}} \frac{\alpha^3}{3!} z^3 + \dots \\
 &\approx \frac{e^{2\alpha d} - R_{23}}{e^{2\alpha d} + R_{23}} \alpha z,
 \end{aligned}
 \tag{9.52}$$

where the coefficient $[(e^{2\alpha d} - R)/(e^{2\alpha d} + R)]\alpha$ is referred as the effective absorbance.

9.7.4 Substrate reflectivity and photoresist absorbance

Because of the addition of the returning wave to the bulk intensity, the intensity drop-off is less steep for more reflective substrates (see Fig. 9.14). This implies that resists will have straighter sidewalls on reflective substrates, provided the standing waves can be diffused out. Also, resists to be used on nonreflective substrates need to be more transparent than those used for highly reflective materials such as aluminum (see Fig. 9.14).

³⁴R. Dammel, “Anti reflection coatings: theory and practice,” SPIE Short Course No. SC118 (2005).

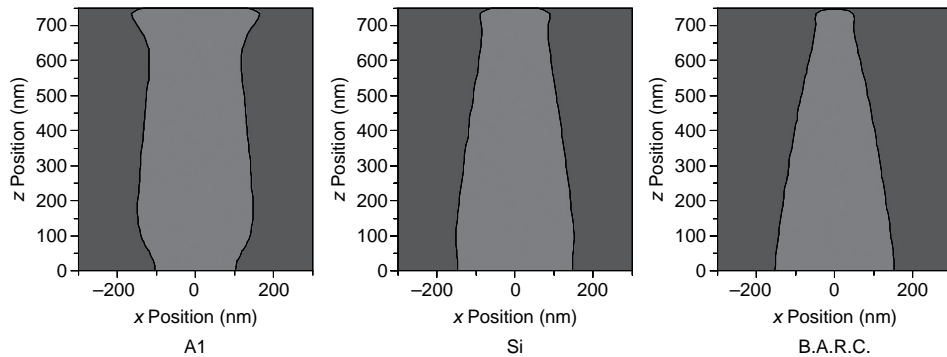


Figure 9.14 PROLITH/2 simulation of the effect of substrate reflectivity on i-line resist sidewall. Simulation parameters: NA 0.55, σ 0.5, 300-nm dense lines, focus in center of resist, at “dose-to-size.” (After R. Dammel.³⁵)

9.7.5 Relative swing amplitude

Using Brunner’s equations for swing amplitude, Eq. (9.1), it is possible to ratio the swing amplitudes for a given thickness of the BARC d_b to that of the substrate without BARC (i.e., $d_b = 0$). In this way, the swing amplitude reduction S_{rel} relative to the substrate is obtained as the square root of the ratio of the reflectivities

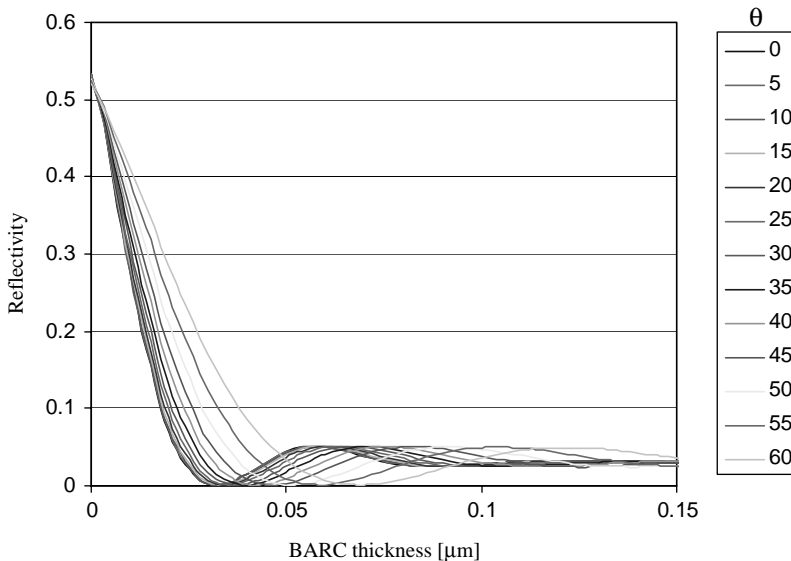


Figure 9.15 Reflectivity as a function of BARC thickness and angle of incidence. (After R. Dammel.³⁶)

³⁵R. Dammel, “Anti reflection coatings: theory and practice,” SPIE Short Course No. SC118 (2005).

³⁶ibid.

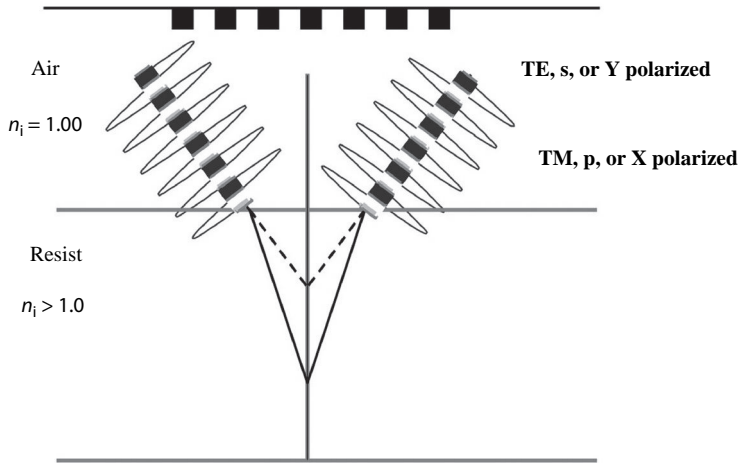


Figure 9.16 Polarization states and interference effects under large-angle imaging condition. (Courtesy of B.W. Smith.)

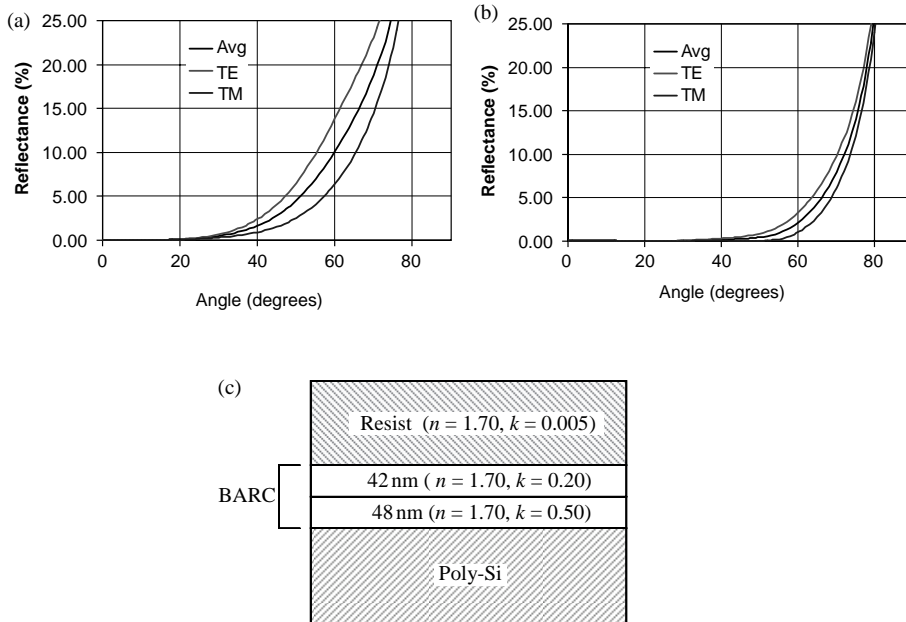


Figure 9.17 Reflectance of TE, TM, and average TE-TM polarization states obtained on optimized multilayer BARC at NA 1.2 and under (a) normal incidence and (b) full angular incidence 0–45 deg. (c) Thickness and optical properties (n and k) values of film stack used in the simulation of (b). The thickness and n and k values of the antireflection coating used in (a) are 35 nm, 1.70, and 0.20, respectively. (Courtesy of B.W. Smith.)

into the resist:

$$S_{\text{BARC}}(d_b) = 4\sqrt{R_t R_{\text{BARC}}(d_b)} e^{-\alpha d_r}, \quad (9.53)$$

$$S_{\text{substrate}} = S_{\text{BARC}}(0) = 4\sqrt{R_t R_{\text{BARC}}(0)} e^{-\alpha d_r}, \quad (9.54)$$

$$S_{\text{rel}}(d_b) = \frac{S_{\text{BARC}}(d_b)}{S_{\text{substrate}}} = \sqrt{\frac{R_{\text{BARC}}(d_b)}{R_{\text{BARC}}(0)}}. \quad (9.55)$$

Similarly, one can define S_{rel} for multiple thin-film stacks versus the substrate.

9.8 Bottom Antireflection Coatings for High-NA Imaging

At high NA, the nonvertical incidence of incoming rays causes a shift in the position of the BARC's reflectance minima. For projection lithography, rays will fall onto the wafer under a range of incident angles θ (see Fig. 9.15). In particular, BARC reflectivity optimization under normal incidence illumination conditions is not adequate for an NA greater than 0.8. Bottom antireflection coating optimization should be over the full angular distribution.

For nonvertical incidence, the transverse electric (TE) and transverse magnetic (TM) waves of light are reflected and refracted differently; their interference properties are also different (Fig. 9.16). The TM state will interfere exactly at normal incidence only. The image in the resist is the sum of the TE and TM images. The use of graded BARCs, multilayer BARCs (in stack configurations: organic-organic, inorganic-organic, inorganic-inorganic) have been found to be effective in reducing BARC reflectivity under hyper-NA conditions (see Fig. 9.17). Polarization effects scale as the cosine of the angle of incidence.

Chapter 10

Stone, Plate, and Offset Lithography

Struggling to be free, art more engaged.

William Shakespeare, *Hamlet*

10.1 Stone and Plate Lithography

Invented in 1798 by Senefelder (as described in Chapter 2), stone lithography¹ was the first printmaking technology that made it possible for an artist to work using traditional techniques to create prints that could rival an original painting in terms of detail, mood, and color variations. Stone lithography rose to prominence in the nineteenth century and is still practiced today by artists and lithography studios, where it is used to create color art for books, as well as for more pedestrian items such as labels, flyers, and posters. Its popularity stems from the fact that it was the first printmaking medium to allow the artist to naturally “paint” or “draw” onto a flat stone to create an image. The artist creates the work directly and naturally.

The basic steps involved in creating stone lithographs comprise the following:²

Step 1. The artist draws or paints on a flat polished stone (typically limestone) with a greasy substance such as a lithographic crayon (a soft waxy/greasy crayon), paint, or pencil. The stone absorbs this greasy substance and retains it.

Step 2. The stone is moistened with water. The parts of the stone that are not protected by the greasy paint absorb the water.

¹Excellent reports on the practice of fine art lithography as practiced in modern times have been written. See, for example, G. Antreasian and C. Adams, *The Tamarind Book of Lithography: Art and Techniques*, Abrams, New York (1971); <http://www.unm.edu/~tamarind/process.html>.

²M. Brain, “How stone lithography works,” Feb. 20, 2007, HowStuffWorks.com, http://entertainment.howstuffworks.com/stone_lithography.htm.

Step 3. Oil-based ink is rolled onto the stone. The greasy parts of the stone pick up the ink, while the wet parts do not.

Step 4. A piece of paper is pressed onto the stone such that the ink transfers from the stone to the paper.

The fundamental principle that underlies this technique is the affinity of oil for oil and the repulsion of oil and water. In the following section, we describe in more detail the process steps that are involved in printing images with the aid of stone lithography. Figure 10.1 shows pictures of these process steps.

Step 1—Preparation of the Stone

The first step in creating a print is the preparation of the stone by the artist (see step 1 of Fig. 10.1). Traditionally, the stone is a flat, polished limestone block, cut into an appropriate size. If the image will contain multiple colors, multiple blocks are used, one for each color. The best stones—Kellhein stones—are obtained from a quarry in Solenhofen, a town in Bavaria. This stone possesses the unique quality that slabs of nearly any thickness can be easily cut and polished to a perfect finish with ease. Already-used stones can be reused simply by grinding and removing the previous image.³

A levigator—a heavy steel plate with a handle on it—is used to grind the surface of the stone with carborundum grit. A lithography image is disposed on the top 1/64 in (about half a millimeter) of the stone. Grinding and polishing the stone are long and arduous processes, taking up several hours on a large stone, such as that shown in step 1 of Fig. 10.1, which in the end removes about a millimeter of the top surface of the stone. If not enough stone is removed, a ghost of the previous artist's work will materialize in the new image.⁴

Step 2—Writing or Drawing on the Stone

Once polishing is completed, the stone is ready to be drawn or painted on by the artist. The artist uses a material that is a mixture of pigment and some form of grease to draw the image on the stone. The drawing material may be used in a solid form called lithographic pencil, chalk, or crayon, or in liquid form called tusche, which is applied with a brush to create the image on the stone (see step 2 of Fig. 10.1). Lithographic pencils are waxy; some can be soft while others can be hard and brittle. On drying, the tusche reticulates, leaving netlike features on the stone, which can show up in the final print, a characteristic unique to stone lithography.⁵

³ibid.

⁴ibid.

⁵ibid.



Figure 10.1 Stone lithographic process steps. Step 1: Polishing of the lithographic stone (today, polishing is done with a levigator). Step 2: The artist draws or paints on the lithographic stone with a greasy substance such as a litho crayon, paint, or pencil; the lithographic stone picks up this greasy substance and holds it. Step 3: Etching of the lithographic stone with a solution of gum arabic and nitric acid to prepare it for printing. The process of etching fixes the artist's image on the stone by making the dark areas very lipophilic and the light areas very hydrophilic. Following etching, the lithographic stone is moistened with water. The parts of the stone not protected by the greasy paint soak up the water. Step 4: Oil-based ink is rolled onto the stone. The greasy parts of the stone pick up the ink, while the wet parts do not. Step 5: A piece of paper is pressed onto the stone, and the ink transfers from the stone to the paper, effectively printing the image on the paper. Step 6: The printed paper is lifted off the lithographic stone, revealing the image. (Published with permission from the Deutsches Museum, Munich.)

In principle, the stone lithography process is extremely natural. There is very little difference between drawing/painting on the stone and doing the same on a piece of paper. However, a few points must be borne in mind: (i) Lettering is drawn on the stone as a mirror image. (ii) For multiple colored images, the artist prepares a different stone for each color, which calls for strict alignment and registration of the stones and their colored inks to their appropriate locations on the printed image on the paper. (iii) There is little room for mistakes, since it is very difficult to correct them once they have been made. This often implies polishing away the entire image and starting all over again.⁶

Step 3—Etching the Stone

After the artist finishes drawing on the stone or plate, the next step is to etch it in order to prepare it for printing. First, rosin is sprinkled on the surface of the stone to protect the drawing; this is followed by the application of talc powder, which helps to stabilize the image. A solution of gum arabic and nitric acid is then applied to the stone and left for about an hour to combine with the greasy particles and the calcium carbonate of the stone (see step 3 of Fig. 10.1). The nitric acid reacts with the grease (oleic acid), forming oleomagnate of lime. The process of etching fixes the artist's image on the stone—makes it a part of the stone, in reality, through a chemical reaction. In the overall process, the acid sensitizes the dark areas such that they accept ink and reject water, and desensitizes the light areas such that they reject ink and accept water. Both the sensitization and desensitization phenomena take place in one step.⁷

Next, the printer wipes off the remaining solution of gum arabic and nitric acid with cheesecloth, after which the entire stone surface is dried, which leaves the greasy image barely visible on the stone. Asphaltum, a naturally occurring petroleum substance, is sometimes applied to the image area of the stone, as a way of keeping the stone surface wet. This tends to prevent ink from adhering to the non-image areas of the stone.⁸

Step 4—Inking the Stone

At the press, the printer sponges the stone or plate first with water (which moistens the nonimage areas), and then rolls it with ink (see step 4 of Fig. 10.1). Being also greasy, the printing ink adheres to the image area, but not to the nonimage areas.⁹

⁶ibid.

⁷ibid.

⁸ibid.

⁹ibid.

Step 5—Creating Prints

If inked properly, appropriately sized papers with registration marks on them are laid on the stone and are printed with the inked stone, using a press, and making sure that the registration marks on the papers align properly with their corresponding marks on the inked stone. Registration marks are particularly important on multistone prints so as to ensure that all of the colors line up properly. The stone is then used to print a series of “trial proofs,” i.e., the same image with different color and paper combinations. When the artist is satisfied with the quality of the print, he or she signs the final print. With this as the standard, the printer is ready to print the edition (see steps 5 and 6 of Fig. 10.1).¹⁰

10.2 Offset Lithography

The first lithographic offset printing press was invented in 1903 by Ira Washington Reubel. Like stone and plate lithography and other types of lithography, offset lithography¹¹ works on a very simple principle: ink and water don't mix. It is also a planographic technique where the image and nonimage areas are, for all practical purposes, in the same geometric plane. Also, like stone and plate lithography, in offset lithography, the image area of a printing plate is made of a material having an ink-receptive oleophilic surface, while the nonimage area is made of a water-receptive, or hydrophilic material. To make a print, a thin film of aqueous solution (called fountain, or dampening solution) is first applied to the plate to wet the nonimage area. Then ink is applied to the plate, where it adheres mainly to the image area.

In offset lithographic presses, the printing plate is attached to a rotating cylinder that transfers the ink to a rubber-covered blanket (called the offset), which in turn transfers the ink to the paper. The process is called “offset” because the image does not print directly to the paper from the plates, as it does in gravure printing or even in stone or plate lithography. Instead, it goes from the printing plate to the rubber blanket cylinder, which serves as an intermediary that transports (offsets) the ink-and-water impression to the paper on the third cylinder, called the impression cylinder (see Fig. 10.2). One revolution of the printing plate cylinder is referred to as an impression.

¹⁰ibid.

¹¹An excellent reference on offset lithography is that by W.C. Browne, “Offset lithography: a treatise on printing in the lithographic manner from metal plates on rubber blanket offset presses, with which is incorporated a comprehensive digest on photolithography and also on tin plate decorating,” *The National Lithographer*, New York (1917).

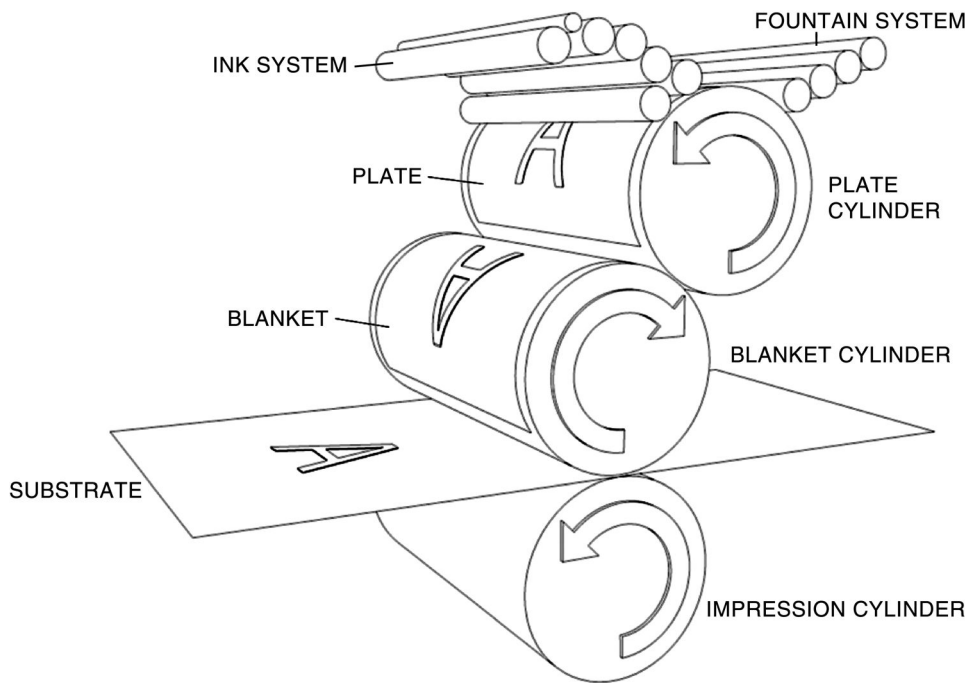


Figure 10.2 Offset lithography rollers. (Drawing courtesy of Boris Listdat.)

10.3 The Offset Lithographic Press

The basis of the rubber blanket offset lithographic press is the substitution of metal plates for lithographic stones. The press consists of three cylinders, one to carry the printing plate (top cylinder), another to carry the rubber blanket (middle cylinder), and a third (the bottom cylinder) to carry the sheet and effect the impression from the rubber blanket to the paper (see Fig. 10.2). Of course, the press is equipped with a certain number of gears, shafts, rollers, etc. Connected to the plate cylinder are a water fountain and a set of water rollers. The surface of the plate (not including the transfer parts, the substances to be printed, and the greasy areas) is dampened.¹² The ink rollers passing over the plate do not deposit ink over the dampened areas, but do ink the transfers to the required strength. The inked-up transfers print on the rubber cylinders, and the sheets fed into the printing cylinder receive their impression from the rubber blanket, completing the printing process.¹³

Certain attributes of the offset lithographic press make it particularly appealing as a means of mass reproduction of printed matter and images. These include extremely high throughput; clear, clean, and sharp impressions; the much lower cost of metal plates relative to stone plates; the ability to handle rough and hard papers; low

¹²ibid., p. 20.

¹³ibid., p. 20.

ink usage relative to stone plate lithography; and the ability to print on uneven-surfaced paper, given the elasticity of the rubber blanket.¹⁴

10.4 Components of an Offset Lithographic Press

The main components of a lithographic offset press include the paper feeding system, the damping system, the inking system, and the drying system.

10.4.1 Paper-feeding system

The two main types of paper-feeding systems in lithographic offset presses comprise the (i) sheet-fed system, where individual sheets are fed successively into the press and (ii) the web system, where a continuous roll of paper, or web, is fed into the press. Papers used in offset lithographic presses are grouped into two categories, namely, coated and uncoated. Both of these paper categories are available in many grades, weights, and finishes. The coatings are mainly made of clay, calcium carbonate, or titanium dioxide dispersed in a suitable binder, usually starch or latex.

10.4.2 Damping system

The damping system consists of a water fountain and water rollers, which deliver fountain solution (aqueous solutions of gum arabic, chromates and/or phosphates, and magnesium nitrate, along with surfactants and emulsifiers) to the plate. The fountain solution is held in the water fountain, from where it is delivered to the plate before each printing run. Quite a good number of configurations for damping systems exist, each differing from the other in the way that they deliver the fountain solution. Some damping systems meter the fountain solution through a series of rollers, while others use a brush system with bristles to do the metering.

10.4.3 Inking system

Equipped with a fountain and ink rollers, the inking system is like the dampening system. Depending on the quantity of ink required, the ink can be supplied to the press fountains via pipes originating from a centralized pumping station, or from point-of-use drum pumps at each press, or even by hand. These inks tend to be very viscous, which makes them rather difficult to be poured.

The ink delivered across the plate from the ink fountain is controlled by a series of blades or ink keys, which limit the volume of ink in discrete areas of the plate to match image requirements. On leaving the ink fountain, the ink is metered through a series of rollers before being applied to the plate as a thin film.

¹⁴ibid.

10.5 Types of Offset Lithographic Inks

Offset lithographic inks are broadly divided into heat-set, cold-set, or energy-curable (such as ultraviolet-curable, electron-beam-curable) inks, depending on the way they are cured. Heat-set inks, as their name implies, are set by applying heat and then rapidly cooling them to catalyze the curing process. They are the most common types of lithographic offset inks, and used in printing magazines, catalogs, and inserts. Cold-set inks are set by absorption into noncoated stocks and are generally used in newspaper and book printing. Energy-curable inks are cured by means of UV radiation and electron beams, and are the highest quality offset lithographic inks.

10.6 Fabrication of Lithographic Offset Plates

As mentioned in Chapter 4, the two main types of lithographic plates used in offset lithography are negative- and positive-working plates. In fabricating negative-working plates (Fig. 10.3), film negatives are used to image unprocessed plates (typically aluminum or zinc substrates) that are generally coated with a photopolymer or monomers with appropriate UV-photosensitive moieties in them. Exposure of the presensitized plate to UV radiation through a film negative disposed over them that serves as a mask causes a cross-linking reaction of the plain monomers or the monomeric units of the photopolymer in the areas under clear areas (image areas) of the film negatives, while the areas under the dark areas of the film negative remain unaltered (nonimage areas). Processing involving dissolution in appropriate developing solvents removes unexposed nonhardened polymer, while leaving

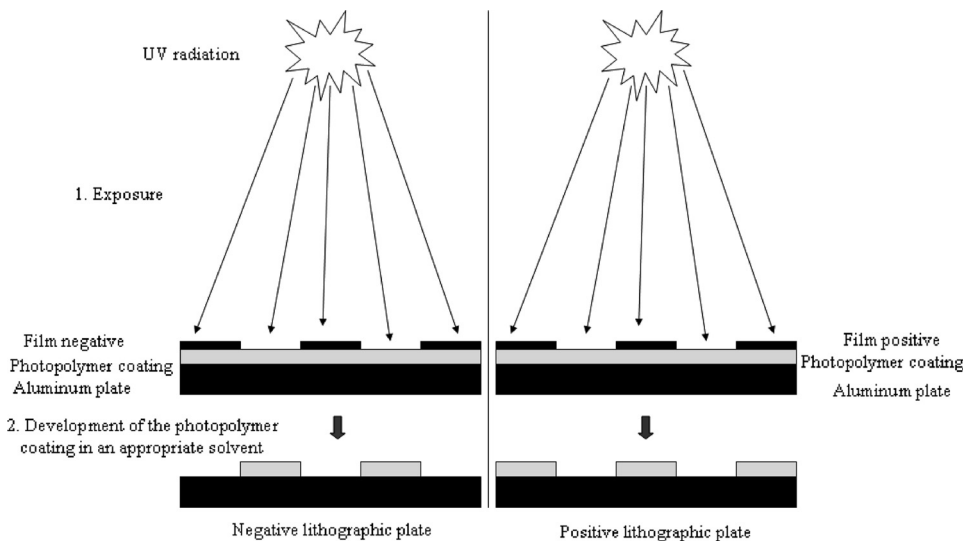


Figure 10.3 Fabrication of an offset lithographic plate.

the exposed part intact on the plate. An application of a gum solution to the non-image areas of the plate makes them water attracting and ink rejecting. The processing does not wash off the hardened polymer image areas of the plate. The negative-working plates are generally inexpensive to fabricate and therefore cost less than their positive-working counterparts.

In fabricating positive-working plates (Fig. 10.3), film positives are used as masks to image the unprocessed plates coated with UV-photosensitive polymers. The exposed parts of photopolymers (i.e., the areas under the clear areas of the mask) become more soluble in the developing solvent and are washed away, while the unexposed areas of the photopolymers remain unaltered and are left on the mask. Following processing, a thin layer of gum is applied over the plate to protect the nonimage areas from ink.

10.7 The Offset Lithographic Process

In this section, we discuss the steps involved in the offset lithography process.

Step 1—Prepress Production

The prepress production step involves the transfer of the information to be printed to a film or a printing plate, as described above in the fabrication of an offset lithographic plate. A measured amount of light is allowed to pass through the film negatives to expose the printing plate, resulting in a chemical reaction that allows an ink-receptive coating to be activated in only the exposed areas, effectively resulting in the transfer of the image from the negative to the plate. For images with multiple colors, a separate plate is used for each color type.

Step 2—Press Run

The press run comprises the set of operations that are used to print the information contained on the printing plate on paper. These operations are highly automated and begin with a huge roll of paper that is fed through banks of rollers. The paper is fed through the press as one continuous stream pulled from the rolls of paper. Each roller adds one color at a time. Some of these operations are briefly described below.

Step 2a—Inking of the Plates

In the inking step, the plates are first dampened by water rollers, followed by ink rollers, which distribute the ink from the ink fountain onto the plates. The image areas of the plate absorb ink from the ink rollers, while the water rollers keep the ink off the nonimage areas of the plate through sheer repulsion between the ink and water. With the image and nonimage areas of the plate now fully defined,

the plate transfers its image to a rubber blanket that in turn transfers the image to the paper. The plate itself does not actually touch the paper, hence the term “offset” lithography.

To facilitate drying of the ink and to prevent it from smudging, the paper is passed through a high-temperature oven. On leaving the oven, the paper is run through chill rollers—a short series of large metal rollers that have refrigerated water flowing through them—that cool the paper down quickly and set the ink into the paper.

Step 2b—Color and Registration Control

Registration involves the precise alignment of the printing plates so that they apply their respective color portions of the image to their appropriate locations on the portion of the image that is being printed. If the plates are not properly aligned, the printed image will not only appear out of focus, but may also print with the wrong color. Color and registration control is a process that is implemented in modern offset lithography with the aid of computers that are part of the registration control system. The routine is one in which the registration control system takes a video image of registration marks that have been placed on the press sheet and compares them, as well as their locations, with those on the printing plate, while at the same time continuing to make necessary adjustments to their positions relative to each other until a perfect alignment is achieved. This routine is extremely fast and takes place while the press is running at full speed.

Color control is achieved through the blending of the ink and is coordinated with plate registration. The image quality is determined by the amount of ink released into the ink rollers, which in turn is adjusted via the control panel, a part of the overall control console. Before being placed on the press, the plates are scanned and the data transferred to a microcassette, which serves as the “master” that directs the release of ink to preset values.

Step 3—Binding

The printing process is completed at the bindery, where the huge rolls of now-printed paper are cut and put together so that the pages fall in the correct order in which they are to be bound, stapled, or glued.

10.8 Waterless Offset Lithography

Waterless offset lithography uses the concept of differential adhesion to keep the image and nonimage areas of the lithographic plate separate during printing (see Fig. 10.4). Unlike standard offset lithography, fountain solution is not used in the waterless offset process. Instead, silicone coating on the surface of the offset plate makes this type of printing possible. The process is such that silicon

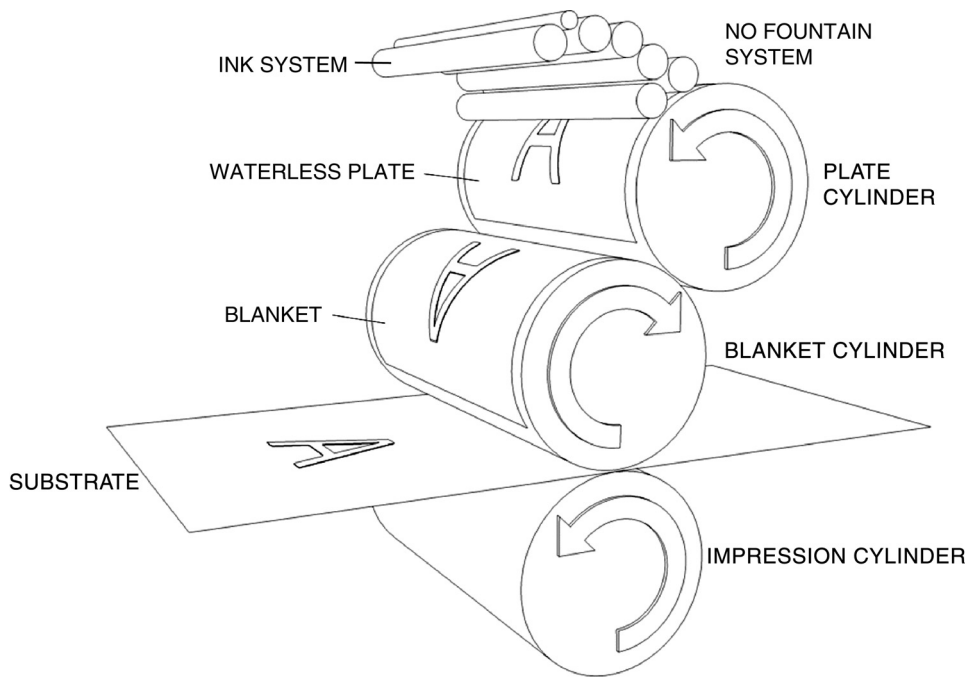


Figure 10.4 Waterless offset lithography rollers. No fountain solution is used. (Drawing courtesy of Boris Listdat.)

is removed from the image area of the plate during plate development—but is not removed, however, from the nonimage areas. This makes the image areas with no silicone slightly deeper than the nonimage silicone area, resulting in very shallow “wells,” which can hold the ink. When ink is subsequently applied to the plate as in standard offset lithography, the ink is retained in these shallow wells containing the image areas and not in the elevated nonimage areas that are covered by silicone. The ink used in waterless offset lithographic presses is formulated to resist adhesion to the silicone, but will deposit only in the nonsilicone shallow well areas. From the waterless plate, the image is transferred to the offset (blanket) plate, from which it is printed on the paper.

Chapter 11

The Semiconductor Lithographic Process

And the atoms that compose this radiance do not travel as isolated individuals but linked and massed together.

Lucretius, *De Rerum Naturae* [*On the Nature of Things*]

11.1 Introduction

Within a semiconductor fabrication facility, popularly called a “fab,” the lithography module occupies a very central position, literally in terms of the device fabrication process flow, as well as in terms of the importance of the role it plays. Lithography is often considered the most critical step in IC fabrication, for it defines the critical dimension—the most difficult dimension to control during fabrication (e.g., polysilicon gate length)—of the device. This is why the critical dimension in lithography is often used to define the device technology node or generation.¹ It is estimated that lithography accounts for nearly one-third of the total wafer fabrication cost.²

The object of semiconductor lithography is to transfer patterns of ICs drawn on the mask or reticle to the semiconductor wafer substrate. The transfer is carried out by projecting the image of the reticle with the aid of appropriate optical elements of an exposure tool onto a radiation-sensitive resist material coated on the semiconductor wafer, typically made of silicon, and stepping the imaging field across the entire wafer to complete a layer. The shape of the IC pattern transferred to the wafer substrate is dependent entirely on the wafer layer being patterned. Examples of patterns include gates, isolation trenches, contacts, metal interconnects, and vias to interconnect metal layers. An advanced CMOS (complementary

¹M. Quirk and J. Serda, *Semiconductor Manufacturing Technology*, pp. 336–337, Prentice Hall, Englewood Cliffs, NJ (2001).

²S. Campbell, *The Science and Engineering of Microelectronic Fabrication*, p. 152, Oxford University Press, New York (1996).

metal-oxide semiconductor) IC can have more than 30 masking layers needed to pattern the multiple layers on a chip.³ Fabrication of an entire layer often entails processing the wafer through lithography before it undergoes subsequent operations in other modules such as etch, implant, etc.

The steps in the semiconductor lithographic process are outlined in Fig. 11.1 and illustrated in Fig. 11.2 for a negative and a positive resist. The chemical and physical principles underlying each step are discussed at length in the following sections. Lithographic modeling comprehending most of these steps is provided in Chapter 12 in a unified manner, with a view to providing a framework for predicting lithographic outcomes, given a defined set of input resist materials and process variables, as well as exposure conditions.

11.2 Adhesion Promotion

The most commonly used insulator in semiconductor devices is silicon dioxide (SiO_2), which is typically formed on the surface of the silicon wafer by thermal oxidation of the surface with oxygen or water vapor at a temperature between 1000 and 1200°C. It is also possible to deposit the oxide layer onto a substrate that is not

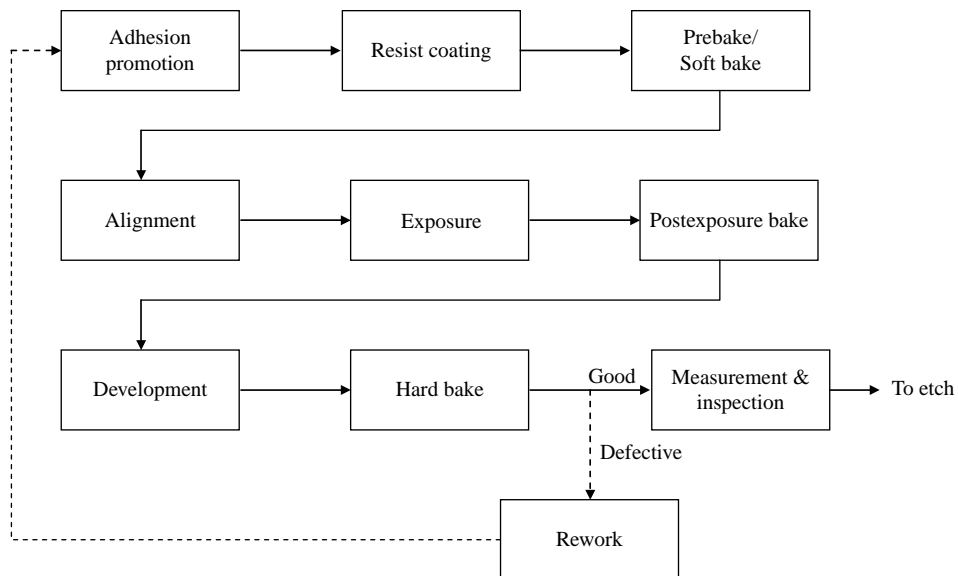


Figure 11.1 Steps of the semiconductor lithographic process. The adhesion promotion step is often skipped when a BARC is applied to the wafer substrate before the resist application step.

³P. Castrucci, W. Henley, and W. Liebmann, "Lithography at an inflection point," *Solid State Technol.*, p. 127, (Nov. 1997).

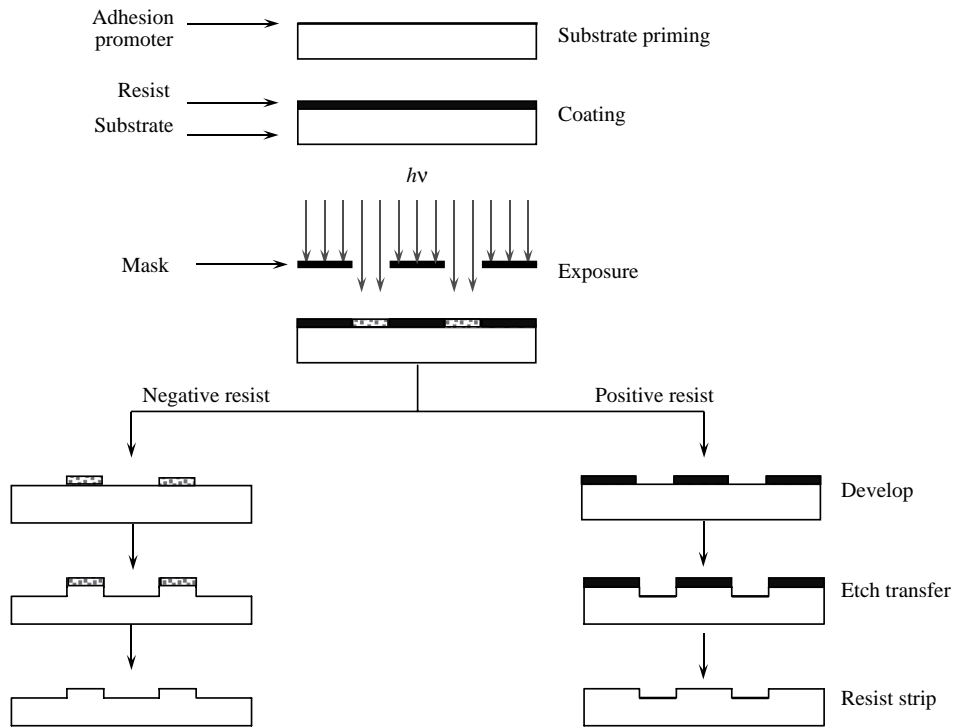


Figure 11.2 The semiconductor lithographic process.

necessarily silicon, basically by the vapor-phase oxidation of silane with oxygen at a temperature between 400 and 500°C.⁴

A fresh surface of thermally grown silicon dioxide, it must be pointed out, is hydrophobic. However, it quickly reacts with water vapor in the atmosphere to form silanol (Si—OH) and gradually becomes hydrophilic. In fact, the chemical vapor deposition of silicon dioxide forms only a silanolated surface. Being fairly hydrophobic, resists do not adhere well to hydrophilic surfaces such as SiO₂. These surfaces contain hydroxyl groups as illustrated in Reaction [11.1]. The adhesion failure of resist films on such surfaces is often observed in the course of development or wet etching. As a result, a surface treatment to promote adhesion is necessary before the resist film is deposited on such surfaces.⁵

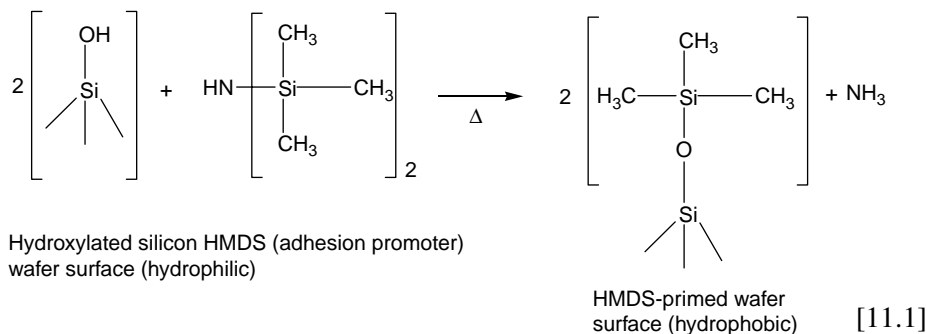
A method for enhancing adhesion of resist materials onto surfaces of silicon dioxide and other semiconducting substrates was invented by Collins and Deverse,⁶ and involves subjecting the surface to an atmosphere containing the

⁴S. Nonogaki, T. Ueno, and T. Ito, *Microlithography Fundamentals in Semiconductor Devices and Fabrication Technology*, p. 133, Marcel Dekker, New York (1998).

⁵ibid.

⁶R.H. Collins and F.T. Deverse, "Process for improving photoresist adhesion," U.S. Patent No. 3,549,368 (1970).

vapor of hexamethyldisilazane (HMDS)⁷ for a period of time at a temperature sufficient for the surface to react with this reagent (see Reaction [11.1]). In this reaction, HMDS acts as a silane-coupling agent that converts hydrophilic silanol groups on the surface into hydrophobic siloxanes.



11.2.1 Priming of silicon dioxide surface with HMDS

Normally, this silyl ether formation reaction is base catalyzed and requires the addition of, for example, an amine, to proceed unless the reagent contains its own base, as is the case with HMDS. The use of HMDS to chemically passivate the hydrophilic surface is notable in another way in that it yields only a gaseous reaction product, ammonia. Other similar adhesion promoters include trimethylsilyldiethylamine (TMSDEA), which can be more effective but also less stable than HMDS. Wafers with inorganic CVD BARCs, such as $\text{Si}_x\text{O}_y\text{N}_z$, Si_xN_y , etc., are also typically primed for similar reasons.

Substrate priming using either HMDS or TMSDEA or similar adhesion promoters can be carried out in either the liquid or the vapor phase. In either case, priming is done at elevated process temperatures $\sim 100^\circ\text{C}$. Substrates are typically cleaned with UV/ozone treatment, HF, plasma, or other “oxidative” cleaning methods, followed by dehydration bake at $\sim 150^\circ\text{C}$ to remove adsorbed moisture before the application of the adhesion promoter. Priming agents are typically best applied using vapor prime methods, either in-line or in batch vacuum ovens, whereby a stream of gaseous adhesion promoter is introduced into the adhesion oven for a set period of time after heating the wafer, which is followed by a N_2 purge and heating. Uniformity and reduced chemical usage make this approach a more attractive option than ambient temperature liquid treatment.⁸

The dilute HF dip is another commonly used approach in priming silicon wafers. The HF dip has been determined not only to remove the surface SiO_x layer, but to generate hydrophobic Si–H and Si–F bonds on the surface.⁹

⁷HMDS is a colorless liquid that boils at 125°C .

⁸B.W. Smith, “Resist Processing,” in *Microlithography: Science and Technology*, pp. 520–521, Marcel Dekker (1998).

⁹M. Grundner, D. Graf, P.O. Hahn, and A. Schnell, “Wet chemical treatments of Si surfaces: chemical composition and morphology,” *Solid State Technol.* **34**, pp. 69–75, (Feb. 1991).

The role of priming, according to Moreau,¹⁰ is to adjust the surface energy of the wafer in a way that makes it comparable to the surface energy of the resist layer. Deviations occurring both at the high and low ends are consequential, i.e., insufficient priming can lead to adhesion failure, while overpriming can lead to dewetting. Priming can also impact the development time in wet processes. In conditions of high fluence exposure such as obtained in heavy UV exposure in ion-implantation steps, overpriming can also lead to a phenomenon known as “popping,” in which nitrogen formed in the DNQ/novolac-type resists may not escape from the film quickly enough through diffusion, but may instead accumulate at the resist-wafer interface, weakening the adhesion between the two surfaces, and resulting in the formation of bubbles there. Under high fluence, these bubbles may explode and deposit resist debris on adjacent substrate areas.¹¹

Remedies for mitigating against overpriming include the use of shorter priming times, resist solvents with lower surface tension, prerinsing the wafer surface with the resist casting solvent before resist coating, and oxygen or ozone plasma treatments of the wafer.¹²

A method for monitoring the adhesion promotion process is through measuring the ability of fluids to wet the surface of the primed surface. This is typically accomplished by placing a sessile droplet of water on a primed wafer and measuring the contact angle (see Fig. 11.3). The shape of the sessile water droplet is governed by free surface energies of the interfaces with which it is in contact. Wetting is described using Young’s equation, relating the equilibrium contact angle θ of the droplet to the surface tensions of the three interfaces (SV for

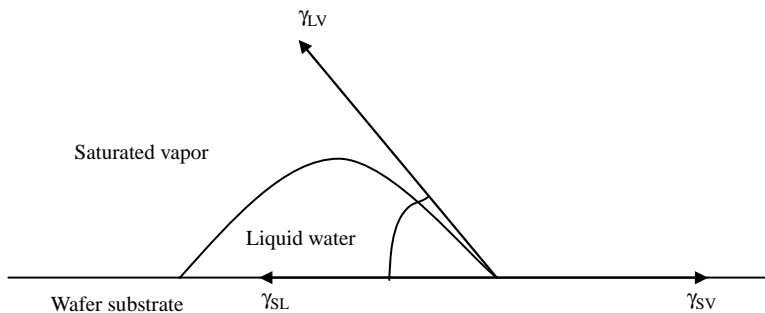


Figure 11.3 A sessile droplet of water on a wafer surface.

¹⁰W.A. Moreau, *Semiconductor Lithography: Principles, Practices and Materials*, pp. 289–291, 651–665, Plenum Press, New York (1988).

¹¹R. Dammel, *Diazonaphthoquinone based Resists*, p. 101, SPIE Press, Bellingham, WA (1993); B.W. Smith, “Resist processing,” in *Microlithography: Science and Technology*, p. 521, Marcel Dekker (1998).

¹²B.W. Smith, “Resist Processing,” in *Microlithography: Science and Technology*, p. 521, Marcel Dekker (1998); H.J. Levinson, *Principles of Lithography*, 2nd ed., pp. 57–59, SPIE Press, Bellingham, WA (2005).

solid/vapor interface, SL for solid/liquid interface, and LV for liquid/vapor interface) in the following way:¹³

$$\gamma_{LV} \cos \theta = \gamma_{SV} - \gamma_{SL}. \quad (11.1)$$

It should be pointed out, however, that a completely wetting fluid does not have an equilibrium contact angle. A properly primed wafer surface typically has water contact angle values of $50 \text{ deg} < \theta < 70 \text{ deg}$. Hydrophobic surfaces are associated with larger contact angles, while hydrophilic surfaces have smaller contact angles.¹⁴

The work of adhesion of the liquid to the solid has been shown to be¹⁵

$$W_A = \gamma_{LV}(1 + \cos \theta). \quad (11.2)$$

11.3 Resist Coating

After priming, the wafer is coated with a liquid solution of BARC (in the case of spin-on BARCs), baked, and cooled, before it is coated with a liquid solution of resist. Wafers with inorganic CVD inorganic BARCs are coated with resists immediately after priming. There are several methods of coating resists on wafers, including spin coating, spray coating, and dip coating. The most widely used methods for coating resist in the semiconductor industry are spin-coating methods.

11.3.1 The resist spin-coating process

In the spin-coating process, a precise amount of liquid resist is dispensed onto a wafer (either statically, i.e., with the wafer at rest, or dynamically, i.e., with the wafer rotating). The wafer is then spun at high speeds until such time that the film thickness reaches a desired value, oftentimes corresponding to a stationary point on the swing curve of the given resist (Fig. 11.4). The process thus uses the dynamics of centrifugal forces to disperse a fluid of polymeric resist material over the entire wafer surface. The flow and rheological properties of the resist do influence the coating process and need to be considered to achieve optimal results.¹⁶

The diagrams in Fig. 11.4 show a schematic of the spin-coating process. The variables and coordinates used in developing the mathematical equations governing this flow are also indicated in the diagrams.

The two main forces governing the spin-coating process are the viscous forces of the fluid that retard the expulsion of material from the wafer and centrifugal

¹³S. Wu, *Polymer Interface and Adhesion*, Marcel Dekker, New York (1982).

¹⁴H.J. Levinson, *Principles of Lithography*, 2nd ed., p. 59, SPIE Press, Bellingham, WA (2005).

¹⁵W.A. Zisman, "Relation of equilibrium contact angle to liquid and solid constitution," in *Contact Angle Wettability and Adhesion, Advances in Chemistry Series*, Vol. 43, American Chemical Society, Washington, DC (1964).

¹⁶D.E. Bornside, C.W. Macosko, and L.E. Scriven, "On the modeling of spin coating," *J. Imag. Tech.* **13**, 123 (1987).

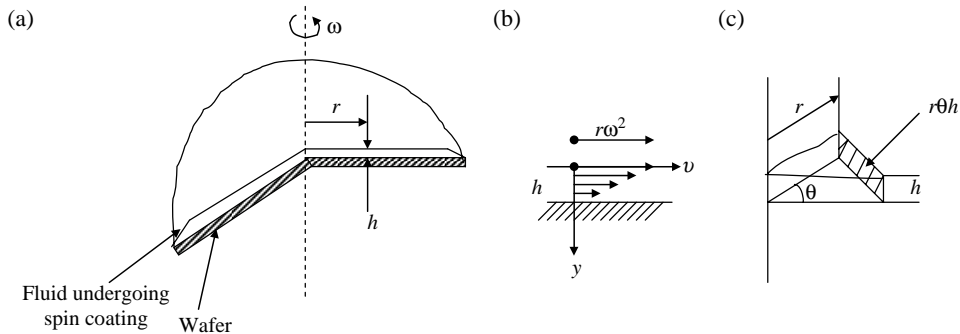


Figure 11.4 Schematics of the spin-coating process, showing (a) liquid flow on a rotating wafer, (b) the velocity profile of the flowing liquid, and (c) cross section of a wedge-shaped portion of the flowing liquid.

force, which serves to throw the fluid material outward, away from the wafer. The balance of viscosity and centrifugal forces at each point during the spin-coating process determines the thickness of the fluid on the wafer substrate.¹⁷ Emslie et al.¹⁸ were the first people to recognize this relationship, the equation of motion of which they reduced to the expression

$$\eta \frac{dv}{dy} = -\rho r \omega^2 y, \quad (11.3)$$

where η is the viscosity of the liquid, ρ is the density of the liquid, ω is the angular velocity of the liquid in radians per second, h is thickness of the liquid at the distance r , v is the velocity of the liquid in the plane (r direction), and r is the distance in the radial direction. In their analysis, Emslie and his co-workers assumed that the resist was a Newtonian fluid (with a linear relationship between shear stress and shear rate) flowing on a rotating infinite plane. In the following section, we examine their analysis in order to understand why a uniform film thickness is achieved by spin coating.

The terms on the right-hand side of Eq. (11.3) represent centrifugal force ($m r \omega^2$) acting at a distance r from the rotation axis; m is the mass of the liquid under consideration. This force creates a shear stress within the liquid, which is expressed as $\rho \omega^2 y$, where y is the depth from the surface of the fluid. The terms on the left-hand side of Eq. (11.3), involving the radial velocity of the liquid at depth y , represent the viscous forces.

If the liquid is Newtonian, the radial velocity of the liquid at depth y of Eq. (11.3) must satisfy the boundary condition

$$v = 0 \quad \text{and} \quad y = h. \quad (11.4)$$

¹⁷Excellent treatment of this subject has been provided elsewhere. See, for example, S. Nonogaki, T. Ueno, and T. Ito, *Microlithography Fundamentals in Semiconductor Devices and Fabrication Technology*, Chapter 5, Marcel Dekker, New York (1998). Here we emphasize only the key facts.

¹⁸A.G. Emslie, F.T. Bonner, and L.G. Peck, "Flow of a viscous liquid on a rotating disk," *J. Appl. Phys.* **29**, 858–862 (1958).

Integration of Eq. (11.3) with respect to y under the boundary condition shown in Eq. (11.4) results in

$$v = r\omega^2 \frac{\rho}{2\eta} (h^2 - y^2). \quad (11.5)$$

Using the kinematic viscosity, $\kappa = \eta / \rho$, Eq. (11.5) becomes

$$v = r\omega^2 \frac{1}{2\kappa} (h^2 - y^2). \quad (11.6)$$

Assuming that the rotational velocity is constant and that the Coriolis force is negligible, the flow of the liquid is confined within a wedge-shaped portion as shown in Fig. 11.4(c). The space velocity V (cm^3/s) of the liquid passing through the cross section of the wedge at the distance r , indicated by the hatching in Fig. 11.4(c) is calculated from Eq. (11.6) as

$$V = r\theta \int_0^h v dy = r^2\theta \frac{\omega^2}{3\kappa} h^3, \quad (11.7)$$

where θ is the wedge angle.

The equation of volume balance in the flow is expressed as

$$r\theta dr \frac{\partial h}{\partial t} = - \frac{\partial V}{\partial r} dr, \quad (11.8)$$

where t is the time.

By using Eqs. (11.7) and (11.8), we obtain the central equation governing spin coating:

$$\frac{\partial h}{\partial t} = - \frac{\omega^2}{3\kappa} \left(2h^3 + 3rh^2 \frac{\partial h}{\partial r} \right). \quad (11.9)$$

Solving Eq. (11.9) under a given initial condition yields the liquid film thickness h at a distance r from the rotation axis at a time t .

Consider the case where the initial film thickness is uniform, that is,

$$h = h_0 = \text{const at } t = 0. \quad (11.10)$$

The last term on the right-hand side of Eq. (11.9) vanishes, and the equation becomes independent of r , yielding an analytical solution of the form:

$$\frac{1}{h^2} = \frac{1}{h_0^2} + \frac{4\omega^2}{3\kappa} t. \quad (11.11)$$

Equation (11.11) shows that the film thickness decreases uniformly with increasing time.

Next, we consider the general case where the initial film thickness varies along the radial direction. Under this case, Eq. (11.9) cannot be solved analytically.

However, numerical calculation shows that the solution approaches very rapidly to a solution with uniform film thickness. Thus, it can be concluded that a spin-coating process using a Newtonian resist solution produces a uniform film thickness regardless of the initial film thickness profile.¹⁹

It should be pointed out, however, that Eq. (11.3) assumes Newtonian behavior, which the complex polymeric resists and BARC fluids do not necessarily exhibit. In particular, mass is not lost, neither from the radial flow of material nor from evaporation of solvent. Meyerhofer²⁰ considered the effects of evaporation on the final film thickness. He reported that the final solid film thickness is inversely proportional to the square root of the rotational velocity. He also developed a model similar to that considered above, but allowed the solvent to evaporate during the spinning process. His central assumption was that the thinning process could be divided into two major stages, namely, one dominated by radial flow outward and another by evaporation of solvent. Effectively, he assumed a constant rate of evaporation and the viscosity concentration relationship expressed as

$$\eta = \eta_{\text{solvent}} + \eta_{\text{solid}}c^\gamma, \quad (11.12)$$

where c is the concentration of the solid and γ has a value around 2.5.

Flack and co-workers²¹ developed a complex model that included the effects of evaporation on the rheological properties of the viscous fluid. Their work established the idea that only fluid viscosity, angular speed, and evaporative effects are important in determining the final film thickness. Dispense volume, dispense rate, and other factors seem not to be particularly critical in determining the final film thickness as long as the wafer is spun for a sufficiently long time. Yet, in spite of evaporative effects, the final thickness h_f of the fluid can be fairly well predicted with an inverse power law relationship [Eq. (11.13)], where C is a constant depending on the viscosity and contains the effects of viscous forces,

$$h_f = C\omega^{-N}. \quad (11.13)$$

The exponent N indicates how inversely related the thickness is to spin speed. Most common fluids behave in a Newtonian manner, with $N = 1/2$. Evaporation may also affect the value of N . Taking the logarithm of both sides of Eq. (11.13) and rearranging yields a linear equation, which can be easily plotted to determine C and N ,

$$\log(h_f) = -N\log(\omega) + \log(C). \quad (11.14)$$

¹⁹S. Nonogaki, T. Ueno, and T. Ito, *Microlithography Fundamentals in Semiconductor Devices and Fabrication Technology*, Chapter 5, Marcel Dekker, New York (1998).

²⁰D. Meyerhofer, "Characteristics of resist films produced by spinning," *J. Appl. Phys.* **49**, 3393–3997 (1978).

²¹W.W. Flack, D.S. Soong, A. Bell, and D.W. Hess, "A mathematical model for spin coating of polymer resists," *J. Appl. Phys.* **56**, 1199–1205 (1984).

11.4 Characterizing Ultrathin Resist Processes

The comprehensive characterization of ultrathin resist (UTR) (≤ 100 nm) processes in terms of defectivity,²² manufacturability,²³ and physical properties (structure, dynamics, stability, thermodynamic behavior, etc.)²⁴ have been a central point of interest in semiconductor microlithography for quite some time. Despite many years of experimental and theoretical efforts along these lines, a number of basic questions still remain to be answered. One of these issues is the fundamental lower physical limit of the resist thickness, below which lithographic patterning is not viable. For resists based on the polyhydroxy styrene platform, this lower limit has been determined to be around 60 nm, with the onset of film instability occurring at around 55 nm.²⁵ For a host of other resist platforms, this lower limit is yet to be determined.

This lower limit of UTR film thickness is of great importance in microlithography, particularly as the critical dimensions required for manufacturing semiconductor devices continue to shrink toward the length scale of individual macromolecules. Because of the considerable optical absorption of conventional resist materials, particularly at 157 nm and 13.5 nm, UTR processes where imaging is confined to a very thin layer (≤ 100 nm) of the resist are promising options for implementing these lithographies. Another consideration for using UTR processes is the reduction of the feature aspect ratio as a way of mitigating pattern collapse associated with high aspect ratios.

In spite of the above-mentioned advantages of UTR processes, practical considerations often impose a choice of resist and substrate that are not fully compatible, resulting in films that are unstable or metastable with finite relaxation time. While thick films (> 300 nm) may be stable or metastable due to gravity,²⁶ for thin films (≤ 100 nm) intermolecular and surface forces dominate.²⁷ UTR films are susceptible to both spontaneous thin-film instabilities due to London–van der

²²S.W.J. Kuan, C.W. Frank, Y.H. Yen Lee, T. Eimori, D.R. Allee, R.F. Pease, and R. Browning, "Ultrathin polymer films for microlithography," *J. Vac. Sci. Technol. B* **6**(6), 2274 (1988); K.P. Muller and H.S. Sachdev, "Defect studies on single and bilayer resist systems," *J. Vac. Sci. Technol. B* **10**, 2560 (1992); K.E. Early, D.M. Tennant, D.Y. Jeon, P.P. Mulgrew, A.A. MacDowell, O.R. Wood II, G.D. Kubiak, and D.A. Tichenor, "Characterization of AZ PN114 resist for soft x ray projection lithography," *Appl. Opt.* **32**(34), 7044 (1993); U. Okoroanyanwu, J. Cobb, P. Dentinger, P.C. Henderson, V. Rao, and C. Pike, "Defects and metrology of ultrathin resist films," *Proc. SPIE* **3998**, 515 (2000).

²³K.B. Nguyen, C. Lyons, J. Schefske, S. Bell, H.J. Levinson, and U. Okoroanyanwu, "Characterization of the manufacturability of ultrathin resist," *J. Vac. Sci. Technol. B* **17**(6), 3039 (1999).

²⁴U. Okoroanyanwu, "Thin film instabilities and implications for ultra thin resist process" *J. Vac. Sci. Technol. B* **18**(6), 3381–3387 (2000); U. Okoroanyanwu, "Limits of ultra thin resist process" *Future Fab. Int.* **10**, 157–163 (2001).

²⁵ibid.

²⁶P. G. de Gennes, "Wetting: statics and dynamics," *Rev. Mod. Phys.* **57**, 827 (1985); F. Brochard, C. Redon, and F.C.R. Rondelez, "Démouillage : régime de gravité," *Acad. Sci., Ser. 2* **306**, 1143 (1988).

²⁷J.N. Israelachvili, *Intermolecular and Surface Forces*, Academic Press, London (1985).

Waals interactions and defects caused by substrate imperfections (topographical features such as pits or mounds).²⁸

Because UTR films have a higher surface-to-volume ratio than their thicker counterparts for any given feature size, they are highly interfacial. Each macromolecular component of a UTR system is close to an interface, either the solid substrate or the free surface interface. In the most extreme case, each macromolecule is confined within the solid interface and the free surface. Consequently, ultrathin film material properties may be quite different from those of the bulk. In particular, the glass transition temperature (T_g) may be depressed or elevated by as much as 40°C relative to the bulk values, depending on the film thickness and the chemical nature of the solid substrate on which the film is deposited.²⁹ This may affect the viscoelastic response of the film during subsequent thermal annealing. The interfacial properties of such polymer-inorganic interfaces often determine their lithographic performance and consequently the performance of devices fabricated with them.

Establishing the lower thickness limit of UTR films, and understanding and controlling the causes of defects associated with such films, are major challenges for the near-term development of UTR process technology. It is difficult to produce ultrathin films that are uniform, continuous, defect free, and stable to changes in shape after aging or thermal processing. These issues together determine the lower thickness limit of a given UTR film below which lithography is not viable.

11.4.1 Instabilities in ultrathin resist films

Instabilities in UTR polymer films are manifested in two main ways, namely, (i) defects resulting from the coating process, substrate nonuniformities, and conjoining pressure, and (ii) discontinuities in the thermophysical properties of the films due to interfacial effects and polymer cooperative and surface dynamics.

11.4.2 Spin coating and instabilities in ultrathin resist films

Consider the spin-coating process, in which centrifugal forces cause the spreading of fluids against viscous resistance. There are at least three definable stages in the process of flow and coating of substrates: movement of the contact line across the substrate, thinning of the film in the liquid state, and curing of the final film. Defects and pinholes can form in all three steps.³⁰ During spin coating, topographical

²⁸T.G. Stange, R. Mathews, D.F. Evans, and W.A. Hendrickson, "Scanning tunneling microscopy and atomic force microscopy characterization of polystyrene spin coated onto silicon surfaces," *Langmuir* **8**, 920 (1992).

²⁹O. Prucker, S. Christian, H. Bock, J. Ruehe, C.W. Frank, and W. Knoll, "On the glass transition in ultrathin polymer films of different molecular architecture," *Macromol. Chem. Phys.* **199**, 1435 (1998); J.N.D'Amour, C.W. Frank, and U. Okoroanyanwu, "Influence of substrate chemistry on the properties of ultra thin polymer films," *Microelectron. Eng.* **73** **74**, 209 217 (2004).

³⁰S. Kalliadasis, C. Bielarz, and G.M. Homsy, "Steady free surface thin film flows over topography," *Phys. Fluids* **12**, 1889 1898 (2000).

features such as crystal-originated pits (COPs) can give rise to pressure-driven ridges, which lead to film instabilities, which in turn lead to dewetting and the formation of pinholes.

Van der Waals forces dominate in determining film stability³¹ of ultrathin films spin coated on nonwetting substrates (“nonwetting” in the sense that a drop of the solution makes a finite contact angle on being placed on the substrate³²). Such films can become unstable, and dewetting can occur. Experimental and theoretical studies suggest that dewetting begins with a nucleation event leading to the formation of a dry patch.³³ The hole grows by transport of material away from the nucleation site to a retreating rim surrounding the hole. As a hole grows, it eventually impinges on adjacent holes, resulting in the formation of ribbons of material along their contact line. Complete dewetting occurs when all holes have coalesced, forming polygons composed of isolated droplets of materials.

For spin-coated ultrathin films, nucleation occurs by a spinodal decomposition phenomena³⁴ or by airborne particles falling on the surface of the film.³⁵ Spinodal decomposition proceeds by amplification of surface disturbances on the free surface of the film due to thermal fluctuations or mechanical vibrations. Conjoining forces overwhelm the tendency for surface tension to level the film, thus driving the growth of the surface modulations until they reach the substrate to nucleate a hole.

11.4.3 Hydrodynamics of ultrathin resist films

The dynamic model of thin-film instabilities has been described in detail elsewhere;³⁶ we briefly summarize the relevant facts here. For an ultrathin film of mean thickness, $h_0 < 100$ nm, with a gas above and a solid substrate beneath, the following is the appropriate film profile equation for film thickness $h(x, t)$, assuming (i) a quadratic velocity profile, (ii) no-slip condition at the solid surface, and

³¹H.S. Khesghi and L.E. Scriven, “Dewetting: Nucleation and growth of dry regions,” *Chem. Eng. Sci.* **46**, 519 (1991).

³²W. Adamson and A.P. Gast, *Physical Chemistry of Surfaces*, 6th ed., John Wiley & Sons, Hoboken, NJ (1997).

³³H.S. Khesghi and L.E. Scriven, “Dewetting: Nucleation and growth of dry regions,” *Chem. Eng. Sci.* **46**, 519 (1991); A. Sharma, “Relationship of thin film stability and morphology to macroscopic parameters of wetting in the apolar and polar systems,” *Langmuir* **9**, 861 (1993); G. Reiter, “Unstable thin polymer films: rupture and dewetting processes,” *Langmuir* **9**, 1344 (1993); C. Redon, F. Brochard Wyart, and F. Rondelez, “Dynamics of dewetting,” *Phys. Rev. Lett.* **66**, 715 (1991).

³⁴F. Brochard Wyart and J. Daillant, “Drying of solids wetted by thin liquid films,” *Can. J. Phys.* **68**, 1084 (1990).

³⁵A. Sharma and E. Ruckenstein, “Dewetting of solids by the formation of holes in macroscopic liquid films,” *J. Colloid Interface Sci.* **133**, 358 (1989); G.I. Taylor and D.H. Michael, “On making holes in a sheet of fluid,” *J. Fluid Mech.* **58**, 625 (1973).

³⁶G.F. Teletzke, L.E. Scriven, and H.T. Davis, “How liquids spread on solids,” *Chem. Eng. Commun.* **55**, 41 (1987).

(iii) no shear condition at the free surface:

$$\frac{\partial h(x, t)}{\partial t} = \frac{\partial}{\partial x} \left[\frac{h^3}{3\eta} \frac{\partial}{\partial x} \left(-\gamma \frac{\partial^2 h}{\partial x^2} - \frac{A}{6\pi h^3} \right) \right], \quad (11.15)$$

where η is the liquid viscosity, A is the Hamaker constant, γ is the surface tension, x is a coordinate parallel to the surface, and t is time. Perturbations of the surface induce a pressure gradient associated with Laplace pressure P_L ³⁷ [Eq. (11.16)] and disjoining pressure Π ³⁸ [Eq. (11.17)]:

$$P_L = \gamma \left[\frac{d^2 h(x, t)}{dx^2} \right], \quad (11.16)$$

$$\Pi = - \left(\frac{A}{6\pi h^3} \right). \quad (11.17)$$

Such perturbations can be schematically described as modulations of the liquid free surface of the form³⁹

$$h(x, t) = h_0 + ue^{st+iqx}, \quad (11.18)$$

with amplitude u , wave number q , and frequency of disturbance s . Linear stability analysis gives the dispersion relation:

$$\frac{1}{\tau} = s = \frac{q^2}{\eta} \left[-\gamma q^2 h_0^3 + \frac{A}{2\pi h_0} \right], \quad (11.19)$$

where τ is the time constant that describes the time scale for the disturbance to grow or decay. The dispersion relationship yields the critical wave number q_c [Eq. (11.20)], which defines the stable and unstable regions of spatial frequencies. The critical wave number increases at the rate $1/h_0^2$ as the film thickness h_0 decreases, suggesting that an increasing region of spatial frequencies will be susceptible to film instabilities:

$$q_c = \frac{1}{h_0^2} \sqrt{\frac{A}{2\pi\gamma}}. \quad (11.20)$$

For $q < q_c$, $(A/2\pi h_0 > \gamma q^2 h_0^3)$, τ is positive, and surface disturbances are amplified exponentially. These disturbances can continue to grow, eventually reaching the substrate and nucleating a hole. The minimum time constant τ_{\min}

³⁷A. Sharma and E. Ruckenstein, "Dewetting of solids by the formation of holes in macroscopic liquid films," *J. Colloid Interface Sci.* **133**, 358 (1989); G.I. Taylor and D.H. Michael, "On making holes in a sheet of fluid," *J. Fluid Mech.* **58**, 625 (1973).

³⁸B.V. Derjaguin, *Kollid. Zh.* **17**, 191 (1955); B.V. Derjaguin, N.V. Churaev, and V.M. Muller, *Surface Forces*, Consultants Bureau, New York (1987).

³⁹A. Sharma and E. Ruckenstein, "Dewetting of solids by the formation of holes in macroscopic liquid films," *J. Colloid Interface Sci.* **133**, 358 (1989); G.I. Taylor and D.H. Michael, "On making holes in a sheet of fluid," *J. Fluid Mech.* **58**, 625 (1973).

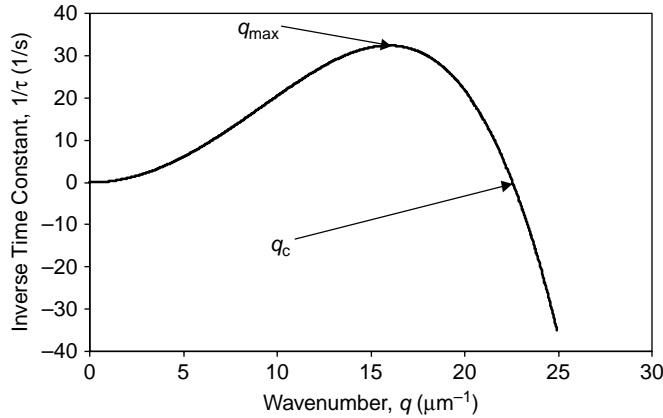


Figure 11.5 Thin-film stability dispersion curve of polystyrene film ($A = 8 \times 10^{-20}$ J, $\gamma = 40 \times 10^{-3}$ J/m²).

for unstable growth is given by Eq. (11.21) and occurs at $q = q_{\max}$, for which the rate of the disturbance growth is a maximum (see Fig. 11.5):

$$\tau_{\min} = \frac{4^2 \pi^2 \eta h_0^5 \gamma}{A^2}. \quad (11.21)$$

q_{\max} is related to q_c as

$$q_c = \sqrt{2} q_{\max}. \quad (11.22)$$

This indicates that disturbances in the frequency band below q_c will grow more rapidly as h_0 shrinks. As long as τ_{\min} is much smaller than the time required for resist spinning, drying, and curing, disturbances will grow exponentially and rupture the film before it has a chance to solidify. This also suggests that the number of pinhole-type defects in UTR films may scale with $1/h_0^2$.

11.4.4 Instabilities and thermophysical properties of ultrathin resist films

Instabilities in UTR films can also be manifested as discontinuities in the thermophysical properties of the films due to interfacial effects and polymer cooperative and surface dynamics. Polymer surfaces are regions of enhanced molecular mobility as compared to the bulk, given the decreased constraints on macromolecules at a free surface. The orientation of the surface groups is affected by the nature of the interfacing environment. This implies that polymeric surfaces can restructure (in terms of orientation of surface functionalities, concentration of surface groups, etc.) in response to a change in the interfacial phase, in order to adjust their surface properties to the properties of the interfacial medium.⁴⁰

Synthetic polymers exhibit substantial dependence of their mechanical, thermal, optical, and electrical properties on chemical composition, processing

⁴⁰F. Garbassi, M. Morra, and E. Ochiello, *Polymer Surfaces: From Physics to Technology*, 2nd ed.; John Wiley & Sons, Hoboken, NJ (1998).

protocol, and morphological structure. Typically, bulk physical properties depend on the macromolecular nature of the material; the characteristic molecular dimension is the radius of gyration R_g , which is proportional to the square root of the molecular weight. The picture of polymers as amorphous solids, first proposed by P.J. Flory in 1953 and subsequently verified by neutron scattering, is well accepted for the bulk state, but inaccurate for polymer films of constrained geometry, such as those whose film thickness is comparable to a small multiple of R_g .⁴¹

These results suggest that material properties of UTR films can differ in significant ways from their bulk counterparts. For example, physical properties such as the degree of crystallinity⁴² cannot only be different in the ultrathin-film state, but these properties become increasingly sensitive to film thickness, substrate surface energy, and local ordering into nonhomogeneous and structured phases. Of particular interest, because of its influence on the viscoelastic behavior of the spin-coated film, is the effect of film thickness on T_g . A variety of experimental methods, including spectroscopic ellipsometry,⁴³ x-ray reflectometry,⁴⁴ positron annihilation lifetime spectroscopy,⁴⁵ and Brillouin scattering,⁴⁶ have shown that T_g depends on film thickness and on the chemical nature of the polymer-substrate interaction. For noninteracting substrates, e.g., a hydrophobic polymer on a hydrophobic substrate, the T_g value can be depressed by as much as 40°C.⁴⁷ For moderately strongly interacting substrates, e.g., an oxide surface interacting with a polymer capable of hydrogen bonding, the T_g value can be elevated by a comparable amount.⁴⁸ Figure 11.6 shows T_g values for polystyrene film on a variety of substrates, including silicon with native oxide, evaporated gold on silicon, and a self-assembled monolayer (SAM) of 1-mercapto hexadecanoic acid. All of the films exhibited a depression in T_g with decreasing film thickness. Films on silicon substrates showed the least T_g depression with decreasing film thickness, while polystyrene film on the SAM showed the greatest drop in T_g , 12.5°C.⁴⁹

⁴¹For a general review, see, for example, I.C. Sanchez, Ed., *Physics of Polymer Surfaces and Interfaces*, Butterworth Heinemann (1992).

⁴²M.M. Despotopoulou, R.D. Miller, J.F. Rabolt, and C.W. Frank, "Polymer chain organization and orientation in ultrathin films: A spectroscopic investigation," *J. Polym. Sci.: Pt. B* **34**, 2335 (1996); C.W. Frank, Stanford University, Private Communication (2001).

⁴³J.L. Keddie, R.A.L. Jones, and R.A. Coury, "Size dependent depression of the glass transition temperature in polymer films," *Europhys. Lett.* **27**, 49 (1994).

⁴⁴J.H. van Zanten, W.E. Wallace, and W.L. Wu, "Effect of strongly favorable substrate interactions on the thermal properties of ultrathin polymer films," *Phys. Rev. E* **53**, R2053 (1996).

⁴⁵G.B. DeMaggio, W.E. Frieze, D.W. Gidley, M. Zhu, H.A. Hristov, and A.F. Yee, "Interface and surface effects on the glass transition in thin polystyrene films," *Phys. Rev. Lett.* **78**, 1524 (1997).

⁴⁶D.B. Hall, J.C. Hooker, and J.M. Torkelson, "Ultrathin polymer films near the glass transition: Effect on the distribution of α relaxation times as measured by second harmonic generation," *Macromolecules* **30**, 667 (1997).

⁴⁷O. Prucker, S. Christian, H. Bock, J. Ruehe, C.W. Frank, and W. Knoll, "On the glass transition in ultrathin polymer films of different molecular architecture," *Macromol. Chem. Phys.* **199**, 1435 (1998).

⁴⁸J.A. Torres, P.F. Nealey, and J.J. de Pablo, "Molecular simulation of ultrathin polymeric films near the glass transition," *Phys. Rev. Lett.* **85**, 3221 (2000).

⁴⁹J.N. D'Amour, C.W. Frank, and U. Okoroanyanwu, "Influence of substrate chemistry on the properties of ultra thin polymer films," *Microelectron. Eng.* **73** **74**, 209 217 (2004).

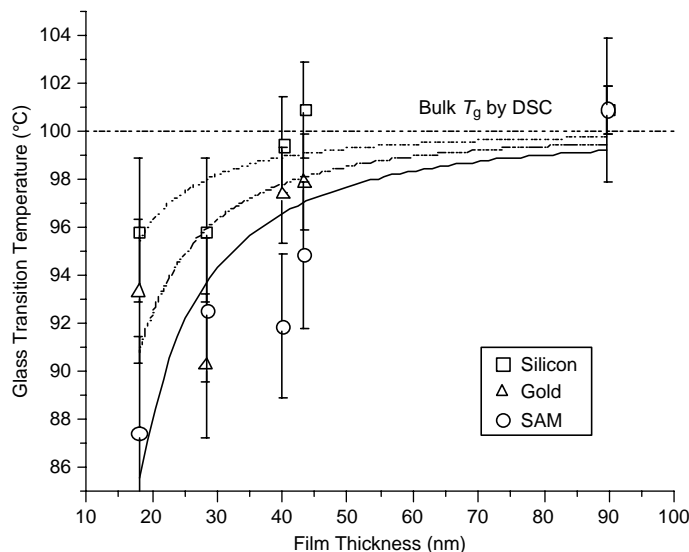


Figure 11.6 The glass transition temperature as a function of film thickness of polystyrene films on silicon, gold, and SAM surfaces. (Reprinted with permission from Ref. 50. © 2004 Elsevier.)

Practical consequences of T_g modification include significant changes to dissolution and etching characteristics, mechanical creep behavior, and adhesion. For example, dissolution rate measurements of spin-coated films of poly(3-methyl-4-hydroxystyrene), a common matrix resin in chemically amplified resists used in DUV lithography, showed dramatic reduction in the diffusion coefficient of the basic developing solution in the region close to the native silicon oxide surface of the solid substrate.⁵¹ This was attributed to enhancement of the hydrogen bonding network due to chain orientation effects. In addition, the interaction of the first few hundred angstroms of the film with the substrate determines its adhesion and can alter its electrical and optical properties, as well as its topographical and surface characteristics.⁵²

A three-layer model was found by the author⁵³ to describe adequately a Shipley's phenolic XP-98248 resist, a commercially available environmentally stable chemically amplified photoresist (ESCAP) film, thus suggesting the presence of three distinct layers for each film: film-substrate interface layer, bulk layer, and surface layer. This three-layer model is consistent with the results of

⁵⁰ibid.

⁵¹C.W. Frank, V. Rao, M.M. Despotopoulou, R.F.W. Pease, W.D. Hinsberg, R.D. Miller, and J.F. Rabolt, "Structure in thin and ultrathin spin cast polymer films," *Science* **273**, 912 (1996).

⁵²L.B. Rothman, "Properties of thin polyimide films," *J. Electrochem. Soc.* **127**, 2216 (1980); M.M. Despotopoulou, R.D. Miller, J.F. Rabolt, and C.W. Frank, "Polymer chain organization and orientation in ultrathin films: A spectroscopic investigation," *J. Polym. Sci.: Pt. B* **34**, 2335 (1996).

⁵³U. Okoroanyanwu, "Thin film instabilities and implications for ultra thin resist processes" *J. Vac. Sci. Technol. B* **18**(6), 3381–3387(2000); U. Okoroanyanwu, "Limits of ultra thin resist processes" *Future Fab. Int.* **10**, pp. 157–163 (2001).

molecular dynamics simulation obtained by Torres et al.,⁵⁴ in which they were able to reveal the existence of low- or high-mobility layers near the substrate or near the air interface by changing the intermolecular potentials acting between the polymer segments and the interface. Also, this experimentally determined three-layer model validates the layer model proposed by Forrest and Mattson⁵⁵ to describe the behavior of T_g in thin polystyrene films in terms of length scales for cooperative dynamics. They considered the film to have a region near the free surface with enhanced mobility (and lower T_g) than the bulk and a region near the substrate with reduced mobility and with a slightly higher T_g than the surface region.

The x-ray reflectivity (XRR) profiles of the films characterized by Okoroanyanwu (see Fig. 11.7)⁵⁶ can be categorized into two different groups: high- and

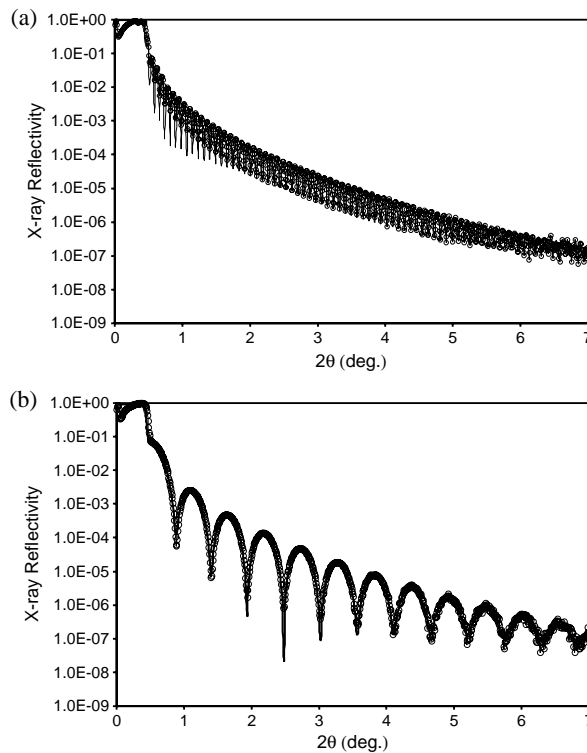


Figure 11.7 (a) X-ray reflectivity profile of 100-nm-thick film. (b) X-ray reflectivity profile of 12.6-nm-thick film. Circles are the experimental data, while the line in each graph represents the model fit. The resist used was Shipley XP-98248 resist.

⁵⁴J.A. Torres, P.F. Nealey, and J.J. de Pablo, "Molecular simulation of ultrathin polymeric films near the glass transition," *Phys. Rev. Lett.* **85**, 3221 (2000).

⁵⁵J.A. Forrest and J. Mattson, "Reductions of the glass transition temperature in thin polymer films: Probing the length scale of cooperative dynamics," *Phys. Rev. E*, **61**, R53 (1999).

⁵⁶U. Okoroanyanwu, "Thin film instabilities and implications for ultra thin resist processes" *J. Vac. Sci. Technol. B* **18**(6), 3381–3387 (2000); U. Okoroanyanwu, "Limits of ultra thin resist processes" *Future Fab. Int.* **10**, 157–163 (2001).

low-reflectivity oscillation fringe groups. The apparent differences are caused by differences in the density of the film-substrate interface layer and the surface layer. On average, weak reflectance fringes were obtained for the film-substrate interface layer in comparison to the bulk and surface layers, suggesting that the interface layer has lower density than the bulk and surface layers. This may also suggest weak adhesion or partial delamination in the film-substrate interface layer, particularly at total film thickness < 53 nm. Variations in the roughness of the surface layer do not appear to change the reflectance fringe amplitude. The “roughness” figures for the film-substrate interface and the bulk layers show rather large values (compared to the surface layer); they represent a density gradient rather than an interface roughness. Bulk film density shows no significant dependence on thickness.⁵⁷

Figure 11.8 shows the thickness of each of the three layers observed by Okoroanyanwu⁵⁸ as a function of total film thickness. The surface layer and substrate-film interfacial layer thickness remain practically constant at roughly ≤ 2 nm for a total film thickness ≥ 30 nm, below which the surface layer thickness increases significantly to ~ 5 nm (nearly 30% of the total film thickness) at total film thickness ~ 16 nm. The ~ 2 -nm thickness of the surface layer is in excellent agreement with the cooperativity length scale in the 2.5–3.5-nm range for polystyrene estimated by Donth⁵⁹ and the 2.5–5.0-nm range estimated by Forest and Mattson.⁶⁰ Since this film-substrate interfacial layer is affected directly by a combination of chain packing constraints and short-range attraction between the substrate and the segments of the polymer, its size will be determined by the persistence length of the polymer. The ~ 2 -nm thickness of the film-substrate interfacial layer is again in excellent agreement with the 2.7 nm reported by Forest and Mattson⁶¹ for polystyrene.

Figure 11.9 shows film density as a function of total film thickness of XP-98248 resist as determined by fitting the XRR data. In the 53–100-nm total film thickness range, the density of the three layers is relatively uniform, with bulk layer density (~ 1.3 g/cm³) greater than that of the surface layer (~ 0.9 – 1.2 g/cm³) and the film-substrate interface layer (~ 0.9 g/cm³). While the density of the bulk layer remains relatively uniform in the 16–100-nm total film thickness range, that of the surface and film-substrate interface layers show significant fluctuations below 53 nm, suggesting the influence of polymer cooperative and surface dynamics on the surface layer and the influence of substrate-film interaction due perhaps to polymer chain packing constraints and short-range attraction between the substrate and the monomeric units of the polymer in this region of

⁵⁷ibid.

⁵⁸ibid.

⁵⁹E. Donth, “Characteristic length of the glass transition,” *J. Polym. Sci., Part B* **34**, 2881 (1996).

⁶⁰J.A. Forrest and J. Mattson, “Reductions of the glass transition temperature in thin polymer films: Probing the length scale of cooperative dynamics,” *Phys. Rev. E* **61**, R53 (1999).

⁶¹ibid.

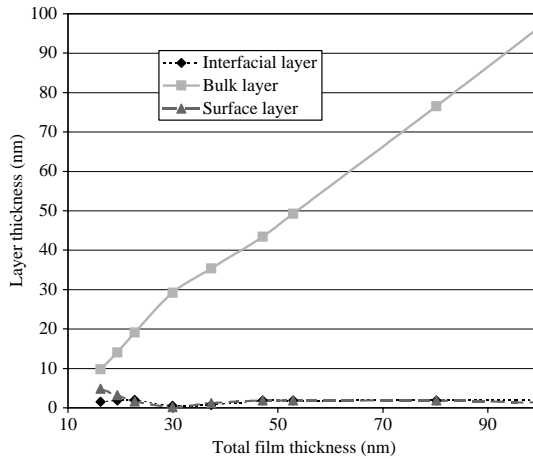


Figure 11.8 Film layer thickness as a function of specific layer thickness. The resist used was Shipley XP-98248 resist. The total film thickness is the sum of the thickness of the film-substrate interfacial, bulk, and surface layers.⁶²

the film. These also suggest the onset of thin-film instabilities in this thickness range.⁶³

Figure 11.10 shows a plot of film layer roughness as a function of total film thickness of XP-98248 resist as determined by fitting the XRR data. While

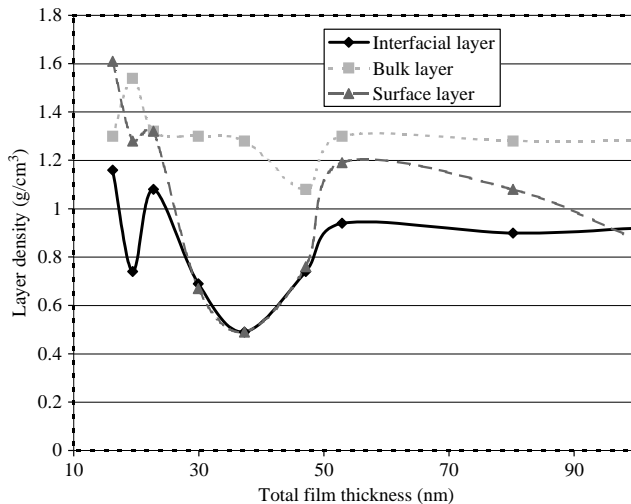


Figure 11.9 Film layer density as a function of total film thickness as determined by x-ray reflectivity. The resist used was Shipley XP-98248 resist.⁶⁴

⁶²U. Okoroanyanwu, “Thin film instabilities and implications for ultra thin resist processes” *J. Vac. Sci. Technol. B* **18**(6), 3381–3387 (2000); U. Okoroanyanwu, “Limits of ultra thin resist processes” *Future Fab. Int.* **10**, 157–163 (2001).

⁶³ibid.

⁶⁴ibid.

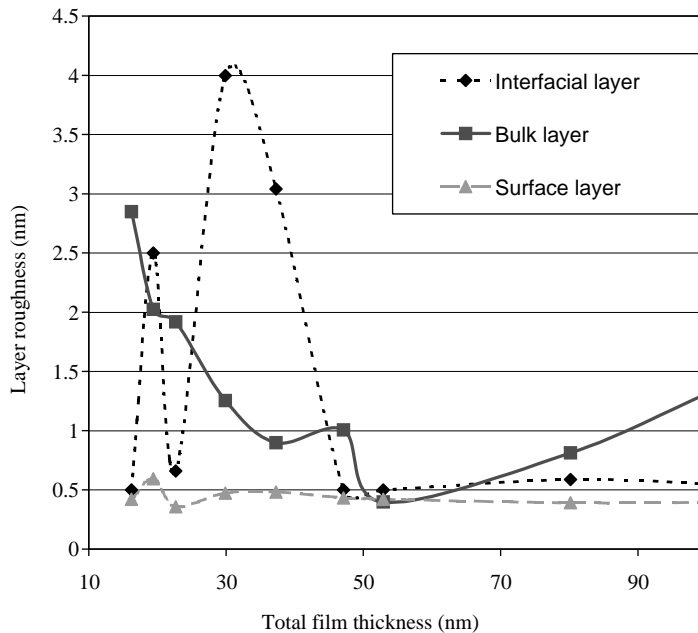


Figure 11.10 Film layer roughness as a function of total film thickness as determined by x-ray reflectivity. The resist used was Shipley XP-98248 resist.⁶⁵

the surface layer is relatively smooth (roughness measured by XRR was ~ 0.4 – 0.5 nm, compared to the ~ 0.2 – 0.3 -nm RMS value obtained with the AFM) through the total film thickness range 16–100 nm, that of the interface between the bulk and surface layer shows significant fluctuations between (~ 0.4 – 2.7 nm) within this thickness range. The film-substrate interface layer, on the other hand, is smooth (roughness ~ 0.5 nm) in the 47–100-nm total film thickness range, below which it shows significant roughness of up to 4.0 nm at a thickness of 30 nm. This result indicates the influence of film-substrate interfacial effects and, consequently, thin-film instabilities.⁶⁶

11.4.5 Ultrathin films and defectivity

Typical examples of UTR defects are shown in Fig. 11.11. The defects are categorized into four types, namely, COPs (associated with substrate imperfections), bubbles (associated with trapped gas), particles, and “fall-on particles” (the last two being associated with discrete particles of various sizes and origins). Bursting of bubbles of the kind shown in Fig. 11.11 will result in holes in the film (see Fig. 11.12).

⁶⁵ibid.

⁶⁶ibid.

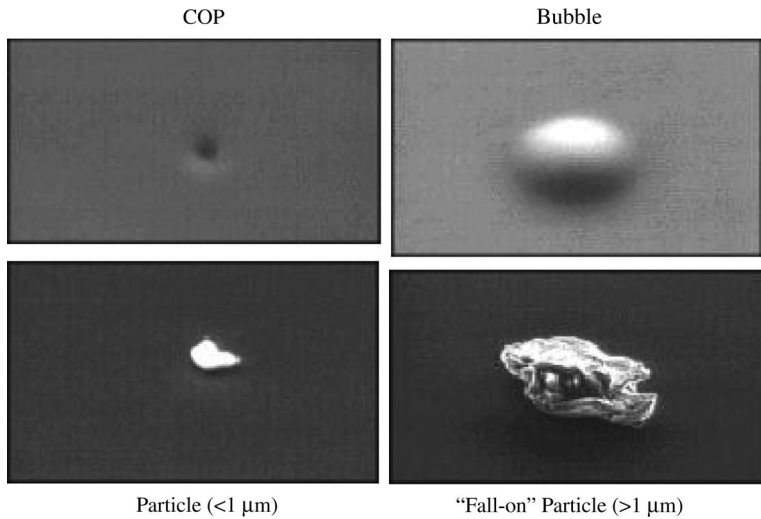


Figure 11.11 SEM review showing four defect classes identified in UTR film of Shipley UV6 and XP-98248 resists.⁶⁷

Other investigators reported pinhole defect density data that scale roughly with the inverse of the square of the film thickness,⁶⁸ which can be derived from dynamic arguments,⁶⁹ as was shown in Eq. (11.20). Spinodal decomposition dominates the nucleation process under clean room conditions, while particle nucleation increases in higher aerosol concentration environments.⁷⁰

Given the enhanced surface mobility, which is a consequence of the decreased surface density, and hence increased free volume of UTR film surfaces relative to the bulk and that of the film-substrate interfacial region, the lithographic properties of UTR films are bound to be dominated by interfacial effects. The surface region of such films is usually saturated with water or other solvents that can act as plasticizers. Thus, the T_g value of the surface chains can be further lowered with

⁶⁷U. Okoroanyanwu, "Limits of ultra thin resist processes" *Future Fab. Int.* **10**, 157-163 (2001).

⁶⁸S.W.J. Kuan, C.W. Frank, C.C. Fu, D.R. Allee, P. Maccagno, R.F. Pease, "Ultrathin polymer films for microlithography," *J. Vac. Sci. Technol. B* **6**(6), 2274 (1988); K.P. Muller and H.S. Sachdev, "Defect studies on single and bilayer resist systems," *J. Vac. Sci. Technol. B* **10**, 2560 (1992); K.E. Early, D.M. Tennant, D.Y. Jeon, P.P. Mulgrew, A.A. MacDowell, O.R. Wood II, G.D. Kubiak, and D.A. Tichenor, "Characterization of AZ PN114 resist for soft x ray projection lithography," *Appl. Opt.* **32**(34), 7044 (1993).

⁶⁹G.F. Teletzke, L.E. Scriven, and H.T. Davis, "How liquids spread on solids," *Chem. Eng. Commun.* **55**, 41 (1987); B.V. Derjaguin, *Kollid. Zh.* **17**, 191 (1955); B.V. Derjaguin, N.V. Churaev, and V.M. Muller, *Surface Forces*, Consultants Bureau, New York (1987); G. Reiter, "Dewetting of thin polymer films," *Phys. Rev. Lett.* **68**, 75 (1993).

⁷⁰T.G. Stange, R. Mathews, D.F. Evans, and W.A. Hendrickson, "Scanning tunneling microscopy and atomic force microscopy characterization of polystyrene spin coated onto silicon surfaces," *Langmuir* **8**, 920 (1992).

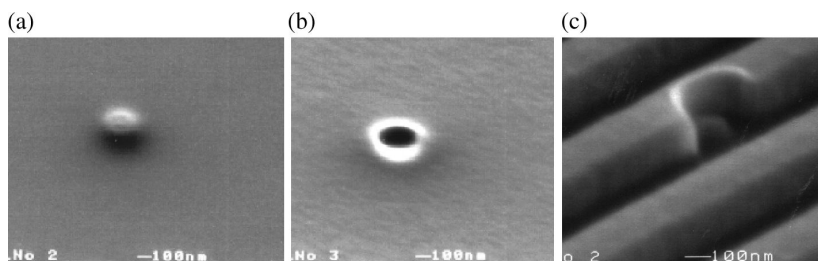


Figure 11.12 Evolution of a bubble defect formed at (a) resist coat, (b) through development, and (c) patterning with ASML PAS5500/300 KrF stepper. Unexposed resist loss for the UTR film was $\sim 6\text{--}10$ nm. The poly-Si patterns are 180-nm lines and spaces. Film thickness was ~ 100 nm.⁷¹

respect to the bulk chains.⁷² The differences between the surface and bulk properties of the UTR films can have significant influence on their dissolution, etching, and diffusional properties.⁷³

Figure 11.13 shows SEM images of line-and-space patterns printed with ~ 60 -nm-thick XP-98248 resist on bare silicon and exposed at 157 nm, highlighting the dominant influence of polymer cooperative and surface dynamics near the surface region and interfacial effects related to polymer packing constraints near the substrate region. Poor profiles such as these are also obtained when the same film is processed on antireflection coatings, implying that the poor lithographic performance of this UTR film cannot be solely due to the reflective swing effects from the silicon substrate. Significant undercutting suggests enhanced dissolution in the film-substrate interfacial region relative to the bulk layer. This is consistent with the XRR results obtained on a similar film of the same resist (see Fig. 11.9), which show the film-substrate interface layer to have a lower density than the bulk layer. It may also be related to polymer chain packing constraints and weak adhesion or even partial delamination between the polymer and the substrate. Lithographic patterning of such films present significant difficulties unless ways to mitigate or eliminate such instabilities, be it by manipulation of substrate energies, orientation effects, and/or temperature, are implemented.⁷⁴

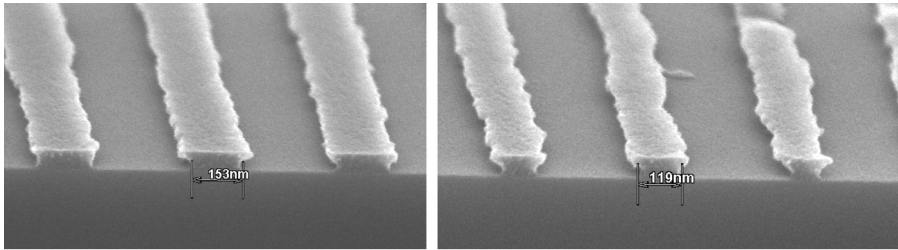
There may also be functional groups in the resist polymer film migrating back and forth on the surface and subsurface region, depending on the environmental conditions. Resist additives such as leveling agents, plasticizers, bases, PAGs, etc., can segregate and partition themselves at different layers of the film, driven by interfacial effects, which in turn are magnified as the film thickness decreases. The significant edge roughness in the resist patterns of Fig. 11.13 is

⁷¹ibid.

⁷²F. Garbassi, M. Morra, E. Ochiello, *Polymer Surfaces: From Physics to Technology*, 2nd ed., John Wiley & Sons, Hoboken, NJ (1998).

⁷³U. Okoroanyanwu, "Thin film instabilities and implications for ultra thin resist processes" *J. Vac. Sci. Technol. B* **18**(6), 3381–3387 (2000); U. Okoroanyanwu, "Limits of ultra thin resist processes" *Future Fab. Int.* **10**, 157–163 (2001).

⁷⁴ibid.



180-nm line-and-space features. 130-nm line-and-space features.

(Pitch = 1:1.5)

(Pitch = 1:2)

Figure 11.13 SEM images of line-and-space patterns printed with ~ 60 -nm-thick Shipley XP-98248 resist on bare silicon and exposed at 157 nm. Process conditions: postapplied bake $130^\circ\text{C}/60$ seconds, postexposure bake $130^\circ\text{C}/90$ seconds, developer 0.26N tetramethylammonium hydroxide (without surfactant) for 20 seconds. Unexposed resist loss ~ 6 nm. Exposure energy 1.35 mJ/cm². Note the significant surface inhibition layer, showing poisoning effects.⁷⁵

consistent with uneven distribution of these additives, particularly the PAG. Uneven distribution of the PAG in the film leads to nonuniform propagation of the chemical amplification reactions and related photochemical processes during the exposure and postexposure bake steps of the film. Eventually, this results in uneven dissolution of the film during the solvent development step. Such UTR films will have higher susceptibility to poisoning effects and unexposed film thickness loss than their thicker counterparts.⁷⁶

11.5 Soft Bake/Prebake

Following the spin coating of the resist on the wafer, the next processing step is the soft bake (also called prebake). The purpose of this bake is to densify the film and drive off residual solvent. Other consequences of soft baking include a reduction of free volume and polymer relaxation, which have been suggested to be useful in improving resist process performance.⁷⁷ The soft bake also improves adhesion of the resist to the substrate, promotes resist uniformity on the wafer, and aids in better line width control during etching.

Figures 11.14(a)–(d) show the mechanisms of different physical processes taking place during the first 10 seconds of soft baking a typical resist on a vacuum hot plate.⁷⁸ Figure 11.14(a) shows that the temperature of the wafer increases with an initial rapid rise during the first seconds of baking, before leveling off after three seconds. Figure 11.14(b) shows that the solvent loss during this time

⁷⁵ibid.

⁷⁶ibid.

⁷⁷P.J. Paniez, G. Festes, and J.P. Cholett, "Physical description of lithographic processes: correlation between bake conditions and photoresist contrast," *Proc. SPIE* **1672**, 623 (1992).

⁷⁸C.A. Mack et al., "Modeling of solvent evaporation effects for hot plate baking of photoresist," *Proc. SPIE* **2195**, 584 (1994).

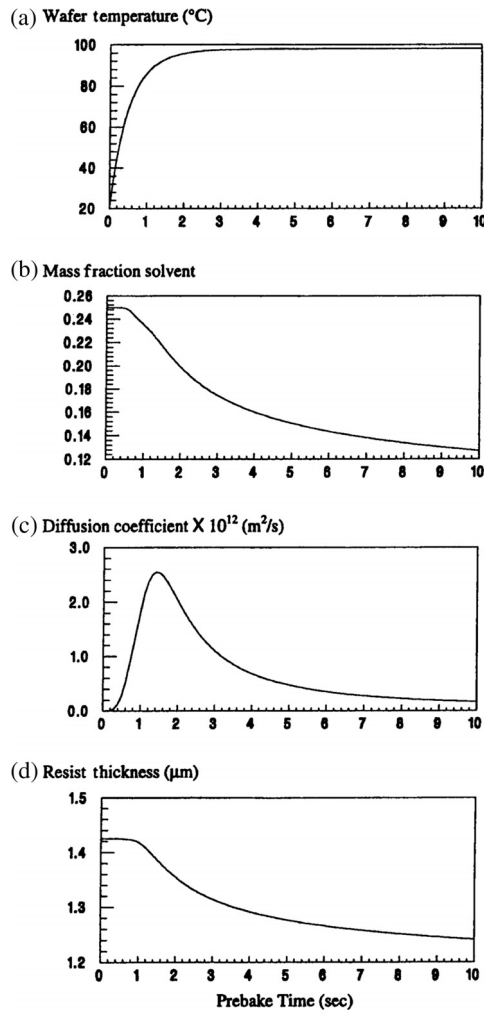


Figure 11.14 Mechanisms of different physical processes taking place during the first 10 seconds of soft baking of a resist: (a) rise in wafer temperature, (b) solvent loss, (c) diffusivity of solvent, and (d) thickness change.⁷⁹

continues to decrease well out to 10 seconds and beyond. Figure 11.14(c) shows the impact of baking time on diffusivity, which rises during the initial few seconds, reaching a maximum at about two seconds, before decreasing, and reaching a steady state at around eight seconds. Figure 11.14(d) shows a typical change in resist thickness during baking, which decreases as the resist density increases.

Typical soft bake temperatures are 90–120°C for 60 seconds on a hot plate, followed by a cooling step on a chill plate to achieve uniform wafer temperature control. The boiling points of most resist solvents are on the order of

⁷⁹ibid.

140°C, far higher than the soft bake temperatures of resists. Temperature control is important for soft baking processes, which become increasingly critical as the IC industry shifts the bulk of production to chemical amplification resists.⁸⁰ To achieve the stringent temperature uniformity specifications necessary for the tight CD control specifications for advanced semiconductor lithography, careful consideration of the vacuum hot plate design including uniform wafer-to-hot-plate contact, airflow, thermal management, and contamination control, is mandated.⁸¹

Even with prebaking, a considerable amount of solvent remains in the resist film⁸² (Fig. 11.15). A small percentage of residual solvent in the film is quite desirable for resists based on DNQ/novolac because it enhances water diffusion within the film, thus making it possible for water to participate in the conversion of ketene (an intermediate in the photolysis of DNQ) to indene carboxylic acid, which enhances the dissolution of the exposed part of the resist. In general, the chemical amplification resists based on poly(hydroxyl styrene) platform designed for 248-nm lithography have much lower residual solvent concentrations than DNQ/novolac films. The difference is due to the higher soft bake temperatures and lower film thickness of the 248-nm resists than their DNQ/novolac resist counterparts. Similar results are found for chemical amplification resists designed for 193-nm lithography as are found for their 248-nm counterparts.⁸³

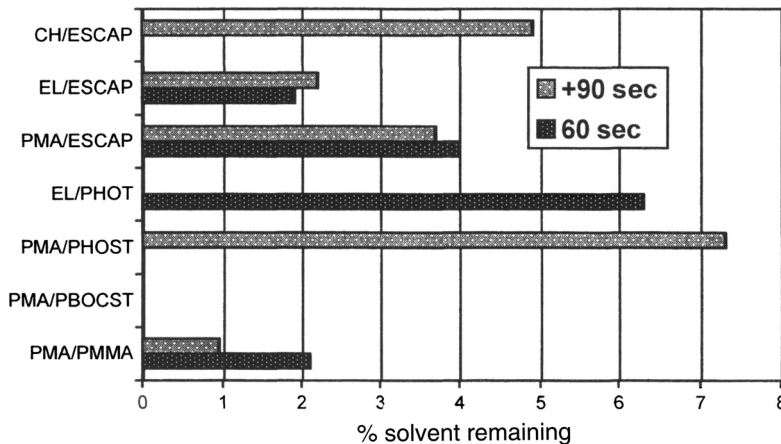


Figure 11.15 Solvent content of baked resist films. The resist films include ESCAP resin, PHOST resin, PBOCST resin, and PMMA resin. The solvents include cyclohexanone (CH), ethyl lactate (EL), and propylene glycol monomethylether acetate (PMA).⁸⁴

⁸⁰B.W. Smith, "Resist processing," in *Microolithography: Science and Technology*, p. 530, Marcel Dekker, New York (1998).

⁸¹ibid., p. 530.

⁸²H. Ito and M. Sherwood, "NMR analysis of chemically amplified resist films," *Proc. SPIE* **3678**, 104 115 (1999).

⁸³ibid.

⁸⁴ibid.

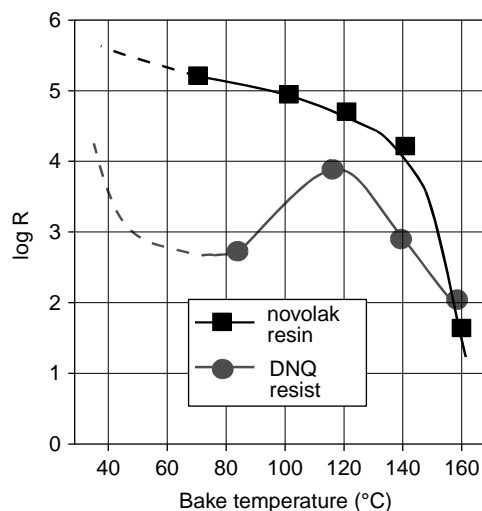


Figure 11.16 Effect of soft bake temperature on dissolution rates of novolak resin and exposed DNQ/novolak resist. (Reprinted with permission from American Chemical Society.⁸⁵)

The soft bake process can affect the solubility properties of some resists in the developing solvent. For instance, in DNQ/novolak resists, the solubility of the exposed resist as a function of prebake temperatures shows a maximum at around 120°C (Fig. 11.16).⁸⁶ Four zones can be distinguished in this plot: (i) a no-bake zone where residual solvent and dissolution rates are high, (ii) a low-temperature zone (up to 80°C) where the dissolution rate shows an appreciable decrease due to solvent removal, (iii) a mid-temperature zone (80–110°C) where the DNQ is thermally and preferentially converted to indene carboxylic acid, leading to an increase in dissolution rate, and (iv) a high-temperature zone (>120°C) where the film densification takes place, DNQ is thermally decomposed, the film is depleted of water, and the novolak resin is cross-linked, resulting in dramatic dissolution inhibition.⁸⁷

11.6 Alignment

Once the resist-coated wafer has been soft baked in the track system, it is cooled and sent into the wafer stage of the exposure tool. Resist processing equipment is commonly interfaced directly with an exposure tool, in which case the wafer

⁸⁵A.C. Ouano, in *Polymers in Microelectronics*, T. Davidson Ed., ACS Symp. Ser. 242, pp. 79–91, American Chemical Society, Washington, DC (1984).

⁸⁶ibid.

⁸⁷M. Koshiba, M. Murata, M. Matsui, and Y. Harita, "Thermally induced and base catalyzed reactions of naphthoquinone diazides," *Proc. SPIE* **920**, 364 (1988).

transfer is automatic. At this point, the wafer is raised or lowered as needed to bring it to within the focal range of the optics of the exposure tool. The wafer is then aligned to patterns on the reticle so as to ensure that the pattern can be transferred to the proper location on the resist-coated wafer surface. Because ICs are fabricated in a series of patterning steps, starting with lithography, followed by etch or ion implantation, and in between the patterning steps, along with operations such as film depositions, planarizations, etc., it becomes absolutely necessary to ensure that each new pattern be placed at the right location on top of the preceding layers. The entire operation that ensures that there is proper overlay⁸⁸ between layers of the IC device is called alignment, and is carried out with specialized equipment that is part of the exposure tool.⁸⁹ Specifically, alignment can be defined as the process of determining the position, orientation, and distortion of select patterns already on the wafer and then placing them in correct relation to the projected image from the reticle. Alignment should be fast, repeatable, accurate, and precise. The outcome of the alignment process, or how accurately each successive pattern is matched to the previous layer, is known as overlay,⁹⁰ and is a critical factor in determining if the final device will function properly or not.

11.7 Exposure

The exposure of the resist-coated wafer follows immediately after the alignment of the wafer to the mask (containing the circuit patterns). It involves illuminating the mask with the exposure radiation and projecting the transmitted/reflected image of the mask (called the aerial image) onto the resist film. Being radiation sensitive, the resist film can be selectively exposed in some areas and not in others, depending on the mask pattern, thus effectively transferring the image of the mask patterns onto the resist. At this stage, the image of the mask in the resist film is the latent image, comprising the spatial distribution of the radiation-generated (most often photogenerated) species, typically acids, within the resist film. These acids are either directly responsible for enhancing the dissolution properties of the exposed part of the resist (as in DNQ/novolac resists) or are involved in subsequent

⁸⁸For details on the differences between overlay and registration, see for example, "Specifications for overlay capabilities of wafer steppers," *The SEMI Standard*, pp. 18–92, Semiconductor Equipment and Materials International, Mountain View, CA. Here, overlay is defined as: "a vector quantity defined at every point on the wafer. It is the difference \vec{O} between the vector position \vec{P}_1 of a substrate geometry and the vector position of the corresponding point \vec{P}_2 in an overlaying pattern, which may consist of the photoresist." Mathematically, it is expressed as $\vec{O} = \vec{P}_2 - \vec{P}_1$. A related quantity, registration, is "a vector quantity defined at every point on the wafer. It is the difference \vec{R} between the vector position \vec{P}_1 of a substrate geometry and the vector position of the corresponding point \vec{P}_0 in a reference grid." Mathematically, it is expressed as $\vec{R} = \vec{P}_1 - \vec{P}_0$. With these definitions, overlay is a relative quantity, while registration is an error compared to an absolute standard \vec{P}_0 .

⁸⁹H.J. Levinson, *Principles of Lithography*, 2nd ed., p. 2, SPIE Press, Bellingham, WA (2005).

⁹⁰G. Gallatin, "Alignment and overlay," in *Microlithography: Science and Technology*, J. Sheats and B. Smith, Eds., pp. 317–366, Marcel Dekker, New York (1998).

chemical reactions that alter the chemical structures of the resins of the resist (as in chemical amplification resists), which in turn alter their dissolution properties in developing solvents.

The transformation of the sinusoidal aerial image into the latent image by the resist and subsequently into a fairly straight-edged developed image is a nonlinear process, one that lies at the heart of semiconductor lithographic imaging phenomena. How good a particular resist is in performing this transformation determines its resolution as well as its process capabilities, both of which depend on many factors, chief among which is its radiation absorption characteristics. Resists whose imaging mechanism is based only on exponential attenuation of radiation (i.e., with no mechanism for photobleaching or chemical amplification, for example) are inherently limited to a certain maximum of allowable contrast, sidewall angle, and ultimate resolution because of the inherent absorption trade-offs required when imaging into the resist film. Because both maximum transmission (to reach to the bottom of the resist) and maximum absorption (to achieve the highest sensitivity) are desired, there is an optimum resist absorbance value for any resist thickness.⁹¹

The exposure radiation flux (energy per unit area) decreases exponentially with penetration depth z according to the integral form of the Lambert's law:

$$I(z) = I_0 e^{-\alpha z}, \quad (11.23)$$

where I_0 is the incident flux (mJ/cm^2) and α is the absorption coefficient (cm^{-1}) of the resist, which is the characteristic inverse length that is proportional to the cross section. The value of α depends on the radiation's wavelength and the resist material.

Equation (11.23) can be re-expressed in terms of Beer-Lambert law as⁹²

$$\log \frac{I}{I_0} = -\epsilon cz, \quad (11.24)$$

where I is the intensity after passage through the resist sample, c is the molar concentration of the absorbing species in the resist film, and ϵ is the molar absorption coefficient (formerly called the extinction coefficient). The molar absorption coefficient depends on the frequency of the incident radiation and is greatest where the absorption is most intense, such that the greater the absorption cross section of the absorbing species in the resist film, the greater the attenuation of the intensity of the beam. Its dimensions are $1/(\text{concentration} \times \text{length})$. The dimensionless product $A = \epsilon cz$ is called the absorbance (formerly called the optical density) of the resist sample, and the ratio I/I_0 is the transmittance T . These two quantities are related as follows:

$$\log T = -A. \quad (11.25)$$

⁹¹B.W. Smith, "Resist processing," in *Microlithography: Science and Technology*, J.R. Sheats and B.W. Smith, Eds., pp. 515–565, Marcel Dekker, New York (1998).

⁹²P.W. Atkins, *Physical Chemistry*, 5th ed., p. 545, W.H. Freeman and Co., New York (1994).

The energy density absorbed in the resist is equal to the reduction in the energy density of the incident exposure beam as it transits the resist:

$$E(z) = \alpha I(z) = \alpha I_0 e^{-\alpha z} = \epsilon c I_0 e^{-\epsilon c z}. \quad (11.26)$$

Several observations can be made from Eq. (11.26). First, the resist exposure always decreases with increasing depth into the resist (assuming α is constant). Second, since α varies with wavelength, a beam containing a spread of wavelengths will undergo selective absorption and be filtered as it progresses through the resist. Third, E varies directly with α so that in lithographies with EUV photons, x-ray photons, and electron beams, where photoelectrons or Auger electrons mediate the exposure process, these electrons can cause enhanced resist exposures anywhere a material with high α comes into contact with the resist such as below the mask,⁹³ at an absorber layer inside the resist,⁹⁴ or at the resist-substrate interface.⁹⁵

It should be pointed out that the basis of the contrast in semiconductor lithographic imaging of any resist occurs in two phases, namely, the light (or radiation) phase and the dark phase. The light phase comprises the chemical and physical transformations taking place during the exposure processes, while the dark phase comprises the changes taking place during the postexposure and development stages (see next section). The kinetics of the light reactions is described by the Dill model, which is discussed in Chapter 12.

11.8 Postexposure Bake

The baking of the exposed but undeveloped resist film is called postexposure bake (PEB). The most important effect of PEB is the smoothing out of standing waves in the resist through thermally induced diffusion of photoacid in DNQ/novolac resists and chemical amplification in chemically amplified resists.⁹⁶ As presented in Chapter 9, the standing waves result from the interference of the incident and reflected waves from a reflective substrate, which creates a non-uniform distribution of the radiation intensity within the resist film. Figure 11.17(a) shows a computer simulation of such a standing wave pattern that compares fairly well with an example of standing waves in a resist that was not postexposure baked [Fig. 11.17(b)]. In Fig. 11.17(c), the dramatic effect of PEB at 115°C for 45 seconds in reducing the standing waves in an identically processed wafer is

⁹³J.R. Maldonado, G.A. Coquin, D. Maydan, and S. Somekh, "Spurious effects caused by the continuous radiation and ejected electrons in x ray lithography," *J. Vac. Sci. Technol.* **12**, 1329 (1975).

⁹⁴A.R. Neureuther, "Simulation of x ray resist line edge profiles," *J. Vac. Sci. Technol.* **15**, 1004 (1978).

⁹⁵P. Tischer and E. Hundt, "Profiles of structures in PMMA by x ray lithography," in *Proc. of 8th Int. Conf. on Electron and Ion Beam Sci. Technol.*, pp. 444-452 (1978).

⁹⁶J.M. Shaw and M. Hatzakis, "Performance characteristics of diazo type photoresists under e beam and optical exposure," *IEEE Trans. Electron. Dev.*, **ED-25**, p. 425 (1978).

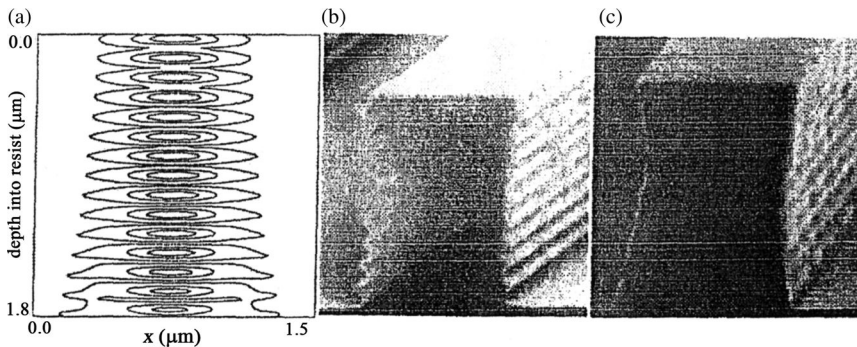


Figure 11.17 Standing waves in DNQ/novolac resists: (a) calculated standing-wave pattern after exposure;⁹⁷ (b) standing-wave patterns observed in a feature developed without PEB; and (c) effect of PEB (1.15°C for 45 seconds).⁹⁸

shown. A similar dramatic effect of PEB, illustrated by the gradual disappearance of the standing waves with increasing temperature, is observed in the dissolution rate of the resist layer (see Fig. 11.18).

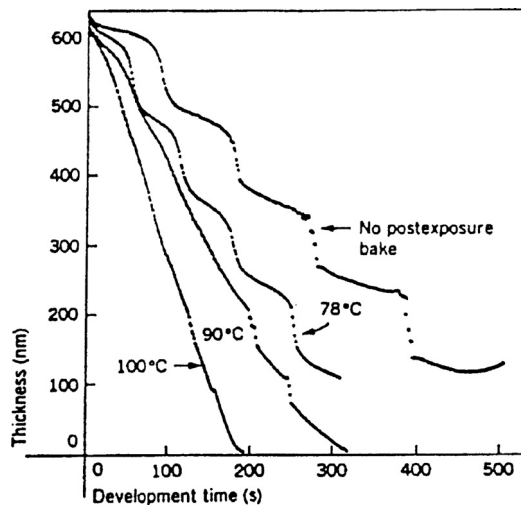


Figure 11.18 Effect of PEB on thickness versus development time curves for AZ 1350J resist on silicon. Resist was exposed at 405 nm with 15 mJ/cm² and developed in a 1:1 mixture of AZ developer/deionized water solution. (Reprinted with permission from Ref. 99. © 1978 IEEE.)

⁹⁷Figure 11.19(a) is reproduced from R. Dammel, *Diazonaphthoquinone based Resists*, p. 110, SPIE Press, Bellingham, WA (1993).

⁹⁸Figures 11.17(b) and 11.17(c) are reproduced from P. Trefonal III, B.K. Daniels, M.J. Eller, and A. Zampini, "Examination of the mechanism of the postexposure bake effect," *Proc. SPIE* **920**, 203 (1988).

⁹⁹Figure is reproduced from J.M. Shaw and M. Hatzakis, "Performance characteristics of diazo type photoresists under e beam and optical exposure," *IEEE Trans. Electron. Dev.* **ED-25**, 425 (1978).

It should be pointed out that the solubility change in all chemically amplified resists (CARs) occurs only in the dark reaction during the PEB. Some of the CARs such as acetal and ketal systems have low activation energy, so deprotection can occur with low-temperature PEBs or even at room temperature. In the absence of thermally driven diffusion such as in acetal and ketal resist systems, BARCs must be used for resists with such low PEB temperatures, which are significantly lower than the soft bake temperature, in order to control reflectivity issues associated with standing waves.

Examples of physical and chemical processes taking place during dark reactions of PEBs include deprotection, acid and quencher (base additive) diffusion, etc. The full description of these processes results in a three-dimensional map of the latent image, comprising the distribution of the radiation- or photogenerated species within the resist film. The consequences of these processes manifest as resolution loss on account of uncontrolled diffusion, line edge roughness, heightened propensity to environmental poisoning (as in PEB delay stability issues), and temperature variation (measured in terms of PEB sensitivity). In the following section, we examine some of these dark phase processes and reactions that are associated with PEB.

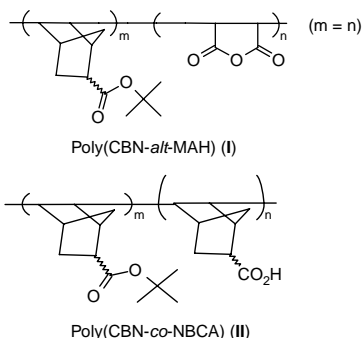
11.8.1 Deprotection kinetics of representative resist polymer systems

Infrared spectroscopy provides a convenient method for studying the deprotection kinetics of resist polymers. For example, the deprotection kinetics¹⁰⁰ of some alicyclic polymer resist systems comprising (i) poly(methylpropyl bicyclo[2.2.1]hept-5-ene-2-carboxylate-*co*-bicyclo[2.2.1]hept-5-ene-2-carboxylic acid) (*trivial name*: poly(carbo-*t*-butoxynorbornene-*co*-norbornene carboxylic acid) [poly(CBN-*co*-NBCA)] (**I**) and (ii) poly(methylpropyl bicyclo[2.2.1]hept-5-ene-2-carboxylate-*co*-maleic anhydride) (*trivial name*: poly(carbo-*t*-butoxynorbornene-*co*-maleic anhydride) [poly(CBN-*alt*-MAH)] (**II**)¹⁰¹ and containing triphenylsulfonium

¹⁰⁰The methodologies reported here follow from U. Okoroanyanwu, J.D. Byers, T. Cao, S.E. Webber, and C.G. Willson, "Deprotection kinetics of alicyclic polymer resist systems designed for ArF (193 nm) lithography," in *Polymers for Micro and Nano Patterning Science and Technology*, H. Itoh, E. Reichmanis, O. Nalamasu, and T. Ueno, Eds., pp. 174-190, American Chemical Society, Washington, DC (1998).

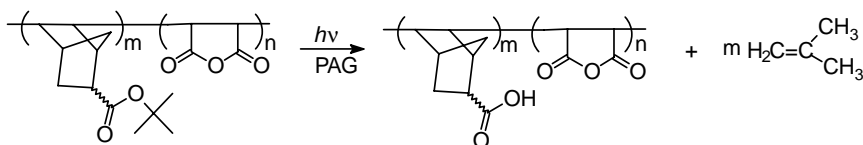
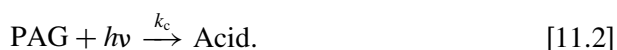
¹⁰¹For details on the synthesis, characterization, and lithographic evaluation of polymers **I** and **II**, see, for example, U. Okoroanyanwu, Ph.D. Thesis, University of Texas at Austin (1997); U. Okoroanyanwu, T. Shimokawa, J.D. Byers, and C.G. Willson, "Alicyclic polymers for 193 nm resist applications: synthesis and characterization" *Chem. Mater.* **10**(11), 3319-3327 (1998); U. Okoroanyanwu, J.D. Byers, T. Shimokawa, and C.G. Willson, "Alicyclic polymers for 193 nm resist applications: lithographic evaluation" *Chem. Mater.* **10**(11), 3328-3333 (1998).

hexafluoroantimonate that were exposed to 248 and 193-nm radiations, was investigated with FTIR spectroscopy.¹⁰²



These resists were formulated by dissolving the alicyclic polymer and a PAG such as triphenylsulfonium hexafluoroantimonate in an appropriate solvent such as propyleneglycol monomethyl ether acetate (PGMEA). On irradiation, the PAG in the resist film generates a latent image of strong acid, which on baking catalyzes the deprotection of the *t*-butyl ester pendant group (as illustrated for a typical photoresist in Scheme [11.1]), leading to the formation of isobutylene and a polymer with a norbornene carboxylic acid unit that has a higher solubility in basic developing solvent than its masked precursor. Development of the exposed and baked film in aqueous base generates a positive tone image of the mask.¹⁰³

On exposure to UV radiation, the PAG decomposes with a rate constant k_c to produce the photoacid (designated as Acid), as illustrated in Reaction [11.2]. Here, $h\nu$ represents photon energy, where h is Planck's constant and ν is the frequency of the radiation.



Scheme 11.1 Deprotection of photoresist film of poly (CBN-*alt*-MAH) by photogenerated acid.

¹⁰²U. Okoroanyanwu, J.D. Byers, T. Cao, S.E. Webber, and C.G. Willson, "Deprotection kinetics of alicyclic polymer resist systems designed for ArF (193 nm) lithography" in *Polymers for Micro and Nano Patterning Science and Technology*, H. Itoh, E. Reichmanis, O. Nalamasu, T. Ueno, Eds., pp. 174–190, American Chemical Society, Washington, DC (1998).

¹⁰³U. Okoroanyanwu, J.D. Byers, T. Shimokawa, and C.G. Willson, "Alicyclic polymers for 193 nm resist applications: lithographic evaluation" *Chem. Mater.* **10**(11), 3328–3333 (1998).

The generally accepted mechanism for the generation of acid from irradiation of the triphenylsulfonium salt was reported by Dektar and Hacker,¹⁰⁴ Knapzyck and McEwen,¹⁰⁵ and Crivello and Lam.¹⁰⁶ The excited state of the sulfonium salt is believed to undergo homolytic cleavage of the carbon-sulfur bond to give an intermediate sulfur-centered radical cation along with a phenyl radical. The photoacid (a Brønsted acid) is believed to arise from hydrogen atom abstraction by the radical cation followed by dissociation.¹⁰⁷ Some investigators have observed phenylthiobiphenyl rearrangement products, which suggest that the acid may arise by photorearrangement followed by dissociation.¹⁰⁸ Also, evidence has been presented that suggests that a phenyl cation is produced by heterolytic cleavage of the excited state of the sulfonium salt.¹⁰⁹

As an example, when the photoacid generator triphenylsulfonium hexafluoroantimonate is exposed to radiation, it decomposes to release the superacid hexafluoroantimonic acid in the resist film. While this photochemical reaction can occur at room temperature, the acid-catalyzed deprotection of the pendant *t*-butyl group of the resist polymer occurs at reasonable rates only at elevated temperature. It is therefore necessary to heat the resist film to an appropriate temperature (PEB) to provide the energy that is required for the acid-catalyzed deprotection of the *t*-butyl group of the ester, which in turn affords the base-soluble norbornene carboxylic acid unit; the isobutylene volatilizes. The extent of deprotection at constant temperature is dependent on the dose of applied radiation. By monitoring the carboxylic acid OH stretch 3000–3600 cm⁻¹ and the ester carbonyl (C=O) around 1735 cm⁻¹, acid carbonyl (C=O) around 1705 cm⁻¹, and ester (C–O–C) stretch around 1150 cm⁻¹, it is possible to determine by means of IR spectroscopy the extent of dose-dependent deprotection, as well as the influence of baking temperature on the extent of deprotection for each resist system. Doses ranging from 0 to 50 mJ/cm² were applied to each resist system, after which they were baked at 120, 130, 140, and 150°C for 60 seconds and analyzed by FTIR.¹¹⁰

Figure 11.19 shows a typical family of IR spectra of a film of resist formulated with triphenylsulfonium hexafluoroantimonate and poly(CBN-*co*-NBCA), samples of which were exposed to 248-nm radiation doses of 0–50 mJ/cm² and

¹⁰⁴J.L. Dektar and N.P. Hacker, "A new mechanism for photodecomposition and acid formation from triphenylsulfonium salts," *J. Chem. Soc., Chem. Commun.* 1591 (1987).

¹⁰⁵J.W. Knapzyck and W.E. McEwen, "Photolysis of triarylsulfonium salts in alcohol," *J. Org. Chem.* **35**, 2539 (1970).

¹⁰⁶J.V. Crivello and H.H.W. Lam, "Photoinitiated cationic polymerization with triarylsulfonium salts," *J. Polym. Sci. Polym. Chem. Ed.* **17**, 977 (1979).

¹⁰⁷J.L. Dektar and N.P. Hacker, "A new mechanism for photodecomposition and acid formation from triphenylsulfonium salts," *J. Chem. Soc., Chem. Commun.* 1591 (1987).

¹⁰⁸ibid.

¹⁰⁹R.S. Davidson and J.W. Goodin, "The polymerization of acrylates using a combination of a carbonyl compound and an amine as a photo initiator system," *Eur. Polym. J.* **18**, 597 (1982).

¹¹⁰U. Okoroanyanwu, J.D. Byers, T. Cao, S.E. Webber, and C.G. Willson, "Deprotection kinetics of alicyclic polymer resist systems designed for ArF (193 nm) lithography" in *Polymers for Micro and Nano Patterning Science and Technology*; H. Itoh, E. Reichmanis, O. Nalamasu, and T. Ueno, Eds., pp. 174–190, American Chemical Society, Washington, DC (1998).

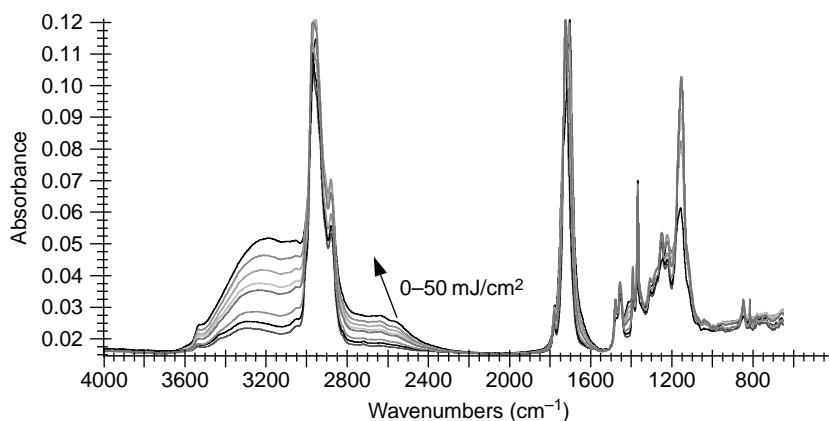


Figure 11.19 Change in FTIR spectra of a typical resist copolymer poly(CBN-co-NBCA) as a function of dose. PEB temperature 130°C, time 60 seconds. Resist was exposed at 248 nm. (Reprinted with permission from American Chemical Society.¹¹¹)

baked at 130°C after exposure. Similar spectra were collected at 120, 140, and 150°C and also under 193-nm exposure for poly(CBN-*alt*-MAH).¹¹²

Figure 11.20 shows the dose-dependent absorbance profiles of the carboxylic OH stretch (3100–3500 cm⁻¹) and the ester C–O–C stretch (around 1150 cm⁻¹) of a poly(CBN-*co*-NBCA) exposed to 248-nm radiation and baked afterward at 120, 130, 140, and 150°C. The carboxylic acid OH stretch and the carboxylic acid carbonyl (C=O) stretch (1695–1705 cm⁻¹) both increase, while the ester carbonyl (C=O) stretch (1730–1735 cm⁻¹) decreases with increasing dose of exposure (0–50 mJ/cm²), which allows us to follow the deprotection of the *t*-butyl ester group and the consequent conversion to a carboxylic acid group. The C–O–C (1150 cm⁻¹) stretch of the ester also decreases with dose of exposure, indicating the loss of the isobutylene group from the resist polymer.¹¹³

Figure 11.21 is an Arrhenius-type plot of the deprotection kinetics of resists formulated with poly(CBN-*co*-NBCA). The activation energy for the deprotection of the pendant-*t*-butyl group of resists formulated with poly(CBN-*co*-NBCA) made by Pd(II)-catalyzed addition and free radical polymerization techniques was determined to be 6.7 and 9.4 kcal/mol, respectively, over the temperature range of 120–150°C. Figure 11.22 is an Arrhenius-type plot of the deprotection kinetics of resist formulated with poly(CBN-*co*-MAH). The activation energy for the deprotection of the pendant-*t*-butyl group of resist polymer was determined to be 18.3 kcal/mol over the temperature range of 120–150°C.

¹¹¹ *ibid.*

¹¹² *ibid.*

¹¹³ *ibid.*

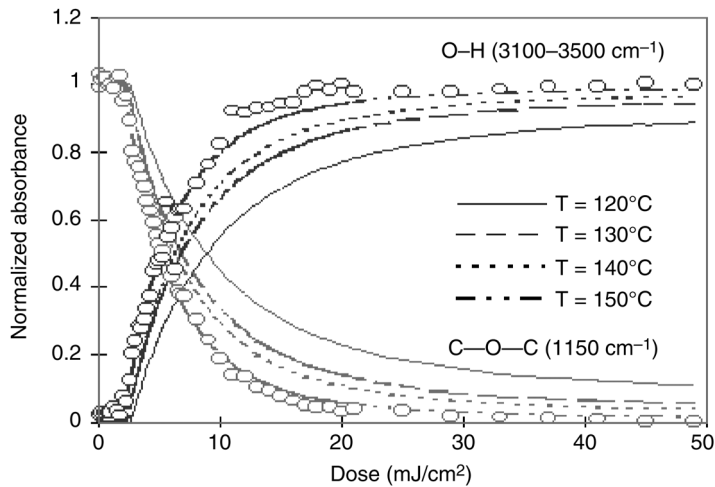


Figure 11.20 The carboxylic OH and ester C–O–C stretch profile on 24-nm irradiation of resist. (Reprinted with permission from American Chemical Society.¹¹⁴)

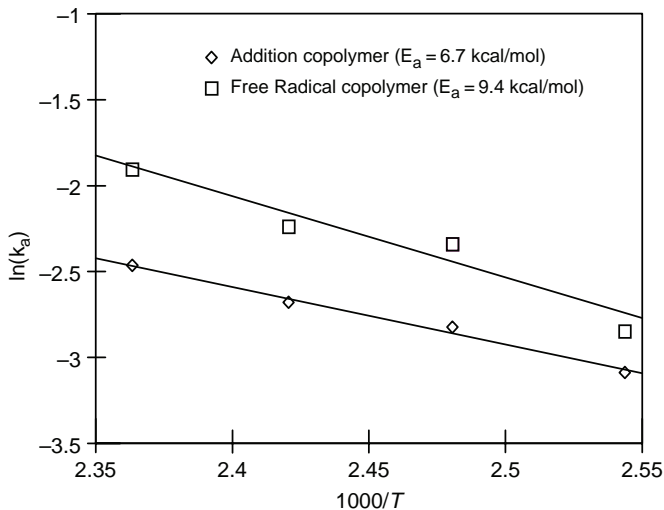


Figure 11.21 Arrhenius plot for resist formulated with poly(CBN-co-NBCA) and 3 wt% of triphenylsulfonium hexafluoroantimonate (TPSHFA), and exposed under 248-nm radiation. (Reprinted with permission from American Chemical Society.¹¹⁵)

This Arrhenius relationship is not considered valid outside of the region experimentally covered.

The thermal decomposition of DNQs in novolac resist film follows pseudo first-order reaction kinetics (see Fig. 11.23.). The 2,1,4-DNQ PAC is more

¹¹⁴ibid.

¹¹⁵ibid.

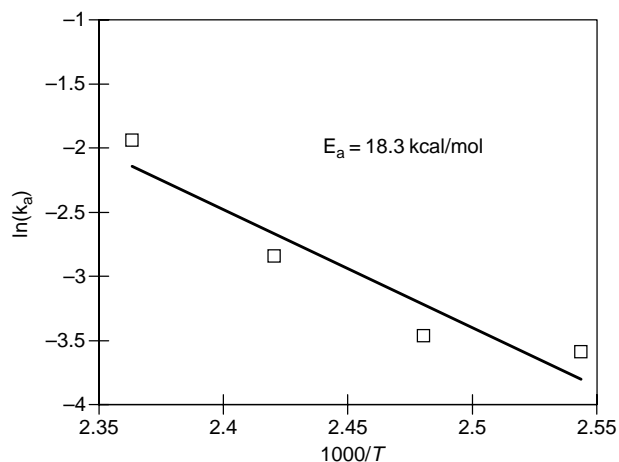


Figure 11.22 Arrhenius plot for resist formulated with poly(CBN-co-MAH) and exposed under 193-nm radiation. (Reprinted with permission from American Chemical Society.¹¹⁶)

thermally stable than the 2,1,5-DNQs, the activation energy difference between the two isomers being 8 kcal/mole.¹¹⁷

11.9 Monitoring Photoacid Generation in Thin Photoresist Films by Means of Fluorescence Spectroscopy

Fluorescence spectroscopic techniques are increasingly being used in a wide range of research fields including biochemical, medical, and chemical research,

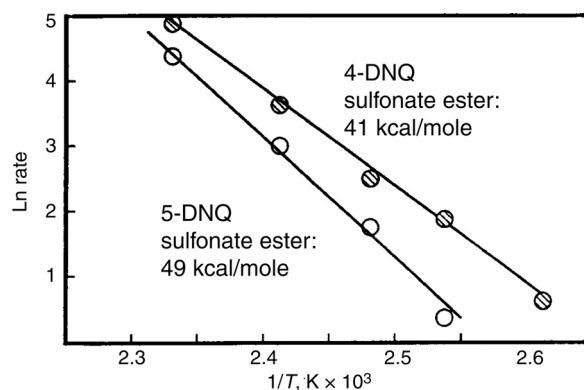


Figure 11.23 Thermal decomposition of DNQs in novolac resist film.¹¹⁸

¹¹⁶ibid.

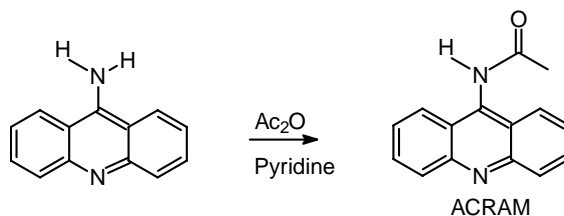
¹¹⁷W.M. Moreau, "Thermal stability of naphthodiazquinone sensitizers," *Proc. SPIE* **3049**, 618–627 (1997).

¹¹⁸ibid.

primarily because of their inherent sensitivity and the favorable time scale of the phenomenon of fluorescence.¹¹⁹ Some fluorophores have dramatically different emission characteristics for their protonated and unprotonated forms. Using this phenomenon, the photoacid concentrations generated within CAR systems can be monitored.¹²⁰ For instance, the photogeneration of acid in some of the above-mentioned alicyclic polymer resist films has been monitored and quantified with this technique.¹²¹

Many molecules with pH-dependent fluorescence properties are known and used only in aqueous media, which essentially precludes them from resist applications. To be of use in resist applications, fluorescent molecules must be soluble in organic solvents of moderate polarity and also be compatible with polymer films.¹²² Aromatic monazines such as acridine have been known to be essentially nonfluorescent in non-hydrogen-bonding solvents, whereas their protonated forms are highly fluorescent in aqueous solutions, which makes this class of materials interesting candidates for potential acid sensors.¹²³

Commercially available acridine is usually provided as the HCl salt; if this acid is not completely removed, it can mask and even become a source of interference when the acridine salt is titrated against the photogenerated acid. N-(9-acridinyl)acetamide (ACRAM) was used in this study. ACRAM is readily obtained from acridine amine with acetic anhydride in pyridine, as shown in Scheme 11.2. The protonation of ACRAM by the photoacid proceeds via Scheme 11.3.



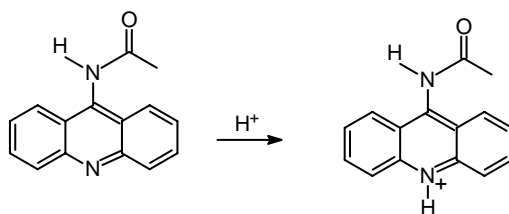
Scheme 11.2 Synthesis of ACRAM from acridine amine.

¹¹⁹J.R. Lackowicz, *Principles of Fluorescence Spectroscopy*, Chapters 1–2, Plenum Press, New York (1986).

¹²⁰G. Pohlert, S. Virdee, J.C. Sciano, and R. Sinta, "Aromatic monoazines as fluorescent sensors for photoacid generation in thin polymer films," *Chem. Mater.* **8**, 2654 (1996); A.Z. Weller, *Elektrochem.* **61**, 956 (1957); K. Kasama, K. Kikuchi, S. Yamamoto, K. Ujiiie, Y. Nishida, and H. Kokubun, "Relaxation mechanism of excited acridine in nonreactive solvents," *J. Phys. Chem.* **85**, 1291 (1981).
¹²¹ibid.

¹²²D.R. McKean, U. Schaedeli, and S.A. MacDonald, "Acid photogeneration from sulfonium salts in solid polymer matrices," *J. Polym. Sci. Part A* **27**, 3927 (1989); W.P. Carey, B.S. Jorgensen, "Optical sensors for high acidities based on fluorescent polymers," *Appl. Spectrosc.* **45**, 834 (1991).

¹²³U. Okoroanyanwu, J.D. Byers, T. Cao, S.E. Webber, C.G. Willson, "Deprotection kinetics of alicyclic polymer resist systems designed for ArF (193 nm) lithography" Ch. 14 in *Polymers for Micro and Nano Patterning Science and Technology*; H. Itoh, E. Reichmanis, O. Nalamasu, T. Ueno, Eds., ACS Books, American Chemical Society, Washington, DC, pp. 174–190 (1998).



Scheme 11.3 Protonation of ACRAM by photogenerated acid.

Figure 11.24 shows the change of fluorescence intensity (normalized to the pure ACRAM spectrum) with the addition of photoresist solution formulated from poly(CBN-*alt*-MAH) and TPSHFA (4.41×10^{-7} M). These spectra show hypsochromic spectral shifts of the peaks around λ_1 : 440 \rightarrow 430 nm and λ_2 : 470 \rightarrow 460 nm, as well as an increase in the intensity of these peaks, indicating the protonation of ACRAM/THF solution by the photogenerated acid.¹²⁴

Table 11.1 summarizes the amount of photoacid generated at 193 nm from photoresists from different PAGs with 50 mJ/cm². Using the values of Table 11.1, the quantum yield for acid production was determined from the number of acid molecules produced per photon absorbed by the film. In this way, a quantum yield of 1.1×10^{-4} was determined for the PAG (TPSHFA) in

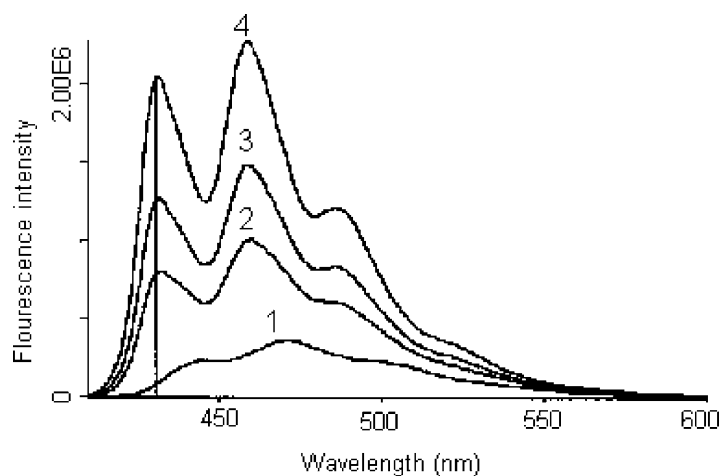


Figure 11.24 Fluorescence spectra of 27.1 nM ACRAM in THF with and without photoresist solution formulated from poly(CBN-*alt*-MAH) and TPSHFA (4.41×10^{-7} M). (1) +0 μ L of photoresist/THF. (2) +35 μ L of photoresist/THF. (3) +60 μ L of photoresist/THF. (4) +120 μ L of photoresist/THF. (Reprinted with permission from American Chemical Society.¹²⁵)

¹²⁴ibid.

¹²⁵ibid.

Table 11.1 Photoacid generation at 193 nm from photoresist formulated with poly (CBN-*alt*-MAH) and different TPSHFA concentrations. The exposure dose was with 50 mJ/cm². (Reprinted with permission from American Chemical Society.¹²⁶)

PAG	Dose (mJ/cm ²)	Conc. of TPSHFA (M)	Conc. of photoacid (M)
TPSHFA	50	4.41×10^{-7}	1.04×10^{-7}
TPSHFA	50	6.61×10^{-8}	4.13×10^{-8}

a poly(CBN-*alt*-MAH) resist system that was exposed to 193-nm radiation. Such a low quantum yield is indicative of the fact that most of the 193-nm radiation that is absorbed by the resist is not utilized in the production of photoacid from the PAG (TPSHFA).¹²⁷

11.10 Postexposure Bake Sensitivity

The CD of features patterned with chemical amplification resists show higher sensitivities to PEB than to the prebake. A very small variation in PEB temperature can result in significant change in the feature CD. In the regime of extremely tight CD control requirements, bake plates must have excellent across-the-plate uniformity, significantly less than 0.5°C (range). Figure 11.25 shows typical PEB sensitivity plots for resists based on acrylate and hybrid alicyclic/acrylate resist polymer platforms used in ArF lithography. PEB sensitivity for these resists is in the range of 4–0 nm/°C. Most current 193-nm resists have PEB sensitivities of no

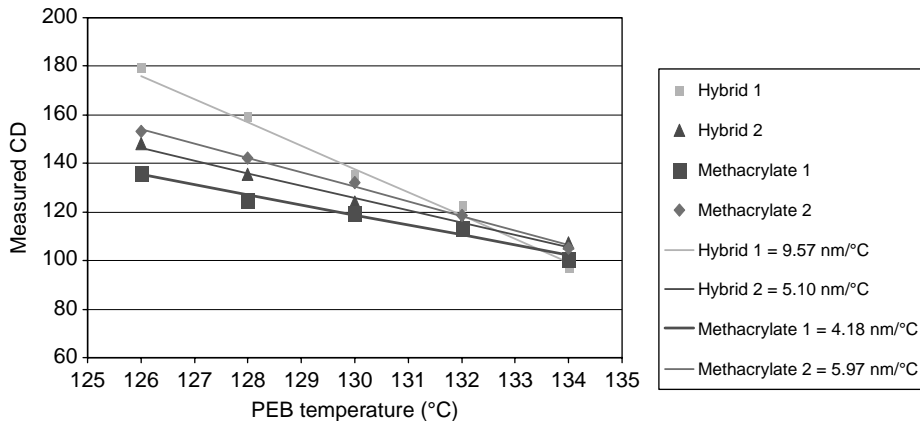


Figure 11.25 PEB sensitivity curves for different acrylate and alicyclic/acrylate hybrid resist polymer platforms used in ArF lithography. The target CD was 120 nm L/S at 1:2 duty cycle. [Reproduced from R. Dammel, “Practical photoresist processing,” SPIE Short Course No. SC616 (2005).]

¹²⁶ibid.

¹²⁷ibid.

Table 11.2 PEB sensitivities of commercially available KrF resists. [Reproduced from H.J. Levinson, *Principles of Lithography*, 2nd ed., p. 82, SPIE Press, Bellingham, WA (2005).]

Resist	Supplier	Line width sensitivity (nm/°C)
Apex E	Rohm and Haas Electronic Materials	16.0
UVIHS	Rohm and Haas Electronic Materials	7.5
UV6	Rohm and Haas Electronic Materials	2.6
TM 461	JSR	2.6
DP 024	TOK	1.8
ARC2	Arch	~0

better than 4–5 nm/°C near their linear resolution limit. The best-in-class resists have PEB sensitivity values around 2 nm/°C.¹²⁸ Table 11.2 shows the PEB sensitivities for commercially available KrF resists.¹²⁹ In general, high-activation energy resist systems tend to have much higher PEB sensitivity than their low-activation energy counterparts because of the role of temperature in photoacid diffusion, already discussed above.

11.11 Consequences of Acid Diffusion

While the increased sensitivity of chemical amplification resists is tied to the ability and the ease of the generated acid to diffuse through the free volume of the resist polymer resin, aided by PEB, to catalyze chemical transformations of the resin that alter their dissolution properties in the developer solution, these same characteristics of chemical amplification can also negatively impact the patterning action of the resist.

First, with the minimum device feature size approaching length scales that are on the same order of magnitude as the diffusion lengths of photoacids generated in CARs, preserving the integrity of the latent image has now become a major concern in microlithography. Diffusion of the photoacid during the time between exposure and development can cause significant contrast loss and ultimately lead to loss of the latent image, especially in CARs that must require a postexposure baking step, which facilitates the diffusion of the acid due to the high temperature normally used.

Next, if neutralization of the acid occurs, the dissolution rate of the exposed part of the resist decreases. If the resist is exposed to airborne molecular bases (such as ammonia and N-methyl pyrillodone) after exposure and prior to PEB (normally called PEB delay), a thin soluble inhibition layer forms on the top surface of the resist, which results in the formation of a characteristic “T-top” on development (see Fig. 11.26). Acid evaporation during PEB can also lead to T-top formation. Early commercial chemical amplification resists had

¹²⁸R. Dammel, “Practical photoresist processing,” SPIE Short Course No. SC616 (2005).

¹²⁹K.G. Kemp, D.J. Williams, J.W. Clayton, P. Steege, S. Slonaker, and R. Eliot, “Effects of DUV resist sensitivities on lithographic process window,” *Proc. SPIE* **3049**, 955–962 (1997); J.M. Parker and D.A. Miller, “Direct temperature metrology helps minimize CA resist CD variation,” *Solid State Technol.* 139–146 (Sept. 2000).

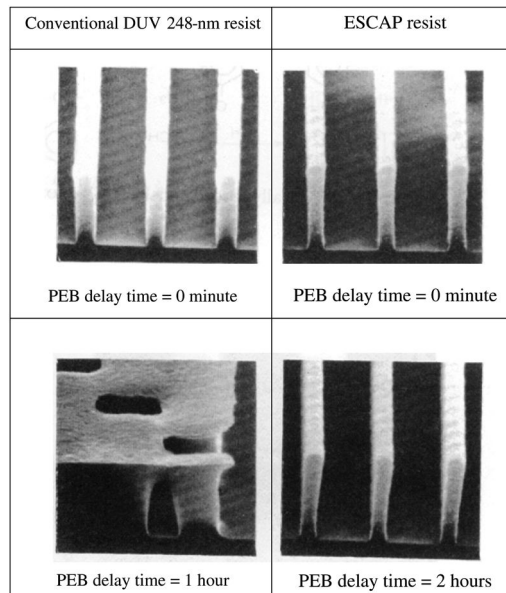


Figure 11.26 PEB stability of a conventional DUV 248-nm resist based on poly(4-hydroxystyrene-co-*tert*-butylcarbonyloxy styrene) versus ESCAP based on poly(4-hydroxystyrene-co-*tert*-butyl acrylate). Note that the acid generated in the conventional DUV resist is trifluoromethane sulfonic acid (a very strong, small, volatile acid), while that of the ESCAP resist is camphor sulfonic acid (a very weak, bulky, nonvolatile acid). While the conventional DUV resist polymer is nonannealing, that of the ESCAP is an annealing polymer. [Reproduced from R. Dammel, “Practical photoresist processing,” SPIE Short Course No. SC616 (2005).]

PEB delay stability of a few minutes; this value is now on the order of hours in current commercial chemical amplification resists.

The improvement in PEB delay stability of current resists is attributed to a few strategies that have been adopted over the years; these include the use of a barrier layer on top of the resist to prevent in-diffusion of airborne bases and out-diffusion of acids, and the use of efficient broad-spectrum filters equipped with activated charcoal media designed to remove airborne bases and acids. Other strategies that have been employed include annealing the resist at high enough temperature near their T_g and softening them to decrease the free volume in the polymer matrix and thereby limiting the effect and extent of acid and airborne base diffusion; the use of acid generators that produce bulky, nonvolatile acids; and the use of base additives and quenchers that scavenge and neutralize the excess acids, preventing them from diffusing to the surface and reacting with airborne bases and creating T-tops or from diffusing into the nonexposed regions, which helps to improve the sidewall angle of the feature (see Fig. 11.27).

The acid can also diffuse from the exposed area to the interface between the resist in the unexposed area and the substrate and interact with basic moieties in the substrate or BARCs, especially inorganic BARCs such as SiON and TiN, leading to the creation of footing.

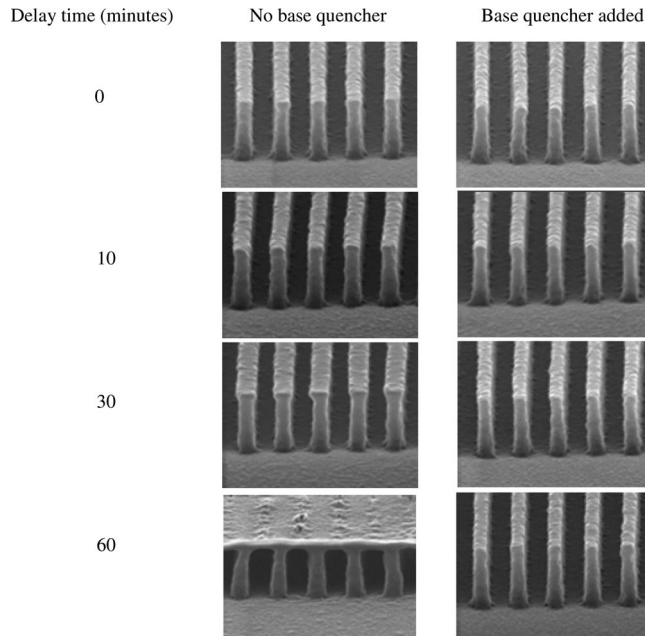


Figure 11.27 Effects of base additives on PEB delay stability of an ArF resist. [Reproduced from R. Dammel, “Practical photoresist processing,” SPIE Short Course No. SC616 (2005).]

11.12 Development

Following the PEB for both conventional and chemical amplification resists, the resist film is developed in a liquid chemical developer to dissolve the soluble regions of the resist film. As stated in Chapter 6, the soluble region of negative resists is the unexposed part, while for the positive resists, it is the exposed part. The primary goal of resist development is to accurately replicate the latent image generated during the PEB step, which is, in effect, the transfer of the aerial image of the mask in the resist. In its essence, the development step completes the imaging process, which effectively results in the transformation of the two-dimensional image of the mask into a three-dimensional relief image of the mask on the resist film.

The liquid chemical developers¹³⁰ that have been in use in the IC industry are basic, aqueous solutions. The main two classes are the buffered metal-ion-containing (e.g., sodium metasilicate) and the metal-ion-free (MIF) developers (e.g., aqueous solutions of TMAH). Both classes of developers are typically formulated with additives such as surfactants to improve wetting.¹³¹ The buffered systems can be used at lower pH for the same normality, and thus offer better

¹³⁰For a general discussion on the constitution of developers, please see Chapter 5.

¹³¹R. Dammel, *Diazonaphthoquinone based Resists*, p. 112, SPIE Press, Bellingham, WA (1993).

discrimination, dark erosion, and contrast.¹³² Although alkali bases such as NaOH and KOH were used as developers in earlier times in device fabrication, they are no longer in use today for this application because alkali metals such as sodium and potassium have been implicated in gate oxide degradation.¹³³

Today, the standard developer used in the IC industry is the MIF 0.26N TMAH solution.¹³⁴ Given the larger cross section of the TMAH cation, TMAH developers show slower development speed than those of NaOH and KOH solutions at the same normality.¹³⁵ Remarkably, when TMAH and metal-ion-containing developers are mixed, even at the parts-per-million level, a substantial decrease of the dissolution rate, well below that of TMAH solution, is observed.¹³⁶ One other remarkable effect is that metal-ion-containing NaOH and TMAH developers also differ substantially in the influence of temperature on the resist dissolution rate. While the development rate decreases with developer temperature for TMAH developers, the trend is opposite that for metal-ion-containing developers such as NaOH and KOH.¹³⁷

11.12.1 Resist development methods

Since the dawn of semiconductor lithography in 1957, resists have been developed by methods ranging from immersion to spray to puddle processes, either in batch mode or in continuous mode. Resist development in the 1970s and early 1980s typically involved immersion development, in which batches of wafers were immersed in tanks of developers for a given length of time. This approach has been largely superseded by puddle development on single-wafer processes because of the superior uniformity and control performance of the puddle single-wafer processes relative to the batch processes. In addition, single-wafer puddle processes are amenable to cluster operation, where the resist processing tracks are interfaced to the exposure tools.¹³⁸

The single-wafer puddle process, operating in an automatic continuous mode in a track system, is now the most commonly used method for resist development. It involves an initial dispense of the developer on each wafer, forming a puddle that covers the entire wafer surface for a period of time on the order of 30–75 seconds, following which the developer is rinsed off with deionized water. Additional

¹³²ibid.

¹³³R. Sze, *Physics of Semiconductor Devices*, 2nd ed., Chapter 7, John Wiley & Sons, Hoboken, NJ (1981).

¹³⁴This standardization has been driven mostly by cost considerations rather than because 0.26 N developer provides superior lithographic performance relative to other normality values. For details on these considerations, see, for example, T. Y. Chu and K. P. Cheng, "Developer concentration influence on DUV process," *Proc. SPIE* **3678**, 448–454 (1999); M. Touky, B. Maxwell, and S. Chanthalyma, "The effect of developer normality on the resist dissolution rate and performance," *Proc. SPIE* **3678**, 721–726 (1999).

¹³⁵R. Dammel, *Diazonaphthoquinone based Resists*, p. 112, SPIE Press, Bellingham, WA (1993).

¹³⁶ibid.

¹³⁷C.M. Garza, C.R. Szamanda, and R.L. Fischer, "Resist dissolution kinetics and submicron process control," *Proc. SPIE* **920**, 321–338 (1988).

¹³⁸H.J. Levinson, *Principles of Lithography*, 2nd ed., p. 80, SPIE Press, Bellingham, WA (2005).

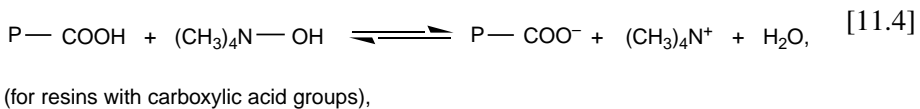
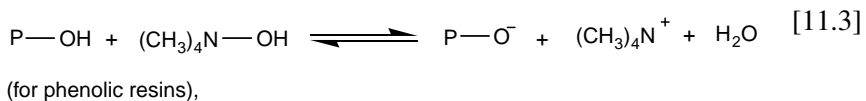
puddles may sometimes be applied to the wafer in order to reduce defects.¹³⁹ The tubes carrying the developer to the wafer are jacketed, and their temperature is actively controlled to within $\pm 0.2^\circ\text{C}$ since resist development involves chemical reactions, often acid-base neutralization reactions, which are temperature dependent.¹⁴⁰ The other reason for controlling the temperature of the developer is evaporation of the developer, often more pronounced at the wafer periphery than at the center; this can cause variations in the concentration of the developer and temperature of the resist film because of evaporative cooling, leading to variations in development rates and ultimately to poor CD uniformity.

11.12.2 Types of development processes

There are two types of resist development processes, namely, chemical development and physical development.

11.12.2.1 Chemical development

In chemical development, the matrix resin of the resist system dissolves in the developer through a chemical reaction. Examples of resists that use chemical development include positive resists composed of novolac resins and DNQs, as well as positive chemical amplification resists based on phenolic, acrylate, and alicyclic polymers. These resists are developed with a 0.26-N aqueous solution of tetramethylammonium hydroxide. The exposed resins with phenolic and acidic functional groups dissolve in the developer via the chemical reactions



where P—OH, P—COOH, P—O[−], and P—COO[−] stand for phenolic resin, resin with carboxylic acid group, resin with phenolate ion functional group, and resin with carboxylate functional group, respectively. The species (CH₃)₄N⁺ stands for the tetramethylammonium ion.

The reaction does not occur in the unexposed areas because of the dissolution inhibition of the DNQs that remains unchanged there, or because of the lack of chemical amplification reaction there. As a result, the unexposed resist film

¹³⁹ibid.

¹⁴⁰J.M. Shaw and M Hatzakis, "Developer temperature effects on e beam and optically exposed positive photoresist," *J. Electrochem. Soc.* **126**(11), 2026–2031 (1979).

neither dissolves nor swells in the developer. It is because of this lack of swelling during development that positive resists generally have higher resolution capability than their traditional negative resist counterparts.

11.12.2.2 Physical development

In physical development, there is no chemical reaction involved in the dissolution process. Instead, the resin dissolves in a solvent (typically organic) with similar solubility parameters through mixing and solvation. Examples of resists that employ physical development include negative resists based on cyclized polyisoprene and aromatic bisazide, or positive chain scission resists such as polymethyl methacrylates, which are developed in xylene and similar organic solvents. In the cyclized polyisoprene resists, the resist film in the exposed areas has been insolubilized by cross-linking reactions, and therefore does not dissolve in the developing solvent. In the case of PMMA, the exposed film has lower molecular weight than their unexposed film, and is therefore soluble in the organic solvent, whereas the unexposed film is not. The insolubilized resist film, however, swells in the developing solvent. This swelling decreases the resolution capability of the resist.¹⁴¹ In instances where a chemical amplification resist is developed in a nonpolar solvent to give a negative pattern, the resist is physically developed.¹⁴²

11.12.3 Development rate characterization

There are a number of reasons that it is important to characterize the dissolution or development rate of any given resist. The main reasons tend to be for process control purposes, given that image discrimination in resists is based on differences in dissolution rates between the image and non-image areas. The two main techniques that are used to characterize the dissolution properties of a resist are laser interferometry and quartz crystal microbalance. Each of these techniques is reviewed below.

11.12.3.1 Laser interferometry

The first use of laser interferometry in monitoring the dissolution rate of a resist during development was by Konnerth and Dill.¹⁴³ The basis of their idea is shown in Fig. 11.28. A laser beam is directed toward the film, which is immersed in the developer. The reflected beam from the surface of the film and that reflected from the interface between resist and substrate interfere constructively or

¹⁴¹S. Nonogaki, T. Ueno, and T. Ito, *Microlithography Fundamentals in Semiconductor Devices & Fabrication Technology*, Chapter 5, Marcel Dekker, New York (1998).

¹⁴²H. Ito and C.G. Willson, "Chemical amplification in the design of dry developing resist materials," *Polym. Eng. Sci.* **23**, 1012–1018 (1983).

¹⁴³K.L. Konnerth and F.H. Dill, "In situ measurement of dielectric thickness during etching or developing processes," *IEEE Trans. Electron. Dev.* **ED-22**, 453 (1975); K.L. Konnerth and F.H. Dill, "IOTA, a new computer controlled thin film thickness measurement tool," *Solid State Electron.* **15**, 371 (1972).

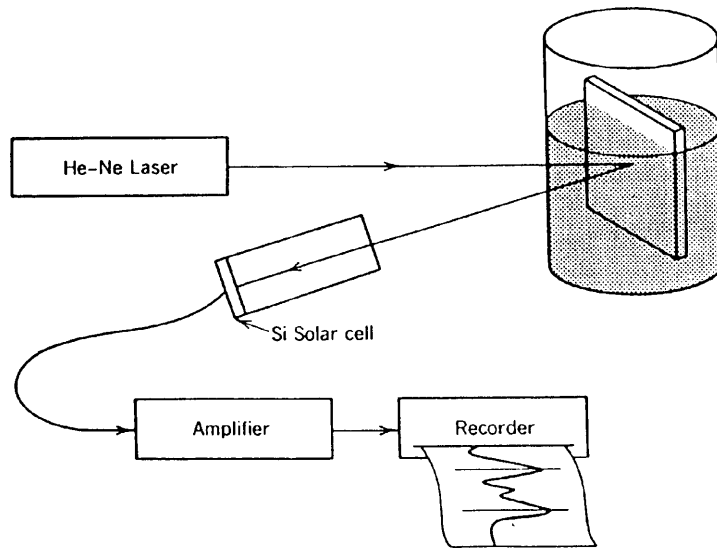


Figure 11.28 Schematic of a laser interferometric apparatus for measuring resist development rate. The beam from a small He-Ne laser is used to illuminate the surface of the resist immersed in developer. The beams reflected from the surface of the resist and from the substrate-resist interface interfere constructively or destructively, depending on the thickness of the resist layer, and the solar cell receives in turn higher and lower light intensities. The corresponding signal is amplified and displayed on a chart recorder. (Reprinted with permission from Ref. 146. © 1980 IEEE.)

destructively,¹⁴⁴ depending on the angle of incidence and on thickness of the film. These reflected beams are directed to the Si solar cell (a photocell), which in turn generates photoelectrons (photocurrents) that are sent to an amplifier, where they are amplified to make them easier to measure as a signal. As the film dissolves in the developer, with the film thickness decreasing accordingly, the Si photocell registers maxima and minima of light intensity, corresponding to the remaining thickness of the resist on the substrate. A typical record trace of this signal as a function of time in the developer is shown in Fig. 11.29. The interval of time Δt between two extrema on the recorder trace corresponds to a change Δr in film thickness, which is determined by the Bragg relation

$$2\Delta r = \frac{m\lambda}{n} \Delta t, \quad (11.27)$$

where n is the index of refraction of the resist, λ is the wavelength of the laser radiation, and m is an integer number. The recorder trace is thus easily transformed into a film thickness-versus-development time curve,¹⁴⁵ as shown in Fig. 11.29.

¹⁴⁴F. Rodriguez, P.D. Krasicky, and R.G. Groele, "Dissolution rates measurements," *Solid State Technol.* **28**(5), 125 (1985).

¹⁴⁵A. Reiser, *Photoreactive Polymers: The Science and Technology of Resists*, pp. 197-199, John Wiley & Sons, Hoboken, NJ (1989).

¹⁴⁶D. Meyerhofer, "Photosolubility of diazoquinone resists," *IEEE Trans. Electron. Dev.* **ED-27**, 921 (1980).

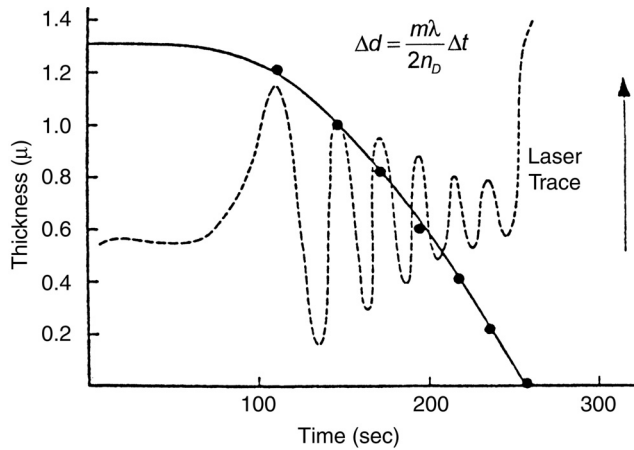


Figure 11.29 Reflectivity versus the time a resist film is immersed in a developer and monitored by laser interferometry during development. The film thickness versus time in developer (solid line) can be derived from the recorder trace as indicated in Eq. (11.27). (Reprinted with permission from American Chemical Society.¹⁴⁷)

The dampening of the interferograms at long dissolution times is attributed to increasing light loss due to diffuse scattering as the resist surface gets roughened up during the course of the dissolution. In the most extreme case, this can prevent meaningful dissolution rates from being determined with this method.¹⁴⁸

Today, more sophisticated versions of the simple Konnerth and Dill¹⁴⁹ instrument are now sold commercially as the Dissolution Rate Monitor by Litho Tech Japan. Equipped with onboard microprocessors, these instruments can simultaneously monitor the dissolution rates of a whole set of locations on a resist-coated wafer, as well as generate the corresponding family of dissolution rate curves in a single run.

11.12.3.2 Quartz crystal microbalance

The use of the quartz crystal microbalance in monitoring resist dissolution rates was first reported in 1985 by W.D. Hinsberg et al.¹⁵⁰ This technique is based on the equation that G. Sauerbrey developed in 1959 as a method for correlating changes in the oscillation frequency of a piezoelectric crystal with the mass

¹⁴⁷C.G. Willson, in *Introduction to Microlithography*, L.F. Thompson, C.G. Willson, and M.J. Bowden, Eds., p. 117, ACS Symp. Ser. 219, American Chemical Society (1984).

¹⁴⁸R. Dammel, *Diazonaphthoquinone based Resists*, p. 50, SPIE Press, Bellingham, WA (1993).

¹⁴⁹K.L. Konnerth and F.H. Dill, "In situ measurement of dielectric thickness during etching or develop processes," *IEEE Trans. Electron. Dev.* **ED-22**, 453 (1975); K.L. Konnerth and F.H. Dill, "IOTA, a new computer controlled thin film thickness measurement tool," *Solid State Electron.* **15**, 371 (1972).

¹⁵⁰W.D. Hinsberg, C.G. Willson, and K.K. Kanazawa, "Use of a quartz crystal microbalance rate monitor to examine photoproduct effects on resist dissolution," *Proc. SPIE* **539**, 6 (1985).

deposited on it.¹⁵¹ In deriving the equation, he treated the mass deposited on the crystal as though it were an extension of the thickness of the underlying quartz. Because of this, the mass-to-frequency correlation (as determined by this equation) is largely independent of electrode geometry. This has the benefit of allowing mass determination without calibration. The Sauerbrey equation is expressed as

$$\Delta f = -\frac{2f_0^2}{A\sqrt{\rho_q\mu_q}}\Delta m, \quad (11.28)$$

where f_0 is the resonant frequency in Hertz of the quartz resonator before the change, Δf is the frequency change in Hertz, Δm is the mass change in grams, A is the piezoelectrically active crystal area (area between the electrodes in m^2), ρ_q is the density of quartz (2.648 g/cm^3), and μ_q is the shear modulus of quartz ($2.947 \times 10^{11} \text{ g/cm} \cdot \text{s}^2$)

In addition to deriving the equation that now bears his name, Sauerbrey also developed a method for measuring the characteristic frequency and its changes by using the crystal as the frequency-determining component of an oscillator circuit. It should be mentioned that the Sauerbrey equation was developed for oscillation in air and only applies to rigid masses attached to the crystal. However, Kanazawa and Gordon have shown that quartz crystal microbalance measurements can be performed in liquid, in which case a viscosity-related decrease in the resonant frequency is observed:¹⁵²

$$\Delta f = -f_0^{3/2} \sqrt{\frac{\eta_l \rho_l}{\pi \rho_q \mu_q}}, \quad (11.29)$$

where Δf is frequency change, f_0 is the resonant frequency, ρ_l is the density of the liquid, and the η_l is the viscosity of the liquid.

In adapting the Kanazawa-Gordon extension of Sauerbrey's equation to operations in liquids, Hinsberg et al.¹⁵³ coated the resist film onto the crystal and monitored the characteristic frequency of the crystal while the system was immersed in the developer. Figure 11.30 shows a schematic of the quartz crystal balance described by Hinsberg et al.¹⁵⁴ The characteristic frequency depends on the mass of the oscillating unit, of which the resist film is a part. As the film dissolves, the mass changes, as does the frequency. Because the frequency shift is linearly dependent on the mass of the cast film [as shown in Eq. (11.28)], it can therefore be used to monitor the dissolution process. The technique offers a number of advantages. It can be used to measure very high dissolution rates, and it can handle thick films, as

¹⁵¹G. Sauerbrey, "The use of quartz crystal oscillators for weighing thin layers and for micro weighing," *Z. Phys.* **155**, 206–222 (1959).

¹⁵²K.K. Kanazawa and J.G. Gordon, "Frequency of a quartz microbalance in contact with liquid," *Anal. Chem.* **57**, 1770–1771 (1985).

¹⁵³W.D. Hinsberg, C.G. Willson, and K.K. Kanazawa, "Use of a quartz crystal microbalance rate monitor to examine photoproduct effects on resist dissolution," *Proc. SPIE* **539**, 6 (1985).

¹⁵⁴ibid.

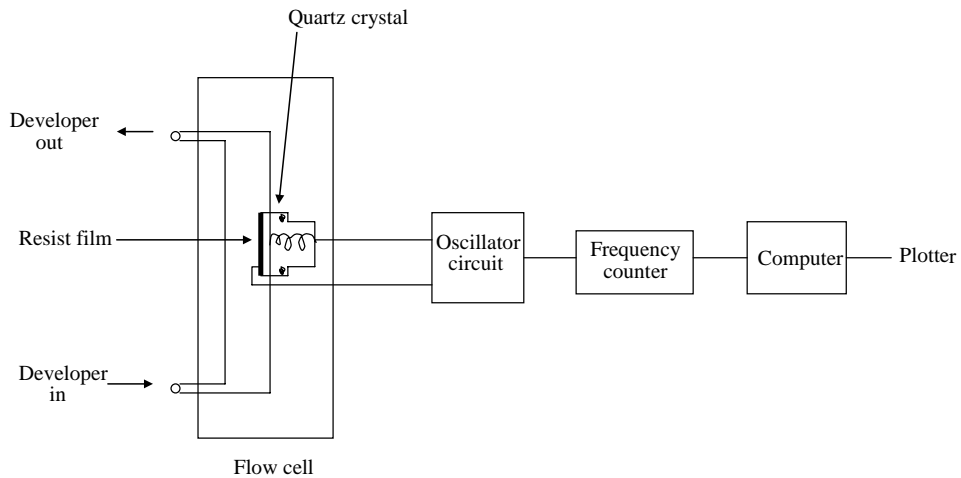


Figure 11.30 Schematic of a quartz crystal microbalance dissolution monitor. The mass of the quartz crystal balance controls the frequency of the oscillating circuit. The change in the total mass of the crystal as the resist film coated on it dissolves is linearly related to the oscillating frequency, which is monitored with the frequency counter. The dissolution rate of the resist is thus monitored by measuring the change in frequency of the oscillator with time as the resist film dissolves. (Adapted from Ref. 153.)

well as opaque films and films with an uneven surface, which are impossible to measure with interference methods.¹⁵⁵

11.13 Dissolution Mechanism of Resist Polymers

Given the fact that the matrix resins of resists are comprised largely of polymers, it is expected that the dissolution of resists will generally follow the same patterns as polymers with fairly high molecular weight. The 1960s saw Ueberreiter and Asmussen¹⁵⁶ investigate the dissolution of high-molecular-weight polymers. They found that polymer dissolution occurs in two stages. In the first stage, solvent penetrates into the glassy polymer, forming a gel layer separating the polymer matrix from the pure solvent. In the second stage, the polymer coils disentangle from the gel, eventually diffusing into the liquid. Three distinct phases in the steady state dissolution process are¹⁵⁷ glassy polymer, swollen gel, and solvent or solution.

¹⁵⁵A. Reiser, *Photoreactive Polymers: The Science and Technology of Resists*, p. 200, John Wiley & Sons, Hoboken, NJ (1989).

¹⁵⁶K. Ueberreiter and F. Asmussen, "Velocity of dissolution of polymers. Part I," *J. Polym. Sci.* **57**, 187 (1962); F. Asmussen and K. Ueberreiter, "Velocity of dissolution of polymers. Part II," *J. Polym. Sci.* **57**, 199 (1962).

¹⁵⁷A. Reiser, *Photoreactive Polymers: The Science and Technology of Resists*, p. 211, John Wiley & Sons, Hoboken, NJ (1989).

Ueberreiter found that in the polymer systems he studied, the diffusion of the solvent across the gel layer is the rate-determining step (i.e., it is the slowest of all the involved steps),¹⁵⁸ and in those cases solvent uptake and the inward movement of the glass-gel interface depend on the square root of time, as is characteristic of Fickian diffusion. In other systems, the processes in the glass-gel interface are rate determining, and solvent uptake and interface movement are linear functions of time. Alfrey et al.¹⁵⁹ termed it case II diffusion or polymer relaxation-controlled mass transfer.¹⁶⁰ Figure 11.31 shows a schematic of time-concentration profiles for the two dissolution modes.

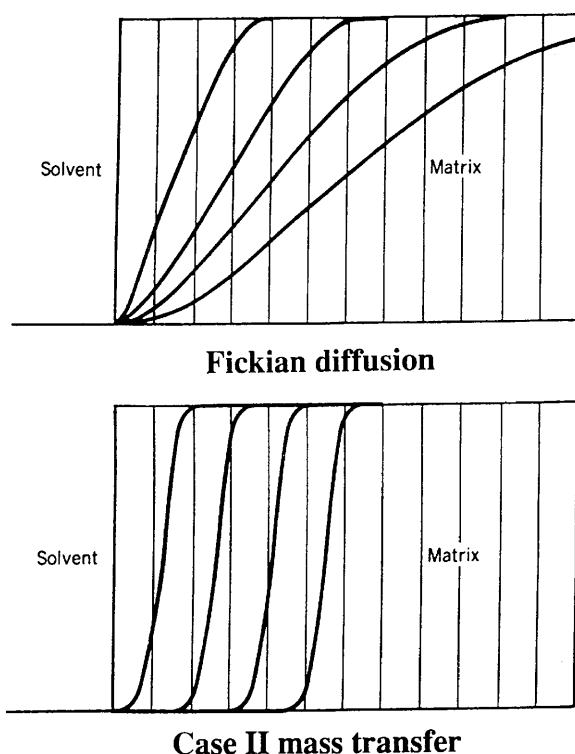


Figure 11.31 Concentration-time profiles for Fickian diffusion and for case II mass transfer. [Reprinted with permission from A. Reiser, *Photoreactive Polymers: The Science and Technology of Resists*, p. 212, John Wiley & Sons, Hoboken, NJ (1989).]

¹⁵⁸K. Ueberreiter, in *Diffusion in Polymers*, J. Crank and S. Park, Eds., Academic Press, New York (1968).

¹⁵⁹T. Alfrey, Jr., E.F. Gurnee, and W.O. Lloyd, "Diffusion in glassy polymers," *J. Polym. Sci., Part C Polymer Symposia*, **12**, 249 (1960).

¹⁶⁰G.C. Sarti, "Solvent osmotic stresses and the prediction of Case II transport kinetics," *Polymer* **20**, 827 (1979); N.L. Thomas and A.H. Windle, "A theory of case II diffusion," *Polymer* **23**, 529 (1982).

In the following section, we discuss in some depth the dissolution mechanism of phenolic polymer resists such as novolac and poly(hydroxy styrene) resins, as well as those of acrylate and alicyclic resist polymer platforms. The development of phenolic polymer resins involves similar dissolution stages. Unlike their counterparts that are solvent developable, such as bis-azide/cis-polyisoprene negative resists that require some degree of swelling for their dissolution, these phenolic polymer resists do not require such adverse swelling for dissolution.¹⁶¹

11.14 Dissolution Mechanism of Phenolic Resists

The mechanism of the phenolic polymer resist dissolution has been a hotly contested and debated concept. Many models have been proposed for how this process plays out. Although all of these models have been successful in explaining different aspects, but not the complete mechanism of novolac dissolution behavior, there is now some consensus on some key general facts surrounding this mechanism. These facts are outlined below.

11.15 Comparison of Dissolution Characteristics of Novolac and Poly(hydroxystyrene)-based Resists

Although there are some structural similarities between novolac resins and poly(hydroxystyrene)-based resists, there exist distinct differences in their dissolution characteristics. Figure 11.32 shows the development rate curves for (a) an i-line DNQ/novolac resist, (b) a poly(hydroxystyrene)/melamine cross-linker resist/photoacid generator (DUV 248-nm chemical amplification negative resist),¹⁶² and (c) a poly(butylcarbonyloxy styrene-co-hydroxystyrene)/photoacid generator (DUV 248-nm chemical amplification positive resist).¹⁶³ The dissolution rate curve for the DNQ/novolac resist exhibits a nonlinear dissolution rate profile consisting of three regions. The steep development rate log slope (DRLS = 5.2) of this resist is indicative of its high contrast. The high development contrast (R_{\max}/R_{\min}) of this resist is associated with high sensitivity and low erosion properties. In contrast, the negative- and positive-tone chemically amplified DUV 248-nm resists have DRLS values of 4.5 and 9.1, respectively, suggesting that the negative resist performs slightly worse than the i-line resist, while the positive

¹⁶¹J.P. Huang, T.K. Kwei, and A. Reiser, "Molecular mechanism of positive novolac resists," *Proc. SPIE* **1086**, 74 (1989); H. Shih, T. Yeu, A. Reiser, "Percolation view of novolac dissolution: 3. dissolution inhibition," *Proc. SPIE* **2195**, 514 (1994); B.W. Smith, "Resist processing," in *Microolithography: Science and Technology*, p. 546, Marcel Dekker (1998).

¹⁶²J.W. Thackeray et al., "Deep UV ANR photoresists for 248 nm excimer laser photolithography," *Proc. SPIE* **1086**, 34 (1989).

¹⁶³O. Nalamasu et al., "Development of a chemically amplified positive resist material for single layer deep UV lithography," *Proc. SPIE* **1262**, 32 (1990).

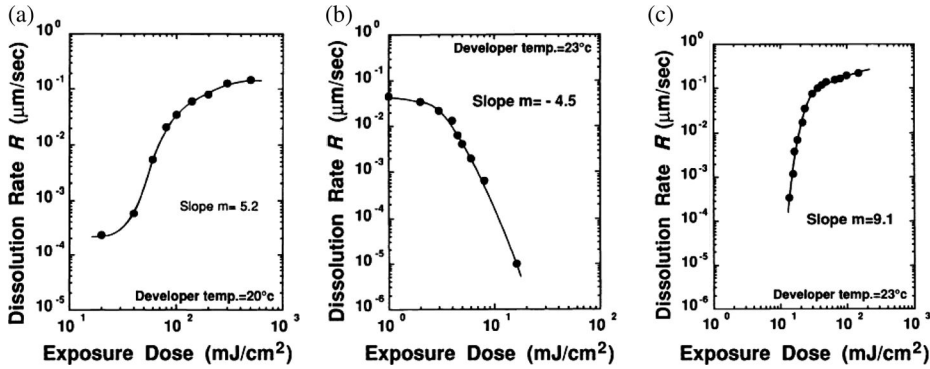


Figure 11.32 Dissolution rate curves for (a) an i-line DNQ/novolac resist, (b) a poly(hydroxystyrene)/melamine cross-linker resist (DUV 248-nm chemical amplification negative resist), and (c) poly(butylcarbonyloxy styrene-co-hydroxystyrene) (DUV 248-nm chemical amplification positive resist). The slope is the development rate log slope.¹⁶⁴

resist performs better than both the i-line and negative DUV 248-nm resists, in terms of lithography. Figure 11.33 shows an Arrhenius plot for the dissolution of i-line resist, with three distinct regions, namely, a high-dose, low-temperature region where the activation energy E_a is small and positive, an intermediate region where E_a is negative and decreasing, and a low-dose, high-temperature region where E_a is positive and comparatively large. In contrast, the plots for the DUV 248-nm resists show a constant E_a , suggesting that only one reaction

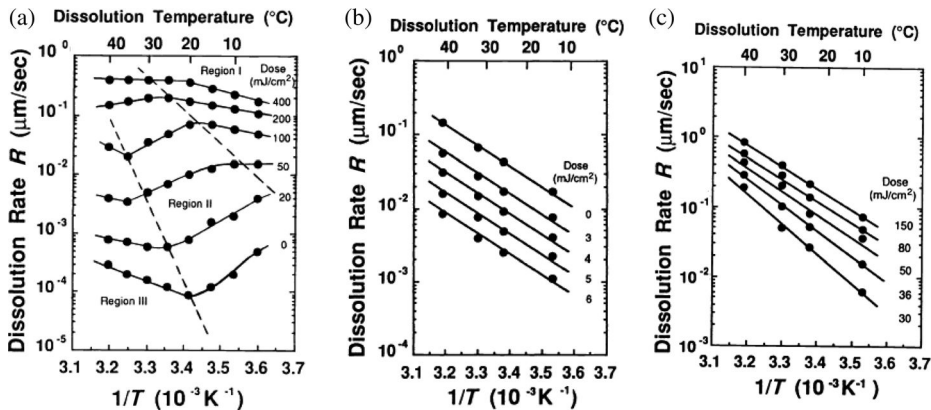


Figure 11.33 Dissolution rate Arrhenius plots (dissolution rate R versus $1/T$ of the developer) for the three resists in Fig. 11.32.¹⁶⁵

¹⁶⁴T. Itani, K. Itoh, and K. Kasama, “Dissolution kinetics of chemically amplified resists,” *Proc. SPIE* **1925**, 388 (1993).

¹⁶⁵ibid.

mechanism governs the development rate of these DUV 248-nm resists, although E_a appears to saturate at high doses. At these high doses, deprotonation of hydroxyl groups at the PHOST becomes rate determining, as in the mechanism for the negative resist.¹⁶⁶

11.16 General Facts about the Dissolution Mechanism of DNQ/Novolac Resists

The key empirical facts surrounding the dissolution of novolac that have been established are outlined below. It was on the basis of these facts that mechanistic models of novolac dissolution were proposed. The dissolution of novolac, with the exception of a brief initial phase, proceeds with a constant rate and follows case II mass transfer kinetics (also called case II Fickian diffusion). In low-molecular-weight novolacs, the width of the gel layer is on the order of 10 nm.¹⁶⁷ Arcus has demonstrated the existence of this gel layer in a high-molecular-weight phenolic novolac resin,¹⁶⁸ as shown in the laser interferogram trace of Fig. 11.34. This interferogram shows three separate sets of reflections, corresponding to the interface between the polymer matrix and the silicon wafer, the interface between the polymer matrix and the swollen gel, and the interface between the gel layer and the developer solution.¹⁶⁹

Unlike classic solvent-developed negative resists such as cyclized rubber/bisazide resist, which swell during development, the positive DNQ/novolac resists do not appreciably swell during their development in aqueous alkaline solutions. It should be emphasized that the dissolution of novolac is not exactly the same as that of the usual case II mass transfer kinetics in that it is not physical relaxation of the polymer molecules that is rate controlling. In case II dissolution, the rate-determining events occur at the polymer-gel interface.¹⁷⁰

Empirical evidence suggests that the dissolution phenomenon of novolacs has some unique characteristics (see below), the interpretation of which have provided valuable insights into the dissolution process. A minimum base concentration is required to dissolve the novolac resin at a reasonable rate, and this minimum concentration varies from one resin to another. The existence of this critical base concentration is related to the fact that the deprotonation of the phenol to the

¹⁶⁶B.W. Smith, "Resist processing," in *Microolithography: Science and Technology*, p. 447, Marcel Dekker (1998).

¹⁶⁷A. Reiser, *Photoreactive Polymers: The Science and Technology of Resists*, p. 211, John Wiley & Sons (1989); see Ref. 116, p. 211.

¹⁶⁸R.A. Arcus, "A membrane model for positive photoresist development," *Proc. SPIE* **631**, 124 (1986).

¹⁶⁹A. Reiser, *Photoreactive Polymers: The Science and Technology of Resists*, p. 211, John Wiley & Sons, Hoboken, NJ (1989); R. Dammel, *Diazonaphthoquinone based Resists*, p. 52, SPIE Press, Bellingham, WA, (1993).

¹⁷⁰R. Dammel, *Diazonaphthoquinone based Resists*, pp. 52–53, SPIE Press, Bellingham, WA (1993).

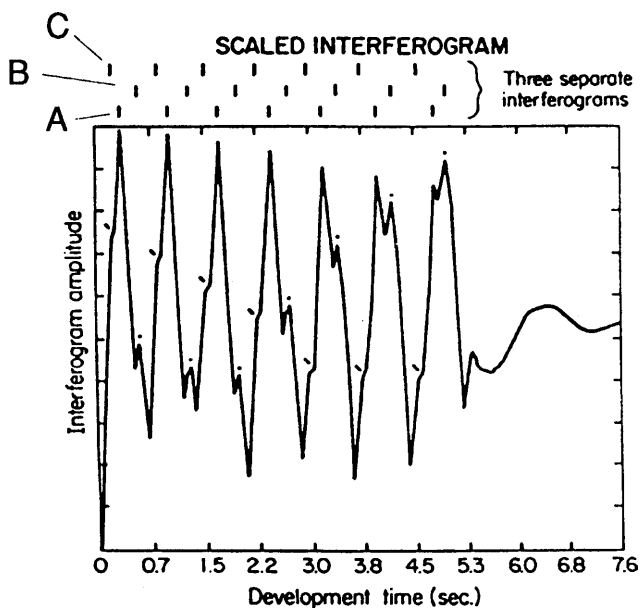
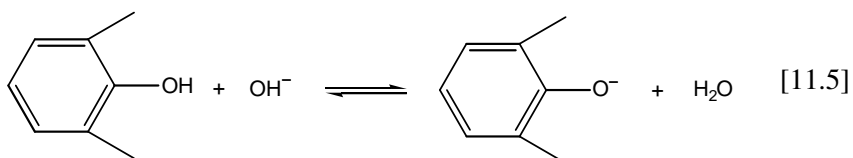


Figure 11.34 Laser interferogram obtained during the dissolution of a phenolic base resin of high molecular weight. The three sets of interferences correspond to reflections from the interfaces between solution and gel layer, gel layer and solid polymer, and polymer and glass substrate.¹⁷¹

phenolate ion must occur at some stage in the dissolution process, as shown below:¹⁷²



Above that critical concentration, the dissolution rate R shows a power law dependence on the base concentration c according to the scaling equation,¹⁷³

$$R = kc^n \quad (11.29)$$

where the constant of proportionality k is the scaling factor and n is the exponent to which c can be raised. Hinsberg and Gutierrez¹⁷⁴ reported that the dissolution

¹⁷¹R.A. Arcus, "A membrane model for positive photoresist development," *Proc. SPIE* **631**, 124 (1986).

¹⁷²A. Reiser, *Photoreactive Polymers: The Science and Technology of Resists*, p. 213, John Wiley & Sons, Hoboken, NJ (1989).

¹⁷³ibid.

¹⁷⁴W.D. Hinsberg and M.L. Gutierrez, "Effect of developer composition on photoresist performance," *Proc. SPIE* **469**, 57 (1984).

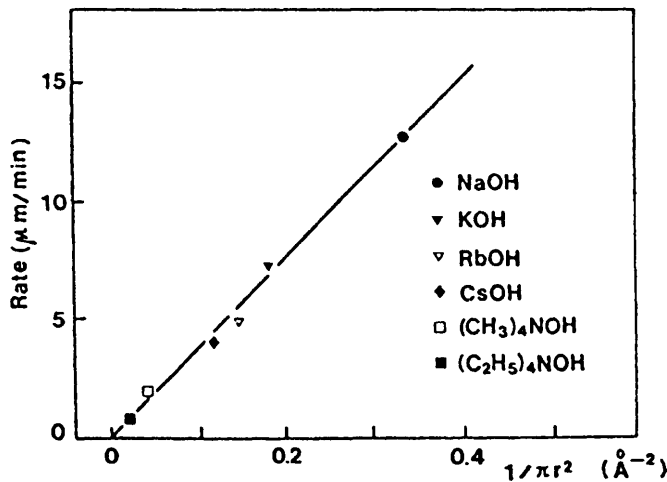


Figure 11.35 Influence of unhydrated cation size on dissolution rate, showing linear correlation between the reciprocal diffusion cross section $1/(\pi r^2)$ of the unhydrated cations and the dissolution rate.¹⁷⁵

rate of novolac is increased if a neutral salt of the base cation is added to the developer. In the systems they investigated, the dissolution rate shows a linear dependence on the concentration of the base cation, but a strongly supralinear dependence on the concentration of OH^- ions. The observations made by Hinsberg and Gutierrez¹⁷⁶ have also been confirmed for other positive resists.¹⁷⁷

Another clue to the nature of the dissolution process was uncovered when it was determined that in many resist systems there exists a linear correlation between the dissolution rate and the reciprocal diffusion coefficient of the unhydrated cation size¹⁷⁸ (see Fig. 11.35).

11.16.1 Mechanistic models for DNQ/novolac dissolution

A number of mechanistic models have been proposed with a view to explaining the above empirical results dealing with novolac dissolution. Taking together the above-outlined empirical observations surrounding novolac dissolution, according

¹⁷⁵ibid.

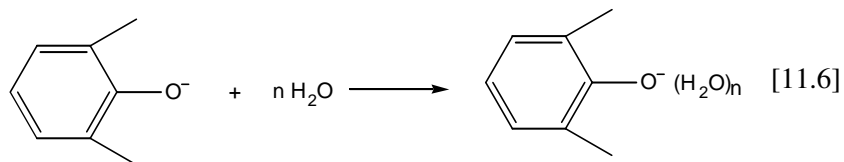
¹⁷⁶ibid.

¹⁷⁷M.J. Hanrahan and K.S. Hollis, "Comparison of the dissolution behavior of poly(p hydroxystyrene) with novolac," *Proc. SPIE* **771**, 128 (1987).

¹⁷⁸J. P. Huang, T.K. Kwei, and A. Reiser, "Molecular mechanism of positive novolac resists," *Proc. SPIE* **1086**, 74 (1989); "On the dissolution of novolac in aqueous alkali," *Macromolecules* **22**, 4106 (1989).

to Reiser,¹⁷⁹ suggests that the novolac dissolution process must contain the following steps:

- (1) The penetration of water and OH^- ions into the glassy matrix, leading to the formation of a narrow penetration zone that is the equivalent of the gel layer observed with high-molecular-weight polymers.
- (2) Deprotonation of phenol as shown in Reaction [11.5].
- (3) The hydration of the phenolate ion as shown below:



- (4) Compensation of the negative charge of the phenolate ion by the base cation.
- (5) Transfer of the hydrated novolac macromolecule into the developer solution.

Examples of models that have been proposed in an attempt to link the above steps into a coherent mechanism include the membrane model, the secondary structure model, the critical deprotonation model, the percolation model, the critical ionization model, and the stone wall model, to mention but a few. In the following sections, we briefly review the aspects of these models.

11.16.1.1 The membrane model

The membrane model, proposed by Arcus,¹⁸⁰ treats the interface between the resin and developer as a partially semipermeable membrane that may “differentiate between the ions of aqueous developers due to variations in size, composition, and charge . . . the membrane properties can be modified by chemical treatments, changes in concentration . . . and most importantly by the photochemistry of the included naphthoquinone-diazide.”¹⁸¹ This model appears to account for a great

¹⁷⁹A. Reiser, *Photoreactive Polymers: The Science and Technology of Resists*, pp. 215–216, John Wiley & Sons, Hoboken, NJ (1989).

¹⁸⁰R.A. Arcus, “A membrane model for positive photoresist development,” *Proc. SPIE* **631**, 124 (1986).

¹⁸¹*ibid.*

Table 11.3 Properties of hydrated alkali ions. (Data used with permission from Ref. 182. © 2000, Oxford University Press.¹⁸²⁾

	Li ⁺	Na ⁺	K ⁺	Rb ⁺	Cs ⁺
Ionic radii (Å) in crystals	0.68	0.98	1.33	1.48	1.67
Radii of hydrated ions	3.4	2.76	2.32	2.28	2.28

many aspects of the empirical observations surrounding the dissolution of novolac resins. It explains why the membrane would allow the passage of OH⁻ ions, while slowing down the diffusion of larger cations. This makes the cation transport through the membrane the rate-determining step and explains the increase in dissolution rate by the addition of neutral salts. Furthermore, it provides a qualitative interpretation of the cation size effect, although in the presence of highly hydrated cations, the membrane diffusion rates would be expected to correlate with the size of the hydrated cations. Yet, in reality, it is the radius of the unhydrated ions derived from crystallographic data that appears to be correlated with the dissolution rates. (see Table 11.3.)¹⁸³

While the membrane model implies that the overall rate of the dissolution process is controlled by the rate of diffusion of developer components into the matrix, another model proposed by Garza et al.¹⁸⁴ maintains that in some resins, the deprotonation of the phenol groups of the novolac can be the rate-determining step (see below).

11.16.1.2 The secondary structure model

The secondary structure model, proposed by Templeton et al.,¹⁸⁵ relates the secondary structures of novolacs [see Figs. 11.36(a) and (b)] to their dissolution behavior. The authors distinguished between structures where intermolecular bonds between novolac molecules predominate and those with predominantly intramolecular hydrogen bonds; and they correlated these to dissolution behavior. They found that, for example, for novolacs made from *p*-cresol, the secondary structure of the resin brings the OH⁻ groups of the phenols together to such an extent that

¹⁸²R.S. Berry, S.A. Rice, and J. Ross, *Physical Chemistry*, p. 422, Oxford University Press, Oxford, UK (2000).

¹⁸³A. Reiser, *Photoreactive Polymers: The Science and Technology of Resists*, p. 216, John Wiley & Sons, Hoboken, NJ (1989).

¹⁸⁴C.M. Garza, C.R. Szmanda, and R.L. Fischer, Jr., "Resist dissolution kinetics and submicron process control," *Proc. SPIE* **920**, 321 (1988).

¹⁸⁵M.K. Templeton, C.R. Szamanda, and A. Zampini, "Dissolution kinetics of positive photoresists: the secondary structure model," *Proc. SPIE* **771**, 136 (1987).

they are linked by a series of intramolecular hydrogen bonds. On deprotonation of the first phenol group of the ensemble, the resulting negative charge is delocalized via the mobile hydrogens over the whole “nest” of participating phenols (Fig. 11.37).¹⁸⁶

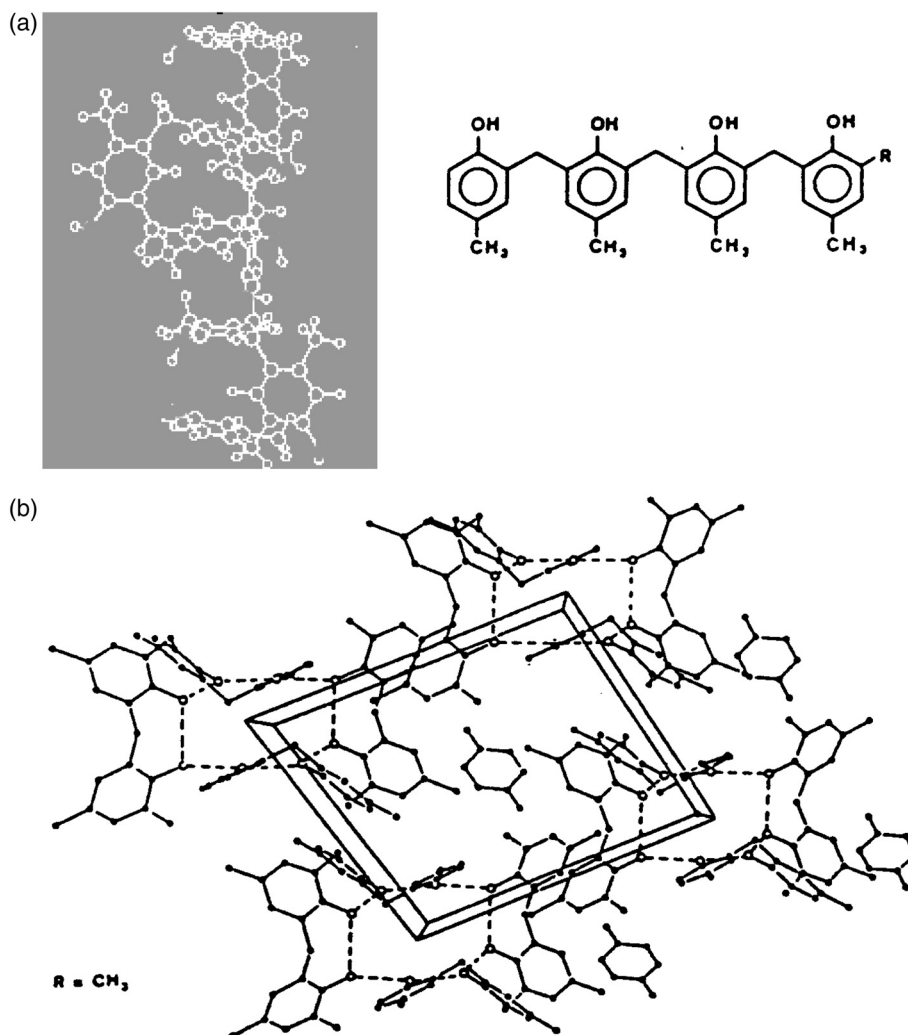


Figure 11.36 (a) Secondary structure of an *ortho-para*-coupled *m*-cresol novolac as calculated by molecular mechanics. (After M.K. Templeton et al.¹⁸⁷) (b) Secondary structure of *p*-cresol novolac tetramer as determined from x-ray crystallography. Hydrogen bonds are indicated with dotted lines.¹⁸⁸

¹⁸⁶A. Reiser, *Photoreactive Polymers: The Science and Technology of Resists*, p. 217, John Wiley & Sons, Hoboken, NJ (1989).

¹⁸⁷M.K. Templeton, C.R. Szamanda, and A. Zampini, “Dissolution kinetics of positive photoresists: the secondary structure model,” *Proc. SPIE* **771**, 136 (1987).

¹⁸⁸*ibid.*

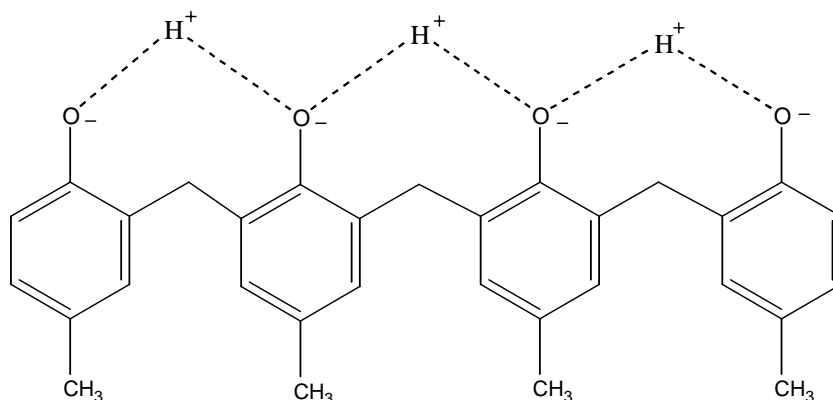


Figure 11.37 Delocalization of negative charges (via mobile hydrogen ions) over different phenol groups of *p*-cresol tetramers of novolac, following deprotonation of one of the phenolic groups.

Arriving at this phenolate site, a small cation will form a tight ion pair with the phenolate ion, binding the charge to a single center. On the other hand, if a large cation arrives at the phenolate site, it will form a loose ion pair, and part of the negative charge of phenolate will remain delocalized over the other phenols of the ensemble, making the second deprotonation step within the group much more difficult. This will effectively slow down the deprotonation of the resin and make the chemical reaction the rate-determining step in the dissolution process.¹⁸⁹

The secondary structure model, it must be pointed out, has been remarkably successful in interpreting the large differences in the dissolution rates between resins based on different cresol isomers; it also has a natural explanation for the cation size effect in *p*-cresol-based novolacs. It does, however, run into difficulties in explaining the known dependence of the dissolution process on the thermal history of the resin and its free volume status. This is not entirely unexpected for a system controlled by chemical reaction.¹⁹⁰

In explaining the results of the secondary structure model, Garza et al.¹⁹¹ suggested that for some resins the deprotonation of the phenol groups of novolacs can be the rate-determining step. In particular, they suggested that the dissolution proceeds in two distinct steps, comprising an initial single deprotonation of a hydrogen-bonded cluster, followed by the removal of the remaining proton, presumably in several smaller steps. Reiser¹⁹² rejected this argument on the grounds

¹⁸⁹A. Reiser, *Photoreactive Polymers: The Science and Technology of Resists*, p. 217, John Wiley & Sons, Hoboken, NJ (1989).

¹⁹⁰*ibid.*, p. 218.

¹⁹¹C.M. Garza, C.R. Szmanda, and R.L. Fischer, Jr., "Resist dissolution kinetics and submicron process control," *Proc. SPIE* **920**, 321 (1988).

¹⁹²A. Reiser, *Photoreactive Polymers: The Science and Technology of Resists*, p. 218, John Wiley & Sons, Hoboken, NJ (1989).

that if the deprotonation reaction is indeed the rate-limiting step and the observed high exponent of $[\text{OH}^-]$ in the rate equation is a true kinetic order, this must imply that the reaction involves the simultaneous extraction of many protons from the resist, as Garza proposed;¹⁹³ this is an event that Reiser considers highly unlikely. Instead, Reiser points out that the very high reaction order found by Garza et al. for the rate-determining step seems to indicate that the dissolution rate is limited by the kinetics of the last step, in which an $n - 1$ times deprotonated novolac reacts to form an n times deprotonated species, which detaches from the polymer matrix and enters into dissolution in the developer.¹⁹⁴

11.16.1.3 The critical deprotonation model

Huang et al.¹⁹⁵ postulated the critical deprotonation model as a way to resolve the difficulties of the Garza model, as long as the assumption is made that the rate-determining event in novolac dissolution is the last step, namely, the detachment of the hydrated novolac molecule from the matrix. According to this model, during development in aqueous base developer, water and OH^- ions of the base simultaneously enter the novolac film matrix, deprotonating some of the phenolic groups of the resin, and forming phenolates. As the water and the OH^- ion penetrate into the film, with the cation of the base following the OH^- ion, a thin penetration zone is formed by these species; this zone is equivalent to the gel layer observed in conventional polymer dissolution. A diffusion path is thus defined by a succession of hydrophilic sites (the phenolate sites), and the developer proceeds deeper into the film as through a set of diffusion channels. The phenolate ions in the diffusion channels bind the water molecules via coordination; the charge of the polymer-bound phenolates is balanced by those of the cations of the developer base. During the early stages of these processes, the deprotonated novolac segments remain attached to the polymer matrix. Only when a sufficient number of novolac segments have been converted to phenolate, can the ionomeric molecule detach itself from the polymer matrix. It is the last critical deprotonation step that makes possible the transfer of polymer into the solvent, resulting in dissolution.¹⁹⁶

It must be emphasized that a critical deprotonation must be reached before the detachment of the hydrated novolac molecule from the matrix, suggesting that the deprotonation equilibrium between phenol and developer base controls the concentration of the deprotonated species P_{n-1} , which is just one deprotonated step

¹⁹³C.M. Garza, C.R. Szmanda, and R.L. Fischer, Jr., "Resist dissolution kinetics and submicron process control," *Proc. SPIE* **920**, 321 (1988).

¹⁹⁴A. Reiser, *Photoreactive Polymers: The Science and Technology of Resists*, p. 218, John Wiley & Sons, Hoboken, NJ (1989).

¹⁹⁵J. P. Huang, T.K. Kwei, and A. Reiser, "Molecular mechanism of positive novolac resists," *Proc. SPIE* **1086**, 74 (1989); "On the dissolution of novolac in aqueous alkali," *Macromolecules* **22**, 4106 (1989).

¹⁹⁶ibid.

away from dissolution. The equilibrium constant K for the specific case of the deprotonation reaction on NaOH developer is given by¹⁹⁷

$$K = \frac{[P_{n-1}]}{[\text{NaOH}]^{n-1}}. \quad (11.30)$$

They reported that the dissolution rate is determined by the kinetics of the last step:

$$R = k_d[P_{n-1}][\text{NaOH}] = k_d K [\text{NaOH}]^n, \quad (11.31)$$

where k_d is the rate constant of the dissolution rate.

Furthermore, the state of critical deprotonation involves a multistage acid-base equilibrium, comprising very fast processes that are diffusion limited, even in fluid solution. The rate of phenolate formation in the penetration zone in this case is determined by the rate of supply of the reactants. Consequently, the rate of dissolution of the resin, which is dependent on the deprotonation process, is controlled by the diffusion of the developer into the polymer matrix.¹⁹⁸

Huang, Kwei, and Reiser¹⁹⁹ have estimated the diffusion coefficient of some cations from the dissolution rate and the width of the penetration zone. Using the observed dissolution rate R (200 Å/s) and an estimated penetration width d of 20–100 Å, the authors have estimated the diffusion coefficient of the cations in novolac resins to be on order of

$$D = Rd = 4 \times 10^{-13} \text{ to } 2 \times 10^{-12} \text{ cm}^2/\text{s}. \quad (11.32)$$

These authors²⁰⁰ have also constructed a model for the diffusion coefficient in terms of the base concentration in the penetration zone $D(c)$ as

$$D(c) = a(c - c')^n, \quad (11.33)$$

where c is the concentration of the developer, c' is the critical concentration of the developer below which no dissolution occurs, and n is a numerical exponent.

When expressed in terms of the diffusion flux, these authors arrive at an equation for the diffusion coefficient as a function of fractional depth x' into the penetration zone that is expressed in the form²⁰¹

$$D = D_0(1 - x')^{n/(n+1)}. \quad (11.34)$$

¹⁹⁷A. Reiser, *Photoreactive Polymers: The Science and Technology of Resists*, p. 218, John Wiley & Sons, Hoboken, NJ (1989).

¹⁹⁸J. P. Huang, T.K. Kwei, and A. Reiser, "Molecular mechanism of positive novolac resists," *Proc. SPIE* **1086**, 74 (1989); "On the dissolution of novolac in aqueous alkali," *Macromolecules* **22**, 4106 (1989).

¹⁹⁹ibid.

²⁰⁰ibid.

²⁰¹ibid.

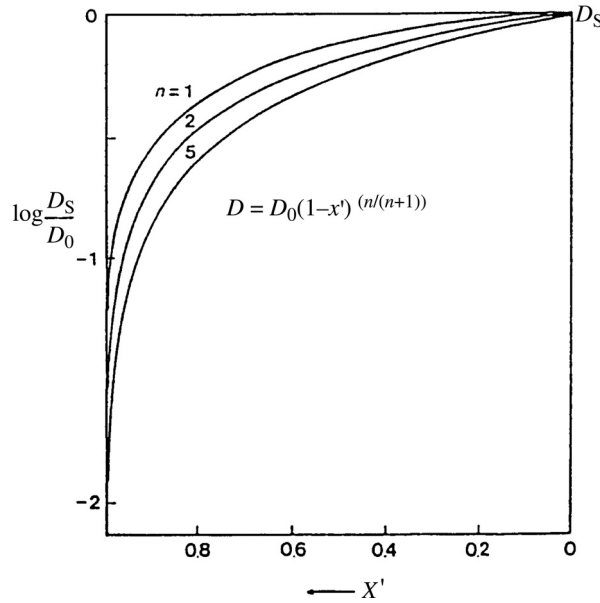


Figure 11.38 Evolution of the diffusion coefficient along the penetration zone, and collapse of the diffusion coefficient at the polymer-gel interface.²⁰²

Figure 11.38 shows the collapse of the diffusion coefficient at the polymer-gel interface (at $x' = 1$). A similar treatment yields an improved equation for the experimentally observed supralinear dependence of dissolution on the base concentration (see Fig. 11.39).

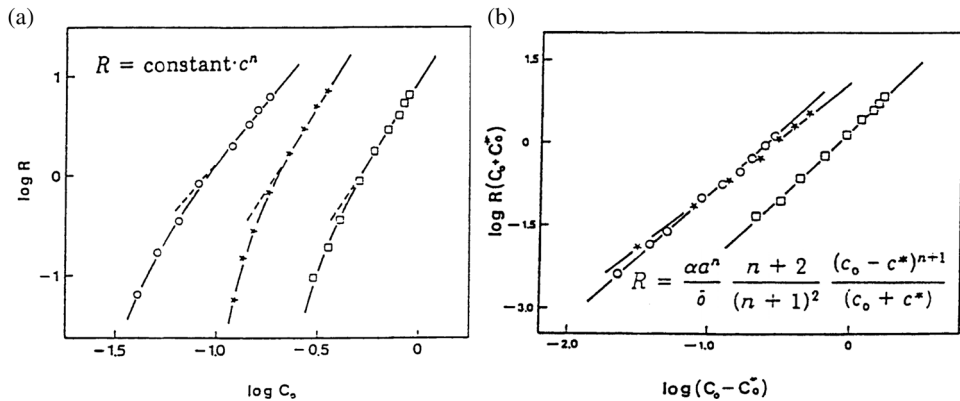


Figure 11.39 Dependence of novolac dissolution rate on the developer base concentration: (a) standard power law model; (b) Huang-Kwei-Reiser model. c^* is the critical concentration below which no development occurs.²⁰³

²⁰²ibid.

²⁰³ibid.

All of the above results, which show the cation transport to be the rate-determining step, are also corroborated by results of the investigations on the effect of added neutral salts (such as NaCl and NaOH) to the developer solution, as reported by Hinsberg and Gutierrez.²⁰⁴ Above a certain threshold, the rate of increase of the dissolution speed is greatly lowered, indicating the saturation of cation transport, a regime in which the dissolution rate is limited by the deprotonation step.²⁰⁵

11.16.1.4 The percolation model of resist dissolution

The idea of novolac as an amphiphilic polymer into which the developer penetrates through a chain of hydrophilic sites has led to a mathematical treatment of resist dissolution as a percolative diffusion process.²⁰⁶ The basic ideas of the percolation theory of dissolution include the following six key facts. (i) The dissolution rate is determined by transport of ions through the percolation zone. (ii) Dissolution occurs only if the percolation field exceeds a critical value. (iii) Molecular weight effects are caused by energy conduction in the chains. (iv) All aqueous dissolution of polymers follows one dimensionless master equation; in other words, the dissolution properties of all polymers scale the same way. (v) Inhibitors work by clustering the percolation sites. (vi) Neutral salts enhance the dissolution by increasing cation flux, and inhibit it by competing with anion movement.

Percolation theory²⁰⁷ predicts for the dissolution rate R an equation of the form

$$R = k(p - p_c)^2, \quad (11.35)$$

where k is a constant, p is the percolation parameter (i.e., the degree of filling of the percolation field), and p_c is the percolation threshold (i.e., the critical value of p above which the cluster size tends to infinity). The percolation parameter is readily determined from the density of hydrophilic sites x from the relation $p = ax + b$, where the constants a and b are determined by setting $p = 1$ for $x = 1$, corresponding to the maximum density of free hydroxyl groups in the group of resins studied, and by setting $p_c = ax_c + (1 - a)$, where x_c is the critical

²⁰⁴W.D. Hinsberg and M.L. Gutierrez, "Effect of developer composition on photoresist performance," *Proc. SPIE* **469**, 57 (1984).

²⁰⁵R. Dammel, *Diazonaphthoquinone based Resists*, p. 58, SPIE Press, Bellingham, WA (1993).

²⁰⁶T.F. Yeh, H.Y. Shi, and A. Reiser, "A percolation view of novolac dissolution and inhibition," *Proc. SPIE* **1672**, 204 (1992); "Percolation view of novolac dissolution and dissolution inhibition," *Macromolecules* **25**, 5345–5352 (1992).

²⁰⁷According to percolation theory, a branch of mathematics dealing with phenomena such as the formation of connected channels (otherwise called "Percolating clusters") from randomly distributed sites on a grid, such a system would be expected to have a strongly nonlinear response if the number of sites per volume (otherwise called "degree of space filling") is close to a threshold value called the "percolation threshold." For more details, see, for example, D. Stauffer, *Introduction to Percolation Theory*, Taylor & Francis, London (1985).

density of percolation sites for which dissolution no longer occurs. The value of x_c is determined for each resin from a plot of $\log R$ versus x , where $\log R$ goes to $-\infty$ for x_c .²⁰⁸ Typically, the values of x_c determined experimentally are consistent with $p_c = 0.2$, a value that is reasonable for a large number of three-dimensional percolation processes.²⁰⁹

Figure 11.40 shows a plot of $\log R$ versus $\log(p - p_c)$ for seven structurally different resins, as well as a dimensionless master curve obtained by taking the ratio of the dissolution rates of the seven structurally different resins relative to R_1 , the dissolution rate of polyhydroxystyrene, i.e., a fully occupied percolation field ($x = p = 1$) versus p , according to the equation²¹⁰

$$\log\left(\frac{R}{R_1}\right) = -2\log(1 - p_c) + 2\log(p - p_c). \quad (11.36)$$

It is remarkable that these seven structurally different resins all yielded a slope of 2 on $\log R$ versus $\log(p - p_c)$ plots for a value of $p_c = 0.2$, all of them mapping perfectly onto the same master curve.²¹¹ It should be pointed out that a major

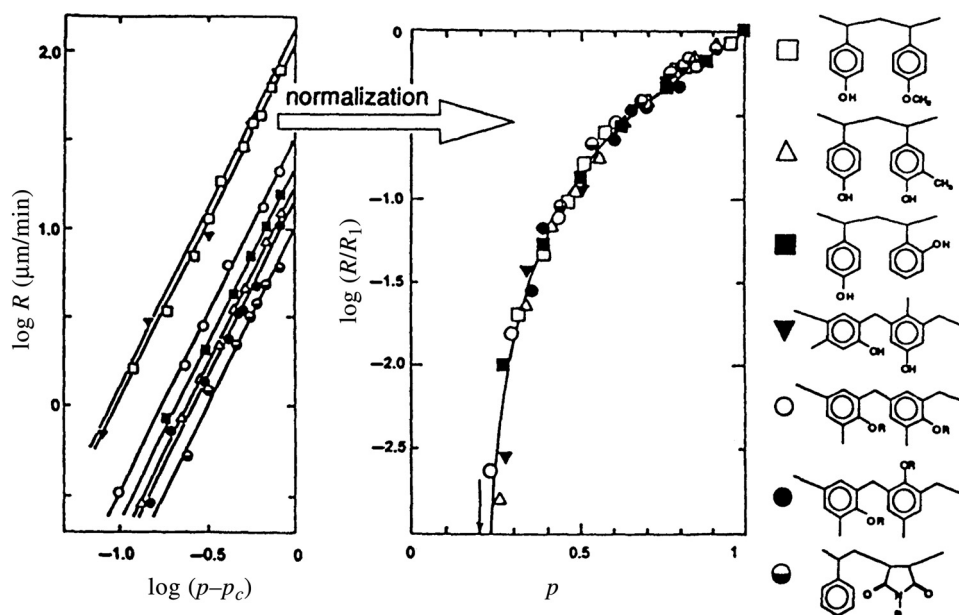


Figure 11.40 The dimensionless master curve for seven structurally different resins.²¹²

²⁰⁸R. Dammel, *Diazonaphthoquinone based Resists*, p. 62, SPIE Press, Bellingham, WA (1993).

²⁰⁹T.F. Yeh, A. Reiser, R.R. Dammel, G. Pawlowski, and H. Roschert, "Scaling law for the dissolution of phenolic resins in aqueous base," *Proc. SPIE* **1925**, 570 (1993).

²¹⁰F. Yeh, A. Reiser, R.R. Dammel, G. Pawlowski, H. Roschert, "Scaling law for the dissolution of phenolic resins in aqueous base," *Proc. SPIE* **1925**, pp. 570–582 (1993); R. Dammel, *Diazonaphthoquinone based Resists*, p. 65, SPIE Press, Bellingham, WA (1993).

²¹¹ibid.

²¹²ibid.

problem with the percolation model is that it predicts a resist contrast that is far lower than what is observed experimentally.

11.16.1.5 The critical ionization model

The critical ionization model proposed by Tsiartas et al.²¹³ states that a resist polymer below its entanglement molecular weight dissolves in a developer whenever a critical fraction of its blocked groups become deblocked. In the specific case of phenolic resins, dissolution proceeds via acid-base reaction between the aqueous developer base and the phenolic group of the resins, leading to deprotonation of the latter and the formation of phenolate ions. Dissolution as a result occurs in the phenolic resins only when a critical fraction of the phenol groups in the polymer is ionized (deprotonated). Below this critical ionization fraction, no dissolution of the resin occurs in the developer. This implies that lower-molecular-weight polymers will require fewer deblocking (deprotonation or ionization) events to become soluble compared to their higher-molecular-weight counterparts.

11.16.1.6 The stone wall model of novolac dissolution

Proposed by Hanabata et al.²¹⁴ in 1988, this model states that during development, the low-molecular-weight novolacs and sensitizer (referred to as the mortar of the wall) in the exposed part of DNQ/novolac resist dissolve quickly; this has the effect of increasing the surface areas of the high-molecular-weight novolac (referred to as the stones of the wall) that is in contact with the developer, and will eventually lead to a breakup of the “stone wall” and result in dissolution (see Fig. 11.41).

11.16.1.7 Effects of resin and inhibitor structure on dissolution rate

There is ample evidence that the structural properties of phenolic resins such as novolac and poly(hydroxystyrene), as well as the inhibitors associated with them, do exert considerable influence on the dissolution properties of the DNQ/novolac resist.²¹⁵

²¹³P.C. Tsiartas, L.W. Flanagan, C.L. Henderson, W.D. Hinsberg, I.C. Sanchez, R.T. Bonnecaze, and C.G. Willson, “The mechanism of phenolic polymer dissolution: a new perspective,” *Macromolecules* **30**, 4656–4664 (1996).

²¹⁴M. Hanabata, Y. Uetani, and A. Furuta, “Novolac design for high resolution positive photoresists. II. stone wall model for positive photoresist development,” *Proc. SPIE* **920**, 349–482 (1990).

²¹⁵C.G. Willson, R. Miller, D. McKean, N. Clecak, T. Tompkins, D. Hofer, J. Michl, and J. Downing, “Design of a positive resist for projection lithography in the mid UV,” *Polym. Sci. Eng.* **23**, 1004 (1983); M.K. Templeton, C.R. Szamanda, and A. Zampini, “Dissolution kinetics of positive photoresists: the secondary structure model,” *Proc. SPIE* **771**, 136 (1987).

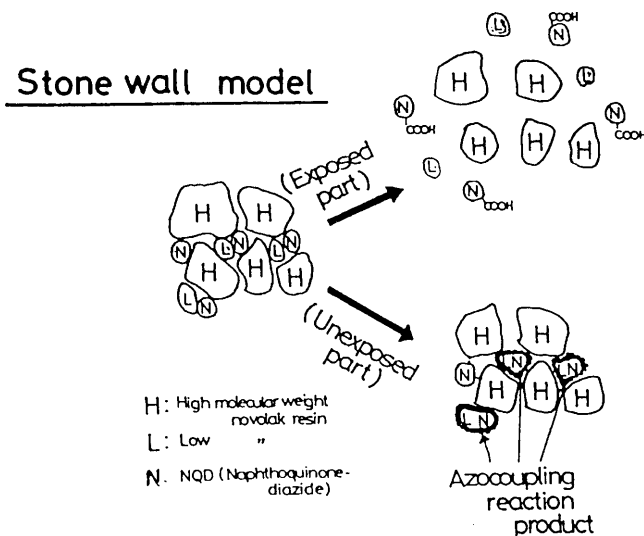


Figure 11.41 Stone wall model of DNQ/novolac resist development.²¹⁶

As discussed earlier in the secondary structure model, Templeton et al.²¹⁷ have shown that the steric arrangement of the methylene links in the novolac resin can have a profound effect on its dissolution rate and on lithographic performance. Using molecular mechanics, these authors have calculated the equilibrium secondary structures of cresol-formaldehyde oligomers.²¹⁸ They found that the secondary structure of these molecules determines the relative positions of the hydroxyl groups in the novolac matrix, and hence the possibility of intramolecular hydrogen bonding.²¹⁹

Figure 11.42 shows the secondary structure of (a) *ortho*-coupled novolac, (b) *ortho-para*-coupled novolac, and (c) poly(hydroxyl styrene). In the model of the *ortho*-coupled *p*-cresol novolac, all four hydroxyl groups are within reach of each other, and intramolecular hydrogen bonding is strongly favored, making this novolac have low T_g , low dissolution rate, and good inhibition properties. In contrast, in the secondary structure of the *ortho-para*-coupled *m*-cresol novolac, the hydroxyl groups are widely separated and located on the periphery of the molecule, a configuration that favors intermolecular hydrogen bonding over

²¹⁶ibid.

²¹⁷M.K. Templeton, C.R. Szamanda, and A. Zampini, "Dissolution kinetics of positive photoresists: the secondary structure model," *Proc. SPIE* **771**, 136 (1987).

²¹⁸E. Paulus and V. Bohmer, "The crystal structure of oligo[(2 hydroxy 1,3 phenylene)methylene]s," *Makromol. Chem.* **185**, 1921 (1984).

²¹⁹A. Reiser, *Photoreactive Polymers: The Science and Technology of Resists*, p. 218, John Wiley & Sons, Hoboken, NJ (1989).

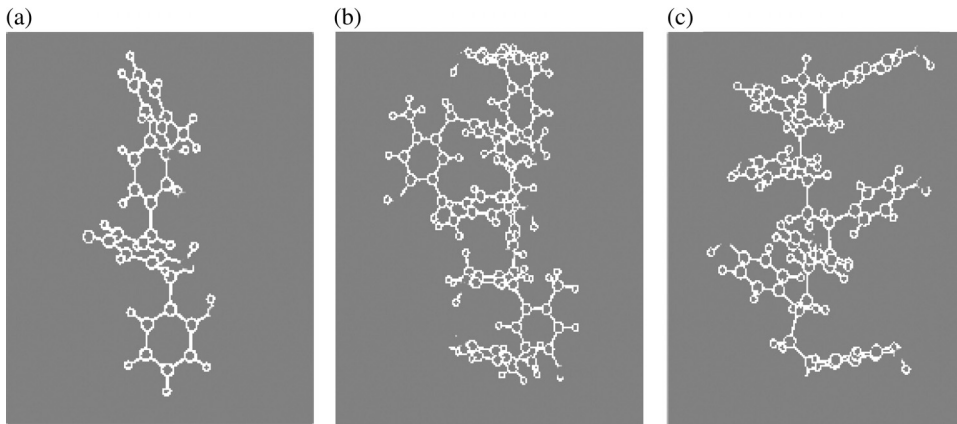


Figure 11.42 Secondary structure of (a) *ortho*-coupled novolac, (b) *ortho-para*-coupled novolac, and (c) poly(hydroxyl styrene). The *ortho*-coupled novolac has a high degree of hydrogen bonding, low T_g , low dissolution rate, and good inhibition properties. The *ortho-para*-coupled novolac has a low degree of intramolecular hydrogen bonding, high T_g , high dissolution rate, and poor dissolution inhibition properties. The poly(hydroxyl styrene) has no intramolecular hydrogen bonding, very high T_g , very fast dissolution, and poor dissolution inhibition properties.²²⁰

intramolecular bonding. The same also applies to poly(hydroxystyrene). As a result, both *ortho-para*-coupled *m*-cresol novolac and poly(hydroxystyrene) have high T_g , high dissolution rate, and poor dissolution inhibition properties. The balance between intra- and intermolecular hydrogen bonding also affects the interaction of the resin with the inhibitor, in other words, the solubility of the DNQ in the novolac.²²¹

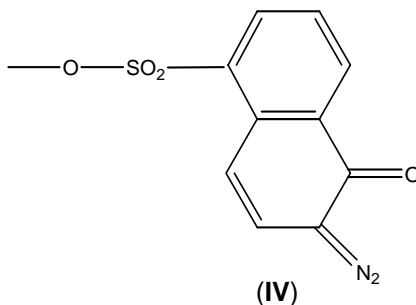
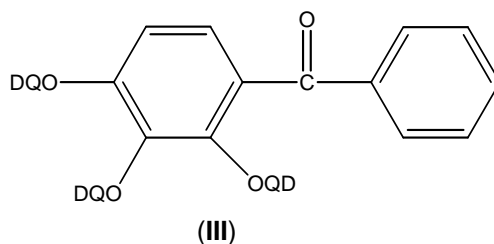
The effect of the structure of the inhibitor on the dissolution rate of the resist and on its lithographic performance has also been reported by Trefonas and Daniels.²²² These investigators studied the effects of the number of diazoquinone units attached to a polyfunctional inhibitor (**III**). For example, with benzophenone as the central component (ballast), they prepared six derivatives by gradually substituting all six hydroxyl groups of hexahydroxybenzophenone by diazoquinone moieties, which yielded six different photoactive species. The ratio q of active groups to ballast thus had values between 1 and 6. They used trisubstituted

²²⁰M.K. Templeton, C.R. Szamanda, and A. Zampini, "Dissolution kinetics of positive photoresists: the secondary structure model," *Proc. SPIE* **771**, 136 (1987).

²²¹*ibid.*, pp. 219–220.

²²²P. Trefonas III and B.K. Daniels, "New principle for image enhancement in single layer positive photoresists," *Proc. SPIE* **771**, 194 (1987).

benzophenone (shown below) as the photoactive species (inhibitor),²²³ where DQ is the moiety (IV).



It should be pointed out that the DQ groups in the resist absorb light independently and decompose independently, so that in a partially exposed resist film there will be a mixture of photoproducts. Assuming that the dissolution rate R is the sum of the dissolution rates r_i associated with each photoproduct, and weighted by the content m_i of the product i in the partially exposed resist, they obtained

$$R = \sum_i m_i r_i. \quad (11.37)$$

The remarkable result of this analysis, which is rather counterintuitive, is the finding that in certain particularly selective novolac resists with a trifunctional inhibitor ($q = 3$), the contribution to the dissolution rate by the fully (i.e., triply) converted inhibitor is much larger than the contributions of the other components.²²⁴ For instance, in the case cited by Trefonas and Daniels,²²⁵ the rate of contribution (r_0) of the fully converted inhibitor ($q = 0$) and those of the others, (r_1, r_2, r_3) are given as²²⁶ $r_0 = 1690 \text{ (}\dot{\text{A}} \cdot \text{s}^{-1}\text{)}$, $r_1 = 24$, $r_2 < 1$, and $r_3 = 0$.

The implication of these results suggests that the dissolution of the resist is controlled almost exclusively by the fully exposed (triply converted) component, the

²²³A. Reiser, *Photoreactive Polymers: The Science and Technology of Resists*, p. 211, John Wiley & Sons, Hoboken, NJ (1989).

²²⁴ibid, p. 223.

²²⁵P. Trefonas III and B.K. Daniels, "New principle for image enhancement in single layer positive photoresists," *Proc. SPIE* **771**, 194 (1987).

²²⁶These are also cited in A. Reiser, *Photoreactive Polymers: The Science and Technology of Resists*, p. 223, John Wiley & Sons, Hoboken, NJ (1989).

concentration of which becomes important in the latter stages of irradiation.²²⁷ Dissolution of the resist is slow initially as the dissolution proceeds, but increases quite dramatically when the third component starts to dominate the composition of the photoproduct. As a result, the resist has a sharp exposure threshold and high development contrast, as observed by Trefonas and Daniels.²²⁸ Figure 11.43 shows the effect of inhibitor functionality on the dimensions and the wall slope of 1.25- μm features in a series of proprietary resist compositions of increasing inhibitor functionality. The improvement in image quality, dimensional accuracy, and sidewall slope in this series is remarkable.²²⁹

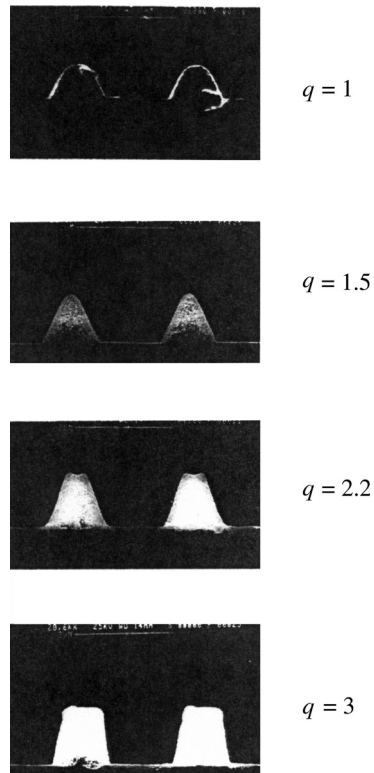


Figure 11.43 Effect of inhibitor functionality on the dimensions and the wall slope of 1.25- μm features in a series of proprietary resist compositions of increasing inhibitor functionality.²³⁰

²²⁷A. Reiser, *Photoreactive Polymers: The Science and Technology of Resists*, p. 223, John Wiley & Sons, Hoboken, NJ (1989).

²²⁸P. Trefonas III and B.K. Daniels, "New principle for image enhancement in single layer positive photoresists", *Proc. SPIE 771*, 194 (1987).

²²⁹A. Reiser, *Photoreactive Polymers: The Science and Technology of Resists*, p. 223, John Wiley & Sons, Hoboken, NJ (1989).

²³⁰P. Trefonas III and B.K. Daniels, "New principle for image enhancement in single layer positive photoresists," *Proc. SPIE 771*, 194 (1987).

11.17 Resist Development Issues

11.17.1 Pattern collapse

The collapse of patterns is a phenomenon that occurs during the rinse step of the development process of resists. As developer and rinse deionized water are removed from the developed wafers, surface tension forces pull closely spaced adjacent lines together (see Fig. 11.44). The outside features are more susceptible to collapse than those on the inside. Factors that influence pattern collapse include the aspect ratio (height/width), pitch, and mechanical properties of the resist.²³¹

The origin of this phenomenon can be traced to the drying step of the liquid development process. During the development step, after the resist-patterned wafer has been contacted with the developer solution for a given length of time and subsequently rinsed with deionized water, the level of the rinse liquid at some point attains a condition similar to that shown in Fig. 11.45, where the space between adjacent resist lines is partially filled with fluid. The fluid meniscus exhibits a curvature due to the differences in pressure across the fluid interface that result from surface tension in the confined space between the resist lines. Tanaka et al.²³² developed a cantilever beam mechanical model for describing pattern collapse. The Laplace equation relates the pressure differential across the meniscus

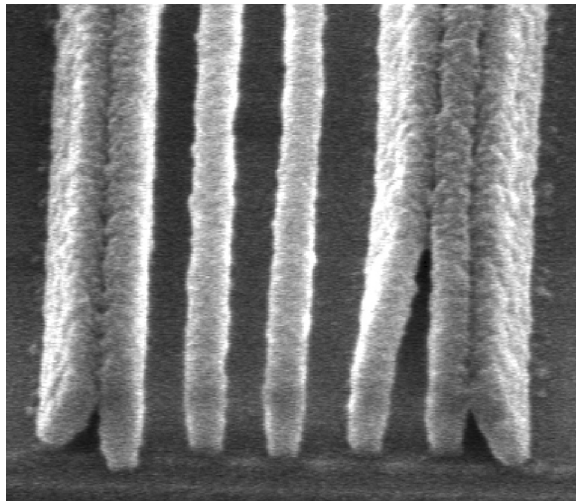


Figure 11.44 Features that have collapsed after liquid development.

²³¹W.D. Domke, V.L. Graffenberg, S. Patel, G.K. Rich, H.B. Cao, and P.F. Nealey, "Pattern collapse in high aspect ratio DUV and 193 nm resists," *Proc. SPIE* **3999**, 313–321 (2000).

²³²T. Tanaka, M. Morgami, and N. Atoda, "Mechanism of resist pattern collapse during development process," *Jpn. J. Appl. Phys.* **32**, 6059–6064 (1993).

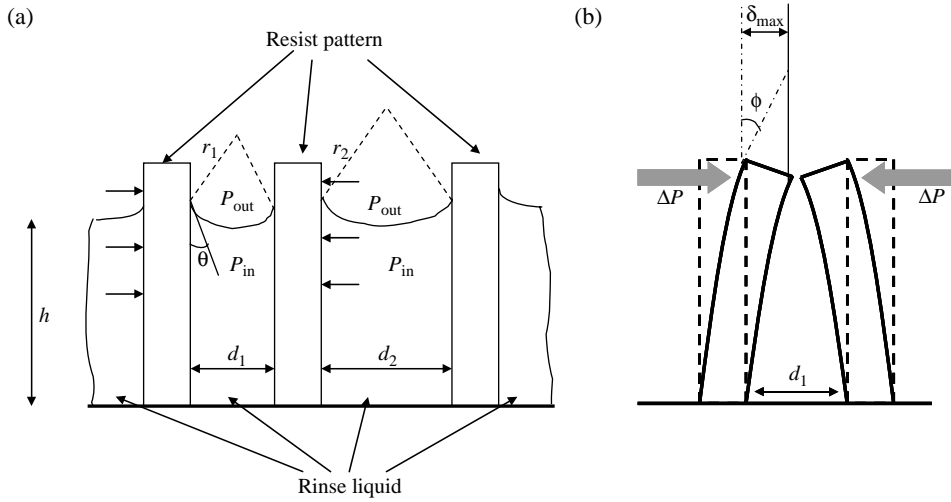


Figure 11.45 Schematic of (a) resist patterns undergoing rinsing during development and (b) the forces acting on the resist patterns due to developer rinse liquid.

to the capillary pressure as²³³

$$\Delta P = \frac{\gamma}{r}, \tag{11.38}$$

where γ is the surface tension and r is the radius of curvature of the fluid’s meniscus. r is related to the space d between the two resist lines (before any bending occurs) as

$$r = \frac{d}{2 \cos \theta}. \tag{11.39}$$

The pressure differential across the meniscus exerts capillary forces that act perpendicularly and inward from the resist sidewall. Thus, the capillary force on the resist line is given by²³⁴

$$F = \Delta P A = \frac{2\gamma \cos \theta}{d} h l, \tag{11.40}$$

where A is the area of the resist line covered by the rinse liquid (height h of the rinse liquid \times length l of the resist line). From the above equation, it can be seen that pattern collapse depends on the spacing distance between the resist lines (this is related to the pitch), as well as the surface tension of the rinse liquid (for water,

²³³P.W. Atkins, *Physical Chemistry*, 5th ed., pp. 963–966, W.H. Freeman & Co., New York (1994).

²³⁴T. Tanaka, M. Morgami, and N. Atoda, “Mechanism of resist pattern collapse during development process,” *Jpn. J. Appl. Phys.* **32**, 6059–6064 (1993).

it is 0.072 N/m or 72 dynes per centimeter at room temperature), and the aspect ratio of the line (h/d).

The capillary force increases as the resist line starts to bend. The radius of curvature of the meniscus decreases as the two resist lines approach each other, causing an increase in the capillary force.²³⁵

The bending of the resist line can be modeled as an elastic cantilever beam.²³⁶ The Young's modulus E , which is a measure of the stiffness of the resist, is the important property that can be used to describe the bending action of the resist. In general, resists have a Young's modulus in the range of 2–6 GPa (with novolac resists occupying the high end of the range and the acrylate resists occupying the low end of the range).²³⁷ The T_g of a resist correlates positively with its Young's modulus; resists with high T_g tend to have high Young's modulus, and those with low glass transition temperature tend to have low Young's modulus.

Applying a capillary force F to a resist line causes that line to move (or sway) into the space by an amount δ given by

$$\delta = \frac{3}{2} \left(\frac{F}{E} \right) \left(\frac{h}{d} \right)^3. \quad (11.41)$$

The fact that the amount of bending is proportional to the cube of the aspect ratio of the resist line implies that bending is very sensitive to the aspect ratio.²³⁸

As the resist line bends, the pulling of the line by the capillary force is opposed by a restoring force caused by the stiffness of the resist. Eventually, a critical point is reached where the capillary force exceeds the restoring force of the resist, resulting in the collapse of the resist pattern.²³⁹ Tanaka et al.²⁴⁰ have calculated this critical point to occur when

$$\frac{E}{\gamma} \leq \frac{4}{d} A_1^3 \left[3A_s \cos \theta + \sin \theta + \sqrt{9A_s^2 \cos^2 \theta + 6A_s \cos \theta \sin \theta} \right], \quad (11.42)$$

where A_s is the aspect ratio of the space and A_1 is the aspect ratio of the line (h/d). In a situation where the contact angle is less than about 80 deg and the aspect ratio of the space is high, the square root term in Eq. (11.42) can be approximated with the

²³⁵C.A. Mack, *Fundamental Principles of Optical Lithography: The Science of Microfabrication*, p. 364, John Wiley & Sons, Hoboken, NJ (2007).

²³⁶T. Tanaka, M. Morgami, and N. Atoda, "Mechanism of resist pattern collapse during development process," *Jpn. J. Appl. Phys.* **32**, 6059–6064 (1993).

²³⁷J. Simons, D. Goldfarb, M. Angelopoulos, S. Messick, W. Moreau, C. Robinson, J. de Pablo, and P. Nealey, "Image collapse issues in photoresist," *Proc. SPIE* **4345**, 19–29 (2001).

²³⁸C.A. Mack, *Fundamental Principles of Optical Lithography: The Science of Microfabrication*, p. 364, John Wiley & Sons, Hoboken, NJ (2007).

²³⁹ibid.

²⁴⁰T. Tanaka, M. Morgami, and N. Atoda, "Mechanism of resist pattern collapse during development process," *Jpn. J. Appl. Phys.* **32**, 6059–6064 (1993).

first terms of the Taylor series to give²⁴¹

$$\frac{E}{\gamma} \leq \frac{4}{d} A_1^3 [3A_s \cos \theta + \sin \theta]. \quad (11.43)$$

Yoshimoto et al.²⁴² have proposed an elastoplastic model for pattern collapse, in which the maximum feature displacement δ_{\max} from mean position arising from pattern-bending deformation is described by the equation

$$\delta_{\max} = \frac{\sigma_Y^2 W}{E \alpha \Delta P} \left\{ \frac{1}{2} - \sqrt{1 - \alpha} \right\}, \quad (11.44)$$

where σ_Y^2 is the yield stress, E is the Young's modulus, ΔP is the pressure difference acting on the features, and α is a parameter ($2/3 < \alpha < 1$). Elastic bending results in a smaller radius of curvature of the meniscus, leading to higher capillary pressure ΔP as

$$\Delta P = \frac{2\gamma \cos(\theta - \phi)}{S - 2\delta_{\max}}, \quad (11.45)$$

where ϕ is the tangential angle made by the feature at the point of maximum displacement. This effect is more pronounced for symmetric structures than asymmetric ones.

The value of any model lies not only in its predictive ability, but also in how it can be used to mitigate the problems it describes. The same is true for the pattern-collapse models presented above. In particular, Eq. (11.43) is a very important equation because it shows the factors that affect pattern collapse and therefore what can be done to reduce it. The factors that affect pattern collapse include surface tension of the rinse fluid, Young's modulus of the resist line, contact angle of water to the resist, and aspect ratios of the line and space, as well as the width of the space.²⁴³ Approaches that are effective in reducing pattern collapse are briefly described below. They include making the resist stiffer by increasing its Young's modulus through increasing its T_g .²⁴⁴ Reducing the air-water surface tension by adding surfactant to the rinse liquid will also reduce pattern collapse.²⁴⁵

²⁴¹C.A. Mack, *Fundamental Principles of Optical Lithography: The Science of Microfabrication*, p. 365, John Wiley & Sons, Hoboken, NJ (2007).

²⁴²K. Yoshimoto et al., "A two dimensional model of the deformation of photoresist structures using elastoplastic polymer properties," *J. Appl. Phys.* **96**(4), 1857 (2004).

²⁴³C.A. Mack, *Fundamental Principles of Optical Lithography: The Science of Microfabrication*, p. 365, John Wiley & Sons, Hoboken, NJ (2007).

²⁴⁴ibid.

²⁴⁵S. Hien, G. Rich, G. Molina, H.B. Cao, and P.F. Nealey, "Collapse behavior of single layer 193 nm and 157 nm resists: use of surfactants to realize the sub 130 nm nodes," *Proc. SPIE* **4690**, 254–261 (2002); K. Tanaka, R. Naito, T. Kitada, Y. Kiba, Y. Yamada, M. Kobayashi, and H. Ichikawa, *Proc. SPIE* **5039**, pp. 1366–1381 (2003); P. Zhang, M. Jaramillo, D. King, B. Ross, D. Witko, T. Paxton,

(Surfactants may pose contamination problems and can also soften the resist, reducing its Young's modulus.) The use of supercritical carbon dioxide (which has no surface tension) to develop the resist will also reduce pattern collapse. Heating the resist during the rinse step has been reported to reduce pattern collapse.²⁴⁶ Given that the worst case for pattern collapse [maximum value of $3A_s(\cos\theta + \sin\theta)$] occurs at an angle of $\tan^{-1}(1/3A_s)$, which is generally less than 10 deg, and which is associated with hydrophilic resists, making the resist more hydrophobic will reduce pattern collapse.²⁴⁷ Although the aspect ratio of the space can impact pattern collapse, it is less so for hydrophobic resists (with small $\cos\theta$). Because the space width has a direct impact on pattern collapse, with smaller spaces increasing the capillary force and thus the propensity to collapse, increasing the space width will reduce pattern collapse. By far, the most critical factor in pattern collapse is the aspect ratio of the line, given that the tendency to collapse increases as the cube of the line aspect ratio; decreasing the aspect ratio of the line will significantly reduce pattern collapse.²⁴⁸

11.18 Postdevelopment Bake and Resist Stabilization Treatments

11.18.1 Postdevelopment bake

In the postdevelopment bake, also called postbake or hard bake, the patterned resist features are subjected to a thermal treatment in a forced air oven or a hot plate. The function of the postdevelopment bake step is to remove residual casting solvent, developer, and water within the resist film,²⁴⁹ as well as to harden the resist film so that it can withstand the rigors of plasma etching and other harsh processes.²⁵⁰ Baking the resist above its T_g also improves the adhesion of the resist to the substrate.²⁵¹ Because the photosensitivity of the resist is no longer required for any of the subsequent process operations, the baking temperature can be elevated to as high as possible, sometimes approaching the solvent boiling point, so as to remove residual solvents from the resist as well as to effect maximal densification. For DNQ/novolac resist, unreacted DNQ compounds can lead to problems in subsequent process steps such as implantation, which may cause the rapid release of

and T. Davis, "The impact of surfactant in developer and rinse solutions on 193 nm lithography performance," *Proc. SPIE* **5039**, 1409–1415 (2003).

²⁴⁶T. Tanaka, M. Morigami, H. Oizumi, T. Soga, T. Ogawa, and F. Murai, "Prevention of pattern collapse by resist heating during rinse," *J. Electrochem. Soc.* **141**(12), L169–L171 (1994).

²⁴⁷C.A. Mack, *Fundamental Principles of Optical Lithography: The Science of Microfabrication*, p. 365, John Wiley & Sons, Hoboken, NJ (2007).

²⁴⁸ibid.

²⁴⁹B.W. Smith, "Resist processing," in *Microlithography: Science and Technology*, Marcel Dekker, p. 561 (1998).

²⁵⁰W.A. Moreau, *Semiconductor Lithography: Principles, Practices, and Materials*, p. 5, Plenum Press, New York (1988).

²⁵¹R. Dammel, *Diazonaphthoquinone based Resists*, p. 118, SPIE Press, Bellingham, WA (1993).

nitrogen from the radiolysis of DNQ. In densified resist films, the nitrogen may not easily diffuse out of the film and may thus cause localized explosive resist popping, dispersing resist particles on the wafer surface. Baking the DNQ/novolac resist above the decomposition temperature of DNQ (110°C) has been reported to destroy the PAC and prevent it from participating in any unwanted reactions.²⁵²

As a rule, novolac resins are not as thermally stable as their poly(hydroxystyrene)-based counterparts. Poly(hydroxystyrene)-based DUV resists have T_g values on the order of 140–180°C, while novolacs have T_g values in the range of 80–120°C.²⁵³ Baking DNQ/novolacs at temperatures above 110°C decomposes the DNQ molecule; in the absence of water, multifunctional DNQs react with novolac hydroxy groups to cause cross-linking, thus, further increasing the thermal stability of the resist patterns. Pure novolac resins also do cross-link at elevated temperatures, via the oxidation of the methylene bridges.²⁵⁴ The temperature required to induce this cross-linking, however, is above the T_g of novolac, which implies that features patterned in novolacs will flow and get distorted before even reaching their cross-linking temperature. This makes thermal cross-linking of novolacs not a viable option for conventional novolac resins.²⁵⁵ It should be pointed out that novolacs with T_g values above 130°C have been reported.²⁵⁶

At temperatures higher than 120–130°C, hardening and flow of the resist patterns are two competing processes in DNQ/novolac resists. Figure 11.46 shows novolac resist patterns before and after postbake; the features postbaked at very elevated temperatures (130°C) have deformed to a rounded shape due to surface tension. The temperature at which the resist feature starts to deform is termed the flow temperature of the resist. Large features are more susceptible to thermally induced deformation than small ones.²⁵⁷

11.18.2 UV radiation curing

To improve the thermal properties of resists and prevent thermal deformation of resist pattern profiles during the dry etching process, where the temperature of the wafer often exceeds the deformation temperature of untreated resist, UV radiation curing that results in cross-linking is sometimes used.²⁵⁸ DNQ/novolac, poly(hydroxystyrene), acrylate, alicyclic, and a whole host of other

²⁵²B.W. Smith, "Resist processing," in *Microlithography: Science and Technology*, p. 562, Marcel Dekker (1998).

²⁵³ibid, p. 562.

²⁵⁴W.A. Moreau, *Semiconductor Lithography: Principles, Practices, and Materials*, Plenum Press, New York, pp. 289–291, 651–665 (1988).

²⁵⁵B.W. Smith, "Resist processing," in *Microlithography: Science and Technology*, p. 562, Marcel Dekker (1998).

²⁵⁶M.A. Toukhy, T.R. Sarubbi, and D.J. Brzozowy, "Technology and chemistry of high temperature positive resist," *Proc. SPIE* **1466**, 497 (1991).

²⁵⁷R. Dammel, *Diazonaphthoquinone based Resists*, p. 118, SPIE Press, Bellingham, WA (1993).

²⁵⁸H. Hiraoka and J. Pakansky, "UV hardening of photo and electron beam resist patterns," *J. Vac. Sci. Technol.* **19**, 1132–1135 (1981).

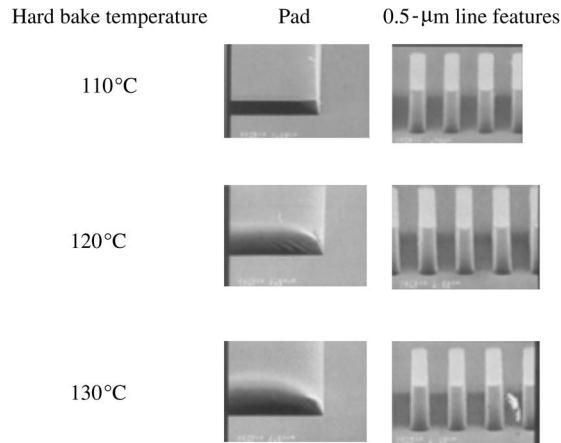


Figure 11.46 Effect of postbake on different feature sizes (0.5 μm and a large pad) patterned on a 1.29- μm -thick DNQ/novolac resist (AZ7512 from AZ Corporation). Processing conditions: prebake 110°C, exposure dose 200 mJ/cm^2 , PEB 110°C, development TMAH puddle for 51 seconds.²⁵⁹

resist platforms described in Chapters 6 and 7 are amenable to UV curing. UV radiation curing of resists has been commonly used to harden the outer shell of the resist, thereby allowing higher postbake temperatures to be attained without destroying the patterned image. The high optical absorbance of resins such as novolac at wavelengths below 300 nm (absorbance $\gg 1 \mu\text{m}^{-1}$) prevents cross-linking to substantial depths.²⁶⁰ Although the efficiency is quite low, novolac resins can be made to cross-link at DUV wavelengths (240–260 nm). Carrying out this process at high temperature facilitates the curing.²⁶¹ Subjecting patterned resist features to DUV exposure at temperatures above 150°C results in a thermally stabilized surface crust. Elevating the temperature of the DUV cure process leads to the oxidation of the bulk of the resist feature, resulting in resist features that can withstand thermal processes up to 210°C without significant resist flow. The process is outlined in Scheme 11.4.²⁶² In particular, the scheme shows that DUV irradiation induces radical chain reactions in novolac, which cross-link the outer resist layer only, given the high absorbance of novolac at 250 nm.²⁶³ Multifunctional DNQs can also undergo DUV curing by cross-linking via novolac ester formation involving mostly radical reactions and oxidation induced in the novolac.²⁶⁴

²⁵⁹ibid., pp. 119–120.

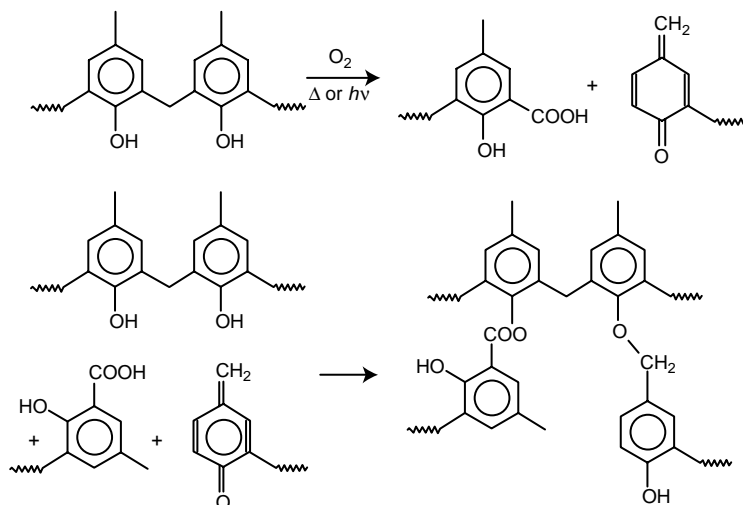
²⁶⁰B.W. Smith, “Resist Processing,” in *Microlithography: Science and Technology*, p. 562, Marcel Dekker New York (1998).

²⁶¹R. Dammel, *Diazonaphthoquinone based Resists*, p. 120, SPIE Press, Bellingham, WA (1993).

²⁶²ibid., p. 121; B.W. Smith, “Resist processing,” in *Microlithography: Science and Technology*, p. 562, Marcel Dekker, New York (1998).

²⁶³R. Dammel, *Diazonaphthoquinone based Resists*, p. 120, SPIE Press, Bellingham, WA (1993).

²⁶⁴ibid., p. 121.



Scheme 11.4 UV curing of novolac resin, showing radical chain reactions and cross-linking via ester formation.²⁶⁵

A low-pressure mercury arc lamp is normally used as a source of short-wavelength UV radiation for curing phenolic resin-based resists. Although the novolac DUV curing chemistry readily takes place in the presence of oxygen, it can also take place in a nitrogen atmosphere, in which case the novolac acts as a self-oxidizer.²⁶⁶ For resist systems based on acrylate, alicyclic, and hybrid acrylate/alicyclic polymers used in DUV 193-nm lithography, as well as 157-nm lithography, which are generally very transparent at DUV wavelengths, they can be cured at the VUV wavelength of 172 nm.

A technique involving the combination of UV radiation curing with hot plate (ramped) baking of the patterned resist, which allows for a more efficient process, has been reported.²⁶⁷ In this technique, a fast cure is obtained by encapsulating the bulk of the resist (which is being cured by the hot plate) with the UV-cured surface film. The bulk resist temperature is ramped from a lower temperature and is kept below the T_g of the surfaced-cured film. The process requires careful balancing of curing of the skin of the pattern (to ensure that it is uniform), while ensuring that the bulk of the resist is prevented from flowing while the hot plate is ramped close to the T_g of the resist. The surface of the resist pattern is given a harder cure (it receives UV + bake) than the bulk (which receives only thermal cure). It should be pointed out that although the harder-cured surface layer may

²⁶⁵ibid.

²⁶⁶ibid.

²⁶⁷J.C. Mathews and J. Wilmott, "Stabilization of single layer and multilayer resist patterns to aluminum etching environments," *Proc. SPIE* **470**, 194 (1984); "Hardening of photoresist," U.S. Patent No. 4,548,688 (1985) (assigned to Fusion Semiconductor).

hold together patterned features, it may also encapsulate some of the volatiles and solvents, which when subjected later to temperatures higher than the postbake temperature (for example, plasma etching or ion implantation), can cause trapped solvent evolution that can wrinkle or crack the brittle surface layer of the resist in a process called reticulation. This problem highlights one of the main drawbacks of UV radiation curing.²⁶⁸

11.18.3 Electron-beam curing of resists

Electron-beam curing of postdeveloped resists is aimed at improving the thermal and etch stabilities of the patterned resist feature.²⁶⁹ An electron beam can interact with a resist polymer primarily in two ways: nuclear and electronic interaction. While nuclear interactions or collisions (also called Rutherford scattering) are elastic and merely change the direction of the electron within the resist, they play no significant role in electron-beam curing of resists. In contrast, it is the electronic interaction between the electron beam and the resist molecules that is utilized in the electron-beam curing of resists.

Electronic collisions are inelastic and slow down the primary electrons, causing them to transfer their energy into excitation energy and kinetic energy of secondary electrons within the resist. These inelastic collisions of the electron beam with the resist molecules lead to the generation of secondary electrons within the resist. The inelastic collisions also slow down the primary electrons (electron beam) as they travel through the resist film, resulting in the primary electrons imparting their energies to the resist molecules, and ionizing them in the process, before they are finally absorbed. The secondary electrons in turn travel away from their point of creation at relatively slower speeds than the primary electrons, while also producing ions along the trajectory of the primary electrons.²⁷⁰ Within an order of a picosecond after ionization, molecular rearrangement takes place in the ions and excited molecules, accompanied by thermal deactivation or the dissociation of valence bonds within the molecules in the resist.²⁷¹ The radicals, created by these broken bonds, may recombine with each other, or form new bonds and reattach themselves to neighboring polymer chains, which also have broken bonds in their side groups, effectively resulting in cross-linking of the polymer.

²⁶⁸W.R. Livesay, A.L. Rubiales, M. Ross, S. Woods, and S. Campbell, "Electron beam hardening of photoresists," *Proc. SPIE* **1925**, 426–436 (1993).

²⁶⁹U. Okoroanyanwu, J. Shields, and C.Y. Yang, "Process for preventing deformation of patterned photoresist features," U.S. Patent No. 6,589,709 (2003); C. Gabriel, H.J. Levinson, and U. Okoroanyanwu, "Selective photoresist hardening to facilitate lateral trimming," U.S. Patent No. 6,716,571 (2004); W.R. Livesay, A.L. Rubiales, M. Ross, S. Woods, and S. Campbell, "Electron beam hardening of photoresists," *Proc. SPIE* **1925**, 426–436 (1993).

²⁷⁰A. Chapiro, *Radiation Chemistry of Polymer Systems*, p. 42, John Wiley & Sons, Hoboken, NJ (1962).

²⁷¹F. Billmeyer, *Textbook of Polymer Science*, p. 372, John Wiley & Sons, Hoboken, NJ (1971).

The cross-linking processes will persist with continued electron-beam irradiation and will stop only when the entire bulk of the film is cross-linked.

The effect of the cross-linking of resist polymer films is to make the film stable to heat such that it cannot be made to flow or melt. A fully cross-linked resist polymer film is practically insoluble in most solvents, although it can be stripped with oxygen plasma etching. Its plasma etch resistance is superior to a similar film that is not cross-linked.

Operationally, electron-beam processing is controlled by beam energy, dose, current, processing gas, and substrate temperature. The penetration depth of the electrons into the target material is determined by the energy of the electron beam according to Grun's formula,²⁷² as follows:

$$R_g = \frac{0.046V_a^{1.75}}{d}, \quad (11.46)$$

where R_g is the Grun range (penetration depth) in μm , V_a is the accelerating voltage or energy in KeV, and d is the density of the target material in g/cm^3 .

Figure 11.47 shows the three possible electron-beam processing schemes, namely, (i) full electron-beam curing, (ii) variable energy electron-beam curing, and (iii) depth-controlled electron-beam curing. In full electron-beam curing, the entire film can be modified by selecting an electron-beam energy such that the penetration depth of the electrons is equal to or larger than the film thickness, thus producing a homogenous film with properties significantly different from the starting material. In the variable energy electron-beam curing scheme, by varying the electron-beam energy with time, it is possible to vary the film properties very gradually as a function of thickness. In depth-controlled electron-beam exposure, the penetration depth is restricted to a certain fraction of the film

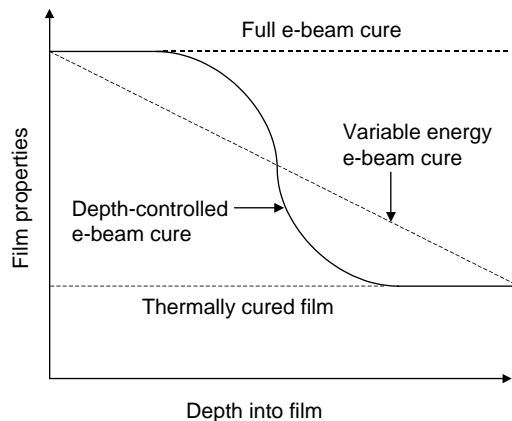


Figure 11.47 Electron-beam processing parameters and film properties such as glass transition temperature, density, Young's modulus, etc.

²⁷²A.E. Grun, "Lumineszenz Photometrische Messungen der Energie absorption im Strahlungsfeld von Elektronequellen Eindimensionaler Fall in Luft," *Z. Naturforsch* **12a**, 89-95 (1957).

thickness, such as the top layer, such that the irradiated top layer of the film is cured, leaving the underlying film unaffected.²⁷³

11.18.3.1 Radiation chemistry of electron-beam curing

Figure 11.48 shows FTIR spectra highlighting the different chemical transformations of different functional groups in the PAR700 resist [formulated from poly(adamantyl methacrylate-*co*-gamma-butyro lactone)] on account of electron-beam curing. This figure shows significant decrease in the intensity of the C–H stretching vibrations' absorption peaks around $2960\text{--}2850\text{ cm}^{-1}$ with increasing electron-beam dose, suggesting possible electron-beam-induced polymer cross-linking. A possible mechanism for this cross-linking reaction could involve the initial abstraction of a hydrogen atom from any of the methylene groups in the polymer backbone, leading to the formation of reactive radical species, which quickly react with similar radicals from different polymer chains, thereby effectively transforming the ordinarily linear polymer chain of the resist resin to three-dimensional, cross-linked network structures.

11.18.3.2 Effects of electron-beam curing

Electron-beam-induced cross-linking of the resist polymer increases the bulk modulus and bulk toughness of the feature pattern, as well as the interfacial

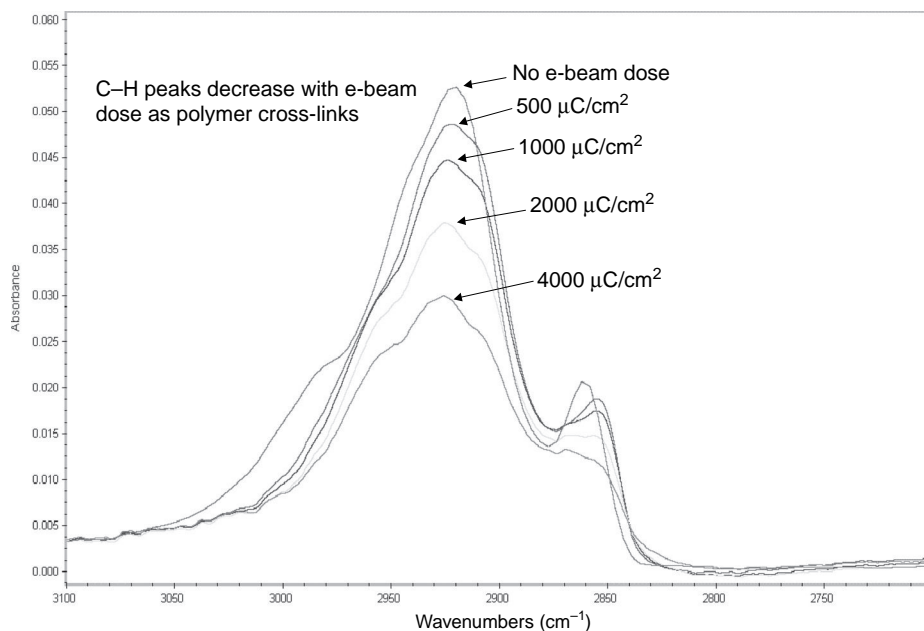


Figure 11.48 FTIR spectra showing electron-beam-induced photochemistry in PAR700 between 3100 and 2750 cm^{-1} .

²⁷³M. Ross, Electron Vision Corp., Private Communication (2000).

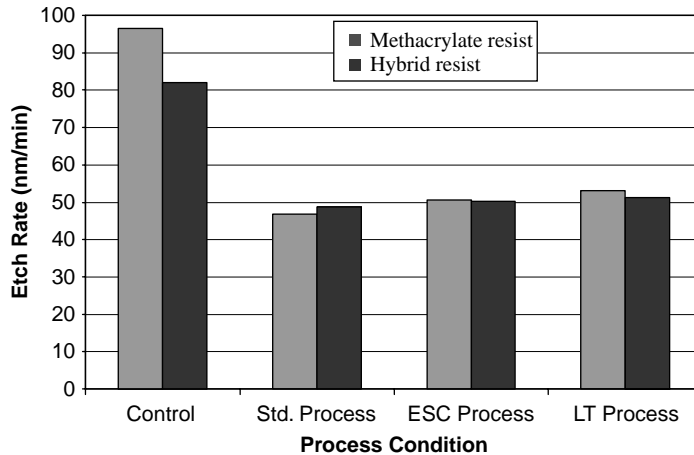


Figure 11.49 Effect of electron-beam curing of resists based on poly(methacrylate) platform and hybrid methacrylate/alcyclic polymer platform on polygate etch. Electron-beam curing improves etch resistance by up to 50% relative to the control (uncured) sample. Processing was done in a nitrogen environment of the ElectronCure Electron Beam Process Chamber utilizing these electron-beam parameters: 3.75 keV, 6 mA, 2000 $\mu\text{C}/\text{cm}^2$. The wafer temperature of the standard (Std.) process was not controlled, that for the electron-beam standard cure (ESC) process was kept at a medium temperature, that for the low-temperature (LT) process was maintained at a low temperature, while that for the control was at room temperature. [After R. Dammel, “Practical resist processing,” SPIE Short Course No. SC616 (2005).]

toughness of the substrate-resist polymer bond, thereby ensuring that patterned resist features will be better able to withstand bending, breaking, collapse, and mechanical deformation of the features during etch processing.²⁷⁴ In addition, cross-linking and decomposing the functional groups in the resist polymer make the patterned features more impervious to etchant species, thereby improving the etch stability of the cured resist (see Fig. 11.49). Other observed effects include film thickness loss (see Fig. 11.50) and an increase in T_g of the electron-beam-cured resist.

11.19 Measurement and Inspection

Following development, the patterned wafer is inspected for defects, and specific CD features are measured to check if they meet preset process control targets. This step is necessary to identify and remove defective wafers before they continue

²⁷⁴U. Okoroanyanwu, J. Shields, and C.Y. Yang, “Process for preventing deformation of patterned photoresist features,” U.S. Patent No. 6,589,709 (2003); C. Gabriel, H.J. Levinson, and U. Okoroanyanwu, “Selective photoresist hardening to facilitate lateral trimming,” U.S. Patent No. 6,716,571 (2004); W.R. Livesay, A.L. Rubiales, M. Ross, S. Woods, and S. Campbell, “Electron beam hardening of photoresists,” *Proc. SPIE* **1925**, 426–436 (1993).

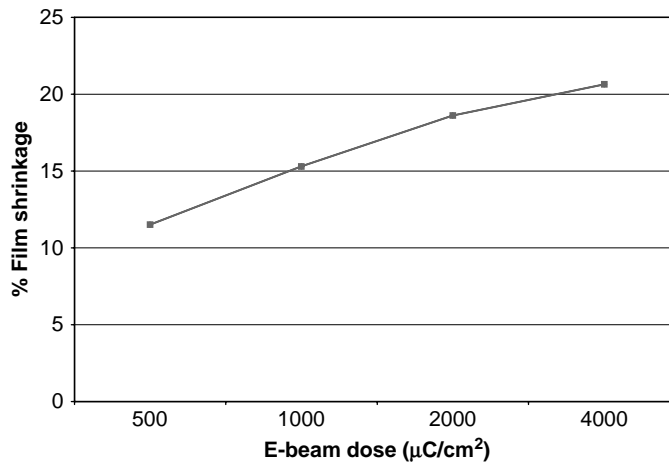


Figure 11.50 Film shrinkage of PAR-700/A4 resist as a function of electron-beam dose. The nominal resist thickness was 400 nm.

to the subsequent processes of etch or implant. This step is also used to characterize the overall lithographic process, with a view to providing information to the lithography production team for corrective action, where and if necessary.

Two possible outcomes exist for a wafer that fails the measurement-and-inspection step. If the wafer has a problem from a previous operation that makes it unacceptable, then it is scrapped. If, however, the problem is associated specifically with the quality of the pattern in the resist film, then the wafer is reworked, which involves essentially stripping off the resist and organic antireflection coatings. Following reworking, such a wafer is reinserted into the lithography process line.

11.20 Etching

Following the resist pattern stabilization steps, an etching process is used to transfer the resist pattern into the underlying semiconductor substrate. There are two main forms of etching processes, namely, wet and dry etching. Before the dry etching techniques were developed, all of the etching processes in semiconductor device fabrication were carried out with wet etching.

11.20.1 Wet etching

In wet etching, the substrate is etched with an etchant solution in a process that involves dipping the patterned resist wafer in the etchant solution and subsequently cleaning and rinsing it with pure deionized water. Wet etch rate is mainly dependent on the composition of the etchant solution and the temperature. Given that

these two factors and the etching time are easily controlled, the reproducibility of the wet etch result is quite good.²⁷⁵

The choice of etchants is dependent on the nature of the substrate to be etched. Silicon dioxide is etched with a mixture of aqueous solution of hydrogen fluoride (HF) and ammonium fluoride (NH₄HF). Parisi et al.²⁷⁶ have reported the following functional expression for the etch rate γ_d in angstroms per minute of silicon dioxide:

$$\gamma_d = 4.5 \times 10^9 [\text{HF}] e^{4980/T}, \quad (11.47)$$

where [HF] is the concentration of hydrogen fluoride in moles per liter and T is the temperature of the etchant in degrees Kelvin.

Silicon is etched with a mixture of aqueous solution of HF and nitric acid (HNO₃).²⁷⁷ The electron concentration, crystal defects, and catalysis by lower oxides of nitrogen all influence the etch rate of silicon by HF/HNO₃ etchant.²⁷⁸

Aluminum is typically etched with a mixture of phosphoric acid, nitric acid, acetic acid, and water, in a volume ratio of 16:1:2:1.²⁷⁹ It should be mentioned that aluminum can be easily etched with an aqueous mixture of a host of the common inorganic acids, but often with poor reproducibility because these acid solutions tend to generate hydrogen bubbles on reaction with aluminum. These hydrogen bubbles tend to interfere and inhibit the diffusion of the etchant species to etching sites on the aluminum substrate. In contrast, in the etchant based on phosphoric acid, nitric acid, acetic acid, and water, hydrogen evolution is eliminated by the oxidative reaction of nitric acid.²⁸⁰

Chromium is readily etched by aqueous solution of ceric salt, prepared from ceric nitrate, perchloric acid, and water. Chrome masks are now being fabricated with this type of etchant solution.²⁸¹

11.20.2 Dry etching

Dry etching is the primary etching method currently used to transfer the resist pattern into underlying semiconducting substrates in an IC device. The pattern transfer is accomplished by removing underlying substrate materials that are not

²⁷⁵S. Nonogaki, T. Ueno, and T. Ito, *Microlithography Fundamentals in Semiconductor Devices & Fabrication Technology*, Chapter 5, Marcel Dekker, New York (1998).

²⁷⁶G.I. Parisi, S.E. Haszko, and G.A. Rozgonyi, "Tapered windows in SiO₂: the effect of NH₄F:HF dilution and etching temperature," *J. Electrochem. Soc.* **124**, 917-921 (1977).

²⁷⁷S. Nonogaki, T. Ueno, and T. Ito, *Microlithography Fundamentals in Semiconductor Devices & Fabrication Technology*, Chapter 5, Marcel Dekker, New York (1998).

²⁷⁸B. Schwartz and H. Robbins, "Chemical etching of silicon IV. etching technology," *J. Electrochem. Soc.* **123**, pp. 1903-1909 (1976).

²⁷⁹S. Nonogaki, T. Ueno, and T. Ito, *Microlithography Fundamentals in Semiconductor Devices & Fabrication Technology*, Chapter 5, Marcel Dekker, New York (1998).

²⁸⁰ibid.

²⁸¹ibid.

protected by the resist. Dry etching techniques fall into three main categories, depending on the mechanism of their etching action: physical etching (also called sputtering), chemical etching, and combination physical and chemical etching.

Physical etching or physical sputtering is a process whereby atoms are ejected from a solid target material due to bombardment of the target by high-energy particles. The basis of physical sputtering is the momentum exchange resulting from collisions between the incident bombarding ions and atoms in the target material. When the target is bombarded, the incident ions set off collision cascades in the target material. When such cascades recoil and reach the target surface with energy that is higher than the binding energy, an atom can be ejected. The primary particles for the sputtering process can be supplied by a variety of methods, including, for example, a plasma source, an ion source, an accelerator, etc.

Sputter etching is chosen in situations where a high degree of etching anisotropy is needed and selectivity is not a concern, as it produces a high etch rate. A major drawback of this technique is wafer damage. Another issue with it is the fact that the species removed by the sputtering are not volatile and may redeposit back on the wafer, causing particulate and chemical contamination.

In the dry chemical etching technique, plasma-generated reactive species (such as free radicals, ions, and atoms) react chemically with the underlying materials on the wafer surface that are not protected by the resist. The precursor gases introduced into the etch chamber are selected to attain high selectivity (in other words, to minimize the chemical reaction between the resist and the underlying wafer layers). Volatile by-products of the reaction are removed by the low-pressure pumping system. Dry chemical etching is very isotropic and as a result produces poor CD control.

It is possible to perform a combined physical and chemical mechanism where ion bombardment improves the chemical etching action. The etch profile is varied from isotropic to anisotropic by adjusting the plasma conditions and gas conditions. Combined physical and chemical etch produces good CD control with reasonable selectivity, and is often preferred for most dry etch processing. Dry chemical etching techniques are categorized, depending on the nature of their etchant, i.e., plasma and reactive-ion etching.

11.20.2.1 Plasma etching

As the name implies, the species that do the etching in this technique are gaseous plasmas generated within an evacuated chamber to which is introduced the etchant precursor gas(es) and which is subjected to high-frequency electric power via external electrodes. These plasmas comprise ionic and neutral fragments. For a precursor etchant gas such as carbon tetrafluoride (CF_4), species including C^+ , CF^+ , CF_3^+ , C, F, CF, CF_2 , and CF_3 have been detected in the generated plasma.²⁸²

²⁸²T.M. Mayer and R.A. Baker, "Reactive ion beam etching with CF_4 : characterization of a Kaufman ion source and details of SiO_2 etching," *J. Electrochem. Soc.* **129**, 585–591 (1982).

In plasma etchers, specific radicals are selected from the mix of the species generated within the chamber to effect the etching action. For the specific case of species generated from CF_4 gas within a plasma chamber, for example, the fluorine radical (F) is selected by means of an appropriately configured perforated aluminum shield or other contraption that blocks the other species from reaching the wafer. In this way, etching of the wafer proceeds only by the reaction of the fluorine radical. Substrates such as silicon, silicon dioxide, and silicon nitride are readily etched by this technique.²⁸³

This was the first dry etching technique introduced into the semiconductor industry. The fact that etching with this technique proceeds isotropically precludes its use in precise pattern-transfer applications. As a result, it has been replaced with an anisotropic-type etching technique called reactive-ion etching.

11.20.2.2 Reactive-ion etching

Reactive-ion etching (RIE) is the most frequently used dry etching technique in the fabrication of semiconductor devices. The etching species are plasma-reactive ions generated between two electrodes in an evacuated chamber by radio-frequency gas discharge. The wafer to be etched is electrically contacted with one of the internal electrodes, ensuring that the ambient condition of the surface of the wafer is the same as that of the electrode.²⁸⁴

Given the significant difference in electron and ion mobilities, an ion-rich layer termed an ion sheath is formed on both sides of the surfaces. When the surfaces of the wafer and the electrode are negatively charged, a large electric potential difference is created across the ion sheath, resulting in the acceleration of the ions in the ion sheath perpendicular to the surface of the wafer. In situations where the etchant gas pressure within the chamber is relatively low, the mean free path of the ions may be comparable to the thickness of the ion sheath, and the accelerated ions will be nearly perpendicularly incident on the wafer. Because the rate of the etching reaction is significantly enhanced by the impact of the incident ions, the RIE proceeds anisotropically.²⁸⁵ Table 11.4 is a list of gases that are commonly used in reactive-ion etching of typical substrates used in semiconductor device fabrication.

Ohnishi and co-workers²⁸⁷ established this empirical relationship between the oxygen RIE rate and the effective amount of carbon in the polymer as

$$\text{ER} \propto \frac{N}{N_C - N_O}, \quad (11.48)$$

²⁸³S. Nonogaki, T. Ueno, and T. Ito, *Microlithography Fundamentals in Semiconductor Devices & Fabrication Technology*, Chapter 5, Marcel Dekker, New York (1998).

²⁸⁴ibid.

²⁸⁵ibid.

²⁸⁶ibid., p. 155.

²⁸⁷H. Gokan, S. Esho, and Y. Ohnishi, "Kinetics of the cubic \rightarrow hexagonal transformation of cadmium sulfide," *J. Electrochem. Soc.* **130**, 423 (1983).

Table 11.4 Common gases used in reactive-ion etching. (Data used with permission from Taylor & Francis Group LLC.)²⁸⁶

Substrate	Gases
Silicon	CF ₄ , SF ₆ , CF ₄ + O ₂ , CCl ₄
Silicon dioxide	CF ₄ + H ₂ , C ₂ F ₆ , C ₃ F ₈ , C ₄ F ₅
Silicon nitride	CF ₄ + H ₂ , CH ₂ F ₂ , CH ₃ F
Aluminum	CCl ₄ , BCl ₃ , Cl ₂
Refractory metals and refractory silicides	CF ₄ , SF ₆ , CCl ₄ , Cl ₂ , Cl ₂ + O ₂

where ER is the etch rate, N is the total number of atoms in the repeating units of the polymer, N_C is the number of carbon atoms in the repeating unit of the polymer, and N_O is the number of oxygen atoms in the repeating unit of the polymer. This relation implies that the etch rates of resist materials in Ar and O₂ RIE processes scale linearly with the effective amount of carbon atom fraction $[N/(N_C - N_O)]$ in the polymer repeat unit. A similar correlation was found for silicon-containing polymers. These results are generally interpreted to mean that RIE speed is controlled by the sputtering phenomena, in contrast to plasma etch rates, which seem to be correlated with the chain scission parameter G_s .²⁸⁸

11.21 Rework/Stripping

Following the etching step, the resist and organic antireflection coatings are stripped from the wafer by either a wet or dry process. Under certain circumstances, in the event of misprocessing or general process drifts due to equipment problems, the processed wafer may be sent to rework for stripping, instead of proceeding to the next processing step.

In the wet process, the resist and organic antireflection coatings are stripped with commercially available resist strippers, which often are mixtures of strong solvents containing wetting agents and basic additives such as amines. If the resist did not undergo extreme postbake, it may simply be stripped with undiluted developers, often accompanied by flood exposure. Cross-linked resists may be stripped with solvents such as acetone, dimethylformamide, N-methylpyrrolidone, or dimethylsulfoxide.²⁸⁹ Stripping is carried out by dipping the wafer with the resist patterns into the stripping solvent maintained at about 100°C for about 20 minutes, washing with a solvent such as methanol, and washing again with pure water, before finally drying. There exist special stripper solutions for removing the silicon-containing “sidewall polymer” that results from redeposition during dry etching.

²⁸⁸R. Dammel, *Diazonaphthoquinone based Resists*, p. 124, SPIE Press, Bellingham, WA (1993).

²⁸⁹ibid.

Oxygen plasma etching is most frequently used in the dry process for stripping resists and organic antireflection coatings. Because all of the practical resist and antireflection coating materials are made of organic compounds, they are stripped from the wafer substrate by the oxidative reaction of oxygen plasma.²⁹⁰ Moreau²⁹¹ has provided an extensive review of stripping processes.

²⁹⁰ibid., S. Nonogaki, T. Ueno, and T. Ito, *Microlithography Fundamentals in Semiconductor Devices & Fabrication Technology*, Chapter 5, Marcel Dekker, New York (1998).

²⁹¹W.A. Moreau, *Semiconductor Lithography: Principles, Practices, and Materials*, pp. 289–291, 779–809, Plenum Press, New York (1988).

Chapter 12

Lithographic Modeling

All physical things, the stars and the universe are mathematically related.

Pythagoras, ca. 581–497 BC

12.1 Introduction

Lithographic modeling has played very critical roles in advancing lithographic science and technology. These roles span many aspects of the patterning process: as a research tool for gaining insight into the outcomes of experiments that are difficult or impossible to execute any other way, as a development tool for evaluating options and optimizing processes, as a manufacturing tool for troubleshooting process problems and determining optimal yield settings, and as a learning tool for studying different aspects of the lithographic process. All of these functions of lithographic modeling are today readily performed on personal computers and engineering workstations. How did all of these come about? What is involved in lithographic modeling? Specifically, what physical models are employed in a typical lithographic simulator? How good is lithographic modeling in predicting lithographic results? And how is lithographic modeling currently employed in the semiconductor industry? These questions and more are addressed in this chapter.

12.2 Historical Background

The roots of lithographic modeling date to the early 1970s when Dill and co-workers at IBM set out to describe the basic steps of the lithographic process with mathematical equations, resulting in a set of publications in 1975, now commonly referred to as the “Dill papers.”¹ Together, the Dill papers not only gave birth to the field of lithographic modeling, they also marked the first time a

¹F.H. Dill, “Optical lithography,” *IEEE Trans. Electron. Dev.* **ED-22**(2), 440–444 (1975); F.H. Dill, W.P. Hornberger, P.S. Hauge, and J.M. Shaw, “Characterization of positive photoresists,” *IEEE Trans. Electron Dev.* **ED-22**(7), 445–452 (1975); K.L. Konnerth and F.H. Dill, “In situ measurement of dielectric thickness during etching or developing processes,” *IEEE Trans. Electron Dev.* **ED-22**(7),

serious attempt was made to describe lithography not as an art, but as a science. In the papers, Dill and his co-workers presented a simple model for image formation with incoherent illumination, namely, “Dill’s first order exposure kinetic model,” and an empirical model for development coupled with a cell algorithm for photoresist profile calculations.²

In order to make their task more tractable, they broke up the lithographic process into a sequence of calculations designed to determine the intensity of light inside the resist (calculation of the standing wave), the chemical concentration of exposure products resulting from this light, the impact of this chemistry on the development rate, and, finally, the integration of the development rate through time to predict the resist thickness after development. A most auspicious event at this time was the development of an automated thin-film thickness measurement tool at IBM; this tool could be used to monitor the effects of lithographic process steps on an exposed resist film.³

When it was observed that the DNQ/novolac resists in use at the time became more transparent on exposure (i.e., they bleached), Dill used this change in optical absorbance as a way of monitoring the kinetics of exposure. He developed a first-order model of exposure consisting of three parameters A , B , and C , now called the “Dill model,” which accurately fit the experimental measurement results of the transmittance of a resist coating on an optically matched glass wafer as a function of exposure dose. The Dill parameters A , B , and C , describe bleachable absorbance, nonbleachable absorbance, and exposure rate constant, respectively.⁴

It should be pointed out that the key to photoresist development modeling was the development of a development rate monitor (DRM), a modified version of the thin-film measurement tool developed at IBM, which was alluded to earlier. This reflectance spectroscopic tool was customized to work through a fluid flow chamber surrounding the wafer. Measurement of the resist thickness in real time during development yielded the development rate, which could be calculated as a function of the depth into the resist. By repeating this measurement for many exposure doses, and employing the Dill exposure model to relate incident dose to the amount of chemical change within the resist, Dill could determine the development rate as a function of the chemical composition of the resist. Assuming that the development rate was surface rate limited, Dill fit his data to a simple second-order polynomial (on a log-development rate scale), from which he deduced his empirical development rate function. Soon afterward, he was able to confirm the accuracy of his models by correctly predicting the depth-dependent development rate of resist on a silicon wafer. By combining the Dill models with a simple coherent

452–456 (1975); F.H. Dill, A.R. Neureuther, J.A. Tuttle, and E.J. Walker, “Modeling projection printing of positive photoresists,” *IEEE Trans. Electron Dev.* **ED-22**(7), 456–464 (1975).

²C.A. Mack, “Optical lithography modeling,” in *Microolithography: Science and Technology*, J.R. Sheats and B.W. Smith, Eds., p. 109, Marcel Dekker, New York (1998); C.A. Mack, “30 years of lithography simulation,” *Proc. SPIE* **5754**, 1–12 (2004).

³ibid.

⁴ibid.

imaging model and a cell algorithm developed by Neureuther (one of Dill's co-workers who was on a one-year sabbatical from the University of California at Berkeley), the first lithographic simulator was at last developed, paving the way for other lithographic modeling and simulation packages to follow soon after.⁵

On returning to Berkeley, Neureuther and one of his colleagues at the University of California, William Oldham, started their own modeling project. In 1979, they published their first paper on the lithographic simulation program called "SAMPLE."⁶ SAMPLE included a number of significant enhancements relative to the Dill simulator. It incorporated partial coherence to the image calculations and a surface inhibition function to the development rate calculation, and it replaced the cell algorithm of the Dill simulator for dissolution calculations with a string algorithm, which gave better results for large grid sizes. Most importantly, SAMPLE was made available to the U.S. semiconductor lithography community, paving the way for researchers in the field to use modeling as a tool to help them to understand and improve their lithographic processes.⁷

The impact of SAMPLE as well as the influence of the SAMPLE research group in advancing lithography research over its 30-year history are substantial. The proposal for the use of dyed photoresists, early proposals for phase-shifting mask schemes, several resolution enhancement techniques, and the design of an aberration-sensitive monitor are a few of the notable contributions made by the SAMPLE research group.⁸ Also, the SAMPLE research group, early on, established that a low value for the Dill parameter B was important for good imaging, which guided early i-line resist development.⁹

Building on the earlier Dill and SAMPLE models, Chris Mack, then at the U.S. National Security Agency, developed the lithographic modeling program PROLITH (which stands for positive resist optical lithography) around 1985.¹⁰ The PROLITH simulator incorporated a simple incoherent imaging model, an analytical expression for the standing wave intensity inside the resist, and a prebake model, as well as a kinetic model for resist development that later came to be called the Mack model, and also a model for contact and proximity printing. While the first-generation PROLITH simulator was released to the public for free in 1985, PROLITH/2 (the second generation of PROLITH software) was commercialized in 1990 by FINLE Technologies, after the U.S. National Security Agency

⁵C.A. Mack, "Optical lithography modeling," in *Microlithography: Science and Technology*, J.R. Sheats and B.W. Smith, Eds., p. 109, Marcel Dekker, New York (1998); C.A. Mack, "30 years of lithography simulation," *Proc. SPIE* **5754**, 1–12 (2004).

⁶W.G. Oldham, S.N. Nandgaonkar, A.R. Neureuther, and M. O'Toole, "A general simulator for VLSI lithography and etching processes: Part 1. application to projection lithography," *IEEE Trans. Electron Dev.* **ED-26**(4), 717–722 (1979).

⁷C.A. Mack, "Optical lithography modeling," in *Microlithography: Science and Technology*, J.R. Sheats and B.W. Smith, Eds., p. 109, Marcel Dekker, New York (1998); C.A. Mack, "30 years of lithography simulation," *Proc. SPIE* **5754**, 1–12 (2004).

⁸ibid.

⁹H.J. Levinson, Global Foundries, Inc., Private Communication (2008).

¹⁰C.A. Mack, "PROLITH: a comprehensive optical lithography model," *Proc. SPIE* **538**, 207–220 (1985).

decided that lithographic modeling was not quite within its charter. FINLE Technologies (which became a division of KLA-Tencor in 2000) subsequently developed later generations of PROLITH that incorporated new models for chemically amplified resists, contrast enhancement materials, the extended source method for partially coherent image calculations, broadband illumination, phase-shifting masks, FLEX-multiple focal plane exposures, high-NA imaging, off-axis illumination, vector imaging, two- and three-dimensional masks and aerial imaging, aberrations, variable diffusivity reaction-diffusion in three dimensions, step-and-scan vibrations, scanner aberration averaging, notch development, base quencher diffusion, immersion lithography, mask topography electromagnetic force simulator, birefringence, etc.¹¹

It should be pointed out that the first commercial simulator was DEPICT, which was based on SAMPLE, and was developed by Bob Pack of Technology Modeling Associates. DEPICT was released to the marketplace in 1986, but eventually faded away into oblivion after a few acquisitions of the parent company by other companies.¹²

Another modeling program of note is TEMPEST, which was developed at the University of California, Berkeley in the early 1990s for modeling polarization and three-dimensional effects at the mask.¹³ TEMPEST has proven particularly useful for analyzing the effects of mask topography associated with phase-shifting masks.¹⁴ Other lithographic simulators that are part of the technology computer-aided design (TCAD) tools, and that were developed within academia (specifically, University of California of Berkeley) include SPLAT and STORM. Together, they simulate the entire lithographic process with efficient numerical models.¹⁵

Other commercial lithography simulators of note include Solid, which was developed by Wolfgang Hencke of the Fraunhofer Institute in 1991. Solid was the first 3D lithography simulator. It was first commercialized in 1992 by Silvaco, but subsequently was released in 1994 as SOLID-C by SIGMA-C.¹⁶

Today, there are several companies that sell lithography simulators (see Table 12.1), and simulation can even be performed over the Internet using programs at a web site at the University of California at Berkeley.¹⁷

12.3 Structure of a Lithographic Model

Lithographic modeling simulates several key steps in the lithographic process comprising image formation, resist exposure, postexposure bake diffusion,

¹¹C.A. Mack, "30 years of lithography simulation," *Proc. SPIE* **5754**, 1–12 (2004).

¹²ibid.

¹³A. Wong and A. Neureuther, "Examination of polarization and edge effects in photolithographic masks using three dimensional rigorous simulation," *Proc. SPIE* **2197**, 521–527 (1994).

¹⁴H.J. Levinson, *Principles of Lithography*, 2nd ed., p. 103, SPIE Press, Bellingham, WA (2005).

¹⁵Berkeley TCAD Software Tools, <http://tanqueray.eecs.berkeley.edu/tcad/tcad.html>.

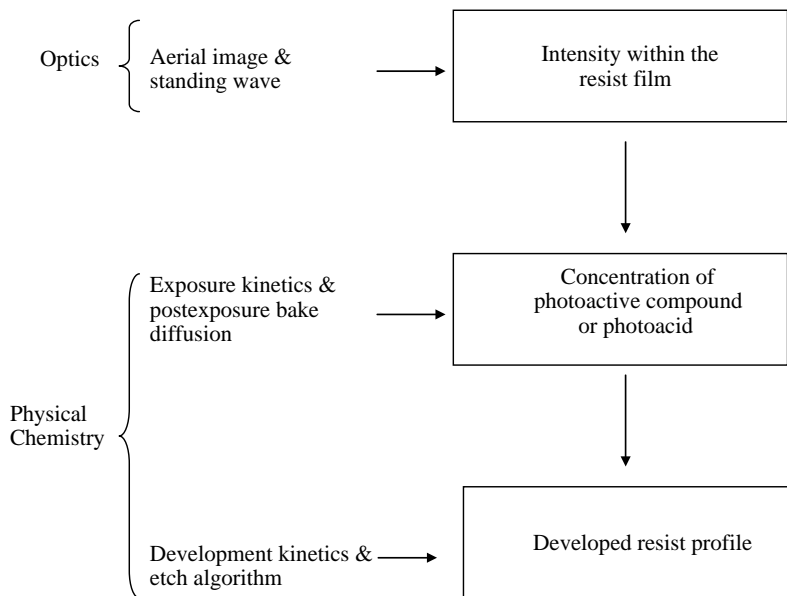
¹⁶SIGMA C, www.sigma-c.de.

¹⁷A.R. Neureuther, C. Hsu, T. Horie, J. Cheng, P. Chien, T. James, V. Lee, M. Li, R. Shen, R. Yang, and V. Wien, "Lithography simulation using the Internet," *Microlithography World*, pp. 18–20 (Winter, 1999).

Table 12.1 Commercially or publicly available lithography modeling programs. (Adapted from Ref. 18.)

Program	Company or organization	Web site
PROLITH	FINLE Division of KLA Tencor (Austin, TX)	www.kla tencor.com
SOLID C	SIGMA C, division of Synopsis (Munich, Germany)	www.sigma c.de
EM Suite and JLith Calibre	Panoramic Technology Mentor Graphics (Wilsonville, Oregon)	www.panoramicttech.com www.mentorgraphics.com
SAMPLE, TEMPEST, STORM, SPLAT Optolith	University of California (Berkeley, California) Silvaco International (Sunnyvale, California)	http://cuervo.eecs.berkeley.edu/ Volcano www.silvaco.com
Proteus	Synopsys (Mountain View, California)	www.synopsys.com

development, and final resist profile. Figure 12.1 is a schematic of the calculation steps, including the disciplines required for lithographic modeling. Following is a brief overview of the physical models found in a typical lithography simulator. A more detailed treatment of these physical models is provided in subsequent sections.

**Figure 12.1** Flow diagram of lithographic modeling. (Adapted with permission from Taylor & Francis Group LLC.¹⁹)

¹⁸H.J. Levinson, *Principles of Lithography*, 2nd ed., p. 103, SPIE Press, Bellingham, WA (2005).

¹⁹C.A. Mack, "Optical lithography modeling," in *Microolithography: Science and Technology*, J.R. Sheats and B.W. Smith, Eds., p. 111, Marcel Dekker, New York (1998).

12.3.1 Aerial image

This is the intensity of the exposure radiation in the plane of the wafer. The extended source method, or Hopkins' method,²⁰ is often used to predict the aerial image of a partially coherent, diffraction-limited, low-numerical-aperture-aberrated projection system based on scalar diffraction theory. For very high NA, vector calculations involving the complete solution of Maxwell's equation are used. The illumination may be of a single wavelength or it may be broadband. The illumination source may be a conventional disk shape or other more complicated shapes as in off-axis illumination.²¹

12.3.2 Standing waves

An analytical expression is often used to calculate the standing wave intensity as a function of depth into the resist, including the effects of resist bleaching, antireflection coatings, dyes in resists, contrast enhancement layers, and the effect of non-vertical light propagation in the case of high-NA systems.²²

12.3.3 Prebake

The thermal decomposition of the resist photoactive compound or radiation-sensitive components during prebake is modeled using first-order kinetics; this often results in a change in the resist's optical properties, mostly the Dill *A* and *B* parameters.²³

12.3.4 Exposure

First-order kinetics is used to model the exposure chemistry resulting from the previously calculated light distributions within the resist film. The standard Dill *A*, *B*, and *C* parameters are used.²⁴

12.3.5 Postexposure bake

The effects of thermally driven diffusion of active chemical species within the resist during the postexposure bake are modeled with appropriate diffusion

²⁰H.H. Hopkins, *Wave Theory of Aberrations*, Clarendon Press (1950).

²¹C.A. Mack, "Optical lithography modeling," in *Microolithography: Science and Technology*, J.R. Sheats and B.W. Smith, Eds., p. 110, Marcel Dekker, New York (1998).

²²*ibid.*, p. 111.

²³F.H. Dill, "Optical lithography," *IEEE Trans. Electron. Dev.* **ED-22**(2), 440–444 (1975); F.H. Dill, W.P. Hornberger, P.S. Hauge, and J.M. Shaw, "Characterization of positive photoresists," *IEEE Trans. Electron Dev.* **ED-22**(7), 445–452 (1975).

²⁴*ibid.*

equations. For chemically amplified resists, this diffusion is associated with acid-catalyzed amplification reactions that lead to cross-linking and deblocking, as well as certain functional group transformations of the polymers in the exposed resists. Typical effects of diffusion include the reduction of standing waves.²⁵

12.3.6 Development

A model that relates resist dissolution to the chemical composition of the film is often used in conjunction with an etching algorithm to determine the final resist profile. Effects such as surface inhibition or enhancement are also incorporated into the model.²⁶

The combination of the models described above provides a fairly complete mathematical description of the optical lithographic process. In the following sections, we discuss each of these models in depth, including their mathematical derivations, as well as the physical basis for their applications.²⁷

12.4 Basic Imaging Theory

Before delving into aerial image models, we consider first the basic theories of how images are formed in a conventional projection imaging system. Shown in Figure 12.2 is a diagram of a projection imaging system of the kind used in advanced semiconductor lithography. It consists of a light source, a condenser lens, the mask, the objective lens, and the resist-coated wafer substrate. The combination of the source and the condenser lens is called the illumination system, and its purpose is to deliver light to the mask and subsequently the objective lens with sufficient intensity, proper directionality and spectral characteristics, and adequate uniformity across the field. Passing through the clear areas of the mask, the light diffracts at apertures on the mask, so that only a portion of the diffracted beam is transmitted through the entrance pupil of the lens, which projects an image of the mask onto the resist-coated wafer.

Because light is a wave, its transmission through apertures is, perforce, described by the wave equation. The presence of an aperture modifies the propagation of such waves relative to transmission through free space or air.

²⁵E.J. Walker, "Reduction of photoresist standing wave effects by post exposure bake," *IEEE Trans. Electron Dev.* **ED-22**(7), 464–466 (1975).

²⁶C.A. Mack, "Optical lithography modeling," in *Microlithography: Science and Technology*, J.R. Sheats and B.W. Smith, Eds., p. 111, Marcel Dekker, New York (1998).

²⁷Many excellent reviews on lithographic modeling have been written, see for example, C.A. Mack, "Optical lithography modeling," in *Microlithography: Science and Technology*, J.R. Sheats and B.W. Smith, Eds., pp. 109–170, Marcel Dekker, New York (1998). In the treatment here, we follow the general methods adopted by the above referenced source.

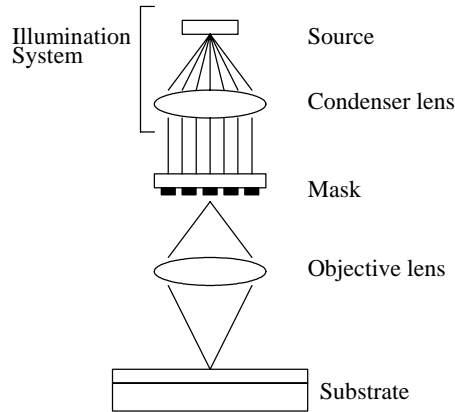


Figure 12.2 Projection imaging system. (Reprinted with permission from Taylor & Francis Group LLC.²⁸)

Mathematically, these modifications serve as the boundary conditions for the wave equation.²⁹

Let us consider the simple case of only the electric field component of light transmittance of a mask pattern, $m(x, y)$, where the mask is in the x - y plane and has both magnitude and phase. For a simple chrome on a glass mask, the mask pattern is binary: either 1 under the glass or 0 under the chrome. Let the x' - y' plane be the diffraction plane, that is, the entrance to the objective lens, and let z be the distance from the mask to the objective lens. Let us further assume that the illuminating light is monochromatic with wavelength λ and that the entire system is in air. Then, the electric field of the diffraction pattern, $E(x', y')$, is given by the Fraunhofer diffraction integral³⁰

$$E(x', y') = \int_{-\infty}^{\infty} \int_{-\infty}^{\infty} m(x, y) e^{2\pi i(f_x x + f_y y)} dx dy, \quad (12.1)$$

where $f_x = x'/z\lambda$ and $f_y = y'/z\lambda$, which are called the spatial frequencies of the diffraction pattern. The above equation for the diffraction pattern (i.e., the electric field distribution of the mask pattern as it enters the objective lens), it should be noted, is the Fourier transform of the mask's transmittance. This implies that

²⁸B.W. Smith, "Optics for photolithography," in *Microlithography: Science and Technology*, J.R. Sheats and B.W. Smith, Eds., p. 172, Marcel Dekker, New York (1998).

²⁹H.J. Levinson, *Principles of Lithography*, 2nd ed., p. 100, SPIE Press, Bellingham, WA (2005).

³⁰C.A. Mack, "Optical lithography modeling," in *Microlithography: Science and Technology*, J.R. Sheats and B.W. Smith, Eds., p. 113, Marcel Dekker, New York (1998).

given a mask in the x - y plane described by the electric field transmission $m(x, y)$, the electric field M as it enters the objective lens (the x' - y' plane) is given by³¹

$$M(f_x, f_y) = F\{m(x, y)\}, \quad (12.2)$$

where F represents the Fourier transform, and f_x and f_y are the spatial frequencies and are simply scaled coordinates in the x' - y' plane.

Since only the diffraction orders that enter the objective lens pupil are used in the imaging, it is necessary to define the maximum angle of diffraction α for which diffracted light just makes it into the lens. This angle is related to the aperture of the lens through the numerical aperture, which is defined as the product of the sine of the maximum half-angle of diffracted light that can enter the lens and the refractive index of the surrounding medium (which is 1 for air). Therefore, $\text{NA} = \sin \alpha$ (since all of the lenses in conventional lithography are in air). Thus, the maximum spatial frequency that can enter the objective lens is NA/λ .³²

Inside the objective lens, the diffraction patterns of the mask (i.e., the Fourier transform of the mask pattern) that pass through the NA of the lens undergo an inverse Fourier transform that recreates to a finite extent the real image of the mask. One can define an ideal imaging lens as one that produces an image that is identical to the Fourier transform of the light distribution entering the lens. Ideal lenses in which the image is limited only by the diffracted light that makes it through the lens are described as diffraction limited.³³

Let us define the objective lens pupil (aperture) function P for an ideal lens as the portion of light that enters the lens; it is 1 inside the aperture and 0 outside.³⁴

$$1, P_{\text{ideal}}(f_x, f_y) \begin{cases} 1, & \sqrt{f_x^2 + f_y^2} < \frac{\text{NA}}{\lambda} \\ 0, & \sqrt{f_x^2 + f_y^2} > \frac{\text{NA}}{\lambda} \end{cases}. \quad (12.3)$$

The product of the pupil function and the diffraction pattern describes the light entering the objective lens. A combination of the pupil function with the inverse Fourier transform of the diffraction pattern gives an expression for the electric field at the wafer plane as

$$E(x, y) = F^{-1}\{M(f_x, f_y)P(f_x, f_y)\}. \quad (12.4)$$

³¹ibid., p. 114.

³²ibid., p. 115.

³³ibid.

³⁴ibid., p. 116.

The aerial image is the intensity distribution at the wafer plane and is the square of the magnitude of the electric field.³⁵

For the special case where the illumination is incident on the mask at some angle θ' , the effect is simply to shift the diffraction pattern with respect to the lens aperture (in terms of spatial frequency) by an amount $\sin(\theta'/\lambda)$. Letting f'_x and f'_y be the shift in the spatial frequency due to the tilted illumination, Eq. (12.4) becomes³⁶

$$E(x, y, f'_x, f'_y) = F^{-1}\{M(f_x - f'_x, f_y - f'_y)P(f_x, f_y)\}. \quad (12.5)$$

If the illumination is incident on the mask from a range of angles, such illumination is called partially coherent, and its effect is to cause a range of shifts, resulting in broadened diffraction orders. (Partial coherence is defined as the sine of the half-angle of the illumination cone divided by the NA of the objective lens.)³⁷

It should be noted that the extended source method for partially coherent image calculations is based on dividing the full source into individual point sources, with each source being coherent and resulting in an aerial image given by Eq. (12.5). Two point sources from the extended source, it must be pointed out, do not interact coherently with each other. For such cases, the contributions of these two sources must be added to each other incoherently (that is, their intensities are additive). The calculation of the full aerial image involves calculating the coherent aerial image from each point on the source and then integrating the intensity over the source.³⁸

12.5 Accounting for Aberrations

Aberrations are deviations of the real behavior of an imaging system from its ideal behavior (the diffraction-limited performance). They can be understood in the context of geometric optics as situations in which all of the light rays originating from a single object point do not converge to a single image point or converge to the wrong point. They are inherent in all practical imaging systems and generally arise from a number of sources: (i) imperfect design, (ii) lens and mirror surfaces that deviate from design specifications, (iii) lens material inhomogeneity, (iv) imperfect lens assembly, and (v) changes in the environmental conditions such as temperature and barometric pressure.³⁹

Because light rays pass through different parts of glass elements and across various points on lens element surfaces, simple variations in the optical constants or curvature of the lens elements' surfaces cause light rays to deviate from their intended paths. Such aberrations can vary substantially across the image field,

³⁵ibid.

³⁶ibid., p. 117.

³⁷ibid.

³⁸ibid.

³⁹H.J. Levinson, *Principles of Lithography*, 2nd ed., p. 105, SPIE Press, Bellingham, WA (2005).

resulting in across-field line width variations.⁴⁰ A full accounting of imaging must therefore include the effects of aberrations.

The effects of aberrations on lithographic performance are determined more generally by incorporating aberrations into the aerial image models. This is done by modifying the pupil function of the lens to include phase error due to aberrations.⁴¹

Mathematically, aberrations are described as wavefront deviations (or errors), i.e., the difference in phase (or path difference) of the actual wavefront emerging from the lens compared to the ideal spherical wavefront. In other words, each primary aberration will produce unique deviations within the lens pupil. This phase difference is a function of position within the lens pupil, which can be described with an aberrated pupil function. An aberrated pupil function is described in terms of wavefront deformation as⁴²

$$P(f_x, f_y) = P_{\text{ideal}}(f_x, f_y)e^{i2\pi W(r, \theta)}, \quad (12.6)$$

where $P_{\text{ideal}}(f_x, f_y)$ is the pupil shape and is given by Eq. (12.3), and $W(r, \theta)$ represents the optical path difference relative to the wavelength (or the wavefront aberration function).

The aberration function is decomposed into sums of mathematical functions, making possible the classification of the aberrations. For this decomposition, it has proven convenient to use particular sets of orthogonal polynomials, the most common of which are the Zernike polynomials.⁴³ With the Zernike polynomials, each polynomial represents a particular type of aberration, having its own characteristic effect on imaging and optical lithography.⁴⁴

The Zernike polynomials are functions of the polar coordinates (r, θ) of positions r and angle θ in the exit pupil. Because the same point in the exit pupil is specified by θ and $(\theta + 360 \text{ deg})$, it is convenient for the polynomials to be expressed as functions of $\sin(n\theta)$ and $\cos(n\theta)$, where n is an integer.⁴⁵ Although the Zernike polynomials comprise an orthogonal polynomial series with an

⁴⁰J.E. Gorytch and D. Williamson, "Effects of higher order aberrations on the process window," *Proc. SPIE* **1463**, 368–381 (1991).

⁴¹C.A. Mack, "Optical lithography modeling," in *Microlithography: Science and Technology*, J.R. Sheats and B.W. Smith, Eds., p. 120, Marcel Dekker, New York (1998).

⁴²ibid., p. 219.

⁴³F. Zernike, "Beugungstheorie des Schneidenverfahrens und seiner verbesserten Form, der Phasenkontrastmethode," *Physica* **1**, 689–704 (1934); M. Born and E. Wolf, *Principles of Optics*, 7th ed., pp. 523–532, Cambridge University Press, New York (1999).

⁴⁴H.J. Levinson, *Principles of Lithography*, 2nd ed., pp. 107–108, SPIE Press, Bellingham, WA (2005).

⁴⁵For tables of the Zernike polynomials, as well as in depth discussion on aberrations in lithographic exposure tools, see, for example, H.J. Levinson, *Principles of Lithography*, 2nd ed., p. 109, SPIE Press, Bellingham, WA (2005); C.A. Mack, "Optical lithography modeling," in *Microlithography: Science and Technology*, J.R. Sheats and B.W. Smith, Eds., pp. 118–119, Marcel Dekker, New York (1998); B.W. Smith, "Optics for photolithography," in *Microlithography: Science and Technology*, J.R. Sheats and B.W. Smith, Eds., pp. 223–226, Marcel Dekker, New York (1998).

infinite number of terms, it is customary to cut off the series after 36 terms. By knowing the numerical values of the 36 Zernike coefficients, one is able to describe to a reasonable level of accuracy the aberration behavior of a lens at a single point.⁴⁶

It is possible to arrange the Zernike polynomial in a number of ways, but the method that has been adopted in most lens design software and lens measuring equipment uses the fringe or circle Zernike polynomial, defined as⁴⁷

$$W(r, \theta) = \frac{\text{OPD}}{\lambda} = \sum_{i=0}^{\infty} Z_i F_i(r, \theta), \quad (12.7)$$

where $W(r, \theta)$ is the optical path difference (OPD) relative to the illuminating wavelength λ , Z_i is the i th Zernike coefficient, and $F_i(r, \phi)$ are polynomial terms, defined in Table 12.2. The phase error due to aberrations is $2\pi W(r, \phi)$, while the polar coordinates on the unit circle (r, ϕ) are related to the Cartesian spatial frequency coordinates by⁴⁸

$$f_x = \frac{\text{NA}}{\lambda} r \cos \phi, \quad (12.8a)$$

$$f_y = \frac{\text{NA}}{\lambda} r \sin \phi. \quad (12.8b)$$

Table 12.2 Polynomial functions and common names for the first 36 terms in the fringe Zernike polynomial. (Adapted with permission from Ref. 49. © 2007 John Wiley & Sons.)

Term	Fringe Zernike formula, F_i	Common name
Z_0	1	Piston
Z_1	$r \cos \phi$	x tilt
Z_2	$r \sin \phi$	y tilt
Z_3	$2r^2 - 1$	Power (paraxial focus)
Z_4	$r^2 \cos 2\phi$	Third order astigmatism
Z_5	$r^2 \sin 2\phi$	Third order 45 deg astigmatism
Z_6	$(3r^2 - 2)r \cos \phi$	Third order x coma
Z_7	$(3r^2 - 2)r \sin \phi$	Third order y coma
Z_8	$6r^4 - 6r^2 + 1$	Third order spherical
Z_9	$r^3 \cos 3\phi$	Trefoil (third order three point)
Z_{10}	$r^3 \sin 3\phi$	45 deg trefoil
Z_{11}	$(4r^2 - 3)r^2 \cos 2\phi$	Fifth order astigmatism

(Continued)

⁴⁶C.A. Mack, *Fundamental Principles of Optical Lithography: The Science of Microfabrication*, p. 79, John Wiley & Sons, Hoboken, NJ (2007).

⁴⁷ibid.

⁴⁸ibid.

⁴⁹ibid, p. 80.

Table 12.2 *Continued.*

Z_{12}	$(4r^2 - 3)r^2 \sin 2\phi$	Fifth order 45 deg astigmatism
Z_{13}	$(10r^4 - 12r^2 + 3)r \cos \phi$	Fifth order x coma
Z_{14}	$(10r^4 - 12r^2 + 3)r \sin \phi$	Fifth order y coma
Z_{15}	$20r^6 - 30r^4 + 12r^2 - 1$	Fifth order spherical
Z_{16}	$r^4 \cos 4\phi$	Quadrafoil (third order four point)
Z_{17}	$r^4 \sin 4\phi$	45 deg quadrafoil
Z_{18}	$(5r^2 - 4)r^3 \cos 3\phi$	Fifth order trefoil (fifth order three point)
Z_{19}	$(5r^2 - 4)r^3 \sin 3\phi$	Fifth order 45 deg trefoil
Z_{20}	$(15r^4 - 20r^2 + 6)r^2 \cos 2\phi$	Seventh order astigmatism
Z_{21}	$(15r^4 - 20r^2 + 6)r^2 \sin 2\phi$	Seventh order 45 deg astigmatism
Z_{22}	$(35r^6 - 60r^4 + 30r^2 - 4)r \cos \phi$	Fifth order x coma
Z_{23}	$(35r^6 - 60r^4 + 30r^2 - 4)r \sin \phi$	Fifth order y coma
Z_{24}	$70r^8 - 140r^6 + 90r^4 - 20r^2 + 1$	Seventh order spherical
Z_{25}	$r^5 \cos 5\phi$	Pentafoil (third order five point)
Z_{26}	$r^5 \sin 5\phi$	45 deg pentafoil
Z_{27}	$(6r^2 - 5)r^4 \cos 4\phi$	Fifth order quadrafoil (fifth order four point)
Z_{28}	$(6r^2 - 5)r^4 \sin 4\phi$	Fifth order quadrafoil
Z_{29}	$(21r^4 - 30r^2 + 10)r^3 \cos 3\phi$	Seventh order trefoil (seventh order three point)
Z_{30}	$(21r^4 - 30r^2 + 10)r^3 \sin 3\phi$	Seventh order 45 deg trefoil
Z_{31}	$(56r^6 - 105r^4 + 60r^2 - 10)r^2 \cos 2\phi$	Ninth order astigmatism
Z_{32}	$(56r^6 - 105r^4 + 60r^2 - 10)r^2 \sin 2\phi$	Ninth order 45 deg astigmatism
Z_{33}	$(126r^8 - 280r^6 + 210r^4 - 60r^2 + 5)r \cos \phi$	Ninth order x coma
Z_{34}	$(126r^8 - 280r^6 + 210r^4 - 60r^2 + 5)r \sin \phi$	Ninth order y coma
Z_{35}	$252r^{10} - 630r^8 + 560r^6 - 210r^4 + 30r^2 - 1$	Ninth order spherical
Z_{36}	$924r^{12} - 2772r^{10} + 3150r^8 - 1680r^6 + 420r^4 - 42r^2 + 1$	Eleventh order spherical

12.6 Aerial Image Formation Models

Aerial image models of varying complexity have been derived over the years to account for a range of physical phenomena involved in image formation. Although certain physical parameters are ignored in some of these models without adversely affecting the accuracy of their predictions, in other models, these physical parameters must be included in order to obtain results at the desired level of accuracy. Such is the case with accounting for the effects of light polarization on predicting the accuracy of the aerial image models.

12.6.1 Scalar models for calculating aerial image intensity

The scalar models for calculating aerial image intensity neglects the effects of polarization of light. This is a legitimate approximation for numerical apertures less than ~ 0.7 . Scalar models are the simplest of the aerial models and come in three main types: the zero-order, first-order, and high-NA scalar models.

12.6.1.1 Zero-order scalar model

Originally proposed by Dill,⁵⁰ and adapted into SAMPLE⁵¹ and the 1985 version of PROLITH,⁵² the zero-order scalar model involves two main calculations: (i) calculation of aerial image intensity $I_i(x)$ as if it were projected into air (x being along the surface of the wafer and perpendicular to the propagation direction of the image) and (ii) calculation of the standing wave intensity $I_s(z)$ assuming a plane wave of light at normal incidence on the photoresist-coated wafer (with z defined to be zero at the top of the resist and positive going into the resist—see the section on standing waves below for the appropriate expression for the standing wave intensity under normal incidence condition). The normal incidence assumption here is valid for low-NA lithographic lenses because at the air-resist interface, the plane wave is refracted toward the optical axis and propagates into the resist at near-normal angles.⁵³

This model embodies the assumption that the actual intensity within the resist film $I(x, z)$ can be approximated by⁵⁴

$$I(x, z) \approx I_i(x)I_s(z). \quad (12.9)$$

This is referred to as the separability assumption in that the aerial image and the standing wave can be calculated independently and then multiplied together to yield the total intensity within the resist.⁵⁵

As stated above, these approximations are valid for low-NA systems, as well as for thin photoresists. They are not valid, however, for situations where the aerial image changes as it propagates through the resist (i.e., defocuses) or when the light entering the resist is at moderate to large angles of incidence.⁵⁶

12.6.1.2 First-order scalar model

Independently proposed by Mack⁵⁷ and Bernard,⁵⁸ this model accounts for the effect of a changing aerial image focus (i.e., defocus effect) as it propagates

⁵⁰W.G. Oldham, S.N. Nandgaonkar, A.R. Neureuther, and M. O'Toole, "A general simulator for VLSI lithography and etching processes: Part 1. application to projection lithography," *IEEE Trans. Electron Dev* **ED-26**(4), 717–722 (1979).

⁵¹ibid.

⁵²C.A. Mack, "PROLITH: a comprehensive optical lithography model," *Proc. SPIE* **538**, 207–220 (1985).

⁵³C. A. Mack, "Optical lithography modeling," in *Microlithography: Science and Technology*, J.R. Sheats & B.W. Smith, Eds., p. 120, Marcel Dekker, New York (1998).

⁵⁴ibid.

⁵⁵ibid.

⁵⁶C.A. Mack, "Optical lithography modeling," in *Microlithography: Science and Technology*, J.R. Sheats and B.W. Smith, Eds., pp. 120, Marcel Dekker, New York (1998).

⁵⁷C.A. Mack, "Understanding focus effects in sub micron optical lithography," *Proc. SPIE* **922**, 135–148 (1988); and *Opt. Eng.* **27**(2), 1093–1100 (1988).

⁵⁸D.A. Bernard and H.P. Urbach, "Thin film interference in photolithography for finite numerical apertures," *J. Opt. Soc. Am. A* **8**(1), 123–133 (1991).

through the resist. The simulator calculates the image as a function of x and the distance δ from the plane of best focus. If the defocus distance of the image at the top of the resist is δ_0 , the defocus within the resist at any position z is given by⁵⁹

$$\delta(z) = \delta_0 + \frac{z}{n}, \quad (12.10)$$

where n is the real part of the index of refraction of the resist. The intensity within the resist is therefore expressed according to the separability assumption,

$$I(x, z) = I_i[x, \delta(z)]I_s(z). \quad (12.11)$$

The expression for the intensity of the standing waves for the normal incidence condition is provided in Section 12.7.

12.6.1.3 High-NA scalar model

Under high-NA imaging, the light illuminates the resist over a wide array of angles ranging from normal to non-normal incidence. This model, like the other scalar models, embodies the separability assumption, where the aerial image and the standing wave are calculated independently and then multiplied together to yield the total intensity within the resist. This model uses an expression for the intensity of the standing wave for the non-normal incidence situation (see Section 12.7). In addition, the model uses the exact defocus expression defined in terms of the OPD as⁶⁰

$$\text{OPD}(\theta) = \delta(1 - \cos \theta), \quad (12.12)$$

where θ is the angle of the light exiting the lens.

12.6.2 Full scalar and vector models

In the full scalar model, the full light intensity inside the resist is calculated, subject to the standard scalar approximation, involving the requirement that the three components of the electric field vector be treated separately as scalar quantities, with each scalar electric field component satisfying the wave equation. In addition, when two fields of light (for example, two plane waves) are added together, the scalar approximation dictates that the sum of the field would simply be the sum of the scalar amplitudes of the two fields. Implicit in the scalar approximation is

⁵⁹H.J. Levinson and W.H. Arnold, "Focus: the critical parameter for submicron lithography," *J. Vac. Sci. Technol. B* **5**, 21–34; 293–298 (1987); C.A. Mack, "Optical lithography modeling," in *Micro lithography: Science and Technology*, J.R. Sheats and B.W. Smith, Eds., pp. 120–121, Marcel Dekker, New York (1998).

⁶⁰ibid., pp. 121–122.

the assumption that the electric field vectors are always parallel and will always give complete interference, which is not the case for electric fields that are at right angles to each other or for plane waves at large angles of incidence to the wafer.⁶¹

For the full vector model, the complete solution of Maxwell's equations is used, while accounting for the vector directions is required.⁶² This model is valid for all angles and numerical apertures.

12.7 Standing Wave Models

The light inside the resist film consists of incident and reflected components. The light intensity within the resist varies in the vertical direction because of absorption and interference effects associated with standing waves. Standing waves are rapidly varying light distribution within the depth of the resist. They result from the interference between the incident and reflected light within the resist. This causes a sinusoidal variation in light intensity, marked by low and high exposure levels, within the depth of the resist.

Standing waves limit the resist exposure process because they disrupt the uniform transmission of light within the depth of the resist, creating uneven exposure levels within the resist that manifest as feature bridging and footing in the least-exposed areas and feature slimming in the overexposed areas. The use of antireflection coatings has proven effective in mitigating the effects of standing waves (see Chapter 9).

The mathematical derivation of the analytical expressions for standing waves in resist films disposed over appropriate substrates is presented in Chapter 9. In this chapter, we will make use of the relevant standing wave expressions for the normal and nonincidence illumination conditions.

For the specific case of normal incidence illumination of a homogenous resist film (see Fig. 12.3), the electric field inside the resist $E_2(z)$ is given by⁶³

$$E_2(z) = E_1(z) \frac{\tau_{12}[e^{(i2\pi n_2 z/\lambda)} + \rho_{23}\tau_D^2 e^{i2\pi n_2 z/\lambda}]}{1 + \rho_{12}\rho_{23}\tau_D^2}, \quad (12.13)$$

where E_1 is the electric field of the incident plane wave at $z = 0$, which is not a function of x and y for the case of normal incidence,

$$\rho_{ij} = \frac{\tilde{n}_i - \tilde{n}_j}{\tilde{n}_i + \tilde{n}_j} \text{ is the Fresnel reflection coefficient,} \quad (12.14)$$

⁶¹ibid., p. 123.

⁶²D.G. Flagello, A.E. Rosenbluth, C. Proglar, and J. Armitage, "Understanding high numerical aperture optical lithography," *Microelectron. Eng.* **17**, 105–108 (1992); C.A. Mack and C. B. Juang, "Comparison of scalar and vector modeling of image formation in photoresist," *Proc. SPIE* **2440**, 381–394 (1995).

⁶³C.A. Mack, "Analytical expression for the standing wave intensity in photoresist," *Appl. Opt.* **25**(12), 1958–1961 (1986).

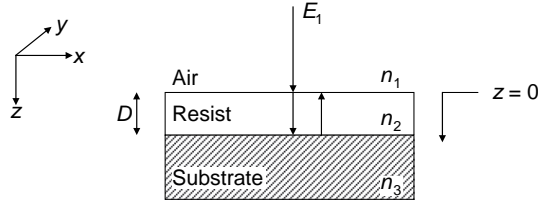


Figure 12.3 Film stack showing the geometry used in deriving the standing wave equations for a normally incident electric field.

$$\tau_{ij} = \frac{2\tilde{n}_i}{\tilde{n}_i + \tilde{n}_j} \text{ is the Fresnel transmission coefficient,} \quad (12.15)$$

$$\tau_D = e^{-ik_2 D} \text{ is the internal transmittance of the film,} \quad (12.16)$$

$$k_i = \frac{2\pi\tilde{n}_i}{\lambda} \text{ is the propagation constant,} \quad (12.17)$$

$\tilde{n}_j = n_j - ik_j$ is the complex refractive index of the j th medium, n_j and k_j are the real refractive index and extinction coefficient of the medium, and λ is the illumination wavelength.

It should be noted that absorption is accounted for in Eq. (12.13) through the imaginary part of the index of refraction. Absorption coefficient α is related to the imaginary part of the refractive index by

$$\alpha = \frac{4\pi\kappa}{\lambda}. \quad (12.18)$$

In the special case where the resist film is not homogenous, such that there is a small variation in the imaginary part of the refractive index along the z direction, with the real part constant, the anisotropic absorbance in that case can be expressed as

$$Abs(z) = \int_0^z \alpha(z') dz'. \quad (12.19)$$

Thus, the electric field intensity can be determined as a function of z by using Eq. (12.19) in Eq. (12.13).⁶⁴ Calculation of the intensity inside the resist from

⁶⁴C.A. Mack, "Optical lithography modeling," in *Microolithography: Science and Technology*, J.R. Sheats and B.W. Smith, Eds., p. 126, Marcel Dekker, New York (1998).

Eq. (12.13) yields a very messy result as

$$\begin{aligned}
 I_2(z) &= |E_2(x, y, z) \cdot E_2^*(x, y, z)| \\
 &= E_1(z) \frac{\tau_{12} [e^{i2\pi n_2 z/\lambda} + \rho_{23} \tau_D^2 e^{i2\pi n_2 z/\lambda}]}{1 + \rho_{12} \rho_{23} \tau_D^2} \\
 &\quad \times E_1(z) \frac{\tau_{12}^* [e^{i2\pi n_2 z/\lambda} + \rho_{23}^* \tau_D^{*2} e^{i2\pi n_2 z/\lambda}]}{1 + \rho_{12}^* \rho_{23}^* \tau_D^{*2}}. \tag{12.20}
 \end{aligned}$$

However, a few algebraic simplifications allow for a reasonably useful form for the relative intensity inside the resist:⁶⁵

$$\begin{aligned}
 I(z) &= \frac{n_2 |E(z)|^2}{n_1 |E_1|^2} = T_{\text{eff}} \left\{ [e^{-\alpha z} + |\rho_{23}|^2 e^{-\alpha(2D-z)}] + 2|\rho_{23}| e^{-\alpha D} \right. \\
 &\quad \left. \times \cos \left[\frac{4\pi n_2 (D-z)}{\lambda} \right] + \phi_{23} \right\}, \tag{12.21}
 \end{aligned}$$

where $\rho_{23} = |\rho_{23}| e^{i\phi_{23}}$,

$$T_{\text{eff}} = \frac{n/n |\tau_{12}|^2}{|1 + \rho_{12} \rho_{23} \tau_D^2|^2} = \frac{T_{12}}{|1 + \rho_{12} \rho_{23}|^2}, \tag{12.22}$$

and T_{eff} is the effective transmittance into the resist.

For the case of non-normal illumination incidence at some angle θ , the Fresnel transmission and reflection coefficients are now functions of the angle of incidence as well as the polarization of the incident light; they are given by⁶⁶

$$\rho_{ij\perp}(\theta) = \frac{\tilde{n}_i \cos(\theta_i) - \tilde{n}_j \cos(\theta_j)}{\tilde{n}_i \cos(\theta_i) + \tilde{n}_j \cos(\theta_j)}, \tag{12.23}$$

$$\rho_{ij\parallel}(\theta) = \frac{\tilde{n}_i \cos(\theta_j) - \tilde{n}_j \cos(\theta_i)}{\tilde{n}_i \cos(\theta_j) + \tilde{n}_j \cos(\theta_i)}, \tag{12.24}$$

$$\tau_{ij\perp}(\theta) = \frac{2\tilde{n}_i \cos(\theta_i)}{\tilde{n}_i \cos(\theta_i) + \tilde{n}_j \cos(\theta_j)}, \tag{12.25}$$

$$\tau_{ij\parallel}(\theta) = \frac{2\tilde{n}_i \cos(\theta_i)}{\tilde{n}_i \cos(\theta_j) + \tilde{n}_j \cos(\theta_i)}, \tag{12.26}$$

⁶⁵C.A. Mack, *Fundamental Principles of Optical Lithography: The Science of Microfabrication*, p. 133, John Wiley & Sons, Hoboken, NJ (2007).

⁶⁶ibid., pp. 137–138.

where θ_i and θ_r represent the incident angle and reflected angle, respectively, that light makes with a normal to the resist surface. Here, the symbol \parallel is used to represent an electric field vector that lies in a plane defined by the direction of the incident light and a normal to the resist surface. Other common names used to represent \parallel polarization include p -polarization and transverse magnetic (TM) polarization. The polarization denoted by \perp is used to represent an electric field vector that lies in a plane perpendicular to that defined by the direction of the incident light and a normal to the resist surface. Other common names used to represent the \perp polarization include s -polarization and transverse electric (TE) polarization.⁶⁷

For the s -polarized light, the intensity of the electric field inside the resist points in the y direction, and is given by an expression similar to Eq. (12.13), but with the position z replaced with $z\cos\theta_2$ as⁶⁸

$$E_y(z, \theta_2) = \frac{\tau_{12}(\theta_2)E_1[e^{i2\pi n_2 z \cos \theta_2/\lambda} + \rho_{23}(\theta_2)\tau_D^2(\theta_2)e^{-i2\pi n_2 z \cos \theta_2/\lambda}]}{1 + \rho_{12}(\theta_2)\rho_{23}(\theta_2)\tau_D^2(\theta_2)}. \quad (12.27)$$

The resulting relative intensity in the resist is given by

$$I(z) = T_{\text{eff}}(\theta_2) \left\{ e^{(\alpha z/\cos \theta_2)} + |\rho_{23}(\theta_2)|^2 e^{[\alpha(2D - z)/\cos \theta_2]} \right. \\ \left. + T_{\text{eff}}(\theta_2) 2|\rho_{23}(\theta_2)| e^{[\alpha D/\cos \theta_2]} \cos \left[4\pi n_2 \cos \theta_2 \left(\frac{D - z}{\lambda} \right) + \phi_{23} \right] \right\}. \quad (12.28)$$

For the p -polarized incident light, the resulting electric field will have both x and z components, which are given by⁶⁹

$$E(x) = \frac{\cos \theta_2 \tau_{12}(\theta_2) E_1 [e^{i2\pi n_2 z \cos \theta_2/\lambda} + \rho_{23}(\theta_2) \tau_D^2(\theta_2) e^{-i2\pi n_2 z \cos \theta_2/\lambda}]}{1 + \rho_{12}(\theta_2) \rho_{23}(\theta_2) \tau_D^2(\theta_2)}, \quad (12.29a)$$

$$E(y) = \frac{\sin \theta_2 \tau_{12}(\theta_2) E_1 [e^{i2\pi n_2 z \cos \theta_2/\lambda} - \rho_{23}(\theta_2) \tau_D^2(\theta_2) e^{-i2\pi n_2 z \cos \theta_2/\lambda}]}{1 + \rho_{12}(\theta_2) \rho_{23}(\theta_2) \tau_D^2(\theta_2)}. \quad (12.29b)$$

⁶⁷C.A. Mack, *Fundamental Principles of Optical Lithography: The Science of Microfabrication*, p. 138, John Wiley & Sons, Hoboken, NJ (2007).

⁶⁸C.A. Mack, "Optical lithography modeling," in *Microolithography: Science and Technology*, J.R. Sheats and B.W. Smith, Eds., p. 126, Marcel Dekker, New York (1998).

⁶⁹C.A. Mack, *Fundamental Principles of Optical Lithography: The Science of Microfabrication*, pp. 139–140, John Wiley & Sons, Hoboken, NJ (2007).

The resulting total standing wave intensity inside the resist, relative to the incident intensity, is given by⁷⁰

$$\begin{aligned}
 I(z) &= \frac{n_2(|E_x|^2 + |E_z|^2)}{n_1|E_1|^2} \\
 &= T_{\text{eff}}(\theta_2) \left\{ e^{(\alpha z / \cos \theta_2)} + |\rho_{23}(\theta_2)|^2 e^{[\alpha(2D - z) / \cos \theta_2]} \right\} \\
 &\quad + T_{\text{eff}}(\theta_2) 2|\rho_{23}(\theta_2)| e^{(\alpha D / \cos \theta_2)} \cos(2\theta_2) \cos \left[4\pi n_2 \cos \theta_2 \left(\frac{D - z}{\lambda} \right) + \Phi_{23} \right].
 \end{aligned}
 \tag{12.30}$$

12.8 Exposure Models

The starting point of lithographic exposure modeling for positive resists is the Dill equations,⁷¹ which characterize the optical and photochemical properties of resist films, the results of which can be used to predict the final shape of the resist image.⁷² These analyses are based on the assumption that the rate of decomposition of a PAC such as DNQ at any location in the resist film is proportional to the radiation intensity prevailing at that location at the given instant of time. Given that only the radiation absorbed by the PAC participates in the photoreaction,⁷³ the changes in the absorbance of the PAC and the changes in the resist composition are linked. These changes may be described by a set of these two simultaneous differential equations:

$$\frac{\partial m(z, t)}{\partial t} = -I(z, t)m(z, t)C, \tag{12.31}$$

$$\frac{\partial I(z, t)}{\partial z} = -I(z, t)[Am(z, t) + B], \tag{12.32}$$

where $m(z, t)$ is the fraction of PAC remaining at depth z in the film at time t [see Eq. (12.34)], and $I(z, t)$ is the radiation intensity at that location and time. It should be pointed out that the square bracket in Eq. (12.32) contains the absorbance of the resist that is made up of two terms, namely, the time-dependent absorbance of the diazoquinone $Am(z, t)$ (also called the bleachable absorbance) and the

⁷⁰ibid, p. 140.

⁷¹F.H. Dill, "Optical lithography," *IEEE Trans. Electron. Dev.* **ED-22**(2), 440–444 (1975); F.H. Dill, W.P. Hornberger, P.S. Hauge, and J.M. Shaw, "Characterization of positive photoresists," *IEEE Trans. Electron Dev.* **ED-22**(7), 445–452 (1975).

⁷²M.A. Narasimham, *IEEE Trans. Electron Dev.* **ED-22**, 478 (1975); F.H. Dill, A.R. Neureuther, J.A. Tuttle, and E.J. Walker, "Modeling projection printing of positive photoresists," *IEEE Trans. Electron Dev.* **ED-22**(7), 456–464 (1975).

⁷³This is a statement of Draper's law of photochemistry, enunciated in the nineteenth century. For more details, see Chapter 3.

time-independent absorbance B (also called nonbleachable absorbance) of the base resin. The dimensionless parameter C is the exposure rate constant and is related to the quantum yield of the reaction. Alternatively, the absorption coefficient α of the resist film is expressed as

$$\alpha = Am(z, t) + B. \quad (12.33)$$

According to Beer's law, in dilute solutions the absorption coefficient is proportional to the concentration c of the absorbing species in the material, and we have

$$\alpha = ac, \quad (12.34)$$

which for a photoresist film comprising four major components—base resin R , which imbues the resist with its structural properties, photoactive compound M , exposure products P generated by the reaction of M with ultraviolet light, and solvent S —the total absorption coefficient of the resist film is therefore a sum of the contribution of all of the individual components in the resist:

$$\alpha = a_M M + a_P P + a_R R + a_S S, \quad (12.35)$$

where a_i represents the molar absorption coefficient of species i . If M_0 is the initial PAC concentration (i.e., with no UV exposure), the stoichiometry of the exposure reaction yields

$$P = M_0 - M. \quad (12.36)$$

Substituting Eq. (12.36) into Eq. (12.35), we obtain

$$\alpha = Am + B, \quad (12.37)$$

where

$$A = (a_M - a_P)M_0, \quad (12.38)$$

$$B = a_P M_0 + a_R R + a_S S, \quad (12.39)$$

$$m = \frac{M}{M_0}. \quad (12.40)$$

The rate of the destruction of the diazoquinone inhibitor under unit radiation intensity is constant and is measured by the dimensionless parameter C , which is related to the quantum yield of the photoreaction.⁷⁴

The changes in the absorptive behavior of the film as well as the changes in the local composition, that is, $m(z, t)$, are obtained as the simultaneous solutions of

⁷⁴A. Reiser, *Photoreactive Polymers: The Science and Technology of Resists*, p. 206, John Wiley & Sons, Hoboken, NJ (1989).

Eqs. (12.31) and (12.32), subject to the initial conditions,

$$m(z, 0) = 1, \quad (12.41)$$

$$I(z, 0) = I_0 \exp[-(A + B)z] \quad (12.42)$$

and the boundary conditions,

$$I(0, t) = I_0, \quad (12.43)$$

$$M(0, t) = \exp(-I_0 C t). \quad (12.44)$$

Although analytical solutions of Eqs. (12.31) and (12.32) exist,⁷⁵ the integration is usually carried out by numerical methods.

The three parameters A , B , and C can also be determined from the dependence of the transmission of the resist film on the exposure dose. To do this, the internal transmission (T) of the film is expressed in the general form

$$Tt = \exp \left\{ - \int_0^d [Am(z, t) + B] dz \right\}, \quad (12.45)$$

which for $t = 0$ and $t = \infty$ reduces to the following expressions:

$$T(0) = \exp[-(A + B)d], \quad (12.46)$$

$$T(\infty) = \exp(-Bd), \quad (12.47)$$

and the initial slope of the transmission curve is given by the expression

$$\frac{dT}{dt}(0) = T(0)[1 - T(0)] \frac{AI_0 C}{A + B}. \quad (12.48)$$

Thus, the parameters A , B , and C may be determined from the initial and the final value of T and from its derivative at time $t = 0$.⁷⁶

The A , B , and C parameters are experimentally measurable quantities⁷⁷ and are typically determined from typical resist absorbance curves. When the resist is fully exposed, i.e., $m = 0$, one obtains

$$\alpha_{\text{exposed}} = B. \quad (12.49)$$

⁷⁵S.V. Babu and V. Srinivasan, "Optical density and contrast for positive resists," *Proc. SPIE* **539**, 36–43 (1985).

⁷⁶A. Reiser, *Photoreactive Polymers: The Science and Technology of Resists*, p. 207, John Wiley & Sons, Hoboken, NJ (1989).

⁷⁷F.H. Dill, W.P. Hornberger, P.S. Hauge, and J.M. Shaw, "Characterization of positive photoresists," *IEEE Trans. Electron Dev.* **ED-22**(7), 445–452 (1975).

Similarly, when the resist is unexposed, $m = 1$ ($M = M_0$), one obtains

$$\alpha_{\text{exposed}} = A + B. \quad (12.50)$$

Substituting Eq. (12.49) into Eq. (12.50) yields A as

$$A = \alpha_{\text{unexposed}} - \alpha_{\text{exposed}}. \quad (12.51)$$

Another exposure model was proposed by Byers et al.⁷⁸ In this model, the exposure dose is first converted into an effective dose, which is coupled into the resist as a function of depth. The depth dependence of the exposure dose $D(z)$ is expressed in terms of a simplified form of the full standing wave equation, given by

$$D(z) = D_s \left[e^{-\alpha(d-z)} + |\tilde{r}|^2 e^{-\alpha(d+z)} - 2|\tilde{r}| e^{-\alpha d} \cos\left(\frac{4\pi n z}{\lambda} + \phi_0\right) \right], \quad (12.52)$$

where D_s is the applied dose in mJ/cm^2 , corrected by the reflectivity at the air-resist interface, α is the absorption coefficient of the resist film in nm^{-1} , d is the film thickness in nm , n is the real part of the refractive index, λ is the exposure wavelength in nm , \tilde{r} is the complex reflectivity coefficient of the resist-underlayer interface, ϕ_0 is the phase shift due to the complex reflectivity coefficient \tilde{r} , and z is the distance from the resist-underlayer interface in the resist. Averaging this dose from 0 to d gives the effective dose D_{eff} coupled into the resist as

$$D_{\text{eff}} = \frac{1}{d} \int_0^d D(z) dz. \quad (12.53)$$

The effective dose is involved in the photoinduced chemistry of the photoactive compound or photoacid generator, which leads to the generation of photoacid, whose concentration is given by

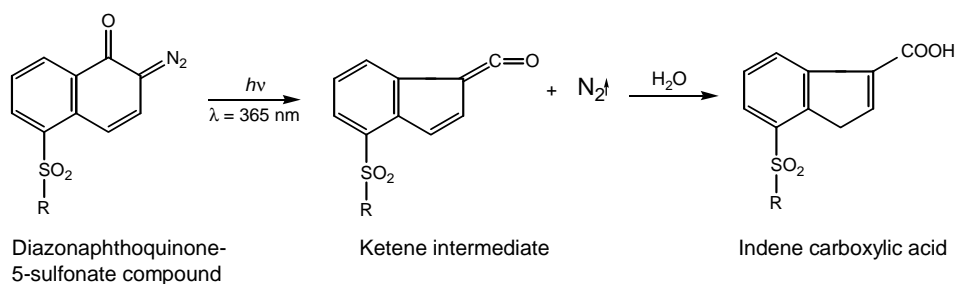
$$[\text{Acid}] = [\text{PAG}]_0 (1 - e^{-C \times \text{Dose}}), \quad (12.54)$$

where $[\text{Acid}]$ is the acid concentration right after exposure, $[\text{PAG}]_0$ is the initial PAG concentration, C is the exposure rate constant, and Dose is the average dose given by Eq. (12.53).

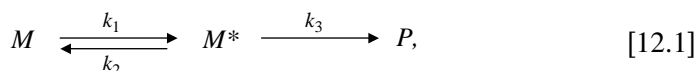
⁷⁸J. Byers et al., "Characterization and modeling of a positive amplified resist," *Proc. SPIE* **2438**, 153–166 (1995).

12.8.1 Adapting exposure kinetics of DNQ to the Dill equations

On irradiation with UV light, the DNQ PAC is converted to indene carboxylic acid through a ketene intermediate as shown in Scheme 12.1 and Reaction [12.1]:



Scheme 12.1 Photolysis of DNQ PAC.



where M is the PAC, M^* is the excited state molecule, P is the indene carboxylic acid, and k_1 , k_2 , k_3 are the rate constants for the reactions. Assuming first-order kinetics, the rate equation for each of the species can be expressed as

$$\frac{dM}{dt} = k_2 M^* - k_1 M, \quad (12.55)$$

$$\frac{dM^*}{dt} = k_1 M - (k_2 + k_3) M^*, \quad (12.56)$$

$$\frac{dP}{dt} = k_3 M^*. \quad (12.57)$$

Applying the Bodenstein pseudo-steady-state approximation, where it is assumed that the excited molecule M^* is formed as quickly as it disappears, yields

$$\frac{dM^*}{dt} = 0. \quad (12.58)$$

Substituting Eq. (12.58) into Eq. (12.56) and solving for M^* yields

$$M^* = \frac{k_1}{k_2 + k_3} M. \quad (12.59)$$

Substituting Eq. (12.59) into Eq. (12.55) yields

$$\frac{dM}{dt} = -KM, \quad (12.60)$$

where K , the overall rate constant, is expressed as

$$K = \frac{k_1 k_3}{k_2 + k_3}. \quad (12.61)$$

Integrating Eq. (12.61) with the assumption that K remains constant with time yields

$$M = M_0 \exp(-Kt). \quad (12.62)$$

Experimental evidence indicates that K is directly proportional to the intensity of the exposing radiation.⁷⁹ The significance of this finding for laser lithography is tremendous, especially considering the pulse nature of laser light, which led to early concerns that it might cause nonlinear effects such as reciprocity failures⁸⁰ at exposure doses of lithographic interests.⁸¹ This implies that Eq. (12.60) can be expressed as

$$\frac{\partial m}{\partial t} = -CIm, \quad (12.63)$$

where $m = M/M_0$ is the relative PAC concentration at depth z in the film and time t , and C is the standard exposure rate constant (as previously defined).

Mack⁸² made the interesting observation that by integrating Eq. (12.63) with respect to time (with the assumption that K remains constant with time) gives

$$m = e^{-Ct}, \quad (12.64)$$

and then differentiating Eq. (12.64) with respect to x produces

$$\frac{\partial m}{\partial x} = m \ln(m) \frac{1}{I} \frac{\partial I}{\partial x}. \quad (12.65)$$

Equation (12.65) represents the variation of the photoactive compound on account of exposure. This expression shows that the latent image gradient $\partial m/\partial x$

⁷⁹C.A. Mack, "Absorption and exposure in positive photoresist," *Appl. Opt.* **27**(23), 4913-4919 (1988).

⁸⁰A resist exposure process is described to obey the law of reciprocity if the product of the light intensity and the required exposure time is intensity independent.

⁸¹K. Jain, C.G. Willson, and B.J. Lin, "Ultrafast deep UV lithography with excimer lasers," *IEEE Electron Device Lett.* **EDL-3**, 53 (1982); S. Rice and K. Jain, "Reciprocity behavior of photoresists in excimer laser lithography," *IEEE Trans. Electron Dev.* **ED-31**, 1 (1984).

⁸²C.A. Mack, "Photoresist process optimization," *KTI Microelectronics Seminar Proc.*, pp. 153-167 (1987).

is directly proportional to the image log-slope [= $\partial \ln(I)/\partial x = (1/I)(\partial I/\partial x)$]. In other words, it shows that the modulation in x results from the pattern on the mask.

The logarithmic slope of the aerial image is typically called the “log-slope,” and it is a good metric of the quality of the latent image. It is customary to normalize the image log-slope by multiplying it by the nominal line width w of the feature to yield the normalized image log-slope (NILS) as⁸³

$$\text{NILS} = w \frac{d \ln(I)}{dx}. \quad (12.66)$$

The NILS is proportional to the exposure latitude and is the best metric for judging the quality of an aerial image. The term $m \ln(m)$ is exposure dependent (with m being the relative amount of resist sensitizer that has not been exposed at the point where the latent image gradient is being described). A plot of $-m \ln(m)$ versus m shows that there is one exposure dose (one value of m) that maximizes the latent image quality (i.e., when the full information of the aerial image is transferred into the resist during exposure), and it occurs when $m = e^{-1} \approx 0.37$.⁸⁴

Defining a lumped parameter, the resist contrast γ that relates the aerial image and the development rate r , one obtains the lithographic imaging equation

$$\frac{\partial \ln(r)}{\partial x} = \gamma \frac{\partial \ln(I)}{\partial x}. \quad (12.67)$$

This equation shows how a gradient in aerial image intensity results in a solubility differential in the resist. The development rate contrast is maximized by a high resist contrast and a large log-slope of the aerial image.⁸⁵

Among the many parameters (resolution, contrast, sensitivity, etch resistance, storage stability, thermal stability, radiation absorption, adhesion to appropriate substrates, solubility in appropriate solvents, etc.) that are used to describe resists, contrast and sensitivity are the two that are most used to describe resist performance.

The sensitivity (or contrast) curves for positive and negative resists are shown schematically in Fig. 12.4.⁸⁶ To generate this curve, the thickness of the exposed resist film after development (normalized to the original thickness

⁸³M.D. Levenson, D.S. Goodman, S. Lindsey, P.W. Bayer, and H.A.E. Santini, “The phase shifting mask ii: imaging simulations and submicrometer resist exposures,” *IEEE Trans. Electron Dev.* **ED-31**(6), 753–763 (1984); H.J. Levinson and W.H. Arnold, “Focus: the critical parameter for submicron lithography,” *J. Vac. Sci. Technol. B* **5**(1), 293–298 (1987); W.H. Arnold and H.J. Levinson, “Focus: the critical parameter for submicron optical lithography: Part 2,” *Proc. SPIE* **772**, 21–34 (1987).

⁸⁴C.A. Mack, *Field Guide to Optical Lithography*, p. 56, SPIE Press, Bellingham, WA (2006).

⁸⁵A.R. Neureuther and C.A. Mack, “Optical lithography modeling,” in *Handbook of Microlithography, Micromachining, and Microfabrication*, Vol. 1, P. Rai Choudhury, Ed., pp. 597–679, SPIE Press, Bellingham, WA (1997).

⁸⁶The curve shown here is a special truncated case of the more general Hurter Driffield curve [see for example: C.A. Mack, *Microelectron. Manuf. Technol.* **14**(1), 36–43 (1991)].

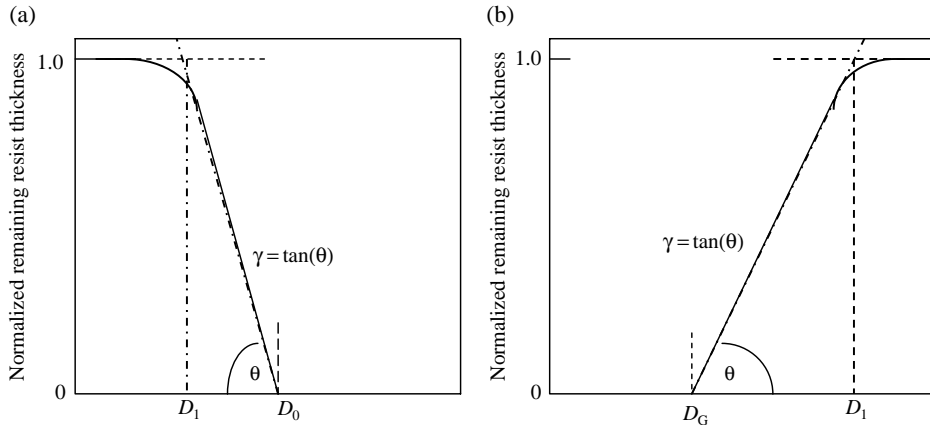


Figure 12.4 Contrast curves for (a) positive-tone and (b) negative-tone resists. The intercept of the curve and abscissa in positive-tone resists is called the “dose to clear” and is designated as D_0 , while in negative resists, it marks the onset of cross-linking, and is designated as D_G . This should not be confused with the lithographic dose to print, which tends to be approximately 1.6–2.2 times higher. The absolute value of the slope of the tangent to the contrast curve at its intercept with the abscissa is defined as the resist contrast. It is usually defined in terms of an auxiliary dose value D_1 , which is obtained by continuing the above tangent line to the full resist film thickness (normalized to 1.0).

before development) is plotted as a function of the logarithm of the exposure dose for the resist. For positive resists, the point of intercept of the curve and abscissa is defined as the “dose to clear” and is usually designated D_0 . The sensitivity is defined as the dose at which the exposed areas are cleanly developed to the substrate with a minimal thickness loss in the unexposed regions. For negative resists, the sensitivity is defined as the dose at which 50% of the thickness is retained in the exposed areas.⁸⁷

The contrast γ is determined as the slope of the tangent to the contrast curve at its intercept with the abscissa at D_0 . It is usually defined by means of an auxiliary dose value D_1 , which is obtained by continuing the tangent to full film thickness (normalized). Mathematically, it is defined as⁸⁸

$$\gamma = \frac{1}{\log\left(\frac{D_0}{D_1}\right)} = \frac{1}{\log D_1 - \log D_0}. \quad (12.68)$$

Although not quite apparent from the above definition, the value of γ depends on resist thickness in two nonobvious ways. First, due to absorption, γ decreases approximately linearly with increasing film thickness, such that the product of

⁸⁷H. Ito, *Chemical Amplification Resists for Microlithography*, Springer Verlag, Berlin, p. 44 (2005).

⁸⁸R. Dammel, *Diazonaphthoquinone based Resists*, p. 11, SPIE Press, Bellingham, WA (1993).

film thickness and γ is a constant. Second, for optical absorption, there may be a periodic variation (with decreasing amplitude) of γ with film thickness that results from thin-film interference effects, and is manifested as the so-called swing curve (see Fig. 12.5), particularly on reflective substrates. Together, these effects cause γ to peak at the inflection points of the swing curve and to be minimal at the stationary points.⁸⁹

In principle, a resist with an infinitely high contrast (in other words, with a contrast curve shaped like a step function) can resolve sinusoidal aerial images of mask features into sharp resist features on the wafer as long as there is a finite intensity difference in the diffracted radiation beams reaching the latter. This is the ultimate goal of resist designers, and it is amazing how tantalizingly close many advanced resists have approached this limit.⁹⁰

While it is simple to solve the exposure rate equation [Eq. (12.63)] in the situation where the intensity within the resist is constant, it is, however, not quite simple to solve for the situation where the intensity within the resist varies with exposure, as is the case when the resist bleaches. For the latter case, the variation of the intensity within the resist with exposure must be accurately known in order to solve the exposure rate equation. The simplest case where the intensity within the resist varies as a function of exposure occurs in situations where absorption is the

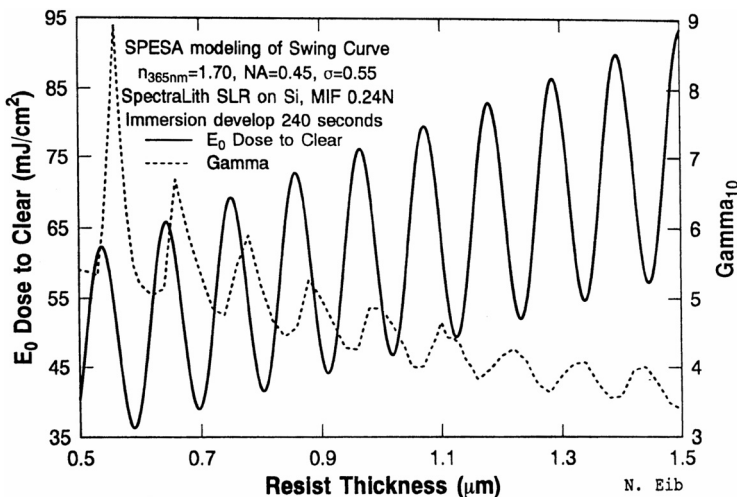


Figure 12.5 Behavior of γ as a function of resist thickness according to model calculations. The exact shape of the curve and positions of the maxima will depend on specific resist properties.⁹¹

⁸⁹ibid.

⁹⁰That most advanced resists today are printing features much smaller than dictated by the Rayleigh resolution criterion is a testament to the extremely high contrast these materials possess. Historically, the contribution of resists and resist processes in resolution of printed features for each technology node far outweighed contributions from exposure tool improvements.

⁹¹R. Dammel, *Diazonaphthoquinone based Resists*, p. 12, SPIE Press, Bellingham, WA (1993).

only factor affecting the intensity within the resist, as is obtained in situations where the resist film is coated over substrates with the same index of refraction. For such a case, Lambert's law of absorption, coupled with Beer's law [see Eq. (12.32)] is applicable.⁹² Equations (12.63) and (12.32) are coupled first-order nonlinear partial differential equations known as "Dill equations" (see above) that must be solved simultaneously. The solution to Eqs. (12.63) and (12.32) was first carried out numerically for the case of lithography simulation,⁹³ although the analytical solution to them was reported many years earlier.⁹⁴ Analytical solutions to the equations were also reported by Diamond and Sheats⁹⁵ and by Babu and Barouch.⁹⁶ These solutions are in the form of a single numerical integration, which is far easier to solve than two partial differential equations.

For the more realistic situation where intensity within the resist varies as a function of exposure as well as on account of standing waves, the solution to Eq. (12.32) becomes extremely difficult to obtain. The approach employed in modern lithographic simulators such as PROLITH is to use the standing wave equations [Eqs. (12.13)–(12.30)] to determine the intensity within the resist as a function of $m(x, y, z, t)$. Initially, the PAC distribution is given by $m(x, y, z, 0) = 1$, and the standing wave equation gives the intensity distribution $I(x, y, z, 0)$. The exposure equation, given by Eq. (12.63), is then integrated over a small increment of exposure time Δt to produce the PAC distribution $m(x, y, z, \Delta t)$, where the assumption is made that over this small increment in exposure time the intensity remains relatively constant, leading to the exponential solution. Next, the new PAC distribution is used to calculate the new intensity distribution $I(x, y, z, \Delta t)$, which in turn is used to generate the PAC distribution at the next increment of exposure time $m(x, y, z, 2\Delta t)$. This process is continued until the final exposure time is reached.⁹⁷

12.9 Postexposure Bake Models

To account for the effect of postexposure bake in reducing standing waves through thermally driven diffusion of the photoacid, lithographic simulators employ models

⁹²C.A. Mack, "Optical lithography modeling," in *Microlithography: Science and Technology*, J.R. Sheats and B.W. Smith, Eds., p. 132, Marcel Dekker, New York (1998).

⁹³F.H. Dill, W.P. Hornberger, P.S. Hauge, and J.M. Shaw, "Characterization of positive photoresists," *IEEE Trans. Electron Dev.* **ED-22**(7), 445–452 (1975).

⁹⁴C.E. Herrick, Jr., "Solution of the partial differential equations describing photodecomposition in a light absorbing matrix having light absorbing photoproducts," *IBM J. Res. Dev.* **10**, 2–5 (1966).

⁹⁵J.J. Diamond and J.R. Sheats, "Simple algebraic description of photoresist and contrast enhancement," *IEEE Electron Device Lett.* **EDL-7**(6), 383–386 (1986).

⁹⁶S.V. Babu and E. Barouch, "Exact solution of Dill's model equations for positive photoresist kinetics," *IEEE Electron Device Lett.* **EDL-7**(4), 252–253 (1986).

⁹⁷C.A. Mack, "Optical lithography modeling," in *Microlithography: Science and Technology*, J.R. Sheats and B.W. Smith, Eds., p. 133, Marcel Dekker, New York (1998).

based on Ficke's second law of diffusion, shown (in one dimension) as

$$\frac{\partial C_A}{\partial t} = D \left(\frac{\partial^2 C_A}{\partial x^2} \right), \quad (12.69)$$

where C_A is the concentration of the species A , D is the diffusion coefficient at some temperature T , and t is the time that the system is at temperature T . It should be pointed out that Eq. (12.69) assumes that diffusivity is independent of concentration. Equation (12.69) is solved with a set of boundary conditions that include: (i) the initial distribution of A and (ii) an impulse source, where at some point x_0 there is an infinite concentration of substance A and at all other points there is no A .⁹⁸

Using the initial distribution of A as the boundary condition, the solution⁹⁹ to Eq. (12.69) is the Gaussian distribution function

$$C_A(x) = \frac{N}{\sqrt{2\pi\sigma^2}} e^{-r^2/2\sigma^2}, \quad (12.70)$$

where $r = x - x_0$ and σ is the diffusion length, which is given by

$$\sigma = \sqrt{2Dt}. \quad (12.71)$$

In reality, impulse sources do not exist under PEB conditions. An impulse source can be approximated as having a concentration C_0 over some small distance Δx centered at x_0 , with zero concentrations outside this range. Using this modified impulse source as a boundary condition, the solution of Eq. (12.69) can be approximated as¹⁰⁰

$$C_A(x) = \frac{C_0 \Delta x}{\sqrt{2\pi\sigma^2}} e^{-r^2/2\sigma^2}. \quad (12.72)$$

Equation (12.72) is fairly accurate if $\Delta x < 3\sigma$. In the situation where there are two impulse sources located at x_1 and x_2 , with initial concentrations C_1 and C_2 , each over a range Δx , the concentration of A at x after diffusion is given by¹⁰¹

$$C_A(x) = \left[\frac{C_1}{\sqrt{2\pi\sigma^2}} e^{-r_1^2/2\sigma^2} + \frac{C_2}{\sqrt{2\pi\sigma^2}} e^{-r_2^2/2\sigma^2} \right] \Delta x, \quad (12.73)$$

where $r_1 = x - x_1$ and $r_2 = x - x_2$.

⁹⁸ibid.

⁹⁹For solutions to the diffusion equation, please see, for example, J. Crank, *The Mathematics of Diffusion*, 2nd ed., Oxford University Press, New York (2003); J. Crank, G.S. Park, *Diffusion in Polymers*, Academic Press, London (1968).

¹⁰⁰ibid.

¹⁰¹ibid.

In situations where there are multiple sources, Eq. (12.73) becomes

$$C_A(x) = \frac{\Delta x}{\sqrt{2\pi\sigma^2}} \sum C_n e^{-(x_n^2/2\sigma^2)}. \quad (12.74)$$

And in situations where there is a continuous initial distribution $C_0(x)$, Eq. (12.74) becomes

$$C_A(x) = \frac{1}{\sqrt{2\pi\sigma^2}} \int_{-\infty}^{\infty} C_0(x-x') e^{-(x'^2/2\sigma^2)} dx', \quad (12.75)$$

where x' is the distance from the point x . A close examination of Eq. (12.75) reveals that it is the convolution of two functions:

$$C_A(x) = C_0(x) * f(x), \quad (12.76)$$

where

$$f(x) = \frac{1}{\sqrt{2\pi\sigma^2}} e^{-(x^2/2\sigma^2)}. \quad (12.77)$$

By analogy, the two-dimensional equivalent of Eq. (12.76) can be expressed as

$$C_A(x, y) = C_0(x, y) * f(x, y), \quad (12.78)$$

where

$$f(x, y) = \frac{1}{2\pi\sigma^2} e^{-(r^2/2\sigma^2)}, \quad (12.79)$$

where

$$r = \sqrt{x^2 + y^2}. \quad (12.80)$$

With the functional expression for $C_A(x, y)$ in Eq. (12.78) established, the next step is to apply it to the diffusion of the photoacid during PEB, with the understanding that after exposure the distribution of the photoactive compound is described by $m(x, z)$, where m is the relative distribution of the photoactive compound. From Eq. (12.78), it is established that the relative distribution of the

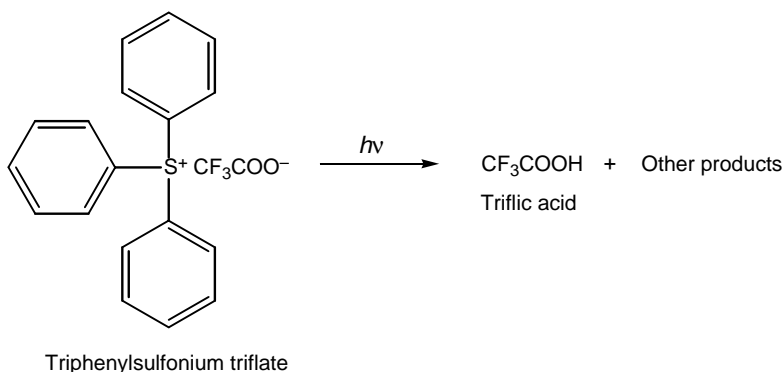
photoactive compound after PEB, $m^*(x, z)$, is given by¹⁰²

$$m^*(x, z) = \frac{1}{2\pi\sigma^2} \int_{-\infty}^{\infty} \int_{-\infty}^{\infty} m(x - x', z - z') e^{-r^2/2\sigma^2} dx' dz'. \quad (12.81)$$

The evaluation of Eq. (12.81) typically involves the replacement of the integrals by summations over intervals Δx and Δz , with the restrictions that $\Delta x < 3\sigma$ and $\Delta z < 3\sigma$. Alternatively, the diffusion equation shown in Eq. (12.69) can be solved directly, using finite difference methods. In lithographic simulators, either Eq. (12.81) or Eq. (12.69) is solved, with the specification of the diffusion length σ , or equivalently, the diffusion coefficient D , which in turn can be determined from appropriate functional models that account for the dependence of diffusion on bake temperature T (discussed in the next section).

12.9.1 Adapting exposure kinetics of chemical amplification resists to the Dill equations

In chemical amplification resist systems,¹⁰³ photoacids are generated from the interaction of radiation with PAGs, which go on to catalyze a number of reactions that transform the solubility properties of the exposed resist resin relative to the unexposed resin. The photoinduced generation of acid from a PAG such as triphenylsulfonium triflate is illustrated in Scheme 12.2.



Scheme 12.2 Photogeneration of triflic acid from triphenylsulfonium triflate.

¹⁰²C.A. Mack, "Optical lithography modeling," in *Microlithography: Science and Technology*, J.R. Sheats and B.W. Smith, Eds., pp. 147, Marcel Dekker, New York (1998); C.A. Mack, *Fundamental Principles of Optical Lithography: The Science of Microfabrication*, pp. 210–212, John Wiley & Sons, Hoboken, NJ (2007).

¹⁰³These resist systems as well as their imaging mechanisms are covered in depth in Chapter 7.

The exposure reaction of chemical amplification resist systems is assumed to follow first-order kinetics, which can be represented as¹⁰⁴

$$\frac{\partial G}{\partial t} = -CIG, \quad (12.82)$$

where G is the concentration of PAG at time t , I is the exposure intensity, and C is the exposure rate constant. Under constant intensity conditions, the rate equation can be solved for G to yield

$$G = G_0 e^{-CIt}, \quad (12.83)$$

where G_0 is the initial concentration of the PAG. The acid concentration H is determined as

$$H = G_0 - G = G_0(1 - e^{-CIt}). \quad (12.84)$$

Exposing the resist to an aerial image $I(x)$ produces an acid latent image $H(x)$. A postexposure bake step is applied to thermally induce a set of chemical reactions, which ultimately lead to the transformation of the solubility properties of resist resin relative to the unexposed part. These reactions may be the activation of a cross-linking agent for a negative resist or the deprotection of the polymer resin for a positive resist. The reaction is catalyzed by the acid, which is not consumed by the reaction, and so the acid concentration remains fairly constant during the course of the reaction. Also, one acid molecule can participate in many of these resin-transformational reactions, so much so that catalytic chain length¹⁰⁵ of the order of hundreds is not uncommon. Hence, these reactions are described as chemical amplification reactions.

To model the amplification reaction, we let M be the concentration of some reactive site within the resist resin; these sites react according to some unknown order in H and first order in M :¹⁰⁶

$$\frac{\partial M}{\partial t'} = -K_{\text{amp}}MH^n, \quad (12.85)$$

where K_{amp} is the rate constant of the amplification reaction. Under the assumption that H is constant, Eq. (12.82) can be solved for the concentration of reacted sites, X , as

$$X = M_0 - M = M_0(1 - e^{-K_{\text{amp}}H^n t'}). \quad (12.86)$$

¹⁰⁴C. A. Mack, "Optical lithography modeling," in *Microlithography: Science and Technology*, J.R. Sheats and B.W. Smith, Eds., p. 133, Marcel Dekker, New York (1998).

¹⁰⁵Catalytic chain length refers to the average number of amplification chemical events caused by one acid molecule.

¹⁰⁶D. Seligson, S. Das, H. Gaw, and P. Pianetta, "Process control with chemical amplification resists using deep ultraviolet and x ray radiation," *J. Vac. Sci. Technol. B* 6(6), 2303–2307 (1988).

It should be pointed out that although H is not consumed by the reaction, its value is not locally constant because diffusion during PEB and evaporation (as well as unwanted side reactions involving the acid, i.e., all acid loss mechanisms) may induce local variations in the concentration of H . This condition necessitates the use of reaction-diffusion equations to accurately model this system. However, the assumption that H is constant is not without merit, for it is valid under certain conditions. Besides, it helps to simplify the problem.

For the ease of calculation, the concentrations of the acid-reacted and unreacted sites are normalized to some initial values, yielding their corresponding values for h , x , and m as¹⁰⁷

$$h = \frac{H}{G_0}, \quad x = \frac{X}{M_0}, \quad m = \frac{M}{M_0}. \quad (12.87)$$

Equations (12.84) and (12.86) are thus transformed into

$$h = 1 - e^{Ct'}, \quad (12.88a)$$

$$m = 1 - x = e^{-\alpha h^n}, \quad (12.88b)$$

where α represents a lumped “amplification” factor equal to $G_0^n K_{\text{amp}} t'$. In effect, the PEB amplifies the latent image $m(x)$, corresponding to an exposed latent image $h(x)$, which in turn results from the aerial image $I(x)$.¹⁰⁸ Note that n is generally assumed to be equal to 1.0.

As stated above, the acid concentration in reality is not locally constant; the acid diffuses during the bake and is also involved in various acid-loss mechanisms. The full accounting of these scenarios in the exposure models of chemical amplification resists is outlined below. First, the diffusion equation is used, which in one dimension takes the form¹⁰⁹

$$\frac{\partial H}{\partial t'} = \frac{\partial}{\partial x} \left(D_H \frac{\partial H}{\partial x} \right), \quad (12.89)$$

where D_H is the diffusivity of acid in the photoresist. The solution to Eq. (12.89) involves the initial condition being the initial acid distribution within the film $H(x, 0)$, and these two boundary conditions: (i) the boundary at the wafer surface is assumed to be impermeable, hence no diffusion of the acid into the wafer occurs, and (ii) the top surface of the resist is assumed to be impermeable to acid; hence, acid loss through evaporation is not allowed.

¹⁰⁷C.A. Mack, “Optical lithography modeling,” in *Microlithography: Science and Technology*, J.R. Sheats and B.W. Smith, Eds., p. 135, Marcel Dekker, New York (1998).

¹⁰⁸ibid.

¹⁰⁹ibid.

Equation (12.89) can be readily solved if the diffusivity of the acid in the resist is known. In reality, diffusivity depends on temperature and is intimately related to the extent of amplification. The connection between diffusivity and the extent of chemical amplification stems from the fact that as the amplification reaction proceeds in the specific case of positive resists based on protection group chemistry, the deprotection events of polymers generate volatile species that leave the film, resulting in a decrease in film thickness and an increase in free volume. An increase in free volume within the film makes it easier for the acid to diffuse through it. Furthermore, given that the temperature of the resist changes with time during PEB, the diffusivity will invariably be time dependent as well. Given that the acid concentration within the film is time and position dependent, in standard lithographic simulators, the diffusivity equation in Eq. (12.89) is determined as part of the solution to Eq. (12.89) by an iterative method. The set of Eqs. (12.85) and (12.89) constitute the reaction-diffusion equations that must be solved simultaneously in order to describe the exposure kinetics of chemical amplification resist systems.¹¹⁰

The temperature dependence of diffusivity is accounted for in lithographic simulators in terms of the Arrhenius expression:

$$D_0(T) = Ae^{-(E_A/RT)}, \quad (12.90)$$

where D_0 is a general diffusivity, A is the Arrhenius constant, R is the universal gas constant, E_A is the activation energy, and T is temperature. While the variation of T with bake time is used in the full treatment of amplification reaction in some lithographic simulators, in others, the simplifying assumption is made that the temperature of the resist remains zero (low enough for no diffusion or reaction to occur) until the start of the PEB, at which time it immediately rises to the final PEB temperature, and stays constant for the duration of the bake, before instantly falling back to zero.¹¹¹

The concentration dependence of diffusivity is accounted for with a number of different models. The diffusivity behavior has been variously described as constant¹¹² or either linearly or exponentially dependent on concentration.¹¹³ The simplest of these models expresses diffusivity as a function of the extent of the amplification reaction. It assumes a linear relationship between diffusion

¹¹⁰C.A. Mack, "Optical lithography modeling," in *Microlithography: Science and Technology*, J.R. Sheats and B.W. Smith, Eds., p. 136, Marcel Dekker, New York (1998).

¹¹¹ibid.

¹¹²Y. Yoshimura, Y. Nakayama, and S. Okazaki, "Acid diffusion effect on nanofabrication in chemical amplification resist," *J. Vac. Sci. Technol. B* **10**, 2615–2619 (Nov. Dec. 1992).

¹¹³J. Byers et al. "Characterization and modeling of a positive amplified resist," *Proc. SPIE* **2438**, 153–166 (1995); C.A. Mack, "Inside PROLITH—a comprehensive guide to optical lithography simulation," (Feb. 1997); M. Zuniga, G. Wallraff, E. Tomacruz, B. Smith, C. Larson, W.D. Hinsburg, and A.R. Neureuther, "Simulation of locally enhanced three dimensional diffusion in chemically amplified resists," *J. Vac. Sci. Technol. B* **11**, 2862–2866 (Nov. Dec. 1993).

and the unreacted sites as

$$D_H = D_0 + x(D_f - D_0), \quad (12.91)$$

where D_0 stands for the diffusivity of the acid in completely unreacted resist, D_f is the diffusivity of the acid in resist that has completely reacted, and x is the normalized reacted sites on the resist polymer.

Another common way to express the concentration dependence of diffusivity is the Fujita-Doolittle equation, which takes the form¹¹⁴

$$D_H = D_0 e^{\alpha x / (1 + \beta x)}, \quad (12.92)$$

where α and β are experimentally determined constants and are, in general, temperature dependent. There are quite a number of expressions for the concentration dependence of diffusivity that have been proposed over the years, some of which are employed in different lithographic simulators.¹¹⁵

As mentioned above, acid loss from the resist film negatively impacts the chemical amplification reaction in the sense that such lost acid does not contribute to the desired reaction. Two basic acid-loss processes have been identified, namely, those that occur between exposure and PEB and those that occur during the PEB. Acid losses occurring between exposure and PEB lead to delay time effects, exemplified by the diffusion of atmospheric-based contaminants into the top surface of the resist, resulting in neutralization of the acid there, accompanied by reduced amplification reaction for positive resists. In the severest form of acid loss, there is a formation of an insoluble skin, referred to as “T-top,” during development. For negative resists, the top portion of the line is not insolubilized, and film thickness is lost from the top portion during development.¹¹⁶

The effects of acid loss due to atmospheric-based contaminants are accounted for in standard lithographic simulators in a simple way. The assumption is made that the concentration of the base contaminant in contact with the top of the resist remains constant, such that the diffusion equation can be solved for the concentration of the base B as a function of depth into the resist as¹¹⁷

$$B = B_0 \operatorname{erfc}\left(\frac{z}{\sqrt{2}\sigma_B}\right), \quad (12.93)$$

¹¹⁴H. Fujita, A. Kishimoto, K. Matsumoto, “Concentration and temperature dependence of diffusion coefficients for systems poly(methylmethacrylate) and n alkyl acetates, *Trans. Faraday Soc.* **56**, 424–437 (1960).

¹¹⁵C.A. Mack, “Optical lithography modeling,” in *Microlithography: Science and Technology*, J.R. Sheats and B.W. Smith, Eds., p. 136, Marcel Dekker, New York (1998).

¹¹⁶C.A. Mack, *Fundamental Principles of Optical Lithography: The Science of Microfabrication*, p. 231, John Wiley & Sons, Hoboken, NJ (2007); C.A. Mack, “Optical lithography modeling,” in *Microlithography: Science and Technology*, J.R. Sheats and B.W. Smith, Eds., Marcel Dekker, New York, p. 137 (1998).

¹¹⁷C.A. Mack, “Optical lithography modeling,” in *Microlithography: Science and Technology*, J.R. Sheats and B.W. Smith, Eds., p. 137, Marcel Dekker, New York (1998).

where B_0 is the base concentration at the top of the resist film (which, according to Henry's law, is directly proportional to the concentration of base in the atmosphere), z is the depth into the resist (with $z = 0$ being at the top of the film), and σ_B is the diffusion length of the base in the resist. The assumption of constant diffusivity implies that the diffusion length follows a square root dependence on the delay time.

Given that the photogenerated acid used in lithography is a strong acid, it is assumed that all of the base contaminants will react with acid if there is sufficient acid present. This implies that the acid concentration at the beginning of the PEB H^* can be related to the acid concentration after exposure H by

$$H^* = H - B \quad \text{or} \quad h^* = h - b, \quad (12.94)$$

where the lowercase symbols are the normalized concentrations relative to the initial photoacid generator concentration.¹¹⁸

As for acid losses during PEB, a few mechanisms have been identified. One mechanism involves trapping of the acid at certain sites as the acid diffuses through the polymer, rendering the acids unusable for further amplification. In the situation where the amount of these traps greatly exceeds the concentration of the acid, the resulting acid-loss rate is assumed to follow first-order kinetics as

$$\frac{\partial h}{\partial t'} = -K_{\text{loss}}h, \quad (12.95)$$

where K_{loss} is the acid-loss reaction rate constant.¹¹⁹

Another mechanism for acid loss occurring during PEB is evaporation from the top of the resist. The amount of evaporation depends on the size of the acid and the degree of its interaction with the resist polymer. A small acid such as trifluoroacetic acid may have appreciable evaporation during PEB. The evaporation rate is expressed as

$$\left. \frac{\partial h}{\partial t'} \right|_{z=0} = -K_{\text{evap}}[h(0, t) - h_{\text{air}}(0, t)], \quad (12.96)$$

where $z = 0$ is the top of the resist, K_{evap} is the evaporation rate constant, and h_{air} is the acid concentration in the atmosphere just above the photoresist surface. Because the PEB takes place in a PEB oven with enough airflow to eliminate any buildup of evaporated acid above the resist, $h_{\text{air}} = 0$. If K_{evap} is negligible, then the top boundary of the resist is treated as being impermeable. If, however, K_{evap} is very large, in which case evaporation is much faster than the rate of acid diffusion, the effect is to reduce the surface concentration of the acid in the resist to zero.¹²⁰

¹¹⁸ibid., p. 138.

¹¹⁹ibid.

¹²⁰ibid.

Furthermore, another acid-loss mechanism occurring during PEB, and one that can in principle also occur during the time between exposure and PEB, is base contamination from the substrate, as has been reported on TiN and S_xN_y substrates and exemplified by a foot at the bottom of the profile.¹²¹ The nitrogen in these substrates acts as trapping sites for acid molecules, effectively resulting in the reduction of the desired amplification reactions, development rate, and consequently, resist footing.

The kinetics of the substrate-induced acid loss depends on the concentration of the acid trap sites at the substrates S , which is expressed relative to the initial concentration of the PAG as¹²²

$$s = \frac{S}{G_0}. \quad (12.97)$$

The assumption is made that one trap site reacts with one acid molecule, such that the rate of acid trapping in the substrates is therefore expressed as¹²³

$$\left. \frac{\partial h}{\partial t'} \right|_{z=D} = -K_{\text{trap}} h(D, t) s. \quad (12.98)$$

The way the above equations are employed in lithographic simulators to model exposure kinetics of chemical amplification resist systems entails the simultaneous solution of Eqs. (12.85) and (12.89), the so-called reaction-diffusion system, using Eq. (12.84) as an initial condition and either Eq. (12.91) or Eq. (12.92) to describe the reaction-dependent diffusivity. Any or all of the acid-loss mechanisms described above may be included, depending on the specific condition. The finite difference method¹²⁴ is often employed to solve these equations, in a way that approximates the differential equations by difference equations. By marching through time and solving for all space at each time step, the final solution is reached after the final time step. The accuracy of the solution depends on the size of the time step, i.e., small time steps give more accurate results. If the spatial dimension of interest is the grid Δx (or Δy or Δz), the recommended time step is chosen such that the diffusion length is less than Δx .¹²⁵

The effects of quenchers are also incorporated into PEB models. When present in a resist film, the quencher can neutralize the photoacid in a typical acid-base

¹²¹K.R. Dean and R.A. Carpio, "Contamination of positive deep UV photorists," in *OCG Micro lithography Seminar Interface '94*, pp. 199–212 (1994).

¹²²C.A. Mack, "Optical lithography modeling," in *Microlithography: Science and Technology*, J.R. Sheats & B.W. Smith, Eds., p. 137, Marcel Dekker, New York (1998).

¹²³ibid., p. 139.

¹²⁴F.P. Incropera and D.P. DeWitt, *Fundamentals of Heat and Mass Transfer*, 3rd ed., John Wiley & Sons, Hoboken, NJ (1990).

¹²⁵C.A. Mack, "Optical lithography modeling," in *Microlithography: Science and Technology*, J.R. Sheats and B.W. Smith, Eds., pp. 139, Marcel Dekker, Hoboken, NJ (1998).

neutralization reaction as follows:



The acid and the quencher concentrations during this process are described by the following differential equation:

$$\frac{\partial}{\partial t} [\text{Acid}]_t = -k_\alpha [\text{Acid}]_t [Q]_t, \quad (12.99)$$

where k_α is the neutralization reaction coefficient modeled by an Arrhenius temperature relation:

$$k_\alpha = A_\alpha \exp\left(-\frac{E_\alpha}{RT}\right) \quad (12.100)$$

and $[\text{Acid}]_t$ and $[Q]_t$ are the acid and quencher concentrations, respectively, at time t . It should be pointed out that the difference between the acid and quencher concentrations remains constant during the PEB as

$$[\text{Acid}]_t - [Q]_t = [\text{Acid}]_0 - [Q]_0, \quad (12.101)$$

where $[\text{Acid}]_0$ and $[Q]_0$ are the initial acid and quencher concentrations before PEB. Solving Eqs. (12.99) and (12.101), we get the acid concentration as a function of the PEB time,

$$[\text{Acid}]_t = \frac{[\text{Acid}]_0 - [Q]_0}{1 - ([Q]_0/[\text{Acid}]_0)e^{-k_\alpha([\text{Acid}]_0 - [Q]_0)t}}, \quad (12.102)$$

where the diffusion of acid and base is ignored.

12.10 Development Models

Development rate models seek to determine the dissolution rate as a function of the PAC or photoacid concentration within the resist after PEB. Many development rate models have been proposed over the years;¹²⁶ a few of them are reviewed here. The first development rate model was proposed by Dill and his co-workers, and is of the form¹²⁷

$$R = e^{E_1 + E_2M + E_3M^2}, \quad (12.103)$$

¹²⁶See, for example, T. Ohfuji, K. Yamanaka, and M. Sakamoto, "Characterization and modeling of high resolution positive photoresists," *Proc. SPIE* **920**, 190 (1988).

¹²⁷F.H. Dill, W.P. Hornberger, P.S. Hauge, and J.M. Shaw, "Characterization of positive photoresists," *IEEE Trans. Electron Dev.* **ED-22**(7), 445–452 (1975).

where R is the development rate, E_1 , E_2 , and E_3 are constants, and M is the PAC concentration.

The most widely used development rate models are the kinetic development rate model,¹²⁸ enhanced kinetic development rate model,¹²⁹ and the lumped parameter model¹³⁰ proposed by Mack. We briefly outline their derivation here.¹³¹

It is assumed that the solution development of a conventional positive resist occurs in three steps, namely, diffusion of developer from the bulk solution to the surface of the resist, reaction of the developer with the resist, and diffusion of the product back into the solution. It is also assumed that the last step, diffusion of the dissolved resist into solution, occurs very rapidly, and therefore can be ignored.¹³²

12.10.1 The kinetic development model or Mack model

The diffusion of the developer to the resist surface can be described with a simple diffusion rate equation as

$$r_D = k_D(D - D_S), \quad (12.104)$$

where r_D is the diffusion rate equation that describes the diffusion of the developer to the resist surface, D is the bulk developer concentration, D_S is the developer concentration at the resist surface, and k_D is the diffusion rate constant.¹³³

For a positive resist based on dissolution inhibition chemistry such as the DNQ/novolac resist system, the rate of the reaction r_R between the developer with the resist (comprised of resin R , a photoactive compound that acts as a dissolution inhibitor M , but which is converted to product P on exposure to UV light, which in turn enhances the dissolution rate of the resin) is given by

$$r_R = k_R D_S P^n, \quad (12.105)$$

¹²⁸C.A. Mack, "Development of positive resist," *J. Electrochem. Soc.* **134**(1), 148–152 (1987).

¹²⁹C.A. Mack, "New kinetic model for resist dissolution," *J. Electrochem. Soc.* **139**(4), L35–L37 (1992).

¹³⁰C.A. Mack, A. Stephanakis, and R. Herschel, "Lumped parameter model of the photolithographic process," in *Kodak Microelectronics Seminar Proc.*, pp. 228–238 (1986), R. Herschel and C.A. Mack, "Lumped parameter model for optical lithography," in *Lithography for VLSI, VLSI Electronics Microstructure Science*, R.K. Watts and N.G. Einspruch, Eds., pp. 19–55, Academic Press, New York (1987); C.A. Mack, "Enhanced lumped parameter model for photolithography," *Proc. SPIE* **2197**, 501–510 (1994).

¹³¹An excellent review of these models is provided in C.A. Mack, "Optical lithography modeling," in *Microlithography: Science and Technology*, J.R. Sheaths and B.W. Smith, Eds., pp. 109–179, Marcel Dekker, New York (1998).

¹³²C.A. Mack, "Optical lithography modeling," in *Microlithography: Science and Technology*, J.R. Sheaths and B.W. Smith, Eds., p. 148, Marcel Dekker, New York (1998).

¹³³ibid.

where k_R is the rate constant and n is the reaction order corresponding to the number of molecules of product P .¹³⁴ From the stoichiometry of the exposure reaction,

$$P = M_0 - M, \quad (12.106)$$

where M_0 is the initial PAC concentration.

It should be noted that the two steps outlined above occur in sequence, with one reaction following the other. Therefore, at steady state, their rates are equal to a value called r :

$$r_R = r_D = r. \quad (12.107)$$

Equating the rate equations, Eqs. (12.104) and (12.105), and solving for D_S and eliminating it from the overall equation, one obtains

$$r = \frac{k_D k_R D P^n}{k_D + k_R P^n}. \quad (12.108)$$

Using Eq. (12.106) and defining $m = M/M_0$ as the relative PAC concentration, Eq. (12.108) becomes

$$r = \frac{k_D D (1 - m)^n}{(k_D/k_R M_0^n) + (1 - m)^n}. \quad (12.109)$$

When $m = 1$ (unexposed resist), the rate is zero. When $m = 0$ (resist completely exposed), the rate is equal to r_{\max} , where

$$r_{\max} = \frac{k_D D}{(k_D/k_R M_0^n) + 1}. \quad (12.110)$$

If a constant a is defined such that

$$a = \frac{k_D}{k_R M_0^n}, \quad (12.111)$$

the rate equation becomes

$$r = r_{\max} \frac{(a + 1)(1 - m)^n}{a + (1 - m)^n}. \quad (12.112)$$

It is important to note that the constant a describes the rate constant of diffusion relative to the surface reaction rate constant. A large value of the constant a

¹³⁴It should be pointed out that Eq. (12.105) is the rate equation for the polyphotolysis model proposed by P. Trefonas, B.K. Daniels, "New principle for image enhancement in single layer positive resists," *Proc. SPIE* **771**, 194–210 (1987).

indicates that the diffusion is very fast, and thus less important, compared to the fastest surface reaction (for completely exposed resist).¹³⁵

The three constants a , n , and r_{\max} must be experimentally determined. The inflection point on the dissolution rate curve can be determined from its second derivative with respect to m as

$$\frac{d^2r}{dm^2} = 0 \quad (12.113)$$

and solving for a to yield

$$a = \frac{n+1}{n-1}(1 - m_{\text{TH}})^n, \quad (12.114)$$

where m_{TH} is the value of m at the inflection point, which is called the threshold PAC concentration.

The model in Eq. (12.112) does not take into account the finite dissolution rate of unexposed resist r_{\min} that is independent of the exposed PAC. A common approach is simply to add this term to Eq. (113), giving

$$r = r_{\max} \frac{(a+1)(1-m)^n}{a+(1-m)^n} + r_{\min}. \quad (12.115)$$

Equation (12.115) is commonly referred to as the “kinetic model” or “Mack model,” named after the scientist who first proposed it.¹³⁶ In the case where the diffusion rate constant is large compared to the surface reaction rate, i.e., $a \gg 1$, Eq. (12.115) reduces to

$$r = r_{\max}(1-m)^n + r_{\min}. \quad (12.116)$$

12.10.2 The enhanced kinetic development model or enhanced Mack model

To explicitly account for the dissolution inhibitory effect of the PAC and the dissolution enhancement of the photogenerated acid from the PAC, Mack proposed the enhanced kinetic model (now called the enhanced Mack model) in 1992¹³⁷ as

$$R = R_{\text{resin}} \left[\frac{1 + k_{\text{enh}}(1-m)^n}{1 + k_{\text{inh}}(m)^l} \right], \quad (12.117)$$

¹³⁵C.A. Mack, “Optical lithography modeling,” in *Microlithography: Science and Technology*, J.R. Sheats and B.W. Smith, Eds., p. 149, Marcel Dekker, New York (1998).

¹³⁶C.A. Mack, “Development of positive resist,” *J. Electrochem. Soc.* **134**(1), 148–152 (1987).

¹³⁷C.A. Mack, “New kinetic model for resist dissolution,” *J. Electrochem. Soc.* **139**(4), L35–L37 (1992).

where k_{enh} is the rate constant for the enhancement mechanism, n is the enhancement reaction order, k_{inh} is the rate constant for the inhibition mechanism, l is the inhibition reaction order, and R_{resin} is the development rate of the resin alone.

For no exposure, $m = 1$, the development rate is at its minimum, and Eq. (12.118) reduces to

$$R_{\text{min}} = \frac{R_{\text{resin}}}{1 + k_{\text{inh}}}. \quad (12.118)$$

When $m = 0$, corresponding to complete exposure, the development rate is at its maximum:

$$R_{\text{max}} = R_{\text{resin}}(1 + k_{\text{enh}}). \quad (12.119)$$

Thus the application of the enhanced Mack model of development rate in lithographic simulators calls for the specification of these five expression parameters: R_{max} , R_{min} , R_{resin} , n , and l .

To account for surface inhibition effects, an assumption is made that the development rate near the surface of the resist exponentially approaches the bulk development rate, giving a rate as a function of depth $r(z)$ as¹³⁸

$$r(z) = r_B [1 - (1 - r_0) e^{-(z/\delta)}], \quad (12.120)$$

where r_B is the bulk development rate, r_0 is the development rate at the surface of the resist relative to r_B , and δ is the depth of the surface inhibition layer.

12.10.3 The lumped parameter model

Based on a simple model for the development rate and a phenomenological description of the development process, the lumped parameter model predicts the change in line width with exposure for a given aerial image. The main advantage of the model is its extreme ease of application to a lithographic process. It can be used to predict the sidewall angle of the resulting resist profile. The model uses two main parameters, resist contrast and effective thickness, which are easily collected.¹³⁹

In deriving the lumped parameter model, it is customary to let E be the nominal exposure energy (i.e., intensity times the exposure time), $I(x)$ be the normalized image intensity, and $I(z)$ be the relative intensity variation with depth into the resist. The exposure energy as a function of position within the resist E_{xz} is

¹³⁸C.A. Mack, "Optical lithography modeling," in *Microolithography: Science and Technology*, J.R. Sheaths and B.W. Smith, Eds., p. 152, Marcel Dekker, New York (1998).

¹³⁹ibid., p. 161.

given by¹⁴⁰

$$E_{xz} = EI(x)I(z), \quad (12.121)$$

where $x = 0$ is the center of the mask feature and $z = 0$ is the top of the resist of thickness D . We define the logarithms of these quantities as

$$\varepsilon = \ln[E] \quad i(x) = \ln[I(x)] \quad i(z) = \ln[I(z)]. \quad (12.122)$$

Taking the logarithm of the energy deposited [Eq. (12.121)], we obtain

$$\ln[E_{xz}] = \varepsilon + i(x) + i(z). \quad (12.123)$$

The photoresist contrast¹⁴¹ γ is defined theoretically as¹⁴²

$$\gamma = \frac{d \ln r}{d \ln E_{xz}}, \quad (12.124)$$

where r is the resulting development rate from an exposure of E_{xz} . It should be noted that contrast is defined in terms of base e in Eq. (12.124). Assuming a constant contrast over the range of energies of interest, Eq. (12.124) can be integrated to yield a simple expression for the development rate, with appropriate values for the integration constant chosen for the energy and the development time and rate. Choosing ε_0 as the log energy required to just clear the resist in the allotted development time t_{dev} and r_0 as the development rate that results from an exposure of this amount, and integrating Eq. (12.124), we obtain

$$r(x, z) = r_0 e^{\gamma[\varepsilon + i(x) + i(z) - \varepsilon_0]} = r_0 \left[\frac{E_{xz}}{E_0} \right]^\gamma, \quad (12.125)$$

where $E_0 = e^{\varepsilon_0}$. By definition, the development rate for an open-frame exposure is expressed as

$$r = \frac{dz}{dt}. \quad (12.126)$$

¹⁴⁰ibid., p. 155.

¹⁴¹The theoretical resist contrast is different from the characteristic resist contrast, which is defined as a slope on a characteristic curve generated from normalized resist thickness versus an exposed log dose plot.

¹⁴²C.A. Mack, "Lithographic optimization using photoresist contrast," in *KTI Microlithography Seminar Proc.*, pp. 1–12 (1990); *Microelectron. Manuf. Technol.* **14**(1), 36–42 (1991).

Equation (12.126) can be integrated over the development time. If $\varepsilon = \varepsilon_0$, the remaining thickness is by definition zero, such that

$$t_{\text{dev}} = \int_0^D \frac{dz}{r} = \frac{1}{r} \int_0^D e^{-\gamma i(z)} dz, \quad (12.127)$$

where $i(x)$ is zero for an open-frame exposure. From Eq. (12.127), an effective resist thickness D_{eff} can be defined as

$$D_{\text{eff}} = r_0 t_{\text{dev}} e^{\gamma i(D)} = e^{\gamma i(D)} \int_0^D e^{-\gamma i(z)} dz = \int_0^D \left[\frac{I(z)}{I(D)} \right]^\gamma dz. \quad (12.128)$$

Accordingly, the effective resist thickness for the case of absorption only causing a variation in intensity with depth in the resist [i.e., the case where $I(z)$ decays exponentially] can be calculated from Eq. (12.128) as

$$D_{\text{eff}} = \frac{1}{\alpha \gamma (e^{\alpha \gamma} - 1)}. \quad (12.129)$$

If the resist is only slightly absorbing, such that $\alpha \gamma D \ll 1$, the exponential can be approximated by the first few terms in its Taylor series expansion as

$$D_{\text{eff}} \cong D \left(1 + \frac{\alpha \gamma D}{2} \right). \quad (12.130)$$

And from Eq. (12.130), it can be seen that the effect of absorption is to make the resist appear thicker than it actually is during the development process.¹⁴³

Consider a situation in which the development process proceeds in two steps, i.e., a vertical development to a depth z , followed by a lateral development to a position x (measured from the center of the mask feature). The time required to develop in both vertical and horizontal directions, t_z and t_x , respectively, can be calculated from Eq. (12.125). The development time per unit thickness of resist is the reciprocal of the development rate, and it is given by

$$\tau(x, z) = \frac{1}{r(x, z)} = \tau_0 e^{-\gamma [\varepsilon + i(x) + i(z)]} \quad (12.131)$$

where

$$\tau_0 = \frac{1}{r_0} e^{\gamma \varepsilon_0}. \quad (12.132)$$

¹⁴³C.A. Mack, "Optical lithography modeling," in *Microlithography: Science and Technology*, J.R. Sheats and B.W. Smith, Eds., p. 156, Marcel Dekker, New York (1998).

The time required to develop to a depth z at some starting position x_0 is given by

$$t_z = \tau_0 e^{-\gamma \varepsilon} e^{-\gamma i(x_0)} \int_0^z e^{-\gamma i(z')} dz'. \quad (12.133)$$

In like manner, the horizontal development time to go from x to x_0 is given by

$$t_x = \tau_0 e^{-\gamma \varepsilon} e^{-\gamma i(z)} \int_{x_0}^x e^{-\gamma i(x')} dx'. \quad (12.134)$$

The sum of t_z and t_x equals the total development time,

$$t_{\text{dev}} = \tau_0 e^{-\gamma \varepsilon} \left[e^{-\gamma i(x_0)} \int_0^z e^{-\gamma i(z')} dz' + e^{-\gamma i(z)} \int_{x_0}^x e^{-\gamma i(x')} dx' \right]. \quad (12.135)$$

Differentiating Eq. (12.135) with respect to log-exposure energy, we obtain

$$\left. \frac{dx}{d\varepsilon} \right|_z = \frac{\gamma t_{\text{dev}}}{\tau(x, z)} = \gamma t_{\text{dev}} r(x, z). \quad (12.136)$$

Taking the log of both sides of Eq. (12.136) and using the development rate expression Eq. (12.125), we obtain

$$\ln\left(\frac{dx}{d\varepsilon}\right) = \ln(\gamma t_{\text{dev}} r_0) + \gamma [\varepsilon + i(x) + i(z) - \varepsilon_0]. \quad (12.137)$$

Equation (12.137) can be rearranged to yield

$$\varepsilon = \varepsilon_0 - i(x) - i(z) + \frac{1}{\gamma} \ln\left(\frac{dx}{d\varepsilon}\right) - \frac{1}{\gamma} \ln(\gamma t_{\text{dev}} r_0), \quad (12.138)$$

where ε is the log-energy needed to expose a feature of width $2x$. Equation (12.138) is the differential form of the lumped parameter model, which relates the CD versus log-exposure curve and its slope to the image intensity.¹⁴⁴

¹⁴⁴C.A. Mack, A. Stephanakis, and R. Herschel, "Lumped parameter model of the photolithographic process," in *Kodak Microelectronics Seminar Proc.*, pp. 228–238 (1986), R. Herschel and C.A. Mack, "Lumped parameter model for optical lithography," in *Lithography for VLSI, VLSI Electronics Microstructure Science*, R.K. Watts and N.G. Einspruch, Eds., pp. 19–55, Academic Press, New York (1987); C.A. Mack, "Enhanced lumped parameter model for photolithography," *Proc. SPIE* **2197**, 501–510 (1994).

The integral form of the lumped parameter model can be derived by applying the definition of the development rate to Eq. (12.136) or solving for the slope in Eq. (12.138) to yield

$$\frac{d\varepsilon}{dx} = \frac{1}{\gamma t_{\text{dev}} r_0} e^{\gamma[\varepsilon+i(x)+i(z)-\varepsilon_0]}. \quad (12.139)$$

The energy to just clear the resist ε_0 is related to the energy that gives zero line width $\varepsilon(0)$ through the relation

$$\varepsilon_0 = \varepsilon(0) + i(x=0). \quad (12.140)$$

Applying the relation in Eq. (12.140) to Eq. (12.139) yields

$$\frac{d\varepsilon}{dx} = \frac{1}{\gamma t_{\text{dev}} r_0} e^{\gamma i(z)} e^{\gamma[\varepsilon(0)-\varepsilon(x)]} e^{\gamma[i(0)-i(x)]}. \quad (12.141)$$

Equation (12.141) can be rearranged in a log form and simplified with Eq. (12.128), with the assumption that the line width is measured at the resist bottom (i.e., $z = D$), to yield

$$\frac{dE}{dx} = \frac{E(x)}{\gamma D_{\text{eff}}} \left[\frac{E(0)I(0)}{E(x)I(x)} \right]^\gamma. \quad (12.142)$$

Integrating Eq. (12.142) as

$$\int_{E(0)}^{E(x)} E^{\gamma-1} dE = \frac{1}{\gamma D_{\text{eff}}} [E(0)I(0)]^\gamma \int_0^x I(x')^{-\gamma} dx'$$

yields

$$\frac{E(x)}{E(0)} = \left[1 + \frac{1}{\gamma D_{\text{eff}}} \int_0^x \left(\frac{I(x')}{I(0)} \right)^\gamma dx' \right]^{1/\gamma}. \quad (12.143)$$

Equation (12.140) is the integral form of the lumped parameter model.¹⁴⁵ With this equation, it is possible to generate a normalized CD versus exposure curve, as long

¹⁴⁵C.A. Mack, A. Stephanakis, and R. Herschel, "Lumped parameter model of the photolithographic process," in *Kodak Microelectronics Seminar Proc.*, pp. 228–238 (1986); R. Herschel, C.A. Mack, "Lumped parameter model for optical lithography," in *Lithography for VLSI, VLSI Electronics Microstructure Science*, R.K. Watts and N.G. Einspruch, Eds., pp. 19–55, Academic Press, New York (1987); C.A. Mack, "Enhanced lumped parameter model for photolithography," *Proc. SPIE* **2197**, 501–510 (1994).

as one knows the image intensity $I(x)$, the effective resist thickness D_{eff} , and the contrast γ .

12.10.4 Resist profile

A good measure of the resist profile is the sidewall angle, which can be predicted with the lumped parameter model. To derive an expression for the sidewall slope, it is customary to rewrite Eq. (12.135) in terms of development rate as

$$t_{\text{dev}} = \int_0^z \frac{dz'}{r(0, z')} + \int_{x_0}^x \frac{dx'}{r(x', z)}. \quad (12.144)$$

By taking the derivative of Eq. (12.144) with respect to z , we obtain

$$0 = \int_0^z \frac{d\tau}{dz} dz' + \frac{1}{r(0, z)} + \int_{x_0}^x \frac{d\tau}{dz} dx' + \frac{1}{r(x, z)} \frac{dx}{dz}. \quad (12.145)$$

The derivative of the reciprocal development rate can be calculated from Eq. (12.131) as

$$\frac{d\tau}{dz} = -\gamma\tau(x, z) \frac{d \ln(E_{xz})}{dz}. \quad (12.146)$$

Equation (12.146) implies that the variation of development rate with depth into the resist depends on the variation of the exposure dose with depth. For the simple case where bulk absorption is the only factor responsible for the variation of exposure with z , we have

$$\frac{d \ln(E_{xz})}{dz} = -\alpha, \quad (12.147)$$

where α is the absorption coefficient of the resist. Applying Eqs. (12.146) and (12.147) to Eq. (12.145), we obtain

$$-\alpha\gamma \left(\int_0^z \tau dz' + \int_{x_0}^x \tau dx' \right) = \frac{1}{r(0, z)} + \frac{1}{r(x, z)} \frac{dx}{dz}. \quad (12.148)$$

The term in parentheses in Eq. (12.148) is the development time. The reciprocal of the resist slope can be given by the expression¹⁴⁶

$$-\frac{dx}{dz} = \frac{r(x, z)}{r(0, z)} + \alpha\gamma t_{\text{dev}} r(x, z) = \frac{r(x, z)}{r(0, z)} + \alpha \frac{dx}{dE}. \quad (12.149)$$

¹⁴⁶C.A. Mack, "Optical Lithography Modeling," in *Microlithography: Science and Technology*, J.R. Sheaths and B.W. Smith, Eds., pp. 160–161, Marcel Dekker, New York (1998).

The two terms in Eq. (12.149) represent the two main contributors to the sidewall angle, i.e., (i) the development effect (captured by the first term as the ratio of the development rate at the edge of the resist feature to the development rate at the center) and (ii) the absorption effect (captured by the second term).

12.11 Accuracy of Lithographic Models

Standard lithographic modeling programs in use today are fairly accurate in simulating experimental data. Figure 12.6 shows the comparison of the accuracy of three popular lithographic models—Dill, Mack, and enhanced Mack models—in simulating experimental dissolution rate data of a conventional resist. Both the Dill and Mack models fairly accurately simulate the dissolution curve at most PAC concentrations, except at the lowest concentration ranges. In contrast, the enhanced Mack model accurately simulates the dissolution curve from the lowest to the highest concentration of the PAC.

Figure 12.7 shows a comparison of PROLITH simulation results with actual SEM pictures of 130-nm isolated and dense lines (1:1.50 duty cycle) printed on a methacrylate resist with an ArF stepper. The similarity between the simulation results and the actual SEM pictures is striking, illustrating the extremely high degree of accuracy of this particular lithographic modeling and simulation program in modeling experimental results.

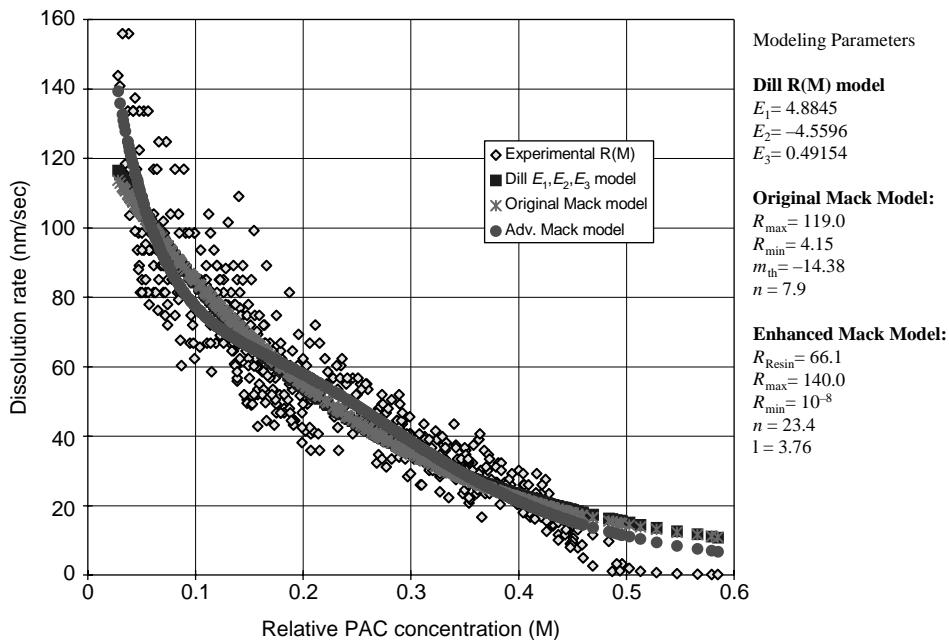


Figure 12.6 Comparison of the accuracy of the Dill model, Mack model, and enhanced (advanced) Mack model in modeling the dissolution rate data of AZ 7908 resist developed in 300-MIF developer. (Courtesy of R. Dammel.)

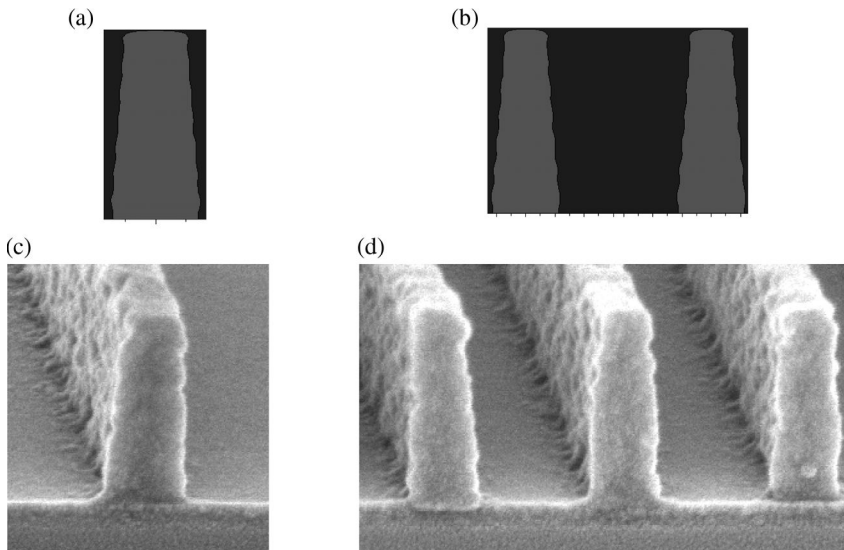


Figure 12.7 (a) and (b) PROLITH simulation results and (c) and (d) SEM pictures of 130-nm isolated line and dense lines (1:1.50 duty cycle) printed on a methacrylate resist on an ArF exposure stepper, using NA = 0.6. The modeling parameters used in this simulation are shown in Table 12.3. (Courtesy of the late Dr. Jeffrey Byers.)

Table 12.3 Parameters used in the simulation of the resist features shown in Figure 12.7. The parameters are defined in the derivations in the preceding section. (Courtesy of the late Dr. Jeffrey Byers.)

Exposure Parameters		PEB Parameters		Development Parameters	
n_{193}	1.703	$[Q]/[PAG]$	0.102	Model Type	Enhanced Mack
k_{193}	0.017	E_A [kcal/mol]	15.034	R_{max} [nm/s]	333.73
α_{193} [$1/\mu\text{m}$]	1.122	$\ln(A_a)$	17.124	R_{min} [nm/s]	0.01
C_{193}	0.068	E_D [kcal/mol]	17.75	R_n	1.77
		$\ln(A_D)$	25.356	R_{resin} [nm/s]	46.25
				R_1	5.63
				R_{inh}	0.16
				R_z	120

12.12 Applications/Uses of Lithographic Modeling

Lithographic modeling and simulation have found wide applications, spanning research, process development, manufacturing process optimization and control, and even education within the semiconductor industry. A few notable examples of these applications and their roles in shaping the evolution of lithography are outlined below.

12.12.1 Research applications

Since its introduction in 1974, lithographic modeling has had a major impact on research in lithography. For instance, lithographic modeling was used to predict the advantages of using dyed photoresist in reducing standing waves,¹⁴⁷ ten years before they were confirmed experimentally.¹⁴⁸

Additionally, lithographic modeling was used extensively to understand the effects of phase-shifting masks,¹⁴⁹ such as their increased defect printability¹⁵⁰ and the utility of assist features.¹⁵¹ In general, lithographic modeling has proved very useful in predicting the printability of defects.¹⁵² The advantages of off-axis illumination in improving resolution and depth of focus were first predicted through lithographic modeling, before this imaging scheme was implemented.¹⁵³ Also, the advantages of using variable numerical aperture and variable partial coherence were all predicted through lithographic modeling, before these systems were implemented in lithographic exposure tools.¹⁵⁴

Furthermore, lithographic modeling is conventionally used to quantify optical proximity effects and for defining algorithms for geometry-dependent mask biasing.¹⁵⁵ It has also been used to study the metrology of lithographic structures.¹⁵⁶

¹⁴⁷A.R. Neureuther and F.H. Dill, "Photoresist modeling and device fabrication applications," in *Optical and Acoustical Micro Electronics*, pp. 233–249, Polytechnic Press, New York (1974).

¹⁴⁸H.L. Stover, M. Nagler, I. Bol, and V. Miller, "Submicron optical lithography: *i* line lens photoresist technology," *Proc. SPIE* **470**, 22–33 (1984); I. Bol, "High resolution optical lithography using dyed single resist," in *Kodak Microelectronics Seminar Interface '84*, pp. 19–22 (1984).

¹⁴⁹M.D. Levenson, N.S. Viswanathan, and R.A. Simpson, "Improving resolution in photolithography with phase shifting mask II. Imaging simulations and submicrometer resist exposures," *IEEE Trans. Electron Dev.* **ED-36**(6), 753–763 (1984).

¹⁵⁰M.D. Pouty and A.R. Neureuther, "Optical imaging with phase shift masks," *Proc. SPIE* **470**, 228–232 (1984).

¹⁵¹*ibid.*

¹⁵²A.R. Neureuther, P. Flanner III, and S. Shen, "Coherence of defect interactions with features in optical imaging," *J. Vac. Sci. Technol. B* **5**(1), 308–312 (1987); J. Wiley, "Effects of stepper resolution on the printability of submicron 5× reticle defects," *Proc. SPIE* **1088**, 58–73 (1989).

¹⁵³C.A. Mack, "Optical stepper performance through image manipulation," in *KTI Microelectronics Seminar Proc.*, p. 209 (1989).

¹⁵⁴*ibid.*; C.A. Mack, "Algorithm for optimizing stepper performance through image manipulation," *Proc. SPIE* **1264**, 71–82 (1990).

¹⁵⁵C.A. Mack and P.M. Kaufman, "Mask bias in submicron optical lithography," *J. Vac. Sci. Technol. B* **6**(6), 2213–2220 (1988); N. Shamma, F. Sporon Fielder, and E. Lin, "A method for correction of proximity effect in optical projection lithography," in *KTI Microelectronics Seminar Proc.*, pp. 145–156 (1991).

¹⁵⁶L.M. Milner, K.C. Hickman, S.M. Gasper, K.P. Bishop, S.S.H. Naqvi, J.R. McNeil, M. Blain, and B.L. Draper, "Latent image exposure monitor using scatterometry," *Proc. SPIE* **1673**, 274–283 (1992); K.P. Bishop, L.M. Milner, S.S.H. Naqvi, J.R. McNeil, and N.L. Draper, "Use of scatterometry for resist process control," *Proc. SPIE* **1673**, 441–452 (1992); L.M. Milner, K.P. Bishop, S.S.H. Naqvi, and J.R. McNeil, "Lithography process monitor using light diffracted from latent image," *Proc. SPIE* **1926**, 94–105 (1993); S. Zidi, S.L. Prins, J.R. McNeil, and S.S.H. Naqvi, "Metrology sensors for advanced resists," *Proc. SPIE* **2196**, 341–351 (1994).

Still further, lithographic modeling has been employed in resist studies to understand the depth of focus loss associated with printing contact holes in negative resists,¹⁵⁷ the basis of the extremely high contrast in resists with surface inhibition,¹⁵⁸ the potential for exposure condition optimization so as to maximize process latitude,¹⁵⁹ and the role of diffusion in chemically amplified resists,¹⁶⁰ as well as in the design and evaluation of new resists.

12.12.2 Process development applications

Lithographic modeling has found widespread applications in the development of new lithographic processes and equipment. Such applications include the optimization of dye loadings in resists,¹⁶¹ the simulation of substrate reflectivity,¹⁶² the applicability and optimization of top and bottom antireflection coatings,¹⁶³ and the simulation of the effect of bandwidth on swing curve amplitude.¹⁶⁴

Furthermore, lithographic modeling is employed by resist manufacturers to evaluate new formulations¹⁶⁵ and to determine adequate measures of resist

¹⁵⁷C.A. Mack and J.E. Connors, "Fundamental differences between positive and negative tone imaging," *Proc. SPIE* **1674**, 328–338 (1992); *Microlithography World* **1**(3), 17–22 (1992).

¹⁵⁸C.A. Mack, "Lithographic optimization using photoresist contrast," in *KTI Microlithography Seminar Proc.*, pp. 1–12 (1990); *Microelectron. Manuf. Technol.* **14**(1), 36–42 (1991).

¹⁵⁹C.A. Mack, "Photoresist optimization," in *KTI Microlithography Seminar Proc.*, pp. 153–167 (1987); P. Trefonas and C.A. Mack, "Exposure dose optimization for a positive resist containing poly functional photoactive compound," *Proc. SPIE* **1466**, 117–131 (1991).

¹⁶⁰J.S. Petersen, C.A. Mack, J. Sturtevant, J.D. Myers, and D.A. Miller, "Non constant diffusion coefficients: short description of modeling and comparison to experimental results," *Proc. SPIE* **2438**, 167–180 (1995).

¹⁶¹J.R. Johnson, G.J. Stagman, J.C. Sardella, C.R. Spinner III, F. Liou, P. Trefonas, and C. Meister, "The effects of absorptive dye loading and substrate reflectivity on a 0.5 μm *i* line photoresist process," *Proc. SPIE* **1925**, 552–563 (1993); W. Conley, R. Akkapeddi, J. Fahey, G. Hefferon, S. Holmes, G. Spinillo, J. Sturtevant, and K. Welsh, "Improved reflectivity control of APEX E positive tone deep UV photoresist," *Proc. SPIE* **2195**, 461–476 (1994).

¹⁶²N. Thane, C.A. Mack, and S. Sethi, "Lithographic effects of metal reflectivity variations," *Proc. SPIE* **1926**, 483–494 (1993).

¹⁶³S. S. Miura, C.F. Lyons, and T.A. Brunner, "Reduction of linewidth variation over reflective topography," *Proc. SPIE* **1674**, 147–156 (1992); H. Yoshino, T. Ohfuji, and N. Aizaki, "Process window analysis of the ARC and TAR systems for quarter micron optical lithography," *Proc. SPIE* **2195**, 236–245 (1994).

¹⁶⁴G. Flores, W. Flack, and L. Dwyer, "Lithographic performance of a new generation *i* line optical system: a comparative analysis," *Proc. SPIE* **1927**, 899–913 (1993); B. Kuyel, M. Barrick, A. Hong, and J. Vigil, "0.5 micron deep UV lithography using micrascan 90 step and scan exposure tool," *Proc. SPIE* **1463**, 646–665 (1991).

¹⁶⁵H. Iwasaki, T. Itani, M. Fujimoto, and K. Kasama, "Acid size effects of chemically amplified negative resist on lithographic performance," *Proc. SPIE* **2195**, 164–172 (1994); U. Schedeli, N. Münzel, H. Holzwarth, S.G. Slater, and O. Nalamasu, "Relationship between physical properties and lithographic behavior in a high resolution positive tone deep UV resist," *Proc. SPIE* **2195**, 98–110 (1994).

performance and quality control.¹⁶⁶ The optimization of the numerical aperture and partial coherence of lithographic steppers and scanners,¹⁶⁷ print bias between dense and isolated lines,¹⁶⁸ and optical proximity correction rules and schemes¹⁶⁹ are all based on lithographic modeling.

12.12.3 Manufacturing and instructional applications

Lithographic modeling and simulations are routinely used in the manufacturing environment for process and quality control purposes.¹⁷⁰ Within the semiconductor industry as well as within academia, lithographic modeling and simulation are used to systematically instruct people about lithography and what role its various aspects play in producing lithographic images, as well as the factors that affect the quality of these images. This learning process is made easier by the speed and the versatility with which the lithographic simulation programs provide feedback to the student.

¹⁶⁶K. Schlicht, P. Scialdone, P. Spragg, S.G. Hansen, R.J. Hurditch, M.A. Toukhy, and D.J. Brzozowy, "Reliability of photospeed and related measures of resist performances, *Proc. SPIE* **2195**, 624–639 (1994).

¹⁶⁷R.A. Cirreli, E.L. Raab, R.L. Kostelak, and S. Vaidya, "Optimizing numerical aperture and partial coherence to reduce proximity effects in deep UV lithography," *Proc. SPIE* **2197**, 429–439 (1994); B. Katz, T. Rogoff, J. Foster, B. Rericha, B. Rolfson, R. Holscher, C. Sager, and P. Reynolds, "Lithographic performance at sub 300 nm design rules using high NA *i* line stepper with optimized NA and sigma in conjunction with advanced PSM technology, *Proc. SPIE* **2197**, 421–428 (1994).

¹⁶⁸V.A. Deshpande, K.L. Holland, and A. Hong, "Isolated grouped linewidth bias on SVGL micras can," *Proc. SPIE* **1927**, 333–352 (1993).

¹⁶⁹R.C. Henderson and O.W. Otto, "Correcting for proximity effect widens process latitude," *Proc. SPIE* **2197**, 361–370 (1994).

¹⁷⁰H. Engstrom and J. Beacham, "Online photolithography modeling using spectrophotometry and PROLITH/2, *Proc. SPIE* **2196**, 479–485 (1994); J. Kasahara, M.V. Dusa, and T. Perera, "Evaluation of a photoresist process for 0.75 micron G line lithography," *Proc. SPIE* **1463**, 492–503 (1991); E.A. Puttlitz, J.P. Collins, T.M. Glynn, and L.L. Linehan, "Characterization of profile dependency on nitride substrate thickness for a chemically amplified *i* line negative resist, *Proc. SPIE* **2438**, 571–582 (1995).

Chapter 13

Optical Lithography

Mehr licht! [More light!]

Attributed dying words of Johann Wolfgang von Goethe (1749–1832)

13.1 Introduction

Lithography using photons,¹ otherwise called photolithography or optical lithography, has been and continues to be the preeminent lithographic technique used in the fabrication of integrated circuit devices in the semiconductor industry since the invention of the transistor and the integrated circuit. Spanning a period of over 50 years and many generations of device technology nodes that have witnessed critical dimension reduction of over three orders of magnitude, and up to now comprising largely photons with wavelengths from the visible (436 nm) through mid-UV (365 nm), DUV (248 nm and 193 nm), and VUV (157 nm) regions of the spectrum, it has demonstrated remarkable longevity that is expected to continue into the foreseeable future.

The remarkable longevity of optical lithography is a direct consequence of the advancements that have been made in optical exposure tools, and resist and process technologies. In particular, technological advancement in lithographic exposure tools has evolved across four broad categories, i.e., how the pattern is transferred from mask to wafer, the type of optics, the exposure medium and area exposed, and the wavelength of light used. Figure 13.1 shows the technologies that fall into these categories. All optical lithographic exposure tools in use today use one technology from each of these categories.

¹The term “optical lithography” as used in this book encompasses all lithographic patterning techniques where photons are used in such a manner that the imaging action obeys the laws of geometric optics—the simple laws of reflection and refraction, to mention but a few. With this usage, the terms photolithography and optical lithography are interchangeable, denoting the fact that photons are the primary agents that initiate the chemical transformations of the resists, resulting in the contrast between the exposed and the unexposed regions, and ultimately leading to the effective transfer of the mask image to the semiconducting substrate.

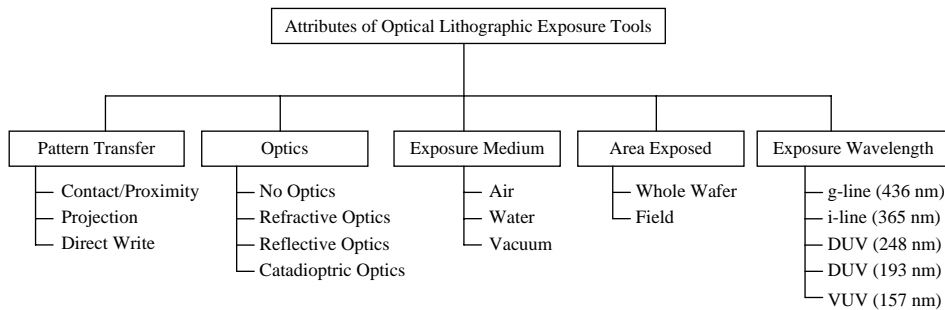


Figure 13.1 Essential attributes of lithographic exposure tools.

The key factors driving the advancements in exposure tool technology are line width resolution, registration, and depth of focus. The ability to decrease device feature line width is beneficial in that it lowers cost, increases the number of dies produced per wafer, and also increases device speed. Registration helps to increase device yield and speed by accurately overlaying one layer on another. Depth of focus control helps to determine CD control and consequently device speed and yield.²

The objective of optical lithography is to transfer the mask pattern to the semi-conducting substrate via photosensitive materials called photoresists. It is a multi-step process that involves making the mask, depositing the resist, exposing the wafer, and developing the resist. Manufacturing an advanced integrated circuit device today requires 30 or more lithographic masking steps. Figure 13.2 shows an optical lithography process flowchart.³

In the remaining sections of this chapter, we present material on the elements of optical lithography and various optical lithographic technologies, along with the physical and chemical basis behind the roles photons play in mediating them. Materials are organized around two main categories of optical lithography, namely, (i) visible light lithography (utilizing exposure wavelength at 436 nm), and (ii) UV lithography (utilizing exposure wavelengths at 365 nm, 248 nm, 193 nm, and 157 nm).

13.2 Elements of Optical Lithography

There are six basic elements of optical lithography, i.e., (i) an exposure source, (ii) an illumination optics system, (iii) a photomask or reticle and its pellicle, (iv) a projection optics system, (v) a wafer stage, and (vi) a photoresist-coated wafer. As shown in Fig. 13.3, the source provides the exposure radiation that, with the aid of the illumination optics, illuminates the photomask and transfers

²“Microlithography & mask making,” VLSI Research Inc. Report (1992).

³A detailed description of the various process steps, except the mask making steps, is provided in Chapter 12.

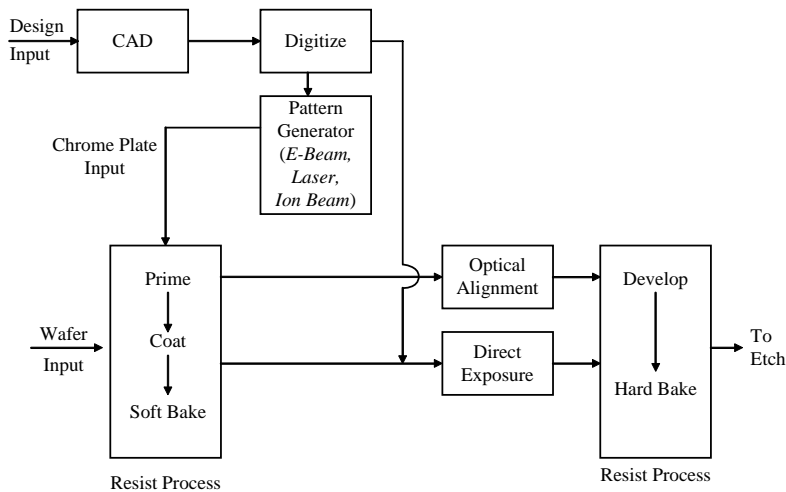


Figure 13.2 Optical lithography process flowchart. (Adapted from VLSI Research Inc. report.⁴)

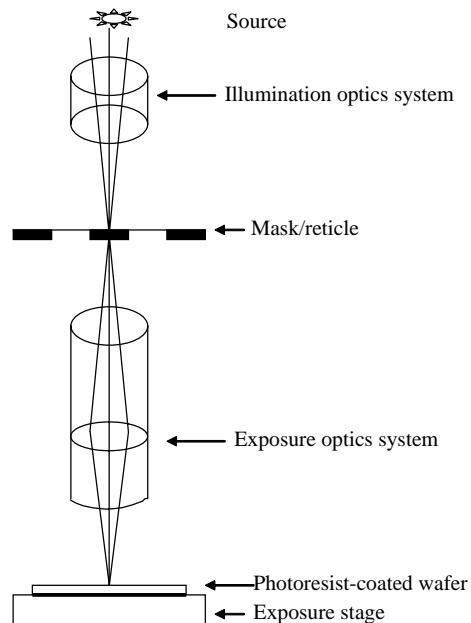


Figure 13.3 Elements of an optical lithographic exposure tool.

the image of the photomask with the aid of projection optics (in projection systems) to a photoresist-coated wafer (in projection systems) or directly to the photoresist-coated wafer in the absence of projection optics (in proximity and contact printing systems). In this way, the patterns on the photomask or reticle are replicated by the

⁴“Microlithography & mask making,” VLSI Research Inc. Report (1992).

exposure system onto the photoresist-coated wafer, resulting in regions of high and low exposure intensity. The resulting latent images are then developed, creating openings in the resist for subsequent processing.

13.2.1 Radiation sources

The varieties of exposure sources that have found applications in UV and visible light optical lithography can be broadly divided into two groups: (i) high-pressure arc lamp or incoherent sources and (ii) laser sources or temporally coherent sources. In the laser-type sources, we include all techniques and devices for radiation generation that have their basis in stimulated emission of radiation.

13.2.1.1 High-pressure arc lamps

The high-pressure arc lamp sources are usually mercury (Hg) or mercury-xenon (Hg-Xe) arc lamps where electric current (input power in the 0.5–1.5-kW range) is passed through two electrodes enclosed in a bulb containing Hg or Hg-Xe gas to create a discharge arc, which emits a characteristic light spectrum with many peaks between 240 nm and 600 nm (see Fig. 13.4). Of the peaks shown in Fig. 13.4, the g-line (436 nm) and the i-line (365 nm) have adequate power output over a narrow bandwidth for lithographic applications in the visible and mid-UV regions of the spectrum; as a result, these lines have been widely used in optical lithography. The electrodes are typically made of refractory metals such as tungsten that can withstand the extremely high temperature of the operation

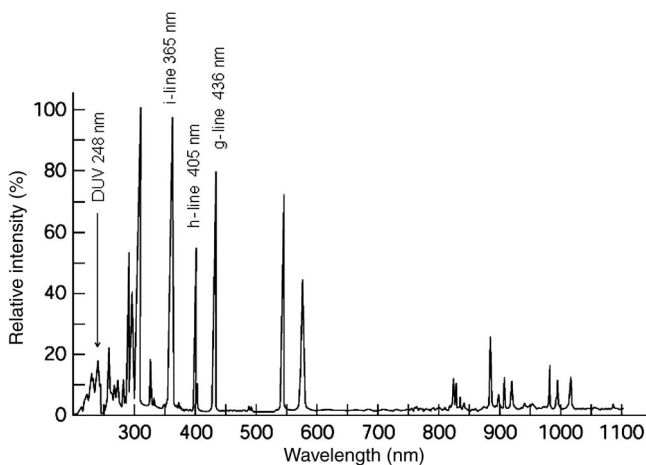


Figure 13.4 Emission spectrum of high-pressure mercury arc lamp. (Source: Ushio Specialty Lighting Products.)

of this equipment. The electrodes are sometimes coated with thorium so as to reduce the electrode work functions and thereby provide electrons to the plasma more easily. The relative partial pressures of Hg and Xe as well as the total pressure of the discharge mixture determine the spectral distribution of the light output of these types of sources in the mid-UV region of the spectrum.⁵

The most attractive features of high-pressure arc lamp sources is the small, well-defined source size, which is usually in the shape of a point or a line; this makes them optically very convenient to handle. A major drawback of these sources is their extremely poor efficiency at shorter wavelengths, which, as a result, severely limits their usefulness in the DUV regions.⁶ In fact, less than 1% of the electrical power supplied to a Hg arc lamp is converted to actinic light. Operation of these lamps leads to gradual deposition of the electrode material on the inside of the bulb, reducing light output. Lamps are therefore replaced after several hundred hours, corresponding to the end of their rated lifetime, in order to maintain high exposure tool throughput and to prevent catastrophic failures such as fracture and explosion of the bulbs.⁷

13.2.1.2 Exciplex and excimer laser sources

Exciplex laser sources used in optical lithography are based on the emission properties of rare-gas monohalides such as KrF (lasing at 248 nm) and ArF (lasing at 193 nm), while the excimer laser sources are based on halogen gases such F₂ gas (lasing at 157 nm). These lasers belong to a class of very efficient and powerful pulsed ultraviolet lasers that became commercially available in the late 1970s.⁸ Table 13.1 is a list of various commercially available exciplex and excimer laser transitions used in lithography, along with their type(s) of excitation schemes. These laser sources provide several options in power output, pulse energy, spectral bandwidth, and pulse repetition rate.⁹ The ArF exciplex lasers are quite similar in overall characteristics to KrF lasers, except for a less robust discharge. They are more prone to contamination effects, and it is more difficult to maintain their performance at high pulse repetition rates. The main difference between ArF and KrF lasers is cost of ownership, with the former having a significantly higher cost of ownership than the latter. Current improvements in these laser systems are focused on reducing optical damage and allowing higher numerical apertures through the use of pulse stretching, multi-kHz repetition rates, and ultranarrow bandwidths (<0.5 pm).

⁵H.J. Levinson, *Principles of Lithography*, 2nd ed., p. 144, SPIE Press, Bellingham, WA (2005).

⁶K. Jain, *Excimer Laser Lithography*, p. 9, SPIE Press, Bellingham, WA (1990).

⁷H.J. Levinson, *Principles of Lithography*, 2nd ed., p. 144, SPIE Press, Bellingham, WA (2005).

⁸See, for example, J.J. Ewing, "Rare gas halide lasers," *Phys. Today* **31**, 32 (May 1978); *Excimer Lasers*, 2nd ed., C.K. Rhodes, Ed., Springer Verlag, New York (1984).

⁹K. Jain, *Excimer Laser Lithography*, p. 93, SPIE Press, Bellingham, WA (1990).

Table 13.1 Commercially available exciplex and excimer laser sources. (Adapted from K. Jain.¹⁰)

Lasing exciplex(*)/ excimer(**) species	Emission wavelength (nm)	Excitation scheme		
		Electric discharge	Electron beam	Electron beam controlled discharge
KrF*	248	Yes	Yes	Yes
ArF*	193	Yes	Yes	
F ₂ **	157	Yes		

13.2.1.2.1 Lasing mechanism of rare-gas halide exciplex and diatomic halogen excimer lasers

Molecules belonging to the rare-gas halide exciplex lasers and diatomic halogen excimer lasers are characterized by a bound or metastable excited upper state and an unstable or very weakly bound ground state. The crucial characteristic of this type of laser is that only when they are electronically excited do they exist in a bound state with a well-defined potential energy minimum; the ground electronic state generally has no potential energy minimum, or else a very shallow one.¹¹ For the specific case of rare-gas halide lasers, the rare gases do not appreciably interact in the ground state, but on excitation they form exciplexes of the type RX (where R denotes a rare-gas atom such as Kr or Ar, and X denotes a halogen atom such as F). These exciplexes have comparatively long lifetimes compared to other laser sources.¹²

Exciplexes are generally formed by chemical reaction between inert gas and halide ions produced by an electrical discharge. Specifically, they are the result of chemical reactions between a ground state halogen atom (produced on excitation from a halogen molecule) with an excited rare-gas atom, where one of the peripheral electrons is promoted into a higher (Rydberg) orbital. The electron vacancy that arises in the excited rare-gas atom is filled by the odd electron of the halogen, resulting in the formation of an excited complex, which on deactivation emits fluorescence (the laser radiation).¹³

A schematic of typical potential energy curves for rare-gas halide exciplex lasers is shown in Fig. 13.5. While the excited state complex, the exciplex, is bonded strongly enough to have a radiative lifetime of 10^{-8} – 10^{-6} s, the lower state reached by the radiative transition is not bonded and dissociates almost instantaneously (within a single vibration, about 10^{-12} s) into free atoms that are again available for excitation. Given the large difference in lifetimes, with the

¹⁰ibid.

¹¹D.L. Andrews, *Lasers in Chemistry*, pp. 39–40, Springer Verlag, Berlin (1986).

¹²K. Jain, *Excimer Laser Lithography*, p. 93, SPIE Press, Bellingham, WA (1990); J. Ewing, "Rare gas halide lasers," *Phys. Today* **31**(5), 93 (1978).

¹³A. Reiser, *Photoreactive Polymers: The Science and Technology of Resists*, p. 254, John Wiley & Sons, Hoboken, NY (1989).

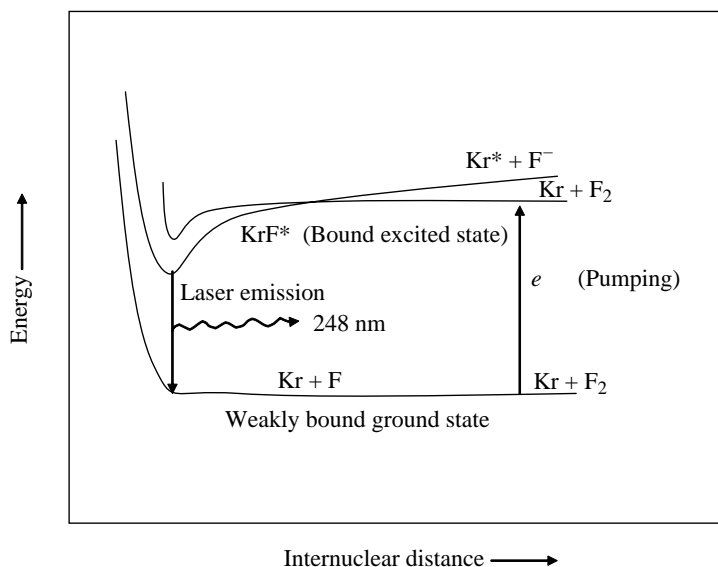
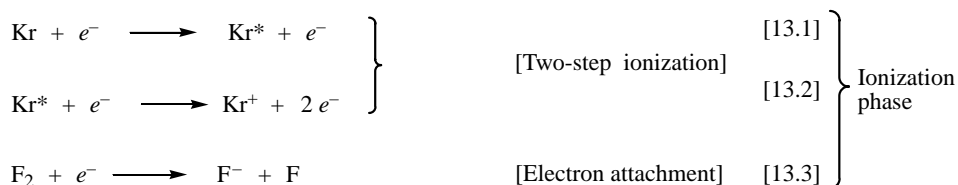


Figure 13.5 Schematic of potential energy curves for a rare-gas monohalide excimer laser based on KrF. KrF^* is formed via two reaction channels. It decays to the ground state via dissociation into Kr and F while emitting a photon at 248 nm. (Adapted with permission from Francis & Taylor Group LLC.¹⁴) The diatomic halogen excimer lasers based on F_2 also have similar potential energy curves.

lower level having a substantially shorter lifetime than the upper level, population inversion between the two states is easily achieved.¹⁵

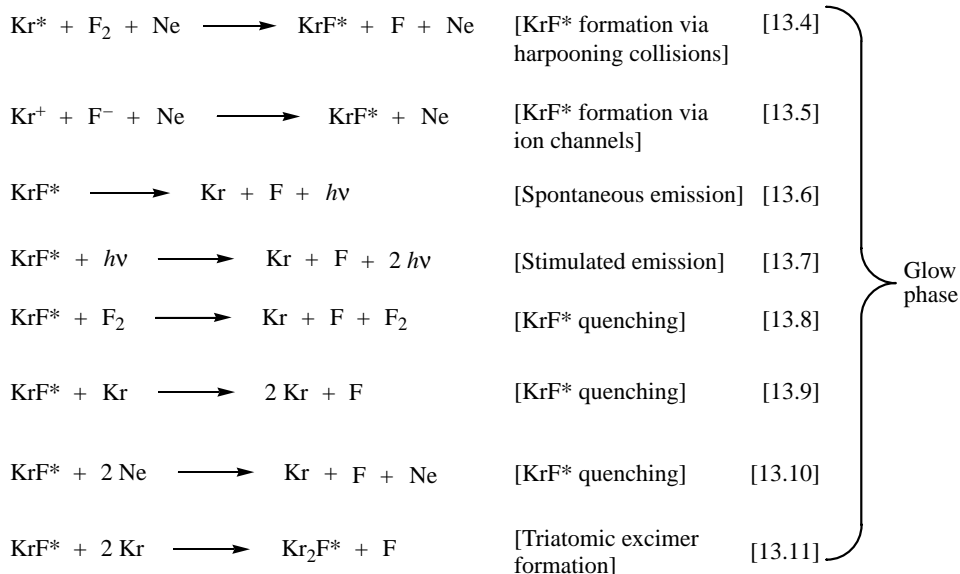
Reactions [13.1]–[13.11] illustrate the specific photochemical reactions involved in the lasing actions of KrF excimer lasers.¹⁶ (Similar reactions are also involved in ArF excimer lasers.)



¹⁴P. Das and U. Sengupta, “Krypton fluoride excimer laser for advanced microlithography,” in *Microlithography: Science and Technology*, p. 280, J.R. Sheats and B.W. Smith, Eds., Marcel Dekker, New York (1998).

¹⁵K. Jain, *Excimer Laser Lithography*, p. 93, SPIE Press, Bellingham, WA (1990); J. Ewing, “Rare gas halide lasers,” *Phys. Today* **31**(5), 32 (1978); A. Reiser, *Photoreactive Polymers: The Science and Technology of Resists*, pp. 254–255, John Wiley & Sons, Hoboken, NJ (1989).

¹⁶P. Das and U. Sengupta, “Krypton fluoride excimer laser for advanced microlithography,” in *Microlithography: Science and Technology*, p. 279, J.R. Sheats and B.W. Smith, Eds., Marcel Dekker, New York (1998).



In the three-body reaction (Reaction [13.5]), the Ne acts as a buffer. Given that the krypton fluoride so produced is electronically excited and has a short lifetime (about 2.5 ns), it rapidly decays by photon emission to the lower energy state as shown in Fig. 13.5. Because this is an unbound state in which the force between the atoms is always repulsive, the exciplex molecule then immediately dissociates into its constituent atoms. As a result, this state never attains a large population, and a population inversion therefore exists between it and the higher energy bound exciplex state. The decay transition can therefore be efficiently stimulated to produce laser emission. One noteworthy characteristic of this particular laser system is that it represents a rare example of a truly two-level laser.¹⁷

It is worth mentioning that because some of the reactions taking place in the glow phase of the laser action regenerate the starting materials, i.e., krypton atom and fluorine molecule, the exciplex laser system can be operated continuously without direct consumption of the active medium, in contrast to other chemical lasers. In this way, a sealed cavity, charged with the right amount of the gas mixtures to the desired pressure level, can be used. As expected, the cavity wall material must be carefully chosen in view of the highly corrosive halogen gas used. In addition, since the walls are rapidly poisoned by the gas, it is not possible to use the same laser tube for different halogens.¹⁸

13.2.1.2.1.1 EXCITATION SCHEMES

The methods that have been reported for exciting exciplex and excimer lasers include (i) direct excitation by a high-energy electron beam, (ii) excitation by an electric discharge controlled by an electron beam, (iii) direct high-voltage electric

¹⁷D.L. Andrews, *Lasers in Chemistry*, pp. 39–40, Springer Verlag, Berlin (1986).

¹⁸ibid.

discharge excitation, and (iv) excitation by optical pumping with another laser beam. Of these, the direct high-voltage electric discharge excitation scheme is the most practical in terms of compactness and ease of operation, and therefore is the method that has found wide application in optical lithography.¹⁹ In this method, a mixture of the laser gases Kr or Ar and F₂ (in the case of rare-gas monohalide exciplex lasers based on KrF and ArF) or pure F₂ gas (in the case of halogen excimer lasers based on F₂) is pumped through an electrode assembly at several atmospheres of pressure. By discharging a condenser across the electrodes, a laser pulse of high intensity and short duration is created. Repetition rates of up to 4 kHz can be achieved.²⁰

A major drawback of the exciplex and excimer lasers concerns the degradation of the gas mixture due to some unwanted photochemistry. This necessitated frequent gas changes in early systems, but with the development of recirculators and purification units, for current state-of-the-art commercial systems, it is possible to operate them on a single gas filling for billions of pulses, without appreciable loss of power.

13.2.1.2.1.2 KEY OPERATIONAL PARAMETERS

The key operational parameters of exciplex and excimer lasers used in optical lithographic applications include exposure-dose-related parameters comprising average power, pulse energy, repetition rate, and pulse width; temporal coherence; spatial coherence including beam dimensions, beam divergence, and beam uniformity; and maintenance and reliability. Table 13.2 lists some of the key operational parameters of KrF, ArF, and F₂ laser systems used in optical lithography.

(i) Spatial coherence

Exciplex and excimer lasers have very poor spatial coherence and therefore do not produce speckles in lithography. Speckles are the random interference patterns that result when, on illumination of an object with a spatially coherent wavefront, any

Table 13.2 Key performance parameters of commercial exciplex and excimer lasers.

	Repetition rate (kHz)	Average power (W)	Pulse energy (mJ)	Bandwidth (FWHM) ^d (pm)	Wavelength (nm)
ArF ^a	4	40	10	<0.25	193
KrF ^b	4	40	10	<0.35	248
F ₂ ^c	1	10	10		157

^aBased on Cymer's XLA 100 laser system.

^bBased on Cymer's ELS 7010 laser system.

^cBased on the Lambda Physik Novaline F1030 F₂ laser system.

^dFull width half maximum.

¹⁹K. Jain, C.G. Willson, and B.J. Lin, "Ultrafast high resolution contact lithography with excimer lasers," *IBM J. Res. Dev.* **26**, 151 (1982).

²⁰See, for example, "Nanolith™ 7000: the world's most advanced 193 nm (ArF) production laser," Cymer Product Brochure, www.cymer.com.

scattering at an optical surface causes different parts of the wavefront to interfere with each other constructively and destructively. They appear as intense image noise. The value of contrast in a speckle pattern is given by $1/\sqrt{N}$, where N is the number of independent, spatially coherent wavefronts, or modes, used to illuminate the object. For exciplex and excimer laser illumination, N may have a value of several thousands or even hundreds of thousands, resulting in an interference pattern with effectively zero contrast; in other words, an exposure free of speckle.²¹

(ii) Spectral bandwidth and temporal coherence

The spectral bandwidth of the radiation emitted by a laser determines its temporal coherence, expressed as a coherence length l_c , and given by

$$l_c = \frac{c}{\Delta f} = \frac{\lambda^2}{\Delta \lambda}, \quad (13.1)$$

where c is the velocity of light, Δf is the frequency spread of the laser output, and $\Delta \lambda$ is the corresponding spread in wavelength. For free-running (i.e., not spectrally narrowed) exciplex and excimer lasers, the lasing bandwidth is typically <1 nm, corresponding to a coherence length of ~ 100 μm .²² In the specific case of free-running KrF exciplex lasers, their natural bandwidth is approximately 300 pm, which is too wide for high-resolution wafer steppers and step-and-scan systems.²³

Figures 13.6 and 13.7 show the spectrum of a free-running ArF exciplex laser (in air and nitrogen) and a line-narrowed laser in air, respectively. The spectral output of free-running lasers overlaps with oxygen Schumann-Runge resonances (at wavelengths between 210 nm and 180 nm). The spectrum shown in Fig. 13.6 is a free-running ArF (193-nm) exciplex-laser-induced excitation profile of molecular oxygen in air, and shows in particular the Schumann-Runge absorption bands between the 192.5-nm and 194-nm wavelengths. These bands play a crucial role in the ArF-laser-induced photochemistry of molecular oxygen, especially as this photochemistry involves the dissociation of oxygen and the formation of ozone. In particular, the bands are indicative of the absorption of laser photons by molecular oxygen, leading to the excitation and subsequent dissociation of molecular oxygen into atomic oxygen, which can in turn react with molecular oxygen to form ozone. The net result of the absorption of laser photons by molecular oxygen, which these bands represent, is a reduction in laser output. Several P and R rotational lines of the (4,0) vibrational band of oxygen are shown in the spectrum of air in the free-running laser of Fig. 13.6. It should be pointed out that the relative intensities of the peaks associated with these bands have their lowest intensity around the 193.0-nm wavelength, and the highest intensity around 193.5 nm. Using a line-narrowed laser with a peak center wavelength

²¹K. Jain, *Excimer Laser Lithography*, p. 101, SPIE Press, Bellingham, WA (1990).

²²ibid., p. 103.

²³H.J. Levinson, *Principles of Lithography*, 2nd ed., p. 150, SPIE Press, Bellingham, WA (2005).

at 193.0 nm and a narrow bandwidth that does not overlap the high-intensity Schumann-Runge bands of molecular oxygen will prevent this reduction of ArF exciplex-laser output. This idea is illustrated in Fig. 13.7.

The impact of using free-running lasers on lithographic performance can range from focus shifts (due to instability of the center wavelength) to chromatic aberration (due to instability in bandwidth) to laser-induced optical damage (related to the laser pulse shape). (Some of these problems also occur in

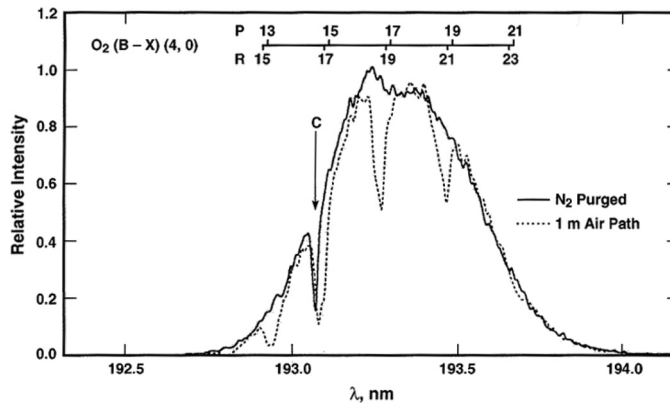


Figure 13.6 Spectrum of a free-running ArF exciplex laser in 1-m air path and in N_2 .²⁴

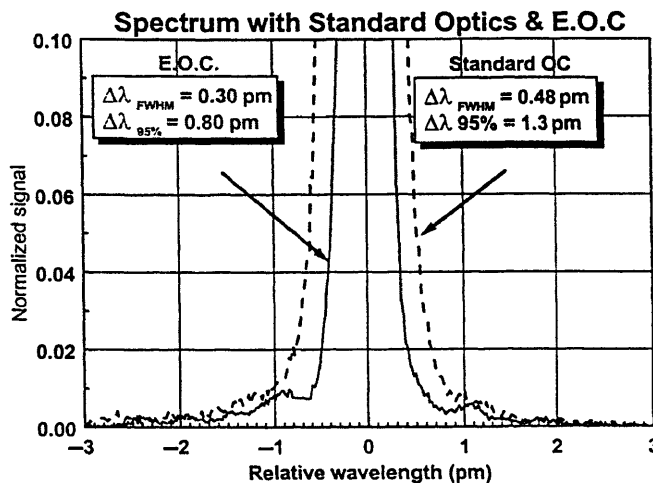


Figure 13.7 Spectra of line-narrowed ArF exciplex laser. The line was narrowed with both a standard output coupler and an etalon output coupler (EOC).²⁵

²⁴R. Sandstrom, "Argon fluoride excimer laser source for sub 0.25 μm optical lithography," *Proc. SPIE* **1463**, 610–616 (1991).

²⁵A.I. Ershov, H. Besaucele, and P.P. Das, "Performance characteristics of ultra narrow ArF laser for DUV lithography," *Proc. SPIE* **3679**, 1030–1037 (1999).

line-narrowed lasers.) It should, however, be pointed out that in many applications in lithography, the temporal characteristics of free-running exciplex and excimer lasers are satisfactory. Such applications include (i) contact and proximity tools, which are “bandwidth insensitive” since no optical image formation takes place in them; (ii) full-wafer scanning projection systems, which have a wide working bandwidth given their all-mirror projection system; (iii) step-and-repeat systems that use achromatic reduction projection lenses made with two optical materials such as quartz and calcium fluoride (these can be designed with color correction over the free-running exciplex and excimer laser bandwidth); and (iv) 1:1 imaging systems based on the catadioptric Wynne-Dyson design with capabilities for color correction over a bandwidth of several angstroms, given that the dominant imaging element is reflective.²⁶

On the other hand, steppers and step-and-scan exposure systems, with monochromatic, all-refractive optics, require a very narrow laser bandwidth, typically <1 pm, while those with catadioptric and moderate NA require bandwidths <100 pm.²⁷ This implies a line narrowing of up to two orders of magnitude relative to the free-running exciplex and excimer lasers. Several methods that have been reported to be effective in narrowing laser bandwidth include gratings,²⁸ prisms,²⁹ and combinations of gratings and Fabry-Perot etalons.³⁰

13.2.2 Illumination system

The functions of the illumination system include (i) spectral filtering, (ii) establishing a specified level of spatial coherence, (iii) controlling the exposure dose, and (iv) providing uniform radiation to the mask.³¹ How the illumination system performs the above functions is briefly discussed below.

The illumination system comprises a series of relay optics and uniformizing optics that project the radiation from the source through the photomask to the entrance pupil of the projection optics of the lithographic lens, where it forms an image of the illumination source (see Fig. 13.8). This type of illumination system is referred to as Köhler illumination.³² The fraction of the pupil filled by the illuminator source’s image determines the degree of coherence in the projection

²⁶K. Jain, *Excimer Laser Lithography*, p. 104, SPIE Press, Bellingham, WA (1990).

²⁷O. Semperez, “Excimer lasers for future lithography light sources,” *Solid State Technol.*, pp. 255–260 (July 2000).

²⁸*ibid.*

²⁹H.J. Kahlert, U. Rebhan, P. Lokai, and D. Basting, “Comparison of 248 nm line narrowing resonator optics for DUV lithography lasers,” *Proc. SPIE* **1463**, 604–609 (1991).

³⁰H.J. Levinson, *Principles of Lithography*, 2nd ed., p. 151, SPIE Press, Bellingham, WA (2005).

³¹*ibid.*, p. 154.

³²A. Köhler, “Gedanken zu Einem Neuen Beleuchtungsverfahren für Mikrographische Zwecke,” *Zeitschrift für wissenschaftliche Mikroskopie* (1893); D.C. O’Shea, *Elements of Modern Optical Design*, p. 113, John Wiley & Sons, Hoboken, NJ (1985).

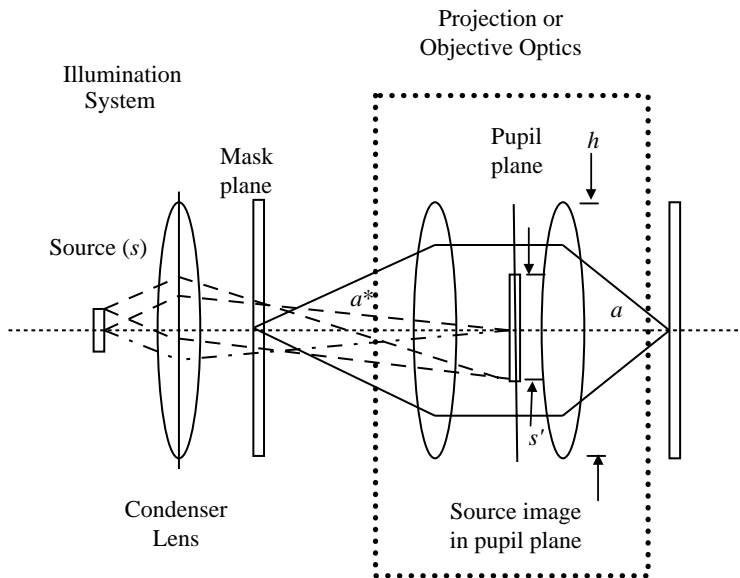


Figure 13.8 Köhler illumination schematic.

optics' image formation. The image of the source is the effective size of the source, and for a circularly shaped source the degree of coherence σ is given by

$$\sigma = \frac{s'}{h} = \frac{\sin \phi_{\max}}{\text{NA}} = \frac{\text{Source Diameter}}{\text{Lens Diameter}}, \quad (13.2)$$

where s' is the diameter of the source at the entrance pupil and h is the diameter of the entrance pupil; ϕ_{\max} is the maximum angle, measured from the normal, of light illuminating the mask, and NA is the numerical aperture of the objective lens.

The radiation traversing the entire chain of illuminator and projection optics forms an aerial image of the mask that is projected onto the resist-coated wafers. A fast shutter within the illuminator assembly exposes the photoresist to the image for a very short period of time, on the order of a few tenths of a second. The integrated energy of each exposure must be repeatable to within 1%, such that the illumination of the reticle is fairly uniform ($< \pm 1\%$) over a large area, a feat it accomplishes with the aid of a number of methods, including the use of fly's eyes³³ and rods.³⁴

A fly's eye arrangement, it should be noted, consists of an array of lenslets, each of which images part of the light source over the entire field to be illuminated, which has the effect of averaging the amount of radiation over the field.³⁵

³³R. Voelkel, H.P. Herzig, P. Nussbaum, R. Daendiliker, and W.B. Hugel, "Microlens array imaging system for photolithography," *Opt. Eng.* **35**, 3323–3330 (1996).

³⁴J. van Schoot, F. Bornebroek, M. Suddendorf, M. Mulder, J. Van der Spek, J. Stoeten, and A. Hunter, "0.7 NA DUV step & scan system for 150 nm imaging with improved overlay," *Proc. SPIE* **3679**, 448–463 (1999).

³⁵H.J. Levinson, *Principles of Lithography*, 2nd ed., p. 155, SPIE Press, Bellingham, WA (2005).

The dose control function of the illuminator is accomplished through real-time measurement of the radiation intensity in a scheme whereby a small fraction ($\leq 1\%$) of the radiation is picked off with the aid of a beam splitter and measured with the aid of appropriate detectors. By integrating the radiation dose from the time the shutter is opened to when it closes, when the correct amount of dose has been delivered, a feedback loop based on the intensity from the picked-off beam is used to control the scanning speed in step-and-repeat systems. Constant dose on the wafer is achieved by decreasing the scanning speed of both the reticle and wafer by an appropriate percentage that compensates for decreases in radiation intensity reaching the wafer plane.³⁶ Most modern lithographic exposure tools based on both step-and-repeat and step-and-scan systems have radiation intensity detectors on the wafer stage, which is used in periodic checks of the dose control system. The calibration of the detector on the wafer stage requires the use of an external energy monitor.³⁷

13.2.3 Mask and reticles

The history of mask-making tools runs somewhat parallel to that of the wafer-exposure tools. Starting from the 1960s, masks were made in a process in which drafting of large drawings of the circuit pattern to be printed were made by hand on Rubylith (masking films), followed by cutting and laying out thin strips of the Rubylith with the circuit pattern. Cameras with reduction lenses were then used to reduce the drawing to appropriate size, and photorepeaters were used to reproduce the circuit image on a resist-coated mask blank, exposing the mask one chip at a time, and resulting in a mask master. The master mask was produced from chrome on glass. Then, film emulsion copies were made from the master. In order to distinguish between the mask with multiple chips and the master object containing the pattern of only one chip, the single-chip mask was called a reticle, while the name mask was reserved for masks with multiple chips.³⁸

The 1970s witnessed the development of the computer-aided design (CAD) system, which created the market for pattern generators—exposure systems capable of taking the bit patterns from a CAD system and directly patterning a 10:1 reticle. Such pattern generators eliminated the need for Rubylith. The reticle generated from the pattern generator was subsequently used in a photorepeater to reduce the image and repeat it over the mask.³⁹

While the original pattern-generation tools of the early 1970s were optical systems, in 1974, AT&T Bell Laboratories introduced an electron-beam direct exposure mask-making system called MEBES,⁴⁰ which was subsequently licensed to ETEC for commercialization. By 1980, electron-beam mask writers became

³⁶ibid., p. 156.

³⁷The U.S. National Institutes of Standards and Technology provides absolute calibration of such detectors; see, for example, R.W. Leonhardt and T.R. Scott, "Deep UV excimer laser measurements at NIST," *Proc. SPIE* **2439**, 448–459 (1995).

³⁸"Microlithography & mask making," VLSI Research Inc. Report (1992).

³⁹ibid.

⁴⁰ibid.

widely accepted because of the flexibility of the equipment and the better registration of electron beam-made masks, as well as the fact that devices could be easily scaled by mere reduction of the spot size on the raster-scanning electron-beam systems. And by the early 1980s, laser direct-write systems were developed by ATEQ that offered a faster and thus less expensive alternative to electron-beam systems. These systems were more stable because laser beams are inherently more stable than electron beams, although they offered lower resolution than electron beams.⁴¹

Masks and reticles contain the blueprints or the patterns of the circuit elements used as templates in the fabrication of IC devices. They provide the templates of the circuit elements from which numerous replications, perhaps numbering in the millions, are made. The object of lithography is to transfer these blueprints to semiconducting substrates such as silicon wafers.

The quality of printed wafer feature patterns, as measured by line width control, overlay, and defects, is strongly dependent on the quality of the corresponding parameters on the masks. For instance, line width variations on the mask result in line width variations on the wafer, just as mask registration errors contribute to overlay errors on the wafer, and mask defects may produce defects on the wafer and may ultimately lead to a nonfunctional device die. All of the above problems are of course magnified in step-and-repeat systems, given the repetitive nature of their imaging. In fact, the very repetitive nature of imaging in both step-and-repeat and step-and-scan systems imposes stringent requirements on masks in terms of line width control, overlay, and defectivity, especially for $1\times$ exposure systems, i.e., printed features having the same size as those on the mask.⁴²

For reduction projection systems, dimensions on the reticle are printed with demagnification onto the wafer. The effective mask dimension error is expected to be reduced by the demagnification factor. For imaging large mask features, a unit of error on the mask corresponds to a unit change in printed size scaled by the reduction ratio of the exposure system.⁴³

$$\Delta CD_{\text{printed}} = \frac{\Delta CD_{\text{mask}}}{M}, \quad (13.3)$$

where the demagnification factor M is typically 4 or 5 in commonly available projection exposure systems.

However, in the imaging of small features [with sizes $<0.75(\lambda/NA)$ for a contact and $<0.5(\lambda/NA)$ for a line and space], the effective mask dimension error is magnified and is described by the mask error enhancement factor (MEEF),⁴⁴ such that the relation between mask dimension error and wafer line

⁴¹ibid.

⁴²H.J. Levinson, *Principles of Lithography*, 2nd ed., p. 243, SPIE Press, Bellingham, WA (2005).

⁴³A.K. K. Wong, *Resolution Enhancement Techniques in Optical Lithography*, 2nd ed., p. 10, SPIE Press, Bellingham, WA (2001).

⁴⁴W. Mauer, "Mask specifications for 193 nm lithography," *Proc. SPIE* **2884**, 562–571 (1996); P. Yan, R. Hainsey, J. Farnsworth, and J. Neff, "Sub micron low k_1 imaging characteristics using a DUV printing tool and binary masks," *Proc. SPIE* **2440**, 270–276 (1995); F. Lo, G. Dao, M. Berube, N. Tam, R. Hainsey, J. Farnsworth, J. Dewitt, R. LaVoy, and S. Daugherty, "Ever increasing role of

width variation is given by⁴⁵

$$\Delta CD_{\text{printed}} = \text{MEEF} \times \frac{\Delta CD_{\text{mask}}}{M}. \quad (13.4)$$

For small features, MEEF is typically greater than 1, and can be as high as 3 or 4.

As a consequence, the reticle dimension control is a major concern with shrinking critical dimension and tolerance. The difference between the effective mask feature size (the reticle dimension divided by the exposure system reduction factor) and the target developed resist dimension is called the mask bias.

13.2.3.1 Classification of masks

Masks are sometimes classified on the basis of their tones into light-field and dark-field masks. If most of the mask area is bright, the mask is called a light-field, bright-field, or clear-field mask. If however, the mask is mostly covered with dark regions, it is called a dark-field mask.

13.2.3.2 Mask types and mask materials

There are two main types of masks, namely, binary intensity masks (BIMs) and phase-shifting masks (PSMs). BIMs have regions that are either transparent or opaque, and usually consist of a coating of a (dark) chromium, a chromium-containing compound layer, or a molybdenum-containing layer approximately 80-nm thick on a (clear) glass substrate.⁴⁶ Chromium and chromium-containing compounds are the most common opaque materials used for fabricating photo-masks. Typically, the films of chromium and chromium-containing compounds are sputtered onto the glass substrates to thicknesses between 50 nm and 110 nm.⁴⁷ The optical constants of chromium at different lithographic wavelengths are given in Table 13.3.

A consequence of the high absorption of chromium at the indicated lithographic wavelengths is mask heating during exposure,⁴⁸ which causes magnification errors, with dark-field masks being more sensitive to this issue than their bright-field counterparts.

mask technology in deep submicron lithography,” *Proc. SPIE* **2254**, 2–13 (1994); P. Yan and J. Langston, “Mask CD control requirement at 0.18 μm design rules for 19 nm lithography,” *Proc. SPIE* **3051**, 164–169 (1997); J. Wiley and J. Reynolds, “Device yield and reliability by specification of mask defects,” *Solid State Technol.* **36**(7), 65–66, 70, 72, 74, 77 (1993); A. Wong, R. Ferguson, L. Liebermann, S. Mansfield, A. Molless, and M. Nessler, “Lithographic effects of mask critical dimension error,” *Proc. SPIE* **3334**, 106–116 (1998); A. Wong, R. Ferguson, and S. Mansfield, “The mask error factor in optical lithography,” *IEEE Trans. Semiconductor Manuf.* **13**(2), 235–242 (2000).

⁴⁵A.K. K. Wong, *Resolution Enhancement Techniques in Optical Lithography*, p. 11, SPIE Press, Bellingham, WA (2001).

⁴⁶*ibid.*, p. 11.

⁴⁷H.J. Levinson, *Principles of Lithography*, 2nd ed., p. 247, SPIE Press, Bellingham, WA (2005).

⁴⁸J. Chang, A. Abdo, B. Kim, T. Bloomstein, R. Englestad, E. Lovell, W. Beckman, and J. Mitchell, “Thermomechanical distortions of advanced optical reticles during exposure,” *Proc. SPIE* **3676**, 756–767 (1999).

Table 13.3 Optical characteristics of chromium films at different lithographic wavelengths.⁴⁹

Wavelength (nm)	Refractive index ⁵⁰	Reflection R from chromium glass interface	Transmission T through a 60 nm film of chromium	$(1 - R) \times T \times 100\%$
436	1.79 4.05 <i>i</i>	0.60	0.0009	0.036
365	1.39 3.24 <i>i</i>	0.56	0.0012	0.055
248	0.85 2.01 <i>i</i>	0.47	0.0022	0.119
193	0.84 1.65 <i>i</i>	0.38	0.0016	0.098
157	0.68 1.11 <i>i</i>	0.32	0.0048	0.310

BIMs are also often called chromium-on-glass (COG) masks. Borosilicate glass was used in some i-line (365-nm) reticles, but because of excessive absorption in the DUV region of the spectrum, they could not be used in KrF and ArF lithographies at 248-nm and 193-nm wavelengths, respectively. Instead, fused silica, which offers the additional advantage of a lower thermal expansion coefficient, became the standard glass material used in reticles for ArF and KrF exciplex laser lithographies, and even for much longer-wavelength lithographies such as g-line and i-line lithographies. At the 157-nm wavelength, fluorine-doped fused silica is used to improve reticle transparency in F₂ excimer laser lithography.⁵¹

PSMs are masks that transmit light consisting of two or more phases. The essence of this type of mask in relation to conventional masks is illustrated in Fig. 13.9. It is well established that light interference occurs during exposure of conventional masks with tight lines and spaces. The amplitude of the light on the wafer blends, resulting in positive intensity across the wafer, which causes some exposure in unintended areas of the resist. The net result is a loss of optical contrast in the center of the dark feature. In contrast, in PSMs, the phase shifter (the added transparent or translucent film) shifts light amplitude of the center mask window to 180 deg out of phase. Because adjacent profiles are 180 deg out of phase, the amplitude in the overlap area under the chrome at the wafer plane is reduced to zero from destructive interference of the light waves, and the resulting contrast of the intensity profile is significantly enhanced over that produced by the BIM. The net result is a significant increase in optical contrast and enhanced resolution for fine dark features.⁵²

The four main types of PSMs include the following: (i) attenuated PSMs⁵³ [Fig. 13.10(a)], which are similar to COG masks except that the opaque chromium

⁴⁹Adapted from H.J. Levinson, *Principles of Lithography*, 2nd ed., p. 247, SPIE Press, Bellingham, WA (2005).

⁵⁰E.D. Palik, Ed., *Handbook of Optical Constants of Solids II*, Academic Press, San Diego (1991).

⁵¹A.K. K. Wong, *Resolution Enhancement Techniques in Optical Lithography*, p. 12, SPIE Press, Bellingham, WA (2001).

⁵²M.J. Bowden, "The lithographic process: the physics," in *Introduction to Microlithography*, 2nd ed., L.F. Thompson, C.G. Willson, and M.J. Bowden, Eds., pp. 78–79, American Chemical Society, Washington, DC (1994).

⁵³B.J. Lin, "The attenuated phase shifting mask," *Solid State Technol.* **35**(1), 43–47 (1992); T. Terasawa, N. Hasegawa, and H. Fukuda, "Imaging characteristics of multi phase shifting and half tone phase shifting masks," *Jpn. J. Appl. Phys.* **30**(11B), 2991–2997 (1991).

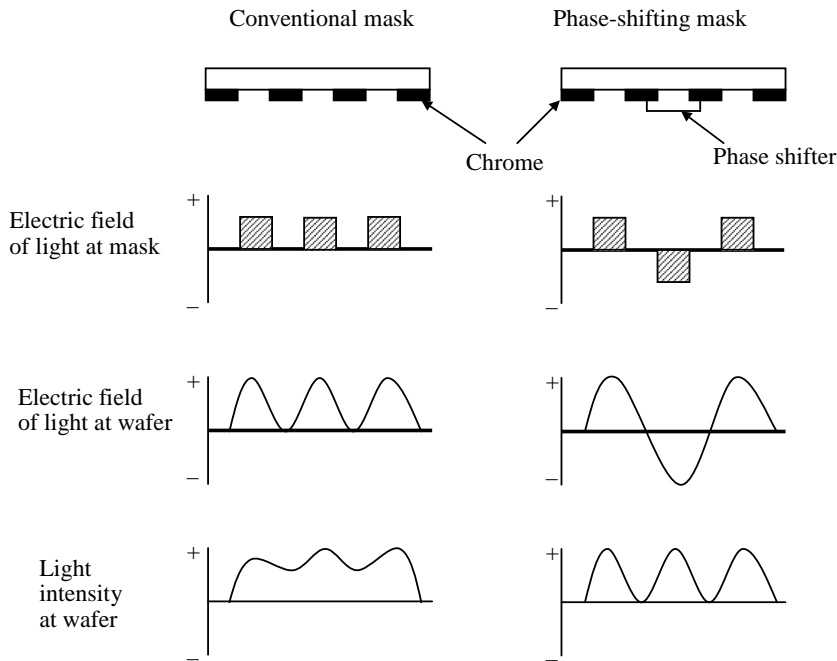


Figure 13.9 Conventional and phase-shifting mask technology basics.

is replaced by a partially transmitting layer with a 180-deg phase difference with respect to the clear regions: (ii) rim PSMs⁵⁴ [Fig. 13.10(b)], with a rim containing subresolution features bordering the phase region and a 180-deg phase difference with respect to the phase region: (iii) alternating PSMs⁵⁵ [Fig. 13.10(c)], with neighboring transmitting regions having the same transmittance but that are 180 deg out of phase (the two phase areas are separated by opaque areas): (iv) chromeless PSMs⁵⁶ [Fig. 13.10(d)] having neighboring phase

⁵⁴A. Nitayama, T. Sato, and K. Hashimoto, "New phase shifting mask with self aligned phase shifters for a quarter micron photolithography," *Tech. Digest Int. Electron Dev. Meet.*, pp. 3.2.1–3.2.4 (1989).

⁵⁵M. Levenson and N. Viswanathan, R. Simpson, "Improving resolution in photolithography with a phase shifting mask," *IEEE Trans. Electron Dev.* **29**(12), 1812–1846 (1982); L. Liebermann, I. Graur, W. Leipold, J. Oberschmidt, D. O'Grady, and D. Regaill, "Alternating phase shifted mask for logic gate levels, design and mask manufacturing," *Proc. SPIE* **3679**, 27–37 (1999); H. Y. Liu, L. Karklin, Y. T. Wang, and Y.C. Pati, "The application of alternating phase shifting masks to 140 nm gate patterning: linewidth control improvements and design optimization," *Proc. SPIE* **3236**, 328–337 (1998); S. Nakao, A. Nakae, K. Tsujita, and W. Wakamiya, "Impact of spherical aberrations on printing characteristics of irregularly aligned patterns of alternating phase shift mask," *Jpn. J. Appl. Phys.* **38**(4A), 1919–1926 (1999); R. Schenker, "Effects of phase shift masks on across field linewidth control," *Proc. SPIE* **3679**, 18–26 (1999).

⁵⁶K. Toh, G. Dao, R. Singh, and H. Gaw, "Chromeless phase shifted masks: a new approach to phase shifting masks," *Proc. SPIE* **1496**, 27–53 (1990).

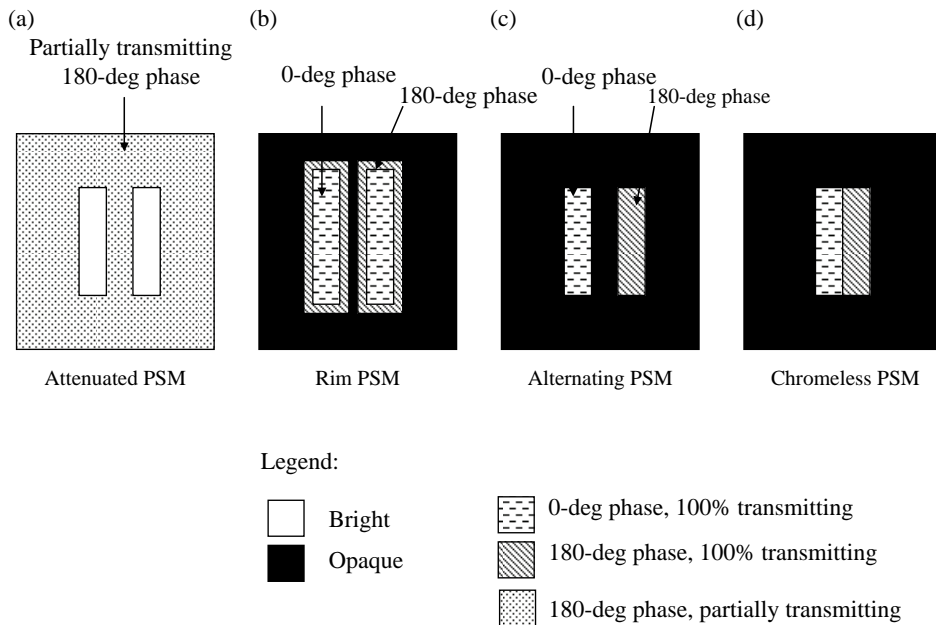


Figure 13.10 Types of phase-shifting masks.⁵⁷

regions forming a border with each other directly, without any opaque area in between. Chromeless PSMs are similar to attenuated PSMs, except that they have 100% transmission.⁵⁸

13.2.3.3 Fabrication of photomasks

The fabrication of a lithographic mask involves the transformation of computer-aided designs of an IC into a physical layout to create a geometrical pattern of the mask. Coordinates of the IC layout are digitized and stored in appropriate electronic storage media such as tapes. The pattern is then transferred onto the surface of chrome-quartz plates or appropriate substrates, depending on the mask type.⁵⁹

The mask-making process consists of generating the pattern of the circuit on a chrome-covered quartz plate coated with a resist film. There are four types of equipment used in writing mask optical pattern generators, electron-beam writers, focused-ion-beam writers, and laser writers. Lithographic exposure of the resist-coated, chrome-covered quartz plate involves the repeated exposure of the circuit pattern with a stepper or a scanner. In earlier times, lithographic

⁵⁷ibid., p. 13.

⁵⁸A.K. K. Wong, *Resolution Enhancement Techniques in Optical Lithography*, pp. 12–13, SPIE Press, Bellingham, WA (2001).

⁵⁹“Microlithography & mask making,” VLSI Research Inc. Report (1992).

exposure of mask-making resists was done with photorepeaters. The choice of specific resist tone is made to be consistent with the mask type. Bright-field masks are generally made with negative resists, and dark-field masks are generally made with positive resists.⁶⁰ The exposed resist is developed, revealing the appropriate areas of the opaque material, which is subsequently etched so as to transfer the resist image into the mask blank.

13.2.3.3.1 Optical pattern generator

This system focuses light through lenses and apertures to create circuit patterns on the mask. Using stored digital patterns to drive a computer-controlled variable aperture, it exposes the photoresist-coated mask blank with the same pattern as the digitized IC layout. Each exposure typically consists of a single rectangle. The mask blank is held on a laser-interferometrically controlled stage and moved between exposures, until the entire circuit pattern is reproduced on the mask blank.⁶¹ Postexposure processing comprising baking and development produces a three-dimensional pattern of the IC design. Limitations in resolution and throughput made these systems obsolete in the mid-1980s.

13.2.3.3.2 Electron-beam writers

In electron-beam writers, electrons are focused into narrow beams and used to expose resist-coated mask blanks with digitized patterns of the IC device layer. Over moderate distances (<1 mm), pixels can be exposed by deflection of the electron beam in contrast to the mechanical stage movement required by optical pattern generators, thereby greatly increasing throughput. In addition to having good sensitivity to an electron beam, the resists used in this application must be resistant to chromium etchants.⁶² The most popular electron-beam patterning tools used in mask making originated in the electron-beam exposure system (EBES) developed at Bell Telephone Laboratories in Murray Hill, New Jersey.⁶³ This technology was eventually licensed by Etec Systems, now a subsidiary of Applied Materials.⁶⁴

There are two methods for scanning electron beams, i.e., the raster method and the vector method. While the raster technique was more often used for mask making until about 2000, vector scanning is now preferred for mask making and for direct wafer exposures. In raster scanning, each pixel in a field is exposed as the beam is scanned back and forth by the electron optics. Simply put, the beam is turned on and off to expose needed pixels on a mask substrate. This approach

⁶⁰ibid.

⁶¹H.J. Levinson, *Principles of Lithography*, 2nd ed., p. 247, SPIE Press, Bellingham, WA (2005).

⁶²ibid., p. 248.

⁶³D.R. Herriot, R.J. Collier, D.S. Allen, and J.W. Stafford, "EBES: a practical electron lithography system," *IEEE Trans. Electron Dev.* **ED-22**, 385–392 (1975).

⁶⁴H.J. Levinson, *Principles of Lithography*, 2nd ed., p. 248, SPIE Press, Bellingham, WA (2005).

makes for easy scaling to smaller dimensions because spot sizes are all that need to be reduced since it is a bit map image.

EBES systems are based on raster scans. In contrast, vector scanning has more resemblance to a small floodlight than a pencil beam. Here, the beam moves on a vector path that directly exposes the entire region needed, before turning on the beam and writing the pattern. Next, the beam is turned off and repositioned over another pattern for exposure. The vector scan is faster because the beam wastes no time rastering over areas that do not need exposure. However, it is more difficult to scale since all vectors must be recalculated to reduce size.⁶⁵

13.2.3.3.3 Laser writers

As their name implies, laser writers use laser beams that are scanned in a raster fashion to write masks. There are two popular designs for mask laser writers; one is based on the ALTA systems⁶⁶ produced by Etec Systems, and the other is based on the Sigma systems produced by Micronic Laser Systems AB. An argon ion laser operating at a wavelength of 364 nm, and the second-harmonic generation of the 514-nm Ar laser line, which produces DUV radiation at 257-nm wavelength,⁶⁷ are good examples of lasers used in the ALTA type of mask writers. The laser radiations from the above sources are passed through conditioning optics and a laser-interferometrically controlled stage. An alignment system that enables the overlay of second patterns to preexisting patterns on the mask is also present in the advanced versions of the ALTA writers.⁶⁸

In laser writers from Micronic Laser Systems AB, patterning is done with the aid of micromirror arrays. The radiation is produced from KrF excimer lasers. After conditioning by the illuminator optics, the light is reflected from a beam splitter onto a spatial light modulator (SLM), which is an array of 10^6 mirrors, each of which is $16\ \mu\text{m} \times 16\ \mu\text{m}$ in size. The mirrors are deflected to produce the desired pattern on the reticle substrate in a manner that is programmable.⁶⁹

In general, laser writers offer some unique advantages. With multiple laser beams (up to 32 in some systems), these systems are capable of high throughput and are therefore considerably faster than their electron-beam-writer counterparts. They are also more accurate than electron-beam writers because they are more stable, a consequence of the facts that electrons are very sensitive to magnetic fields and also tend to scatter. The very small effective address unit is useful for fine adjustment of line widths on the mask, which makes it easier to implement optical proximity correction schemes in these masks than in masks produced from other mask writers. Furthermore, laser writers operating at 364-nm and

⁶⁵“Microlithography & mask making,” VLSI Research Inc., Report (1992).

⁶⁶H.C. Hamaker and P.D. Buck, “Performance of a new high NA scanned laser mask lithography system,” *Proc. SPIE* **3236**, 42–54 (1997).

⁶⁷P.C. Allen, “Laser pattern generation technology below 25 μm ,” *Proc. SPIE* **3334**, 460–468 (1998).

⁶⁸H.J. Levinson, *Principles of Lithography*, 2nd ed., p. 258, SPIE Press, Bellingham, WA (2005).

⁶⁹*ibid.*, p. 259.

257-nm wavelengths make use of well-characterized optical resists used in wafer patterning.⁷⁰ They are also less expensive. A major limitation of laser writers is their lower resolution than electron-beam writers.

13.2.3.4 Mask-making resists

The choice of a particular mask-making resist⁷¹ is determined by the sensitivity of the particular resist to the mask-writing exposure wavelength or charged particles, temperature variation, and environmental contamination. For many years, the standard practice was for mask makers to use mask blanks precoated with resist by the blank supplier. Since standard i-line resists are sufficiently stable, this presented no problem. However, as the IC industry migrated to resists based on chemical amplification principles (to take advantage of their superior sensitivity to conventional resists), which by nature tend to be sensitive to environmental contamination, the necessity arose for the mask shops to coat the mask blanks themselves, immediately prior to exposure. This also required baking the resists after exposure at well-controlled temperatures, a rather difficult undertaking, given that glass substrates are quite thick.⁷²

Typical optical and laser writer mask-making resists include 895i from ARCH (formerly OCG and now Fuji Films) and iP3500 from TOK for 364-nm exposure systems. Typical resists for electron-beam writers include poly(butene-1-sulfone) (PBS) developed at Bell Laboratories, EBR-900 M1 (novolac-based resist) from Toray Industries, ZEP 7000 from Nippon Zeon, and KRS-XE from IBM.⁷³

13.2.3.5 Etching of mask-making resists

Following development of the exposed features, etching of the resist patterns on the mask for many years was done with wet etchants based on a mixture of ceric ammonium nitrate $[\text{Ce}(\text{NH}_4)_2(\text{NO}_3)_6]$ and nitric acid, perchloric acid, or acetic acid.⁷⁴ Resist patterns subjected to wet etching are susceptible to undercut, which invariably contributes to line width variations on the mask. For this reason, masks for critical applications are dry etched. Because CrO_xCl_y species are volatile,⁷⁵ typical chromium etches involve mixtures of Cl_2 and O_2 , with additional

⁷⁰ibid., p. 258.

⁷¹The chemistry of negative tone and positive tone mask making resists is covered in Chapters 6 and 7, respectively.

⁷²H.J. Levinson, *Principles of Lithography*, 2nd ed., SPIE Press, Bellingham, WA, p. 259 (2005).

⁷³ibid., pp. 259–261.

⁷⁴See, for example, “Chromium etchants applications notes,” Cyanetec Corp., Fremont, CA [cited in H.J. Levinson, *Principles of Lithography*, 2nd ed., p. 261, SPIE Press, Bellingham, WA (2005)].

⁷⁵B.J. Curtis, H.R. Brunner, and M. Ebnoether, “Plasma processing of thin chromium films for photo masks,” *J. Electrochem. Soc.* **130**(11), 2242–2249 (1983).

gases added to reduce etch loading effects that can negatively impact isolated dense bias in the CD of patterned features.⁷⁶

Furthermore, because chromium has proven difficult to dry etch, there have been considerable efforts expended in finding alternative mask opaque absorber materials. Molybdenum silicide (MoSi) appears to be gaining traction in certain applications, particularly in attenuated phase-shifting mask (att-PSM) and EUV mask applications (see Section 14.3), and even for binary masks.⁷⁷

13.2.4 Pellicles

Pellicles, which were introduced in the early 1980s,⁷⁸ keep dust particles and other hard defects far enough off the reticle surface that their image prints out of focus and not on the resist. This improves yields substantially, which was responsible for their widespread deployment across the industry.

Pellicles are thin ($\sim 1 \mu\text{m}$) polymer films (mostly nitrocellulose and Teflon) stretched across a frame that is attached to the mask (see Fig. 13.11). Frame heights are typically in the 5–10-mm range, with 6.35 mm (the thickness of the mask blank) being the most common. Particles deposited on the pelliclized mask fall onto the pellicle or glass back side of the mask, and being several millimeters away from the chrome features that are being imaged, will print out of focus and therefore not affect the image quality.⁷⁹

Pellicle frames are usually made of anodized aluminum, into which are drilled small holes for equalizing the pressure of air in the space enclosed by the mask and pellicle with that of the ambient air pressure.⁸⁰ These holes are extremely small, in

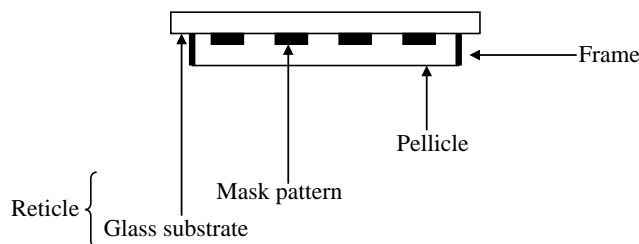


Figure 13.11 Cross-sectional view of a reticle with an attached pellicle.

⁷⁶S. Aoyama, S. Sakamoto, T. Koike, N. Yoshioka, N. Harashima, A. Hayashi, and T. Sasaki, “Advanced Cr dry etching process,” *Proc. SPIE* **3748**, 137–146 (1999).

⁷⁷H.J. Levinson, *Principles of Lithography*, 2nd ed., SPIE Press, Bellingham, WA, p. 262 (2005).

⁷⁸R. Hershel, “Pellicle protection of integrated circuit (IC) masks,” *Proc. SPIE* **275**, 23–28 (1981).

⁷⁹H.J. Levinson, *Principles of Lithography*, 2nd ed., p. 262, SPIE Press, Bellingham, WA (2005).

⁸⁰R.W. Murphy and R. Boyd, “The effect of pressure differentials on pelliclized photomasks,” *Proc. SPIE* **2322**, 187–210 (1994).

order to prevent them from becoming routes for particles to enter the space between the pellicle and mask.⁸¹

While the holes in the pellicle frame are effective in preventing particles from entering the space between the pellicle and mask, they are not effective in preventing airborne molecular contaminants such as ammonia, sulfur dioxide, water vapor, etc. from reaching this space. Under DUV illumination, these contaminants react together to form ammonium sulfate crystals on the reticle, discussed in Section 13.3.4.⁸² In addition, molecular contaminants can outgas from pellicle adhesives and from degradation products of the interaction of pellicles with DUV radiation.

It should be pointed out that because mask substrates are made of glass, which is an insulator, they are very susceptible to damage from electrostatic discharge (ESD).⁸³ Sparks from discharges can cause the mask absorber material to melt and can lead to bridging across gaps on the mask.⁸⁴ Another mask problem related to ESD damage is electric-field-induced metal (EFM) migration.⁸⁵ In photomasks, this problem manifests as the migration of chromium ions from the mask absorbers and their deposition and oxidation in and around features in the clear areas of the mask (see Section 13.3.5). The result is a degradation of CD uniformity of mask patterns.

13.2.5 Exposure optics system

The exposure optics system comprises the set of optics (mirrors and lenses) that delivers the aerial image of the mask to the resist-coated wafer on the exposure stage. There are two categories of such systems. Contact and proximity optics systems are the simplest and the least expensive of the systems, but are not well suited for high-volume IC manufacture because of their high level of defectivity. The other system, the projection optics system, is predominantly used in modern semiconductor manufacturing. Both systems rely on the entire mask, or at least a portion of it, to be imaged simultaneously.

The use of optical lithography in silicon IC device fabrication dates back to the mid-1950s when Andrus employed it at Bell Laboratories to define precise

⁸¹H.J. Levinson, *Principles of Lithography*, 2nd ed., pp. 262–263, SPIE Press, Bellingham, WA (2005).

⁸²B.J. Grenon, C. Peters, K. Battacharyya, and W. Volk, “Formation and detection of sub pellicle defects by exposure to DUV systems illumination,” *Proc. SPIE* **3873**, 162–176 (1999); B.J. Grenon, C. Peters, K. Battacharyya, W. Volk, and A. Poock, “Reticle surface contaminants and their relationship to sub pellicle particle formation,” *Proc. SPIE* **5256**, 1103–1110 (2003).

⁸³A.C. Rudack, L.B. Levit, and A. Williams, “Mask damage by electrostatic discharge: a reticle print ability evaluation,” *Proc. SPIE* **4691**, 1340–1347 (2002).

⁸⁴H.J. Levinson, *Principles of Lithography*, 2nd ed., p. 267, SPIE Press, Bellingham, WA (2005).

⁸⁵G. Rider, “Estimation of the field induced damage thresholds in reticles,” *Semicond. Manuf.*, pp. 80–94 (Feb., 2004).

windows on silicon oxide substrates that were subsequently opened by chemical etching, and through which dopant impurities were diffused into the underlying silicon to establish the *n*-type and *p*-type regions needed in semiconductor devices.⁸⁶ This event aided the development of the mesa transistor at Texas Instruments in 1957, which first made use of thermally grown silicon oxides in conjunction with a photoresist, followed by an etch step, as well. It was, however, the subsequent development of the planar transistor by Hoerni at Fairchild in 1959 that provided the impetus for growth and paved the way for the development of ICs.⁸⁷ Since that seminal event, both ICs and optical lithographical exposure tools have developed together, hand-in-glove fashion.

In the following sections, we delve a little more in depth into lithographic exposure tool photochemistry, lithographic optical materials, and the different modes of lithographic printing, along with the historical background surrounding them. We will also discuss the various forms of optical lithography, emphasizing unique attributes of the equipment and materials, and the process issues involved in each form.

13.3 UV Photochemistry in the Exposure Chamber Environment of Optical Lithographic Tools

The exposure chambers of optical lithographic tools used in UV lithography, in particular mid-UV (365 nm) and DUV (248 nm and 193 nm), contain clean dry air at approximately atmospheric pressure. Those operating in VUV (157 nm) contain nitrogen at roughly one atmosphere of pressure. Those operating in EUV (13.5 nm) are under vacuum, at roughly 10^{-6} torr, while those in x-ray lithographic tools contain air at one atmosphere of pressure. The interactions of the exposure photons with the above contaminants in the ambient environments within the above tools result in unique photochemistries that have significant implications for the quality of the printed features,⁸⁸ the contamination of optical elements, and the degradation of bulk optical materials and mask absorber materials, as well as the overall lifetime of various components of exposure tools. These interactions also present radiation hazards to humans working with such tools.⁸⁹

⁸⁶J. Andrus, "Fabrication of semiconductor devices," U.S. Patent No. 3,122,817 (1964); J. Andrus and W.L. Bond, "Photoengraving in transistor fabrication," in *Transistor Technology*, Vol. III, F.J. Biondi et al. Eds., Van Nostrand, Princeton, pp. 151–162 (1958).

⁸⁷J.A. Hoerni, "Planar silicon transistors and diodes," *IRE Int. Electron Devices Meet.*, Washington, DC (1960).

⁸⁸U. Okoroanyanwu, P. Kunze, K. Al Shamery, J. Romero, and J. Bernard, "Impact of photoinduced species in O₂ containing gases on lithographic patterning at 193 nm wavelength" *Proc. SPIE* **4691**, 746 (2002).

⁸⁹See, for example, P. Veechia, H. Hiatenen, B.E. Stuck, E.V. Denventer, and S. Niu, Eds., "Protecting Workers from Ultraviolet Radiation," Int. Commission on Non Ionizing Radiation (ICNIR) Report No. 14/2007, <http://www.icnirp.org/documents/UVWorkers.pdf> (2007).

The ambient environment within exposure tools typically contains residual amounts of airborne gases such as H₂O, O₂, CO, and CO₂, volatile and condensable organic compounds, inorganic acidic gases such as SO₂ and NO_x, and Si–O compounds such as silicones and siloxanes. These not only can attenuate the exposure light, but can on interaction with the DUV and VUV photons serve as precursors for photoinduced species that can directly degrade optical elements, or that on reaction with each other may form stable contamination layers on optical surfaces. Because of their compositional inhomogeneities, coupled with the differences in their refractive indices relative to that of the optical elements, these contamination layers invariably cause light scattering, thereby reducing image contrast. In the extreme case, contamination can render the optical elements unusable, thereby necessitating their replacement. Most frequently, contamination causes significant variation in CD uniformity, due largely to light scattering off of contaminated optical surfaces or due to variation in the intensity of the radiation flux reaching the wafer plane on account of light absorption by volatile molecular contaminants. The contaminants may be introduced into the exposure tool from a variety of sources such as outgassing of the tool's construction materials, sealing compounds and adhesives, purge nitrogen, filter breakthrough, outgassing from photoresist, etc. Table 13.4 is a summary of the types of common airborne molecular contaminants (AMCs) in the clean room, their sources, and effects.⁹⁰

Although contamination control is implemented in these exposure tools with on-board purge control units, which are equipped with gas purifiers that remove contaminants such as H₂O, O₂, CO, CO₂, hydrocarbons, H₂, and sulfur compounds, these control units are oftentimes not 100% efficient. Typical benefits of molecular contamination control include improved process yield and greater process control.

13.3.1 UV absorption properties of typical gases in lithographic exposure tools

Figure 13.12 shows the UV absorption profile of typical gases found (O₂, H₂O) and formed (O₃) in the ambient environment of exposure tools. The Schumann-Runge band (180–210-nm) and continuum (<180-nm) regions dominate the photochemistry of molecular oxygen around 193 nm (of ArF excimer laser) and 157 nm (of F₂ excimer laser), respectively.

The absorption coefficient of oxygen at 193.1 nm was reported to be 0.0186 cm⁻¹ atm⁻¹, while the quantum yield of ozone formation at 193.1 nm by decomposition of excited oxygen molecules was reported to be 0.3 between 300 and 1300 torr.⁹¹ The low bond strength of ozone and its large absorption

⁹⁰U. Okoroanyanwu, P. Kunze, K. Al Shamery, J. Romero, and J. Bernard, "Impact of photoinduced species in O₂ containing gases on lithographic patterning at 193 nm wavelength," *Proc. SPIE* **4691**, 746 (2002).

⁹¹N. Washida, Y. Mori, and I. Tanaka, "Quantum yield of ozone formation from photolysis of the oxygen molecule at 1849 and 1931 Å," *J. Chem. Phys.* **54**(3), 1119–1122 (1970).

Table 13.4 A airborne molecular contaminants in the clean room.

Class	Contaminant	Source	Effects
Molecular acids	Fluorides, chlorides, bromides, sulfates, phosphates, nitrogen/oxygen compounds	Etch chambers, diffusion furnaces, CVD processes, buffered oxide etch, wet benches using HCl, HF	Forms haze crystals on reticles, wafers, and exposure tool optical elements, causes corrosion of Al and Cu metal lines
Molecular bases	Ammonia	CVD, HMDS, CMP slurries, wafer cleaning processes, TiN and Si ₃ N ₄ films deposition, TMAH decomposition	Neutralizes photoacids in resists, reacts with molecular acids to form haze crystals on optical elements
	Amines	Resist strippers	
	Amides	NMP, dimethyl acetamide, polyimides	
Molecular condensables	Phthalates, organophosphates, silicones, siloxanes	Outside air, air filters, sealants, adhesives, flame retardants, FOUPs, gaskets	Delaminates resist and ARC films
Molecular dopants	Boron, phosphorus, organophosphates, arsenic, antimony	Outside air, degradation of HEPA and ULPA filters, exhaust from RIE, EPI, and CVD processes	Causes unwanted <i>n</i> - and <i>p</i> -doping of wafers
Metals	Organometallic compounds	Cross-contamination of wafers, plastic additives containing organotin, organobismuth compounds, corroding ductwork	Forms particulates in air and on wafers

Legend: CVD (chemical vapor deposition), CMP (chemical mechanical polishing), HMDS (hexamethylene disilazane), TMAH (tetramethyl ammonium hydroxide), NMP (N-methyl pyrrolidone), ARC (antireflection coating), RIE (reactive-ion etching), EPI (epitaxial), HEPA (high-efficiency particulate air), ULPA (ultralow-penetration air)

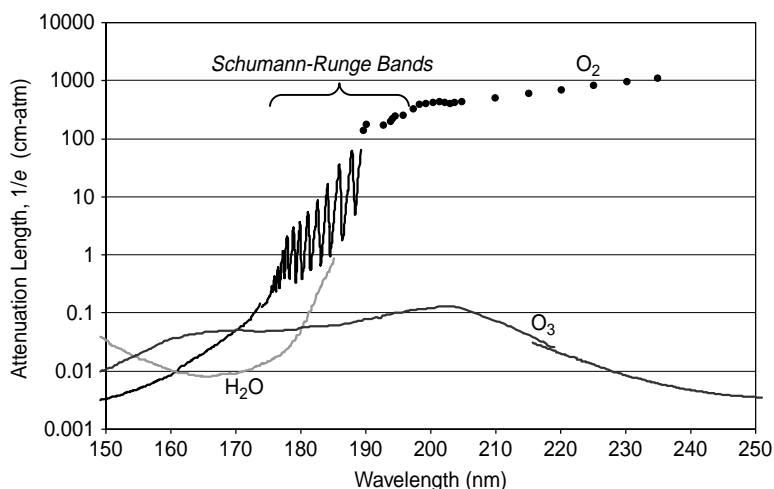


Figure 13.12 UV absorption spectrum of typical gases found in the ambient environments of exposure chambers of lithographic tools. (Courtesy of R. Kunz and R. Dammel.⁹²)

coefficient in the Hartley band readily permit production of excited oxygen atoms and molecules at 193 nm.

Although the absorption cross section of oxygen at 193 nm is relatively small ($\sim 10^{-23}$ cm²), since it comprises 21% of air, its overall effect in the attenuation of photons and the production of reactive excited-state species is quite significant. Its contribution to absorption shows a marked increase from 200 nm to 180 nm and a marked decrease from 200 nm to 250 nm in the Herzberg continuum, where the ozone absorption becomes significant.

13.3.2 Photodissociation of molecular oxygen

The potential energy curves for the three lowest electronic states of molecular oxygen are shown in Fig. 13.13. Molecular oxygen plays a very significant role in photochemical processes because of its high chemical energy content, its unique reactivity characteristics, its low-lying excited states, and its ubiquity as an impurity in reaction systems. It is unique in the sense that it is one of the very few natural molecules whose ground state has triplet multiplicity ($^3\Sigma_g$), instead of singlet multiplicity. The lowest excited state of molecular oxygen is the singlet $^1\Delta_g$, which lies only 94 kJ mole⁻¹ above the $^3\Sigma_g$. The next excited state of molecular oxygen is the $^1\Sigma_g$, which lies 157 kJ mole⁻¹ above the $^3\Sigma_g$. Due to

⁹²R.R. Kunz and R. Dammel, "193 nm lithography: fundamentals and issues," SPIE Short Course No. SC120 (2005).

the very weak electronic coupling between the $^3\Sigma_g$ and $^1\Delta_g$ states of molecular oxygen, even simple collisions provide significant spin-orbit perturbation mechanisms to mix these two states.⁹³ Radiationless conversion of $^1\Delta_g$ to $^3\Sigma_g$ is spin-forbidden, and is therefore expected to be quite slow.⁹⁴ Herein lies the reason why most reactions of oxygen with organic compounds, although exergonic, do not proceed at room temperature, except on heating or in the presence of catalysts. ArF laser photons and other UV radiations shorter than 240 nm can readily

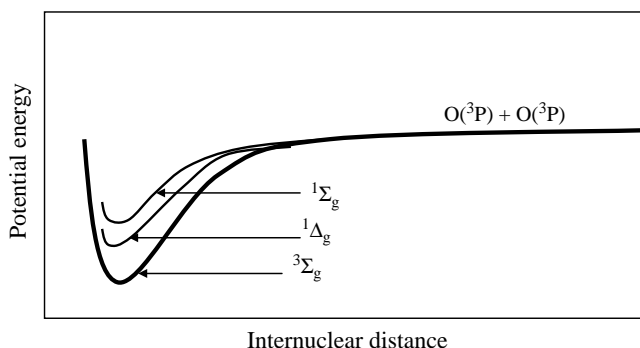


Figure 13.13 Schematic of potential energy curves of the photodissociation of molecular oxygen, showing some of the electronic states of oxygen. (Reprinted with permission from University Science Books.⁹⁵)

dissociate molecular oxygen ($^3\Sigma_g$, binding energy 5.1 eV) into atomic oxygen O (3P) as shown in Reaction [13.12].

The main reactions of oxygen induced by 193-nm photons are summarized below. Atomic oxygen [O(3P)], singlet molecular oxygen [1O_2 ($^1\Delta_g$, $^1\Sigma_g$)], and ozone (O₃) are readily formed from the interaction of UV photons with sufficient energy (e.g., 193-nm photons) with molecular oxygen. Once formed, these species participate in photo-oxidative degradation of resist features even in unpatterned areas.⁹⁶ Of these species, atomic oxygen is believed to play the dominant role. These species are readily formed during exposure of photoresists from the 6.4-eV ArF laser photons' irradiation of triplet molecular oxygen (3O_2) (ground

⁹³S.R. Lanhoff, "Ab initio evaluation of the fine structure of the oxygen molecule," *J. Chem. Phys.* **61**, 1708 (1974); P.B. Merkel and D.R. Kearns, "Radiationless decay of singlet molecular oxygen in solution. Experimental and theoretical study of electronic to vibrational energy transfer," *J. Am. Chem. Soc.* **94**, 7244 (1972); T.G. Slinger, P.C. Cosby, D.L. Huestis, and T.A. Bida, "Discovery of the atomic oxygen green line in the Venus night airglow," *Science* **291**, 463 (2001).

⁹⁴N.J. Turro, *Modern Molecular Photochemistry*, p. 587, University Science Books, Sausalito, CA (1991).

⁹⁵*ibid.*, p. 587.

⁹⁶U. Okoroanyanwu, P. Kunze, K. Al Shamery, J. Romero, and J. Bernard, "Impact of photo induced species in O₂ containing gases on lithographic patterning at 193 nm wavelength," *Proc. SPIE* **4691**, 746 (2002).

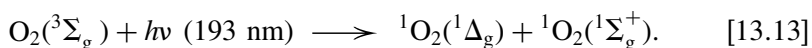
state) in the clean dry air used to purge exposure scanners and steppers in order to prevent contaminants and impurities from being deposited on the optical elements of the tool. Specifically, the ArF laser photons can do the following:

- (1) Dissociate molecular oxygen in air into atomic oxygen [O(³P)]:⁹⁷



where the absorption cross sections (σ_{O_2}) of oxygen at 193.3 nm, 193.4 nm, and 248 nm are $2 \times 10^{-23} \text{ cm}^2$, $8 \times 10^{-22} \text{ cm}^2$, and $5 \times 10^{-24} \text{ cm}^2$, respectively. Niwa et al.⁹⁸ reported the following values for the absorption cross section of oxygen: $\sigma(\lambda = 193 \text{ nm}) \cong (3.2 \pm 0.2) \times 10^{-22} \text{ cm}^2 \text{ molecule}^{-1}$ for the Schumann-Runge band ($v' = 4$) and $\sigma(\lambda = 193 \text{ nm}) \cong (1.2 \pm 0.1) \times 10^{-23} \text{ cm}^2 \text{ molecule}^{-1}$ for the Schumann continuum. The rate constant of the predissociation of O₂ has been obtained to be $6.40 \times 10^{-5} \text{ cm}^2 \text{ J}^{-1}$ at 22.1°C.⁹⁹

- (2) Excite molecular oxygen from its ground state to singlet oxygen:

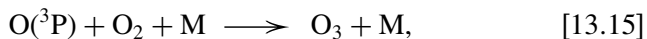


- (3) Photodissociate ozone:



where the absorption cross sections (σ_{O_3}) of ozone at 193 nm and 248 nm are $8 \times 10^{-19} \text{ cm}^2$ and $1 \times 10^{-17} \text{ cm}^2$, respectively.

- (4) Form ozone from reactions between atomic and molecular oxygen:¹⁰⁰



where M is a third collision partner such as O₂ or N₂.

It should be pointed out that of the four above reactions, Reactions [13.12], [13.14], and [13.15] directly participate in the dissociation of molecular oxygen, with the attendant formation of ozone, as well as the attenuation of the laser

⁹⁷For a comprehensive review of photochemistry of small molecules, see, for example, H. Okabe, *Photochemistry of Small Molecules*, John Wiley & Sons, Hoboken, NJ (1978); D.H. Volman, "Photochemical evidence relative to the excited states of oxygen," *J. Chem. Phys.* **24**(1), 122–124 (1956).

⁹⁸Y. Niwa, A. Matsuzaki, S. Nishio, and H. Sato, "Ozone formation by photodissociation of oxygen molecule with a 193 nm excimer laser," *J. Phys. Chem. A* **101**(4), 668–671 (1997).

⁹⁹ibid.

¹⁰⁰For a comprehensive review of photochemistry of small molecules, see, for example H. Okabe, *Photochemistry of Small Molecules*, John Wiley & Sons, Hoboken, NJ (1978); D.H. Volman, "Photochemical evidence relative to the excited states of oxygen," *J. Chem. Phys.* **24**(1), 122–124.

beam. Under laser irradiance, the rate equations for the formation of the main active species—O(³P) and O₃—are as follows:

O(³P) formation

$$\frac{d[\text{O}]}{dt} = 2\Phi\sigma_{\text{O}_2}[\text{O}_2] - k_1[\text{O}][\text{O}_2][\text{M}], \quad (13.5)$$

where k_1 is the rate constant for the formation of ozone in reaction 4 and Φ is laser flux.

Ozone (O₃) formation:

$$\frac{d[\text{O}_3]}{dt} = k_1[\text{O}][\text{O}_2][\text{M}] - \Phi\sigma_{\text{O}_3}[\text{O}_3]. \quad (13.6)$$

By solving Equations (13.5) and (13.6), it can be shown that

$$[\text{O}_3] \approx 2\left(\frac{\sigma_{\text{O}_2}}{\sigma_{\text{O}_3}}\right)[\text{O}_2](1 - 10^{-\Phi\sigma_{\text{O}_3}t}) \quad (\text{at } t > 1 \text{ ms}), \quad (13.7)$$

and at steady state,

$$t = \infty, P_{\text{O}_3} \approx 2\left(\frac{\sigma_{\text{O}_2}}{\sigma_{\text{O}_3}}\right)P_{\text{O}_2}, \quad (13.8)$$

where P_{O_3} and P_{O_2} are the partial pressures of ozone and molecular oxygen, respectively.

Equation (13.8) implies that ozone is generated at a rate that is 50 times greater at the 193-nm wavelength than at 248-nm wavelength. It also indicates that the steady state absorbance (attenuation) depends on the ratio of the absorption cross section of molecular oxygen to ozone, molecular oxygen partial pressure, and purge rate of beam line gas; it is independent of laser power and laser repetition rate. The absorption cross section is dependent on laser wavelength (see Fig. 13.14).

Once formed, the above active species mediate photo-oxidative degradation processes of resist polymers, including cross-linking, chain scission, oxidation, and other secondary reactions by free radical mechanisms, resulting in resist feature erosion and poor resist feature profiles, particularly under bright-field illumination in full-field scanners and steppers. These photo-oxidative degradation reactions are essentially the same type of reactions that are involved in the VUV¹⁰¹ and EUV¹⁰² cleaning of organics in the presence of oxygen.

¹⁰¹Z. Falkenstein, "Effects of the O₂ concentration on the removal efficiency of volatile organic compounds with dielectric discharges in Ar and N₂," *J. Appl. Phys.* **85**, 525 (1999).

¹⁰²M. Malinowski, P. Grunow, C. Steinhaus, M. Clift, and L. Klebanoff, "Use of molecular oxygen to reduce EUV induced carbon contamination of optics," *Proc. SPIE* **4343**, 347 (2001).

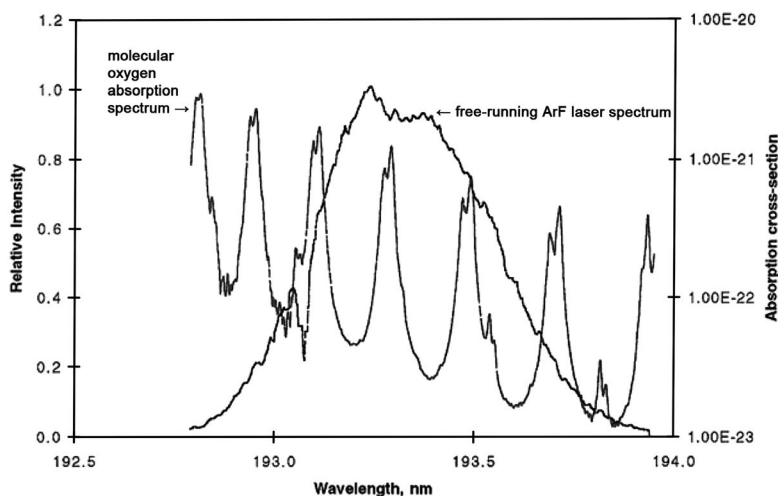


Figure 13.14 Molecular oxygen absorption spectrum over the spectrum of a free-running ArF exciplex laser. The absorption peaks in the molecular oxygen spectrum are Schumann-Runge absorption bands. (Courtesy of R. Kunz and R. Dammel.¹⁰³)

13.3.3 Photo-oxidative degradation of photoresist polymers

Photo-oxidative degradation of resist polymers, including such processes as photo-oxidation, chain scission, cross-linking, and secondary reactions, occurs by free radical mechanisms during ArF laser illumination in oxygen-containing gaseous environments within the exposure chamber of the stepper or scanner. Photo-oxidative degradation processes are initiated at the surface of the resist polymers by photoinduced species such as atomic oxygen, singlet oxygen, ozone, etc., and proceed inward, giving rise to a gradient of deteriorated material across the resist thickness. Oxidation will occur if unstabilized polymer is exposed to gases containing even parts-per-million levels of oxygen for prolonged periods above 80°C, and over the course of months or years at ambient temperatures.¹⁰⁴

The photochemical sequence involved in photo-oxidative degradation of resist polymers can be divided into the following three stages:

- (1) The absorption of photons by molecular oxygen and the chromophores in the resist polymers, leading to the formation of electronically excited states of oxygen species and chromophoric groups of the polymer, respectively.
- (2) The primary photochemical processes, which involve the electronically excited states.
- (3) The secondary or “dark” (thermal) reactions of the radicals, radical ions, ions, and electrons produced by the primary photochemical process.

¹⁰³R.R. Kunz and R. Dammel, “193 nm Lithography: fundamentals and issues,” SPIE Short Course No. SC120 (2005).

¹⁰⁴ibid., p. 2.

13.3.3.1 General mechanism of patterned resist polymer photo-oxidative degradation

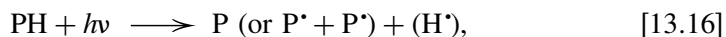
While many excellent reviews¹⁰⁵ and books¹⁰⁶ on the photo-oxidative degradation of polymers have been published, in this book, we concentrate on reactions

¹⁰⁵For a comprehensive review of photodegradation of polymers, see, for example, D.J. Carlsson and D.M. Wiles, "The photooxidative degradation of polypropylene. Part I. Photooxidation and photoinitiation processes," *J. Macromol. Sci. Rev. Macromol. Chem.* **C14**, 65 (1976); A. Garton, D.J. Carlsson, and D.M. Wiles, Polymer oxidation and secondary cage combination of peroxy radicals, *Makromolekulare Chemie* **181**(9), 1841 (1980); G. Geuskens and C. David, "The photo oxidation of polymers. A comparison with low molecular weight compounds," *Pure Appl. Chem.* **51**, 233 (1979); G. Geuskens and C. David, "Recent advances in the photo oxidation of polymers," *Pure Appl. Chem.* **51**, 2385 (1979); J.E. Guillet, "Fundamental processes in the UV degradation and stabilization of polymers," *Pure Appl. Chem.* **30**, 135 (1972); J.E. Guillet, "Photochemistry in macromolecular systems," *Naturwissensch.* **59**, 503 (1972); J.E. Guillet, "Photochemistry in the solid phase," *Polym. Eng. Sci.* **14**, 482 (1974); J.E. Guillet, "Fundamental processes in the photo degradation of polyolefins," *Adv. Chem. Ser.* **169**, 1 (1978); J.E. Guillet, J. Dhanraj, F.J. Golemba, and G.H. Hartely, "Fundamental processes in the photodegradation of polymers," *Adv. Chem. Ser.* **85**, 272 (1968); W.B. Hardy, *Dev. Polym. Photochem.* **3**, Ch. 8, p. 287 (1980); D.A. Holden, *Encycl. Polym. Sci. Eng.* **11**, 154 (1987); J. Lemaire and R. Arnaud, "Primary hydroperoxidation in photooxidation of polyolefins and polyamides," *Polym. Photochem.* **5**, 243 (1984); L.A. Linden, J.F. Rabek, H. Kaczmarek, A. Kaminska, and M. Scoconi, "Photooxidative degradation of polymers by HO_{xxx} and HO_{2xxx} radicals generated during the photolysis of H₂O₂, FeCl₃, and Fenton reagents," *Coord. Chem. Rev.* **125**, 195 (1993); J.R. MacCallum, W.W. Wright, "Photo and photo oxidative degradation of polymers," *Macromol. Chem. (London)* **3**, 331 (1984); J.R. MacCallum, in *Comprehensive Polymer Science*, G. Allen and J.C. Bevington, Eds., Vol. 6, p. 529, Pergamon Press, New York (1989); J.F. Rabek, in *Polymer Additives*, p. 1, J.E. Kresta, Ed., Plenum, New York (1984); J.F. Rabek, G. Canback, and B. Ranby, *J. Appl. Polym. Sci. Polym. Symp.* **35**, 299 (1979); J.F. Rabek and B. Ranby, in *ESR Applications to Polymer Research, Nobel Symp.* **22**, P.O. Kinell, and B. Ranby, Eds., p. 201, Almqvist & Wiksel, Stockholm (1973); B. Ranby and J.F. Rabek, *J. Appl. Polym. Sci.* **35**, 243 (1979); B. Ranby and J.F. Rabek, in *Comprehensive Polymer Science*, G. Allen, Ed., p. 253, Pergamon Press, Oxford (1992); G. Scott, "Photoinitiated degradation of polymers," *Macromol. Chem.* **8**, 319 (1973); M. Shimoyama, H. Niino, and A. Yabe, "A KrF excimer laser induced dehydrochlorination of a chlorinated poly(vinyl chloride): preparation of a conjugated diene," *Makromol. Chem.* **193**, 569 (1992); K. Tsuji, "ESR study of photodegradation of polymers," *Polym. Plast. Technol. Eng.* **9**, 1 (1977).

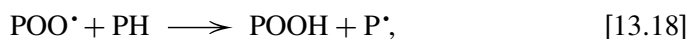
¹⁰⁶For books on photodegradation of polymers, see, for example, J.F. Rabek, *Photodegradation of Polymers: Physical Characteristics & Applications*, Springer, New York (1996); N.S. Allen and M. Edge, *Fundamentals of Polymer Degradation and Stabilization*, Elsevier, London (1992); G. Geuskens, Ed., *Degradation and Stabilization of Polymers*, John Wiley & Sons, Hoboken, NJ (1975); N. Grassie and G. Scott, *Polymer Degradation and Stabilization*, Cambridge University Press, Cambridge (1985); H.H.G. Jellinek, Ed., *Aspects of Degradation and Stabilization of Polymers*, Elsevier, Amsterdam (1979); H.H.G. Jellinek, Ed., *Degradation and Stabilization of Polymers*, Vol. 1, Elsevier, Amsterdam (1989); H.H.G. Jellinek and H. Kachi, Eds., *Degradation and Stabilization of Polymers*, Vol. 2, Elsevier, Amsterdam (1989); J.F. McKellar and N.S. Allen, *Photochemistry of Man Made Polymers*, Applied Science, London (1979); Z. Osazawa, *Photodegradation and Stabilization of Polymers: Fundamentals and Practice of Photostabilization Techniques*, CMC Co., Japan (1986); A.D. Patsis, *Advances in Stabilization and Controlled Degradation of Polymers*, Technomic, Lancaster (1989); J.F. Rabek, *Mechanisms of Photophysical Processes and Photochemical Reactions in Polymers: Theory and Applications*, John Wiley & Sons, Chichester (1987); J.F. Rabek, *Photostabilization of Polymers: Principles and Applications*, Elsevier, London (1990); J.F. Rabek,

engendered during UV exposures of photoresists from ArF and KrF exciplex lasers, as well as the role of these reactions on patterned photoresist feature profile degradation and erosion. The mechanistic steps of photo-oxidation includes the following:¹⁰⁷

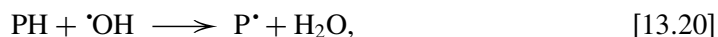
Initiation:



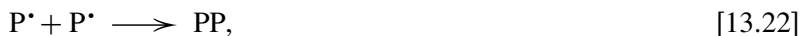
Chain propagation:



Chain branching:



Termination:



where PH is the polymer, P^{*} is the polymer alkyl radical, PO^{*} is the polymer alkoxy radical, POO^{*} is the polymer peroxy radical, POOH is the polymer hydroperoxide, and HO^{*} is the hydroxy radical. Photo-oxidative degradation generally causes main chain scission and cross-linking, the former being more generally predominant in the presence of oxygen.

Photodegradation of Polymers: Mechanisms and Experimental Methods, Chapman & Hall, London (1995); B. Ranby and J.F. Rabek, *Photodegradation, Photooxidation and Photostabilization of Polymers: Principles and Applications*, John Wiley & Sons, London (1975); D.V. Rosato and R.T. Schwartz, Eds., *Environmental Effects on Polymeric Materials*, John Wiley & Sons, Hoboken, NJ (1968); G. Scott, Ed., *Mechanisms of Polymer Degradation and Stabilization*, Elsevier, London (1990); J. Voigt, *Die Stabilisierung der Kunststoffe gegen Licht und Wärme*, Springer, Berlin (1966); J. Wypych, *Weathering Handbook*, Chemtec, Toronto (1990).

¹⁰⁷J.F. Rabek, *Photodegradation of Polymers: Physical Characteristics & Applications*, p. 60, Springer, New York (1996).

Figure 13.15 shows the effects of different gaseous environments (dry air and nitrogen) on PAR710 resist during ArF exposure. The significant decrease in the signal peak intensity around 1792 cm^{-1} , corresponding to C=O bending vibration, and around 1157 cm^{-1} , corresponding to C-C(=O)-O stretching vibration, in the wafer exposed in a dry air environment relative to that in nitrogen is suggestive of higher photo-oxidative degradation of the resist in the dry air environment than in nitrogen.¹⁰⁸ This finding is in agreement with published results.¹⁰⁹ Another direct evidence of photo-oxidative degradation of the resist film exposed in dry

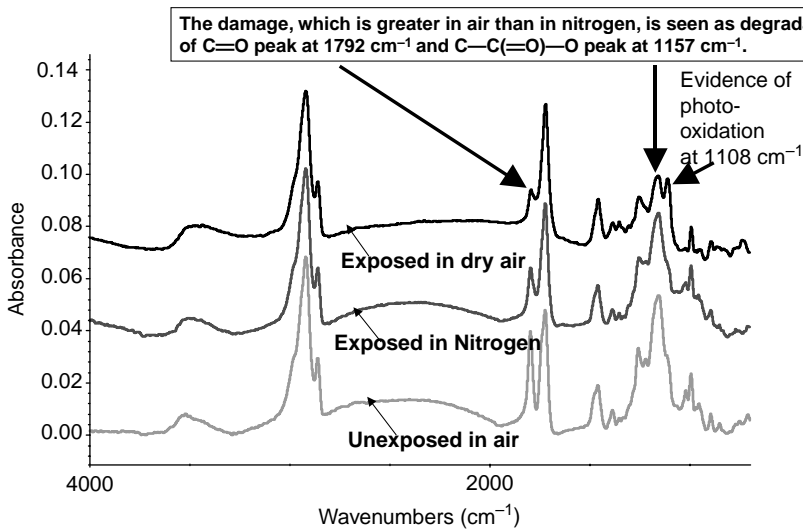


Figure 13.15 FTIR spectra showing the effects of different gaseous environments on resist during exposure (damage in dry air versus damage in nitrogen environment).¹¹⁰

¹⁰⁸U. Okoroanyanwu, P. Kunze, K. Al Shamery, J. Romero, and J. Bernard, "Impact of photoinduced species in O₂ containing gases on lithographic patterning at 193 nm wavelength," *Proc. SPIE* **4691**, 746 (2002).

¹⁰⁹L.L. Fewell and L. Finney, "An ESCA study of atomic oxygen interactions with phosphazene coated polymeric films," *Polym. Commun.* **32**, 393 (1991); A. Garton, P.D. McLean, W. Wiebe, R.J. Densely, "Exposure of cross linked epoxy resins to the space environment," *J. Appl. Polym. Sci.* **32**, 3941 (1986); M.A. Golub and T. Wydeven, "Reactions of atomic oxygen [O(³P)] with various polymer films," *Polym. Degrad. Sci.* **22**, 325 (1988); R.H. Hansen, in *Interface Conversion*, P. Weiss and G.D. Cheever, Eds., p. 287, Elsevier, New York (1968); R.H. Hansen, in *Thermal Stability of Polymers*, R.T. Conley, Ed., p. 153, Dekker, New York (1970); R.H. Hansen, J.V. Pascale, T. Debendicitis, and P.M. Rentzepsis, "Effect of atomic oxygen on polymers," *J. Polym. Sci. Chem. Ed.* **3**, 2205 (1965); E.L. Lawton, "Oxidation of polymers by radiofrequency plasma," *J. Polym. Sci. Chem. Ed.* **10**, 1857 (1972); J. Lucki, B. Ranby, and J.F. Rabek, "Comparative studies of reactions of commercial polymers with molecular oxygen, singlet oxygen, atomic oxygen and ozone II. Reactions with 1,2 polybutadiene," *Eur. Polym. J.* **15**, 1101 (1979); J.R. MacCallum and C.T. Rankin, "A novel method for modifying surfaces," *J. Polym. Sci. Polym. Lett.* **9**, 751 (1971); D.H. Reneker and L.H. Bolz, "Effect of atomic oxygen on the surface morphology of polyethylene," *J. Makromol. Chem. Sci. Chem.* **A10**, 599 (1976); A.G. Shard and J.P.S. Badyal,

air is the presence of the peak around 1108 cm^{-1} , which is absent in both the spectra of the unexposed part of the film in dry air and the exposed part of the film in nitrogen.

13.3.3.1.1 Atomic oxygen reactions with polymers

It has been reported that atomic oxygen $\text{O}(^3\text{P})$ reacts with almost all polymers (PH), causing surface erosion (etching and material loss):¹¹¹



A polymer mass loss rate of $10^{-6}\text{ kgh}^{-1}/\text{area}$ and an activation energy of 21.1 kJ/mol for atomic oxygen-exposed poly(methyl methacrylate) was reported by Whitaker et al. The mass loss rate was found to be directly related to the exposure area and to be independent of sample thickness.¹¹²

13.3.3.1.2 Photo-oxygenation of polymers by singlet oxygen

Singlet oxygen species $^1\text{O}_2(^1\Delta_g)$ and $^1\text{O}_2(^1\Sigma_g^+)$ undergo versatile reactions with polymers containing allylic and/or diene unsaturated bonds.¹¹³ Depending on

“Plasma oxidation versus photo oxidation of polystyrene,” *Polym. Commun.* **32**, 217 (1991); A.F. Whitaker and B.Z. Jang, “The mass loss mechanisms of polymers in a radio frequency induced atomic oxygen environment,” *J. Appl. Polym. Sci.* **48**, 1341 (1993).

¹¹⁰U. Okoroanyanwu, P. Kunze, K. Al Shamery, J. Romero, and J. Bernard, “Impact of photoinduced species in O_2 containing gases on lithographic patterning at 193 nm wavelength” *Proc. SPIE* **4691**, 746 (2002).

¹¹¹ibid.

¹¹²A.F. Whitaker and B.Z. Jang, “The mass loss mechanisms of polymers in a radio frequency induced atomic oxygen environment,” *J. Appl. Polym. Sci.* **48**, 1341 (1993).

¹¹³B. Ranby and J.F. Rabek, *Photodegradation, Photooxidation and Photostabilization of Polymers: Principles and Applications*, John Wiley & Sons, London (1975); D.J. Carlsson and D.M. Wiles, “Importance of singlet oxygen in the degradation of rubber and plastics,” *Rubb. Chem. Technol.* **47**, 991 (1974); M.A. Golub, “Photosensitized oxidation of unsaturated polymers,” *Pure Appl. Chem.* **52**, 305 (1980); M.L. Kaplan and A.M. Trozzolo, in *Singlet Oxygen*, H.H. Wasserman and R.W. Murray, Eds., p. 575, Academic Press (1979); J.R. MacCallum and C.T. Rankin, “Reaction of excited oxygen species with polymer films,” *Makromol. Chem.* **175**, 2477 (1974); J.F. Pratte and S.E. Webber, “Molecular weight effects on triplet sensitization of poly(2 vinylnaphthalene) in benzene,” *Macromolecules* **15**, 417 (1982); J.F. Rabek, J. Lucki, and B. Ranby, “Comparative studies of reactions of commercial polymers with molecular oxygen, singlet oxygen, atomic oxygen and ozone I. Reactions with cis 1,4 polybutadiene,” *Eur. Polym. J.* **15**, 1089 (1979); J.F. Rabek and B. Ranby, “Role of singlet oxygen in photo oxidative degradation and photostabilization

the availability of an allylic hydrogen, substituent polymers react with it to produce either dioxetanes or hydroperoxides, whereas polydienes yield endoperoxides.¹¹⁴ In polymers, light-absorbing impurities (external and/or internal structure irregularities) have been reported to act as potential photosensitizers for the generation of singlet oxygen.¹¹⁵

13.3.4 Inorganic salt formation on DUV exposure tool lenses and reticles

Accumulating experimental evidence suggests the formation of inorganic crystals that cause haze defects on 193-nm and 248-nm exposure reticles¹¹⁶ and lenses. These haze defects have been termed progressive defects because they cause catastrophic defect growth over the course of production usage of the lens and reticle in the fab. Although these progressive defects have been observed at almost all lithographic wavelengths, the problem is especially severe in 193-nm lithography because of the highly energetic (6.4-eV) photons and the concurrent transition to 300-mm wafers, which require photomasks and lenses to endure more prolonged exposure compared to 200-mm wafers. Raman spectroscopic compositional analyses of these crystals have shown them to be made primarily of ammonium sulfate $[(\text{NH}_4)_2\text{SO}_4]$.¹¹⁷

of polymers," *Polym. Eng. Sci.* **15**, 40 (1975); J.F. Rabek and B. Ranby, "Studies on the photooxidation mechanism of polymers. V. Oxidation of polybutadienes by singlet oxygen from microwave discharge and in dye photosensitized reactions," *J. Polym. Sci. Chem. Ed.* **14**, 1463 (1976); J.F. Rabek and B. Ranby, "Studies on the photo oxidative mechanism of polymers. VII. The role of singlet oxygen in the dye photosensitized oxidation of *cis* 1,4 and 1,2 polybutadienes and butadiene styrene copolymers," *J. Appl. Polym. Sci.* **23**, 2481 (1979); J.F. Rabek, Y.J. Shur, and B. Ranby, in *Singlet Oxygen: Reactions with Organic Compounds and Polymers*, B. Ranby and J.F. Rabek, Eds., p. 264, John Wiley & Sons, Chichester (1978); G. Scott, in *Singlet Oxygen: Reactions with Organic Compounds and Polymers*, B. Ranby and J.F. Rabek, Eds., p. 230, John Wiley & Sons, Chichester (1978); A. Zwiag and W.A. Henderson, "Singlet oxygen and polymer photooxidations. I. Sensitizers, quenchers, and reactants," *J. Polym. Sci. Chem. Ed.* **13**, 717 (1975).

¹¹⁴M.L. Kaplan and P.G. Kelleher, "Photo oxidation of polymers without light: Oxidation of polybutadiene and an ABS polyblend with singlet oxygen," *J. Polym. Sci. Chem. Ed.* **8**, 3163 (1970); H.C. Ng and J.E. Guillet, "Singlet oxygen initiation of polymer photooxidation: photolysis of *cis* 1,4 polyisoprene hydroperoxide," *Macromolecules* **11**, 929 (1978); C. Tanielian and J. Chaineaux, "Singlet oxygen reactions with model compounds of *cis* and *trans* polyisoprene containing two units," *J. Photochem.* **9**, 19 (1978).

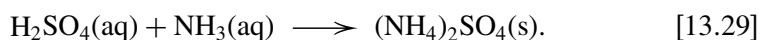
¹¹⁵J.F. Rabek, *Photodegradation of Polymers: Physical Characteristics & Applications*, p. 87, Springer, New York (1996).

¹¹⁶B. Grenon, K. Bhattacharyya, W. Volk, and A. Poock, "Reticle surface contaminants and their relationship to subpellicle particle formation," *Proc. SPIE* **5256**, 1103 (2003); E. Johnstone, L. Dieu, C. Chovino, J. Reyes, D. Hong, P. Krishnan, D. Coburn, and C. Capella, "193 nm haze contamination: a close relationship between mask and its environment," *Proc. SPIE* **5256**, 440 (2003).

¹¹⁷*ibid.*

13.3.4.1 Mechanism of ammonium sulfate crystal formation on DUV lithographic exposure lenses and reticles

Physical and chemical processes in the exposure chamber of DUV steppers and scanners are responsible for the formation of inorganic salts from precursor gases (SO_2) contained in the purge air of the tool. These precursor gases, buoyed by atmospheric processes, are oxidized to H_2SO_4 by oxidants (OH^- , O_3 , H_2O_2) generated from O_2 and H_2O by the exposure tool laser. Once formed, the H_2SO_4 reacts with NH_3 to form the corresponding salt, i.e., ammonium sulfate $(\text{NH}_4)_2\text{SO}_4$ as



It should also be mentioned that there are many chemical pathways through which SO_2 in the purge air of the exposure tool can be oxidized into sulfates, including homogenous processes that take place in the gas phase and in liquid droplets or heterogeneous processes that take place on the surface of particles or droplets.

13.3.4.1.1 Reaction pathways leading to the formation of ammonium sulfate crystals in DUV lithographic exposure tools

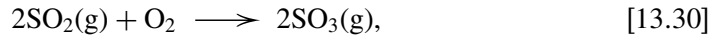
A wide variety of interrelated homogenous gas-phase, solution-phase, and heterogeneous chemistry may ultimately result in oxidation of SO_2 to sulfuric acid in DUV exposure tools. The three main possible reaction pathways for the oxidation of sulfur dioxide to sulfuric acid in the exposure chamber may include (i) direct oxidation of sulfur dioxide by stable atmospheric oxygen, (ii) catalyzed oxidation of sulfur dioxide by metal ions, and (iii) photochemical oxidation of sulfur dioxide by ozone and hydroxyl radical.

13.3.4.1.1.1 DIRECT OXIDATION OF SULFUR DIOXIDE BY STABLE ATMOSPHERIC OXYGEN

Thermodynamic considerations indicate that sulfur dioxide has a strong tendency to react with oxygen in the air within the exposure chamber, as it does under normal tropospheric conditions,¹¹⁸ as shown in Reaction [13.30]. Thermodynamics arguments also inform us that at humidities normally encountered in the exposure chamber, the SO_3 produced by Reaction [13.30], can be converted efficiently to

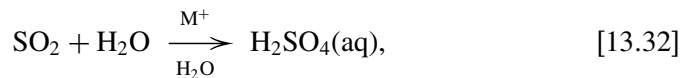
¹¹⁸These reactions are similar to those governing the acid deposition processes as reported in "Acid deposition: atmospheric processes in eastern North America," Natl. Academy of Sciences Commission on Physical Sciences, Mathematics, and Applications (CPSMA) Report, pp. 1–373, National Academy Press, Washington, DC (1983).

sulfuric acid, H_2SO_4 (aq), according to Reaction [13.31]:



13.3.4.1.1.2 CATALYZED OXIDATION OF SULFUR DIOXIDE BY METAL IONS

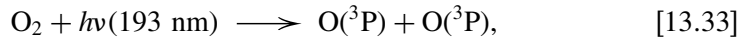
Certain metal ions (Cr^+ , Mn^{2+} , Fe^{3+} , Mo^+ , etc.) in aqueous solutions of SO_2 (HSO_3) can catalyze the overall sequence of Reaction [13.32]:¹¹⁹



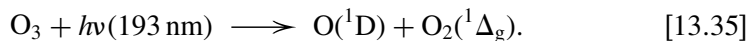
where M^+ is a metal ion catalyst such as Cr^+ and Mo^+ found on photomasks. Other active catalysts include Mn^{2+} , Fe^{3+} , Cu^{2+} , etc.

13.3.4.1.1.3 PHOTOCHEMICAL OXIDATION OF SULFUR DIOXIDE BY OZONE AND HYDROXYL RADICAL

The photochemical generation of ozone in the exposure chamber involves the 193-nm light dissociation of molecular oxygen in the air to ground-state atomic oxygen species $\text{O}({}^3\text{P})$ (Reaction [13.33]), which in turn reacts with molecular oxygen to form ozone (Reaction [13.34]):



The photodecomposition of ozone may form electronically excited oxygen atoms, $\text{O}({}^1\text{D})$, and excited molecular oxygen with absorption of the 193-nm radiation (Reaction [13.35]). The $\text{O}({}^1\text{D})$ species formed in Reaction [13.35] is much more reactive than the ground-state oxygen atoms [$\text{O}({}^3\text{P})$]:



$\text{O}({}^1\text{D})$ reacts efficiently when it collides with a water molecule to form a highly important transient in atmospheric chemistry, the hydroxyl radical HO^{\bullet} (Reaction [13.36]):¹²⁰



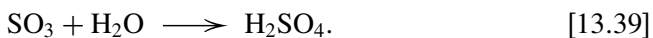
¹¹⁹ibid., p. 156.

¹²⁰ibid., p. 160.

The HO radical reacts efficiently with SO₂ in the presence of a third body, M, such as the exposure reticle or exposure lens to form the free radical HOSO₂, an unstable and highly reactive molecule (Reaction [13.37]), which reacts with oxygen to form SO₃ (Reaction [13.38]):



The SO₃ generated in Reaction [13.38] is then easily oxidized to sulfuric acid (Reaction [13.39]),



It should be pointed out that the various pathways that lead to the oxidation of SO₂ are coupled by common products and reactants that can directly and indirectly influence the rates of reaction by other pathways. Shown in Fig. 13.16 is a schematic of the reaction mechanism that may lead to the formation of ammonium sulfate in the exposure tool, the main elementary reactions of which are shown in Reactions [13.30]–[13.39]. A few of the notable facts about these pathways are summarized below.

- (A) Reaction [13.29] is the overall haze formation reaction, which is a neutralization reaction between the sulfuric acid and ammonia to form ammonium sulfate crystals.

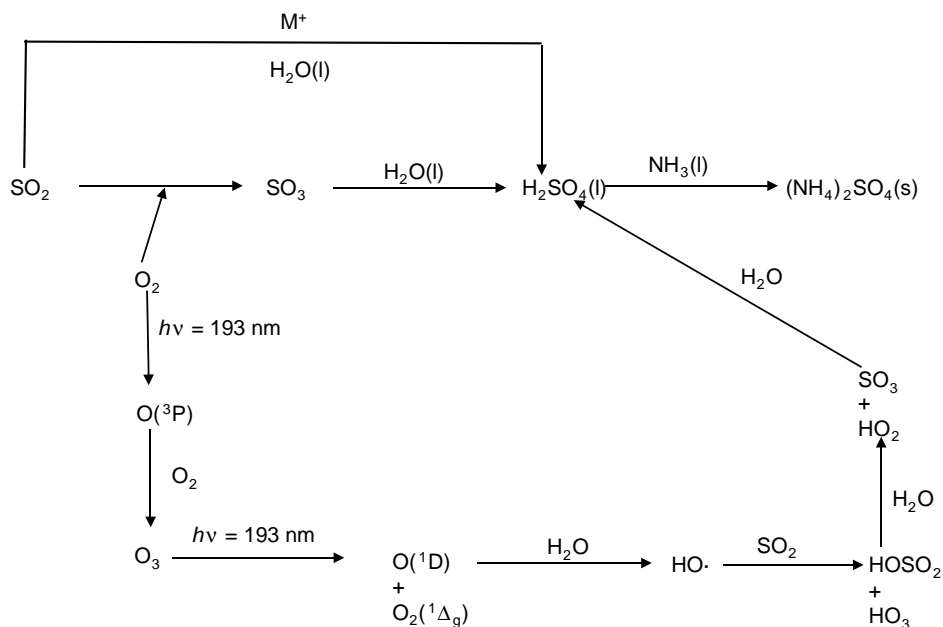


Figure 13.16 Ammonium sulfate formation mechanism in ArF lithographic exposure tools.

- (B) The elementary reactions in the reaction mechanism represent the various reactions involved in the oxidation of SO_2 to H_2SO_4 in three main reaction pathways, namely, (i) direct oxidation of SO_2 , (ii) metal-ion-catalyzed oxidation of SO_2 to H_2SO_4 , and (iii) photochemical oxidation of SO_2 to H_2SO_4 by means of oxidants such as hydroxyl radical and ozone. Once formed, the H_2SO_4 will react readily with NH_3 to form the ammonium sulfate haze crystals. All three of these reaction pathways are operative in the DUV (193-nm and 248-nm) exposure tools, and the interplay between them as they react with photons and ultimately with NH_3 , as well as the concentration of the reactants at each point in time, are responsible for the progressive growth nature of these haze crystals.
- (C) Reactions [13.30] and [13.31] make up the pathway that involves direct gas-phase oxidation of SO_2 to H_2SO_4 .
- (D) Reaction [13.32] makes up the pathway that involves the mask metallic-component-catalyzed solution phase oxidation of SO_2 to H_2SO_4 . This explains why we see these crystals only on the chrome side of binary masks or on the metallic structures of embedded masks, and not on the pellicle side.
- (E) Reactions [13.33]–[13.39] make up the photochemical pathways for the oxidation of SO_2 to H_2SO_4 mediated by hydroxyl radical and ozone, which are generated from the interaction of the exposure light with moisture and oxygen, respectively, in the exposure chamber.

13.3.5 Corrosion and oxidation of chrome structures in DUV lithographic masks

The degradation of chrome structures on lithographic masks is a new and emerging problem in advanced lithography using the DUV 193-nm wavelength.¹²¹ Its main attributes are progressive growth of chromium oxide (Cr_xO_y) scale on the sidewalls and base of chrome structures of masks (see Fig. 13.17). There is a distinct difference in the growth rate of this Cr_xO_y scale between the features at the center of the mask and those at the periphery, with the center features having a faster growth rate and therefore larger accumulation of the Cr_xO_y than those at the periphery. This degrades the CD uniformity of features patterned on the wafer with such a degraded mask. The scale is composed of Cr_xO_y and has an amorphous morphology. It does appear that the exposure condition somehow enhances the growth of this scale in the presence of ambient oxygen, suggesting some photochemical

¹²¹A. Tchicioulaeva, A. Holfeld, M. Arend, and E. Foca, "ACLV degradation: root cause analysis and effective monitoring strategy," *Proc. SPIE* **7028**, 702816 (2008); G. Rider, "Reticle ESD modules 1, 2, 3," presented at SEMATECH ESD Workshop (Dec. 2003); G. Rider, "Experimental quantification of reticle electrostatic damage below the threshold for ESD events," *Proc. SPIE* **6922**, 69221Y (2008).

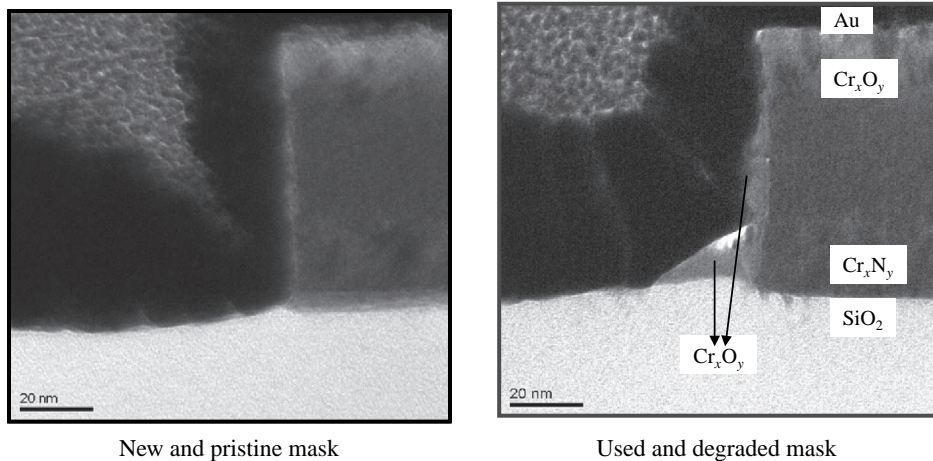


Figure 13.17 Transmission electron microscopy (TEM) image of a cross section of a chrome line feature of on a degraded gate mask and an unused mask blank.¹²²

contribution to the problem. The chromium oxide growths can be cleaned off with standard mask-cleaning procedures.¹²³

It should be mentioned that chromium oxide (Cr_2O_3) is among the ten most abundant compounds in the Earth's crust. When exposed to air, chromium forms an invisible thin oxide, which makes the metal extremely resistant to corrosion and also very useful as a decorative and protective coating over other metals such as brass, bronze, and steel.¹²⁴ Called a spinel, this protective oxide is very dense and therefore can prevent the diffusion of oxygen into underlying layers in materials such as steel, on which it is typically coated. In contrast to other metals such as iron and nickel, chromium does not suffer from hydrogen embrittlement. It does, however, suffer from nitrogen embrittlement, which may have implications for the degradation problem in lithographic masks. To date, no straight chromium alloy has ever been developed because of this embrittlement problem.¹²⁵

13.3.5.1 Mechanism of lithographic mask chrome structure oxidation

The chromium oxide footing seen between the line chrome structures and SiO_2 surface on gate masks and on the SiO_2 surface at the bottom of vias with chromium sidewalls (see Fig. 13.16) are Cr_xO_z scale growths arising from the oxidation of the Cr and Cr_xN_y sidewall of these features. The whole process is perhaps initiated in a

¹²²A. Tchicioulaeva, A. Holfeld, M. Arend, and E. Foca, "ACLV degradation: root cause analysis and effective monitoring strategy," *Proc. SPIE* **7028**, 702816 (2008).

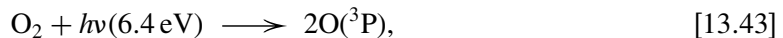
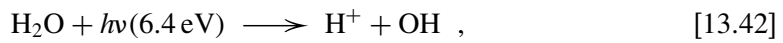
¹²³ibid.

¹²⁴A. Swertka, *A Guide to the Elements*, 2nd ed., pp. 85–86, Oxford University Press, Oxford (2002).

¹²⁵ibid.

photoelectric effect under exposure conditions, in which the 6.4-eV photons eject photoelectrons (~ 1 eV) from chrome nitride (Reaction [13.40]) and chrome oxide (Reaction [13.41]) surfaces, oxidizing them into higher oxidation states (Cr^{+n} or perhaps Cr^{+6}). Under the influence of the electric field, the Cr^{+n} ions migrate out from the chrome structure lattices via grain boundaries and dislocation sites. Water vapor and molecular oxygen may in turn be dissociated by the 6.4-eV photons under exposure conditions to hydroxyl radicals (OH^-) (Reaction [13.42]) and atomic oxygen (O) species (Reaction [13.43]), which diffuse inward toward the chrome structures through the same grain boundaries and dislocation sites. On meeting, the Cr^{+n} species O and OH species react to form the Cr_xO_y scale growths (Reactions [13.44] and [13.45]). The source of the electric field could be from electrostatic discharge processes. The sources of the oxygen and hydroxyl radicals are molecular oxygen and water vapor, respectively, in the compressed dry air of the exposure tool. Molecular oxygen dissociation can also be catalyzed by the pure Cr surface.

The relevant elementary reactions occurring at each location on each film surface interface are outlined as follows:



It should be noted that Cr^{+n} ions, perhaps generated from the interaction of ArF photons and Cr_xO_z or with Cr_xN_y film and the displacement of nitrogen by oxygen, are mobile and can migrate from the films at the feature edge to the SiO_2 layer, where they can get oxidized into Cr_xO_z , causing the footing or residues that are observed on the mask structures. Repeated cycles of this reaction over time will lead to the growth of the chromium oxide residues and footings seen in line and via structures of masks.

The differences in the chrome oxide growth rate between the chrome features located in the center of the mask relative to those at the edge are related to the differences in the availability of chromium ions from the surrounding features in the areas in question. The spaces surrounding the features at the center have a higher amount of available sources of chromium ions than comparable features at the edge. Once released from the sources of the chromium, the chromium ions migrate and settle on the available surfaces where they form seed nuclei, which are then oxidized by oxygen. The overall growth rate of the formed oxide is determined by the slow migration of the chromium cation through the oxide and nitride layers.

13.4 Optical Materials for UV and Visible Light Lithographies

The main optical materials used in UV and visible light lithographic exposure tools fall into two categories, namely, reflective optical materials (mirrors) and refractive optical materials (lenses). Reflective optical materials are advantageous because broadband illumination can be used with them. However, it is very difficult to design and build high-NA, all-reflective optics because of physical interference; some mirrors will block the light path of others. For this reason, lithographic exposure tools utilizing all-reflective optics such as EUV exposure tools have low NA (0.14–0.25); they achieve very high resolution because of their short exposure wavelength (13.5 nm). As a consequence, DUV lithographic lenses that employ mirrors also contain some refractive elements; such systems containing both mirrors and lenses are called catadioptric.¹²⁶

The refractive optical materials requirement for lithographic applications comprises high transmission, low birefringence, good index homogeneity to minimize wavefront distortion, and durability (where projected lifetime is up to 10 years and delivering 40–100 billion pulses at 0.1 to 5 mJ/cm²/pulse for state-of-the-art 193-nm exposure tools). Amorphous SiO₂ (also called fused silica) and crystalline CaF₂ are the only practical candidates (see Table 13.5 for their bulk optical properties). Table 13.6 shows a list of potential optical materials for use in UV lithography, along with their bandgaps, physical properties, areas of applications, and specific issues.

The optical elements in conventional g-line, i-line, KrF laser, ArF laser, and F₂ laser lithographic exposure tools are made of refractive lenses, which have been traditionally made of transmitting glasses in the particular wavelength of the exposure tool. These refractive lenses generally provide good imaging over a narrow band of wavelengths. Typical bandwidths for g-line and i-line lenses are 4–6 nm full width half maximum (FWHM). Fused silica was for many years the only available material with sufficient transparency and quality for making 248-nm lenses, and such lenses required very narrow bandwidth, typically

Table 13.5 Bulk optical properties of amorphous SiO₂ and crystalline CaF₂ at the 193-nm wavelength.

Property at 193 nm	Fused Silica, SiO ₂	CaF ₂
Refractive index	1.56	1.5
dn/dT (ppm/°K)	22	5.9
Homogeneity index (ppm)	<0.5	<1.0
Stress birefringence (nm/cm)	<1	1 4

¹²⁶In lithography, catadioptric lenses were used almost exclusively in Ultratech and SVG (now part of ASML) lithographic exposure tools. Now, all immersion lithographic exposure tool lenses with NA > 1, except for the S609 from Nikon, are catadioptric.

Table 13.6 Optical materials used in UV lithography.

Material	Bandgap (eV)	Comments	Applications
Fused silica, SiO ₂	~9.0		Stepper optics, mask blanks
Calcium fluoride, CaF ₂	10.3		Laser optics, stepper optics
Barium fluoride, BaF ₂	9.2	Crystal growth issues	
Lithium fluoride, LiF	12.0	Hygroscopic	
Sodium fluoride, NaF	~10.5	Soft and hygroscopic	
Magnesium fluoride, MgF ₂	11	Birefringent	Laser optics, antireflection coatings
Sapphire, Al ₂ O ₃	8.3	Birefringent, absorbs at 193 nm because of impurities	

<1 pm (FWHM). Lenses in 193-nm lithographic exposure tools typically use both fused silica and a small amount of CaF₂. In spite of their shorter wavelengths and higher resolution, lenses for 193-nm lithography have bandwidth requirements that are comparable to the single-material 248-nm lenses of comparable numerical apertures.¹²⁷

It is practical to operate lenses used in 248-nm and 193-nm lithographic exposure tools over very narrow ranges of wavelength (<1 pm) because adequate intensity from excimer and excimer lasers can be obtained over such narrow bandwidths. This contrasts with i-line lenses, which operate over much wider bandwidths of between 4 and 6 nm. At shorter wavelengths, impurities in lithographic glass materials absorb light. This absorption is small in stepper lenses; it does not have a major impact on lens transmission. Lenses containing absorbing impurities may heat up¹²⁸ and expand during exposure, causing defocus,¹²⁹ changes in magnification, and other aberrations. This type of heating is common in i-line lenses. A similar problem occurs in 193-nm lenses because fused silica becomes slightly absorbing at that wavelength (in contrast to what happens at 248 nm, where fused silica is extremely transparent)¹³⁰ (see Fig. 13.18).

Birefringence (a property in which the index of refraction varies along various crystal axes) is another problem that degrades the performance of lithographic lenses. Many crystalline materials exhibit birefringence, and as such are not suitable for use in lithographic exposure tools designed for high-resolution

¹²⁷H.J. Levinson, *Principles of Lithography*, 2nd ed., p. 162, SPIE Press, Bellingham, WA (2005).

¹²⁸Software is often used to compensate for the effects of lens heating, see for example, P. van Oorshot, B. Kock, J. van der Spek, E. Stuijver, H. Franken, H. Bother, and R. Garreis, "Performance of an I line step and scan system for sub 0.25 μm mix and match application," *Proc. SPIE* **3334**, 423–436 (1998).

¹²⁹T.A. Brunner, S. Cheng, and A.E. Norton, "A stepper image monitor for precise setup characterization," *Proc. SPIE* **4691**, 687–695 (2002).

¹³⁰H.J. Levinson, *Principles of Lithography*, 2nd ed., p. 163, SPIE Press, Bellingham, WA (2005).

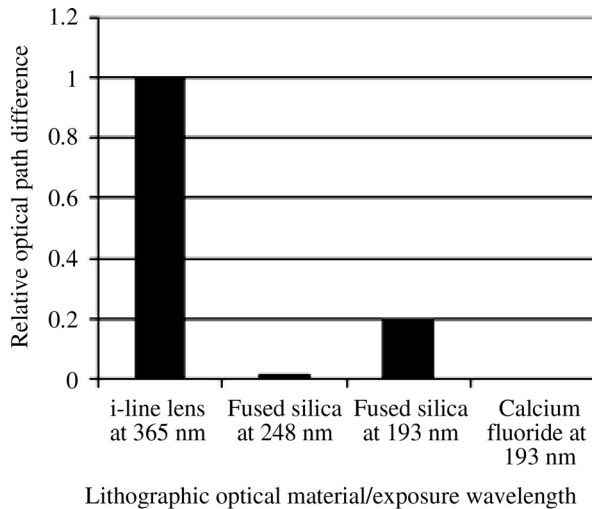


Figure 13.18 Lens heating of various optical materials as measured by OPD at i-line (365 nm), 248-nm, and 193-nm exposure wavelengths. (Adapted with permission from Ref. 131.)

imaging. For instance, SiO_2 in its purely crystalline form, quartz, is extremely difficult to incorporate into lenses because it is birefringent, while in an amorphous state (such as amorphous fused silica), it is not birefringent and is thus used extensively in lenses. Other lens materials such as MgF_2 and LiF have adequate transparency at 193-nm and 157-nm wavelengths, but are too birefringent for use in high-resolution lenses. CaF_2 has negligible intrinsic birefringence at long wavelengths, but at 193 nm and 157 nm, has appreciable birefringence.¹³² Remarkably, the birefringence of CaF_2 can be easily corrected by using different [111]-oriented CaF_2 lens elements with their crystallographic axes rotated by 60 deg relative to each other, and also by including pairs of elements of [100]-oriented material with the two elements in the pair rotated 45 deg with respect to each other.¹³³ BaF_2 has also been reported to have higher intrinsic birefringence than CaF_2 .¹³⁴

¹³¹J. Mulken et al., "Step and scan technology for the 193 nm era," Abstract from the Third Symposium on 193 nm Lithography, Onuma, Japan (1997).

¹³²J.H. Burnett, Z.H. Levine, and E.L. Shirley, "Intrinsic birefringence in calcium fluoride and barium fluoride," *Phys. Rev. B* **64**, pp. 1–4 (2001).

¹³³J.H. Burnett, Z.H. Levine, and E.L. Shirley, "Hidden in plain sight: calcium fluoride's intrinsic birefringence," *Photon. Spectra*, pp. 88–92 (Dec. 2001).

¹³⁴J.H. Burnett, Z.H. Levine, E.L. Shirley, and J.H. Brunning, "Symmetry of spatial dispersion induced birefringence and its implications for CaF_2 ultraviolet optics," *J. Microlith. Microfab. Microsyst.* **1**(3), 213–224 (2002).

It should be noted that low levels of birefringence can be induced by mechanical stresses in materials that are not birefringent in their perfect crystalline state.¹³⁵ Such stresses are typically created if there are large thermal inhomogeneities in the furnaces in which the crystal of fused silica are grown.¹³⁶

13.4.1 Fused silica

Fused silica is by far the primary optical material for lens manufacturing. Its mechanical and thermal properties are well known, and its grinding and polishing infrastructure are well established. It is relatively inexpensive and has good index homogeneity over large areas. Lens-grade fused silica, however, is an expensive material. The temperature-dependent properties of fused silica are summarized in Table 13.7.

Figure 13.19 shows the wavelength dependence of the refractive index and the thermal coefficient refractive index in the mid-UV spectral region for amorphous (fused) silica for a mean temperature of 25°C.¹³⁷ Figure 13.20 shows the attenuation mechanisms (scattering,¹³⁸ defects,¹³⁹ hydroxyl ion impurity,¹⁴⁰ exciton absorption, etc.) of fused silica. Figure 13.21 is a plot of the Rayleigh-scattering-induced attenuation as a function of wavelength of bulk fused silica. It should be pointed out that Rayleigh scattering in a single-component glass such as silica

Table 13.7 Thermal properties of fused silica at 298°K.

Property	Value
Thermal conductivity (W/m °K)	1.30 ^a
Average coefficient of thermal expansion (10 ⁻⁶ /°K) or (ppm/°K)	0.52 ^a
Specific heat (J/Kg °K)	740

^aExcerpted from Corning Corporation HPFS[®] Fused Silica ArF Grade Product Catalog (2003).

¹³⁵B. Wang, "Birefringence in fused silica and CaF₂ for lithography," *Solid State Technol.*, 77–82 (Feb. 2000).

¹³⁶H.J. Levinson, *Principles of Lithography*, 2nd ed., p. 163, SPIE Press, Bellingham, WA (2005).

¹³⁷For a comparison of refractive index data of fused silica from different suppliers, see for example, J. Malitson, "Interspecimen comparison of the refractive index of fused silica," *J. Opt. Soc. Amer.* **35**, 1205 (1965).

¹³⁸S. Sakaguchi, S. Todoroki, and S. Shibata, "Rayleigh scattering in silica glasses," *J. Amer. Ceramic Soc.* **79**, 2821 (1996).

¹³⁹Defects in glasses can include vacancies, interstitials, dangling bonds, over coordinated atoms, uncoordinated atoms, etc. See, for example, D.L. Griscom, "Defect structure of glasses," *J. Non Crystall. Solids* **73**, 51 (1985).

¹⁴⁰S. Sakaguchi, S. Todoroki, and S. Shibata, "Rayleigh scattering in silica glasses," *J. Amer. Ceramic Soc.* **79**, 2821 (1996); D.L. Griscom, "Defect structure of glasses," *J. Non Crystall. Solids* **73**, 51 (1985).

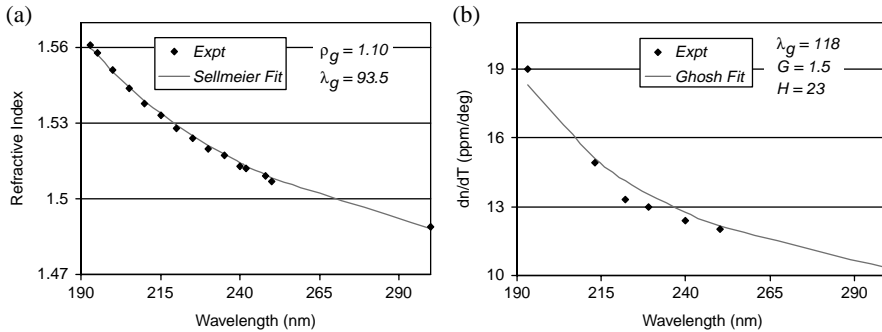


Figure 13.19 (a) Refractive index and (b) thermal coefficient of index of refraction in the mid-UV spectral region for amorphous (fused) silica for a mean temperature of 25°C. The fitting curve for Fig. 13.19(a) is based on the Sellmeier dispersion equation, while that for Fig. 13.19(b) is based on the Ghosh equation. [Adapted with permission from J. Malitson, “Interspecimen comparison of the refractive index of fused silica,” *J. Opt. Soc. Amer.* **35**, 1205 (1965). Copyright 1965, Optical Society of America. Reproduced with permission from R. Kunz and R. Dammell, 193-nm lithography: fundamentals and issues, SPIE Short Course SC120 (2005).]

glass arises from statistical density fluctuations in the sample, which is frozen in the glass at a fictive temperature that is generally represented as the glass transition temperature T_g . Rayleigh scattering depends to a great extent on the techniques used in fabricating the sample. The scattering is believed to be affected by the optical inhomogeneity induced by granularity and glass properties such as refractive index n and T_g . The light loss due to Rayleigh scattering α is given by

$$\alpha = \frac{8\pi^3}{3\lambda^4} n^8 p^2 k T_g \beta_T, \quad (13.9)$$

where n is the refractive index, λ is the exposure wavelength, p is the photoelastic constant, k is the Boltzmann constant, T_g is the glass transition temperature, and β_T is the isothermal compressibility at T_g .

13.4.1.1 Fused-silica degradation mechanisms

On laser irradiation of fused silica at 193 nm, structural rearrangement occurs in the material leading to changes in its density; this is often accompanied by changes in its refractive index, and may cause stress-induced birefringence. Two different mechanisms have been reported to be associated with these changes. One mechanism is compaction, where the fused silica becomes denser (indicating a shortened optical path and increased refractive index) with increasing exposure, while the other is exactly opposite, with rarefaction or decompaction.

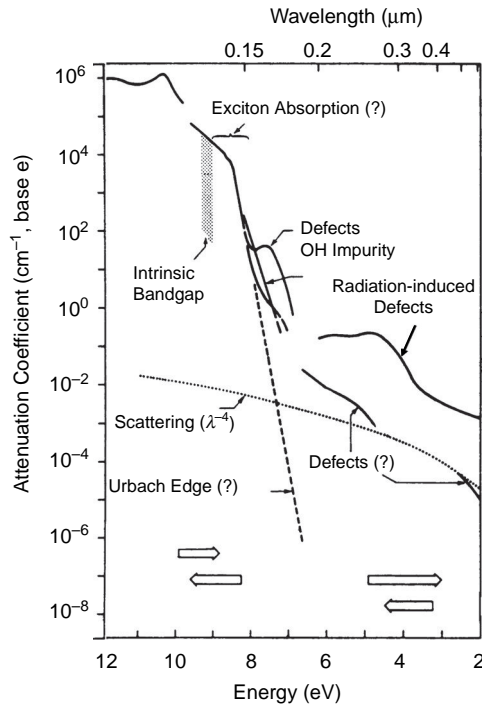


Figure 13.20 Attenuation mechanism of fused silica. [Adapted with permission from D.L. Griscom, "Defect structure of glasses," *J. Non-Crystal. Solids* **73**, 51 (1984). Copyright 1984, Elsevier. Reproduced with permission from R. Kunz and R. Dammel, 193-nm lithography: fundamentals and issues, SPIE Short Course SC120 (2005).]

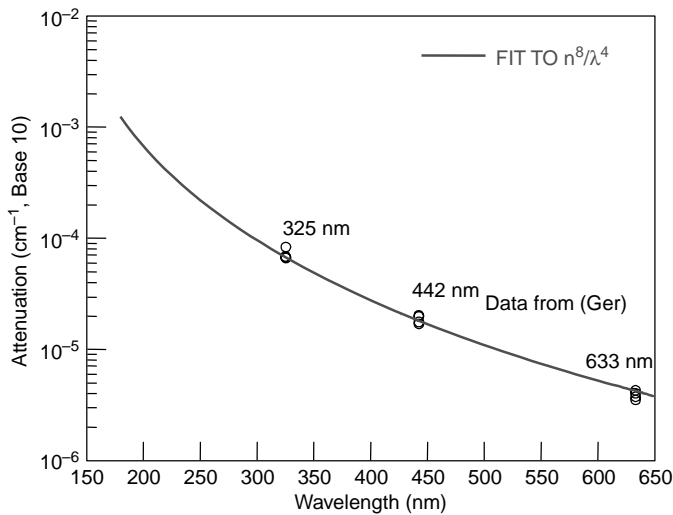


Figure 13.21 Rayleigh scattering of bulk fused silica. (Courtesy of R. Kunz and R. Dammel.)

The change in the refractive index Δn (in ppb) is expressed as¹⁴¹

$$\Delta n = k_1(NI)^a + \left(k_2 \frac{NI^2}{\tau} \right)^b, \quad (13.10)$$

where τ is the pulse length (in nanoseconds), N is the number of pulses, I is the energy density (J/cm^2) per pulse, while k_1 , k_2 , a , and b are fitting parameters that vary from sample to sample. The first term on the right-hand side of Eq. (13.10) represents the rarefaction, while the second term represents compaction. These two terms have different functional dependencies. Even the manufacturing process for the fused silica can influence the rate of its compaction. Optics lifetime can be maximized by optimizing peak power and pulse duration.¹⁴²

The lithographically useful lifetime of fused silica is dependent on many parameters, including (i) lens design as it relates to peak laser fluence, polarization and temperature sensitivity, and phase error tolerance, and (ii) laser parameters such as pulse duration (higher peak fluences must be applied in shorter pulses).

Given the susceptibility of fused silica to laser-induced damage, particularly at high fluences at 193-nm wavelength, it is not used in the illuminator lenses. Rather, at present, calcium fluoride is used in most 193-nm illumination systems for elements where fused silica's lifetime has been projected to be unacceptably short. Also, when necessary, optical coatings that are laser resistant and can function as antireflection coatings are coated on fused silica lenses to protect them from surface damage. Typically, fused silica lenses are used in the projection optics where fluences are much lower than in the illuminator lenses.¹⁴³

An important example of a problem caused by surface damage, especially of the roughening kind, of the exposure lens elements or nonoptimized antireflection coatings is flare.¹⁴⁴ This refers to light scattered in the optical system that reaches areas that are not intended to be exposed at the image plane. Flare can also occur from scattering at surfaces or at defects in the lens materials' substrates. Other causes of scattering from lens surfaces include contamination arising from DUV light-induced photochemical reactions that deposit materials on the lens surfaces.¹⁴⁵ When such deposited materials coalesce, light is scattered by the resulting particles.¹⁴⁶

¹⁴¹It is possible to estimate scattering loss from refractive index dispersion. See, for example, S. Saka guchi, S. Todoroki, and S. Shibata, "Rayleigh scattering in silica glasses," *J. Amer. Ceramic Soc.* **79**, 2821 (1996).

¹⁴²H.J. Levinson, *Principles of Lithography*, 2nd ed., p. 165, SPIE Press, Bellingham, WA (2005).

¹⁴³ibid., p. 166.

¹⁴⁴P. Bousquet, F. Flory, and P. Roche, "Scattering from multilayer thin films: theory and experiment," *J. Opt. Soc. Am.* **71**(9), 1115–1123 (1981).

¹⁴⁵R.R. Kunz, V. Lieberman, and D.K. Downs, "Photoinduced organic contamination of lithographic optics," *Microolithography World*, pp. 2–8 (Winter, 2000).

¹⁴⁶H.J. Levinson, *Principles of Lithography*, 2nd ed., p. 166, SPIE Press, Bellingham, WA (2005).

Flare can occur over long and short distances, hence the types called long-range and short-range flare. Long-range flare leads to a fairly uniform background of light throughout the imaged area, resulting in reduced image contrast, as shown below. In a flare-free exposure system, image contrast is given by

$$C = \frac{I_{\max} - I_{\min}}{I_{\max} + I_{\min}}, \quad (13.11)$$

where I_{\max} and I_{\min} are the maximum and minimum intensity of the image, respectively.

In an exposure system with flare (δ), the intensity is given by

$$I_{\text{flare}} = (1 - \delta)I + \delta, \quad (13.12)$$

where I is the intensity in a flare-free system. The contrast in an exposure system with flare is therefore given by

$$C_{\text{flare}} = \frac{I_{\max} - I_{\min}}{I_{\max} + I_{\min} + \sum_{i=1}^n X_i}, \quad (13.13)$$

where X_i is flare from source i , and n is the total number of sources of flare in the system.

13.4.2 Calcium fluoride

High-purity, single-crystal CaF_2 is an alternative lens material to fused silica in UV lithography, particularly DUV and VUV lithographies. It has higher transmission at 193 nm than fused silica. It is the only material transparent enough to be used as a lens material in 157-nm lithography. It has high damage resistance since it does not suffer from laser-induced compaction like fused silica. It suffers from color center formation to a lesser degree than fused silica, and at 193 nm it does not form color centers. The main drawbacks of CaF_2 include its high residual index inhomogeneity (roughly 1 ppm), spatial dispersion-induced (intrinsic) birefringence¹⁴⁷ (see Table 13.8), poor quality control, difficulty of polishing it, low yield, and high cost.

The difficulties associated with producing high-yield CaF_2 crystals are related to a number of factors. First, obtaining smooth CaF_2 surfaces is difficult because the hardness of CaF_2 depends on crystallographic orientation, which results in uneven surfaces during polishing, particularly across unevenly shaped bulk CaF_2 samples. Special techniques have been developed, however, for polishing CaF_2 .¹⁴⁸ Second, the thermal gradients in the furnace not only limit crystal quality, but necessitate the use of long cooling processes that can last several weeks so as to prevent

¹⁴⁷J.H. Burnett, Z.H. Levine, and E.L. Shirley, "Intrinsic birefringence in calcium fluoride and barium fluoride," *Phys. Rev. B* **64**, 1–4 (2001).

¹⁴⁸D. Golini, M. DeMarco, W. Kordonski, and J. Brunning, "MRF polishes calcium fluoride to high quality," *Laser Focus World*, pp. S5–S13 (July, 2001).

Table 13.8 Spatial dispersion-induced birefringence of CaF₂ at different UV wavelengths.¹⁴⁹

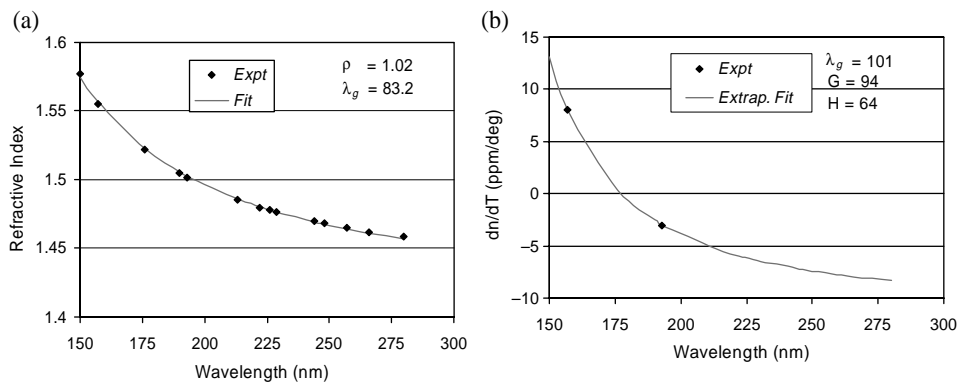
Wavelength (nm)	Birefringence	
	$n_{[110]}$	$n_{[001]}$ (ppm)
253.65		0.055
193.09		0.34
157.63		1.18

thermal stresses. These long times for growing CaF₂ crystals contribute significantly to the high cost of CaF₂ lenses.

The temperature-dependent properties of CaF₂ are summarized in Table 13.9. Figure 13.22 shows the wavelength dependence of refractive index and refractive index change per unit temperature change in the mid-UV spectral region for CaF₂. Figure 13.23 shows the durability of CaF₂ as a function of 193-nm laser pulses. Showing the initial and induced absorption of CaF₂ as a function of number of

Table 13.9 Select properties of CaF₂.¹⁵⁰

Property	Value
Thermal conductivity (W/m °K) at 273°K	10
Linear expansion coefficient (ppm/°K) at 293°K	18.7
Solubility in water (g/100 g of H ₂ O) at 298°K	0.015
Crystal structure	Cubic

**Figure 13.22** (a) Refractive index and (b) refractive index change per unit temperature change in the DUV and VUV spectral regions for CaF₂. (Courtesy of R. Kunz and R. Dammel.¹⁵¹)

¹⁴⁹R. Kunz and R. Dammel, "193 nm Lithography: fundamentals and issues," SPIE Short Course No. SC120 (2005).

¹⁵⁰Linear expansion coefficient and solubility values excerpted from Corning Corporation's H0607[®] CaF₂ Product Catalog (2003).

¹⁵¹ibid.

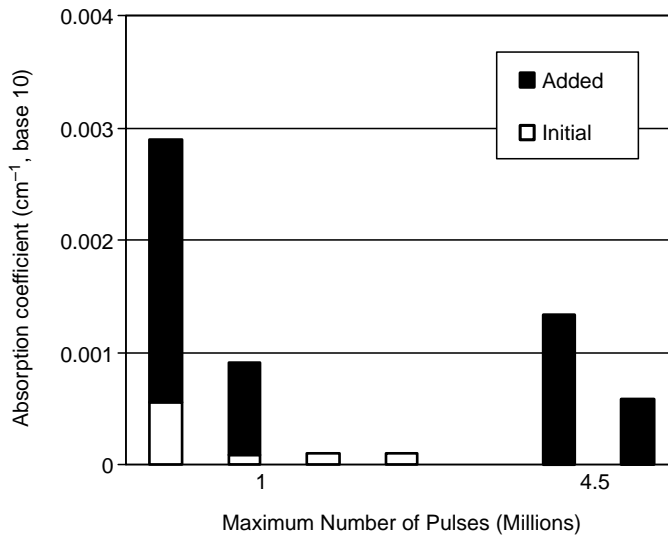


Figure 13.23 Durability of different CaF₂ samples under 193-nm laser irradiation (at 1 mJ/cm²/pulse). (Courtesy of R. Kunz and R. Dammel.¹⁵²)

laser pulses, this plot indicates that after about 1 billion pulses (at 1 mJ/cm²/pulse), the total bulk absorption of fused silica is significantly less than 0.001 cm⁻¹. The total absorption in CaF₂ is dominated by added (laser-induced) losses.

13.4.3 Optical coatings

In order to ensure good transmission, and to some degree to protect the optical elements of lithographic exposure tools, particularly in high-radiation fluence situations, optical coatings are nearly always applied to these optical elements. The common types of UV optical coatings include antireflection (AR) coatings (used to enhance throughput and reduce ghost images), full reflectors (used in laser windows and tuning mirrors), partial reflectors (used in beam delivery systems and catadioptric imaging systems), and filters. The applications of coatings fall into two categories, namely, (i) aluminum mirrors with dielectric overcoat and (ii) dielectric coatings.

13.4.3.1 Aluminum mirrors

Aluminum mirrors are designed for broadband exposure (or equivalently, a broad range of angles of incidence), and have greater than 85% reflectance over the UV range. They are inexpensive and simple to deposit. Their durability under

¹⁵²ibid.

long-term laser irradiance is inferior to those of dielectric-based optical coatings (see next section) because of their higher absorption.

13.4.3.2 Dielectric optical coatings

These are based on constructive and/or destructive interference effects of incident and reflected light. These antireflection coatings have bandwidths of a few nanometers for optimal operation. With appropriate material selection, their absorption can be minimized, and excellent durability can be achieved. They are, however, more complicated to deposit, requiring precise knowledge of the optical constants of the films, endpoint monitoring for determining the correct thickness of the film, and optimization of deposition conditions for denser defect-free films. For these reasons, they cost more than aluminum mirrors.

The basic design of these coatings involves alternating quarter-wave layers of higher- and lower-index materials as compared to the substrate, i.e., 2–5 layers for antireflection designs, and up to 40 layers for highly reflective applications. The layer thicknesses are typically in the tens of nanometers, depending on wavelength and layer indices. For fused silica or calcium fluoride substrates, fluoride or oxide layer materials can be used. Specifically, for high-index applications, fluorides such as LaF_3 , GdF_3 , and NdF_3 or oxides such as Al_2O_3 , HfO_2 , and ZrO_2 are coated over the fused silica or calcium fluoride substrate. For low-index applications, fluorides such as MgF_2 , LiF , and AlF_3 or oxides such as SiO_2 are coated over fused silica or calcium fluoride substrate.¹⁵³

13.4.4 Pellicle materials

Pellicles used in UV lithography such as 193 nm are generally made of perfluorinated polymers. Irradiation of pellicles over time induces small but measurable changes in their physical properties, i.e., they become thinner due to polymer photovolatilization, their refractive indices decrease due to increased porosity, and their absorbance increases due to formation of new chemical bonds. All of these changes in physical properties are affected by the exposure ambient, with exposures in nitrogen experiencing degradation acceleration relative to those in oxygen ambient, perhaps due to the healing effect of photogenerated radicals via peroxy formation in oxygen ambient.¹⁵⁴

13.5 Printing Modes

As stated above, there are three main lithographic printing modes, namely, contact printing, proximity printing, and projection printing (see Fig. 13.24).

¹⁵³ibid.

¹⁵⁴ibid.

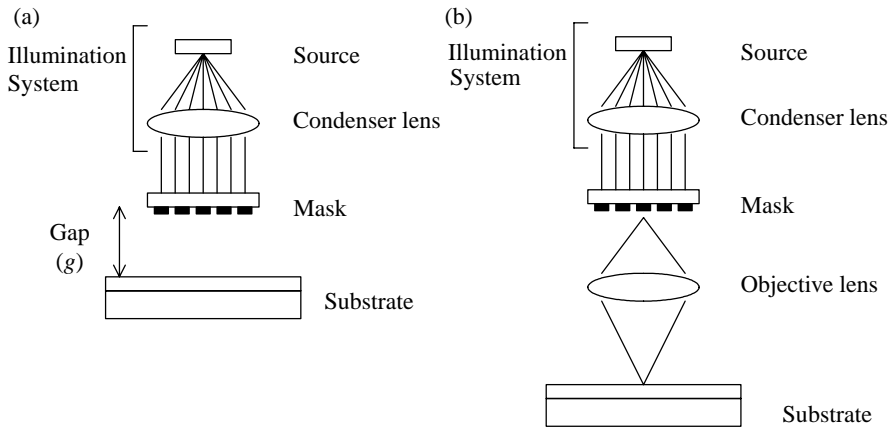


Figure 13.24 Schematic of (a) contact ($z = 0$) and proximity printing and (b) projection printing. (Adapted with permission from Taylor & Francis Group LLC.¹⁵⁵)

13.5.1 Contact and proximity printing

In contact printing [see Fig. 13.24(a)] the mask and the photoresist-coated substrate are in direct contact during exposure, with the mask held chrome-side down on the resist film. Patterns on the mask are transferred to the entire wafer by broadband radiation. The theoretical resolution limit of contact printing is given by¹⁵⁶

$$CD \cong \frac{3}{2} \sqrt{\frac{\lambda z}{2}}, \quad (13.14)$$

where CD is the minimum critical dimension (assuming that the feature is a grating with a period of twice the CD), λ is the exposure wavelength, and z is the photoresist thickness. As alluded to above, the act of bringing the mask and the wafer into contact causes damage to the mask and creates defects, which are reproduced in subsequent exposures. In addition, wafer and mask nonflatness results in alignment errors that degrade the resolution capability of the technique.¹⁵⁷

The early 1960s saw the development of the contact aligners, the first practical exposure systems that were sold commercially by companies such as Microtech, Electroglas, Preco, and Kulicke & Soffa. In these contact aligners, patterns were imaged and exposed in a photoresist via a mask that was in intimate physical contact with the upper surface of the photoresist. Such exposures created yield

¹⁵⁵B.W. Smith, "Optics for photolithography," in *Microlithography: Science and Technology*, J.R. Sheats and B.W. Smith, Eds., p. 172, Marcel Dekker, New York (1998).

¹⁵⁶M.J. Bowden, "The lithographic process: the physics," in *Introduction to Microlithography*, L.F. Thompson, C.G. Willson, and M.J. Bowden, Eds., pp. 22–23, American Chemical Society, Washington, DC (1994).

¹⁵⁷A.K. K. Wong, *Resolution Enhancement Techniques in Optical Lithography*, p. 14, SPIE Press, Bellingham, WA (2001).

degrading problems, because the contact caused mask scratches and resist lifting. With the introduction in 1971 of the 4-KB DRAM by Mostek and the first microprocessor by Intel—the 4004—the need for a new generation of contact printers that could pattern tens of thousands of transistors became all too apparent. This need was met with the introduction of the Cobit soft contact aligner around 1972, which had a resolution of about five microns.¹⁵⁸

However, due to the defectivity problem associated with contact printing, as discussed above, the first noncontact aligners, called proximity aligners, were introduced in 1973 by Kasper Instruments. In proximity printing mode, the mask does not come into direct physical contact with the wafer [see Fig. 13.24(a)]. Rather, it is held 10–25 μm above the upper surface of the resist-coated wafer. This gap, however, limited resolution on account of diffraction. The theoretical resolution limit of proximity printing is given by the expression¹⁵⁹

$$\text{CD} \cong \frac{3}{2} \sqrt{\lambda \left(g + \frac{z}{2} \right)}, \quad (13.15)$$

where g is the distance between the mask and the resist surface. The square root dependence of the resolution is a consequence of the Fresnel diffraction theory, which is valid in the near-field region, just below the mask openings.

The proximity printers achieved a resolution of roughly 4–6 μm ; they had higher yield than the contact aligners. Their yield was limited because of the difficulties associated with controlling the gap spacing between the mask and the resist-coated wafer.¹⁶⁰

13.5.2 Projection printing

Technical difficulties associated with proximity printing and stringent resolution requirements led to the introduction of scanning projection printing¹⁶¹ in 1973 by Perkin-Elmer. In this system, the image of the mask is projected through a slit onto the wafer surface as the mask and wafer are moved simultaneously by the slit [see Fig. 13.24(b)].¹⁶² The exposure dose was determined by the intensity of the light, the slit width, and the speed at which the wafer was scanned. These systems offered much better resolution and yield, as well as higher throughput than the contact and proximity aligners. They, however, suffered from limited registration accuracy. In fact, the early scanning projection systems were designed

¹⁵⁸“Microlithography & mask making,” VLSI Research Inc. Report (1992).

¹⁵⁹M.J. Bowden, “The lithographic process: the physics,” in *Introduction to Microlithography*, L.F. Thompson, C.G. Willson, and M.J. Bowden, Eds., pp. 24, American Chemical Society, Washington, DC (1994).

¹⁶⁰“Microlithography & mask making,” VLSI Research Inc. Report (1992).

¹⁶¹The first scanning projection system was developed under the auspices of a joint project between Perkin Elmer and Intel Corporation.

¹⁶²R.M. Scott, “Annular field optical imaging systems,” U.S. Patent No. 3,821,763 (1974); A. Offner and C.T. Darien, “Unit power imaging catoptric anastigmat,” U.S. Patent No. 3,748,015 (1973).

to provide full-wafer exposure without demagnification. These $1\times$ systems were amenable to simple optical designs, which permitted the use of a relatively broad light spectrum.¹⁶³

With the trend in increasing wafer size and the reduction of feature dimension, full-wafer printing without demagnification became increasingly difficult to implement due to mask dimension control and pattern placement difficulties. Reduction projection printing was therefore introduced to alleviate these problems.¹⁶⁴ These reduction projection systems were called steppers [see Fig. 13.25(a)] and were introduced in the early 1970s first by Kasper Instruments and in 1976 by the GCA Corporation.¹⁶⁵ GCA's first commercial stepper, the DSW4800,¹⁶⁶ was based on the multiple-aperture step-and-repeat projection systems for reticle making (also called photorepeaters) that GCA was already producing. The DSW4800 could handle 3-, 4-, or 5-in wafers and was equipped with a $10\times$ reduction, 0.28 NA, g-line lens (supplied by Carl Zeiss of Oberkochen,

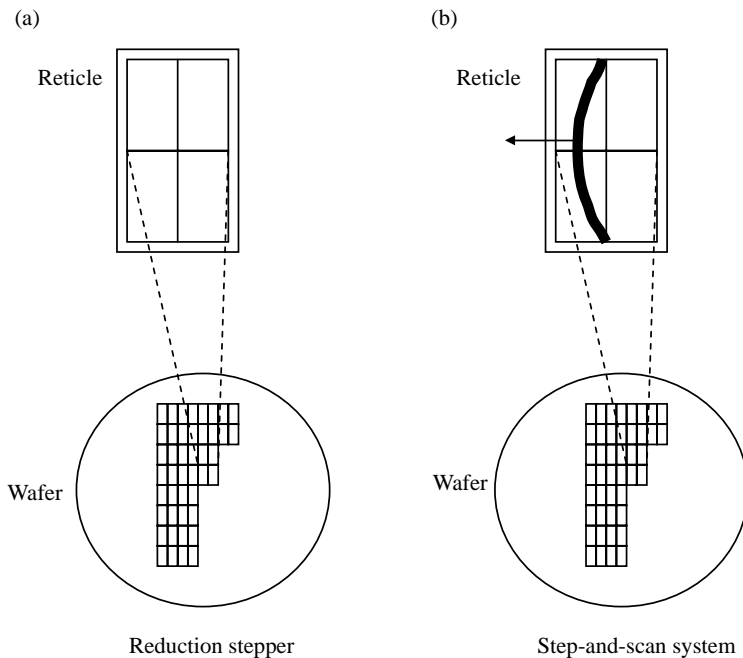


Figure 13.25 How (a) steppers and (b) step-and-scan tools expose a large wafer with a small image field.

¹⁶³A.K. K. Wong, *Resolution Enhancement Techniques in Optical Lithography*, p. 15, SPIE Press, Bellingham, WA (2001); "Microlithography & mask making," VLSI Research Inc. Report (1992).

¹⁶⁴A.K. K. Wong, *Resolution Enhancement Techniques in Optical Lithography*, p. 15, SPIE Press, Bellingham, WA (2001).

¹⁶⁵"Microlithography & mask making," VLSI Research Inc. Report (1992).

¹⁶⁶The abbreviation DSW of GCA's first stepper stood for Direct Step on the Wafer, an allusion to the stepper's origin in mask making.

Germany) that could pattern a maximum square field of 10 mm × 10 mm. It could achieve overlay of 0.7 μm and a resolution of 1.25 μm. The development of the DSW4800, it should be pointed out, was preceded by systems designed and built by several semiconductor companies, including Philips, Thomson CSF, and IBM,¹⁶⁷ who built steppers for their own use and did not sell them commercially, although the Philips stepper technology was eventually commercialized by ASM Lithography.¹⁶⁸

Wafer steppers expose one rectangular section of a wafer (called an image field) at a time, i.e., on a field-by-field basis using a step, expose, and repeat method [see Fig. 13.25(b)]. This method offered better alignment accuracy and focus control than the preceding techniques by aligning and exposing only a portion of the wafer at a time. The image could be reduced from a larger mask, offering increased resolution and much higher yields, because defect printing would be reduced by the reduction ratio, so much so that some of the defects would not be able to print. This greatly relaxed the burden on mask makers. Substantial performance benefits were soon realized with them in practice as improvements in masks, lenses, light sources, numerical aperture, focus control, and registration were implemented over time.¹⁶⁹ From the mid-1980s through most of the 1990s, when device critical dimension reached 250 nm, steppers dominated the IC industry.

The design of reduction projection optics, even with reduced image field, it should be pointed out, is not trivial because of the drive toward higher numerical aperture lenses for improved resolution and the need for aberration correction of the image field area. At sub-300-nm wavelengths, fused silica and CaF₂ are the only practical lens materials, which makes chromatic (color) aberration correction impossible in refractive exposure systems. Although reflective or catadioptric (i.e., utilizing both reflective and refractive elements) methods can be used, the required surface finish of the aspheric mirrors in such systems is extremely difficult to achieve.¹⁷⁰

Another approach that has been adopted in the IC industry for mitigating the effects of aberration, particularly chromatic aberration, is line narrowing of the incident radiation. The basis of this approach derives from the realization that an illumination radiation with extremely narrow spectral bandwidth is associated with very low chromatic aberration, obviating the need for color correction of the refractive elements associated with such a system. The required degree of spectral purity increases with increasing NA. For instance, KrF (248-nm) exposure systems with NA ~0.7 require spectral bandwidth on the order of a picometer

¹⁶⁷A. Bouwer, G. Bouwhuis, H. Van Heek, and S. Wittkoek, "The silicon repeater," *Philips Tech. Rev.* **37**(11/12), 330–333; S. Wittkoek, "Optical aspects of the silicon repeater," *Philips Tech. Rev.* **41**, 268 (1983/84); H. Binder and M. Lacomat, "Step and repeat projection printing for VLSI circuit fabrication," *IEEE Trans. Electron Dev.* **ED-26**(4), 698–704 (1979); J. Wilcynski, "Optical step and repeat camera with dark field automatic alignment," *J. Vac. Sci. Technol.* **16**, 1929–1933 (1979).

¹⁶⁸H.J. Levinson, *Principles of Lithography*, 2nd ed., p. 141, SPIE Press, Bellingham, WA (2005).

¹⁶⁹"Microlithography & mask making," VLSI Research Inc. Report (1992).

¹⁷⁰A. K. K. Wong, *Resolution Enhancement Techniques in Optical Lithography*, p. 15, SPIE Press, Bellingham, WA (2001).

(10^{-12} m).¹⁷¹ Such a narrow spectrum requires high spectral power, which is readily achieved with high-repetition-rate exciplex laser sources.¹⁷²

In 1989, Perkin-Elmer introduced the first step-and-scan system (a hybrid between a stepper and scanning projection system) to address the ever-increasing chip size problem and the ever-more stringent dimension control requirements. These issues were mitigated in the step-and-scan tool through the reduction of the exposure area.¹⁷³ Developed under the auspices of a joint venture between IBM and Perkin-Elmer in the mid-1980s, the tool was sold under the brand name of Micrascan.¹⁷⁴ The step-and-scan system uses a fraction of a normal stepper field (for example, 26 mm × 8 mm), then scans this field in one direction to expose the entire 4× reduction mask (to produce, for example, a 26 mm × 33 mm field on the wafer). The wafer is then stepped to a new location, and the scan is repeated. In other words, the reticle is scanned rather than exposed all at once. Step-and-scan systems offer many technical advantages such as greater overlay, better imaging capability, and higher productivity than the first GCA stepper (see Table 13.10). The smaller imaging field simplifies the design and fabrication of the lens, but at the expense of a more complicated wafer stage and reticle. It is the exposure system of choice for printing device critical dimensions <250 nm.

Influenced by the success of the GCA steppers, several companies began to produce wafer steppers and market them commercially. The major stepper suppliers today for advanced lithographic patterning applications include ASM Lithography (ASML), Nikon, and Canon.

Modern steppers have considerably greater capability than the original GCA DSW4800, but the operating principles remain essentially the same. The exposure wavelength of tools used in production has evolved from 436 nm through 365 nm, and 248 nm to 193 nm. In the meantime, the numerical aperture of the projection tool has increased from 0.16 (with the first projection systems) to 1.35 in water-

¹⁷¹ibid.

¹⁷²A.I. Ershov, T. Hofmann, W.N. Partlo, I.V. Formenkov, G. Everage, P.R. Das, and D. Myers, "Feasibility studies of operating KrF lasers at ultra narrow spectral bandwidths for 0.18 μm linewidths," *Proc. SPIE* **3334**, 1021–1030 (1998); U. Stamm, R. Pätzelt, J. Kleinschmidt, K. Vogler, W. Zschocke, I. Bragin, and D. Basting, "ArF excimer laser for 193 nm lithography," *Proc. SPIE* **3334**, 1010–1013 (1998).

¹⁷³S. Hirukawa, K. Matsumoto, and K. Takemasa, "New projection optical system for beyond 150 nm patterning with KrF and ArF sources," *Proc. SPIE* **3334**, 414–422 (1998); D. Cote, K. Andersen, D. Cronin, H. Harold, M. Himmel, J. Kane, J. Lyons, L. Markoya, C. Mason, D. McCafferty, M. McCarthy, G. O'Connor, H. Sewell, and D. Williamson, "Micrascan III performance of a third generation, catadioptric step and scan lithographic tool," *Proc. SPIE* **3051**, 806–816 (1997); J. van Schoot, F. Bornebroek, M. Suddendorf, M. Mulder, J. Van der Spek, J. Stoeten, and A. Hunter, "0.7 NA step and scan system for 150 nm imaging with improved overlay," *Proc. SPIE* **3679**, 448–463 (1999); N. Deguchi and S. Uzawa, "150 nm generation lithographic equipment," *Proc. SPIE* **3679**, 464–472 (1999).

¹⁷⁴Following the introduction of the Micrascan, Perkin Elmers Optical Lithography Group was acquired by Silicon Valley Group (SVG) in May of 1990. Subsequent generations of the Micrascan tools were produced and marketed by SVG.

Table 13.10 Comparison of the attributes of the commercially available step-and-scan 193-nm exposure tools and the first commercial wafer stepper (GCA's DSW4800). It should be noted that both Canon and Nikon specify their throughput using 64 and 65 exposure fields ("shots") per wafer, respectively, while ASML specifies throughput with 125 shots per wafer.¹⁷⁵

	GCA	Canon	Nikon	ASML
Model	DSW4800	AS4	NSR S307E	XT:1250D
M:1	10×	4×	4×	4×
Wavelength (nm)	436	193	193	193
Maximum lens NA	0.28	0.85	0.85	0.85
Field size (mm)	10 × 10	26 × 33	26 × 33	26 × 33
Overlay, machine to itself (nm)	500	10	8	8
Wafer size (mm except for GCA)	3 in, 4 in, 5 in	200, 300	200, 300	200, 300
Throughput (300 mm wafers per hour, except for GCA)	20 (4 in wafers)	140	140	114

immersion ArF lithographic exposure systems currently used to fabricate devices at the 45-nm technology node. Leading-edge steppers also come in the step-and-scan and the step-and-repeat configurations.

Figure 13.26 shows pictures of a state-of-the-art advanced step-and-scan 193-nm exposure tool based on the TWINSCAN XT:1900Gi model from ASML. This tool is rated by the supplier as a high-productivity, dual-stage

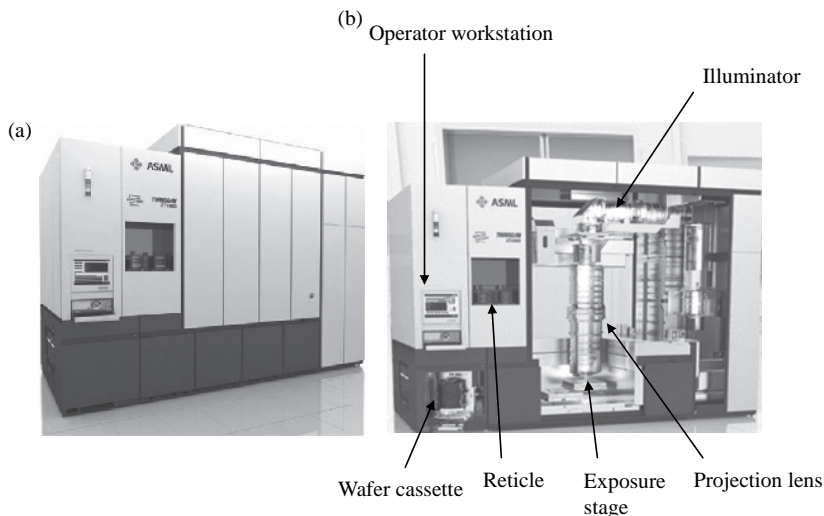


Figure 13.26 ASML Twinscan XT:1900Gi 193-nm step-and-scan lithographic exposure tool, with (a) the chassis closed and (b) showing the optical path. (Photos courtesy of ASML.)

¹⁷⁵H.J. Levinson, *Principles of Lithography*, 2nd ed., p. 141, SPIE Press, Bellingham, WA (2005).

water-immersion lithography tool designed for volume 300-mm wafer production at 45-nm resolution and below. Utilizing an in-line catadioptric projection lens design with 1.35 NA, this tool supports 26-mm \times 33-mm field, 4 \times reduction imaging. The illuminator features polarization at maximum throughput of ≥ 131 wafers per hour (using 30 mJ/cm² exposure dose delivered on 300-mm wafers integrated from 125 shots from a 6-KHz ArF exciplex laser system).¹⁷⁶ It should be pointed out that normal NA (< 1) exposure tool designs based on the twin-scan and single-stage models exist for dry 193-nm, 248-nm, and 365-nm wavelength lithographies; although they differ mainly in their exposure wavelength, sources, and lens design, their configuration is essentially similar.

13.6 General Considerations on Optics Relevant to Lithography

13.6.1 Image formation

It is well established that the diffraction of light by an object, e.g., a mask, plays a very critical role in image formation in optical systems,¹⁷⁷ including those used in optical lithography.¹⁷⁸ When a beam of light encounters the edge of an opaque obstacle (e.g., a mask) placed an appreciable distance away from the recording plane (wafer), rectilinear propagation does not occur, contrary to the assumptions of geometric optics. The variation in intensity produced at some distance from the obstacle depends on a number of factors, including the coherency of the light, its wavelength, and the distance the light travels before being observed.¹⁷⁹ Figure 13.27 shows the situation for a coherently illuminated mask, along with the resulting intensity pattern observed at increasing distances.

In coherent illumination, fringes are created in the diffuse shadowing between light and dark, as a result of interference. Only when there is no separation between the obstacle and the recording plane does rectilinear propagation actually occur. As the distance between the recording plane and the obstacle increases, there occurs a region in which the geometrical shadow is still discernible. Beyond this region, far from the obstacle, the intensity pattern at the recording plane is no longer similar to the geometrical shadow, but instead contains areas of light and dark fringes.¹⁸⁰ As the separation distance between the obstacle and the recording plane becomes extremely close, such that geometric shadowing is still recognizable, near-field diffraction or Fresnel diffraction dominates;¹⁸¹ this is the situation obtained in contact printing. At greater separation distance between the recording plane and the

¹⁷⁶Source: ASML 2008 Product Catalog.

¹⁷⁷E. Abbe, *Archiv. Mikrosk. Anat. Entwicklungsmech* **9**, 413 (1904).

¹⁷⁸B.W. Smith, "Optics for photolithography," in *Microlithography: Science and Technology*, J.R. Sheats and B.W. Smith, Eds., p. 183, Marcel Dekker, New York (1998).

¹⁷⁹*ibid.*, p. 183.

¹⁸⁰*ibid.*

¹⁸¹*ibid.*

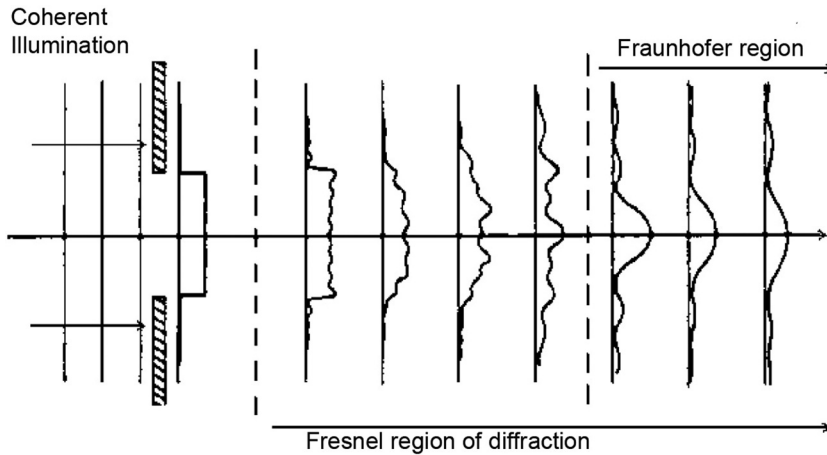


Figure 13.27 Diffraction pattern of a coherently illuminated mask opening at near (Fresnel) and far (Fraunhofer) distances. (Reprinted with permission from Taylor & Francis Group LLC.¹⁸²)

obstacle, far-field diffraction or Fraunhofer diffraction dominates; this is the situation obtained in projection lithography.¹⁸³ Since optical projection lithography is the dominant printing technique currently in use in the fabrication of IC devices, the analysis in this section will be concentrated on this technique.

In a projection lithographic exposure tool, when light is incident on a mask, it is diffracted toward the objective lens in the projection system. The light propagation inside the tool determines how the tool ultimately performs, depending on the coherence of the light that illuminates the mask.

It can be shown that for a coherently illuminated single space mask opening of width d , as shown in Figure 13.28, the OPD between two waves, w_1 and w_2 , exists whenever one wave travels farther than the other by any amount. Such a path difference can be expressed as $(d/2)\sin\theta$. When the resulting OPD is one-half wavelength or any multiple of one-half wavelength, the waves will interfere destructively. In like manner, an OPD of $d\sin\theta$ exists between any two waves that originate from points separated by the full space width. The destructive interference of the waves from the top portion of the mask opening with those from the bottom portion of the mask opening occurs when¹⁸⁴

$$d \sin \theta = m\lambda \quad (m = \pm 1, \pm 2, \pm 3, \dots), \quad (13.16)$$

¹⁸²ibid., p. 183.

¹⁸³ibid.

¹⁸⁴B.W. Smith, "Optics for photolithography," in *Microlithography: Science and Technology*, J.R. Sheats and B.W. Smith, Eds., pp. 186–187, Marcel Dekker, New York (1998).

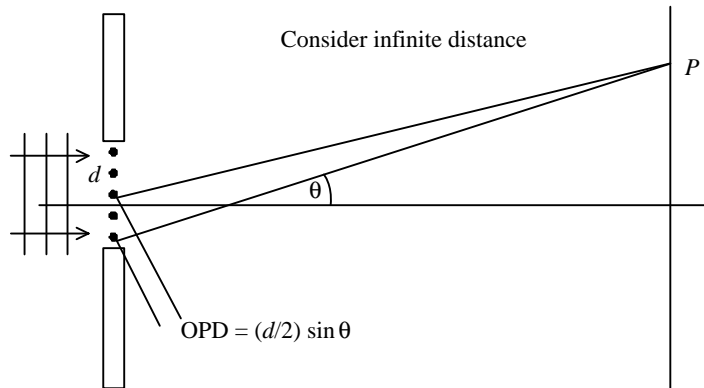


Figure 13.28 Determination of Fraunhofer diffraction effects for a coherently illuminated single mask opening. (Reprinted with permission from Taylor & Francis Group LLC.¹⁸⁵)

where

$$|m| \leq \frac{d}{\lambda}. \quad (13.17)$$

From Eq. (13.16), the positions of dark fringes in the Fraunhofer diffraction pattern can be readily determined. The resulting diffraction pattern from a single space is shown in Fig. 13.29, where a broad central bright fringe exists at positions corresponding to $\theta = 0$, and where dark fringes occur when θ satisfies the destructive interference condition.¹⁸⁶

It should be noted that Fraunhofer diffraction represents spatial frequency spectrum or pattern detail. It is essentially the Fourier transform of the mask

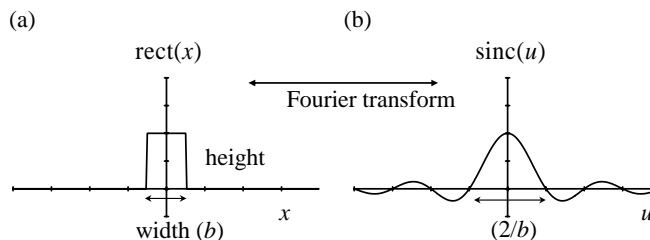


Figure 13.29 (a) A single space mask pattern and (b) its corresponding Fraunhofer diffraction pattern. These are Fourier transform pairs. (Reprinted with permission from Taylor & Francis Group LLC.¹⁸⁷)

¹⁸⁵ibid., p. 186.

¹⁸⁶ibid., p. 187.

¹⁸⁷B.W. Smith, "Optics for photolithography," in *Microlithography: Science and Technology*, J.R. Sheats and B.W. Smith, Eds., p. 187, Marcel Dekker, New York (1998).

function. If $m(x, y)$ is a two-dimensional mask function or electric field distribution across the x - y mask plane and $M(u, v)$ is the coherent field distribution across the u - v Fraunhofer diffraction plane, then the Fourier transform operation is given by

$$M(u, v) = \mathfrak{F}\{m(x, y)\}, \quad (13.18)$$

where

$$u = \frac{x'}{\lambda z}, \quad (13.19a)$$

$$v = \frac{y'}{\lambda z}, \quad (13.19b)$$

where (x', y') are coordinates in the diffraction plane and z is the distance from the mask to the diffraction plane. Both $m(x, y)$ and $M(u, v)$ have amplitude and phase components. For the specific case of an isolated space, the distribution of the amplitude of the interference pattern is the Fourier transform of an even, one-dimensional, nonperiodic, rectangular pulse, commonly referred to as a rect function, $\text{rect}(x)$. The Fourier transform of $\text{rect}(x)$ is a $\text{sinc}(u)$, where¹⁸⁸

$$\text{sinc}(u) = \frac{\sin(\pi u)}{\pi u}, \quad (13.20)$$

which is shown in Fig. 13.28. The intensity of the pattern is proportional to the square of the amplitude or a $\text{sinc}^2(u)$ function, which corresponds to the power spectrum.¹⁸⁹

13.6.1.1 The role of the objective lens

The process of image formation in optical systems, such as projection lithographic exposure tools, consists of diffraction of light by the mask, followed by recombination of that light at the image plane with the aid of the projection lens. All of the light that goes to form the image of the mask on the wafer plane passes through the focal plane of the projection lens.¹⁹⁰ This connection between diffraction and image formation was first proposed in 1870 by Ernst Abbe,¹⁹¹ who was working on image formation in microscopes at the time. He showed that the diffraction maxima formed in the back focal plane of the objective lens are critical to the formation of the image, with the higher orders controlling the finer detail in the image. He also determined that perfect image formation requires all of the

¹⁸⁸ibid., p. 189.

¹⁸⁹ibid.

¹⁹⁰M.J. Bowden, "The lithographic process: the physics," in *Introduction to Microlithography*, 2nd ed., L.F. Thompson, C.G. Willson, M.J. Bowden, Eds., p. 49, American Chemical Society, Washington, DC (1994).

¹⁹¹E. Abbe, *Archiv. Mikrosk. Anat. Entwicklungsmech* **9**, 413 (1904).

diffracted orders to be collected and combined with all other orders at the image plane, unless, of course, there are no higher orders, as is usually the case for state-of-the-art optical lithography. In fact, the $+1$, 0 , and -1 diffraction orders contain information about the fundamental periodicity of the mask grating, whereas the higher orders define the edge slope.¹⁹²

In projection printing, the role of the objective lens is therefore to collect a finite amount of diffracted information from a mask, determined by its maximum acceptance angle, otherwise called the numerical aperture (see Fig. 13.30). In this capacity, the objective lens behaves as a linear filter for a diffraction pattern propagating from a mask. By limiting high-frequency diffraction orders, it acts as a low-pass filter, blocking out the orders that propagate at angles beyond its numerical aperture. The orders that are passed through the numerical aperture of the lens are acted on by the lens to produce a second inverse Fourier transform operation, which partially reconstructs the mask image at the image plane (see Fig. 13.31). The mask image reconstruction is carried out on a partial basis because of the loss of higher-frequency diffraction orders, on account of the finite nature of the numerical aperture, as well as degradation resulting from lens aberration.¹⁹³

In mathematical terms, the low-pass filtering function of the projection lens can be described in the following manner for the special case of a rectangular grating, where $p \sin \theta = m\lambda$ describes the positions of the discrete coherent diffraction orders. If the lens is described in terms of a two-dimensional pupil function $H(u, v)$,

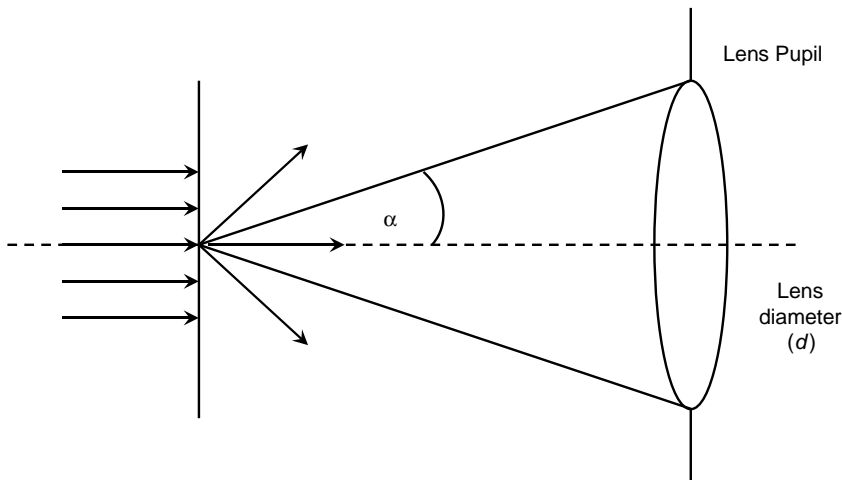


Figure 13.30 Schematic representation of the NA of a lens. $NA = n_i \sin(\alpha)$, where n_i is the refractive index of the medium and α is one-half the acceptance angle.

¹⁹²M.J. Bowden, "The lithographic process: the physics," in *Introduction to Microlithography*, 2nd ed., L.F. Thompson, C.G. Willson, and M.J. Bowden, Eds., p. 49, American Chemical Society, Washington, DC (1994).

¹⁹³B.W. Smith, "Optics for photolithography," in *Microlithography: Science and Technology*, J.R. Sheats and B.W. Smith, Eds., p. 195, Marcel Dekker, New York (1998).

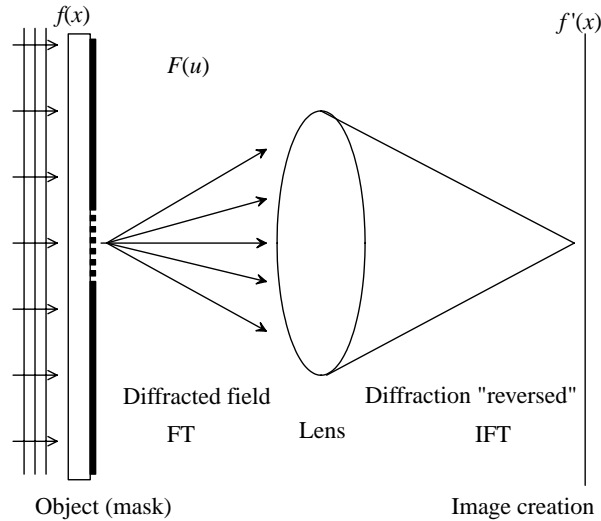


Figure 13.31 Image formation in a projection lens.

which is limited by its scaled numerical aperture, NA/λ , then the expressions

$$\begin{aligned} H(u, v) &= 1 \quad \text{if} \quad \sqrt{u^2 + v^2} < \frac{NA}{\lambda} \\ &= 0 \quad \text{if} \quad \sqrt{u^2 + v^2} > \frac{NA}{\lambda} \end{aligned} \quad (13.21)$$

describe the behavior of the lens as a low-pass filter. The image amplitude produced by the lens is the inverse Fourier transform of the mask's Fraunhofer diffraction pattern multiplied by the lens pupil function:¹⁹⁴

$$A(x, y) = \mathfrak{F}^{-1}\{M(u, v) \cdot H(u, v)\}. \quad (13.22)$$

The image intensity distribution, otherwise called the aerial image, is given by the square of the image amplitude:¹⁹⁵

$$I(x, y) = |A(x, y)|^2. \quad (13.23)$$

13.6.1.2 Partial coherence theory of image formation

The concept of degree of coherence is of great utility in the description of illumination conditions. Our starting point for this analysis is Abbe's theory of microscope imaging, which is applicable to optical lithographic imaging with coherent or

¹⁹⁴B.W. Smith, "Optics for photolithography," in *Microlithography: Science and Technology*, J.R. Sheats and B.W. Smith, Eds., p. 195, Marcel Dekker, New York (1998).

¹⁹⁵ibid., p. 196.

partially coherent illumination.¹⁹⁶ Abbe showed that when a ruled grating is coherently illuminated and imaged through an objective lens, the resulting image is dependent on the numerical aperture of the lens. The minimum resolution that can be obtained for such a condition is a function of both the illumination wavelength and the NA of the lens, as shown in Fig. 13.32, for coherent illumination.¹⁹⁷

Given that imaging is not possible in a situation in which no more than the undiffracted beam (the zero order) is accepted by the lens, it thus follows that a minimum of the first diffraction order is required for resolution. The position of this first diffracted order is given by¹⁹⁸

$$\sin(\theta) = \frac{\lambda}{p}. \quad (13.24)$$

By definition, the numerical aperture of a lens is the sine of one-half its acceptance angle (θ), so it follows that the minimum resolvable line width ($hp_{\min} = p/2$) should be

$$hp_{\min} = \frac{p}{2} = 0.5 \frac{\lambda}{\text{NA}}. \quad (13.25)$$

It should be pointed out that Abbe used a uniform source (a lamp) and a sub-stage condenser to form the image in the object plane. For nonuniform sources,

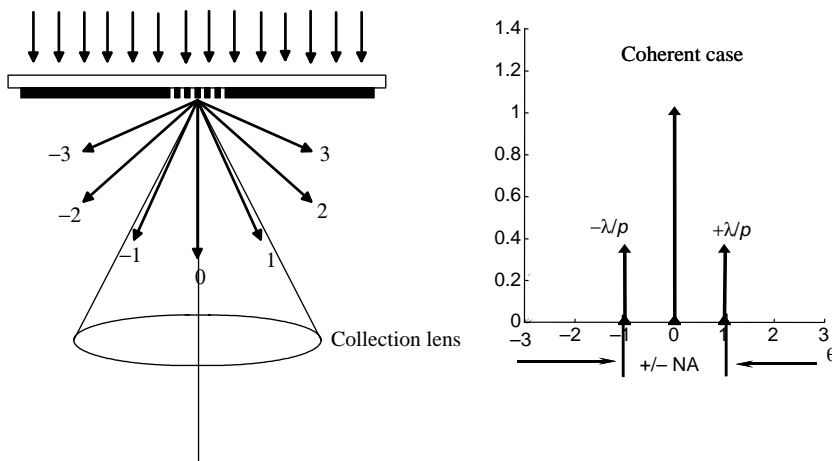


Figure 13.32 The diffraction orders associated with coherent illumination of a grating mask, illustrating the condition for minimum diffraction-limited resolution. (Reprinted with permission from Taylor & Francis Group LLC.¹⁹⁹)

¹⁹⁶R. Kingslake, *Optical System Design*, p. 196, Academic Press, London (1983).

¹⁹⁷B.W. Smith, "Optics for photolithography," in *Microlithography: Science and Technology*, J.R. Sheats and B.W. Smith, Eds., pp. 197–199, Marcel Dekker, New York (1998).

¹⁹⁸ibid.

¹⁹⁹ibid., p. 199.

Köhler devised a two-stage illuminating system to form an image of the source in the entrance pupil of the objective lens, as was shown in Fig. 13.8.²⁰⁰ Such a pupil at the condenser lens can control the numerical aperture of the illumination system. As the size of the pupil is decreased, the source size and the effective source size are decreased accordingly, resulting in an increase in the degree of coherency. In this way, the Köhler illumination scheme makes possible the control of partial coherence in the exposure system. The degree of partial coherence σ is expressed as the ratio of the effective source size to the full objective aperture size, as shown in Eq. (13.2). As σ approaches the value zero, a condition of coherent illumination exists. As σ approaches infinity, incoherent illumination exists. In lithographic projection systems, practical σ values are generally in the range of 0.3 to 0.9. Values below 0.3 lead to “ringing” in the images; these are fringes that result from coherent interference effects.²⁰¹

A notable effect of partial coherence on imaging is the spreading of each diffraction order about their discrete coherent frequencies, as illustrated in Fig. 13.33, which shows the diffraction orders for a rectangular wave mask pattern illuminated with σ values greater than zero. In this situation, the zeroth order is centered on axis but with a width >0 , a result of the extent of partially coherent illumination angles. In like manner, each higher diffraction order also has a width >0 , an effective spreading of the discrete orders.²⁰²

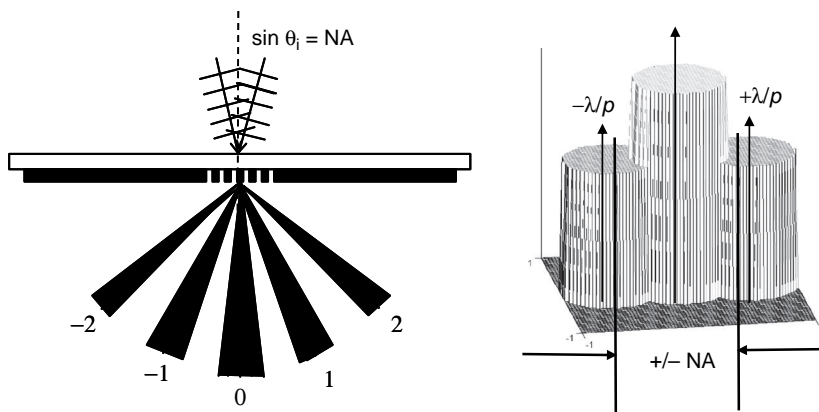


Figure 13.33 Spread of diffraction orders for partially coherent illumination. (Reprinted with permission from Taylor & Francis Group LLC.²⁰³)

²⁰⁰A. Köhler, “Gedanken zu Einem Neuen Beleuchtungsverfahren für Mikrographische Zwecke,” *Zeitschrift für wissenschaftliche Mikroskopie* (1893); D.C. O’Shea, *Elements of Modern Optical Design*, p. 113, John Wiley & Sons, New York (1985).

²⁰¹B.W. Smith, “Optics for photolithography,” in *Microlithography: Science and Technology*, J.R. Sheats and B.W. Smith, Eds., p. 200, Marcel Dekker, New York (1998).

²⁰²ibid.

²⁰³ibid.

It can be shown that the minimum resolvable pitch p_{\min} for partial coherent illumination is given by

$$p_{\min} = \frac{\lambda}{(\sigma + 1)NA}. \quad (13.26)$$

There are some conditions in which the performance of partial coherent imaging is superior to coherent imaging. An example is a situation involving coherent illumination of a rectangular grating mask where the ± 1 diffraction orders fall just outside the NA of a projection lens system. With coherent illumination, imaging is not possible because the size of the mask feature falls below the $R = 0.5(\lambda/NA)$ limit. In contrast, with partial coherent illumination, part of the ± 1 diffraction order information can be captured by the lens, affording reasonable imaging of the features. Partially coherent illumination is therefore recommended when mask features fall below $R = 0.5(\lambda/NA)$ in size. An optimum degree of coherence can be determined for a feature based on its size, the illumination wavelength, and the NA of the objective lens. Figure 13.34 illustrates the effect of partial coherence on imaging of large features $[0.6(\lambda/NA)]$ and small features $[0.4(\lambda/NA)]$. In the case of the large features, with aerial images larger than the resolution possible for coherent imaging, an increase in values of partial coherence above $\sigma = 0$ results in the degradation of the aerial image. In contrast, in the case of the smaller features, they become resolvable as partial coherence levels increase above $\sigma = 0$.²⁰⁴

13.6.2 Image quality

There are quite a few metrics that lithographers use to quantify the quality of an image. These include the contrast, modulation transfer function, exposure latitude,

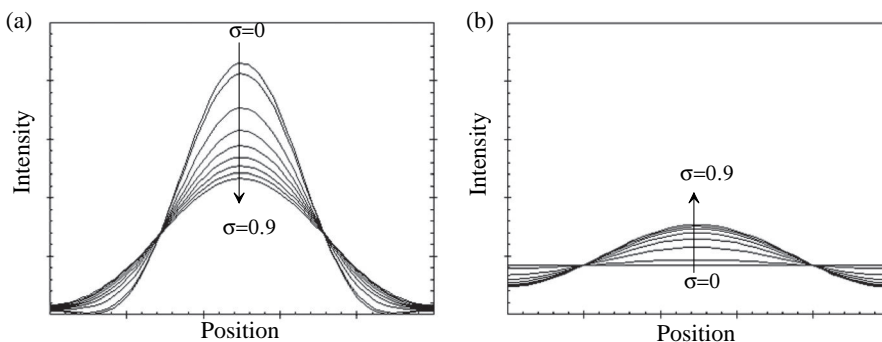


Figure 13.34 Aerial image intensities for (a) large features $[0.6(\lambda/NA)]$ and (b) small features $[0.4(\lambda/NA)]$ with varying levels of partial coherence. (Reprinted with permission from Taylor & Francis Group LLC.²⁰⁵)

²⁰⁴ibid., p. 201.

²⁰⁵ibid., p. 202.

normalized image log-slope, depth of focus, exposure-defocus window, and CD uniformity, each of which is addressed in the following sections.

13.6.2.1 Contrast

The image contrast is defined mathematically in Eq. (13.11). Contrast is a measure of modulation; the higher the contrast, the more distinctly defined are the bright and dark regions, and hence the better the image quality. It should be pointed out, however, that the image contrast metric is only strictly defined for equal line and space patterns, and is only useful for patterns near the resolution limit. For large features, it is essentially 1.0, regardless of the image quality. And finally, it is not directly related to practical metrics of lithographic quality, such as line width control.²⁰⁶

13.6.2.2 Modulation transfer function

An ideal imaging system such as an ideal lens transmits 100% of the incident light that passes through it. Real lenses are not perfect; they lose a fraction of the incident light on them due to aberrations and diffraction, while transmitting the rest. When these losses are measured in terms of contrast, it is called the modulation of the contrast. In other words, modulation describes how much contrast is lost by a given lens. The modulation transfer function (MTF) is the spatial frequency response of an imaging system; it is the contrast at a given spatial frequency relative to low frequencies. It is useful for calculating the fraction of radiation transmitted through the optical system at a particular frequency.²⁰⁷ Above all, it is used to characterize the resolution and performance of an imaging system. It does not, however, make any prediction as to how well a feature will image because of the fact that a pattern is generally composed of multiple sinusoidal frequencies.²⁰⁸

Mathematically, the MTF is expressed as the ratio of the modulation of the relative image contrast (M_{image}) to the relative object contrast (M_{object}) for a given spatial frequency when the illumination is incoherent:²⁰⁹

$$\text{MTF}(v) = \frac{M_{\text{image}(v)}}{M_{\text{object}(v)}}. \quad (13.27)$$

²⁰⁶C.A. Mack, *Fundamental Principles of Optical Lithography: The Science of Microfabrication*, p. 371, John Wiley & Sons, Hoboken, NJ (2007).

²⁰⁷M.J. Bowden, "The lithographic process: the physics," in *Introduction to Microlithography*, 2nd ed., L.F. Thompson, C.G. Willson, and M.J. Bowden, Eds., p. 61, American Chemical Society, Washington, DC (1994).

²⁰⁸A.K. K. Wong, *Resolution Enhancement Techniques in Optical Lithography*, p. 60, SPIE Press, Bellingham, WA (2001).

²⁰⁹M.J. Bowden, "The lithographic process: the physics," in *Introduction to Microlithography*, 2nd ed., L.F. Thompson, C.G. Willson, and M.J. Bowden, Eds., p. 61, American Chemical Society, Washington, DC (1994).

By convention, the MTF is normalized to unity at zero spatial frequency. At low spatial frequencies, the MTF is close to 1.0 (100%); it generally falls as the spatial frequency increases, until it reaches zero. Higher spatial frequencies have lower contrast values than lower spatial frequencies. As spatial frequencies increase, the MTF curve falls until it reaches zero. This represents the limit of the resolution for the given optical system, and the associated frequency is called the cutoff frequency.²¹⁰

A concept that is related to MTF is the critical modulation transfer function (CMTF), which is a useful approximation for determining minimum modulation required for a photoresist. The minimum required modulation of a resist with (base 10) contrast γ is expressed as²¹¹

$$\text{CMTF} = \frac{10^{1/r} - 1}{10^{1/r} + 1}. \quad (13.28)$$

13.6.2.3 Exposure latitude

Exposure latitude is the maximum amount of dose variation that can be tolerated before a pattern prints out of specification (see Fig. 13.35). A $\pm 10\%$ dimension

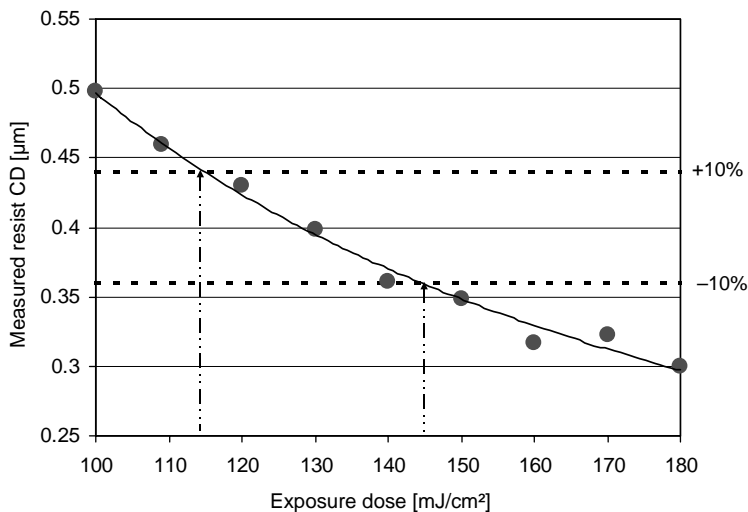


Figure 13.35 Exposure latitude for printing a feature of target size $0.4 \mu\text{m}$. If the dose to print the feature target is $128 \text{ mJ}/\text{cm}^2$, then the exposure latitude $(145 - 114)/128 \times 100\% = 24.2\%$.

²¹⁰A. Reiser, *Photoreactive Polymers: The Science and Technology of Resists*, p. 240, John Wiley & Sons, Hoboken, NJ (1989).

²¹¹B.W. Smith, "Optics for photolithography," in *Microlithography: Science and Technology*, J.R. Sheats and B.W. Smith, Eds., p. 207, Marcel Dekker, New York (1998).

tolerance is typical for photolithography. Exposure latitude is applicable to all feature types. Given topography and reflectivity fluctuations, dose setting error, illumination nonuniformity, flare, and mask CD error, a manufacturable process requires at least 6–10% exposure latitude.²¹²

13.6.2.4 Normalized image log-slope

The quality of a printed resist image depends on the sharpness of its edges relative to the unexposed surrounding areas. What determines this edge is related to the steepness of the transition from bright (exposed) to dark (unexposed) within the aerial image. The steeper the aerial image intensity transition, the better the edge definition of the resist pattern. The steepness of this transition is the slope of the aerial image intensity near the desired resist edge (dI/dx). Dividing the slope of the aerial image intensity at the resist edge by the intensity associated with the edge (threshold) normalizes the effect of the exposure dose. The result is called the image log-slope, which is proportional to the dose sensitivity at the edge position.²¹³

$$\text{Image log-slope} = \frac{1}{I_{\text{threshold}}} \left. \frac{dI}{dx} \right|_{\text{threshold}} = \left. \frac{d \ln I}{dx} \right|_{\text{threshold}}, \quad (13.29)$$

where the log-slope is measured at the nominal (desired) line edge position. Multiplying the log-slope by the CD of the feature yields the normalized image log-slope (NILS):

$$\text{NILS} = \text{CD} \left. \frac{d \ln I}{dx} \right|_{I_{\text{threshold}}}. \quad (13.30)$$

The NILS is usually the best single metric for judging the lithographic usefulness of an aerial image.²¹⁴

13.6.2.5 Depth of focus

The depth of focus (DOF) image quality metric refers to the maximum amount of focus change that can be tolerated before the printed pattern size falls outside the specification. It is defined as the distance along the optical axis that produces an image of some suitable quality. The Rayleigh depth of focus for a feature at

²¹²A.K. K. Wong, *Resolution Enhancement Techniques in Optical Lithography*, p. 61, SPIE Press, Bellingham, WA (2001).

²¹³C.A. Mack, *Field Guide to Optical Lithography*, p. 53, SPIE Press, Bellingham, WA (2006); A.K. K. Wong, *Resolution Enhancement Techniques in Optical Lithography*, p. 60, SPIE Press, Bellingham, WA (2001); C.A. Mack, *Fundamental Principles of Optical Lithography: The Science of Microfabrication*, p. 123, John Wiley & Sons, Hoboken, NJ (2007).

²¹⁴C.A. Mack, *Field Guide to Optical Lithography*, p. 53, SPIE Press, Bellingham, WA (2006).

the resolution limit is expressed as²¹⁵

$$\text{DOF} = \pm \frac{k_2 \lambda}{\text{NA}^2} \quad (\text{for } \text{NA} \leq 0.7), \quad (13.31)$$

where k_2 is a process-dependent factor, also known as an unknown variable.

13.6.2.6 Exposure-defocus window

The analysis of the exposure-defocus window image quality metric involves the determination of the simultaneous influence of focus and dose on feature line width.²¹⁶ In generating this plot, a Bossung plot²¹⁷ of the measured line width at various focus levels is first determined. Very flat curves suggest that the printed size is less focus sensitive, and therefore will have a large DOF. Similarly, closely packed curves indicate that the feature size fluctuates less rapidly with dose changes; this is associated with large exposure latitude.²¹⁸ From the Bossung plot, contours of the feature size as a function of focus and dose can be determined, and the exposure-defocus window can be derived, such that two curves offset from the nominal CD by $\pm 10\%$ bound an area in which the focus and dose values afford the feature size that meets the specification. These two curves define the exposure-defocus window.²¹⁹

13.6.2.7 Critical dimension uniformity

In the CD uniformity metric, the variation of feature CD is experimentally determined from measurement, and relevant population statistics are applied to characterize it in terms of range and standard deviation. Good image quality is associated with tight CD uniformity.

13.7 Optical Lithographic Technologies and Their Performance

13.7.1 i-line (365-nm) lithography

As stated earlier, i-line lithography uses the emission from an Hg arc lamp at 365 nm to expose resists, mostly based on DNQ/novolac systems (see Chapter 7

²¹⁵A.K. K. Wong, *Resolution Enhancement Techniques in Optical Lithography*, pp. 62–63, SPIE Press, Bellingham, WA (2001).

²¹⁶B.J. Lin, "Partially coherent imaging in two dimensions and theoretical limits of projection printing in microfabrication," *IEEE Trans. Electron Dev.* **27**(5), 931–938 (1980).

²¹⁷J.W. Bossung, "Projection printing characterization," *Proc. SPIE* **100**, 80–84 (1977).

²¹⁸A.K. K. Wong, *Resolution Enhancement Techniques in Optical Lithography*, pp. 64–65, SPIE Press, Bellingham, WA (2001).

²¹⁹ibid., pp. 64–66.

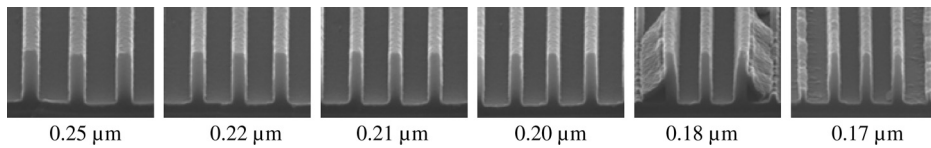


Figure 13.36 Resolution capability of AZ HiR 1075 i-line photoresist used in printing line/space features with 1:1.5 pitch. Processing conditions: Film thickness 0.66 μm on 1300 \AA AZ BARLi II BARC, soft bake (proximity) 90°C/60 seconds (proximity). Exposure tool ASML/400 Scanner. Exposure conditions: Dose 170 mJ/cm^2 , annular illumination, NA 0.65, partial coherence σ (outer/inner) 0.85/0.55. Postexposure bake (proximity) 110°C/90 seconds. Development 2.38% tetramethyl ammonium hydroxide developer/single puddle for 60 seconds at 21.0°C. (Courtesy of R. Dammel.²²⁰)

for the chemistry of this resist system). For over a quarter of a century, from the early 1970s to the late 1990s, the DNQ/novolac resist system was the dominant resist technology, and was used in h-, g-, and i-line lithographic technologies. Figures 13.36 and 13.37 show the i-line lithographic resolution and depth of focus capability of a state-of-the-art i-line resist.

13.7.2 KrF (248-nm) lithography

KrF lithography succeeded i-line lithography as the patterning option for printing device-critical IC layers around the late 1990s at the 0.25- μm device technology node, and remained the dominant technology until 2003. Using exposure tools similar to those shown in Fig. 13.26 (with the exception that the tools are equipped with a KrF excimer laser source), as well as chemical amplification resists based on a polyhydroxystyrene resist platform (see Chapter 7), this lithography was deployed in the patterning of critical device layers spanning many generations: 0.25- μm , 0.18- μm , 0.15- μm , and 0.13- μm technology nodes. Figure 13.38 shows the resolution capability of this lithographic technology.

13.7.3 Dry ArF (193-nm) lithography

At the heart of dry ArF lithography lies an exposure tool equipped with ArF excimer laser source (emitting 193-nm wavelength photons). The insertion of ArF (193-nm) lithography into production was originally expected to take place in

²²⁰R. Dammel, "Diazonaphthoquinone based resists," SPIE Short Course No. SC104 (2002).

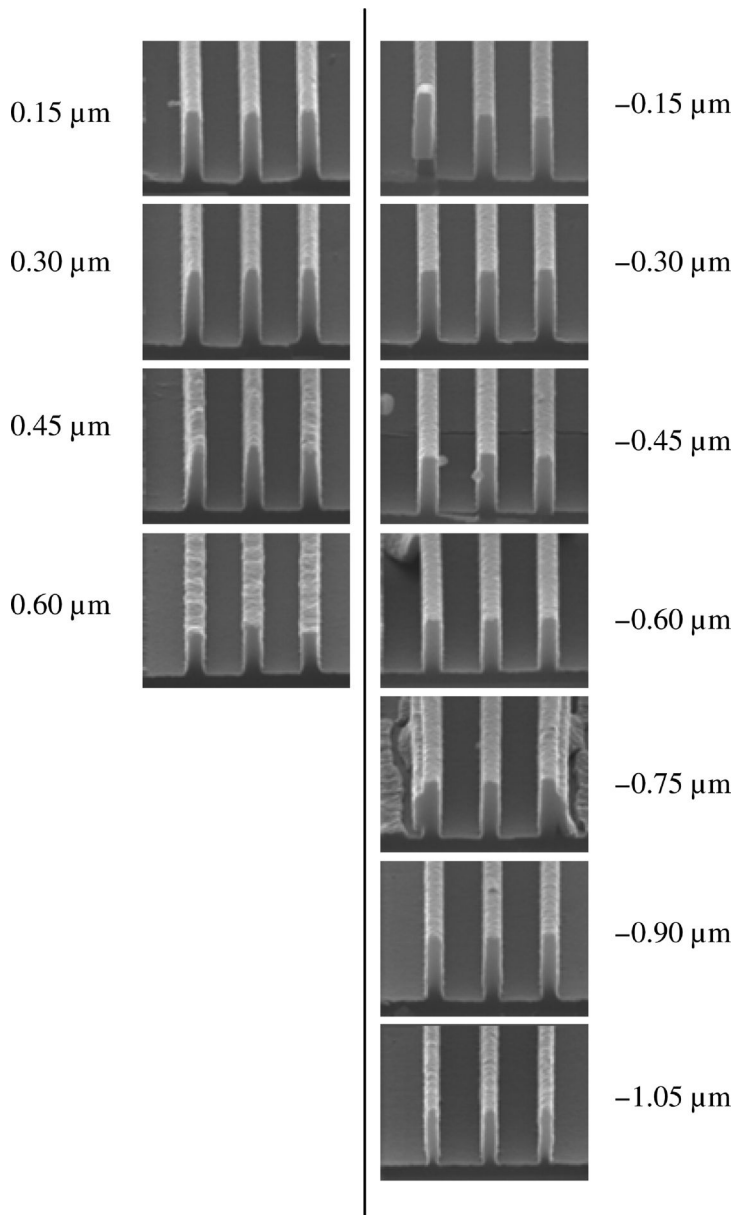


Figure 13.37 Depth of focus capability of AZ HiR 1075 i-line photoresist used in printing 0.22- μm line features with 1:1.5 pitch. Processing conditions: Film thickness 0.66 μm on 1300 \AA AZ BARLi II BARC, soft bake (proximity) 90°C/60 seconds (proximity). Exposure tool ASML/400 Scanner. Exposure conditions: Dose 170 mJ/cm^2 , annular illumination, NA 0.65, partial coherence σ (outer/inner) 0.85/0.55. Postexposure bake (proximity) 110°C/90 seconds. Development 2.38% tetramethyl ammonium hydroxide developer/single puddle for 60 seconds at 21.0°C. (Courtesy of R. Dammel.²²¹)

²²¹R. Dammel, "Practical resist processing," SPIE Short Course No. SC616 (2005).

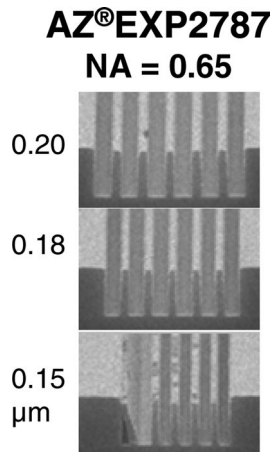


Figure 13.38 Resolution capability of AZ EXP 2787 DUV 248-nm photoresist used in printing line/space features with a 0.65-NA KrF excimer laser tool. (Courtesy of R. Dammel.²²²)

2001 at the 130-nm technology node.²²³ Instead, KrF (248-nm) lithography was extended, aided by improvements in resist materials, availability of high-NA exposure tools, and successful implementation of resolution enhancement techniques such as phase-shifting masks, off-axis illumination, and OPC schemes. The large-scale insertion of ArF lithography into production in many of the leading semiconductor companies started around 2003 at the 90-nm technology node for logic devices.²²⁴ It was also used in the fabrication of critical layers at the 65-nm technology node around 2005.

The two most commonly cited reasons for this delayed introduction of ArF lithography into volume production include the lack of adequate supply of CaF_2 for exposure tool lenses and the immaturity of ArF resist materials²²⁵ and related infrastructure. Another less well-known but important reason was the tendency of many IC manufacturing companies to impose process technologies that have worked well for 365-nm (i-line) and 248-nm (DUV) on ArF resists with the hope of obtaining the same level of performance as in the longer-wavelength resist materials, even though the material properties of these resists are different from their longer-wavelength counterparts. But to achieve the optimal performance of ArF resists, lithographic, etch and ion implant process technologies had to be

²²²R. Dammel, “Diazonaphthoquinone based resists,” SPIE Short Course No. SC104 (2002).

²²³The International Technology Roadmap for Semiconductors, Semiconductor Industry Association (1999).

²²⁴Some of the leading edge memory device makers actually inserted ArF lithography into limited production runs at the 130 nm half pitch around 2002.

²²⁵K. Ronse, P. De Bisschop, A.M. Goethals, I. Pollentier, and G. Vandenberghe, “On the maturing of ArF resists: when can they be implemented in manufacturing?” *Future Fab. Int.* **10**, 175 (2001).

specifically tuned to match the chemical and material properties of ArF resists.²²⁶ This was a lesson that was learned.

Different ARC materials from those used in KrF lithography drove process integration changes involved with ArF excimer laser patterning. Successful implementation of ArF lithography in large-scale device patterning required those integration issues to be resolved. Such issues include (i) ARC reflectivity control and thickness, and the trade-offs between using organic and inorganic ARCs; (ii) resist optical absorption, feature CD profile, CD uniformity, line edge and sidewall roughness, and line feature slimming under SEM inspection and analysis; and (iii) resist erosion, line thinning, end cap pullback, and line edge and sidewall roughening during etch. The issues were not so much about the material and process technology limitations of ArF lithography, as they were about working around these limitations while meeting the stringent specifications for production.

While the limitation of ArF resist materials and issues of ArF lithography have been treated to varying degrees elsewhere,²²⁷ here we will focus on how these resist material issues intersect with device process technologies. The approach will involve analyses of lithographic patterning, etch patterning, and metrology issues of ArF resist materials and related processes used in the fabrication of polygate, contact, via, and trench layers of a CMOS logic device. In addition, we will briefly review the state of the art in ArF SLR (single-layer resist) materials, along with the strengths and weaknesses of the resist polymer platforms. The scope of the treatment is limited to the SLR approach since that is by far the most popular option used in ArF lithography.

13.7.3.1 ArF resist material chemistry

The history of the development and chemistry of various resist polymer platforms of ArF resist materials has been reviewed in detail elsewhere,²²⁸ as well as in Chapter 7. Here, we briefly summarize the main attributes of each platform with a view to relating aspects of their physical and chemical properties to lithographic and etch performance. Figure 13.39 shows the three main polymer platforms [acrylate, cycloolefin (CO), and cycloolefin-maleic anhydride (COMA)] on which most of the commercially available ArF resists today are based.

The acrylate platform is characterized by the presence of pendant aliphatic and alicyclic units with acid labile groups on an acrylate backbone. These resist polymers have high transparency at 193 nm, excellent adhesion properties, and high

²²⁶U. Okoroanyanwu, "Materials and process issues delaying the Introduction of ArF lithography into production (Part 1)," *Future Fab Int.* **12** (2002); U. Okoroanyanwu, "Materials and process issues delaying the introduction of ArF lithography into production (Part 2)," *Future Fab Int.* **13** (2002).

²²⁷K. Ronse, P. De Bisschop, A.M. Goethals, I. Pollentier, and G. Vandenberghe, "On the maturing of ArF resists: when can they be implemented in manufacturing?" *Future Fab Int.* **10**, 175 (2001); U. Okoroanyanwu, H.J. Levinson, C. Y. Yang, S. Pangrle, J. Schefske, and E. Kent, "Integration considerations for 130 nm device patterning using ArF lithography," *Proc. SPIE* **4000**, 423 (2000).

²²⁸U. Okoroanyanwu, H.J. Levinson, A.M. Goethals, and F. Van Roey, "Progress in 193 nm photo resists and related process technologies," in *OMM Interface'98 Proc.*, 1 (1998).

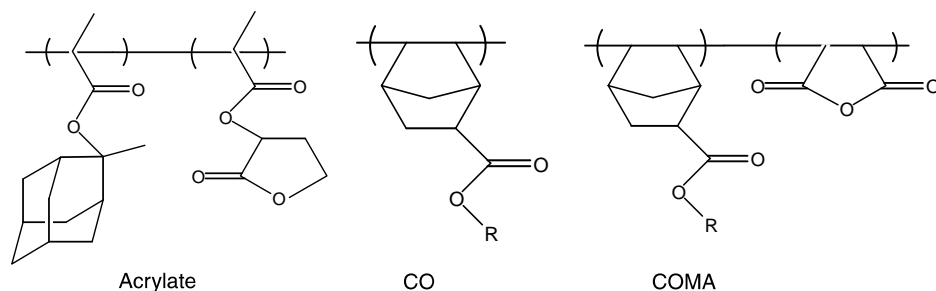


Figure 13.39 Chemical platforms of ArF resist polymers.

imaging resolution. However, they tend to suffer from significant line edge and sidewall roughness, and significant line slimming during SEM inspection (see Section 13.7.3.2.8). Due to their limited mechanical stability, they tend to be susceptible to pattern collapse at aspect ratios typically greater than 3.

The backbone of the CO polymer platform is alicyclic units with pendant ester-protecting groups, acidic groups, and adhesion-promoting groups. Resist polymers of this platform generally have higher plasma etch stability, but are also more hydrophobic than their acrylate and COMA counterparts.

The backbone of the COMA polymer platform comprises cycloolefins with acid labile groups and maleic anhydride. These resists have generally good etch resistance, high mechanical stability, and good resolution, but only moderate transparency. Both CO and COMA platform resists are less susceptible to pattern collapse and show less line width slimming during SEM inspection than their acrylate counterparts.

13.7.3.2 ArF lithographic patterning issues

The ultimate goal of lithographic patterning at every technology node is to achieve tight CD control with sufficiently wide process latitude. Some of the main lithographic patterning issues with ArF resists that contribute to CD variation include compatibility with dielectric ARC materials and reflectivity effects (swing effects and notching), bulk effects,²²⁹ optical proximity effects (OPEs),²³⁰ PEB delay and sensitivity effects, excessive line edge roughness, and pattern collapse.

²²⁹M. Op de Beeck et al., "Lithographic strategies for 0.35 μm polygates for random logic applications," *Proc. SPIE* **2195**, 407–421 (1994); K. Ronse, M. Op de Beeck, A. Yen, H. H. Kim, and L. Van den Hove, "Characterization and optimization of CD control for 0.25 μm CMOS applications," *Proc. SPIE* **2726**, 555–563 (1996).

²³⁰R. Pforr, A. Wong, K. Ronse, L. Van den Hove, A. Yen, S. Palmer, G. Fuller, and O. Otto, "Feature biasing versus feature assisted lithography—a comparison of proximity correction methods for 0.5*(λ /NA) lithography," *Proc. SPIE* **2440**, 150–170 (1995); P. Tziatkov et al., "0.3 μm and sub 0.30 μm *i* line lithography for random logic poly gates," in *Proc. of Interface'95 Microlithography Seminar*, 1 (1995); A. Yen et al., "Optical proximity correction for 0.3 μm *i* line lithography," *Microelectron. Eng.* **30**, 141 (1996).

In the following sections, these issues are illustrated for the particular device layer where their effect is most acute, using the best performing resists.

As stated above, the large-scale insertion point of ArF lithography into production was in gate patterning applications, starting at the 90-nm technology node for logic devices. Resolution enhancement techniques such as phase-shifting masks and optical proximity correction, as well as the use of thin-layer resist imaging over hard mask, did improve the process margin at the 90-nm technology node. Decreasing the resist thickness also did reduce the aspect ratio and decrease the likelihood of pattern collapse due to mechanical forces. However, the smaller the structure and the thinner the resist, the more the properties become surface dominated, thus posing a new set of integration problems. Contact hole and via patterning applications with ArF lithography, on the other hand, are resolution limited because of their high MEEF, typically greater than 4.

13.7.3.2.1 CD uniformity and control

The top-down SEM pictures of Fig. 13.40 show slightly sloped profiles of different gate layer structures patterned in an acrylate resist with ArF lithography. Corner rounding [Figs. 13.40(a) and 13.40(c)] and line-end pullback [Fig. 13.40(b)] are evident in these images. The slight slope in the profile is due to different intensity of light reaching different levels in the resist film, creating a gradient in the chemical amplification reactions on which this lithography is based. Profiles such as these translate to poor CD uniformity and control.²³¹

Figure 13.41 shows a top-down SEM image of 160-nm vias (string, isolated, and dense) printed with an acrylate resist. Note the absence of significant CD bias between these structures.

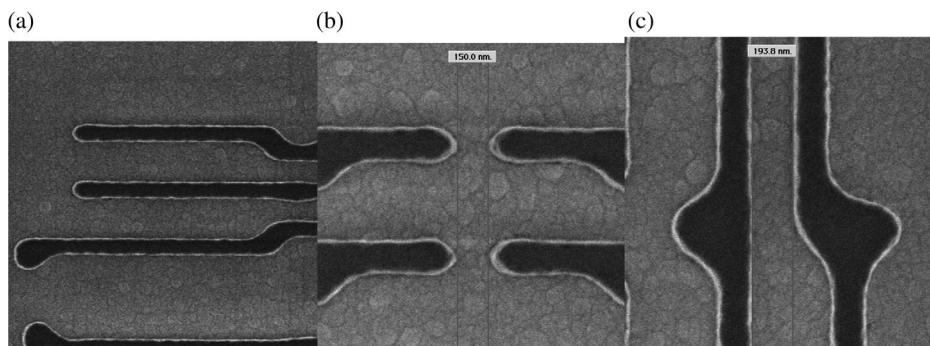


Figure 13.40 Top-down SEM images of different gate structures patterned in acrylate resist, showing (a) and (c) corner rounding and (b) line-end shortening and pull back. Experimental conditions: ASML PAS5500/900 scanner, NA 0.63, σ 0.6, conventional illumination, binary mask, acrylate resist.

²³¹U. Okoroanyanwu, H.J. Levinson, B. Singh, and S.J. Lee, "Impact of optical absorption on process control for sub 150 nm device patterning using 193 nm lithography," *Proc. SPIE* **3998**, 781 (2000).

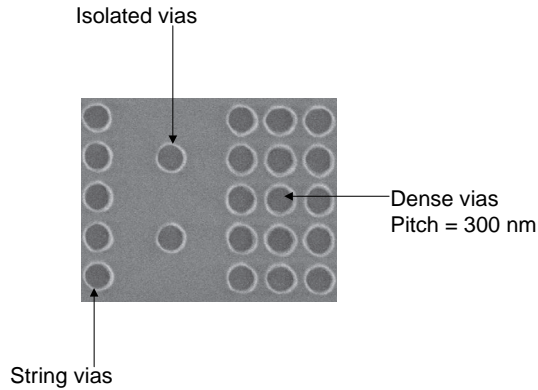


Figure 13.41 Top-down SEM image of 160-nm string, isolated, and dense vias printed on an acrylate resist. Experimental conditions: ASML PAS5500/900 scanner, NA 0.63, σ 0.5, conventional illumination, att-PSM with 6% transmission, dose 21 mJ/cm².

13.7.3.2.2 Optical proximity effects

OPEs become severe as the printed feature sizes approach the $\lambda/2$ -NA resolution limit of the imaging tool. OPEs are due to the fact that the point spread function of the imaging tool ($\sim\lambda/NA$) is no longer small compared to the aerial images of the features being printed, thus higher diffraction orders are not used in the formation of the images. The fidelity of the images of these features is thus highly influenced by the presence and/or absence of neighboring features. The main factors that contribute to proximity effects include optical effects or aerial image (NA and partial coherence σ of the exposure tool and mask tonality), resist processing conditions, substrate effects, and etch processing conditions. Typically, OPEs occur in three forms, namely, line width differences between similar (with same mask CD) structures with varying pitch densities, line-end shortening or end of line (EOL) effects, and corner rounding (see Fig. 13.40).

13.7.3.2.3 Postexposure bake sensitivity

Tables 13.11 and 13.12 show the feature-dependent PEB sensitivity of typical acrylate and COMA resists, respectively. The high PEB sensitivities of the different feature size and/or pitch combinations have significant implications in CD control and overall process integration. A 1.0°C change in PEB temperature results in a CD fluctuation of roughly 9–10 nm (for the acrylate resist) and 17–19 nm (for the COMA resist) for the indicated features.

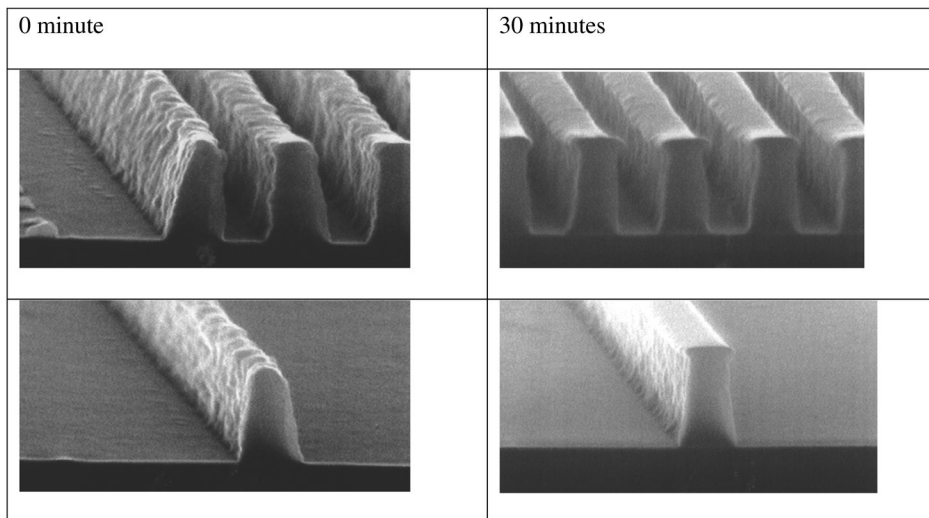
Figure 13.42 illustrates the environmental stability of a typical acrylate resist. T-topping is evident after 30 minutes in an environment with 0.6 ppb of ammonia and 0.08 ppb of N-methyl pyrrolidone (NMP). At much longer time frames (60 minutes or greater), these structures experience space closure and catastrophic failure.

Table 13.11 PEB sensitivity of features patterned with an acrylate resist.

Feature	PEB Sensitivity (nm/°C)
130 nm lines/360 nm pitch	9.3
150 nm lines/360 nm pitch	8.8
130 nm lines/420 nm pitch	8.9
150 nm lines/420 nm pitch	9.8
150 nm isolated lines	9.0

Table 13.12 PEB sensitivity of features patterned with a typical COMA resist.

Feature	PEB Sensitivity (nm/°C)
120 nm lines/280 nm pitch	18.6
120 nm isolated lines	17

**Figure 13.42** PEB delay effects on acrylate resist #3 on AR19 BARC (820 Å). Ammonia concentration 0.6 ppb, NMP concentration 0.08 ppb.

13.7.3.2.4 Line edge and sidewall roughness

Line edge and sidewall roughness in the range of 6–8 nm ($3 \times$ standard deviation) have been observed for most ArF resist materials. Figure 13.42 (with no delay time) shows a typical level of line edge and surface roughness of a typical acrylate resist. This level of edge roughness constitutes a significant portion of the lithographic CD budget. Although etch processing tends to smooth the line edge and side wall

roughness of features, resists with the lowest line edge and sidewall roughness after lithographic processing also generally tend to have the lowest line edge and sidewall roughness after etch processing. The impact of line edge and sidewall roughness on device performance has elicited great debate in recent times.²³²

13.7.3.2.5 Pattern collapse

Minimum gate CD and pitch are today limited by resist mechanical stability. Pattern collapse, particularly at aspect ratios greater than 3.5, is a common problem with most ArF resists, as it is with other resist types. Figure 13.43 is a good illustration of this problem. The features were patterned in an acrylate resist. The outer features on the left collapsed and fell on the inner line structure due likely to a number of factors, some of which include (i) capillary and mechanical forces during drying of the rinse liquid,²³³ (ii) adhesion loss between the patterned resist structures due to the interaction of the developer and rinse additives with specific chemical moieties in the resist polymer and the underlying substrate,²³⁴ and (iii) unfavorable aspect ratio and pitch of the line structure.²³⁵

13.7.3.2.6 Defectivity issues

Defects in ArF lithography, as in other optical lithographic technologies, can be categorized into three broad categories, namely, (i) intrinsic defects, (ii) particle defects, and (iii) process (coat, bake, and develop unit operations)-induced defects. While process-induced and intrinsic defects make up the bulk of the

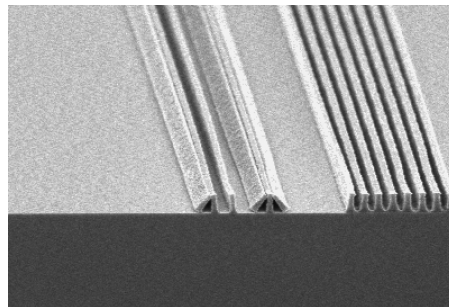


Figure 13.43 Pattern collapse of 130-nm lines printed in an acrylate resist.

²³²C.H. Diaz, H. J. Tao, Y. C. Ku, A. Yen, and K. Young, "An experimentally validated analytical model for gate line edge roughness (LER) effects on technology scaling," *IEEE Electron Device Lett.* **22**(6), 287 (2001).

²³³T. Tanaka et al., "Mechanism of resist pattern collapse," *J. Electrochem. Soc.* **140**, 115 (1993).

²³⁴A. Kawai, "Adhesion of resist micropatterns during drying after water rinse," *Jpn. J. Appl. Phys.* **34**, 1093 (1995); U. Okoroanyanwu, C. Pike, and H.J. Levinson, "Process induced defects in sub 150 nm device patterning using 193 nm lithography," *Proc. SPIE* **3998**, 277 (2000).

²³⁵M. McCallum, K.R. Dean, and J.D. Byers "Integration considerations for 193 nm photoresists," *MNE* **46**, 335–338 (1999).

subject matter of this section, particle type defects are also described in the context of their interaction with the above standard unit operations in lithographic processing.

Some intrinsic defects originate from the substrate-resist film interfacial interactions and can be controlled with appropriate surface-energy-matching schemes. Others originate from compositional inhomogeneities in the resist solution. Particle defects are extraneous materials that find their way into the resist either at the vendor's manufacturing facility or at the point of use of the resist. Usually, these can be removed by filtration. The presence of such particles on the surface of wafers can lead to thin film instabilities. Process-induced defects originate from coating, baking, and development unit operations in lithographic processing, during pattern transfer to the underlying substrates by plasma etching, and during resist removal by either plasma etching or solution stripping.

Decreasing the thickness of photoresists in order to accommodate the absorption problem of 193-nm resists makes such films susceptible to both spontaneous thin-film instabilities (due to London–van der Waals interactions) and defects driven by substrate imperfections (topographical features such as pits or mounds).²³⁶ Thin-film instabilities can lead to complete dewetting and related defects. Finally, the combination of contact line dynamics, partial wetting, and the presence of a surface feature may result in trapping of nanopackets of gas, leading to blistering and/or bubbles.

The physical size of some of the process-induced defects is beyond the physical resolution and detection limits of the traditional optical inspection techniques. The way in which each of the patterning processes contributes to defectivity in ArF-lithography-based device manufacture is related to the constituent materials in the photoresist and to the interaction of the photoresist with the substrate or ARC.

Photoresists used in ArF lithography are solution mixtures of polymeric resins, photoacid generators, base additives, stabilizers, surface-leveling agents, unreacted initiators, and monomeric impurities. There are bound to be chemical and even physical interaction between the various functional groups in these compounds and with the developer. Side reactions between these impurities, especially after the PEB process and during the development processes, can generate unwanted residues on the wafer. The molecular structure of the photoresist polymeric resin can also have profound influences on its thermophysical properties and its propensity to form a given type of defect. Depending on whether the photoresist is formulated with a random or a block polymer, its ability to form insoluble complexes in the developer can be dramatically affected. Other factors that can influence process-induced defects include the soft and PEB temperatures, pH of the deionized rinse water, temperature of the developer, etc.

The photoacid generators used are mostly organic-based onium salts, designed to be soluble in both the casting and the developing solvent. Remarkably, some of

²³⁶T.G. Strange, R. Mathews, D.F. Evans, and W.A. Hendrickson, "Scanning tunneling microscopy and atomic force microscopy characterization of polystyrene spin coated onto silicon surfaces," *Langmuir* **8**, 920 (1992); U. Okoroanyanwu, J. Cobb, P. Dentinger, P. C. Henderson, V. Rao, and C. Pike, "Defects and metrology of ultrathin resist films," *Proc. SPIE* **3998**, 515 (2000).

these photoacids are not very soluble in the developer, and thus leave residues on patterned wafers.²³⁷

13.7.3.2.6.1 COAT-PROCESS-INDUCED DEFECTS

The spin-coating operation can be a significant source of defects in a resist process. Insufficient exhaust in the spin cup for a given rotational speed can lead to resist aerosol particles redepositing on the wafer surface. Poor filtration of the resist or dried polymer on the resist nozzle tip will result in undesirable material becoming embedded in the polymer film. Air in the resist delivery system will produce bubbles in the resist coating and will produce radial streaking if severe. Solvent for cleaning the back of the wafer or removal of the edge bead can splash onto the top surface, causing localized film thickness variations.

13.7.3.2.6.2 DEVELOP-PROCESS-INDUCED DEFECTS

Inadequate developer coverage will produce macroscopic pattern defects. Dissolved gases in the developer can form bubbles on the resist surface, preventing development. Poor filtration of developer may deposit particles on the wafer surface, causing micromasking during etch or implantation processes. Carbon dioxide can react with the developer to form an insoluble compound on the developer nozzle tip that may redeposit on the wafer. Sudden changes in the pH (otherwise called shock) within the resist and/or developer solution during the initial stages of the deionized water rinsing sequence of the development process can cause precipitation of dissolved resists from the developer solution. Defects can also arise from resist and by-product solubility problems due to unwanted side reactions²³⁸ (see Fig. 13.44).

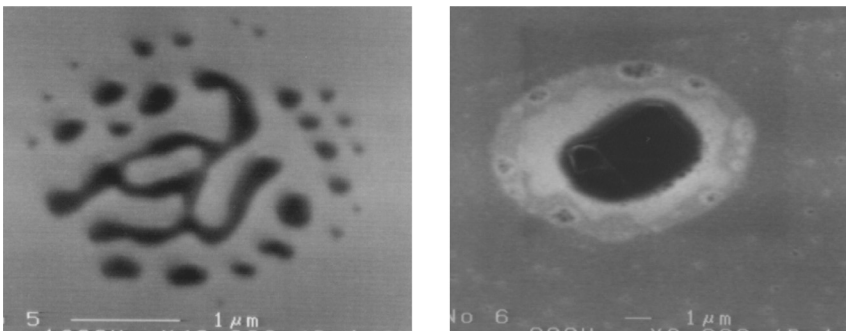


Figure 13.44 SEM images of residue defects.

²³⁷C.L. Pike and J. Erhardt, "Understanding the DUV resist development process using a develop residue monitoring technique," presented at Olin Interface '99 (1999).

²³⁸ibid.

13.7.3.2.7 Etch patterning issues

In the following sections, the etch performance as well as the main etch patterning issues are illustrated for the gate, contact hole, via, and trench layers of a CMOS device, using the typical ArF resists.

13.7.3.2.7.1 GATE ETCH PATTERNING APPLICATIONS

Minimum gate CDs are limited by resist mechanical and etch stability. McCallum et al.²³⁹ have shown that a resist with adequate etch stability and thickness of approximately three times greater than that of the gate electrode is sufficient for pattern transfer into a polysilicon gate down to the 100-nm node. The main gate etch patterning issues include end cap pull back, pattern distortion, and microloading effects. Figure 13.45(a) is a SEM micrograph showing 132-nm etched lines printed on an acrylate resist on top of SiON film, which in turn is coated on top of polysilicon. There is no significant line thinning on step areas observed in these structures, which is indicative of the good reflectivity control with the SiON BARC. These polysilicon line profiles are vertical and smooth, and do show slight end cap pull back.

Figure 13.45(b) is a tilt SEM micrograph of shallow trench isolation topographic structures patterned with an acrylate resist, and showing 130-nm dense

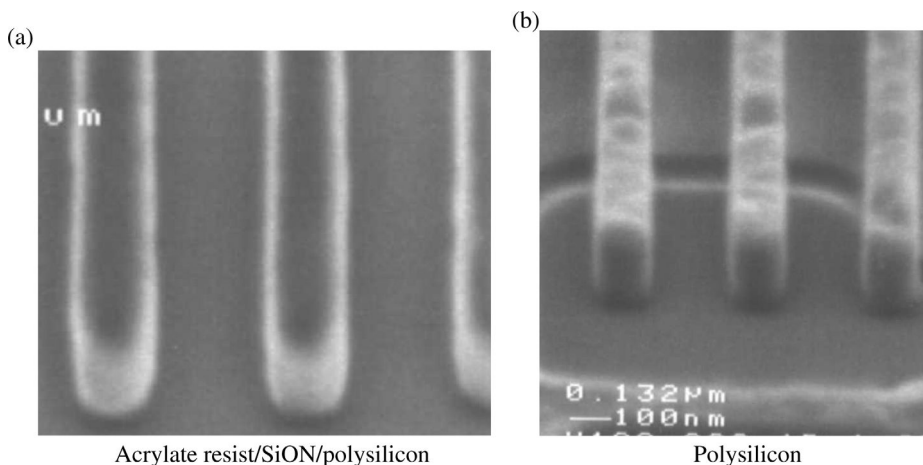


Figure 13.45 SEM micrographs showing 132-nm etched lines of (a) acrylate resist/SiON/polysilicon and (b) polysilicon. In (b), the resist and SiON have been stripped.

²³⁹M. McCallum, K.R. Dean, and J.D. Byers, "Integration considerations for 193 nm photoresists," *MNE* **46**, 335–338 (1999).

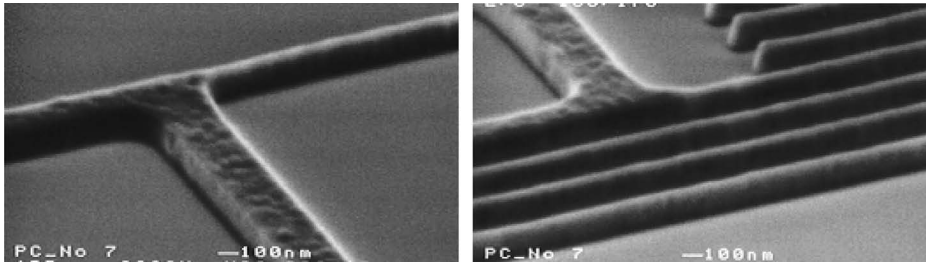


Figure 13.46 SEM micrographs showing sub-100-nm isolated and dense etched polysilicon lines patterned with acrylate resist. The resist has been stripped.

polysilicon lines at 360-nm pitch. In this figure, the resist and SiON materials have been stripped. The polysilicon lines are shown running over the field and active areas. Note the significant granularity of the polysilicon lines. Figure 13.46 is SEM micrographs of sub-100-nm isolated and dense etched polysilicon lines patterned with an acrylate resist, showing the patterning potential of ArF resists when lithographic and etch processes are tuned to match the properties of the resists.

13.7.3.2.7.2 CONTACT HOLE AND VIA ETCH PATTERNING APPLICATIONS

The main contact hole and via etch patterning issues include pattern distortion, proximity, and microloading effects. Figure 13.47 shows cross-sectional SEM images of 110-nm, 160-nm, and 200-nm contact holes patterned into SiO₂ substrate with an acrylate resist. Note that the resist has been stripped off. The sidewalls of the features are smooth and nearly vertical.

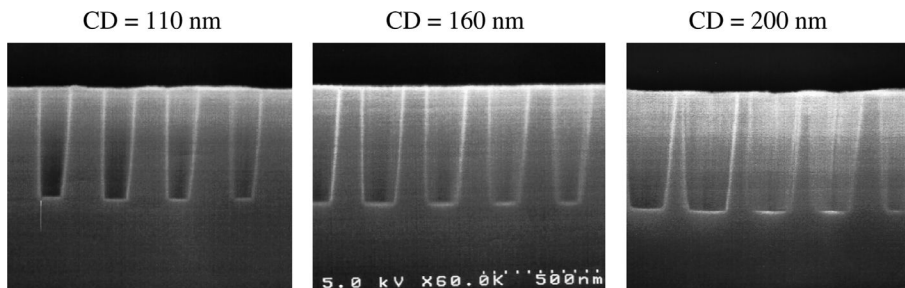


Figure 13.47 Cross-sectional SEM images of 110-nm, 160-nm, and 200-nm contact holes patterned into SiO₂ substrate with an acrylate resist. Pitch = 300 nm. The resist has been stripped.

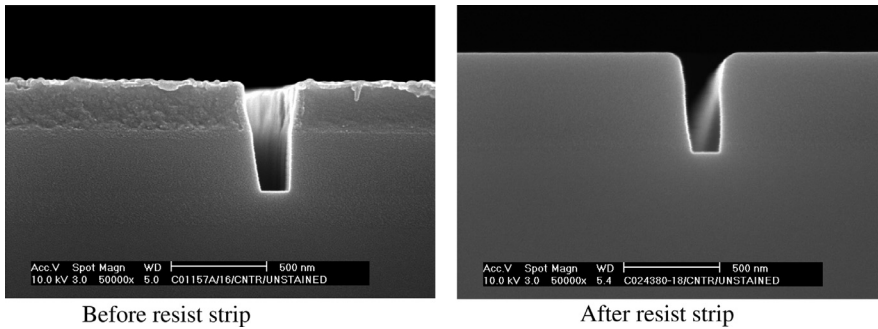


Figure 13.48 Cross-sectional SEM images of 160-nm trench patterned into SiO_2 substrate with an acrylate resist.

13.7.3.2.7.3 TRENCH ETCH PATTERNING APPLICATIONS

The main trench etch patterning issues include pattern distortion, proximity, and microloading effects. Figure 13.48 shows cross-sectional SEM images of a 160-nm trench patterned into SiO_2 substrate with an acrylate resist, showing smooth feature sidewalls.

13.7.3.2.8 Metrology issues

Line slimming under SEM tool inspection and analysis of resist features is a major problem affecting most ArF resists. While a number of papers have been published on this subject,²⁴⁰ we briefly review the main facts. The main cause of line slimming is the interaction of the low-energy primary electron beam of the SEM tool with the resist material, leading to the generation of secondary electrons, which in turn mediate the chemical transformation of the resist feature, typically by decarboxylation and cross-linking. The process is irreversible. Figure 13.49 is a plot of the CD of line features printed with an acrylate resist versus the number of SEM measurements of the same site on the wafer, illustrating this problem. Figure 13.50 shows a plot of CD shrinkage as a function of number of SEM measurements of the same site on the wafer and the SEM tool acceleration voltage of the electron beam, for an acrylate resist and a COMA resist. The lower the acceleration voltage, the lower is the extent of line slimming. In general, COMA-type resists experience a lower degree of line slimming relative to their acrylate counterparts.

²⁴⁰T. Sarubbi, M. Ross, M. Neisser, T. Kocab, B. Beauchemin, W. Livesay, S. Wong, and W. Ng, "Mechanism studies of scanning electron microscope measurement effects on 193 nm photoresists and the development of improved line width measurement methods," *Proc. SPIE* **4345**, 211 (2001); M. Neisser, T. Kocab, B. Beauchemin, T. Sarubbi, S. Wong, and W. Ng, "Mechanism studies of SEM measurement effects on 193 nm photoresists and the development of improved line width measurement methods," in *Proc. Interface 2000 Microlithography Seminar*, 233 (2000).

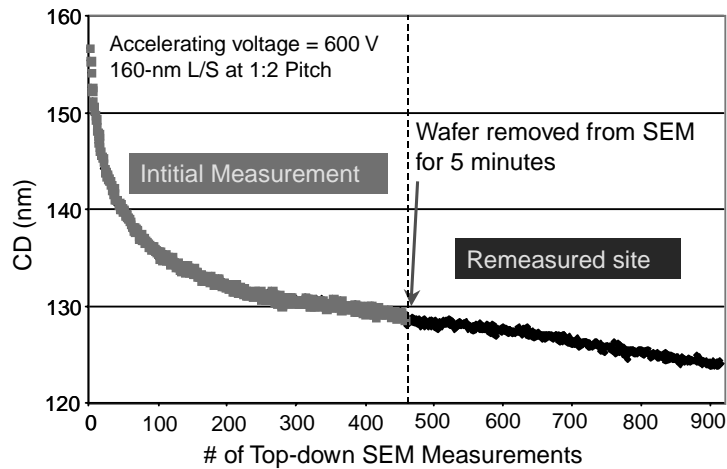


Figure 13.49 Typical CD slimming curve during top-down SEM analysis of an acrylate resist. (Courtesy of Neisser et al.²⁴¹)

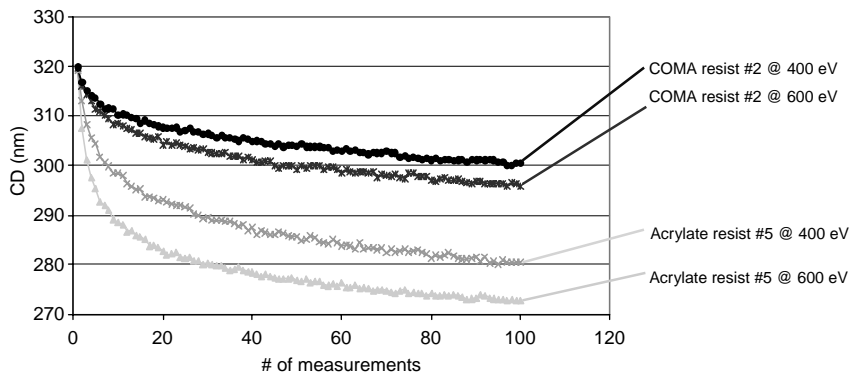


Figure 13.50 CD slimming of COMA- and acrylate-type resists as a function of acceleration voltage. (Courtesy of Neisser et al.²⁴²)

13.7.4 Water immersion ArF (193-nm) lithography

Water immersion ArF lithography²⁴³ was deployed for the first time in large-scale fabrication of critical layers of IC devices at the 45-nm technology node in 2008,

²⁴¹M. Neisser, T. Kocab, B. Beauchemin, T. Sarubbi, S. Wong, and W. Ng, "Mechanism studies of SEM measurement effects on 193 nm photoresists and the development of improved linewidth measurement methods," in *Proc. Interface 2000 Microlithography Seminar*, 233 (2000).

²⁴²*ibid.*

²⁴³The roots of immersion lithography date back to the invention of immersion microscopy by Ernst Abbe (1840–1905) in 1878, since he sought ways to increase the resolving power of optical

and is expected to be used in the fabrication of devices at the 32-nm technology node. The only difference between it and dry ArF lithography is the fact that the last lens element of the projection system is in water, while it is in air in the case of the dry ArF lithography. Figure 13.51 is a schematic showing the main physical and optical differences between the two forms of ArF lithography.

The basis of the imaging performance similarities and differences in terms of resolution and depth of focus, respectively, between immersion and dry lithography can be derived as follows. The nonparaxial scaling equations (applicable in systems with high angles of incidence) for resolution in dry and immersion lithographies are given by²⁴⁴

$$R_{\text{air}} = k_1 \frac{\lambda}{\sin \theta} = k_1 \frac{\lambda_0/n_{\text{air}}}{\sin \theta_{\text{air}}} = k_1 \frac{\lambda_0}{\text{NA}} \quad (\text{dry lithography in air}), \quad (13.32)$$

where $\lambda = \lambda_0/n_{\text{air}}$ and λ is the wavelength in the imaging medium (air), θ_{air} is the refracted angle in air, k_1 is a process-dependent constant and is a measure of the difficulty of the printing, and n_{air} is the refractive index of air (which is nearly

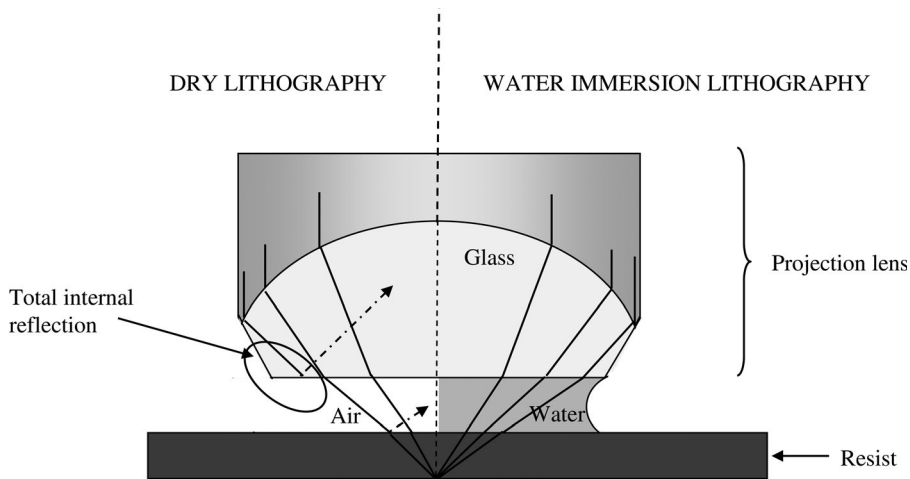


Figure 13.51 Schematic showing the main physical and optical differences of water immersion and dry ArF lithographies.

microscopes. He had observed an enhancement of resolution and depth of focus when he placed a thin liquid film between the final lens element of the microscope objective and the specimen. Abbe's invention was inspired by the earlier work along the same lines by Giovanni Battista Amici (1786–1863).

²⁴⁴B.J. Lin, "The K_3 coefficient in non paraxial λ/NA scaling equations for resolution, depth of focus, and immersion lithography," *J. Microlith. Microfab. Microsyst.* **1**(1), 7 (2002); "New λ/NA scaling equations for resolution and depth of focus," *Proc. SPIE* **4000**, 759 (2000).

equal to 1.0).

$$R_{\text{immersion}} = k_1 \frac{\lambda_{\text{water}}}{\sin \theta_{\text{water}}} = k_1 \frac{\lambda_0/n_{\text{water}}}{\sin \theta_{\text{water}}} = k_1 \frac{\lambda_0}{\text{NA}} \quad (\text{water immersion lithography}). \quad (13.33)$$

Similarly, the nonparaxial scaling equations for depth of focus in dry and immersion lithographies are given by

$$\begin{aligned} \text{DOF}_{\text{dry}} &= k_3 \frac{\lambda_{\text{air}}}{\sin^2(\theta_{\text{air}}/2)} = k_3 \frac{\lambda_0/n_{\text{air}}}{\frac{1}{n_{\text{air}}^2} [n_{\text{air}}^2 \sin^2(\theta_{\text{air}}/2)]} \\ &= k_3 \frac{n_{\text{air}} \lambda_0}{\text{NHA}^2} = k_3 \frac{\lambda_0}{\text{NHA}^2} \quad (\text{dry lithography in air}), \end{aligned} \quad (13.34)$$

$$\begin{aligned} \text{DOF}_{\text{immersion}} &= k_3 \frac{\lambda_{\text{water}}}{\sin^2(\theta_{\text{water}}/2)} = k_3 \frac{\lambda_0/n_{\text{water}}}{\frac{1}{n_{\text{water}}^2} [n_{\text{water}}^2 \sin^2(\theta_{\text{water}}/2)]} \\ &= k_3 \frac{n_{\text{water}} \lambda_0}{\text{NHA}^2} \quad (\text{water immersion lithography}), \end{aligned} \quad (13.35)$$

where NHA is the numerical half-aperture and k_3 is a process-dependent constant.

From Eqs. (13.32)–(13.35), resolution in dry and immersion lithographies are equal for the same wavelength and NA, while the DOF of immersion lithography is greater than that of dry lithography by a factor that is at least as great as the refractive index of water (which is 1.44 at $\lambda = 193$ nm at standard atmospheric temperature and pressure). Effectively, the higher refractive index of water in immersion lithography is able to couple the higher spatial frequencies (higher diffraction orders) into the resist for a given NA, whereas in the case of dry lithography, these orders are simply internally reflected into the lens for a lens with $\text{NA} > 1$, instead of being coupled into the resist. In other words, for a given diffraction order of light from the mask, the angle of the light inside the immersion fluid is less than in dry lithography. These smaller angles in the immersion fluid result in smaller optical path differences between the various diffraction orders when they are out of focus; the result is a smaller degradation of the image for a given amount of defocus. In this way, immersion lithography provides a greater depth of focus for a given NA than dry lithography (see Fig. 13.52). It also enables hyper-NA imaging ($\text{NA} > 1.0$), with attendant resolution enhancement.

13.7.4.1 Resists and topcoats

The main difference between dry and immersion lithography is the fact that the exposure is done in air in dry lithography and in a liquid (water) in immersion lithography. To prevent the leaching of resist components into the immersion water, topcoats are often used. It should be mentioned that topcoats do not prevent water from leaching into the resist film. The topcoat layer is removed after the exposure and PEB steps, but before development.

AT:1150i, 90-nm dense lines and spaces

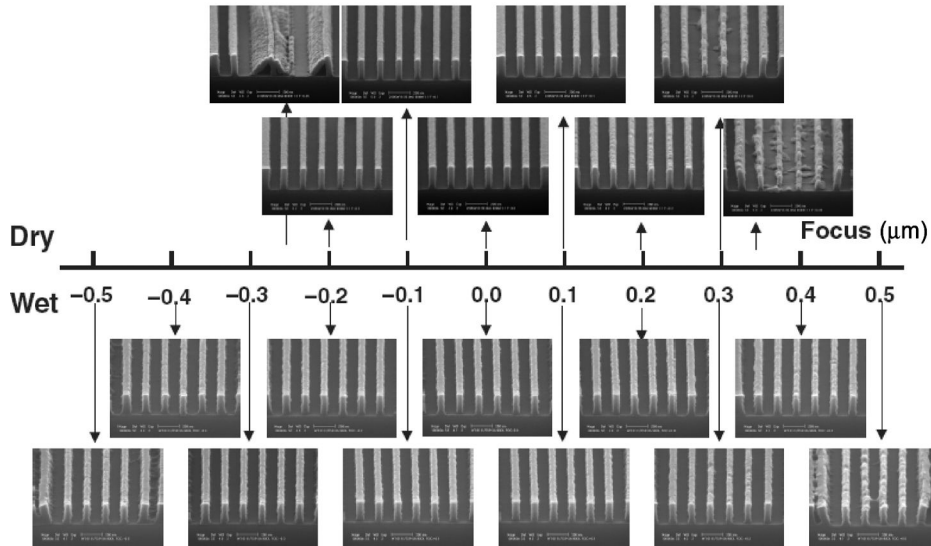


Figure 13.52 Depth of focus performance of dry and water immersion (wet) lithography at NA 0.85. Note the significant enhancement in depth of focus obtained with immersion lithography ($\sim 1 \mu\text{m}$) relative to dry lithography ($\sim 0.06 \mu\text{m}$) for NA 0.85. (Photo courtesy of ASML.)

There are two types of topcoats, namely, developer-soluble and solvent-soluble topcoats. While the developer-soluble topcoat can be removed during the resist develop process in standard 0.26N TMAH solution, the solvent-soluble topcoat can only be removed with an organic solvent before the resist development step. This means that for the developer-soluble topcoat, the topcoat removal step can be done in the develop module and integrated into the development step, while for the solvent-developable topcoat, a different topcoat stripping module has to be installed as part of the unit operations of the track-processing sequences. Because of the ease of implementation and cost considerations, the developer-soluble topcoat approach is the preferred option for ArF water immersion lithography involving the use of topcoats. Even more ideal are resists that have been designed to have low levels of leaching, and therefore do not require topcoats.

The typical sequence is to coat the topcoat over the resist, which is in turn coated over a BARC. The topcoat solvent is chosen so that it does not dissolve the resist layer in order to prevent the formation of an intermixing layer between the two layers. Most 193-nm resists use PGMEA and propylene glycol monomethylether (PGME) as solvent, and topcoats have an alcohol-based solvent system. To plumb in a new topcoat, the line has to be carefully and thoroughly cleaned in order to avoid unwanted interactions between incompatible solvents.

13.7.4.2 Postexposure bake delay stability

Topcoats also provide a protective function against airborne molecular contaminants such as amines. Figure 13.53 shows PEB delay stability of up to 15 minutes obtained on a resist film protected with a topcoat. Following the indicated PEB delay times, the resist film was postexposure baked and developed. Even after 15 minutes, the CD values of the 80-nm and 90-nm lines/space features remained remarkably stable. This is considerably better performance than that achieved when topcoat is not used.

13.7.4.3 Defectivity

The main immersion-specific lithography defects reported in the literature fall into these general types: particles, bubbles, water marks, extra patterns, resist residues, line thinning and swelling, bridging, BARC blobs, and aerosols. Although the nature, origins, formation mechanisms, and effects of immersion defects have been reported elsewhere,²⁴⁵ we here trace the evolution of these defects

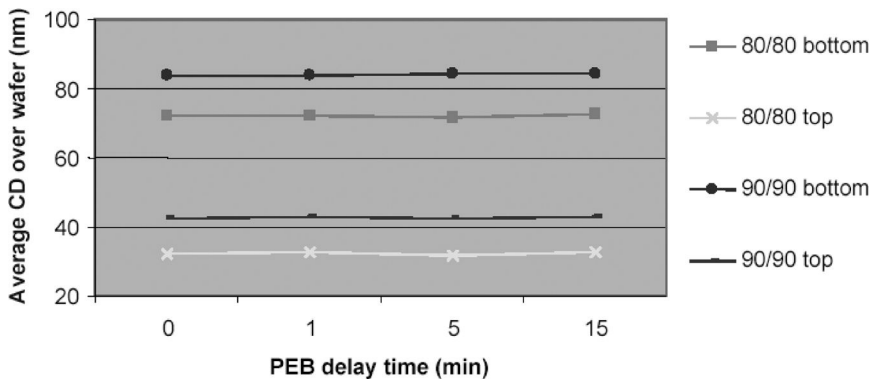


Figure 13.53 Measured average CD across the wafer versus PEB delay time obtained on ASML AT:1150 immersion exposure tool with NA 0.85.

²⁴⁵U. Okoroanyanwu, J.Kye, N. Yamamoto, and K. Cummings, "Defectivity in water immersion lithography," *Microlithography World* (Nov. 2005); U. Okoroanyanwu, J.Kye, N. Yamamoto, H.J. Levinson, K. Cummings, "Prospects & challenges of defectivity in water immersion lithography," *Proc. of 2nd Symp. on Immersion Lithography*, Brugge, Belgium, Sept. 2005; F. J. Liang, H. Chang, L. H. Shiu, C. K. Chen, L. J. Chen, T. S. Gau, and B.J. Lin, "Immersion defect reduction, part I: analysis of water leaks in an immersion scanner," *Proc. SPIE* **6520**, 65204U (2007); M. Erckens, M. Maenhoudt, and M. van Bavel, "Progress in understanding and reducing immersion related defectivity and resist leaching," *Semiconductor Fabtech*, 31st ed., pp. 66–70 (2006); L. H. Shiu, F. J. Liang, H. Chang, C. K. Chen, L. J. Chen, T. S. Gau, and B.J. Lin, "Immersion defect reduction, part II: the formation mechanism and reduction of patterned defects," *Proc. SPIE* **6520**, 652012 (2007); M. Kobayashi, H. Nakano, M. Arakawa, M. Tanabe, K. Toyoda, T. Chibana, Y. Matsuoka, and Y. Kawasaki, "Contamination and particle control system in immersion exposure

from their very formation to their ultimate manifestation on the patterned wafer. Most importantly, we present the subtleties inherent in the defect metrology of immersion lithography, particularly with respect to inspection and monitoring of immersion defects relative to those of dry lithography. We also provide an overview of the evolutionary tree of immersion lithography defects, which should make for easy classification and characterization of defects, as well as aid in the debugging of immersion-lithography-based process technologies.

13.7.4.3.1 Origins and evolution of immersion lithographic defects

Defects seen on the immersion lithography cluster generally fall into two categories, depending on which part of the cluster they originate, namely, scanner-generated defects and track (resist process)-generated defects (see Fig. 13.54 for the evolutionary tree of defects in immersion lithography).²⁴⁶

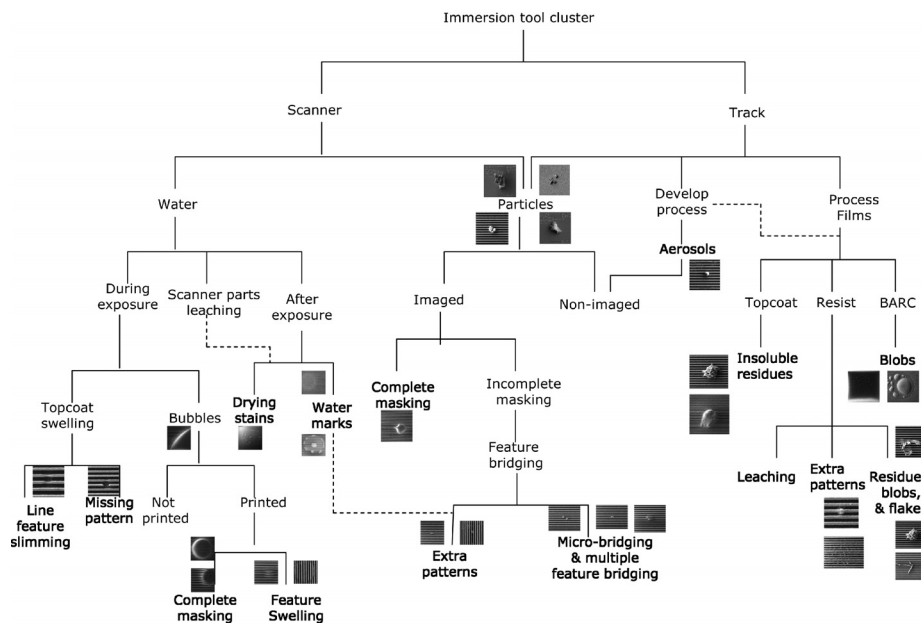


Figure 13.54 Evolutionary tree of defects in an immersion lithography cluster. Actual defects on wafers are indicated in bold.

tool,” *Proc. SPIE* **6520**, 652014 (2007); R.D. Watso, T. Laursen, B. Pierson, and K.D. Cummings, “Defect testing using an immersion exposure system to apply immediate pre exposure and post exposure water soaks,” *Proc. SPIE* **6520**, 65204V (2007).

²⁴⁶U. Okoroanyanwu, R. Kirsch, R. Wirtz, M. Grundkowsky, and W. Grundke, “Defect metrology in water immersion lithography,” *Semiconductor Fabtech* (Nov. 2007).

13.7.4.3.1.1 SCANNER-GENERATED DEFECTS

Scanner-generated defects can further be classified as originating from immersion water or from particles shed from the scanner. Immersion water can cause defects through three primary modes: during exposure, after exposure, or through leaching of scanner construction parts. During exposure, the immersion water can cause defects through swelling of the topcoat or through formation of bubbles. Topcoat swelling when imaged leads to line thinning and/or slimming, missing patterns, and contact hole enlargement because of the enhanced coupling of the incident rays toward the optical normal of the rays on account of the higher refractive index of the topcoat relative to water—as predicted by geometric optics. Bubbles on the other hand, when printed, can cause magnification of the features. Bubbles mostly appear when there is too much dissolved gas in the immersion water, resist outgassing during exposure,²⁴⁷ or cavitation due to local lowering of pressure in the water flow,²⁴⁸ particularly over topographic features on a wafer.

Particles can be generally divided into organic and inorganic (metallic) particles. While metallic particles (mostly iron and nickel) can be directly identified to originate from the scanner, organic particle origins are attributed to resist/BARC/topcoat residues. While pre- and postrinse sequences should remove most of the particles before and after the exposure step, particles can lead to shadowing of the exposure itself, if they are already on the wafer surface during the exposure process. This will normally lead to unwanted printed structures. In principle, it should be possible to distinguish inorganic particles originating from the scanner from organic particles originating from the track by processing uncoated wafers directly through the scanner. However, loose organic residues can be transferred from a coated wafer during normal lithographic processing in the track onto the wafer stage and surrounding mechanical systems by the immersion water. These residues can then be picked up by subsequent wafers processed through the exposure tool, for instance, an uncoated wafer, processed as part of the scanner particle test or even patterned product wafers. Some cleaning protocols that automatically clean off these particles have proved effective in reducing the number of these particles.²⁴⁹

Bubbles are typically spherical. Their overall impact on imaging is dependent on their location relative to the surface of the resist. Bubbles close to the resist surface cause underexposure and nonexposure of the patterns in the area under the bubble.²⁵⁰ They may also be associated with local magnification (swelling)

²⁴⁷R. Kunz, “Photoresist outgassing: a potential achilles heel for short wavelength optical lithography,” *Proc. SPIE* **5376**, 1–15 (2003).

²⁴⁸B. Streefkerk, J. Baselmans, W. Gehoel van Ansem, J. Mulkens, C. Hoogendam, M. Hoogendorp, D. Flagello, and H. Sewel, “Extending optical lithography with immersion,” *Proc. SPIE* **5377**, 285–305 (2004).

²⁴⁹U. Okoroanyanwu, R. Kirsch, R. Wirtz, M. Grundkowsky, and W. Grundke, “Defect metrology in water immersion lithography,” *Semiconductor Fabtech* (Nov. 2007).

²⁵⁰P. De Bisschop, A. Erdman, and A. Rathsfeld, “Simulation of the effect of a resist surface bound air bubble on imaging in immersion lithography,” *Proc. SPIE* **5754**, 243–253 (2004).

of line features, particularly those at the edge of the bubble. In contrast, bubbles that are a significant distance from the top of the resist may be printed out of focus and away from the wafer, and therefore may not affect resist printing at all. The immersion water can also cause defects such as drying stains and water marks after exposure of the wafer when residual water droplets are not properly evaporated before the wafer goes back to the track for PEB and develop processing.

Drying stains have their origin in the natural tendency for solids dispersed in a drying drop of immersion water to migrate to the edge of the drop to form a solid ring.²⁵¹ The solutes or the dissolved or dispersed solids could be dissolved tool construction materials, leached resist ingredients, particles shed from mechanical systems or from improperly filtered coating solutions, impurities in the immersion water, or even bacterial growth.

Water marks originate from water droplets on exposed wafers that are not completely dried before the wafer leaves the scanner. During the baking of the exposed wafer in the PEB oven, photoacids generated within the area directly under the water droplet during the exposure are extracted. Once extracted from the resist, these acids are no longer available to deprotect the exposed areas, resulting in an undeprotected mass of resist under the water mark that is insoluble in the developing solvent. Typically, water marks are circular defects that block the formation of resist images, although usually one can see pattern formation at their edges. Their surface morphology is typically amorphous, with the appearance of surface residues that may look like an insoluble mass. Unlike bubbles and topcoat swelling, they are not associated with magnification and demagnification of features. Tiny water marks and/or water droplets that extract the photoacid, locally preventing deprotection of the resist polymer, can also cause extra pattern and bridging defects.

The other defect types from the scanner are particles, typically shed by components of the exposure tool during mechanical movements. When imaged, these particles can occlude the exposure light, effectively causing micromasking that can result in feature distortion (line bridging and extra patterns). While most of the particles shed from components of the exposure tool or picked up from the immersion water after exposure are washed away during development, some do manage to stick. Others may fall on the wafer during postexposure processing, and all can cause micromasking during etching.

13.7.4.3.1.2 TRACK-GENERATED DEFECTS

Track-generated defects are classified as originating from the process films (topcoat, resist, and BARC), develop process, or from particles shed from track construction materials. When they are imaged, particles shed from the track will manifest the same types of defects as those from the scanner, as explained

²⁵¹R.D. Deegan, O. Bakajin, T.F. Dupont, G. Huber, S.R. Nagel, and T.M. Witten, "Contact line deposits in an evaporating drop," *Phys. Rev. E* **62**(1), 1063–651 (2000).

above. Aerosols are the main defects generated from the develop process, and by their nature, they occur after exposure and are not strictly immersion related. Under certain circumstances involving nonuniform resist dissolution during the develop process, bridging defects and extra pattern defects can arise.

Defects originating from process films include: insoluble residues (from topcoat, resist, and BARC); leaching of additives (from resist); BARC blobs on account of chunks of resist materials being washed away during the develop process and redepositing on the hydrophilic BARC surface, and sticking to it; and resist flakes from resist fragments of dried-up resist materials flaking off, perhaps from the dispense nozzle, and landing on the fully processed wafer. These flakes can even land en route to the scanner, before the wafer is exposed.

13.7.4.3.1.3 IMPACTS OF IMMERSION LITHOGRAPHY DEFECTS

The lithographic impacts of characteristic defects seen on the immersion lithography cluster are many and varied. Bubbles can cause pattern distortion such as feature swelling and, in the most extreme case, can prevent patterns from printing. Topcoat swelling can cause line thinning, missing patterns, and contact hole swelling. Water marks can cause insoluble surface residues, webbing of features, and bridging, and can also prevent features from printing. The impact of shed particles from the movement of the exposure tool mechanical systems is to occlude the exposure light from exposing the areas where they land, often resulting in pattern bridging and lack of pattern definition, as stated above.

13.7.5 F₂ excimer laser (157-nm) lithography

Before the introduction of water immersion ArF lithography into the semiconductor industry, lithography using 157-nm photons from F₂ excimer laser sources was heavily researched between 1999 and 2003 as a potential bridging technology between dry ArF lithography and one of the next-generation lithographies.²⁵² After it became apparent that there were significant technical challenges that may not be resolved in time for the technology to intersect the semiconductor technology roadmap,²⁵³ the industry resolved to abandon it in 2003. The main technical challenges of this technology that were identified included the lack of an adequate infrastructure for manufacturing high-purity CaF₂ for the lens elements, the intrinsic birefringence of CaF₂,²⁵⁴ immaturity of the resists, etc.

On the whole, the design and configuration of the 157-nm lithographic exposure tool are similar to those of 248-nm and 193-nm lithographies, except in

²⁵²J.A. McClay and A.S.L. McIntyre, "157 nm optical lithography: the accomplishments and the challenges," *Solid State Technol.*, p. 57 (June, 1999).

²⁵³International Technology Roadmap for Semiconductors (ITRS), Lithography Chapter (2002).

²⁵⁴J.H. Burnett, Z.H. Levine, and E.L. Shirley, "Intrinsic birefringence in calcium fluoride and barium fluoride," *Phys. Rev. B* **64**, 1–4 (2001).

a few main facts. Because of the high absorptivity of 157-nm photons in air at VUV wavelengths, 157-nm lithographic exposures are done in nitrogen atmosphere instead of air, as in 248-nm and 193-nm lithographies. All of the refractive optical elements are made of CaF_2 , instead of fused silica. Also, the resist platforms for 157-nm lithography are based on fluorinated analogs of their 193-nm counterparts, since these are the only reasonably transparent materials at 157 nm (see Chapter 7). Molecular contamination, mostly of hydrocarbons, of the optical elements as well as the reticles is a far more pronounced problem in 157-nm lithography in contrast to its longer-wavelength counterparts. This necessitated the implementation of active contamination control schemes for protecting the optical elements and reticles including in situ cleaning protocols for cleaning contaminated optics and reticles; it also necessitated unique reticle handling schemes that employed the continuous purging of the reticle holder/box with nitrogen.²⁵⁵ Figure 13.55 shows the performance of a typical 157-nm resist.

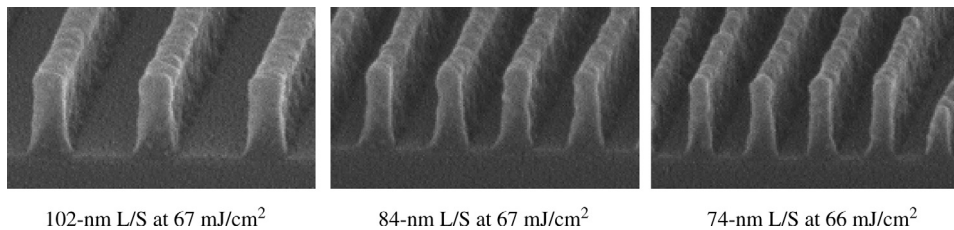


Figure 13.55 Performance of Shipley's XP0589A resist on SiON BARC on Excitech 157-nm microexposure tool with NA 0.85 and σ 0.3. Reticle phase-shifting mask. Soft bake 110°C/60 seconds. PEB 110°C/60 seconds. Resist thickness 200 nm. (Courtesy of the Shipley Corporation.)

²⁵⁵U. Okoroanyanwu, N. Stepanenko, B. Vereecke, A. Eliat, M. Kocsis, Y.S. Kang, R. Jonkheere, T. Conard, and K. Ronse, "Experimental investigation of fabrication process, transportation, storage, and handling induced contamination of 157 nm reticles and vacuum UV cleaning," *Proc. SPIE* **5377**, 487–503 (2004).

Chapter 14

X-Ray and Extreme Ultraviolet Lithographies

I saw eternity the other night,
Like a great ring of pure and endless light

Henry Vaughan, "The World"

14.1 Introduction

Like their conventional optical lithography counterparts (discussed in Chapter 13), EUV lithography and x-ray lithography utilize photons to image and pattern devices. But unlike their conventional optical lithography counterparts, they utilize extremely short-wavelength photons in the soft (for EUV lithography) and hard x-ray (for x-ray lithography) regions of the electromagnetic spectrum. Of these two lithographies, x-ray lithography was the first to be successfully demonstrated to be useful in lithographic patterning.¹

The resolution potential of both x-ray and EUV lithographies, given their short wavelengths, was the main motivation for their development. The two main printing modes of these lithographies are in proximity mode (for x-ray lithography) and projection mode (for soft x-ray lithography, also called EUV lithography). In the following sections, we discuss the essential attributes of these lithographies.

¹D.L. Spears and H.I. Smith, "High resolution pattern replication using soft X rays," *Electron Lett.* **8**, 102 (1972); B. Fay, J. Trotel, Y. Petroff, R. Pinchaux, and P. Thiry, "X ray replication of masks using the synchrotron radiation produced by the ACO storage ring," *Appl. Phys. Lett.* **29**, 370 (1976); J.R. Maldonado, G.A. Coquin, D. Maydan, and S. Somekh, "Spurious effects caused by the continuous radiation and ejected electrons in x ray lithography," *J. Vac. Sci. Technol.* **12**, 1329 (1975); A. Huerberger "X ray lithography," *Solid State Technol.* **29**(2), 93 (1986); J.R. Maldonado, A. Reisman, H. Lezec, L.K. Williams, and S.S. Iyer, "X ray damage considerations in MOSFET devices," *J. Electrochem. Soc.* **133**, 628 (1986); A.P. Neukermans, "Current status of x ray lithography," *Solid State Technol.* **27**(11), 213 (1984); D. Fleming, J.R. Maldonado, and M. Nessler, "Prospects for x ray lithography," *J. Vac. Sci. Technol. B* **10**(6), 2511 (1992); C.N. Archie, J.I. Garanlund, R.W. Hill, and A.D. Wilson, "Installation and early operating experience with the Helios compact synchrotron x ray source," *J. Vac. Sci. Technol. B* **10**(6), 3224 (1992).

14.2 Proximity X-Ray Lithography

Lithography using x-ray photons with extremely short wavelengths in the range of 0.4 nm to 2 nm can inherently overcome the diffraction effects associated with imaging features with sizes comparable to the exposure wavelengths of UV lithographies. This was the main motivation underlying x-ray lithography. However, at x-ray wavelengths, there are no known materials for making image-forming lenses or mirrors. Consequently, proximity x-ray lithography (see Fig. 14.1), where the mask is brought to within a few microns of the wafer and the x rays are passed directly through the mask and onto the wafer, was invented.

The year 1972 witnessed the invention of proximity x-ray lithography by Hank Smith at Massachusetts Institute of Technology. Many companies (IBM, Canon, Nikon), universities (MIT and the University of Wisconsin), and governments (United States and Japan) spent well over a billion dollars on its development.² The first attempts at production of x-ray aligners were made in the mid-1970s by AT&T and MIT, and in the early 1980s by Micronix Partners, Hampshire Instruments, Nikon, and Karl Suss. X-ray step-and-repeat and step-and-scan systems were eventually made commercially available.³

The promise of x-ray lithography lies in the fact that it offers the shortest optical wavelength, and theoretically the highest resolution of all of the other optical lithographies. The minimum resolvable linewidth w in x-ray lithography is given by

$$w = \sqrt{\frac{\lambda z}{\alpha}}, \quad (14.1)$$

where λ is the x-ray exposure wavelength, z is the gap between the x-ray mask and the wafer, and α is a parameter that is a measure of the contributions from the resists. Typically, α ranges between 0.5 and 1.5.⁴

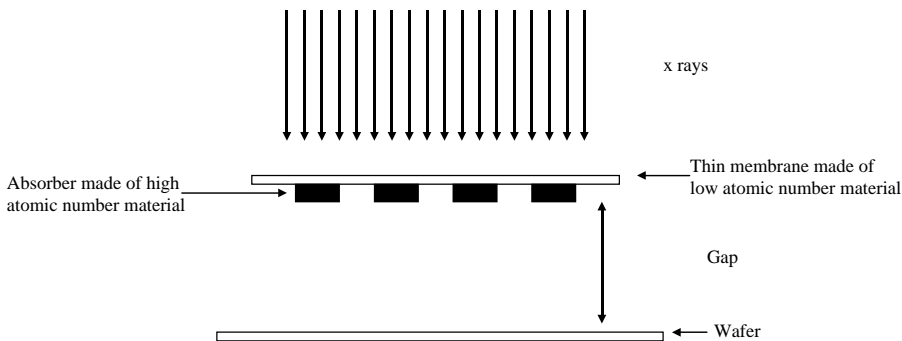


Figure 14.1 Schematic of x-ray proximity lithography with a collimated x-ray source.

²"Microlithography & mask making," VLSI Report (1992).

³K. Uda, N. Mizusawa, Y. Tanaka, Y. Watanabe, H. Ina, and S. Uzawa, "X ray stepper development for volume production at Cannon," *Proc. SPIE* **3331**, 689–697 (1998); Q. Leonard, J. Wallace, O. Vladimirsky, K. Simon, and F. Cerrina, "X ray mask replication using a Suss stepper at CXrL," *Proc. SPIE* **3048**, 299–303 (1997).

⁴H.J. Levinson, *Principles of Lithography*, 2nd ed., p. 381, SPIE Press, Bellingham, WA (2005).

Furthermore, x-ray lithography offers excellent CD control, superior depth of focus, and the ability to project through surface contamination on wafers and masks. By using x rays, wavelength-related diffraction problems, which limit resolution of other optical lithographies, are eliminated. High-aspect-ratio pattern fabrication can be achieved with x-ray lithography, given the high transparency of resist films to x rays. In addition, there are no field size limitation issues in x-ray lithography. Unwanted scattering and reflection are negligible in x-ray lithography because the index of refraction is about the same (close to unity) for all materials in the x-ray spectral region.⁵ As a result, standing wave effects and other reflection-based problems that limit resolution in other optical lithographies are eliminated in x-ray lithography.

There are, however, some major limitations of x-ray lithography, and these include the difficulty of fabricating $1 \times$ masks, the high cost of generating the x rays at sufficient power, penumbral and diffraction blurs that limit resolution (in the case of point sources), and overlay control.⁶

14.2.1 Synchrotron sources

Synchrotron storage rings produce x rays (0.1–10-nm wavelength) that have been used in x-ray lithography. In the synchrotron, electrons are accelerated to up to 1 GeV and maintained at that energy, and circulate in an evacuated ring of pipe surrounded by a strong magnetic field. As the orbiting electrons in the storage ring change direction in the magnetic field, they emit shortwave dipole radiation. Under certain conditions, when the electron velocity approaches the velocity of light, the radiation pattern changes from dipole type to a forward lobe, resulting in a strong continuous output of an almost parallel (collimated) beam of radiation with a wide range of wavelengths.⁷ One synchrotron storage ring can produce up to 20 beam lines that can be used in as many x-ray exposure tools.⁸ X rays produced in the synchrotron are ideally suited for proximity lithography.⁹ Because they are naturally collimated, x rays produced in synchrotrons do not

⁵H.I. Smith, M.L. Schattenberg, S.D. Hector, J. Ferrera, E.E. Moon, I.Y. Yang, and M. Burkhardt, "X ray nanolithography: Extension to the limits of the lithographic process," *Microelectron. Eng.* **32**, 143 (1996).

⁶M.J. Bowden, "The lithographic process: the physics," in *Introduction to Microlithography*, 2nd ed., L.F. Thompson, C.G. Willson, and M.J. Bowden, Eds., p. 121, American Chemical Society, Washington, DC (1994).

⁷S. Doniach, I. Lindau, W.E. Spicer, and H. Winick, "Synchrotron radiation as a new tool within photon beam technology," *J. Vac. Sci. Technol.* **12**, 1123 (1975); P. Pianetta, R. Redaelli, R. Jaeger, and T.W. Barbee, Jr., "X ray lithography at the Stanford Synchrotron Radiation Laboratory (SSRL)," *Proc. SPIE* **537**, 69 (1985); I. Okada, S. Saitoh, S. Itabashi, and H. Yoshihara, "A plasma x ray source for x ray lithography," *J. Vac. Sci. Technol. B* **4**, 243 (1986).

⁸M.S. Hibbs, "Overview of optical steppers and scanners," in *Microlithography: Science and Technology*, J.R. Sheats, B.W. Smith, Eds., p. 25, Marcel Dekker, New York (1998).

⁹*ibid.*; A. Heuberger, "X ray lithography," *Solid State Technol.* **29**(2), 93 (1986); W.D. Grobman, in *Handbook on Synchrotron Radiation*, E.E. Koch, D.E. Eastman, and Y. Farge, Eds., North Holland, Amsterdam (1981).

cause penumbra; but they produce deep resist profiles with vertical sidewalls and astonishing aspect ratios. In addition, because of the extremely short wavelength of x rays, diffraction effects caused by the mask-substrate gap in proximity printing are minimized.¹⁰

Synchrotrons are not without drawbacks. One of their major limitations is their extremely large size and the huge cost of ownership associated with them. Reliability is also a concern with these systems. For instance, a synchrotron can take a whole day or more to be brought up because they operate at 10^{-9} torr or higher vacuum, and beam lifetimes last only 24 hours.¹¹

14.2.2 X-ray masks

Given that there are no materials that have excellent transparency to x rays, x-ray masks are comprised of very thin membranes (with thickness $< 2 \mu\text{m}$), typically made of low-atomic-number materials, on which the circuit patterns are placed in the form of high-atomic-number absorber materials. A high percentage of the x rays pass through the low-atomic-number material, but are absorbed or scattered by the high-atomic-number materials, thus generating a contrast for the pattern.¹² Typical materials used as x-ray mask membranes include silicon, boron nitride, silicon carbide, diamond, and silicon nitride. Typical materials used as x-ray mask absorbers include gold,¹³ tungsten,¹⁴ Ta, TaN,¹⁵ TaSiN,¹⁶ and Ta₄B,¹⁷ with the last four materials being the most preferable because they are compatible with various etch and cleaning processes.¹⁸

Membrane materials must have a high Young's modulus (for silicon carbide, the value is 450 GPa, while it is 900 GPa for diamond), a characteristic that minimizes mechanical distortion as well as makes the membrane damage resistant to prolonged exposure to x rays.¹⁹

¹⁰A. Reiser, *Photoreactive Polymers: The Science and Technology of Resists*, p. 337, John Wiley & Sons, Hoboken, NJ (1989).

¹¹"Microlithography & mask making," VLSI Report (1992).

¹²H.J. Levinson, *Principles of Lithography*, 2nd ed., SPIE Press, Bellingham, WA, p. 375 (2005).

¹³G.E. Georgiou, C.A. Jankowski, and T.A. Palumbo, "DC electroplating of sub micron gold patterns on x ray masks," *Proc. SPIE* **471**, 96 (1984).

¹⁴P.A. Seese, K.D. Cummings, D.J. Resnik, A.W. Yanfo, W.A. Johnson, G.M. Welss, and J.P. Wallace, "Accelerated radiation damage testing of x ray mask membrane materials," *Proc. SPIE* **1924**, 457–466 (1993).

¹⁵J.T. Sheu, A. Chu, J.H. Ding, and S. Su, "Characteristics of sputtered TaX absorbers for x ray masks," *Proc. SPIE* **3676**, 42–45 (1999).

¹⁶J.M. Rocque, D.M. Puisto, D.J. Resnick, K.D. Cummings, W. Chuc, and P.A. Seese, "SNR200 chemically amplified resist optimization," *Proc. SPIE* **3048**, 90–99 (1997).

¹⁷C.J. Brooks, K.C. Racette, M.J. Lercel, L.A. Powers, and D.E. Benoit, "Advanced refractory metal and process technology for the fabrication of x ray masks," *Proc. SPIE* **3676**, 14–23 (1999).

¹⁸H.J. Levinson, *Principles of Lithography*, 2nd ed., p. 367, SPIE Press, Bellingham, WA (2005).

¹⁹P.A. Seese, K.D. Cummings, D.J. Resnik, A.W. Yanfo, W.A. Johnson, G.M. Welss, and J.P. Wallace, "Accelerated radiation damage testing of x ray mask membrane materials," *Proc. SPIE* **1924**, 457–466 (1993).

The use of thin membranes in x-ray masks presents many challenges. These challenges include film deformation because of stresses, and susceptibility to vibration when stepped or scanned in an exposure tool.²⁰ Mask deformation is particularly problematic in x-ray lithography, given that the imaging is 1:1 printing, with no reduction. This necessitates very tight tolerances for x-ray masks relative to reduction printing systems.²¹

On the other hand, there are no lens distortions or feature-size-dependent pattern-placement errors associated with x-ray lithography since there are no lenses involved. This implies that a significant portion of the overlay budget can be allocated to the mask in x-ray lithography.²²

14.3 Extreme Ultraviolet Lithography

Projection soft x-ray lithography, also called EUV lithography, was invented independently in the 1980s by research teams at NTT²³ in Japan and at Bell Laboratories in the United States,²⁴ who were inspired by the availability of mirrors of reasonable efficiency at soft x-ray wavelengths ($\lambda \approx 4\text{--}40\text{ nm}$).²⁵ Summarized below are the basic attributes of EUV lithography.

EUV lithography uses photons with 13.5-nm wavelength to expose wafers. It has higher resolution (with suitable numerical aperture) than longer-wavelength photons used in conventional DUV lithography. For the same k_1 factor for EUV and 193-nm lithographies, the resolution of the EUV imaging system relative to that of the state-of-the-art advanced immersion 193-nm imaging system is given by

$$\frac{w_{\text{EUV}}}{w_{193}} = \frac{k_1 13.5 / \text{NA}_{\text{EUV}}}{k_1 193 / \text{NA}_{193}} \approx \frac{1}{5}, \quad (14.2)$$

which is for numerical aperture values of $\text{NA}_{\text{EUV}} = 0.45$ and $\text{NA}_{193} = 1.35$ (hyper-NA imaging with immersion lithography). This result indicates that the resolution potential of the EUV system is approximately five times better than

²⁰M.P. Schlax, E.L. Engelstadt, E.G. Lovell, and C.J. Brooks, "Predicting mechanical distortions in x ray mask membranes," *Proc. SPIE* **3331**, 629–637 (1998).

²¹H.J. Levinson, *Principles of Lithography*, 2nd ed., p. 376, SPIE Press, Bellingham, WA (2005).

²²*ibid.*, p. 367.

²³H. Kinoshita, T. Kaneko, H. Takei, N. Takeuchi, and S. Ishihara, "Study on x ray reduction projection lithography," *Proc. of 47th Autumn Meeting of the Japan Soc. of Appl. Phys.*, Paper No. 28 ZF 15 (1986); H. Kinoshita, K. Kurihara, Y. Ishii, and Y. Torii, "Soft x ray reduction lithography using multilayer mirrors," *J. Vac. Sci. Technol. B* **7**, 1648 (1989); T. Namioka, "Current research activities in the field of multilayer for soft x rays in Japan," *Revue Phys. Appl.* **23**, 1711–1726 (1988).

²⁴W.T. Silfvast, O.R. Wood II, "Tenth micron lithography with a 10 Hz 37.2 nm sodium laser," *Microelectron Eng.* **8**, 3–11 (1988); A.M. Hawryluk and L.G. Seppala, "Soft x ray projection lithography using an x ray reduction camera," *J. Vac. Sci. Technol. B* **6**, 2162–2166 (1988).

²⁵For an excellent historical account of the development of EUV lithography, see for example, H. Kinoshita and O. Wood, "EUV lithography: an historical perspective," in *EUV Lithography*, V. Bakshi, Ed., pp. 1–54, SPIE Press, Bellingham, WA (2009).

that of the hyper-NA immersion 193-nm lithography system, provided that the resist process used to print the EUV image can support the same k_1 factor as the 193-nm lithographic process. Designing and fabricating such a resist that can enable such enhanced resolution is one of the main difficulties in implementing EUV lithography in manufacturing. In addition, producing an imaging system that can exploit the advantages of the short EUV wavelength is a very complex undertaking in light of the fact that traditional materials used to fabricate lenses and mirrors do not have the required optical characteristics in the EUV range.²⁶

EUV lithography uses a $4\times$ demagnification factor, consistent with the current (2008) International Technology Roadmap for Semiconductors (ITRS) mask development roadmap.²⁷ In some aspects, the fabrication of EUV masks will be simpler than for leading-edge masks used in longer-wavelength optical lithographies such as DUV lithography because the OPC features are much fewer and less complicated. Unlike conventional DUV lithography, the source of EUV radiation used in EUV lithography is not a laser; instead, it is a dense hot plasma that can be formed by laser plasmas or electrical discharges.

The source chamber cannot be separated from the main chamber by a physical barrier because no known material has sufficient transparency to EUV photons. This places a significant challenge in being able to prevent debris in the form of particles, energetic ions, and neutrals generated by the hot plasma from getting into the main chamber where the illumination optics are housed. Vacuum clamping cannot be used in EUV exposure tools because of the risk of generating particles. Therefore, electrostatic clamping must be used in the EUV exposure tool. Components in the EUV exposure chamber are not accessible for maintenance and/or adjustment, necessitating remote control of subsystems, diagnostics, etc.

EUV radiation cannot be transmitted through air, which makes it necessary to maintain the entire EUV exposure tool in a vacuum environment (10^{-9} mbar). Outgassing of resists and components of the exposure tool inside the exposure chamber therefore poses a significant contamination risk to the EUV optics, which are completely based on mirrors. Furthermore, hydrocarbons and water vapor are cracked by EUV radiation, contaminating mirror surfaces via carbon deposition and oxidation of multilayer coatings. Both carbon deposition and oxidation of the surfaces of EUV optical elements reduce the reflectivity of the mirrors and introduce wavefront aberrations to the projection optics. The overall effect decreases not only the throughput of the exposure tool, but also the imaging performance.²⁸ Thus, it is necessary to minimize hydrocarbons and water vapor content in the tool. This is yet another reason that imaging in EUV lithography is done in vacuum.

There are no reasonably EUV-transmissive refractive materials that can be used in EUV optics. Instead, most naturally occurring materials reflect only a very small fraction of the incident EUV photons, and tend to absorb most of

²⁶B. La Fontaine, "EUV optics," in *Extreme Ultraviolet Lithography*, B. Wu, A. Kumar, Eds., Chapter 4, McGraw Hill, New York (2009).

²⁷International Technology Roadmap for Semiconductors, Lithography Section (2008).

²⁸A. Barty and K.A. Goldberg, "Effects of radiation induced carbon contamination on the performance of an EUV lithographic optic," *Proc. SPIE* **5037**, 450–459 (2003).

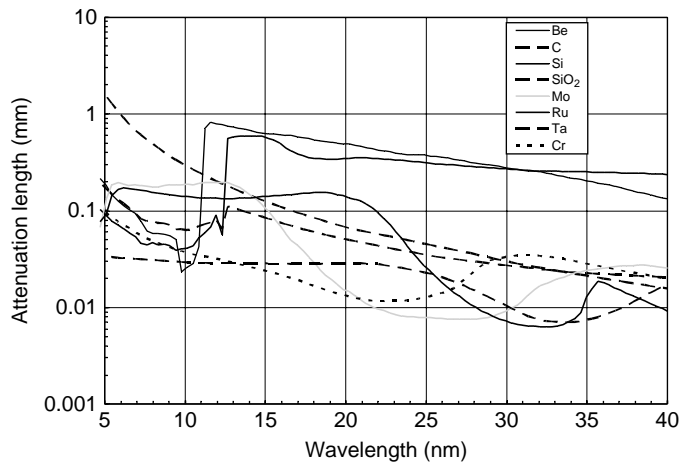


Figure 14.2 Attenuation length of EUV radiation for selected elements. (Reprinted with permission from Ref. 30. © 2009 McGraw-Hill.)

them within a fraction of a micron from their surface²⁹ (see Fig. 14.2). Therefore, only precisely figured reflective optics (with reflectivity on the order of 70%) comprising mirrors and reticles can be used in the EUV tool. Even with reflective optics of moderate reflectivity, there are still significant photon losses through the exposure optics after reflection from multiple mirror surfaces, i.e., only about 6% of the photons incident on the reflective mirrors reach the wafer plane.³¹

Also, because of the high EUV absorptivity of solid materials, including thin polymer films, there are no materials currently demonstrated with sufficient transparency that can be used as EUV pellicles. As a result, there are no pellicles for EUV masks, which presents significant defect control challenges in EUV lithography.

Furthermore, EUV photons are sufficiently energetic to interact directly with bound electrons of the individual atoms of any given material. In this spectral range, there are a large number of atomic resonances, which leads to strong absorption.³²

Given the small scattering cross section in the 10–15-nm wavelength range, the refractive indices of available materials approach unity; as a result, materials tend to exhibit low reflectivity in the EUV region of the spectrum. The reflectivity R at normal incidence for an interface between vacuum and a given material is expressed as

$$R = \left(\frac{1 - n}{1 + n} \right)^2, \quad (14.3)$$

²⁹B. La Fontaine, “EUV optics,” in *Extreme Ultraviolet Lithography*, B. Wu and A. Kumar, Eds., Chapter 4, McGraw Hill, New York (2009).

³⁰ibid.

³¹ibid.

³²ibid.

where n is the refractive index of the material and 1 is the refractive index of vacuum.

In general, R increases roughly as the fourth power of the wavelength in this regime.³³ The influence of atomic resonances also increases significantly at extremely short wavelengths. For example, at 12.4 nm, silicon has an absorption edge associated with photoionization of its $2p$ electrons, and its index of refraction is greater than 1, while its reflectivity shows a significant decrease,³⁴ as can be seen in Fig. 14.3.

It must be emphasized that the short attenuation length and low normal-incidence reflectivity of materials in the EUV range present very difficult problems regarding fabricating single-surface mirrors or lenses. The main solution to this problem is the use of multilayer reflectors. Absent these reflectors, EUV lithography as currently practiced would not be possible.

14.3.1 EUV multilayer mirrors

The main optical elements used in EUV optics are based on multilayer (ML) film reflectors. As stated above, at 13.5 nm, a single-surface reflector made of any material has very low reflectivity. For instance, at normal incidence, the reflectivity of molybdenum is about 10^{-3} at 13.5 nm (see Fig. 14.3), which corresponds to an electric field amplitude reflectivity of about 3%. By constructing a smooth substrate, comprising a multilayer stack of alternating thin (a few nanometers) layers of molybdenum and silicon, with negligible photon absorption, it is possible to

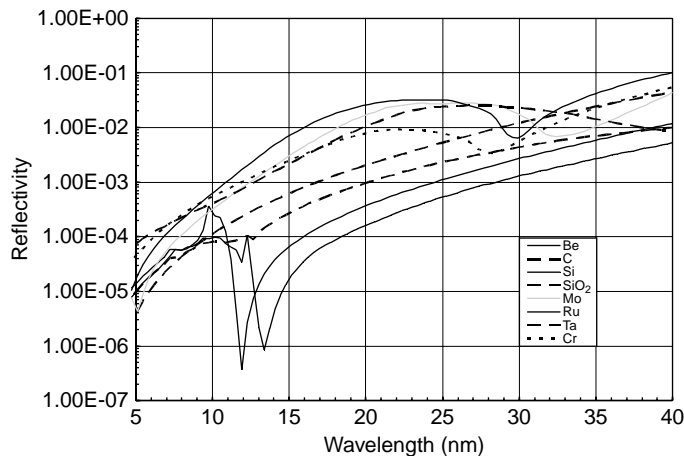


Figure 14.3 Reflectivity at normal incidence of selected materials in the EUV range, for normal incidence. (Reprinted with permission from Ref. 35. © 2009 McGraw-Hill.)

³³ibid.

³⁴ibid.

³⁵ibid.

significantly increase the reflectivity from such structures through constructive additions of the amplitudes of the multiply reflected waves³⁶ (see Fig. 14.4). The Bragg equation expresses the condition for coherent addition of the EUV radiation reflected from these multiple interfaces:

$$2d = \frac{m\lambda}{\sin \theta}, \quad (14.4)$$

where $2d$ is the period or spacing of the reflecting planes, θ is the angle of incidence of the light, and m is the order of diffraction from this periodic structure.

Practically all materials have very short attenuation lengths in the EUV range; this significantly limits the reflectivity of actual multilayer film reflectors. Maximizing reflectivity at each interface and minimizing absorption of the spacer material makes the choice of the materials to be used for this purpose extremely critical.³⁷ The reflectivity at the interface between two different materials is expressed as³⁸

$$R = \frac{|n_2 - n_1|^2}{|n_2 + n_1|^2} = \frac{(\delta_2 - \delta_1)^2 + (\beta_2 - \beta_1)^2}{4}, \quad (14.5)$$

where β_i is the imaginary part of the refractive index of component i , and δ_i is the real part of the refractive index of component i .

From the above equation, it can be seen that having low component absorption and maximizing the difference between the real part of the refractive indices of the two components provide the overall maximum reflectivity for the multilayer.³⁹

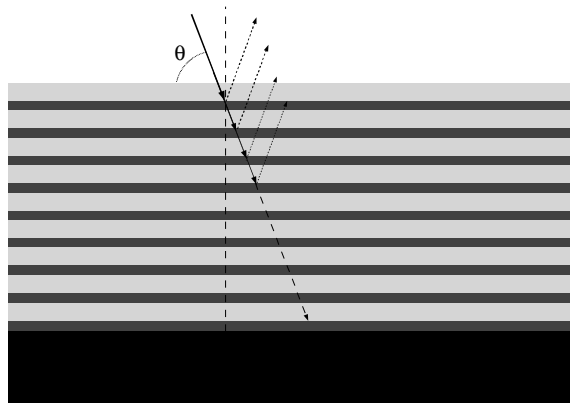


Figure 14.4 Schematic cross-sectional view of a multilayer film reflector. θ is the angle of incidence of the light relative to the surface. Reflection from the first few interfaces between the more reflective material (dark gray) and the more transparent material (light gray) are shown. (Reprinted with permission from Ref. 40. © 2009 McGraw-Hill.)

³⁶ibid.

³⁷ibid.

³⁸ibid.

³⁹ibid.

⁴⁰ibid.

At 13.5-nm wavelength, silicon and molybdenum make an excellent pair of materials for an EUV multilayer mirror. The real part of their refractive indices is quite different in the EUV spectral region; in addition, molybdenum has the lowest absorption at EUV relative to other alternative metals with reasonable single interface reflectivity.⁴¹

In fact, normal incidence multilayer mirrors with reflectivity approaching 70% at 13.5 nm have been fabricated using the molybdenum-silicon pair.⁴² Figure 14.5 shows the calculated reflectivity curve for perfectly smooth interfaces of 50 alternating pairs of molybdenum (2.5 nm) and silicon layers (4.2 nm), indicating a theoretical peak reflectivity of 74%. It must be noted, however, that the theoretical reflectivity cannot be achieved in practice due to the roughness of the interfaces, which may result from a number of factors such as substrate roughness, the material deposition process, and interfacial chemistry between the pairs of materials.⁴³

Given that multilayer reflectors are resonant structures, they typically operate within a narrow range of wavelengths around the Bragg condition

$$2d = \frac{m\lambda}{\sin \theta}, \quad (14.6)$$

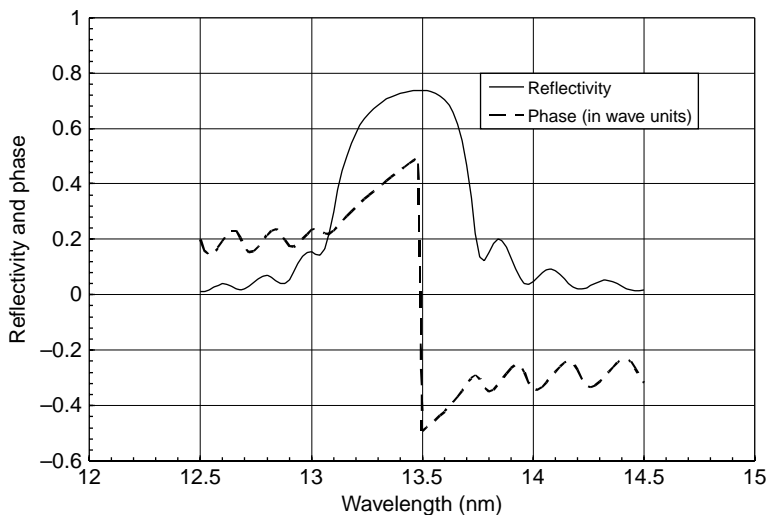


Figure 14.5 Calculated normal incidence reflectivity curve for a molybdenum-silicon multilayer mirror with number of bilayers = 50. The molybdenum thickness is 2.7 nm and the silicon thickness is 4.2 nm. (Reprinted with permission from Ref. 44. © 2009 McGraw-Hill.)

⁴¹ibid.

⁴²C. Montcalm, S. Bajt, P.B. Mirkarimi, E. Spiller, F.J. Weber, and J.A. Folta, "Multilayer reflective coatings for extreme ultraviolet lithography," *Proc. SPIE* **3331**, 42–51 (1998).

⁴³B. La Fontaine, "EUV optics," in *Extreme Ultraviolet Lithography*, B. Wu, A. Kumar, Eds., Chapter 4, McGraw Hill, New York (2009).

⁴⁴ibid.

where $2d$ is the period or spacing of the reflecting planes, θ is the angle of incidence of the EUV radiation, and m is the diffraction order from the periodic structure. For a multilayer mirror with N bilayers, the accumulated phase error for a wavelength offset $\Delta\lambda$ is $\Delta\phi = 2\pi N\Delta\lambda/\lambda$. Assuming a maximum phase shift of π from one side of the spectrum to the other, the bandwidth of the multilayer reflector is expressed as⁴⁵

$$\frac{2\Delta\lambda}{\lambda} = \frac{1}{N}. \quad (14.7)$$

To protect the ML coating that is part of an EUV optic or EUV reticle, a capping layer is often deposited on top of its surface. Bajt et al.⁴⁶ have identified the properties that good capping layers must possess. They must possess the right optical properties at EUV wavelength, i.e., they should increase or at the very least have no effect on the reflectivity (at $\lambda = 13.5$ nm) of the entire ML coating. They must make continuous and smooth films, even at extremely thin thicknesses. To avoid intermixing in the underlying ML stack, they must be able to be deposited at low temperatures ($<200^\circ\text{C}$). In the most ideal case, their surface chemistry must be such that carbon and oxygen atoms recombine on their surfaces to form carbon dioxide, which could be easily desorbed thermally or by electron- or photon-stimulated desorption processes associated with the incident EUV flux. They must be impermeable to carbon or oxygen diffusion, either into the ML or out, from the ML to the surface. If the capping layer is polycrystalline, a specific crystallographic texture might be required. And if the capping layer is amorphous, it should be defect free. The capping layers should also be chemically inert with respect to the stack materials underneath; they must be thermally stable, and must generate minimal stresses in the film stack during deposition. Finally, they must be cost effective and consistent with environmental, health, and safety regulations during their manufacture and use.

14.3.2 Fabrication of Mo-Si multilayer mirrors

The fabrication of Mo-Si multilayer optics involves the alternating deposition of Mo and Si on highly polished substrates, often low-thermal-expansion glass, using a range of deposition techniques based on DC magnetron sputtering,⁴⁷ ion-beam sputtering,⁴⁸ or e-beam evaporation combined with ion-beam

⁴⁵ibid.

⁴⁶S. Bajt, N.V. Edwards, and T.E. Madey, "Properties of ultrathin films appropriate for optics capping layers exposed to high energy photon irradiation," *Surf. Sci. Rep.* **63**, 73–99 (2008); S. Bajt, "Optics contamination," in *EUV Lithography*, V. Bakshi, Ed., pp. 227–259, SPIE Press, Bellingham, WA (2009).

⁴⁷C. Montcalm, S. Bajt, P.B. Mirkarimi, E. Spiller, F.J. Weber, and J.A. Folta, "Multilayer reflective coatings for extreme ultraviolet lithography," *Proc. SPIE* **3331**, 42–51 (1998).

⁴⁸K. Murakami, T. Oshino, H. Kondo, H. Chiba, H. Komatsuda, K. Nomura, and H. Iwata, "Development status of projection optics and illumination optics for EUV1," *Proc. SPIE* **6921**, 69210Q (2008).

polishing.⁴⁹ A combination of these techniques is often used to achieve high reflectivity, while maintaining low stress. Current coating chambers are capable of handling large substrates (up to ~ 600 mm) that are also fairly heavy (several kilograms) and are characterized by large curvatures.⁵⁰ Figure 14.6 shows a multi-layer defect resulting from a particle on the substrate. This type of multilayer defect can produce phase defects during imaging.

14.3.3 EUV masks

Figure 14.7 shows the cross section of a typical EUV mask. It comprises an absorber layer (typically Ta, TaN, or CrN), which is deposited on top of the buffer layer (typically SiO_2) that separates it from the Mo-Si multilayer reflector. Note that the absorber material in Fig. 14.7 is TiN. A capping layer (typically Ru or Si) is often deposited on top of the Mo-Si stack to protect it from reflectivity-degradative carbon deposition and oxidation reactions.

Fabrication of EUV masks involves the deposition of the buffer layer on the mask blank, followed by the deposition of the absorber layer, and finally the deposition of the capping layer. By coating an appropriate resist over the capping layer and exposing (with electron-beam lithography) and developing away the exposed areas of the resists, a relief image comprising the open areas (without resist) and the resist-covered absorber areas is printed on the mask blank. Pattern transfer into underlying layers through the open areas over the capping layer, absorber, and buffer layer is effected by means of appropriate etching, in a subtractive manner. Here, the resist protects the capping layer and absorber–buffer layer stack under it.

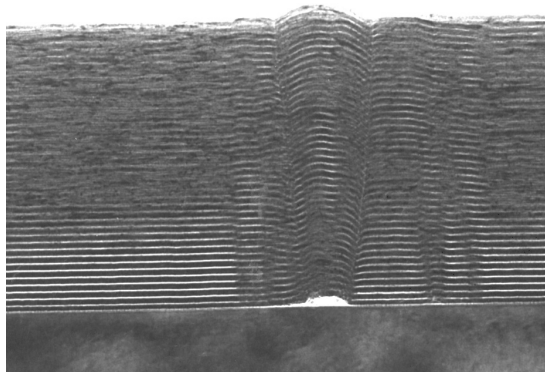


Figure 14.6 Propagating defect resulting from the deposition of Mo-Si multilayers over a bump.

⁴⁹R. Soufli, S.L. Baker, D.L. Windt, E.M. Gullikson, J.C. Robinson, W.A. Podgorski, and L. Golub, “Atomic force microscopy characterization of Zerodur mirror substrates for the extreme ultraviolet telescopes aboard NASA’s Solar Dynamics Observatory,” *Appl. Opt.* **46**(16), 3156–3163 (2007).

⁵⁰B. La Fontaine, “EUV optics,” in *Extreme Ultraviolet Lithography*, B. Wu, A. Kumar, Eds., Chapter 4, McGraw Hill, New York (2009).

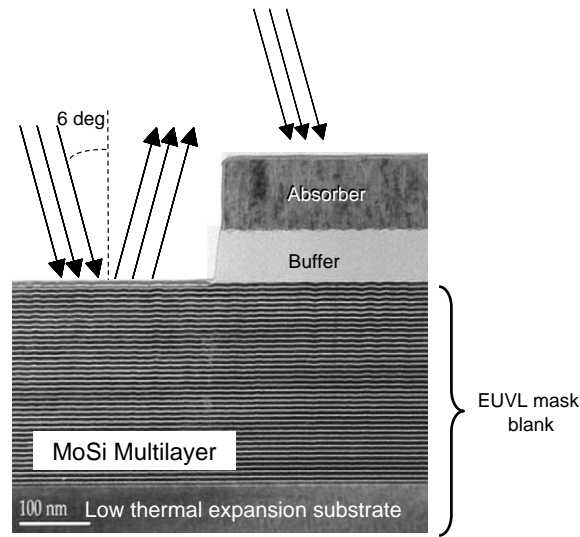


Figure 14.7 EUV mask architecture. (TEM picture courtesy of J. Gray.)

14.3.4 The EUV exposure system

The EUV exposure system comprises the plasma source (for generating the plasma that in turn emits EUV photons), the source collection optics (comprising the condenser and illumination optics), and the projection optics. A schematic of an EUV exposure tool is shown in Fig. 14.8.

Specially designed optics are used to collect EUV photons generated in the plasma source. The collector optics directs the EUV photons from the plasma source to the intermediate focus, which is the entrance to the illumination optical system. It is conventional to use the power level measured at the intermediate focus to specify the source power. The intermediate focus is also where étendue (a measure of how spread out the radiation is in area and angle) matching between the collector and the illuminator is implemented in order to ensure that all of the collected EUV photons (from the collector) are accepted into the illuminator to avoid being wasted. The function of the illumination system is to provide uniform EUV irradiation of the reticle, as well as the required degree of partial coherence for imaging. The projection optics constitutes the last part of the exposure tool and is designed to produce a high-resolution image of the reticle. It should also have very low distortion and aberration levels.⁵¹ Figure 14.9 shows an optical design similar to the one adopted by ASML in the design of the first full-field EUV exposure tool called the ASML Alpha Demonstration Tool.⁵²

⁵¹B. La Fontaine, "EUV optics," in *Extreme Ultraviolet Lithography*, B. Wu, A. Kumar, Eds., Chapter 4, McGraw Hill, New York (2009).

⁵²H. Meiling, J.P.H. Benschop, U. Dinger, and P. Kurz, "Progress of the EUVL alpha tool," *Proc. SPIE* **4343**, 38 (2001).

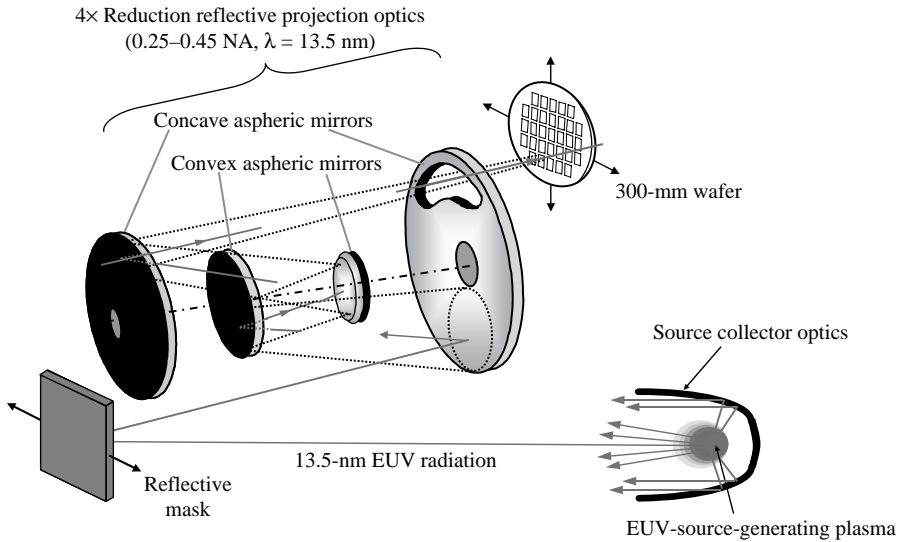


Figure 14.8 Schematic of an EUV lithography exposure system.

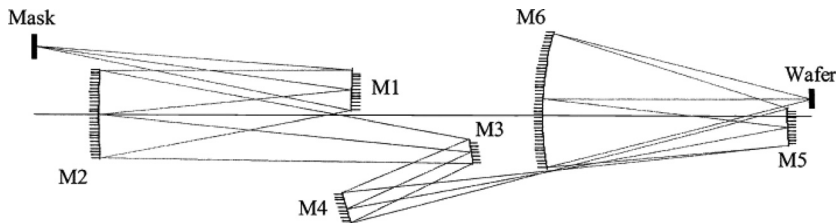


Figure 14.9 4 \times design similar to that of the ASML Alpha Demo Tool. NA = 0.25, 25 m λ rms wavefront error, 2-mm ring field width, <1-nm dynamic distortion, \sim 1.4-m overall length (M stands for mirror).⁵³

14.3.5 Sources for EUV lithography

The two main sources used in commercial EUV lithographic exposure tools comprise laser-produced plasma sources⁵⁴ and discharge-produced plasma sources.⁵⁵

⁵³R.M. Hudyma, "An overview of optical systems for 30 nm resolution lithography," *Proc. SPIE* **4832**, 137–148 (2002); R.M. Hudyma, H. J. Mann, U. Dinger, and P. Kurz, "Projection system for EUV lithography," U.S. Patent No. 6,985,210 (2006).

⁵⁴U. Stamm, J. Kleinschmidt, K. Gabel, et al., "EUV source power and lifetime: the most critical issues for EUV lithography," *Proc. SPIE* **5374**, 133–144 (2004); M. Richardson, C. S. Koay, K. Takenoshita, et al., "Laser plasma EUVL sources—progress and challenges," *Proc. SPIE* **5374**, 447–453 (2004).

⁵⁵U. Stamm, J. Kleinschmidt, K. Gabel, et al., "EUV source power and lifetime: the most critical issues for EUV lithography," *Proc. SPIE* **5374**, 133–144 (2004).

14.3.5.1 Laser-produced plasma sources

In laser-produced plasma (LPP) sources, a high-intensity laser radiation (typically from a pulsed Nd-YAG laser, CO₂ laser, or diode-pumped fiber laser) is used to create a plasma from target materials such as Sn,⁵⁶ Li,⁵⁷ and Xe⁵⁸ (see Fig. 14.10), with Sn being preferred because of its higher conversion efficiency (3%) compared to that of Xe (1%) and the highly reactive Li (2–3%). It must be mentioned that Sn has several critical challenges, the main one of which is the fact that it is a condensable fuel that deposits on surfaces under standard EUV tool operating conditions.⁵⁹ Not only does the Sn deposition contaminate optical surfaces, it also degrades the reflectivity of the affected optics. In addition, high-energy Sn ions or neutrals can contaminate optical surfaces, making them rougher while also eroding them.⁶⁰ Xe, on the other hand, offers some advantages, i.e., it produces relatively strong EUV emissions and is also chemically inert in its electrically neutral state, which makes it less likely to generate debris that can contaminate and degrade EUV optics. However, EUV radiation is produced by the highly charged Xe⁺¹⁰ ionic state, which has been reported to sputter solid

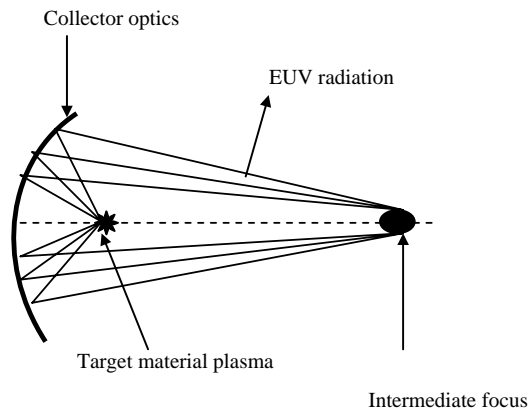


Figure 14.10 Schematic of an EUV laser-produced plasma source.

⁵⁶T. Tomie, T. Aota, Y. Ueno, G. Nimi, H. Yashiro, J. Lin, I. Matsushima, K. Komiyama, D. Lee, K. Nishigori, and H. Yokota, "Use of tin as a plasma source material for high conversion efficiency," *Proc. SPIE* **5037**, 147–155 (2003).

⁵⁷W. Parlo, I. Formenkov, R. Olivier, and D. Birs, "Development of an EUV (13.5 nm) light source employing a dense plasma focus in lithium vapor," *Proc. SPIE* **3997**, 136–156 (2000).

⁵⁸G. Schriever, M. Rahe, W. Neff, K. Bergmann, R. Lebert, H. Lauth, and D. Basting, "Extreme ultraviolet light generation based on laser produced plasmas (LPP) and gas discharge based on pinch plasmas: a comparison of different concepts," *Proc. SPIE* **3997**, 162–168 (2000); L. Rymell, M. Berglund, B.A.M. Hansson, and H.M. Hertz, "X ray and EUV laser plasma sources based on cryogenic liquid jet target," *Proc. SPIE* **3676**, 421–424 (1999).

⁵⁹D.N. Ruzic and S.N. Srivastava, "Normal incidence (multilayer) collector contamination," in *EUV Lithography*, V. Bakshi, Ed., 285–323, SPIE Press, Bellingham, WA (2009).

⁶⁰ibid.

surfaces.⁶¹ Debris-mitigation schemes are implemented in these EUV sources, particularly those that use materials other than noble gases.

Figure 14.11 shows the normalized EUV emission spectrum in the region from 8 to 20 nm obtained from a Sn target in an LPP system under development for high-volume manufacturing at Cymer. The peak emission of the CO₂-laser-produced plasma occurs at 13.5 nm and matches well to the reflectivity curve of multilayer coated mirrors designed for this wavelength.

Due to their isotropic radiation, LPP sources allow for the use of normal incident collectors; thus, higher collection efficiency can be achieved with LLP sources as opposed to DPP sources, which tend to be directional. Because LPP sources do not require electrodes, there is no concern about electrode debris being generated from them. In addition, LLP sources have potential for easier and better thermal management than DPP sources because the plasma they generate is isolated from the collection optics, which is designed to capture the emission from the plasma and relay it to the intermediate focus from where it is relayed to the exposure tool.

14.3.5.2 Discharge-produced plasma sources

Discharge-produced plasma (DPP) sources employ extremely high electrical voltages to ionize and discharge fuel materials such as xenon gas or tin confined within an electrode assembly, resulting in the creation of plasmas comprising

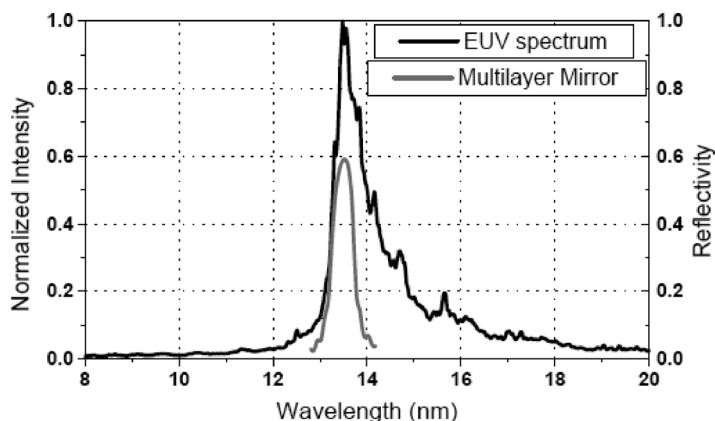


Figure 14.11 EUV spectrum for a Sn droplet obtained with a CO₂ drive laser of an LPP system during high-repetition-rate operation in comparison with a high-temperature stable multilayer mirror reflectance curve. (After D.C. Brandt et al.⁶²)

⁶¹P.A. Grunov, L.F. Klebanoff, S. Graham, Jr., S.J. Haney, and W.M. Clift, “Rates and mechanisms of optics contamination in the EUV engineering test stand,” *Proc. SPIE* **5037**, 418–428 (2003).

⁶²D.C. Brandt, I.V. Formenkov, A.I. Ershov, N.P. William, D.W. Myers, N.R. Bowering, A.N. Bykanov, G.O. Vaschenko, O.V. Khodykin, J.R. Hoffman, E. Vargas, R.D. Simmons, J.A. Chavez, and C.P. Chrobak, “LPP EUV source development for HVM,” *Proc. SPIE* **6517**, 65170Q (2008).

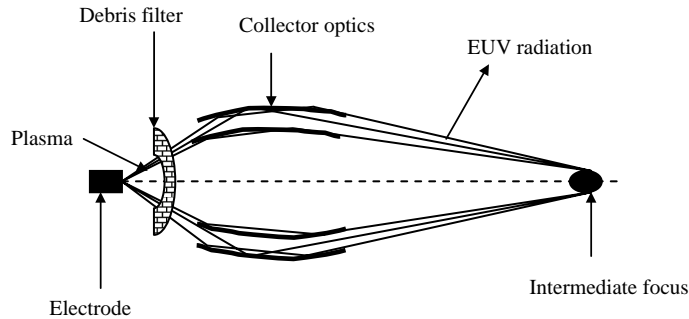


Figure 14.12 Schematic of an EUV DPP source.

ionic species, which are compressed with some type of pinch (dense plasma focus, z-pinch) to high temperatures, ultimately resulting in the emission of characteristic EUV radiations at 13.5 nm (see Fig. 14.12). Like their LPP counterparts, the DPP sources produce strong electric fields during plasma expansion that can accelerate the fuel ions to extremely high energies. These energetic ions bombard the mirror surfaces of the collector optics, causing surface erosion, roughening, deposition, and implantation of impurities onto them, and consequently degrading their reflectivity. Low-energy sputtered debris can degrade reflectivity through deposition and coating processes, but these effects are judged to be minimal compared to erosive fluxes encountered in the source chamber. Just as in LPP sources, debris mitigation is a major challenge in DPP sources because expansion occurs during the postemission time frame, accelerating the gases away from the pinch location.⁶³ Many debris mitigation schemes have been developed. Mechanical debris mitigation uses fins to deflect the debris from the optic. Other schemes are based on the use of electric and/or magnetic fields to deflect charged particles and ions away from the optic.

Due to their directional pattern of radiation, DPP sources can afford smaller collection angles than their laser-produced counterparts, which radiate in an almost isotropic manner. This explains the use of grazing incidence optics as the collector for DPP sources. Also, DPP sources generate additional debris from the eroded electrodes, which are absent in LLP sources. The conversion efficiency (electricity to EUV radiation) of DPP sources is $<1.5\%$ (into 2π sr), with transmission to intermediate focus of about 6%.

14.4 Optics Lifetime

Optics lifetime refers to the length of time a given optics can be used within the exposure environment before it has to be replaced or repaired so as to maintain a specified level of the element's reflectivity and, consequently, wafer throughput.

⁶³D.N. Ruzic and S.N. Srivastava, "Normal incidence (multilayer) collector contamination," in *EUV Lithography*, V. Bakshi, Ed., SPIE Press, Bellingham, WA, pp. 285–323 (2009).

It is one of the critical challenges that must be mitigated if EUV lithography is to be deployed in high-volume manufacturing (HVM). Despite recent progress made on this front, largely by combining an oxidation-resistant capping layer with in situ cleaning strategies that attempt to leverage chamber gas-surface interactions to impede oxidation and contamination,⁶⁴ optics lifetimes still fall short of specifications for HVM by nearly two orders of magnitude.⁶⁵

Condenser optics have short lifetimes; their optics specifications are less stringent than those for the projection optics. The condenser optical components are considered consumable and are replaced on a regular basis. In contrast, projection optics have extremely tight specifications and are difficult and time consuming to fabricate and to align.

In EUV lithography, optics lifetime (as monitored by reflectivity level) is limited by surface contamination, oxidation, radiation-induced damage (nonthermal and thermal), surface composition changes, and surface roughening. These reflectivity-degradation processes affect the collector and projection optics to different degrees, in part because of their different locations in the EUV exposure tool, and also because of the composition of these mirrors. While the projection optics are normal-incidence ML mirrors, those of the collector optics may have both normal-incidence and grazing-incidence mirrors that are not ML mirrors. The grazing-incidence mirrors have lower reflectivity than their normal-incidence counterparts. For the grazing-incidence mirrors of the collector optics, sputter-induced roughness and contamination are the main causes of reflectivity degradation. The sputtering is caused by debris generated from the source fuel (ions and neutrals from xenon, tin, or lithium), which erodes electrodes and other materials in the source (in the case of DPP systems). For normal-incidence mirrors of the projection optics, erosion, roughness, and contamination are responsible for reflectivity degradation.⁶⁶

⁶⁴M. Malinowski, C. Steinhaus, M. Clift, L.E. Klebanoff, S. Mrowka, and R. Soufli, "Controlling contamination in Mo/Si multilayer mirrors by Si surface capping modifications," *Proc. SPIE* **4688**, 44–453 (2002); M. Malinowski, P. Grunow, M. Clift, and L. Klebanoff, "Use of molecular oxygen to reduce EUV induced carbon contamination of optics," *Proc. SPIE* **4343**, 347–356 (2001); S. Graham, C. Steinhaus, M. Clift, and L. Klebanoff, "Radio frequency discharge clearing of silicon capped Mo/Si multilayer extreme ultraviolet optics," *J. Vac. Sci. Technol. B* **20**(6), 2393–2401 (2002); B. Mertens, B. Wolshrijn, R. Jansen, N. Koster, M. Weiss, M. Wedowski, R. Klein, R. Bock, and R. Thornagel, "EUV time resolved studies on carbon growth and cleaning," *Proc. SPIE* **5037**, 95–102 (2003); K. Hamamoto, T. Tanaka, T. Watanabe, N. Sakaya, M. Hosoya, T. Shoki, H. Hada, N. Hishinuwu, H. Sugahara, and H. Kinoshita, "Cleaning of extreme ultraviolet lithography optics and masks using 13.5 nm and 172 nm radiation," *J. Vac. Sci. Technol. B* **23**, 247–252 (2005).

⁶⁵S. Bajt, "Optics contamination," in *EUV Lithography*, V. Bakshi, Ed., Chapter 6A, SPIE Press, Bellingham, WA, 227–259 (2009).

⁶⁶D.N. Ruzic and S.N. Srivastava, "Normal incidence (multilayer) collector contamination," in *EUV Lithography*, V. Bakshi, Ed., pp. 285–323, SPIE Press, Bellingham, WA (2009); V. Rigato, "Grazing angle collector contamination," in *EUV Lithography*, V. Bakshi, Ed., SPIE Press, Bellingham, WA, Chp. 6B, pp. 261–284 (2009).

14.5 Contamination Processes

In the absence of an ultrahigh-vacuum environment, the EUV lithographic projection optics and reticles are exposed to water, hydrocarbon, and other contaminants in the presence of EUV photons.⁶⁷ Oxidation and carbon deposition are the two contamination processes that have been identified to limit an EUV projection optics' lifetime.⁶⁸ Oxidation is thought to be the most severe of the two problems because it is considered to be difficult to remove.⁶⁹ Understanding the scaling laws governing the growth of contamination layers on EUV optics is critical to obtaining an accurate assessment of optics lifetime in a given EUV exposure environment of residual gases and photon fields. Several studies have shown a nonlinear relationship between reflectivity loss and incident EUV dose, as well as with partial pressure of hydrocarbons or water;⁷⁰ all of these make extrapolations to a realistic HVM environment somewhat unreliable.

14.5.1 Carbon deposition

Carbon deposition occurs when EUV photons crack residual hydrocarbons in the vicinity of an EUV optic or reticle. These hydrocarbons may originate from a number of sources such as outgassing of resists or other materials inside the scanner environment, residual air in the exposure chamber, etc. Once deposited, these carbon deposits can be cleaned with minimal or no damage to the underlying multilayer film. This could allow repeated cleaning cycles to be performed to extend the lifetime of an optics system. In this scenario, the frequency and duration of the cleaning procedure could be integrated into the operation of the tool in such a way that acceptable productivity and cost of ownership are maintained.⁷¹

The carbon-deposition process of EUV optics has been described to involve adsorption, diffusion, and dissociation of hydrocarbons at the surface of the

⁶⁷S. Bajt, "Optics contamination," in *EUV Lithography*, V. Bakshi, Ed., pp. 227–259, SPIE Press, Bellingham, WA (2009).

⁶⁸S. Bajt, H.N. Chapman, N. Nguyen, J. Alameda, J.C. Robinson, M. Malinowski, E. Gullikson, A. Aquila, C. Tarrío, and S. Grantham, "Design and performance of capping layers for extreme ultraviolet multilayer mirrors," *Appl. Opt.*, **42** (28), 5750–5758 (2003).

⁶⁹S. Bajt, "Optics contamination," in *EUV Lithography*, V. Bakshi, Ed., pp. 227–259, SPIE Press, Bellingham, WA (2009).

⁷⁰S.B. Hill, N.S. Faradzhev, C. Tarrío, T.B. Lucatorto, T.E. Madey, B.V. Yakshinskiy, E. Loginova, and S. Yulin, "Accelerated lifetime metrology of EUV multilayer mirrors in hydrocarbon environments," *Proc. SPIE* **6921**, 692117 (2008).

⁷¹B.J. Lin, "Sober view on extreme ultraviolet lithography," *J. Microlith., Microfab., Microsyst.* **5**, 033005 (2006).

optics, followed by the cross-linking of graphite-like molecules.⁷² In the absence of radiation, the adsorbed hydrocarbons have a fairly large desorption rate and do not tend to stick to the surface. However, in the presence of EUV photons, these adsorbed hydrocarbons are dissociated into smaller, more reactive species and fragments that readily interact with the surface and with each other, forming graphite-like films on the surface as a result. The dissociation of the adsorbed hydrocarbons is mediated via either direct absorption⁷³ or ionization by EUV photons or through the generation of secondary electrons.⁷⁴

Malinowski and co-workers at Sandia National Laboratories have established a correlation between the electric field at the surface of the multilayer film, the photoelectron yield, and the carbon growth rate, indicating that the photoelectrons play a critical role in cracking hydrocarbons.⁷⁵ Figure 14.13 is a plot of the electric

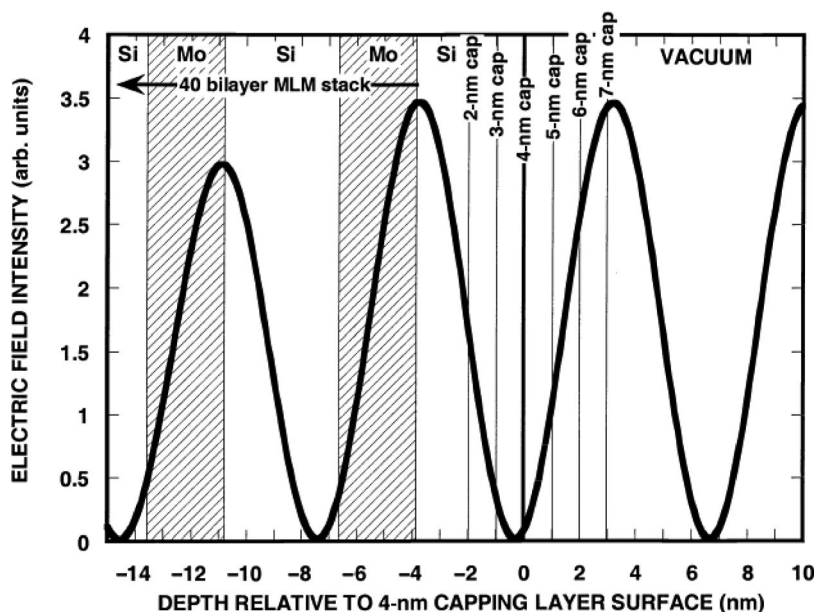


Figure 14.13 Electric field at the surface of a multilayer reflector resulting from the standing waves created by the incident and reflected beams.⁷⁶

⁷²J.T. Hollenshead and L. E. Klebanoff, "Modeling carbon contamination of extreme ultraviolet (EUV) optics," *Proc. SPIE* **5374**, 675 (2004).

⁷³J. Hollenshead and L. Klebanoff, "Modeling radiation induced carbon contamination of extreme ultraviolet optics," *J. Vac. Sci. Technol. B* **24**, 64–82 (2006).

⁷⁴K. Boller, R.P. Haelbich, H. Hogrefe, W. Jerk, and C. Kunz, "Investigation of carbon contamination of mirror surfaces exposed to synchrotron radiation," *Nucl. Instrum. Method.* **208**, 273–279 (1983).

⁷⁵M.E. Malinowski, C. Steinhaus, W.M. Clift, L.E. Klebanoff, S. Mrowka, and R. Soufli, "Controlling contamination in Mo/Si multilayer mirrors by Si surface capping modifications," *Proc. SPIE* **4688**, 442 (2002).

⁷⁶ibid.

field at the surface of a multilayer reflector due to the standing wave created by the incident and reflected beams.

Malinowski and co-workers⁷⁷ showed that, depending on the thickness of the capping layer, the electric field at the surface can be adjusted to minimize the photoelectron yield (see Fig. 14.13). They measured and correlated the reflectivity change of the mirror with photoelectron (PE) yield from a film of carbon grown at the surface of a multilayer mirror. The correlation between reflectivity loss and photoelectron current suggests that electrons play an important role in hydrocarbon cracking when a mirror is irradiated at the actinic wavelength. The results, shown in Fig. 14.14, indicate that a faster reflectivity decrease is associated with a high PE yield, while a slower reflectivity decrease is associated with a lower PE yield.⁷⁸

The carbon growth on optics has also been shown to be dependent on the mass of the hydrocarbon contaminant and the partial pressure of hydrocarbons, as well as on the EUV radiation dose and intensity.⁷⁹ Experimental results obtained with model hydrocarbon compounds and showing the trends of carbon growth as a function of these parameters are shown in Fig. 14.15. EUV radiation intensity has a pronounced effect on contamination, which appears to initially grow rapidly as the intensity is increased, eventually reaching a plateau. In a similar manner,

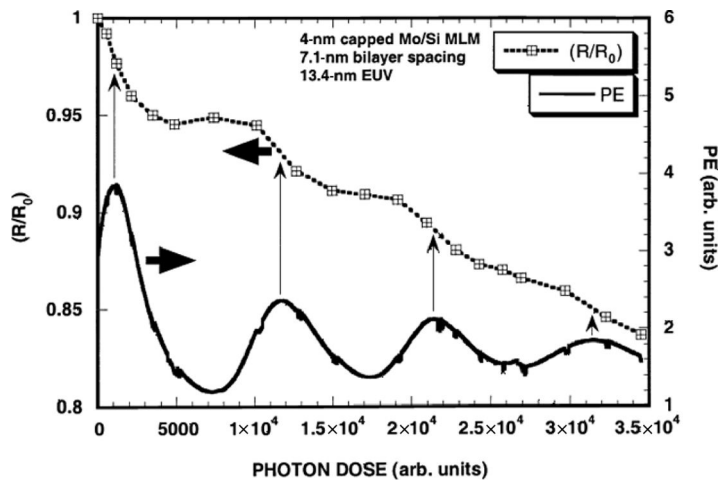


Figure 14.14 Reflectivity and photoelectron current as a function of the photon dose (which is proportional to the thickness of the carbon contamination on the surface of the multilayer mirror).⁸⁰

⁷⁷ibid.

⁷⁸ibid.

⁷⁹S. Matsunari, T. Aoki, K. Murakami, Y. Gomei, S. Terashima, H. Takase, M. Tanabe, Y. Watanabe, Y. Kakutani, M. Niibe, and Y. Fukuda, "Carbon deposition on multi layer mirrors by extreme ultra violet ray irradiation," *Proc. SPIE* **6517**, 65172X (2007).

⁸⁰ibid.

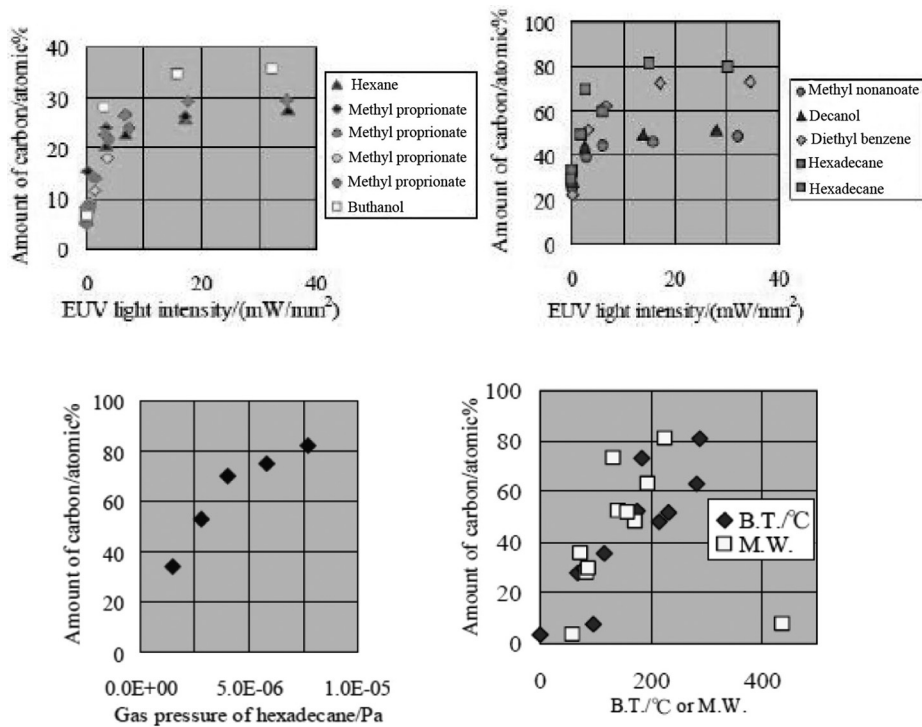


Figure 14.15 Contamination trends as a function of EUV intensity, hydrocarbon partial pressure, boiling temperature, and molecular weight.⁸¹

carbon contamination shows a marked increase with hydrocarbon partial pressure initially; it saturates at high gas pressure. And finally, the results show a dependence of carbon contamination on both the molecular weight and boiling temperature of the hydrocarbon, with higher contamination levels observed with larger molecular weight hydrocarbons, which also have higher boiling temperatures. This result is consistent with the fact that larger-molecular-weight hydrocarbons generally have longer residence times on the EUV optics surface, as well as higher adsorption enthalpy; they will more easily adhere to the surface than their lighter counterparts.

Taken together, these results support the hypothesis that EUV photoinduced hydrocarbon cracking, mediated by photoelectrons, is responsible for carbon contamination in EUV optics. This is referred to as the hydrocarbon cracking model. These results are supported by the model on a number of grounds. First, for a fixed amount of hydrocarbons in the vicinity of the mirror surface, the carbon growth increases with the number of photons and/or photoelectrons

⁸¹S. Matsunari, T. Aoki, K. Murakami, Y. Gomei, S. Terashima, H. Takase, M. Tanabe, Y. Watanabe, Y. Kakutani, M. Niibe, and Y. Fukuda, "Carbon deposition on multi layer mirrors by extreme ultra violet ray irradiation," *Proc. SPIE* **6517**, 65172X (2007).

available for cracking the hydrocarbons (as measured by EUV intensity) until these photoelectrons have all been used up. In like manner, for a fixed intensity or number of electrons, the fraction of hydrocarbons cracked increases with their probability of being near the surface (as measured by hydrocarbon gas pressure). The dependence on the molecular weight of the hydrocarbons is explained on the basis of the fact that a larger number of fragments can be cracked by the EUV radiation and photoelectrons when larger molecules are present in the environment.⁸²

14.5.2 Oxidation

Under EUV photon irradiation in the presence of oxygen or oxidizing agents, the surfaces of EUV optics and reticles are easily oxidized, leading to reflectivity loss of such surfaces. Oxides strongly absorb EUV radiation, and a small increase in oxide film thickness (~ 1.5 nm) can decrease EUV multilayer mirror reflectivity by up to 1.6% (absolute).⁸³ Because oxidation is difficult to remove, even small amounts of oxidation can negatively affect the EUV optics lifetime. The oxidation of silicon-capped EUV multilayer reflectors has been reported to show similar trends as those observed for carbon deposition. In particular, the rate of reflectivity loss due to oxidation of EUV mirrors has been observed to increase with the partial pressure of water in the optics environment, as well as with the EUV radiation intensity (see Fig. 14.16).⁸⁴

Given the high oxidation rates of silicon-terminated multilayer films, other capping layer materials have been studied extensively.⁸⁵ Oxidation can be appreciably reduced with protective capping layers. Extended lifetimes have been reported for ruthenium (Ru)-capped⁸⁶ and carbon-capped ML mirrors.⁸⁷ Ruthenium embodies many useful attributes of a good capping layer. Its optical constants

⁸²B. La Fontaine, "EUV optics," in *Extreme Ultraviolet Lithography*, B. Wu and A. Kumar, Eds., Chapter 4, McGraw Hill, New York (2009).

⁸³S. Bajt, H.N. Chapman, N. Nguyen, J. Alameda, J.C. Robinson, M. Malinowski, E. Gullikson, A. Aquila, C. Tarrío, and S. Grantham, "Design and performance of capping layers for extreme ultraviolet multilayer mirrors," *Appl. Opt.* **42**(28), 5750–5758 (2003).

⁸⁴M. Niibe, Y. Kakutani, S. Terashima, H. Takase, Y. Gomei, S. Matsunari, T. Aoki, K. Murakami, and Y. Fukuda, "New contamination experimental equipment in the new SUBARU and evaluation of Si capped multilayer mirrors using it," *Proc. SPIE* **6151**, 615134 (2006).

⁸⁵S. Bajt, Z. Dai, E.J. Nelson, M.A. Wall, J. Alameda, N. Nguyen, S.L. Baker, J.C. Robinson, J.S. Taylor, M. Clift, A. Aquila, E.M. Gullikson, and N.V. Edwards, "Oxidation resistance of Ru capped EUV multilayers," *Proc. SPIE* **5751**, 118–127 (2005).

⁸⁶S. Bajt, H.N. Chapman, N. Nguyen, J. Alameda, J.C. Robinson, M. Malinowski, E. Gullikson, A. Aquila, C. Tarrío, and S. Grantham, "Design and performance of capping layers for EUV multilayer mirrors," *Proc. SPIE* **5037**, 236–248 (2003); S. Bajt, H.N. Chapman, N. Nguyen, J. Alameda, J.C. Robinson, M. Malinowski, E. Gullikson, A. Aquila, C. Tarrío, S. Grantham, "Design and performance of capping layers for extreme ultraviolet multilayer mirrors," *Appl. Opt.* **42**, 5750–5758 (2003).

⁸⁷B.M. Mertens, B. Wolshrijn, R. Jansen, N. Koster, M. Weiss, M. Wedowski, R. Klein, T. Bock, R. Thornagel, "EUV time resolved studies on carbon growth and cleaning," *Proc. SPIE* **5037**, 95 (2003).

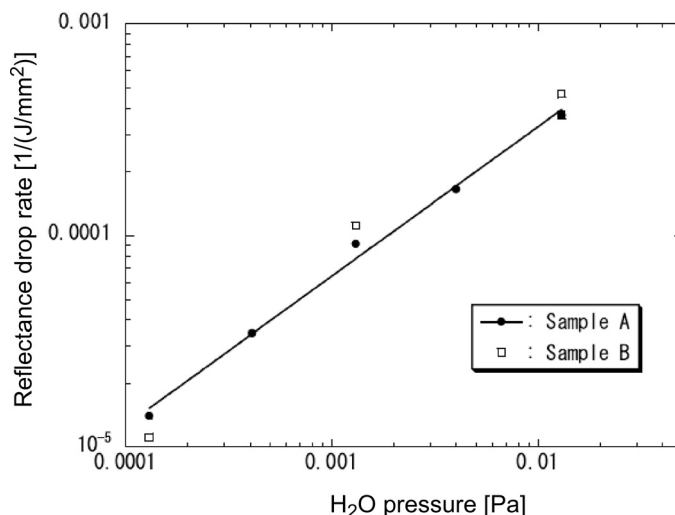


Figure 14.16 The rate of reflectivity degradation increases with water pressure inside the vacuum chamber.⁸⁸

make it a good reflective layer for EUV radiation. It has good stability in air and to EUV radiation. It can be deposited with the standard DC-magnetron sputtering technique and forms a continuous and relatively smooth layer at a thickness of only a few nanometers. Its oxidation processes are complex, but in general, forms RuO₂ only at high temperatures and high oxygen pressures.

It has also been established that Ru surfaces are very efficient heterogeneous catalysts.⁸⁹ In particular, numerous investigators have studied the surface chemistry of small molecules such as H₂O, O₂, CO₂, H₂, and N_xO_y on Ru surfaces.⁹⁰ The majority of the data they collected, however, were collected under ideal conditions, mostly with clean, single-crystal surfaces. Most of the investigations were performed on Ru(0001) surfaces, although limited data exist for a Ru(10 $\bar{1}$ 0) surface. A 2-nm-thick Ru capping layer has been shown through TEM studies

⁸⁸ibid.

⁸⁹S.E. Soiporin, R.J. David, W. Rarog Pilecka, D. Szmiegl, and Z. Kowalczyk, "Isotopic transient analysis of ammonia synthesis over Ba or Cs promoted Ru/carbon catalysts," *Catal. Lett.* **93**(1-2), 61-65 (2004); R.B. Anderson, *The Fischer-Tropsch Synthesis*, Academic Press, New York (1984).

⁹⁰D.L. Doering and T.E. Madey, "The adsorption of water on clean and oxygen dosed Ru(011)," *Surf. Sci. Rep.* **123**, 305-337 (1982); P.A. Thiel, and T.E. Madey, "The interaction of water with solid surfaces: fundamental aspects," *Surf. Sci. Rep.* **7**, 211-385 (1987); M. Henderson, "The interaction of water with solid surfaces: fundamental aspects revisited," *Surf. Sci. Rep.* **46**, 1-308 (2003); I.J. Malik and J. Hrbek, "Very high atomic oxygen coverages on Ru(001)," *J. Vac. Sci. Technol. A* **10**, 2565-2569 (1992); A. Bottcher, H. Conrad, and H. Niehus, "Characterization of oxygen phases created during oxidation of Ru(0001)," *J. Chem. Phys.* **112**(10), 4779-4787 (2000); H. Over, A. P. Seitsonen, "Oxidation of metal surfaces," *Science* **297**, 2003-2005 (2002); A. Baraldi, S. Lizzit, G. Comelli, and G. Paolucci, "Oxygen adsorption and ordering on Ru(10 $\bar{1}$ 0)," *Phys. Rev. B* **63**, 115-410 (2001).

to be polycrystalline with a variety of crystallographic orientations; the same study also established a correlation between these crystallographic orientations and lifetime performance.⁹¹ Ru capping layers with large grains and the close-packed plane (0001) orientation were shown to have the best lifetime performance, perhaps due to their lower reactivity with background gases than other planes, such as Ru(10 $\bar{1}$ 0) and Ru(10 $\bar{1}$ 1).⁹²

Ru capping layers are now accepted within the semiconductor industry as a benchmark for the development and performance of other capping layers.⁹³ They are by no means a perfect solution to the lifetime problem of EUV optics, since they also can be degraded through a combination of oxidation caused by the interaction of water vapor and EUV radiation, and carbon deposition associated with hydrocarbon dissociation.⁹⁴ Both of these processes can be caused by thermal⁹⁵ and nonthermal excitations.⁹⁶

Under nonthermal conditions, optics exposed to EUV radiation absorb photons, which cause valence and core photoexcitations of electrons in surface and subsurface atoms,⁹⁷ engendering both direct and indirect excitation processes. For most cases, indirect excitation processes involving secondary electrons dominate over direct photoexcitation processes.⁹⁸ The low-energy secondary electrons (<10 eV) have very high molecular dissociation cross section and therefore play a significant role in EUV radiation-induced processes at a surface. A significant fraction of these electrons reach the surface and escape as secondary electrons, which in turn induce electronic excitations in surface molecules (such as adsorbed molecules), which in turn cause their further dissociation and subsequent reaction.⁹⁹ Direct processes involving photoexcitation of substrate core electronic levels by EUV photons, on the other hand, can cause photon-stimulated desorption of oxygen from oxides, which can affect the stoichiometry, lifetime, and surface

⁹¹S. Bajt, Z.R. Dai, E.J. Nelson, M.A. Wall, J.B. Alameda, N.Q. Nguyen, S.L. Baker, J.C. Robinson, J.S. Taylor, A. Aquila, and N.V. Edwards, "Oxidation resistance and microstructure of ruthenium capped extreme ultraviolet lithography multilayers," *J. Microlithogr. Microfabri. Microsyst.* **5**, 023004 (2006).

⁹²ibid.

⁹³S. Bajt, "Optics contamination," in *EUV Lithography*, V. Bakshi, Ed., pp. 227–259, SPIE Press, Bellingham, WA (2009).

⁹⁴ibid.

⁹⁵There is little or no data on thermally induced oxidation of Ru surfaces in a water environment.

⁹⁶S. Bajt, "Optics contamination," in *EUV Lithography*, V. Bakshi, Ed., pp. 227–259, SPIE Press, Bellingham, WA (2009).

⁹⁷N. Itoh, A.M. Stoneham, *Materials Modification by Electronic Excitation*, Cambridge University Press, Cambridge (2001); L. Sanche, *Excess Electrons in Dielectric Media*, p. 1, CRC Press, Boca Raton (1991); A.D. Bass and L. Sanche, "Dissociative electron attachment and charge transfer in condensed matter," *Radiat. Phys. Chem.* **68**(1–2), 3–13 (2003).

⁹⁸X.L. Zhou, X.Y. Zhu, and J.J. White, "Photochemistry at adsorbate/metal interfaces," *Surf. Sci. Rep.* **13**(3–6), 73–220 (1991).

⁹⁹S. Bajt, "Optics contamination," in *EUV Lithography*, V. Bakshi, Ed., pp. 227–259, SPIE Press, Bellingham, WA (2009).

chemistry of such materials.¹⁰⁰ Thus, the EUV photons excite the adsorbed water by direct and indirect processes and cause dissociation, with the resulting atomic oxygen reacting with the mirror surfaces.¹⁰¹

In the final analysis, the main radiation damage mechanism for surface oxides occurs via the formation of oxygen vacancies (surface defects). Background gas molecules (such as water, hydrocarbons, etc.) are generally more reactive with defects than with stoichiometric surfaces, a situation that alters the surface chemistry of the capping layer.¹⁰² A number of kinetic models have been proposed for EUV mirror degradation; these models incorporate key processes contributing to oxide growth¹⁰³ and carbon growth.¹⁰⁴

14.5.3 Impact of contamination

There are quite a few consequences of EUV optics contamination. First, EUV optics and reticle molecular contamination can cause reflectivity loss, which in turn reduces the throughput (productivity) of the exposure tool. In other words, it takes longer to expose a wafer with contaminated optics and reticles. Figure 14.17 shows reflectivity loss data measured on Ru-capped ML mirrors in a standard EUV tool (ASML's EUV Alpha Demonstration Tool) under typical use conditions, showing that reflectivity loss is primarily from carbon and not on account of oxidation from water-EUV photon interaction. This result contradicts the results of Niibe et al.¹⁰⁵ obtained on Si-capped MLs (see Fig. 14.16), which showed that reflectivity loss was due to oxidation resulting from the interaction of water and EUV photons in their EUV exposure tool. Perhaps the differences in the results of the two experiments could be due to the differences in the surface chemistries of the capping layers used in the MLs. A Ru capping layer is known to be more stable and protective toward oxidation than a Si capping layer.

¹⁰⁰T.E. Madey, N.S. Faradzhev, B.Y. Yakshinsky, and N.V. Edwards, "Surface phenomena related to mirror degradation in extreme ultraviolet (EUV) lithography," *Appl. Surf. Sci.* **253**, 1691–1708 (2006).

¹⁰¹S. Bajt, "Optics contamination," in *EUV Lithography*, V. Bakshi, Ed., pp. 227–259, SPIE Press, Bellingham, WA (2009).

¹⁰²ibid.

¹⁰³J. Hollenshead and L. Klebanoff, "Modeling extreme ultraviolet/H₂O oxidation of ruthenium optic coatings," *J. Vac. Sci. Technol. B* **24**, 118–130 (2006); Y. Gomei, H. Takase, T. Aoki, Y. Kakutani, and M. Niibe, "Scaling law in acceleration test of extreme ultraviolet lithography projection optics mirror contamination," *J. Vac. Sci. Technol. B* **23**, 2848–2851 (2005); A.N. Broers, W.W. Molzen, J.J. Cuomo, N.D. Wittels, "Electron beam fabrication of 80Å metal structures," *Appl. Phys. Lett.* **29**, 596–598 (1976).

¹⁰⁴J. Hollenshead and L. Klebanoff, "Modeling radiation induced carbon contamination of extreme ultraviolet optics," *J. Vac. Sci. Technol. B* **24**, 64–82 (2006).

¹⁰⁵M. Niibe, Y. Kakutani, S. Terashima, H. Takase, Y. Gomei, S. Matsunari, T. Aoki, K. Murakami, and Y. Fukuda, "New contamination experimental equipment in the new SUBARU and evaluation of Si capped multilayer mirrors using it," *Proc. SPIE* **6151**, 615134 (2006).

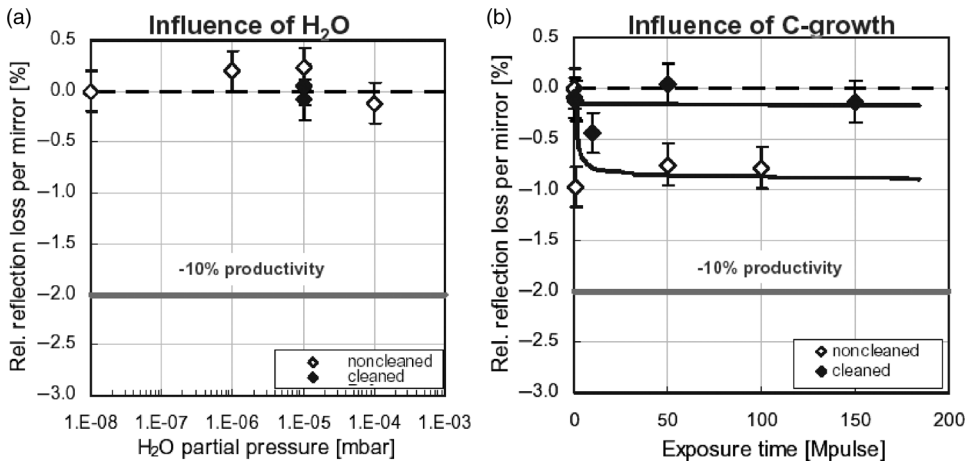


Figure 14.17 The influence of (a) oxidation from water and (b) carbon growth on the reflectivity loss of EUV ML in the ASML Alpha Demonstration Tool under pulsed EUV irradiation. Note the significant reflectivity loss due to carbon growth and the insensitivity of the ML reflectivity on the water concentration, an indicator for the extent of oxidation of the MLs. (Figure courtesy of K. Cummings.)

Figure 14.17 also shows that in situ cleaning with EUV radiation in the presence of a residual amount of molecular oxygen is effective in restoring lost reflectivity.

Second, because contamination resulting from carbon deposition depends on the local intensity of the EUV radiation at the surface of the mirror, it is possible that certain parts of the mirror surface in the projection optics may experience a local reduction in reflectivity that is larger than that occurring at other locations. The result is apodization of the projection optics, which can cause CD variation across the chip that is printed with EUV lithography.¹⁰⁶

Third, contamination resulting from EUV exposure can lead to roughening of the EUV multilayer surface (see Fig. 14.18). Surprisingly, the angle-resolved scattering measurements of the multilayer surface after irradiation reveal a lower scatter level than the as-deposited mirror (Fig. 14.19).¹⁰⁷ This suggests that morphological changes in the coatings are only confined to the uppermost interfaces, which contribute very little to the total scattering. In contrast, scattering from the buried interfaces is reduced as a result of enhanced absorbance in the uppermost layers. Consequently, the observed reduction in radiation scattering from the interfaces within the multilayer film in the contaminated sample is attributed to

¹⁰⁶B. La Fontaine, "EUV optics," in *Extreme Ultraviolet Lithography*, B. Wu and A. Kumar, Eds., Chapter 4, McGraw Hill, New York (2009).

¹⁰⁷S. Schroder, N. Benoit, T. Feigl, A. Duparre, and A. Tunnermann, "Scattering of EUV optics: substrate, coating, and degradation effects," *Proc. SPIE* **6921**, 69212Q (2008).

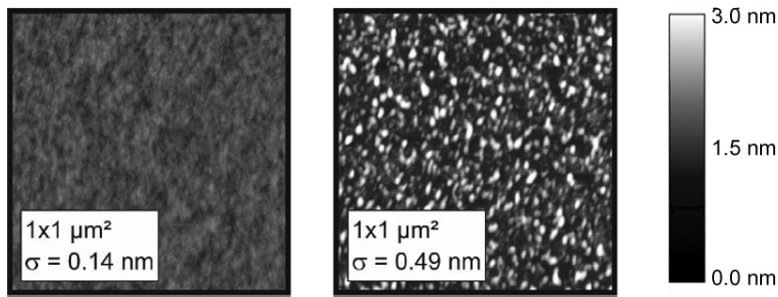


Figure 14.18 AFM images in $1 \times 1 \mu\text{m}^2$ scan areas of Mo-Si coatings before (left) and after (right) irradiation. The AFM scans of the two samples show that the contaminated or irradiated sample is rougher ($\sigma = 0.49 \text{ nm}$) than the pristine sample ($\sigma = 0.14 \text{ nm}$).¹⁰⁸

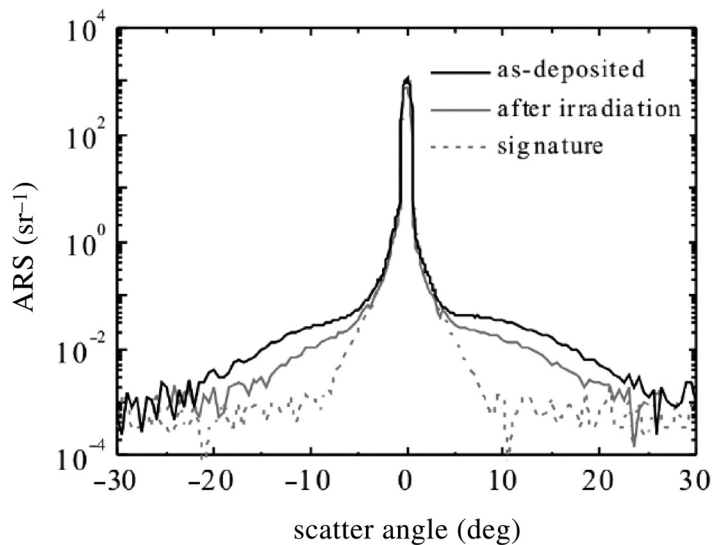


Figure 14.19 Angle-resolved scattering from an unirradiated (uncontaminated) and irradiated (contaminated) Mo-Si coating at 13.5 nm .¹⁰⁹

oxidation-induced absorption of the uncapped Mo-Si multilayer coating during irradiation.¹¹⁰

14.6 Contamination Mitigation Strategies

Contamination mitigation is required to maintain EUV exposure tool and mask productivity. A number of mitigation strategies have been reported for tackling

¹⁰⁸ibid.

¹⁰⁹ibid.

¹¹⁰ibid.

oxidation and carbon growth contamination of EUV optics and masks. These strategies can be broadly classified into five main approaches: exposure chamber environmental control methods, use of oxidation-resistant capping layers, thermal processes, nonthermal processes, and reactive-ion etching processes. In the following sections, we examine aspects of the chemistry underlying these processes that have been reported in the literature as reasonably effective EUV contamination mitigation strategies.

14.6.1 Exposure chamber environment control

The mitigation strategies involved in this method include controlling the vacuum chamber environment through the use of resist materials with low outgassing rates, and using background gases in the vicinity of the projection optics to competitively scavenge contaminants before they contaminate optics.

14.6.2 Use of oxidation-resistant capping layers

Oxidation-resistant capping layers (made of Ru, RuO₂, or TiO₂) that serve as a diffusion barrier to prevent the oxidation have been reported to be effective in mitigating oxidation of EUV multilayer coatings.¹¹¹ In particular, high reflectivity values have been reported to be achieved with good resistance to oxidation with TiO₂- and RuO₂-capped EUV multilayers.¹¹²

14.6.3 Thermal processes used in EUV optics contamination mitigation

Thermal processes used in EUV optics contamination mitigation are processes in which heat is used to either inhibit or clean off contaminants, without introducing a new set of problems. Taking a Ru-capped EUV multilayer reflector as our target surface, we examine here aspects of the surface reactions involved in removing carbon deposits and surface oxides from model Ru and RuO₂ surfaces.

¹¹¹L.E. Klebanoff, P.A. Grunow, S. Graham, Jr., W.M. Clift, A.H. Leung, and S.J. Haney, "Environmental data from the engineering test stand," *Proc. SPIE* **4688**, 310 (2002); K. Koida, M. Niibe, Y. Kakutani, S. Matsunari, T. Aoki, S. Terashima, T. Nakayama, H. Takase, and Y. Fukuda, "Protection from surface oxidation of Ru capping layers for EUVL projection optics mirrors by introducing hydrocarbon gas," *Proc. SPIE* **6921**, 69213C (2008); B.V. Yakshinskiy, I. Nishiyama, A. Wuest, and T.E. Madey, "Surface phenomena related to degradation of EUV mirrors: interaction of ethyl alcohol with ruthenium surfaces," *Proc. SPIE* **6921**, 69213E (2008).

¹¹²H. Takase, S. Terashima, Y. Gomei, M. Tanabe, Y. Watanabe, T. Aoki, K. Murakami, S. Matsunari, M. Niibe, and Y. Kakutani, "Study of ruthenium capped multilayer mirror for EUV irradiation durability," *Proc. SPIE* **6151**, 615135 (2006).

A good starting point is the investigation of Koch et al.¹¹³ involving the water-formation reaction between gas-phase molecular H₂ and adsorbed O on Ru(0001). They observed that molecular hydrogen dissociates on the Ru surface into atomic H, which then proceeds to react with adsorbed O in a reaction that proceeds as (2H + O → H₂O). The weakly bound H₂O desorbs readily at typical reaction temperatures (300–500 K). It must be stated that the reaction rate is low at 300 K, but optimal at ~ 450 K, and depends strongly on oxygen coverage. Also, the sticking probability of molecular hydrogen decreases as O coverage increases, so much so that an oxygen-saturated surface is not reactive with molecular hydrogen—an observation made by Hrbek.¹¹⁴

On the (110) surface of RuO₂, a hydrogen transfer reaction between adsorbed hydrogen and adsorbed oxygen appears to be involved in the formation of H₂O. At 300 K, adsorbed hydrogen on the RuO₂ surface has been reported not to be effective in reducing the oxide on heating in the absence of excess oxygen.¹¹⁵ However, a dilute amount of H₂ (~10⁻⁵ mbar) at elevated temperatures may be able to reduce thin films of RuO₂. Also, RuO₂ nanoparticles have also been reported to be completely reduced to Ru at temperatures in excess of 400 K, in the presence of H₂.¹¹⁶

Atomic hydrogen is effective at removing adsorbed O from a Ru(0001) surface at low temperatures. Weinberg and co-workers¹¹⁷ have demonstrated that as gas-phase H atoms (produced by dissociation of H₂ on a hot W wire) impinge on a 0.5 monolayer of oxygen at surface temperatures below 100 K, they react directly to form surface OH ions via the Eley-Rideal mechanism, in which the H atoms react with O before being accommodated on the surface. The OH ion eventually reacts with the H atom to form water, which readily desorbs from the surface as the latter warms up (at temperatures greater than 200 K).

An important reaction by which O is removed from many transition metal surfaces involves the oxidation of CO to CO₂ as in (CO + O → CO₂). Remarkably, Ru exhibits a somewhat anomalous behavior in this reaction. Under UHV conditions, the rate of CO₂ production on Ru(0001) has been reported to be very low, but at high CO gas pressures (10 torr), the catalytic formation of CO₂ is

¹¹³M.H. Koch, P. Jakob, and D. Menzel, "The influence of steps on the water formation reaction on Ru(001)," *Surf. Sci.* **367**, 293–306 (1996).

¹¹⁴J. Hrbek, "Weakly bound hydrogen on oxygen modified Ru(001) surface," *J. Catal.* **100**, 523 (1986).

¹¹⁵M. Knapp, D. Crihan, A.P. Seitsonen, and H. Over, "Hydrogen transfer reaction on the surface of an oxide catalyst," *J. Am. Chem. Soc.* **127**, 3236 (2005).

¹¹⁶J. Assmann, V. Narkhede, L. Khodeir, E. Löffler, O. Hinrichsen, A. Birkner, H. Over, and M. Muhler, "On the nature of the active state of supported ruthenium catalysts used for the oxidation of carbon monoxide: Steady state and transient kinetics combined with in situ infrared spectroscopy," *J. Phys. Chem. B* **108**, 14634 (2004).

¹¹⁷M. Schick, J. Xie, W.J. Mitchell, and W.H. Weinberg, "Interaction of gas phase atomic deuterium with the Ru(001) p(1 × 2) O surface: Kinetics of hydroxyl and water formation," *J. Chem. Phys.* **104**, 7713–7718 (1996); J. Xie, W.J. Mitchell, K.J. Lyons, Y. Wang, and W.H. Weinberg, "Observation of the reaction of gas phase atomic hydrogen with Ru(001) p(1 × 2) O at 100 K," *J. Vac. Sci. Technol. A* **12**, 2210–2214 (1994).

quite high.¹¹⁸ It was recently discovered that the “active catalytic” surface is not metallic Ru, but rather the ordered ruthenium oxide RuO₂.¹¹⁹ As an example, the RuO₂(110) surface grows on Ru(0001) and exposes bridging oxygen atoms as well as Ru atoms that are not capped by oxygen. It is these coordinatively unsaturated Ru (called *cus* Ru) sites that are responsible for the high reactivity observed on RuO₂ surfaces. CO adsorbs at *cus* Ru and reacts with neighboring lattice O to form CO₂.¹²⁰ A few key facts are, however, not clearly known with this CO oxidation reaction on Ru surfaces, i.e., at what point does it stop, how much oxygen can be removed from O-covered Ru by this mechanism, and how does the atomic structure of the exposed oxide surface affect the reflectivity.¹²¹

In a related reaction, a C deposit can be cleaned from many metals through combustion in oxygen to make CO. However, this reaction occurs most effectively on a heated surface, at temperatures in excess of 500–600 K, which may not be ideally suited for EUV multilayer mirrors. Reactions involving reactive oxygen species, generated from VUV lamps or plasma discharge sources involving molecular oxygen, ozone, etc., can also remove C from surfaces, but at the risk of accelerated oxidation of the substrate, which makes this option less attractive as a mitigation strategy.

14.6.4 Nonthermal processes used in EUV optics contamination mitigation

Contamination mitigation strategies based on radiation-induced or nonthermal processes involving electron- and photon-induced chemistry on surfaces have

¹¹⁸C. Stampfl and M. Scheffler, “Anomalous behavior of Ru for catalytic oxidation: A theoretical study of the catalytic reaction $\text{CO} + 1/2\text{O}_2 \rightarrow \text{CO}_2$,” *Phys. Rev. Lett.* **78**, 1500–1503 (1997); H. Over, Y.D. Kim, A.P. Seitsonen, S. Wendt, E. Lundgren, M. Schmid, P. Varga, A. Morgante, and G. Ertl, “Atomic scale structure and catalytic reactivity of the RuO₂(110) surface,” *Science* **287**, 1474–1476 (2000).

¹¹⁹H. Over, Y.D. Kim, A.P. Seitsonen, S. Wendt, E. Lundgren, M. Schmid, P. Varga, A. Morgante, and G. Ertl, “Atomic scale structure and catalytic reactivity of the RuO₂(110) surface,” *Science* **287**, 1474–1476 (2000); J. Wang, C.Y. Fan, K. Jacobi, and G. Ertl, “The kinetics of CO oxidation on RuO₂(110): Bridging the pressure gap,” *J. Phys. Chem. B* **106**, 3422–3427 (2002); J. Assmann, D. Crihan, M. Knapp, E. Lundgren, E. Löffler, M. Muhler, V. Narkhede, H. Over, M. Schmid, A.P. Seitsonen, and P. Varga, “Understanding the structural deactivation of ruthenium catalysts on an atomic scale under both oxidizing and reducing conditions,” *Angew. Chemie Int. Ed.* **44**, 917–920 (2005).

¹²⁰H. Over, Y.D. Kim, A.P. Seitsonen, S. Wendt, E. Lundgren, M. Schmid, P. Varga, A. Morgante, and G. Ertl, “Atomic scale structure and catalytic reactivity of the RuO₂(110) surface,” *Science* **287**, 1474–1476 (2000); J. Wang, C.Y. Fan, K. Jacobi, and G. Ertl, “The kinetics of CO oxidation on RuO₂(110): Bridging the pressure gap,” *J. Phys. Chem. B* **106**, 3422–3427 (2002).

¹²¹J. Assmann, D. Crihan, M. Knapp, E. Lundgren, E. Löffler, M. Muhler, V. Narkhede, H. Over, M. Schmid, A.P. Seitsonen, and P. Varga, “Understanding the structural deactivation of ruthenium catalysts on an atomic scale under both oxidizing and reducing conditions,” *Angew. Chemie Int. Ed.* **44**, 917–920 (2005).

been demonstrated to be reasonably effective in cleaning contaminated EUV optics and extending their lifetime. As a strategy, the radiation-induced mitigation involves a competition between adsorption, decomposition, reaction (e.g., oxidation of the substrate, or of surface C), and desorption. These are complex processes whose rates depend sensitively on the surface composition (e.g., extent of oxidation, or of C coverage), surface temperature, composition and relative pressures of background gases, and radiation flux. As is typical of surface reactions, the reaction rates of the species often do not scale linearly with the partial pressure of a component gas (as observed recently and demonstrated for Ru-capped mirrors¹²²); rates of processes involving two or more reactants (e.g., a Langmuir-Hinshelwood reaction) can have an unusual reaction profile, with a maximum at an intermediate pressure.¹²³

It has been reported that carbon deposits on EUV optics can be removed with molecular oxygen,¹²⁴ RF-O₂, RF-H₂,¹²⁵ ozone, and atomic hydrogen.¹²⁶ Other methods that have been reported for removing carbon deposits include in situ cleaning using EUV radiation and high oxygen pressure (5×10^{-2} Pa).¹²⁷

Although there is much empirical evidence that a judicious choice of gas mixtures can have a positive effect on mitigation, overall, very little is known about the detailed mechanism of mitigation via radiation-induced surface chemistry. Other examples of empirical evidence on radiation-induced cleaning or mitigation of EUV contamination are outlined below. In particular, the use of oxygen in combination with irradiation has been reported to be effective in removing carbon contamination, both for Ru- and TiO₂-capped multilayer films.¹²⁸ The repeated use

¹²²S. Hill, C. Tarrío, S.E. Grantham, T.B. Lucatorto, T. Madey, I. Ermanoski, S. Bajt, M. Chandhok, P. Yan, O.R. Wood II, S. Wurm, and N.V. Edwards, "EUV testing of multilayer mirrors: critical issues," *Proc. SPIE* **6151**, 61510F (2006).

¹²³R.P.H. Gasser, *An Introduction to Chemisorption and Catalysis by Metals*, Clarendon Press, Oxford (1985).

¹²⁴M. Malinowski, P. Grunow, C. Steinhaus, M. Clift, and L. Klebanoff, "Use of molecular oxygen to reduce EUV induced carbon contamination of optics," *Proc. SPIE* **4343**, 347–356 (2001).

¹²⁵S. Graham, C. Steinhaus, M. Clift, and L. Klebanoff, "Radio frequency discharge cleaning of silicon capped Mo/Si multilayer extreme ultraviolet optics," *J. Vac. Sci. Technol. B* **20**(6), 2393–2401 (2002).

¹²⁶S. Graham, C. Steinhaus, M. Clift, and L. Klebanoff, "Radio frequency discharge cleaning of silicon capped Mo/Si multilayer extreme ultraviolet optics," *J. Vac. Sci. Technol. B* **20**, 2393–2400 (2002); S. Graham, C. Steinhaus, M. Clift, L. Klebanoff and S. Bajt, "Atomic hydrogen cleaning of EUV multilayer optics," *Proc. SPIE* **5037**, 460–468 (2003); S. Oestreich, R. Llein, F. Scholze, J. Jonkers, E. Louis, A. Yakshin, P. Gorts, G. Ulm, M. Haidl, and F. Bijkerk, "Multilayer reflectance during exposure to EUV radiation," *Proc. SPIE* **4146**, 64–71 (2000); H. Oizumi, H. Yamanashi, I. Nishiyama, K. Hashimoto, S. Ohsono, A. Masuda, A. Izumi and H. Matsumura, "Contamination removal from EUV multilayer using atomic hydrogen generated by heated catalyzer," *Proc. SPIE* **5751**, 1147–1154 (2005).

¹²⁷K. Hammamoto, T. Tanaka, T. Watanabe, N. Sakaya, M. Hosoya, T. Shoki, H. Hada, N. Hishinuma, H. Sugihara, and H. Kinoshita, "Cleaning of extreme ultraviolet lithographic optics and masks using 13.5 nm and 172 nm radiation," *J. Vac. Sci. Technol. B* **23**, 247–252 (2005).

¹²⁸B.V. Yakshinskiy, M.N. Hedhili, S. Zalkind, M. Chandhok, and Theodore E. Madey, "Radiation induced defect formation and reactivity of model TiO₂ capping layers with MMA: A comparison with Ru," *Proc. SPIE* **6921**, 692114 (2008).

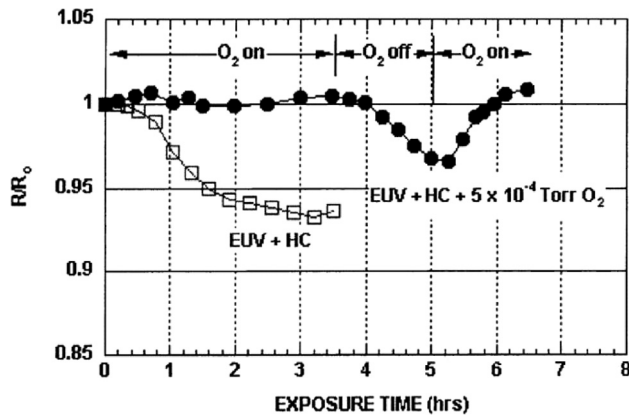


Figure 14.20 Cleaning of hydrocarbon-contaminated EUV mirrors with oxygen and EUV radiation.¹²⁹

of in-situ O₂ and/or EUV radiation cleaning of a carbon-contaminated EUV mirror without mirror degradation has been demonstrated (see Fig. 14.20).¹³⁰ In addition, the repeated use of cleaning on carbon-contaminated EUV mirrors has been demonstrated to extend optics lifetime.¹³¹

With respect to mitigating oxidation, Bajt et al.¹³² have reported that oxides, once formed, are difficult to remove, while Nishiyama et al.¹³³ reported that Ru oxidized by electron cyclotron resonance (ECR) O₂ plasma can be successfully reduced by exposure to atomic H, raising the hopes for a practical mitigation method. Mertens et al.¹³⁴ have reported that under identical gas exposure and radiation conditions, a Si-terminated mirror shows oxidation, whereas a (unspecified) capped mirror shows carbon growth, implying that the surface chemistry plays a critical role in determining the nature of the contamination process a particular surface will undergo under EUV exposure conditions.

¹²⁹M.E. Malinowski, P. Grunow, C. Steinhaus, M. Clift, and L. Klebannoff, "Use of molecular oxygen to reduce EUV induced carbon contamination of optics," *Proc. SPIE* **4343**, 347 (2001).

¹³⁰ibid.

¹³¹H. Meiling, H. Meijer, V. Banine, R. Moors, R. Groeneveld, H. J. Voorma, U. Mickan, B. Wolschrijn, B. Mertens, G. van Baars, P. Kurz, and N. Harned, "First performance results of the ASML alpha demo tool," *Proc. SPIE* **6151**, 615108 (2006).

¹³²S. Bajt, H.N. Chapman, N. Nguyen, J. Alameda, J.C. Robinson, M. Malinowski, E. Gullikson, A. Aquila, C. Tarrío, and S. Grantham, "Increasing the range of unambiguity in step height measurement with multiple wavelength interferometry application to absolute long gauge block measurement," *Appl. Opt.* **42** (28), 5750–5758 (2003).

¹³³I. Nishiyama, H. Oizumi, K. Motai, A. Izumi, T. Ueno, H. Akiyama, and A. Namiki, "Reduction of oxide layer on Ru surface by atomic hydrogen treatment," *J. Vac. Sci. Technol. B* **23** (2005).

¹³⁴B. Mertens, M. Weiss, H. Meiling, R. Klein, E. Louis, et al., "Progress in EUV optics lifetime expectations," *Microelectron. Eng.* **73-74**, 16–22 (2004).

It has also been reported that EUV optics oxidation during exposure can be suppressed by means of gas mixtures of H₂O vapor¹³⁵ and carbon-containing gases such as methanol¹³⁶ and ethanol.¹³⁷ Figure 14.21 shows the effect of using ethanol in combination with Ru-capped multilayers in mitigating the oxidation problem.

Furthermore, Hill et al.¹³⁸ reported that mitigation of Ru-capped multilayers by carbon-containing species may result from water-induced desorption and/or displacement of carbon compounds from the exposure chamber and other surfaces therein. Atomic hydrogen has been reported to be effective in cleaning Sn as well as carbon contaminants from EUV mirrors.¹³⁹

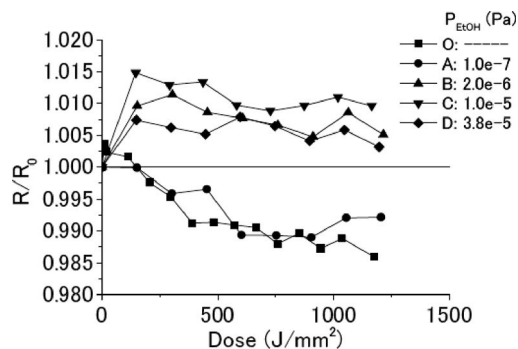


Figure 14.21 Mitigation of oxidation on ruthenium-capped EUV multilayer reflectors. The decrease in reflectivity of a Ru-capped multilayer as a function of EUV dose is shown for different ethanol pressure values. A partial pressure of 2×10^{-6} Pa of ethanol was found to be optimal for simultaneously minimizing oxidation and carbon deposition on the mirror.¹⁴⁰

¹³⁵M. Malinowski, P. Grunow, C. Steinhaus, M. Clift, and L. Klebanoff, "Use of molecular oxygen to reduce EUV induced carbon contamination of optics," *Proc. SPIE* **4343**, 347–356 (2001).

¹³⁶L.E. Klebanoff, W.M. Clift, M.E. Malinowski, C. Steinhaus, P. Grunow, and S. Bajt, "Radiation induced protective carbon coating for extreme ultraviolet optics," *J. Vac. Sci. Technol. B* **20**, 696–703 (2002).

¹³⁷S. Hill, C. Tarrío, S.E. Grantham, T.B. Lucatoro, T. Madey, I. Ermanoski, S. Bajt, M. Chandhok, P. Yan, O.R. Wood II, S. Wurm, and N.V. Edwards, "EUV testing of multilayer mirrors: critical issues," *Proc. SPIE* **6151**, 61510F (2006).

¹³⁸ibid.

¹³⁹D.J.W. Klunder, M.M.J.W. van Herpen, V.Y. Banine, K. Gielissen, "Debris mitigation and cleaning strategies for Sn based sources for EUV lithography," *Proc. SPIE* **5751**, 943–951 (2005); S. Graham, C. Steinhaus, M. Clift, L. Klebanoff, and S. Bajt, "Atomic hydrogen cleaning of EUV multilayer optics," *Proc. SPIE* **5037**, 460–469 (2003).

¹⁴⁰H. Takase, S. Terashima, Y. Gomei, M. Tanabe, Y. Watanabe, T. Aoki, K. Murakami, S. Matsunari, M. Niibe, and Y. Kakutani, "Study of ruthenium capped multilayer mirror for EUV irradiation durability," *Proc. SPIE* **6151**, 615135 (2006).

14.6.5 Reactive-ion etching processes for cleaning contaminated optics

Reactive-ion etching (RIE) of debris is a potential method for cleaning contaminated mirror surfaces. In particular, RIE with Ar/Cl₂ can selectively etch Sn, offering the potential for using this approach to clean contaminated mirrors.¹⁴¹

14.6.6 Debris-mitigation schemes

A number of concepts for debris mitigation in EUV exposure systems have been proposed. These include the use of tape targets, ambient gas for moderating the species, foil traps, cavity confinement, electrostatic repeller fields, magnetic field, and mass-limited targets.¹⁴²

14.7 EUV Resists and Imaging Performance

Given that the absorption phenomenon at EUV is atomic, almost every element is opaque at EUV (see Fig. 14.22) except thin films of polymers with high carbon content (as in aromatic polymers based on PHOST) and silicon (see Fig. 14.23). Polymers containing high amounts of oxygen and fluorine have very high absorptivity at EUV (see Fig. 14.23).

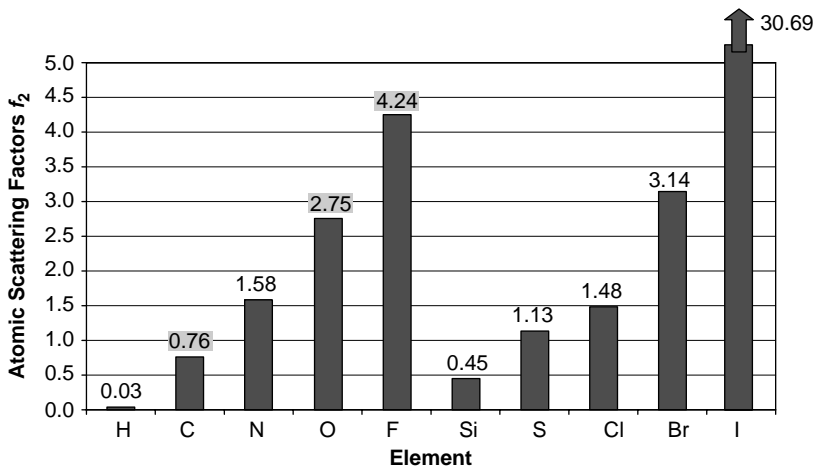


Figure 14.22 Atomic scattering factors, f_2 , of elements at EUV (13.5 nm).

¹⁴¹D.N. Ruzic and S.N. Srivastava, "Normal incidence (multilayer) collector contamination," in *EUV Lithography*, V. Bakshi, Ed., pp. 285–323, SPIE Press, Bellingham, WA (2009).

¹⁴²S.S. Harilal, M.S. Tillack, Y. Tao, et al., "Extreme ultraviolet spectral purity and magnetic ion debris mitigation with low density tin targets," *Opt. Lett.* **31**, 1549 (2006).

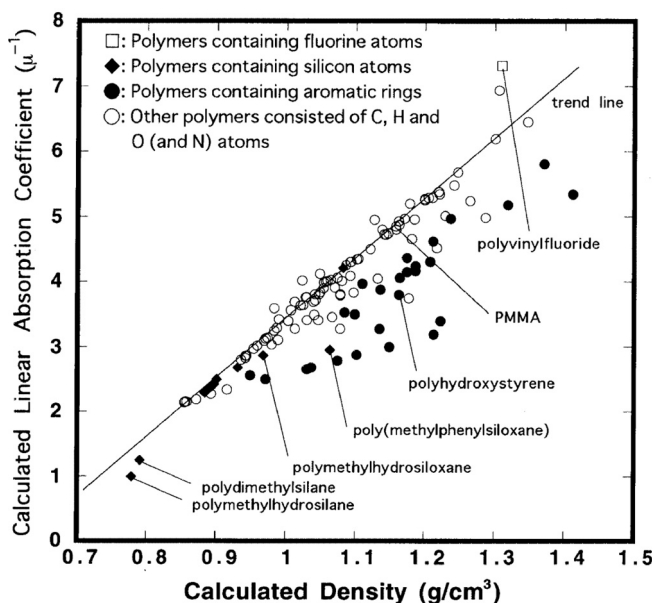


Figure 14.23 Absorbance of different polymers at EUV. (Reprinted with permission from Japan Science and Technology Agency.¹⁴³)

Resins for EUV resists are mostly hydroxystyrene,¹⁴⁴ acrylate,¹⁴⁵ and alicyclic¹⁴⁶ polymers of the kinds in use in KrF and ArF lithographic resists. The photoacid generators are also based on similar chemistries as those used in KrF and ArF lithographies, although they are optimized to tune their sensitivity to EUV radiation. Their imaging mechanism is also based on chemical amplification. While maximizing the sensitivity of these resists, attempts are made to control their photoacid diffusion in order to mitigate the resolution-loss issue of chemical amplification resists, particularly as the feature geometries approach a few multiples of the radius of gyration of the resist polymer. Common approaches employed toward this end include the use of polymer-tethered photoacid generators (which limits the diffusion range of the photoacid), hybrid resists composed of polymers with high and low activation energy deprotection groups, low activation energy resists based on acetals, and acid-catalyzed polymer-breakable groups.

Figures 14.24–14.26 show the performance of representative EUV resists on different EUV exposure tools, ranging from an interferometric exposure tool with microexposure field (Fig. 14.24) to full-field EUV exposure scanners

¹⁴³N.N. Matsuzawa, H. Oizumi, S. Mori, S. Irie, E. Yano, S. Okazaki, and A. Ishitani, "Theoretical estimation of absorption coefficients of various polymers at 13 nm," *J. Photopol. Sci. Technol.* **12**(4), 571–576 (1999).

¹⁴⁴For the chemistry of these resist polymers, see Chapter 7.

¹⁴⁵ibid.

¹⁴⁶ibid.

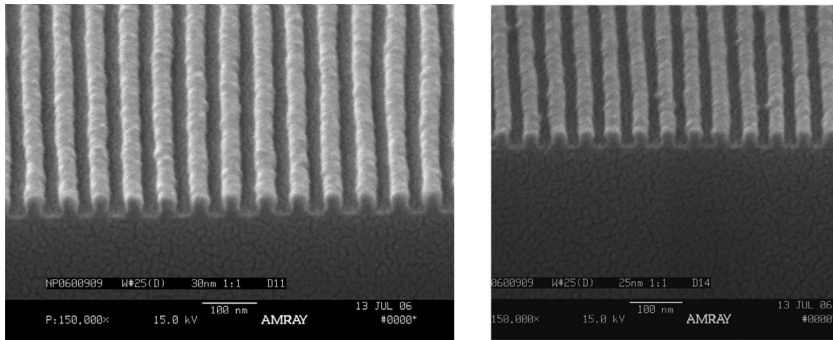


Figure 14.24 Resolution capability of XP6627 EUV resist from Rohm and Haas, showing 25-nm and 30-nm dense (1:1) line/space features, with less than 2.5-nm line edge roughness and 3.5-nm line width roughness. Imaging was done on an EUV interferometric tool at Paul Scherrer Institute in Switzerland. (Courtesy of J. Thackeray.)

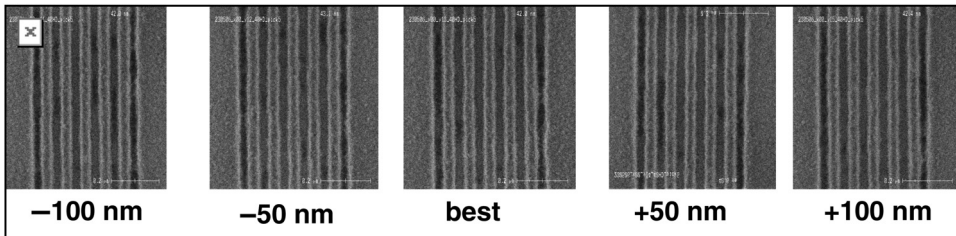


Figure 14.25 SEM images of 40-nm 1:1 lines and spaces through focus printed on the first full-field EUV exposure tool from ASML. Exposure conditions: 18 mJ/cm², NA 0.25, partial coherence 0.5, conventional illumination. Resist: MET-2D. (Courtesy of Rohm and Haas.)

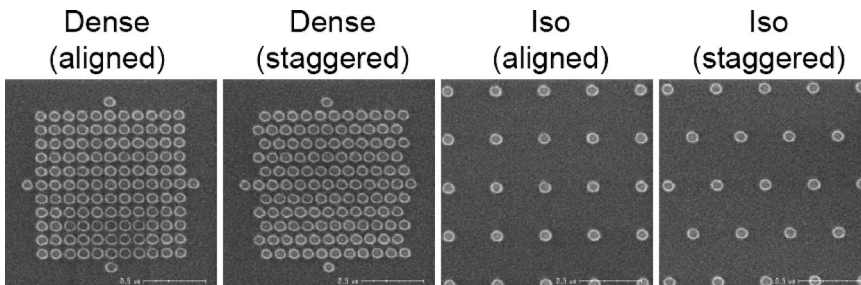


Figure 14.26 SEM images of 55-nm contacts in dense and sparse arrays printed on the first full-field EUV exposure tool with 0.25 NA from ASML. (Courtesy of ASML.)

(Figs. 14.25 and 14.26). Dense line/space resolution down to 25-nm (Fig. 14.24), greater than 200-nm depth of focus for 40-nm line/space features (Fig. 14.25), and contact hole resolution down to 55 nm (Fig. 14.26) have been demonstrated with this technology.

Chapter 15

Charged Particle Lithography

So free we seem, so fettered fast we are

Robert Browning

15.1 Introduction

Charged particle lithography comprises lithographic patterning techniques in which the imaging action is mediated by charged particles such as electrons (as in electron-beam lithography) and ions (as in ion-beam lithography). Some of the key concepts and methods employed in these lithographies are similar to those of optical lithography. However, there are some distinct differences between each of the lithographies that make up charged particle lithography, as well as between them and those that make up optical lithography. In the following sections, we explore these differences in more detail, from the point of view of how they are implemented as a lithographic strategy. We start with electron-beam lithography and end with ion-beam lithography.

15.2 Electron-Beam Lithography

Electron-beam lithography (EBL) refers to a lithographic patterning technique in which a focused beam of electrons is used to expose and pattern resist-coated semiconductor substrates as part of a number of steps used in the fabrication of IC devices. Its introduction into IC fabrication dates back to 1957.¹ Today, electron-beam lithography is used primarily in fabrication of masks used in optical lithography and x-ray lithography. It is also used in low-volume fabrication of exploratory IC device layers with extremely small features; it has also found application in nanotechnology research.

Like photons, electrons exhibit particle and wavelike properties, but their wavelength (0.012–0.024 nm, corresponding to 50–100-keV of energy for

¹D.A. Buck and K. Shoulders, “An approach to microminiature systems,” in *Proc. of Eastern Joint Computer Conf.*, ATEE, p. 55 (1957).

electrons used in EBL) is three orders of magnitude shorter than the wavelength of UV radiation used in optical lithographic exposure tools, and hence their resolution is not limited by diffraction.² Only features with atomic-scale dimensions are able to diffract electron beams.³ Electron-beam lithography therefore has the potential for extremely high resolution. In fact, features as small as 10 nm have been successfully fabricated with electron-beam lithography.⁴ In addition, electron beams image with extremely large depth of focus, providing relief from one of the most challenging problems of optical lithography.⁵

Irradiation of resist coatings with electron beams produces in the polymeric resin microstructural changes such as chain scissioning, cross-linking, or selective bond breaking. With the aid of PEB (where necessary) these microstructural changes result in some sort of polarity change in the exposed region of the resist during development. The final resist patterns on the wafer represent either a positive tone (same as the image of the electron-beam pattern from the electron-beam writer) or a negative tone (reverse of the image of the electron-beam pattern from the electron-beam writer), depending on the chemistry of the resist.⁶

Given that electrons can be focused to a few nanometers in diameter, resolution approaching the diameter of the electron beam might in principle be expected to be possible. Unfortunately, many factors other than the size of the electron beam determine the extent of the exposed volume in the resist, and consequently, the developed profile of the resist. The conventional technique for fabricating IC circuits with electron-beam lithography uses an electron beam with relatively low acceleration voltages in the range of 50–100 keV, as well as thick resists; these are conditions that favor electron scattering and make it the dominant factor in limiting resolution in this lithographic technique.⁷ A technique called low-energy electron projection lithography (LEEPL) uses low electron-beam acceleration voltages (~ 100 eV) to fabricate IC devices.

15.2.1 Electron scattering

When an electron beam is irradiated on a resist polymer film (or any solid material for that matter), it loses energy via elastic and inelastic collisions collectively called electron scattering. Elastic collisions lead only to a change of direction of the electrons, whereas inelastic collisions result in energy loss. These scattering

²M.J. Bowden, "The lithographic process: the physics," in *Introduction to Microlithography*, L.F. Thompson, C.G. Willson, and M.J. Bowden, Eds., p. 85, American Chemical Society, Washington, DC (1994).

³E.E. Anderson, *Modern Physics and Quantum Mechanics*, W.B. Saunders, Philadelphia (1971).

⁴H.G. Craighead, "10 nm resolution electron beam lithography," *J. Appl. Phys.* **55**(2), 4430–4435 (1984).

⁵H.J. Levinson, *Principles of Lithography*, 2nd ed., p. 393, SPIE Press, Bellingham, WA (2005).

⁶M.J. Bowden, "The lithographic process: the physics," in *Introduction to Microlithography*, L.F. Thompson, C.G. Willson, and M.J. Bowden, Eds., pp. 85–86, American Chemical Society, Washington, DC (1994).

⁷*ibid.*, p. 86.

processes cause broadening or spreading of the beam in the transverse or lateral direction to the original beam direction, which leads to exposure of the resist at points significantly distant from the point of initial electron entry.⁸ As a result, the developed positive resist image is wider than expected⁹ if it is a trench or a contact hole feature, or smaller if it is a line feature. The converse is true for negative resists.

There are three main types of scattering processes in electron-beam lithography, i.e., forward scattering in the resist, backscattering usually from the substrate but also from the resist, and stochastic scattering. Given that most of the electrons are scattered in the forward direction through small angles (less than 90 deg) relative to their original direction, this type of scattering increases the effective beam width at the bottom of the resist layer.¹⁰ In backscattering, some electrons experience large-angle scattering (approaching 180 deg), often within the underlying substrate; this causes them to return to the resist.¹¹

Stochastic scattering refers to the random electron-electron interactions that result from when an electron beam is focused into a small volume, where the individual electrons experience the electric fields of the other electrons. For electrons traveling with a velocity v , given by

$$v = \left(\frac{2qV}{m} \right)^{1/2}, \quad (15.1)$$

and constituting a beam current i , the mean axial separation Δ between electrons is expressed as

$$\Delta = \frac{qv}{i} = \frac{1}{i} \left(\frac{2q^3V}{m} \right)^{1/2}, \quad (15.2)$$

where V is the kinetic energy of the electrons in volts, q is the magnitude of the electronic charge, and m is the electronic mass. At high current levels, the electron-electron interactions are quite significant, with the major effect of the forces between the electrons being to push them out radially, and leading to the broadening of the diameter of the beam.¹² Crewe has reported an analytical expression for estimating beam broadening resulting from the electron-electron interaction as¹³

$$\Delta r = \frac{1}{8\pi\epsilon_0} \left(\frac{m}{q} \right)^{1/2} \frac{Li}{\alpha V^{3/2}}, \quad (15.3)$$

⁸ibid.

⁹ibid.

¹⁰ibid.

¹¹ibid.

¹²L.R. Harriot, S.D. Berger, J.A. Liddle, G.P. Watson, and M.M. Mkrtychyan, "Space charge effects in projection charged particle lithography systems," *J. Vac. Sci. Technol. B* **13**(6), 2404–2408 (1995).

¹³A.V. Crewe, "Some space charge effects in electron probe devices," *Optik* **52**, 337 (1978).

where α represents the numerical aperture of the electron optics, L represents the total length of the column, and ϵ_0 is the permittivity of free space. It must be mentioned that neither the positions of the lenses nor their optical properties appear in Eq. (15.3). It is only the total distance from source to workpiece that is important.¹⁴

The magnitude of the electron scattering at any spatial position within the resist-substrate stack depends on parameters such as the atomic number and density of the resist and substrate, as well as the velocity (accelerating voltage) of the electron. A partially processed wafer containing several materials (for example, polysilicon, silicon dioxide, tungsten, resist polymer made of mostly carbon, etc.) will possess different scattering properties from one area to another, dictated by the location of these materials in the resist-wafer substrate stack.¹⁵ Planarization with a thick organic film does not in the main eliminate scattering effects; however, because organic resist polymers are relatively low-density films (density $<1.5 \text{ g/cm}^3$), scattering effects are reduced and made uniform across a partially processed wafer.¹⁶

The greater the incident electron-beam energy, the narrower is the width of the forward-scattered electron distribution and the broader is the backscattered electron distribution. The broadening of the backscattered electron distribution with increasing incident electron energy is related to the fact that high-incident-energy electron beams pass through the resist and deposit their energy in the underlying substrate, from which electrons can be backscattered. In contrast, low-incident-energy electrons may not even reach the underlying substrate; as a result, these low-incident energy electrons will generate little or no backscattered electrons from the underlying substrate.¹⁷ Also, the extent of forward scattering is reduced for thinner resists relative to thicker ones.¹⁸

These scattering processes lead to practical problems, particularly for adjacent patterns where the exposure of one pattern contributes to the exposure of another nearby pattern located within the scattering range of the electrons. Termed proximity effects, such scattering processes impose certain restrictions on the size and shape of relief structures that can be successfully patterned in electron-beam resists, particularly for complex patterns with high packing densities and sub-micrometer dimensions.¹⁹ Electron scattering that originates within a pattern feature gives rise to intraproximity effects, while those that originate from adjacent features give rise to interproximity effects.²⁰ As a result, the total amount of energy deposited within a feature pattern depends on both the size of the feature

¹⁴G. Owen and J.R. Sheats, "Electron beam lithography systems," in *Microlithography: Science and Technology*, J.R. Sheats and B.W. Smith, Eds., p. 379, Marcel Dekker, New York (1998).

¹⁵L.F. Thompson, "Resist processing," in *Introduction to Microlithography*, L.F. Thompson, C.G. Willson, and M.J. Bowden, Eds., p. 354, American Chemical Society, Washington, DC (1994).

¹⁶ibid.

¹⁷ibid., p. 88.

¹⁸ibid.

¹⁹ibid.

²⁰ibid.

(intraproximity) and the magnitude of the distance of the neighboring features (interproximity).²¹ The influence of proximity effects is thus dependent on the size and spacing of the feature patterns in question.²²

Furthermore, although the high-energy electrons that pass through the resist film (with minimal interaction) and deposit their energy in the underlying substrate may be problematic when used to pattern wafers, they may not be problematic for mask making for a number of reasons.²³ First, electrons with energies greater than 50 keV are typically not used in mask fabrication because the resolution requirements for mask making are less stringent than those for writing on wafers, due to reduction lithography. In contrast, higher-energy electrons may be required for direct electron-beam writing of wafers, and more energy is thus deposited into wafer substrates than is typically deposited in mask making. Second, being typically made of fused silica, which has a low coefficient of thermal expansion (~ 0.5 ppm/ $^{\circ}\text{C}$), photomasks have nearly an order of magnitude lower thermal expansion coefficient than silicon. Also, photomasks in general have much greater thermal capacity than wafers. The combination of lower thermal expansion coefficient and greater thermal capacity offsets fused silica's lower thermal conductivity, relative to silicon. As a result, photomasks mechanically distort less than silicon wafers on account of energy deposition; they will also have lower magnitude of registration errors than silicon wafers.²⁴

Another problem related to the effects of energy deposition on the resist, dielectric films, and underlying substrate by highly energetic electrons is charging. These highly energetic electrons deposit a net negative charge to the substrate and the intervening resist and dielectric films, resulting in the buildup of a potential gradient that can approach the beam voltage. Ultimately, these negative charges on the substrate and the dielectric and resist films will electrostatically deflect the incident electron beam, causing inaccurate image placement and distortion of the edge.²⁵ In addition, the deflection of the beam causes defocus errors, which result in a change in feature size.²⁶

Fortuitously, the good electrical conductivity of silicon prevents these charges from building up to dangerous levels, which explains why the reported pattern placement errors due to such hypothesized deflections have been smaller than measurement capability (20 nm).²⁷ Another method for minimizing charging

²¹ *ibid.*

²² *ibid.*

²³ B. Shamoun, R. Engelstadt, and D. Trost, "Assessment of thermal loading induced distortions in optical photomasks due to e beam multi pass patterning," *J. Vac. Sci. Technol. B* **16**(6), 3558-3562 (1998).

²⁴ H.J. Levinson, *Principles of Lithography*, 2nd ed., p. 393, SPIE Press, Bellingham, Washington (2005).

²⁵ L.F. Thompson, "Resist processing," in *Introduction to Microlithography*, L.F. Thompson, C.G. Willson, and M.J. Bowden, Eds., American Chemical Society, Washington, DC, p. 354 (1994).

²⁶ *ibid.*

²⁷ M. Bai and R.F. Pease, "Resist charging in electron beam lithography," *SRC Technon* (Sept. 2000).

effects in trilevel resist systems is by inserting a thin conductive film as the intermediate pattern transfer layer.²⁸ A similar improvement may be realized with the use of a conductive resist.²⁹ In the case of electron-beam writing of masks, charge build-up may be prevented by means of conducting grounding wires that connect the electron-beam tool to the chrome or molybdenum-silicon structures of the mask. These grounding wires conduct the built-up charges.

15.2.2 Electron-beam lithography systems

Figure 15.1 shows a schematic diagram of an EBL exposure system, which consists of three main subsystems, namely, the electron source (gun), electron optical column (beam-forming system), and exposure stage. A computer is used to control the various machine subsystems and transfer pattern information to the beam deflection coils.

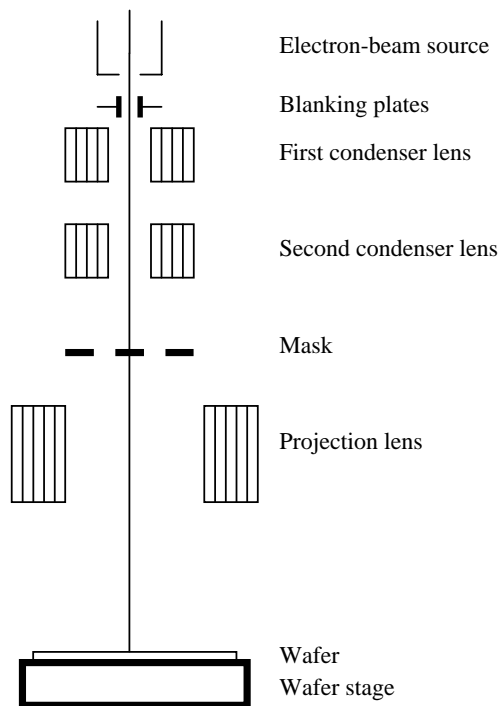


Figure 15.1 A schematic diagram of an EBL exposure system.

²⁸L.F. Thompson, "Resist processing," in *Introduction to Microlithography*, L.F. Thompson, C.G. Willson, and M.J. Bowden, Eds., p. 354, American Chemical Society, Washington, DC (1994).

²⁹*ibid.*, p. 354.

15.2.2.1 Electron sources

Electron sources used in EBL exposure tools are similar to those used in conventional electron microscopes. They can be divided into two main groups—thermionic or field emission—depending on the way in which they emit electrons.³⁰ The sources that rely on the emission of electrons from a material that is heated to a temperature at which electrons are emitted from the surface are referred to as thermionic sources. These sources are fabricated from materials such as tungsten, thoriated tungsten, or lanthanum hexaboride (LaB_6).³¹

Tungsten emission sources have fairly good current stability and tolerance to variations in vacuum conditions. They can be easily fabricated and maintained.³² Thoriated tungsten sources have a work function that is lower than that of pure tungsten sources; they also emit equivalent electron current at lower temperatures than pure tungsten sources. As a result, they have a much longer lifetime and are more stable than pure tungsten sources. However, they do require a stable vacuum (10^{-7} – 10^{-9} torr) and are more difficult to fabricate than pure tungsten sources.³³

Lanthanum hexaboride has a much lower work function than either tungsten or thoriated tungsten, which makes such sources brighter than those made from either pure tungsten or thoriated tungsten. The lanthanum hexaboride source requires a better vacuum than that required for a thoriated tungsten source and as a result is less stable than sources made from the latter. It is preferred for illuminating shaped-beam systems because its emission uniformity can be maintained over a larger area compared with that from the other sources.³⁴

Field-emission sources use a high electric field surrounding a very sharp point of tungsten to extract electrons at the tip of the source, forming a Gaussian spot only a few nanometers in diameter. The energy spread of the electrons emitted from a field-emission source is less than that from a thermionic source; this enables the field-emission source to have less chromatic aberration (where electrons of slightly different energies are focused at different image planes) and higher resolution than the thermionic emission sources. These field-emission sources are also considerably brighter than any of the thermionic emitters. However, they are more difficult to fabricate and must be operated in vacuums of the order of 10^{-8} – 10^{-10} torr. They are widely used in electron-beam-scanning lithographic exposure tools.³⁵

³⁰D.R. Herriot and G.R. Brewer, in *Electron Beam Technology in Microelectronic Circuit Fabrication*, G.R. Brewer, Ed., pp. 141–216, Academic Press, Orlando (1981).

³¹M.J. Bowden, “The lithographic process: the physics,” in *Introduction to Microlithography*, L.F. Thompson, C.G. Willson, and M.J. Bowden, Eds., p. 111, American Chemical Society, Washington, DC (1994).

³²*ibid.*

³³*ibid.*

³⁴*ibid.*, pp. 111–112.

³⁵*ibid.*, pp. 112–113.

15.2.2.2 Electron optical components

The electron optical components comprise lenses (used to focus and define the spot of the electron beam), beam blanker (for modulating the beam), beam-limiting apertures, and a beam-deflection unit to position the beam precisely and accurately over the scan field. The configuration of these elements can vary, depending on the purpose and design of the particular column and system.³⁶ Typically, the column is designed to minimize aberrations so that a spot or an edge profile equivalent to the desired address feature can be achieved.³⁷ The intended use of the machine—whether for mask making or wafer printing applications—determines the form of the edge profile.³⁸

The exposure of an entire wafer necessarily involves the movement of the beam over the entire area. The deflection of the beam by the electromagnetic or electrostatic scan coils is not without errors because of the inherent limits to how far these coils can accurately and precisely deflect the beam. Good pattern quality requires the edge gradient of the electron-beam profile, the distortion of the exposed pattern, and the positional stability of the beam to be held below a small fraction of the minimum feature size. These considerations mandate that the size of the scan field be limited to a few millimeters at most and necessitate mechanical exposure stages to move the substrate through the deflection field of the electron-beam column.³⁹

15.2.2.3 Exposure stage

The exposure stage positions the resist-coated substrate to be exposed at the right location under the electron column. It can be operated in a step-and-repeat mode in which the field containing a circuit, or a portion of a circuit, is exposed on the substrate by deflecting the electron beam over the field, while the exposure stage is stationary. The exposure stage is then stepped to the adjacent field, and the next circuit or portion is exposed. This operation is continued until the entire substrate is exposed.⁴⁰ The correct positioning of the exposure stage is critical to successful registration and is typically controlled by means of laser interferometry. Laser interferometers are used for monitoring the exposure stage position continuously, such that the substrate position errors can be compensated for by electronic deflection of the electron beam.⁴¹

³⁶M. Born and E. Wolf, *Principles of Optics*, 4th ed., p. 559, Pergamon Press, New York (1970); P. Givet, *Electron Optics*, Pergamon Press, Oxford, (1965); H.C. Pfeiffer, "Variable spot shaping for electron beam lithography," *J. Vac. Sci. Technol.* **15**(3), 887 (1978).

³⁷M.J. Bowden, "The lithographic process: the physics," in *Introduction to Microlithography*, L.F. Thompson, C.G. Willson, and M.J. Bowden, Eds., p. 113, American Chemical Society, Washington, DC (1994).

³⁸*ibid.*

³⁹*ibid.*

⁴⁰*ibid.*

⁴¹*ibid.*

An alternative method of operating the exposure stage in a continuous mode is one in which the pattern is written on the substrate while the stage is moving. This strategy was developed at Bell Laboratories in the 1970s⁴² and is employed today on all MEBES⁴³ mask-making machines.

15.2.2.4 Computer

A computer controls all of the above-named subsystems. It does this by monitoring in real time the various operating parameters of the column and stage position. In addition, it transfers the primary operating data directly to the electron deflection system in a feedback loop mechanism that ultimately dictates the writing rate of the tool. In other words, the rate at which the data can be transmitted to the electron optical column ultimately determines the modulation rate of the electron-beam machine, that is, the writing rate (and hence the dwell time t). While the maximum current i that can be delivered to a unit area a of the resist-coated substrate is limited by the brightness of the source, the parameters a , i , and t determine the maximum dose (D_{\max}) per unit dwell time in coulombs per square centimeter, which is given by

$$D_{\max} = \frac{it}{a}. \quad (15.4)$$

The maximum dose delivered by the exposure tool per unit dwell time defines the resist sensitivity required to maximize the throughput of the tool.⁴⁴

15.3 Types of Electron-Beam Lithographies

Following the invention of the SEM, it was quickly realized that the same instrument could be used to expose resists. This realization not only influenced the design of the first electron-beam tool, employing Gaussian beams in 1974, but it also influenced the design of subsequent tools employing shaped beams in 1979, the cell or character projection in 1990, and scattering contrast projection in 1996.

Figure 15.2 shows the different types of EBLs, along with their writing strategies. This figure also illustrates how the exposure tool has evolved from being a tool that used a Gaussian beam (in raster scan or vector scan mode) to print one pixel at a time on the wafer, to one that used a shaped beam (with fixed or variable shape) to print one pixel at a time on the wafer, then to one that used a shaped beam to project and print an entire cell or character at a time on the wafer, and then to one

⁴²D.S. Alles, C.J. Biddick, J.H. Bruning, J.T. Clemens, R.J. Collier, E.A. Gere, L.R. Harriot, F. Leone, R. Liu, T.J. Mulrooney, R.J. Nielsen, N. Paras, R.M. Richman, C.M. Rose, D.P. Rosenfeld, D.E.A. Smith, M.G.R. Thompson, "EBES4: A new electron beam exposure system," *J. Vac. Sci. Technol. B* 5(1), 47 (1987).

⁴³MEBES is the commercial adaptation of the Bell Laboratories's Electron Beam Exposure System (EBES). It was licensed by Etec Systems, Inc., which is now a division of Applied Materials, Inc.

⁴⁴M.J. Bowden, "The lithographic process: the physics," in *Introduction to Microlithography*, L.F. Thompson, C.G. Willson, and M.J. Bowden, Eds., p. 110, American Chemical Society, Washington, DC (1994).

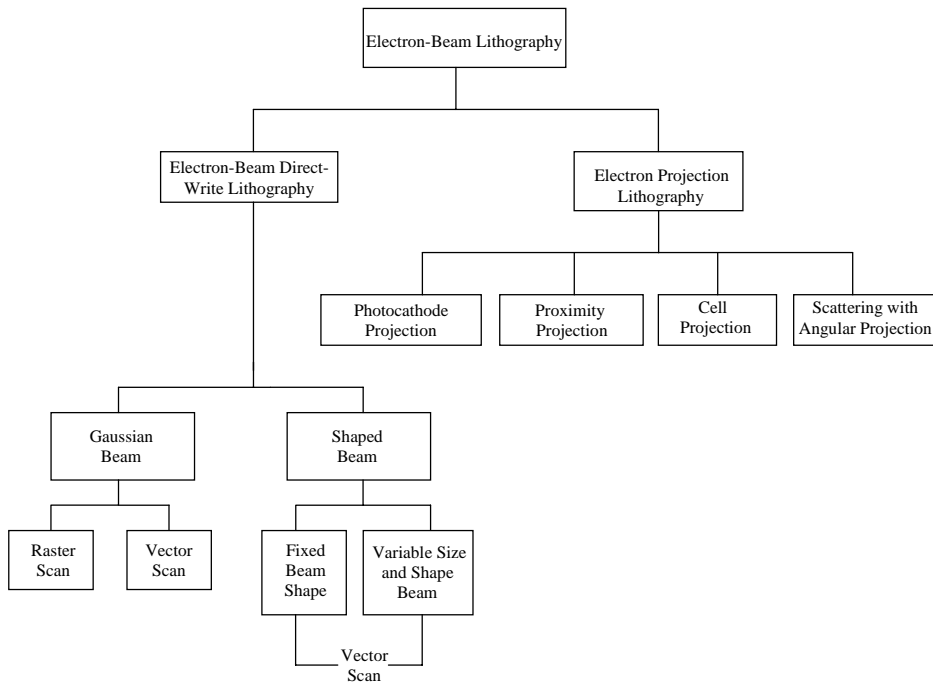


Figure 15.2 Varieties of EBLs, along with their writing strategies.

that uses scattering contrast between components of its mask to project and print a pixel at a time on the wafer, and now to multibeam systems that print a multitude of pixels simultaneously and in parallel fashion on the wafer.

Electron-beam lithography can be divided into two broad categories, namely, (i) electron-beam direct-write lithography utilizing scanning systems of focused electron beams to expose the resist-coated substrate in a serial manner, and (ii) electron projection lithography utilizing systems that project the entire pattern simultaneously onto the substrate. The projection systems utilizing parallel-exposure techniques have been investigated extensively because they offer the advantage of higher exposure throughput when compared with the serial exposure technique, in which only small features or portions of a feature are written at a time.⁴⁵

15.3.1 Electron-beam direct-write lithography

In electron-beam direct-write lithography, the scanning electron beam of the exposure systems is focused to a small spot that is controlled [i.e., deflected and turned on and off (blanked)] by a computer as it is scanned across the surface of the resist film. Masks are not used in this exposure process. Two beam-forming approaches are employed. The first uses a Gaussian round beam. The second

⁴⁵ibid., p. 109.

approach uses a shaped beam that is imaged to a square or rectangular spot on the writing surface, thereby allowing several pixels to be printed in parallel. The Gaussian beam exposure systems have demonstrated the highest resolution of all of the electron-beam exposure systems.

15.3.2 Scanning strategies

Raster and vector scanning are the two basic scanning methods used in EBL exposure tools. In the raster-scanning strategy, the electron beam is deflected such that the entire scan field is scanned serially along parallel strips until the entire field is written. This is accomplished in a scheme that first breaks the area to be scanned into parallel strips, with the pattern in one strip being decoded with a computer during stage retrace and stored in memory from which it is subsequently read and used in writing. The exposure stage moves with almost constant velocity, and information is read from a memory buffer in a serial fashion, minimizing the frequency response or bandwidth required of the deflection system.⁴⁶

The vector-scanning strategy calls for the electron beam to be deflected sequentially to individual elements of the pattern, which are then written in a raster scan fashion. Exposure time is saved with this approach through limiting exposure only to the areas of the substrate to be patterned (in contrast to scanning serially over the entire scan field as is done with full raster scanning). This scanning method requires complex beam deflection systems to compensate for hysteresis effects and large angle deflections. Furthermore, the vector-scanning technique is very well suited to the use of shaped beams and variable-shaped beams for exposing feature patterns instead of the more conventional round beams.⁴⁷

The shaped beam systems have an aperture of a given geometric configuration (typically rectangular or square) that is imaged through electromagnetic lenses and projected onto a wafer surface. These systems can pattern sharper corners than Gaussian beam systems. The key advantage of this strategy is the fact that it can expose several address units simultaneously.

A notable improvement in the vector-scanning strategy that has been reported involves the imaging of two apertures simultaneously, which enables the size and shape of the beam to be varied, thereby minimizing the number of flashes of the electron beam required to expose the area to be patterned.⁴⁸

15.4 Electron Projection Lithography

In order to address the low throughput issues of electron-beam direct-write lithography, without multiple columns and the attendant complexity, electron

⁴⁶ibid., p. 117.

⁴⁷H.C. Pfeiffer, T.R. Groves, and T.H. Newman, "High throughput, high resolution electron beam lithography," *IBM J. Res. Dev.* **32**(4), 494 (1988).

⁴⁸ibid.

projection lithography (EPL) involving masks was developed. The EPL systems can be classified into four broad categories, namely, photocathode projection lithography,⁴⁹ proximity projection lithography (or shadow mask proximity printing),⁵⁰ cell projection lithography,⁵¹ and scattering with angular limitation projection electron-beam lithography (SCALPEL).⁵² The first three of these techniques use stencil masks; some use very small fields ($\leq 5 \mu\text{m} \times 5 \mu\text{m}$), while others use considerably larger fields of the order of a few millimeters.⁵³ A stencil mask consists of a thin (but opaque) membrane through which holes are etched to provide regions of the mask through which electrons can pass. The small-field techniques have limited applicability in the fabrication of IC circuits because of their small fields; some have nevertheless found use in some niche applications. In particular, in certain applications such as patterning the repetitive core cells of memories, the cell projection system has been used to make prototype high-bit-count DRAMS.⁵⁴ The SCALPEL technology uses much larger masks of the order of a few square millimeters that are made of membranes. In the following section, we briefly review the main attributes of each of these systems.

The 1:1 photocathode projection scheme uses UV radiation to irradiate a CsI photocathode, which is masked by a thin metal pattern. Photoelectrons are ejected from the cathode and accelerated to the wafer, which acts as the anode. A uniform magnetic field is used to focus the electrons at the wafer. Chromatic aberrations tend to limit resolution in these systems. Other problems that have been identified to hamper this technique include issues such as the uniformity of the electric and magnetic fields, substrate flatness requirements, and poor cathode life.⁵⁵

The shadow mask proximity printing technique projects the shadow image of the transmission mask onto a resist-coated wafer by scanning a 1-mm-diameter

⁴⁹J.P. Scott, "Photocathodes for use in an electron image projector," *J. Appl. Phys.* **46**, 661 (1975); I. Mori, K. Sugihara, C. Itoh, M. Tabata, and T. Schinozaki, "An electron beam image projection system with automatic wafer handling," *Microelectron. Eng.* **3**, 69 (1985); T.W. O'Keefe, J. Vine, and R.M. Handy, "An electron imaging system for the fabrication of integrated circuits," *Solid State Electron.* **52**, 841 (1969).

⁵⁰H. Bohlen, J. Greschmer, W. Kulcke, P. Nehmiz, W. Zapka, U. Behringer, W. Haug, and J. Keyser, "Electron beam proximity printing: step and scan technique for future small groundrule lithography," *Proc. Microcircuit Eng.*, Vol. 84, A. Heuberger and H. Beneking, Eds., p. 265, Academic Press, Orlando (1985).

⁵¹Y. Nakayama, S. Okazaki, N. Saitou, and H. Wakabayashi, "Electron beam cell projection lithography: A new high throughput electron beam direct writing technology using a specially tailored Si aperture," *J. Vac. Sci. Technol. B* **8**(6), 1836 (1990).

⁵²S.D. Berger and J.M. Gibson, "New approach to projection electron lithography with demonstrated 0.1 μm linewidth," *Appl. Phys. Lett.* **57**, 153 (1990).

⁵³H.J. Levinson, *Principles of Lithography*, 2nd ed., p. 395, SPIE Press, Bellingham, WA (2005).

⁵⁴H. Yasuda, K. Sakamoto, A. Yamada, and K. Kawashima, "Electron beam block exposure," *Jpn. J. Appl. Phys.* **30**(11B), 3098–3102 (1991).

⁵⁵M.J. Bowden, "The lithographic process: the physics," in *Introduction to Microlithography*, L.F. Thompson, C.G. Willson, and M.J. Bowden, Eds., p. 119, American Chemical Society, Washington, DC (1994).

collimated electron beam across the mask, which is separated from the substrate by a gap of about 500 μm . It uses a 2- μm -thick stencil mask, configured in the form of two complimentary masks that are required to facilitate the exposure of ring-shaped structures. The substrate is mounted on a laser-interferometer-controlled x - y stage, which makes possible the stitching of complementary masks and step-and-repeat exposure of the whole substrate.⁵⁶

Cell projection lithography⁵⁷ incorporates elements of image projection into the variable-shaped beam approach. Here, the shaped beam is created by an aperture, formed from single-crystal silicon, containing various shapes coinciding with the array of each unit cell of an integrated circuit device pattern such as the repetitive core cells of memory chips.⁵⁸

15.4.1 Scattering with angular limitation projection electron-beam lithography (SCALPEL)

The significant benefits of projection electron-beam lithography such as high resolution, wide process latitude, and good depth of focus were well recognized for several decades⁵⁹ following the development of the first electron-beam exposure tools (described above). However, attempts to exploit these benefits met with failure, primarily on account of two main problems. The first problem has to do with absorbing stencil masks used in projection electron-beam lithography. These stencil masks are susceptible to heating,⁶⁰ which limits the acceleration voltage that can be employed, and cannot support patterns containing closed curves (the doughnut problem) unless complementary mask pairs are used. The second problem concerns the fact that full-field optics, which do not scale with increasing die sizes and decreasing feature sizes, require the use of such small numerical apertures to control optical aberrations that, at the beam currents necessary for acceptable throughput in electron-beam exposure systems, space charge effects destroy the resolution.⁶¹

⁵⁶ibid.

⁵⁷Y. Nakayama, S. Okazaki, N. Saitou, and H. Wakabayashi, "Electron beam cell projection lithography: A new high throughput electron beam direct writing technology using a specially tailored Si aperture," *J. Vac. Sci. Technol. B* **8**(6), 1836 (1990).

⁵⁸M.J. Bowden, "The lithographic process: the physics," in *Introduction to Microlithography*, L.F. Thompson, C.G. Willson, and M.J. Bowden, Eds., p. 119, American Chemical Society, Washington, DC (1994).

⁵⁹R.P. Feynman in *Miniaturization*, H.D. Gilbert, Ed., Rheinhold, New York (1961); M.B. Heritage, "Electron projection microfabrication system," *J. Vac. Sci. Technol.* **12**, 1135 (1975).

⁶⁰H. Bohlen, J. Greschner, W. Kulcke, and P. Nehmiz, "Electron beam step and repeat proximity printing, presented at *Proc. of 8th Symp. on Electron and Ion Beam Science and Technology*, Seattle (1978).

⁶¹J.A. Liddle and S.D. Berger, "High throughput projection electron beam lithography employing SCALPEL," *Proc. SPIE* **2014**, 66–76 (1993); L.R. Harriot, "SCALPEL: Projection electron beam lithography," *Proc. 1999 Particle Accelerator Conference*, New York, pp. 595–599 (1999).

To overcome the above two problems associated with stencil masks, in 1989 Steven Berger and Murray Gibson at Bell Laboratories invented the SCALPEL mask concept (described below).⁶² It was quickly realized, soon after the invention of the SCALPEL mask, that thin membrane masks were not sufficiently stable over a large area to meet error budget requirements, without the addition of some supporting structure. This necessitated the development of the strutted mask concept, which was compatible with the need to move away from full-field optics. Next, the step-and-scan writing strategy was adopted into the SCALPEL tool. Together, the SCALPEL mask and step-and-scan writing strategy proved effective in overcoming the main limitations that had prevented earlier attempts at projection electron-beam lithography from working.⁶³

Figure 15.3 shows a schematic of a SCALPEL exposure system,⁶⁴ comprising the mask, projection lens, limiting aperture, objective lens, and wafer stage. The mask is made of a low-atomic-number membrane comprising 100 nm of silicon nitride, 5 nm of chromium, and 25 nm of tungsten or diamondlike carbon⁶⁵ covered with a patterned layer of high-atomic-number material (called a scatterer) such as tungsten, tantalum, or other materials used for x-ray masks. While the mask is almost completely transparent at the energies employed in SCALPEL (100 keV), contrast is generated from the difference in the electron scattering characteristics between the low-atomic-number membrane material and the patterned high-atomic-number material. The membrane material scatters electrons weakly and to small angles; in contrast, the patterned layer scatters them strongly and to large angles. A physical aperture positioned in the back focal (pupil) plane of the projection optics blocks the strongly scattered electrons; it allows only a small fraction of the scattered electrons to pass through. This leads to the formation of a high-contrast aerial image at the wafer plane. With this design, the functions of contrast generation and energy absorption are separated between the mask and the physical aperture. This implies that very little of the incident energy is actually absorbed by the mask, which significantly minimizes thermal instabilities in the mask.⁶⁶

It should be mentioned that although the membrane scatters electrons weakly compared to the scatterer, a major fraction of the electrons passing through the membrane are scattered sufficiently to be stopped by the physical aperture. The fraction absorbed in the physical aperture depends on factors such as the thickness and composition of the membrane, as well as the angular size of the physical

⁶²S.D. Berger and J.M. Gibson, "New approach to projection electron lithography with demonstrated 0.1 μm linewidth," *Appl. Phys. Lett.* **57**, 153 (1990).

⁶³J.A. Liddle and S.D. Berger, "High throughput projection electron beam lithography employing SCALPEL," *Proc. SPIE* **2014**, 66–76 (1993); L.R. Harriot, "SCALPEL: Projection electron beam lithography," *Proc. 1999 Particle Accelerator Conference*, New York, pp. 595–599 (1999).

⁶⁴*ibid.*, pp. 595–599.

⁶⁵I. Anemiya, H. Yamashita, S. Nakatsuka, M. Tsukahara, and O. Nagerekawa, "Fabrication of a continuous diamondlike carbon membrane mask for electron projection lithography," *J. Vac. Sci. Technol. B* **21**(6), 3032–3036 (2003).

⁶⁶L.R. Harriot, "SCALPEL: Projection electron beam lithography," *Proc. 1999 Particle Accelerator Conference*, New York, pp. 595–599 (1999).

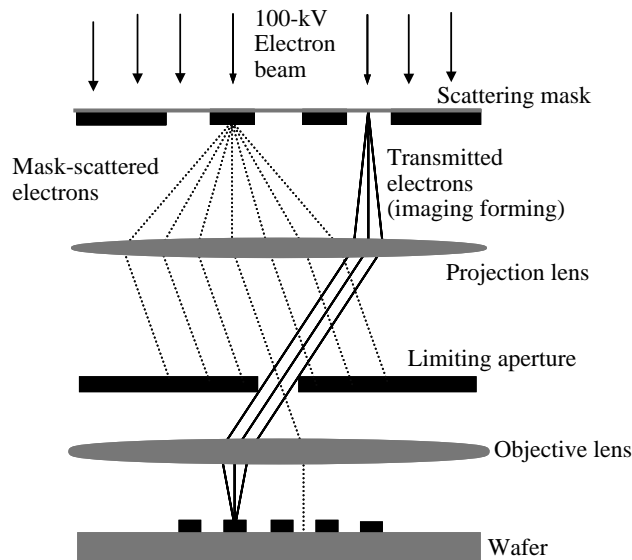


Figure 15.3 Schematic of a SCALPEL exposure system. (Adapted with permission from Ref. 67. © 1999 IEEE.)

aperture. Those portions of the mask corresponding to regions of the IC design that are supposed to be exposed on the wafer allow electrons to penetrate with little scattering.⁶⁸

As mentioned above, the SCALPEL mask is uniformly illuminated by a parallel beam of 100-keV electrons. In the SCALPEL exposure tool, a reduction-projection optic in a telecentric doublet arrangement produces a 4:1 demagnified image of the mask at the wafer plane. Given that the features to be printed are much larger than the wavelength of the electrons ($\lambda = 3.7$ pm) used, the full benefits of the reduction ratio are realized, especially in terms of the mask, because imaging is aberration limited, not diffraction limited. Also, because the illumination in the SCALPEL exposure tool is incoherent, there are no interference effects.⁶⁹

By design, the SCALPEL exposure tool employs a small (1 mm \times 1 mm) electron optical field, which is consistent with the strutted mask design and step-and-scan writing strategy. Since the electron optical field is the same width as the pattern area between the mask struts, die exposure is accomplished by mechanically scanning the mask and wafer through the effective electron optical field.⁷⁰

Shown in Fig. 15.4 are 80-nm contacts printed with SCALPEL technology, illustrating the resolution capability of this technology.

⁶⁷L.R. Harriot, "SCALPEL: Projection electron beam lithography," *Proc. 1999 Particle Accelerator Conference*, New York, pp. 595–599 (1999).

⁶⁸ibid.

⁶⁹ibid.

⁷⁰ibid.

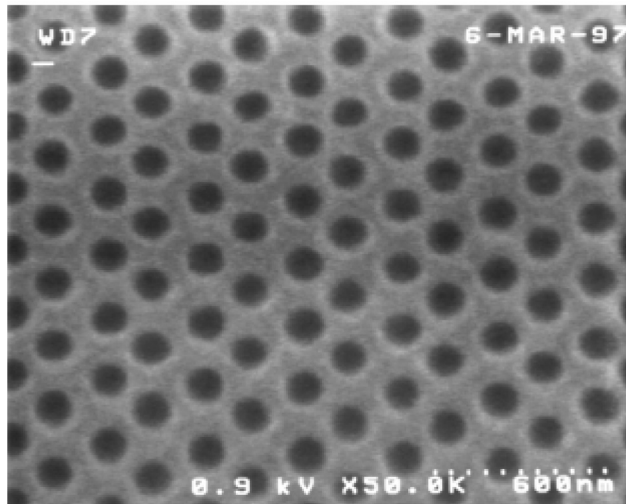


Figure 15.4 SEM image of 80-nm contacts printed with the SCALPEL exposure tool in 750-nm-thick DUV resist. (Reprinted with permission from Ref. 71. © 1999 IEEE.)

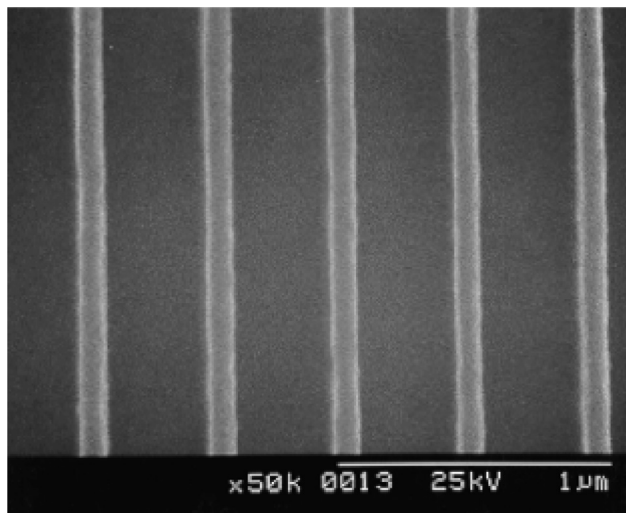


Figure 15.5 SEM images of 100-nm isolated lines printed with SCALPEL exposure tool in NEB-22A resist from Sumitomo.⁷²

⁷¹L.R. Harriot, "SCALPEL: Projection electron beam lithography," *Proc. 1999 Particle Accelerator Conference*, New York, pp. 595–599 (1999).

⁷²Reproduced with permission from Alcatel Lucent.

15.4.1.1 SCALPEL technology challenges

SCALPEL technology faces many challenges that are unique to it and some that are not. Some of these challenges are discussed in the following paragraphs. One of these challenges is the fact that the device pattern is segmented on the mask in two dimensions by the struts and must be reassembled or stitched to form a continuous image on the wafer.⁷³ This stitching is essential to ensure that the critical dimension of any feature crossing a stitching boundary is maintained to within the tolerances specified by the error budget.⁷⁴ Heating of the mask and the wafer that occurs during exposure makes it difficult to successfully stitch two adjoining fields together. While very little energy is deposited on the SCALPEL mask, the fact that the membranes are so thin means that they have very little thermal mass and as a result will heat up appreciably during exposures.⁷⁵ Published simulation results show that the temperature increase, which occurs nonuniformly across the mask during SCALPEL exposure, can exceed 7°C and can cause deformations of up to 20 nm.⁷⁶

In a related manner, most of the energy of the 100-keV electrons used in SCALPEL technology is deposited into the silicon wafer, which can cause temperature rises of up to several degrees (in Celsius).⁷⁷ This wafer heating can result in mechanical distortions that depend significantly on how the wafers are chucked.⁷⁸

Another challenge faced by SCALPEL technology is related to the fact that the SCALPEL mask is not protected by pellicles, making particulate and airborne molecular contamination a major issue. In particular, many components of the SCALPEL tool are sensitive to the presence of charged particulates; these include electrostatic chucks, electrostatic optics, and apertures. The fact that the SCALPEL tool is designed to operate in a vacuum environment (10^{-7} torr) has been reasonably effective in limiting the amount of particulate and molecular contamination, but has not eliminated them entirely.

Low throughput is another major challenge faced by SCALPEL technology. Given the very high beam currents used in the modest field size used in SCALPEL technology, the problem of stochastic scattering is particularly severe. The amount of blur that can be tolerated decreases with shrinking feature sizes, mandating that the beam current be reduced in order to image smaller features with a given electron-optical system. This establishes the operational relation

⁷³J.A. Liddle, L.R. Harriot, A.E. Novembre, and W.K. Waskiewicz, "SCALPEL: a projection electron beam approach to sub optical lithography," http://www.bel_labs.com/project/SCALPEL.

⁷⁴H.J. Levinson, *Principles of Lithography*, 2nd ed., p. 396, SPIE Press, Bellingham, WA (2005).

⁷⁵ibid.

⁷⁶C.J. Martin, W.H. Semke, G.A. Dicks, R.L. Englestad, E.G. Lovell, J.A. Liddle, and A.E. Novembre, "Mechanical and thermal modeling of the SCALPEL mask," *J. Vac. Sci. Technol. B* **17**(6), 2878–2882 (1999).

⁷⁷B. Kim, R.L. Englestad, E.G. Lovell, S.T. Stanton, J.A. Liddle, and G.M. Gallatin, "Finite element analysis of SCALPEL wafer heating," *J. Vac. Sci. Technol. B* **17**(6), 2883–2887 (1999).

⁷⁸H.J. Levinson, *Principles of Lithography*, 2nd ed., p. 396, SPIE Press, Bellingham, WA (2005).

between throughput and resolution that underpins SCALPEL technology; i.e., throughput decreases in order to print smaller features.⁷⁹ It was the inability to resolve this trade-off that ultimately led to the demise of SCALPEL technology.

Another effect limiting resolution in SCALPEL as in other electron-beam and ion-beam exposure systems is shot noise,⁸⁰ which is dependent on resist sensitivity. The relationship between resist sensitivity and shot noise can be understood from the following analysis. Let us suppose that an area to be exposed with electron beams consists of a grid of addressable locations called pixels whose dimensions (l_p) correspond to the minimum resolution element that can be printed by the presence or absence of electrons striking that element. Furthermore, let us suppose that the exposure process is binary such that a minimum number (N_{\min}) of electrons striking the pixel is required for it to be regarded as exposed. Cognizant that the scenario we have painted is really a simplification in that resist contrast is finite, the conclusions we shall draw from our analysis are nevertheless quite valid. If the number of electrons striking the pixel is less than N_{\min} , the pattern will not be printed. For a resist with sensitivity D (in C/cm^2), N_{\min} is expressed as⁸¹

$$N_{\min} = \frac{Dl_p^2}{e}, \quad (15.5)$$

where e is the electronic charge and l_p^2 corresponds to the area of the pixel.

An examination of Eq. (15.5) reveals the connection between sensitivity and resolution, as well as how the product of sensitivity and pixel size (resolution) is determined by N_{\min} . A highly sensitive resist will require far fewer electrons to expose the pixel compared with the number required for an insensitive resist for the same pixel size. Ordinarily, that is not problematic as long as each pixel receives the same average number of electrons required for exposure. However, in real physical systems, electrons are emitted randomly from the cathode, not in a series of emission events equally spaced in time. This implies that the number of electrons arriving at the pixel per unit time varies statistically. For a large number of electrons N_e , the uncertainty surrounding their number is given by $\sqrt{N_e}$, and the ratio of N_e to the uncertainty is $N_e/\sqrt{N_e}$, which is simply $\sqrt{N_e}$. This value is analogous to a signal-to-noise ratio.⁸²

To properly expose a resist, $\sqrt{N_e}$ should therefore be large. The foregoing analyses lead to the conclusion that resist sensitivity sets the minimum resolution that can be written in the resist with electrons.⁸³

⁷⁹ibid., p. 398.

⁸⁰G.R. Brewer, *Electron Beam Technology in Microelectronic Circuit Fabrication*, G.R. Brewer, Ed., pp. 141–216, Academic Press, Orlando (1981).

⁸¹M.J. Bowden, "The lithographic process: the physics," in *Introduction to Microlithography*, L.F. Thompson, C.G. Willson, and M.J. Bowden, Eds., p. 108, American Chemical Society, Washington, DC (1994).

⁸²ibid.

⁸³ibid.

15.4.2 Projection reduction exposure with variable axis immersion lens (PREVAIL) lithography

An electron-beam technology that succeeded SCALPEL was based on projection reduction exposure with variable axis immersion lens (PREVAIL). It was developed at IBM in the early 1990s and included the essential elements of SCALPEL such as a scattering mask and focal plane aperture, as well as IBM electron-optical technology.⁸⁴ Shown in Fig. 15.6 is a SEM image of 80-nm line and space features printed with the PREVAIL technology, illustrating the resolution capability of this technology. Unfortunately, it suffers from the same limitations as SCALPEL.

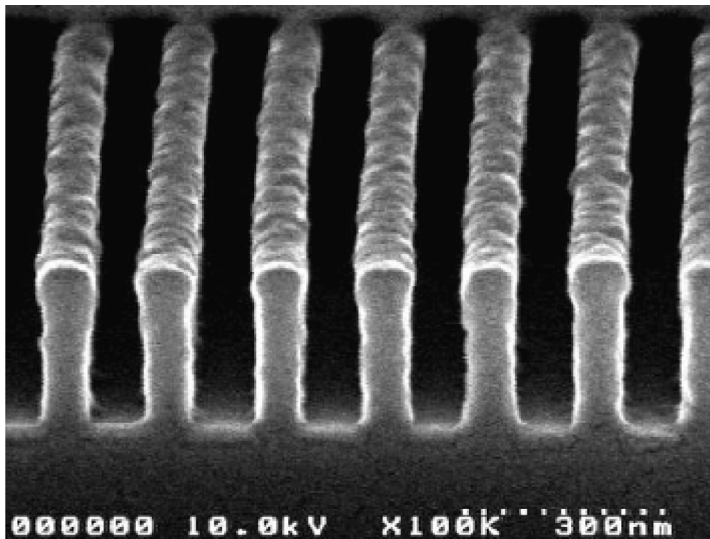


Figure 15.6 SEM image of 80-nm line and space features patterned with PREVAIL technology.⁸⁵

15.5 Ion-Beam Lithography

An energetic ion incident on a solid resist-coated substrate can interact with the latter in a variety of phenomena that include sputtering of neutral atoms, emission of electrons, lattice damage, heat generation, and ion implantation, as shown in Fig. 15.7. In addition, the beam can produce secondary electrons that participate in the chemical transformations of the resist, such as bond breaking, of the kind that can expose the resist. It is this flexibility and effectiveness of ions in

⁸⁴H.J. Levinson, *Principles of Lithography*, 2nd ed, p. 398, SPIE Press, Bellingham, WA (2005).

⁸⁵H.C. Pfeiffer, "PREVAIL IBM's e beam technology for next generation lithography," *Proc. SPIE* **3997**, 206–213 (2000).

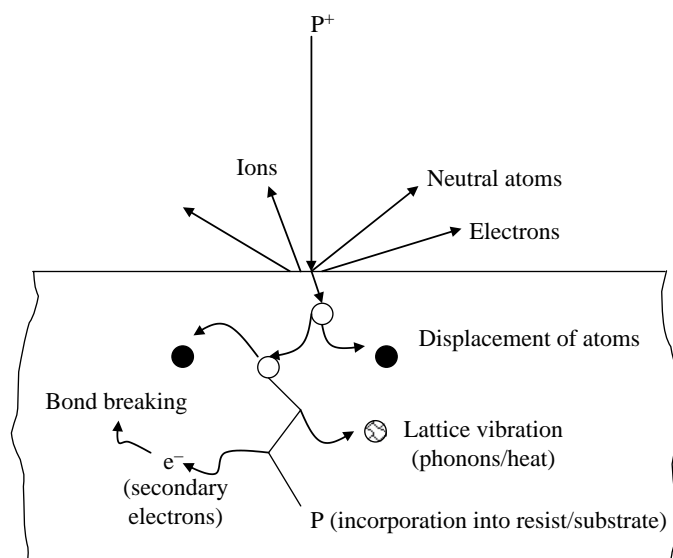


Figure 15.7 Schematic of an ion-resist interaction, showing sputtering of neutral atoms, emission of electrons, lattice damage, heat generation, and implantation. In addition, the beam can generate secondary electrons that participate in bond-breaking reactions in resist molecules.

modifying the properties of the resist, a direct consequence of the fact that they can deliver both mass and energy to the latter, that make them attractive tools for lithography.⁸⁶ Other applications of ion beams include ion implantation and ion milling.⁸⁷

The ion-beam lithographic exposure tool is similar to that of electron-beam exposure systems, the major differences being in the source and deflection lenses. The key advantages of ion-beam lithography are high resolution and the fact that it can be used with resists with poor sensitivities. These advantages are a result of their negligible scattering, which stands in stark contrast to what is obtained in electron-beam lithography, where scattering constitutes a primary factor limiting resolution. The large effective mass of an ion and its greater cross section of interaction with atoms of the resist when compared with that of an electron result in energy being deposited in a much smaller volume in ion-beam lithography than in electron-beam lithography. As a result, energy penetration is more limited and takes place over a well-defined range in ion-beam lithography.⁸⁸

⁸⁶T.M. Hall, A. Wagner, and L.F. Thompson, "Ion beam exposure characteristics of resists," *J. Vac. Sci. Technol. B* **6**, 1889 (1979); T. Kaneko, T. Umegaki, and Y. Kawakomi, in *Proc. Kodak Interface*, Vol. 80, p. 25 (1980).

⁸⁷W.L. Brown, "Recent progress in ion beam lithography," *Microcirc. Eng.* **9**, p. 269 (1989).

⁸⁸M.J. Bowden, "The lithographic process: the physics," in *Introduction to Microlithography*, L.F. Thompson, C.G. Willson, and M.J. Bowden, Eds., p. 132, American Chemical Society, Washington, DC (1994).

This implies that minimum energy is delivered to the substrate, in contrast to high-energy electrons used in electron-beam lithography, which penetrate relatively deeply into the substrate and lose only a small fraction of their energy in exposing the resist. Thus, resolution in ion-beam lithography is primarily limited by the range of the secondary electrons produced as the ion loses energy in the resist; in contrast, in electron-beam lithography, resolution is primarily limited by scattering of the much more energetic primary electrons.⁸⁹

Ion-beam lithography is not without its drawbacks, especially when compared to electron-beam lithography. Shot noise is a major issue for ion-beam lithography, just as it is for electron-beam lithography. Ion current densities are significantly lower than electron current densities, a limitation that is somewhat offset by the fact that each ion deposits more energy into the resist than an electron deposits, which implies that lower doses are needed to produce the same exposure effect when using ions relative to when electrons are used.⁹⁰

Furthermore, the energy spread of the ion beam (particularly metallic sources) is significantly greater than that of electrons such that chromatic aberrations play a dominant role in limiting performance in ion-beam lithography compared to electron-beam lithography.⁹¹ And finally, since energetic ions carry enough energy to displace crystal lattice atoms, they can also cause considerable damage to the substrate when subjected to very thin resists.⁹²

15.5.1 Types of ion-beam lithographies

There are three ways in which ion beams are employed in lithography (see Fig. 15.8). A point beam can be focused to a fine spot (~ 10 nm) from a bright “point” source and deflected on the surface, in an arrangement called focused ion beam (FIB),⁹³ to expose the resist directly without a mask.⁹⁴ Two types of ion sources, liquid metal⁹⁵ and gaseous (cryogenic) field ion source,⁹⁶ have been successfully used in this technology. Of these two sources, liquid metal has

⁸⁹ibid.

⁹⁰ibid.

⁹¹ibid.

⁹²J. Melngailis, “Applications of ion microbeams in lithography and direct processing,” *Handbook of VLSI Microlithography*, 2nd ed., J.N. Helbert, Ed., William Andrew Inc., pp. 790–855 (2001).

⁹³Other applications of focused ion beam in integrated circuit industry include device repair, failure analysis, and direct implantation of ions into substrates.

⁹⁴See, for example, E. Platzgummer, H. Loeschner, and G. Gross, “Projection maskless patterning (PMLP) for the fabrication of leading edge complex masks and nano imprint templates,” *Proc. SPIE* **6730**, 673033 (2007).

⁹⁵P. Prewett and G. Maier, *Focused Ion Beams from Liquid Metal Ion Sources*, Research Studies Press (1991).

⁹⁶J. Melngailis, “Applications of ion microbeams in lithography and direct processing,” *Handbook of VLSI Microlithography*, 2nd ed., J.N. Helbert, Ed., William Andrew Inc., pp. 790–855 (2001).

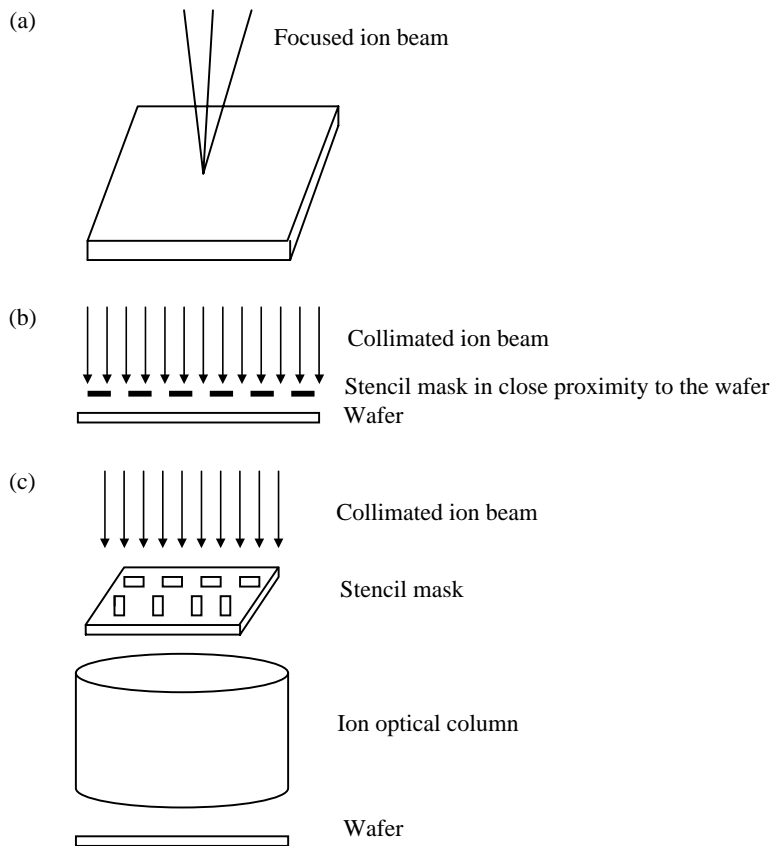


Figure 15.8 Schematic of three ways of employing ion beams in lithography: (a) focused ion beam lithography, (b) proximity ion-beam lithography, (c) ion projection lithography.

proven more widely used.⁹⁷ Typical liquid metal sources include Ga, AuSi, AuSiBe,⁹⁸ PdAs,⁹⁹ PdAsB,¹⁰⁰ NiB,¹⁰¹ etc.

The second way to employ ion beams in lithography is to place a stencil mask in close proximity to a surface and irradiate the mask with a collimated beam of ions. This is referred to as proximity ion-beam lithography, and it is a 1:1

⁹⁷ibid.

⁹⁸J. Kurihara, "A focused ion beam system for submicron lithography," *J. Vac. Sci. Technol. B* **3**, 41 (1985); E. Miyauchi, H. Hashimoto, and T. Utsumi, "Lateral spreads of Be and Si in GaAs implanted with a maskless ion implantation system," *Jpn. J. Appl. Phys.* **22**, L225 (1983); K. Gamo, T. Matsui, and S. Namba, "Characteristics of Be Si Au ternary alloy liquid metal ion sources," *Jpn. J. Appl. Phys.* **22**, L692 (1983).

⁹⁹W. Clark, R.L. Seliger, M.W. Utlaut, A.E. Bell, L.W. Swanson, G.A. Schwind, and J.B. Jorgensen, "Long lifetime, reliable liquid metal ion sources for boron, arsenic, and phosphorus," *J. Vac. Sci. Technol. B* **5**, 197 (1987).

¹⁰⁰ibid.

¹⁰¹L.W. Swanson, A.E. Bell, and G.A. Schwind, "A comparison of boron emission characteristics for liquid metal ion sources of PtB, PdB, and NiB," *J. Vac. Sci. Technol. B* **6**, 491 (1988).

shadow mask printing, quite similar to x-ray proximity printing, except that the ions, typically protons with energies between 10 and few hundred keV, can be collimated and controlled by electrostatic deflection and focusing. It uses the channeling mask technique, which involves aligning the ion beam with the lattice of a thin crystal silicon membrane such that the protons are “channeled” through the silicon with minimal scattering. This technique permits the use of relatively thick membranes ($\sim 0.5 \mu\text{m}$), while keeping scattering angles to less than 0.3 deg .¹⁰²

The third way to employ ion beams in lithography is to combine the first two techniques and use an ion optical column to project the image of the pattern of a stencil mask onto a wafer. This is called ion projection lithography (IPL), which was pioneered at Ion Microfabrication Systems (IMS) of Austria in the late 1980s.¹⁰³ Because IPL is the most technologically important of the three versions of ion-beam lithographies, we shall discuss it in much greater detail.

15.5.2 Ion projection lithography

Ion projection lithography can be implemented either with masks or without masks (the latter is called maskless lithography). Both techniques have found niche applications in the fabrication of leading-edge complex masks, nanoimprint templates, and exploratory research in nanostructured surfaces. Figure 15.9 shows a schematic of an IPL system in which ions with a small energy spread ($\sim 1 \text{ eV}$) from the ion source are used to uniformly illuminate the stencil mask¹⁰⁴ with the aid of electrostatic lenses. Some of the ions pass through the open areas of the stencil mask, while others are blocked in the absorber sections of the mask.¹⁰⁵ The mask substrate is made of single-crystal silicon wafer that is about $4\text{-}\mu\text{m}$ thick. Ion-beam energies are typically in excess of 250 keV in these systems. Another set of electrostatic lenses farther down the ion-optic column projects a demagnified ($4\times$ reduction) ion-beam image of the mask and focuses the ions onto the wafer, positioned on the x - y stage, which is laser-interferometrically controlled.¹⁰⁶ Features as low as 65-nm resolution have been patterned in DUV resists with mask IPL technology.¹⁰⁷

¹⁰²M.J. Bowden, “The lithographic process: the physics,” in *Introduction to Microlithography*, L.F. Thompson, C.G. Willson, and M.J. Bowden, Eds., p. 133, American Chemical Society, Washington, DC (1994).

¹⁰³G. Stengl, H. Löschner, and P. Wolf, “Ion projection lithography machine IPLM 01: A new tool for sub 0.5 micron modification of materials,” *J. Vac. Sci. Technol. B* **6**, 194 (1986).

¹⁰⁴A. Erhmann, A. Elsner, R. Liebe, T. Struck, J. Butschke, F. Letzkus, M. Irmscher, R. Springer, E. Haygeneder, and H. Löschner, “Stencil mask key parameter measurement and control,” *Proc. SPIE* **3997**, 373–384 (2000); R. Kaesmaier and H. Loschner, “Overview of the Ion Projection Lithography European MEDEA and International Program,” *Proc. SPIE* **3997**, 19–32 (2000).

¹⁰⁵J. Melngailis, “Applications of ion microbeams in lithography and direct processing,” *Handbook of VLSI Microlithography*, 2nd ed., J.N. Helbert, Ed., William Andrew Inc., pp. 790–855 (2001).

¹⁰⁶H.J. Levinson, *Principles of Lithography*, 2nd ed., pp. 398–400, SPIE Press, Bellingham, WA (2005).

¹⁰⁷W. Bruenger, L.M. Buchmann, M. Torkler, and S. Sinkwitz, “HPR 506 photoresist used as a positive tone ion resist,” *J. Vac. Sci. Technol. B* **14**, 3924 (1996); W.H. Bruenger, M. Torkler,

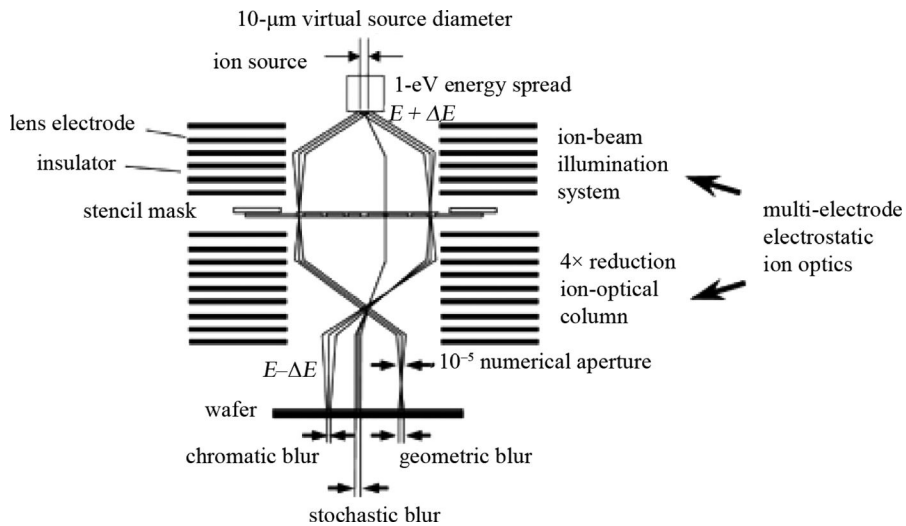


Figure 15.9 Schematic of an ion projection lithography system.¹⁰⁸

The principle of maskless ion projection lithography is illustrated in Fig. 15.10. A broad ion beam is used to illuminate a programmable aperture plate with thousands of apertures of micrometer-scale dimensions, generating up to 4000 beams. In the vicinity of the apertures are tiny deflection plates, each of which can be individually controlled with the aid of integrated CMOS electronics. The slightly deflected beams are blocked at the stopping plate, and the nondeflected

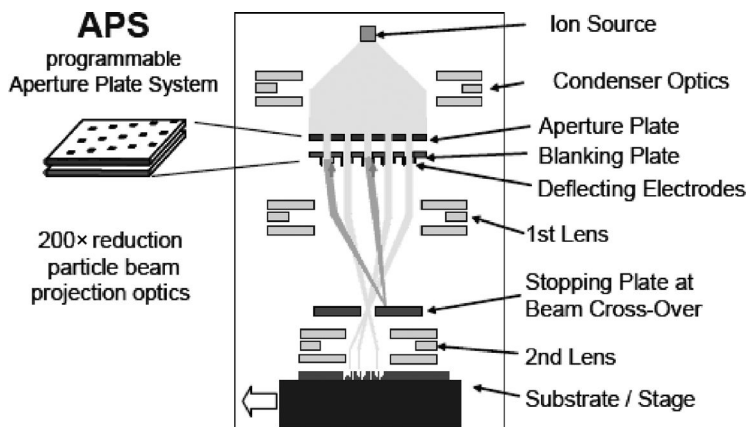


Figure 15.10 Schematic of a maskless ion projection lithography system developed at IMS, Vienna, Austria. (Courtesy of G. Gross.)

L.M. Buchmann, and W. Finkelstein, "Chemically amplified deep ultraviolet resist for positive tone ion exposure," *J. Vac. Sci. Technol. B* **15**, 2355 (1997).

¹⁰⁸R. Kaesmaier and H. Loschner, "Overview of the Ion Projection Lithography European MEDEA and International Program," *Proc. SPIE* **3997**, 19–32 (2000).

beams are projected to the substrate, with $200\times$ demagnification. Resistless direct patterning of surfaces of Si, GaAs, glass, Cr, and MoSi layers have been successfully demonstrated with this technique.¹⁰⁹

Figures 15.11–15.13 show the patterning capabilities of this technique. Varieties of structures of different sizes and intricate shapes have been directly patterned on different substrates with this technique.

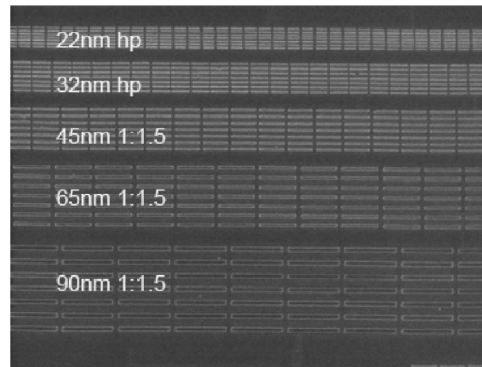


Figure 15.11 Resolution SEM images of features ranging in size from 22-nm half-pitch (hp) to 90 nm (1:1.5 pitch), printed with maskless ion projection lithography system on 20-nm hydrosilesquixane resist, using 10-keV argon ions at an exposure dose of $5.6 \mu\text{C}/\text{cm}^2$.¹¹⁰

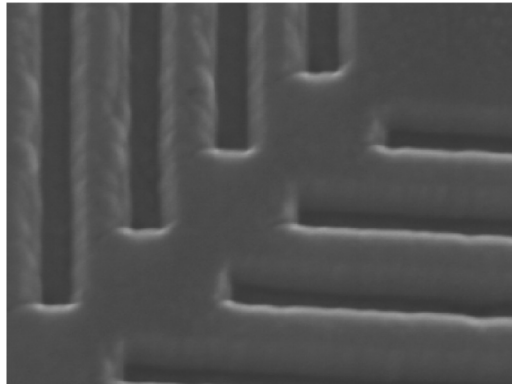


Figure 15.12 SEM image of directly patterned 70-nm Cr on quartz mask blanks with maskless ion projection lithography system, using 10-keV argon ions at a sputtering dose of $39 \mu\text{C}/\text{cm}^2$.¹¹¹

¹⁰⁹E. Platzgummer, H. Loeschner, and G. Gross, “Projection mask less patterning (PMLP) for the fabrication of leading edge complex masks and nano imprint templates,” *Proc. SPIE* **6730**, 673033 (2007).

¹¹⁰ibid.

¹¹¹ibid.

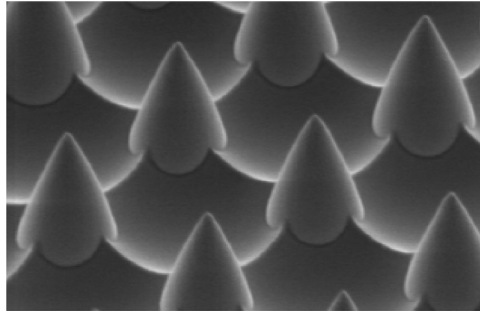


Figure 15.13 SEM image of directly patterned cone structures (formed by redeposition processes at the lens edges following prolonged sputtering GaAs substrate) with maskless ion projection lithography system, using 250,000 parallel 10-keV argon ions.¹¹²

Ion sources such as inert ions including H, He, Ne, Ar, and Xe have been successfully used in these systems.¹¹³ The interaction of ions with each other within the ion optical column leads to resolution limit issues, the main one of which is stochastic blur.

15.5.3 Stochastic blur

There are two main ways in which coulomb interaction between ions manifests itself. The first is the global effect, which results from displacement of a given ion due to the combined effect of all the other ions traveling in the beam. The second is the individual random ion-ion scattering, which makes some ions suffer enough trajectory displacement that they do not arrive at their intended location. This is referred to as stochastic blur. This effect is particularly pronounced in the densest locations of the beam, namely, at the beam crossover point, usually in the field-free region between the two lenses of the column. A way to minimize stochastic blur is to increase the ion energy in the crossover as much as possible.¹¹⁴

¹¹²ibid.

¹¹³G. Stengl, H. Loeschner, W. Maurer, and P. Wolf, "Ion projection lithography machine IPLM 01: A new tool for sub 0.5 micron modification of materials," *J. Vac. Sci. Technol.* **B4**, 194 (1986).

¹¹⁴J. Melngailis, "Applications of ion microbeams in lithography and direct processing," *Handbook of VLSI Microlithography*, 2nd ed., J.N. Helbert, Ed., William Andrew Inc., pp. 790–855 (2001).

Chapter 16

Lithography in Integrated Circuit Device Fabrication

To see a world in a grain of sand
And a heaven in a wild flower
Hold infinity in the palm of your hand
And eternity in an hour.

William Blake, "Auguries of Innocence"

16.1 Introduction

The fabrication of IC devices used in the analog and digital electronics on which modern life so greatly depends involves a sequence of chemical and physical operations that are performed on silicon¹ wafers with the object of establishing connections between functional units such as amplifiers, inverters, adders, flip-flops, multiplexers, etc., designed to collectively perform predefined tasks, oftentimes involving logic or memory operations. These physical operations are grouped into four categories, namely, layering, lithographic patterning, etching, and doping.² The functional units are implemented by devices such as transistors, diodes, resistors, capacitors, and sometimes inductors. Of these devices, diodes

¹The choice of silicon as the substrate for building IC devices is not accidental. Silicon offers major processing advantages. It can be easily oxidized to form silicon dioxide, which is not only a high quality insulator but also an excellent barrier layer for the selective diffusion steps employed in IC fabrication. Furthermore, silicon is a very abundant element in nature, providing the possibility of a low cost starting material. In addition, it has a wider bandgap than germanium (the alternative material) and can therefore operate at higher temperatures than germanium.

²M. Quirk and J. Serda, *Semiconductor Manufacturing Technology*, p. 199, Prentice Hall, Englewood Cliffs, NJ (2001).

and transistors represent the main active³ components, while resistors, capacitors, and inductors represent passive⁴ components.

Figure 16.1 shows a layout of the various process modules used in the fabrication of IC devices in a typical semiconductor wafer fabrication facility. As discussed in Chapter 11, the lithography module plays a very critical role in the fabrication of these devices.

There are a variety of ways transistors can be categorized, including the following:

- (1) In terms of semiconductor material as silicon, germanium, gallium arsenide, and silicon carbide transistors.
- (2) In terms of structure as bipolar junction transistor (BJT), metal-oxide semiconductor field-effect transistor (MOSFET), etc.
- (3) In terms of polarity as NPN and PNP (for BJTs), *n*-channel and *p*-channel [for field-effect transistors (FETs)].

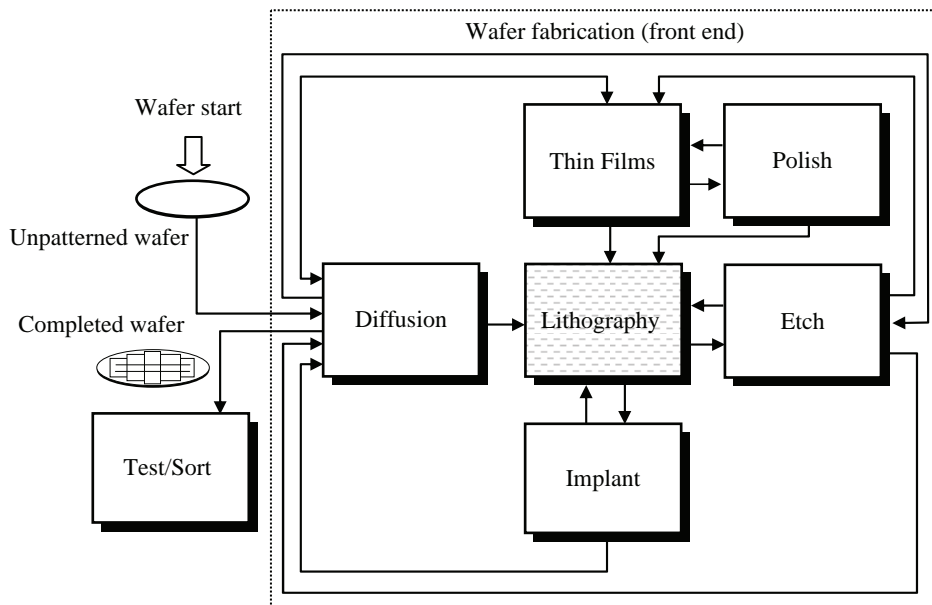


Figure 16.1 Wafer fabrication process flow. (Reproduced with permission from Advanced Micro Devices.)

³Active components can control voltages or currents and can also create switching action in electrical circuits. They are often used to control the direction of current flow; they are also used to amplify small signals and to create more complicated circuits such as current and voltage regulators, oscillators, and logic gates.

⁴Passive components contribute no power gain (or amplification) to an electrical circuit or system. They cannot perform control action and do not require any input other than a signal to perform their functions.

- (4) In terms of maximum power rating as low, medium, or high.
- (5) In terms of application as switch, general purpose, high voltage, audio, super-beta, or matched pair.
- (6) In terms of maximum operating frequency as low, medium, high, radio-frequency, microwave, etc.

While there are many different types of transistors, the two most widely used are the BJTs and the FETs, both of which have three electrodes, i.e., emitter, base, and collector in the case of BJTs, and source, gate, and drain in the case of FETs. Both are constructed on the surface of a monocrystalline silicon substrate. While the BJT requires input current at the base to turn on, the FET turns on as a result of an electric field created when an input voltage is applied to the gate, hence the name field-effect transistor. BJTs are primarily used in radios, tape recorders, automotive electronics, aircraft control systems, biomedical instrumentation, robotics, and wherever there is a need for high-power control. In contrast, FETs are widely used in linear and/or analog circuits and as a switching component in digital electronics, especially where low voltage and low power are required. In particular, they are widely used in instrumentation and communications applications. The low power consumption and compactness make FETs extremely suitable for the ever-shrinking dimensions of IC technology.⁵

FETs are of two basic types, namely, the junction FET (JFET) and the insulated gate FET (IGFET), the latter known generally as the metal-oxide semiconductor field-effect transistor (MOSFET). MOSFET was named based on its original construction as a layer of metal (the gate), a layer of oxide (the insulator), and a layer of semiconductor. As the thickness of silicon dioxide gate dielectric in advanced IC devices has reached dimensions (~ 2 nm) in which leakage current becomes a major concern, it is now being replaced with high-dielectric constant materials that allow for increased gate capacitance and thus increased device speed and performance, but without current leakage problems.

The main difference between the JFET and the MOSFET is that the gate on the MOSFET, which is the input to the FET, is insulated by a thin dielectric material (silicon dioxide, referred to as gate oxide) from the other two electrodes of the transistor. In contrast, the gate of the JFET forms a physical p - n junction⁶ with the other electrodes of the transistor. JFETs are used extensively in GaAs integrated circuits.⁷

MOSFETs gained wide acceptance in logic applications in the 1970s and have since remained the workhorse transistor in IC products. They are of two types,

⁵M. Quirk and J. Serda, *Semiconductor Manufacturing Technology*, p. 52, Prentice Hall, Englewood Cliffs, NJ (2001).

⁶A p n junction is formed wherever a region of n type semiconductor is adjacent to a region of p type semiconductor. p n junctions play important roles in the operation of all transistors.

⁷M. Quirk and J. Serda, *Semiconductor Manufacturing Technology*, p. 52, Prentice Hall, Englewood Cliffs, NJ (2001).

namely, nMOS (*n*-channel) and pMOS (*p*-channel). Each type is characterized by its majority current carriers.⁸ Figure 16.2 shows the cross sections of the two types of MOSFETs.

The gate is the input electrode in each MOSFET. The source and the drain electrodes are heavily doped with *n*-type or *p*-type dopants, respectively, consistent with the type of the transistor. These two electrodes supply the majority current carriers in the transistor. Because the nMOSFET uses electrons as the primary carriers, its channel is termed *n*-type. In contrast, the pMOSFET has a *p*-channel, formed by holes from the source to the drain. The *n*-channel MOSFET is fabricated inside a *p*-well, while the *p*-channel MOSFET is fabricated inside an *n*-well.⁹

While nMOSFETs and pMOSFETs were each separately used in making integrated circuits, starting from the 1970s, the nMOSFET systems outperformed and thus found wider applications than the pMOSFETs. Since the early 1980s, devices incorporating both nMOSFETs and pMOSFETs in the same integrated circuit, called CMOSs (complementary metal-oxide semiconductors), have become extremely popular, driven largely by the combination of power efficiency, design scaling techniques, and improved manufacturing. In particular, CMOS is currently the preferred IC technology for fabricating electronic products such as calculators, clocks, cellular telephones, computers, etc.¹⁰

Figure 16.3 is a cross-sectional diagram of a simple CMOS inverter circuit, showing its two transistors—pMOS and nMOS transistors. The gates serve as a single input to the inverter. The inverter's output is taken out of the two drains, which are tied together. Isolation regions are referred to as the field oxide and insulate transistors from each other in order to prevent the flow of undesirable leakage current between transistors. The metal layer serves to make electrical connections between the pMOS and nMOS transistors.¹¹

Given that CMOS technology is the most popular process technology for making ICs, we will use it to illustrate how IC devices are made. Specifically, we illustrate in the following sections the fabrication process steps of a 90-nm CMOS microprocessor device based on copper interconnect technology, with particular emphasis on how lithography is implemented in the entire process flow.

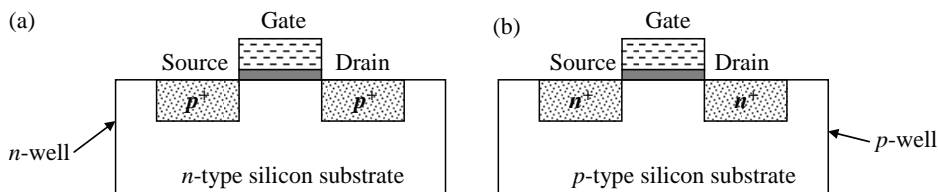


Figure 16.2 Two types of MOSFETs: (a) p-MOSFET (*p*-channel transistor) and (b) n-MOSFET (*n*-channel transistor).

⁸ibid., p. 53.

⁹ibid.

¹⁰ibid., p. 58.

¹¹ibid., p. 57.

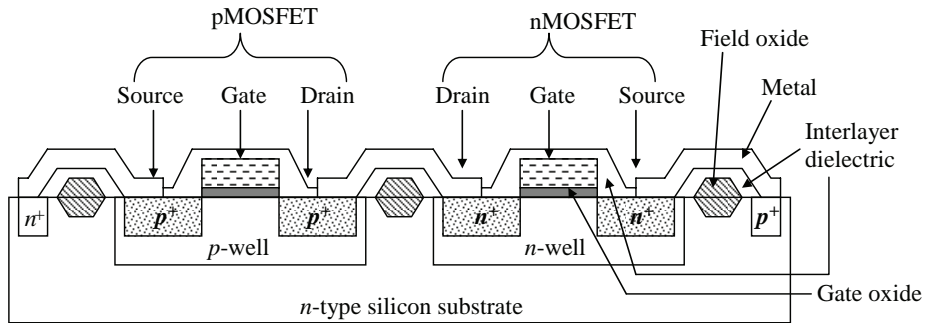


Figure 16.3 Schematic of a CMOS inverter.

The manufacture of the CMOS microprocessor, just like every other IC device, comprises the three phases of design, fabrication, and testing shown in Fig. 16.4. The first phase is the design phase, comprising the definition, circuit design and analysis, layout synthesis, verification, and tape-out¹² of the microprocessor from the design house. This phase relies heavily on CAD software.

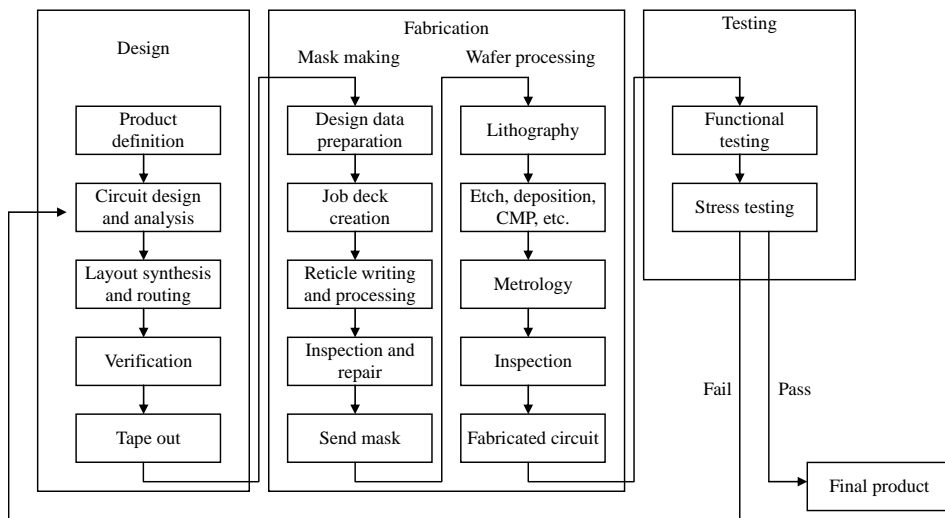


Figure 16.4 Steps used in the manufacture of an IC device. (Adapted from Ref. 13.)

¹²Tape out is the final stage of the IC design cycle, where the description of the IC device's design is sent to the fabrication facility to be manufactured. The root of the term dates back to the early era of PCB design, when an enlarged (to improve precision) drawing of the PCB was manually "taped out" of tape and adhesive covered PCB footprints on sheets of polyethylene terephthalate film. Following tape out, the drawing was reduced in size photographically to the appropriate size and subsequently used to create the lithographic mask of the device.

¹³A.K. K. Wong, *Resolution Enhancement Techniques in Optical Lithography*, p. 3, SPIE Press, Bellingham, WA (2001).

Following the tape-out of the microprocessor, the design is transferred from the computer to the mask in the mask house, through a series of steps that involve design data preparation, job deck creation, reticle writing and processing, inspection, and repair. If the reticle is judged to be an accurate representation of the microprocessor design, it is sent to the fab for wafer processing, i.e., to be transferred from the mask to the silicon wafer and used to fabricate the device structures. The structures are fabricated layer by layer through the repeated application of a number of basic processing steps that involve epitaxy, oxidation, lithography, etching, diffusion, evaporation or sputtering, ion implantation, CVD, chemical mechanical polishing, etc.¹⁴

The oxidation process involves heating the silicon wafer to a temperature of 1000–1200°C in the presence of oxygen to form silicon dioxide. Metal films are deposited by means of sputtering. Earlier, evaporation involving heating the metal to its melting point in a vacuum was used to deposit metal films. Thin films of silicon nitride, silicon dioxide, and polysilicon are formed through CVD, in which the material is deposited out of a gas mixture onto the surface of the wafer. It is also possible to deposit some insulators by sputtering,¹⁵ and some metals via CVD.¹⁶

The formation of shallow *n*- and *p*-type layers and junctions is now exclusively done by ion implantation, in which the wafer is bombarded with high-energy donor or acceptor atoms generated in a high-voltage particle accelerator.¹⁷

The fabrication of IC devices requires that the *n*- and *p*-type regions be formed selectively in the surface of the wafer. Silicon dioxide, silicon nitride, polysilicon, and especially resists are typically used to mask (or cover) specific areas of the wafer surface to prevent them from being penetrated by impurities during ion implantation or diffusion. The wafer areas to be implanted or deposited with conducting metals are defined with the aid of lithography.

Lithography in general includes the overall process of mask fabrication as well as the process of transferring patterns from the mask to the surface of the wafer. The lithographic process is very critical to the production of ICs, so much so that the number of lithographic masking steps is often used as a measure of complexity when comparing fabrication processes.¹⁸ Dry etch processing is used to open the windows of the areas defined by lithography into the underlying layers.

At the end of the wafer processing, the wafer with the IC devices is inspected for defects and reviewed with relevant metrology. If the defect level is acceptable, the IC wafer is sent to the testing facility, where it is electrically probed to check for electrical performance. Next, the IC wafer is stress tested, which involves operating it at the extremes of its specified typical use conditions. If the IC wafer passes the functional and stress tests, it is sent to the packaging facility, where bond pad

¹⁴R.C. Jaeger, *Introduction to Microelectronic Fabrication*, Vol. V, in Modular Series on Solid State Devices, G.W. Neudeck and R.F. Pierret, Eds., p. 4, Addison Wesley, New York (1987).

¹⁵*ibid.*, pp. 5–6.

¹⁶*ibid.*, p. 5.

¹⁷*ibid.*, pp. 5–6.

¹⁸*ibid.*, p. 6.

metals are bonded to it at the relevant locations, followed by the application of a passivation layer to protect it from environmental and particulate hazards and contamination.

16.2 Fabrication of a 90-nm CMOS Microprocessor

A possible fabrication process flow for a single 90-nm technology node microprocessor CMOS inverter, consisting of two transistors—nMOS and pMOS—is presented in this section. Cross-sectional views of the inverter are provided for each major operation, with the operations involving lithographic masking called out with thicker lines, where possible. It must be noted that the illustration is for only a small microscopic area of a microprocessor that is one of hundreds of microprocessors that may populate a given 300-mm wafer at the end of the fabrication process.

The CMOS manufacturing steps¹⁹ to be described below include: (i) twin-well process, (ii) shallow trench isolation process, (iii) polygate process, (iv) lightly doped drain (LDD) implant process, (v) sidewall spacer formation process, (vi) source/drain (S/D) implant processes, (vii) contact formation process, (viii) via and tungsten plug formation processes, (ix) copper interconnect wiring formation by means of a dual damascene process, (x) bond pad metal formation and packaging processes, and (xi) wafer testing and sorting.

16.2.1 Twin-well process

The twin-well process is typically the first step in CMOS wafer fabrication and is used to define the active regions of the nMOS and pMOS transistors. A twin well consists of a p -well and an n -well, with each well requiring some number of steps to fabricate. The twin-well process thus consists of two processes: n -well formation and p -well formation.

16.2.1.1 n -well formation

Figure 16.5 shows the process sequence executed in n -well formation. Six distinct processes are implemented: epitaxial growth, initial oxide growth, n -well lithographic masking, n -well implantation, resist stripping and cleaning, and annealing.

¹⁹There are many excellent books on CMOS fabrication; see, for example, M. Quirk and J. Serda, *Semiconductor Manufacturing Technology*, Prentice Hall, Englewood Cliffs, NJ (2001); S. Gandhi, *VLSI Fabrication Principles: Silicon and Gallium Arsenide*, 2nd ed., John Wiley & Sons, Hoboken, NJ (1994); R.C. Jaeger, *Introduction to Microelectronic Fabrication*, Vol. V, in Modular Series on Solid State Devices, G.W. Neudeck, R.F. Pierret, Eds., Addison Wesley, New York (1993). For our purposes in this chapter, we adapt the methods described by Quirk and Serda in the above named book.

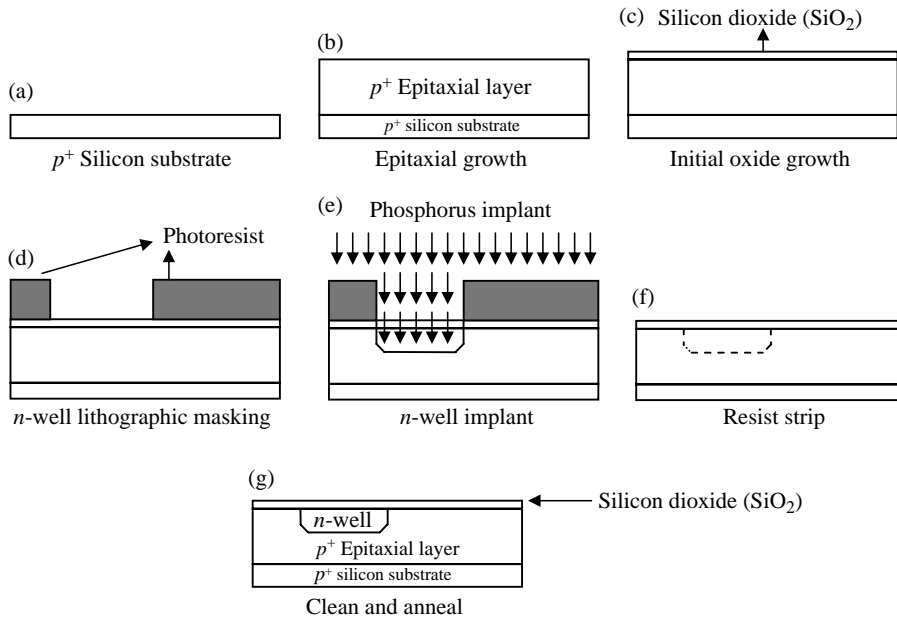


Figure 16.5 Process sequence for n -well formation: (a) p^+ silicon substrate, (b) epitaxial growth, (c) initial oxide growth, (d) n -well lithographic masking that defines the area to be implanted, (e) n -well implantation with phosphorus ions, (f) resist stripping and cleaning, and (g) annealing of the implanted wafer.

The starting silicon wafer that has been lightly doped with a p -type dopant (boron) is first subjected to a deposition of a thin layer of epitaxial silicon (epilayer). The epilayer has the same crystal structure as the silicon substrate, except that it is purer and has fewer crystal defects than a pure silicon wafer. After cleaning the epitaxial silicon wafer in a series of chemical baths to remove particles, organic and inorganic contaminants, and native oxide growth, the wafer is oxidized in a high-temperature ($\sim 1000^\circ\text{C}$) furnace in the presence of oxygen to form a thin layer of silicon dioxide (SiO_2), which protects the epitaxial silicon surface from contamination, prevents its excessive damage during implantation, and serves as a screen oxide that helps to control the depth of the dopants during implantation.

The n -well lithographic masking step (involving mask #1; These mask numbers denote the sequence/order in which the lithographic masks are used in the IC device fabrication process flow, highlighting each lithographic masking step. They also indicate that these masks are different from one another, each playing a distinct role in defining the features to be fabricated. By their sheer number—nine in the case described in this chapter—one gets a sense of how critical lithography is in device fabrication.) defines the areas of the inverter to be implanted in order to form the n -well for the pMOS transistor, while covering with the resist the areas that are not to be implanted with the ions. A high-energy phosphorus implantation is performed that implants phosphorus ions into the

n-well region through the openings created in the resist layer with the aid of lithography. The implanting dopant ions penetrate the crystal lattice of the silicon, causing damage to the covalent atomic structure. This damage will be repaired in the annealing step.

Following the phosphorus ion implantation, the resist layer is stripped off in an oxygen-plasma etcher, and subsequently cleaned by a wet chemical process to remove residual resists and polymers created by the plasma process. The silicon dioxide on the wafer surface is also removed during this step.

Finally, the wafer is annealed in a high-temperature furnace. The annealing process accomplishes the following three objectives: (i) The high temperature causes the diffusion of the dopants, resulting in their uniform distribution within the target area. (ii) It repairs the damage caused by the implant. (iii) It activates the bonds between the dopant atoms and the silicon atoms, making the dopant atoms a part of the silicon crystal lattice structure.

16.2.1.2 *p*-well formation

Figure 16.6 shows the process sequence executed in *p*-well formation. The lithographic masking step (involving mask #2) is the same as that for the *n*-well implant mask. It defines the area of the inverter to be implanted to form the *p*-wells for the nMOS transistors. A boron implantation is performed, followed by resist stripping and cleaning. Annealing is done in basically the same manner as described above for the *n*-well.

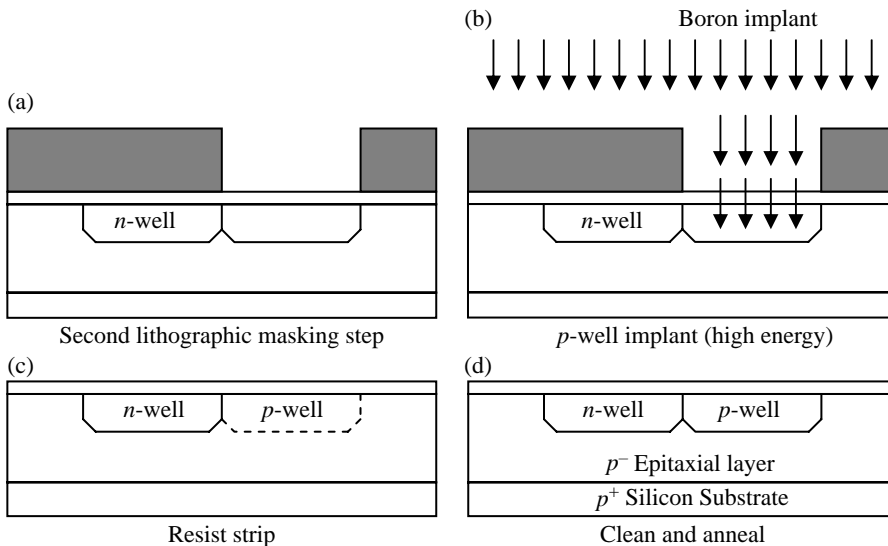


Figure 16.6 Process sequence for *p*-well formation: (a) *p*-well lithographic masking step (mask #2), (b) *p*-well implantation with boron ions, (c) resist stripping and cleaning, and (d) annealing of the implanted wafer.

16.2.2 Shallow trench isolation process

Following the *n*-well and *p*-well formations, the wafer undergoes the shallow trench isolation (STI) process, which serves to create isolation regions between active transistor areas on the substrate. It comprises three major steps that follow each other sequentially, namely, trench etch, oxide fill, and oxide polish (see Fig. 16.7). The trench etch begins with the wafer being cleaned to remove contamination and oxide, after which the wafer undergoes a high-temperature oxidation in a furnace in the presence of oxygen. A thin layer of silicon dioxide forms on the surface of the wafer. This layer will form a barrier to protect active regions from chemical contamination during the nitride stripping process later. Silicon nitride (Si_3N_4) is then deposited by a low-pressure chemical vapor deposition (LPCVD) process involving high-temperature reaction of ammonia and dichlorosilane gases. The nitride serves as both an implantation mask and an oxidation mask, preventing oxygen diffusion into the active regions during STI oxide deposition; it also serves as a polish-stop material during the chemical mechanical polishing (CMP) step.

The STI lithographic masking step (involving mask #3) is next implemented to define the location of the STI trench, while covering and/or protecting with resist the other areas of the silicon that are not to be etched. Following lithographic masking, plasma etching is used to etch away the nitride layer and the underlying silicon in the isolation regions. The slanted profile and the rounded bottoms of the trenches are designed to improve the filling process and the electrical characteristics of the isolation structure. At the completion of the etch operation, the wafer is stripped of resist and wet cleaned.

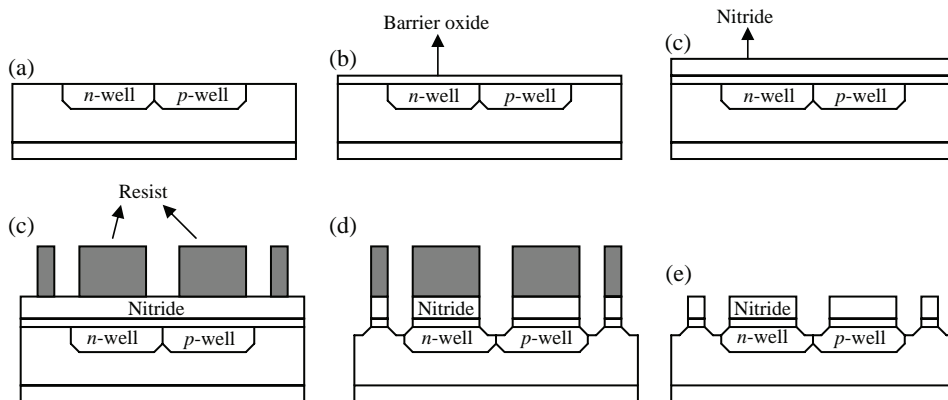


Figure 16.7 Process sequence for STI trench etch: (a) cleaning of the wafer, (b) barrier oxide deposition, (c) nitride deposition, (d) STI lithographic masking (involving mask #3) to define isolation region, and (e) selective opening of isolation areas in the epitaxial layer by the STI trench etch. Then the wafer is stripped of resist and finally, cleaned.

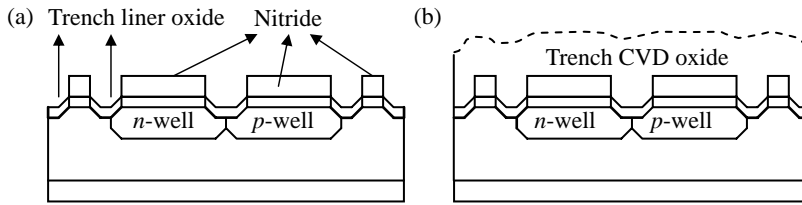


Figure 16.8 Process sequence for STI oxide fill: (a) trench liner oxide deposition and (b) trench oxide fill with CVD oxide.

16.2.2.1 STI oxide fill

Following the STI etch operation, the wafer is again cleaned to remove contamination and surface oxide, after which it undergoes a high-temperature oxidation in a furnace in the presence of oxygen. This results in the growth of a thin layer of silicon dioxide (called the liner oxide) in the exposed walls of the isolation trenches. The liner oxide serves to improve the interface between the silicon and the trench CVD oxide that will be subsequently deposited. The trench is then filled with CVD oxide (see Fig. 16.8).

16.2.2.2 STI oxide polish and nitride strip

The next operation after the deposition of the trench CVD oxide is polishing its surface to planarize it (see Fig. 16.9). This is done in a CMP operation, in which the wafer is turned upside down and is polished with a polishing pad with the aid of a chemical slurry that controllably abrades the surface of the oxide until it reaches the nitride layer. Being harder than the oxide, the nitride layer serves as the polish-stop material to prevent overpolishing the isolation structures. After polishing, the wafer is thoroughly cleaned to remove the particles and chemical contaminants that are generated during CMP.

The nitride stripping operation completes the STI process. Hot phosphoric acid is used to strip the nitride film from the wafer, after which the wafer is cleaned and dried.

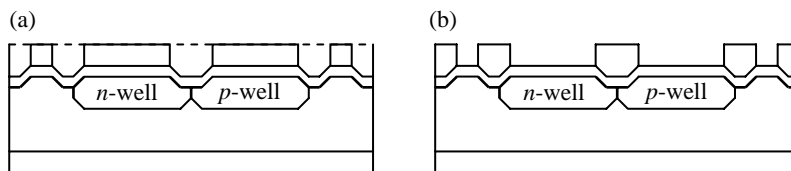


Figure 16.9 Process sequence for STI oxide polish and nitride stripping: (a) CMP of trench oxide and (b) nitride stripping with hot phosphoric acid.

16.2.3 Polysilicon gate process

The polysilicon gate process (see Fig. 16.10) begins with a high-temperature oxidation of the cleaned wafer following the STI process in an oxidation furnace. This results in the growth of a thin layer of silicon dioxide on the epitaxial silicon layer over the *n*-well and *p*-well regions. Polysilicon is then deposited over the entire wafer by means of an LPCVD-process-induced dissociation of silane (SiH_4) gas. The gate lithographic masking step (involving mask #4) is used to define the polysilicon gate region of the transistors. Using anisotropic plasma etching, polysilicon is etched away everywhere on the wafer, except the gate regions. Following plasma etching, the remaining resist and antireflection coating are stripped and cleaned off the wafer.

16.2.4 Lightly doped drain implant processes

The next process after the gate process is used to define the source and drain regions of the transistors. Each pMOS and nMOS transistor is implanted twice—once with a shallow implant process called the lightly doped drain (LDD) implant, and subsequently with a medium or high dose S/D implant (see Section 16.2.6 below). The LDD implant process uses considerably larger dopant species—arsenic and boron difluoride—to create an amorphous upper layer of silicon. It is the combination of large mass and amorphous surface conditions that helps to maintain a shallow junction, which in turn helps to reduce channel current leakage between the source and drain, an emerging problem, particularly as the gate width (and hence

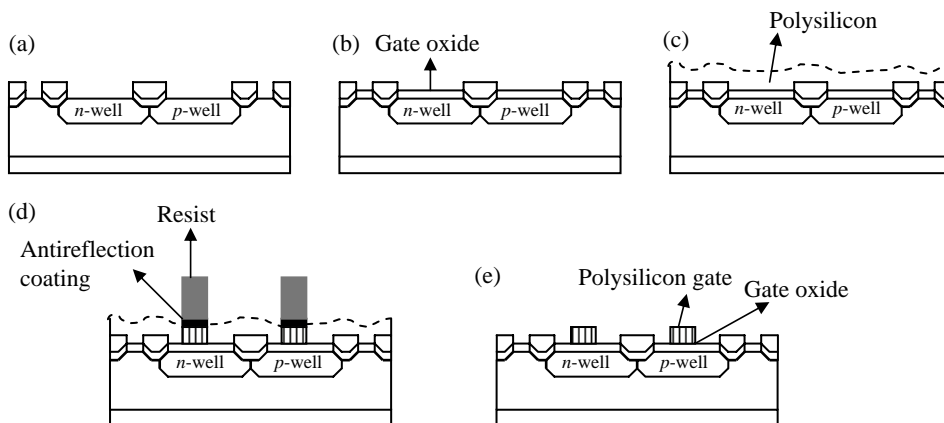


Figure 16.10 Process sequence for gate process: (a) cleaning of the STI wafer, (b) gate oxide growth, (c) polysilicon deposition by means of an LPCVD process involving silane, (d) gate lithographic masking (involving mask #4), (e) polygate etch process, in which polysilicon is etched away everywhere on the wafer except over the gate regions and the active areas. Then the wafer is stripped of resist and antireflection coating, and finally cleaned.

the channel length below the gate structure) becomes increasingly smaller. The LDD implant process comprises two main steps: n^- LDD implant and p^- LDD implant. LDD is used to reduce short channel effects and hot carrier effects.

16.2.4.1 n^- LDD implant

The n^- LDD implant lithographic masking process step (involving mask #5) is the first step in the n^- LDD implant process (see Fig. 16.11), and is used to define the n -channel transistor regions, which involves opening up windows in the n -channel transistor areas while protecting all other areas with resist. Next, arsenic ions are selectively implanted through the windows in the patterned resist layer. It should be noted that arsenic is preferred over phosphorus because with its larger mass, it is able to amorphize the silicon surface in such a manner as to create a uniform dopant distribution at the target depth.

16.2.4.2 p^- LDD implant

The p^- LDD implant lithographic masking step (involving mask #6) is first used to define the p -channel transistor regions; this involves opening up windows in the p -channel transistor areas while protecting all other areas with resist. Boron difluoride (BF_2) is then used to implant the p -channel transistor region through the windows created above. The use of the heavier BF_2 (instead of boron) is intended to amorphize the silicon. The process ends with the stripping and cleaning of the layer off the wafer (see Fig. 16.12).

16.2.5 Sidewall spacer formation

Sidewall spacers are formed alongside the polygates to prevent the high-dose dopants used in the S/D implant step from penetrating too close to the channel where S/D punch-through could occur. The sidewall spacer formation process comprises two major process steps. These include the deposition of a CVD oxide layer across the surface of the wafer, followed by etching back of this

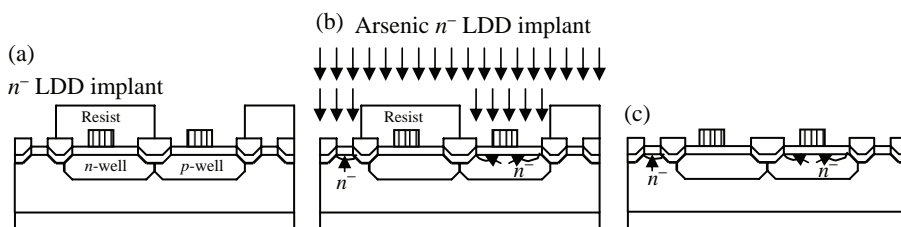


Figure 16.11 Process sequence for the n^- LDD implant process: (a) n^- LDD implant lithographic masking (involving mask #5), (b) n^- LDD implant with arsenic, and (c) resist stripping and cleaning.

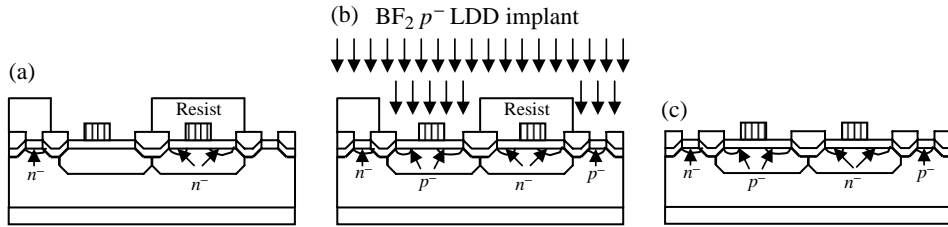


Figure 16.12 Process sequence for p LDD implant process: (a) p LDD implant lithographic masking (involving mask #6), (b) n LDD implant with BF_2 , and (c) resist stripping and cleaning.

oxide by means of anisotropic plasma etching that is stopped when the polysilicon is exposed. No lithographic masking step is performed in this step because the anisotropic etch process sputters away most of the oxide. The etch process does leave behind a thicker oxide on the sidewalls of the polysilicon gates (see Fig. 16.13).

16.2.6 Source/drain implant process

Following the spacer formation, medium-dose implants are made to penetrate the silicon slightly beyond the LDD junction depth, but not as deep as the original twin-well implants (see Section 16.2.1). The spacer oxide from the previous step serves to protect the channel from the dopant atoms during the implant process. There are two S/D implant processes, namely, n^+ S/D implant and p^+ S/D implant.

16.2.6.1 n^+ S/D implant

The n^+ S/D implant lithographic masking (involving mask #7) is first used to define areas of the nMOS transistors that are to be implanted, following which arsenic dopants of medium energy are implanted through the windows created by the preceding lithographic masking step (see Fig. 16.14). At the end of the process, the resist layer protecting the areas that were not implanted is stripped off the wafer, followed by cleaning of the wafer.

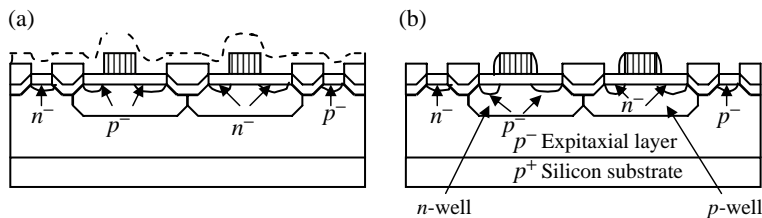


Figure 16.13 Process sequence for the sidewall spacer formation: (a) spacer oxide deposition and (b) spacer oxide etch back.

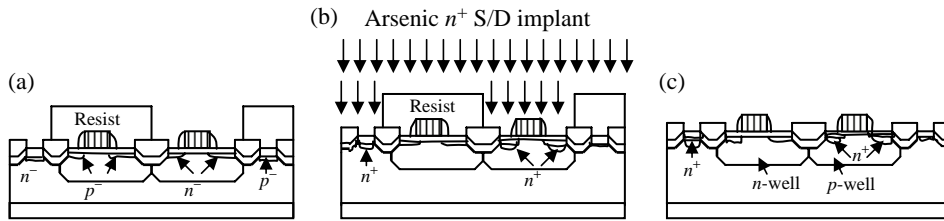


Figure 16.14 Process sequence for n^+ S/D implant formation: (a) n^+ S/D implant lithographic masking (involving mask #7), (b) arsenic n^+ S/D implant, and (c) resist stripping and cleaning.

16.2.6.2 p^+ S/D implant

The formation of the p^+ S/D regions begins with the p^+ S/D implant lithographic masking step (involving mask #8), which defines the areas of the pMOS transistors that are to be implanted. Next, the boron p^+ dopants are implanted through the windows created by the lithographic step above. Again, the spacer oxide prevents boron dopant from encroaching into the narrow channel. Then, the wafer is annealed in a rapid thermal process in which the temperature quickly reaches up to 1000°C and is maintained at that temperature for several seconds (see Fig. 16.15). This condition prevents spreading of dopants and helps to control diffusion of dopants in the S/D regions.

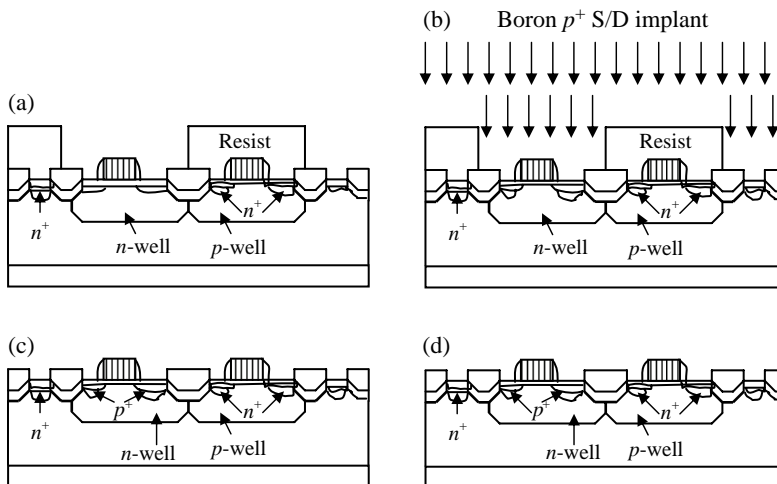


Figure 16.15 Process sequence for p^+ S/D implant formation: (a) p^+ S/D implant lithographic masking (involving mask #8), (b) boron p^+ S/D implant, (c) resist stripping and cleaning, and (d) annealing of the wafer.

16.2.7 Contact formation

Metal contacts are formed on all active areas of silicon during the contact formation process steps. The metal contacts serve to provide a low-resistance path between the silicon and the metal conductor material that is subsequently deposited. Titanium or cobalt are typically used. Both metals have low resistivity characteristics and do react very well with silicon to form titanium silicide (TiSi_2) and cobalt silicide (CoSi_2) compounds, respectively. Neither titanium nor cobalt reacts with SiO_2 ; therefore, no chemical bonding or physical connection is established between these metals and SiO_2 . As a result, both metals can be easily etched off SiO_2 without the need for a lithographic masking step. TiSi_2 and CoSi_2 remain at all locations where active silicon exists, such as at the source, drain, and gate areas.

The contact formation process steps (see Fig. 16.16) begin with titanium or cobalt deposition, as the case may be, after the wafer has been thoroughly cleaned of contaminants and surface oxides. The deposition is typically by sputtering, resulting from a physical vapor deposition (PVD) process in which energetic argon ions bombard the metal target, releasing metal atoms, which deposit on the wafer. Next, the wafer is annealed at a high temperature, which triggers a chemical reaction between the titanium (or cobalt) with silicon that forms their corresponding silicide. Then, chemicals are used to etch away unreacted titanium (or cobalt), leaving behind TiSi_2 or CoSi_2 over the active areas of the silicon wafer.

16.2.8 Via-1 and tungsten plug formation

With the titanium silicide contacts in place, the next step in the CMOS fabrication process flow is the via-1 and tungsten plug formation, which involves the formation of metal connecting lines between transistors and other titanium silicide contacts.

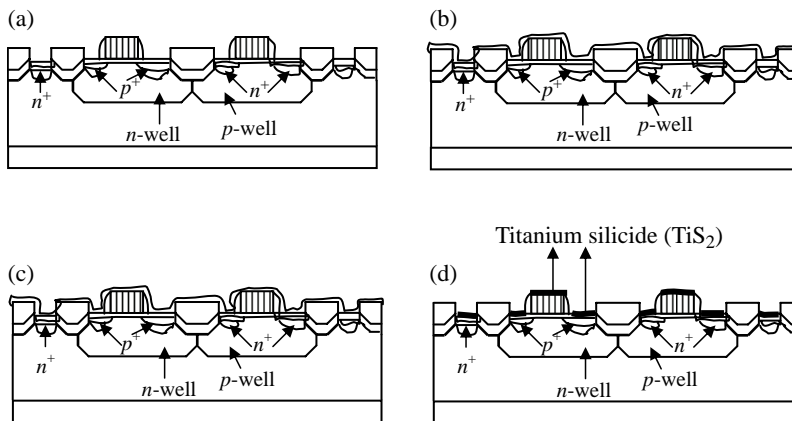


Figure 16.16 Process sequence for contact formation: (a) wafer cleaning, (b) titanium deposition, (c) high-temperature anneal leading to the formation of TiSi_2 , and (d) titanium etch. Cobalt can be used in place of titanium.

The via-1 and tungsten plug formation process begins with the deposition of dielectric films, followed by CMP, lithographic patterning, etch processing step, tungsten deposition, and ending with tungsten polishing. These processes are grouped into two categories, involving the via-1 formation and the tungsten plug formation. A description of the processes involved in each of the categories is provided below.

16.2.8.1 Via-1 formation

The via-1 formation process (see Fig. 16.17) begins with the deposition of an inter-layer dielectric (ILD), ILD-1 oxide, on the wafer with a CVD tool. This layer serves as the dielectric material in which vias are to be formed. Vias are openings created in the ILD to provide an electrical pathway from one metal layer to adjacent metal layers. CMP is used to polish off the ILD-1 oxide to planarize the surface, following which the wafer is cleaned to remove particles generated during the polishing process. The via-1 lithographic masking step (involving mask #9) is used to define via windows in the dielectric oxide. An etch step is used to transfer the via-1 openings into the ILD-1 oxide layer, following which the wafer is cleaned.

16.2.8.2 Tungsten plug formation

First, a thin barrier layer of titanium is deposited by PVD on the wafer to line the bottom and the inside walls of the via-1 holes. The titanium serves to improve the adhesion of the tungsten plug to the ILD-1 oxide. Next, titanium nitride (TiN) is immediately deposited over the titanium as a diffusion barrier for the tungsten metal. Then, tungsten metal is deposited by CVD to fill the via-1 holes and coat the entire wafer. Finally, the tungsten is polished down to the upper surface of

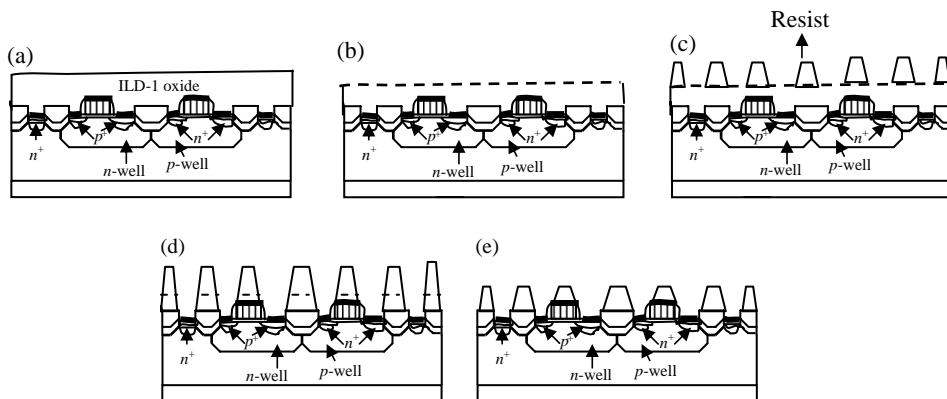


Figure 16.17 Process sequence for via-1 formation: (a) ILD-1 oxide (SiO_2) deposition, (b) CMP of ILD-1 oxide, (c) via-1 lithographic masking (involving mask #9) to define the via-1 windows in which the tungsten plug will be subsequently deposited, (d) etch step to open up via holes in the ILD-1 oxide, and (e) resist strip and clean.

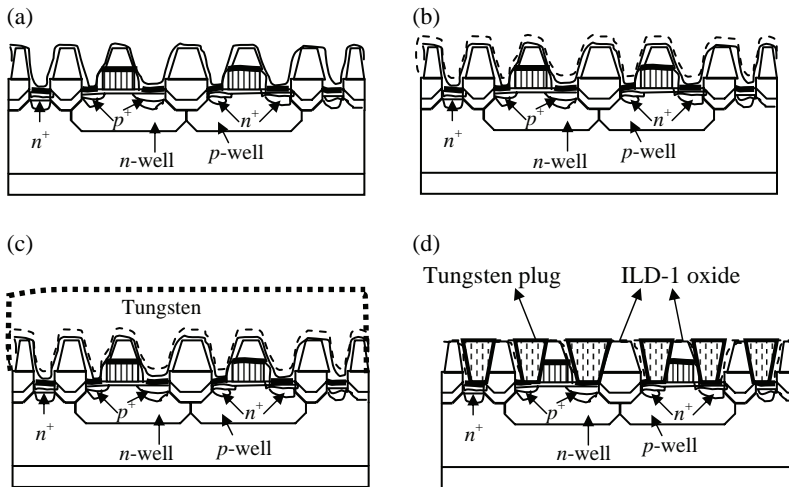


Figure 16.18 Process sequence for tungsten plug formation: (a) titanium barrier metal deposition by means of PVD, (b) titanium nitride deposition, (c) tungsten deposition by means of CVD, and (d) tungsten polish.

the ILD-1 oxide (see Fig. 16.18). Tungsten offers some unique advantages as a plug: It fills holes and/or trenches without leaving voids in the formed metal plug; it also has good polishing characteristics.

16.2.9 Copper interconnect wiring formation by means of the dual damascene²⁰ technique

Copper interconnect formation relies on the dual damascene technique, which creates both the vias and lines for each metal layer by etching holes and trenches in the ILD, depositing copper in the etched features, and using CMP to remove the excess copper. This differs from the traditional metallization scheme in which a blanket layer of aluminum alloy metal is deposited on the dielectric layer and then patterned and etched to form the metal lines. The unique attribute of the dual damascene approach deals with the fact that the dielectric etch defines the critical line width and spacing, instead of the metal etch. Also, in contrast to the traditional metallization, which relies on metallic etching, the copper interconnect using damascene avoids any kind of metallic etching, including copper.²¹

²⁰The name damascene derives from a technique of making inlaid metals that originated in ancient Damascus, now in present day Syria. See, for example, P. Singer, "Making the move to dual damascene processing," *Semiconductor Int.*, pp. 70–82 (Jan. 1999).

²¹M. Quirk, J. Serda, *Semiconductor Manufacturing Technology*, p. 326, Prentice Hall, Englewood Cliffs, NJ (2001).

Copper interconnect technology was adopted in the IC industry starting from about the 150-nm technology node. Technology nodes of 180 nm and larger were based on aluminum interconnect technology. Copper interconnect technology offers several advantages over the older aluminum interconnect technology, and it was for these advantages that the IC industry shifted from aluminum to copper interconnect technology. First, copper has lower resistivity ($1.678 \mu\Omega\text{-cm}$) than aluminum ($2.65 \mu\Omega\text{-cm}$) at 20°C , which means that its lower resistance reduces the resistance-capacitance (RC) signal delay, thereby increasing the speed of ICs fabricated with it relative to those fabricated with aluminum. Copper is a relatively soft metal, and thus can be easily polished and planarized by CMP. Copper has superior resistance to electromigration, a common reliability problem with aluminum.²² This implies that ICs fabricated with copper can handle higher electrical power densities, permitting the development of new products when compared to systems fabricated with aluminum interconnects.²³

Copper interconnect technology is, however, not without drawbacks.²⁴ Copper diffuses readily in oxides and silicon, a major problem if it diffuses into the active region of the device (such as the source, drain, and gate regions of the transistor), where it will create junction or oxide leakage. It cannot be easily etched with regular plasma etching because it does not produce a volatile by-product from its chemical reaction with the plasma. Although it oxidizes quickly in air at low temperatures ($<200^\circ\text{C}$), it does not form a protective layer to stop further oxidation.²⁵

All of these challenges and/or drawbacks are addressed by dual damascene processing with special barrier metals optimized for copper. In particular, the dual damascene processing approach to copper metallization eliminates the need to etch copper, as stated above. A second advantage to dual damascene processing is that it eliminates the need for a dielectric gap fill between etched metal lines, since the dielectric is applied as a blanket and then etched. Furthermore, it uses 20–30% fewer steps than a traditional aluminum interconnect, leading to significantly reduced manufacturing costs compared with those associated with the former.²⁶ In addition, the use of tungsten plugs (described above) overcomes the concern of copper contaminating the silicon.

The essential detail in the dual damascene technique is outlined in Fig. 16.19. It begins with the deposition of a blanket SiO_2 ILD oxide by means of the plasma-enhanced chemical vapor deposition (PECVD) technique to the desired thickness for the via. Next, a dense thin film of SiN is deposited on the ILD oxide by means of the high-density chemical vapor deposition (HDPCVD) technique.

²²A. Sethuram, J.F. Wang, and L. Cook, "Copper vs. aluminum: a planarization perspective," *Semiconductor Int.*, p. 178 (June 1996).

²³M. Quirk and J. Serda, *Semiconductor Manufacturing Technology*, pp. 305–306, Prentice Hall, Englewood Cliffs, NJ (2001).

²⁴X. Lin and D. Pramanik, "Future interconnect technologies and copper metallization," *Solid State Technol.*, p. 63 (Oct. 1998).

²⁵M. Quirk and J. Serda, *Semiconductor Manufacturing Technology*, p. 307, Prentice Hall, Upper Saddle River, NJ (2001).

²⁶*ibid.*, pp. 306–308.

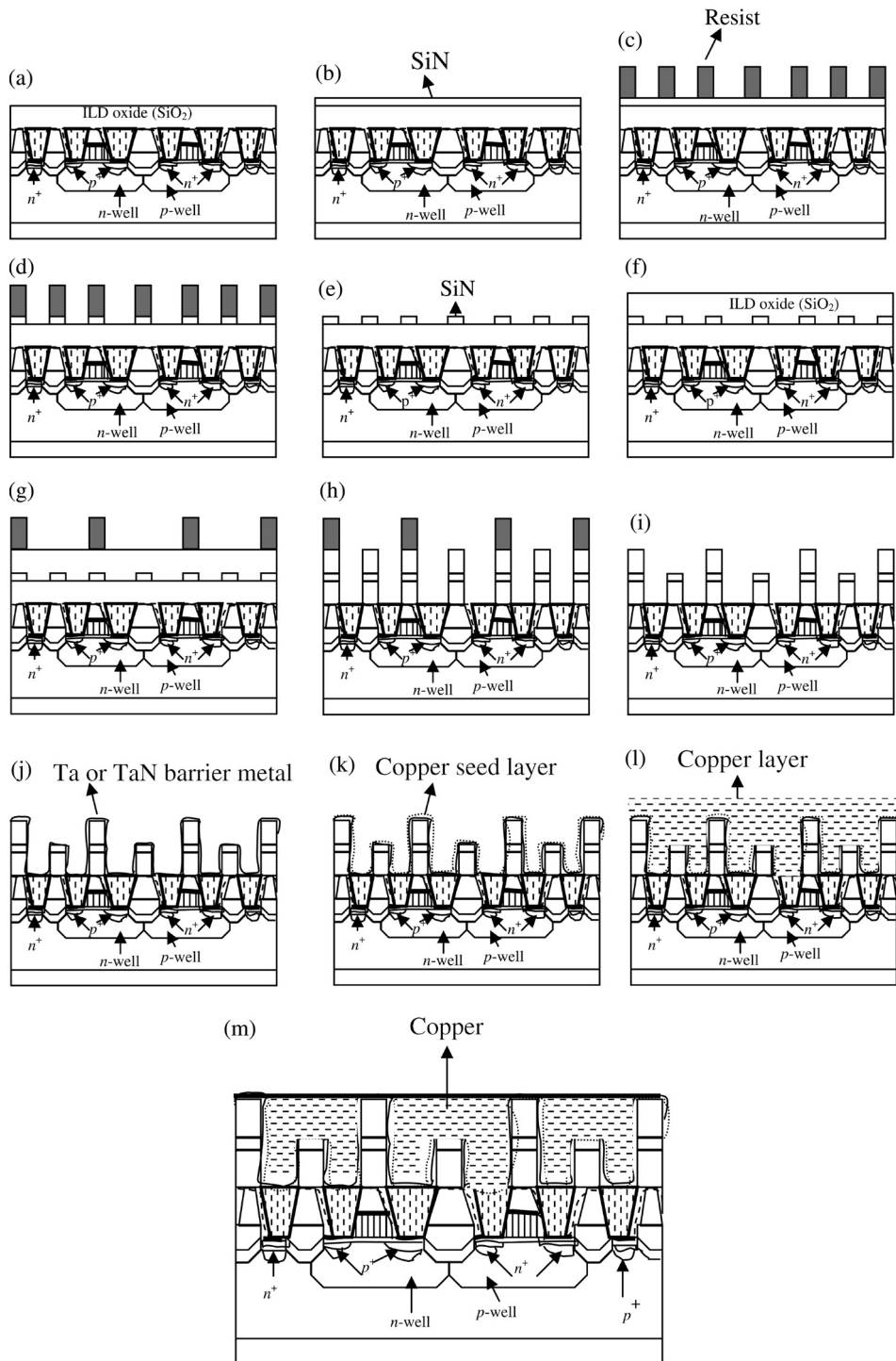


Figure 16.19 Process steps for dual damascene copper interconnect formation: (a) ILD oxide (SiO_2) deposition by means of PECVD; (b) silicon nitride (SiN) deposition

This SiN will serve as an etch-stop layer. Then, lithographic masking is used to pattern via openings on the SiN with resist. This is followed by a dry etch step to pattern transfer the via openings into the underlying SiN, at the completion of which the remaining resist is stripped. Next, additional ILD oxide is deposited by means of PECVD over the entire structure. Then, the second lithographic masking is used to pattern the SiO₂ trench with resist. The previously patterned via openings are now located under the trench. A dry etch process step is used to pattern transfer the trench into the underlying ILD oxide, stopping on the SiN layer, but continuing to form via openings by passing through the opening in the SiN, until it reaches the metal-1 (tungsten plug). This is called the “trench-first” approach. An alternate method, called the “via-first” approach patterns the via first, before opening up the trench.²⁷

Tantalum (Ta) or tantalum nitride (TaN) is deposited into the hole created by the previous etch process, covering the bottom and sidewalls of the trench and vias. This film serves as a barrier metal for copper. Next, a copper seed layer is deposited on top of the Ta or TaN barrier layer. Then, copper is electrochemically deposited into the trench and via openings, filling both. This electroplating of copper is accomplished in a way that immerses the wafer with a conductive surface into an aqueous solution of copper sulfate (CuSO₄), which contains copper ions to be deposited. The wafer and its seed layer are connected electrically to an external power supply as a negatively charged electrode, or cathode. A solid piece of copper is configured as the positively charged electrode, or anode, and immersed in a copper sulfate solution. When electrical current is passed through the wafer, into the solution, and through the copper anode, the following reduction reaction occurs at the wafer surface, depositing copper metal inside the trench and via openings created above:²⁸

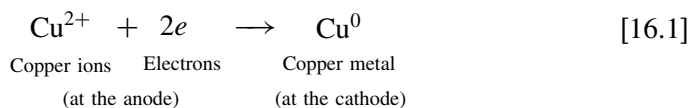


Figure 16.19 (Continued) by means of HDPCVD; (c) lithographic masking to define via openings; (d) dry etch process to open and pattern transfer via openings into SiN layer; (e) resist stripping and cleaning; (f) ILD oxide (SiO₂) deposition by means of PECVD; (g) lithographic masking to define trench openings. Previously patterned via openings are located in the ILD layer under the trench; (h) dry etch process to open and transfer trench into ILD oxide, stopping on the SiN layer, while continuing on to underlying ILD through via openings in SiN; (i) resist stripping and cleaning; (j) deposition of Ta or TaN barrier metal; (k) deposition of copper seed layer; (l) electrochemical deposition of copper, filling both via opening and trench, and (m) chemical mechanical polishing to remove excess copper and planarize the surface.

²⁷:ibid., pp. 326–327.

²⁸:ibid., p. 324.

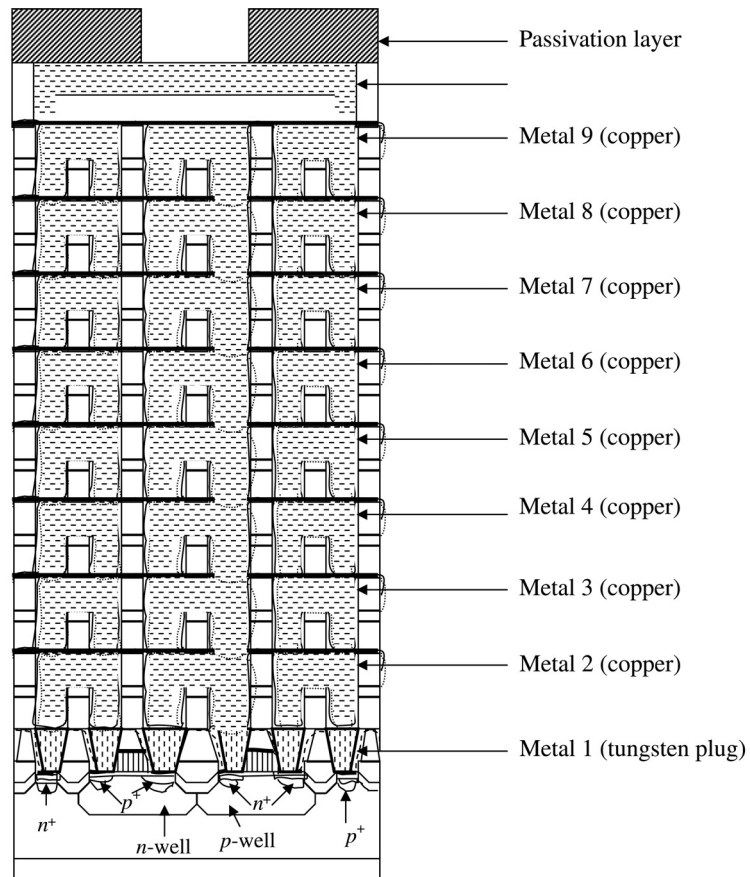


Figure 16.20 Cross section of a full 90-nm IC CMOS inverter with nine copper metal layers.

In this reaction, the anode generates copper ions and electrons, and undergoes oxidation. These copper ions migrate to the cathode (the wafer), where they are reduced to metallic copper. Using Faraday's law of electrolysis, which states that the quantity of copper deposited is directly proportional to the current delivered to the wafer, it is possible to control the amount of copper and the rate of its deposition into the trench and via openings by adjusting the amount of current and time duration of the deposition process.²⁹

Finally, the excess copper is polished away by means of CMP. This process step planarizes the surface and prepares it for the next level. The dual damascene technique can be repeated as many times as necessary, until the required number of copper metal layers are formed.

²⁹ibid., p. 325.

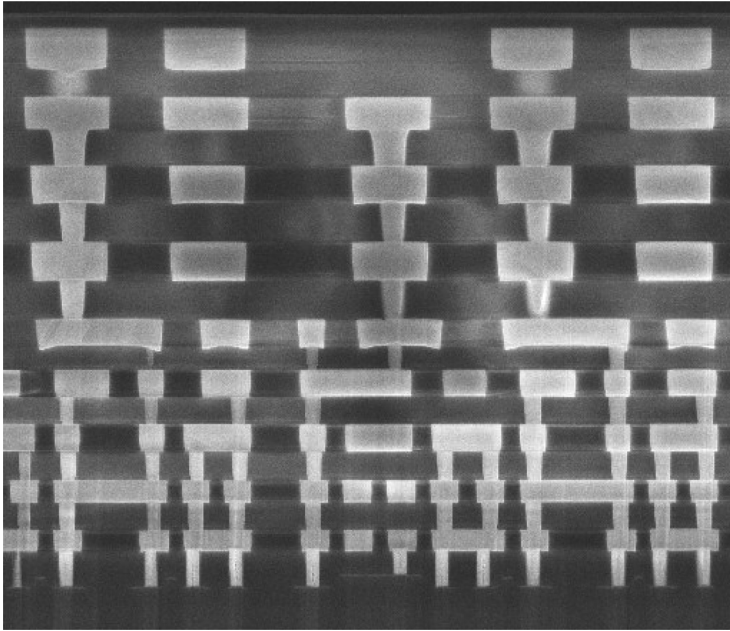


Figure 16.21 SEM micrograph of a cross section of a 90-nm technology node AMD microprocessor, with nine copper metal layers, fabricated with copper interconnect technology. (Reproduced with permission from AMD.)

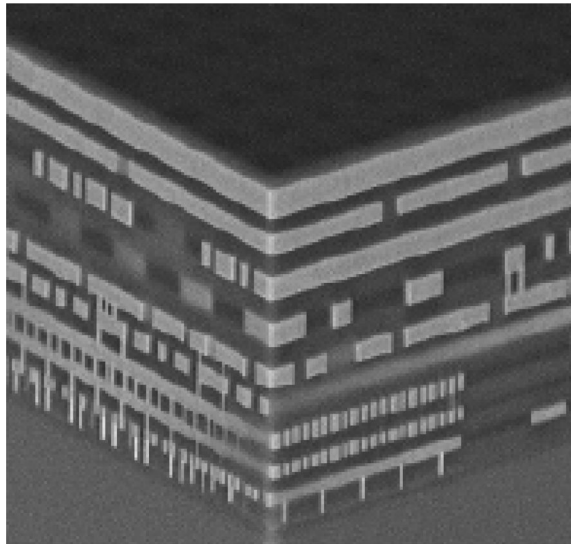


Figure 16.22 SEM micrograph of a three-dimensional cross-sectional view of a 90-nm technology node AMD microprocessor, with nine copper metal layers, fabricated with copper interconnect technology. (Reproduced with permission from AMD.)

The resulting multilevel structure comprises a series of planar metallic layers with metal inlays in the dielectric, forming the circuitry (see Fig. 16.20). Figures 16.21 and 16.22 show SEM micrographs of a cross section of a 90-nm technology node AMD microprocessor, with nine copper metal layers, fabricated with dual damascene copper interconnect technology.

16.2.10 Bond pad metal formation and packaging

Following the formation of all of the required metal layers (see Fig. 16.20), lithographic masking is used to define windows for the bonding pad metal, to which electrical connections can be made by means of bonding wires attached on the periphery of the IC die. Bumps usually formed from tin/lead solder are used to interconnect the chip bonding pads to the packaging substrate. Next, the chip is encapsulated in a plastic or ceramic package designed to provide environmental protection. Note that there are many, many variations in package types and the resulting bonding requirements.

16.2.11 Wafer testing and sorting

The wafer is tested twice to determine yield—once after the deposition of the first metal (referred to as in-line parametric testing) and again after the completion of the last fabrication process (referred to as wafer sort). The first test is also referred to as the wafer electrical test (WET) and is performed in line. In the last test, each die on the wafer is tested for electrical functionality, and the obtained data is used to compute the die yield.

Chapter 17

Advanced Resist Processing and Resist Resolution Limit Issues

In nature's infinite book of secrecy
A little can I read

William Shakespeare, *Anthony and Cleopatra*

17.1 Introduction

Shrinking integrated circuit devices, fueled by the need to increase device speed and density, are approaching dimensions that are considerably smaller than the practical resolution limit of conventional lithography. A number of advanced resist-processing schemes have been proposed to accommodate the resolution requirements for IC devices at such extremely small technology nodes. The 32-nm and sub-32-nm technology nodes are particularly affected. Lithographic resolution patterning of the IC device features at these nodes is extremely difficult because of the mask error enhancement factor (MEEF), which increases as k_1 decreases.

In addition, aspect ratio considerations, dependent on mechanical stability and pattern collapse propensity of resist lines, limit the thickness of resists designed for these technology nodes to ultrathin resist thickness regimes (~ 100 nm and lower). However, the aspect ratio considerations must be balanced against the etch stability requirements that ensure successful pattern transfer to underlying substrates in a device. Both the aspect ratio and etch stability requirements must be balanced against the intrinsic resolution, particularly pitch resolution, of the resist in question. Hence, there is a trade-off between aspect ratio requirements and etch stability requirements on the one hand, and pitch resolution on the other. Therein lies the motivation for these advanced resist-processing schemes.

Another type of balance that is struck in resist design for these advanced technology nodes concerns the trade-off between resolution, line edge roughness, and sensitivity. Empirical evidence shows that it is extremely difficult to

simultaneously meet the 2008 ITRS¹-specified recommendations for these three resist metrics in EUV lithography.

How the balance between the above-named requirements are struck in each of the major advanced resist-processing schemes in use today is discussed below, along with the advantages and drawbacks of each technique. In particular, we discuss the material basis of the resolution limit issues of resists, especially as they concern those based on chemical amplification systems, since these constitute the majority of resists in use in advanced lithographic processing today.

17.2 Resist Systems

Resist systems may be classified into two broad categories, namely, SLR (single-layer resist) systems and ML (multilayer) resist systems.

17.2.1 Single-layer resist systems

Single-layer resist systems, involving the use of an imaging layer that may be paired with antireflection coatings—be it at the top or at the bottom of the layer, or both—have been the dominant resist systems used in the fabrication of devices since the beginning of the semiconductor industry in the early 1950s. They were the workhorse resist system employed in h-line, g-line, i-line, KrF exciplex laser, ArF exciplex laser, electron-beam, ion-beam, and x-ray lithographies. Today, they are employed in patterning leading-edge IC devices, with the aid of hyper-NA immersion lithography at the 45-nm and 32-nm nodes, and with the aid of EUV lithography at the sub-32-nm nodes. Chapters 11–13 of this book cover in detail different aspects of these resist systems.

17.2.2 Multilayer resist systems

There are three main approaches to ML resist imaging systems (see Fig. 17.1); these include: (i) HM (hard mask) processes, (ii) top surface imaging (TSI) processes, requiring latent image formation only near the surface of the resist, thus circumventing any transparency requirements, and (iii) BLR (bilayer resist) processes that use thin imaging layers to accommodate strong absorption at the lithographic wavelength of interest. Historically, TSI and BLR approaches have been investigated and pursued at near-UV and DUV lithographies for reasons such as improved depth of focus and resolution, and elimination of problems associated with substrate reflectivity; but in the regime of EUV lithography, the HM approach is the preferred option for reasons of resist transparency and improved depth of focus.

¹International Technology Roadmap for Semiconductors, ITRS, <http://www.itrs.net/Links/2008ITRS/Home2008.htm> (2008).

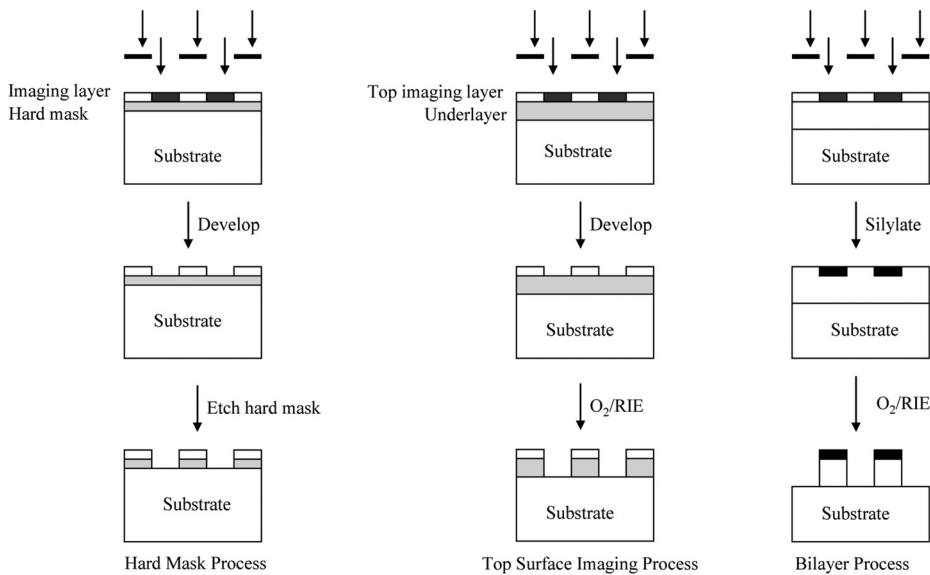


Figure 17.1 Approaches to multilayer resist imaging systems.

In each of these approaches, the lithographically formed image is confined to a thin imaging layer disposed on the top of the stack, and is then transferred into a second nonimaging layer beneath the top layer, the latter of which serves as an etch-resistant mask for final substrate etching. The initially formed image in the top layer is usually transferred to the underlayer by means of selective anisotropic etch processes. By judicious selection of etch chemistries and materials design, the final relief image can provide a robust barrier for the final image transfer into the underlying device layer substrates. The added complexity of multilayer resist approaches, it should be mentioned, presents some significant drawbacks, but is offset by their inherent advantages over SLR approaches (see the remainder of this section).

The major differences in the approaches are primarily related to the film thickness used for the individual layers and the lithographic function that each layer is designed to perform. The top thin layer of the HM, BLR, and TSI configurations is responsible for imaging and good etch resistance (in the bilayer scheme, it also acts as a mask to transfer the image into the bottom layer by dry development in an oxygen-containing plasma), while the underlayer is responsible for imparting good plasma resistance and for reflectivity control.

Each approach has its characteristic advantages and disadvantages due to the underlying technology and the materials issues involved (see the remainder of this section). In contrast, SLR schemes are relatively simple processes, can have moderate levels of resolution and etch resistance, and good linearity, but they suffer from reflective swing problems and small depths of focus, and are limited to low aspect ratios. Irrespective of the resist process approach chosen, chemical amplification continues to be the dominant exposure mechanism of the imaging layer.

17.2.2.1 Hard mask resist system

The HM approach² employs ultrathin resist films, typically $\sim \leq 100$ nm coated over inorganic substrates such as silicon oxynitride, silicon nitride, amorphous carbon, etc. The HM approach offers advantages of thin-film imaging, which eases the requirements for high transparency and reduces the impact on image quality of focus drift; furthermore, the combination of the imaging layer and the HM constitutes a rather thick, high-aspect ratio film, which improves the integrity of the protecting pattern, while mitigating against pattern collapse. The major limitations of HM processes deal with the increased complexities associated with maintaining adequate process control over etching the different films involved, particularly in the regime of tight device CD tolerances.

The adoption of HM processes in IC device manufacture started around the 45-nm technology node; they are expected to become the dominant resist process technology in technology nodes ≤ 32 nm because of their compatibility with double-patterning technology as well as for the reasons stated above.

17.2.2.2 Top surface imaging resist system

In TSI processes, the resist is exposed to form a latent image in the top layer of the resist film. The resist is then silylated in vapor or liquid phase to introduce silicon into the exposed region selectively. The silylated resist is subsequently dry developed with oxygen plasma to transfer the patterns. Typical vapor-phase silylating agents include dimethylsilyldimethylamine (DMSDMA),³ trimethylsilyldiethylamine,⁴ and trimethylsilyldimethylamine.⁵ Typical liquid-phase silylating

²K.B. Nguyen, C. Lyons, J. Schefske, S. Bell, H.J. Levinson, and U. Okoroanyanwu, "Characterization of the manufacturability of ultra thin resist," *J. Vac. Sci. Technol. B* **17**(6), 3039 (1999); C. Pike, K.B. Nguyen, M.V. Plat, C.F. Lyons, P. King, K.A. Phan, U. Okoroanyanwu, and H.J. Levinson, "Manufacturability of the ultrathin resist process," *J. Vac. Sci. Technol. B* **18**(6), 3381–3387(2000).

³S.C. Palmateer, R.R. Kunz, M.W. Horn, A.R. Forte, and M. Rothschild, "Optimization of a 193 nm silylation process for sub 0.25 μm lithography," *Proc. SPIE* **2438**, 455 (1995).

⁴M.A. Hartney, D.W. Johnson, and A.C. Spencer, "Evaluation of phenolic resists for 193 nm surface imaging," *Proc. SPIE* **1466**, 238 (1991); T.T. Dao, C.A. Spence, and D.W. Hess, "Study of silylation mechanisms and kinetics through variations in silylating agent and resin," *Proc. SPIE* **1455**, 257 (1991); D.W. Johnson, R.R. Kunz, and M.W. Horn, "Further developments in surface imaging resists," *J. Photopolym. Sci. Technol.* **6**, 593 (1993); D.W. Johnson, and M.A. Hartney, "Surface imaging resists for 193 nm lithography," *Jpn. J. Appl. Phys.* **31**, 4321 (1992).

⁵M.A. Hartney, D.W. Johnson, and A.C. Spencer, "Evaluation of phenolic resists for 193 nm surface imaging," *Proc. SPIE* **1466**, 238 (1991); T.T. Dao, C.A. Spence, and D.W. Hess, "Study of silylation mechanisms and kinetics through variations in silylating agent and resin," *Proc. SPIE* **1455**, 257 (1991).

agents include 1,1,3,3,5,5-hexamethylcyclotrisilazane⁶ and bis(dimethylamino)-dimethylsilane with N-methyl-2-pyrrolidone (NMP) as a diffusion promoter.⁷ Typical polymer resins include polyvinyl phenol and novolac/diazoquinone polymer resins.

While initially proposed by Taylor and co-workers⁸ in 1984, TSI involving silylation processes for ArF lithography was first reported by Hartney and co-workers in 1990.⁹ As surface imaging techniques, silylation processes for ArF and KrF lithographies were developed as alternatives to bulk imaged resists. They offer a technique for (i) working around the resin transparency requirement at 193 nm, (ii) working within the small depths of focus found with the larger-numerical-aperture lenses mandated by higher-resolution requirements, and (iii) eliminating reflection problems and standing-wave effects. In particular, TSI offers good resolution, high aspect ratio, and high etch resistance. Its major drawback is the fact that it suffers from poor linearity and has line edge roughness problems and poor contrast; it also suffers from equipment performance and/or reliability issues, as well as materials and process defects. Since their introduction, silylation processes for ArF lithography have received considerable attention both in the laboratory and in evaluation for production.¹⁰

⁶M.A. Hartney, R.R. Kunz, L.M. Eriksen, and D.C. LaTulipe, "Comparison of liquid and vapor phase silylation processes for 193 nm positive tone lithography," *Proc. SPIE* **1925**, 270 (1993).

⁷K. H. Baik, L. Van den Hove, and B. Roland, "Comparative study between gas and liquid phase silylation for the diffusion enhanced silylated resist process," *J. Vac. Sci. Technol. B* **9**, 3399 (1991); K. H. Baik, K. Ronse, L. Van den Hove, and B. Roland, "Liquid phase silylation for the DESIRE process," *Proc. SPIE* **1672**, 362 (1992).

⁸G.N. Taylor, L.E. Stillwagon, and T. Venkatesen, "Gas phase functionalized plasma developed resists: Initial concepts and results for electron beam exposure," *J. Electrochem. Soc.* **131**, 1658 (1984).

⁹M.A. Hartney, R.R. Kunz, D.J. Ehrlich, and D.C. Shaver, "Silylation processes for 193 nm excimer laser lithography," *Proc. SPIE* **1262**, 119 (1990).

¹⁰G.N. Taylor, L.E. Stillwagon, and T. Venkatesen, "Gas phase functionalized plasma developed resists: Initial concepts and results for electron beam exposure," *J. Electrochem. Soc.* **131**, 1658 (1984); M.A. Hartney, R.R. Kunz, D.J. Ehrlich, and D.C. Shaver, "Silylation processes for 193 nm excimer laser lithography," *Proc. SPIE* **1262**, 119 (1990); M.A. Hartney and J.W. Thackeray, "Silylation processes for 193 nm lithography using acid catalyzed resists," *Proc. SPIE* **1672**, 486 (1992); N. Benjamin, B. Chapman, and R. Boswell, "Progress of an advanced diffusion source plasma reactor," *Proc. SPIE* **1392**, 95 (1990); M.W. Horn, M.A. Hartney, and R.R. Kunz, "Comparison of etching tools for resist pattern transfer," *Proc. SPIE* **1672**, 448 (1992); S.C. Palmateer, R.R. Kunz, M.W. Horn, A.R. Forte, and M. Rothschild, "Optimization of a 193 nm silylation process for sub 0.25 μm lithography," *Proc. SPIE* **2538**, 455 (1995); M.A. Hartney, D.W. Johnson, and A.C. Spencer, "Evaluation of phenolic resists for 193 nm surface imaging," *Proc. SPIE* **1466**, 238 (1991); T.T. Dao, C.A. Spence, and D.W. Hess, "Study of silylation mechanisms and kinetics through variations in silylating agent and resin," *Proc. SPIE* **1466**, 257 (1991); A.M. Goethals, K.H. Baik, K. Ronse, J. Vertommen, and L. Van den Hove, "Proximity effects in dry developed lithography for sub 0.35 μm application," *Proc. SPIE* **2195**, 394 (1994); J. Dijkstra, G. Van de Ven, and H. Kalter, "Dry development of the DESIRE process in a DECR reactor," *Microelectronic Eng.* **13**, 455 (1991).

17.2.2.3 Bilayer resist system

Since the imaging is done in a thin silicon-containing top layer, the advantages of the bilayer scheme include high aspect ratio, excellent resolution, good plasma etch resistance, and good linearity, while the disadvantage involves the fact that it is slightly more complex than the single-layer scheme, requiring additional etching steps.

The portable conformable mask (PCM) concept proposed by Burn J. Lin in 1980 was the first reported bilayer resist system.¹¹ This system comprises a top imaging resist layer and a photosensitive planarizing layer. The top imaging layer is designed to be opaque at the exposure wavelength of the planarizing layer. This allows the imaged top layer to serve as a contact mask for exposure of the underlying planarizing layer. It must be mentioned, however, that the pattern transfer to the underlying layer in the PCM concept is by optical exposure and not by reactive-ion etching as is now the case in conventional bilayer resist systems.

The conventional bilayer resist systems in which the top imaging layer (typically organosilicon polymer) also serves as an etch mask was first proposed by Hatzakis et al.¹² in 1981, ostensibly for electron-beam lithography. Since then, a number of organosilicon resists for bilayer resist systems have been reported for use in near-UV, DUV, mid-UV, electron-beam, and x-ray applications, a good review of which has been provided by Ohnishi et al.¹³ In recent times, negative-tone resist systems and processes based on silicon-backbone polymers such as polysilanes,¹⁴ polysilynes,¹⁵ and plasma-deposited polymers¹⁶ have been developed for 193-nm lithography.

It should be mentioned that these silicon-backbone polymers are highly absorptive, and must therefore be used in very thin films (~ 30 nm), which can be prone to defects. Also, the principal electronic transition in these polysilane (with two-dimensional silicon backbone) and polysilane (three-dimensional silicon backbone) polymers when irradiated at 193 nm is most likely a σ - σ^* transition involving the all-silicon backbone.¹⁷ Due to this excitation, reaction pathways leading to scission of the Si-Si bonds lead to photodegradation of the polymer.

¹¹B.J. Lin, "AZ1350J as a deep UV mask material," *J. Electrochem. Soc.* **127**, 202 (1980).

¹²M. Hatzakis, J. Paraszczak, and J. Shaw, "Double layer resist systems for high resolution lithography," in *Proc. Microelectronics Engineering*, p. 386 (1981).

¹³Y. Ohnishi, M. Suzuki, K. Saigo, Y. Saotome, and H. Gokan, "Postirradiation polymerization of e beam negative resists: Theoretical analysis and method of inhibition," *Proc. SPIE* **539**, 62 (1985).

¹⁴R.R. Kunz, M.W. Horn, R.B. Goodman, P.A. Bianconi, D.A. Smith, J.R. Eshelman, G.M. Wallraff, R.D. Miller, and E.J. Ginsberg, "Surface imaged silicon polymers for 193 nm excimer laser lithography," *Proc. SPIE* **1672**, 385 (1992).

¹⁵R.R. Kunz, M.W. Horn, R.B. Goodman, P.A. Bianconi, D.A. Smith, and J.R. Eshelman, "Wet developed bilayer resists for 193 nm excimer laser lithography," *J. Vac. Sci. Technol. B* **10**, 2554 (1992).

¹⁶M.W. Horn, S.W. Pang, and M. Rothschild, "Plasma deposited organosilicon thin films as dry resists for deep ultraviolet lithography," *J. Vac. Sci. Technol. B* **8**, 1493 (1990).

¹⁷R.D. Miller and J. Michl, "Polysilane high polymers," *Chem. Rev.* **89**, 1359 (1989).

In the presence of oxygen, this photodegradation results in siloxane (Si-O-Si) formation within the polymer, and in the case of the three-dimensional network polymers, an increase in molecular weight is the result. This combination of both molecular weight and structural changes on irradiation allow for either solvent- or plasma-based development. Both approaches lead to negative-tone imaging.¹⁸

Figure 17.2 shows SEM images of 130-nm line and space features printed with a bilayer resist, comprising a 250-nm imaging layer and a 500-nm underlayer, both from ARCH Chemicals, and based on the above bilayer resist platform.

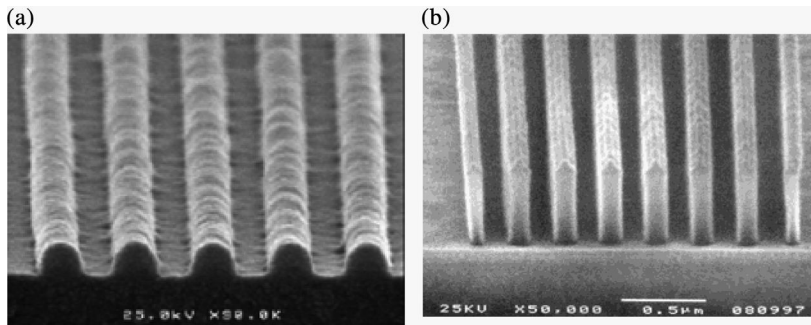


Figure 17.2 SEM images of 130-nm line and space features printed with a bilayer resist, comprising a 250-nm imaging layer and a 500-nm underlayer, both from ARCH Chemicals. (a) Lithographic image printed on the imaging layer with ISI ArF stepper, using NA = 0.6 and partial coherence = 0.7. (b) After etching of the underlayer.

17.3 Advanced Resist Processing Techniques

Advanced processing techniques targeted at 32-nm and sub-32-nm patterning applications fall into roughly three broad categories, namely, single-exposure techniques, double-exposure techniques, and double-patterning techniques. Figure 17.3 shows the different advanced processing techniques targeted at the 32-nm and sub-32-nm technology nodes.

17.3.1 Single-exposure techniques

The single-exposure techniques comprise those techniques in which there is only a single mask exposure process, following which the resist is developed and the wafer prepared for subsequent processing. These techniques do not alter the pattern density or the pitch. Single-exposure techniques are divided into three broad categories, namely, hyper-NA imaging, short-wavelength imaging, and postexposure CD shrink techniques.

¹⁸R.R. Kunz, M.A. Hartney, M.W. Horn, C.L. Keast, M. Rothschild, and D.C. Shaver, "Resist processes for ArF excimer laser lithography," *J. Photopolym. Sci. Technol.* **4**, 490 (1993).

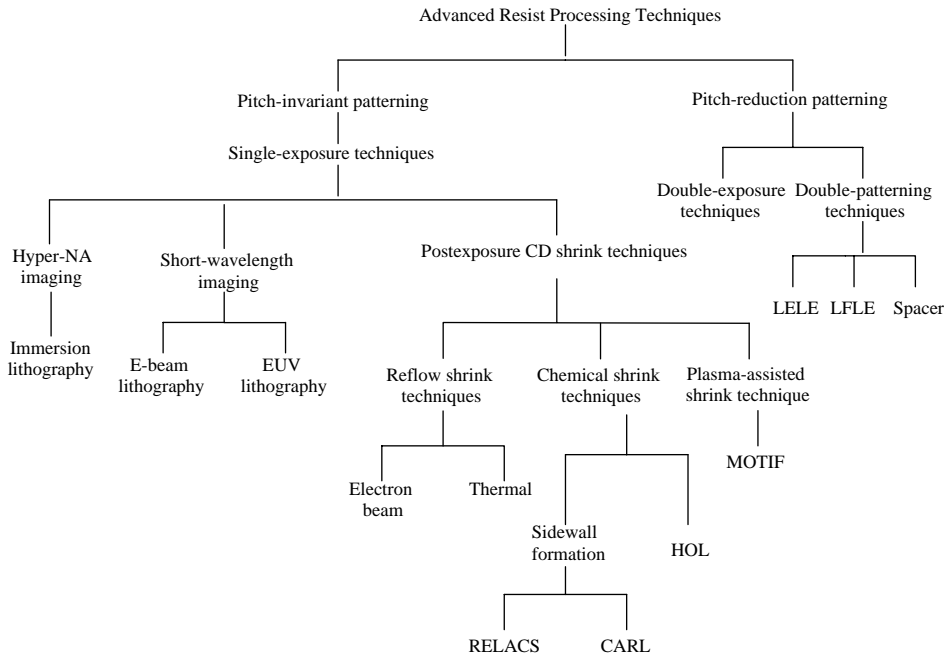


Figure 17.3 Advanced resist processing techniques.

The single-exposure techniques are based on the lithographic resolution R equation

$$R = k_1 \frac{\lambda}{\text{NA}}, \quad (17.1)$$

where λ is the exposure wavelength, NA is the numerical aperture and k_1 is the process-dependent parameter that is a measure of the difficulty of the patterning process.

In general, the single-exposure techniques rely on the use of either hyper-NA >1.0 as implemented in immersion lithography (see Chapter 13) or exposure wavelength reduction as implemented in EUV lithography (see Chapter 14) and electron-beam lithography (see Chapter 15). These techniques may be complemented with reticle-based resolution-enhancement techniques such as phase-shifting masks and the like.

17.3.1.1 Hyper-NA imaging resist processing techniques

Resist processing for hyper-NA imaging incorporates bottom antireflection coatings specially designed to accommodate nonnormal incidence of exposing rays, as well as polarization effects. Graded BARCs and multilayer BARCs have been found to be effective in reducing BARC reflectivity under hyper-NA imaging conditions. In addition, the resists are formulated to be compatible with imaging under water. Some of the resists can be imaged under water with topcoats to prevent resist

additives from leaching into the water medium, while others are topcoatless and are designed not to leach resist additives into the water medium.

17.3.1.2 EUV lithography resist processing technique

Resist processing for EUV lithography is executed exactly as the conventional SLR processing discussed in Chapter 14, except that the photogenerated acids in these resists are designed to have a relatively shorter diffusion length than their conventional counterparts. The reduction of diffusion length in these resists is accomplished through the use of PAGs that are tethered to the backbone of the resist polymer, or through the use of low-activation-energy resists that can be processed at low temperatures and therefore have low diffusion blur.

17.3.1.3 Postexposure-based CD shrink techniques

As shown in Eq. (17.1), resolution can be improved by a combination of these methods: reducing the exposure wavelength, increasing the NA, and decreasing the k_1 factor. Unfortunately, reducing the exposure wavelength and increasing the NA are very expensive and complex options. The postexposure-based CD shrink techniques improve CD resolution by lowering the k_1 factor.

The imaging of small contact holes is one of the most challenging areas in low- k_1 lithography. It is extremely difficult to pattern sub-100-nm contact holes with conventional lithographic technologies, mostly because of the high MEEF. Postexposure CD shrink technologies have emerged in recent years as process enablers for patterning small contact holes. In general, these CD shrink techniques do not improve pitch resolution, only feature size resolution of holes and trenches.

The postexposure-based techniques are grouped into three broad categories, namely, reflow-based shrink techniques, chemical-based shrink techniques, and plasma-assisted shrink techniques. The reflow-based shrink techniques comprise thermally induced reflow and electron-beam heating-induced reflow of patterned resist features. The chemical-based shrink techniques comprise those techniques that either increase or decrease the sidewall thickness of already patterned resist features, thus effectively altering their critical dimension. Examples of chemical-based shrink techniques that result in an increase in the sidewall of the patterned features include techniques based on RELACS (resolution enhancement of lithography assisted by chemical shrink)¹⁹ and CARL (chemical amplification of resist lines).²⁰ Examples of chemical-base shrink techniques that result in decrease

¹⁹T. Toyoshima, T. Ishibashi, N. Yasuda, S. Tarutani, T. Kanda, K. Takahashi, Y. Takano, and H. Tanaka, "Below 100 nm hole pattern formation using resolution enhancement lithography assisted by chemical shrink (RELACS)," *J. Photopolym. Sci. Technol.* **15**(3), 377–378 (2002).

²⁰M. Sebald, R. Sezi, R. Leuschner, H. Ahne, and S. Birkle, "Chemical amplification of resist lines (CARL)," *Microelectronic Eng.* **11**, 531 (1990); M. Sebald, R. Leuschner, R. Sezi, H. Ahne, and

in the sidewalls of the patterned features include the hydrophilic overlayer (HOL) process.²¹

The plasma-assisted shrink techniques (e.g., MOTIF²²) use plasma to deposit a thin film that conformally coats contact holes and spaces printed in resists, which on dry etching result in smaller contact holes and spaces. In the remainder of this section, we provide a more detailed treatment of the postexposure-based single-layer exposure techniques employed in advanced resist processing.

17.3.2 Reflow CD shrink techniques

17.3.2.1 Thermal reflow shrink technique

The thermal reflow shrink technique is mostly targeted at shrinking the CD of contact holes. It involves baking the already-printed contact holes at a temperature above the glass transition temperature (or softening temperature at which the resist polymer transforms from a solid film to a glassy material) to melt the resist materials surrounding the contact holes, such that the melted resist materials flow vertically down the sidewall of the contact holes due to gravity, thereby leading to shrinkage of the size of the contact hole. The flow process also causes the densification of the film as the resist polymer melt flows into the free volume (voids) in the polymer. Film densification imbues the resist patterns with enhanced structural, mechanical, and etch stability. Figure 17.4 shows cross-sectional SEM micrographs of contact holes printed in a resist that was not subjected to reflow heating and another that was subjected to reflow heating at 170°C for 60 seconds, which resulted in 70% shrinkage in the CD and 56% decrease in the thickness of the contact hole resist pattern. Given that the film thickness decrease is mostly associated with deprotection of the resist polymer, a way of mitigating this problem involves the use of resist matrix resins, formulated from low-glass transition polymers, which can be thermally reflowed and annealed at temperatures well below their deprotection temperature.

S. Birkle, "Chemical amplification of resist lines: a novel sub half micron bilayer resist technique for NUV and deep UV lithography," *Proc. SPIE* **1262**, 528 (1990); M. Sebald, H. Berthold, M. Beyer, R. Leuschner, Ch. Nölscher, U. Scheler, R. Sezi, H. Ahne, and S. Birkel, "Application aspects of the Si CARL bilayer process," *Proc. SPIE* **1466**, 227–237 (1991); R. Leuschner, M. Beyer, H. Borndorfer, E. Kühn, Ch. Nölscher, M. Sebald, and R. Sezi, "CARL resist: A technology for optical quarter micron resolution and below," in *Proc. SPE Reg. Tech. Conf. Photopolym.*, Ellenville, NY, pp. 215–224 (1991).

²¹U. Okoroanyanwu, "Materials and methods for sub lithographic patterning of contact, via, and trench structures in integrated circuit devices," U.S. Patent No. 6,767,693 (2004); U. Okoroanyanwu and A. Acheta "Materials and methods for sublithographic patterning of gate structures in integrated circuit devices," U.S. Patent No. 6,884,735 (2005).

²²MOTIF is a trademark of Lam Research Corporation.

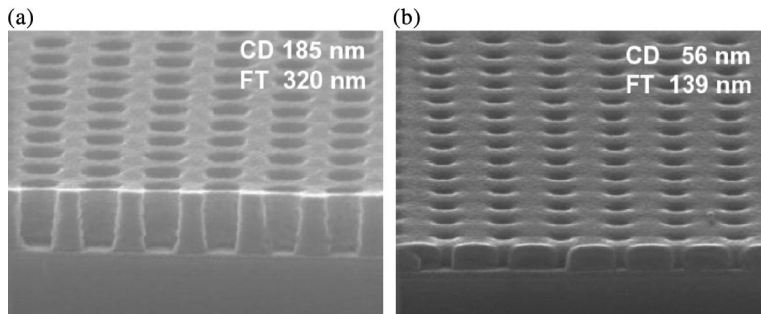


Figure 17.4 Cross-sectional SEM micrographs of (a) unbaked 185-nm contact holes printed in a 320-nm-thick 193-nm resist (AZ EXP AX 1050P) that was coated on a 39-nm-thick BARC (AZ EXP ArF-1C1B), both from AZ Corporation. (b) 56-nm contact holes in 139-nm dense resist film thickness, resulting from the thermally induced contact hole CD shrink of 185-nm contact holes originally printed in a 320-nm-thick 193-nm resist of the same resist as in (a), but baked at 170°C for 60 seconds. The resist was exposed on the ISI ArF laser lithographic exposure tool with NA 0.6, partial coherence 0.7, using a half-tone mask, with +40-nm mask bias. Processing condition: soft bake 130°C/60 seconds, PEB 120°C/60 seconds, developer 0.26N AZ 300MIF/60 seconds. Note the significant shrinkage of the CD of the baked contact hole, from an original value (unbaked CD) of 185 nm to 56 nm, representing a CD change of 129 nm (70% CD shrink). Equally noteworthy is the significant difference between the film thickness of the unbaked film (320 nm) and the baked film (139 nm), representing a film thickness change of 181 nm (56% film thickness decrease). (Courtesy of R. Kunz and R. Dammel.²³)

17.3.2.2 Electron-beam-induced CD shrink techniques

Electron-beam-mediated heating and flowing of patterned resist features has been demonstrated as a viable technique for shrinking the size of contact hole and via structures to sub-90-nm dimensions, thereby overcoming the mask error factor problem of printing these features.²⁴ While the CD uniformity of electron-beam-shrunk contact holes and vias is comparable to that obtained on the same structures that have not been irradiated with electron beam, the iso-dense bias does increase with the dose of electron-beam irradiation.

The MEEF is a major problem limiting the printing of contact hole and via structures. A way of overcoming the MEEF problems of contact hole, via, and trench printing is to first lithographically pattern large sizes of such features, and

²³R. Kunz and R.R. Dammel, “193 nm lithography: fundamentals and issues,” SPIE Short Course No. SC120 (2005).

²⁴U. Okoroanyanwu, “Process for reducing critical dimensions of contact holes, vias, and trench structures in integrated circuits,” U.S. Patent No. 6,518,175 (2003); U. Okoroanyanwu, “Process for reducing the pitch of contact holes, vias, and trench structures in integrated circuits,” U.S. Patent No. 6,589,713 (2003).

then use electron-beam-mediated heating and flow to shrink them down to desired sizes.

Figures 17.5 and 17.6 show the effect of electron-beam-mediated shrinking of 160-nm contact holes. By irradiating the patterned wafer with electron-beam accelerating voltage 20 KeV, current 4 mA, dose $750 \mu\text{C}/\text{cm}^2$ and 20 KeV, current 5 mA, dose $1000 \mu\text{C}/\text{cm}^2$, the hole size was shrunk down to 115 nm and 90 nm, respectively. The nearly circular, doughnut-shaped electron-beam-treated features in the top-down SEM picture of Fig. 17.5, with a lighter outer annulus surrounding a dark interior circle, is indicative of sloped resist sidewall, caused by the flow of the electron-beam-heated and melted resist, which subsequently flows down due to gravity. In contrast, the uncured features have fairly straight sidewall profiles.

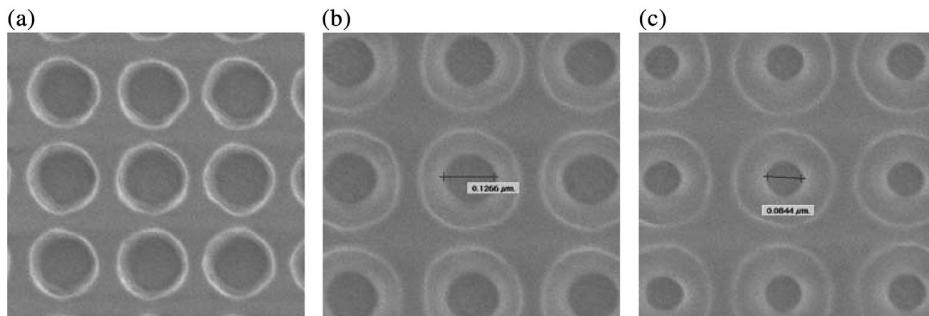


Figure 17.5 Top-down SEM images of (a) 160-nm dense patterned contact holes that were not irradiated with electron beam, (b) same size contact holes as in (a) after irradiation with electron beam of 20-KeV accelerating voltage, 4-mA current, and dose of $750 \mu\text{C}/\text{cm}^2$, and (c) same size contact holes as in (a) after irradiation with electron beam of 20-KeV accelerating voltage, 5-mA current, and dose of $1000 \mu\text{C}/\text{cm}^2$.

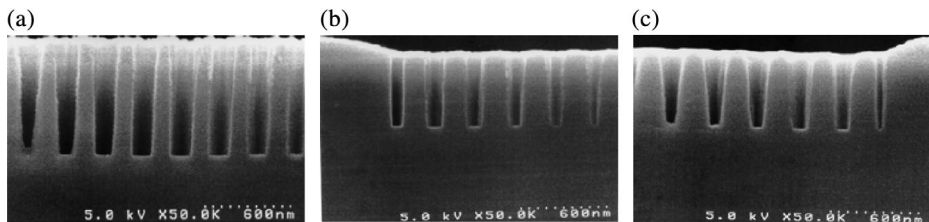


Figure 17.6 Cross-sectional SEM images of (a) 160-nm dense patterned contact holes that were not irradiated with electron beam, and (b) 115-nm contact holes resulting from electron-beam-induced CD shrink. Electron-beam irradiation parameters: 20-KeV accelerating voltage, 4-mA current, and dose of $750 \mu\text{C}/\text{cm}^2$. (c) 90-nm contact holes resulting from electron-beam-induced CD shrink. Electron-beam irradiation parameters: 20-KeV accelerating voltage, 5-mA current, and dose of $1000 \mu\text{C}/\text{cm}^2$.

Proximity effects are also evident in the electron-beam-treated features in Fig. 17.6, where the outer holes adjoining large pad areas of resist are considerably smaller than the ones in the inner areas separating adjacent holes, because more melted resist flows down into these outer holes from these pads than from the areas separating the internal holes. A possible way of solving this electron-beam-induced proximity effect is to incorporate outer dummy contact holes in the mask during fabrication, such that during electron-beam treatment of the patterned features, the melted resist from the pad area adjoining these dummy holes will flow into the latter, without distorting the inner holes. Another possible solution is to size up the outer holes during lithographic patterning.

17.3.3 Chemically induced CD shrink techniques

The two main approaches employed in chemically induced CD shrink techniques are based on sidewall formation and sidewall erosion, respectively.

17.3.3.1 Chemically induced CD shrink techniques based on sidewall formation

As the name implies, this technique increases the thickness of the sidewall, resulting in a decrease in the diameter of the hole or trench opening. It is used in reducing the CD of contact hole and trench features. The resolution enhancement of lithography assisted by chemical shrink (RELACS) is a good example of this technique.

17.3.3.1.1 Resolution enhancement of lithography assisted by chemical shrink (RELACS)

The process flow for RELACS is shown in Fig. 17.7. Based on the thermal cross-linking reaction between RELACS coating material and the photoacid present at the resist sidewall of the contact hole, the technique has been demonstrated to pattern 100-nm and smaller contact holes.²⁵ Following the patterning of contact holes or trenches, the solution of RELACS polymeric material is coated over the hole, filling the latter. Next, the mixture of the resist pattern and RELACS polymer is heated to an appropriate temperature, so much so that unreacted photoacid generated in the original exposure of the contact hole resist patterns catalyze a cross-linking reaction between the polymers on the wall of the contact hole and those of the RELACS polymeric material. This forms a cross-linked layer on the wall of the contact hole. The process is completed by rinsing off the uncross-linked RELACS polymeric material with appropriate solvents.

²⁵T. Toyoshima, T. Ishibashi, N. Yasuda, S. Tarutani, T. Kanda, K. Takahashi, Y. Takano, and H. Tanaka, "Below 100 nm hole pattern formation using resolution enhancement lithography assisted by chemical shrink (RELACS)," *J. Photopolym. Sci. Technol.* **15**(3), 377–378 (2002).

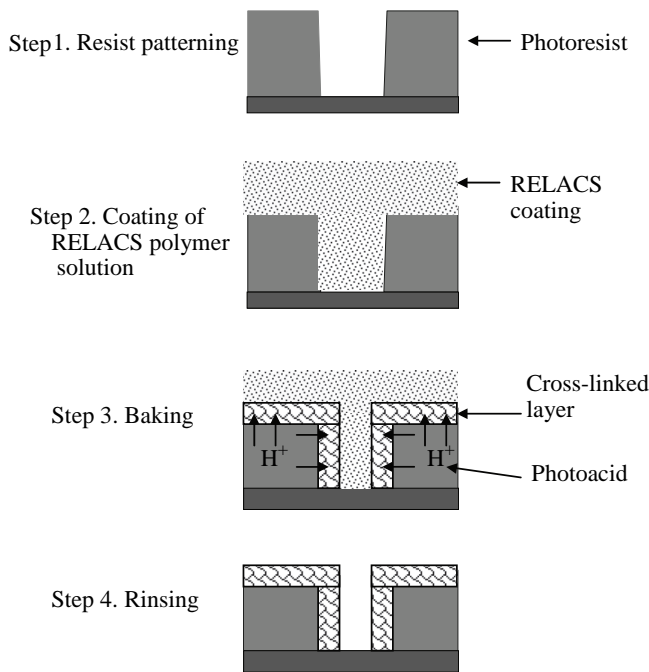


Figure 17.7 RELACS process flow (Reprinted with permission from the Conference of Photopolymer Science and Technology.²⁶)

The RELACS technique offers many advantages over a thermal shrink approach. For example, it reduces iso-dense bias when compared to thermal shrink techniques, has very low pitch dependence, reduces LER and line width roughness (LWR), and improves etch resistance.

17.3.3.1.2 Chemical amplification of resist lines (CARL) process scheme

An interesting variation on the bilayer resist concept is the chemical amplification of resist lines (CARL) process, developed at Siemens (see Fig. 17.8).²⁷ In the CARL process, a top imaging layer resist formulated from an alternating polymer of maleic anhydride and an appropriate monomer, depending on the

²⁶ibid.

²⁷M. Sebald, R. Sezi, R. Leuschner, H. Ahne, and S. Birkle, "Chemical amplification of resist lines (CARL)," *Microelectron. Eng.* **11**, 531 (1990); M. Sebald, R. Leuschner, R. Sezi, H. Ahne, and S. Birkle, "Chemical amplification of resist lines: a novel sub half micron bilayer resist technique for NUV and deep UV lithography," *Proc. SPIE* **1262**, 528 (1990); M. Sebald, H. Berthold, M. Beyer, R. Leuschner, Ch. Nölscher, U. Scheler, R. Sezi, H. Ahne, and S. Birkel, "Application aspects of the Si CARL bilayer process," *Proc. SPIE* **1466**, 227-237 (1991); R. Leuschner, M. Beyer, H. Borndorfer, E. Kühn, Ch. Nölscher, M. Sebald, and R. Sezi, "CARL resist: A technology for optical quarter micron resolution and below," in *Proc. SPE Reg. Tech. Conf. Photopolym.*, Ellenville, NY, pp. 215-224 (1991).

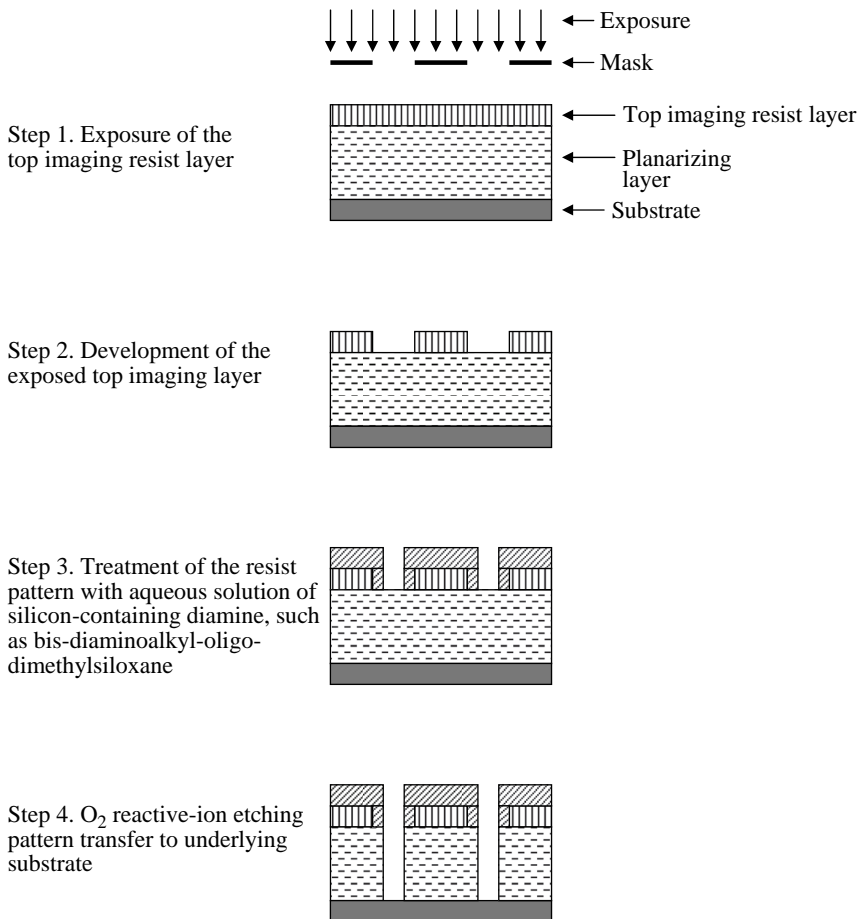


Figure 17.8 Process sequence for the CARL process.

exposure wavelength, is exposed and developed. The resulting resist patterned features are then treated with an aqueous solution containing a silicon-substituted diamine such as bis-diaminoalkyl-oligo-dimethylsiloxane and a dissolution promoting alcohol (see Fig. 17.9). The diamine reacts with the anhydride functional group in the resist to form amide groups, which may be located on different polymer chains; this results in cross-linking of the resist. In this way, a substantial amount of silicon (up to 20%) may be incorporated into the top and sidewall of the resist-patterned features, leading to the swelling of their CDs and a decrease in the space between them. Etch pattern transfer through these shrunken spaces produces extremely small contact holes and trenches.

Although originally developed for i-line lithography, the CARL process has been extended to ArF lithography.²⁸

²⁸U. Okoroanyanwu and R. Subramanian, "Interconnect structure with silicon containing alicyclic polymers and low k dielectric materials and method of making same with single and dual damascene techniques," U.S. Patent No. 6,475,904 (2002).

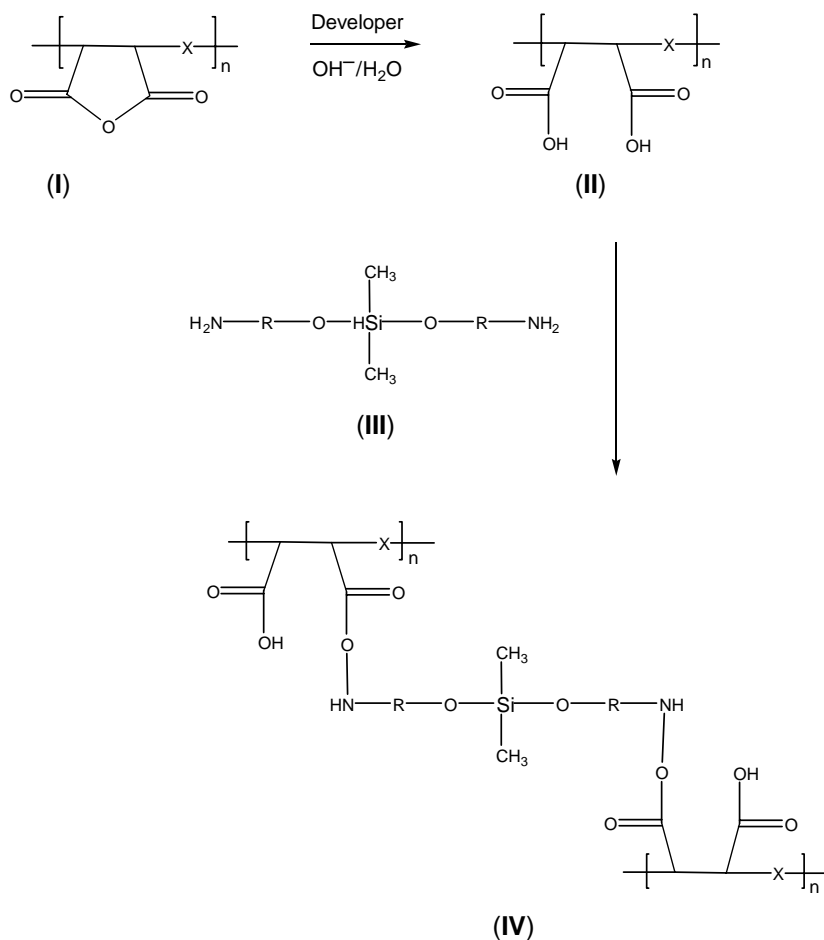


Figure 17.9 The chemistry of the CARL process scheme.²⁹ *x* may stand for hydroxystyrene, acrylates, and alicyclic monomeric units, etc. *R* represents an alkyl group. Structure (I) is the alkaline-insoluble resist resin, consisting of an alternating polymer of maleic anhydride and an appropriate monomer. Structure (II) is the product of the base-catalyzed hydrolysis of the anhydride resin. Structure (III) is the bis-diaminoalkyl-oligo-dimethylsiloxane, the CARL process silylating agent. Structure (IV) is the cross-linked product of silylating agent and the hydrolyzed anhydride resist resin.

17.3.3.2 Chemically induced CD shrink techniques based on sidewall erosion

Chemically induced CD shrink techniques based on sidewall erosion rely on chemical reactions that preferentially take place at the sidewalls of already-patterned resist features, leading to their erosion. The hydrophilic overlayer process is a good example of this technique.

²⁹ibid.

17.3.3.2.1 Hydrophilic overlayer process

Figure 17.10 shows the process sequence of the hydrophilic overlayer (HOL) process.³⁰ First, a chemically amplified or non-chemically amplified positive-tone photoresist comprising hydrophobic polymer and appropriate PAG is coated to a nominal thickness on an appropriate substrate such as a silicon wafer, followed by a soft bake to dry out the nonaqueous solvent. Next, the photoresist film is exposed to radiation of appropriate wavelength to generate photoacid from the PAG. Then the exposed film is again baked (called PEB) at the standard temperature to enhance the diffusion of the photoacid and thermolysis of the acid-labile protecting groups of the polymers.

The next sequence calls for the coating of a thin layer of a hydrophilic polymer from an appropriate solvent on top of the photoresist. The polymeric HOL must have a lower glass transition temperature (T_g) than the photoresist polymer; it must be able to diffuse into the photoresist polymer on baking; and it must be phase compatible with the photoresist polymer. Suitable hydrophilic polymers include, but are not limited to, polymers and copolymers of fluoroalkyl methacrylic acid, fluoroalkyl acrylic acid, etc. Surfactants may be used to improve the wettability of the HOL over the resist polymer layer.

Then, the hydrophilic polymer/hydrophobic photoresist coating is baked at an appropriate temperature above the T_g of the hydrophilic polymer, but below or at the T_g of the photoresist polymer. Baking will enhance the diffusion of the melted glassy hydrophilic polymer into the photoresist polymer, leading to the

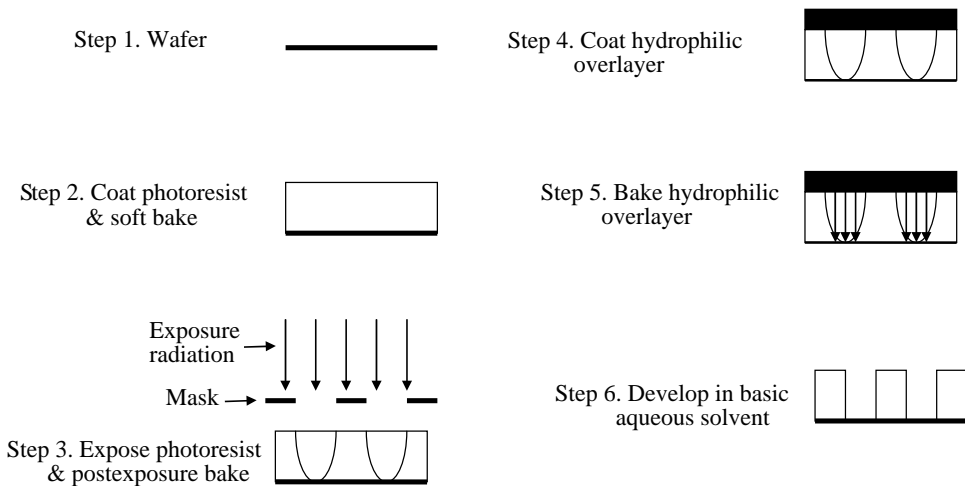


Figure 17.10 HOL process scheme.

³⁰U. Okoroanyanwu, "Materials and methods for sub lithographic patterning of contact, via, and trench structures in integrated circuit devices," U.S. Patent No. 6,767,693 (2004); U. Okoroanyanwu, A. Acheta "Materials and methods for sub lithographic patterning of gate structures in integrated circuit devices," U.S. Patent No. 6,884,735 (2005).

plasticization of the polymer in the exposed part of the photoresist relative to the unexposed part on the same wafer, and even to the exposed part of a wafer processed without HOL. Plasticization decreases the T_g and enhances the diffusion of the photoacid within the exposed part of the photoresist relative to the unexposed part. Increased diffusion of the photoacid increases the deprotection of the hydrophobic *t*-butyl ester group or any of the chemical-amplification-related reactions of the plasticized photoresist polymer, leading to the increased formation of hydrophilic carboxylic acid moieties within the photoresist polymer, relative to an exposed area of the same photoresist without the HOL.

The degree of diffusion of the hydrophilic polymer into the hydrophobic photoresist polymer is temperature dependent. The higher the temperature, the greater is the degree of plasticization and diffusion. Also, the diffusion is a self-limiting process, since it terminates when the melted hydrophilic polymer HOL concentration is exhausted. Therefore, the thicker the hydrophilic polymer to begin with, the greater will be the extent of diffusion of the plasticizer into the photoresist polymer, and consequently the greater is the extent of the plasticization of the photoresist polymer, as well as the greater the enhancement of diffusion of the photoacid within the photoresist polymer, and also the greater the enhancement of the deprotection reaction. Therefore, the bake temperature of the HOL/photoresist layer and the exposure dose delivered to the photoresist can be used to control the CD of the structure to be patterned.

The last step calls for the development of the HOL polymer/photoresist film stack in an aqueous basic solvent such as 0.26 N tetramethylammonium hydroxide. This will dissolve and wash away the exposed part of the resist, comprising the carboxylic acid moieties. The preferential diffusion of the HOL into the exposed area of the photoresist results in deprotection of the photoresist polymer at the edge of the unexposed features, leading to their dissolution. This is the basis of the CD reduction, improved process window, and exposure latitude, and smoother sidewall and line edge profile of photoresist features processed with HOL relative to the features processed without HOL.³¹

Figure 17.11 shows SEM micrographs of line features printed on PAR707 resist from Sumitomo, using conventional lithographic processing, as well as the HOL process following lithographic exposure at 193 nm, under the same exposure conditions as the conventional process. It is noteworthy that the HOL process reduced the CD of the feature from 170 nm to approximately 90 nm. It is also noteworthy that the sidewall of the feature printed with the HOL process has a nearly vertical profile relative to that obtained with the conventional process.

17.3.3.3 Plasma-assisted CD shrink technique

The plasma-assisted CD shrink technique was introduced by Lam Research Corporation, using a Lam Research 2300 MOTIF patterning system to deposit a

³¹U. Okoroanyanwu and A. Acheta "Materials and methods for sub lithographic patterning of gate structures in integrated circuit devices," U.S. Patent No. 6,884,735 (2005).

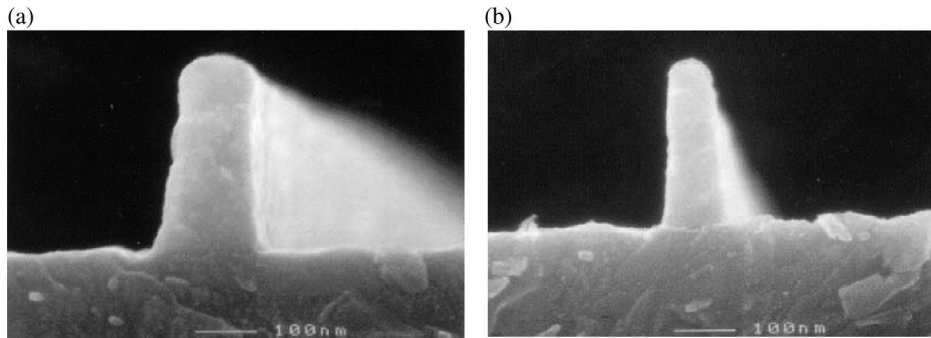


Figure 17.11 SEM micrographs of line structures obtained with (a) the conventional process and (b) the HOL process following lithographic exposure. The resist/HOL system was baked at 125°C following lithographic exposure on an ASML PAS5500/900 scanner with NA 0.63, partial coherence 0.5, and exposure wavelength 193 nm. The HOL process reduced the CD of the feature from 170 nm to approximately 90 nm. Note the smoothness of the sidewall and the nearly vertical sidewall profile of the feature obtained with the HOL process relative to that obtained with the conventional process.³²

plasma-generated polymeric coating over the top and sidewalls of patterned resist features. The coating reduces the size of the hole or space between the feature sidewalls, which on transfer to underlying layers produces much smaller hole and space sizes than would otherwise be the case were they patterned in the conventional fashion. The MOTIF polymeric coating has high etch resistance and can be removed with a standard resist strip process. The amount of CD reduction can be controlled through the number of shrink process cycles applied.

Figure 17.12 shows the process flow for this patterning scheme. First, the hole or space to be shrunk is lithographically patterned with appropriate resist for the given exposure wavelength. Next, a plasma-generated polymeric coating is deposited in a conformal fashion over the sidewalls and top of the resist features, reducing the size of the holes or space between the sidewalls. An etch step is used to transfer the reduced hole or space opening into the underlying substrate. The process ends with stripping both the plasma-generated polymeric coating and the resist features. Figure 17.13 shows SEM images of significantly smaller contact holes (~40 nm) produced with this technique when contrasted with those obtained in the conventional manner (~100 nm) under identical conditions.

17.3.4 Double-exposure techniques

Double-exposure techniques (see Fig. 17.14) comprise a sequence of two separate exposures of the same resist layer, with the same mask or two different masks.

³²ibid.

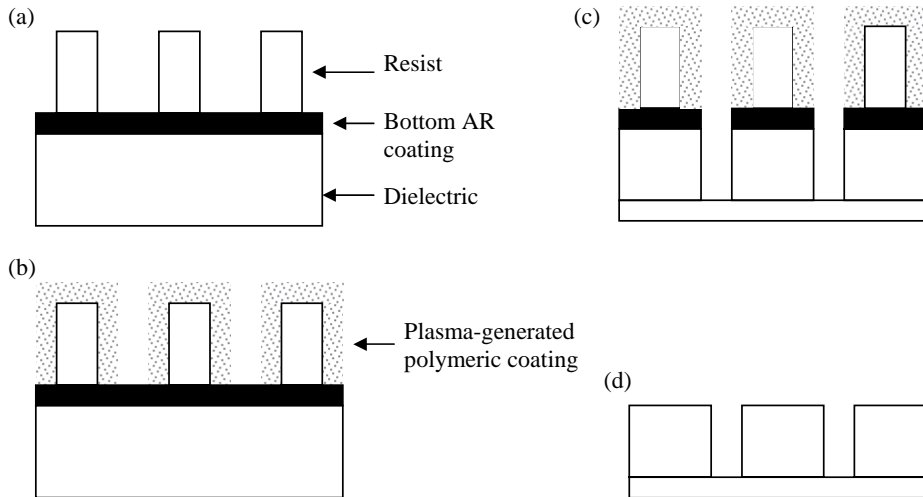


Figure 17.12 Process flow for Lam Research Corporation's 2300 MOTIF system plasma-assisted CD shrinking of hole and space features, showing: (a) lithographic patterning, (b) deposition of the plasma-generated polymeric coating, (c) etching into the dielectric, and (d) stripping of the resist, coating, and the plasma-generated polymeric coating.

Double exposure is commonly used to pattern features in the same layer that are different or have incompatible densities or pitches. A good example might be the situation where two exposures are made such that one exposure is used to define features oriented in one direction, while the other exposure is used to define the other set of features oriented in another direction that is perpendicular to the first direction. In this way, two-dimensional patterns can be decomposed into two one-dimensional patterns, which are considerably easier to print. In other words, the double-exposure technique enables the patterning of minimum pitch features

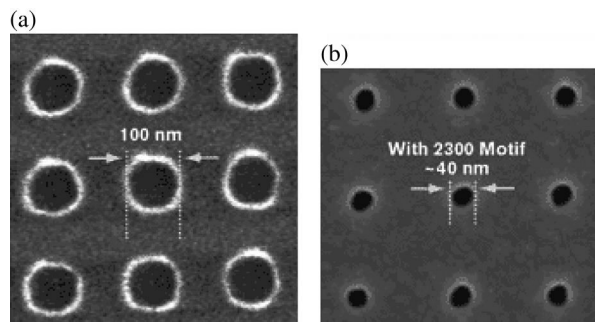


Figure 17.13 Top-down SEM images of contact hole images (a) processed conventionally (CD 100 nm) and (b) processed with MOTIF plasma-assisted CD shrink technique (CD 45 nm). Note the significant shrinkage of the CD of the contact hole from 100 nm to 45 nm obtained with the MOTIF process. (Source: Lam Research Corporation.)

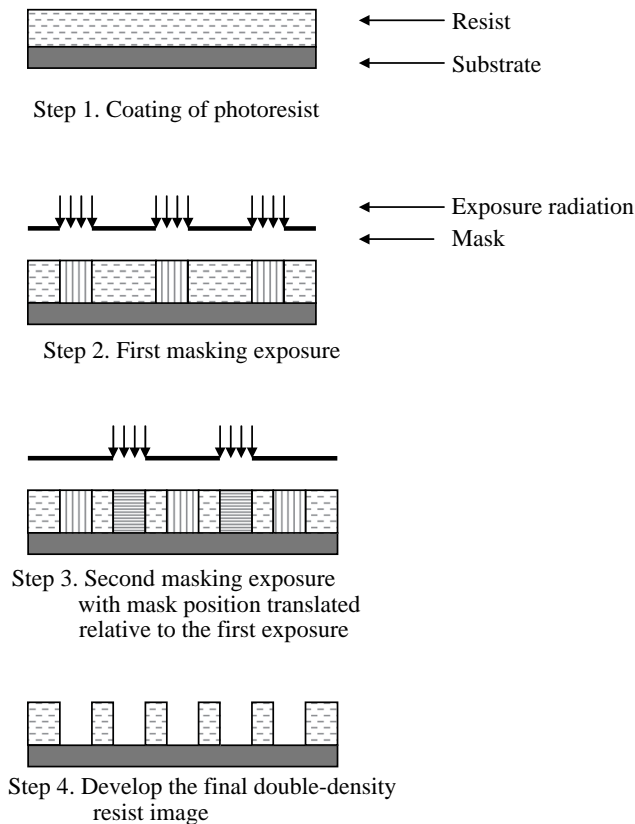


Figure 17.14 Double-exposure scheme.

in a layout that may contain a variety of features. It should be pointed out that the use of an alternating phase-shifting mask in IC device patterning typically involves a double-exposure process, in which one exposure with one mask is used to define the main features, and a second exposure with a different mask, often referred to as a cut mask or a trim mask, is used to define and remove the phase edges associated with these features. It must also, however, be pointed out that the sum of the double exposures cannot improve the minimum resolution limit unless the photoresist response is not a simple addition of the two exposures. It does reduce the pitch of the features, as long as the features have the same orientation (as shown in Fig. 17.14).

Relative to the other double-patterning approaches, the double exposure is the simplest to implement since it does not require additional follow-up process steps. Its main challenge is meeting alignment tolerance requirements.

17.3.5 Double-patterning techniques

Designed to overcome the problem of printing at small pitches, double-patterning techniques typically comprise those techniques in which two cycles each of

lithography and etch processing are used to pattern the design of IC device features. (In some variants of double-patterning techniques, there might be less than two cycles of lithography or etch.) Splitting the pattern into two printing steps ensures that the lithography can be printed at twice the desired final pitch, which helps to alleviate some of the process constraints and limitations associated with printing at small pitches—critical requirements for device scaling. The implementation of this technique effectively results in the doubling of the pattern density and a twofold reduction in the pitch of the final pattern.

It is the above-mentioned reasons, coupled with the realization that EUV lithography will not be ready for the 32-nm half-pitch node, account for the emergence of double patterning between 2008 and 2010 as a viable means of extending the resolution capability of currently available lithography tools.³³ A state-of-the-art 193-nm water immersion lithographic exposure tool with a NA of 1.35 can potentially extend its resolution to 22-nm half-pitch with double patterning, although at considerable mask and process cost.

³³P. Nikolsky, N. Davydova, and R. Goosens, “Topological and model based approach to pitch decomposition for double patterning,” *Proc. SPIE* **6792**, 679205 (2008); K. Monahan and A. Widmann, “Enabling immersion lithography and double patterning,” *Proc. SPIE* **6518**, 65181M (2007); S. Mimotogi, T. Higaki, H. Kanai, S. Tanaka, M. Satake, Y. Kitamura, K. Kodera, K. Ishigo, T. Kono, M. Asano, K. Takahata, and S. Inoue, “Impact of patterning strategy on mask fabrication beyond 32 nm,” *Proc. SPIE* **7028**, 702814 (2008); A. Hazelton, S. Wakamoto, S. Hirukawa, M. McCallum, N. Migome, J. Ishikawa, C. Lapeyre, I. Guilmeau, S. Barnola, and S. Gaugiran, “Double patterning requirements for optical lithography and prospects for optical extension without double patterning,” *Proc. SPIE* **6924**, 69240R (2008); M.C. Chiu, B.S. M. Lin, M.F. Tsai, Y.S. Chang, M.H. Yeh, T.H. Ying, C. Ngai, J. Jin, S. Yuen, S. Huang, Y. Chen, L. Miao, K. Tai, A. Conley, and I. Liu, “Challenges of 29 nm half pitch patterning with 193 nm dry lithography and self aligned double patterning,” *Proc. SPIE* **7140**, 714021 (2008); S. Corbo, C. MacNaughton, T. Gubiotti, and M. Wollenweber, “Using scatterometry to improve process control during the spacer pitch splitting process,” *Proc. SPIE* **7140**, 714025 (2008); S. M. Kim, S. Y. Koo, J. S. Choi, Y. S. Hwang, J. W. Park, E. K. Kang, C. M. Lim, S. C. Moon, and J. W. Kim, “Issues and challenges of double patterning lithography in DRAM,” *Proc. SPIE* **6520**, 65200H (2007); M.O. Beeck, J. Versluijs, V. Wiaux, T. Vanderweyer, I. Ciofi, H. Struyf, D. Hendrickx, and J.V. Olmen, “Manufacturability issues with double patterning for 50 nm half pitch single damascene applications, using RELACS shrink and corresponding OPC,” *Proc. SPIE* **6520**, 65200I (2007); W. Y. Jung, S. M. Kim, C. D. Kim, G. H. Sim, S. M. Jeon, S. W. Park, B. S. Lee, S. K. Park, J. S. Kim, and L. S. Heon, “Patterning with amorphous carbon spacer for expanding the resolution limit of current lithography tool,” *Proc. SPIE* **6520**, 65201C (2007); H. Nakamura, M. Omura, S. Yamashita, Y. Taniguchi, J. Abe, S. Tanaka, and S. Innoue, “Ultra low k1 oxide contact hole formation and metal filling using resist contact hole pattern by double L&S formation method,” *Proc. SPIE* **6520**, 65201E (2007); H.J. Liu, W.H. Hsieh, C.H. Yeh, J.S. Wu, H.W. Chan, W.B. Wu, F.Y. Chen, T.Y. Huang, C.L. Shin, and J.P. Lin, “Double patterning with multilayer hard mask shrinkage for sub .25k1 lithography,” *Proc. SPIE* **6520**, 65202J (2007); A. Vanleenhove and D.V. Steenwinckel, “A litho only approach to double patterning,” *Proc. SPIE* **6520**, 65202F (2007); M. Crouse, R. Uchida, Y. van Dommelen, A. Tomoyuki, E. Schmitt Weaver, M. Takeshita, S. Wu, and R. Routh, “Litho only double patterning approaches: positive negative versus positive positive tone,” *J. Micro/Nanolith. MEMS MOEMS* **8**, 011006 (2009); T. B. Chiou, R. Socha, H. Y. Kang, A.C. Chen, and S. Hsu, “Full chip pitch/pattern splitting for lithography and spacer double patterning techniques,” *Proc. SPIE* **7140**, 71401Z (2008).

Double patterning is not without drawbacks. One of its main weaknesses relates to the fact that overlay errors between the two lithographic steps translate directly into CD errors in the final pattern, except for the case of the self-aligned double-patterning technique (described in Section 17.3.5.3). A very tight overlay tolerance is therefore required in order to successfully implement double patterning in IC device manufacture. Another weakness of double patterning when compared to single-exposure patterning concerns the fact that some schemes of the former, such as the lithography-etch-lithography-etch scheme, increases processing steps (such as coating, lithography, etching) by a factor of two for linear (i.e., one-dimensional) pattern layers.

The three commonly practiced approaches to double patterning include: (i) the lithography-etch-lithography-etch (LELE) patterning scheme, (ii) the lithography-freeze-lithography-etch (LFLE) patterning scheme, and (iii) the self-aligned double-patterning (SADP) scheme. In the following sections, we discuss the main attributes of each scheme, along with their potential applications and drawbacks. The choice of which double-patterning scheme is chosen relies heavily on trade-offs—especially between process complexity and materials complexity. The choice also depends on the device design, i.e., whether it is for logic or memory application.

17.3.5.1 Lithography-etch-lithography-etch patterning scheme

Figure 17.15 shows the process sequence for the LELE scheme. The scheme begins with a lithographic exposure of the resist and BARC coated on top of a HM, which in turn is deposited on other substrates such as polysilicon. An etch step is used to transfer the image on the resist layer to an underlying HM, following which the resist is stripped. A second layer of HM is coated over the first patterns, following which BARC, followed by resist are coated over the second HM and then exposed at locations in between the features patterned in the HM layer. A second etch is used to transfer the final, double density patterns into the polysilicon layer. Finally, the remaining HM is stripped off.

Although this scheme uses materials that are readily available, it suffers from low throughput and significant process complexity. In addition, discrepancy and delay between the second resist pattern and the first HM pattern are significant contributors to process variation. Figure 17.16 shows SEM images of 22-nm dense line and space features obtained with this technique.

17.3.5.2 Lithography-freeze-lithography-etch patterning scheme

The first step in the LFLE patterning scheme (see Fig. 17.17) is the resist-masking exposure, similar to the first lithography step of LELE. Next, the created resist image is frozen in place by means of photochemical or radiation curing or thermal curing and hardening methods. This allows the coating of a second resist layer over the patterned resist features without intermixing issues between the two resist materials. This step also eliminates the first HM etch as in the LELE

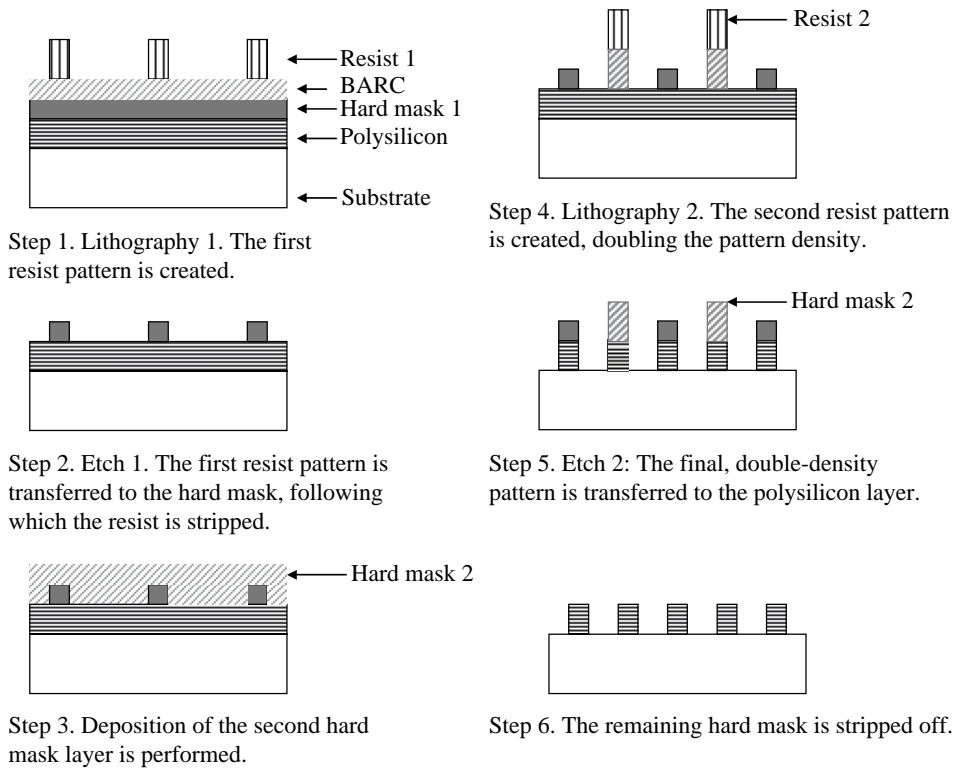


Figure 17.15 Process sequence for LELE double-patterning technique.

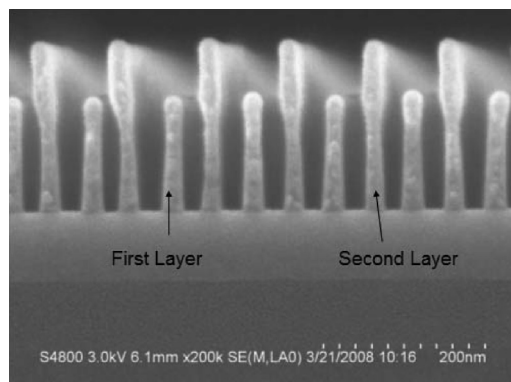


Figure 17.16 SEM cross section of 25-nm half-pitch lines patterned with LELE double-patterning technique. The line profiles were obtained after the final pattern transfer to the underlying substrate. The second-layer patterns after the second etch step are considerably longer than the first-layer patterns because they are capped with the second HM material. (Courtesy of S. Holmes.)

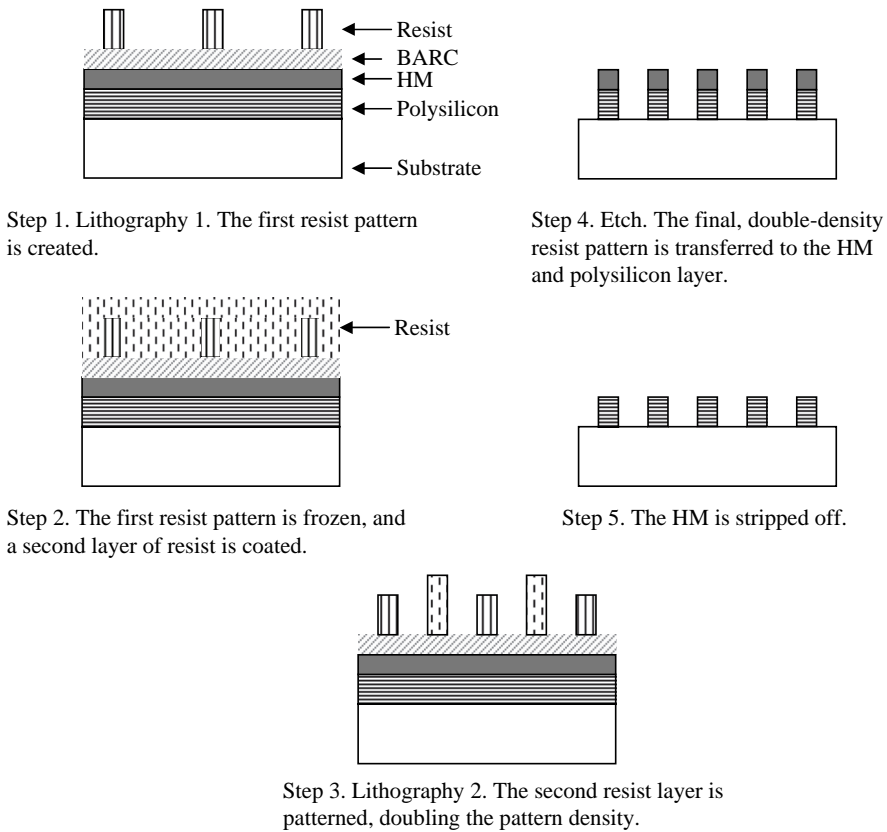


Figure 17.17 Process sequence for LFLE double-patterning technique.

patterning scheme. Then, the second resist layer is exposed through a mask that is translated by a distance corresponding to the half-pitch of the original pitch of the resist image in the first exposure. A development step completes the second lithographic step. An etch process step is used to transfer the final, double density resist pattern into the HM and polysilicon layers. The entire process ends with stripping of the remaining resist and the HM.

Although this technique requires fewer steps in comparison to the LELE and SADP techniques, the materials issues associated with freezing the first image, without unduly affecting the overall patterning process, are significant. Figure 17.18 shows top-down SEM images of 22-nm dense line and space features obtained with this technique.

17.3.5.3 Self-aligned double-patterning (SADP) scheme

Figure 17.19 shows the processing scheme for the SADP scheme. The process scheme begins with the first lithographic masking exposure to create resist images on a HM that is disposed on top of suitable semiconductor substrates such

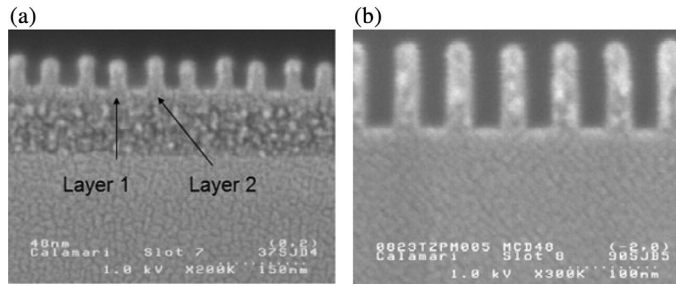


Figure 17.18 Cross-sectional SEM image of 32-nm half-pitch lines patterned with LFLE double-patterning technique. (a) Line profiles of the two resist layers following the second lithographic exposure. (b) Line profiles after the final pattern transfer to underlying substrate. (Courtesy of S. Holmes.)

as polysilicon. An etch step is used to transfer the resist image created above into the HM layer, following which the remaining resist is stripped off.

The next step is the conformal deposition of a spacer material, oftentimes a nitride film, over the HM patterns. A second etch step, called the etch back step, is implemented in such a way as to remove the thickness of the spacer material corresponding to the thickness only on the horizontal surfaces, while leaving intact

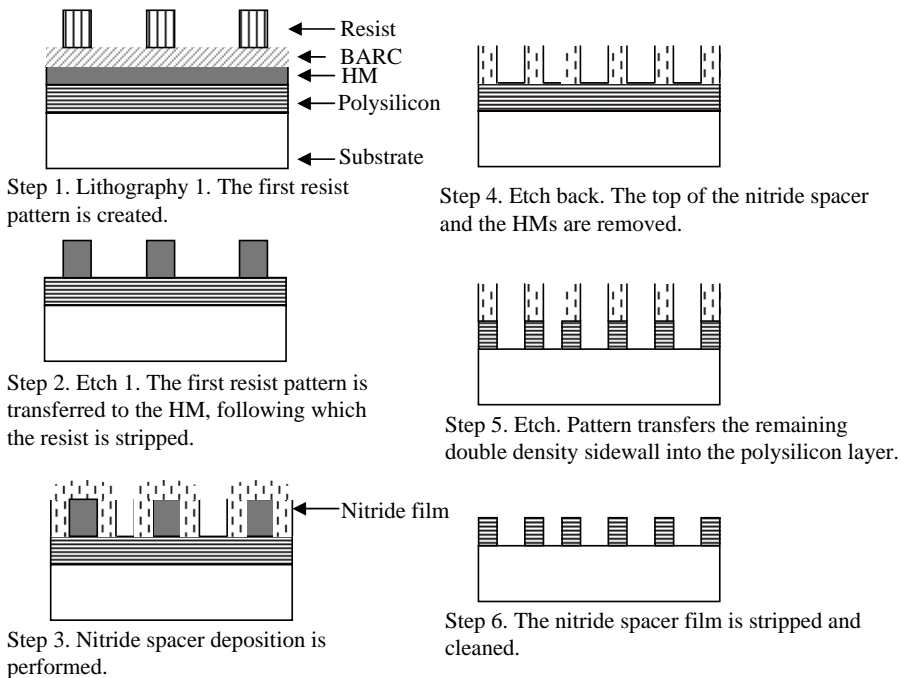


Figure 17.19 Process sequence for self-aligned double-patterning technique by means of sidewall spacer formation.

the thicker spacer material on the sidewalls. A third etch step is used to remove the HM pattern, while leaving the spacer sidewalls intact. This etch step also transfers the double density feature pattern to the underlying polysilicon substrate. And because there are two spacers for every HM pattern or line pattern, the overall feature pattern density is now doubled. The spacer double-patterning technique has found applications in patterning of extremely small gates at half the original lithographic pitch.

The spacer technique is unique in that with one lithographic exposure, the pitch can be reduced by a factor of two indefinitely, just with the application of a succession of spacer-formation and pattern-transfer processes. Furthermore, because spacer materials are mostly drawn from HM materials, their postetch pattern quality tends to be superior, especially in terms of line edge roughness and CD control, when compared to corresponding resist profiles after etch. It is also not sensitive to interlayer alignment.

The spacer double-patterning approach has some issues, the main one of which concerns placement accuracy of the features, which requires excellent dose and etch uniformity control. Equally problematic is the fact that the spacers may not stay in place at the proper location after the material to which they are attached (the HM pattern) is removed. Forming acceptable uniform spacer profiles that will yield uniform CDs is not a trivial exercise. In addition, the etch pattern transfer steps, often involving delicate removal of materials adjacent to the spacers, place unusually tight etch process tolerance on this technique, in order to have a successful outcome.

Figure 17.20 shows SEM images of shallow trench isolation structures patterned with the self-aligned double-patterning technique at various stages of the process flow, and ending in 22-nm half-pitch structures. Figure 17.21 shows SEM images of 22-nm half-pitch gridded design structures patterned into silicon, with the aid of the SADP spacer HM scheme in conjunction with a cut mask. This figure illustrates the versatility with which the 22-nm half-pitch trench array can be employed in the fabrication of a usable IC device.

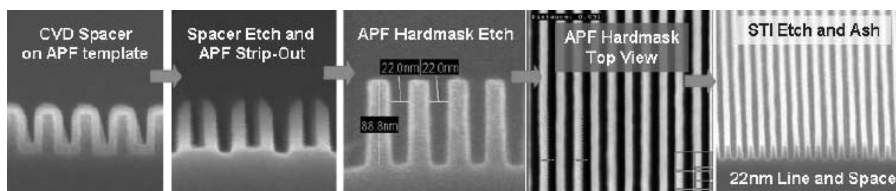


Figure 17.20 SEM images of shallow trench isolation structures patterned with self-aligned double-patterning technique through various stages of the process flow, and ending in 22-nm half-pitch structures. The HM used is Applied Materials Corporation's advanced patterning film (APF).³⁴

³⁴C. Bencher, Y. Chen, H. Dai, W. Montgomery, and L. Huli, "22 nm half pitch patterning by CVD spacer self aligned double patterning," *Proc. SPIE* **6924**, 69244E (2008).

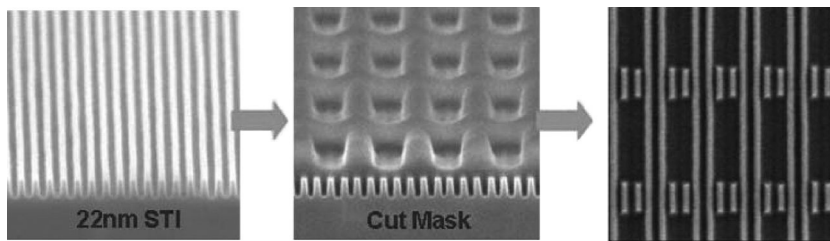


Figure 17.21 SEM images of 22-nm half-pitch gridded design structures patterned into silicon. The structures were fabricated with a SADP spacer HM scheme in conjunction with a cut mask.³⁵

17.4 Resolution Limit Issues of Resists

The resist specifications of the 2008 ITRS³⁶ for the 32- and sub-32-nm technology nodes address many challenges and stumbling blocks that must be overcome in order to successfully manufacture devices at these technology nodes. Some of these specifications, especially those for the 22-nm and smaller technology nodes call for near-atomic-scale resolution—something that is nearly impossible with conventional resist design concepts and imaging mechanisms. The key 2008 ITRS resist specifications by product type for the 32-nm and 22-nm technology nodes are summarized in Table 17.1. These stumbling blocks are intimately

Table 17.1 Key resist requirements by product type for the 32-nm and 22-nm technology nodes. (Adapted from 2008 ITRS.³⁷)

Lithography related characteristic	32 nm technology node	22 nm technology node
DRAM half pitch (nm) (contacted)	32	22
MPU/ASIC metal 1 (M1) half pitch (nm) (contacted)	32	22
MPU printed gate length (nm)	25	18
MPU physical gate length (nm)	18	14
Resist thickness (nm)	50 90	35 65
Low frequency line edge roughness (nm, 3σ) $<8\%$ of CD	2.0	1.4
Gate critical dimension control (nm, 3σ)	1.9	1.5
Contact in resist (nm)	39	28
Contact after etch (nm)	36	25
Resist sensitivity (193 nm lithography) (mJ/cm^2)	20 50	20 50
Resist sensitivity (13.5 nm, EUV lithography) (mJ/cm^2)	5 30	5 30

³⁵ibid.

³⁶International Technology Roadmap for Semiconductors 2008 Update, <http://www.itrs.net/Links/2008ITRS/Home2008.htm> (2008).

³⁷This table was adapted from the ITRS 2008 Update, <http://www.itrs.net/Links/2008ITRS/Home2008.htm> (2008). In the generation of this table, we use the factor 0.7 as the scaling factor between successive technology nodes.

tied to the nature of the resist chemical amplification imaging mechanism, thin-film confinement effects, and polymer molecular properties. Acting either separately or in concert, these stumbling blocks are resolution limiting, with disastrous consequences such as poor CD control, line edge roughness, pattern collapse, and the inability to simultaneously meet resolution, line edge roughness and sensitivity targets. How these resist properties and issues limit resolution are discussed in more detail in the following sections.

17.4.1 Resolution limits due to chemical amplification in resists

While the chemical amplification concept has served the semiconductor industry very well since its invention in the 1970s and development in the 1980s,³⁸ in terms of high sensitivity and resolution, it is now well established experimentally that the very attributes of this concept that made resists based on it become the workhorse of the industry for the last 25 years are unfortunately resolution limiting on account of diffusion, image spreading, or resist blur.³⁹ The implications of the uncontrolled diffusion for the semiconductor industry is significant, particularly

³⁸H. Ito and C.G. Willson, "Chemical amplification in the design of dry developing resist materials," *Polym. Eng. Sci.* **23**, 1012 (1983); H. Ito, C.G. Willson, and J.M.J. Frechet, "Positive and negative working resist compositions with acid generating photoinitiator and polymer with acid labile groups pendant from polymer backbone," U.S. Patent No. 4,491,628 (1985).

³⁹K.E. Mueller, W.J. Koros, C.A. Mack, and C.G. Willson, "Diffusivity measurements in polymers, Part IV: acid diffusion in chemically amplified resists," *Proc. SPIE* **3049**, 706–711 (1997); G.M. Schmid, M.D. Stewart, C. Y. Wang, B.D. Vogt, V.M. Prabhu, E.K. Lin, and C.G. Willson, "Resolution limitations in chemically amplified photoresist systems," *Proc. SPIE* **5736**, 333–342 (2004); M.D. Stewart, H.V. Tran, G.M. Schmid, T.B. Stachowiak, D.J. Becker, and C.G. Willson, "Acid catalyst mobility in resist resins," *J. Vac. Sci. Technol. B: Microelec. Nan. Struct.* **20**(6), 2946–2952 (2002); M.D. Stewart, M.H. Sommervell, H.V. Tran, S.V. Postnikov, and C.G. Willson, "Study of acid transport using IR spectroscopy and SEM," *Proc. SPIE* **3999**, 665–674 (2000); P.L. Zhang, A.R. Eckert, C.G. Willson, S.E. Webber, and J. Byers, "Acid diffusion through polymer films," *Proc. SPIE* **3049**, 898–909 (1997); F.A. Houle, W.D. Hinsberg, and M.I. Sanchez, "Acid base reactions in a positive tone chemically amplified photoresist and their effects on imaging," *J. Vac. Sci. Technol. B* **22**(2), 747–757 (1997); F.A. Houle, W.D. Hinsberg, M.I. Sanchez, and J.A. Hoffnagle, "Influence of resist components on image blur in a patterned positive tone chemically amplified photoresist," *J. Vac. Sci. Technol. B* **20**(3), 924–931 (2002); F.A. Houle, W.D. Hinsberg, M.I. Sanchez, G. Wallraff, C. Larson, and J. Hoffnagle, "Determination of coupled acid catalysis diffusion processes in a positive tone chemically amplified photoresist," *J. Vac. Sci. Technol. B* **18**(4), 1874–1885 (2000); C.P. Umbach, A.N. Broers, C.G. Willson, R. Koch, and R.B. Laibowitz, "Nanolithography with an acid catalyzed resist," *J. Vac. Sci. Technol. B* **6**, 319–322 (1988); C.P. Umbach, A.N. Broers, C.G. Willson, R. Koch, and R.B. Laibowitz, "Nanolithography with a high resolution stem," *IBM J. Res. Dev.* **32**(4), 454–461 (1988); W. Hinsberg, F. Houle, M.I. Sanchez, J. Hoffnagle, G. Wallraff, D.R. Medeiros, G. Gallatin, and J. Cobb, "Extendibility of chemically amplified resists: another brick wall?" *Proc. SPIE* **5039**, 1–14 (2003); J. Hoffnagle, W. Hinsberg, M.I. Sanchez, and F. Houle, "Liquid immersion deep ultraviolet interferometric lithography," *J. Vac. Sci. Technol. B* **17**, 3306 (1999); M. Swittkes, M. Rothschild, "Resolution enhancement of 157 nm lithography by liquid immersion," *Proc. SPIE* **4691**, 459 (2002).

given that with aggressive scaling of the gate length, CD control will present a very difficult challenge at the 22-nm and sub-22-nm nodes.

Empirical evidence suggests that chemical amplification starts to limit resolution in high-activation-energy resist systems such as those based on *t*-BOC resist systems as the pitch approaches 80 nm.⁴⁰ For instance, the blur at FWHM of state-of-the-art DUV 248 nm and 193 nm is around 50 nm,⁴¹ while that of a state-of-the-art low-activation-energy resist is less than 20 nm.⁴² Lithographic patterning at the 22-nm node will require blur that should not exceed 15 nm, in order to capture the high-resolution aerial image. A blur value of less than 15 nm may be difficult to achieve at high throughput, especially with weak EUV sources. Changing exposure wavelength does not address any of these issues. All of the issues are increasingly problematic as feature sizes shrink.

The design concept of chemical amplification is based on generation of a chemically stable catalytic species (commonly referred to as a photoacid and designated as a proton H^+ , as illustrated in Fig. 17.22 for a resist system comprising a copolymer—poly(4-hydroxystyrene-*co*-4-*t*-butyloxycarbonyloxystyrene)—in

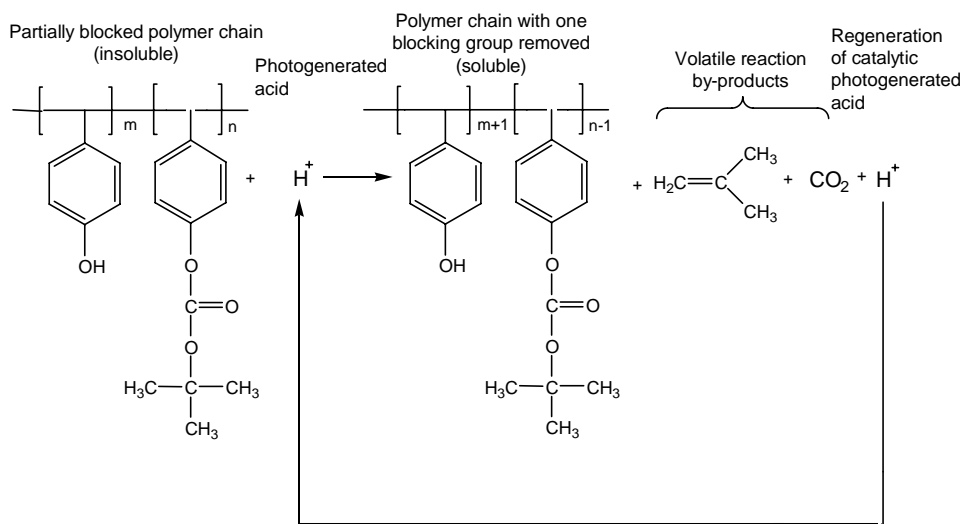


Figure 17.22 Catalytic deprotection reaction of a photoresist system based on copolymer poly(4-hydroxystyrene-*co*-4-*t*-butyloxycarbonyloxystyrene).

⁴⁰C.P. Umbach, A.N. Broers, C.G. Willson, R. Koch, and R.B. Laibowitz, "Nanolithography with an acid catalyzed resist," *J. Vac. Sci. Technol. B* **6**, 319–322 (1988); C.P. Umbach, A.N. Broers, C.G. Willson, R. Koch, and R.B. Laibowitz, "Nanolithography with a high resolution stem," *IBM J. Res. Dev.* **32**, 454–461 (1988); W. Hinsberg, F. Houle, M.I. Sanchez, J. Hoffnagle, G. Wallraff, D.R. Medeiros, G. Gallatin, and J. Cobb, "Extendibility of chemically amplified resists: another brick wall?" *Proc. SPIE* **5039**, 1–14 (2003).

⁴¹J.A. Hoffnagle, W.D. Hinsberg, F.A. Houle, and M.I. Sanchez, "Characterization of photoresist spatial resolution by interferometric lithograph," *Proc. SPIE* **5038**, 464–472 (2003).

⁴²W.D. Hinsberg of IBM Corp., Private Communication (2002).

regions of the photoresist film that are irradiated. The catalytic action of the catalyst on the photoresist polymer or copolymer causes a change in the dissolution rate in the irradiated regions of the film. Rather than using exposure energy to directly cause a solubility switch, chemically amplified resists use exposure energy only to generate a catalytic species. The photogenerated catalyst then initiates a chain reaction or promotes a cascade of solubility-switching reactions in the exposed regions of the photoresist. The apparent quantum efficiency for the solubility-switching reaction in such a system is the product of the quantum efficiency for catalyst generation and the catalytic chain length. Catalytic chain lengths in the many hundreds are common; so, in effect, the quantum efficiency can be greater than one. One photochemical conversion can cause several chemical reactions, and thus the exposure can be said to have been “chemically amplified.” In this manner, lithographic imaging can be accomplished with very low exposure doses, saving time and money in manufacturing.⁴³

While chemically activated resists (CARs) have many advantages, they have one major limitation, namely, it is possible for the catalyst generated in exposed regions to diffuse into unexposed regions, causing blurring of the latent image (see Fig. 17.23). The migration of the photoacid effectively results in a bias between the distribution of exposure energy and the final distribution of exposure

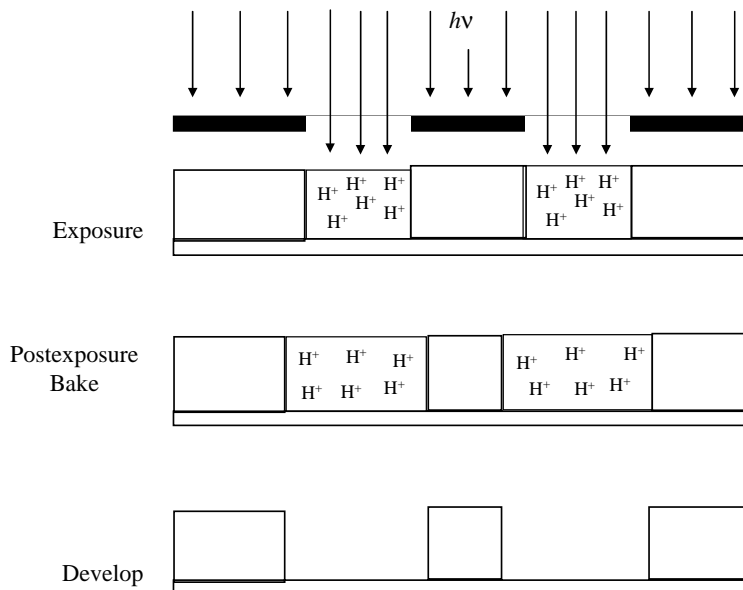


Figure 17.23 Exposure process of a CAR, illustrating photoacid diffusion beyond the exposed areas.

⁴³G.M. Schmid, M.D. Stewart, C. Y. Wang, B.D. Vogt, V.M. Prabhu, E.K. Lin, and C.G. Willson, “Resolution limitations in chemically amplified photoresist systems,” *Proc. SPIE* **5736**, 333–342 (2004).

photoproducts. This bias depends on the photoresist chemistry and the processing conditions, but is largely independent of the exposure conditions and therefore cannot be eliminated by improving the exposure process.

It is, however, possible to reduce catalyst migration by increasing the size of the catalyst or by reducing the temperature of the PEB step. Another approach for mitigating the problem of feature dimension bias due to migration of acid catalyst is to incorporate base additives into the photoresist formulation. These approaches for reducing acid catalyst migration also generally reduce the catalytic efficiency of each photoproduct and therefore increase the total dose of exposure energy that is required to pattern the film. Increases in required exposure dosage effectively reduce the throughput of the expensive exposure tools and can seriously reduce the profitability of the manufacturing process.⁴⁴

As a thermally driven process, the photoacid diffusion length and rate in CARs is temperature dependent, as illustrated in Fig. 17.24 for the diffusion of perfluorooctane sulfonate photoacid in partially protected poly(4-*t*-butyloxycarbonyloxystyrene)-based resist. Within normal processing conditions, the higher the PEB temperature, the faster is the rate of the photoacid diffusion and the longer is the diffusion length. Although the PEB temperature can be used to modulate photoacid diffusion and consequently resist sensitivity, it nevertheless involves a trade-off

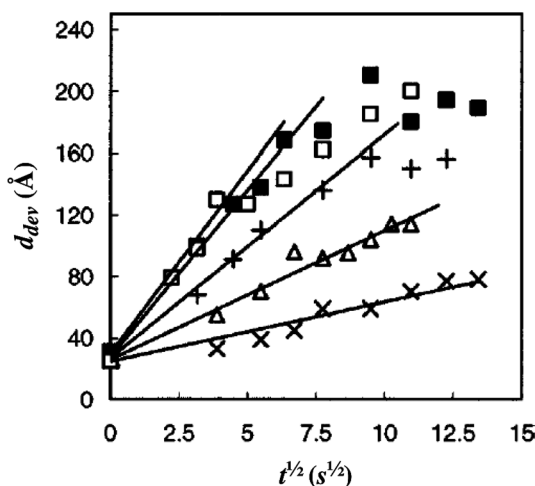


Figure 17.24 Diffusion length of perfluorooctane sulfonate photoacid in partially protected poly(4-*t*-butyloxycarbonyloxystyrene)-based resist at different temperatures. (×) 90°C, (Δ) 100°C, (+) 110°C, (□) 120°C, (■) 130°C. The standard uncertainty in the d_{dev} measurement is ± 10 Å. (Adapted with permission from Ref. 45. © 2001 American Institute of Physics.)

⁴⁴ibid.

⁴⁵D.L. Goldfarb and M. Angelopoulos, "Confinement effects on the spatial extent of the reaction front in ultrathin chemically amplified photoresists," *J. Vac. Sci. Technol. B* **19**(6), 2699 (2001).

with line edge roughness and CD uniformity. While high-activation-energy resists based on *t*-butyl ester and butoxycarbonyl protecting groups typically need a high PEB temperature to be deprotected, low-activation-energy resists based on acetal and ketal protecting groups typically need a low PEB temperature, oftentimes at room temperature, while within the exposure chamber to be deprotected. Because of their high PEB temperatures, the high-activation-energy resists have much higher blur values and lower line edge roughness than their low-activation-energy counterparts, which suffer more from high LER and outgassing. So, in principle, the chemical amplification concept is extendible to the 22-nm and sub-22-nm technology nodes with the low-activation-energy, low-blur, high-LER, and bad outgassing resists of the acetal and ketal platforms. Conventional high-activation-energy resists are not extendible to the 22-nm node because of their high blur.⁴⁶

17.4.1.1 Elucidating how photoacid diffusion leads to resist contrast and resolution loss

During PEB, the resist polymer experiences the time-averaged acid concentration c , which deprotects the polymer or transforms it in a way that alters its solubility properties. For line and space structures, the Gaussian function can be used to approximate the response to the initial acid concentration $c(x, y, 0) = \delta(x)$ (where δ is the Dirac delta function), which evolves over time to establish an average acid concentration field. The one-dimensional time-averaged concentration field, otherwise known as the line spread function, is given by Eq. (17.2) and illustrated in Fig. 17.25, where the variable x is the spatial coordinate, t is time, and D is the diffusion coefficient:

$$\bar{c}(x, t_f) = \frac{1}{2} \sqrt{\frac{1}{Dt_f}} \left[\frac{2}{\sqrt{\pi}} e^{-x^2/(4Dt_f)} + \frac{|x| \operatorname{erf}\left(\frac{x}{2\sqrt{Dt_f}}\right)}{\sqrt{Dt_f}} \right]. \quad (17.2)$$

Applying the superposition principle, the response to an initially sinusoidal modulation of the photoacid concentration, also called the modulation transfer function (MTF), can be calculated with Eq. (17.3):

$$\operatorname{MTF}_{\text{diff}} = \frac{p^2}{4\pi^2 Dt_f} [1 - e^{-(4\pi^2 Dt_f/p^2)}]. \quad (17.3)$$

For example, suppose that one wants to know which diffusion length is allowed if one accepts a relative 20% reduction of the resist image MTF due to diffusion. Then the diffusion length $L_d = \sqrt{2Dt}$ may be as large as 0.16 times the pitch (see Fig. 17.26).

⁴⁶U. Okoroanyanwu and J.H. Lammers, "Resist road to the 22 nm technology node," *Future Fab Int.* **17**, 68–71 (2004).

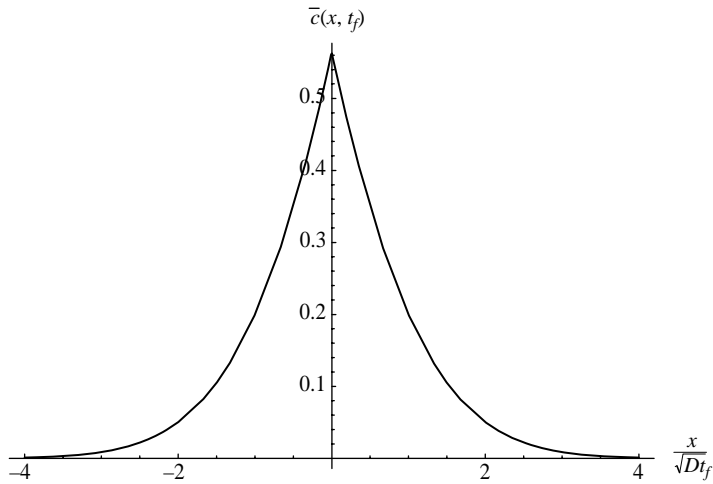


Figure 17.25 Average photoacid concentration, or line spread function, due to photoacid diffusion as a function of scaled coordinate $x/\sqrt{Dt_f}$. (Adapted from Ref. 47.)

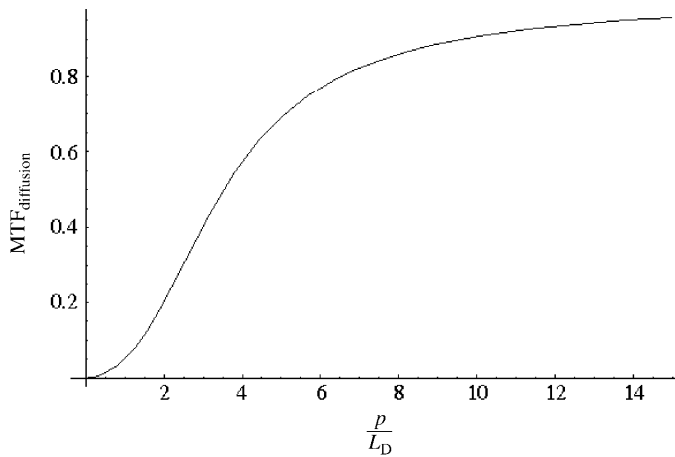


Figure 17.26 Modulation transfer function due to diffusion (MTF_{diff}) versus pitch (p)/diffusion length (L_D).⁴⁸

An important result from the application of the continuum theory to this diffusion problem is the fact that shrinking the feature pitch can only be accommodated as long as the photoacid diffusion length is also comparably shrunk. For a pitch of 45 nm, one requires a diffusion length of about 7 nm or less. The diffusion

⁴⁷U. Okoroanyanwu and J.H. Lammers, “Resist road to the 22 nm technology node,” *Future Fab Intl.* **17**, 68–71 (2004).

⁴⁸ibid.

length is roughly equal the FWHM of the line spread function. Even by tuning the size of the anion, the PEB temperature, and the coating thickness, the diffusion length of this magnitude is nearly impossible to achieve with high-activation-energy resist systems, but seems achievable with low-activation-energy, low-PEB chemical amplification resist systems.

17.4.2 Resolution limits due to line edge roughness

Line edge roughness (LER) (see Fig. 17.27), defined as “local line edge variation evaluated along a distance equal to four times the technology node,” in the ITRS 2008 update, has been implicated in transistor performance degradation due mostly to leakage current.⁴⁹ A number of factors have been reported to contribute to or influence LER in printed resist features, some of them include resist processing

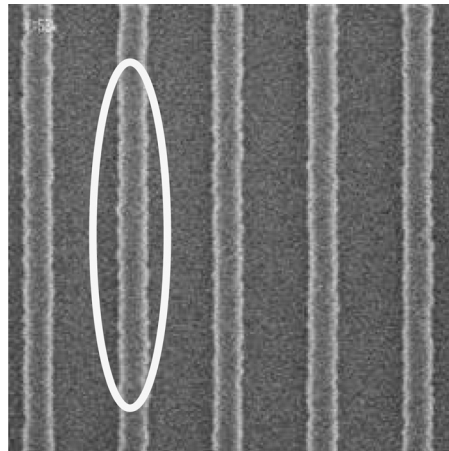


Figure 17.27 LER of 65-nm line features. LER = 4.6 nm (3 sigma).

⁴⁹X. Xiong, J. Bokor, Q. Xiang, P. Fisher, I.M. Dudley, and P. Rao, “Gate line edge roughness effects in 50 nm bulk MOSFET devices,” *Proc. SPIE* **4689**, 733–741 (2002); K. Shibata, N. Izumi, and K. Tsujita, “Influence of line edge roughness on MOSFET devices with sub 50 nm gates,” *Proc. SPIE* **5375**, 865–873 (2004); J.A. Croon, G. Storms, S. Winkelmeier, I. Pollentier, M. Ercken, S. Decoutere, W. Sansen, and H.E. Maes, “Line edge roughness: characterization, modeling and impact on device behavior,” *IEDM '02 Digest* (2002); C.H. Diaz, H. J. Tao, Y. C. Ku, A. Yen, and K. Young, “An experimentally validated analytical model for gate line edge roughness (LER) effects on technology scaling,” *IEEE Electron Device Lett.* **22**, 287–289 (2001); K. Patterson, J.L. Sturtevant, J.R. Alvis, N. Benavides, D. Bonser, N. Cave, C. Nelson Thomas, W.D. Taylor, and K.L. Turnquest, “Experimental determination of the impact of polysilicon LER on sub 100 nm transistor performance,” *Proc. SPIE* **4344**, 809–814 (2001).

conditions,⁵⁰ acid diffusion,⁵¹ polydispersity⁵² of the resist polymer,⁵³ shot noise,⁵⁴ mask effects, and aerial image contrast.⁵⁵ In the following sections, we examine the role of base loading, polymer molecular weight, shot noise, and quantum yield on LER.

17.4.2.1 Base quenchers

The addition of base quenchers to resists has been shown to improve LER at the expense of photospeed⁵⁶ (see Fig. 17.28). This stems from the neutralization reaction between the photoacid and the base quencher within the exposed area, resulting in the increase in the photogenerated acid concentration gradient, as well as chemical contrast at the feature edge. The enhanced chemical contrast at the feature edge translates into enhanced development contrast between the exposed and the unexposed areas of the film; the result is a much sharper edge (lower LER) than would otherwise be the case.

⁵⁰D. He and F. Cerrina, "Process dependence of roughness in a positive tone chemically amplified resist," *J. Vac. Sci. Technol. B.* **16**(6), 3748 (1998).

⁵¹T. Itani, H. Yoshino, S. Hashimoto, M. Yamana, N. Samoto, and K. Kasama, "Acid and base diffusion in chemically amplified DUV resists," *Microelectron. Eng.* **35**, 149 (1997); T. Itani, H. Yoshino, and S. Hashimoto, "Photoacid bulkiness effect on dissolution kinetics in chemically amplified deep ultraviolet resists," *J. Vac. Sci. Technol. B.* **13**(6), 3026 (1995).

⁵²Polydispersity of a polymer is the ratio of its weight average molecular weight to its number average molecular weight. It is a measure of the molecular weight distribution of a polymer, with very tight and narrow distribution associated with a uniform distribution of similarly sized polymers, having a polydispersity of 1.0, while polymers with larger polydispersity values (greater than 1.0) have broader molecular weight distributions, comprised of polymers with varying molecular weight sizes.

⁵³T. Yoshimura, H. Shiraiishi, J. Yamamoto, and S. Okazaki, "Correlation of nano edge roughness in resist patterns with base polymers," *Jpn. J. Appl. Phys.* **32**, 6065 (1993); T. Itani, H. Yoshino, S. Hashimoto, M. Yamama, N. Samoto, and K. Kasama, "Polymer structure effects on dissolution characteristics and acid diffusion in chemically amplified deep ultraviolet resists," *J. Vac. Sci. Technol. B.* **15**(6), 2541 (1997).

⁵⁴J.M. Hutchinson, "Shot noise impact on resist roughness in EUV lithography," *Proc. SPIE* **3331**, 531 (1998); N. Rau, F. Stratton, C. Fields, T. Ogawa, A. Neureuther, R. Kubena, and G. Willson, "Shot noise and edge roughness effects in resists patterned at 10 nm exposure," *J. Vac. Sci. Technol. B.* **16**(6), 3784 (1998).

⁵⁵W. Lawrence, "Spatial frequency analysis of line edge roughness in nine chemically related photo resists," *Proc. SPIE* **5039**, 713–724 (2003); T. Azuma, K. Chiba, M. Imbeppu, D. Kawamura, and Y. Ohnishi, "Line edge roughness of chemically amplified resists," *Proc. SPIE* **3999**, 264–269 (2000); A.R. Pawloski, A. Acheta, I. Lalovic, B.M. LaFontaine, and H.J. Levinson, "Characterization of line edge roughness in photoresist using an image fading technique," *Proc. SPIE* **5376**, 414–425 (2004); M.I. Sanchez, W.D. Hinsberg, F.A. Houle, J.A. Hoffnagle, H. Ito, and C. Nguyen, "Aerial image contrast using interferometric lithography: effect on line edge roughness," *Proc. SPIE* **3678**, 160–171 (1999).

⁵⁶W. Lawrence, "Spatial frequency analysis of line edge roughness in nine chemically related photo resists," *Proc. SPIE* **5039**, 713–724 (2003); R. Brainard, P. Trefonas, J.H. Lammers, C.A. Cutler, J.F. Mackevich, A. Trefonas, and S.A. Robertson, "Shot noise, LER and quantum efficiency of EUV photoresists," *Proc. SPIE* **5374**, 74–85 (2004).

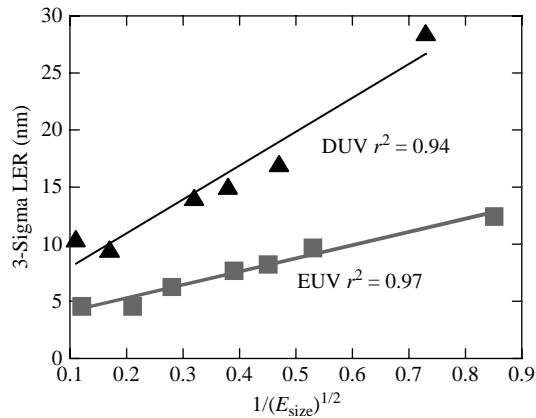


Figure 17.28 LER versus $1/\sqrt{E_{size}}$ for DUV 248-nm and EUV 13.4-nm exposure of EUV 2D resists formulated with seven different concentrations of base quencher.⁵⁷

17.4.2.2 Polymer size

The influence of polymer molecular weight (a measure of the size of the polymer) on the LER has been reported by a number of investigators.⁵⁸ In particular, the size of the polymer grains or aggregates has been related to the magnitude of the LER.⁵⁹ In a study involving the AFM examination of patterned resist feature sidewalls, Yamaguchi et al.⁶⁰ attribute the cause of the LER to aggregates trapped in the pattern sidewall of the resist. In another study, Yamaguchi et al.⁶¹ link resist LER directly to aggregate size, which in turn increases with molecular weight.

⁵⁷R. Brainard, P. Trefonas, J.H. Lammers, C.A. Cutler, J.F. Mackevich, A. Trefonas, and S.A. Robertson, "Shot noise, LER and quantum efficiency of EUV photoresists," *Proc. SPIE* **5374**, 74–85 (2004).

⁵⁸S. Mori, T. Morisawa, N. Matsuzawa, Y. Kaimoto, M. Endo, T. Matsuo, K. Kuhara, and M. Sasago, "Reduction of line edge roughness in the top surface imaging process," *J. Vac. Sci. Technol. B* **16**(6), p. 3739 (1998); W. Hinsberg, F. Houle, G. Wallraff, M. Sanchez, M. Morison, J. Hoffnagle, H. Ito, C. Nguyen, C.E. Larson, P.J. Brock, and G. Breyta, "Factors controlling pattern formation in chemically amplified resists at sub 100 nm dimensions," *J. Photopolym. Sci. Technol.* **12**(4), 649 (1999); V. Rao, J. Hutchinson, S. Holl, J. Langston, C. Henderson, D.R. Wheeler, G. Cardinale, D. O'Connell, J. Goldsmith, J. Bohland, G. Taylor, and R. Sinta, "Top surface imaging process and materials development for 193 nm and extreme ultraviolet lithography," *J. Vac. Sci. Technol. B* **16**(6), 3722 (1998); S. Mori, N. Matsuzawa, Y. Kaimoto, M. Endo, T. Matsuo, T. Morisawa, K. Kuhara, and M. Sasago, "Study of high photo speed top surface imaging process using chemically amplified resist," *J. Photopolym. Sci. Technol.* **11**(4), 613 (1998).

⁵⁹H. Namatsu, M. Nagase, T. Yamaguchi, K. Yamazaki, and K. Kurihara, "Influence of edge roughness in resist patterns on etched patterns," *J. Vac. Sci. Technol. B* **16**(6), 3315 (1998).

⁶⁰T. Yamaguchi, H. Namatsu, M. Nagase, K. Kurihara, and Y. Kawai, "Line edge roughness characterized by polymer aggregates in photoresists," *Proc. SPIE* **3678**, 617 (1999).

⁶¹T. Yamaguchi, H. Namatsu, M. Nagase, K. Kurihara, K. Yamazaki, and K. Kurihara, "Nanometer scale linewidth fluctuations caused by polymer aggregates in resist films," *Appl. Phys. Lett.* **71**(16), 2388 (1997).

They observed that the aggregates trapped in the pattern sidewalls were similar to those in the unexposed regions of the film.

17.4.2.3 Shot noise

Given the inherent statistical nature of the discrete processes (such as photon absorption, secondary electron generation, PAG excitation, acid-quencher annihilation, deprotection, etc.) involved in advanced resist imaging, say, with EUV lithography, a credible concern has been reported that resists may reach a “shot noise limit” whereby low doses of high-energy EUV photons may cause the number of photons to fall to such low levels that the statistical variations inevitably will cause the LER to increase beyond an acceptable limit.⁶² This acceptable limit is referred to as the shot noise limit, and it is defined as the limit imposed by the statistical probability of underexposing a pixel.⁶³

For a Poisson process such as photon absorption, the statistical variation in the number of absorbed photons σ_N is equal to the square root of the number of absorbed photons, N , and is expressed as

$$\sigma_N = \sqrt{N}. \quad (17.4)$$

The relative dose variation $\frac{\sigma_N}{N}$ is proportional to the shot noise and has been determined to scale with the LER (see Fig. 17.28) as

$$\text{LER} \propto \text{shot noise} \propto \frac{\sigma_N}{N} \propto \frac{1}{\sqrt{\text{dose}}}. \quad (17.5)$$

In other words, the LER decreases as the dose increases.⁶⁴ Also, the LER has been determined to exhibit a reciprocal relationship with contrast and image log-slope; i.e., a higher contrast image or an image with higher image log-slope has a lower LER⁶⁵ and is also less sensitive to shot noise.⁶⁶

⁶²A.R. Neurerther and C.G. Willson, *J. Vac. Sci. Technol. B* **6**(1), 167 (1988); J.M. Hutchinson, “Shot noise impact on resist roughness in EUV lithography,” *Proc. SPIE* **3331**, 531 (1998); S.C. O’Brien and M.E. Mason, *Proc. SPIE* **4346**, 534 (2001).

⁶³A.R. Neurerther and C.G. Willson, “Reduction in x ray lithography shot noise exposure limit by dissolution phenomena,” *J. Vac. Sci. Technol. B* **6**(1), 167 (1988).

⁶⁴ibid.

⁶⁵W. Lawrence, “Spatial frequency analysis of line edge roughness in nine chemically related photo resists,” *Proc. SPIE* **5039**, 713–724 (2003); T. Azuma, K. Chiba, M. Imbeppu, D. Kawamura, and Y. Ohnishi, “Line edge roughness of chemically amplified resists,” *Proc. SPIE* **3999**, 264–269 (2000); A.R. Pawloski, A. Acheta, I. Lalovic, B.M. LaFontaine, and H.J. Levinson, “Characterization of line edge roughness in photoresist using an image fading technique,” *Proc. SPIE* **5376**, 414–425 (2004); M.I. Sanchez, W.D. Hinsberg, F.A. Houle, J.A. Hoffnagle, H. Ito, and C. Nguyen, “Aerial image contrast using interferometric lithography: effect on line edge roughness,” *Proc. SPIE* **3678**, 160–171 (1999).

⁶⁶P.M. Dentinger, L.L. Hunter, D.J. O’Connell, S. Gunn, D. Goods, T.H. Fedynshyn, R.B. Goodman, and D.K. Astolfi, “Photospeed considerations for extreme ultraviolet lithography

17.4.3 Resolution limits due to confinement effects in resists

Resist technologies that will enable EUV lithographic patterning at the sub-22-nm technology nodes must be capable of exceptional CD control, in addition to having low LER. Given the significant attenuation of EUV radiation in organic materials, ultrathin resist (thickness ≤ 100 nm) imaging appears to be the only viable option for single-exposure patterning at the sub-22-nm technology nodes. The 2008 ITRS specifications call for a resist thickness of 35–65 nm for the 22-nm technology node. However, the stability of ultrathin resist films presents very difficult challenges due primarily to confinement effects. In addition, ultrathin resist (UTR) imaging will require materials (resists and underlayers such as HMs) with superb etch selectivity and etch processes that lead to negligible roughness transfer between layer stacks.

As discussed in Chapter 11, experimental results suggest that material properties of UTR films can differ in significant ways from their bulk counterparts. Of particular interest, because of its influence on the viscoelastic behavior of the spin-coated films, is the effect of film thickness on T_g (see Fig. 17.29), which decreases with film thickness for the particular substrate investigated in the study.

Practical consequences of T_g modification in polymer films include significant changes of dissolution, diffusional and etching characteristics, mechanical creep behavior, and adhesion. Figure 17.30 shows a plot of the effective diffusion coefficient of perfluorooctane sulfonate photoacid as a function of film thickness of partially protected poly(4-*t*-butyloxycarbonyloxystyrene).⁶⁷ The profile shows asymptotic behavior at ~ 600 Å, below which diffusion slows down remarkably, probably due to interfacial and confinement effects. Clearly, the interaction of the first few hundred angstroms of the film with the substrate determines its adhesion and can alter its electrical and optical properties as well as its topographical and surface characteristics.⁶⁸

Resist additives such as leveling agents, plasticizers, bases, PAGs, etc. can segregate and partition themselves at different layers of the film, driven by interfacial effects, which are magnified as the film thickness decreases.⁶⁹ As a result, UTR films tend to have higher LERs than their thicker counterparts. They also tend to have higher susceptibility to poisoning effects and unexposed film thickness loss

resists," *J. Vac. Sci. Technol. B* **20**, 2962–2967 (2002); G.M. Gallatin, F.A. Houle, and J.L. Cobb, "Statistical limitations of printing 50 and 80 nm contact holes by EUV lithography," *J. Vac. Sci. Technol. B* **21**, 3172–3176 (2003); G. Han, M. Khan, and F. Cerrina, "Stochastic modeling of high energy lithographies," *J. Vac. Sci. Technol. B* **21**, 3166–3171 (2003).

⁶⁷D.L. Goldfarb and M. Angelopoulos, "Confinement effects on the spatial extent of the reaction front in ultrathin chemically amplified photoresists," *J. Vac. Sci. Technol. B* **19**(6), 2699 (2001).

⁶⁸M.M. Despotopoulou, R.D. Miller, J.F. Rabolt, and C.W. Frank, "Polymer chain organization and orientation in ultrathin films: A spectroscopic investigation," *J. Polym. Sci.: Pt. B* **34**, 2335 (1996); L.B. Rothman, "Properties of thin polyimide films," *J. Electrochem. Soc.* **127**, 2116 (1980).

⁶⁹U. Okoroanyanwu, "Thin film instabilities and implications for ultrathin resist processes," *J. Vac. Sci. Technol. B* **18**(6), 3381–3387 (2000); U. Okoroanyanwu, "Limits of ultrathin resist processes," *Future Fab Int.* **10**, 157–163 (2001).

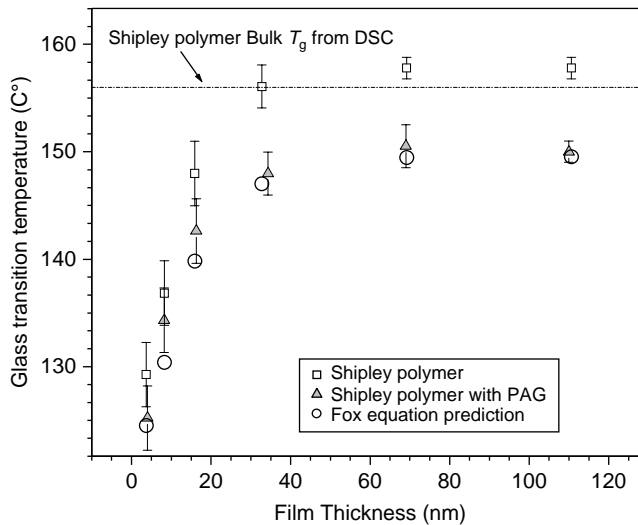


Figure 17.29 Glass transition temperature of resist polymer and resist polymer with PAG as a function of film thickness.⁷⁰

than their thick resist counterparts.⁷¹ It is widely appreciated that understanding and controlling the causes of defects associated with ultrathin films are major challenges for the near-term development of UTR process technology. It is difficult to produce ultrathin films that are uniform, continuous, defect free, and stable to changes in shape after aging or thermal processing.⁷²

17.4.4 Resolution limits due to resist polymer molecular properties

As shown in Table 17.1, the CD and LER tolerances of resist features are smaller than the dimensions of the polymer molecules in today's resists.⁷³ A CD of 22 nm is only a small multiple of the radius of gyration r_g in Å ($r_g \sim 0.6 \times MW^{0.5}$, where MW is molecular weight) of typical amorphous polymers used in resists today. And given a typical carbon-carbon bond length of 0.13–0.15 nm,⁷⁴ the 2008 ITRS specifications call for near-atomic-scale resolution, which is realistically untenable. Resist material parameters such as the polymerization length distribution, the end-to-end distance, and the radius of gyration, along with the effects

⁷⁰J.N. D'Amour, C.W. Frank, and U. Okoroanyanwu, "Measuring thermophysical properties of ultra thin photoresist films," *Proc. SPIE* **4690**, 936–942, 2002; "Modifications to thermophysical behavior in ultrathin polymer films," *Proc. SPIE* **5039**, 996–1007 (2003).

⁷¹ibid.

⁷²ibid.

⁷³F. Billmeyer, *Textbook of Polymer Science*, 2nd ed., pp. 154–157, John Wiley & Sons, Hoboken, NJ (1984).

⁷⁴G. Castellan, *Physical Chemistry*, 2nd ed., p. 578, Addison Wesley, Reading, MA (1971).

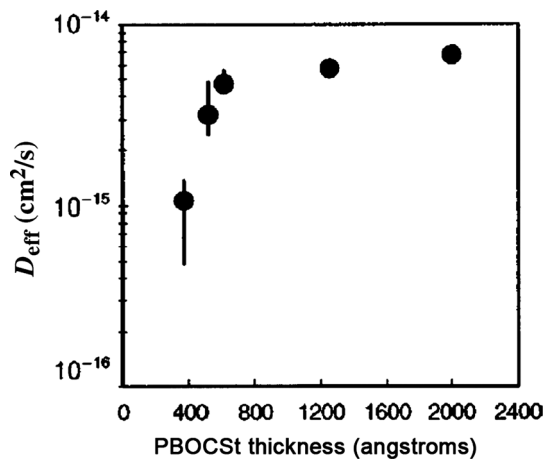


Figure 17.30 Effective diffusion coefficient of perfluorooctane sulfonate photoacid as a function of film thickness of a partially protected poly(4-*t*-butyloxycarbonyloxystyrene). (Reprinted with permission from Ref. 75. © 2001 American Institute of Physics.)

of the lithographic processes, especially dissolution, will affect resolution as well as surface and LER at the 22-nm and sub-22-nm technology nodes.

17.4.5 Resolution – line edge roughness – sensitivity trade-off

It is now well established that no resist at the present time simultaneously meets the ITRS 2008 specifications for resolution, LER, and sensitivity for patterning at the 22-nm and sub-22-nm nodes with EUV lithography. The correlation between resist sensitivity (E_{size} at 40-nm half-pitch) and limiting resolution for EUV resists evaluated on the EUV microexposure tool (MET) at Lawrence Berkeley National Laboratory (LBNL) in the United States in 2007 is shown in Fig. 17.31. As is evident in this graph, the resists with the highest resolution tend to be the least sensitive. The correlation between LER and sensitivity for a large selection of EUV resists that were also evaluated on the EUV MET at LBNL is shown in Fig. 17.32. The solid curve in Fig. 17.32 is the prediction of a simple model for the shot-noise-limited LER. Given its short exposure wavelength, it is expected that EUV lithography could have additional contribution to LER due to shot noise since for the same exposure energy, an EUV image will have a smaller number of photons per pixel than a comparable image obtained with longer wavelength lithographies. The LER for the most sensitive resist formulations tends to be dominated by shot noise, while that for the slower resists appears not to be as sensitive to shot noise, but rather to other effects (see Fig. 17.32).⁷⁶

⁷⁵D.L. Goldfarb and M. Angelopoulos, “Confinement effects on the spatial extent of the reaction front in ultrathin chemically amplified photoresists,” *J. Vac. Sci. Technol. B* **19**(6), 2699 (2001).

⁷⁶O. Wood, Global Foundries, Private Communication.

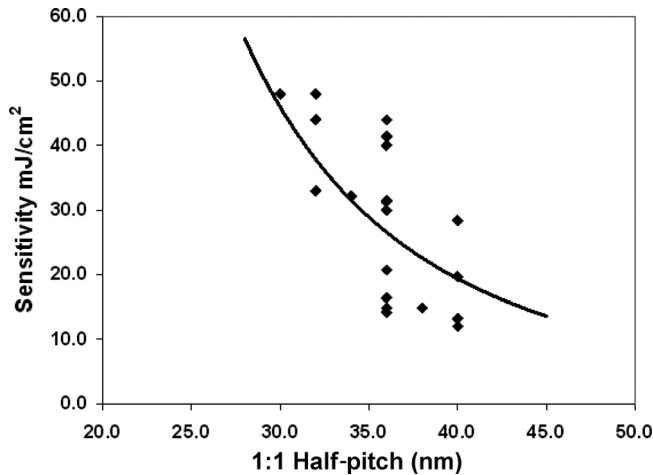


Figure 17.31 The correlation between resist sensitivity and limiting resolution for EUV resists evaluated with the EUV MET at LBNL in 2007.⁷⁷

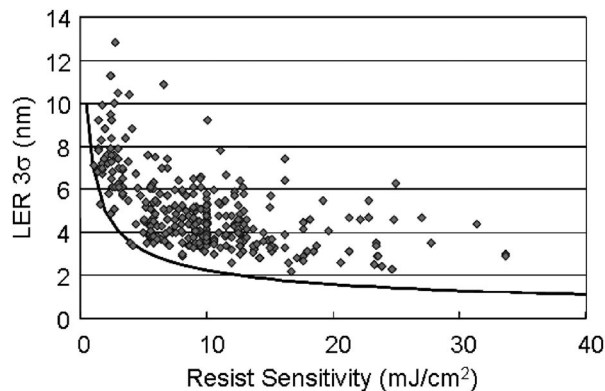


Figure 17.32 LER and sensitivity for a large selection of EUV resists evaluated with the EUV MET at LBNL.⁷⁸

Attempts have been made to model the relationship between these three critical performance parameters: resolution, LER, and sensitivity. Among these, the lithographic uncertainty principle (K_{LUP}) proposed by van Steenwinckel et al.⁷⁹

⁷⁷T. Wallow, C. Higgins, R. Brainard, K. Petrillo, W. Montgomery, C. S. Koay, G. Denbeaux, O. Wood, and Y. Wei, "Evaluation of EUV resist materials for use at the 32 nm half pitch node," *Proc. SPIE* **6923** (2008).

⁷⁸H. Levinson, "EUV lithography's future," presented at EUVL Symp., Lake Tahoe, Sept. 30, 2008.

⁷⁹D. van Steenwinckel, et al., "A novel method for characterizing resist performance," *Proc. SPIE* **6519**, 65190V (2007).

and the Z -constant proposed by Wallow,⁸⁰ where $Z \propto [\text{Pitch}/2]^3 \times [\text{LER}]^2 \times \text{Sensitivity}$, have proved to be relatively useful when comparing the performance of EUV resists.

The fact that these three critical parameters are in opposition raises some serious questions as to whether the resist infrastructure will be mature enough to support high-volume manufacturing at these nodes targeted for EUV lithography. Empirical evidence suggests that increased base loading cannot be used to improve the trade-off, but that it does improve LER and resolution at the cost of sensitivity. In like manner, PAG loading has been found to improve the resolution–LER–sensitivity trade-off. Furthermore, improving the quantum yield of the resist has also been shown to improve the trade-off.⁸¹

Of all the three performance metrics discussed above, LER continues to be the most challenging metric to meet for the 22-nm nodes and beyond.

17.5 Resist Materials Outlook for the 22-nm and Smaller Technology Nodes

Image blur caused by acid diffusion into unexposed areas of resists can only be limited, but not eliminated, if high sensitivity due to chemical amplification is to be maintained. This is because the mechanisms responsible for high sensitivity in CARs are intimately tied to the processes that lead to image blurring, making it extremely difficult, if not impossible, to have a highly sensitive, high-resolution chemically amplified resist based on the conventional design concepts. Therefore, novel resist design concepts incorporating different polymer architectures and PAGs that can achieve high sensitivity are currently under serious exploration. Such alternative resist design concepts could incorporate photocatalysts with well-defined limited lifetimes, whose diffusion length at nominal processing temperature could be targeted to match the resolution requirements of 22-nm and smaller design rules. This will ensure that at the barest minimum, the acid can only diffuse to a manageable distance that should fall within the geometry of the 22-nm and smaller design rules.

Another approach is to tether the PAG to the backbone of the resist polymer. In this way, the electrostatic interactions between the photoacid and its polymer-backbone-bound counter-ion will limit the diffusion of the photoacid to within a very short radial distance from where it is generated.

The use of PAGs that generate bulky photoacid is also a potential approach. Such bulky photoacids will have shorter diffusion lengths than their smaller-sized counterparts.

⁸⁰T. Wallow, C. Higgins, R. Brainard, K. Petrillo, W. Montgomery, C. S. Koay, G. Denbeaux, O. Wood, and Y. Wei, "Evaluation of EUV resist materials for use at the 32 nm half pitch node," *Proc. SPIE* **6923** (2008).

⁸¹G. Gallatin, Private Communication.

Another approach is to process the resists at low temperatures in order to reduce the thermally driven diffusion of the photoacids. The prime examples of this approach are found in low-activation-energy chemical amplification resists such as those based on acetal and ketal chemistry. These low-activation-energy resist platforms are in principle extendible to the 22-nm and sub-23-nm technology nodes, if ways are found to mitigate their outgassing and LER problems. It is of course possible for exposure tools to be designed such that outgassed species from resists are prevented from reaching the optical elements. Because these low-activation-energy chemical amplification resists can be processed at low temperatures, they have short diffusion lengths, and therefore have extremely low blur.

It is also possible to smoothen the walls of patterned resist features, using standard post-lithographic processing techniques such as UV hardening, electron-beam irradiation, and thermal flow. The use of surfactant rinse liquids has also been shown to improve LER of patterned resist features to acceptable values.⁸²

Finally, non-CARs are in principle extendible to the 22-nm and sub-22-nm technology nodes, with high exposure doses and low throughput, if the exposure tools can support that.

17.6 Resist Processing Outlook for the 22-nm and Smaller Technology Nodes

Double-patterning techniques will in all likelihood be used for device patterning at the 32-nm and 22-nm nodes, using hyper-NA immersion ArF lithography and resolution enhancement techniques. For the nodes of 15 nm and smaller, the single-exposure technique, using EUV lithography in combination with resolution enhancement techniques, appears to be the dominant resist processing technology. It is also conceivable that some of the layers for these sub-15-nm node devices might be patterned with a combination of single and double-patterning techniques. At some point, it will become nearly impractical to employ top-down patterning approaches as is currently done in conventional lithography. At such a point, the semiconductor industry may make the transition to bottom-up, hierarchical molecular self-assembly techniques.

⁸²D.L. Goldfarb, S.D. Burns, R.L. Burns, C.J. Brodsky, M.C. Lawson, and M. Angelopoulos, "Rinse additives for line edge roughness control in 193 nm lithography," *Proc. SPIE* **5376**, 343–351 (2004); P. Zhang, L. M. Jaramillo, M.B. Rao, C. Yates, D.M. King, B.F. Ross, and B.L. O'Brien, "Surface conditioning solutions to reduce resist line roughness," *Proc. SPIE* **5376**, 801–806 (2004).

Afterword

Here, on the level sand,
Between the sea and land,
What shall I build or write
Against the fall of night?

Tell me of runes to grave
That hold the bursting wave,
Or bastions to design
For longer date than mine.

A.E. Housman, from "Smooth Between Sea and Land"

We have come to the end of our long journey of exploration of the role of chemistry in lithography. Our journey has led us to many important destinations that mark the trail of the story of lithography. We started off by exploring the events that led to the invention of lithography, and from there we wandered farther afield in search of its chemical and optical origins. There we discovered a long chain of connected roads, built with physical and chemical ideas and concepts, spanning over 3000 years, stretching all the way back to the Greek era, through the scientific revolutions of the eighteenth and nineteenth centuries, that made possible the invention and development of lithography.

Next, we explored the evolution of lithography into the myriad strands that are practiced today, aided in large part by advancements in chemistry and physics, especially optical physics. In particular, we explored the roles of chemicals in lithographic patterning. We went a step further and explored each major lithographic technology in depth, examining the chemical and physical basis of their imaging mechanisms, and highlighting in the process how each imaging mechanism is made possible by the successful marriage between chemistry and optics. In addition, we examined how lithography is implemented in the fabrication of IC devices, using as an illustrative example the case of a complementary metal-oxide semiconductor device built from a 90-nm technology node inverter. This semiconductor device uses transistors to mediate computational functions in microprocessors used in computers that have done so much to enhance our modern lives. Finally, we examined the main approaches of advanced resist

processing and resolution limit issues of resists in the context of the trade-offs between resolution, line edge roughness, and sensitivity.

I have enjoyed being your guide through this journey. I hope you have enjoyed it as well. If through the course of this book, you, dear reader, have gained a better appreciation of the important role of chemistry in mediating lithography, then the efforts that have gone into writing it have been well worth it.

Index

- 1,1-diphenyl-2-picrylhydrazyl (DPPH), 220
1,1-diphenylethylene, 237
1,1,3,3,5,5-hexamethylcyclotrisilazane, 393, 795
1,2-diazepines, 232–233
1,3-dimethyl-1-tetrahydropyrimidinone, 191
1,3-dimethyl-2-imidazolidinone (DMI), 191
1,3-dimethyl-2-imidazolinone, 191
1,4-di(acetoxymethyl) benzene, 240
1H,1H-perfluorooctyl methacrylate, 250, 251
1-mercapto hexadecanoic acid, 477
1-phenyl-1,2-propanedione-2-*O*-benzoyloxime (PPO), 261
1-vinylnaphthalene, 404
2,1,4-diazonaphthoquinone sulfonate, 295
2,1,5-diazonaphthoquinone sulfonate, 295
2,2,6,6-tetramethylpiperidine-1-oxyl, 350
2-(2-aminoethoxy) ethanol (AEE), 191
2,2'-azobis(isobutyronitrile) (AIBN), 259
2,2'-dimethoxy-2-phenylacetophenone (DMPA), 260
2,3,4-trihydroxy benzophenone, 293
2,6-bis(4-azidobenzal)-4-methylcyclohexanone, 212
2-benzyloxy-protected poly(*p*-hydroxystyrene) (BOP), 381–382
2-chlorothioxanthone, 265
2-diazodimedones, 317
2-ethoxyethanol, 323
2-ethoxymethyl acetate, 185
2-ethylethoxy propionate, 185
2-heptanone, 185
2-isopropylthioxanthone, 265
2-methoxyethylether, 185
2-methoxypropyl-protected poly(*p*-hydroxystyrene) (MOP), 381–382
3,3'-diazodiphenylsulfone, 217
3- β -acryloyloxyandrosterone, 247
4,4'-bis(dimethylamino)benzophenone, 264–265
4,4'-diazidobenzalacetone, 215
4,4'-diazidobenzophenone, 215
4,4'-diazidostilbene, 215
4,6-bis(trichloromethyl)-1,3,5-triazine, 341
4-acetoxystyrene, 244
4-(aminomethyl)benzoate, 264
4-azidochalcone, 217
4-(dimethylamino)benzaldehyde, 264
4-(dimethylamino)methylbenzoate, 264
4-dimethylaminophenyldiazonium chloride, 234
4-ethylphenol, 348
4-hydroxy-4-methyl-2-pentanone, 185
4-hydroxybenzaldehyde, 350
4-*tert*-butyl(dimethyl)siloxy styrene, 350
4-vinylbenzene acetate, 240
5-(2-trifluoromethyl-1,1,1-trifluoro-2-hydroxypropyl)-2-norbornene (NBHFA), 236
5-*tert*-butyl(dimethyl)silyloxystyrene, 352
5-trifluoromethyl-5-hydroxy-2-norbornene, 377–378
 α chloroacrylate, 325
 β -elimination, 357
 γ -butyrolactone, 191
 π - π^* electronic transition, 314
 σ - σ^* transition, 796
A
Abbe sine condition, 89
aberration, 162, 554
aberration correction, 163
aberration-sensitive monitor, 553
absolute temperature, 67
absorbance, 490
absorption, 44
— bleachable, 552
— nonbleachable, 552
— of light, 58
absorption bands, 295

- absorption coefficient, 58, 490
— molar, 58, 490
absorption cross section, 632
absorption edge, 710
absorption layer, 714
absorption lines, 72
absorption spectrum, 400
accelerating voltage, 744
acetal-protected chemical amplification
 resists, 381–383
acetic acid, 350, 626
acetone, 190
acetophenone derivatives, 261
achromatic lens, 86
acid generators, 336–343
— classification of, 337
acid sensors, 499
acid-catalyzed thermolysis, 226, 357
acidolysis, 341
acid-quencher annihilation, 828
acridine, 499
acridine dyes, 268
acridine orange, 276
acridine yellow, 276
acriflavin, 268
across-field line width variations, 561
acrylamide, 266
acrylated polyol-based negative resists,
 219
acrylonitrile, 266, 325
actinic radiation, 285
action spectrum, 406
activation energy, 496
activity coefficients, 120
acyloximino groups, 326
acylsilane resists, 218
adhesion, 184
— work of, 468
adhesion promoters, 466
adsorption enthalpy, 724
advanced processing techniques, 797
aerial image, 490, 556
aerial image models, 563
aerosols, 696
affinities, 115
agar, 209
air, 102
airborne molecular base, 424
airborne molecular contaminants
 (AMCs), 630
albumin, 145
alchemy, 98–99
aldehyde, 207
alicyclic polymers, 183
alignment, 160, 488–489
aliphatic polymers, 183
alkane thiols, 177
alkoxymethylmelamine, 224
allyl methacrylate, 221
alpha rays, 64
alternating phase-shifting masks
 (PSMs), 622–623, 811
aluminum mirrors, 657–658
amidation, 135
ammonia, 104, 300, 424, 776
ammonium cyanate, 117
ammonium dichromate, 182, 209
ammonium hydroxide, 190
ammonium sulfate crystals, 628, 641
amorphous carbon, 431
amorphous silicon, 186
amplifier, 147, 767
amyl acetate, 185
angular momentum l , 75
anionic polymerization, 351
annealing, 775
anode, 788
antenna, 405
anthracene, 398, 428–429
anthraquinone, 263
antifoaming agents, 194
antioxidants, 182
antireflection coatings, 181, 186
— graded-index, 435
— organic and inorganic, 186
aperture function, 559
APEX-ETM, 357
apodization, 729
ArF (193 nm) exciplex lasers, 94, 183
ArF (193 nm) line-narrowed exciplex
 lasers, 164
ArF (193 nm) lithography, 118
aromatic monazines, 499
aromatic monobenzoid, 428
aromatic multibenzoid, 428
aromatics, 428
arsenic, 778
arsenic acid, 103
arsenic anhydride, 103–104
aryldiazonium salts, 274

- ascorbic acid, 268
aspect ratio, 532
asphaltum, 454
aspherical lens elements, 94
atmosphere, composition of, 103
atom lithography, 175–176
atomic bomb, 133
atomic energy levels, 78
atomic force microscopy (AFM), 165
atomic orbital, 131
atomic oxygen, 636
atomic theory, 99, 109, 111–113
— origin of, 111–113
atomic volume curve, 125
atomic weights, 125
atomic-scale resolution, 173
atoms, 5
attenuated phase-shifting mask (PSM),
165, 621–623
attenuation length of EUV radiation,
709
attenuation mechanism of fused silica,
653
Auger electrons, 415
average power, 613
Avogadro's hypothesis, 116–117
AZ Photoresist™, 291
azide resists, 208
azimuthal quantum number l , 131
azo compounds, 118
azobisisobutyronitrile (AIBN), 365
- B**
- back end of line (BEOL), 189
backbone scission, 411
backscattering, 743
Baekelite, 288
Balmer series, 77
barium fluoride, 649
barium platinocyanide, 63
base, 114, 769
base quenchers, 826–827
base-catalyzed esterification, 292
bas-relief master, 171
beam blanker, 748
beam-deflection unit, 748
beam-limiting apertures, 748
Beer-Lambert law, 490
benzene, 118, 428–429
benzoflavin, 276
benzoin, 259–260
benzoyl peroxide, 258
benzyl acetate, 225
benzyltrimethylstannane, 268
bilayer resist (BLR), 391
bilayer resist (BLR) system, 796–797
bimetallic plates, 141
binary intensity masks (BIMs), 620
binders, 280
biochips, 172
bipolar junction transistor (BJT), 768
birefringence, 48, 649
— stress-induced, 652
biradical, 274
bis(4-*tert*-butylphenyl)iodonium
cyclamate, 379
bis-diaminoalkyl-oligo-
dimethylsiloxane, 805
bis(dimethylamino)dimethylsilane, 393,
795
bisphenol A, 289
bis-tetrafluoroborate-tetrakis
(cyanomethane) palladium, 369
bit line contacts, 436
bitumen of Judea, 22, 182
blackbody radiation, 65, 66–69
— Planck's quantum hypothesis for,
67–69
bleachable absorbance, 552
bleaching, 295
blur, 757
Bodenstein pseudo-steady-state
approximation, 574
Bohr frequency condition, 77
Bohr orbits, 76
Bohr radius, 76
Bohr's model of the hydrogen atom, 75
boiling point, 185
Boltzmann constant, 67, 652
bond pad metal formation, 773
bond scission, 5
bonds
— covalent, 129
— dative, 129
— ionic and nonionic, 129
— mixed double, 129
— valence, 132
boron difluoride (BF₂), 778, 779
boron implantation, 775
boron trifluoride (BF₃), 275

- borosilicate glass, 620
 Bossung plot, 677
 bottom antireflection coating (BARC),
 186, 428
 — blobs, 696
 — developer-soluble, 430
 — graded, 798
 — multilayer, 798
 — organic and inorganic, 428
 — photosensitive, 430
 bound state, 77
 Boyle's law, 99
 Bragg equation, 711
 Bragg relation, 508
 branched polymers, 197
 bridging defects, 696
 bright-field mask, 620
 Brillouin scattering, 477
 broadband illumination, 163
 bromine, 61
 Brownian motion, 70
 Brunner's formula, 420
 bubbles, 696
 buffer layer, 714
 buffering agents, 142, 188, 194
 burning glass, 60
 butoxycarbonyloxystyrene (BOCST),
 240
 butyl carbitol, 190
 butyl cellosolve, 190
 butyllithium, 351
- C**
- cache memories, 156
Caesalpiniaceae, 289
 cage effect, 343
 calcination, early theories of, 99–100
 calcinations, 97
 calcium carbonate, 454
 calcium fluoride (CaF₂), 7, 163
 calcogenide glass, 227
 calixerenes, 241
 C-alkylation, 240, 245
 camera lucida, 10
 camera obscura, 10
 camphor, 118
 camphor sulfonic acid, 503
 canola oil, 194
 capacitors, 147, 767
 capillary pressure, 533
 capping layer, 713
 carbenes, 218, 296–297
 carbohydrates, 133
 carbon deposition on EUV optic,
 721–725
 carbon dioxide, 102
 carbon growth on EUV optic, 722
 carbon tetrafluoride, 546
 carbon-carbon bond length, 830
 carbonium ion, 343
 carborundum grit, 452
 carbo-*t*-butoxy norbornene (CBN), 367
 CARL (chemical amplification of resist
 lines), 799, 804
 Carl Zeiss Foundation, 92
 Carruther's equation, 272
 case II diffusion, 512
 casein, 104, 209
 casting solvents, 181
 castor oil, 194
 catadioptric systems, 163
 catalyzed oxidation of sulfur dioxide,
 642
 cathode, 788
 cathode ray, 61–63
 cathode ray tube, 61–62
 cationic polymerization, 208, 350
 — coordination, 365
 cationic ring-opening polymerization,
 257
Catoptrica, Euclid, 34
 catoptrics, early studies in, 34
 ceiling temperature T_c , 387, 390
 cell algorithm, 553
 cell projection lithography, 752
 cellosolve acetate, 187
 centrifugal force, 468–469
 ceric ammonium nitrate, 626
 chain scission mechanism, 324
 charged particle lithography, 741
 charging, 745
 charging effect, 224
chēmeia, 98
 chemical amplification, 335–336
 chemical amplification of resist lines
 (CARL), 799, 804
 chemical amplification resist
 — acetal-protected, 381–383
 — based on Claisen rearrangement,
 385–386

- chemical amplification resist (*cont.*)
— based on depolymerization, 387–389
chemical contrast, 826
chemical development, 506–507
chemical effects of light, 33, 58–61
— on certain salts, 55
chemical equivalents, 109
chemical etching, 546
chemical mechanical polishing (CMP),
151, 772
chemical printing [*chemische
druckerey*], 15
chemical reactions, laws of, 110–111
chemical transformations, 5
chemical vapor deposition (CVD), 432,
772
chemical-based shrink techniques, 799
chemically amplified resists, 226
chemische druckerey [chemical
printing], 15
chemistry, 4
— post-Lavoisian evolution of, 109–110
chlorine, 61, 103
chlorobenzene, 184
chlorofluorocarbons (CFCs), 186, 422
chloroform, 190
chloromethyltriazine, 240
chromatic aberrations, 86, 163, 752
chrome on a glass mask, 558
chromeless masks, 165
chromeless phase-shifting masks
(PSMs), 622–623
chromic acid, 190
chromium (Cr), 119, 367
chromium (III) ions, 208
chromium oxide, 645
chromium-on-glass (COG) masks, 621
chromospheres, 72
cinnamic acid, 202
citric acid, 104
Claisen rearrangement, 286
cleaners, 142
clear-field mask, 620
CMOS (complimentary metal-oxide
semiconductor), 149, 463–464
CO₂ laser, 717
coal gas, 102
coat-process-induced defects, 688
cobalt (Co), 782
cobalt silicide (CoSi₂), 782
coconut oil, 194
coherence length, 614
coherent illumination, 672
cold-set inks, 458
collector, 768
colligative properties, 133
colloids, naturally occurring, 145
collophonium, 288
color center formation, 655
colors of the rainbow, 39
combustion, early theories of, 99–100,
106
compaction, 652
complex refractive index, 424
complimentary metal-oxide
semiconductor (CMOS), 149, 463–
464
compound microscope, 86
compounds, 5, 113
— coordination, 129
— molecular, 130
computer, general-purpose, 154
computer clock speeds, 154
condensation/intermolecular
dehydration, 208, 224
condenser lens, 557
conductive electron-beam resists, 224
conductive paste, 142
conductivity, 53
— electrical, 124
— specific, κ , 123
conductivity equivalent, 123
confinement effects in resists, 829–830
conjoining forces, 474
conjoining pressure, 473
conservation of energy, law of, 121
conservation of mass, 108
contact aligners, 659
contact formation process, 773
contact printing, 160, 658
— theoretical resolution of, 160
contacts, 463, 782
contamination mitigation strategies,
730–737
contamination processes, 721–728
contrast, 184, 673
contrast enhancement layers, 556
controllers, 138
conversion efficiency, 719
cooperativity length, 480

- coordination cationic polymerization, 365
- coordination compounds, 129
- copper, electroplating of, 787
- copper arsenite, 104
- copper ferrocyanide, 122
- copper interconnect, 784
- copper interconnect wiring formation, 773
- copper metallization, 143
- copper seed layer, 787
- copper sulfate (CuSO₄), 787
- Coriolis force, 470
- corn oil, 194
- corrosion,
— lithographic mask degradation due to, 124
- corrosion inhibitors, 194
- cottonseed oil, 194
- coulombic interactions, 396
- cresols, 288
- critical dimension (CD), 160, 463
- critical dimension (CD) uniformity, 674, 677
- critical deprotonation model, 518
- critical ionization model, 518
- critical modulation transfer function, 675
- critical wave number, 475
- Crookes tube, 92
- cross-linking, 411
- cross-linking reactions, 5
— radiation-induced, 200
- cross-linking yield G_x , 413
- crown glass, 86, 90
- crystallinity, degree of, 477
- crystallization, 97
- crystal-originated pits (COPs), 474
- cut mask, 811
- cyclohexanone, 184, 185, 187
- cyclopentadiene, 367
- cyclopolymerization, 387
- D**
- daguerreotype process, 17, 25
- dampening solutions, 455
- dark reaction, 211
- dark-field mask, 620
- debris-mitigation schemes, 718, 737
- decompaction, 652
- decomposition temperature, 369
- deep ultraviolet (DUV), 183
- deep ultraviolet (DUV) lithography, 792
- defectivity control, 422
- defects, 473
- definite proportions, law of, 110
- degree of coherence, 616–617
- degree of crystallinity, 477
- degree of polymerization, 272
- degree of spectral purity, 163
- degrees of freedom, 122
- dehydrogenation, 348
- deionized water, 189
- dendrimers, 241
- Dennard's scaling rules, 155
- DEPICT, 554
- depolymerization, 286
— chemical amplification resists based on, 387–389
- deprotection, 5, 286
- deprotection kinetics, 493
- deprotection temperature, 369
- depth of focus, 674
- desensitizing gums, 142
- desilylation, 351
- developer selectivity, 360
- developers, 181
— metal-ion-free (MIF), 504
- development, 504–511
— chemical, 506–507
— physical, 507
— puddle, 505
— resist, 505–506
- development models, 589–599
- development rate r , 576
- development rate monitor (DRM), 552
- develop-processed-induced defects, 688
- device miniaturization, 153
- device technology node, 463
- dewetting, 474
- di(α -methylbenzene)ether, 245
- diacetone alcohol, 185
- dialkyldisulfides, 177
- dialkylphenacylsulfonium salts, 279
- diaryliodonium sulfonates, 340
- diazo compounds, light-sensitive, 141
- diazo plates, 141
- diazo resists, 233–234
- diazo-Meldrum's acid, 316

- diazo-Meldrum's acid-based resists, 316–317
- diazonaphthoquinone (DNQ), 182
- chemistry of, 292
 - photolysis of, 296
- diazonaphthoquinone (DNQ) ballast compounds, 294
- diazonaphthoquinone (DNQ) sensitizer, 118
- diazonaphthoquinone-4-sulfonate, 292
- diazonaphthoquinone-5-sulfonate, 290, 292
- diazonaphthoquinone/novolak, 145
- diazonaphthoquinone/novolak resists, 286–292
- diazonium salts, 287
- diazopiperidine dione, 317
- diazopyrazolidine dione (DPD), 317
- diazoresin, 233
- diazotetramic acid, 317
- diazotization, 292
- dichlorosilane gases, 776
- dichromate resists, 208
- dichromated gelatin, 209
- dielectric constant, 53, 409
- dielectric material, 53
- dielectric optical coatings, 658
- Diels-Adler reaction, 367
- diethylene glycol dialkyl ether, 191
- diethylene glycol monobutyl ether, 191
- diethylene glycol monoethyl ether, 191
- diffraction, 42
- diffraction limitations, 30
- diffraction order, 713
- diffraction patterns, 559
- diffraction-limited system, 94
- diffusion, 772
- case II, 512
- diffusion barrier, 783
- diffusion coefficient, 478, 580
- diffusion lengths, 502, 823
- diffusion promoter, 795
- digital waterless plates, 141
- diglyme, 185
- Dill model, 552
- Dill papers, 551
- Dill parameters *A*, *B*, and *C*, 552
- dimethyl formamide, 190
- dimethylsilyldimethylamine, (DMSDMA), 393, 794
- diode-pumped fiber laser, 717
- diodes, 147, 767
- dioxane, 190
- dioxycyclopentadiene, 275
- dip coating, 468
- diphenyl hexafluoroarsenate, 387
- diphenylbenzofuran, 270
- diphenyliodonium hexafluoroarsenate, 389
- dipolar interaction, 400
- dipole, oscillating, 400
- dipole radiation, 705
- dipole resonance transfer, 400
- dipole-dipole interactions, 135
- dipotassium hexachloroiridate, 369
- dip-pen lithography, 175
- Dirac delta function, 823
- direct oxidation of sulfur dioxide, 642
- direct photoexcitation processes, 727
- direct-current (DC) magnetron sputtering, 713
- directed self-assembly lithography, 177
- directed valencies, theory of, 132
- discharge-produced plasma (DPP) sources, 716, 718–719
- discrete electronic components, 147
- discrete transistors, limits of, 147
- disjoining pressure, 475
- dispersion relation, 475
- dissociative electron attachment (DEA), 418
- dissolution inhibition behavior 183
- dissolution inhibition resists, 286–292
- dissolution inhibitor, 293
- dissolution properties, 507
- dissolution rates, 308
- distillation, 97
- di-*tert*-butyl dicarbonate, 352
- di-*tert*-butyl peroxide, 351
- di-*tert*-butyl peroxide initiators, 365
- di(*tert*-butylphenyl) iodonium perfluorobutanesulfonate (nonaflate) (DTBPIONf), 340
- Döbreiner's triads, 125
- dose to clear, 577
- dosimetry, 411
- double patterning, 794, 797
- double-exposure techniques, 797
- drain, 769

- DRAM (dynamic random access memory), 150
- dry ArF (193-nm) lithography, 678–692
- dry etching, 151, 545–546
- dry resists, 280–282
- drying stimulators, 194
- dual damascene processes, 429, 773, 784
- dualistic theory, 113–115
- DUV (deep ultraviolet), 183
- dwell time, 749
- dynamic random access memory (DRAM), 150
- E**
- edge sharpening, 230
- egg albumin, 209
- Einstein mass-energy equivalence law, 85
- Einstein's theory of relativity, 83
- elastic collisions, 742
- elastoplastic model for pattern collapse, 535
- electric charge density ρ , 52
- electric current density J , 52
- electric displacement D , 52
- electric field, 54
- electric permittivity of vacuum, 54
- electric switch, 147
- electric vector, 425
- electric-field-induced metal (EFM) migration, 628
- electrochemical series, 115
- electrochemical theory, 113–115
- electrode potentials, 115
- electroless copper deposition, 143
- electrolysis, 52, 115
- Faraday's law of, 788
- laws of, 116
- electrolytic dissociation, theory of, 123–124
- electromagnetic induction, 116
- electromagnetic spectrum, 55–57
- electromagnetic theory, 50–55
- electromagnetic units, 54
- electromagnetism, 50
- equations of, 47
- electromigration, 152
- of chromium ions, 124
- electromotive force, 115
- electron, 5, 127
- Auger, 415
- discovery of, 61–62
- low-energy, 415
- outer-shell, 5
- secondary, 415
- thermalization distance of, 417
- valence, 127
- electron acceptor, 398
- electron affinities, 398
- electron donor, 398
- electron microscopy, 80
- electron optical column, 746
- electron optical components, 748
- electron projection lithography, 749, 751–753
- electron scattering, 742–746
- electron source, 746
- electron-beam (e-beam) curing, 540–543
- electron-beam (e-beam) direct-write lithography, 750
- electron-beam (e-beam) evaporation, 713
- electron-beam (e-beam) heating-induced reflow, 799
- electron-beam (e-beam) lithography, 167–169, 741, 746–749
- electron-beam (e-beam) machines
- mask-based, 168
- maskless direct-write, 168
- electron-beam (e-beam) resists, conductive, 224
- electron-beam (e-beam) system cell-projection, 168
- electron-beam (e-beam) writers, 623, 624–625
- electron-electron interaction, 743
- electronic charge, 409, 743
- electronic orbit, 82
- electronic shells, 78
- electrophile, 238
- electrophilic aromatic substitution, 225
- electrophilic substitution reaction, 226, 238
- electrophotographic plates, 141
- electroplating of copper, 787
- electrostatic chucks, 757
- electrostatic discharge (ESD), 628
- electrostatic lenses, 763

- electrostatic units, 54
 - elements [*stoicheia*], 95, 99
 - transmutation of the, 96
 - embossing, 165
 - emission bands, 295
 - emitter, 769
 - empirical formula, 133
 - encapsulation of IC devices, 207
 - end cap pull back, 689
 - end-to-end distance, 830
 - energy migration
 - down-chain, 405
 - in resist polymer, 403–406
 - energy transfer, 399–403
 - sensitization by, 407–409
 - energy-curable inks, 458
 - enhanced kinetic development rate model, 590
 - epilayer, 774
 - epitaxial silicon, 774
 - epitaxy, 772
 - epoxy-based negative resists, 219
 - equilibrium contact angle θ , 467
 - equilibrium reaction, 120
 - equivalents, law of, 111
 - ESCAP (environmentally stable chemically amplified photoresist), 358
 - esterification, 135, 208, 246
 - base-catalyzed, 292
 - ester-protected chemical amplification resists, 357–360
 - ester-protected poly(hydroxy styrene)-based resists, 357–360
 - ester-protected poly(methacrylate)-based resist platform, 360–364
 - etch resistance, 184
 - etching of mask-making resists, 626
 - etching process, 544, 772
 - chemical, 546
 - dry, 151, 545–546
 - physical, 546
 - plasma, 546–547
 - reactive-ion, 232, 547–548
 - wet, 544–545
 - etch-stop layer, 787
 - ethanol, 323
 - ether winds, 46
 - ether-protected chemical amplification resists, 344–345
 - ethyl cellulose acetate, 185
 - ethyl lactate, 185
 - ethyl pyruvate, 185
 - ethylacrylate, 221
 - ethylene glycol, 194
 - ethylenediamine, 191
 - EUV (extreme ultraviolet) lithography, 164
 - evaporation, 772
 - exchange transfer, 401–403
 - excimer laser sources, 609
 - excimer-binding energy *B*, 397
 - excimers, 397–398
 - exciplex laser sources, 7, 609
 - exciplexes, 398–399
 - excitation schemes, 612–613
 - excited chromophore, 201
 - excited state, 77
 - excited state complexes, 397–399
 - exciton, 403
 - exciton traps, 405
 - exothermic reaction, 402
 - exponential attenuation of radiation, 490
 - exposure, 489–491
 - exposure latitude, 576, 673
 - exposure mechanism of resists, 415–418
 - exposure models, 570
 - exposure optics system, 628–629
 - exposure rate constant, 552
 - exposure-defocus window, 674, 677
 - extended source method, 556
 - extra pattern defects, 696
 - extreme ultraviolet (EUV) emission spectrum, 718
 - extreme ultraviolet (EUV) exposure system, 715–716
 - extreme ultraviolet (EUV) lithography, 164, 170, 703
 - sources for, 716–719
 - extreme ultraviolet (EUV) mirrors, 710–713
- F**
- F₂ excimer laser (157 nm), 7
 - line-narrowed, 164
 - F₂ excimer laser (157-nm) lithography, 700–701
 - Faraday's law of electrolysis, 788

- far-field diffraction, 666
fermentation, 102
fiber optics, 94
Fick's second law of diffusion, 580
field emission, 747
field oxide, 770
field-effect transistors (FETs), 768
field-emission sources, 747
film-forming resin, 181
filtration, 97
fine art printing, 5
first-order scalar model, 564–565
fish glue, 209
fixed air (CO₂), 102
FLEX, 554
flare, 654
— long-range and short-range, 655
flint glass, 86, 90
flip-flops, 767
floating gate, 150
flow temperature, 537
fluorescein, 266, 268
fluorescence, 396
— delayed, 404
— emission, 397
— lifetime, 400
— spectroscopy, 498–501
fluorescent screen glow, 63
fluorine-doped fused silica, 621
fluorocarbons, 184
fluorspar, 103
fly's eyes, 617
focused ion beam (FIB), 761
focused-ion-beam (FIB) writers, 623
footing defects, 430, 503
formamides, 190
forward scattering, 743
fountain solutions, 141, 194, 455
four-element theory, 95–96
Fourier optics, 93
Fourier transform, 558
— inverse, 559
Fourier transform infrared (FTIR)
 spectroscopy, 310
Fraunhofer diffraction, 666
Fraunhofer diffraction integral, 558
Fraunhofer diffraction pattern, 667
Fraunhofer lines, 72
free energy, 409
free radical polymerization, 257, 365
freezing point, depression of the, 123
— molecular projection of the, 122
Fresnel diffraction, 665
Fresnel equations, 440
fringes, 43
front end of line (FEOL), 189
Fujita-Doolittle equation, 586
full scalar model, 565–566
full width half maximum (FWHM), 648
full-wafer printing, 163
fungicides, 194
furans, 275
fused silica, 163, 621, 649
— attenuation mechanism of, 653
— degradation mechanisms, 652
— thermal properties of, 651
fusion, 97
- G**
- gallic acid, 104
gallium, 126
galvanic cells, theory of, 124
gamma rays, 64
gate, 463, 769
gate length, polysilicon, 463
Gaussian beam, 749
Gaussian distribution function, 580
gel curve, 254
gel point, 252
gelatin, 145, 209
gelation theory, 254
germanium, 126
germinate recombination, 410
ghost images, 657
glass prism, 37
glass temperature transition T_g , 350
glasses, planed and curved, 36
glassmaking technologies, 33
g-line, 183, 608
glycerol, 104
glycidyl ether bisphenol-A novolak, 414
glycidyl methacrylate, 220
glycol ethers, 188, 190, 194
glycol monoalkyl ethers, 191
gold, 706
graded bottom antireflection coating
 (BARC), 798
gravure painting, 455
grazing-incidence mirrors, 720
Grignard reagent, 31

- ground state, 77
Grun's formula, 541
gum arabic, 453
G-value, 411
- H**
- Hamaker constant, 475
hard bake, 536
hard mask (HM), 391, 435
hard mask (HM) resist system, 794
Hartley band, 630
haze defects, 641
HCl (hydrogen chloride), 350
heat-set inks, 458
heat theorem, 124
Heisenberg's uncertainty principle, 81
heliography, 22
heptanone, 187
Herzberg continuum, 623
Hess's law, 121
heterojunction bipolar transistor, 149
heterolysis, 343
hexafluoroalcohol, 376
hexafluoroantimonic acid, 495
hexahydroxy benzophenone derivatives, 294
hexamethyldisilazane (HMDS), 466
Hg (mercury) arc lamps, 164
high-activation-energy resists, 823
high-numerical-aperture (NA) scalar model, 565
high-pressure arc lamp, 608
high-repetition-rate laser sources, 163
h-line lithography, 183
holography, 94
homolytic cleavage, 495
Hopkins' method, 556
Hückel diagram, 401–402
Hund's rule of maximum multiplicity, 396
hydrazine, 369
hydrocarbon cracking model, 724
hydrocarbons, polynuclear aromatic 276
hydrofluoric acid (HF), 103, 191
hydrogen, 102
hydrogen bonds, 135
hydrogen peroxide, 190
hydrogen silsesquioxane (HSQ), 245
hydrogen sulfide, 104
hydrolytic stability, 336
hydrophilic over layer (HOL) process, 800
hydrophobic–hydrophilic interactions, 137
hydroquinone, 266
hydroxyethyl methacrylate, 221
hydroxymethyl melamine, 224
hyper-numerical-aperture imaging, 50, 435, 797
hypsochromic spectral shifts, 500
- I**
- IC (integrated circuit), 3, 148, 605
IC devices, fabrication of, 767
Icelandic spar, 47
i-line (365 nm), 183, 608
i-line (365-nm) lithography, 183, 677–678
illumination system, 557, 616–618
image formation, 554, 665–673
— theory of, 93
image log-slope, 576
image quality, 673–677
image reversal, 218, 300
image spreading, 819
imaging theory, 557–560
imidazole, 300
imides, 340
immersion optics, 165
impression, 455
in situ cleaning, 720
incoherent illumination, 672
incoherent sources, 608
indene carboxylic acid, 238, 295
indene-1-carboxylic acid and indene-3-carboxylic acid, 297
indenone, 327
indestructibility of matter, law of, 107
index of refraction, 37
indirect excitation processes, 727
inductors, 147, 767
inelastic collisions, 742
inelastic scattering, 416
inertial resistance, 84
inflammable air (H₂), 102
infrared radiation, 55
infrared spectroscopy, 493
initiators, 258
inks, 137, 181
inspection and measurement, 543–544

- insulated gate field-effect transistor (IGFET), 769
- integrated circuit (IC), 3, 148, 605
- integrated circuit (IC) devices, fabrication of, 767
- intensity match conditions, 427
- interconnects, 29
- interfacial tension, 137
- interference phenomenon, 40
- interferometer, 46
- interferometric lithography, 47
- interlayer dielectric (ILD), 783
- intermolecular forces, 134–135
- internal conversions, 396
- International Technology Roadmap for Semiconductors (ITRS), 8
- intersystem crossings, 396
- intramolecular dehydration, 208, 236
- intramolecular esterification, 246–247
- intramolecular potentials, 479
- intrinsic defects, 687
- intrinsic viscosity, 252
- inverse Fourier transform, 559
- inverters, 767
- iodine, 61
- iodonium, 275
- ion beams, 760
- ion implantation, 760, 772
- ion milling, 760
- ion projection lithography (IPL), 763
- ion-beam lithography, 169–170, 741, 759–766
- ion-beam polishing, 715
- ion-beam sputtering, 713
- ionization, 124
- degree of, 124
- ionization energy, 410
- ionizing radiation, 409
- ions, 5
- Ir (iridium), 367
- Ir(IV)-based catalysts, 365
- isobenzofurane, 268
- isomerism, 130
- optical, 130
- isoprene, 133
- isopropyl alcohol, 194
- isothermal compressibility, 652
- J**
- junction field-effect transistor (JFET), 768
- junction transistors, 146
- K**
- k_1 as a process-dependent parameter, 7
- Kellheim limestone, 12, 452
- ketal resist system (KRS), 381
- ketal-protected chemical amplification resists, 381–383
- ketene, 296–297
- ketocoumarins, 265–266
- ketones, 190
- ketoxime esters, 261
- kinematic viscosity, 470
- kinetic chain length, 272
- kinetic development rate model, 590
- kinetics, 120
- Kirchoff's law, 73
- Kodak positive resists, 145
- Kodak Thin Film™ resist (KTFR), 212
- Köhler illumination, 616, 672
- kopals, 289
- KrF (248-nm) exciplex lasers, 94, 183
- KrF (248-nm) line-narrowed exciplex lasers, 164
- KrF (248-nm) lithography, 678
- L**
- lactic acid, 104
- Lambert's law, 58, 490
- lampblack, 12
- lanthanum hexaboride (LaB₆), 747
- Laplace pressure, 475
- laquer, 288
- laser, 94
- laser interferometry, 310, 507
- laser plates, 141
- laser sources, 608
- laser writers, 623, 625–626
- laser-produced plasma (LPP) sources, 716–718
- latent electrophile, 238
- latent heat, 102
- latent image, 489
- lawrencium, 126

- leakage current, 925
 - lens heating, 650
 - leveling agents, 182
 - levigator, 452
 - Lewis acid, 275
 - lift-off processes, 299
 - light
 - nature of, 38
 - polarization of, 47–50
 - speed of, 37, 67
 - velocity of, 44–47
 - wavelength of, 44
 - light and color, 39
 - light as a wave or particle, 40
 - light waveguides, 94
 - light waves, 50
 - light-field mask, 620
 - lightly doped drain (LDD) implant process, 773
 - line edge roughness (LER), 804, 825
 - line slimming, 691
 - line spectra, dark and light, 71–74
 - line spread function, 823
 - line thinning, 696
 - line width roughness (LWR), 804
 - linear polymers, 197
 - linear stability analysis, 475
 - line-narrowed F_2 excimer laser, 164
 - line-narrowed KrF and ArF excimer lasers, 164
 - liner oxide, 777
 - linseed oil, 184, 194
 - liquid contact potentials, 124
 - liquid phase silylating agents, 794–795
 - liquification of gases, 116
 - lithium, (Li), 717
 - lithium fluoride, 649
 - lithographic crayon, 451
 - lithographic imaging equation, 576
 - lithographic modeling, 551
 - lithographic pencil, 452
 - lithographic simulator, first, 553
 - lithographic simulators, 582
 - lithographic stones, 16
 - lithographic uncertainty principle, 832
 - lithographie* [writing with stone], 19
 - lithography, 3, 772
 - fine art, 451
 - immersion, 50
 - invention of, 4, 10
 - stone, 451
 - stone plate, 5
 - lithography-etch-lithography-etch (LELE) double-patterning process, 813
 - lithography-freeze-lithography-etch (LFLE) double-patterning process, 813
 - logic circuits, 147
 - London forces, 135
 - longitudinal wave, 49
 - long-range and short-range flare, 655
 - Lorentz space and time transformations, 83
 - low-activation-energy resists, 823
 - low-energy secondary electrons, 727
 - low-pressure chemical vapor deposition (LPCVD), 776
 - low-thermal-expansion glass, 713
 - Lucifer lacca*, 288
 - luminescent effect, 63
 - luminiferous ether, 43, 50
 - lumped parameter model, 590
 - Lyman series, 77
- ## M
- Mack model, 553, 590–593
 - magnesium fluoride, 649
 - magnetic field, 54
 - magnetic induction B , 52
 - magnetic permeability, 53
 - magnetic quantum number m , 131
 - malic acid, 104
 - manganese, 103
 - mask, 463, 557, 618–623
 - mask bias, 620
 - mask error enhancement factor (MEEF), 619, 791
 - mask making, 745
 - mask-making resists, 626–627
 - etching of, 626
 - mass action, law of, 120
 - matter waves, 79
 - McLaurin series, 444
 - mean free path, 547
 - measurement and inspection, 543–544
 - MEBES (multiple electron-beam exposure system), 749
 - melamine cross-linker, 239
 - membrane model, 518

- memory bottleneck, 155
memory chips, 138
mercury (Hg) arc lamps, 164
metacresol, 303
metal interconnects, 463
metal-chalcogenide resists, 227, 230
metal-ion-free (MIF) developers, 504
metal-organic chemical vapor
 deposition (MOCVD), 151
metal-oxide semiconductor field-effect
 transistor (MOSFET), 149, 768, 769
meta-PHOST isomers, 351
methides, 340
methyl isobutyl ketone (MIBK), 190,
 245
methylamylethanol, 191
methylene, 268
methylene chloride, 190
methylethyl ketone, 190
methylmethoxy propionate, 185
Michelson-Morley experiment, 47
Michler's ketone, 264
microcontact printing, 171
microelectronics, 29
microfluidics, 172
microloading effects, 689
micromolding in capillaries, 171–172
microprocessors, 138
microscope, invention, 38
minimum resolvable pitch, 673
mirrors, 36
modern chemistry, foundation of, 104–
 109
modulation transfer function, 673, 674–
 675
molar absorption (extinction)
 coefficient, 58, 490
molarity, 256
molding, 165
molecular beam epitaxy, 151
molecular contaminants, 628
 — airborne, 630
molecular self-assembly lithography,
 176–177
molecular theory of matter, 64, 65
molecular weight, 830
molecules, 5
molybdenum (Mo), 710
molybdenum silicide (Mo-Si), 714
molybdic acid, 103
momentum p , 79
monazoline, 300
monobenzoid aromatics, 428
monoethanolamine (MEA), 191
monolithic integrated circuit (IC), 148
monopropanolamine, 191
Moore's law, 6
MOSFET (metal-oxide semiconductor
 field-effect transistor), 149, 768, 769
mucic acid, 104
multibenzoid aromatics, 428
multilayer bottom antireflection coating
 (BARC), 798
multilayer resist systems, 792–793
multilevel metallization, 152
multiple proportions, law of, 111
multiplexers, 767
- N**
- N-(9-acridinyl acetamide (ACRAM),
 499
nanofluids, 172
nanoimprint lithography, 172–173
nanoskiving, 171, 172
naphthol, 287
natural calcite, 47
near-field diffraction, 665
near-UV lithography, 792
negative resist, 159
 — radiation-induced, 200–224
negative resist composition, 280
negative resist developers, 187
negative/positive process, 17
network polymer, 197
neutron scattering, 477
neutrons, 75
Newtonian fluid, 469
Newton's rings, 41
N-iminopyridinium ylides, 232–233
nitrene, 214
nitric acid, 453
nitric oxide, 92
nitrogen, 106
nitromethane, 190, 369
N-methoxymethylated melamine, 238
N-methylacetamide (Mac), 191
N-methyldiethanolamine, 264
N-methyl-N-ethylpropionamide, 191
N-methylpyrrolidone (NMP), 356, 424,
 795

- nMOS (*n*-channel MOSFET), 149, 770
N,N-diethylbutylamide, 190
N,N-dimethylacetamide (DMAc), 191
N,N-dimethylpropionamide, 191
nonbleachable absorbance, 552
non-chemically amplified negative resists, 226
non-radiation-based negative resists, 199–200
nonradiative transition, 396
nonvolatile semiconductor memory (NVSM), 150
norbornene, 367
norbornene hexafluoroisopropanol, 373
norbornene-derived monomers, 183
normal butyl acetate, 187
normal paraffins, 194
normal-incidence multilayer mirrors, 720
normalized image log-slope (NILS), 576, 647
Norrish-type I process, 323
Norrish-type II process, 331
notch development, 554
novolak, 288
nuclear energy, 133
nuclear model of the atom, 74
nucleic acids, 133
nucleophilicity, 274
nucleus, 78, 127
numerical aperture (NA), 7
- O**
- O₂ ashing, 190
o-(α -methylbenzyl)phenol, 245
O-alkylation, 240, 245
objective lens, 556
off-axis illumination, 165, 554
offset lithographic inks, 193, 458
offset lithography, 3, 455
— waterless, 460–461
offset lithography rollers, 456
offset printing press, 455
oil paints, 289
oleic acid, 454
oleomagnate of lime, 454
onium salts, 273
optical activity, 118, 119
optical coatings, 657–658
optical density, 490
optical fingerprints, 86
optical lithography, 160–166, 605
— elements of, 606–608
optical materials used in UV lithography, 649
optical path difference (OPD), 562
optical pattern generators, 623, 624
optical proximity correction (OPC), 165
optical proximity effects, 684
optics, 4
— early studies in, 34
Optics, Euclid, 34
optics lifetime, 719–720
organic chemistry, 4
— development of, 117–118
— ortho-nitrobenzyl chemistry, resists based on, 318–322
ortho-PHOST isomers, 351
osmium (Os), 367
osmotic pressure, 122
overlay, 489
overpriming, 467
oxalic acid, 104
oxidation, 720, 721, 725–728, 772
oxidation potential, 409
oxidation-resistant capping layers, 731
oxycyclohexene, 275
oxygen, 102, 106
oxygen plasmas, 193
ozalid process, 285
Ozatec™, 290
ozone, 636
- P**
- packaging process, 773
para-PHOST isomers, 351
partial coherence, 553, 560
particle accelerator, 772
particle defects, 687
particle (corpuscular or emission) theory, 40–42
passive components, 768
path difference, 561
pattern collapse, 532–536, 686
— elastoplastic model for, 535
pattern distortion, 689
pattern generators, 618
Pauli's exclusion principle, 130
Pd(II)-based catalysts, 365
pellicles, 627–628

- perchloric acid, 626
percolation model, 518
perfluorinated compounds, 421
perfluoroalkanesulfonic acids (PFAS), 421
perfluoroalkanoic acid (PFAA), 421
perfluorooctane sulfonate photoacid, 822
perfluorooctanesulfonate, 340
perfluorooctanesulfonic acid, 421
perfluorooctanoic acid, 421
perfluorooctyl sulfonate, 340
periodic law, 124–129
periodic table, 124–129
— theory of the, 130–132
permeability of vacuum, 54
permittivity of free space, 744
peroxides, 258
Perrin formula, 402–403
persistence length, 480
perspective, laws of, 34
perylene, 276
pewter plate, 22
phase defects, 714
phase edges, 811
phase error, 562
phase match condition for zero reflectivity, 426
phase rule, 122
phase-contrast microscope, 93
phase-shifting masks (PSMs), 165, 553, 620–623, 798
phenols, 190
phenylene diacrylates, 205
phenylsilanediol, 245
philosopher's stone, 98
phlogiston theory, 100
phosphorescence, 396
phosphoric acid, 777
phosphorous, 103
phosphorous implantation, 774
photoacid generation monitoring, 498–501
photoacid generator, 181
photoactive compound, 73
photobleaching, 230
photocathode projection lithography, 752
photochemical oxidation of sulfur dioxide, 62
photochemistry, 33
photodecomposable base, 380
photodimerization reaction, 203
photodissociation of molecular oxygen, 632–636
photodoping, 227
photoelastic constant, 652
photoelectric effect, 69–71, 416, 647
photoelectricity, 65
photoelectron yield, 722
photoelectrons, 415
photofragmentation, 258
photo-Friess rearrangement, 286
— resists based on, 322
photogeneration of radicals, 258–262
photograph
— the first, 22
— the first permanent, 17
photography, 4
photoimageable polyimides, 206
photoinitiation, 258
photoinitiator, 181, 182
photoionization, 409
photolithography, 4, 160–166, 605
— invention of, 17
— limits of, 165
— step-and-repeat, 163
photolysis, 274
photomasks, fabrication of, 623–626
photomechanical reproductions, 287
photometry, 33
photonic devices, 151
photons, 5
photon-stimulated desorption, 727
photo-oxidative degradation, 633
photo-oxygenation of polymers, 640–641
photopolymer plates, 141
photopolymer printing plate, 256
photopolymer resins, 141
photoreduction, 210
photorepeaters, 618
photoresist, inorganic, 55
— dyed, 553
photosensitization, 406
photospeed, 315
photosphere, 72
photosynthesis, 103
physical chemistry, development of, 120–133

- physical development, 507
physical etching, 546
physical vapor deposition (PVD), 782
pinacol rearrangement, 208, 234–235
pinacol-pinacolone rearrangement
 reaction, 208
pinholes, 473
pitch, 6
planarizing layer, 421
Planck's constant, 69
Planck's distribution law, 69
Planck's quantum hypothesis for
 blackbody radiation, 67–69
planographic printing technique, 17,
 455
plasma etching, 546–547
plasma stripping, 193
plasma-assisted shrink techniques, 799
plasma-deposited polymers, 796
plasticization, 808
plasticizer, 808
pMOS (*p*-channel MOSFET), 149, 770
p-n junction, 147
p-n junction transistors, 146
point de vue du Gras [view from the
 window at Le Gras], 22
poisoning from airborne molecular
 bases, 356
polarity changes
 — radiation-induced, 226
 — reverse, 235
polarization, 44
polarization plane, 49
poly(1,3-cyclopentylenevinylene), 367
poly(2-methyladamantyl methacrylate-
 co-gamma butyrolactone), 361
poly(2,7-bicyclo[2.2.1]hept-2-ene), 368
poly[3-methyl-2-(4-vinylphenyl)-2,3-
 butanediol], 235
poly(3-methyl-4-hydroxy styrene), 478
poly[4-(1-hydroxyethyl)styrene], 244
poly[4-(2-hydroxy-2-propyl)styrene],
 236
poly(4-hydroxy- α -methylstyrene), 352
poly[4-hydroxystyrene-*co*-4-(3-furyl-3-
 hydroxypropyl)styrene], 243
poly(4-hydroxystyrene sulfone), 352
poly(4-*tert*-butoxy- α -methylstyrene),
 353
poly(4-*tert*-butoxycarbonyloxystyrene
 sulfone), 353
poly(4-vinyl benzoate), 358
poly(4-vinylbenzoic acid), 358
poly(acrylamide), 217
polyacrylics, 145
poly(allyl methacrylate-*co*-
 hydroxyethyl methacrylate), 221
polyamic acids, 206
polyamides, 135
poly(butene sulfone) (PBS), 329, 332
poly(carbo-*t*-butoxynorbornene-*co*-
 maleic anhydride), 493–494
poly(carbo-*t*-butoxynorbornene-*co*-
 norbornene carboxylic acid), 493
poly(chloromethyl styrene-*co*-vinyl
 naphthalene), 223
poly(chloromethylstyrene), 222
poly(*cis*-isoprene) rubber, 208
poly(*cis*-isoprene)-bisazide negative
 resists, 208
polydimethylsiloxane, 165
poly(dinorbornene-*alt*-maleic
 anhydride), 373
polydispersity, 350
polyesters, 135, 205
polyfluoroalkylethers, 186, 422
poly(fluorobutyl-*co*-maleic anhydride),
 330
polygate process, 773
poly(glycidyl methacrylate) (PGMA),
 220
poly(glycidyl methacrylate-*co*-
 ethylacrylate), 221
poly(hexafluoro methacrylate), 328, 330
polyhydroxybenzophenone, 293
poly(hydroxyphenyl methacrylate), 353
polyhydroxystyrene (PHOST), 348–349
polyhydroxystyrene (PHOST) resists,
 183
poly(hydroxystyrene-*co-tert*-butyl
 acrylate), 359
polymer chemistry, development of,
 133–135
polymer cooperative dynamics, 473
polymer degradation, 411
polymer grains, 827
polymer relaxation-controlled mass
 transfer, 512

- polymer surface dynamics, 473
- polymer-bound dyes, 429
- polymerization length distribution, 830
- polymers, synthetic, 145
- polymer-tethered photoacid generators, 738
- poly(methyl methacrylate) (PMMA), 323, 330
- poly(methylisopropenyl ketone), 313
- poly(methylpentene sulfone) (PMPS), 334
- poly(methylpropyl bicyclo[2.2.1]-hept-5-ene-2-carboxylate-*co*-bicyclo[2.2.1]hept-5-ene-2-carboxylic acid, 493
- poly(methylpropyl bicyclo[2.2.1]-hept-5-ene-2-carboxylate-*co*-maleic anhydride, 493
- poly(*N*-hydroxyphenyl methacrylate), 353
- polynuclear aromatic hydrocarbons, 276
- poly(*N*-vinyl pyrrolidone), 234
- poly(*p*-acetoxystyrene), 322
- poly(perfluorobutyl methacrylate), 327–328
- poly(propargyl methacrylate-*co*-hydroxyethyl methacrylate), 221
- polysilanes, 393, 796
- polysilicon gate length, 463
- polysilynes, 393, 796
- polystyrene, cross-linking of, 222
- poly(styrene-*co*-maleimide), 352
- poly[styrene-*co*-*N*-(4-hydroxyphenyl)maleimide], 352
- poly(*t*-BOC-styrene-*co*-4-acetonxystyrene-*co*-styrene sulfone), 353
- poly(*tert*-butoxycarbonyl oxystyrene) (PBOCST), 322, 346
- poly(trifluoromethyl-*o*-chloroacrylate), 328
- poly(vinyl alcohol), 145, 209
- poly(vinyl butyral), 145, 209
- poly(vinyl cinnamate), 145, 201
- poly(vinyl cinnamate) resist system, 203
- poly(vinyl cinnamylidene acetate), 203, 205
- poly(vinyl ether-*alt*-maleic anhydride (VEMA), 364
- poly(vinyl naphthalene), 223
- poly(vinyl phenol), 217
- poly(vinyl pyridine), 208
- poly(vinyl pyrrolidone), 145, 209, 217
- popping, 467
- population inversion, 612
- portable conformable mask (PCM), 796
- positive resist, 159
- positive resist developers, 187
- positive-working reprographic plates, 287
- positron annihilation lifetime spectroscopy, 477
- postbake, 536–537
- postdevelopment bake, 536–537
- postexposure bake (PEB), 491
- postexposure bake (PEB) delay stability, 696
- postexposure bake (PEB) diffusion, 554
- postexposure bake (PEB) models, 579
- postexposure bake (PEB) sensitivity, 493, 684–685
- postexposure critical dimension (CD) shrink techniques, 797
- postexposure thermal processing, 5
- potassium carbonate, 104
- potassium hydroxide, 189
- potential diagram, 397
- potential energy, 397
- potential well, 397
- power density, 156
- power spectrum, 668
- p*-phenylenediacyrylic acid (PDDA), 205
- p*-polarization, 569
- prebake, 485
- precoated lithographic printing plates, 205
- presensitized lithographic plate, 211
- PREVAIL (projection reduction exposure with variable axis immersion lens), 759
- principal quantum number *n*, 130
- principle of continuity, 68
- printed circuit board (PCB), 138, 142–145
- printing modes, 658
- process-induced defects, 687
- processing speed, 156
- projection imaging system, 557
- projection printing, 162, 658

- projection reduction exposure with
variable axis immersion lens
(PREVAIL), 759
- projection soft x-ray lithography, 707
- PROLITH, 553
- propargyl methacrylate, 221
- propyleneglycol monoethylether acetate
(PGMEA), 185
- proteins, 133
- protons, 75, 127
- proximal probe lithography, 173–175
- proximity effects, 744, 803
- proximity ion-beam lithography, 762
- proximity printing, 162, 658
— theoretical resolution of, 162
- proximity projection lithography, 752
- prussic acid, 104
- puddle development, 505
- pulse energy, 609, 613
- pulse repetition rate, 609
- pulse width, 613
- pulsed Nd-YAG laser, 717
- pulsed photomagnetic curing, 306
- pupil function, 559
- pyréolophore, 19
- pyridine, 218
- pyrogalllic acid, 104
- Q**
- quantum effect devices, 151
- quantum theory, 64–65
— of light, 79–83
- quantum yield, 255, 500
- quartz crystal, 119
- quartz crystal microbalance, 308, 507
- quaternary pyridinium salts, 207
- quenching sphere, 403
- R**
- radiation, exponential attenuation of,
490
- radiation absorption, 184
- radiation chemical yield, 411
- radiation-induced cross-linking
reactions, 200
- radiation-induced negative resists, 200–
224
- radiation-induced polarity changes, 226
- radical polymerization, 350
- radical scavengers, 220
- radicals, 219
- radio frequency (RF) field, 193
- radio waves, 64
- radioactivity, 62–64
- radius of gyration R_g , 477, 830
- Raoult's law, 124
- rarefaction, 652
- rare-gas halide exciplex lasers, 610
- rare-gas monohalides, 609
- raster scan, 749
- raster scanning, 751
- rate constant, 494
- Rayleigh scattering, 652
- Rayleigh-Jeans law, 66–67
- Rayleigh's resolution criterion, 7
- reactions, law of, 109, 124
- reactive-ion etching (RIE), 232, 547–
548
- reciprocal portions, law of, 111
- reciprocity failures, 575
- rectilinear propagation of light, 41
- red shift, 397
- reduction optics, 163
- reduction potential, 409
- reduction projection printing, 163, 661
- reflecting telescope, 86
- reflection, law of, 34
- reflection amplitudes, 425
- reflection coefficients r_{12} , 425
- reflective notching, 420
- reflective systems, 163
- reflectivity R , 425
- reflow-based shrink techniques, 799
- refracting telescope, 86
- refraction, 35
— degrees of, 39
— double, 48
— laws of, 36, 37
- refractive index, complex, 424
- refrangibility, degrees of, 39
- registration, 160
- RELACS (resolution enhancement of
lithography assisted by chemical
shrink), 799
- relativistic mechanics, 84
- relativity, theories of, 70
- repetition rate, 613
- residence times, 724
- resist, 181

- resist (*cont.*)
- acetal-protected chemical amplification, 381–383
 - confinement effects in, 829–830
 - dry, 280–282
 - ester-protected chemical amplification, 357–360
 - ester-protected poly(hydroxy styrene)-based, 357–360
 - ester-protected poly(methacrylate)-based, 360–364
 - ether-protected chemical amplification, 344–345
 - high-activation-energy, 823
 - ketal-protected chemical amplification, 381–383
 - low-activation-energy, 823
 - manufacture of, 184–186
 - mask-making, 626
 - multicomponent, 182
 - one-component, 182
 - poly(chloroacrylate-*co*- α -methylstyrene), 334–335
 - poly(hydrostyrene) (PHOST), 183, 346–357
 - carbonate-protected, 346–348
 - poly(methyl isopropenyl ketone), 331
 - poly(olefin sulfone), 331–334
 - polyphthaldehyde, 387
 - poly(tetrahydrofuran-*co*-novolak), 344–345
 - resolution limit issues of, 792
 - single-layer (SLR), 360
 - sulfone/novolak system (SNS), 334
- resist based on ortho-nitrobenzyl chemistry, 318–322
- resist based on photo-Friess rearrangement, 322
- resist blur, 819
- resist classifications, 182
- resist contrast γ , 576
- resist developers and rinses, 187–189
- resist development, 505–506
- resist exposure, 415–418, 554
- resist sensitizer, 73, 398
- resist solvents, 184
- resist stabilization treatments, 536–543
- resist strippers and cleaners, 189–193
- resist stripping, 775
- resist stripping solutions, broad-spectrum, 190
- resistors, 147, 767
- resolution, 184
- resolution enhancement of lithography assisted by chemical shrink (RELACS), 799
- resolution enhancement techniques, 165, 798
- resolution limit issues of resists, 792
- respiration, 102
- rest mass, 85
- reticle, 164, 463
- reticulation, 540
- reverse polarity switch, 235
- rework/stripping, 438, 548–549
- rheological properties, 468
- riboflavin, 268
- rim phase-shifting masks (PSMs), 622–623
- ring-opening metathesis polymerization, 365, 367
- ring-shaped image field, 162
- Riston®, 145, 219
- Riston LUV®, 282
- Riston LV®, 268, 282
- rose bengal, 266, 268
- rosin, 454
- rubber, 133
- rubylith, 618
- ruthenium (Ru), 367
- Rutherford scattering, 540
- Rutherford's planetary model of the atom, 75
- ## S
- safflower oil, 194
- salt, 113–114, 188
- SAMPLE, 553
- sapphire, 649
- Sauerbrey equation, 510
- scalar diffraction theory, 556
- SCALPEL (scattering with angular limitation projection electron-beam lithography), 752
- SCALPEL mask, 754
- scandium, 126
- scanner-generated defects, 698
- scanning probe lithography, 165
- scanning strategies, 751

- scanning tunneling microscopy (STM), 165, 173
- scattering processes, 743
- scattering with angular limitation
 projection electron-beam lithography (SCALPEL), 752
- Schiemann reaction, 274–275
- Schrödinger equation, 130
- Schumann-Runge band, 614–615, 630
- scintillation counting, 356
- scission yield, determination of, 412
- screen printing, 144
- scumming, 420
- secondary structure model, 518
- second-harmonic generation, 625
- second-harmonic generators, 94
- selenium, 119
- self-aligned double patterning, 813
- self-aligned gate process, 151
- self-assembled monolayer (SAM), 171
- self-developed images, 387
- self-propagating chain reaction, 272
- semiconductor lithography, 3, 157–160
- semipermeable membrane, 122
- Senefelder, Alois, 11
- sensitivity, 184, 577
- sensitization
 — direct and indirect, 416
 — spectral, 406
 — triplet, 407
- sensitization by electron transfer, 408–409
- sensitization by energy transfer, 407–408
- sensitizer, 181, 182
- separability assumption, 564
- shadow mask proximity printing, 752
- shallow trench isolation process, 773
- shaped beam, 749
- shear rate, 469
- shear stress, 469
- sheet-fed system, 457
- shelf life, 212
- shellac, 145, 209
- short-wavelength imaging, 797
- shot noise, 758, 828
- shot noise limit, 828
- sidewall erosion, 803
- sidewall formation, 803
- sidewall spacer formation process, 773
- sighting tubes, 36
- silane (SiH_4) gas, 778
- silane-coupling agent, 466
- silanol, 465
- silanol polymers, 184
- silicon dioxide (SiO_2), 464
- silicon fluoride (SiF_4), 103
- silicon nitride (Si_3N_4), 776
- silicon oxynitride, 186, 431
- siloxane, 394, 796
- siloxycarbenes, 218
- silsesquioxanes, 245
- silver halide plates, 141
- silver metal, 227
- silver nitrate, darkening of, 55
- silylating agents, 794
 — liquid and vapor phase, 393
- silylation processes, 795
- SiN , 787
- single-electron memory cell (SEMC), 150
- single-exposure techniques, 797
- single-layer resist (SLR), 360
- singlet oxygen, 636
- singlet S_1 , 395
- singlet-triplet splitting, 408
- Snell's law, 37
- sodium ammonium racemate, 119
- sodium fluoride, 649
- sodium metasilicate, 504
- soft bake, 485
- soft lithography, 165, 170–171
- soft x rays, 170
- soft x-ray lithography, 703
- softening point, 212
- solar cell, 149
- solar spectrum, 74
- solder mask, 283
- solid state electronics, 146
- solid state photodimerization, 202
- solid-film resists, 145
- solubility, 184
- solubility parameter, 356
- solution, 97
- solution pressure, 124
- solutions, theory of, 122–123
- solvation, 507
- solvent, 181
- sorting, 773
- sound wave, 49

- source, 768
 source/drain (S/D) implant process, 773
 soy oil, 194
 space velocity, 470
 space-charge effects, 169, 753
 spark discharge plates, 141
 spatial coherence, 613
 spatial filtering, 93
 spatial frequencies, 558
 specific conductivity κ , 123
 specific heats, 102
 speckles, 613
 spectral bandwidth, 609
 spectral sensitization, 203, 406
 spectroscopic ellipsometry, 477
 spherical aberration, 36
 spherical wavefront, 561
 spin coating, 468
 spin-forbidden plane vibrations, 396
 spinodal decomposition, 474
 SPLAT, 554
 s-polarization, 569
 spray coating, 468
 sputtering, 546, 772
 stabilizers, 182
 stamping, 165
 standing-wave effects, 166
 standing-wave models, 566–570
 standing waves, 419, 556
 — reduction of, 557
 starch, 209
 state-mixing effects, 396
 statistical mechanics, 65
 statistical theory of heat, 65
 statistical thermodynamics, 64
 steady state approximation, 270–271
 steam lithographic press, 16
steindruck [stone printing], 13
 stencil masks, 752
 step-and-flash imprint lithography, 172
 step-and-repeat systems, 691
 step-and-scan systems, 164, 619
 step-and-scan tools, 661
 steppers, 661
 stereochemistry, 119
 stereolithography, 176
 stochastic blur, 766
 stochastic scattering, 743
 Stockmayer's rule, 255
stoicheia [elements], 95
 stone lithography, 451
 stone plate lithography, 137
 stone printing [*steindruck*], 13
 stone wall model, 518
 storage cell, 436
 storage stability, 184
 STORM, 554
 stress-induced birefringence, 652
 string algorithm, 553
 strippers, 181
 stripping issues, 438, 548–549
 strutted mask, 754
 styrylpyridine, 206
 styrylpyridinium, 208
 styrylquinolinium, 208
 SU8™, 277
 sublimation, 97, 428
 subsidiary quantum number l , 131
 substitution, theory of, 117
 substrate preparation, 5
 substrate priming, 466
 sugars, 118
 sulfinic acids, 341
 sulfonal ester of cumylphenol, 293
 sulfone/novolak system (SNS) resists, 334
 sulfonic acid, 190, 341
 sulfonic acid chloride, 292
 sulfonium salts, 275
 sulfurane, 191
 sulfur, 119
 sulfuric acid, 190
 sunflower oil, 194
 supercritical (SC) carbon dioxide (CO₂), 247, 536
 superposition principle, 823
 surface contamination, 720
 surface dynamics, 473
 surface energy, 467
 surface inhibition effects, 593
 surface inhibition function, 553
 surface tension, 467
 surfactants, 182
 sweet PAG, 379
 swelling, 507, 696
 swing amplitude S , 420
 swing curve effects, 420
 switching delay, 155, 156
 synchrotron sources, 705–706
 synchrotron storage ring, 705

Syrian asphalt, 182

T

tactile and emission theories of light, 33

talc powder, 454

tantalum (Ta), 706, 787

tantalum boride (Ta₄B), 706

tantalum nitride (TaN), 706, 787

tantalum silicide (TaSi₂), 186, 431

tantalum silicide nitride (TaSiN), 706

target materials, 717

tartaric acid, 104, 118

t-butoxycarbonyl oxystyrene, 352

t-butyl methacrylate, 250

technology computer-aided design (TCAD), 554

Teflon-based materials, 186, 422

telescope, invention of, 36

TEMPEST, 554

temporal coherence, 613

temporally coherent sources, 608

tert-butyl acrylate, 367

tert-butyl-2-trifluoromethylacrylate (TBTfMA), 377

tetrabromobisphenol A, 341

tetracene, 398

tetrachloroethylene, 190

tetrafluoroethylene (TFE), 375

tetrahydropyranal ether, 344

tetrahydropyranal methacrylate, 250

tetramethylammonium hydroxide (TMAH), 188, 504

thermal expansion coefficient, 745

thermal oxidation, 464

thermal properties of fused silica, 651

thermal stability, 184

thermalization distances of electrons, 417

thermally induced reflow, 799

thermionic emission, 747

thermionic sources, 747

thermochemistry, 121–122

— foundations of, 107

thermodynamics, third law of, 124

thermogravimetric analysis (TGA) profile, 369

thermolysis, acid-catalyzed, 226

thermoplastics, 197

thermosets, 198

thiazines, 268

thiol-ene system, 272–273

thionyl chloride, 292

thiourea, 306

thioxanthenes, 265

thoriated tungsten, 747

thyristor, 149

time constant, 475

tin (Sn), 119, 717

titanium (Ti), 782

titanium nitride, 186, 431

titanium silicide (TiSi₂), 782

TMAH (tetramethylammonium hydroxide), 188, 504

top antireflection coatings, 186

— theory of, 424

— water-based, 423

top surface imaging (TSI), 391

top surface imaging (TSI) resist system, 794–795

topcoats, 694–696

transesterification, 247

transfer functions, 93

transistor, 138, 767

— bipolar, 147

— first point contact, 146

— invention of, 146–147, 605

transistor action, 146

transistor effect, 146

transistor gate width, 156

transition dipole moments, 400

transmission amplitudes, 424–427

transmission coefficients, t_{12} , 425

transmittance, 490

transmutation of elements, 133

transport number n , 123

transuranium elements, 133

transverse electric (TE) field, 448

transverse electric (TE) field polarization, 569

transverse magnetic (TM) field, 448

transverse magnetic (TM) field polarization, 569

transverse wave, 49

trench isolation, 151

trenches, 463

trench-first approach, 787

triarylsulfonium salts, 276

triazines, 261–262

trichloroethylene, 190

trichromatic theory of color vision, 43

- triethanolamine, 300
triethylamine, 264
trifluoromethane sulfonic acid, 503
trim mask, 811
trimethylsilyldiethylamine (TMSDEA),
393, 466, 794
trimethylsilyldimethylamine
(TMSDMA), 393, 794
triphenyl sulfonium
hexafluoroantimonate, 278
triphenyl sulfonium
trifluoromethanesulfonate, 340
triphenyl sulfonium salts, 343
triplet, T_1 , 395
triplet sensitization, 407
triplet-to-singlet energy transfer, 402
truxillate, 202
truxinate, 202
T-topping, 315
tung oil, 194
tungsten (W), 367, 706, 747
tungstic acid, 103
tunnel diode, 149
turpentine, 118, 184
tusche, 452
twin-well process, 773
Tyndall phenomenon, 116
- U**
- ultraviolet (UV) lithography, 606
— optical materials used in, 649
ultraviolet (UV) radiation, 55
ultraviolet (UV) radiation curing,
537–540
undercutting, 430
undulatory theory of light, 40, 42–44
universal gas constant, 121
uranium, 64, 133
urea, 117
uric acid, 104
- V**
- vacuum tubes, 147
valency, electronic theory of, 129
van der Waals radii, 397
vapor pressure, lowering of, 123
vector scan mode, 749
vector scanning, 751
via and tungsten plug formation
processes, 773
via-first approach, 429, 787
vias, 463, 783
vinyl addition polymerization, 368
viscosity, 185, 469
— kinematic, 470
viscous forces, 468
visible light lithography, 606
vital force, 117
- W**
- W (tungsten), 367, 706, 747
wafer, 543
wafer testing, 773
water, 184
water marks, 696
water-based top antireflection coating
materials, 423
water-immersion ArF (193-nm)
lithography, 164, 692–700
waterless offset lithography, 460–461
waterless plates, 141
water-processable resists, 207, 217
wave theory of light, 40, 42–44
wavefront aberration, 708
wavefunction ψ , 132
wavelength markers, 86
wave-particle duality, 81
wax-lampblack-soap resists, 199–200
web system, 457
weight-average molecular weight, 252
wet etching, 544–545
wetting agents, 194
Wittig reaction, 350
Wolf rearrangement, 296
Wollaston doublet lens for microscopes,
50
work function, 747
work of adhesion, 468
writing rate, 749
- X**
- xanthenes, 268
xenon (Xe), 717
x rays, 5, 63
— soft, 170
x-ray diffraction, 91
x-ray lithography, 165–166, 703
x-ray mask absorbers, 706
x-ray mask membranes, 706
x-ray masks, 166, 706–707

x-ray reflectivity, 479
x-ray reflectometry, 477
xylene, 184, 187

Y

ylide resists, 232–223
Young's equation, 467
Young's modulus, 534, 706
Young's two-slit experiment, 73

Z

Z-constant, 833
Zernike coefficient, 562
Zernike polynomials, 93, 561
zero reflectivity, phase match condition
 for, 426
zero-order scalar model, 564
Ziegler-Natta catalysts, 367
zinc chloride, 234



Uzodinma Okoroanyanwu is a senior member of the technical staff in the Technology Research Directorate of GLOBALFOUNDRIES, a company that is partly owned by AMD. He worked at AMD from 1997 to 2009, during which time, he conducted research in KrF, ArF (dry and immersion), F₂, and EUV lithographic process technologies, organic electronics, and electro-chemistry. He was a research scientist (on assignment from AMD) at IMEC in Belgium between 2002 and 2004, at Fachbereich Physikalische Chemie, Universität Oldenburg, Germany, in 2001, and at Fujitsu Laboratories in Mie, Japan, in 1998. He has published extensively

on lithography science and technology, polymer science and engineering, and organic electronics. He holds 27 U.S. patents. He is a member of the American Chemical Society, the American Association for the Advancement of Science, Deutsche Bunsen Gesellschaft für Physikalische Chemie, e.V. and SPIE. He holds the following degrees from The University of Texas at Austin: PhD in physical chemistry (1997), MS in chemical engineering (1995), MA in physical chemistry (1994), and BS in chemistry and chemical engineering (1991).